RIKEN Accelerator Progress Report

2021

Vol. 55

国立研究開発法人理化学研究所　仁科加速器科学研究センター
RIKEN Nishina Center for Accelerator-Based Science

RIKEN Accelerator Progress Report 2021

Vol. **55**

国立研究開発法人理化学研究所　仁科加速器科学研究センター
RIKEN Nishina Center for Accelerator-Based Science
Wako, Saitama, 351-0198 JAPAN

RIKEN Accelerator Progress Report 2021 Vol. 55

This is an unabridged version of the 55th volume of RIKEN Accelerator Progress Report (hereinafter referred to as APR), the official annual report of the Nishina Center for Accelerator-Based Science.

A PDF version of APR can be downloaded from our website.
http://www.nishina.riken.jp/researcher/APR/index_e.html

Published by
RIKEN Nishina Center for Accelerator-Based Science
2-1 Hirosawa, Wako-shi, Saitama 351-0198 JAPAN

Director of RIKEN Nishina Center for Acclerator-Based Science
Hiroyoshi Sakurai

Contact
progress@ml.riken.jp

RIKEN Nishina Center for Accelerator-Based Science, November 2022

PREFACE

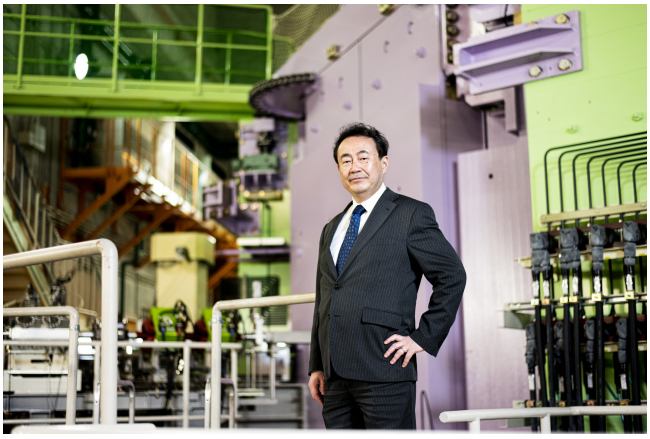

The RIKEN Accelerator Progress Report is the annual report of all the research activities conducted at the RIKEN Nishina Center for Accelerator-Based Science (RNC). This volume covers the activities conducted during the Japanese fiscal year 2021 (i.e., April 2021 to March 2022).

Masaaki Kimura launched a new laboratory, "Nuclear Many-body Theory Laboratory," in October 2021 to further strengthen nuclear theory activities cooperating with experimental programs at Radioactive Isotope Beam Factory (RIBF). Yoshitaka Hatta has been appointed as Group Leader of Theory Group in RIKEN BNL Research Center (RBRC) as of May 2021.

Two years have passed since restrictions on social activities were first imposed due to the coronavirus crisis. However, we are yet to know what changes the pandemic will bring for us in future.

The COVID-19 vaccination drive began in 2021 along with implementation of other measures to prevent the spread of the virus. Although we managed to overcome a huge rise in the coronavirus cases last summer, we had to face the spread of a new variant, Omicron, at the end of the year. The emergence of new variants of coronavirus counters the effect of the vaccine. However, this cannot be prevented. Therefore, it is imperative to find ways to adapt to living alongside the coronavirus.

Our society is progressively becoming polarized in the way people think: "virus" vs "vaccination," "justice" vs "injustice," "restriction" vs "ease," "wealth" vs "poverty," "authentic" vs "fake," and "nation" vs "individual." Because science and technology always seek "authenticity," according to me, the pandemic has not significantly changed how science and technology is viewed. I believe that science and technology originate from curiosity and ideas of an "individual" and its end goal is welfare of humanity. Consequently, I anticipate that science and technology connecting "individual" with humanity will play a vital role despite the pandemic.

Many outstanding research results were obtained at RNC last year, some of which took less than a year since their inception, while others were the fruition of research that took more than several decades. We will continue to strive to contribute significantly to research, which we hope will yield results in future.

Eleven press releases were disseminated in FY2020. Selected strides made in 2020 have been compiled in the "Highlights of the Year" section in this volume, which show successful multi-disciplinary activities of RNC for science, technology, and innovation. It is noteworthy that these were achieved not only the in-house researchers and engineers in RNC but also by collaborating users at RIBF, RBRC, and Rutherford Appleton Laboratory. "Measurement of neutron-rich high-dense matter pressure," published in Physical Review Letters is a result obtained with the SπRIT TPC in the SAMURAI magnet to give the information on equation-of-state in asymmetric nuclear matter. The heavy-ion beam breeding successfully created a new type of Satsuma mandarin orange, which will have a huge impact on the orange market in Japan. RNC has started delivering ^{211}At for an investigator-initiated trial at Osaka University Hospital for refractory thyroid cancer.

Colleagues of RNC were awarded: Tomoko Abe for the "IAEA Women in Plant Mutation Breeding Award," and Ryo Taniuchi for "Inoue Research Award for Young Scientist." "Young Scientist Award of the Physical Society of Japan" was given to Tokuro Fukui, Junki Tanaka and Takumi Yamaga. Masaomi Tanaka was awarded the "RIBF Thesis Award." "Student Presentation Award of the Physical Society of Japan" and "2021 Symposium on Nuclear Data Poster Presentation Award" were given to Akira Hirayama and Kenta Sugihara, respectively. The "2021 RIKEN Awards" included the "EIHO Award," which was given to Kazuhide Tsuneizumi *et al*. "BAIHO Award" was given to Tadaaki Isobe and Junki Tanaka, and "OHBU Award" to Momo Mukai and Minori Tajima.

Hiroyoshi Sakurai
Director
RIKEN Nishina Center for Accelerator-Based Science

C O N T E N T S

Ⅱ. RESEARCH ACTIVITIES I (Nuclear, Particle and Astro-Physics)

1. Nuclear Physics

2. Nuclear Physics (Theory)

3. Nuclear Data

4. Hadron Physics

Ⅲ. RESEARCH ACTIVITIES II (Material Science and Biology)

1. Atomic and Solid State Physics (Ion)

2. Atomic and Solid State Physics (Muon)

3. Radiochemistry and Nuclear Chemistry

4. Radiation Chemistry and Biology

Ⅳ. OPERATION RECORDS

Ⅴ. EVENTS

Ⅵ. ORGANIZATION AND ACTIVITIES OF RIKEN NISHINA CENTER (Activities, Members, Publications & Presentations)

Ⅶ. APPENDICES

ImPACT Data are taken at RIBF

Photo : Inside the accelerating cavity of Superconducting Ring Cyclotron

RNC's initiatives in the ImPACT program

The ImPACT Program

Since 2007, Radioactive Isotope Beam Factory (RIBF) [1] has been one of the world-leading heavy-ion accelerator facilities for low-energy nuclear physics. RIBF has contributed to the expansion of the nuclear chart by producing more than 150 new isotopes and has provided a multitude of opportunities to discover new phenomena originating from high isospin asymmetry. In parallel to such pure nuclear physics activities, a new and national program of nuclear engineering was launched for social benefits. In the period of 2014–2018, the program entitled "Reduction and Resource Recycling of High-level Radioactive Wastes through Nuclear Transmutation" [2] was carried out as one of the ImPACT R&D programs conducted by the Cabinet of Japan.

Since Hideki Yukawa left the Japan Atomic Energy Commission in 1957, the nuclear physics and nuclear engineering communities have been separated in Japan. The incident of the Fukushima Dai-ichi Unit in 2011, however, impelled Japanese nuclear physicists to seriously consider possible contributions to nuclear engineering. In 2014, a demonstration experiment was performed with RIBF. In this experiment, the inverse kinematics with energetic radioactive-isotope (RI) beams of ^{137}Cs and ^{90}Sr was employed to study spallation reaction to find an efficient reaction pathway for reduction of the radioactivity.[3] The experiment provided an opportunity to the physicists and engineers to work together. The potentials of RI beams at RIBF were also demonstrated, and the fundamental reaction data obtained with RI beams were found highly useful for designing an accelerator-based transmutation system.

High-level radioactive waste has two main components: long-lived fission products (LLFPs) and minor actinides (MAs). The transmutation of MAs has been studied in detail for the purpose of reprocessing spent nuclear fuel under the concept of using fast-breeder reactors or accelerator-driven systems. The LLFP nuclides are supposed to create risks in the geological disposal strategy because their half-lives are much longer than those of MAs. However, the transmutation of LLFPs has not been studied extensively. Considering the present situation of R&D activities in the field of the radioactive waste, the ImPACT program was jointly proposed by the nuclear physicists and engineers, to focus on accelerator-based transmutation of LLFPs.

The ImPACT program emphasized on the "resource recycle" of radioactive waste. Thus, ^{107}Pd and ^{93}Zr were highly prioritized as objectives. The program consisted of five projects as follows:

Project-1: Development of separation and recovery technologies,

Project-2: Production of nuclear reaction data and new nuclear reaction control methods,

Project-3: Reaction theory modeling and simulation,

Project-4: Evaluation of the nuclear transmutation system and development of elemental technologies, and

Project-5: Process design concept by nuclear engineers.

All the projects were managed coherently, and Project-2 and Project-4 were conducted by RIKEN Nishina Center.

An overview of the activities in Project-2 and -4 is presented in this article.

Transmutation Reactions for Accelerator System

To design an accelerator system for the transmutation, the possible reactions for the transmutation were intensively discussed at an early stage of the ImPACT program.

First, we adopted nuclear reactions, not electromagnetic reactions. In the case of nuclear reactions induced by "hadron" particles, which interact strongly with LLFP nuclei, several reactions, such as spallation, knockout reactions, are applied with reaction cross sections of the order of 1 barn. Conversely, in the case of electromagnetic reactions, the reaction candidate is only the photoabsorption process (γ, n), and its cross section is approximately 0.2 barns for LLFPs. To induce the (γ, n) reaction, secondary high-energy photons, of which energy is more than 10 MeV, should be produced by high-energy electron beams through the bremsstrahlung process in a converter material or through the inverse Compton process with intense laser lights. However, the high-energy photons are wasted to create the electron-positron pairs, simply because the cross section of the pair creation is 10 barns, much higher than that of the photoabsorption. Thus, most of the electron-beam energy is wasted in creating the electron-positron pairs, not in transmuting LLFP nuclides significantly.

Next, several types of nuclear reactions were considered for transmutation and were categorized with respect to transmutation throughput and reaction controllability. The candidate reactions are spallation reaction, neutron knockout reaction, such as $(n, 2n)$, and muon capture reaction. The spallation reaction induced by high-energy proton- or deuteron-beams is very promising in terms of throughput, but it is not excellent in terms of controllability. When the spallation reaction is applied, the beams are irradiated directly to LLFP materials, and the target thickness is determined from the stopping range of the beams. Higher energy beams lead to thicker targets, and hence, the throughput is increased as a function of beam energy. However, according to the results obtained in Project-2, higher beam energy produces more nuclides as spallation products, because a

higher energy beam deposits higher energy in the target nuclei, and the higher deposited energy in the nuclei is used to emit more protons and more neutrons from the nuclei. Thus, in the case of the spallation reaction, the optimal beam-energy should be carefully considered in terms of not only the throughput but also the costs necessary to treat radioactive nuclides produced in LLFP materials after long-term irradiation.

The neutron knockout reaction is induced by high-energy neutrons with energy more than 8 MeV. In the case of even-odd separated LLFP, especially for the Pd nuclides, the neutron knockout reaction has very high reaction controllability. After the even-odd separation, ^{105}Pd and ^{107}Pd are left as nuclear waste (^{105}Pd is a stable nuclide, and ^{107}Pd is a long-lived one). The $(n, 2n)$ reaction produces ^{104}Pd and ^{106}Pd which are both stable, and $(n, 3n)$ reaction also could be applied to produce ^{103}Pd and ^{105}Pd. The ^{103}Pd nuclide is not stable, but its half-life is as short as approximately 17 days. The neutron energy range appropriate for $(n, 2n)$ is 8–18 MeV, and it gives the cross section of approximately 2 barns. Higher energy neutron beams also induce $(n, 3n)$. The high energy neutron beams could be created by high energy deuteron beams via breakup reaction. The broad energy range of neutrons is very useful because this leads to the generation of high flux neutron for transmutation. The target thickness for the neutron knockout reaction is determined from the mean-free path of the reaction, which is of the order of 100 g/cm^2 in Pd metal.

The other reaction candidate is the negative muon capture reaction. The negative muon capture process also has high reaction controllability. A negative muon is a unique particle, which interacts electromagnetically and can form a muonic atom where, like an electron, the negative muon is trapped by a nucleus. Then, the muon is captured by a proton inside the nucleus by weak interaction, and the proton is converted to a neutron. The capture probability per muon is almost 100% for $Z >$ 40 nuclides, when the negative muons are implanted to the material with $Z > 40$. Because s muon is approximately 100 times heavier than an electron, the energy transfer in the process is rather high, and a few neutrons are emitted from the nucleus. Hence, the muon capture has reaction controllability for the proton number and decrements the number by one. This feature of the muon capture is very useful for chemical separation. In the case of Pd with atomic number of 46, the products are only Rh with atomic number of 45. Although the negative muon is very promising in terms of controllability, the production of a muon is rather energy consuming; the production of one muon needs 5 GeV. A negative muon is created through decay of a negative pion, and the pion is created by a high-energy nuclear reaction, for example, proton induced nucleus collision, in which the proton energy should be higher than 300 MeV. The pion production cross section highly depends on the energy of beams and isospin of beams. Accelerator facilities for muons, such as TRIUMF, PSI, RAL, and J-PARC, deliver high-energy and intense proton beams with energy of more than 500 MeV, and the target thickness is limited to avoid pion capture in the target. These facilities are not optimized for negative muon productions. Instead of proton beams, deuteron beams can produce four times more negative muons than proton beams because of the isospin effects.

Negative muons are also useful to produce 14 MeV neutrons via muon catalyzed fusion of $d + t$. In the process, one muon can create approximately 100 14 MeV neutrons. Thus, the energy cost for a 14 MeV neutron is approximately 50 MeV. This value is smaller than that in case of an accelerated deuteron beam inducing $d + t$ fusion, which is approximately 2 GeV.

Regarding the neutron capture process, it is noted that neutron capture cross section for ^{107}Pd is higher than 1 barn at a neutron energy below 100 keV and 10 barns at 10 eV to 1 keV. Thus, neutrons produced via spallation reaction are also very useful for transmutation. In the case of the even-odd separation scheme for the Pd nuclides, the neutron capture changes ^{105}Pd and ^{107}Pd to ^{106}Pd and ^{108}Pd, respectively, which are both stable nuclides. Thus, a combination of the knockout reaction and neutron capture could lead to high throughput for transmutation. Considering all the above, we have decided to design an accelerator system for deuteron beams. The deuteron beams are utilized for a variety of applications: spallation reaction in direct irradiation as well as spallation neutron production, high energy neutron production via the deuteron breakup reaction, and efficient production of negative muons.

Nuclear Reaction Data with RIBF

Project-2 aimed to produce reaction data of the LLFPs that could be evaluated and utilized as input for a simulation code as part of Project-3. As introduced in the previous section, all the possible reactions for transmutation were discussed: proton-, deuteron-, and neutron-induced reactions and muon capture reactions.

In the case of direct irradiation of charged-particles into an LLFP material, an energy-dependence study of the reaction is quite important because of the stopping power in the material. This argument is also applied for the high-energy neutron-induced spallation reaction. A challenge for the energy-dependence study is to build a bridge over the Fermi energy; at a lower energy, the collective natures of the reaction are dominant and at a higher energy, the nucleon-based natures become dominant.

According to the experiences in the previous experiment of ^{137}Cs and ^{90}Sr,[3] the reaction study for proton-, deuteron-, and neutron-induced reactions was conducted in inverse kinematics at RIBF under a large domestic collaboration comprising the University of Tokyo, Tokyo Institute of Technology, Kyushu University, Miyazaki University, Niigata University, and RIKEN. Compared with the traditional activation method via normal kinematics

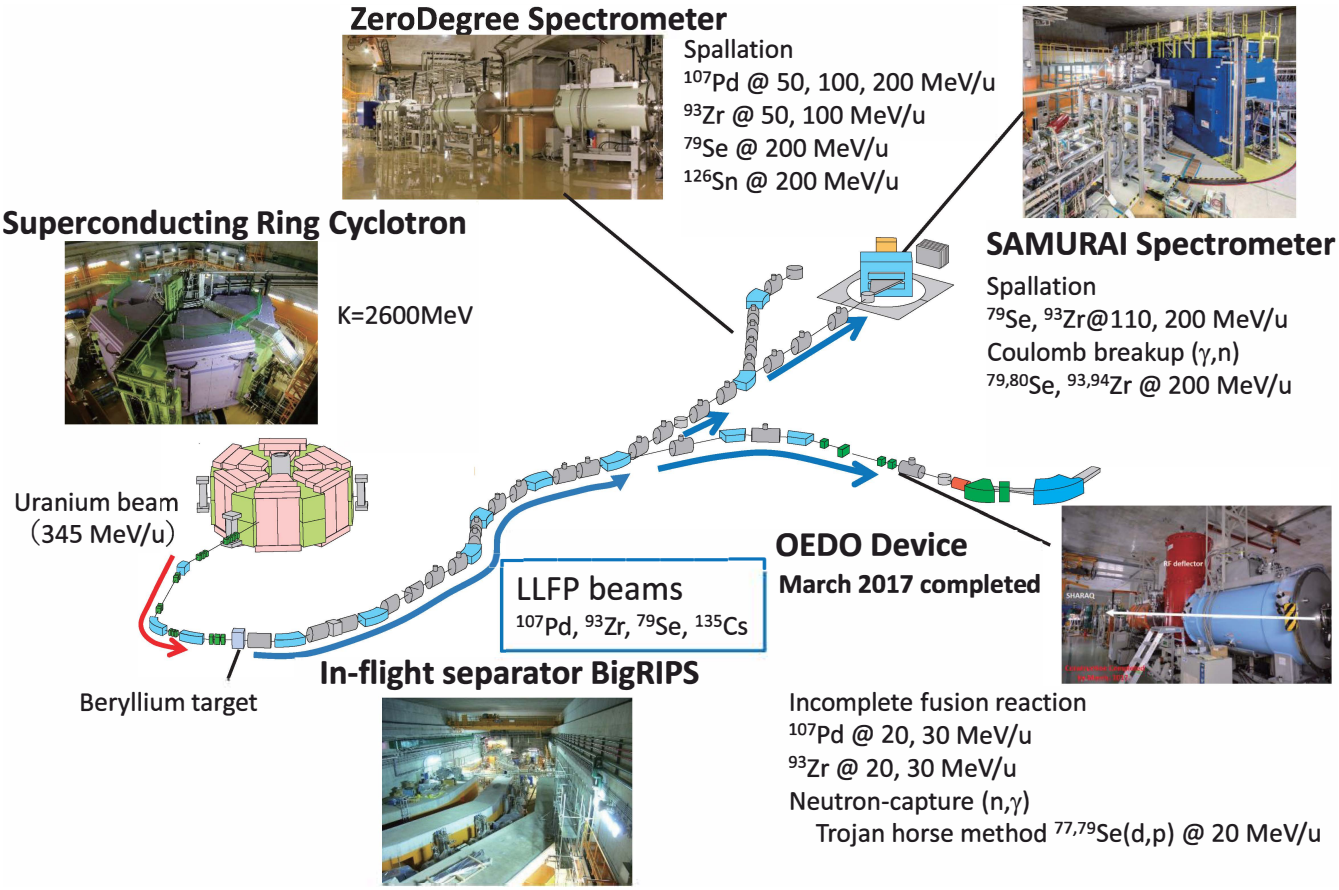

Fig. 1. Reaction study for long-lived fission products at RIBF in the ImPACT program. Major spectrometers such as, ZeroDegree, SAMURAI, and SHARAQ, were utilized.[4)]

with stable beams and RI targets, the inverse kinematics technique gives clear particle identification for reaction products and easy control of RI beam energies for the study of energy-dependence. In addition, we do not have to prepare RI targets but stable-isotope targets, such as protons and deuterons. All these advantages of inverse kinematics result in reaction data of excellent quality at RIBF.

As shown in Fig. 1, intense beams of LLFPs, such as ^{107}Pd and ^{93}Zr were produced at the in-flight separator "BigRIPS" via fission reactions with a uranium beam accelerated at Superconducting Ring Cyclotron (SRC), and then were delivered to three spectrometers (ZeroDegree, SAMURAI, and SHARAQ), which were utilized to identify and analyze the reaction products.[5–9)] ZeroDegree is suitable for inclusive measurements with relatively heavy fragments. SAMURAI has a wide acceptance in both momentum and scattering angle for reaction products. Hence, semi-exclusive measurements were performed to detect reaction products as well as neutrons in the projectile frame. At the SHARAQ spectrometer, CNS, the University of Tokyo and RIKEN worked together to develop an efficient deceleration scheme for RI beams. A new device "OEDO"[10)] was installed in the SHARAQ beamline to control emittance growth by transverse RF electric fields. An operation mode of BigRIPS was developed to realize energy-decelerated beams.[11,12)] The combination of OEDO and energy-decelerated beams successfully led to a reaction study at an energy of 20 MeV/nucleon.

Enhancement of element production by incomplete fusion reaction with weakly bound deuteron was observed at 50 MeV/nucleon,[9)] as shown in Fig. 2, and the incident energy was much higher than the energy scale of complete fusion reaction. The reaction mechanism could be applied to produce a higher Z element by increasing the atomic number by 2 via heavy loosely bound nuclei such as ^{9}Be and ^{6}He. Another highlight is a deduction of neutron capture reaction via the Trojan horse method with a low energy RI beam at 20 MeV/nucleon.[13)] In future, the new method can be widely applied not only for nuclear engineering but also for nuclear astrophysics.

All these data stimulated theoretical works, and the JAEA nuclear data group developed a new data library "JENDLE/ImPACT–2018" for proton- and neutron-induced reactions up to 200 MeV/nucleon.[14)] The new library has been built in as a package of PHITS simulation code.[15)]

A test of ^{107}Pd transmutation with macroscopic quantities was conducted with normal kinematics by utilizing

a low energy deuteron beam at the AVF cyclotron at RIBF.[16] Almost 100% enriched ^{107}Pd was prepared as a target and irradiated for several days. After the irradiation, the reaction products were identified from gamma-ray and ICP-MS measurements. The production yields were found consistent with PHITS predictions.[15]

Accelerator System

Project-4 proposes an accelerator-based transmutation system for LLFPs, and focuses on three objectives: (1) to design an accelerator system with a possible transmutation scenario, (2) to develop essential technologies for a high-power accelerator system, and (3) to encourage ideas for new high-power and energy-saving accelerators. Four activities by the RIKEN Nishina Center are selected and briefly introduced.

Linear accelerator system ImPACT2017

Delivering high-energy and intense deuteron beams is essentially important for the nuclear transmutation as described in the second section. The next question is the intensity of deuteron beams. In the existing facilities in operation, the maximum intensity of proton beams is of the order of 1 mA. As discussed in the ImPACT project, the beam intensity necessary for the transmutation is at least 1 A, which is three orders of magnitude higher than that of the present facilities. It should be noted that 1 A corresponds to approximately 1 mol/day. If all the beams contribute to the transmutation, the throughput would be approximately 100 g/day for the mass number of 100, which corresponds to 36 kg/year.

To achieve a 1-A deuteron beam, we have made a conceptual design for a linear accelerator system called "ImPACT2017,"[17] as shown in Fig. 3. There are a few key aspects of ImPACT2017. First, the system does not start with a radio-frequency quadrupole (RFQ). Second, the RF cavity of the linear accelerator is made as a single cell. The RFQ device is convenient and widely employed because a single RFQ device has three functions: beam bunching, acceleration, and focusing. However, a small beam aperture of RFQ (~1 cm) limits the beam current due to the space charge effect. Thus, we must develop other types of acceleration scheme, which is capable for a large size beam. To accelerate a high-intensity beam, we must supply high RF power to the cavities. A standard configuration has several cells in one cavity, and the RF power is supplied to the cavity through RF couplers. Each RF coupler has a limitation for transmitted power; hence, many RF couplers should be attached to the cavity. In this case, a multi-cell configuration may cause problems in operation. Decrease the number of RF couplers is significant for reasonable operation of the linear accelerator, and we have decided to employ a single cell configuration for the cavity. Further details of the new idea are found in Ref. 17).

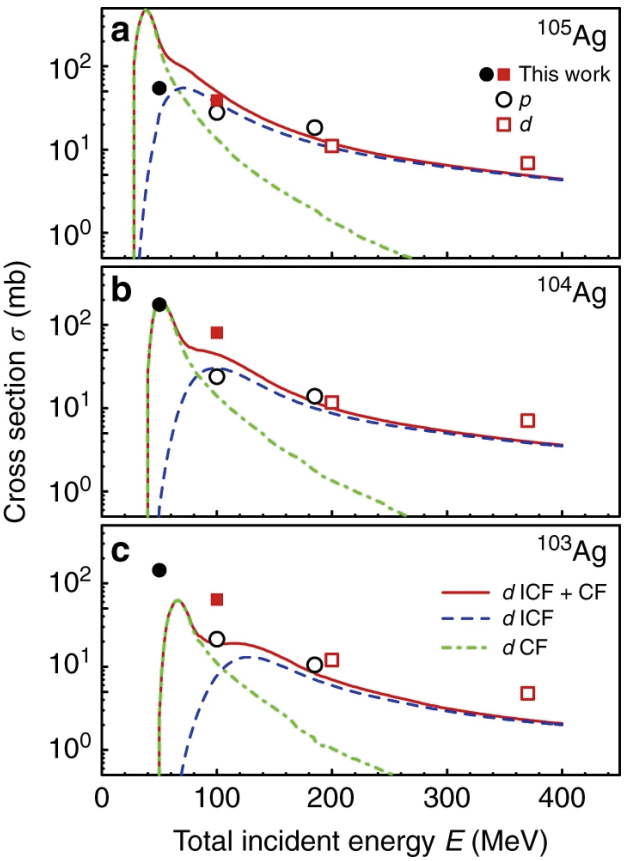

Fig. 2. Proton-induced and deuteron-induced cross sections for the ^{103,104,105}Ag isotopes produced by ^{107}Pd as a function of total incident energy, taken from Ref. 9). Cross sections on proton and deuteron are displayed by circles and squares, respectively. Enhancement of the ^{103,104}Ag cross sections with deuterons is clearly observed at the incident energy of 100 MeV, *i.e.*, 50 MeV/nucleon for deuterons.

R&D of key technologies for high-power accelerator system

As essential components for high power accelerator systems, a superconducting RF cavity for low-velocity charged-particles, material-free window-system for vacuum sealing, and liquid-target system for production targets have been developed by the RIKEN accelerator group.

R&D of a quarter-wave superconducting RF-cavity for low-velocity charged-particles[18] is essential to achieve low power consumption and space-saving. A prototype of the cavity was designed, constructed, and tested. The cavity was successfully cooled down to 4 K with liquid He, and acceptably high values of Q (~10^9) and acceleration electric field (up to 9 MV/m) were achieved. Based on the experiences in this R&D process, the linear accelerator RILAC has been recently upgraded by installing a similar type of superconducting RF-cavities.[19]

A plasma-window with a diameter of up to 20 mm was developed as the material-free window system for vacuum sealing. The achieved pressure and the V-I characteristics as a function of diameter were investigated.

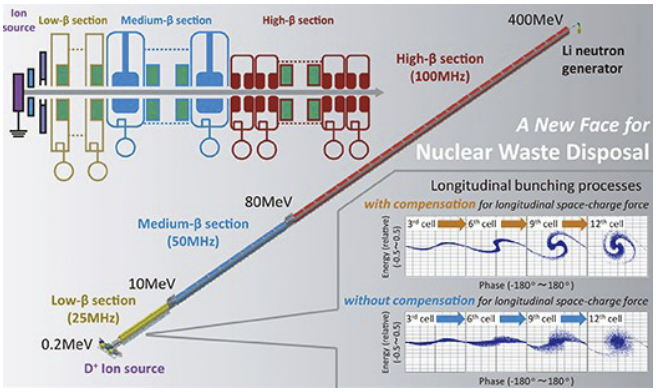

Fig. 3. Schematic of the 1-A Linac, taken from the cover page of Proc. Jpn. Acad. Ser. B **95**(7).[17)]

Detailed information can be found in Ref. 20).

The new idea of a target accepting the high intensity beam was proposed and published as patent.[21)]

Summary and Future Perspectives

The ImPACT program ran from 2014 to 2018 as the first step in the nuclear transmutation of LLFPs and successfully stimulated the interest of the nuclear chemists, nuclear physicists, accelerator physicists, and nuclear engineers in Japan. The program created new data as well as new ideas. In the second step, it is necessary to identify R&D items and proceed. For example, the transmutation scenario with high-energy neutrons still needs nuclear reaction data with ^{99}Tc and other nuclides. In addition, 1-A Linac would be highly desirable. R&D for a target to accept the very intense deuteron beam must be conducted in the future. It should be noted that these R&D can be linked to our future of pure nuclear physics, where high intensity beams may become necessary. The methodology of inverse kinematics can also be extended to a reaction study for MAs.

In the program, as an alternative scenario, a transmutation with 14 MeV neutrons produced via muon-catalyzed fusion was also discussed; for which, an efficient production of negative pions has been proposed with an FFAG accelerator.[22)] To promote further the muon scenario, production cross sections of negative pions with a deuteron beam would be highly desirable. A negative muon was also recognized as a charming particle that causes muon capture reaction and changes the atomic number of nuclei capturing the muon. Based on the muon capture reaction, a new application of muons was proposed to produce the isotope ^{99}Mo for medical use, where ^{99}Tc in the waste is utilized as the substance for ^{99}Mo production via muon capture.[23)] Experiments of muon capture were organized at the facility of RCNP Osaka University, RAL muon facility, and J-PARC. The results are being published.[24,25)]

The future role of nuclear reactors is being intensively discussed in conjunction with the realization of a carbon-free society to avoid global warming. However, risk management in reactor operation has become a serious concern since the Fukushima incident, and the cost of nuclear energy has increased. Regardless of the promotion of or opposition to nuclear energy, the problem of high-level radioactive waste needs to be solved because the waste already exists. In Japan, approximately 18,000-tons of spent fuel exists, and the location for the geographical disposal has not been decided. Mitigating the risk of the waste is an important issue because this negative legacy should be left to posterity. Pure nuclear physics is now playing an important role in realizing a radioactive-waste free society.

Acknowledgment

The works introduced here were funded by the ImPACT Program of Council for Science, Technology, and Innovation (Cabinet Office, Government of Japan).

References

1) Y. Yano, Nucl. Instrum. Methods Phys. Res. B **261**, 1009 (2007).
2) ImPACT: "Reduction and Resource Recycling of High-level Radioactive Waste through Nuclear Transmutation," https://www.jst.go.jp/impact/hp_fjt/en/.
3) H. Wang *et al.*, Phys. Lett. B **754**, 104 (2016).
4) H. Sakurai, Nucl. Phys. News **31**, 26 (2021).
5) H. Wang *et al.*, Prog. Theor. Exp. Phys. **2017**, 021D01 (2017).
6) S. Kawase *et al.*, Prog. Theor. Exp. Phys. **2017**, 093D03 (2017).
7) K. Nakano *et al.*, Phys. Rev. C **100**, 044605 (2019).
8) S. Takeuchi *et al.*, Prog. Theor. Exp. Phys. **2019**, 013D02 (2019).
9) H. Wang *et al.*, Comm. Phys. **2**, 78 (2019).
10) S. Michimasa *et al.*, Nucl. Instrum. Methods Phys. Res. B **463**, 143 (2020).
11) J. Hwang *et al.*, Prog. Theor. Exp. Phys. **2019**, 043D02 (2019).
12) T. Sumikama *et al.*, Nucl. Instrum. Methods Phys. Res. A **986**, 164687 (2021).
13) N. Imai *et al.*, in preparation.
14) S. Kunieda *et al.*, J. Nucl. Sci. Technol. **56**, 1073 (2019).
15) T. Sato *et al.*, J. Nucl. Sci. Technol. **50**, 913 (2013).
16) Y. Miyake *et al.*, J. Nucl. Sci. Technol., published online (2022), https://doi.org/10.1080/00223131.2022.2072012.
17) H. Okuno *et al.*, Proc. Jpn. Acad. Ser. B **95**, 430 (2019).
18) K. Yamada *et al.*, Proc. 28th Linear Accelerator Conference (LINAC2016), TUPLR061, p. 598 (2019).
19) N. Sakamoto *et al.*, Proc. 19th Int. Conf. RF Superconductivity (SRF19), https://accelconf.web.cern.ch/srf2019/doi/JACoW-SRF2019-WETEB1.html.
20) N. Ikoma *et al.*, Rev. Sci. Instrum. **91**, 053503 (2020).
21) H. Okuno *et al.*, Patent Publication PCT/JP2020/003988.
22) Y. Mori *et al.*, JPS Conf. Proc. **21**, 011063 (2018).
23) T. Matsuzaki *et al.*, 10th Int. Sym. on Technetium and Rhenium—Science and Utilization (ISTR2018), October 3–6, 2018, Moscow, Russia.
24) T. Y. Saito *et al.*, submitted to Phys. Rev. C.
25) M. Niikura *et al.*, in preparation.

I. HIGHLIGHTS OF THE YEAR

<< Selection process of highlights >>

Highlights are selected by a two-step process. In the first step, a referee who reviews a manuscript decides whether she/he would recommend it as one of the highlights.
Members of the editorial board then make additional recommendations if they think an important contribution has not been recommended by the referee.

The second step involves the editor-in-chief proposing a list of highlights based on the recommendation given above to the editorial board. After discussing the scientific merits and uniqueness of the manuscripts from viewpoints of experts/non-experts, the editorial board makes the final decision.

Investigation of a new production and separation technique for RI beams at BigRIPS, "In-separator two-step method"

H. Suzuki,[*1] N. Fukuda,[*1] H. Takeda,[*1] Y. Shimizu,[*1] M. Yoshimoto,[*1] K. Yoshida,[*1] Y. Yanagisawa,[*1] and H. Sato[*1]

A new production and separation method of neutron-rich medium-heavy radioactive-isotope (RI) beams "in-separator two-step method" was proposed, and its usefulness was investigated. The beam intensities of such RIs produced by this new method are expected to be higher than those produced by the standard method, in-flight fission of a ^{238}U beam, when its intensity reaches the goal value of 2000 particle nA in the RIBF upgrade project and RI-beam total rates are limited at 1 kHz by data acquisition (DAQ).

In the standard method, as shown in Fig. 1(a), an objective RI beam (*e.g.*, ^{128}Pd) is produced by in-flight fission at the F0 Be target. When the magnetic rigidity ($B\rho$) of the first dipole is set at the momentum peak of ^{128}Pd to maximize its yield, the total rate of the secondary beams becomes too high for DAQ or detectors even with the current ^{238}U-beam intensity of 80 particle nA. To reduce the total rate below 1 kHz, the $B\rho$ setting should be higher than the momentum peak. The ^{128}Pd yield decreases with such adjustment; however, the total rates can be decreased more efficiently. When the primary-beam intensity increases in the future, this $B\rho$-setting shift should be larger. Thus, the ^{128}Pd yield will increase only by a factor of 9, although the ^{238}U-beam intensity will be 25 times larger than the current.

To produce the RI beams more efficiently within the total-rate limit, the in-separator two-step method was proposed, as shown in Fig. 1(b). The Be target is divided into two at F0 and F2 for the first and second reactions, respectively. In the first step, less-exotic RIs (*e.g.*, ^{133}Sn and neighboring RIs) relative to the objective RI are produced and roughly separated. In the second step, the objective RI is produced at the secondary target at F2 and separated.

Through a simulation, the ^{128}Pd yield with the new method is expected to be ∼3 times larger than that obtained using the standard method with a 2000-particle nA ^{238}U beam and 1-kHz total-rate limit.

A test experiment was performed at BigRIPS. The yield of ^{128}Pd with the new method was measured with 2- and 3-mm Be targets located at F0 and F2, respectively, and 2- and 4-mm degraders at F1 and F5, respectively. The RI beams along the central trajectories in the first and second stages were ^{133}Sn and ^{128}Pd, respectively. The measured ^{128}P (total) rate was 0.19 Hz (1 kHz) per 2000 particle nA. For comparison, the ^{128}Pd yield obtained using the standard method was simulated with the LISE^{++} code.[1] A 5-mm F0 Be target, 5-mm F1 degrader, and 1-mm F5 degrader were used. Here, the sums of thicknesses of the targets and degraders were the same in both the methods. The ^{128}Pd rate was estimated to be 0.074 Hz per 2000 particle nA. From these results, an improved setting with the new method was obtained to produce ^{128}Pd, under the conditions of the 2000-particle nA ^{238}U beam and the 1-kHz total-rate limit.

The region in the nuclear chart where the new method is favorable will be searched using the LISE^{++} simulation. However, we have found that some problems should be solved to perform reliable simulations. First, the momentum distribution and yields of fission products from ^{238}U are not reproduced well. Second, the RI production cross-sections from RI beams are not well known, except for a ^{132}Sn-beam case.[2] For further investigation, such basic data should be measured experimentally.

References

1) O. B. Tarasov, D. Bazin, LISE^{++} site, `https://lise.nscl.msu.edu/lise.html`.
2) H. Suzuki *et al.*, Phys. Rev. C **102**, 064615 (2020).

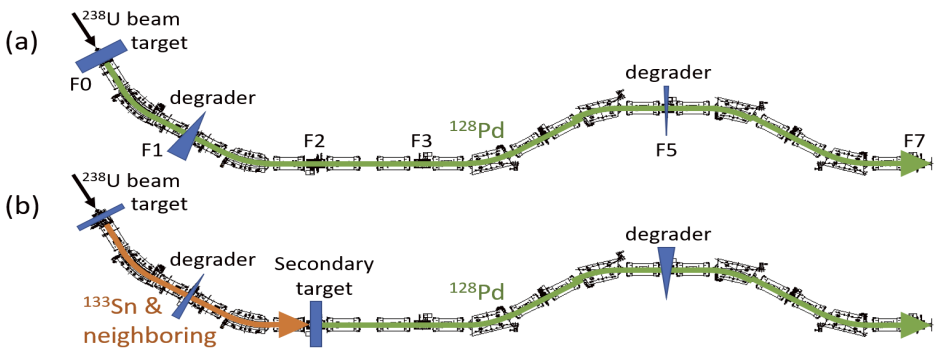

Fig. 1. Schematics of RI-beam productions at BigRIPS. (a) Standard method. An objective RI beam is produced from a ^{238}U beam in one step. (b) New method, "In-separator two-step method." An objective RI beam is produced via less-exotic RIs with two targets in two steps.

*1 RIKEN Nishina Center

Three quasiparticle isomers in odd-even ^{159,161}Pm: Calling for modified spin-orbit interaction for the neutron-rich region†

R. Yokoyama,[*1,*2] E. Ideguchi,[*3,*8] G. Simpson,[*4] Mn. Tanaka,[*3] Y. Sun,[*5] C. -J. Lv,[*5] Y. -X. Liu,[*6] L. -J. Wang,[*7] S. Nishimura,[*8] P. Doornenbal,[*8] G. Lorusso,[*8] P. -A. Söderström,[*8] Z. Y. Xu,[*11,*2] J. Wu,[*10,*8] T. Sumikama,[*8] N. Aoi,[*3,*8] H. Baba,[*8] F. L. Bello-Garrote,[*12] G. Benzoni,[*13] F. Browne,[*14,*8] R. Daido,[*15] Y. Fang,[*15] N. Fukuda,[*8] A. Gottardo,[*16,*17] G. Gey,[*18,*8] S. Go,[*1] S. Inabe,[*8] T. Isobe,[*8] D. Kameda,[*8] K. Kobayashi,[*19] M. Kobayashi,[*1] I. Kojouharov,[*20] T. Komatsubara,[*21,*22] T. Kubo,[*8] N. Kurz,[*20] I. Kuzi,[*23] Z. Li,[*10] M. Matsushita,[*1] S. Michimasa,[*1] C. B. Moon,[*24] H. Nishibata,[*15] I. Nishizuka,[*9] A. Odahara,[*15] Z. Patel,[*8,*25] S. Rice,[*8,*25] E. Sahin,[*12] H. Sakurai,[*8,*11] H. Schaffner,[*26,*8] L. Sinclair,[*26,*8] H. Suzuki,[*8] H. Takeda,[*8] J. Taprogge,[*27,*28] Zs. Vajta,[*23] H. Watanabe,[*29,*8] and A. Yagi[*15]

Nuclear properties of neutron-rich rare-earth nuclei at $Z \approx 60$ could be the possible key to answer one of the longstanding astrophysical questions: the formation of the $A \approx 160$ (rare-earth) peak observed in the elemental abundance distribution. From the nuclear-structure perspective, the formation of a peak in elemental abundance originates in extra stability of local nuclei. For example, in r-process, the neutron magic number $N = 82$ and $N = 126$ are responsible for the prominent abundance peaks at $A \approx 130$ and $A \approx 195$, respectively. Mumpower *et al.* identified that the nuclear properties of nuclei at $N \approx 100$ are critical to the rare-earth peak formation.[1)] In the case of the deformed rare-earth nuclei, a large shell gap between Nilsson single-particle orbitals stabilizes the nuclear shape at large deformation. Several theoretical works have predicted the existence of the deformed shell gaps at $N \approx 100$.[2)] Recently, a 6^- $\nu(5/2[523] \otimes 7/2[633])$ state was discovered in ^{162}Gd$_{98}$,[3)] indicating the large shell gap at $N = 98$.

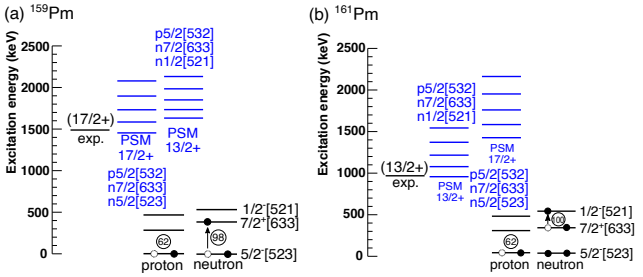

Fig. 1. Excitation energies of the isomers in (a) ^{159}Pm and (b) ^{161}Pm compared with the PSM calculation with the modified Nilsson parameters.

The spectroscopic study on neutron-rich rare-earth nuclei was performed at RIBF using the in-flight fission of ^{238}U^{86+} beam. The delayed γ rays were measured using a Ge detector array, EURICA.[4)] Accordingly, we discovered new quasi-particle isomers in ^{159,161}Pm$_{98,100}$. The 3-qp isomers involve one quasi-proton plus two quasi-neutrons near the Fermi surface as shown in Fig. 1. A calculation employing the projected shell model (PSM)[5)] was performed to understand the isomers. The observation of the (17/2+) isomers cannot be explained by the PSM calculation with traditional Nilsson parameters. We demonstrate that to explain the observation, the strength of the spin-orbit interaction needs to be changed according to the neutron number in exotic nuclei, as suggested by Liu *et al.*[6)] Furthermore, we also confirmed that the reported deformed shell gap at $N = 98$[3)] is present both in even-even and odd-mass nuclei.

† Condensed from the article in Phys. Rev. C **104**, L021303 (2021)

*1 Center for Nuclear Study, University of Tokyo
*2 Department of Physics and Astronomy, University of Tennessee, Knoxville
*3 Research Center for Nuclear Physics, Osaka University
*4 LPSC, Université Grenoble-Alpes, CNRS/IN2P3
*5 School of Physics and Astronomy, Shanghai Jiao Tong University
*6 School of Physics, Huzhou University
*7 School of Physical Science and Technology, Southwest University, Chongqing
*8 RIKEN Nishina Center
*9 Department of Physics, Tohoku University
*10 Department of Physics, Peking University
*11 Department of Physics, University of Tokyo
*12 Department of Physics, University of Oslo
*13 INFN, Sezione di Milano
*14 School of Computing Engineering and Mathematics, University of Brighton
*15 Department of Physics, Osaka University
*16 Dipartimento di Fisica dell Universitá degli studi di Padova
*17 INFN, Laboratori Nazionali di Legnaro
*18 Institut Laue-Langevin, Grenoble
*19 Department of Physics, Rikkyo University
*20 GSI Helmholtzzentrum für Schwerionenforschung GmbH
*21 Department of Physics, University of Tsukuba
*22 RISP, Institute for Basic Science, Daejeon
*23 Institute for Nuclear Research (ATOMKI)
*24 Department of Display Engineering, Hoseo University
*25 Department of Physics, University of Surrey
*26 Department of Physics, University of York
*27 Instituto de Estructura de la Materia, CSIC
*28 Departamento de Física Teórica, Universidad Autónoma de Madrid
*29 IRCNPC, Beihang University

References

1) M. R. Mumpower *et al.*, Phys. Rev. C **86**, 035803 (2012).
2) S. K. Ghorui *et al.*, Phys. Rev. C **85**, 064327 (2012).
3) D. J. Hartley *et al.*, Phys. Rev. Lett. **120**, 182502 (2018).
4) P. A. Söderström *et al.*, Nucl. Instrum. Methods Phys. Res. B **317**, 649 (2013).
5) Y. Sun, Phys. Scr. **91**, 043005 (2016).
6) Y. X. Liu *et al.*, J. Phys. G **47**, 055108 (2020).

Pairing forces govern population of doubly magic ^{54}Ca from direct reactions†

F. Browne,[*1] S. Chen,[*2,*1,*3] P. Doornenbal,[*1] A. Obertelli,[*4,*5,*1] K. Ogata,[*6,*7] Y. Utsuno,[*8,9*] K. Yoshida,[*9] and the SEASTAR2017 Collaboration

In exotic nuclei, the proton-neutron attraction between orbits of the same angular momentum, but different intrinsic spin directions ($j_> = \ell + s$ and $j_< = \ell - s$) can affect the evolution of single-particle energies.[1)] Tensor-driven shell evolution is responsible for the emergence of two non-canonical nuclear magic numbers, $N = 34$ in ^{54}Ca[2)] and $N = 16$ in ^{24}O.[3)] In these nuclei a lack of $\pi 0f_{7/2}$ and $\pi 0d_{5/2}$ occupation, respectively, allows their neutron $j_<$ orbits to increase through the absence of the tensor attraction.

Single-proton knockouts from the valence orbital of ^{25}F (^{24}O plus one proton in $\pi 0d_{5/2}$) have shown a reduction of spectroscopic strength to the ground state compared to expectation.[4)] The explanation of this was due to the mixing of the neutron configurations resulting from the tensor attraction between the $\pi 0d_{5/2}$ and $\nu 0d_{3/2}$ orbitals. In ^{55}Sc (^{54}Ca plus one proton in $\pi 0f_{7/2}$), a similar erosion of the $N = 34$ shell gap is observed (*e.g.* Ref. 5)), therefore, a similar reduction of spectroscopic strength as in ^{25}F might be expected.

A primary beam of ^{70}Zn of intensity 240 particle nA was accelerated to 345 MeV/nucleon and underwent fragmentation on a 10-mm-thick ^{9}Be target. From the secondary beam, ^{55}Sc isotopes were selected and transported to the MINOS LH_2 target system where they underwent knockout reactions at ∼200 MeV/nucleon. Populated states of ^{54}Ca were measured through γ-ray detection with the DALI2$^+$ array, and invariant-mass spectroscopy through detection of residual nuclei and their emitted neutrons in the SAMURAI set-up. Parallel momentum distributions were measured to determine the ℓ-value of the knocked out proton.

Level energies were calculated from the nuclear shell model employing the GXPF1Br interaction.[2)] Theoretical cross sections to states were calculated from DWIA estimates multiplied by shell model spectroscopic factors, which quantify the overlap of the ^{55}Sc and ^{54}Ca wavefunctions. A comparison between the observed and predicted cross sections is shown in Fig. 1.

Despite the shell model calculations showing a significant amplitude of excited neutron configurations in the ground-state of ^{55}Sc, removing the $\pi 0f_{7/2}$ valence proton populated predominantly the ground-state of ^{54}Ca. This counter-intuitive result is attributed to the off-diagonal matrix elements of the pairing interaction leading to a dominance of the ground-state spectroscopic factor.[6)] Owing to the ubiquity of the pairing interaction, this argument should be generally applicable to direct knockout reactions from odd-even to even-even nuclei.

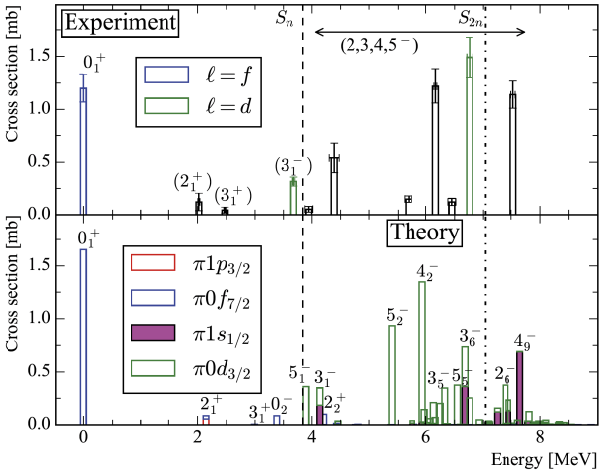

Fig. 1. (Top panel) Observed cross sections to states following the ^{55}Sc$(p, 2p)$ reaction. Above S_n the cross sections are shown at the energy centroids of fitted values and likely represent contributions from several states. States with conclusive ℓ-value assignments are colored accordingly, otherwise are black. (Bottom panel) Theoretical predictions of state energies and their population cross sections. Contributions to cross sections from proton removals from the different orbitals are indicated.

† Condensed from the article in Phys. Rev. Lett. **126**, 252501 (2021)

*1 RIKEN Nishina Center
*2 Department of Physics, University of Hong Kong
*3 State Key Laboratory for Nuclear Physics and Technology, Peking University
*4 Institut für Kernphysik, Universität Darmstadt
*5 IRFU, CEA, Univerité Paris-Saclay
*6 Research Center for Nuclear Physics, Osaka University
*7 Department of Physics, Osaka City University
*8 Center for Nuclear Study, University of Tokyo
*9 Advanced Science Research Center, Japan Atomic Energy Agency

References

1) T. Otsuka *et al.*, Rev. Mod. Phys. **92**, 015002 (2020).
2) D. Steppenbeck *et al.*, Nature (London) **502**, 207 (2013).
3) R. Kanungo *et al.*, Phys. Rev. Lett. **102**, 152501 (2009).
4) T. L. Tang *et al.*, Phys. Rev. Lett. **124**, 212502 (2020).
5) E. Leistenschneider *et al.*, Phys. Rev. Lett. **126**, 042501 (2021).
6) S. Yoshida, Nucl. Phys. **33**, 685 (1962).

Structure of ^{17}B studied by the quasifree neutron knockout reaction†

Z. H. Yang,[*1,*2] Y. Kubota,[*2,*3] A. Corsi,[*4,*2] K. Yoshida,[*5] X. -X. Sun,[*6,*7] J. G. Li,[*8] M. Kimura,[*9,*10,*1] N. Michel,[*11,*12] K. Ogata,[*1,*13] C. X. Yuan,[*14] Q. Yuan,[*8] G. Authelet,[*4] H. Baba,[*2] C. Caesar,[*15] D. Calvet,[*4] A. Delbart,[*4] M. Dozono,[*3] J. Feng,[*8] F. Flavigny,[*16] J. -M. Gheller,[*4] J. Gibelin,[*17] A. Giganon,[*4] A. Gillibert,[*4] K. Hasegawa,[*18] T. Isobe,[*2] Y. Kanaya,[*19] S. Kawakami,[*19] D. Kim,[*20] Y. Kiyokawa,[*2] M. Kobayashi,[*2] N. Kobayashi,[*21] T. Kobayashi,[*18,*2] Y. Kondo,[*22,*2] Z. Korkulu,[*20,*23] S. Koyama,[*21,*2] V. Lapoux,[*4] Y. Maeda,[*19] F. M. Marqués,[*17] T. Motobayashi,[*2] T. Miyazaki,[*21,*2] T. Nakamura,[*22,*2] N. Nakatsuka,[*24,*2] Y. Nishio,[*25] A. Obertelli,[*4,*2] A. Ohkura,[*25] N. A. Orr,[*17] S. Ota,[*3] H. Otsu,[*2] T. Ozaki,[*22] V. Panin,[*2] S. Paschalis,[*15] E. C. Pollacco,[*4] S. Reichert,[*26] J. -Y. Roussé,[*4] A. T. Saito,[*22,*2] S. Sakaguchi,[*25,*2] M. Sako,[*2] C. Santamaria,[*4] M. Sasano,[*2] H. Sato,[*2] M. Shikata,[*22,*2] Y. Shimizu,[*2] Y. Shindo,[*25] L. Stuhl,[*20,*2] T. Sumikama,[*18,*2] Y. L. Sun,[*4] M. Tabata,[*25] Y. Togano,[*22,*27,*2] J. Tsubota,[*22] F. R. Xu,[*8] J. Yasuda,[*25] K. Yoneda,[*2] J. Zenihiro,[*2] S. -G. Zhou,[*6,*7] W. Zuo,[*11,*12] and T. Uesaka[*2,*28]

The halo structure of weakly bound nuclei has been a topic of great interest in recent decades not only as a novel phenomenon in itself, but also provides an important terrestrial model system to study the correlations and properties of dilute neutron-rich matter.[1)]

In the present work, we have studied the structure of the halo nucleus ^{17}B by using the quasi-free (p, pn) reaction. This study concerns a kinematically complete measurement, combining the high-intensity beams provided by the RIBF and the state-of-the-art detector instruments including the vertex-tracking liquid hydrogen target MINOS, in-beam γ-ray spectrometer DALI2, and the SAMURAI spectrometer.[2)]

Shown in Fig. 1 is the relative-energy ($E_{\rm rel}$) spectrum of ^{15}B+n. It is well fitted using four ^{16}B resonances, after considering the experimental acceptance and resolutions. For each state of ^{16}B, the transverse momentum distribution and production cross section were analyzed by the distorted-wave impulse approximation (DWIA) reaction model.[3)] And the corresponding $1s_{1/2}$ and $0d_{5/2}$ spectroscopic factors of the knockout neutron were thus determined, giving a surprisingly small $1s_{1/2}$ component ($\sim$9%) in ^{17}B.

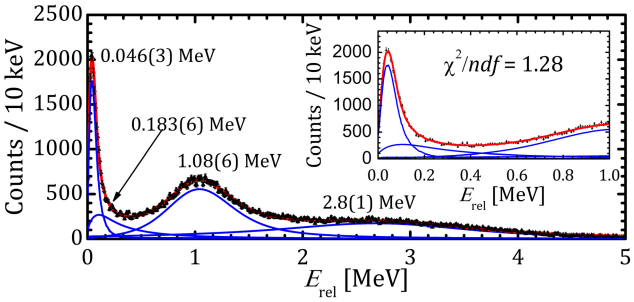

Fig. 1. ^{16}B $E_{\rm rel}$ spectrum fitted with a sum of four resonances (inset is a zoom-in view of the 0–1 MeV region).

Our finding of such a small $1s_{1/2}$ component and the previously reported halo features in ^{17}B (*e.g.*, Ref. 4)) can be well explained by the deformed relativistic Hartree-Bogoliubov theory in continuum (DRHBc),[5)] revealing a definite but not dominant halo component in ^{17}B. Our result gives the smallest s- or p-orbital component among known nuclei exhibiting halo features and implies that the dominant occupation of s or p orbitals is not a prerequisite for the occurrence of halo. The halo component, whether or not dominant, results in a distinctive diffused surface and, thus, manifests itself in reactions sensitive to the surface properties.

References
1) I. Tanihata *et al.*, Prog. Part. Nucl. Phys. **68**, 215 (2013).
2) T. Kobayashi *et al.*, Nucl. Instrum. Methods Phys. Res. B **317**, 294 (2013).
3) T. Wakasa *et al.*, Prog. Part. Nucl. Phys. **96**, 32 (2017).
4) A. Estradé *et al.*, Phys. Rev. Lett. **113**, 132501 (2014).
5) X. -X. Sun *et al.*, Phys. Lett. B **785**, 530 (2018).

† Condensed from the article in Phys. Rev. Lett. **126**, 082501 (2021)

*1 Research Center for Nuclear Physics, Osaka University
*2 RIKEN Nishina Center
*3 Center for Nuclear Study, University of Tokyo
*4 IRFU, CEA, Université Paris-Saclay
*5 Advanced Science Research Center, Japan Atomic Energy Agency
*6 Institute of Theoretical Physics, Chinese Academy of Sciences
*7 School of Physical Sciences, University of Chinese Academy of Sciences
*8 School of Physics and SKLNPT, Peking University
*9 Department of Physics, Hokkaido University
*10 Nuclear Reaction Data Centre, Hokkaido University
*11 Institute of Modern Physics, Chinese Academy of Sciences
*12 School of Nuclear Science and Technology, University of Chinese Academy of Sciences
*13 Department of Physics, Osaka City University
*14 Sino-French Institute of Nuclear Engineering and Technology, Sun Yat-Sen University
*15 Institut für Kernphysik, Technische Universität Darmstadt
*16 IPN Orsay, Université Paris Sud
*17 LPC Caen, Université de Caen Normandie
*18 Department of Physics, Tohoku University
*19 Department of Applied Physics, University of Miyazaki
*20 Center for Exotic Nuclear Studies, Institute for Basic Science
*21 Department of Physics, University of Tokyo
*22 Department of Physics, Tokyo Institute of Technology
*23 Institute for Nuclear Research, Hungarian Academy of Sciences
*24 Department of Physics, Kyoto University
*25 Department of Physics, Kyushu University
*26 Physik Department, Technische Universität München
*27 Department of Physics, Rikkyo University
*28 Cluster for Pioneering Research, RIKEN

Probing the symmetry energy with the spectral pion ratio†

J. Estee,[*1,*2,*3] W. G. Lynch,[*2,*3] C. Y. Tsang,[*2,*3] J. Barney,[*1,*2,*3] G. Jhang,[*1,*2,*3] M. B. Tsang,[*2,*3] R. Wang,[*2] M. Kaneko,[*1,*4] J. W. Lee,[*1,*5] T. Isobe,[*1] M. Kurata-Nishimura,[*1] T. Murakami,[*1,*4] H. Baba,[*1] G. Cerizza,[*1,*2,*3] N. Fukuda,[*1] B. Hong,[*5] T. Kobayashi,[*6] P. Lasko,[*7] J. Łukasik,[*7] A. B. McIntosh,[*8] H. Otsu,[*1] P. Pawłowski,[*7] H. Sakurai,[*1] C. Santamaria,[*1,*2] R. Shane,[*2] D. Suzuki,[*1] S. Tangwancharoen,[*2] Z. G. Xiao,[*9] S. J. Yennello,[*8,*10] Y. Zhang,[*9] for the SπRIT Collaboration and D. Cozma[*2,*11]

Many neutron star properties, such as the proton fraction, reflect the symmetry energy contributions to the equation of state that dominate when neutron and proton densities differ strongly. To constrain these contributions at suprasaturation densities, we measure the spectra of charged pions produced by colliding rare isotope tin (Sn) beams of 270 MeV/nucleon with isotopically enriched Sn targets at RIBF.

Light charged particles, including π^- and π^+, were detected in the SπRIT time projection chamber,[1,2] placed inside the SAMURAI spectrometer.[3] Charged particles were identified by their electronic stopping powers dE/dx and magnetic rigidities.[4] We focus on the most central collisions with the highest charged particle multiplicities while retaining good statistical accuracy, corresponding to impact parameters of $b < 3$ fm.[1]

Using ratios of the charged pion spectra measured at high transverse momenta, we deduced the symmetry energy constraints of $42 < L < 117$ and $32.5 < S_0 < 38.1$ MeV. We used the dcQMD semiclassical quantum molecular dynamics model,[5] which has provided reasonable predictions of the pion multiplicities and ratios in the previous publication.[6] By interpolating the results of dcQMD calculations (typical examples are shown in Fig. 1) with various values for L and Δm^*_{np}, *i.e.* the scaled difference between neutron and proton effective masses, we fit the single ratios $SR(\pi^-/\pi^+) = [dM(\pi^-)/dp_T]/[dM(\pi^+)/dp_T]$ for both the neutron rich ^{132}Sn+^{124}Sn system and the nearly symmetric ^{108}Sn+^{112}Sn system at $p_T > 200$ MeV/c, where we could avoid complications arising from poorly determined Δ baryon potentials. The results suggest a representative symmetry pressure of $P_{sym} = 12 \pm 10$ MeV/fm^3 at $\rho/\rho_0 = 1.5$. These L values are smaller than the values $L = 206 \pm 37$ and $S_0 = 38.3 \pm 4.7$ MeV [7] extracted from a new measurement of the neutron skin thickness of ^{208}Pb,[8] but close to the values $70 < L < 101$ and $33.5 < S_0 < 36.4$ MeV[9] extracted from charge exchange reactions and elastic scattering.

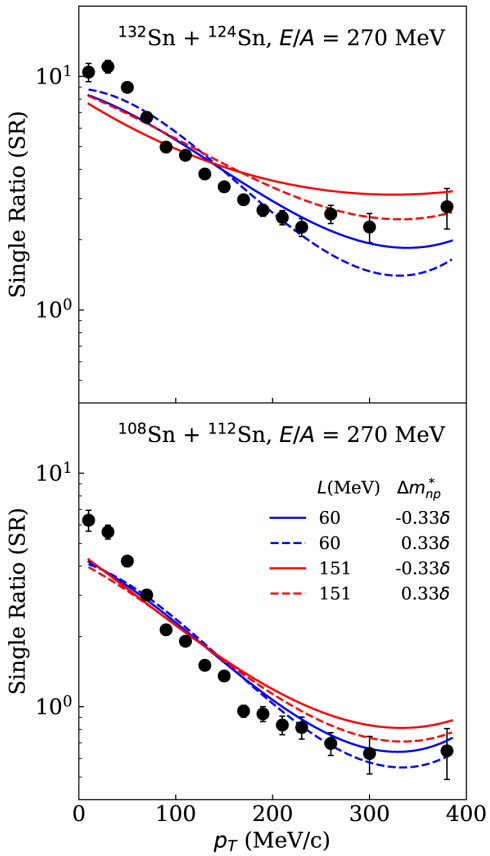

Fig. 1. Single pion spectral ratios for ^{132}Sn + ^{124}Sn (top) and ^{108}Sn + ^{112}Sn (bottom) reactions. The curves are dcQMD predictions from different L and Δm^*_{np} values listed in the bottom panel. Taken from the published article.†

† Condensed from the article in Phys. Pev. Lett. **126**, 162701 (2021)

*1 RIKEN Nishina Center
*2 National Superconducting Cyclotron Laboratory, Michigan State University
*3 Department of Physics, Michigan State University
*4 Department of Physics, Kyoto University
*5 Department of Physics, Korea University
*6 Department of Physics, Tohoku University
*7 Institute of Nuclear Physics PAN
*8 Cyclotron Institute, Texas A&M University
*9 Department of Physics, Tsinghua University
*10 Department of Chemistry, Texas A&M University
*11 Horia Hulubei National Institute for R&D in Physics and Nuclear Engineering

References
1) J. Barney *et al.*, Rev. Sci. Instrum. **92**, 063302 (2021).
2) R. Shane *et al.*, Nucl. Instrum. Methods Phys. Res. A **784**, 513 (2015).
3) H. Otsu *et al.*, Nucl. Instrum. Methods Phys. Res. B **376**, 175 (2016).
4) J. Lee *et al.*, Nucl. Instrum. Methods Phys. Res. A **965**, 163840 (2020).
5) M. D. Cozma, M. B. Tsang, Eur. Phys. J. A **57**, 309 (2021).
6) G. Jhang *et al.*, Phys. Lett. B **813**, 136016 (2021).
7) B. T. Reed *et al.*, Phys. Rev. Lett. **126**, 172503 (2021).
8) D. Adhikari *et al.*, Phys. Rev. Lett. **126**, 172502 (2021).
9) P. Danielewicz *et al.*, Nucl. Phys. A **958**, 147 (2017).

Rapidity distributions of $Z = 1$ isotopes and the nuclear symmetry energy from Sn + Sn collisions with radioactive beams at 270 MeV/nucleon†

M. Kaneko,[*1,*2] T. Murakami,[*1,*2] T. Isobe,[*1] M. Kurata-Nishimura,[*1] A. Ono,[*3] N. Ikeno,[*4] J. Barney,[*5] G. Cerizza,[*5] J. Estee,[*5] G. Jhang,[*5] J. W. Lee,[*6] W. G. Lynch,[*5] C. Santamaria,[*5] C. Y. Tsang,[*5] M. B. Tsang,[*5] R. Wang,[*5] D. S. Ahn,[*1,*7] L. Atar,[*8,*9] T. Aumann,[*8,*9] H. Baba,[*1] K. Boretzky,[*9] J. Brzychczyk,[*10] N. Chiga,[*1] N. Fukuda,[*1] I. Gašparić,[*11] B. Hong,[*6] A. Horvat,[*8,*9] T. Ichihara,[*1] K. Ieki,[*12] N. Inabe,[*1] Y. J. Kim,[*13] T. Kobayashi,[*3,*1] Y. Kondo,[*14,*1] P. Lasko,[*15] H. S. Lee,[*13] Y. Leifels,[*9] J. Łukasik,[*15] J. Manfredi,[*5] A. B. McIntosh,[*16] P. Morfouace,[*5] T. Nakamura,[*14,*1] N. Nakatsuka,[*14,*1] S. Nishimura,[*1] R. Olsen,[*16] H. Otsu,[*1] P. Pawłowski,[*15] K. Pelczar,[*17] D. Rossi,[*9] H. Sakurai,[*1] H. Sato,[*1] H. Scheit,[*8] R. Shane,[*5] Y. Shimizu,[*1] H. Simon,[*9] T. Sumikama,[*1] D. Suzuki,[*1] H. Suzuki,[*1] H. Takeda,[*1] S. Tangwancharoen,[*5] Y. Togano,[12,*14,*1] H. Törnqvist,[*8,*9] Z. Xiao,[*18] S. J. Yennello,[*16,*19] J. Yurkon,[*5] and Y. Zhang[*18] for the SπRIT Collaboration

Heavy-ion collisions at intermediate energies provide a unique laboratory probe for the nuclear symmetry energy at suprasaturation densities. A copious production of light cluster nuclei is one of the distinctive characteristics in this energy domain, and needs to be understood for reliably extracting the symmetry energy.[1)] This is because an explicit consideration of cluster correlations in the collision dynamics may influence physical quantities sensitive to the stiffness of the symmetry energy, such as the neutron-proton dynamics and the consequent charged pion ratio.[2)] Thus, we measured the rapidity distributions of hydrogen isotopes emitted from head-on collisions of ^{132}Sn + ^{124}Sn and ^{108}Sn + ^{112}Sn systems at 270 MeV/nucleon with the SπRIT time projection chamber[3)] installed inside the SAMURAI magnet at RIBF.

The experimental results are compared with the antisymmetrized molecular dynamics (AMD) calculations, and the measured rapidity distributions can be reasonably reproduced by the model after adjusting the in-medium two-nucleon cross section and the bound phase space for $A = 2, 3$ clusters. To investigate the dependence on the symmetry-energy stiffness, two cases of the symmetry energy with slope parameters $L = 46$ MeV and $L = 108$ MeV were assumed in calculations. Figure 1 presents the deuteron-to-proton and triton-to-proton double spectral ratios ($DR_{d/p}$ and $DR_{t/p}$) together with the AMD predictions. A positive slope of the rapidity-dependent double ratios indicates a partial isospin mixing between the projectile and target nuclei. As shown in the right panel of Fig. 1, the experimental $DR_{t/p}$ supports the calculation with $L = 46$ MeV, rather than $L = 108$ MeV. The adjustments applied in calculations do not significantly influence $DR_{t/p}$, and its symmetry-energy dependence. To constrain the symmetry energy more accurately, a more comprehensive set of data including global observables, *e.g.*, collective flows, will be analyzed, and a comparison with different models for deducing theoretical uncertainties is desired.

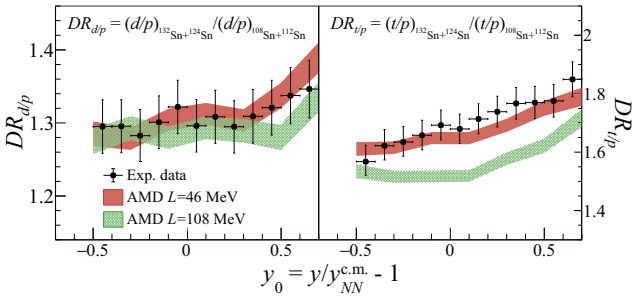

Fig. 1. Double ratio for the cluster-to-proton relative yield in the ^{132}Sn + ^{124}Sn system divided by that in the ^{108}Sn + ^{112}Sn, and the AMD predictions for two cases of the symmetry energy. Left: the deuteron-to-proton double ratio ($DR_{d/p}$). Right: the triton-to-proton double ratio ($DR_{t/p}$).

References

1) A. Ono *et al.*, EPJ Web Conf. **117**, 07003 (2016).
2) N. Ikeno *et al.*, Phys. Rev. C **97**, 066902(E) (2018).
3) J. Barney *et al.*, Rev. Sci. Instrum. **92**, 063302 (2021).

† Condensed from the article in Phys. Lett. B **822**, 136681 (2021)

*1 RIKEN Nishina Center
*2 Department of Physics, Kyoto University
*3 Department of Physics, Tohoku University
*4 Department of Life and Environmental Agricultural Sciences, Tottori University
*5 NSCL and Department of Physics and Astronomy, Michigan State University
*6 Department of Physics, Korea University
*7 Korea Basic Science Institute
*8 Institut für Kernphysik, Technische Unicersität Darmstadt
*9 GSI Helmholtzzentrum für Schwerionenforschung GmbH
*10 Faculty of Physics, Astronomy and Applied Computer Science, Jagiellonian University
*11 Division of Experimental Physics, Ruđer Bošković Institute
*12 Department of Physics, Rikkyo University
*13 Rare Isotope Science Project, Institute for Basic Science
*14 Department of Physics, Tokyo Institute of Technology
*15 Institute of Nuclear Physics, Polish Academy of Sciences
*16 Cyclotron Institute, Texas A&M University
*17 INFN-Laboratori Nazionali del Gran Sasso
*18 Department of Physics, Tsinghua University
*19 Department of Chemistry, Texas A&M University

Estimation of radiative half-life of ^{229m}Th by half-life measurement of other nuclear excited states in ^{229}Th†

Y. Shigekawa,[*1] A. Yamaguchi,[*2,*3] K. Suzuki,[*4] H. Haba,[*1] T. Hiraki,[*4] H. Kikunaga,[*5] T. Masuda,[*4] S. Nishimura,[*1] N. Sasao,[*4] A. Yoshimi,[*4] and K. Yoshimura[*4]

The first excited state in the ^{229}Th nucleus (^{229m}Th) has an excitation energy of ∼8 eV.[1–4] This low-lying isomeric state allows the laser excitation and spectroscopy of the nucleus, potentially leading to an ultraprecise optical nuclear clock.[5] This radiative half-life of ^{229m}Th, which determines the natural linewidth of the nuclear transition between the ground state and ^{229m}Th, is an important parameter to estimate the performance of the nuclear clock. The radiative half-life has yet to be determined experimentally; however, it can be estimated from the reduced transition probabilities $B(X\lambda)$ of the inter-band transitions between the $5/2^+[633]$ and $3/2^+[631]$ rotational bands beginning with higher excited states than ^{229m}Th by applying the Alaga rule.[6] The Alaga rule states that the ratio of two $B(X\lambda)$ values for a pair of intra- or inter-band transitions equals the ratio of the squares of Clebsch-Gordan coefficients based on the assumption of the separable rotational motion of a nucleus. In this study, we measured the half-lives of the excited states in the $5/2^+[633]$ and $3/2^+[631]$ bands to determine the $B(X\lambda)$ values required to estimate the radiative half-live of ^{229m}Th.

To determine the half-lives, we performed a coincidence measurement between γ rays and α particles emitted from a ^{233}U source, as described in Ref. 7). First, we obtained the time trace of the 42.43-keV γ rays following the 4783.5-keV α particles (see Fig. 1 in this paper and Fig. 2 in Ref. 7)). By fitting a single exponential decay function convoluted with a Gaussian function to the time trace, the half-life of the 42.43-keV state was determined to be 169(4) ps, which is consistent with the value of 172(6) ps reported previously.[8] Next, we performed fitting to the time trace of the 54.70-keV γ rays following the 4729-keV α particles, yielding a half-life of 103(12) ps. Moreover, by selecting the 97.14-keV γ rays, we obtained a half-life of 88(9) ps. From the weighted average of these values, the half-life of the 97.14-keV state was determined to be 93(7) ps. In the same manner, the half-life of the 71.82- and 163.25-keV states were determined for the first time to be 120(40) and 220(30) ps by fitting to the time traces of the 71.82- and 66.12-keV γ rays following the 4754-keV and 4664-keV α particles, respectively.

We derived the $B(X\lambda)$ values using the obtained half-lives, experimental γ branching ratios,[1,9,10] mixing ratios,[9,10] and internal conversion coefficients.[10,11] First, for the intra-band transitions, we found that the B(M1) and B(E2) values of the transitions starting with the 29.19-, 42.43-, 71.83-, and 97.14-keV states were consistent with the values estimated from the Alaga rule. By contrast, for the transitions starting with the 163.25-keV state, the B(M1) and B(E2) values deviated from the estimation based on the Alaga rule, as it often appears with increasing nuclear spins. Next, to investigate the validity of the Alaga rule for the inter-band transitions, we calculated the B(M1; ^{229m}Th→^{229g}Th) values from the B(M1) values of the 29.19→0, 71.83→42.43, and 97.14→71.83 keV transitions based on the Alaga rule. The values obtained from the 29.19→0 and 71.83→42.43 keV transitions agreed with each other (0.014(4) and 0.013(4) $\mu_N{}^2$, respectively). This indicates that the contribution of the Coriolis interactions is insignificant and the Alaga rule is applicable for the inter-band transitions between those low-spin states. The weighted average of B(M1; ^{229m}Th→^{229g}Th) obtained from these transitions was 0.014(3) $\mu_N{}^2$, from which we estimated the radiative half-life of ^{229m}Th to be $5.0(11) \times 10^3$ s.

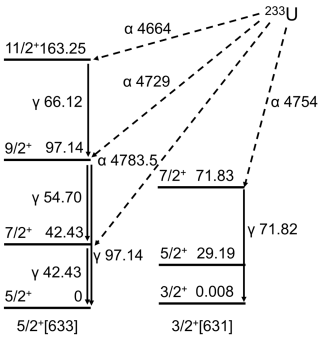

Fig. 1. Energy levels of the ^{229}Th nucleus grouped into rotational bands, as well as the α and γ transitions used for determining the half-lives of the excited states (units: keV).

References
1) B. R. Beck *et al.*, Phys. Rev. Lett. **98**, 142501 (2007).
2) B. Seiferle *et al.*, Nature **573**, 243 (2019).
3) A. Yamaguchi *et al.*, Phys. Rev. Lett. **123**, 222501 (2019).
4) T. Sikorsky *et al.*, Phys. Rev. Lett. **125**, 142503 (2020).
5) E. Peik, C. Tamm, Europhys. Lett. **61**, 181 (2003).
6) G. Alaga *et al.*, Dan. Mat. Fys. Medd. **29** (No.9), 1 (1955).
7) Y. Shigekawa *et al.*, RIKEN Accel. Prog. Rep. **53**, 51 (2020).
8) H. Ton *et al.*, Nucl. Phys. A **155**, 245 (1970).
9) V. Barci *et al.*, Phys. Rev. C **68**, 034329 (2003).
10) T. Masuda *et al.*, Nature **573**, 238 (2019).
11) E. Browne, J. K. Tuli, Nucl. Data Sheets **109**, 2657 (2008).

† Condensed from the article in Phys. Rev. C **104**, 024306 (2021)

*1 RIKEN Nishina Center
*2 Quantum Metrology Laboratory, RIKEN
*3 PRESTO, Japan Science and Technology Agency
*4 Research Institute for Interdisciplinary Science, Okayama University
*5 Research Center for Electron-Photon Science, Tohoku University

Toward *ab initio* charge symmetry breaking in nuclear energy density functionals†

T. Naito,[*1,*2] G. Colò,[*3,*4] H. Z. Liang,[*1,*2] X. Roca-Maza,[*3,*4] and H. Sagawa[*5,*2]

The parameter sets of energy density functionals (EDFs) of the nuclear density functional theory (DFT) are commonly determined phenomenologically to reproduce experimental masses and charge radii as well as nuclear matter properties. To establish a link between microscopic approaches and EDFs, an *ab initio* determination of the parameters of EDFs, as well as their functional forms, is highly desired. To date, however, a direct correspondence between *ab initio* and DFT remains elusive. A sophisticated yet practical approach to pin down the EDF parameters is to combine the *ab initio* and phenomenological EDF calculations.

Even though the isospin symmetry breaking (ISB) terms are small parts of the nuclear interaction, effects of the ISB terms on nuclear properties have received attention, while the ISB terms have often been neglected in EDFs. The ISB interaction can be divided into two parts: the charge symmetry breaking (CSB) and the charge independence breaking (CIB) interactions.

Our aim in this study is to propose a comprehensive methodology to determine the CSB terms in nuclear EDFs adopting the *ab initio* results. We implement the ISB terms in a Skyrme EDF to demonstrate our methodology. We will show that the mass difference of mirror nuclei $\Delta E_{\rm tot}$ and the neutron-skin thickness ΔR_{np} of doubly-magic nuclei calculated by *ab initio* methods without and with the CSB terms, once they are available, enable us to determine the CSB strength in the EDF with an uncertainty of less than 6%, independently from other ISB forces such as CIB and Coulomb forces.

The Skyrme-like CSB and CIB interactions read[1)]

$$v_{\rm CSB}\left(\boldsymbol{r}_1,\boldsymbol{r}_2\right)=\frac{\tau_{1z}+\tau_{2z}}{4}s_0\left(1+y_0P_\sigma\right)\delta\left(\boldsymbol{r}_1-\boldsymbol{r}_2\right), \tag{1a}$$

$$v_{\rm CIB}\left(\boldsymbol{r}_1,\boldsymbol{r}_2\right)=\frac{\tau_{1z}\tau_{2z}}{2}u_0\left(1+z_0P_\sigma\right)\delta\left(\boldsymbol{r}_1-\boldsymbol{r}_2\right), \tag{1b}$$

respectively, where τ_{iz} is the z-direction of the isospin operator of nucleon i ($i=1,\,2$) and P_σ is the spin-exchange operator. For simplicity, in the SAMi-ISB EDF,[2)] $y_0=z_0=-1$ are chosen to select the spin-singlet channel. The CIB strength $u_0=25.8$ MeV fm^3 has been previously determined using the Brueckner Hartree-Fock calculation of symmetric nuclear matter.[2,3)] The CSB strength $s_0=-26.3$ MeV fm^3 has been determined to reproduce the isobaric analog energy of ^{208}Pb.[2)] In this study, as u_0 has been already determined microscopically, we propose a way to determine s_0 microscopically. Because the isobaric analog energy is not available using *ab initio* methods at this moment, we focus on alternative well-established observables: the nuclear radius and mass, which are more easily accessible than any *ab initio* method.

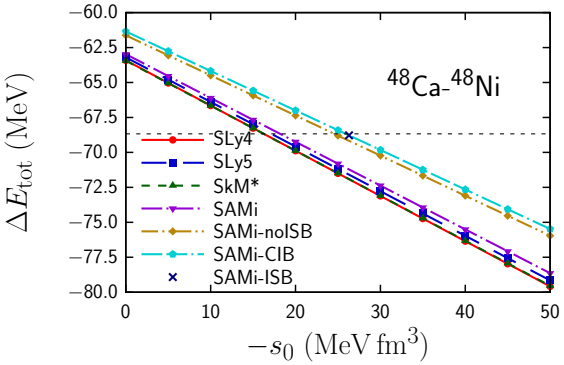

Fig. 1. Dependence of mass difference of mirror nuclei ^{48}Ca and ^{48}Ni, $\Delta E_{\rm tot}=E_{\rm tot}^{\rm Ca48}-E_{\rm tot}^{\rm Ni48}$, on CSB strength s_0.

The dependence of the mass difference of mirror nuclei ^{48}Ca and ^{48}Ni, $\Delta E_{\rm tot}=E_{\rm tot}^{\rm Ca48}-E_{\rm tot}^{\rm Ni48}$, on the CSB strength s_0 is shown in Fig. 1. For comparison, results calculated with the original SAMi-ISB and experimental data (AME2020) are also shown using crosses and horizontal lines, respectively. Remarkably, one can note that $\Delta E_{\rm tot}$ has a strong linear correlation to the CSB strength s_0, and the correlation is universal among the functionals. Thus, the calculated results are fitted to $\Delta E_{\rm tot}=a-bs_0$. As seen in the figure, s_0 and $\Delta E_{\rm tot}$ are highly correlated ($r=1.000$), and the slope b is almost universal among Skyrme EDFs. Note that the parameters a and b are determined with a 0.5% error. Accordingly, among these functionals, the slope b deviates within $\lesssim$6% around the average value of b. Thus, once the *ab initio* results for $\Delta E_{\rm tot}$ calculated without and with the bare CSB interaction, $\Delta E_{\rm tot}^{\rm w/o\ CSB}$ and $\Delta E_{\rm tot}^{\rm w/\ CSB}$, are obtained, using $\bar{b}$, we can determine s_0 as $-s_0=\left(\Delta E_{\rm tot}^{\rm w/\ CSB}-\Delta E_{\rm tot}^{\rm w/o\ CSB}\right)/\bar{b}$. As the uncertainty of $\bar{b}$ is $\lesssim$6%, the expected uncertainty of s_0 is also $\lesssim$6%, assuming that the uncertainty associated with the *ab initio* calculations is negligible.

† Condensed from the article in Phys. Rev. C **105**, L021304 (2022)

*1 Department of Physics, University of Tokyo
*2 RIKEN Nishina Center
*3 Dipartimento di Fisica, Università degli Studi di Milano
*4 INFN, Sezione di Milano
*5 Center for Mathematics and Physics, University of Aizu

References

1) H. Sagawa *et al.*, Phys. Lett. B **353**, 7 (1995).
2) X. Roca-Maza *et al.*, Phys. Rev. Lett. **120**, 202501 (2018).
3) H. Müther *et al.*, Phys. Lett. B **445**, 259 (1999).

Total reaction cross sections in the island of inversion near $N = 40$[†]

W. Horiuchi,[*1,*2] T. Inakura,[*3] and S. Michimasa[*4]

A systematic analysis of the deformation phenomena of Ti, Cr, and Fe isotopes is performed to understand the nuclear structure in the "island of inversion"[1] near the neutron number $N = 40$. As large nuclear deformations are expected in this mass region, we describe various nuclear deformations using the Skyrme-Hartree-Fock method in the three-dimensional coordinate space.[2] A detailed analysis of the obtained nuclear structure information not only the quadrupole deformation but also the hexadecapole deformation increases significantly in the island of inversion. This is because of the excess neutrons occupying elongated intruder orbits. This characteristic is manifested as a change in the density distribution at the nuclear surface and can be observed as a significant increase in the total reaction cross section (σ_R).

Figure 1 plots the quadrupole (β_2) and hexadecapole (β_4) deformation parameters of Ti, Cr, and Fe isotopes as a function of the neutron number N. The results with two Skyrme density functionals, SkM*[3] and SLy4,[4] are shown. SkM* predicts large quadrupole deformation for $N > 34$, which is consistent with empirical $|\beta_2|$ values found in Ref. 5), while the SLy4 results show less deformed ground states for those isotopes. We find that the hexadecapole deformation also enhances for $N > 34$ with SkM* owing to the occupation of the $[nn_z\Lambda]\Omega = [330]1/2$ Nillson orbit, where the hexadecapole moment becomes the largest for the most prolately elongated orbitals among the orbits belonging to the same n, *i.e.*, for $n = n_z$ and $\Lambda = 0$.

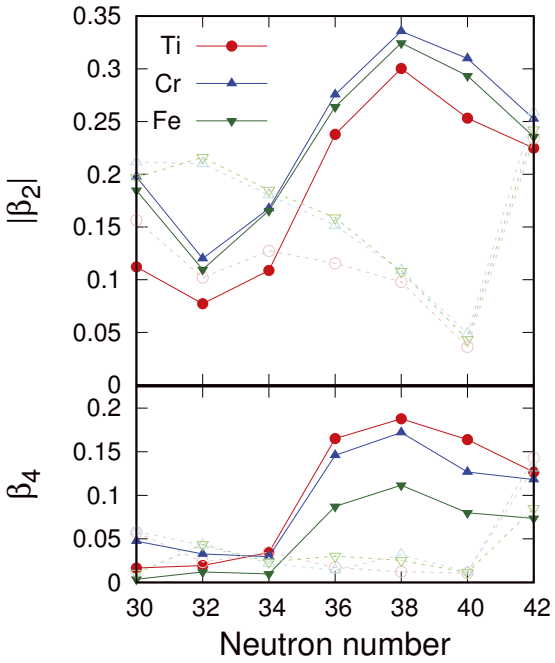

Fig. 1. Quadrupole (β_2) and hexadecapole (β_4) deformation parameters of Ti, Cr, and Fe isotopes calculated with SkM* (closed symbols with solid lines) and SLy4 (open symbols with dashed lines).

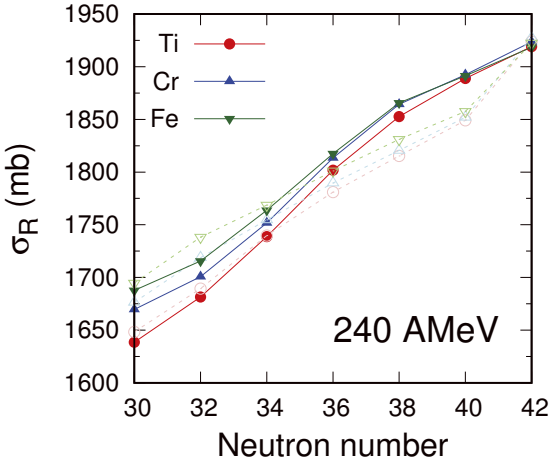

Fig. 2. Total reaction cross sections of Ti, Cr, and Fe isotopes calculated with SkM* (closed symbols with solid lines) and SLy4 (open symbols with dashed lines).

These different deformations are well reflected in the density profiles near the nuclear surface and can be distinguished by total reaction or interaction cross section measurements. Figure 2 displays the calculated σ_R on a carbon target at 240 MeV/nucleon of these nuclei. The cross sections with SkM* are significantly larger than those obtained with SLy4 for $N = 36$–40, where the magnitudes of the nuclear deformations are quite different. The difference is at most approximately 2%, which is significant considering the precision of recent interaction cross section measurements was $\lesssim 1\%$.[6] Such a systematic cross section measurement is desired to clarify the nuclear properties in the island of inversion near $N = 40$.

† Condensed from the article in Phys. Rev. C **105**, 014316 (2022)

*1 Department of Physics, Hokkaido University
*2 Department of Physics and NITEP, Osaka Metropolitan University
*3 Laboratory for Zero-Carbon Energy, Tokyo Institute of Technology
*4 Center for Nuclear Study, University of Tokyo

References
1) E. K. Warburton *et al.*, Phys. Rev. C **41**, 1147 (1990).
2) T. Inakura *et al.*, Nucl. Phys. A **768**, 61 (2006).
3) J. Bartel *et al.*, Nucl. Phys. A **386**, 79 (1982).
4) E. Chanbanat *et al.*, Nucl. Phys. A **627**, 710 (1997).
5) B. Pritychenko *et al.*, At. Data Nucl. Data Tables **107**, 1 (2016).
6) M. Tanaka *et al.*, Phys. Rev. Lett. **124**, 102501 (2020).

Asymmetry of antimatter in the proton†

Y. Goto,[*1] S. Miyasaka,[*2] K. Nagai,[*2] F. Sanftl,[*2] Y. Kudo,[*3] Y. Miyachi,[*3] K. Nakano,[*1,*2] S. Nara,[*3] S. Sawada,[*4] and T. -A. Shibata[*1,*2] for the SeaQuest Collaboration

The structure of the proton is a prototypical example of a strongly coupled and correlated system with quarks and gluons interacting according to quantum chromodynamics (QCD). An essential feature of QCD is its ability to create matter-antimatter quark pairs inside the proton that exist only for a very short time. Their fleeting existence makes the antimatter quarks within protons difficult to study, but their existence is discernible in reactions in which a matter-antimatter quark pair annihilates. In this picture of quark-antiquark creation by the strong force, the probability distributions as a function of momentum for the presence of up and down antimatter quarks should be nearly identical, given that their masses are very similar and small compared to the mass of the proton.[1)] Here, we provide evidence from muon-pair production measurements that these distributions are considerably different, with down antimatter quarks more abundant than up antimatter quarks over a wide range of momenta.

In the Drell-Yan process in hadron-hadron collisions, a quark and an antiquark annihilate into a virtual photon, which decays into a lepton-antilepton pair.[2)] The ratio of the Drell-Yan cross-section on a deuterium target to that on a hydrogen target has a direct sensitivity to $\bar{d}(x)/\bar{u}(x)$, where $\bar{u}(x)$ and $\bar{d}(x)$ are the distributions of up and down antiquarks in the proton, respectively, as a function of the fractional momentum (x) of the proton. The ratio $\bar{d}/\bar{u}$ from the Drell-Yan process was first reported by NA51 at CERN.[3)] This result is consistent with the down antiquark dominance reported in deep inelastic scattering by NMC at CERN.[4)] The Fermilab NuSea experiment[5)] was able to measure the x dependence of the down antiquark dominance with an 800-GeV proton beam in the kinematic range of $0.015 < x < 0.35$.

The Fermilab SeaQuest experiment was designed to investigate the flavour asymmetry at higher x values than NuSea with the newly constructed experimental apparatus. With a proton beam at an energy of 120 GeV, liquid hydrogen and deuterium targets, and a focusing magnet of 10 Tm after the target region, the experiment was optimized for the study of target antiquarks in the intermediate region, with x around 0.3, by detecting muon ($\mu^+\mu^-$) pairs from decays of the virtual photons produced in the Drell-Yan process.

Figure 1 shows the ratios $\bar{d}(x)/\bar{u}(x)$ in the proton

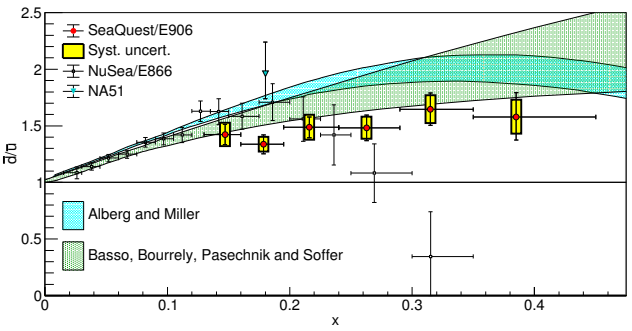

Fig. 1. Ratios $\bar{d}(x)/\bar{u}(x)$.

(red filled circles) with their statistical (vertical bars) and systematic (yellow boxes) uncertainties extracted from the present data based on next-to-leading-order calculations of the Drell-Yan cross-sections. Also shown are the results obtained by the NuSea experiment (open black squares) with statistical and systematic uncertainties added in quadrature. The trends between the two experiments at higher x are quite different. No explanation has been found yet for these differences. The horizontal bars on the data points indicate the width of the bins.

The present data are reasonably described by the predictions of the statistical parton distributions of Basso *et al.*[6)] (green band) and by the chiral effective perturbation theory of Alberg & Miller[7)] (cyan band), which are also shown in Fig. 1. These two calculations emphasize rather different non-perturbative mechanisms that lead to the differences in $\bar{d}(x)$ and $\bar{u}(x)$. The present data show that $\bar{d}$ is greater than $\bar{u}$ for the entire x range measured in this experiment. This provides important support for these and other non-perturbative mechanisms of the QCD structure of the proton that were disfavoured by the NuSea results.

References

1) D. A. Ross, C. T. Sachrajda, Nucl. Phys. B **149**, 497 (1979).
2) S. D. Drell, T. M. Yan, Phys. Rev. Lett. **25**, 316 (1970); erratum **25**, 902 (1970).
3) A. Baldit *et al.*, Phys. Lett. B **332**, 244 (1994).
4) P. Amaudruz *et al.*, Phys. Rev. Lett. **66**, 2712 (1991); M. Arneodo *et al.*, Phys. Rev. D **50**, R1 (1994).
5) R. S. Towell *et al.*, Phys. Rev. D **64**, 052002 (2001).
6) E. Basso *et al.*, Nucl. Phys. A **948**, 63 (2016).
7) M. Alberg, G. A. Miller, Phys. Rev. C **100**, 035205 (2019).

† Condensed from the article in Nature **590**, 561 (2021)

*1 RIKEN Nishina Center
*2 Department of Physics, Tokyo Institute of Technology
*3 Department of Physics, Yamagata University
*4 Institute of Particle and Nuclear Studies, KEK

Gluon EMC effects in nuclear matter†

X. -G. Wang,[*1] W. Bentz,[*2] I. C. Cloët,[*3] and A. W. Thomas[*1]

The European Muon Collaboration (EMC) effect, which refers to the observation that spin-independent structure functions of nuclei differ from the naive sum of structure functions of their constituents, is still one of the most challenging topics in modern nuclear physics. Previous calculations[1] have demonstrated that the Nambu-Jona-Lasinio (NJL) model, when used as an effective quark theory of QCD to describe the quark substructure of hadrons, successfully reproduces the unpolarized EMC data across the periodic table. The key mechanism is the in-medium modification of the quark substructure of nucleons arising from scalar and vector mean fields acting on the quarks. The same framework was used to predict a significant medium modification of the polarized structure functions - the polarized EMC effect. An experiment at Jefferson Lab is planned to measure this effect.[2]

While the EMC effects associated with the quark content of nuclei have been investigated extensively, there have been very few studies of the nuclear modification of the gluon distribution or the "gluon EMC effect." Exploring such changes is one of the primary scientific goals of the planned Electron-Ion-Collider (EIC). In this work we focus on the gluon EMC effect within the framework of the NJL model and the QCD evolution of parton distributions. By evolving our medium modified quark distributions from the NJL model scale ($Q_0^2 = 0.16$ GeV^2) to a scale of $Q^2 = 5$ GeV^2 by using the QCD evolution code of Ref. 3) in next-to-leading order (NLO) and next-to-next-to-leading order (NNLO), we generate the medium modified gluon distributions.

The solid lines in Figs. 1 and 2 show our previous results for the unpolarized EMC ratio F_{2N}^A/F_{2N} and the polarized EMC ratio g_{1p}^A/g_{1p} in nuclear matter. Here F_{2N} is the average of proton and neutron unpolarized structure functions in vacuum while F_{2N}^A is the same quantity in nuclear matter, and g_{1p} is the polarized structure function of the proton in vacuum while g_{1p}^A is the same quantity in nuclear matter. The dashed lines in Figs. 1 and 2 show the ratio g_p^A/g_p for the unpolarized case and $\Delta g_p^A/\Delta g_p$ for the polarized case. Here g_p (Δg_p) is the unpolarized (polarized) gluon distribution in the proton in vacuum while g_p^A (Δg_p^A) is the same quantity in nuclear matter.

It is clear from the figures that our analysis predicts for the first time a sizable gluon EMC effect, both for the unpolarized and the polarized case. We finally mention two points: First, our evolved NJL model results for all quark and gluon distributions agree very well with the phenomenological results of the NNPDF Collaboration.[5] Therefore the assumption that at the NJL model scale the gluons are frozen into the interactions between quarks is not unreasonable. Second, we obtain almost the same results by using the Q^2 evolution in NLO and NNLO. This reflects the fact that $\alpha_s/4\pi$, which is the relevant parameter for Q^2 evolution, is sufficiently small to apply perturbative QCD to models based on quark degrees of freedom.

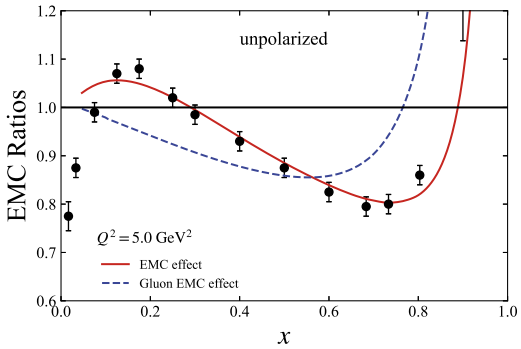

Fig. 1. Unpolarized EMC ratios in nuclear matter for the structure functions (solid line) and the gluon distributions (dashed line) as functions of the Bjorken variable x in NLO. The empirical data points are from Ref. 4).

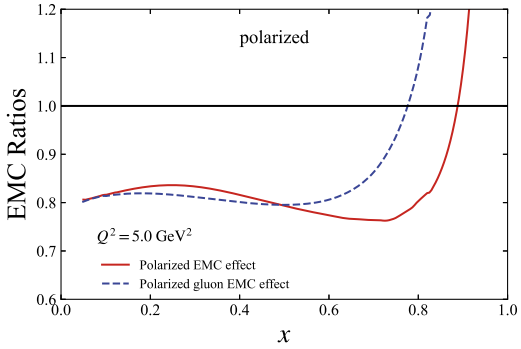

Fig. 2. Polarized EMC ratios in nuclear matter for the structure functions (solid line) and the gluon distributions (dashed line) as functions of x in NLO.

† Condensed from the article by J. Phys. G **49**, 03TL01 (2022)
*1 Department of Physics, University of Adelaide
*2 Department of Physics, Tokai University
*3 Physics Division, Argonne National Laboratory

References

1) I. C. Cloët *et al.*, Phys. Lett. **642**, 210 (2006).
2) The EMC Effect in Spin Structure Functions, `https://www.jlab.org/exp_prog/proposals/14/PR12-14-001.pdf`.
3) V. Bertone *et al.*, Comput. Phys. Commun. **185**, 1647 (2014).
4) I. Sick, D. Day, Phys. Lett. **274**, 16 (1992).
5) R. D. Ball *et al.*, J. High Energy Phys. **2015**, 40 (2015); E. R. Nocera *et al.*, Nucl. Phys. B **887**, 276 (2014).

Production of highly charged calcium-ion beam using high-temperature oven

T. Nagatomo,[*1] Y. Higurashi,[*1] J. Ohnishi,[*1] and T. Nakagawa[*1]

The calcium-48-ion beam is one of the indispensable beams for studying light nuclei with excess neutrons. Before the upgrade of RILAC with superconducting (SC) acceleration cavities[1] to provide calcium (Ca) beams for experiments at RIBF, a Ca^{11+} beam was extracted from a normal-conducting electron-cyclotron-resonance ion source (ECRIS) with a low-temperature oven as an evaporator of Ca,[2] accelerated by RILAC, following which a Ca^{16+} beam was produced through a carbon-foil charge stripper. However, due to the upgrade of RILAC, the charge stripper is no longer available, because the materials sputtered from the stripper into the beam pipe are adsorbed on the cryogenic surface of SC cavities, resulting in a serious reduction in the acceleration voltage. Meanwhile, the ECRIS for RILAC was also upgraded with the SC technology, and the performance of the ion source has been improved significantly. Therefore, we conducted a test to directly extract Ca^{16+} ions from the new SC-ECRIS.

It is also necessary to reduce the consumption of the Ca sample as much as possible because of the recent worldwide shortage of ^{48}Ca samples. Various ovens to evaporate Ca[2–4] were developed worldwide, but we selected a high-temperature oven (HTO)[5] because it was able to achieve a high enough temperature to directly decompose the CaO sample. We tested whether a Ca^{16+} beam of sufficient intensity can be obtained with a small Ca consumption using the HTO as the evaporator.

The experiment was conducted using an SC-ECRIS for RILAC (R28G-K).[6,7] The magnetic mirror was set to the same field as that for the uranium-beam production, which is suitable for producing multiply charged ion beams. An ion-extraction voltage of 9.99 kV was applied to fit to the case of ^{48}Ca-ion acceleration. A tablet-shaped CaO (natural Ca) sample, which was calcined at 1000°C for 2 h in the ambient atmosphere, was placed directly into a tungsten crucible of HTO, which was surrounded by a molybdenum heat shield. In addition, by calcining with an HTO heating power below 200 W for 6 h in vacuum ($\sim 10^{-4}$ Pa) in R28G-K, H_2O and CO_2, which were contained in the CaO sample, were completely eliminated.

High-intensity $^{40}Ca^{16+}$-ion beams were successfully extracted from R28G-K as a function of the total power of microwaves at frequencies of 18 and 28 GHz to heat the ECR plasma, as shown in Fig. 1. The ECR plasma was stabilized by the O_2 support gas. The heating power of HTO (P_{HTO}) was changed from 300 W to 720 W, and the corresponding consumption rates (C.R.) are summarized in Table 1. The results clearly indicate that C.R. depends on the transmission efficiency through the accelerators and the beam lines, and we expect to provide a Ca-ion beam of more than 0.5 particle μA on the target with a Ca consumption of 0.5 mg/h. Furthermore, we plan to study other support gases such as N_2 and different crucible shapes to improve the ionization efficiency to reduce the Ca consumption further.

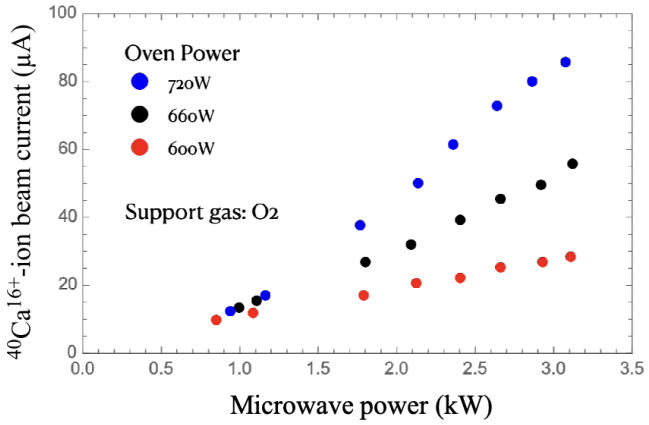

Fig. 1. Obtained $^{40}Ca^{16+}$-beam currents as a function of the total power of the 18- and 28-GHz microwaves. The red, black, and blue points show HTO heating powers of 600, 660, and 720 W, respectively.

Table 1. Total consumption of the CaO sample ΔW as a function of the HTO heating power P_{HTO} and the operation time Δt. The consumption rate (C.R.) was estimated from the ratio of the atomic weights of Ca and O.

P_{HTO}(W)	Δt(hours)	ΔW(CaO, mg)	C.R.(Ca, mg/h)
300.	167.0	6.	0.03
600.	71.3	23.	0.23
660.	40.6	29.	0.51
720.	18.6	20.	0.78

*1 RIKEN Nishina Center

References
1) N. Sakamoto *et al.*, Proc. SRF2019, Dresden, Germany, (2019), pp. 750–757.
2) K. Ozeki *et al.*, Rev. Sci. Instrum. **86**, 016114 (2015).
3) D. Wutte *et al.*, Rev. Sci. Instrum. **73**, 521 (2002).
4) J. Y. Benitez *et al.*, Rev. Sci. Instrum. **85**, 02A961 (2014).
5) J. Ohnishi *et al.*, Proc. ECRIS2018, Catania, Italy, (2018), p. 180.
6) T. Nagatomo *et al.*, Rev. Sci. Instrum. **91**, 023318 (2020).
7) G. D. Alton *et al.*, Rev. Sci. Instrum. **65**, 775 (1994).

First transport of unstable nuclei into SCRIT system

Y. Abe,[*1] T. Ohnishi,[*1] S. Ichikawa,[*1] A. Enokizono,[*1,*2] R. Ogawara,[*1,*3] K. Tsukada,[*1,*3] H. Wauke,[*1,*4] M. Watanabe,[*1] and M. Wakasugi[*1,*3]

The electron-beam-driven RI separator for the SCRIT (ERIS)[1] at the SCRIT electron scattering facility[2] is an online isotope separator system. It is used to produce low-energy RI beams via photofission of uranium. This year, we transported a pulsed ^{137}Cs beam, which was produced by a surface-ionization ion source and using ion-stacking and pulse-extraction systems,[3,4] into the SCRIT system. We report the results obtained from the experiments.

Details of the RI production method and the surface-ionization ion source of the ERIS are reported in Refs. 4) and 5). In the measurements, self-made 43 uranium carbide disks[6] were used as production targets. The total amount of uranium was approximately 28 g. We measured the production rate of Cs isotopes using a particle identification (PID) system[1] located at the exit of the FRAC[3] to estimate the rate of ^{137}Cs, because the life of ^{137}Cs is extremely long to measure γ-rays. In the measurements, the electron beam power was adjusted to approximately 1 W to reduce background events. The target and the ionization chamber were heated to 1500–2000°C by resistive heating. The electric currents applied to the ionization chamber and the target heater were 120 A and 750 A, respectively. Ionized RIs were extracted by the exit grid of the ionization chamber, accelerated to 10 keV, and transported to the PID system. PID was performed by measuring specific γ-rays corresponding to the decay of the RIs using a Ge detector. The measurement process is reported in Ref. 7). Figure 1 shows the isotope dependence of the rate of Cs obtained from the experiments. The mass dependence is similar to the trend reported from the ALTO[8], which is expected to become flat for masses lower than 139. From this result, the rate of ^{137}Cs ion is estimated as approximately 1×10^5 atoms/s with an electron beam power of 1 W under the ionization chamber and target condition.

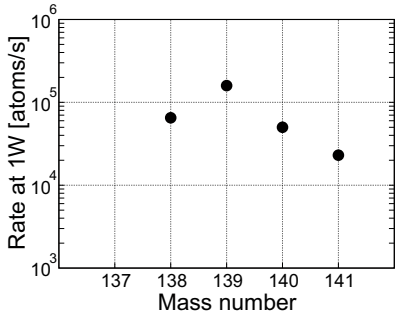

Fig. 1. Isotope dependence of rate of Cs. Electron beam power is approximately 1 W. Total amount of uranium is 28 g.

After adjusting the electric currents of the ionization chamber and target heater to 150 A and 900 A, respectively, the rate of the RIs increased by approximately one order, and we transported the ^{137}Cs beam to the SCRIT system by monitoring it using Faraday cups in the beamline. To produce ^{137}Cs ions, an electron beam was irradiated was at a power of approximately 15 W. The produced ^{137}Cs ions were stacked in the ERIS with a 50 ms stacking time. The pre-pulsed ^{137}Cs ions were injected into the FRAC and subsequently stacked and extracted from the FRAC as a pulsed beam in a cycle of 1 s. The pulsed ^{137}Cs beam was successfully transported from the FRAC to the SCRIT system with approximately 100% transmission efficiency by carefully adjusting the optical parameters. Figure 2 shows the signal of the ^{137}Cs beam at the position monitor located at entrance of the SCRIT device. The number of ^{137}Cs ions transported to the SCRIT system was 9.8×10^6 atoms/pulse. The yield of ^{137}Cs may be improved by optimizing the optical parameters from the ERIS to the FRAC and the stacking conditions of the FRAC. It can also be increased by optimizing the temperature of the ionization chamber and the target heater.

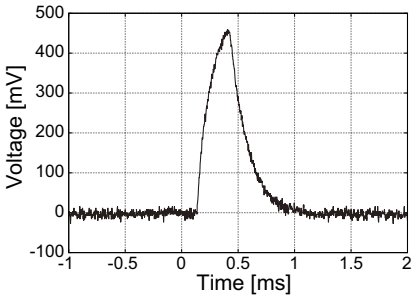

Fig. 2. Signal of ^{137}Cs beam at position monitor located at entrance of SCRIT device.

The ERIS is almost ready for the world's first electron scattering experiment with unstable nuclei, which will be conducted in the future.

*1 RIKEN Nishina Center
*2 Department of Physics, Rikkyo University
*3 Institute for Chemical Research, Kyoto University
*4 Research Center for Electron Photon Science, Tohoku University

References
1) T. Ohnishi *et al.*, Nucl. Instrum. Methods Phys. Res. B **317**, 357 (2013).
2) M. Wakasugi *et al.*, Nucl. Instrum. Methods Phys. Res. B **317**, 668 (2013).
3) M. Wakasugi *et al.*, Rev. Sci. Instrum. **89**, 095107 (2018).
4) T. Ohnishi *et al.*, RIKEN Accel. Prog. Rep. **52**, 142 (2019).
5) T. Ohnishi *et al.*, RIKEN Accel. Prog. Rep. **48**, 229 (2015).
6) T. Ohnishi *et al.*, RIKEN Accel. Prog. Rep. **47**, xiii (2014).
7) T. Ohnishi *et al.*, RIKEN Accel. Prog. Rep. **53**, 110 (2020).
8) S. Essabaa *et al.*, Nucl. Instrum. Methods Phys. Res. B **317**, 218 (2013).

Performance study of wide dynamic range photon detection system using Ge detectors for muonic X-ray spectroscopy

R. Mizuno,[*1] T. Ikeda,[*2] S. Go,[*2] T. Y. Saito,[*1] H. Sakurai,[*1,*2] M. Niikura,[*1] T. Matsuzaki,[*2] and S. Michimasa[*3]

We are planning spectroscopy of the muonic atom of heavy nuclei and muon-induced fission reaction. The energy of muonic X rays of heavy elements, such as actinides, is above 6 MeV.[1)] Therefore, we develop a wide dynamic range X-ray and γ-ray detection system to detect such high energy X-rays. Evaluations of the detector's efficiency and energy resolution are required to understand the performance of the detector in a wide dynamic range. While standard γ-ray sources can be used to evaluate detector performance in low energy regions below 1.8 MeV, there are no sources available for above a few MeV. Therefore, we performed an experiment using the 992-keV resonance in the ^{27}Al$(p,\gamma)^{28}$Si reaction, primarily because the reaction emits several γ rays over a wide energy range from 1.5 to 10.8 MeV, and their energies and relative intensities are well known.[2,3)]

The experiment was performed at the RIKEN Pelletron facility. The proton beam at 1 MeV irradiated a 0.8-μm thick Al target. The energy loss of the beam in the target was estimated as 36 keV. The target thickness and beam energy were sufficient to induce a 992-keV resonance and not excite the nearest resonances at 937 and 1025 keV. The proton beam intensity was approximately 300 nA, and the measurement time was 6.5 h. The experimental setup is shown in Fig. 1. The photon detectors in the system consist of high-purity Ge detectors with high energy resolution. Two Ge detectors, GMX80 (Ortec) and GX5019 (Canberra), were used for γ-ray detection. GMX80 and GX5019 are an n-type 80% coaxial detector and a p-type 50% coaxial detector, respectively. The distances from the target to the detectors were 5 cm (GMX80) and 10 cm (GX5019), respectively. To suppress the Compton component, the main background of the Ge detector's spectrum, BGO detectors were used as a Compton suppressor. In this experiment, GX5019 was surrounded by the BGO Compton suppressors to test the performance of Compton suppression in such a high energy region. Signals from the detectors were acquired by a waveform digitizer (Caen V1730B).

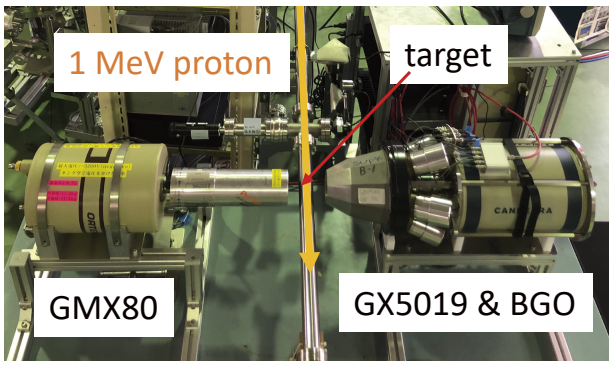

Fig. 1. Photograph of the experimental setup. Two Ge detectors were set next to the target and at an angle of 90-degrees to the beam.

The spectrum of the γ-ray energy acquired with GX5019 after Compton suppression is illustrated in Fig. 2. Figure 2 shows 13 γ-ray peaks in 1.5–10.8 MeV obtained more than 1000 counts for each peak for less than 3% statistical accuracy. Single escape peaks (SE) and double escape peaks (DE) were also observed in the spectrum. Detailed analyses of the γ-ray spectrum are carried out to estimate the Ge detectors' photopeak efficiencies and energy resolutions. Accordingly, we will discuss the performance of the photon detection system in a wide energy range below 10.8 MeV.

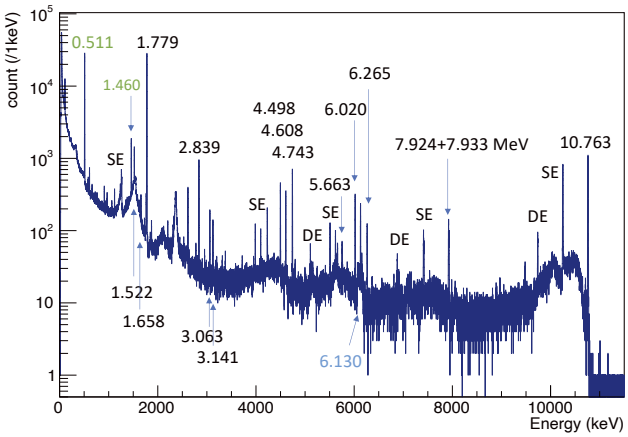

Fig. 2. γ-ray energy spectrum measured by GX5019 suppressed by a compton suppressor. The γ rays from 511 keV to 10.7 MeV can be observed. In the spectrum, SE (DE) means single (double) escape peaks corresponding γ-rays.

*1 Department of Physics, University of Tokyo
*2 RIKEN Nishina Center
*3 Center for Nuclear Study, University of Tokyo

References

1) G. Fricke *et al.*, At. Data Nucl. Data Tables **60**, 177 (1995).
2) A. Anttila *et al.*, Nucl. Instrum. Methods Phys. Res. **147**, 501 (1977).
3) P. M. Endt, Nucl. Phys. A **521**, 1 (1990).

Development of inspection system for bus extender cable of RHIC-sPHENIX INTT detector

H. Imai,[*1,*6] Y. Akiba,[*1] D. Cacace,[*2] K. Cheng,[*3] H. En'yo,[*1] T. Hachiya,[*1,*4] S. Hasegawa,[*1,*5] M. Hata,[*4] T. Kondo,[*7] C. Kuo,[*3] H. -S. Li,[*8] R. -S. Lu,[*9] E. Mannel,[*2] C. Miraval,[*2] M. Morita,[*1,*4] I. Nakagawa,[*1] Y. Nakamura,[*1,*6] G. Nakano,[*1,*6] Y. Namimoto,[*1,*4] R. Nouicer,[*2] G. Nukazuka,[*1] R. Pisani,[*2] M. Shibata,[*1,*4] C. Shih,[*3] M. Shimomura,[*4] M. Stojanovic,[*8] Y. Sugiyama,[*4] R. Takahama,[*1,*4] W. -C. Tang,[*3] M. Watanabe,[*4] and X. Wei[*8]

The sPHNEIX experiment is scheduled to begin at Brookhaven National Laboratory (BNL) in 2023, study quark-gluon plasma (QGP) by using a heavy-ion accelerator.[1)] We have developed a long, high-signal-line-density, flexible substrate cable to transmit data from one of the tracking detectors, INTermediate Tracker (INTT), to a downstream data-processing circuit board. The cable is called Bus Extender (BEX), which is 111 cm long and comprises 124 signal lines separated by a space of 130 μm.

After five years of research and development, the cable is meets the specifications required by sPHENIX in terms of both mechanical and electrical performances. However, there is one remaining technical issue, namely, a poor yield rate (30–50%) in mass production mainly due to dust contamination during signal-line patterning. The contaminated dust causes abnormal patterns in the signal lines, which tends to result in either short or broken signal lines. The anomaly used to be manually inspected using a magnifying glass during the prototyping stage of the cable, which is not practical for mass production because of the large area (a pattern sheet accommodates four BEXs and the size is about 120 cm $\times$ 25 cm) to be inspected for 120 BEXs in total. The motivation of this study was to establish a semi-automated process for pattern inspection.

For this purpose, we developed an inspection fixture, which consists of a high-resolution microscope camera on a moving aluminum frame, as shown in Fig. 1. The aluminum base frame is set along the BEX signal line, and the camera moves along the base frame, as shown with the red arrow. A pattern image taken by the camera is then analyzed using a pattern-recognition software developed by us. The algorithm for anomaly detection from the image is as follows. First, the color image is converted to black and white. Next, the number of pixels for each line and space in a direction perpendicular to the signal lines is counted for both black and white zones and fill number of pixel histograms,

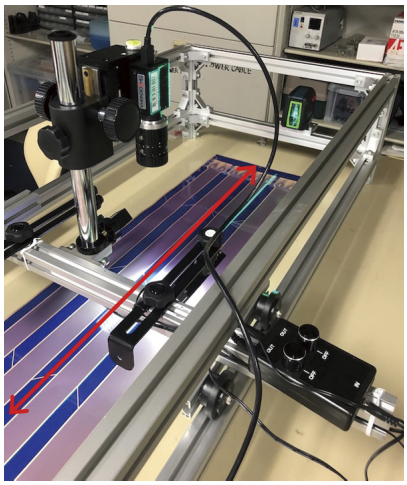

Fig. 1. Inspection fixture and camera for the signal-line pattern of BEX.

respectively, to evaluate the mean and standard deviations of the number of pixels as references. Finally, the algorithm detects anomaly spots on the image, where the pattern deviates by more than 5σ from the reference. The process described above is repeated to scan through the 111-cm-long signal lines. One of the abnormal patterns detected with this algorithm is indicated using the red circle in Fig. 2. This technique facilitated inspections in mass production, which would have been impossible otherwise.

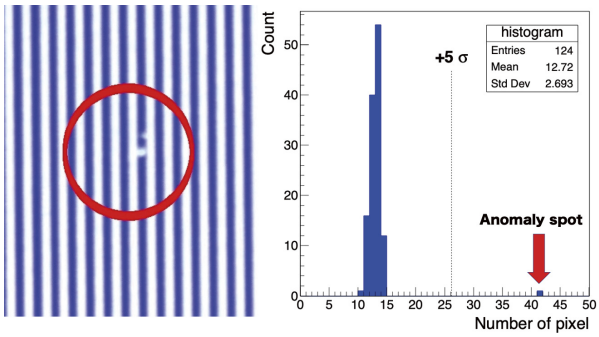

Fig. 2. Example of anomaly spot and histogram of signal-line pattern detected by the algorithm.

*1 RIKEN Nishina Center
*2 Physics Department, Brookhaven National Laboratory
*3 Department of Physics, National Central University
*4 Department of Mathematical and Physical Sciences, Nara Women's University
*5 Japan Atomic Energy Agency
*6 Department of Physics, Rikkyo University
*7 Tokyo Metropolitan Industrial Technology Research Institute
*8 Department of Physics and Astronomy, Purdue University
*9 Department of Physics, National Taiwan University

Reference
1) I. Nakagawa *et al.*, in this report.

Simple cubic self-assembly of PbS quantum dots by fine ligand control†

J. Liu,*1 K. Enomoto,*1 K. Takeda,*1 D. Inoue,*1 and Y. -J. Pu*1

Colloidal quantum dots (QDs) have attracted substantial attention due to their characteristic optoelectronic properties based on the size confinement effect.[1] They are also known to self-assemble into highly ordered superlattices.[2] The geometry of such self-assembled QDs has been explored to better understand the ensemble effects on their optical and electrical properties.[3] Accordingly, it is essential to prepare two-(2D) and three-dimensional (3D) QD superlattices with different geometry for their solid-state device applications.

Most colloidal quantum dots with a *quasi*-spherical shape readily self-assemble into 3D face-centered cubic (fcc) or body-centered cubic (bcc) superlattices.[4] In contrast, 3D simple cubic (sc) superlattices are difficult to obtain from sphere-like QDs because of their relatively low packing fraction of 0.52 and the low stability by entropy.[5] Therefore, sc superlattices have been expected to have different optical and electronic properties from other packing structures, and the quest has been on to achieve 3D self-assembled sc superlattices. Here, we achieve the selective control of the geometry of the *quasi*-spherical PbS QDs in highly-ordered 2D and 3D superlattices: Disorder, sc, and fcc by selectively removing the ligands from the QD surface through gel permeation chromatography (GPC).

The uniform sphere-like PbS QDs with an average diameter of 7.3 nm were synthesized. The QD sample was purified once by precipitation/redissolution process prior to the GPC process (before-GPC). In the GPC process, the eluted QD solution was collected in 5 consecutive portions (GPC-1 to GPC-5).

The thermogravimetric analysis (TGA) was carried out to evaluate weight ratios of oleic acid (OA) ligands bound to QD surface (Fig. 1a) which gradually increase from GPC-1 to GPC-5. To further determine the ligand density, the atomic Pb/S ratios of GPC-2 and before-GPC were obtained from Rutherford backscattering (RBS) spectrometry in RIKEN Pelletron accelerator facility (Fig. 1b).[6] An average Pb/S ratio (1.27) combined with TGA results was used for estimating the ligand density. The TGA results (Fig. 1c) demonstrate that the ligand density of the PbS QDs gradually increases from GPC-1 (0.6 nm^{-2}) to GPC-5 (7.1 nm^{-2}) and that the GPC method can precisely and continuously control the ligand density of the PbS QDs. We also estimated the ligand density by nuclear magnetic resonance spectroscopy. The obtained results are consistent with the ligand density obtained from TGA (Fig. 1c).

Based on the difference in their ligand density, the 2D self-assembly of these QDs was achieved by drop-casting dilute solutions onto solid substrates. GPC-1–5 formed 2D superlattices with different and unique geometries.

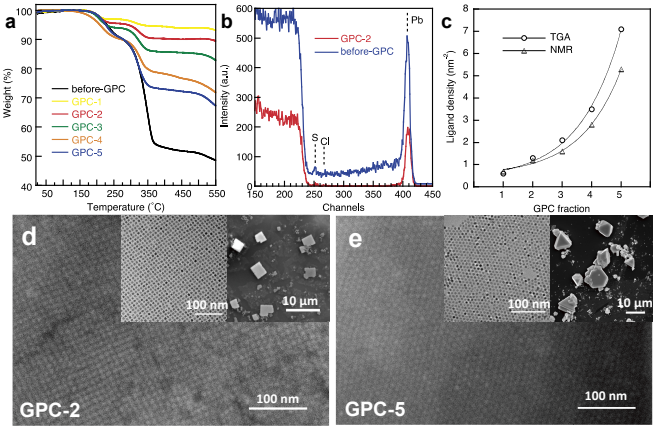

Fig. 1. (a) TGA curves of before-GPC and GPC1-5; (b) RBS spectra of GPC-2 and before-GPC; (c) Ligand density of PbS QDs as a function of the GPC fraction; The scanning electron microscopy (SEM) images of the supercrystal surfaces for GPC-2 (d) and GPC-5 (e); inset: their 2D self-assembled TEM images and SEM images of 3D supercrystals.

GPC-1 QDs showed a random assembly due to insufficient ligands on the QD surface. However, GPC-2 QDs (inset of Fig. 1d) formed a square self-assembled geometry without the fusion between QDs. Also, the GPC-2 QDs in the square superlattice are highly oriented along QD [100] facets. The GPC-3–5 QDs with sufficient ligands formed the hexagonal assemblies with non-oriented facets (inset of Fig. 1e).

Furthermore, the long-range-ordered 3D self-assembled supercrystals for GPC-2 and GPC-5 QDs were prepared by solvent evaporation. GPC-5 QDs can form triangular or hexagonal fcc supercrystals with a hexagonal arrangement on the crystal surface (Fig. 1e). It is noteworthy that GPC-2 QDs self-assembled in cubic supercrystals with sc packing on account of finely controlled ligand removal by GPC, which is usually difficult for quasi-spherical QDs.

In this report, we develop GPC as a method to control the ligand density of the *quasi*-spherical PbS QDs and achieve the selective control of the geometry of QDs in 2D and 3D superlattices: Disorder, sc, and fcc. The precise control of QD self-assembled geometry is expected to greatly improve the performance of next-generation semiconductor devices and photocatalysis.

References
1) C. R. Kagan *et al.*, Science **353**, 885 (2016).
2) M. A. Boles *et al.*, Chem. Rev. **116**, 11220 (2016).
3) C. S. S. Sandeep *et al.*, ACS Nano **8**, 11499 (2014).
4) K. Bian *et al.*, Chem. Mater. **30**, 6788 (2018).
5) M. Boles, D. Talapin, J. Am. Chem. Soc. **137**, 4494 (2015).
6) I. Moreels *et al.*, ACS Nano **3**, 3023 (2009).

† Condensed from the article in Chem. Sci. **12**, 10354 (2021)
*1 RIKEN Center for Emergent Matter Science

Co-precipitation behaviour of single atoms of rutherfordium in basic solutions†

Y. Kasamatsu,[*1] K. Toyomura,[*1] H. Haba,[*2] T. Yokokita,[*1] Y. Shigekawa,[*1] A. Kino,[*1] Y. Yasuda,[*1] Y. Komori,[*1] J. Kanaya,[*2] M. Huang,[*2] M. Murakami,[*2] H. Kikunaga,[*3] E. Watanabe,[*1] T. Yoshimura,[*4] K. Morita,[*2] T. Mitsugashira,[*5] K. Takamiya,[*6] T. Ohtsuki,[*6] and A. Shinohara[*1]

In heavy atoms, the relativistic effects are strong, which would result in deviations of their chemical behaviours from those expected by simple extrapolation of the characteristics of the lighter homologues.[1)] It is very challenging to perform chemical experiments on the heavy elements, because their nuclides are produced with extremely low production rates and tend to decay rapidly; only one atom can be usually treated at a time. Thus, rapid transportation system of the nuclear reaction products and automated chemical separation apparatuses specialized for such elements are needed. Chemical studies of heavy elements have mainly been conducted by two-phase partition methods. In particular, the formation of fluoride, chloride, nitrate, and sulfide complexes of Rf has been investigated in solution chemistry.[1)]

We focused on a precipitation approach to study heavy element chemistry. In a previous study, a co-precipitation method with Sm, 10–20 μg, was developed, and the method was applied to various elements using a multiple radiotracer source. The yields of co-precipitate formed in solutions with several concentrations of ammonia (NH_3) and sodium hydroxide (NaOH) were determined for elements from various groups in the periodic table.[2)] From the consistent co-precipitation yields with their properties in hydroxide precipitation and ammine complexation, it was concluded that the hydroxide and ammine complexation of heavy elements can be qualitatively investigated on the basis of their co-precipitation behaviours with Sm. Based on these findings, the purpose of the present study is to investigate the co-precipitation behaviour of Rf with samarium hydroxide and get an insight into the properties of its hydroxide and ammine complex formation.

^{261}Rf was produced by the ^{248}Cm(^{18}O, $5n$) reaction using the AVF cyclotron at RIKEN RIBF. ^{169}Hf was simultaneously produced to check the status of the online filtration apparatuses[2)] by monitoring Hf behaviour. After dissolution of the transported nuclear reaction products in the dissolution apparatus, a basic solution (aq. NH_3 or NaOH) was added to produce the hydroxide precipitate. The co-precipitation yields, Y, were determined from the radioactivity of precipitate and total radioactivity.

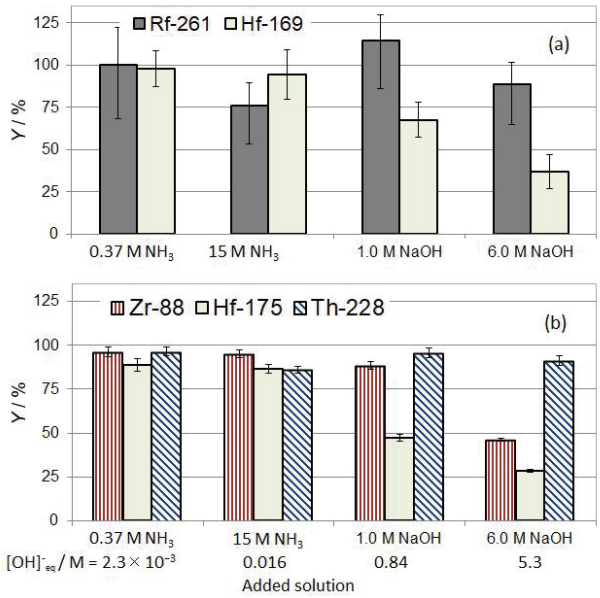

Fig. 1. The Y values of ^{261}Rf and ^{169}Hf (a) and those of ^{88}Zr, ^{175}Hf, and ^{228}Th (b).

The co-precipitation yields evaluated for ^{261}Rf and ^{169}Hf are shown in Fig. 1(a). The yields of ^{88}Zr, ^{175}Hf, and ^{228}Th previously obtained[2)] are also shown in Fig. 1(b). The co-precipitation yields of ^{169}Hf determined in this study typically agreed with previously obtained values for ^{175}Hf, suggesting that the online experiment on ^{261}Rf was successful. In dilute OH^- solutions (aq. NH_3), the Y values of all the elements were high (76–100%), suggesting predominant precipitation. This indicates that the chemical properties of Rf allow for the formation of a hydroxide precipitate; namely, we extrapolate that Rf would form a hydroxide precipitate if in macro amounts. This behaviour is typical of the hydroxides of group 4 elements, precipitation as $M(OH)_4$ (M^{4+} = metal ion of group 4 element). In addition, the yield of Rf in concentrated NH_3 solution was not markedly lower than the yields in other concentrations, suggesting that Rf does not strongly coordinate with NH_3 molecules, similar to its homologues. In concentrated OH^- solutions (NaOH), the Y values of Zr and Hf decreased with increasing

† Condensed from the article in Nature Chem. **13**, 226 (2021)

*1 Graduate School of Science, Osaka University
*2 RIKEN Nishina Center
*3 Research Center for Electron Photon Science, Tohoku University
*4 Radioisotope Research Center, Osaka University
*5 Institute for Material Research, Tohoku University
*6 Institute for Integrated Radiation and Nuclear Science, Kyoto University

OH^- concentration due to the formation of hydroxide complex ions such as $[M(OH)_5]^-$ and $[M(OH)_6]^{2-}$, whereas the yields of Rf and Th remained high. Indeed, the solubility products of $[M(OH)_5]^-$ ($\log K_{s5} = [M(OH)_5]^-/[OH]^-$) for Zr, Hf, and Th are -3.6, -3.2, and -5.8, respectively, and this sequence is consistent with their Y values obtained with 6.0 M NaOH. We can deduce that $\log K_{s5}$ of Rf would be lower than those of Zr and Hf. It suggests a weaker tendency of Rf toward hydroxide complexation than those of Zr and Hf.

References

1) M. Schädel, Phil. Trans. R. Soc. A **373**, 20140191 (2015).
2) Y. Kasamatsu, J. Nucl. Radiochem. Sci. **18**, 24 (2018).

Sodium ascorbate protects ^{211}At-labeled antibodies from reactive oxygen species damage†

S. Manabe,[*1,*2,*3] H. Takashima,[*4] Y. Koga,[*4,*5] K. Onuki,[*6] R. Tsumura,[*4] T. Anzai,[*4] N. Iwata,[*4] M. Yasunaga,[*4] Y. Wang,[*7] T. Yokokita,[*7] Y. Komori,[*7] D. Mori,[*7] H. Haba,[*7] H. Fujii,[*6] and Y. Matsumura[*4]

Radioimmunotherapy (RIT) is synonymous with next-generation antibody medication. α-particles are particularly suited to RIT on account of their potent linear energy transfer (LET) and short path range. Among the several α-emitter nuclei, ^{211}At is preferable to the rest owing to its short half-life (7.2 h) and inability to yield cytotoxic daughter isotopes during decay. Successful delivery of α-particles to the tumor site is a key requisite for effective cancer treatment, which can be achieved by using specific antibodies against tumor antigens.

We investigated ^{211}At-labeled antibodies for cancer therapy.[1)] Briefly, ^{211}At, generated by the RIKEN AVF cyclotron, was conjugated to trastuzumab, a therapeutic antibody targeted against breast and stomach cancer. ^{211}At was immobilized onto trastuzumab carrying trimethylstannyl benzoate via an ^{211}At-Sn exchange reaction, followed by purification using size-exclusion column chromatography. However, using sodium dodecyl sulfate polyacrylamide gel electrophoresis (SDS-PAGE) analyses, we discovered that the ^{211}At-labeled trastuzumab thus obtained was damaged. Further, flow cytometry revealed that the binding affinity of ^{211}At-labeled trastuzumab to human epidermal growth factor receptor 2 (HER2) expressing SK-BR-3 cells was drastically compromised (Fig. 1).

We speculated that damage to the ^{211}At-conjugated antibodies may have been caused by reactive oxygen species (ROS), that were generated from water radiolysis by α-particles released from ^{211}At. Consequently, we established an ROS detection system based on the chemiluminescence luminol assay. Aqueous ^{211}At solutions tested positive in the luminol assay, thereby indicating the presence of ROS. Further, the assay revealed the quenching of ROS in the presence of 6×10^{-2} mg/mL sodium ascorbate.

^{211}At-labeled trastuzumab in the presence of more than 6×10^{-2} mg/mL sodium ascorbate was stable as seen using SDS-PAGE analyses, and its binding affinity was maintained. In addition, WST-8 assays demonstrated more potent cytocidal effects of ^{211}At-labeled trastuzumab in the presence of sodium ascorbate, against high HER2-expressing SK-BR-3 cells than those exerted by the immunoconjugate that was not under the protection (Fig. 2). These results conclusively demonstrated that quenching of ROS is essential for efficacious RIT. Moreover, the cytocidal effects seemed to be dependent on the level of HER2 on the cancer cells. Compared with free ^{211}At, ^{211}At-labeled trastuzumab more efficiently killed SK-BR-3 cells, whereas the cytotoxicity was mitigated against MCF-7 cells that express lower levels of HER2 (Fig. 2).

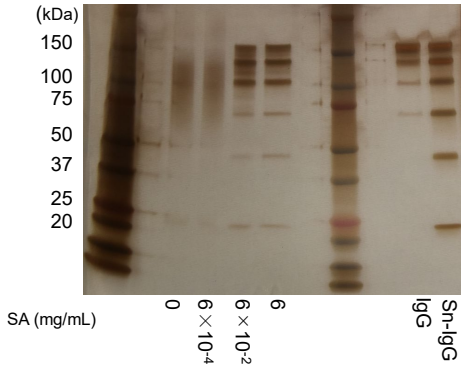

Fig. 1. SDS-PAGE showing damaged ^{211}At-labeled trastuzumab after 1 day.

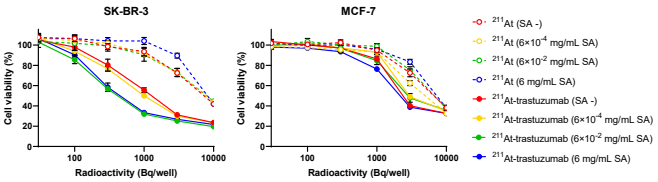

Fig. 2. Cytotoxic effects of ^{211}At-labeled trastuzumab.

While the reducing agent L-cysteine demonstrated similar ROS-quenching activity as sodium ascorbate, others such as sodium hydrosulfite and maltose, had a weaker effect.

We therefore conclude that ^{211}At-labeled antibodies are damaged by ROS that are generated by the action of ^{211}At on water. The presence of sodium ascorbate resulted in the quenching of ROS, which prevented ^{211}At-labeled antibody damage, and maintained its function. The present data warrant further studies for development of the above-described cancer therapy.

This manuscript has been condensed from the article in ACS Omega. Figures are reproduced with permission from American Chemical Society.

Reference

1) H. Takashima *et al.*, Cancer Sci. **112**, 1975 (2021).

† Condensed from the article in ACS Omega **6**, 14887 (2021)

*1 Pharmaceutical Department, Hoshi University
*2 Research Center for Pharmaceutical Development, Tohoku University
*3 Glycometabolic Biochemistry Laboratory, Cluster for Pioneering Research, RIKEN
*4 Division of Developmental Therapeutics, Exploratory Oncology Research and Clinical Trial Center, National Cancer Center
*5 Department of Strategic Programs, Exploratory Oncology Research and Clinical Trial Center, National Cancer Center
*6 Division of Functional Imaging, Exploratory Oncology Research and Clinical Trial Center, National Cancer Center
*7 RIKEN Nishina Center

Intratumoral administration of astatine-211-labeled gold nanoparticle for alpha therapy†

H. Kato,[*1] X. Huang,[*2] Y. Kadonaga,[*3] D. Katayama,[*1] K. Ooe,[*1] A. Shimoyama,[*2] K. Kabayama,[*2] A. Toyoshima,[*3] A. Shinohara,[*3] J. Hatazawa,[*4] and K. Fukase[*2,*3]

As a local radiation therapy for cancer and in addition to external irradiation with γ-rays or X-rays, the effectiveness of brachytherapy using a sealed X-ray source for prostate cancer, breast cancer, uterine cancer, head and neck cancer, and brain tumors is well known. However, the invasiveness of the procedure, extra-lesion displacement of the sealed radiation source, or adverse effects caused by the leakage of X-rays from radionuclides with a long half-life into adjacent organs are problematic issues. α-ray-emitting nuclides have a high linear energy transfer (LET) and relative biological effectiveness and are particularly toxic to proliferating cells. Because of the short range of α-ray emitters, normal tissues are minimally exposed if the radiation sources are appropriately distributed. ^{211}At is a high-energy α-ray emitter with a relatively short half-life and a high cytotoxicity for cancer cells. Its dispersion can be imaged using clinical scanners, and it can be produced in cyclotrons without the use of nuclear fuel material.

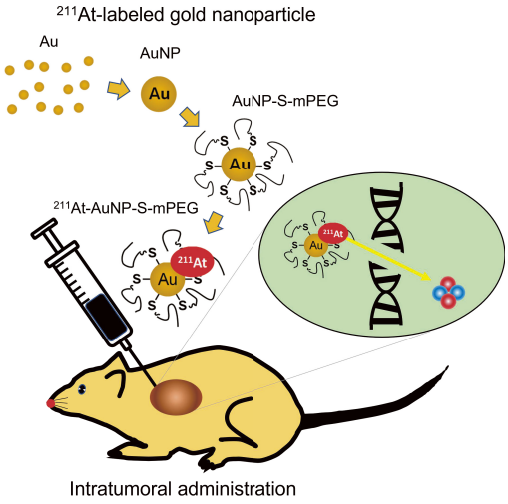

Fig. 1. ^{211}At-labeled gold nanoparticles administered intratumorally. α-ray caused DNA double-strand break and kill the malignant cells.

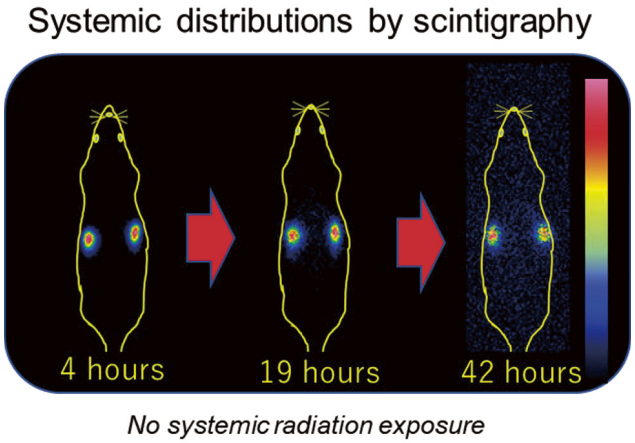

Fig. 2. The radioactivity distributions at 4, 19, and 42 hours after the administration of ^{211}At-AuNP-S-mPEG are shown. Strong radioactivity was found at the transplanted tumor sites. No systemic accumulation of radioactivity was observed in any of the organs.

The objective of this study was to propose an effective nanoseed brachytherapy with significantly reduced radiation exposure. In the present study, we investigated the systemic and intratumoral distributions and verified the antitumor effect of ^{211}At-labeled AuNP administered intratumorally (Fig. 1).

AuNP with a diameter of 5, 13, 30, or 120 nm that had been modified with poly (ethylene glycol)

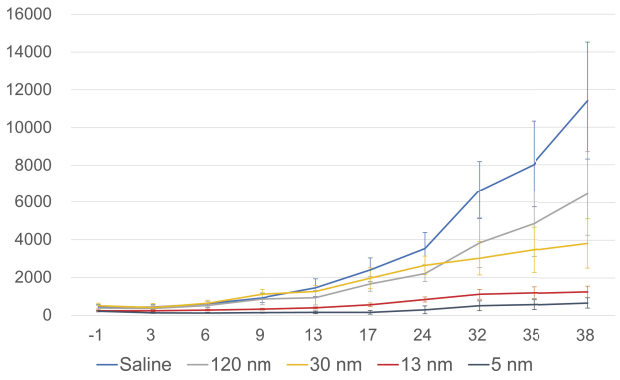

Fig. 3. Changes in the tumor volumes of the C6 glial cells after intratumoral administration (1.4±0.4 MBq/tumor for rats). The C6 gliomas treated with the 5 nm particles had the lowest growth rate, based on tumor size.

† Condensed from the article in J. Nanobiotechnology **19**, 223 (2021)

*1 Department of Nuclear Medicine and Tracer Kinetics, Osaka University Graduate School of Medicine
*2 Department of Chemistry, Graduate School of Science, Osaka University
*3 Division of Science, Institute for Radiation Sciences, Osaka University
*4 Research Center for Nuclear Physics, Osaka University

methyl ether (mPEG) thiol and labeled with ^{211}At (^{211}At-AuNP-S-mPEG) were intratumorally administered to C6 glioma subcutaneously transplanted into rodent models. A part of ^{211}At used in this work was produced in the ^{209}Bi$(\alpha, 2n)^{211}$At reaction using the RIKEN AVF cyclotron. After intratumoral administration, ^{211}At-AuNP-S-mPEG became localized in the tumor and did not spread to systemic organs during a time period equivalent to 6 half-lives of ^{211}At (Fig. 2). Tumor growth was strongly suppressed by ^{211}At-AuNP-S-mPEG without any critical side effects. In the C6 glioma model, the strongest antitumor effect was observed in the group treated with ^{211}At-AuNP-S-mPEG with the smallest diameter of 5 nm (Fig. 3).

The intratumoral single administration of a simple nanoparticle, ^{211}At-AuNP-S-mPEG, was shown to suppress the growth of tumor tissue strongly in a particle size-dependent manner without radiation exposure to other organs caused by systemic spread of the radionuclide.

Activation cross sections of proton-induced reactions on praseodymium up to 30 MeV†

M. Aikawa,[*1,*2,*3] Y. Hanada,[*2,*3] H. Huang,[*2,*3] and H. Haba[*3]

The medical radionuclide ^{140}Nd ($T_{1/2}$ = 3.37 d) is expected to be used as a ^{140}Nd/^{140}Pr in-vivo generator for positron emission tomography (PET).[1] It can be produced via charged-particle-induced reactions. Among the possible production reactions, we focused on the proton-induced reaction of ^{141}Pr. A survey revealed three experimental studies of the reaction for ^{140}Nd production.[2–4] However, the experimental cross sections in the literature are largely scattered. Therefore, we performed an experiment to obtain the cross sections of the ^{141}Pr$(p, 2n)^{140}$Nd reaction up to 30 MeV. The production cross sections of $^{141, 139m}$Nd and ^{139}Ce were also determined.

We conducted an experiment using a 30-MeV proton beam at the AVF cyclotron in RIKEN. We adopted the stacked-foil activation technique and high-resolution gamma-ray spectrometry to determine the excitation functions. The target consisted of pure metallic thin foils of ^{141}Pr (99% purity), ^{nat}Ti (99.5% purity), and ^{27}Al (>99% purity), which were purchased from Nilaco Corp., Japan. The ^{nat}Ti foil was used for the ^{nat}Ti$(p, x)^{48}$V monitor reaction to assess beam parameters and target thicknesses. The ^{27}Al foil was interleaved to catch recoiled products. The side lengths and weight of each foil were measured to obtain the average thicknesses. The measured thicknesses of the two ^{141}Pr, ^{nat}Ti and ^{27}Al foils were 68.6 and 68.5 mg/cm^2, 9.1 mg/cm^2, and 2.2 mg/cm^2, respectively. The large foils were cut into small pieces of 8 × 8 mm^2 to fit a target holder. Eighteen sets of the Pr-Al-Ti-Ti-Al foils were stacked in the target holder, which served as a Faraday cup.

The stacked target was irradiated with a proton beam for 15 min. The average intensity and primary energy of the beam were measured to be 201 nA and 30.2 MeV, respectively. Energy degradation in the stacked target was calculated using stopping powers obtained from the SRIM code.[5]

Gamma-ray spectrometry was performed using a high-purity germanium detector. Each ^{141}Pr foil was measured together with the next ^{27}Al foil that caught the recoiled products. The ^{141}Pr foils were measured 3–9 times to assess the decay curves of the products. The cooling times were from 1.7 h to 31.9 d, and the dead time was maintained below 7.5%.

Cross sections of the ^{nat}Ti$(p, x)^{48}$V monitor reaction were derived for comparison with the IAEA recommended values.[6] Based on the comparison, the thicknesses of the ^{141}Pr foils and the beam intensity were corrected by +2% and −7% within the uncertainties. The measured thicknesses of ^{nat}Ti and ^{27}Al were used without any correction.

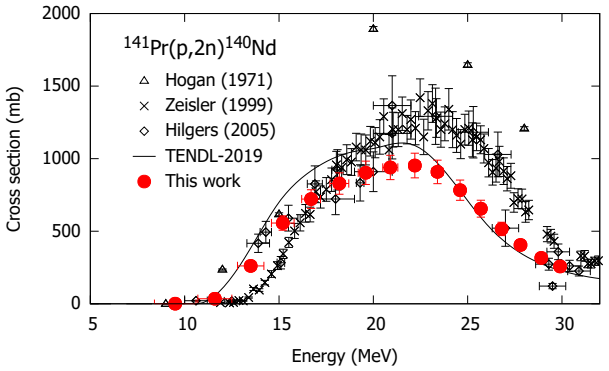

Fig. 1. Cross sections of the ^{141}Pr$(p, 2n)^{140}$Nd reaction with the previous data[2–4] and the TENDL-2019 values.[7]

^{140}Nd has the ground state ($T_{1/2}$ = 3.37 d) and the metastable state at 2.221 MeV ($T_{1/2}$ = 0.60 ms). The isomer fully decays to the ground state via the IT transition (IT: 100%). Because there are no measurable gamma lines from ^{140}Nd, gamma rays with the decay of ^{140}Pr ($T_{1/2}$ = 3.39 min) were instead measured under secular equilibrium with the decay of ^{140}Nd. Direct production of ^{140}Pr during irradiation was negligible because the cooling times were much longer than its half-life. We measured the gamma line at 511 keV (I_γ = 102%) emitted from the irradiated foils, which were sandwiched between copper plates to force positron annihilation. The result is compared with those of the previous studies[2–4] and the TENDL-2019 values[7] in Fig. 1. Our excitation function is largely different from those of the previous studies. The TENDL-2019 values slightly overestimate our experimental data below 23 MeV.

References
1) S. K. Zeisler *et al.*, Clin. Positron Imaging. **2**, 324 (1999).
2) J. J. Hogan, J. Inorg. Nucl. Chem. **33**, 3627 (1971).
3) S. K. Zeisler *et al.*, J. Label. Compd. Radiopharm. **42**, Suppl. 1, S921 (1999).
4) K. Hilgers *et al.*, Radiochim. Acta **93**, 553 (2005).
5) J. F. Ziegler *et al.*, Nucl. Instrum. Methods Phys. Res. B **268**, 1818 (2010).
6) F. Tárkányi *et al.*, IAEA-TECDOC-1211 (2007).
7) A. J. Koning *et al.*, Nucl. Data Sheets **155**, 1 (2019).

† Condensed from the article in Nucl. Instrum. Methods Phys. Res. B **508**, 29 (2021)

*1 Faculty of Science, Hokkaido University
*2 Graduate School of Biomedical Science and Engineering, Hokkaido University
*3 RIKEN Nishina Center

Activation cross section measurement of alpha-particle induced reactions on natural neodymium†

M. Sakaguchi,[*1,*2] M. Aikawa,[*3,*2] N. Ukon,[*4,*2] Y. Komori,[*2] H. Haba,[*2] N. Otuka,[*5,*2] and S. Takács[*6]

Some samarium radionuclides can be used for nuclear medicine. ^{153}Sm ($T_{1/2}$ = 46.3 h) is a beta and gamma emitter available to treat bone metastases.[1] ^{145}Sm ($T_{1/2}$ = 340 d) decays with the emission of low-energy X rays, which is applicable in brachytherapy.[2] These samarium radionuclides can be generated simultaneously in alpha-particle-induced reactions on natural neodymium. Highly accurate cross sections of the reactions are indispensable for practical use. However, there is only one previous experimental study on the $^{\rm nat}$Nd$(\alpha,x)^{153}$Sm reaction up to 26.2 MeV.[3] Further, the literature survey did not reveal any experimental research on the $^{\rm nat}$Nd$(\alpha,x)^{145}$Sm reaction. Therefore, we measure the cross sections of the alpha-particle-induced reactions on natural neodymium up to 51 MeV.

The experiment was performed at the RIKEN AVF cyclotron. The stacked-foil activation technique and high-resolution gamma-ray spectrometry were adopted for the experiment. The target consisted of pure metal foils of $^{\rm nat}$Nd (99.0% purity, Goodfellow Co., Ltd., UK) and $^{\rm nat}$Ti (99.6% purity, Nilaco Corp., Japan). The thicknesses of the $^{\rm nat}$Nd and $^{\rm nat}$Ti foils were 16.7 and 2.35 mg/cm^2, respectively, which were deduced from the measurement of their weights and surface areas. Twenty-one Nd and fourteen Ti foils were arranged in seven sets of Nd-Nd-Nd and Ti-Ti pairs. The second and third Nd foils and the second Ti foil of each pair were assumed to compensate the recoiled products. The $^{\rm nat}$Ti foils were inserted for the $^{\rm nat}$Ti$(\alpha,x)^{51}$Cr monitor reaction to assess the measured beam parameters and target thicknesses.

The stacked target was irradiated with an alpha-particle beam for 60 min. The measured beam energy and intensity were 51.1 ± 0.2 MeV and 172 nA, respectively. Energy degradation through the stacked target was calculated using the SRIM code.[4] The gamma-ray spectra were acquired for the recoil-compensated foils by an HPGe detector without chemical separation. Measurements were performed several times after cooling from 0.7 h to 4.0 d to follow the decay of the produced radionuclides with different half-lives. The distances between the foils and the detector were adjusted to keep the dead time less than 5%.

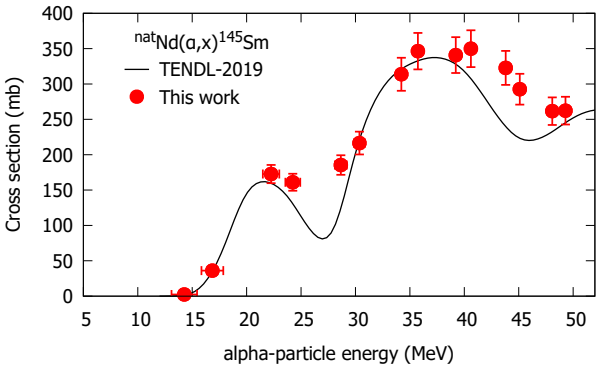

Fig. 1. Excitation function of the $^{\rm nat}$Nd$(\alpha,x)^{145}$Sm reaction compared with the TENDL-2019 data.[6] No experimental data published earlier was found in a survey.

The derived cross sections of the $^{\rm nat}$Ti$(\alpha,x)^{51}$Cr monitor reaction were compared with the IAEA recommended values.[5] The observed shift on the energy scale was corrected by changing the thickness of the Nd foils by −1.5% within its 2% uncertainty to 16.4 mg/cm^2. No additional adjustments were adopted for the data analysis to determine the cross sections of the alpha-particle-induced reactions on natural neodymium.

^{145}Sm ($T_{1/2}$ = 340 d) can be produced in (α,xn) reactions on the stable isotopes of ^{142,143,144,145,146}Nd below 51 MeV. The gamma line at 61.2265 keV (I_γ = 12.15%) emitted with the decay of ^{145}Sm was measured after cooling for 1.4–4.0 days. The net counts of the gamma line were corrected by +8.4% because of the self-absorption effect in the $^{\rm nat}$Nd foils. The cross sections of the $^{\rm nat}$Nd$(\alpha,x)^{145}$Sm reaction were derived from the corrected net counts. The result is shown in Fig. 1 in comparison with theoretical values from the TENDL-2019 library.[6] The TENDL-2019 values are almost consistent with our experimental data. Activation cross sections for other radionuclides ^{153}Sm, ^{151,150,149,148m,148g,144,143}Pm, and ^{149,147}Nd were also determined.

† Condensed from the article in Appl. Radiat. Isot. **176**, 109826 (2021)

*1 Graduate School of Biomedical Science and Engineering, Hokkaido University
*2 RIKEN Nishina Center
*3 Faculty of Science, Hokkaido University
*4 Advanced Clinical Research Center, Fukushima Medical University
*5 Nuclear Data Section, IAEA
*6 Institute for Nuclear Research (ATOMKI)

References

1) I. G. Finlay *et al.*, Lancet Oncol. **6**, 392 (2005).
2) R. G. Fairchild *et al.*, Phys. Med. Biol. **32**, 847 (1987).
3) S. Qaim *et al.*, Radiochim. Acta **95**, 313 (2007).
4) J. F. Ziegler *et al.*, Nucl. Instrum. Methods Phys. Res. B **268**, 1818 (2010).
5) A. Hermanne *et al.*, Nucl. Data Sheets **148**, 338 (2018).
6) A. J. Koning *et al.*, Nucl. Data Sheets **155**, 1 (2019).

Argon-ion-induced mutations in *Arabidopsis EGY1* gene affect chloroplast development in leaf guard cells†

A. Sanjaya,[*1] R. Muramatsu,[*1] S. Sato,[*1] M. Suzuki,[*1] S. Sasaki,[*1] H. Ishikawa,[*1] Y. Fujii,[*1] M. Asano,[*1] R. Itoh,[*2] K. Kanamaru,[*3] S. Ohbu,[*4] T. Abe,[*4] Y. Kazama,[*4,*5] and M. Fujiwara[*1,*4]

Leaf tissues of higher plants such as *Arabidopsis thaliana* contain chloroplasts in the mesophyll and epidermis. Until now, it has been indicated that there exists a tissue- or cell-type-dependent control of chloroplast division in leaves. This raises a fundamental question about the control of chloroplast development in the leaf epidermis, or, more specifically, whether chloroplast biogenesis-related factors in leaf mesophyll cells play an equivalent role in the leaf epidermis.

To address this issue, we examined the phenotype of leaf epidermal chloroplasts using two argon ion irradiation-derived, pale green mutants of *A. thaliana*, Ar50-33-pg1 and Ar-28-pg1 (*egy1-4*).[1–3] Both represent loss-of-function mutants of the *Ethylene-dependent Gravitropism-deficient and Yellow-green 1* (*EGY1*) gene, which encodes a thylakoid membrane-localized protease for chloroplast development in the mesophyll.[4] Moreover, the defects in the thylakoid structure and pigmentation in the mutant mesophyll chloroplasts are known to be pronounced during the later stages of leaf (seedling) development.[3,4]

Fluorescence microscopy observations indicated severe chlorophyll deficiency in the chloroplasts of leaf guard cells and guard mother cells of *egy1* (Fig. 1). This finding was in contrast to that observed in mesophyll cells, which retained a considerable amount of chlorophyll. Labeling of plastids with stroma-targeted fluorescent proteins revealed that *egy1* guard cells contained a normal number of plastids; however, their size was moderately reduced compared to those of the wild-type guard cells (Fig. 1). Transmission electron microscopy further revealed that, in the *egy1* chloroplasts, thylakoid development was impaired not only in mature guard cells but also in the guard mother cell (Fig. 2). Thus, the disorganization of the thylakoid structure and the reduction in the chlorophyll contents showed a positive correlation.

Collectively, these observations demonstrate that *EGY1* is critical for chloroplast differentiation in guard cells: *egy1* guard cell chloroplasts apparently exhibit permanent defects, starting from their development. This prompts a revision to the current understanding of chloroplast development, which has been based mainly from on studies using mesophyll cells.

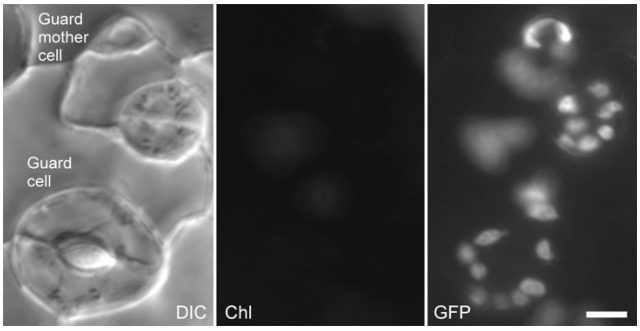

Fig. 1. Fluorescence microscopy images of chloroplasts during guard cell development in Ar50-33-pg1 expressing a stroma-targeted GFP. Bright field (DIC), chlorophyll autofluorescence (chl), and GFP images of leaf epidermis from 18-day-old seedlings are shown. Bar = 10 μm.

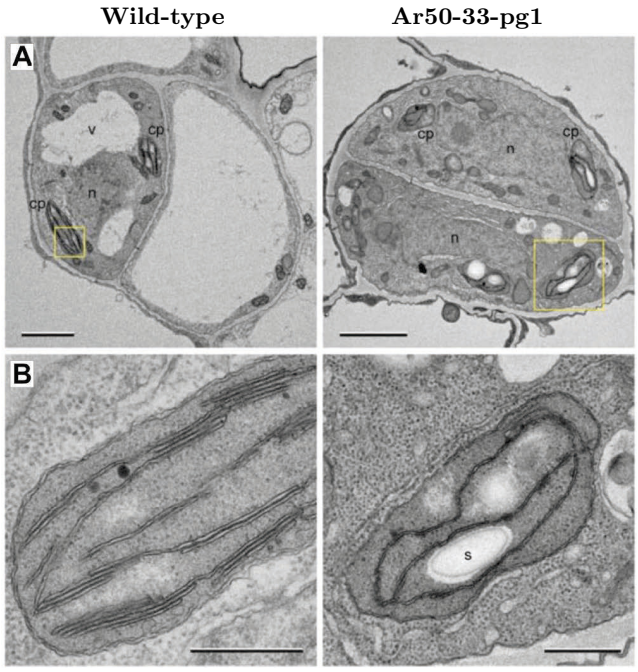

Fig. 2. Transmission electron microscopy analysis of chloroplasts in dividing guard mother cells of expanding leaves. Primary leaves of 10-day-old wild-type and Ar50-33-pg1 plants were analyzed. Guard mother cells (A) and the chloroplasts therein (B). cp, chloroplast; n, nucleus; s, starch; v, vacuole. Bar = 2 μm (A) and 0.5 μm (B).

† Condensed from the article in Plants **10**, 1254 (2021)
*1 Faculty of Science and Technology, Sophia University
*2 Faculty of Science, University of the Ryukyus
*3 Faculty of Agriculture, Kobe University
*4 RIKEN Nishina Center
*5 Faculty of Bioscience and Biotechnology, Fukui Prefectural University

References

1) Y. Kazama *et al.*, RIKEN Accel. Prog. Rep. **43**, 283 (2010).
2) T. Hirano *et al.*, Mutat. Res. **735**, 19 (2012).
3) A. Sanjaya *et al.*, Plants **10**, 848 (2021).
4) G. Chen *et al.*, Plant J. **41**, 364 (2005).

II. RESEARCH ACTIVITIES I
(Nuclear, Particle and Astro-Physics)

1. Nuclear Physics

RI beam production at BigRIPS in 2021

H. Takeda,[*1] N. Fukuda,[*1] H. Suzuki,[*1] Y. Shimizu,[*1] M. Yoshimoto,[*1] N. Inabe,[*1] K. Kusaka,[*1] M. Ohtake,[*1] Y. Yanagisawa,[*1] H. Sato,[*1] K. Yoshida,[*1] and T. Uesaka[*1]

Radioactive isotope (RI) beam production at the BigRIPS fragment separator[1] in 2021 is presented here. Table 1 summarizes the experimental programs that involved the use of the BigRIPS separator in this period and the RI beams produced for each experiment.

In the spring beamtime, the ^{238}U beam campaign was conducted in the first half, followed by the light-ion beam campaign in the second half.

The ^{238}U beam campaign started in April. A ^{80}Zn beam was produced for a HiCARI experiment using ZeroDegree spectrometer to study γ-ray spectroscopy in the vicinity of double-magic ^{78}Ni. During this experiment, mass measurements with a multi-reflection time-of-flight mass spectrometer (MRTOF-MS) located downstream of ZeroDegree spectrometer were performed symbiotically. ^{74}Ni, ^{75}Ni, and ^{76}Ni beams were produced for mass measurements using the Rare RI Ring. Two BRIKEN experiments were then conducted. A ^{156}La beam was produced to measure masses, half-lives, and β-delayed neutron emission probabilities. An ^{202}Os beam was produced to study β-decay spectroscopy in the vicinity of the $N = 126$ closed shell. The symbiotic MRTOF-MS experiment was performed again during these BRIKEN experiments. At the end of the ^{238}U campaign, two machine studies were performed; an in-separator two-step method to produce and separate neutron-rich mid-heavy RI beams with a ^{133}Sn beam[2] and an automation tuning of the primary beamline using a machine learning technique with a ^{238}U primary beam.

The light-ion beam campaign was started in May. In the first two experiments, search for the double Gamow-Teller giant resonances (DGTGR) in $\beta\beta$-decay with a ^{12}C primary beam and high precision spectroscopy of pionic atoms with a ^{2}H primary beam, the BigRIPS F0-F5 section was used as a spectrometer in the dispersion matched operation to analyze the momentum of ejected particles produced at the F0 target. ^{8}Li, ^{9}Li, ^{10}Be, ^{12}B, and ^{3}He beams produced with the ^{12}C primary beam were used for the ion-optical tuning and detector setup for these experiments. The DGTGR experiment was performed with ^{12}B and ^{12}Be settings. After switching to the ^{2}H primary beam, the pionic atom experiment was performed with the ^{3}He setting.

Table 1. List of experimental programs with RI beams produced at the BigRIPS separator in 2021.

Primary beam (Period)	Proposal No.	Spokesperson	Course	RI beams
^{238}U 345 MeV/nucleon (Apr. 8 – May 5)	NP1912-RIBF181-02	R. Taniuchi	ZeroDegree	^{80}Zn
	PE21-01	M. Wada	ZeroDegree	(symbiotic)
	NP1612-RIRING02-02	A. Ozawa	Rare RI Ring	^{74}Ni, ^{75}Ni, ^{76}Ni
	NP1612-RIBF148-07	G. Kiss	ZeroDegree	^{156}La
	NP1712-RIBF158-02	J. Wu	ZeroDegree	^{202}Os
	PE21-02	M. Wada	ZeroDegree	(symbiotic)
	MS-EXP21-01	H. Suzuki	ZeroDegree	^{133}Sn
	MS-EXP21-03	T. Nishi	BigRIPS	(primary)
^{12}C 250 MeV/nucleon (May 20 – May 29)	NP1712-RIBF141R1-01	T. Uesaka	ZeroDegree	^{8}Li, ^{9}Li, ^{10}Be, ^{12}Be, ^{12}B
	NP1912-RIBF135R1-01	K. Itahashi	BigRIPS	^{3}He
^{2}H 250 MeV/nucleon (May 31 – Jun. 9)	NP1912-RIBF135R1-02	K. Itahashi	BigRIPS	^{3}He
^{4}He 200 MeV/nucleon (Jun. 12 – Jun. 21)	NP1712-SHARAQ11-01	K. Miki	SHARAQ	^{3}H
	MS-EXP21-06	S. Michimasa	SHARAQ	^{3}H
	MS-EXP21-07	K. Yoshida	BigRIPS	^{3}H
^{238}U 345 MeV/nucleon (Nov. 20 – Dec. 3)	DA21-04-02	H. Otsu	ZeroDegree	(BigRIPS tuning only)
	NP2012-RIBF199-01	M. Wada	ZeroDegree	^{203}Re
	NP2012-RIBF202-01	M. Rosenbusch	ZeroDegree	^{79}Ni
	INSPECTION21-03	K. Tanaka	BigRIPS	^{75}Zn
	NP1712-RIBF166-05	T. Sonoda	PALIS	^{191}Bi
	NP1712-RIRING01R1-02	S. Naimi	Rare RI Ring	^{124}Pd, ^{125}Pd
	NP2012-RIBF202-02	M. Rosenbusch	ZeroDegree	^{79}Ni

[*1] RIKEN Nishina Center

After switching to a ^{4}He primary beam, a search for three-neutron resonant states was performed with a ^{3}H beam. A machine study for the development of a dispersion matched beam transport of the OEDO beamline was conducted using another ^{3}H beam setting. At the end of the light-ion beam campaign, a machine study was conducted with the two ^{3}H beams and the ^{4}He primary beam to investigate the vertical (Y) axis misalignment.[3)]

In the autumn beamtime, the ^{238}U campaign was conducted again from November. During the BigRIPS tuning, the performance of a newly developed ionization chamber specialized in high-Z beams installed at F7 was examined with the ^{238}U primary beam.[4)] The productions of an ^{237}Np beam and a reduced-energy uranium beam were also tested. Two MRTOF-MS experiments were then performed in ^{203}Re and ^{79}Ni centered beam settings, respectively. A facility inspection was conducted using a ^{75}Zn beam. A PALIS experiment was then performed with a ^{191}Bi beam, and a Rare RI Ring experiment was conducted with ^{124}Pd and ^{125}Pd beams. The auto-focusing and auto-centering systems were tested[5)] in the BigRIPS tuning for the next MRTOF-MS experiment. During the MRTOF-MS experiment with the ^{79}Ni beam, a serious problem occurred on the refrigerator of the BigRIPS separator making it inoperable. The remainder of the scheduled experiments were therefore canceled.

RI beam production at BigRIPS from the start of operation in March 2007 is summarized in our database[6)] available at `https://ribeam.riken.jp/`.

References

1) T. Kubo, Nucl. Instrum. Methods Phys. Res. B **204**, 97 (2003).
2) H. Suzuki *et al.*, in this report.
3) K. Yoshida *et al.*, in this report.
4) M. Yoshimoto *et al.*, in this report.
5) Y. Shimizu *et al.*, in this report.
6) Y. Shimizu *et al.*, Nucl. Instrum. Methods Phys. Res. B **463**, 158 (2020).

Status of the mass measurement of neutron-rich nuclei at $A \sim 50$–60 using SLOWRI/ZD-MRTOF

S. Iimura,[*1,*2,*3] M. Rosenbusch,[*3] A. Takamine,[*1] D. Hou,[*4,*3,*5] M. Wada,[*3] S. Chen,[*3,*6] J. Liu,[*4] W. Xian,[*3,*6] S. Yan,[*7,*3] P. Schury,[*3] S. Kimura,[*1] T. Niwase,[*8,*1,*3] Y. Ito,[*9] T. Sonoda,[*1] T. M. Kojima,[*1] Y. X. Watanabe,[*3] S. Naimi,[*1] S. Michimasa,[*10] S. Nishimura,[*1] A. Odahara,[*2] and H. Ishiyama[*1]

An RF carpet-type helium gas cell combined with an MRTOF mass spectrograph, the ZD-MRTOF, has been installed downstream of the ZeroDegree spectrometer at the RIBF and is under operation as a collaboration between the RNC and KEK/WNSC. Mass measurement using the ZD-MRTOF can be performed parasitically during other experiments at BigRIPS. During experiments for gamma-ray spectroscopy (HiCARI campaign), the first online commissioning of the system and mass measurements of neutron-rich nuclei were performed symbiotically using the ZD-MRTOF system.[1,2] The detailed experimental information including the experimental setup is available in other papers.[3–6] Overall, masses of more than 70 isotopes have been measured successfully. We have completed the analysis and determination of masses of the measured isotopes.

Figure 1 shows an example of a measured TOF spectrum for isobars with $A = 56$. The ZD-MRTOF yielded a mass resolving power of approximately 500,000 during the online commissioning, resulting in high precision mass determinations.

At approximately $A = 50$–60, the masses of 15 radioactive neutron-rich nuclei have been determined. Figure 2 shows the measured nuclei indicated with colored circles on a nuclear chart.

For nuclei enclosed with green circles, the uncertainties of masses determined with the MRTOF are less than

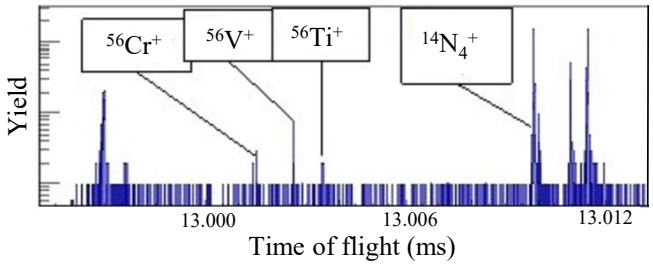

Fig. 1. Example of measured TOF spectrum on isobars with $A = 56$.

*1 RIKEN Nishina Center
*2 Department of Physics, Osaka University
*3 Wako Nuclear Science Center (WNSC), IPNS, KEK
*4 Institute of Modern Physics, Chinese Academy of Sciences
*5 School of Nuclear Science and Technology, Lanzhou University
*6 Department of Physics, University of Hong Kong
*7 Institute of Mass Spectrometer and Atmospheric Environment, Jinan University
*8 Department of Physics, Kyushu University
*9 Advances Science Research Center, Japan Atomic Energy Agency
*10 Center for Nuclear Study, University of Tokyo

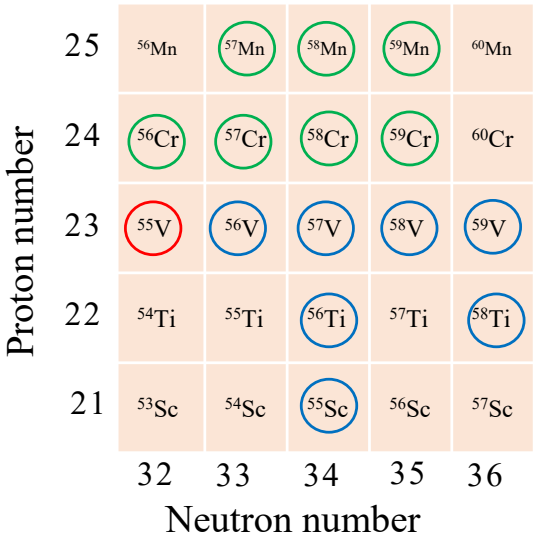

Fig. 2. Nuclei at approximately $A = 50$–60, for which the masses were measured using the ZD-MRTOF (circles with colors: see text).

30 keV but larger than the uncertainties of AME2020. These determined masses are well consistent with the values on AME2020 within their uncertainties. For ^{55}V, indicated with a red circle, the uncertainty is approximately 90 keV owing to the low statistics. For nuclei enclosed with blue circles, the uncertainties are less than 30 keV and are smaller than the uncertainties of AME2020. It is interesting to note that the values of masses of ^{58,59}V and ^{58}Ti determined using the ZD-MRTOF deviate from ones of AME2020 by 100 keV or more. As a result, the uncertainties of the masses on seven nuclei can be improved significantly.

These updated mass values enable us to discuss the magicites for $N = 32$ and 34 of Sc, Ti, and V isotopes, using two neutron separation energies, empirical shell gaps, and other finite difference of binding energies. A detailed discussion is in progress.

References

1) M. Rosenbush *et al.*, RIKEN Accel. Prog. Rep. **54**, S18 (2021).
2) S. Iimura *et al.*, RIKEN Accel. Prog. Rep. **54**, 98 (2021).
3) M. Rosnebucsh *et al.*, Nucl. Instrum. Methods Phys. Res. B **463**, 184 (2020).
4) W. Xian *et al.*, RIKEN Accel. Prog. Rep. **54**, 94 (2021).
5) D. Hou *et al.*, RIKEN Accel. Prog. Rep. **54**, 96 (2021).
6) S. Chen *et al.*, RIKEN Accel. Prog. Rep. **54**, 97 (2021).

Highly precise mass measurements of neutron-rich nuclei at A = 82–92 at ZeroDegree-MRTOF(ZD-MRTOF)

W. Xian,[*1,*2] M. Rosenbusch,[*2] S. Chen,[*1,*2] D. Hou,[*3,*2] S. Iimura,[*5,*4] H. Ishiyama,[*4] Y. Ito,[*6] S. Kimura,[*4] T. M. Kojima,[*4] J. Liu,[*3] J. Lee,[*1] H. Miyatake,[*2] S. Michimasa,[*10] S. Nishimura,[*4] T. Niwase,[*7,*4,*2] S. Naimi,[*4] P. Schury,[*2] T. Sonoda,[*4] A. Takamine,[*4] M. Wada,[*2] Y. X. Watanabe,[*2] H. Wollnik,[*8] and S. Yan[*9]

A state-of-art multi-reflection time-of-flight (TOF) mass spectrograph (MRTOF-MS) coupling to a cryogenic helium filled gas catcher (gas cell) was developed and prepared for on-line tests prior to the launch of the HiCARI campaign 2020[1] for γ-ray spectroscopy. For the first time, the ZD-MRTOF system was operated on-line running as parasitic experiment downstream of the ZeroDegree (ZD) spectrometer. Produced by in-flight fission of ^{238}U primary beam with ^{9}Be target, radioactive ions were selected, identified, and guided by BigRIPS to the focal plane F8, where the exotic ions reacted with a secondary target for in-beam γ-ray research. Reaction products were then analyzed using the ZD spectrometer before they were finally entrapped by the gas cell and measured by the MRTOF-MS.

Abundant stable molecules contribute to strong peaks with long tails in a TOF spectrum, which causes difficulties identifying the much weaker peaks of the ions of interest. Benefiting from the introduction of a new mass filter method,[2] we obtained low-contaminant-background with high resolution isobaric TOF spectrums, as shown in Fig. 1. In this spectrum, in addition to isobaric ions from the on-line beam, stable molecules from background contaminations in the gas were also observed in the same measurement as several species can

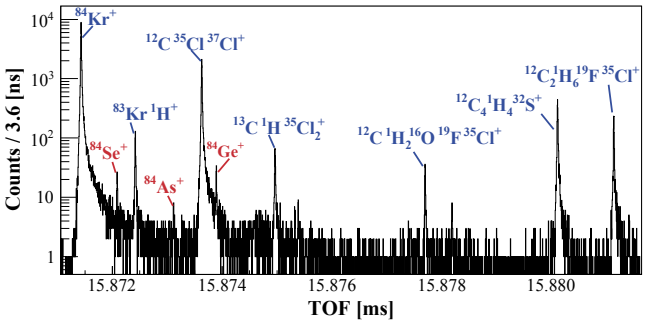

Fig. 1. TOF spectrum at A = 84 with radioactive ions (red) and stable molecules (blue).

*1 University of Hong Kong
*2 Wako Nuclear Science Center (WNSC), IPNS, KEK
*3 Institute of Modern Physics, Chinese Academy of Sciences
*4 RIKEN Nishina Center
*5 Osaka University
*6 Advanced Science Research Center, Japan Atomic Energy Agency
*7 Department of Physics, Kyushu University
*8 Department of Chemistry and Biochemistry, New Mexico State University
*9 Jinan University
*10 University of Tokyo

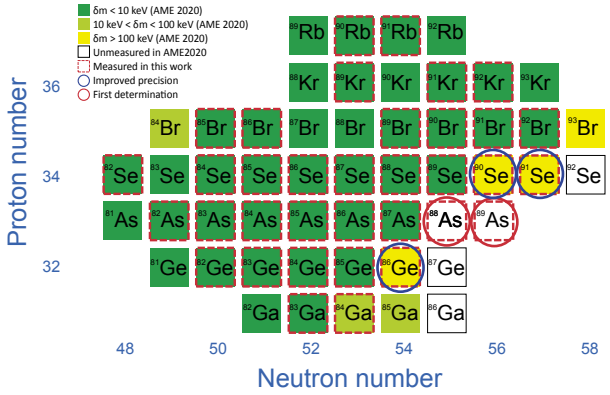

Fig. 2. Meassured isotopes (A = 82–92) in on-line tests.

be measured simultaneously. Stable molecules provided isobaric references for extracting masses of ion of interest. On the other hand, the stable molecules also served as benchmarks for the evaluation of the systematic uncertainties.

In total, the HiCARI campaign 2020 had five separate experiments, covering four different regions. The results introduced in this report were from the data acquired during NP1912-RIBF196 and NP1912-RIBF190. Among other mass regions, abundant species of isotopes have been observed in the mass range A = 82–92. In total, 35 nuclides were measured in a neutron-rich region of Ga, Ge, As, Se, Br, Kr, and Rb in which ^{84}Ga, ^{86}Ge, ^{89}As, ^{91}Se, and ^{92}Br are the most exotic isotopes (see Fig. 2). Among those isotopes, mass uncertainties of ^{86}Ge, ^{90}Se, and ^{91}Se, could be reduced significantly to less than 5 keV. Moreover, for the first time, the masses of ^{88,89}As were unveiled. In addition to radioactive ions, at least one stable atomic or molecular ion was found for each mass number, *e.g.*, ^{82}Kr^{1}H$^+$, ^{83}Kr^{1}H$^+$, ^{12}C^{37}Cl$_2^+$, *etc.* The mass deviations of these ions from AME2020 enable an evaluation of system accuracy of the new ZD-MRTOF system. The weighted mean deviation of the measured masses from the precisely known values was found to be approximately only 2 keV, which proves a very high accuracy for future measurements.

References

1) M. Rosenbusch *et al.*, RIKEN Accel. Prog. Rep. **54**, S18 (2021).
2) S. X. Yan *et al.*, RIKEN Accel. Prog. Rep. **54**, S28 (2021).

Mass measurements of neutron-rich nuclei around $A = 112$ with ZD-MRTOF-MS system

D. Hou,[*1,*2] A. Takamine,[*4] S. Iimura,[*4,*5] S. Chen,[*2,*6] Y. Hirayama,[*2] H. Ishiyama,[*4] Y. Ito,[*7] S. Kimura,[*4] T. M. Kojima,[*4] J. Liu,[*1] H. Miyatake,[*2] S. Michimasa,[*8] T. Niwase,[*4,*2] S. Nishimura,[*4] S. Naimi,[*4] M. Rosenbusch,[*2] P. Schury,[*2] T. Sonoda,[*4] M. Wada,[*2] Y. X. Watanabe,[*2] H. Wollnik,[*9] W. Xian,[*2,*6] and S. Yan[*2,*9]

The ZeroDegree-MRTOF (ZD-MRTOF) system combined with a gas catcher cell with radio-frequency ion guide method has been developed at the downstream of ZeroDegree spectrometer in RIKEN Nishina Center.[1] An online test for this system was performed with fission reactions symbiotically with the in-beam γ-ray spectroscopy experiments[2] at the end of 2020. The reaction products after the second target at the focal plane F8 were selected and guided by the ZeroDegree spectrometer, then they were captured by the gas cell and transported to the MRTOF for precise mass measurement. We measured more than 70 masses in total, and in this work, we concentrated on the masses in the range of neutron-rich isotopes $A = 111$–113.

In Fig. 1, an example of the TOF spectra obtained from the experiments is shown. In the spectra, it can be seen that the beam's ions and their β-decay products were observed. To fit the peaks in the spectra, a Gaussian function coupled with two exponential tails[3] was employed during the data analysis process. The definition of the fitting function is shown in Eq. (1),

$$f(t) = A \cdot \begin{cases} \exp\left(\frac{\Delta_L(2t-2t_c+\Delta_L)}{2\sigma^2}\right) & t \le t_L \\ \exp\left(\frac{-(t-t_c)^2}{2\sigma^2}\right) & t_L < t < t_R \\ \exp\left(\frac{\Delta_R(-2t+2t_c+\Delta_R)}{2\sigma^2}\right) & t \ge t_R \end{cases} \quad (1)$$

where A and t_c are the amplitude and maximum position of this function, σ is the width of the central Gaussian part, t_L ($t_L = t_c - \Delta_L$) and t_R ($t_R = t_c + \Delta_R$) are the transition points of the left and right side of the Gaussian function, where the Gaussian function smoothly changes to an exponential function. The function value and its first derivative are continuous at the transition points. Compared to Gaussian and exponential-Gaussian hybrid functions, the accuracy of fitting results can be significantly improved[4] using the function described in Eq. (1). We can calculate the ion mass accurately after measuring the ions' exact time-of-flight.

*1 Institute of Modern Physics, Chinese Academy of Sciences
*2 Wako Nuclear Science Center (WNSC), IPNS, KEK
*3 RIKEN Nishina Center
*4 Department of Physics, Osaka University
*5 Department of Physics, University of Hongkong
*6 Advanced Science Research Center, Japan Atomic Energy Agency
*7 Center for Nuclear Study, University of Tokyo
*8 Department of Chemistry and Biochemistry, New Mexico State University
*9 Institute of Mass Spectrometry and Atmospheric Environment, Jinan University

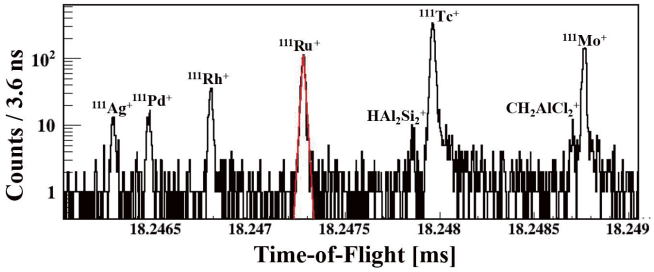

Fig. 1. An example of TOF spectrum at $A = 111$ with radioactive ions and stable molecules. The red line indicates the fit function defined in Eq. (1).

In this work, we measured 15 masses of radioactive neutron-rich nuclei ^{111,113}Ag, ^{111,113}Rh, $^{111-113}$Pd, $^{111-113}$Ru, and ^{111,112}Mo (see in Fig. 2). Compared with the mass values listed in AME2020, an excellent agreement between our results and previously reported values has been observed. The mass measurement of ^{113}Ru was improved, and the ^{112}Mo mass was measured for the first time. Based on our results, we investigated the double neutron separation energy (S_{2n}) and empirical neutrons shell gap (δ_{2n}), and the results will be presented in a future publication.

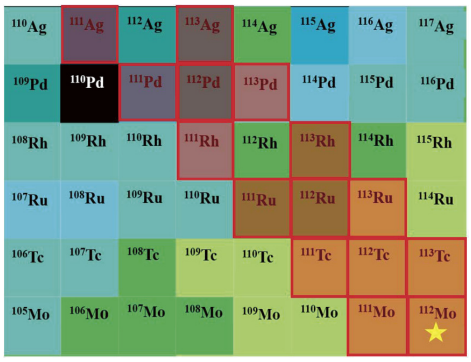

Fig. 2. Nuclei chart $A \sim 110$, nuclei measured with ZD-MRTOF are in red square, and the new mass is marked with a star.

References

1) M. Rosenbusch *et al.*, Nucl. Instrum. Methods Phys. Res. B **463**, 184 (2020).
2) M. Rosenbusch *et al.*, RIKEN Accel. Prog. Rep. **54**, S18 (2021).
3) M. Rosenbusch *et al.*, Phys. Rev. C **97**, 064306 (2018).
4) P. Schury *et al.*, Nucl. Instrum. Methods Phys. Res. B **335**, 39 (2014).

Improved mass measurement of ^{257}Db by decay-correlated mass spectroscopy

P. Schury,[*1] T. Niwase,[*1,*2,*3] M. Wada,[*1] P. Brionnet,[*2] S. Chen,[*4] T. Hashimoto,[*5] H. Haba,[*2] Y. Hirayama,[*1] D. S. Hou,[*6,*7,*8] S. Iimura,[*9,*2,*1] H. Ishiyama,[*2] S. Ishizawa,[*10,*2] Y. Ito,[*11,*2,*1] D. Kaji,[*2] S. Kimura,[*2] H. Koura,[*11] J. J. Liu,[*4,*1] H. Miyatake,[*1] J. -Y. Moon,[*5] K. Morimoto,[*2] K. Morita,[*12,*13] D. Nagae,[*13] M. Rosenbusch,[*1] A. Takamine,[*2] Y. X. Watanabe,[*1] H. Wollnik,[*14] W. Xian,[*4,*1] and S. X. Yan[*15]

We present an improved direct measurement of the atomic mass of the superheavy nuclide ^{257}Db. Atoms of ^{257}Db ($Z = 105$) were produced online at the RIKEN Nishina Center for Accelerator-Based Science using the fusion-evaporation reaction ^{208}Pb(^{51}V, $2n$)^{257}Db. The gas-filled recoil ion separator GARIS-II was used to suppress both the unreacted primary beam and some transfer products, prior to delivering the energetic beam of ^{257}Db ions to a helium gas-filled ion stopping cell wherein they were thermalized. Thermalized ^{257}Db^{2+} ions were then transferred to a multi-reflection time-of-flight mass spectrograph (MRTOF) for mass analysis. An alpha particle detector embedded in the ion time-of-flight detector allowed disambiguation of the rare ^{257}Db^{2+} time-of-flight detection events from background by means of correlation with characteristic α-decays. The extreme sensitivity of this technique,[1] allowed a precision atomic mass determination from 22 decay-correlated events.

In our previous measurement of this nuclide,[2] metallic Pb targets were utilized, limiting the permissible primary beam intensity to below 500 particle nA. In this measurement we tested PbS targets produced via sputtering. The targets were capable of withstanding 2 particle μA primary beam without degradation in their performance. This allowed for twice as many events in half as much time as the previous measurement, while the MRTOF's mass resolving power was significantly improved. Additionally, the implementation of a pulsed deflector,[3] inside the MRTOF allowed selective rejection of transfer products such as ^{211}Po which had previously produced some spurious decay correlations.

Using the same correlation method as previously employed,[2] a mass was determined for the detected ion in each decay-correlated event. A histogram of the masses is shown in Fig. 1. A Gaussian fit to the histogram data, shown in violet, indicates that a mass resolving power of $m/\Delta m = 800\,000$ was achieved; the flight time was $t \approx 17$ ms. The shape of the distribution indicates that either only a single state was present or the isomeric excitation energy is below 300 keV. The centroid of the histogram indicates a mass excess of 100 408(75) keV/c^2 for the possible mixed ensemble of states. Regardless, however, the measured mass is not in agreement with the Atomic Mass Evaluation.[4]

Within the new set of data, only 8 decay-correlated events were determined to have had observed α-decays from ^{257}Db—the others having observed decays of ^{253}Lr or ^{249}Md. A further followup effort to gather more data and better determine the state ordering via decay-correlated mass analysis is planned for FY2022.

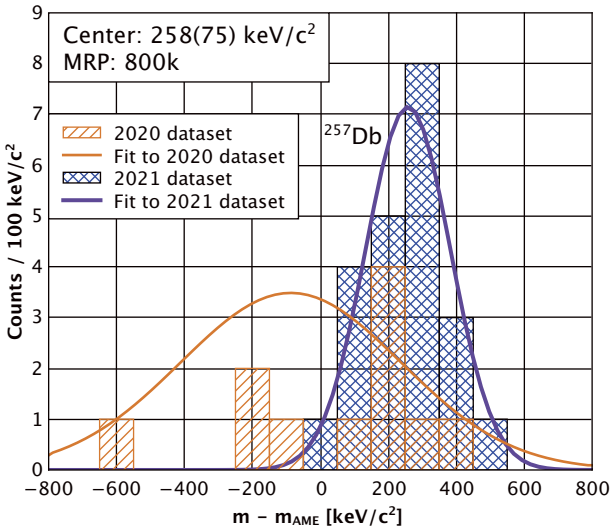

Fig. 1. Histograms of evaluated atomic masses for ions detected with subsequent α-decays consistent with ^{257}Db, ^{253}Lr, or ^{249}Md. If present, isomeric state must have excitation below 300 keV. In the legend, "MRP" refers to mass resolving power.

*1 Wako Nuclear Science Center (WNSC), IPNS, KEK
*2 RIKEN Nishina Center
*3 Department of Physics, Kyushu University
*4 Department of Physics, University of Hong Kong
*5 Institute for Basic Science
*6 Institute of Modern Physics, Chinese Academy of Sciences
*7 University of Chinese Academy of Sciences
*8 School of Nuclear Science and Technology, Lanzhou University
*9 Department of Physics, Osaka University
*10 Graduate School of Science and Engineering, Yamagata University
*11 Advanced Science Research Center, Japan Atomic Energy Agency
*12 Department of Physics, Kyushu University
*13 Research Center for SuperHeavy Elements, Kyushu University
*14 New Mexico State University
*15 Institute of Mass Spectrometer and Atmospheric Environment, Jinan University

References
1) T. Niwase *et al.*, Nucl. Instrum. Methods Phys. Res. A, **953**, 163198 (2020).
2) P. Schury *et al.*, Phys. Rev. C **104**, L021304 (2021).
3) M. Rosenbusch *et al.*, submitted to Nucl. Instrum. Methods Phys. Res. A.
4) M. Wang *et al.*, Chinese Phys. C **41**, 030003 (2017).

Initial mass measurement of ^{258}Db by decay-correlated mass spectroscopy

P. Schury,[*1] T. Niwase,[*1,*2,*3] M. Wada,[*1] P. Brionnet,[*2] S. Chen,[*4] T. Hashimoto,[*5] H. Haba,[*2] Y. Hirayama,[*1] D. S. Hou,[*6,*7,*8] S. Iimura,[*9,*2,*1] H. Ishiyama,[*2] S. Ishizawa,[*10,*2] Y. Ito,[*11,*2,*1] D. Kaji,[*2] S. Kimura,[*2] H. Koura,[*11] J. J. Liu,[*4,*1] H. Miyatake,[*1] J. -Y. Moon,[*5] K. Morimoto,[*2] K. Morita,[*12,*13] D. Nagae,[*13] M. Rosenbusch,[*1] A. Takamine,[*2] Y. X. Watanabe,[*1] H. Wollnik,[*14] W. Xian,[*4,*1] and S. X. Yan[*15]

We present the first direct measurement of the atomic mass of the superheavy nuclide ^{258}Db. Atoms of ^{257}Db ($Z = 105$) were produced online at the RIKEN Nishina Center for Accelerator-Based Science using the fusion-evaporation reaction ^{208}Pb(^{51}V, $1n$)^{258}Db. The gas-filled recoil ion separator GARIS-II was used to suppress both the unreacted primary beam and some transfer products, prior to delivering the energetic beam of ^{258}Db ions to a helium gas-filled ion stopping cell wherein they were thermalized. Thermalized ^{258}Db^{2+} ions were then transferred to a multi-reflection time-of-flight mass spectrograph (MRTOF) for mass analysis. An alpha particle detector embedded in the ion time-of-flight detector allowed disambiguation of the rare ^{258}Db^{2+} time-of-flight detection events from background by means of correlation with characteristic α-decays. The extreme sensitivity of this technique[1] allowed a precision atomic mass determination from 22 decay-correlated events.

This measurement was made simultaneously with ^{257}Db while testing PbS targets produced via sputtering. The targets were capable of withstanding 2 particle μA primary beam without degradation in their performance. The pulsed deflector[2] inside the MRTOF was operated to allow passage of $A/q = 128.5$ and $A/q = 129$ while rejecting transfer products such as ^{211}Po that had previously produced spurious decay correlations. The observed rate of ^{258}Db relative to ^{257}Db is within expectations based on the excitation functions.[3]

Using a similar correlation method as employed for ^{257}Db,[4] extended to encompass spontaneous fission events, a mass was determined for the detected ion in each decay-correlated event. A histogram of the masses is shown in Fig. 1. Based on the mass resolving power seen for ^{257}Db^{2+},[5] there appears to be an excess of events in the low-mass tail. Applying two-peak fitting with fixed resolution results in a good reproduction of the observed distribution. Presuming this is not a statistical anomaly, it would indicate the isomeric excitation to be 300 (150) keV, a significant deviation from the α-decay derived NUBASE value[6] of 53 (14) keV.

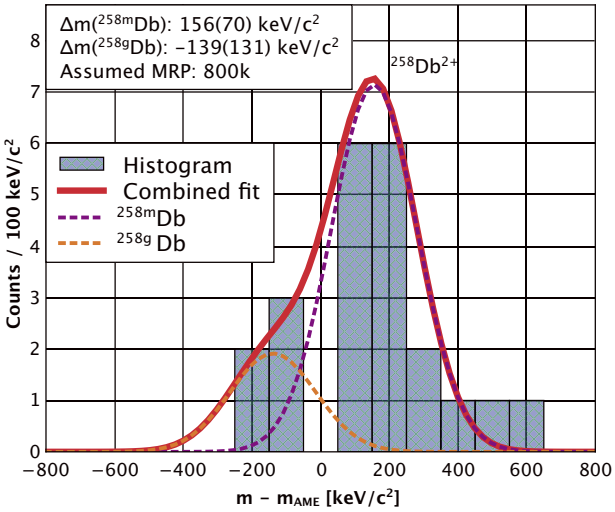

Fig. 1. Histograms of evaluated atomic masses for ions detected with subsequent α-decays consistent with ^{258}Db, ^{254}Lr, or ^{250}Md, ^{258}Rf, and spontaneous fission. The two-peak structure could indicate the isomeric excitation exceeds NUBASE estimates.[6]

A further followup effort to gather more data in order to better determine the isomeric excitation is planned for FY2022. However, due to the small differences between α-particle energies emitted from the two states, determination of the state ordering via precision decay-correlated mass spectroscopy will require a considerably improved detector station. Such a detector station is presently in the initial design phase.

*1 Wako Nuclear Science Center (WNSC), IPNS, KEK
*2 RIKEN Nishina Center
*3 Department of Physics, Kyushu University
*4 Department of Physics, University of Hong Kong
*5 Institute for Basic Science
*6 Institute of Modern Physics, Chinese Academy of Sciences
*7 University of Chinese Academy of Sciences
*8 School of Nuclear Science and Technology, Lanzhou University
*9 Department of Physics, Osaka University
*10 Graduate School of Science and Engineering, Yamagata University
*11 Advanced Science Research Center, Japan Atomic Energy Agency
*12 Department of Physics, Kyushu University
*13 Research Center for SuperHeavy Elements, Kyushu University
*14 New Mexico State University
*15 Institute of Mass Spectrometer and Atmospheric Environment, Jinan University

References
1) T. Niwase *et al.*, Nucl. Instrum. Methods Phys. Res. A **953**, 163198 (2020).
2) M. Rosenbusch *et al.*, submitted to Nucl. Instrum. Methods Phys. Res. A.
3) J. M. Gates *et al.*, Phys. Rev. C **78**, 034604 (2008).
4) P. Schury *et al.*, Phys. Rev. C **104**, L021304 (2021).
5) P. Schury *et al.*, in this report.
6) M. Wang *et al.*, Chin. J. Phys. C, **45** 030001 (2021).

Status of the study of masses and half-lives of ^{252}Cf fission fragments by the MRTOF-MS

S. Kimura,[*1] M. Wada,[*2] H. Haba,[*1] S. Ishizawa,[*3] T. Niwase,[*2] M. Rosenbusch,[*2] and P. Schury[*2]
for the SHE-Mass Collaboration

The nuclear data of neutron-rich nuclei, *e.g.*, mass, lifetime, and neutron-capture cross section, are important for understanding the rapid neutron-capture (r-) process, because a balance of net neutron-capture rate and β^--decay rate is crucial to determine its path. Thus, accurate and high-precision nuclear data about both neutron-rich isotopes' mass and half-life are required.[1)]

The multi-reflection time-of-flight mass spectrograph (MRTOF-MS) has been developed for not only mass measurement but also isobar separation. Here, we briefly report the present status of the mass measurement of neutron-rich isotopes and, in addition, the half-life measurement as an application of the MRTOF-MS.

The mass measurement study of the neutron-rich ^{252}Cf-fission-fragments with the MRTOF-MS[2)] was presented in the previous report.[3)] We had used the 350 kBq ^{252}Cf source and newly installed a more intense source (9.25 MBq). More than 200 isotopes have been confirmed in the time-of-flight spectra and are shown in Fig. 1. In addition, many long-lived isomers were also observed during the measurements. The mass resolving power of the MRTOF-MS reaches $R_m > 5 \times 10^5$; thus, the measurements were achieved with precision better than 10^{-7} in most of the cases.

We have developed a decay-scheme-independent half-life measurement method with the MRTOF-MS. The experimental setup consists of a cryogenic gas-cell, the MRTOF-MS, and a suite of ion traps with a quadrupole ion guide (QPIG), a linear trap, and a flat trap used as an injector for the MRTOF-MS. By changing the operation cycle of the linear trap, the ion storage time of the linear trap can be changed, making it possible to measure the lifetimes of short-lived isotopes. We briefly discuss here the lifetime measurement of ^{92}Br as an example of this "storage method." Figure 2 shows the storage time dependence of the yields of ^{92}Br$^+$ ions normalized by the ^{92}Rb$^+$ ion yields for canceling out the efficiency reduction due to increasing of the storage time. A decreasing trend of ^{92}Br$^+$ ion yields is clearly observed and the ^{92}Br$^+$'s half-life is measured to be 349(178) ms through a fit with the theoretical curve. This value is in agreement with the value in the literature of 314(16) ms. In this analysis, we assumed that an influence of the decay loss of the ^{92}Rb$^+$ ion is negligibly small because its half-life (4.48 s) is sufficiently long compared to the storage time.

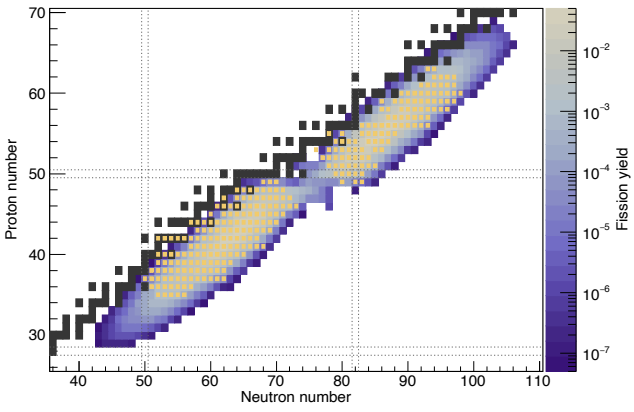

Fig. 1. Location of the observed isotopes on the nuclear chart. The observed isotopes are indicated with orange-colored squares. The black squares represent the stable isotopes. The contour map shows the fission yield of ^{252}Cf.[4)]

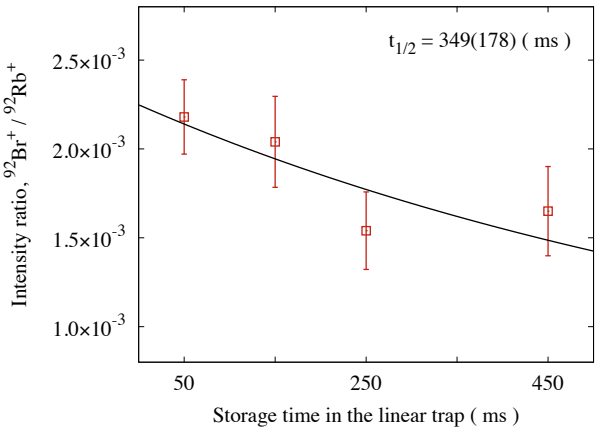

Fig. 2. Intensity ratio of ^{92}Br$^+$/^{92}Rb$^+$ as a function of storage time in the linear trap. A black line shows a fit result. The measured half-life, 349(178) ms, is consistent with the value in the literature of 314(16) ms.

*1 RIKEN Nishina Center
*2 Wako Nuclear Science Center (WNSC), IPNS, KEK
*3 Institute for Materials Research, Tohoku University

References

1) M. R. Mumpower *et al.*, Prog. Part. Nucl. Phys. **86**, 86 (2016).
2) P. Schury *et al.*, Nucl. Instrum. Methods Phys. Res. B **335**, 39 (2014).
3) S. Kimura *et al.*, RIKEN Accel. Prog. Rep. **53**, 52 (2019).
4) J. Katakura, JAEA-Data/Code 2011-025.

First measurement of double Gamow-Teller giant resonance at RIBF

A. Sakaue*[1] for the RIBF-141R1 Collaboration

The double Gamow-Teller (DGT) transition is a nuclear process characterized by a $(\sigma\tau)^2$ operator in which both the spin and isospin change twice. Experimental information about the DGT transition is currently limited to data of double β decays, whose transition strength accounts for only a small proportion of the entire transition strength of the DGT transition. The remainder of the strength is expected to form a giant resonance in a high-excitation energy region. This resonance, called the DGT giant resonance (DGTGR), was proposed in 1989[1)] and is still undiscovered experimentally. The aim of this research was to observe the evidence of the DGTGR for the first time, thereby extending the study on two-phonon excitations to a regime in which the spin-degrees of freedom contribute. Although knowledge of the anharmonicity of the nuclear response in such a domain is scarce, observables of the DGTGR, such as the centroid energy or the width, might provide its information.

Experimental information of the DGTGR is also potentially important for determining the nature of neutrinos. The transition strength and centroid energy of the DGTGR are suggested to be strongly correlated with the nuclear matrix element of a neutrinoless double β decay.[2)] Theoretically predicted values of the nuclear matrix element have a large uncertainty depending on the chosen model.[3)] Experimental information of the DGTGR will provide reference for the calculation of the nuclear matrix element.

In this study, the DGTGR was observed by missing mass spectroscopy using a double-charge exchange reaction (^{12}C, ^{12}Be(0_2^+)). We utilized an isomeric decay of ^{12}Be(0_2^+), for event selection. ^{12}Be(0_2^+) has a lifetime of 331 $\pm$ 12 ns and decays into the ground state by emitting an electron-positron pair.[4)] Detecting back-to-back photons with an individual energy of 511 keV from the positron served to tag the events of the double spin-flip mode.

In May 2021, we performed the first measurement of the (^{12}C, ^{12}Be(0_2^+)) reaction at the RI Beam Factory (RIBF). A ^{12}C primary beam with an intensity of 500 particle nA was accelerated to 250 MeV/nucleon and impinged on a target at F0 focal plane of the BigRIPS separator. We used ^{48}Ca or ^{116}Cd as the target, which are important double β decaying nuclei. The thickness of the target was 10 mg/cm^2 for ^{48}Ca and 50 mg/cm^2 for ^{116}Cd. The ^{48}Ca target was sandwiched between 4-micrometer-thick graphene sheets for preventing oxidation and nitridization when installing in the F0 vacuum chamber. Momentum spread of the primary beam was suppressed by dispersion-matching optics. The momentum of the ejected particle was measured by using F0-F5 as a spectrometer, as established in pionic atoms experiments.[5)] After passing through the tracking detectors of low-pressure multiwire drift chambers (MWDCs) at F5 focal plane, a particle was transferred to F8 focal plane and stopped in a ^{9}Be stopper with a thickness of 18.8 mm.

Delayed γ rays were detected by a DALI2 array at F8. During the beam time, we measured the double-charge exchange reaction for 40 hours for ^{48}Ca and 20 hours for ^{116}Cd, respectively. The left panel of Fig. 1 shows the energy spectrum of the photons measured by DALI2 for the ^{48}Ca target. A peak at the energy of 511 keV is noticeable in the spectrum. The right panel of Fig. 1 shows the timing of the photon detection relative to the signal from a plastic scintillator at F7. Here, the timing distribution of the events in the energy region of 500 $\pm$ 100 keV is also shown. The decay histogram is fitted by an exponential curve and a constant background. The decay constant is 302.3 $\pm$ 8.2 ns, which is close to the known value of the lifetime of ^{12}Be(0_2^+). This suggests that ^{12}Be(0_2^+) is successfully detected.

The analysis is ongoing. The excitation energy spectrum of ^{48}Ti will be obtained from the position measured by the MWDCs at F5. Currently, we are analyzing the MWDCs at F5.

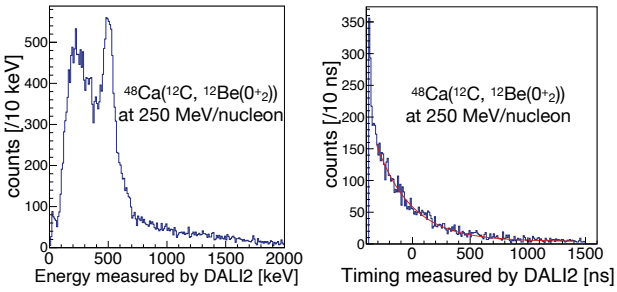

Fig. 1. (Left) Energy distribution of delayed γ rays measured by DALI2. (Right) Timing distribution of delayed γ rays for events in energy region of 500 $\pm$ 100 keV. Red curve is fitting result.

References
1) N. Auerbach, L. Zamick, D. Zheng, Ann. Phys. (Leipzig) **192**, 77 (1989).
2) N. Shimizu *et al.*, Phys. Rev. Lett. **120**, 142502 (2018).
3) J. Engel, J. Menéndez, Rep. Prog. Phys. **80**, 046301 (2017).
4) S. Shimoura *et al.*, Phys. Lett. B **654**, 87 (2007).
5) T. Nishi *et al.*, Nucl. Instrum. Methods Phys. Res. B **317**, 290 (2013).

*1 Center for Nuclear Study, University of Tokyo

Spectroscopy of pionic atoms in tin isotopes by (d, ^{3}He) reactions

S. Y. Matsumoto,[*1] H. Asano,[*2] H. Baba,[*2] G. P. A. Berg,[*3] M. Dozono,[*1,*2] H. Fujioka,[*2,*4] N. Fukuda,[*2] N. Fukunishi,[*2] H. Geissel,[*5] S. Hanai,[*6] T. Harada,[*2,*7] T. Hashimoto,[*8] S. Hayakawa,[*5] K. Higuchi,[*4] Y. Hijikata,[*1,*2] K. Horikawa,[*4] N. Inabe,[*2] K. Itahashi,[*2] K. Kusaka,[*2] Y. Ma,[*2] R. Matsumura,[*9,*2] S. Michimasa,[*6] N. Nakatsuka,[*4,*2] T. Nishi,[*2] S. Ota,[*10] A. Sakaue,[*6] F. Sakuma,[*2] M. Sasano,[*2] R. Sekiya,[*1,*2] Y. Shimizu,[*2] T. Sumikama,[*2] D. Suzuki,[*2] H. Suzuki,[*2] H. Takeda,[*2] Y. K. Tanaka,[*2] J. Tanaka,[*2] R. Tsuji,[*1,*2] T. Uesaka,[*2] K. Yako,[*6] Y. Yanagisawa,[*2] H. Weick,[*5] K. Yoshida,[*2] M. Yoshimoto,[*2] and J. Zenihiro[*1,*2]

We performed systematic spectroscopy measurements of pionic tin isotopes by (d, ^{3}He) reactions. We measured the masses of the reaction products, *i.e.*, pionic atoms, by missing mass spectroscopy. The incident deuteron beam energy was chosen as 500 MeV to enhance the formation cross-sections of the pionic atoms. We installed $A = 112, 115, 117, 119, 122$, and 124 tin isotopes at F0.

^{3}He emitted by an energy of ∼360 MeV was momentum-analyzed by using the BigRIPS. We installed two low-pressure multi-wire drift chambers[1] (MWDCs) at F5, and measured ^{3}He tracks. The MWDCs were operated with 30 kPa isobutane and had sufficient efficiency. We installed plastic scintillators at F5 and F7 for time-of-flight measurements. Combining the time-of-flight information with the measured energy loss at each scintillator, ^{3}He particles were identified.

One of the largest sources of resolution is the momentum spread of the primary beam, which was determined as $\delta p/p = 0.03\%$ (σ). We constructed dispersion matching optics by analyzing the beam momentum at F0 to have a dispersion of 44.6 mm/%. We developed a novel method of tuning the optical condition, called "trace-back method."[2] In this method, the particle tracks at F3 and F5 are measured and the matrix elements in F0-F3-F5 are evaluated. Finally the trajectories are traced back to F0, and the phase distributions are deduced.

Figure 1 shows the position spectra of $p(d, ^3\mathrm{He})\pi^0$ reactions at F5 using a CH_2 target. The spectra were measured by placing the target at horizontal positions −3, 0, and +6 mm from the beam center. The beam spot size was enlarged to approximately 15 mm (σ) for the very large dispersion of 44.6 mm/% at the target. Without the dispersion matching conditions, the displacement of 3.0 mm at the target position causes a 5.5-mm shift at the F5 focal plane and severe deterioration of the energy resolution. In the spectra, we observe similar position distributions for the three target positions, which suggesting a nearly perfect realization of the dispersion matching conditions.

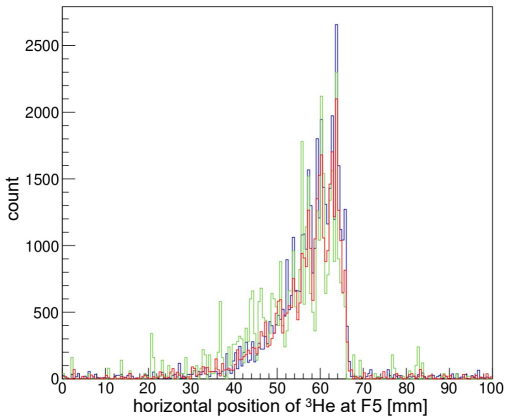

Fig. 1. Position distribution observed by $p(d, ^3\mathrm{He})\pi^0$ reactions. Blue, red and green lines represent data with CH_2 target at −3, 0, and +6 mm from beam center, respectively.

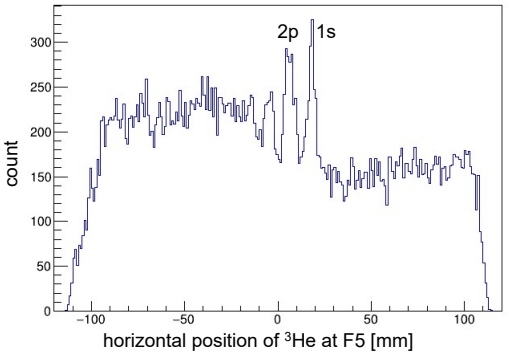

Fig. 2. Position spectrum measured using ^{124}Sn target.

Figure 2 shows a typical position spectrum observed in the production setting. We employed an ^{124}Sn target with a width of 6 mm and accumulated the data for approximately 50 min. Pionic atoms in $1s$ and $2p$ states are noticeable as peak structures.

We will continue the data analysis in terms of energy calibration, resolution improvement, and other factors.

*1 Department of Physics, Kyoto University
*2 RIKEN Nishina Center
*3 JINA and Department of Physics, University of Notre Dame
*4 Department of Physics, Tokyo Institute of Technology
*5 GSI Helmholtzzentrum für Schwerionenforschung GmbH
*6 Center for Nuclear Study, University of Tokyo
*7 Department of Physics, Toho University
*8 Japan Atomic Energy Agency
*9 Department of Physics, Saitama University
*10 Research Center for Nuclear Physics, Osaka University

References

1) S. Y. Matsumoto *et al.*, RIKEN Accel. Prog. Rep. **50**, 205 (2017).
2) A. Sakaue *et al.*, RIKEN Accel. Prog. Rep. **54**, 86 (2021).

Spectroscopy of three-neutron system via the ^{3}H$(t, ^3$He$)3n$ reaction

K. Miki,[*1,*2] K. Kameya,[*1,*2] N. Imai,[*3] S. Michimasa,[*3] S. Ota,[*3] M. Sasano,[*2] H. Takeda,[*2] T. Uesaka,[*2] Y. Hatano,[*4] M. Hara,[*4] H. Haba,[*2] T. Hayamizu,[*2] T. Chillery,[*3] M. Dozono,[*5,*2] N. Fukuda,[*2] J. Gao,[*6] S. Hanai,[*3] S. Hayakawa,[*3] Y. Hijikata,[*5,*2] K. Himi,[*7] J. Hwang,[*8] T. Kawabata,[*7,*2] K. Kishimoto,[*9,*2] S. Kitayama,[*1,*2] K. Kusaka,[*2] J. Li,[*3] Y. Maeda,[*10,*2] Y. Maruta,[*1,*2] T. Matsui,[*1,*2] H. Nishibata,[*9,*2] M. Otake,[*2] H. Sakai,[*2] A. Sakaue,[*3] H. Sato,[*2] K. Sekiguchi,[*1,*2] Y. Shimizu,[*2] S. Shimoura,[*3] L. Stuhl,[*8,*2] T. Sumikama,[*2] H. Suzuki,[*2] R. Tsuji,[*5,*2] S. Tsuji,[*7] H. Umetsu,[*1] R. Urayama,[*1,*2] Y. Utsuki,[*1,*2] T. Wakasa,[*9] K. Yako,[*3] Y. Yanagisawa,[*2] N. Yokota,[*9,*2] C. Yonemura,[*9,*2] K. Yoshida,[*2] and M. Yoshimoto[*2]

Can we find a nucleus that consists only of neutrons? This is a long-standing question in nuclear physics. If any signature of multi-neutron bound or resonant states exists, it is a challenge to the current description of nuclei. In particular, it has a significance on the understanding of high-isospin systems such as neutron stars. In a recent study,[1] a candidate of the tetra-neutron resonance was found in the ^{4}He$(^8$He$, ^8$Be$)4n$ spectrum. This peak located at $E_x = 0.83 \pm 0.65$ (stat) $\pm$ 1.25 (syst) MeV has not been understood yet with the theoretical calculations based on first principles. To investigate the simpler and more fundamental case, we focused on the three-neutron ($3n$) system and performed a ^{3}H$(t, ^3$He$)3n$ experiment at the incident energy of 170 MeV/nucleon.

The schematic layout of our experimental setup is shown in Fig. 1. The primary ^{4}He beam of 200 MeV/nucleon impinged on the ^{9}Be target with a thickness of 6 cm. Among the reaction fragments, the triton beam of 170 MeV/nucleon was selected using the BigRIPS separator with a purity higher than 99%. A high intensity of 5×10^7 particles/sec was obtained owing to the cooperation of the accelerator and radiation-safety group at the RIBF. The beam was transported to the SHARAQ target position in the achromatic ion-optics mode. The beam tuning was performed with low-pressure MWDCs and PPACs installed at each focal plane of the beamline. The scattered ^{3}He particles from the target were momentum-analyzed using the SHARAQ spectrometer and detected by the CRDCs and plastic scintillators. A pair of liquid scintillation detectors were installed around the target, which counted the decay neutrons from the $3n$ system in coincidence with the focal plane detectors.

For the target, we have newly developed a tritiated titanium (Ti-^{3}H) target and used it for the first time at RIBF. The thickness of tritium is 3.5 mg/cm^2, which is almost two orders of magnitude larger than those used in RI beam experiments in the past. This thick target enables us to find rare process such as the production of $3n$ system in this study.

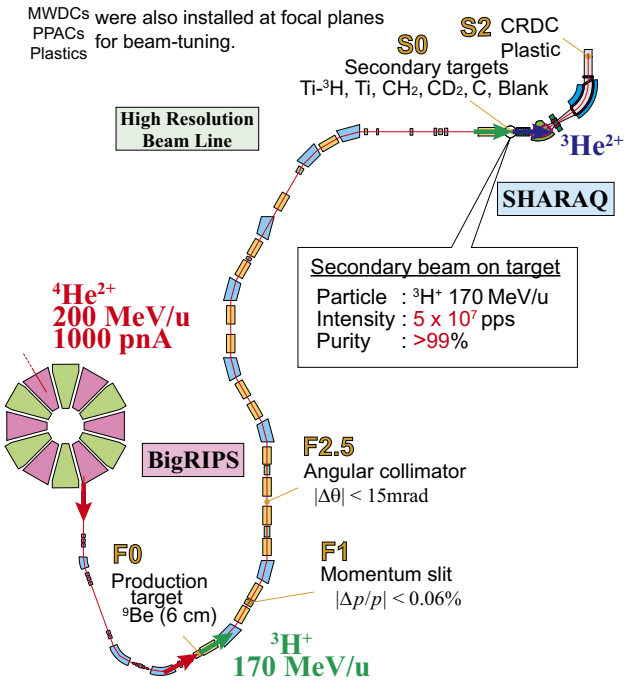

Fig. 1. Schematic layout of the experimental setup. The detector layout is similar to the previous $(t, ^3$He$)$ experiment.[2]

With this setup, the double differential cross section spectra for the ^{3}H$(t, ^3$He$)3n$ reaction were obtained for the excitation energy of $0 \leq E_x \leq 20$ MeV and the scattering angle of $0 \leq \theta \leq 4$ degrees. The ^{1}H$(t, ^3$He$)1n$ and ^{2}H$(t, ^3$He$)2n$ spectra were also obtained in the same beamtime. This aids us to argue the $1n$, $2n$, and $3n$ systems on an equal basis. Detailed analyses are in progress.

*1 Department of Physics, Tohoku University
*2 RIKEN Nishina Center
*3 Center for Nuclear Study, University of Tokyo
*4 Hydrogen Isotope Research Center, University of Toyama
*5 Department of Physics, Kyoto University
*6 School of Physics, Peking University
*7 Department of Physics, Osaka University
*8 Center for Exotic Nuclear Studies, Institute for Basic Science
*9 Department of Physics, Kyushu University
*10 Faculty of Engineering, University of Miyazaki

References

1) K. Kisamori *et al.*, Phys. Rev. Lett. **116**, 052501 (2016).
2) K. Miki *et al.*, Phys. Rev. Lett. **108**, 262503 (2012).

Re-measurement of the ^{4}He(^{8}He, ^{8}Be) reaction

S. Masuoka,[*1,*2] S. Shimoura,[*1,*2] M. Takaki,[*1] S. Ota,[*1] S. Michimasa,[*1] M. Dozono,[*1] C. Iwamoto,[*1,*2] K. Kawata,[*1,*2] N. Kitamura,[*1] M. Kobayashi,[*1] R. Nakajima,[*1] H. Tokieda,[*1] R. Yokoyama,[*1] D. S. Ahn,[*2] H. Baba,[*2] N. Fukuda,[*2] T. Harada,[*2,*3] E. Ideguchi,[*2,*4] N. Imai,[*1] N. Inabe,[*2] Y. Kondo,[*2,*5] T. Kubo,[*2] Y. Maeda,[*2,*6] F. M. Marqués,[*7] M. Matsushita,[*1] T. Nakamura,[*2,*5] N. Orr,[*7] H. Sakai,[*2] H. Sato,[*2] P. Schrock,[*1] L. Stuhl,[*1,*2] T. Sumikama,[*2] H. Suzuki,[*2] H. Takeda,[*2] K. Taniue,[*6] T. Uesaka,[*2] K. Wimmer,[*2,*8] K. Yako,[*1] Y. Yamaguchi,[*1] Y. Yanagisawa,[*2] K. Yoshida,[*2] and J. Zenihiro[*2]

In our previous study, the candidate resonance of the $4n$ system (tetra-neutron) was found using the ^{4}He(^{8}He, ^{8}Be)$4n$ reaction with a 186-MeV/nucleon ^{8}He beam.[1)] A new measurement improved in terms of data statistics and energy accuracy was performed to confirm the existence of tetra-neutron resonance.[2)]

To obtain the mass of tetra-neutrons by the missing mass method, it is necessary to determine the energy and scattering angle of the recoiling particle ^{8}Be. Because ^{8}Be is unbound, it decays into two alpha particles immediately. In this experiment, the pair of alpha particles was simultaneously detected at the final focal plane S2 of the SHARAQ spectrometer to reconstruct the invariant mass of ^{8}Be.

At S2, two cathode readout drift chambers (CRDCs) were installed. One CRDC has two segments for the horizontal direction, and it can provide the beam position in the horizontal and vertical directions. The horizontal and vertical positions are given by the induced charge distribution over the cathode pads and by the drift time of the anode wires, respectively. The horizontal position can be determined by fitting the charge distribution with the SECHS function.

$$f(x) = \frac{p_0}{\cosh^2\left(\frac{x-p_1}{p_2}\pi\right)} \tag{1}$$

To apply for two-particle tracking, the summation of Eq. (1) was used.

$$f(x) = \frac{p_0}{\cosh^2\left(\frac{x-p_1}{p_2}\pi\right)} + \frac{p_0 p_3}{\cosh^2\left(\frac{x-p_4}{p_5}\pi\right)} \tag{2}$$

Figure 1 shows an example of the fitting results. The data are well reproduced by the fitting function in red. The charge can be obtained by integrating each SECHS function in Eq. (2).

As the next analysis step, we consider the reliable identification of two tracks by a ^{8}Be particle. Some events contain the overwrapped tracks on the same direction. Figure 2 shows typical patterns of two-particle tracking. Proper identification of the ^{8}Be events will be confirmed by combining the tracking and charge-deposit data.

Data analysis is in progress toward the final result.

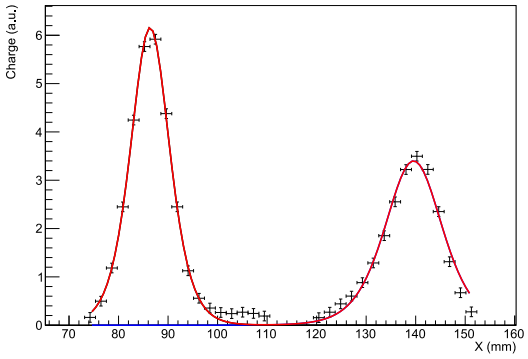

Fig. 1. Example of the charge distribution measured by CRDC. The fitting function is shown by the red line.

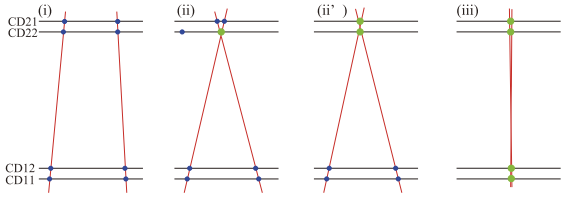

Fig. 2. Two-particle tracking patterns. The filled circles indicate the hit points of alpha particles in the pair of CRDCs. The green circles represent the crossing of two tracks. (i) Two tracks are completely divided. (ii) and (ii') Two tracks cross at one or two segments. (iii) Two tracks are completely overwrapped.

*1 Center for Nuclear Study, University of Tokyo
*2 RIKEN Nishina Center
*3 Department of Physics, Toho University
*4 Research Center for Nuclear Physics, Osaka University
*5 Department of Physics, Tokyo Institute of Technology
*6 Faculry of Engineering, University of Miyazaki
*7 Laboratorie de Physique Corpusculaire, IN2P3-CNRS, ENSICAEN et Université de Caen
*8 Department of Physics, University of Tokyo

References

1) K. Kisamori *et al.*, Phys. Rev. Lett. **116**, 052501 (2016).
2) S. Masuoka *et al.*, RIKEN Accel. Prog. Rep. **50**, 198 (2017).

Mass measurements of neutron-rich Ni isotopes in Rare-RI Ring II

A. Ozawa,[*1,*2] Y. Yamaguchi,[*2] N. Kaname,[*1] T. Moriguchi,[*1,*2] A. Yano,[*1] Y. Abe,[*2] N. Fukuda,[*2] Y. Hijikata,[*2,*3] S. Naimi,[*2] D. Shimizu,[*2] F. Suzaki,[*2,*4] H. Suzuki,[*2] H. Takeda,[*2] T. Uesaka,[*2] M. Yoshimoto,[*2] M. Wakasugi,[*2] Y. Nagata,[*5] D. Nagae,[*5,*2] M. Kanda,[*6,*2] Y. Koizumi,[*6,*2] S. Okubo,[*6] M. Otsu,[*6,*2] H. Seki,[*6,*2] N. Shinozaki,[*6,*2] T. Suzuki,[*6] T. Yamaguchi,[*6,*2] T. Chillery,[*7] M. Dozono,[*7] S. Hanai,[*7] N. Imai,[*7] J. Li,[*7] S. Ota,[*7,*8] S. Michimasa,[*7] R. Yokoyama,[*7] H. F. Li,[*9] and S. Suzuki[*9]

In spring 2021, we conducted an experiment at the Rare-RI Ring (R3) to measure the masses of neutron-rich Ni isotopes. Some of these nuclei were measured before at R3,[1] but the mass values of ^{74}Ni and ^{76}Ni showed large systematic uncertainties. Since the top of the waveform in the previous kicker system is not flat, it causes a fluctuation of approximately 10% in the kick angle within an effective duration of 100 ns.[2] Since the kick angle affects the orbit inside R3, this fluctuation was suspected to be a major source of systematic uncertainties. The kicker magnet system was successfully upgraded in the fall of 2020.[2] For injection, a 100 ns flat top was realized, and the kick angle fluctuation is expected to be 1%. For ejection, a long flat top of approximately 400 ns was realized, enabling the extraction of all stored events in a single step.

The experimental setup was essentially the same as that in the previous experiments.[1] A primary beam of ^{238}U accelerated in the Superconducting Ring cyclotron (SRC) to 345 MeV/nucleon impinged on a Be target with a thickness of 8 mm. Secondary beams, including ^{74}Ni isotopes, were produced via in-flight fission. We adjusted the thickness of degraders located at F1 and F2 in BigRIPS such that the beam energies of ^{76}Zn became approximately 150 MeV/nucleon, which was the proper energy for individual ion injection. Particle identification was performed up to F3 in BigRIPS.[1] The plastic scintillator at F3 provided trigger signals for the kicker magnets to inject particles of interest into R3. To maintain the trigger rate of the kicker magnets within 80 Hz, we applied TOF-ΔE gates[3] for the trigger signals. In this experiment, the momentum-dispersive focus was at F5 in BigRIPS. We placed two parallel-plate avalanche counters (PPACs) there to measure the beam momentum. At S0, the entrance of SHARAQ, we located a TOF counter,[4] which provided the start signal of the TOF in R3. We also measured the TOFs of each particle between F3 and S0, which is used for β calibration. The particles injected into R3 were extracted after approximately 700 μs by using the same kicker magnets. After the extraction, the particle impinged on a plastic scintillator, which provided a stop signal for the TOF in R3; finally, it was stopped in a NaI scintillator.

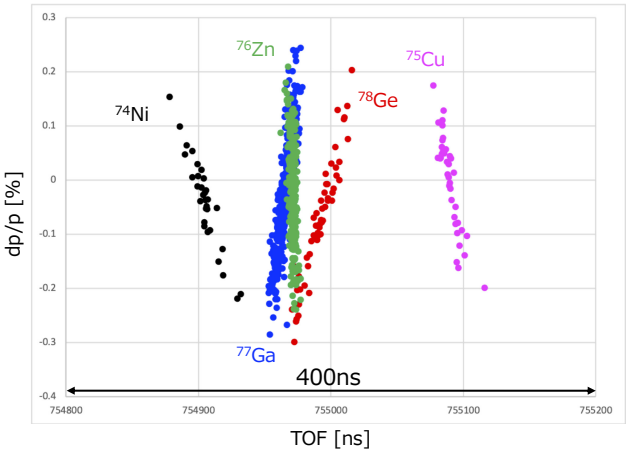

Fig. 1. TOF in R3 (ns) versus momentum difference (%) for extracted events in the experiment. Different colors show different species. All species are extracted within a time window of 400 ns.

In this experiment, we successfully extracted 5 species (^{78}Ge, ^{77}Ga, ^{76}Zn, ^{75}Cu, and ^{74}Ni). The isochronous optics of R3 was tuned using ^{76}Zn such that the width of the TOF in R3 was the narrowest for this nucleus. The observed momentum dependence of TOF in R3 in this experiment is shown in Fig. 1. All species were extracted within a time window of 400 ns. By careful tuning for trim coils, we achieved better isochronicity than in the previous experiment. To deduce the masses, the TOF in R3 should be corrected by the corresponding β or $B\rho$.

Data analysis is ongoing. At this moment, it is unclear whether the kicker upgrade affects the systematic uncertainties.

*1 Institute of Physics, University of Tsukuba
*2 RIKEN Nishina Center
*3 Department of Physics, Kyoto University
*4 Advanced Science Research Center, JAEA
*5 Faculty of Sciences, Kyushu University
*6 Department of Physics, Saitama University
*7 Center for Nuclear Study, University of Tokyo
*8 Research Center for Nuclear Physics, Osaka University
*9 Institute of Modern Physics, Chinese Academy of Science

References

1) A. Ozawa *et al.*, RIKEN Accel. Prog. Rep. **52**, 5 (2019).
2) Y. Yamaguchi *et al.*, RIKEN Accel. Prog. Rep. **54**, 100 (2021).
3) Y. Abe *et al.*, RIKEN Accel. Prog. Rep. **52**, 15 (2019).
4) S. Suzuki *et al.*, Nucl. Instrum. Methods Phys. Res. A **965**, 163807 (2020).

Mass measurements with the Rare-RI ring for the $A = 130$ r-process abundance peak II

S. Naimi,[*1] Y. Yamaguchi,[*1] Y. Nagata,[*2] D. Nagae,[*2,*1] Y. Abe,[*1] F. Suzaki,[*1,*3] M. Wakasugi,[*1] N. Kaname,[*4] S. Suzuki,[*4] A. Yano,[*4] T. Moriguchi,[*4] A. Ozawa,[*4] M. Kanda,[*5] Y. Koizumi,[*5] K. Okubo,[*5] M. Otsu,[*5] K. Sasaki,[*5] H. Seki,[*5] N. Shinozaki,[*5] T. Suzuki,[*5] T. Yamaguchi,[*5] T. Chillery,[*6] S. Hanai,[*6] Y. Hijitaka,[*7,*1] J. Li,[*6] R. Yokoyama,[*6] M. Dozono,[*6] S. Ota,[*6,*8] S. Michimasa,[*6] H. Suzuki,[*1] N. Fukuda,[*1] Y. Shimizu,[*1] H. Takeda,[*1] M. Yoshimoto,[*1] H. F. Li,[*9] and T. Uesaka[*1]

In the fall of 2021, we conducted an experiment at the Rare-RI Ring (R3) aiming to measure masses of neutron-rich silver (Ag) and palladium (Pd) isotopes. The first part of this experiment was conducted in the fall of 2018.[1)] Some of these nuclei were measured at that time, however, the mass values of ^{125}Ag and ^{124}Pd showed large systematic uncertainties that were suspected to be due to the narrow extraction timing of the storage ring. Upgrade of the kicker magnets system was successfully conducted in the fall of 2020[2)] and extraction timing window was extended from 100 ns to 400 ns, leading to extraction of all stored events at the same time.

Particles of interest for this experiment were produced at RIBF by impinging a 60 particle nA Uranium beam on a 5-mm thick Be target. Particles were identified at BigRIPS by energy loss in an Ionization Chamber (IC) placed at F3 and their Time-of-Flight (ToF) from F3 to F5. The ToF was measured by a 0.2 mm thick plastic scintillator at F3 and the PPAC's anode at F5. The particles were then transported to the SHARAQ spectrometer and then injected into the ring. After injection into the R3 and storage for about 1 ms, equivalent to almost 2000 turns, the particles were extracted. To determine the mass, the total ToF inside the ring is necessary. For this purpose, a timing detector[3)] was placed a the focal plane S0 of the SHARAQ spectrometer for the start signal, while a thin plastic detector was placed at the exit of the R3 for the stop signal.

Figure 1 shows the PID at F3 of all events produced at BigRIPS and the extracted events from R3, which are indicated by open black circles. These events were selected by using the so-called TOF/dE gate method that is necessary for the individual injection method.[4)] To estimate the extracted events for each isotone, a PID gate of $\pm 2\sigma$ for ToF from F3 to F5 as well as a $\pm 2\sigma$ gate for energy loss at F3 IC were performed. Unfortunately, no events of ^{124}Pd were extracted, however, sufficient events of ^{125}Ag and reference particles were extracted. Due to technical issues during the beam transport from BigRIPS to R3 and circulation inside the ring, the total efficiency was lower compared to previous experiments.[1,5)]

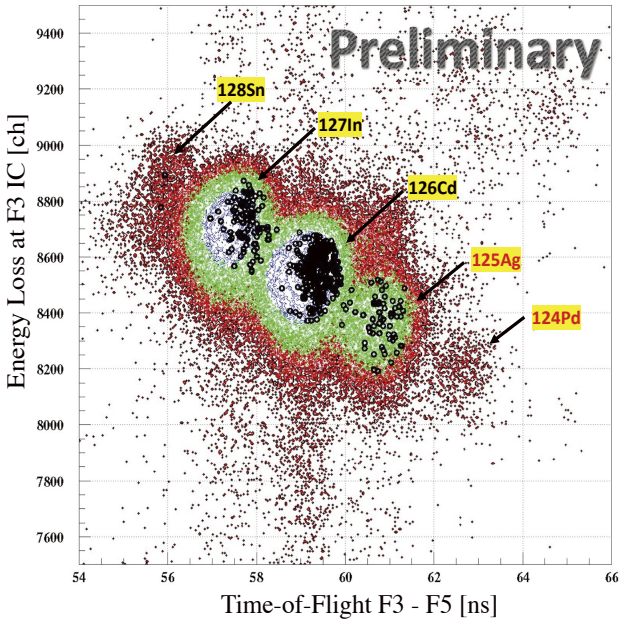

Fig. 1. Particle Identification (PID) showing the energy loss in the Ionizarion Chamber (IC) at F3 and ToF from F3 to F5. Extracted particles from R3 are shown in black empty circles.

In the near future, we will focus our efforts on solving the technical issues encountered during the experiment. We then plan to continue mass measurements of neutron-rich nuclei as well as neutron-deficient nuclei.

*1 RIKEN Nishina Center
*2 Faculty of Sciences, Kyushu University
*3 Advanced Science Research Center, Japan Atomic Energy Agency
*4 Institute of Physics, University of Tsukuba
*5 Department of Physics, Saitama University
*6 Center for Nuclear Study, University of Tokyo
*7 Department of Physics, Kyoto University
*8 Research Center for Nuclear Physics, Osaka University
*9 Institute of Modern Physics, Chinese Academy of Sciences

References

1) H. F. Li *et al.*, Phys. Rev. Lett. **128**, 152701 (2022).
2) Y. Yamaguchi *et al.*, RIKEN Accel. Prog. Rep. **54**, 100 (2021).
3) S. Suzuki *et al.*, Nucl. Instrum. Methods Phys. Res. A **965**, 163807 (2020).
4) Y. Abe *et al.*, RIKEN Accel. Prog. Rep. **52**, 15 (2019).
5) A. Ozawa *et al.*, RIKEN Accel. Prog. Rep. **52**, 5 (2019).

Decay spectroscopy in exotic neutron-rich nuclei near the $N = 50$ shell closure

C. J. Griffin,[*1] G. Carpenter,[*1,*2] R. Caballero-Folch,[*1] I. Dillmann,[*1] R. K. Grzywacz,[*3] K. P. Rykaczewski,[*4] J. L. Tain,[*5] and S. Nishimura[*6] for the BRIKEN Collaboration

β-decay and β-delayed neutron emission play key roles in determining the final elemental abundances of the rapid neutron-capture (r-) process. Current r-process models rely heavily on theoretical data but, with new generations of radioactive ion beam facilities coming online, swaths of neutron-rich nuclei will become available for experimental study. Delayed neutron emission is expected to be the dominant decay mode for these newly-accessible nuclei and has been shown to be crucial in determining r-process abundances.[1)]

In 2016, the BRIKEN collaboration constructed and commissioned the world's most efficient β-delayed neutron detector[2,3)] at RIBF to conduct a wide-ranging and systematic study into the decay properties of hundreds of the most exotic neutron-rich nuclei currently available. The BRIKEN detector consists of 140 ^{3}He tubes within a HDPE moderator surrounding the highly-segmented active stopper AIDA[4)] and two HPGe clover detectors in close geometry.

The NP1412-RIBF127R1 experiment implemented the BRIKEN detector to measure β-delayed neutron emission probabilities and half-lives, as well as conduct decay spectroscopy studies, around the $N = 50$ shell closure near the doubly-magic ^{78}Ni. This region has been highlighted as sensitive to β-decay properties,[5)] however, little to no spectroscopy data exist in this region.

The TRIUMF-based analysis focuses on γ-ray decay spectroscopy of $^{85-90}$Ge, $^{88-92}$As, $^{91-95}$Se and $^{94-97}$Br isotopes, with some high-statistics known cases at lighter masses studied for calibration. During the experiment, approximately $7.5 \cdot 10^{4}$ ^{85}Ge nuclei and $5.75 \cdot 10^{6}$ ^{86}Ge nuclei were implanted into AIDA. Figures 1 and 2 show preliminary decay spectra for the de-excitation of states within ^{85}As and ^{86}As, chosen as two of the few isotopes in this region with any previous spectroscopic data and also relatively high statistics.

With approximately two orders of magnitude fewer ^{85}Ge implants compared to ^{86}Ge, a significant fraction of the decays to ^{85}As are expected to come from the βn decay of ^{86}Ge, with its P_{1n} value of 45%.[6)]

Many of the peaks identified in ^{85,86}As by Mazzocchi *et al.*[7)] are labelled in the spectra, as well as peaks identified from decays into the daughter nuclei ^{85,86}Se.[8,9)]

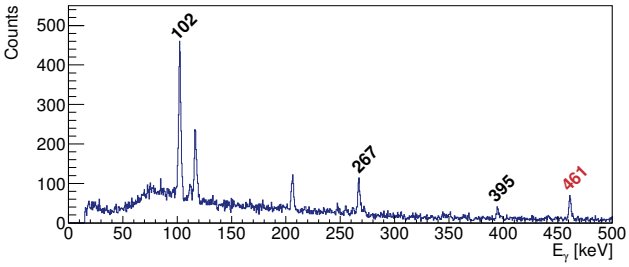

Fig. 1. Preliminary γ-spectrum for decays into ^{85}As, considering both β- and βxn-decay modes from parent nuclei. Known peaks in ^{85}As are labelled in black and peaks identified from the decay of ^{85}As into ^{85}Se are in red.

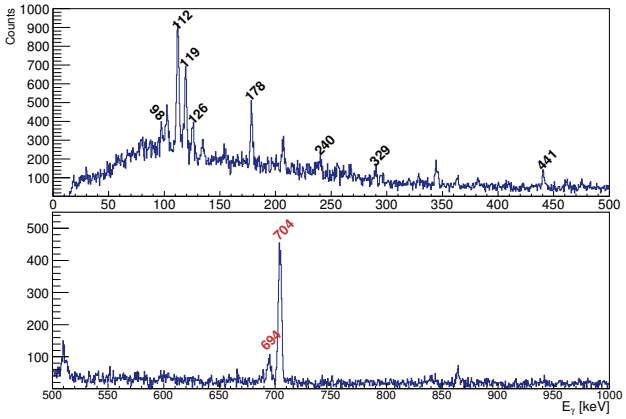

Fig. 2. Preliminary γ-spectrum for decays into ^{86}As, considering both β- and βxn-decay modes from parent nuclei. Known peaks in ^{86}As are labelled in black and peaks identified from the decay of ^{86}As into ^{86}Se are in red.

Analysis of the Ge, As, Se and Br isotopes of interest is on-going and we expect to obtain the first spectroscopic data for some of these isotopes.

*1 Physical Sciences Division, TRIUMF
*2 School of Physics and Astronomy, University of Edinburgh
*3 Depatment of Physics and Astronomy, University of Tennessee
*4 Oak Ridge National Laboratory
*5 Instituto de Física Corpuscular (IFIC)
*6 RIKEN Nishina Center

References
1) M. R. Mumpower *et al.*, Phys. Rev. C **85**, 045801 (2012).
2) A. Tarifeño-Saldivia *et al.*, J. Instrum. **12**, P04006 (2017).
3) A. Tolosa-Delgado *et al.*, Nucl. Instrum. Methods Phys. Res. A **925**, 133 (2019).
4) C. J. Griffin *et al.*, Proc. XIII Nuclei in the Cosmos, PoS (NIC XIII), 097 (2015).
5) T. Shafer *et al.*, Phys. Rev. C **94**, 055802 (2016).
6) K. Miernik *et al.*, Phys. Rev. Lett. **111**, 132502 (2013).
7) C. Mazzocchi *et al.*, Phys. Rev. C **92**, 054317 (2015).
8) Evaluated Nuclear Structure Data File (ENSDF).
9) J. V. Kratz *et al.*, Nucl. Phys. A **250**, 13 (1975).

Half-lives and β-delayed neutron emission for the most exotic neutron-rich Se and Br isotopes

R. Caballero-Folch,[*1] I. Dillmann,[*1] S. Devinyak,[*1] C. J. Griffin,[*1] L. Sexton,[*1,*2] J. Agramunt,[*3] R. K. Grzywacz,[*4] M. Pallas,[*5] K. P. Rykaczewski,[*6] J. L. Taín,[*3] A. Tarifeño-Saldivia,[*5] A. Tolosa-Delgado,[*3] S. Nishimura,[*7] and the BRIKEN Collaboration.

The BRIKEN collaboration performed measurements on several neutron-rich nuclei regions across the nuclear chart during the period 2017–2021. Focused on the double magic ^{78}Ni region, the experiment RIBF127 aimed to determine experimental β-decay half-lives, neutron emission probabilities, and γ spectroscopy of isotopes beyond the $N = 50$ neutron shell, which are all important parameters to provide reliable data for models of the astrophysical rapid-neutron capture process. The most neutron-rich isotopes of elements from Fe ($Z = 26$) to Kr ($Z = 36$) were identified using the BigRIPS spectrometer on an event-by-event basis with the $B\rho$–ΔE–ToF method.[1)] At the end of the beamline, the detection setup consisted of the Advanced Implantation and Detector Array (AIDA)[2)] surrounded by the BRIKEN detector.[3)] The AIDA consists of an array of six highly segmented layers of double-sided Si detectors (DSSSD), enabling the detection of the implants of the ions and their β-decays. The BRIKEN array is a high efficiency neutron detector based on 140 ^{3}He counters embedded in a polyethylene matrix to moderate the emitted neutrons, and two HPGe clover γ detectors. It enabled the detection of the neutrons and the γ-rays emitted after the β-decays.

The isotopic species of interest in this study are $^{91–94}$Se and $^{94–96}$Br. They have been implanted in AIDA (see Table 1), and for most of them, the decay properties were determined for the first time. The data analysis is based on the time correlation of the implants and β-decays registered in AIDA, and the neutrons and γ-rays detected with the BRIKEN detector. In addition to the time correlation, spatial correlations between implants and β-decays are studied owing to the DSSSD's segmentation. This allowed us to adjust the best signal-to-noise rate in the correlations.[4)] Using the Bateman equations and corrections due to the physical limitations of the detection systems,[5,6)] the half-life and the β-delayed neutron emission probability, P_{1n}-value, were determined. Figure 1 shows the analysis of ^{91}Se, in which multiple simultaneous fits of implant-β and implant-β-neutron correlation histograms were performed to determine its properties. Preliminary results show slightly shorter half-life and higher P_{1n}-value compared with the literature for ^{91}Se. An upcoming publication will report new half-lives and P_{1n} values in the region, some of them for the first time.

Table 1. Number of implants of the isotopes of interest and available data in the literature.

Nucleus	Number of ions implanted	Previous literature values half-life (s)	P_{1n} value (%)
^{91}Se	59728	0.27(5)	21(10)[7)]
^{92}Se	340337	-	-
^{93}Se	16631	-	-
^{94}Se	525	-	-
^{94}Br	2627	0.070(20)	30(10)[7)]
^{95}Br	2289	-	-
^{96}Br	159	-	-

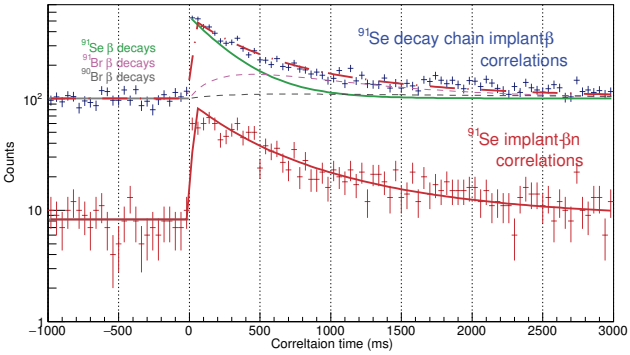

Fig. 1. Implant-β (blue) and implant-β-neutron (red) correlation histograms for ^{91}Se. Fitted curves obtained by simultaneously sharing common parameters, from which the half-life and the P_{1n}-value were determined.

*1 Physical Science Division, TRIUMF
*2 Department of Physics, University of Surrey
*3 Institut the Física Corpuscular de València
*4 Department of Physics and Astronomy, University of Tennessee
*5 Universitat Politècnica de Catalunya
*6 Oak Ridge National Laboratory
*7 RIKEN Nishina Center

References
1) N. Fukuda *et al.*, Nucl. Instrum. Methods Phys. Res. B **317**, 323 (2013).
2) C. Griffin *et al.*, POS (NIC-XIII), 097 (2014).
3) A. Tarifeño-Saldivia *et al.*, J. Instrum. **12**, (2017).
4) R. Caballero-Folch *et al.*, Phys. Rev. C **95**, 064322 (2017).
5) A. Tolosa-Delgado *et al.*, Nucl. Instrum. Methods Phys. Res. A **925**, 133 (2019).
6) J. Agramunt *et al.*, Nucl. Instrum. Methods Phys. Res. A **807**, 69 (2016).
7) J. Liang *et al.*, Nucl. Data Sheets **168**, 1 (2020).

Identification of a new μs-isomer in the REP region

A. Vitéz-Sveiczer,[*1,*2] G. G. Kiss,[*1] A. Tarifeño-Saldivia,[*3] M. Pallas,[*3] J. L. Tain,[*4] A. Estrade,[*5] S. Nishimura,[*6] J. Agramunt,[*4] A. Algora,[*4] N. T. Brewer,[*7] R. Caballero-Folch,[*8] F. Calvino,[*3] T. Davinson,[*9] I. Dillmann,[*8] N. Fukuda,[*6] R. K. Grzywacz,[*10] O. Hall,[*7] A. I. Morales,[*4] A. Navarro,[*3] N. Nepal,[*6] B. C. Rasco,[*7] K. P. Rykaczewski,[*7] N. T. Szegedi,[*1] A. Tolosa-Delgado,[*4] P. Vi,[*11] R. Yokoyama,[*10] K. Wang,[*5] M. Wolinska-Cichocka,[*12] and P. Woods[*9] for the BRIKEN collaboration

The solar r-process abundance distribution has two characteristic maxima at $A \approx 130$ and $A \approx 195$, which can be explained by neutron shell closures at $N = 82$ and $N = 126$, respectively. A smaller peak also exists between these two maxima at $A \approx 160$, which is known as the rare-earth peak (REP). The formation of the REP is sensitive to parameters that control the neutron density and neutron-to-seed ratio Y_e in the late stages of the r-process, such as the timescale for the expansion of the material. However, these astrophysical conditions are entangled with nuclear physics processes that provide additional neutrons, of which β-delayed neutron emissions can be a main contributor.[1)] The mass region responsible for the formation of the REP has previously been inferred.[2)]

During the NP1612-RIBF148 experiment's heavier setting, exotic neutron-rich $^{159–166}$Pm, $^{161–168}$Sm, $^{165–170}$Eu, and $^{167–172}$Gd isotopes were produced (among others) at RIKEN Nishina Center by the fragmentation of a ^{238}U primary beam with an intensity of approximately 60 particle nA to produce isotopes as close to the aforementioned region of nuclei as possible. The fission fragments were selected and identified using the standard ΔE-$B\rho$-ToF method by BigRIPS. The radioactive ions were implanted in the AIDA implantation detector[3,4)] after adjusting their kinetic energy with aluminum degraders placed at the F11 focal point. The AIDA implantation detector was centered in the BRIKEN neutron counter,[5)] which consisted of 140 ^{3}He-filled proportional counters embedded in a large polyethylene moderator matrix. Moreover, two CLARION-type clover detectors[6)] were inserted horizontally from the left and right sides into holes in the matrix that allowed facing the center of the stack of double-sided silicon strip detectors (DSSSD).

Half-lives and P_{1n} values were deduced from implantation–β correlations and implantation–β–neutron correlations for the produced isotopes. These results were used for variance-based sensitivity analysis to reveal the influence of nuclear physics inputs on the calculated abundance pattern for the case of REP.[7)] Beta-delayed γ-spectroscopy was also performed using the CLARION-type clover detectors. In most of the studied nuclei, there was a significant number of newly identified γ-ray transitions. In order to build decay-schemes, γ–γ coincidence analysis was performed as well.

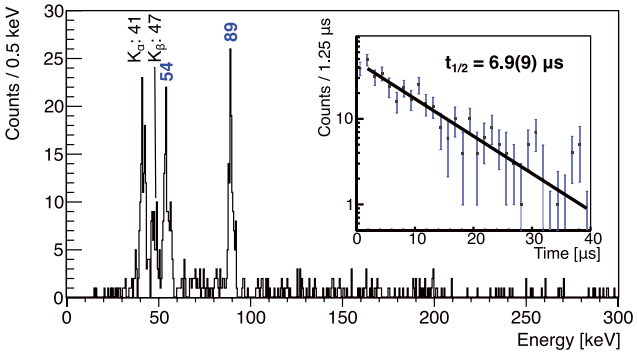

Fig. 1. Energy spectrum of isomer-delayed γ-rays from ^{164}Eu*. Inset: exponential function fit to the isomeric decay curve.

A μs-isomer candidate of ^{164}Eu was identified earlier using implantation–γ correlations; however, no half-life nor exact energy level was reported.[8)] We found that the ^{164}Sm $\rightarrow$ ^{164}Eu* β-decay populates a low-lying isomeric state located at $E_{exc.} = 143.7(3)$ keV, which de-excites through $E_\gamma = 54$ keV and $E_\gamma = 89$ keV γ-transitions. The half-life of this isomeric state was found to be 6.9(9) μs. Figure 1 shows the measured gamma spectra and the isomeric decay curve.

*1 Institute for Nuclear Research (ATOMKI)
*2 Department of Physics, University of Debrecen
*3 Universitat Politècnica de Catalunya (UPC)
*4 Instituto de Física Corpuscular (IFIC)
*5 University College of Science and Engineering, Central Michigan University (CMU)
*6 RIKEN Nishina Center
*7 Oak Ridge National Laboratory
*8 Physical Sciences Division, TRIUMF
*9 School of Physics and Astronomy, University of Edinburgh
*10 Department of Physics and Astronomy, University of Tennessee
*11 Faculty of Physics, VNU University of Science
*12 HIL, University of Warsaw

References

1) A. Arcones *et al.*, Phys. Rev. C **83**, 045809 (2011).
2) M. Mumpower *et al.*, Phys. Rev. C **85**, 045801 (2012).
3) C. J. Griffin *et al.*, Proc. XIII Nuclei in the Cosmos, PoS(NIC XIII), 097 (2015).
4) O. Hall *et al.*, Phys. Lett. B **816**, 136266 (2021).
5) A. Tolosa-Delgado *et al.*, Nucl. Instrum. Methods Phys. Res. A **925**, 133 (2019).
6) C. J. Gross *et al.*, Nucl. Instrum. Methods Phys. Res. **450**, 12 (2000).
7) G. G. Kiss *et al.*, in preparation.
8) Z. Patel *et al.*, Phys. Rev. C **96**, 034305 (2017).

RIBF181: γ-ray spectroscopy in the vicinity of ^{78}Ni

R. Taniuchi,[*1,*2] S. Franchoo,[*3,*2] D. Suzuki,[*2] N. Aoi,[*4,*2] H. Baba,[*2] F. Browne,[*2] C. M. Campbell,[*5] S. Chen,[*1,*6] R. Crane,[*1,*2] H. L. Crawford,[*5] H. de Witte,[*7,*2] P. Doornenbal,[*2] C. Fransen,[*8] N. Fukuda,[*2] H. Hess,[*8,*2] E. Ideguchi,[*4,*2] S. Iwazaki,[*4,*2] J. Kim,[*9] A. Kohda,[*4,*2] T. Koike,[*10,*2] T. Koiwai,[*11,*2] B. Mauss,[*2] R. Mizuno,[*11,*2] B. Moon,[*2] M. Niikura,[*11,*2] D. Nishimura,[*12,*2] T. Parry,[*13,*2] M. Petri,[*1] P. Reiter,[*8] H. Sakurai,[*11,*2] Y. Shimizu,[*2] H. Suzuki,[*2] H. Takahashi,[*12,*2] H. Takeda,[*2] S. Thiel,[*8] K. Wimmer,[*14,*2] Y. Yamamoto,[*4,*2] and M. Yoshimoto[*2] for the RIBF 181 Collaboration

The NP1912-RIBF181 experiment with the HiCARI setup[1] was conducted for 7 days in April 2021. Its objective is the spectroscopy of the nuclei in the vicinity of ^{78}Ni, which is expected to be doubly magic ($Z = 28$, $N = 50$).[2,3] The experiment aimed to prove for the possible shape coexistence phenomena associated with shell-quenching in both proton and neutron gaps at and beyond this anchor-point nucleus, especially by the detailed spectroscopy of the proton single-particle states in ^{79}Cu. ^{80}Zn and the one-proton removal channels were centered in the BigRIPS and ZeroDegree (ZD) spectrometers, respectively.

The secondary beam was produced with a 4-mm beryllium target at the F0 focal plane by a 90-particle nA ^{238}U primary beam at an energy of 345 MeV/nucleon. The beam was purified using the $B\rho$-ΔE-$B\rho$ method through the first stage of BigRIPS with a wedge-shaped 8-mm aluminium degrader installed at F1 and the second stage with a 2-mm aluminium degrader at F5. To enhance the production yield of the ^{80}Zn beam, we selected the magnetic rigidity for a high total beam rate at F7 of about 5×10^4 counts per second (cps). This is much higher than the upper limit (10 kcps) of the previous in-beam γ-ray spectroscopy experiments at the ZD spectrometer. A secondary target consisting of 6.8-mm-thick beryllium was selected for an efficient population yield of the γ rays after the secondary reaction without eroding the advantage of the high-resolution spectrometer array.

The data acquisition (DAQ) system consisted of two parts, the BigRIPS and HiCARI DAQs. The former processed all the data except the data from the HiCARI detector arrays, *i.e.*, the data from the beamline detectors and the timestamp values of the HiCARI DAQ with a shared dead-time mode within the subsystems. The latter recorded the waveforms of the HPGe detector signals with a certain time window generated from the external trigger pulse with practically no dead time. A live-time ratio of ≈87% with a trigger rate greater than 5 kHz was achieved in the BigRIPS DAQ owing to a recently developed data acquisition system, MPV.[5] To establish both good timing and energy measurements with a high beam rate in each plastic detector, a charge-to-time converter (QTC) module[6] was utilized in addition to the standard circuits.

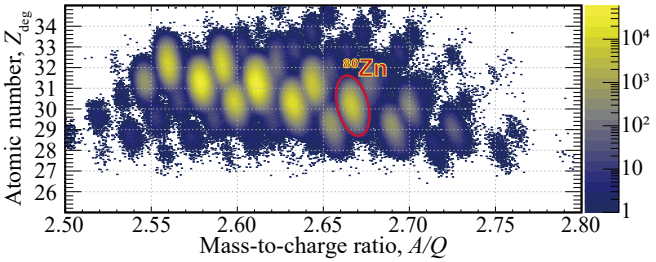

Fig. 1. Preliminary particle identification plot in BigRIPS with the $Z_{\rm deg}$ method. ^{80}Zn is highlighted with a red ellipse.

The particle identification for the secondary beams was performed with the TOF-$B\rho$-ΔE technique. Instead of using the standard MUSIC detector at F7, which suffered from a large number of pile-up hits, the $Z_{\rm deg}$ technique was confirmed to be functional with a reasonable resolution (Fig. 1). This method is to calculate the energy loss in the degrader at F5 from the difference in the reconstructed momenta between F3-F5 and F5-F7 and has been applied before in other experiments in higher Z regions around $Z \approx 50$.[4] The purity of the ^{80}Zn beam is tentatively deduced as 4.8%. The same method was applied to the scattered particles with the ZD spectrometer. As a backup for the energy loss measurement, another 1-mm plastic scintillator was installed at F11 after the standard one.

A set of high-statistics data is expected to provide not only γ-ray energy spectra disentangling high density levels that were not resolved in the previous studies[2,3] but also systematic inclusive nucleon-removal reaction cross sections with a variety of isotopes in the vicinity of ^{78}Ni.

*1 Department of Physics, University of York
*2 RIKEN Nishina Center
*3 IJCLab
*4 Research Center for Nuclear Physics, Osaka University
*5 Nuclear Science Division, Lawrence Berkeley National Laboratory
*6 Department of Physics, University of Hong Kong
*7 Instituut voor Kern- en Stralingsfysica, KU Leuven
*8 Institut für Kernphysik, Universität zu Köln
*9 Department of Physics, Korea University
*10 Department of Physics, Tohoku University
*11 Department of Physics, University of Tokyo
*12 Department of Natural Sciences, Tokyo City University
*13 Department of Physics, University of Surrey
*14 IEM-CSIC

References

1) K. Wimmer *et al.*, RIKEN Accel. Prog. Rep. **54**, S27 (2021).
2) R. Taniuchi *et al.*, Nature **569**, 53 (2019).
3) L. Olivier *et al.*, Phys. Rev. Lett. **119**, 192501 (2017).
4) Y. Shimizu *et al.*, J. Phys. Soc. Jpn. **87**, 014203 (2018); N. Fukuda *et al.*, J. Phys. Soc. Jpn. **87**, 014202 (2018).
5) H. Baba *et al.*, IEEE Trans. Nucl. Sci. **68**, 1841 (2021).
6) T. Ishikawa *et al.*, Nucl. Instrum. Methods Phys. Res. A **875**, 193 (2017).

Neutron intruder states and collectivity beyond $N = 50$ towards ^{78}Ni

L. Plagnol,[*1] F. Flavigny,[*1] for the RIBF196 and HiCARI collaborations

Recent spectroscopy studies in the vicinity of ^{78}Ni[1,2] hint to the presence of low-lying deformed configurations. These intruder configurations are predicted to originate from the multiparticle-multihole excitations[3] of nucleons above the $N = 50$ and $Z = 28$ shell gaps becoming competitive in energy owing to neutron-proton correlations enhancing quadrupole collectivity. The quantification of collective effects above $N = 50$ is crucial since it directly impacts binding energies, drip-line limits,[4] and consequently r-process nucleosynthesis calculations. Because these states involve many-particle excitations, their theoretical description is very challenging: thus, identifying them experimentally is of prime interest to constrain models.

We report here on the analysis status of the RIBF196 experiment to identify and characterize 2p-1h intruder states above $N = 50$ in ^{83}Ge and ^{81}Zn for the first time using a neutron knockout reaction from $N = 52$ isotopes. This selective reaction enables neutron removal from the $g_{9/2}$ orbital populating preferentially $9/2^+$ states with a significant intruder $\nu(g_{9/2})^{-1}(s_{1/2}d_{5/2})^{+2}$ configuration. Simultaneously, low-lying states in ^{82}Zn were populated using proton removal from ^{83}Ga, and their lifetimes will be extracted using line-shape analysis to better characterize the onset of deformation developing in Zn above $N = 50$.[5]

To attain these scientific objectives, a secondary cocktail beam containing ^{84}Ge, ^{83}Ga, and ^{82}Zn was produced and purified in the BigRIPS spectrometer to induce knockout reactions on a secondary 6-mm thick Be target. De-excitation γ-rays of the reaction products ^{83}Ge, ^{82}Zn, and ^{81}Zn were detected using the HiCARI germanium array[6] surrounding the secondary reaction target. Event-by-event particle identification for beam nuclei and reaction products was achieved in the BigRIPS and ZeroDegree spectrometers by reconstructing their atomic number (Z) and their mass-to-charge ratio (A/Q) using the TOF-$B\rho$-ΔE method combined with a two-fold $B\rho$ method.

We performed higher-order optical corrections of the A/Q values to compensate for remaining dependencies on spectrometer variables such as as positions and angles at the focal planes. This additional correction is equivalent to a higher-order determination of optical transfer matrices and improves the identification. It was performed using a multi-dimensional fitting procedure, considering cross-terms. An optically corrected particle identification diagram (PID) is shown in Fig. 1.

The A/Q resolution achieved through this optical correction procedure is of 7.10^{-2}% calculated on the identification of ^{84}Ge in BigRIPS with an amelioration of approximately 14% compared with the uncorrected

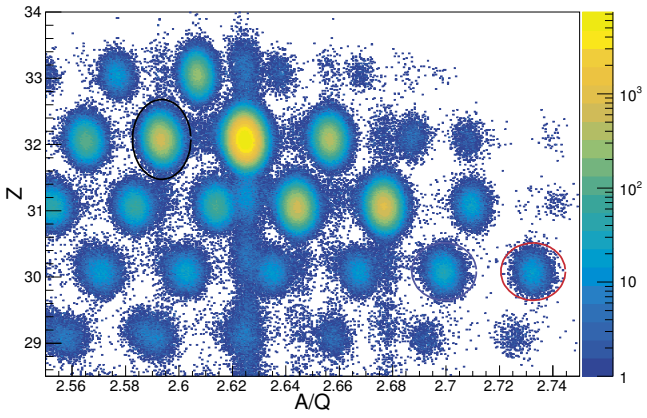

Fig. 1. Particle identification of the reaction products in the ZeroDegree spectrometer. The black, red, and purple ellipsoids indicate ^{83}Ge, ^{82}Zn, and ^{81}Zn, respectively: see text for details.

A/Q resolution, and 9.10^{-2}% on ^{83}Ge in ZeroDegree spectrometer with an amelioration of more than 50%. In addition, we cleaned the PID by removing unwanted events such as delta rays in PPAC detectors, pileup events in plastic detectors and ionisation chambers, and change in charge states. The most impacting selection is the pileup events removal cutting away approximately 10% of events on the total PID.

The HiCARI detectors have been aligned in time, calibrated in energy (38 crystals and 376 segments) using sources of ^{60}Co, ^{152}Eu, and ^{133}Ba, and the array efficiency was determined (2.9% at 1 MeV with a 0.5 mm Pb shield). The non-linearities of the ADCs were quantified from the residuals of the energy calibrated spectra and exhibit a saw-tooth pattern with variations up to 2–3 keV.[7] Their impact on Doppler corrected spectra will be quantified using simulations. Finally, a preliminary Doppler-corrected gamma spectrum has been produced using photogrammetry positions of the clusters and a fixed velocity at the target, but we aim at improving this result using event-by-event Doppler correction using the measured velocity distributions in the BigRIPS and ZeroDegree spectrometers.

*1 LPC Caen, CNRS/IN2P3

References
1) R. Taniuchi *et al.*, Nature **569**, 53 (2019).
2) X. F. Yang *et al.*, Phys. Rev. Lett. **116**, 219901 (2016).
3) K. Heyde, J. L. Wood, Rev. Mod. Phys. **83**, 1467 (2011).
4) J. Erler *et al.*, Nature **486**, 509 (2012).
5) C. Shand *et al.*, Phys. Lett. B **773**, 492 (2017).
6) K. Wimmer *et al.*, RIKEN Accel. Prog. Rep. **54**, S27 (2020).
7) K. Dolde *et al.*, Nucl. Instrum. Methods Phys. Res. A **848**, 127 (2017).

Charge state separation in the ZD spectrometer for the ^{132}Sn region

T. Parry,[*1] Zs. Podolyák,[*1] G. Bartram,[*1] Z. Q. Chen,[*1] M. Górska,[*2] M. Armstrong,[*2] A. Yaneva,[*2] K. Wimmer,[*3,*4] P. Doornenbal,[*4] N. Aoi,[*5,*4] H. Baba,[*4] F. Browne,[*4] C. Campbell,[*6] H. Crawford,[*6] H. De Witte,[*7] C. Fransen,[*8] H. Hess,[*8] S. Iwazaki,[*5,*4] J. Kim,[*4] A. Kohda,[*5,*4] T. Koiwai,[*9,*4] B. Mauss,[*4] B. Moon,[*4] P. Reiter,[*8] D. Suzuki,[*4] R. Taniuchi,[*10,*4] S. Thiel,[*8] and Y. Yamamoto[*5,*4]

Isotopes produced in charge states become increasingly more common amongst higher mass beams. The ability to separate and identify different charges is important in preventing particle identification contamination. In this report, we briefly outline a commonly used method of charge state separation which was utilised during the analysis of the RIBF-189 experiment conducted in November 2020 during the HiCARI campaign.[1,2] The aim of the experiment was to study excited states in $N = 82$ nuclei, focusing on ^{129}Ag. A primary 345 MeV/nucleon beam of ^{238}U was used and the fission fragments were identified in BigRIPS, which was tuned for ^{130}Cd. After the secondary target, the reaction products were identified by the ZeroDegree (ZD) spectrometer. Here the energy of the reaction products was relatively low at around 150 MeV/nucleon, which means that only about 80% of them were fully stripped. Charge state separation is based on magnetic rigidity measurements in the two parts of the separator FP8-FP9 and FP9-FP11. δ is calculated as $\delta = (B\rho - B\rho_0)/B\rho_0$. $B\rho$ denotes the measured magnetic rigidity for individual particles. $B\rho_0$ is the magnetic rigidity for the central path. Figure 1 shows the charge state separation where the structures correspond to different changes of the charge state (ΔQ) in the middle of the ZD spectrometer (FP9). Figure 2, showing Z vs A/Q identification plots, demonstrates the effect of selecting $\Delta Q = 0$ and $\Delta Q = +1$. Note $\Delta Q = 0$ contains ions which are fully stripped (labelled in black) and hydrogen like throughout the ZD spectrometer (red). Similarly $\Delta Q = +1$ includes ions which change from fully stripped to H-like (black) and H-like to He-like (red). Using these identification plots, one obtains γ-ray spectra associated to the nucleus of interest free from the contributions of other isotopes.

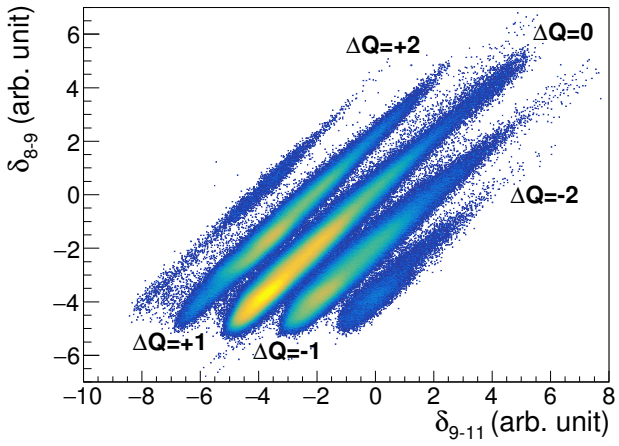

Fig. 1. Charge state separation in ZD spectrometer.

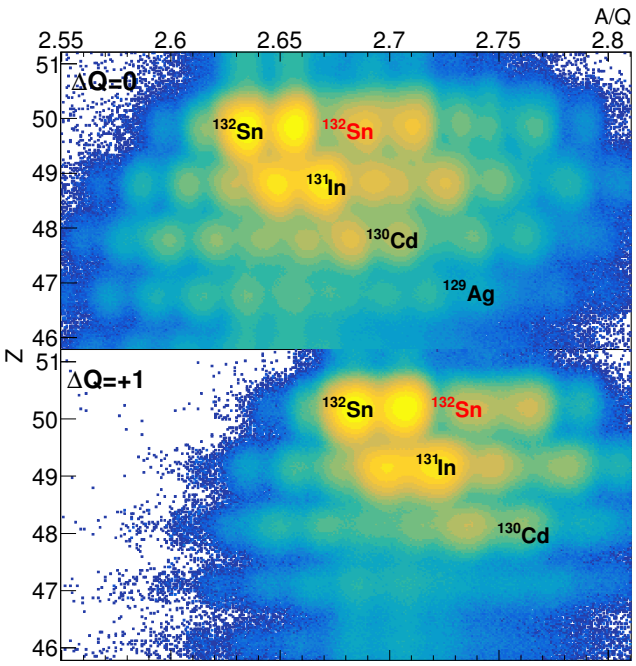

Fig. 2. ZD spectrometer particle identification plots for $\Delta Q = 0$ (upper) and $\Delta Q = +1$ (lower). $N = 82$ nuclei are highlighted.

*1 Department of Physics, University of Surrey
*2 GSI Helmholtzzentrum für Schwerionenforschung GmbH
*3 IEM-CSIC
*4 RIKEN Nishina Center
*5 Research Center for Nuclear Physics, Osaka University
*6 Nuclear Science Division, LBNL
*7 Instituut voor Kern- en Stralingsfysica, KU Leuven
*8 Institut für Kernphysik, Universität zu Köln
*9 Department of Physics, University of Tokyo
*10 Department of Physics, University of York

References

1) T. Parry *et al.*, RIKEN Accel. Prog. Rep. **54**, 9 (2021).
2) K. Wimmer *et al.*, RIKEN Accel. Prog. Rep. **54**, S27 (2021).

Observation of low-lying dipole states in the ^{11}Li(p,n) reaction

L. Stuhl,[*1,*2,*3] M. Sasano,[*3] J. Gao,[*3,*4] Y. Hirai,[*5] K. Yako,[*2] T. Wakasa,[*5] D. S. Ahn,[*3] H. Baba,[*3] A. I. Chilug,[*6,*3] S. Franchoo,[*7] Y. Fujino,[*8] J. Gibelin,[*9] I. S. Hahn,[*1,*10] Z. Halász,[*11] T. Harada,[*12] M. N. Harakeh,[*13,*14] D. Inomoto,[*5] T. Isobe,[*3] H. Kasahara,[*5] D. Kim,[*1,*15] G. G. Kiss,[*11] T. Kobayashi,[*16,*3] Y. Kondo,[*17,*3] Z. Korkulu,[*1,*3] S. Koyama,[*18,*3] Y. Kubota,[*3] A. Kurihara,[*17] H. N. Liu,[*19] M. Matsumoto,[*17] S. Michimasa,[*2] H. Miki,[*17,*3] M. Miwa,[*20,*3] T. Motobayashi,[*3] T. Nakamura,[*17,*3] M. Nishimura,[*3] H. Otsu,[*3] V. Panin,[*3] S. Park,[*10] A. T. Saito,[*17,*2] H. Sakai,[*3] H. Sato,[*3] T. Shimada,[*17] Y. Shimizu,[*3] S. Shimoura,[*2] A. Spiridon,[*6] I. C. Stefanescu,[*6] X. Sun,[*3,*4] Y. L. Sun,[*19] H. Suzuki,[*3] E. Takada,[*21] Y. Togano,[*8,*3] T. Tomai,[*17,*3] L. Trache,[*6] D. Tudor,[*6,*3] T. Uesaka,[*3] H. Yamada,[*17] M. Yasuda,[*17] K. Yoneda,[*3] K. Yoshida,[*3] J. Zenihiro,[*3] and N. Zhang[*22,*2]

The SAMURAI30 experimental program aims to systematically investigate the isovector response of light nuclei near the neutron drip line.[1)] No data are available on spin-isospin collectivity for nuclei with large isospin asymmetry factors, where $(N-Z)/A > 0.25$. Gamow-Teller (GT) and spin-dipole (SDR) transitions, including their giant resonances, were studied on ^{11}Li and ^{14}Be using charge-exchange (p,n) reactions in inverse kinematics combined with the missing-mass technique.[2)] The setup of the PANDORA low-energy neutron time-of-flight counter[3)] and SAMURAI magnetic spectrometer,[4)] as well as a thick liquid hydrogen target, enables us to perform measurements with high luminosity. In our previous experiments at RIKEN RIBF on ^{132}Sn, we successfully demonstrated[5)] that we can obtain data on unstable nuclei in the giant-resonance region with similar statistics as data obtained on stable nuclei.

Preliminary results on GT giant resonance are already detailed in a previous report.[6)] More than fifteen different decay channels were identified for the ^{11}Be reaction product. A strong GT transition at 19 MeV, in agreement with previous beta-decay studies, was observed. We showed experimental evidence for the GT peak shifting below the Isobar Analog State (IAS).

In ^{11}Be,^{10}Be, and ^{9}Be related decay channels, low-lying states were also identified in the excitation energy range below 10 MeV. The angular-momentum distributions of these states show a peak at backward angles, which is characteristic of dipole transitions. Similar low-lying SD states were predicted in previous theoretical calculations on ^{11}Li by Suzuki[7)] in connection to the neutron-halo structure.

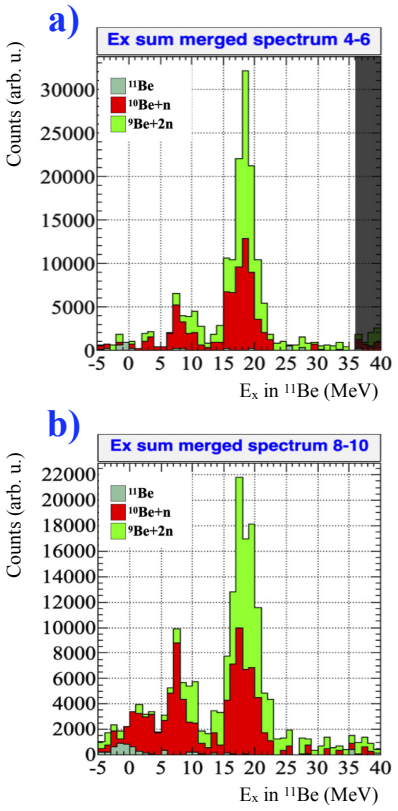

Fig. 1. Low-liying dipole states in excitation energy spectrum in the 4°–6° (a) and 8°–10° (b) center-of-mass angular bins for beryllium-related decay channels.

*1 Center for Exotic Nuclear Studies, Institute for Basic Science
*2 Center for Nuclear Study, University of Tokyo
*3 RIKEN Nishina Center
*4 School of Physics, Peking University
*5 Department of Physics, Kyushu University
*6 Horia Hulubei National Institute for R&D in Physics and Nuclear Engineering
*7 Institut de Physique Nucléaire, Université Paris-Saclay
*8 Department of Physics, Rikkyo University
*9 Nuclear Physics Laboratory, LPC CAEN
*10 Department of Physics, Ewha Womans University
*11 Institute for Nuclear Research (ATOMKI)
*12 Department of Physics, Toho University
*13 Department of Physics, University of Groningen
*14 GSI Helmholtzzentrum für Schwerionenforschung
*15 Department of Physics, Korea University
*16 Department of Physics, Tohoku University
*17 Department of Physics, Tokyo Institute of Technology
*18 Department of Physics, University of Tokyo
*19 Département de Physique Nucléaire, CEA, Université Paris-Saclay
*20 Department of Physics, Saitama University
*21 National Institute of Radiological Sciences (NIRS)
*22 Institute of Modern Physics, Chinese Academy of Sciences

References

1) L. Stuhl *et al.*, RIKEN Accel. Prog. Rep. **48**, 54 (2015).
2) M. Sasano *et al.*, Phys. Rev. Lett. **107**, 202501 (2011).
3) L. Stuhl *et al.*, Nucl. Instrum. Methods Phys. Res. A **866**, 164 (2017).
4) T. Kobayashi *et al.*, Nucl. Instrum. Methods Phys. Res. B **317**, 294 (2013).
5) J. Yasuda *et al.*, Phys. Rev. Lett. **121**, 132501 (2018).
6) L. Stuhl *et al.*, RIKEN Accel. Prog. Rep. **53**, 38 (2019).
7) T. Suzuki *et al.*, Nucl. Phys. A **662**, 282 (2000).

Analysis of ^{48}Cr(p,n) reaction in inverse kinematics

M. Sasano,[*1] J. Gao,[*1,*3] L. Stuhl,[*9,*22] Y. Hirai,[*4] T. Wakasa,[*4] D. S. Ahn,[*1] J. K. Ahn,[*13] H. Baba,[*1] K. Chae,[*20] A. Chilug,[*5,*1] K. Cook,[*15] Y. Fujino,[*7] N. Fukuda,[*1] B. Gao,[*19] S. Goto,[*4] I. S. Hahn,[*8,*22] Y. Hamano,[*4] Z. Halász,[*9] T. Harada,[*10,*1] S. Hong,[*20] S. Huang,[*1,*3] N. Inabe,[*1] D. Inomoto,[*4] T. Isobe,[*1] H. Kasahara,[*4] D. Kim,[*8] T. Kobayashi,[*14,*1] Y. Kondo,[*15,*1] Z. Korkulu,[*1] A. Krasznahorkai,[*9] H. Miki,[*15] K. Miki,[*14,*1] S. Mitsumoto,[*4] M. Miwa,[*18,*1] T. Motobayashi,[*1] T. Nakamura,[*15,*1] M. Nishimura,[*1] H. Oshiro,[*4] H. Otsu,[*1] V. Panin,[*1] S. Sakaguchi,[*4,*1] D. Sakai,[*14] H. Sakai,[*1] S. Sakaki,[*4] H. Sato,[*1] T. Shimada,[*15] Y. Shimizu,[*1] B. Sun,[*21] X. Sun,[*1,*3] H. Suzuki,[*1] J. Tanaka,[*1] Y. Togano,[*7,*1] T. Tomai,[*15,*1] T. Uesaka,[*1] Y. Utsuki,[*14] H. Wang,[*15] X. Xu,[*19] K. Yako,[*2] A. Yasuda,[*15] K. Yoneda,[*1] K. Yoshida,[*1] Y. Yoshitome,[*15] and J. Zenihiro[*1]

In this report, we present the progress of data analysis of the SAMURAI11 experiments performed at the RI Beam Factory of RIKEN Nishina Center in the spring of 2019. These experiments were conducted to measure the (p,n) reaction on $N = Z$ unstable nuclei, ^{48}Cr and ^{64}Ge. Previously, in Refs. 1) and 2), we reported the experimental setup and the particle identification (PID) analysis of the reaction residues using the SAMURAI spectrometer,[3] respectively. Herein, we present the analysis of the data recorded using the particle analyzer neutron detector of real-time acquisition (PANDORA)[4] system.

The PANDORA neutron detector setup consists of 37 plastic scintillators and was placed on the left and right sides of a liquid hydrogen target.[5] The neutron-gamma pulse-shape discrimination method was employed to separate low-energy neutrons from the gamma-ray background. The neutron kinetic energies were deduced employing the time-of-flight method, whereas the neutron scattering angles of the (p,n) reaction in the laboratory frame were determined from the scintillator bar positions.

Figure 1 shows the kinetic curve for the ^{48}Cr$(p,n)^{48}$Mn reaction. Here, the reaction residue ^{47}Cr was selected from the PID analysis. ^{47}Cr is produced via the proton emission from the excited states of ^{48}Mn populated by the (p,n) reaction. The proton separation energy of ^{48}Mn is 2.05 MeV. We successfully identify a locus along the curve corresponding to 4 MeV excitation energy of ^{48}Mn, above the separation energy. Figure 1 shows events due to the background in a low kinetic-energy region below 500 keV. A further analysis is ongoing to substract the background.

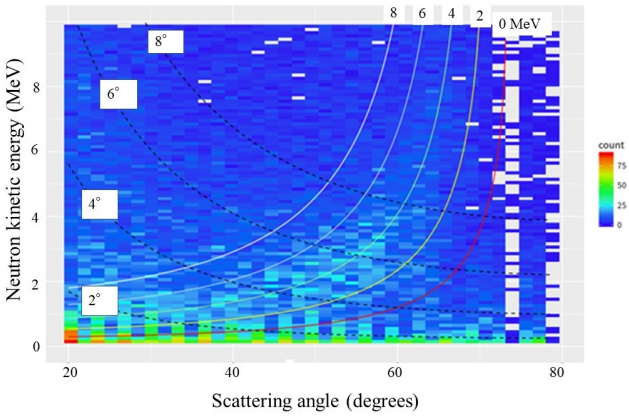

Fig. 1. Two-dimensional plot of neutron kinetic energy vs. neutron scattering angle in the laboratory frame. Solid and dashed curves represent the excitation energies and scattering angles in center-of-mass system of ^{48}Cr(p,n) reaction, respectively.

We are grateful to the RIKEN accelerator staff and the CNS, University of Tokyo, for their continuous efforts to accomplish this stable beam acceleration.

References

1) M. Sasano *et al.*, RIKEN Accel. Prog. Rep. **53**, 40 (2019).
2) J. Gao *et al.*, RIKEN Accel. Prog. Rep. **54**, 14 (2020).
3) T. Kobayashi *et al.*, Nucl. Instrum. Methods Phys. Res. B **317**, 294 (2013).
4) L. Stuhl *et al.*, Nucl. Instrum. Methods Phys. Res. A **866**, 164 (2017).
5) M. Miwa *et al.*, RIKEN Accel. Prog. Rep. **52**, 149 (2018).

*1 RIKEN Nishina Center
*2 Center for Nuclear Study, University of Tokyo
*3 School of Physics, Peking University
*4 Department of Physics, Kyushu University
*5 Horia Hulubei National Institute for R&D in Physics and Nuclear Engineering
*7 Department of Physics, Rikkyo University
*8 Department of Physics, Ewha Womans University
*9 Institute for Nuclear Research, Hungarian Academy of Sciences
*10 Department of Physics, Toho University
*11 KVI - CART, University of Groningen
*12 GSI Helmholtzzentrum für Schwerionenforschung
*13 Department of Physics, Korea University
*14 Department of Physics, Tohoku University
*15 Department of Physics, Tokyo Institute of Technology
*16 Department of Physics, University of Tokyo
*18 Department of Physics, Saitama University
*19 Institute of Modern Physics, Chinese Academy of Sciences
*20 Department of Physics, Sungkyunkwan University
*21 School of Physics and Nuclear Engineering, Beihang University
*22 Center for Exotic Nuclear Studies, Institute for Basic Science

Measurement of proton elastic scattering from ^{132}Sn at 300 MeV/nucleon in inverse kinematics

T. Harada,[*1,*2] J. Zenihiro,[*3,*2] Y. Matsuda,[*4,*2] S. Terashima,[*5,*2] H. Sakaguchi,[*6] N. Aoi,[*6,*2] H. Baba,[*2] M. Dozono,[*7] F. Endo,[*8,*2] S. Enyo,[*3] Y. Fujikawa,[*3] S. Hanai,[*7] S. Hayakawa,[*7] Y. Hijikata,[*3,*2] J. W. Hwang,[*7] N. Imai,[*7] K. Inaba,[*3] S. Ishida,[*4] T. Isobe,[*2] T. Kawabata,[*9,*2] S. Kiyotake,[*10] A. Kohda,[*6,*2] H. Kurosawa,[*4] R. Kojima,[*7] R. Maeda,[*4] Y. Maeda,[*10] S. Y. Matsumoto,[*3,*2] R. Matsumura,[*1,*2] B. Mauss,[*2] S. Michimasa,[*7] T. Murakami,[*3] D. Nishimura,[*11,*2] T. Nishimura,[*10] K. Nosaka,[*4] S. Ota,[*7] K. Sakanashi,[*3] H. Shimizu,[*7,*2] D. Suzuki,[*2] J. Tanaka,[*2] R. Tsunoda,[*7] T. Uesaka,[*2] and K. Yamamoto[*4]

We report on the progress of data analysis of the RIBF79 experiment performed at the RI Beam Factory of RIKEN Nishina Center in 2019. In this experiment, inverse kinematics proton elastic scattering measurements were performed using a high-intensity beam of ^{132}Sn at approximately 600 kcps. The double magic nucleus ^{132}Sn has a larger isospin asymmetry than ^{208}Pb. Therefore,^{132}Sn is expected to have a larger neutron skin thickness, which is defined as the difference between the neutron and proton root-mean-square radii. Furthermore, ^{132}Sn is a flagship nucleus of the equation of state of nuclear matter study. The goal of this experiment is to extract the neutron density distribution of ^{132}Sn from the inverse kinematics proton elastic scattering of ^{132}Sn.

In the previous reports,[1,2] we discussed particle identification for beam particles and the experimental setup. Herein, we report on the analysis of the recoil proton spectrometer (RPS). RPS consists of a 1-mm-thick solid hydrogen target,[3] two multi-wire drift chambers, two plastic scintillators, and fourteen NaI(Tl) calorimeters. The recoil angle and kinetic energy of recoil protons were measured using RPS. By using missing mass spectroscopy, the excitation energy spectrum of ^{132}Sn was obtained. Figure 1 shows the scattering angle distribution spectrum when elastic scattering is selected from the excitation energy obtained. The pattern of increase and decrease corresponding to the interference is clearly visible. Above 80°, the kinetic energy of the recoil protons was low and could not be detected by NaI calorimeters. Figure 2 shows the excitation energy spectrum of the proton scattering from ^{132}Sn in the recoil angle 78°–79°. Data analysis for determining the angular distribution of the cross sections and the density distribution of ^{132}Sn is now in progress.

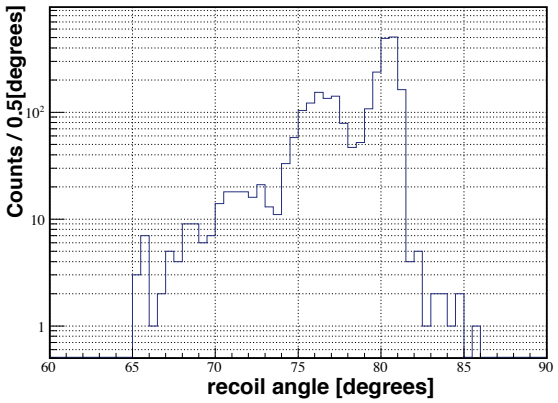

Fig. 1. Angular distribution spectrum for selected elastic scattering events using NaI(TI) calorimeters.

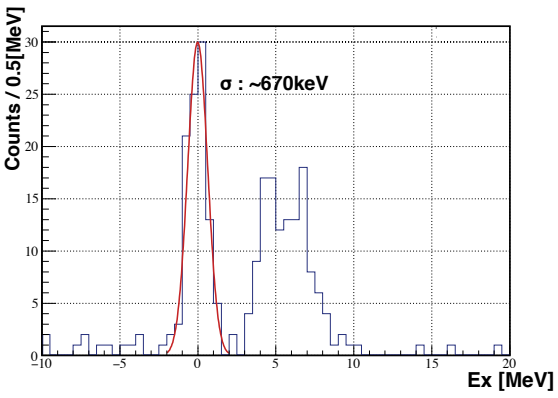

Fig. 2. Excitation energy spectrum of ^{132}Sn at recoil angles in the range of 78°–79°.

References
1) J. Zenihiro *et al.*, RIKEN Accel. Prog. Rep. **53**, 44 (2019).
2) T. Harada *et al.*, RIKEN Accel. Prog. Rep. **54**, 18 (2020).
3) Y. Matsuda *et al.*, Nucl. Instrum. Methods Phys. Res. A **643**, 6 (2011).

*1 Department of Physics, Toho University
*2 RIKEN Nishina Center
*3 Department of Physics, Kyoto University
*4 Cyclotron and Radioisotope Center, Tohoku University
*5 School of Physics, Beihang University
*6 Research Center for Nuclear Physics, Osaka University
*7 Center for Nuclear Study, University of Tokyo
*8 Department of Physics, Tohoku University
*9 Department of Physics, Osaka University
*10 Department of Applied Physics, Miyazaki University
*11 Department of Natural Sciences, Tokyo City University

Commissioning study of SCRIT facility with ^{138}Ba nucleus

K. Tsukada,[*1,*2] Y. Abe,[*2] A. Enokizono,[*2] T. Goke,[*3] Y. Honda,[*2,*3] Y. Ito,[*1] K. Kurita,[*4] Y. Maehara,[*1] T. Ohnishi,[*2] R. Ogawara,[*1,*2] T. Suda,[*2,*3] M. Watanabe,[*2] M. Wakasugi,[*1,*2] and H. Wauke[*2,*3]

The Self-Confining RI Ion Target (SCRIT) electron scattering facility was constructed to realize electron scattering experiments for short-lived unstable nuclei.[1] SCRIT uses a novel technique to achieve a luminosity of 10^{27} cm^{-2}s^{-1}, which is sufficient to perform elastic electron scattering experiments by trapping a small number of target ions, typically 10^{8} particles/pulse, along the electron beam.

In 2021, we performed electron scattering from ^{138}Ba for two electron beam energies, 150 and 300 MeV, as a commissioning experiment. ^{138}Ba is stable, and its charge density distribution is known.[2] This is the first time experiment with the gas target trapped in the SCRIT since the present SCRIT device was installed in 2020, and a drift chamber of the electron spectrometer was replaced with a new one in 2018. The present SCRIT device has a larger cross-section and less material around the trapping region, and it provides much better uniformity of the electric potential compared to the previous device. The present drift chamber in front of the spectrometer magnet provides both vertical and horizontal information of the trajectories of scattered electrons, whereas the previous one provided only horizontal information.

The data for 150 MeV is analyzed in this report. The beam current was 250 mA at the beginning of the data acquisition and dropped to 150 mA at the end. The achieved luminosity was approximately 1×10^{27} cm^{-2}s^{-1} on average.

Figure 1 shows the reconstructed vertex-point distribution along the beam line after the spectrometer acceptance correction. It is found that the target length in the SCRIT device is about 300 mm and the distribution is almost flat. Compared to the previous data,[3] the apparent bump structure caused by the distortion of the electric potential disappears, which makes the data easier to analyze and interpret.

Figure 2 shows the yield distribution after the acceptance correction and background subtraction. The solid line represents a calculation using a phase-shift calculation code, DREPHA,[4] with the charge-density distribution of ^{138}Ba.[2] The distribution of our data is well reproduced by the calculation, except for the foremost point, which corresponds to the end of the acceptance.

In summary, the target ions are trapped in the present SCRIT device almost uniformly as expected,

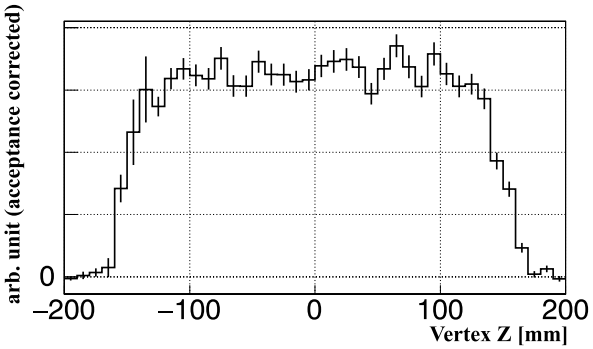

Fig. 1. Reconstructed vertex-point distribution along the beam line after acceptance correction.

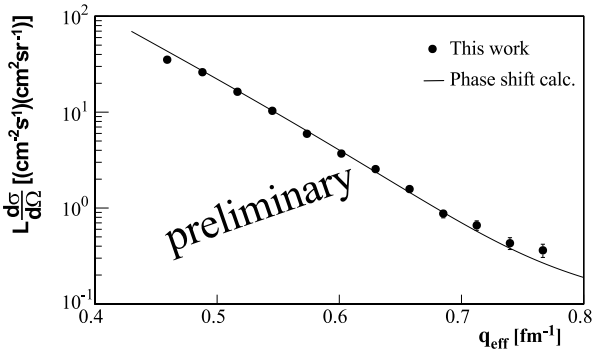

Fig. 2. Yield distribution with varying effective momentum transfer after acceptance corrections. The solid line is a phase-shift calculation obtained using a charge-density distribution of ^{138}Ba.[2]

and the angular distribution is well reproduced by our spectrometer. We are almost ready and will soon start the world's first electron scattering experiment with an unstable nuclear target.

References

1) M. Wakasugi *et al.*, Nucl. Instrum. Methods Phys. Res. **317**, 357 (2013).
2) H. de Vries *et al.*, At. Data Nulc. Data Table **36**, 495 (1987).
3) K. Tsukada *et al.*, Phys. Rev. Lett. **118**, 262501 (2017).
4) B. Drepher, A phase-shift calculation code for elastic electron scattering (private communication with J. Friedrich).

*1 Institute for Chemical Research, Kyoto University
*2 RIKEN Nishina Center
*3 Research Center for Electron-Photon Science, Tohoku University
*4 Department of Physics, Rikkyo University

Yield measurements for ^{86}Kr + ^{198}Pt at KISS

Y. X. Watanabe,[*1] Y. Hirayama,[*1] M. Mukai,[*2] T. Niwase,[*1] P. Schury,[*1] M. Rosenbusch,[*1] M. Wada,[*1] H. Miyatake,[*1] S. C. Jeong,[*1] S. Iimura,[*2,*3] M. Oyaizu,[*1] and A. Taniguchi[*4]

We have been developing the KEK Isotope Separation System (KISS) for spectroscopic studies of neutron-rich nuclei around $N = 126$. These neutron-rich nuclei are considered to be efficiently produced by multinucleon transfer reactions with the target nucleus ^{198}Pt. We have successfully extracted and performed nuclear spectroscopy for neutron-rich nuclei, such as $^{199–201}$Pt, $^{196–200}$Ir, and $^{193–198}$Os using the ^{136}Xe beam.[1] The yield development is essential for KISS to expand the research region toward $N = 126$. We attempted to use the ^{238}U beam, with which the GRAZING calculations[2] predict more production yields. However, we observed that the growth of the extraction yields slows down at an intensity of approximately 30 particle nA in contrast to 50 particle nA for the ^{136}Xe beam. Furthermore, the yields for various extracted isotopes were approximately ten times smaller than those with the ^{136}Xe beam.[3]

The reaction products are first thermalized and neutralized in the argon gas filled in a gas cell at KISS. They are transported via a laminar gas flow and are irradiated using lasers to be element-selectively ionized using the laser resonance ionization technique immediately before they exit the gas-cell orifice. These ions are transported by several RF ion guides and are accelerated with a high voltage of 20 kV to be transmitted to measurement areas. The reduction of the extraction yields for the ^{238}U beam may be attributed to the reneutralization of the laser-ionized isotopes by free electrons generated via radiation from more dense plasma in the gas induced by the elastic scattering of heavier beams. We have performed yield measurements using the ^{86}Kr beam to study the systematics of the extraction yields among different types of beams for the origin of the yield reduction with the ^{238}U beam.

The ^{86}Kr beam with an energy of 10.75 MeV/nucleon from the RRC was decelerated using three 5-μm titanium foils and impinged on a ^{198}Pt target with a thickness of 12.5 mg/cm^2 at an energy of 8.8 MeV/nucleon. Radioactive nuclei ^{199,200,202}Pt, $^{196–198}$Ir, and ^{195,196}Os were extracted. They were identified by measuring their lifetimes at the β-decay station or their masses using the MRTOF-MS. The top panel of Fig. 1 shows the beam intensity dependence of the extraction rates of ^{199}Pt for the ^{86}Kr, ^{136}Xe, and ^{238}U beams. The energies of the ^{136}Xe and ^{238}U beams are 9.4 and 8.9 MeV/nucleon, respectively. The rates for the ^{136}Xe beam are scaled by 0.3. The growth of the rates for the ^{86}Kr beam slows down at an intensity of approximately 80 particle nA, which is 30 particle nA larger than that of the ^{136}Xe beam. However, the extraction rates for the ^{86}Kr beam are smaller than those for the ^{136}Xe beam. The bottom panel shows a comparison of extraction rates for various radioactive isotopes for the ^{86}Kr (80 particle nA), ^{136}Xe (50 particle nA), and ^{238}U (26 and 36 particle nA) beams. The extraction yields of ^{196,197}Ir and ^{195,196}Os are comparable for the ^{86}Kr and ^{136}Xe beams. The extraction yields of ^{199,200}Pt and ^{198}Ir for the ^{86}Kr beam are smaller than those for the ^{136}Xe beam; however, the reduction is smaller than that for the ^{238}U beam for ^{199}Pt. The comparison of the extraction rates for various isotopes does not indicate any significant increase in the extraction efficiency using the lighter beam than ^{136}Xe. Further investigation including the gas-cell design, in-gas-jet ionization, and helium gas cell will be conducted to increase the extraction yields at KISS.

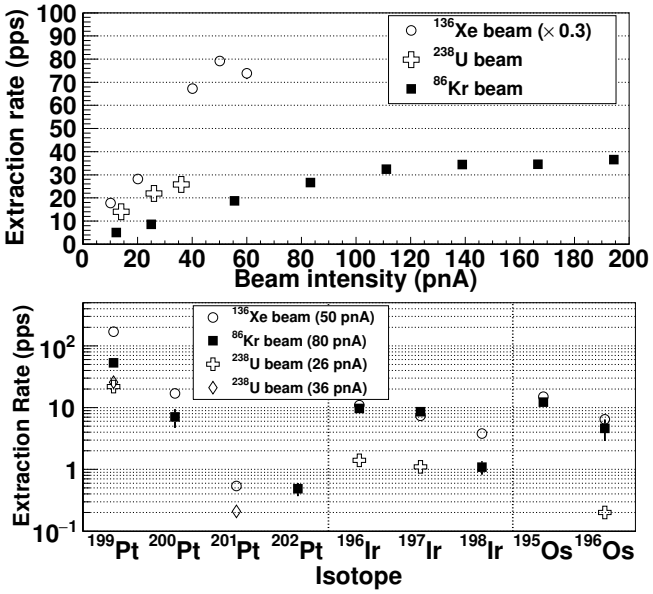

Fig. 1. (Top) Beam intensity dependence of the extraction rates of ^{199}Pt for the ^{86}Kr (squares), ^{136}Xe (circles), and ^{238}U (crosses) beams. The rates for ^{136}Xe (circles) are scaled by 0.3. (Bottom) Extraction rates of various isotopes for the ^{86}Kr (squares), ^{136}Xe (circles), and ^{238}U (crosses and diamonds) beams.

*1 Wako Nuclear Science Center (WNSC), IPNS, KEK
*2 RIKEN Nishina Center
*3 Department of Physics, Osaka University
*4 Institute for Integrated Radiation and Nuclear Science, Kyoto University

References
1) Y. Hirayama *et al.*, Nucl. Instrum. Methods Phys. Res. B **463**, 425 (2020).
2) A. Winther, Nucl. Phys. A **572**, 191 (1994); Nucl. Phys. A **594**, 203 (1995).
3) Y. X. Watanabe *et al.*, RIKEN Accel. Prog. Rep. **51**, 71 (2018).

In-gas-cell laser ionization spectroscopy of ^{200g}Pt using MRTOF-MS at KISS

Y. Hirayama,[*1] M. Mukai,[*2] Y. X. Watanabe,[*1] P. Schury,[*1] J. Y. Moon,[*3] T. Hashimoto,[*3] S. Iimura,[*2] S. C. Jeong,[*1] M. Rosenbusch,[*1] M. Oyaizu,[*1] T. Niwase,[*1] M. Tajima,[*2] A. Taniguchi,[*4] M. Wada,[*1] and H. Miyatake[*1]

Laser spectroscopy can be used to effectively investigate the nuclear structure througth the measured isotope shifts (IS) $\Delta\nu$, changes in the mean-square charge radii $\delta\langle r^2\rangle$, and quadrupole deformation parameters $|\langle\beta_2^2\rangle|^{1/2}$. In previous work[1] related to ^{199g,199m}Pt at the KEK Isotope Separation System (KISS),[2] we reported the constant trend of $|\langle\beta_2^2\rangle|^{1/2} \sim 0.14$ ($N \geq 115$) approaching $N = 126$ deduced from the measured $\delta\langle r^2\rangle$ values using a droplet model. As a continuation of this work followed by ^{199g,199m}Pt laser ionization spectroscopy toward $N = 126$ to investigate the trend of $\delta\langle r^2\rangle$ and $|\langle\beta_2^2\rangle|^{1/2}$ values and the nuclear structure of neutron-rich platinum nuclei, we performed the first laser ionization spectroscopy on ^{200}Pt ($I^\pi = 0^+$ and $T_{1/2} = 12.6(3)$ h) using a multi-reflection time-of-flight mass spectrograph (MRTOF-MS) at KISS.

^{200g}Pt isotopes were produced via multi-nucleon transfer reactions by impinging a stable ^{136}Xe beam (50 particle nA) with an energy of approximately 10 MeV/nucleon on a ^{198}Pt target (12.5 mg/cm^2, enriched 91% and approximately 3% for each ^{194,195,196}Pt). The singly charged isotopes, produced by the in-gas-cell laser ionization technique, with an energy of 20 keV were extracted from the KISS gas cell for hyperfine structure measurements. Using the MRTOF-MS, the extracted ions were identified and the number of the ions was determined. Futher details regarding the MRTOF-MS system can be found in Ref. 3).

Figure 1 shows the measured TOF spectrum of ^{200g}Pt^{2+} using the MRTOF-MS at KISS. The ^{200g}Pt^{2+} isotope can be clearly identified with the contaminant peaks of ^{200g}Au^{2+} and ^{200m}Au^{2+} ions ("g" and "m" indicate the ground and isomeric states, respectively), which were transported to the MRTOF-MS as the survived ions. The masses of these nuclei have already been precisely reported. To acculately evaluate the laser resonance spectrum of ^{200g}Pt, we gated the relative time between 200 and 500 ns in Fig. 1 to deduce the number of ions detected by the MRTOF-MS. The laser resonance spectrum, shown in Fig. 2, was obtained by measuring the number of laser-ionized ^{200g}Pt as a function of the laser wavelength. One resonance peak was observed, which stemmed from the atomic transition of ^{200g}Pt due to $I^\pi = 0^+$. The fitting function was determined from the measured resonance spectrum of the stable nucleus of ^{198}Pt with the same experimental conditions during beam time. From the measured peak position, we can determine the isotope shift value of ^{200g}Pt to deduce the change in charge radius and discuss nuclear deformation. Using these results, we plan to investigate the systematic trend of IS values toward $N = 126$.

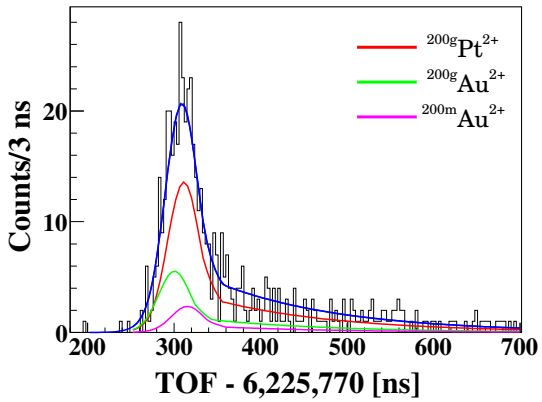

Fig. 1. Measured TOF spectrum of ^{200g}Pt^{2+}.

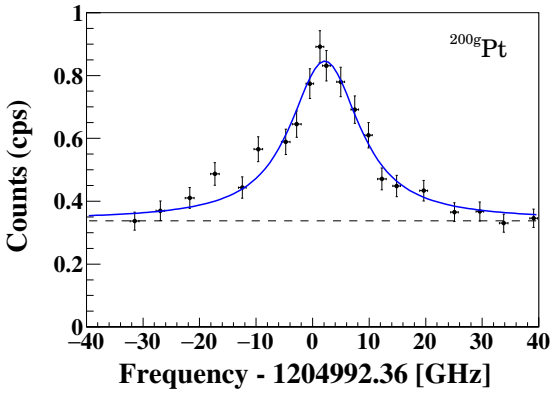

Fig. 2. Measured HFS spectrum of ^{200g}Pt ($I^\pi = 0^+$). Horizontal uncertainty estimated from the accuracy of a wavemeter.

[*1] Wako Nuclear Science Center (WNSC), Institute of Particle and Nuclear Studies (IPNS), High Energy Accelerator Research Organization (KEK)
[*2] RIKEN Nishina Center
[*3] Institute for Basic Science (IBS)
[*4] Institute for Integrated Radiation and Nuclear Science, Kyoto University (KURNS)

References

1) Y. Hirayama *et al.*, Phys. Rev. C **96**, 055805 (2017).
2) Y. Hirayama *et al.*, Nucl. Instrum. Methods Phys. Res. B **412**, 11 (2017).
3) J. Y. Moon *et al.*, RIKEN Accel. Prog. Rep. **53**, 128 (2019).

Isomer spectroscopy using multi-nucleon transfer reaction on ^{248}Cm

S. Go,[*1,*2,*3] R. Orlandi,[*4] T. Niwase,[*5,*3] K. Sugiyama,[*1] T. Tomimatsu,[*1] T. Kai,[*1] K. Hirose,[*4] E. Ideguchi,[*6,*3] Y. Ishibashi,[*1] Y. Ito,[*4] H. Makii,[*4] S. Matsunaga,[*1] K. Morita,[*1,*3] D. Nagae,[*2,*3] Y. Nagata,[*1] H. Nishibata,[*1,*3] K. Nishio,[*4] T. T. Pham,[*6] S. Sakaguchi,[*1,*3] T. K. Sato,[*4] T. Shizuma,[*7] F. Suzaki,[*4] K. Tsukada,[*4] K. Washiyama,[*2] and M. Asai[*4,*2]

The Island of Stability, which is linked to the predicted doubly closed proton and neutron shells in superheavy nuclei, is still an unexplored region in nuclear physics. Owing to low expected cross sections with current experimental techniques, the region has not been accessible for detailed decay studies. Excited states in actinide nuclei can have an important role in characterizing the stability of the island, as part of degenerate orbitals above predicted energy gaps at $Z = 114$ and $N = 184$ can appear as excited states owing to the systematic development of quadrupole deformation. Pioneering studies[1,2] identified a large component of high-j quasiparticle states originating from the $\nu k_{17/2}$ orbital above the gap in ^{249}Cm. Thus, data around this region can provide benchmarks for theoretical calculations of the location and properties of the Island of Stability.

One method to study the region of heavy actinides is to produce them via the transfer reactions of heavy ions onto radioactive actinide targets. The difficulty of using actinide targets lies in their strong radioactivity. An experimental method, called the isomer-scope method,[3] is one of measurements to avoid this problem with the space-time separation. This method was originally developed at JAEA to investigate isomeric states via deep inelastic collisions. The combination of γ-ray detectors and absorbers significantly enhanced the peak-to-background ratio of the delayed γ-ray component. We applied this method to perform isomer spectroscopy of nuclei produced via multi-nucleon transfer reactions on actinide targets.

The experiment was performed at the JAEA tandem accelerator facility in May 2021. An actinide target of ^{248}Cm was prepared via electrodeposition onto a 1.8 μm aluminium backing. The target was irradiated using a ^{18}O beam with an energy of 96.5 MeV with an intensity of approximately 2.0 particle nA. The beam energy was set to detect the light ejectiles identified at backward angles. The produced nuclei were identified via specific transfer channels using an array of ΔE-E telescopes. The selection of the beam energy enabled us to place the telescope at the backward angles, which effectively reduced the radiation damage on the silicon detectors. An ejectile passing through one of the four ΔE detectors (20 μm thick) was stopped in the E detector (300 μm thick) to measure the residual energy. Heavier nuclei were scattered in the forward direction and stopped in a catcher foil. Four germanium and four $LaBr_3$ detectors were placed close to the foil to detect the delayed γ rays. A tungsten shield was placed between the target and γ-ray detectors to absorb the strong γ-radiation around the target.

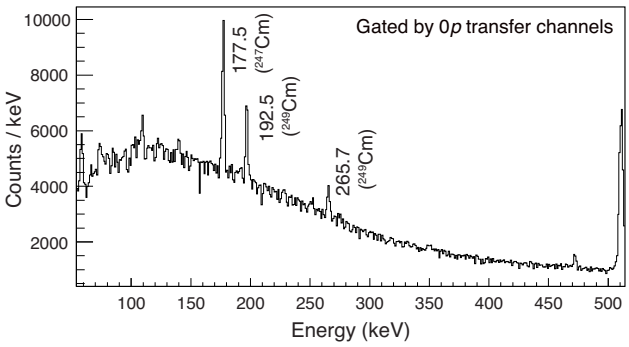

Fig. 1. Delayed γ-ray spectrum gated using $0p$ transfer channels by the ΔE-E silicon telescope. The 177.5- and 265.7-keV peaks resulted from the isomeric state of ^{247}Cm with a half-life of 100.6 ns.[4] The 192.5- and 265.7-keV peaks resulted from the isomeric state of ^{249}Cm with 19-ns half-life.[2]

Several known isomers belonging to nuclei in the region of ^{248}Cm were successfully observed in this study. An example of the delayed γ-ray spectrum is shown in Fig. 1. The 178-keV peak correspond to the γ-ray transition from the isomeric state of ^{247}Cm.[4] The half-life value deduced by the preliminary analysis agreed well with the literature value of 100.6 ns.[4] The 192.5- and 265.7-keV peaks corresponded to transitions from an isomeric state in ^{249}Cm.[2] This short-lived 19-ns isomer was successfully identified in this experimental setup. Further analysis to identify new isomeric states is in progress.

*1 Department of Physics, Kyushu University
*2 Research Center for Superheavy Elements, Kyushu University
*3 RIKEN Nishina Center
*4 Advanced Science Research Center, Japan Atomic Energy Agency
*5 Wako Nuclear Science Center (WNSC), IPNS, KEK
*6 Research Center for Nuclear Physics, Osaka University
*7 Tokai Quantum Beam Science Center, National Institute for Quantum Science and Technology

References

1) I. Ahmad *et al.*, Nucl. Phys. A **646**, 175 (1999).
2) T. Ishii *et al.*, Phys. Rev. C **78**, 054309 (2008).
3) T. Ishii *et al.*, Nucl. Instrum. Methods Phys. Res. A **395**, 210 (1997).
4) I. Ahmad *et al.*, Phys. Rev. C **68**, 044306 (2003).

Proton entropy excess and possible signature of pairing reentrance in hot nuclei†

B. Dey,[*1] S. Bhattacharya,[*2] D. Pandit,[*3,*4] N. D. Dang,[*5] N. N. Anh,[*6] L. T. Phuc,[*7,*8] and N. Q. Hung[*7,*8]

We conducted a systematic study to understand the proton entropy excess ΔS_p obtained for different pairs of odd-even and odd-odd nuclei ranging from $A = 90$ to 238 (^{90}Y and ^{91}Zr, ^{196}Pt and ^{197}Au, ^{211}Po and ^{212}At, ^{231}Th and ^{232}Pa, ^{237}U and ^{238}Np). The proton entropy excess determined from the existing experimental nuclear level density (NLD) data was compared with the microscopic calculation obtained within the exact pairing plus independent particle model (EP+IPM). The latter has predicted an enhanced peak of ΔS_p at an excitation energy $E^* \simeq 1$ MeV in near spherical nuclei (^{90}Y and ^{91}Zr, ^{211}Po and ^{212}At), indicating a possible signature of pairing reentrance in hot nuclei. In the cases under consideration, pairing reentrance occurs because of the weakening of the blocking effect caused by the odd nucleon in odd nuclei. As a result, the pairing gap of odd nuclei, which is finite at $T = 0$, slightly increases at low $T \neq 0$, and decreases as T increases further, as explained in Ref. 1).

We found that the experimental value of ΔS_p as a function of E^* exhibits a strong fluctuation at $E^* < 1$ MeV and reaches saturation at high $E^* > 3$–6 MeV. The analysis using the microscopic EP+IPM calculations shows that the proton entropy excess is approximately 0.1–0.5 k_B for spherical systems and approximately 1.0–1.2 k_B for the deformed ones, which is in good agreement with the experimental data, as shown in Figs. 1(a) and 1(b). These values of proton entropy excess are smaller than the neutron ones owing to the effect of the Coulomb interaction and proton single-particle level density, which is less than the the neutron one. Moreover, the peak-like structure, which is seen in the proton entropy excess obtained within the EP+IPM at low energy $E^* < 1$ MeV, is explained by the pairing reentrance phenomenon caused by the weakening of the blocking effect of an odd nucleon [See Figs. 1(c) and 1(d)].

This peak-like structure is found to be more pronounced in the spherical systems than in the deformed ones because the pairing reentrance is stronger in spherical nuclei than in deformed ones. However, this theoretical peak-like structure is not well supported by the experimental observation owing to the strong fluctuations in the measured data. Therefore, more precise and direct experimental measurements in the low-energy region ($E^* < 1$ MeV) are required in order to confirm our theoretical predictions.

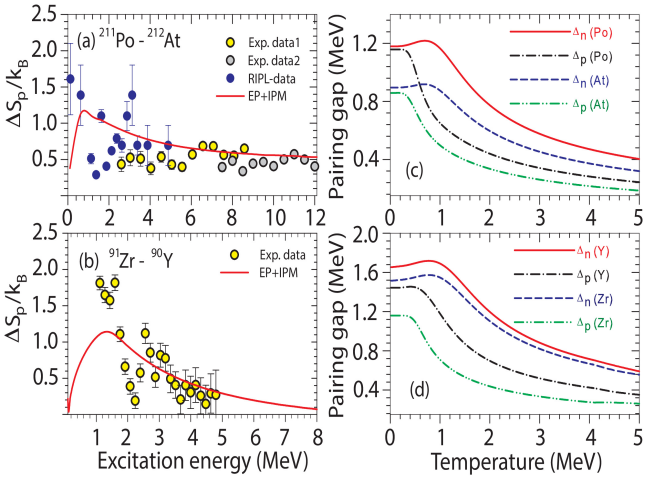

Fig. 1. [(a) and (b)] Proton entropy excesses ΔS_p as functions of excitation energy E^* along with the results of EP+IPM calculations for ^{211}Po–^{212}At and ^{90}Y–^{91}Zr. [(c) and (d)] Exact proton Δ_p and neutron Δ_n pairing gaps as functions of temperature T for different nuclei. Exp. data1 and Exp. data2 in (a) are obtained by using the associated NLD data from Refs. 2) and 3), respectively, whereas RIPL-data are calculated by using the low-energy data taken from RIPL-3[4] averaged over the angular-momentum distribution as in Ref. 2). Exp. data in (b) are obtained by using the NLD data from Refs. 5) and, 6).

References
1) N. Q. Hung *et al.*, Phys. Rev. C **94**, 024341 (2016).
2) B. Dey *et al.*, Phys. Lett. B **789**, 634 (2019).
3) P. Roy *et al.*, Phys. Rev. C **94**, 064607 (2016).
4) `www-nds.iaea.org/RIPL-3/`.
5) M. Guttormsen *et al.*, Phys. Rev. C **90**, 044309 (2014).
6) M. Guttormsen *et al.*, Phys. Rev. C **96**, 024313 (2017).

† Condensed from the article in Phys. Lett. B **819**, 136445 (2021)
*1 Department of Physics, Bankura University
*2 Department of Physics, Barasat Government College
*3 Variable Energy Cyclotron Centre
*4 Homi Bhabha National Institute
*5 RIKEN Nishina Center
*6 Dalat Nuclear Research Institute
*7 Institute of Fundamental and Applied Sciences, Duy Tan University
*8 Faculty of Natural Sciences, Duy Tan University

The ONOKORO project—Toward comprehensive understanding on clustering in heavy nuclei

T. Uesaka,[*1] J. Zenihiro,[*2,*1] K. Ogata,[*3] J. Tanaka,[*1] R. Tsuji,[*2,*1] Y. Hijikata,[*2,*1] K. Higuchi,[*1,*4] S. Takeshige,[*1,*5] K. Yahiro,[*2] S. Kurosawa,[*6] K. Yoshida,[*7] Y. Chazono,[*3] M. Takano,[*8] S. Typel,[*9] and H. Baba[*1] for the ONOKORO Collaboration

A new research project, "ONOKORO project," has started to investigate clustering in heavy nuclei using cluster knockout reactions. Do nuclear systems, in general, have an inherent orientation that breaks uniformity? In this research, we try to answer this question by studying formation mechanisms of deuteron, triton, ^{3}He, and α clusters in stable and unstable nuclei in a wide mass range.

Since early days of nuclear physics, α cluster in nuclei have been discussed, first to explain α decays of heavy nuclei, while clustering is now mainly discussed for light nuclei with masses lighter than 30. On the other hand, there are significant progress in theories of cluster formation in infinite nuclear matter.[1,2] Important predictions of the theories are that clusters develop significantly in the low-density region below 1/10 of the saturation density, and the cluster abundances change significantly with the neutron-proton asymmetry. Typel predicted also such a phenomenon would also occur in the low-density surface of heavy nuclei.[3] Our previous experiment for the $^{112-124}$Sn$(p,p\alpha)$ reaction has confirmed Typel's prediction and has demonstrated the existence of α clusters in those nuclei.[4]

The ONOKORO project will extend the scope to all the light clusters of d, t, ^{3}He, α in stable and unstable nuclei from calcium ($Z = 20$) to heavy nuclei beyond lead ($Z = 82$). The (p,pX) cluster knockout reactions, where X denotes d, t, ^{3}He or α, are used to extract information of clusters in nuclei. Characteristic points of the ONOKORO project are:

- d, t, ^{3}He, α clusters are studied on the same footing
- Both stable and unstable nuclei are covered
- Normal and inverse kinematics experiments are combined

Simultaneous studies of d, t, ^{3}He, α are essentially important because the different clusters would manifest different aspects of clustering depending on its spin and isospin. As is discussed in Refs. 2) and 3), dependence on neutron excess is essential in studies of clustering in heavy finite nuclei and in nuclear matter, and thus the access to unstable nuclei is the core of the project.

In order to cover both stable and unstable nuclei, we will perform experiments at intermediate-energy accelerator facilities in Japan, the RIKEN RIBF, the QST HIMAC, and the Osaka University RCNP cyclotron facility. At RCNP, knockout reaction experiments under normal kinematics for stable nuclear targets are conducted using proton beams and double-arm magnetic spectrometers, Grand Raiden and LAS, to obtain high energy-resolution data. State-by-state separation of the final states enabled by the high resolution is a unique capability in experiments at RCNP. At RIBF and HIMAC, inverse-kinematics experiments will be carried out using unstable and stable heavy-ion beams, respectively. The inverse kinematics experiment has the advantage of covering a broad kinematic region and simultaneous measurements for all clusters of d, t, ^{3}He, α.

In this project, we will construct a detector array, TOGAXSI,[5] designed specifically for inverse kinematics knockout reaction experiments. The array consists of 100-μm pitch silicon strip detectors and GAGG:Ce scintillators. GAGG:Ce scintillators have a good time response of 1 ns rise time and <100 ns decay time. Another good feature of GAGG:Ce is no hygroscopic nature.

The cluster knockout reaction theory based on the impulse approximation will be refined to derive the cluster abundance from the experimental cross sections accurately. In particular, a theory that treats the breakup effect, which is essential in the knockout reaction of weakly-bound deuterons, will be developed using the continuum-discretized coupled-channel method.[6]

By comparing the cluster abundance obtained from the experimental data and the reaction theory with the nuclear structure and nuclear matter theories, we will verify the hypothesis of cluster formation in nuclear matter and clarify the mechanism of cluster formation.

*1 RIKEN Nishina Center
*2 Department of Physics, Kyoto University
*3 Research Center for Nuclear Physics, Osaka University
*4 Department of Physics, Toho University
*5 Department of Physics, Rikkyo University
*6 Institute for Materials Research, Tohoku University
*7 Advanced Science Research Center, Japan Atomic Energy Agency
*8 Department of Physics, Waseda University
*9 Institut für Kernphysik, Technisch Universität Darmstadt

References

1) S. Typel *et al.*, Phys. Rev. C **81**, 015803 (2010).
2) Z. -W. Zhang, L. -W. Chen, Phys. Rev. C **95**, 064330 (2017).
3) S. Typel, Phys. Rev. C **89**, 064321 (2014).
4) J. Tanaka *et al.*, Science **371**, 260 (2021).
5) T. Uesaka *et al.*, RIBF Construction proposal NP2112-SAMURAI72.
6) Y. Chazono *et al.*, in this report.

2. Nuclear Physics (Theory)

Practical method for decomposing discretized breakup cross sections into components of each channel†

S. Watanabe,[*1,*2] K. Ogata,[*3,*4,*5] and T. Matsumoto[*6]

The continuum-discretized coupled-channel method (CDCC)[1] is one of the most powerful tools for describing breakup reactions. In the 1980s, three-body CDCC was first applied to d scattering by assuming the $n+p+T$ three-body model, where T denotes a target. Three-body CDCC has been successful in describing many kinds of three-body reactions. Nowadays, three-body CDCC has been developed mainly in two directions. One is four-body CDCC[2] and the other is three-body CDCC with core excitation.[3] These methods address breakup reactions including multi-breakup channels. For example, for ^{6}Li scattering in the four-body model ($n+p+\alpha+T$), the four-body channel ($^6\mathrm{Li}+T \to n+p+\alpha+T$) and the three-body channel ($^6\mathrm{Li}+T \to d+\alpha+T$) coexist and couple each other during scattering. In CDCC, these breakup channels are precisely considered on an equal footing. However, the corresponding breakup cross sections (BUXs) are obtained as an admixture of these channels owing to the discretization in the calculations. In this work, we propose a practical method for decomposing discretized BUXs into components of each channel. This method is referred to as the "probability separation (P separation)."

Before going to four-body scattering, we first consider $^{11}\mathrm{Be}+T$ scattering in the three-body model with core excitation ($^{10}\mathrm{Be}+n+T$) because this scattering provides an analogy regarding the mixture of different channels as

$$^{11}\mathrm{Be}+T \to ^{10}\mathrm{Be(g.s.)}+n+T \quad \text{(core-ground channel)},$$
$$^{11}\mathrm{Be}+T \to ^{10}\mathrm{Be}^*+n+T \quad \text{(core-excited channel)},$$

where g.s. represents the ground state. This scattering has an advantage in that it allows us to easily obtain each channel's exact breakup wave functions for the ^{11}Be two-body projectile, unlike the ^{6}Li three-body projectile. In the actual analysis,the BUXs are calculated using extended distorted-wave Born approximation (xDWBA)[4] with the particle-rotor model. The xDWBA enables us to calculate both the *exact* (continuous) and the *approximate* (discretized) T-matrix elements. Then, we can compare the approximate BUXs with the exact ones quantitatively. In this report, we show only the validity of the P separation.

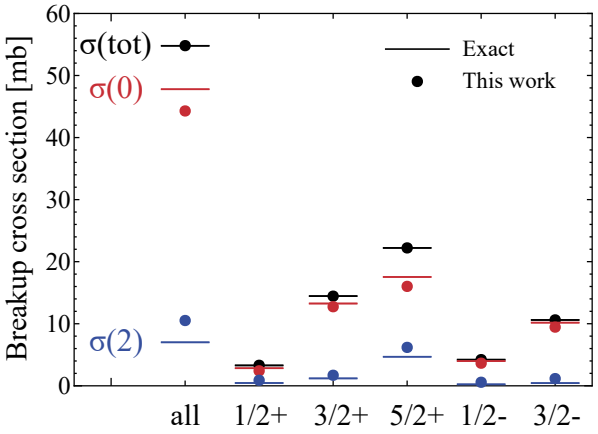

Fig. 1. Decomposition of the breakup cross sections for the scattering of $^{11}\mathrm{Be}+p$ at 63.7 MeV/nucleon. The solid lines represent the exact BUXs (σ), whereas the solid circles correspond to the approximate BUXs ($\hat{\sigma}$).

Figure 1 shows the decomposition of the breakup cross sections. The spin-parities $J^\pi = 1/2^+$, $3/2^+$, $5/2^+$, $1/2^-$, and $3/2^-$ are considered for ^{11}Be. First, the discretized total BUX $\hat{\sigma}(\mathrm{tot})$ is compared with the exact BUX $\sigma(\mathrm{tot})$. For the total breakup cross sections), $\hat{\sigma}(\mathrm{tot}) = \sigma(\mathrm{tot})$ is satisfied, which suggests that the model space is sufficiently large for calculating the BUX. Next, the discretized BUX is decomposed into the core-ground and the core-excited BUXs with the P separation. The total [σ(tot)], core-ground [$\sigma(0)$], and core-excited [$\sigma(2)$] BUXs are shown from top to bottom. The approximate BUXs are in good agreement with the corresponding exact ones for each spin parity. Thus, the P separation is found to work for the discretized BUX.

The P separation has an advantage that it is easily applied to four-body scattering for which the exact breakup wave functions for the three-body projectile are difficult to obtain. The systematic analysis for the validation and the application to four-body CDCC are presented in the original paper.†

† Condensed from the article in Phys. Rev. C **103**, L031601 (2021)

*1 National Institute of Technology, Gifu College
*2 RIKEN Nishina Center
*3 Research Center for Nuclear Physics, Osaka University
*4 Department of Physics, Graduate School of Science, Osaka City University
*5 Nambu Yoichiro Institute of Theoretical and Experimental Physics (NITEP), Osaka Metropolitan University
*6 Department of Physics, Kyushu University

References

1) M. Kamimura *et al.*, Prog. Theor. Phys. Suppl. **89**, 1 (1986).
2) T. Matsumoto *et al.*, Phys. Rev. C **70**, 061601(R) (2004).
3) R. de Diego *et al.*, Phys. Rev. C **89**, 064609 (2014).
4) A. M. Moro, R. Crespo, Phys. Rev. C **85**, 054613 (2012).

Effects of the Skyrme tensor force on 0^+, 2^+, and 3^- states in ^{16}O and ^{40}Ca nuclei with second random phase approximation†

M. J. Yang,[*1] C. L. Bai,[*1] H. Sagawa,[*2] and H. Q. Zhang[*3]

The effects of Skyrme tensor force on the natural parity 0^+, 2^+, and 3^- states of ^{16}O and ^{40}Ca were studied via the subtract second random-phase approximation (SSRPA) by adopting Skyrme energy density functionals (EDFs). To avoid the double counting and divergence in SRPA, the subtracting procedure was adopted in SSRPA calculations; consequently, SSRPA calculations can quickly converge with respect to the the energy cut-off. In the calculations, two tensor parameterizations, SGII+Te1 and SGII+Te3, were adopted, whose triplet-odd tensor terms have different signs, *i.e.*, $U = -350.0$ MeVfm^5 and $+200.0$ MeVfm^5, respectively.

In the SRPA model,[1,2] the particle-hole (p-h) excitation operator, $Q^\dagger_\nu$, can be written as,

$$\begin{aligned} Q^\dagger_\nu =& \sum_{ph}(X^\nu_{ph}a^\dagger_p a_h - Y^\nu_{ph}a^\dagger_h a_p) \\ &+ \sum_{\substack{p_1<p_2\\ h_1<h_2}}(X^\nu_{p_1p_2h_1h_2}a^\dagger_{p_1}a^\dagger_{p_2}a_{h_2}a_{h_1} \\ &- Y^\nu_{p_1p_2h_1h_2}a^\dagger_{h_1}a^\dagger_{h_2}a_{p_2}a_{p_1}). \end{aligned} \tag{1}$$

Suffixes p, p_1, p_2 denote the particle states, while h, h_1, h_2 denote the hole states; X and Y denote forward and backward amplitudes, respectively. The SRPA equation has the same matrix form as the RPA equation:

$$\begin{bmatrix} A & B \\ -B^* & -A^* \end{bmatrix}\begin{bmatrix} X^\nu \\ Y^\nu \end{bmatrix} = \hbar\omega_\nu \begin{bmatrix} X^\nu \\ Y^\nu \end{bmatrix}, \tag{2}$$

where

$$\begin{aligned} A = \begin{pmatrix} A_{11} & A_{12} \\ A_{21} & A_{22} \end{pmatrix}, B = \begin{pmatrix} B_{11} & B_{12} \\ B_{21} & B_{22} \end{pmatrix}, \\ X = \begin{pmatrix} X^\nu_1 \\ X^\nu_2 \end{pmatrix}, Y = \begin{pmatrix} Y^\nu_1 \\ Y^\nu_2 \end{pmatrix}. \end{aligned} \tag{3}$$

Indices 1 and 2 denote the shorthand notations for 1p-1h and 2p-2h configurations, respectively. Matrices A_{12}, B_{12} represent the coupling of 1p-1h and 2p-2h configurations, and A_{22}, B_{22} denote the coupling between 2p-2h configurations. In SSRPA, A_{11} and B_{11} are modified as:

$$\begin{aligned} A^S_{11'} =& A_{11'} + \sum_2 A_{12}(A_{22})^{-1}A_{21'} + \sum_2 B_{12}(A_{22})^{-1}B_{21'}, \\ B^S_{11'} =& B_{11'} + \sum_2 A_{12}(A_{22})^{-1}B_{21'} + \sum_2 B_{12}(A_{22})^{-1}A_{21'}. \end{aligned}$$

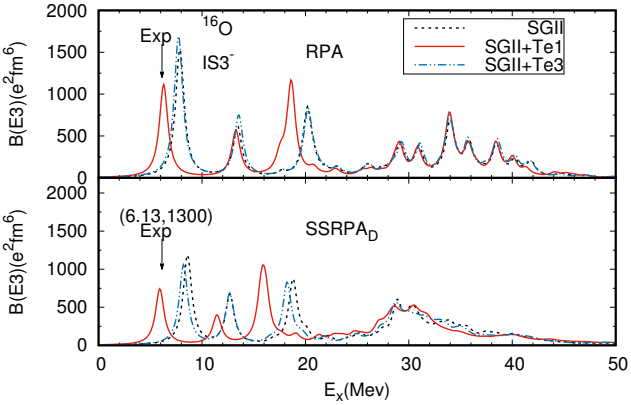

Fig. 1. Isoscalar octupole strength distributions in ^{16}O calculated by RPA (upper panel) and SSRPA (lower panel). Black dashed, red solid, and blue dashed-dotted lines represent the results of SGII, SGII+Te1, and SGII+Te3, respectively. Experimental data are denoted by $(E_x, B(E3))$ in units of MeV and e^2fm^6.

where the diagonal approximation is adopted in A_{22} matrix,

$$A^D_{22} = \delta_{p_1p_1'}\delta_{p_2p_2'}\delta_{h_1h_1'}\delta_{h_2h_2'}(E_{p_1} + E_{p_2} - E_{h_1} - E_{h_2}), \tag{4}$$

while we fully take into account the coupling between the 2p-2h configurations in A_{22} in SRPA Eq. (2).

SSRPA calculations demonstrate a clear difference between the effects of two tensor interactions in SGII+Te1 and SGII+Te3. The effects of triplet-even and triplet-odd tensor forces of SGII+Te3 on the 0^+, 2^+, and 3^+ states cancel each other and no significant effect is observed. In contrast, in the case of SGII+Te1, two tensor terms are added coherently, which improve remarkably the numerical results. Figure 1 presents an example of IS 3^- excitations in ^{16}O. These results indicate the importance of the triplet-odd and triplet-even terms for realistic calculations of collective states.

We adopted two extreme cases in this study to demonstrate how the energies and the strengths are affected by the tensor forces. Accordingly, we showed that the tense effects are observed even in the natural parity states of SSRPA results, while they are negligible in RPA, except the case of 3^-. Thus, by setting appropriate tensor parameters, we will be able to improve further descriptions of the transition probabilities of low-lying collective states. This study remains for the future work.

† Condensed from the article in Phys. Rev. C **103**, 054308 (2021)

*1 College of Physics, Sichuan University
*2 RIKEN Nishina Center
*3 China Institute of Atomic Energy

References

1) D. Gambacurta *et al.*, Phys. Rev. C **81**, 054312 (2010).
2) C. Yannouleas, Phys. Rev. C **35**, 1159 (1987).

On the deformability of atoms†

T. Naito,[*1,*2] S. Endo,[*3,*4] K. Hagino,[*5] and Y. Tanimura[*3,*6]

Atoms and atomic nuclei share common features as quantum many-body systems of interacting fermions. In atoms, the inter-particle interaction is the repulsive Coulomb interaction, and there exists the spherical external Coulomb potential due to the nucleus. In contrast, in atomic nuclei, the inter-particle interaction is the attractive nuclear force, with no external potential. Despite the differences in the fundamental interactions, many similar properties have been observed in both systems, such as the shell structure and the associated magic numbers.

One of the most important properties of atomic nuclei is collective nuclear deformation. It was discussed that this collective deformation originates from the strong attractive interaction between protons and neutrons.[1,2] A natural question then arises: Can atoms be deformed collectively as in atomic nuclei? Calculations of the atomic structure have been frequently conducted by assuming spherical symmetry, and the non-sphericity has been addressed only in a few studies. Thus, it is widely believed that atoms are rather spherical, in stark contrast to deformed atomic nuclei. What is the physical origin of this difference? To what extent can electron density distributions in atoms be deformed collectively?

To answer these questions, we calculate electron density distributions of atoms and their deformation parameters without assuming spherical symmetry. By estimating the change in the energy induced by the deformation, in nuclear systems, we find that the spin-up and spin-down particles tend to be deformed in the same manner due to the attractive inter-particle nuclear interaction. In contrast, in atomic systems, we find that the spin-up and spin-down particles prefer to be deformed in the opposite manner, cancelling each other and resulting in a small deformation as a whole owing to the repulsive inter-particle Coulomb interaction. Thus, the difference between atoms and atomic nuclei in their deformability primarily originates from the different natures of the inter-particle interactions.

Figure 1 shows the deformation parameters β for atoms from Li to Kr calculated using the unrestricted Hartree-Fock method with the 6-31+G basis.[3] All the noble-gas atoms are spherical ($\beta = 0$). For the other atoms, the electronic configuration of their cores is the same as that of the noble-gas atoms. Hence, as long as the core density is not deformed owing to non-trivial many-body effects, the deformation of the atom is expected to result only from the valence electrons. The valence electrons of the s-block atoms only occupy an s orbital, and the many-body effects between the valence electrons and spherically symmetric core necessarily result in a spherical electron density distribution. This is also true for the half-closed-shell atoms.

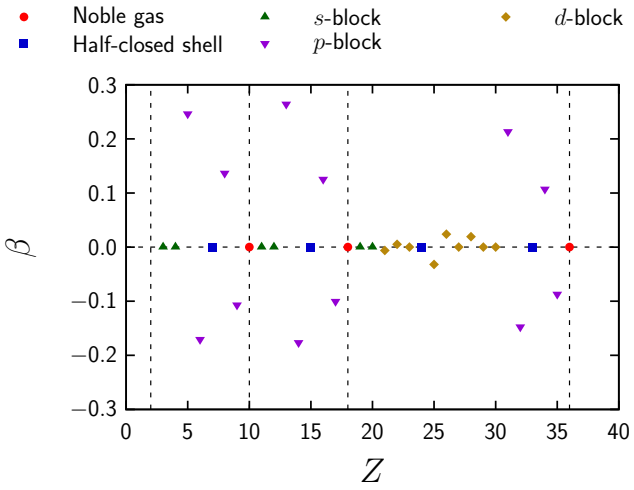

Fig. 1. Deformation parameters β calculated using the unrestricted Hartree-Fock method with the 6-31+G basis.

For the other open-shell atoms, the deformation parameters β are generally non-zero. The deformation parameters for the atoms with the same group exhibit similar tendencies, *i.e.*, $|\beta| \simeq 0.1$–0.3 for the p-block atoms and $|\beta| \lesssim 0.01$ for the d-block atoms. This indicates that the nature of the few valence open-shell electrons contributes significantly to determining β of the whole atom. This deformation originates from single-particle valence orbitals and thus it is misleading to regard it as collective deformation. For example, the deformation of the p-block atoms can be understood as the valence p orbitals that primarily contribute to the deformation. Indeed, $|\beta| \simeq 0.1$–0.3 of the p-block atoms are similar values in order of magnitude to that of a single p orbital, although $|\beta| \simeq 0.3$ might appear a large collective deformation in nuclear physics sense. We conclude in this paper that the p-block atoms can be regarded as an almost inert core plus valence p-electrons, while many-body effects between the core and the valence electrons are relevant in the d-block atoms. In the d-block atoms, the core electrons tend to collectively cancel the deformation of the valence d orbitals.

† Condensed from the article in J. Phys. B **54**, 165201 (2021)
*1 Department of Physics, University of Tokyo
*2 RIKEN Nishina Center
*3 Department of Physics, Tohoku University
*4 Frontier Research Institute for Interdisciplinary Science, Tohoku University
*5 Department of Physics, Kyoto University
*6 Graduate Program on Physics for the Universe, Tohoku University

References

1) P. Federman, S. Pittel, Phys. Rev. C **20**, 820 (1979).
2) J. Dobaczewski *et al.*, Phys. Rev. Lett. **60**, 2254 (1988).
3) W. J. Hehre *et al.*, J. Chem. Phys. **56**, 2257 (1972).

Comparative study of the dineutron in Borromean nuclei ^{11}Li and ^{22}C

M. Yamagami*[1]

A recent knockout-reaction experiment for ^{11}Li measured the mean correlation angle between the momenta of two emitted neutrons,[1] which is considered to reflect the mean opening angle $\langle\theta_{nn}\rangle_0$ between the momenta $\mathbf{k}_1$ and $\mathbf{k}_2$ of valence neutrons in the ground state. In the current study, I discuss how $\langle\theta_{nn}\rangle_0$ reflects the momentum-space structure of the dineutron in the Borromean nuclei ^{11}Li and ^{22}C.

The three-body model calculation is performed using a finite-range n-n interaction,[3] which reproduces the ground-state properties of these nuclei. For example, the distance between the core and the center of mass (cm) of the dineutron in ^{11}Li is 5.00 fm, which is in agreement with the observed value of 5.01(32) fm.[2] $\langle\theta_{nn}\rangle_0$ for each core-n momentum k_n is defined by $\cos\langle\theta_{nn}\rangle_0 = \langle\!\langle\cos\theta_{12}D_{k_n}\rangle\!\rangle/\langle\!\langle D_{k_n}\rangle\!\rangle$. Here, $\langle\!\langle f\rangle\!\rangle = \int d^3k_1 d^3k_2 \rho_2(\mathbf{k}_1,\mathbf{k}_2) f(\mathbf{k}_1,\mathbf{k}_2)$ is the mean value of a function $f(\mathbf{k}_1,\mathbf{k}_2)$ for the two-neutron density distribution $\rho_2(\mathbf{k}_1,\mathbf{k}_2)$. θ_{12} is the opening angle between $\mathbf{k}_1$ and $\mathbf{k}_2$. $D_{k_n}(\mathbf{k}_1,\mathbf{k}_2) = \delta(k_n - |\mathbf{k}_1|)\delta(k_n - |\mathbf{k}_2|)$ picks up the component of $k_n = |\mathbf{k}_1| = |\mathbf{k}_2|$ in ρ_2.

Here, $\mathbf{k}_1$ and $\mathbf{k}_2$ can be expressed as $\mathbf{k}_{\{1\atop 2\}} = \pm\mathbf{k}_{\rm rel} + \mathbf{q}_{\rm cm}/2$ with the relative and cm momenta $\mathbf{k}_{\rm rel}$ and $\mathbf{q}_{\rm cm}$, respectively. As shown below, $\langle\theta_{nn}\rangle_0$ for a given k_n contains the various $q_{\rm cm}$ components of different neutron-pair structures. To illustrate this, Fig. 1(a) shows the density distribution $\rho_{\rm cm} = \langle\!\langle\delta(q_{\rm cm} - |\mathbf{k}_1 + \mathbf{k}_2|)\rangle\!\rangle$ as a function of $q_{\rm cm}$. The root-mean-square core-n momentum $\bar{k}_n$ is defined for each $q_{\rm cm}$ in a similar manner. Together with the associated opening angle $\bar{\theta}_{\rm cm} = 2\cos^{-1}(q_{\rm cm}/2\bar{k}_n)$, the parametric curve of $(\bar{k}_n, \bar{\theta}_{\rm cm})$ is shown in Fig. 1(b). For ^{11}Li, symbol A corresponds to the peak position of $\rho_{\rm cm}$. $\bar{k}_n$ has a local maximum (minimum), as indicated by the symbol B (C). The corresponding cm momenta $q^{(\rm A)}$, $q^{(\rm B)}$, and $q^{(\rm C)}$ are 0.20, 0.47, and 0.65 fm^{-1}, respectively. $\bar{\theta}_{\rm cm} > 90°$ at $q_{cm} < q^{(\rm C)}$ indicates the dineutron configuration. The symbols a, b, and c for ^{22}C have the same meaning as A, B, and C for ^{11}Li, respectively.

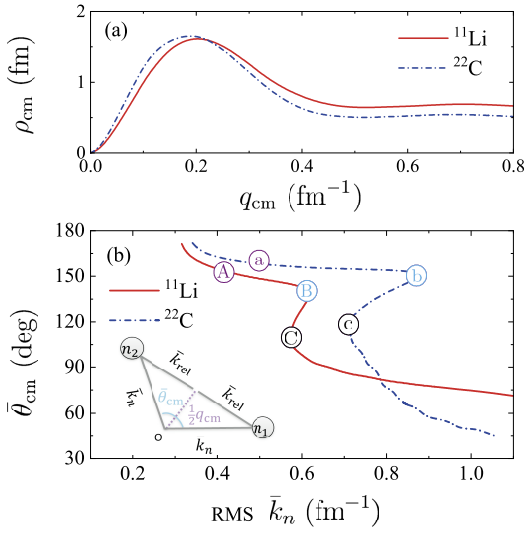

Fig. 1. (a) Two-neutron density distribution $\rho_{\rm cm}$ as a function of $q_{\rm cm}$ in ^{11}Li and ^{22}C. (b) Parametric curve of $(\bar{k}_n, \bar{\theta}_{\rm cm})$. See the text for details.

*1 Department of Computer Science and Engineering, University of Aizu

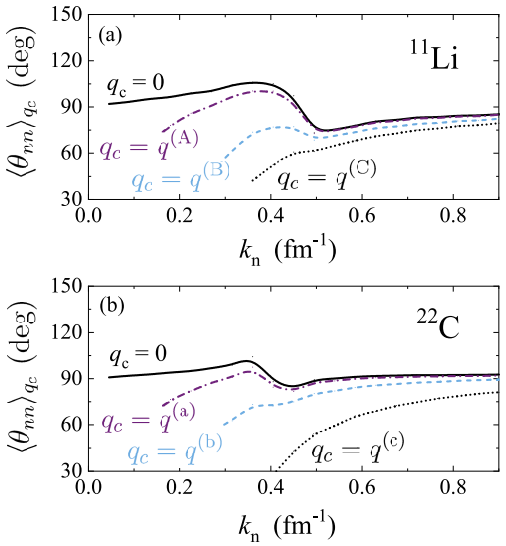

Fig. 2. (a) Mean opening angle $\langle\theta_{nn}\rangle_{q_c}$ in ^{11}Li as a function of k_n. The dependence on the lower cutoff q_c is shown. (b) The same as (a) but for ^{22}C. See the text for details.

The mean opening angle $\langle\theta_{nn}\rangle_{q_c}$, which takes into account the component of $q_{cm} > q_c$ in ρ_2, is also defined. Here, q_c is a lower cutoff. Figure 2 shows $\langle\theta_{nn}\rangle_{q_c}$ in ^{11}Li and ^{22}C. $\langle\theta_{nn}\rangle_0$ has a peak at $k_n \approx 0.35$ fm^{-1}. The peak of $\langle\theta_{nn}\rangle_0$ is cooperatively created by the peak component of $\rho_{\rm cm}$ and the large $\bar{\theta}_{\rm cm}$ in the region of $q_{\rm cm} < q^{(\rm C)}$ ($q^{(\rm c)}$) in ^{11}Li (^{22}C). In ^{22}C, the enlargement of $\langle\theta_{nn}\rangle_0$ due to the low-$q_{\rm cm}$ component appears up to $k_n \approx 0.9$ fm^{-1}, which corresponds to the local maximum value of $\bar{k}_n$. This high local maximum value of $\bar{k}_n$ is due to the d-wave contribution. Such enlargement of $\langle\theta_{nn}\rangle_0$ is not observed at high k_n in ^{11}Li.

In conclusion, I discussed how the mean opening angle $\langle\theta_{nn}\rangle_0$ depends on the momentum-space structure of the dineutron in ^{11}Li and ^{22}C. $\langle\theta_{nn}\rangle_0$ can be a promising probe for revealing the characteristic structure of the dineutron in each Borromean nucleus.

References

1) Y. Kubota *et al.*, Phys. Rev. Lett. **125**, 252501 (2020).
2) T. Nakamura *et al.*, Phys. Rev. Lett. **96**, 252502 (2006).
3) M. Yamagami, RIKEN Accel. Prog. Rep. **54**, 37 (2021).

Nuclear surface diffuseness of Ne and Mg isotopes in the island of inversion†

V. Choudhary,[*1] W. Horiuchi,[*2,*3] M. Kimura,[*2,*4] and R. Chatterjee[*1]

It had been suggested in the literature,[1] that the island of inversion close to $N = 20$ and 28 arises because of the $\nu(sd)^{-2}(fp)^2$ intruder configurations. It was proposed that two neutrons from the *sd*-shell are excited to the *fp*-shell become so low in energy that they manifest as the ground state of $Z = 10$–12 and $N = 20$–22 nuclei. This proposition was confirmed by mass measurements and reactions involving neutron rich isotopes of Ne, Na and Mg, especially at RIBF. This change in occupation of nucleons in different energy levels not only results in large deformations but also affects the nuclear density profile, particularly the nuclear surface diffuseness. In this work, we attempt to systematically investigate the connection between the nuclear surface diffuseness and various spectroscopic information of Ne and Mg isotopes ($N = 19$–28) at or near the island of inversion. We calculate the density and spectroscopic information of Ne and Mg isotopes using the antisymmetrized molecular dynamics (AMD) model.[2,3] We then construct a two-parameter Fermi density distribution (2 pF), with adjustable radius and diffuseness parameters. These parameters are then estimated using two complementary methods - one analyzing the static structure and the other dynamical, in which reaction observables involving these nuclei are analyzed. In the first method, the optimized radius and diffuseness parameters of the 2 pF are estimated by minimizing the difference between densities obtained by AMD and 2 pF density distributions. In the second, both the AMD and 2 pF densities are taken as inputs to calculate the proton-nucleus elastic scattering differential cross section using the Glauber model. We then demand that the first peak position and its magnitude are reproduced for both these densities as prescribed.[4] We have verified that the parameters estimated using these complementary methods agree within a margin of 1–3%.

The nuclear surface diffuseness, *i.e.*, the diffuseness parameter of the 2 pF density of Ne and Mg isotopes extracted from the matter density distribution of AMD is plotted in Fig. 1. The diffuseness parameter has similar dependency on neutron number, illustrating the similarity in nuclear deformations for both Ne and Mg isotopes.[2,3] We observe that the neutron occupancy of

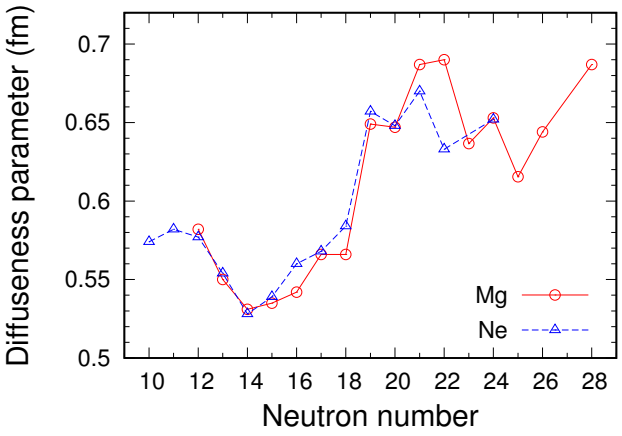

Fig. 1. Diffuseness parameters of Ne and Mg isotopes as a function of neutron number. The figure is adopted from the original article.†

the weakly-bound $1p_{3/2}$ orbit has a significant impact on the global behavior of the diffuseness parameter. The absence of intruder orbitals till $N = 18$ results in normal shell filling and hence diffuseness parameters are very similar to the standard value of 0.54 fm. The effect of the intruder orbitals begins to be felt from $N = 19$ onwards resulting in strong quadrupole deformation and mixing of *p*- and *f*-waves. ^{29}Ne and ^{31}Mg ($N = 19$) have predominant 2p3h configurations in which two particles are promoted from the *sd*- to *pf*-shell. The increasing occupation probability of the $1p_{3/2}$ orbit not only results in a large diffuseness but also the breakdown of the $N = 20$ and 28 magic numbers in this region. An exception, however, is noted for $^{35–37}$Mg where the filling up the holes in the deeply bound *sd*-shell somewhat compensates the increase in diffuseness due to filling up of the $1p_{3/2}$ orbit. Noticeably, for $N = 22$, ^{34}Mg has predominant 4p2h configuration, whereas ^{32}Ne has an admixture of 4p2h and 2p0h configurations. This could be the reason why ^{34}Mg is more diffused than ^{32}Ne.

In conclusion our work shows that information about the nucleus surface diffuseness in exotic neutron rich nuclei can be extracted from the first diffraction peak of nucleon-nucleus elastic scattering differential cross section.

† Condensed from the article in Phys. Rev. C. **104**, 054313 (2021)

*1 Department of Physics, Indian Institute of Technology Roorkee
*2 Department of Physics, Hokkaido University
*3 Department of Physics and NITEP, Osaka Metropolitan University
*4 RIKEN Nishina Center

References

1) E. K. Warburton *et al.*, Phys. Rev. C **41**, 1147 (1990).
2) T. Sumi *et al.*, Phys. Rev. C **85**, 064613 (2012).
3) S. Watanabe *et al.*, Phys. Rev. C **89**, 044610 (2014).
4) S. Hatakeyama *et al.*, Phys. Rev. C **97**, 054607 (2018).

Study of β-delayed one-neutron emission probabilities using a neural network model†

D. Wu,[*1] C. L. Bai,[*1] H. Sagawa,[*2] S. Nishimura,[*2] and H. Q. Zhang[*3]

The β-delayed neutron emission is a key ingredient in astrophysical r-process nucleosynthesis, whose theoretical model predictions still contain large uncertainties. In this work, we applied a novel feed-forward neural network (FNN) model to accurately calculate β-delayed one-neutron emission probabilities.

We considered a three-layer FNN architecture consisting of input, hidden, and output layers with N_{in}, N_h, and N_o neurons, respectively. The model was trained with a set of input data of known physical quantities, namely, one-neutron emission Q-value, Q-value difference between the one- and two-neutron emissions, β-decay half-life, $T_{1/2}$, the distance from the least neutron-rich nucleus with $Q_{\beta 1n} > 0$ in each isotope, $N - N_D$, and the exponential form of the ratio of Q-value, $\exp(-Q_{\beta 2n}/Q_{\beta 1n})$. The learning process was performed to minimize the loss function via proper optimization methods. We used the root mean squared prop (RMSProp) method to obtain the optimal network parameters.

First, we calculated the one-neutron emission probabilities, P_{1n}, of the nuclei, which have only one-neutron emission channels. The input data contain 127 nuclei and the size of the training set is 89. The following inputs are given in the network: $Q_{\beta 1n}$, $\Delta E_w^3 T_{1/2}$, $\mathcal{G}(Z,N) = \Delta E_w \Delta S_{2n}$, and $N - N_D$, where $\Delta E_w = Q_{\beta 1n} - Q_{\beta 2n}$ is actually $Q_{\beta 1n}$ in this special case, and $\Delta S_{2n} = S_{2n}(Z+1,N) - S_{2n}(Z+1,N-2)$. The input, hidden, and output layers contain 4, 40, and 1 neurons, respectively. The P_{1n} differences between the present ML-FNN and experimental data of these nuclei are shown in Fig. 1, together with those obtained by the FRDM12+(Q)RPA+HF[1)] and RHB+RQRPA models.[2)] It can be observed that the results of the three models are reasonable consistent with the experimental data. The differences between ML-FNN and experimental data are distributed over -25% to 25% and densely concentrated around 0, especially when $N > 40$. The RMSD values of ML-FNN are 8.5% and 9.0% for the training and for testing sets, respectively, and 11.8% and 13.4% for the FRDM12+(Q)RPA+HF and RHB+RQRPA models, respectively. A remarkable improvement of ML-FNN model can be seen in the RMSD compared to the other two models.

The waiting-point nuclei are the key elements to determine the time scale of r-process and strongly affect the final abundance of elements in the solar system. The experimental and theoretical P_{1n} values of the waiting-point nuclei at the magic neutron numbers $N = 50$ and 82 are listed in Table 1. It can be observed that the proposed ML-FNN model provides the P_{1n} values of the waiting-point nuclei at $N = 50$ and 82 with the highest accuracy, both qualitatively and quantitatively.

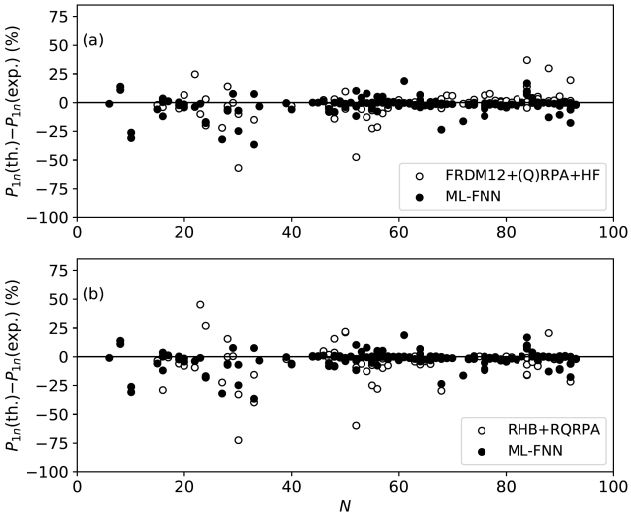

Fig. 1. Differences of P_{1n} between theoretical results and experimental data for the nuclei, which have only one-neutron emission channels. The data of FRDM12+(Q)RPA+HF and RHB+RQRPA are taken from Refs. 1) and 2), respectively.

Table 1. P_{1n} of waiting-point nuclei at magic neutron numbers $N = 50$ and 82. Three theoretical models, FRDM12+(Q)RPA+HF,[1)] RHB+RQRPA,[2)] and ML-FNN, are listed with experimental data with errors in the brackets. The values are given in %.

Nuclides	FRDM12	RHB	ML-FNN	Exp.
$^{79}_{29}Cu_{50}$	30.0	56.5	40.1	66(12)
$^{80}_{30}Zn_{50}$	11.0	22.5	1.6	1.36(12)
$^{81}_{31}Ga_{50}$	7.0	34.3	14.1	12.5(8)
$^{128}_{46}Pd_{82}$	9.0	1.8	11.8	10(7)
$^{129}_{47}Ag_{82}$	10.0	13.2	21.2	17.9(14)
$^{130}_{48}Cd_{82}$	6.0	0.7	1.6	3.0(2)

References

1) P. Möller *et al.*, At. Data Nucl. Data Tables **125**, 1 (2019).
2) T. Marketin *et al.*, Phys. Rev. C **93**, 025805 (2016).

† Condensed from the article in Phys. Rev. C **104**, 054303 (2021)

*1 College of Physics, Sichuan University
*2 RIKEN Nishina Center
*3 China Institute of Atomic Energy

Reentrant of the pairing gap and α-correlation in ^{108}Cd

K. Sugawara-Tanabe[*1,*2] and K. Tanabe[*3]

Motivated by the experimental data of the reaction ^{112}Sn$(p, p\alpha)^{108}$Cd,[1] we solved the number- and angular-momentum-constrained Hartree–Fock–Bogo liubov equation for ^{108}Cd by using the signature-invariant representation. We started from the spherical single-particle energies and included all the direct and exchange contributions from the residual monopole and quadrupole pairing, and quadrupole–quadrupole interactions among the same isospin shells and between the proton (p) and neutron (n) shells. The canonical base represents the diagonalization of densities in the generalized density matrix[2] at the minimum point of the total Hamiltonian determined under the constraints self-consistently. We found, for the first time, the canonical base including the Coriolis coupling term, which provides details of the nuclear structure that depends not only on the particle number, but also on the angular-momentum I.

In Fig. 1(A), we compare the theoretical backbending curve with the experimental one.[3] The theoretical values (squares) reproduce the experimental ones (circles) reasonably well. The backbending appears from the 6^+ state and the yrast level jumps to the new band at the 10^+ state. In Fig. 1(B), the average pairing gap $\bar{\Delta}_{\tau\pm} = \sum_{i\epsilon\tau\pm} \bar{\Delta}_{\hat{i}i}/N_{\tau\pm}$ is calculated for each shell, where $\bar{\Delta}_{\hat{i}i}$ represents the level-dependent gap in the canonical base, τ indicates p or n shell, and $\pm$ the parity of the shell. $N_{\tau\pm}$ is the total level number belonging to the $\tau\pm$ shell. The gradual decrease in $\bar{\Delta}_{\tau\pm}$ for $\tau = p$ or n is due to the Coriolis anti-pairing effect. The figure shows a sudden increase in the proton gap between the 8^+ and 10^+ states, which indicates that the reentrant of the proton pairing gap appears in high-spin states in ^{108}Cd. The single-particle energies in the canonical base, which includes self-energy, chemical potential, and the cranking term, show that the $1g_{7/2,\,1/2}$ level in the $p+$ shell comes down to the Fermi surface suddenly from the 8^+ state to the 10^+ state. This triggers the reentrant of the proton gap. The single-particle energy in the canonical base also indicates that the $1h_{11/2,\,1/2}$ level in the $n-$ shell causes the backbending.

Owing to the reentrant of the proton pairing gap, the α-correlation defined by $\langle \sum_{i>0} C_{i\epsilon p} C_{\hat{i}\epsilon p} C_{i\epsilon n} C_{\hat{i}\epsilon n} \rangle = \sum_{i>0} \kappa^p_{\hat{i}i} \kappa^n_{\hat{i}i}$ as a function of I has two peaks, one at the 0^+ state and the bump at the 10^+ state (∼3.4 MeV), where $C_{i\epsilon\tau}$ denotes the spherical single-particle operator, $\rangle$ denotes the quasiparticle vacuum corresponding to I, and $\kappa^\tau_{\hat{i}i}$ denotes the pairing matrix in the τ-shell.

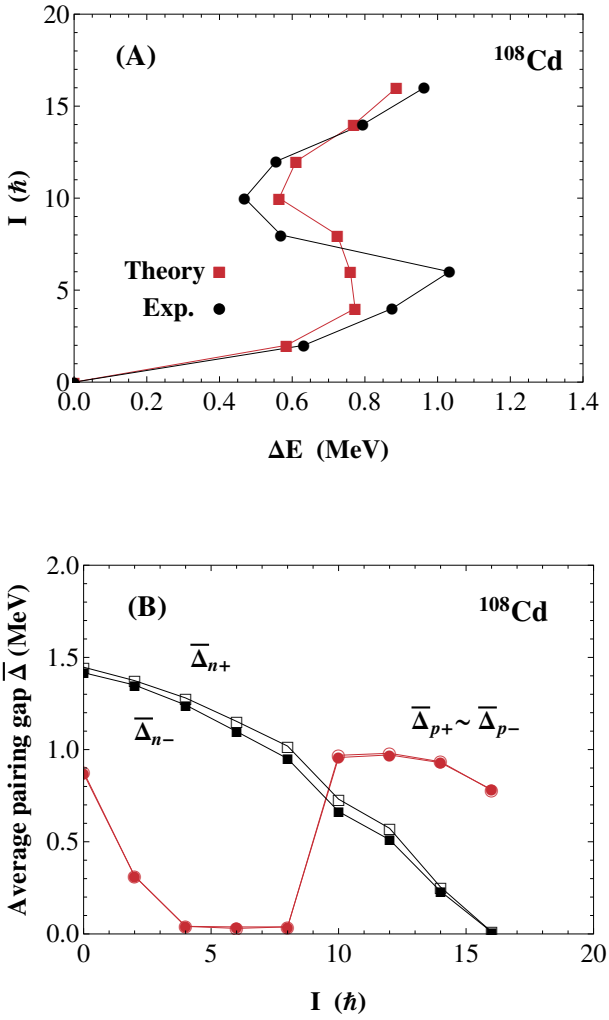

Fig. 1. (A): Comparison of the theoretical backbending plot for ^{108}Cd with the experimental data.[3] The abscissa represents the total energy difference $\Delta E = E(I) - E(I-2)$ for $I \geq 2$, and the ordinate the total angular momentum I. Theoretical values are indicated by squares, and experimental ones by circles. (B): The average pairing gap $\bar{\Delta}$ in each shell as a function of angular momentum I. Solid and open symbols indicate the results on "−" and "+" parity shells, respectively. The squares indicate the values for the n shell, and the circles for the p shell.

*1 RIKEN Nishina Center
*2 Department of Information Design, Otsuma Women's University
*3 Department of Physics, Saitama University

References
1) J. Tanaka *et al.*, Science **371**, 260 (2021).
2) C. Bloch, A. Messiah, Nucl. Phys. **39**, 95 (1962).
3) R. B. Firestone, V. S. Shirley, *Table of Isotopes* (John Wiley and Sons INC, 1996).

α-correlation in ^{108}Cd excitation energy spectrum of α removal from ^{112}Sn

K. Sugawara-Tanabe,[*1,*2] K. Tanabe,[*3] J. Tanaka,[*1] and T. Uesaka[*1]

We employed number- and angular-momentum-constrained Hartree-Fock-Bogoliubov (CHFB) equations for ^{108}Cd and ^{112}Sn using the same set of parameters. The parameters were quadrupole-quadrupole force strength $\chi_p = \chi_n = -0.04$ and $\chi_{pn} = -0.13$ in unit of MeV/b^4, monopole-pairing force $g_p = -0.24$ and $g_n = -0.18$ in unit of MeV, and quadrupole-pairing force with 10% g in unit of MeV/b^4, where b is the oscillator length. We excluded a tensor-type force between proton-neutron pairs. Figure 1(A) shows a comparison of the theoretical and experimental backbending curves[1] of ^{108}Cd (circles) and ^{112}Sn (triangles). The theoretical values (solid) match the experimental ones (open) reasonably well for both nuclei. For ^{112}Sn, a vibrational level scheme with a constant energy shift after the 2^+ state is observed, whereas ^{108}Cd shows a rotational one in which the proton pairing gap reoccures at the 10^+ state. For ^{108}Cd, the deformation parameter β_2 is almost constant (~ 0.15) in the range of $0^+ \sim 16^+$ states, whereas γ ranges from $-2°$ to $5°$ depending on total angular momentum I (almost prolate shape). In contrast, for ^{112}Sn, β_2 remains zero, and γ is zero in the 0^+ state (prolate shape) and approximately $60°$ in the $2^+ \sim 10^+$ states (oblate shape). For ^{112}Sn, the proton pairing gap vanishes as a natural result of the magic number, and its neutron pairing gap of 1.61 MeV is 1.2 times that of ^{108}Cd in the 0^+ state. We consider that the microscopic process creates an α-particle by the reaction, ^{112}Sn$(p, p\alpha)^{108}$Cd[2] is as follows. We assume a physical picture that ^{112}Sn is composed of excited ^{108}Cd and an α particle, and that the final stage is the energy spectrum of the observed ^{108}Cd. The overlap between the initial and final states includes the α-correlation, $\langle \sum_{i>0}(4/(2j_i+1))C_{i\in p}C_{\hat{i}\in p}C_{i\in n}C_{\hat{i}\in n} \rangle = \sum_{i>0}(4/(2j_i+1))\kappa^p_{ii}\kappa^n_{ii}$. In the expression, the factor comes from the Clebsch−Gordan coefficient to form iso-triplet pairs, $C_{i\in\tau}$ is the spherical single-particle operator belonging to τ (proton or neutron), ket $\rangle$ is the quasivacuum of the yrast state of I, and κ^τ_{ii} is the pairing matrix for the τ-shell in ^{108}Cd. In Fig. 1(B), the square of the α-correlation is shown as a function of the excitation energy. Owing to the recurrence of the proton pairing gap, the square of the α-correlation has two peaks as a function of I, one at the 0^+ state and another bump at the 10^+ state (~ 3.4 MeV). The highly excited state corresponds to the high-spin states of Cd in the final stage of the reaction. The ratio of the ground state peak to the second peak at 3.4 MeV is approximately 0.45, which coincides with the experimental value of 0.43 from Fig. 3A in Ref. 2). Summarizing we show that the CHFB calculation reproduces the basic feature of the reaction as well as the high spin states of ^{112}Sn and ^{108}Cd; however, the r-coordinate and/or a finite range formalism are required particularly for the description of an α particle.

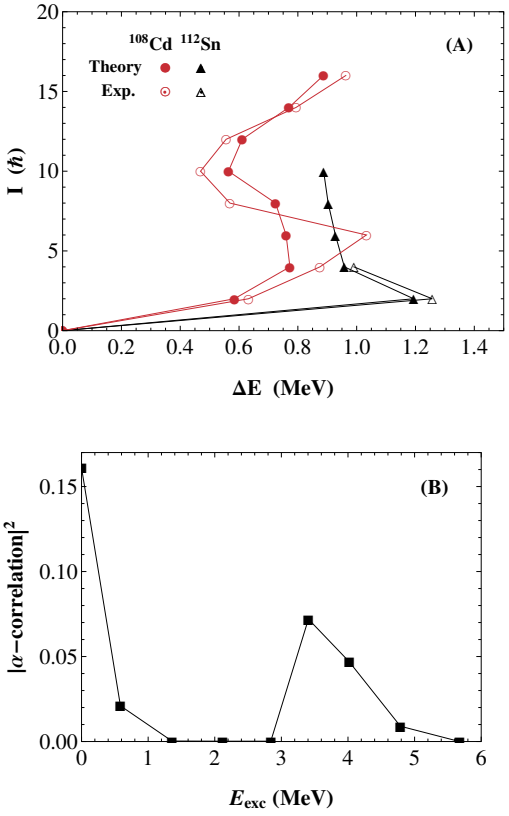

Fig. 1. (A): Comparison of theoretical backbending plots of ^{108}Cd (closed circles) and ^{112}Sn (closed triangles) with experimental data (open symbols) from isotope table.[1] Abscissa is total energy difference $\Delta E = E(I) - E(I-2)$ for $I \geq 2$. Ordinate is for total angular momentum I. (B): A square of α-correlation in ^{108}Cd as functions of $E_{\rm exc} = E(I) - E(0)$, where $E(I)$ is the total energy of $\langle H \rangle$ at I.

*1 RIKEN Nishina Center
*2 Department of Information Design, Otsuma Women's University
*3 Department of Physics, Saitama University

References
1) R. B. Firestone, V. S. Shirley, *Table of Isotopes*, 8th ed. (John Wiley and Sons, INC, 1996).
2) J. Tanaka *et al.*, Science **371**, 260 (2021).

Proof-of-principle calculations in the *ab initio* no-core Monte Carlo shell model†

T. Abe,[*1] P. Maris,[*2] T. Otsuka,[*3,*1,*4] N. Shimizu,[*5] Y. Utsuno,[*4,*5] and J. P. Vary[*2]

Understanding of nuclear structure from first principles is a major challenge in low-energy nuclear theory. This challenge includes not only the confirmation of existing experimental data but also the predictions where the experimental information has not been available yet. In addition, one hopes to extract a detailed understanding of a variety of complex nuclear phenomena, described by successful nuclear models, from the underlying microscopic descriptions. Under these motivations, a number of *ab initio* investigations have been actively done for more than a decade. This trend in *ab initio* studies has been supported by the rapidly growing computational power of supercomputers and continuing improvements of *ab initio* techniques for nuclear many-body calculations.

Here we report the proof-of-principle calculations in the *ab initio* no-core Monte Carlo shell model (MCSM).[1] This is the extension of the MCSM with an assumed inert core[2–4] to the *ab initio* no-core shell model.[3–5] Ground-state energies are obtained in the basis spaces up to seven harmonic oscillator (HO) major shells ($N_{\rm shell} = 7$) with several HO energies, $\hbar\omega$, around the optimal $\hbar\omega$ for the convergence of ground-state energies. These energy eigenvalues are extrapolated to obtain estimates of converged ground-state energies in each basis space using energy variances of computed energy eigenvalues. We further extrapolate these energy-variance-extrapolated energies obtained in the finite basis spaces to infinite basis-space results.

Figure 1 shows our results with two nonlocal NN interactions[6,7] in comparison with the experimental data.[8] In Fig. 1, the JISP16[6] and Daejeon16[7] results are shown by blue and red symbols, respectively, with estimated error bars from our fit to $N_{\rm shell} = 4$–7 results at their respective optimal $\hbar\omega$ values. From Fig. 1, the JISP16 results yield overbinding at ^{12}C and beyond. An improved picture emerges using Daejeon16 with some overbinding still evident when compared with experiments. There are encouraging trends with the Daejeon16 results compared with the JISP16 results. However, this finding suggests the necessity of further revisions of nonlocal NN interactions for the heavier-mass region beyond the p shell and/or the explicit inclusion of a $3N$ interaction. Note that the no-core MCSM results are in reasonable agreement with the other *ab initio* results with the same interactions where those are available.

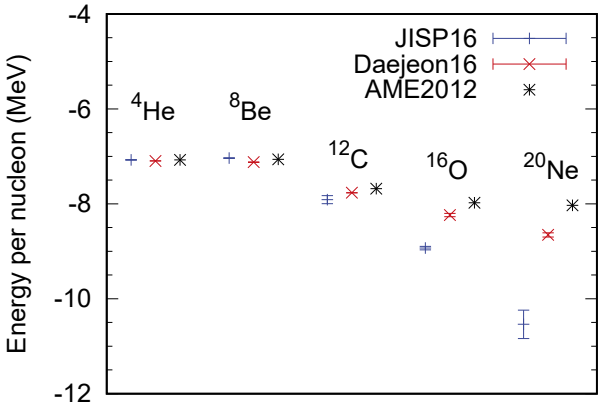

Fig. 1. Comparison of the no-core MCSM results for the energy per nucleon with the JISP16[6] and Daejeon16[7] NN interactions to experimental data.[8] The MCSM results are shown for the basis-space extrapolations using the $N_{\rm shell} = 4$–7 energy-variance-extrapolated results with the respective optimal $\hbar\omega$ values.

The current study offers a foundation for pathways to investigate nuclear structure from first principles, for instance, α-cluster structure and dineutron correlations of valence neutrons on the p-shell nuclei. Also the sd-shell nuclei and beyond continue to provide rich insights into emergent nuclear phenomena. With improved nuclear interactions and increasingly precise *ab initio* tools for nuclear many-body calculations such as the no-core MCSM, we expect an opportunity to probe these emergent phenomena and, at the same time, to probe the limits of our knowledge of the strong and electroweak interactions.

References
1) T. Abe *et al.*, Phys. Rev. C **104**, 054151 (2021).
2) T. Otsuka *et al.*, Prog. Part. Nucl. Phys. **47**, 319 (2001).
3) N. Shimizu *et al.*, Prog. Theor. Exp. Phys. **2012**, 01A205 (2012).
4) N. Shimizu *et al.*, Phys. Scr. **92**, 063001 (2017).
5) T. Abe *et al.*, Phys. Rev. C **86**, 054301 (2012).
6) A. M. Shirokov *et al.*, Phys. Lett. B **644**, 33 (2007).
7) A. M. Shirokov *et al.*, Phys. Lett. B **761**, 87 (2016).
8) G. Audi *et al.*, Chin. Phys. C **36**, 1603 (2012).

† Condensed from the article in Phys. Rev. C **104**, 054315 (2021)

*1 RIKEN Nishina Center
*2 Department of Physics and Astronomy, Iowa State University
*3 Department of Physics, University of Tokyo
*4 Advanced Science Research Center, Japan Atomic Energy Agency
*5 Center for Nuclear Study, University of Tokyo

Structure of few-alpha systems in cold neutron matter†

H. Moriya,[*1] H. Tajima,[*2] W. Horiuchi,[*1,*3] K. Iida,[*4] and E. Nakano[*4]

The first 0^+ excited state of ^{12}C, the Hoyle state,[1] is important for generating ^{12}C elements in the triple alpha (^{4}He nucleus) reaction via the resonant ground state of ^{8}Be, where alpha clusters are well developed. An accurate description of such alpha-induced reactions in the astrophysical environment, such as core-collapse supernovae and neutron star mergers, is required.[2] Recently, the quasiparticle properties of an alpha particle in dilute cold neutron matter have been discussed in terms of a Fermi polaron,[3] where an alpha particle is treated as an impurity in majority neutron matter. In the polaron picture, the effective mass of the alpha particle depends on the density of neutron matter. We introduce medium-induced two- and three-alpha interactions considering simple Feynman diagrams wherein few-alpha particles exchange momenta.

This study investigates two- and three-alpha systems in dilute neutron matter at zero temperature by precisely solving a few-alpha problem, including the quasiparticle properties of an alpha particle. We consider the density of neutron matter up to 1/100th of the saturation density, $\rho_0 \sim 0.16$ fm^{-3}, which corresponds to the Fermi momentum, $k_F \sim 0.360$ fm^{-1}. We discuss the possible stability and structure changes in the Hoyle state and ground state of ^{8}Be.

The effective Hamiltonian for two- and three-alpha systems is given by:

$$H = \sum_i \frac{\boldsymbol{p}_i^2}{2M^*} - T_{\rm cm} + \sum_{i>j} \left(V_{\alpha\alpha,ij} + V^{(2)}_{{\rm eff},ij} \right) + V_{\alpha\alpha\alpha} + V^{(3)}_{\rm eff},$$

where M^* is the effective mass of alpha particles, $\boldsymbol{p}_i$ is the momentum operator of the ith alpha particle, and $T_{\rm cm}$ is the center-of-mass kinetic energy: moreover, $V_{\alpha\alpha}$ and $V_{\alpha\alpha\alpha}$ are the direct two- and three-alpha interactions, while $V^{(2)}_{\rm eff}$ and $V^{(3)}_{\rm eff}$ are the medium-induced two- and three-alpha interactions, respectively. Note that $V_{\alpha\alpha}$ is deep and has forbidden states owing to the Pauli principle. The physical constants and further calculation settings are given in Refs. 4) and 5). The wave function of the few-alpha system can be expressed by superpositioning the correlated Gaussian basis functions, whose parameters are obtained by the stochastic variational method.[6]

Figure 1 shows the in-medium energies and root-mean-square (rms) pair distance of the Hoyle state, labeled C*, and the ground state of ^{8}Be as functions of the Fermi momentum of background neutron matter. The energies of the Hoyle state and ^{8}Be decreased for larger values of k_F owing to the short-range attractive medium-induced two-alpha interaction. Eventually, ^{8}Be and the Hoyle state were bound in neutron matter with $k_F \geq 0.08$ fm^{-1} and 0.16 fm^{-1} corresponding to $\approx 10^{-4}\rho_0$ and $10^{-3}\rho_0$, respectively. Moreover, in terms of structural change, it can be observed that the size of the Hoyle state and ^{8}Be decreased. The rms pair distance monotonically decreased for larger k_F because the internal amplitude of wave functions was strongly modified by the medium-induced interactions. Notably, the shrinkage is consistent with the study investigating the finite system, *i.e.*, the $\alpha-\alpha-n$ cluster system.[7]

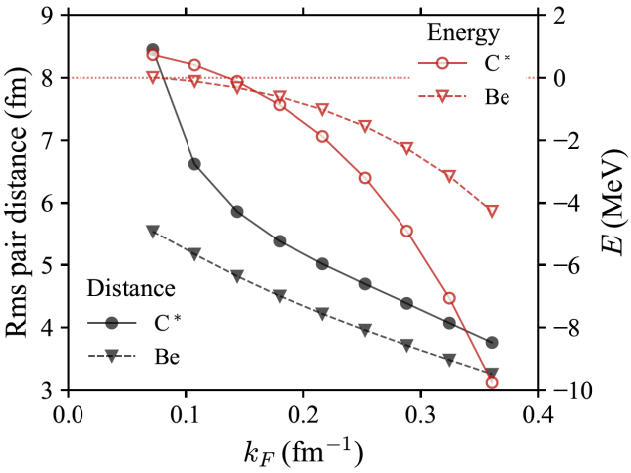

Fig. 1. Energies measured from two- and three-alpha threshold, E (right-hand scale) and rms pair distance (left-hand scale) of the Hoyle state, and ground state of ^{8}Be as functions of the neutron medium Fermi momentum, k_F. The dotted line indicates $E = 0$ MeV.

Thus, we point out the possible stability of fundamental light nuclear ingredients, the Hoyle state, and ^{8}Be. This could significantly impact the modeling of stellar collapse and neutron star mergers, as well as relevant nucleosynthesis.

References
1) F. Hoyle, Astrophys. J. Suppl. Ser. **1**, 12 (1954).
2) M. Oertel *et al.*, Rev. Mod. Phys. **89**, 015007 (2017).
3) E. Nakano *et al.*, Phys. Rev. C **102**, 055802 (2020).
4) K. Fukatsu, K. Katō, Prog. Theor. Phys. **87**, 151 (1992).
5) L. H. Phyu *et al.*, Prog. Theor. Exp. Phys. **2020**, 093D01 (2020).
6) K. Varga, Y. Suzuki, Phys. Rev. C **52**, 2885 (1995).
7) M. Lyu *et al.*, Phys. Rev. C **91**, 014313 (2015).

† Condensed from Phys. Rev. C **104**, 065801 (2021)
*1 Department of Physics, Hokkaido University
*2 Department of Physics, Graduate School of Science, University of Tokyo
*3 Department of Physics and NITEP, Osaka Metropolitan University
*4 Department of Mathematics and Physics, Kochi Univerisity

Second and fourth moments of the charge density and neutron-skin thickness of atomic nuclei†

T. Naito,[*1,*2] G. Colò,[*3,*4] H. Z. Liang,[*1,*2] and X. Roca-Maza[*3,*4]

Recently, the fourth moment of the charge distribution has been highlighted as a possible proxy to access information of the neutron root-mean-square radius.[1–3] This is because the neutron distributions ρ_n of atomic nuclei do contribute to their charge density distributions $\rho_{\rm ch}$. In other words, precise measurements of $\rho_{\rm ch}$ may provide information on ρ_n as well as ρ_p. For instance, Ref. 3) showed the feasibility to extract $\langle r^2\rangle_n$ using $\langle r^2\rangle_{\rm ch}$ and $\langle r^4\rangle_{\rm ch}$. This, however, relies on a correlation for specific nuclei based on a specific type of models, and hence, it is questionable whether that method can be applied, in general.

To answer this question, in this paper, we discuss the feasibility of extracting $\langle r^2\rangle_n$ from the second and fourth moments of $\rho_{\rm ch}$, avoiding as much as possible the use of model-induced correlations. We also explore a method to extract the neutron-skin thickness by employing the information of $\rho_{\rm ch}$ of two neighboring even-even isotopes to cancel a large part of the spin-orbit contributions and reduce the uncertainty due to the nucleon form factors and the pairing correlation. We will show that the key issue is to extract $\langle r^2\rangle_n$ from $\langle r^2\rangle_{\rm ch}$ and $\langle r^4\rangle_{\rm ch}$ to accurately determine $\langle r^4\rangle_p$.

The second and fourth moments of $\rho_{\rm ch}$ read

$$\langle r^2\rangle_{\rm ch} = \langle r^2\rangle_p + \left(r^2_{{\rm E}p} + \frac{N}{Z} r^2_{{\rm E}n}\right) + \langle r^2\rangle_{{\rm SO}p} + \frac{N}{Z}\langle r^2\rangle_{{\rm SO}n}\,, \tag{1a}$$

$$\langle r^4\rangle_{\rm ch} = \langle r^4\rangle_p + \frac{10}{3}\left(r^2_{{\rm E}p}\langle r^2\rangle_p + \frac{N}{Z} r^2_{{\rm E}n}\langle r^2\rangle_n\right) + \left(r^4_{{\rm E}p} + \frac{N}{Z} r^4_{{\rm E}n}\right) + \langle r^4\rangle_{{\rm SO}p} + \frac{N}{Z}\langle r^4\rangle_{{\rm SO}n}\,, \tag{1b}$$

where $r^2_{{\rm E}\tau}$ and $r^4_{{\rm E}\tau}$ are the second and fourth moments of the charge distribution of the nucleon τ, respectively. The spin-orbit contributions $\langle r^n\rangle_{{\rm SO}\tau}$ read

$$\langle r^2\rangle_{{\rm SO}\tau} \simeq \frac{\kappa_\tau}{M_\tau^2 N_\tau}\sum_{a\in{\rm occ}} \mathcal{N}_{a\tau}\langle \boldsymbol{l}\cdot\boldsymbol{\sigma}\rangle\,, \tag{2a}$$

$$\langle r^4\rangle_{{\rm SO}\tau} \simeq \frac{10}{M_\tau^2 N_\tau}\left[\frac{\kappa_\tau}{5}\langle r^2\rangle_\tau + \frac{r^2_{{\rm M}\tau} - r^2_{{\rm E}\tau}}{3} + \frac{\kappa_\tau}{2M_\tau^2}\right] \times \sum_{a\in{\rm occ}} \mathcal{N}_{a\tau}\langle \boldsymbol{l}\cdot\boldsymbol{\sigma}\rangle\,, \tag{2b}$$

where $N_\tau = Z$ for the proton ($\tau = p$) distribution and $N_\tau = N$ for the neutron ($\tau = n$) distribution, κ_τ is the anomalous magnetic moment of the nucleon τ, and $r^2_{{\rm M}\tau}$ is the second moment of magnetic distribution of the nucleon τ. The index $a = (n, \kappa, m)$ is the set of quantum numbers of a single-particle orbital, the occupation number of which is $\mathcal{N}_{a\tau}$. It is also assumed that the second moment of a single-particle orbital is approximately equal to $\langle r^2\rangle_\tau$, which is probably a good approximation except in weakly bound systems.

We then consider whether $\langle r^2\rangle_n$ can be extracted from experimental data of $\langle r^2\rangle_{\rm ch}$ and $\langle r^4\rangle_{\rm ch}$ by using Eqs. (1a) and (1b). Our goal was to reduce model assumptions to a minimum. To this end, we have discussed in detail two contributions to the neutron moment: $\langle r^n\rangle_{{\rm SO}\tau}$ and $\langle r^4\rangle_p$. As for the latter, we have seen that it can be related to $\langle r^2\rangle_p$ in a quite robust manner. Therefore, we deem that we have been able to determine the mildest assumptions under which the $\langle r^2\rangle_n$ of a single isotope can be extracted.

Our main result has been the introduction of a novel method to extract $\langle r^2\rangle_n$ from $\rho_{\rm ch}$ using the information of two neighboring even-even nuclei. The uncertainties due to the nucleon form factors and the approximation for $\langle r^n\rangle_{{\rm SO}\tau}$ are suppressed, whereas the uncertainties introduced by the pairing are negligible. We advocate that this method, namely the consideration of two neighboring isotopes, is more reliable.

Despite our efforts, we conclude that the main obstacle to an accurate determination of the neutron radius is the contribution from $\langle r^4\rangle_p$. Even if it is strongly correlated to $\langle r^2\rangle_p$, the resulting uncertainty cannot be neglected. This uncertainty is strongly enhanced when propagated from the fourth moment to the neutron radius. Eventually, extracting the neutron radius or the neutron-skin thickness from $\langle r^2\rangle_{\rm ch}$ and $\langle r^4\rangle_{\rm ch}$ does not seem to be feasible based on the present discussion. Despite these pessimistic conclusions, the equations derived in this paper may be useful for further understanding and investigation and even more useful if, in the future, a clever way to better determine the proton fourth moment can be envisaged.

† Condensed from the article in Phys. Rev. C **104**, 024316 (2021)

*1 Department of Physics, University of Tokyo
*2 RIKEN Nishina Center
*3 Dipartimento di Fisica, Università degli Studi di Milano
*4 INFN, Sezione di Milano

References

1) H. Kurasawa, T. Suzuki, Prog. Theor. Exp. Phys. **2019**, 113D01 (2019).
2) P. -G. Reinhard *et al.*, Phys. Rev. C **101**, 021301 (2020).
3) H. Kurasawa *et al.*, Prog. Theor. Exp. Phys. **2021**, 013D02 (2021).

Comment on "Breakdown of the tensor component in the Skyrme energy density functional"†

H. Sagawa,[*1] G. Colò,[*2,*3] and L. Cao[*4]

In a recent paper published in Phys. Rev. C[1)], hereafter referred to as Dong and Shang, the authors claim in the abstract that "the Skyrme original tensor interaction is invalid." One should note that, although the original idea by Skyrme dates back to the 1950s and the Skyrme tensor force has been written out in Ref. 2), there have been many studies on how to implement it and fit its parameters since then, even in recent years. In 2014, some of us published a review paper on the tensor force within mean-field and density functional theory (DFT) approaches to the nuclear structure.[3)] In that review, we quoted ≈30–40 papers where the Skyrme tensor is implemented and studied, authored by different colleagues. The conclusion of that review paper is that evidences for a strong neutron-proton tensor force exist, even in mean-field and DFT studies. Therefore, if the tensor force proposed by Skyrme were "invalid," this would impact on a considerable number of published works and conclusions drawn so far. Accordingly, it would be appropriate to have a strong argument regarding this "invalidity."

The argument against the Skyrme tensor force in Ref. 1) was given as: "The Skyrme original tensor force was introduced in an unreasonable way, because the tensor-force operator S_{12} in momentum space but with an r-dependent strength, *i.e.*, $f_T(r)S_{12}(\mathbf{k})$, is applied as a starting point." We note that $S_{12}(\mathbf{k})$ can be expressed as, $S_{12}(\mathbf{k}) = (\sigma_1 \cdot \mathbf{k})(\sigma_2 \cdot \mathbf{k}) - k^2 \frac{\sigma_1 \cdot \sigma_2}{3}$. We do not see any logic behind the sentence by Dong and Shang. In physics, nothing forbids an interaction to be position-dependent and momentum-dependent at the same time. Bethe[4)] was one of the first to advocate that this ought to be the case if one wishes to introduce an effective potential for finite nuclei. Skyrme echoed this at the beginning of his first paper on this topic, and it is useful at this stage to quote literally the sentence from Ref. 5): "in the case of a finite system the effective potential must depend upon both momenta and coordinate."

Several authors have proposed Skyrme-type forces with terms that have both momentum- and density-dependence. If the Skyrme tensor force is unreasonable because of the reason advocated by Dong and Shang, the whole Skyrme force will be unreasonable. If this were the case, this would discredit not only the results of a few hundred papers in which Skyrme tensor terms are introduced but also some more $\approx 10^3$ papers in which Skyrme forces are used.

In the paper by Dong and Shang, it is also claimed that the Skrme-type tensor interaction is introduced in an unreasonable way since the Fourier transform of such tensor interaction is difficult or even impossible. We disagree on this claim based on the procedure that we discuss explicitly as follows. We show that if we start from a general central, spin-orbit or tensor interaction with a radial dependence such that the range is very short, the Fourier transform produces the Skyrme force in momentum space. Let us write the Fourier transform of an interaction $V(r)$ as

$$V(\mathbf{q}) = \int e^{i\mathbf{q}\cdot\mathbf{r}} V(r) d\mathbf{r}, \tag{1}$$

where $\mathbf{q} = \mathbf{k} - \mathbf{k}'$ is the momentum transfer ($\mathbf{k}$ and $\mathbf{k}'$ are the initial and final relative momenta, respectively). The tensor interaction in the coordinate space is expressed as

$$V_T(r) = f_T(r) S_{12}(\mathbf{r}), \tag{2}$$

where $S_{12}(\mathbf{r}) = (\sigma_1 \cdot \mathbf{r})(\sigma_2 \cdot \mathbf{r}) - r^2 \frac{\sigma_1 \cdot \sigma_2}{3} = \sqrt{\frac{8\pi}{3}}[(\sigma_1 \cdot \sigma_2)^{(2)} \times r^2 Y_2(\hat{r})]^{(0)}$ with the spherical harmonics $Y_{2\mu}$. The Fourier transform can be evaluated as

$$V_T(\mathbf{q}) \propto \int r^4 dr f_T(r) j_2(qr) [(\sigma_1 \cdot \sigma_2)^{(2)} \times Y_2(\hat{q})]^{(0)}. \tag{3}$$

using the multipole expansion of a plane wave. The spherical Bessel function $j_2(qr)$ is proportional to q^2, as $j_2(qr) \sim (qr)^2/5!!$ in the lowest order of expansion, and $V_T(\mathbf{q})$ becomes

$$V_T(\mathbf{q}) \simeq -\frac{4\pi}{15}\sqrt{\frac{8\pi}{3}} [(\sigma_1 \cdot \sigma_2)^{(2)} \times q^2 Y_2(\hat{q})]^{(0)} \int r^6 f_T(r) dr. \tag{4}$$

In this way, we obtain the tensor interaction in momentum space. This is a further, more detailed, and mathematically rigorous way to show that the arguments in the paper by Dong and Shang are invalid.

† Condensed from the article in Phys. Rev. C **104**, 039801 (2021)

*1 RIKEN Nishina Center
*2 Dipartimento di Fisica "Aldo Pontremoli," Università degli Studi di Milano
*3 INFN, Sezione di Milano
*4 College of Nuclear Science and Technology, Beijing Normal University

References
1) J. M. Dong, X. L. Shang, Phys. Rev. C **101**, 014305 (2020).
2) T. H. R. Skyrme, Nucl. Phys. **9**, 615 (1959).
3) H. Sagawa, G. Colò, Prog. Part. Nucl. Phys. **76**, 76 (2014).
4) H. Bethe, Phys. Rev. **103**, 1353 (1956).
5) T. H. R. Skyrme, Philos. Mag. **1**, 1043 (1956).

3. Nuclear Data

Production of ^{93}Zr sample in the ^{93}Nb(n, p) reaction towards accurate determination of ^{93}Zr half-life

A. Takamine,[*1] H. Iimura,[*1,*2] M. Tajima,[*1] H. Haba,[*1] N. Sato,[*1] S. Go,[*1] K. Imamura,[*1] A. Gladkov,[*1] H. Yamazaki,[*1] and H. Ueno[*1]

The half-live of a long-lived fission product (LLFP) is not reliable, even though it is one of the important basic data to evaluate the long-term radiological risk of nuclear fuel waste. For example, although ^{93}Zr will be the second significant contributor to the fission product activity of nuclear wastes in 1000 years[1] due to its long half-life, the half-life of ^{93}Zr has been reported as 1.53 Myr,[2] 1.13(11) Myr,[3] and 1.64(6) Myr,[1] and the discrepancy between these values is as large as 30%.

Because it is impossible to measure the decay of radioactivity directly by observing it, the half-lives of LLFPs have been deduced by the formula $T_{1/2} = (\ln 2)N/A$ where N is the number of the atoms and A the radioactivity. In the measurements of A and N, impurities in samples cause unpredictable errors, such as isobar impurities in a mass spectrometry. To reduce such errors and to obtain reliable half-lives, we plan to establish a new method using the collinear laser spectroscopy technique for the accurate determination of half-lives of LLFPs, starting with ^{93}Zr. The ^{93}Zr samples in the previous measurements were chemically separated from a spent nuclear fuel and a zircaloy cladding, but both of them contain many nuclides which may lead to unexpected error. We instead prepared a ^{93}Zr sample using the ^{93}Nb(n, p) ^{93}Zr reaction. Because other radioactive nuclides produced simultaneously by fast neutron beams on this target are almost limited to the Nb isotopes from the (n, xn) reaction, pure radioactivity of ^{93}Zr can be obtained by the chemical separation. The number of ^{93}Zr will be determined from the resonance peak intensities in spectra measured by a collinear laser spectroscopy using the ^{93}Zr sample added with a quantified neutral Zr standard. This can avoid the errors from isobar impurities that could occur in a mass spectrometry.

We conducted a 1-day beam time test in October 2021. Neutrons with an energy of approximately 10 MeV were produced in the ^{9}Be(d, n) reaction by irradiating a 30-MeV d beam from the AVF cyclotron onto a beryllium target of 1.85 g/cm^2. The ^{93}Zr isotopes were then produced in the ^{93}Nb target behind the ^{9}Be target by the ^{93}Nb$(n, p)^{93}$Zr reaction. We prepared a ^{93}Nb target of 102.8 g/cm^2, which was composed of 120 layers of 1-mm thick and ϕ15 mm ^{93}Nb disks. During the beam time, the d beam intensity was measured using a ^{9}Be target holder as a Faraday cup. We evaluated that the ^{9}Be target was irradiated with 5.8×10^{18} deutrons in total. Based on the production cross section data from JENDL-4.0, ^{92m}Nb ($T_{1/2} = 10.15$ d) was expected to be the most abundant radioactive source in the target.

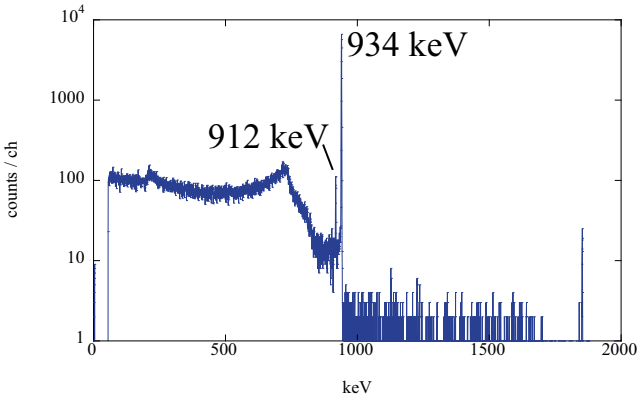

Fig. 1. Example γ-ray spectrum for the neutron-irradiated ^{93}Nb target.

We started γ-ray measurements for the ^{93}Nb targets 5 days after the irradiation. The 120 ^{93}Nb targets were measured one by one using a Ge detector. Figure 1 shows the γ-ray spectrum from the most downstream ^{93}Nb target, as an example, which presents intense peaks of ^{92m}Nb at 934 keV and 912 keV. Using the γ-ray yields of 934 keV from ^{92m}Nb, we evaluated the ^{92m}Nb radioactivity of each target at the end of the beam time, taking into account the measurement date, peak count rates, half-life, γ-ray intensity, and detector efficiency. The total radioactivity was found to be 27.39(9) MBq. A further detailed analysis is in progress.

The target will be chemically separated to extract ^{93}Zr after cooling down to reduce its radioactivity. Then, β-particles from the ^{93}Zr sample will be measured by liquid scintillation counting to measure the ^{93}Zr radioactivity. If we find that the amount of ^{93}Zr is sufficient, we will proceed to the number measurement using our collinear laser spectroscopy setup.[4,5]

The production yields and their dependences on the target thickness obtained in this experiment for ^{92m}Nb and other nuclides can be used to check the validity of the evaluated fast neutron cross section data. We will compare the present results with the predictions using, for example, PHITS[6] with the JENDL data library.

*1 RIKEN Nishina Center
*2 Advanced Science Research Center, Japan Atomic Energy Agency

References
1) P. Cassette *et al.*, Appl. Radiat. Isot. **68**, 122 (2010).
2) K. F. Flynn, private communication to NNDC (1972).
3) J. Yang *et al.*, Radiochim. Acta **98**, 59 (2010).
4) M. Tajima *et al.*, RIKEN Accel. Prog. Rep. **53**, 15 (2020).
5) M. Tajima *et al.*, in this report.
6) T. Sato *et al.*, J. Nucl. Sci. Technol. **55**, 684 (2018).

EXFOR compilation of data from RIBF in 2021

T. Tada,[*1] M. Kimura,[*1,*3,*4] M. Aikawa,[*2,*4] and N. Otuka[*4,*5]

A nuclear database is the compilation of measured reaction data and plays an essential role in providing the best estimate for the safety and effective use of nuclear reactions for various purposes. Thus, nuclear reaction databases support the most fundamental aspect of nuclear sciences and technologies, such as nuclear physics, astrophysics, nuclear reactor development, environmental monitoring, dosimetry, radioisotope production, and radiotherapy.

One of the largest and globally used public nuclear reaction databases is the EXchange FORmat (EXFOR) library for experimental nuclear reaction data.[1)] The EXFOR library is a universal common repository for nuclear reactions. It was established in 1967. The International Network of Nuclear Reaction Data Centres (NRDC) maintains the EXFOR library under the supervision of the International Atomic Energy Agency (IAEA).[2)] The EXFOR library covers a wide range of nuclear reactions, such as neutron-, charged-particle-, and photon-induced reactions.

The Hokkaido University Nuclear Reaction Data Centre (JCPRG),[3)] founded in 1973, is responsible for the compilation of the charged-particle- and photon-induced nuclear reaction experiments conducted in Japanese accelerator facilities.[4)] Our contributions to the EXFOR database constitutes approximately 10% of the total amount of the data records. The database covers papers published in peer-reviewed journals, and a unique EXFOR entry number is assigned to each paper. Each record includes the information of the bibliography, experimental setup, reaction code, measured numerical data, and uncertainties for the reaction. For the compilation of each record, we usually request the corresponding authors to provide us the original data for the numerical accuracy of the database.

Since 2010, JCPRG and RIKEN Nishina Center have been cooperating for the compilation of data obtained by RIBF, which aims to enforce the availability of RIBF data. In 2021, we compiled 33 new articles published by Japanese facilities. These include 16 articles from RIKEN, 4 registered articles, and 12 articles still in the process of registration. The compiled data are accessible by entry numbers, which are listed in Table 1.

Table 1. Entry numbers with references compiled from RIBF data in 2021.

		Entries	
New	E2670[5)]	E2671[6)]	E2672[7)]
	E2676[8)]	E2682[9)]	E2685[10)]
	E2687[11)]	E2689[12)]	E2693[13)]
	E2697[14)]	E2698[15)]	E2703[16)]
	E2704[17)]	E2705[18)]	E2713[19)]
	E2715[20)]		
Total		16	

We acknowledge that collaboration with RIKEN is helpful for us to establish an effective procedure for the compilations. Most RIKEN data are very quickly compiled after publication, and end-users can easily access them. We also thank all authors of articles from RIKEN, who provided us the numerical data. This greatly helps increase the accuracy and quality of the database.

References
1) N. Otuka *et al.*, Nucl. Data Sheets **120**, 272 (2014).
2) `https://www-nds.iaea.org/`.
3) Hokkaido University Nuclear Reaction Data Centre, `https://www.jcprg.org/`.
4) M. Kimura, AAPPS Bulletin **28**, 24 (2018).
5) K. J. Cook *et al.*, Phys. Rev. Lett. **124**, 212503 (2020).
6) T. L. Tang *et al.*, Phys. Rev. Lett. **124**, 212502 (2020).
7) S. Bagchi *et al.*, Phys. Rev. Lett. **124**, 222504 (2020).
8) H. Haba *et al.*, Phys. Rev. C **102**, 024625 (2020).
9) Z. Tsoodol *et al.*, Appl. Radiat. Isot. **168**, 109448 (2021).
10) H. Suzuki *et al.*, Phys. Rev. C **102**, 064615 (2020).
11) L. Yang *et al.*, Phys. Lett. B **813**, 136045 (2021).
12) Z. H. Yang *et al.*, Phys. Rev. Lett. **126**, 082501 (2021).
13) M. Aikawa *et al.*, Nucl. Instrum. Methods Phys. Res. B **498**, 23 (2021).
14) D. Ichinkhorloo *et al.*, Nucl. Instrum. Methods Phys. Res. B **499**, 46 (2021).
15) M. M. Juhász *et al.*, Phys. Lett. B **814**, 136108 (2021).
16) M. Sakaguchi *et al.*, Appl. Radiat. Isot. **176**, 109826 (2021).
17) M. M. Juhász *et al.*, Phys. Rev. C **103**, 064308 (2021).
18) D. Bazin *et al.*, Phys. Rev. C **103**, 064318 (2021).
19) F. Browne *et al.*, Phys. Rev. Lett. **126**, 252501 (2021).
20) M. Aikawa *et al.*, Nucl. Instrum. Methods Phys. Res. B **508**, 29 (2021).

*1 Graduate School of Science, Hokkaido University
*2 Faculty of Science, Hokkaido University
*3 Research Center for Nuclear Physics, Osaka University
*4 RIKEN Nishina Center
*5 Nuclear Data Section, International Atomic Energy Agency

4. Hadron Physics

Simulation study of the charged current DIS cross-section measurement at the EIC

S. Shimizu*1,*2 for the ECCE inclusive reaction group

The precise understanding of the proton structure is one of the keys to answering what matter is made of. Precision is also an important factor as an input in the LHC experiments[1,2] that investigate new physics from TeV-scale proton-proton collisions. While recent LHC results have improved the precision, the electron-proton (ep) scattering data from HERA[3] is still the most important input in the determination of the parton distribution in protons.

The primary process of interest at ep scattering is the deep inelastic scattering (DIS). It is an electroweak process via the exchange of a virtual photon or weak boson between the electron and a parton in the proton. The kinematic variables used to describe DIS are the energy scale Q^2, Bjorken x, and the inelasticity y. Charged current (CC) DIS proceeds via a $W^{\pm}$ boson exchange and hence is a charge selective process. It has a sensitivity to the distribution of quarks with the opposite charge of the incoming lepton.

The Electron Ion Collider (EIC) is the next collider scheduled to be built at the Brookhaven National Laboratory in US. The EIC performs collisions of electrons and protons or nuclei. It has a few beam-energy settings and the highest centre-of-mass energy is 141 GeV. The value is smaller than that of HERA; however, the high luminosity allows a measurement at the edge of the kinematic coverage of the EIC. The EIC is expected to have ep DIS cross-section measurements at the region with higher x values than the HERA data.

The ECCE detector[4] is a multi-purpose detector proposed at the EIC. The full detector simulation is available, and the CC DIS analysis is performed using the simulated samples. CC DIS events are generated as the signal events and neutral current DIS and photoproduction events are generated as background events for ep scattering at the highest beam-energy setting of 18 GeV $\times$ 275 GeV.

In CC DIS, the incoming electron is scattered as a neutrino and cannot be detected. The kinematic variables are reconstructed only from the information of the hadronic final state.[a] Resolution of the reconstructed variables are found to be typically at 15–25%, except for the region corresponding to the calorimeter edges. A large reconstruction bias is observed, possibly due to the insufficient calibration of the calorimeters.

The escaping neutrino creates an imbalance in transverse momentum (p_{T}) in the detected final state. Events with p_{T} imbalance are selected. Further criteria to ensure the quality of p_{T} imbalance are defined for the background rejection. The measurement is restricted to the region $Q^2 > 100$ GeV^2 and $y < 0.9$. The extraction of the cross section is conducted in bins of (x, Q^2). Owing to the large reconstruction bias, a coarse binning is set to avoid unreasonably large event migration. The uncertainties in the energy scale, energy resolution, and background estimation are propagated to the extracted cross section. The values of $\pm 2\%$ and 5% are *arbitrarily* assigned as the scale and resolution uncertainties, respectively.

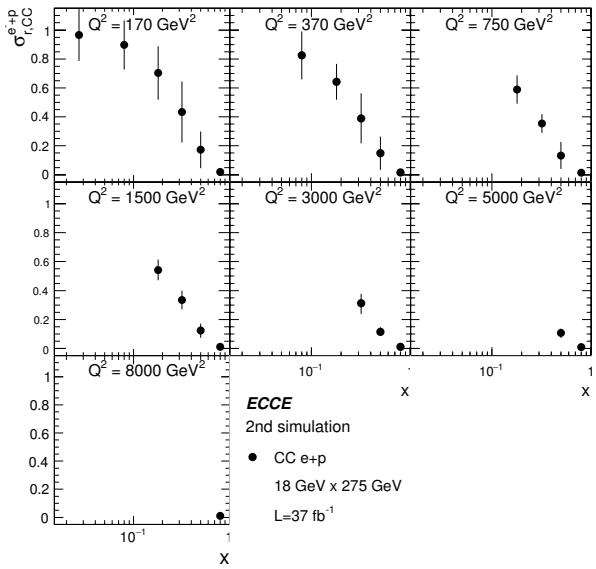

Fig. 1. Reduced CC DIS cross section for $e + p$ collisions at 18 GeV $\times$ 275 GeV extracted from the ECCE 2nd simulation samples. The total uncertainties are shown by vertical error bars. The statistical uncertainties are smaller than the size of markers.

Figure 1 shows the resulting cross section for 37 fb^{-1} of simulated collisions. The measurement reaches $(x, Q^2) = (0.8, 8000\ \mathrm{GeV}^2)$. The statistical uncertainty is small and the maximum value is given as 4% at $(x, Q^2) = (0.8, 170\ \mathrm{GeV}^2)$. The study covers a region of higher x values than that of the HERA data,[3] especially at the mild Q^2 region.

The EIC explores a region of high x, offering further information on the proton structure. Once the detector is adequately understood and properly calibrated, the measurement would be substantially improved with finer binning and smaller uncertainties.

*1 RIKEN Nishina Center
*2 Japan Society for the Promotion of Science

a) Calorimeter clusters are used with zero-mass assumption. In the future, tracking information could be included.

References
1) ATLAS collaboration, J. Instrum. **3**, S08003 (2008).
2) CMS collaboration, J. Instrum. **3**, S08004 (2008).
3) H1 and ZEUS collaborations, Eur. Phys. J. C **75**, 580 (2015).
4) `https://www.ecce-eic.org/`.

Resolution studies for the ECCE EIC detector proposal

R. Seidl*[1]

As the preparation for the electron-ion collider, EIC, is progressing, detector proposals were submitted in December 2021 to the EIC Project. One of these proposals is the ECCE consortium[1] that has based its proposal around re-using the 1.5 T BaBar magnet that is currently prepared for the sPHENIX experiment and also the outer sPHENIX hadronic calorimeter. Re-using these two components allows for more resources to concentrate on the main detector components needed for a deeply inelastic scattering (DIS) collider experiments, namely tracking, electromagnetic calorimetry and particle identification. Given the ongoing involvement of Japanese groups in PHENIX and sPHENIX, it is only natural to continue on the ECCE proposal.

The main part of the proposal concentrated on the technical solutions to fulfill the scientific goals that were formulated in the EIC white paper,[2] the National Academy of Science report and the Yellow Report.[3] All of the key measurements were studied in full GEANT4 simulations of the ECCE detector. In DIS, the main process is the incoming lepton scattering off a quark from the incoming proton or nucleus. As such, the simplest way to reconstruct the hard interaction is by measuring the scattered lepton energy and scattering angle and reconstruct the momentum transfer Q^2 and the momentum fraction x that the quark carried relative to the proton momentum. Figure 1 shows the fraction of events that get reconstructed in the same x and Q^2 bin as the true kinematics (bin retention fraction) for a fine binning that was used in many impact studies of the Yellow Report. As can bee seen, the DIS kinematics can be reconstructed very well over a large range of the phase space, but toward the bottom right corner (at low inelasticity y) the resolution suffers at very small scattering angles. Here other reconstruction methods that also make use of the hadronic final state are preferable.

Next, for many studies related to the spin and three-dimensional structure of the nucleon, semi-inclusive DIS measurements also make use of detecting at least a final-state hadron as well. One of the most important quantities is the momentum fraction z this final-state hadron carries relative to the struck quark. At higher z the hadron is more likely to carry the struck quark and therefore acts as flavor analyzer. Other relevant variables are the transverse momentum relative to the virtual photon from the hard lepton-quark interaction and the azimuthal angles of hadron and incoming proton spin orientation relative to the scattering plane.

In Fig. 2 the average resolution of z for pions in the same fine x and Q^2 binning can be seen. It also suffers somewhat at lower z due to the scattered lepton reconstruction but otherwise is very well reconstructed. The other semi-inclusive variables are even more robust. Using these resolution studies the same impact studies as in the Yellow Report were revisited using a realistic detector simulation and show that the ECCE proposal is capable to carry out these measurements successfully.

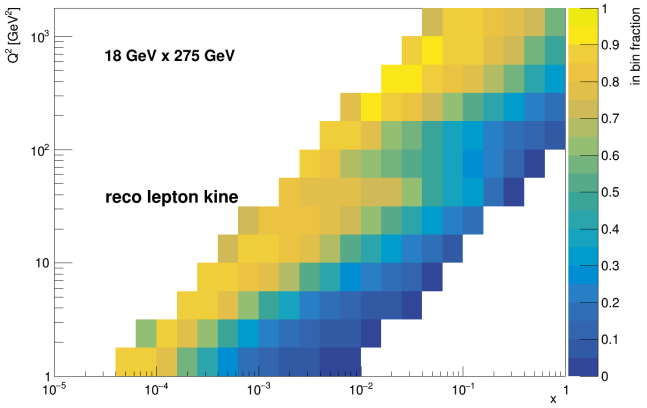

Fig. 1. Bin retention fractions in DIS events of 18 GeV on 275 GeV e-p collisions in bins of x and Q^2 when using the scattered lepton to calculate the DIS kinematics.

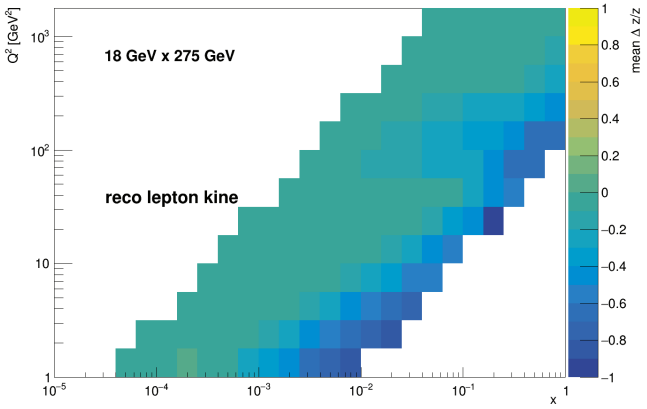

Fig. 2. z resolutions for pions in DIS events of 18 GeV on 275 GeV e-p collisions in bins of x and Q^2 when using the scattered lepton to calculate the DIS kinematics.

References

1) https://www.ecce-eic.org/.
2) A. Accardi *et al.*, Eur. Phys. J. A **52**, 268 (2016).
3) R. Abdul Khalek *et al.*, arXiv:2103.05419.

*1 RIKEN Nishina Center

Design of the zero degree calorimeter for the EIC

S. Shimizu,[*1,*2] Y. Goto,[*1] and Y. Yamazaki[*3] for the EIC Japan group and the EIC eRD27 collaboration

The Electron Ion Collider (EIC) is a future particle collider scheduled for construction in the US. By colliding electrons and protons or nuclei, the EIC will be a powerful tool to examine the structure inside of protons and nuclei. A new electron beam facility is planned to be built and will be operated together with the existing ion beams at the Brookhaven National Laboratory. The expected beam energies are 5–18 GeV for electrons and 41–275 GeV for protons, providing the highest centre-of-mass energy of 141 GeV. The EIC will cover a large kinematic region, which allows for the investigation of the parton dynamics in protons and nuclei.

In some of the key EIC physics programs,[1] it is essential to detect hadrons or photons from collisions in the far-forward region of the ion-beam direction. A suite of detectors will be placed there, in addition to the central detector at the collision point. The Zero Degree Calorimeter (ZDC) is one of the far-forward detector systems and will detect photons and neutrons. It will be placed ∼40 m downstream of the collision point, with an aperture of ∼4.5 mrad.

The first ZDC design is considered based on the physics requirements for the ZDC. Examples of measurements that need the ZDC are as follows:[1]

- Exclusive vector meson production in $e + A$ collisions, which is sensitive to gluon saturation,[2]
- Spectator-neutron-tagged e+d deep inelastic scattering, which is sensitive to the nuclear effect in deuterons,
- Meson structure measurements,
- Leading neutron measurements.

The required performance is as follows:

- Tagging of $O(100)$ MeV photons with >90% efficiency and an energy resolution of 20–30%,
- Detection of 20–40 GeV photons with an energy resolution of $\frac{35\%}{\sqrt{E(\mathrm{GeV})}}$ and a good position resolution of $O(1)$ mm,
- Detection of neutrons with energy up to the ion beam energy with an energy resolution of $\frac{50\%}{\sqrt{E(\mathrm{GeV})}} + 5\%$, a position resolution of $\frac{3\mathrm{mrad}}{\sqrt{E(\mathrm{GeV})}}$, and a large lateral size of 60 cm × 60 cm.

To fulfill these requirements, the ZDC is designed as a complex of detectors, namely a Crystal calorimeter and three types of sampling calorimeters: ALICE FoCal-E[3] style Tungsten-Silicon (W/Si), Lead-Silicon (Pb/Si), and Lead-Scintillator (Pb/Sci) calorimeters.

*1 RIKEN Nishina Center
*2 Japan Society for the Promotion of Science
*3 Department of Physics, Kobe University

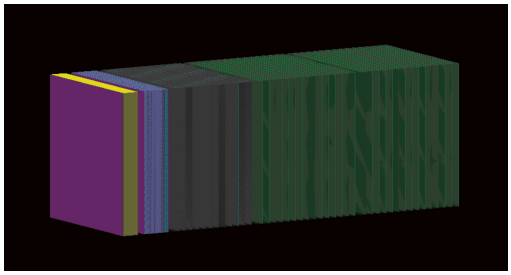

Fig. 1. ZDC design. Particles arrive from the left side of the figure. The detector consists of a 7 cm crystal layer (yellow) with a silicon pixel layer attached in front (magenta), 22 layers of tungsten/silicon planes (light purple) with an additional silicon pixel layer in front, 12 layers of lead/silicon planes (gray), and 30 layers of lead/scintillator planes (green), corresponding to a thickness of $8X_0$, $22X_0$, $2\lambda_I$, and $5\lambda_I$, respectively. The total size is 60 cm × 60 cm × 162 cm. The segmentation on each layer is as follows: 3 cm × 3 cm for the crystal, 1 cm × 1 cm for standard silicon layers, 3 mm × 3 mm for silicon pixel layers, and 10 cm × 10 cm for scintillators.

The Crystal calorimeter is intended for the energy measurement of low-energy photons. The W/Si calorimeter will measure the rest of the photon energy and the shower development of photons and neutrons. Silicon pixel layers are inserted for position measurement. Silicon layers are used in the Pb/Si calorimeter for radiation hardness and for the neutron shower measurement. The last Pb/Sci calorimeters are intended to measure the neutron energy.

The design is studied and optimized using the Geant4[4] simulation. The simulation has a few missing pieces, *e.g.*, no readout materials included for crystals and scintillators. However, it allows the study of baseline performance of the detector complex. Figure 1 shows the optimized design. The performance is studied against single photons and single neutrons. It has an energy resolution better than the requirement and a position resolution for photons better than 2 mm.

The design will be further optimized based on its cost, radiation hardness, and the full simulation. The optimization includes the choice of materials for the crystal, such as $PbWO_4$ (this study) and LYSO.

References

1) R. A. Khalek *et al.*, arXiv:2103.05419.
2) A. Accardi *et al.*, Eur. Phys. J. A **52**, 268 (2016).
3) ALICE collaboration, ALICE-PUBLIC-2019-005, (2019) `https://cds.cern.ch/record/2696471` .
4) S. Agostinelli *et al.*, Nucl. Instrum. Methods Phys. Res. A **506**, 250 (2003).

Preparation for very-forward particle measurements in RHICf-II experiment

M. H. Kim*[1] for the RHICf-II Collaboration

In June 2017, the RHIC-forward (RHICf) experiment[1] measured the very-forward neutral particles in polarized $p+p$ collisions at $\sqrt{s} = 510$ GeV by installing an electromagnetic calorimeter (RHICf detector) 18 m downstream of the STAR experiment. The RHICf experiment has two experimental goals. The first one is the cross-section measurement to constrain the hadronic interaction model, which is necessary to study the origin of ultra high-energy cosmic-rays.[2] The other one is the transverse single spin asymmetry (A_N)[3] measurement to understand the spin-involved production mechanism.

The first result[4] of the RHICf experiment showed non-zero A_N of the very forward π^0, which shows a possibility of the diffractive contribution to the A_N of π^0. To study the underlying interaction of the first result in more detail and also measure various particles, a follow-up experiment, RHICf-II, is being prepared.

Compared to the RHICf experiment, the RHICf-II experiment will be performed at $\sqrt{s} = 200$ GeV. The A_N of the very-forward π^0 at $\sqrt{s} = 200$ GeV and 510 GeV will be compared for testing the x_F scaling at the different energies using the correlation with the STAR detectors. The RHICf-II experiment will possibly include polarized proton-nucleus ($p+A$) collisions. The ultra peripheral collision and the hadronic contributions to the very-forward neutron A_N in polarized $p+A$ collisions[5] can be studied in more detail with wider p_T coverage. We will also measure the A_N of the very-forward π^0 in polarized $p+A$ collisions for the first time to study the relation between the very-forward π^0 and neutron A_N.

We are also planning to measure Λ and K^0_S. Cross-section of K^0_S is an important observable to study the atmospheric neutrino flux background of the cosmic neutrino detection. A_Ns of Λ and K^0_S will enable to extend our understanding of the particle production mechanism because the A_N of Λ is a possible origin of that of the very-forward π^0.

Because the acceptance of the RHICf detector was not enough for Λ and K^0_S measurements, a new larger detector (RHICf-II detector) of 8 cm × 18 cm size is being developed. With the larger detector, we can measure Λ decay into $n + 2\gamma$ and K^0_S decay into 4γ. Because their particle yields in the RHICf-II detector are expected to be one order of magnitude lower than that of π^0, a trigger logic to more effectively measure Λ and K^0_S is being studied.

We are developing the RHICf-II detector by transferring the technology of the ALICE FoCal-E detector.[6] Figure 1 shows the longitudinal composition of the ALICE FoCal-E. It is a sampling electromagnetic calorimeter which is composed of tungsten and silicon layers. Each layer is made up of high granularity layer (30 μm × 30 μm) for position measurement and low granularity layer (1 cm × 1 cm) for energy measurement. To more effectively measure neutron, the interaction length of the RHICf-II detector will be increased compared to that of the RHICf detector.

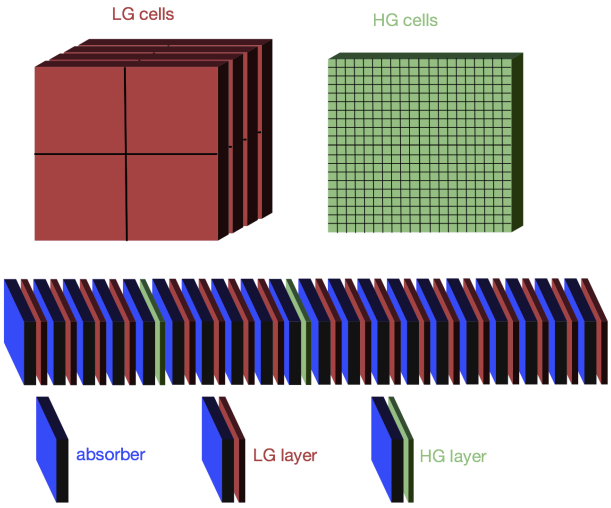

Fig. 1. Longitudinal composition of ALICE FoCal-E detector.[6]

We are proposing to perform the RHICf-II experiment at STAR in 2024. Currently, we're discussing the detailed plan with the STAR and ALICE FoCal members. Two modules of the ALICE FoCal-E will be used to cover the RHICf-II acceptance. A prototype of the first module is being developed now and its full prototype will be prepared in 2022. The other prototype will be prepared in the next year while the first one is in the commissioning.

*1 RIKEN Nishina Center

References
1) RHICf Collaboration, arXiv:1409.4860v1.
2) O. Adriani *et al.*, J. High Energy Phys. **2018**, 73 (2018).
3) M. H. Kim *et al.*, in this report.
4) M. H. Kim *et al.*, Phys. Rev. Lett. **124**, 252501 (2020).
5) C. Aidala *et al.*, Phys. Rev. Lett. **120**, 022001 (2018).
6) ALICE Collaboration, CERN-LHCC-2020-009.

Measurement of J/ψ and ψ' productions in p+d and p+p at SeaQuest

K. Nakano,[*1,*2] Y. Goto,[*2] Y. Miyachi,[*3] K. Nagai,[*4] S. Sawada,[*2,*5] and T. -A. Shibata[*2,*6]
for the E906/SeaQuest Collaboration

The partonic structure of the proton is one of the most vital topics in hadron physics. The SeaQuest (E906) experiment at the Fermi National Accelerator Lab (FNAL) in USA is aimed at measuring the flavor asymmetry of light antiquarks in the proton, $\bar{d}(x)/\bar{u}(x)$, at large Bjorken x ($\gtrsim 0.3$). It utilizes the 120-GeV proton beam from the FNAL Main Injector and targets of liquid hydrogen and liquid deuterium. The result of $\bar{d}(x)/\bar{u}(x)$ using the Drell-Yan process is being reported.[1,2)]

The data recorded by SeaQuest include J/ψ and ψ' productions. The production cross sections of J/ψ and ψ' are sensitive to distributions of both antiquarks and gluons through the $q\bar{q}$ annihilation ($q\bar{q} \to J/\psi$ or ψ') and gluon fusion ($gg \to J/\psi$ or ψ'), as shown in Fig. 1. The $q\bar{q}$ annihilation dominates in the region of large Feynman x ($x_F \gtrsim 0.4$) where SeaQuest can measure. Therefore, the measurement of J/ψ is expected to provide additional constraints on parton distribution functions (PDFs), particularly of antiquarks at middle values of Bjorken x. Furthermore, the measurement of ψ' helps us disentangle the antiquark and gluon contributions because the ratio of the $q\bar{q}$ and gg sub-processes in the ψ' production is different from that in the J/ψ production, as evaluated by a calculation based on non-relativistic quantum chromodynamics (NRQCD).[3)]

Muon pairs from J/ψ and ψ' decays were detected by the SeaQuest spectrometer.[4)] SeaQuest acquired physics data from 2013 to 2017 to record 1.4×10^{18} beam protons on targets. The first half of the recorded data waw analyzed. The detection efficiency of J/ψ was corrected by simulation. The beam intensity was measured with a secondary-electron emission monitor (SEM) for normalizing the p+d and p+p cross sections.

We have reported the p+d/p+p ratio of the J/ψ cross sections.[5)] It is sensitive to the relative sizes of the $\bar{q}$ and g distributions.

On the other hand, the absolute cross section of the J/ψ production in p+p is sensitive to the absolute sizes of the $\bar{q}$ and g distributions. Figure 2 shows the preliminary result measured by SeaQuest as a function of x_F. The solid line is the theory prediction based on the NRQCD framework and the CT14nlo PDF. It shows fair agreement with the measured result. The dashed line is the theory prediction for the ψ' production. Further analysis of the SeaQuest data is underway to extract the ψ' absolute cross section.

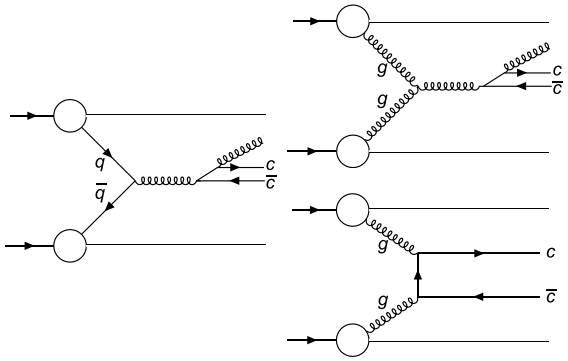

Fig. 1. Leading diagrams of J/ψ productions in proton+proton reaction.

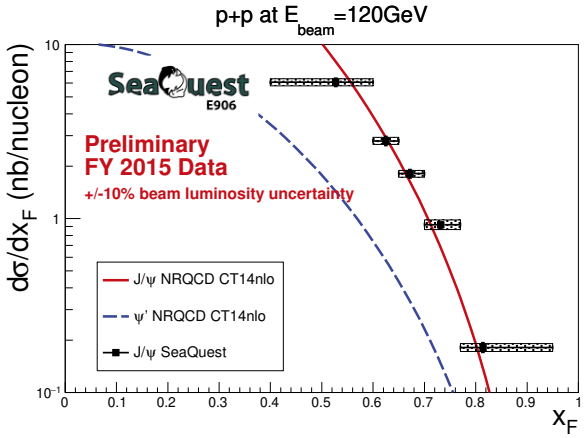

Fig. 2. Absolute cross section of J/ψ and ψ' productions vs. x_F. The points are experimental J/ψ data obtained by SeaQuest, with the statistical and systematic uncertainties drawn as vertical bars and shaded boxes, respectively. The two lines are theory predictions for the J/ψ and ψ' production.[3)]

*1 Department of Physics, University of Virginia
*2 RIKEN Nishina Center
*3 Faculty of Science, Yamagata University
*4 High Energy Nuclear Physics, Los Alamos National Laboratory
*5 Institute of Particle and Nuclear Studies, KEK
*6 College of Science and Technology, Nihon University

References

1) Y. Goto *et al.*, in this report.
2) J. Dove *et al.*, Nature **590**, 561 (2021).
3) C. Y. Hsieh *et al.*, Chin. J. Phys. **73**, 13 (2021).
4) C. A. Aidala *et al.*, Nucl. Instrum. Methods Phys. Res. A **930**, 49 (2019).
5) K. Nakano *et al.*, RIKEN Accel. Prog. Rep. **54**, 60 (2021).

Transverse single spin asymmetries of forward neutrons in $p+p$, $p+$Al and $p+$Au collisions at $\sqrt{s_{NN}} = 200$ GeV as a function of transverse and longitudinal momenta†

R. Seidl*1 and the PHENIX Collaboration

In 2015 the PHENIX collaboration took data with transversely polarized proton beams in proton-proton, proton-Al and proton-Au collisions at center-of-mass energies of 200 GeV per nucleon. One of the mesurements that were performed with this dataset are very forward neutron single-spin asymmetries that were detected with the zero-degree calorimeter in the direction of the polarized proton beam. It is located ca 18m downstream of the beam collision point. As reported, nonzero single spin asymmetries for proton-proton collisions were already known,[1] but the fact that sign and magnitude of such asymmetries were different in proton-nucleus collisions[2] initially came as a surprise. Since then it has been realized, that apart from meson interchange,[3] in p-A collisions increasingly also ulatraperipheral collisions (UPC) can create such asymmetries.[4] In UPC, a nucleus emits virtual photons that can collide with the proton and create final states with forward neutrons, most notably via the production of a Delta resonance.

Previously, these results were extracted integrated over the transverse momentum p_T of the neutron and the longitudinal momentum fraction x_F relative to the proton beam momentum and its direction. Using Bayesian unfolding as implemented in ROOT the PHENIX experiment has now extracted also the explicit x_F and p_T dependence of these asymmetries for the first time. Additionally, the asymmetries were calculated in (anti) correlation with activity in other forward detectors (beam-beam counters, BBC) that are predominantly sensitive to hard collisions and thus allow to enhance or reduce the contribution of the mostly very soft UPC events.

It was found that the meson-based calculations describe the proton-proton data very well, showing roughly a linear transverse momentum dependence with very little x_F dependence. A comparison between inclusive and hard-collision enahanced (BBC tagged) asymmetries shows that some UPC contributions may be present. In p+Al collisions the inclusive asymmetries are comparable with zero over most of the phase-space while the hard-collision enhanced sample is comparable to the $p+p$ case. In contrast, the BBC-vetoed sample (softer processes such as UPC enhanced) shows already positive asymmetries as shown in Fig. 1. The asymmetries in this case are initially rising but do show an indication of a decrease at higher transverse momenta. Theoretical calculations[4] that include both effects qualitatively describe the behavior but do not reproduce the details very well. However, the UPC based calculations only take decays of resonances with one pion in addition to the neutron into account while unpolarized MCs show that other contributions are also present. This likely explains the very sharp kinematic dependence of the theory calculations as the phase-space for neutrons from Delta decays is very limited.

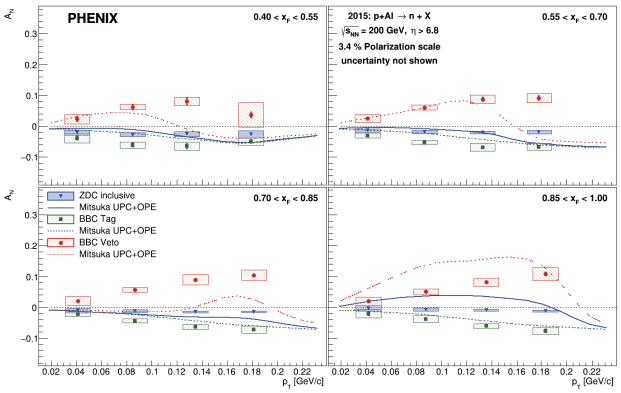

Fig. 1. Neutron single spin asymmetries for p+Al collisions either measured inclusively (blue), enhancing hard collisions (green, labelled BBC tagged) or enhancing UPC events (red, labeled BBC veto) as a function of transverse momentum p_T in bins of x_F.

In p+Au collisions the contributions from UPC are even larger as they increase quadratically with the charge of the nucleus. Here, even some UPC events seem to remain in the hard-collision enhanced data sample where the asymmetries are nearly vanishing while both inclusive and UPC enhanced asymmetries are positive. They reach up to 40% and show a similar behavior as in the UPC enhanced p+Al case.

These results will help further understand the mechanisms that create very forward neutron single spin asymmetries.

References
1) Y. Fukao *et al.*, Phys. Lett. B **650**, 325 (2007).
2) C. Aidala *et al.*, Phys. Rev. Lett. **120**, 022001 (2018).
3) B. Z. Kopeliovich *et al.*, Phys. Rev. D **84**, 114012 (2011).
4) G. Mitsuka, Phys. Rev. C **95**, 044908 (2017).

† Condensed from the article in Phys. Rev. D **105**, 032004 (2022)

*1 RIKEN Nishina Center

Analysis of transverse single spin asymmetry for the forward neutron at the RHICf experiment

M. H. Kim*1 for the RHICf Collaboration

In high energy p+p collision, a spin-involved production mechanism of the forward (pseudo-rapidity $\eta > 6$) neutron can be studied by the transverse single spin asymmetry (A_N), which is defined by the left-right cross section asymmetry with respect to the beam polarization. The forward neutron A_N was measured by the PHENIX experiment at the Relativistic Heavy Ion Collider (RHIC) at three different collision energies, 62.4, 200, and 500 GeV. Recently, the A_N at 200 GeV was unfolded as functions of longitudinal momentum fraction (x_F) and transverse momentum (p_T).[1)]

The non-zero neutron A_N is explained by an interference between the spin-flip and non-flip amplitudes with non-zero phase shift. The model using the π and a_1 meson exchanges between two protons for the spin-flip and non-flip showed a good agreement with the p_T dependence of the data.[2)]

In June 2017, the RHICf experiment[3)] measured the A_N of the forward neutral particles in polarized $p + p$ collisions at $\sqrt{s} = 510$ GeV. We installed an electromagnetic sampling calorimeter[4)] (RHICf detector) at the zero-degree area which was 18 m away from the interaction point of the STAR experiment at RHIC. We measured the neutrons of $0 < p_T < 1$ GeV/c which was a wider p_T coverage than those of previous measurements at PHENIX. The RHICf data can be compared with them and the validity of the π and a_1 exchange model in the higher p_T range can be also tested. In this article, we report the analysis status of the neutron A_N measurement.

First, the neutron candidate is separated from the electromagnetic event using the difference between their shower developments in the detector. A variable called L_{2D} which is defined by the correlation between the longitudinal depth of the detector where the accumulated energy deposit reaches 20% and 90% of the total was used for this separation.

RHICf detector has limited interaction length (1.6 λ_I) for the neutron energy measurement. The x_F and p_T distribution is obtained by the Bayesian unfolding[5)] method. Neutron Monte Carlo sample generated by randomizing the energy and direction was used for the input distribution. Figure 1 shows the p_T projections of the input and unfolded distributions of neutrons. The input distribution was made based on the QGSJET-II 04 model.[6)] One can see the unfolded distribution reproduces the input well. If the $\langle p_T \rangle$s of each bin are estimated based on the unfolded distribution, their differences to the original mean values are smaller than 0.02 GeV/c.

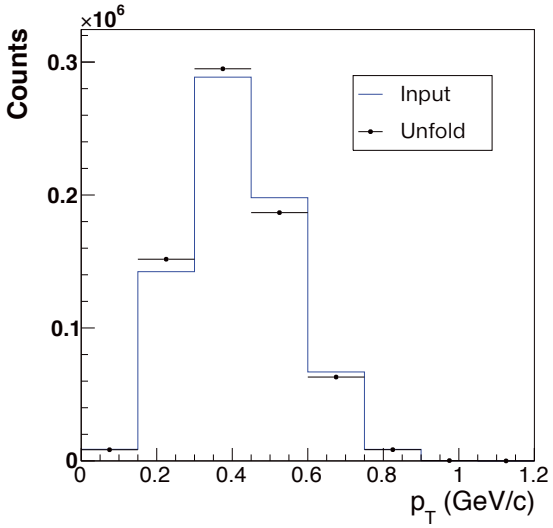

Fig. 1. Input and unfolded p_T distribution of neutron.

After the unfolding, it is necessary to subtract the background A_N because the electromagnetic contamination and the hadronic backgrounds like proton and charged pion are still included in the unfolded distribution. Each background fraction was estimated based on the Monte Carlo samples generated by QGSJET-II 04. The electromagnetic background A_N was calculated by fitting the L_{2D} distributions of the neutron candidates in the up and down polarizations using the shape of the hadronic and electromagnetic samples studied from the QGSJET-II 04 model. Since the backgrounds hadrons cannot be separated from the true neutron, their A_N was assumed as a value which was bigger than the one of the neutron candidates where they belonged to but smaller than 1 which was the maximum A_N a particle can have.

Currently, we are estimating the systematic uncertainties through the analysis procedures described above. It is expected that the analysis will be complete and the result for the neutron A_N covering the highest p_T range ever will be obtained soon.

*1 RIKEN Nishina Center

References

1) U. A. Acharya *et al.*, Phys. Rev. D, in press.
2) B. Z. Kopeliovich *et al.*, Phys. Rev. D **84**, 114012 (2011).
3) RHICf Collaboration, arXiv:1409.4860v1.
4) K. Kawade *et al.*, J. Instrum. **9**, P03016 (2014).
5) G. D'Agostini, Nucl. Instrum. Methods Phys. Res. A **362**, 487 (1995).
6) S. Ostapchenko, Nucl. Phys. B, Proc. Suppl. **151**, 143 (2006).

Status of the J-PARC E16 experiment in 2021

S. Yokkaichi*1 for the J-PARC E16 Collaboration

We proposed the experiment E16[1] to measure the vector meson decays in nuclei in order to investigate the chiral symmetry restoration in dense nuclear matter. The experiment started at the J-PARC Hadron Experimental Facility.

This experiment aims to systematically study the spectral modification of vector mesons in nuclei, particularly the ϕ meson, using the e^+e^- decay channel with statistics that are two orders larger in magnitude than those of the prior E325[2] experiment performed at KEK–PS. In other words, it aims to accumulate 1×10^5 to 2×10^5 events for each nuclear target (H, C, Cu, and Pb) and deduce the dependence of the spectral modification on the size of nucleus and meson momentum. The number of modified mesons could be larger for larger nucleus and lower meson momentum because the decay probability inside the nucleus is enhanced for such cases.

Our proposed spectrometer consists of 26 modules. As shown in Fig. 1, a module consists of Lead-glass calorimeter (LG) and Hadron-blind detector (HBD) for electron identification, as well as three-layers of GEM Trackers (GTR) and a single layer of silicon strip detector (SSD) as the tracking devices.

The first commissioning run of E16 experiment, called Run-0a, was successfully performed in June 4–20, 2020, with the newly constructed 'High-momentum beam line.'[3] Owing to budget limitations, a limited number of modules were installed in the commissioning run.

The second half, called Run-0b, was performed in Feb. 11–28, 2021, with the newly installed modules, namely, 6(SSD)-8(GTR)-6(HBD)-6(LG) modules. Unfortunately, the beam time was aborted, after only 109.5 h of execution, because of a malfunction of MR ESS.[a] To compensate for the unexecuted beam time, Run-0c was performed in May 29–June 9, 2021, for 134 h. In these two runs, 28 and 46 TB of raw data were recorded. In our beam time, approximately 24 h were required to start-up the GEM-detectors under the beam environment. The beam intensity was gradually increased during this period, and the amplification voltage of GEM was also increased carefully to avoid discharges. Furthermore, another 24 h were required to confirm the satisfactory performance of electron ID counters. Thus, for each divided beam time, we required at least 48 h for the tuning of the GEM-detectors.

In Run0-c, we made the two-electron trigger to accumulate the physics data, and found the DAQ live time was reduced to 15%, which contradicted with the measured DAQ dead-time length and trigger accept rate. This was caused by the higher trigger-request rate, localized in time, over the Poisson distribution, owing to the beam micro structures of 5 ms and 5.2 μs cycles. The latter was newly found in this beam line, while the former was also observed in another beam line (K1.8) with lesser strength. As a result of our analysis, origins of both structures were estimated, and countermeasures were prepared. Moreover, DAQ upgrade to reduce the data transfer time is on-going, and the live time is 55% in the simulation, assuming the present beam structure. If the structures are reduced, the live time is recovered to 75% or more.

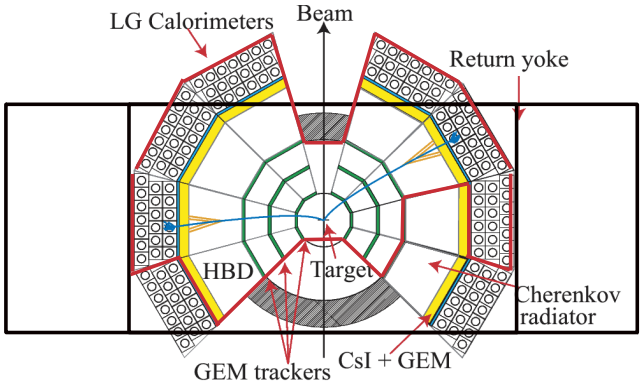

Fig. 1. Plan view of the E16 spectrometer in the eight-module configuration for Run-1. The red lines show the parts that have been operated in Run-0b/c in 2021. The SSD located in the innermost layer is not shown.

After Run-0c, the HBD and GTR were uninstalled for maintenance, including exchange of the damaged GEMs. The maintenance of the GTR is performed in J-PARC, whereas the HBD maintenance should be performed at the Main Bldg. in RIKEN Wako, using an N_2-filled glove box located in a class-1000 clean room. In November 2021, two LG modules are newly installed in the spectrometer. Re-installation of the GTR (HBD) will be completed in Aug. (Nov.) 2022.

The next beam time of J-PARC is planned to start in Dec. 2022, or later. Before Run-1 (physics run), we plan to perform a beam study to check whether the countermeasures can improve the DAQ performance, in cooperation with Beam line group and accelerator group at J-PARC. Subsequently, Run-1 could be performed. This plan has not been endorsed by PAC yet, thus a review will be performed in 2022.

*1 RIKEN Nishina Center

a) J-PARC 30-GeV Main Ring Accelerator, Electro-static septum for the slow extraction.

References

1) S. Yokkaichi *et al.*, J-PARC proposal No. 16 (`http://j-parc.jp/researcher/Hadron/en/pac_0606/pdf/p16-Yokkaichi_2.pdf`); S. Ashikaga *et al.*, JPS Conf. Proc. **26**, 024005 (2019).
2) R. Muto *et al.*, Phys. Rev. Lett. **98**, 042501 (2007).
3) S. Yokkaichi, RIKEN Accel. Prog. Rep. **54**, 107 (2021).

Analysis of Quark-Gluon plasma properties based on jets with ALICE experimental data

T. Kumaoka,[*1,*2] for the ALICE Collaboration

Quark-Gluon plasma (QGP) is defined as a matter phase at high temperatures and high densities. It is predicted using quantum chromodynamics. A few QGP evidences have been discovered through the LHC and RHIC experiments. However, QGP features are not revealed, and various measurements are performed to clarify QGP properties. Among these properties, the stopping power and jet quenching mechanism can be clarified by measuring the nuclear modification factor (R_{AA}) in a wide jet transverse momentum (p_{T}) range. R_{AA} is the ratio of the jet yield in nuclear-nuclear collisions to that in p-p collisions (Fig. 1). When R_{AA} is less than 1, it implies that jets are suppressed by the QGP created owing to nuclear collisions. Measured distributions can restrict theoretical models and clarify the jet quenching mechanism.

In this study, we measure R_{AA} in Pb-Pb collisions at $\sqrt{s_{\mathrm{NN}}} = 5.02$ TeV by using the ALICE experimental data of 2018. This data set possesses an integrated luminosity of 0.4 nb^{-1}, which is larger compared to the previous study.[1)] The data are expected to include rare high-p_{T} jets than the previous measurements, extending the R_{AA} measurements to the higher p_{T} region.[a)] Moreover, the large data statistics enables the study on R_{AA} at various centralities (Fig. 2), which were limited owing to the large number of background particles along the low p_{T} direction in the case of the previous study. As peripheral collisions provide a smaller background than central collisions, studies in the lower p_{T} region become possible. This study clarifies the correlation between the parton energy suppression and centrality.

Data quality requirements were applied to the data, and those marked as good demonstrate three times larger statistics than the previous study.[1)] Jets were reconstructed using the anti-k_{T} algorithm[2)] of the fast-jet package[3)] without any modification. The expected contribution to the jet p_{T} based on background particles was estimated for each jet on an event-by-event basis. By subtracting the background, we obtained jet p_{T} spectra for various centralities. Figure 3 shows the normalized jet p_{T} spectrum for various centralities. Moreover, it shows that jets are more suppressed in the central collisions compared with that in the peripheral collisions.

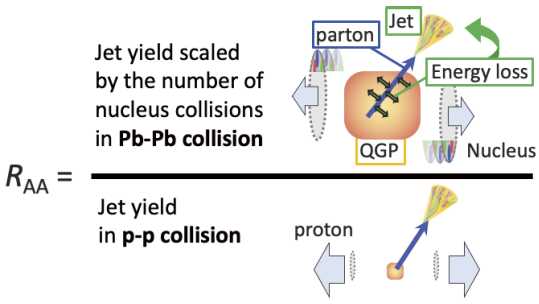

Fig. 1. R_{AA} definition. The numerator and denominator demonstrate the jet yields in heavy ion collisions and p-p.

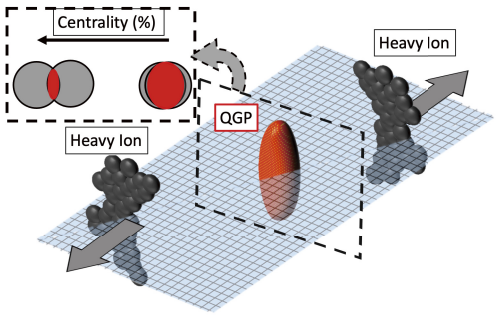

Fig. 2. Collision centrality. The overlap of heavy ions is known as centrality. In other words, centrality is defined as the percentile of the hadronic cross section corresponding to particle multiplicity, considering the count from the most central collisions.

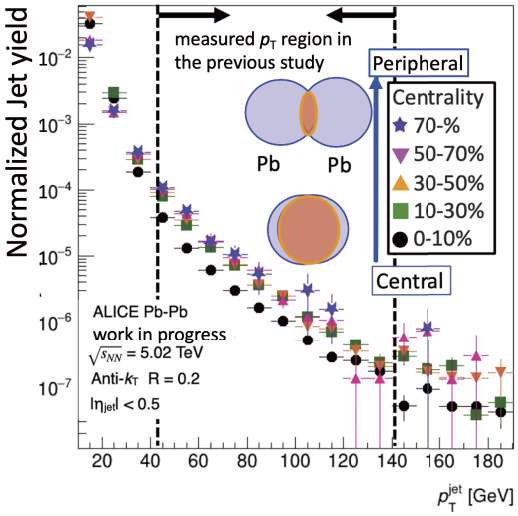

Fig. 3. Jet p_{T} spectrum for each centrality. The horizontal axis denotes jet p_{T} and the vertical axis denotes jet yields normalized by the pseudorapidity range and number of binary collisions. In the previous study, R_{AA} was measured in the area between the two dashed lines.

*1 Department of Physics, University of Tsukuba
*2 RIKEN Nishina Center

a) In this measurement, we will use the jet p_{T} spectrum in p-p collisions at $\sqrt{s} = 5.02$ TeV, which derived from the ALICE experiment conducted in 2018, as the denominator of R_{AA}.

References
1) S. Acharya *et al.*, Phys. Rev. C **101**, 034911 (2020).
2) M. Cacciari *et al.*, J. High Energy Phys. **4**, 063 (2008).
3) M. Cacciari *et al.*, Eur. Phys. J. C **72**, 1896 (2012).

Performance evaluation for sPHENIX-INTT ladder with a beta source

Y. Namimoto,[*1,*4] Y. Akiba,[*1] D. Cacace,[*2] K. Cheng,[*3] H. En'yo,[*1] T. Hachiya,[*1,*4] S. Hasegawa,[*1,*5] M. Hata,[*4] H. Imai,[*1,*6] T. Kondo,[*7] C. Kuo,[*3] H. -S. Li,[*8] R. -S. Lu,[*9] E. Mannel,[*2] C. Miraval,[*2] M. Morita,[*1,*4] I. Nakagawa,[*1] Y. Nakamura,[*1,*6] G. Nakano,[*1,*6] R. Nouicer,[*2] G. Nukazuka,[*1] R. Pisani,[*2] M. Shibata,[*1,*4] C. Shih,[*3] M. Shimomura,[*4] M. Stojanovic,[*8] Y. Sugiyama,[*4] R. Takahama,[*1,*4] W. -C. Tang,[*3] M. Watanabe,[*4] and X. Wei[*8]

The INTermadiate Tracker (INTT) is one of the three tracking detectors for the sPHENIX experiment which will be started in 2023 at the Relativistic Heavy Ion Collider in Brookhaven National Laboratory (BNL). It comprises 56 ladders, and each is composed of two silicon strip sensor modules. One module is divided into 26 cells, and each cell contains 128 readout strips. One readout chip reads the signals from one cell, 128 strips. The quality of all ladders need to be evaluated to be ready for detector construction scheduled for Spring 2022. Dead strips are one of the critical parameters. We developed the test procedure using a beta ray source ^{90}Sr to check for dead strips in a reasonable time scale.

All the strips need to be exposed by beta ray to locate the dead strips. For that purpose, we developed the source test fixture shown in Fig. 1. In the fixture, an INTT ladder was placed with the sensor side down. The source was placed on a movable stage in the fixture and moved from left to right during the measurement. Its moving speed and movable range are adjustable.

Using the fixture, we measured hit counts in each strip, both with and without the source. The hit counts without the source provide background hits. In these measurements, the trigger was provided by the sensor module and it is called "self-trigger mode." Figure 2 depicts the hit counts, the red (light blue) histogram corresponds to that with (without) the source. In these measurements, one can distinguish the hit by the source from the background even though the background is also visible since data was acquired by the self-trigger with relatively low hit threshold. The hit counts are statistically subtracted and shown as the blue histogram in Fig. 2 to show the signal. If the difference is consistent with zero, the strip can be regarded as "dead strip." Accordingly measured the dead strips for a ladder in September 2021 and found no dead strips. The result is better than the requirement of less than 1% dead strips rate in a ladder.

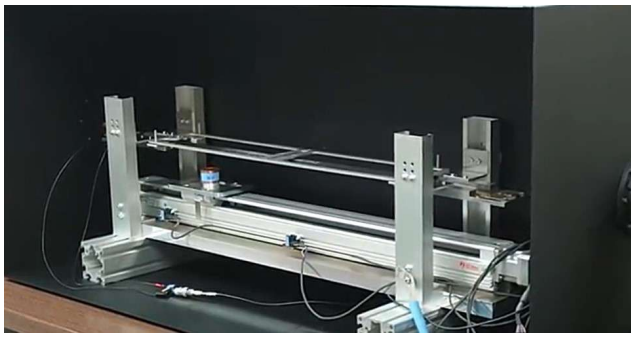

Fig. 1. Source test fixture.

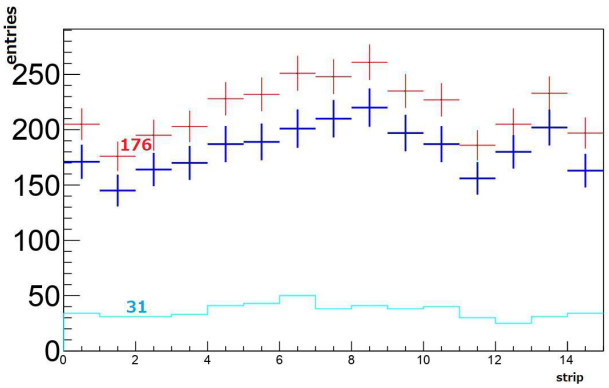

Fig. 2. Number of hit distributions with and without thre beta ray source (red or light blue) and their differences (blue).

The measurements took eight hours for one sensor module, therefore an INTT ladder needs 16 h two modules, approximately one day. It is planned that 80 and 40 ladders will be produced at BNL and National Taiwan University, respectively. Therefore, we can complete the quality evaluation within 80 days at most for all ladders evaluation.

In summary, we developed a procedure to evaluate the dead strips using a beta source. The ladder production is in progress and the evaluation with this procedure will commence soon.

Reference

1) I. Nakagawa *et al.*, in this report.

*1 RIKEN Nishina Center
*2 Physics Department, Brookhaven National Laboratory
*3 Department of Physics, National Central University
*4 Department of Mathematical and Physical Sciences, Nara Women's University
*5 Japan Atomic Energy Agency
*6 Department of Physics, Rikkyo University
*7 Tokyo Metropolitan Industrial Technology Research Institute
*8 Department of Physics and Astronomy, Purdue University
*9 Department of Physics, National Taiwan University

6. Particle Physics

Search for an effective change of variable in QCD simulations

P. Boyle,[*1,*2] T. Izubuchi,[*1,*3] L. Jin,[*4,*3] C. Jung,[*1] C. Lehner,[*5,*1] N. Matsumoto,[*3] and A. Tomiya[*6]

Lattice calculations of quantum chromodynamics (QCD) suffers from the critical slowing down as the continuum limit is approached. Furthermore, the topological sectors in the gauge field space become apparent due to the separation by potential barriers in this limit, and this fact makes it difficult to explore the entire field space in the simulation.

To circumvent these issues, Lüscher proposed[1] using the *trivializing map*[2] in lattice QCD. The idea is to map the system of interest to a trivial system, where the simulation can be performed efficiently. Precisely, we evaluate the expectation value expressed in terms of the following path integral:

$$\langle \mathcal{O} \rangle_S \equiv \frac{\int \mathcal{D}U\, e^{-S(U)} \mathcal{O}(U)}{\int \mathcal{D}U\, e^{-S(U)}}, \tag{1}$$

where $S(U)$ is the lattice QCD action. The trivializing map[1] $U = \mathcal{F}(V)$ is defined such that

$$\begin{aligned} \langle \mathcal{O} \rangle_S &= \frac{\int \mathcal{D}V\ \det \mathcal{F}_*(V)\, e^{-S(\mathcal{F}(V))} \mathcal{O}(\mathcal{F}(V))}{\int \mathcal{D}V\ \det \mathcal{F}_*(V)\, e^{-S(\mathcal{F}(V))}} \\ &= \int \mathcal{D}V\, \mathcal{O}(\mathcal{F}(V)), \end{aligned} \tag{2}$$

where $\mathcal{F}_*(V)$ is the Jacobian matrix of the map $\mathcal{F}$. In other words, we construct a map $\mathcal{F}$ that makes the effective action

$$S_{\mathcal{F}}(V) \equiv S(\mathcal{F}(V)) - \ln \det \mathcal{F}_*(V) \tag{3}$$

the target action $S_{\rm tg}(V) \equiv$ const: $S_{\mathcal{F}} = S_{\rm tg}$.

Lüscher explicitly constructed the trivializing map as a flow $\mathcal{F}_t$ for the pure Yang-Mills theory, which was given in the form of an expansion with the flow time t. To the zeroth order in t, this map becomes the *Wilson flow*, the gradient flow for the Wilson action. Combining the Hybrid Monte Carlo (HMC) with the Wilson flow[1] seems promising, based on the observation of positive effects in the topological tunneling rate.[4] The subject of this study is to investigate the effectiveness of the field transformation in lattice QCD along this line, extending the code to cover more general flow kernels for the trivializing maps.

To design an approximated map, we consider a different strategy from that of Lüscher's. We first prepare a finite basis $\{W_i\}$ and define the truncated effective action:

$$S'_{\mathcal{F}} \equiv {\sum_i}' \beta'_i W_i, \tag{4}$$

where the prime indicates quantities for the finite basis. The coefficients β'_i can be determined with the Schwinger-Dyson equation:[5,6]

$${\sum_j}' \beta'_j \langle \partial^A W_j \partial^A W_i \rangle_{S_{\mathcal{F}}} = \langle (\partial^A)^2 W_i \rangle_{S_{\mathcal{F}}}. \tag{5}$$

This determination gives the best approximation of $S_{\mathcal{F}}$ in the sense that it minimizes the norm

$$||S_{\mathcal{F}} - S'_{\mathcal{F}}||^2 \equiv \langle (\partial^A S_{\mathcal{F}} - \partial^A S'_{\mathcal{F}})^2 \rangle_{S_{\mathcal{F}}}. \tag{6}$$

This is a calculable norm of the HMC force.

We use Eq. (5) to design the approximated map. We define the infinitesimal map $\mathcal{F}_{t,\epsilon}$, which evolves the parameter t by ϵ as

$$\mathcal{F}_{t,\epsilon}(V)_{x,\mu} \equiv e^{\epsilon T^a Z^a_{t,x,\mu}(V)}\, V_{x,\mu}. \tag{7}$$

Here $Z^a_{x,\mu}$ is the kernel

$$Z^A_i \equiv -{\sum_i}' \gamma_{i,t}\, \partial^A W_i, \tag{8}$$

where the label A corresponds to (x, μ, a). Since γ_i can be related to β'_i by

$$\begin{aligned} &{\sum_k}' \gamma_{k,t} \big\langle \partial^A W_k \partial^A [-(\partial^B)^2 W_i + \partial^B S'_{\mathcal{F}} \partial^B W_i] \big\rangle_{S_{\mathcal{F}}} \\ &\quad = -(d\beta'_{j,t}/dt) \langle \partial^B W_j \partial^B W_i \rangle_{S_{\mathcal{F}}}, \end{aligned} \tag{9}$$

we can determine $\gamma_{i,t}$ by specifying the functional form of $\beta'_{i,t}$, or equivalently the target action $S_{{\rm tg},t}$ for all t. In the case where the truncation error is negligible, the above framework provides a way to construct the trivializing map with a large freedom of choosing the intermediate trajectory in the space of actions.[7] The authors thank the US DOE for the resources, which have been necessary for the work.

*1 Physics Department, Brookhaven National Laboratory
*2 School of Physics and Astronomy, University of Edinburgh
*3 RIKEN Nishina Center
*4 Physics Department, University of Connecticut
*5 Universität Regensburg, Fakultät für Physik
*6 Department of Information Technology, International Professional University of Technology

References
1) M. Luscher, Commun. Math. Phys. **293**, 899 (2010).
2) H. Nicolai, Phys. Lett. B **89**, 341 (1980).
3) S. Duane *et al.*, Phys. Lett. B **195**, 216 (1987).
4) L. Jin, The 38th International Symposium on Lattice Field Theory, ZOOM/GATHER@MIT, 2021.
5) A. Gonzalez-Arroyo, M. Okawa, Phys. Rev. D **35**, 672 (1987).
6) QCD-TARO Collaboration, P. de Forcrand *et al.*, Nucl. Phys. B **577**, 263 (2000).
7) N. Matsumoto, BNL-HET & RBRC Joint Workshop "DWQ@25," online, 2021.

Radiative corrections to Landau levels of a single electron revisited

R. Yamazaki[*1] and M. Nio[*1,*2]

The deviation of the g value of the electron from Dirac's prediction, $a_e \equiv (g-2)/2$, is known as the anomalous magnetic moment. A comparison between the measured value of a_e and its theoretical prediction provides the most stringent test of quantum electrodynamics (QED) and, hence, the standard model of elementary particles.

The value of a_e is experimentally determined by trapping a single electron in a Penning trap and by measuring the difference in energy between different eigenstates. The latest measurement leads to[1)]

$$a_e = 1\ 159\ 652\ 180.73\ (28) \times 10^{-12} \quad [0.24\ \text{ppb}]. \quad (1)$$

A new experiment aiming at a 20-fold improvement of the uncertainty is in progress.[2)]

Considering the accuracy to be realized in future experiments, we revisited the theoretical background of the measurement. In a Penning trap, an electron is confined in the xy plane owing to the static constant magnetic field B along the z direction. Vertical confinement along the z direction is realized by the hyperbolic potential of the quadrupole electric field E. The latter effect is so small that we can ignore the E field when radiative corrections of QED to the energy levels of an electron in a Penning trap are considered.

The energy eigenvalues of an electron in the static constant magnetic field B are well known as the Landau levels in the study of quantum mechanics when its velocity v is much less than the speed of light c (see Fig. 1). The energy eigenvalue of the state with a principal quantum number $n \geq 0$ of a simple harmonic oscillator and a spin direction $\sigma_z = \pm 1$ is given by

$$E(n, \sigma_z) = \hbar\omega_c \left(n + \frac{1}{2} - \frac{g}{4}\sigma_z \right), \quad (2)$$

where $\omega_c = eB/(mc)$ with $eB > 0$ is the cyclotron frequency of an electron. The spin-flipping and anomalous frequencies are defined as $\omega_s = (g/2)\omega_c$ and $\omega_a = \omega_s - \omega_c$, respectively. The anomalous magnetic moment a_e is obtained as the ratio $a_e = \omega_a/\omega_c$.

In the early literature,[3,4)] the radiative correction to the Landau levels due to one virtual photon spanning over an electron was calculated using the electron propagator in an external magnetic field. In the weak magnetic field approximation, the correction was obtained as

$$\Delta E(n, \sigma_z) = \frac{\alpha}{2\pi} m \left[-\sigma_z \frac{eB}{2m^2} + \left(\frac{eB}{m^2}\right)^2 \left(\frac{4}{3} \ln \frac{m^2}{2eB} - \frac{13}{18} \right) + \mathcal{O}\left(\left(\frac{eB}{m^2} \right)^3 \right) \right], \quad (3)$$

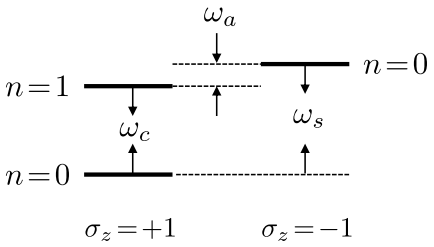

Fig. 1. Energy levels of an electron in a static constant magnetic field, known as the Landau levels. The frequency ω_c is the cyclotron frequency due to the Lorentz force acting on a charged particle. The frequency ω_s is the spin-flipping frequency of an electron with spin 1/2. The eigenvalue σ_z is the direction of the spin. Two frequencies $\omega_a \equiv \omega_s - \omega_c$ and ω_c are measured to determine the anomalous magnetic moment a_e.

with $c = 1$ and $\hbar = 1$. The first term proportional to σ_z is due to the Schwinger term of a_e. In realistic experiments, the magnetic field B is about 5 T, and we find $eB/m^2 \sim 1.1 \times 10^{-9}$, which is bigger than the current precision of a_e, 0.24×10^{-9}. The second term, however, does depend on neither n nor σ_z; thus, it does not contribute to the transition frequencies between different eigenstates, which are to be measured. The third term depends on both n and σ_z, but its magnitude is negligible. Thus, for the current precision of a_e, we need not consider the QED binding corrections to the Landau levels at all.

For the ongoing measurement of a_e, the fourth-order QED binding corrections to the Landau levels might become relevant. In order to investigate the α^2 correction, we have started reinterpreting (3) in terms of NRQED,[5)] which is suitable to describe QED corrections to non-relativistic systems. As expected, the second term of (3) is an analogue of the Lamb shift of a Coulomb-bound system. Applying Bethe's method of NRQED, we should be able to reproduce not only the logarithmic enhancement term but also the finite term of (3). Once the mechanism of QED corrections to the Landau levels is clarified, we expect that the α^2 correction will not be difficult to determine completely.

*1 Department of Physics, Saitama University
*2 RIKEN Nishina Center

References
1) D. Hanneke *et al.*, Phys. Rev. Lett. **100**, 120801 (2008).
2) X. Fan, G. Gabrielse, Phys. Rev. Lett. **126**, 070402 (2021).
3) R. G. Newton, Phys. Rev. **96**, 523 (1954).
4) W. Tsai, A. Yildiz, Phys. Rev. D **8**, 3446 (1973).
5) T. Kinoshita, M. Nio, Phys. Rev. D **53**, 4909 (1996).

Quarternion-spin-isospin model

Y. Akiba *1

The standard model (SM) successully describes the nature, but it has at least 25 free parameters. Simple formulas with no free parameter for 24 SM parameters have been reported:[1] 15 particle masses, four Cabbibo-Kobayashi-Maskawa (CKM) quark mixing parameters, three neutrino mixing angles, the fine structure constant, and the strong coupling constant. Moreover, the quarternion-spin-isospin (QST) model that predicts these formulas,[2] and its implication to gravity and cosmology[3] have also been reported. This article reports an update of the model.

In the QST model, the Planck time $t_{\rm pl} = 5.3912 \times 10^{-44}$ s is the minimum time period in nature. $t_{\rm pl}$ is a fundamental constant in nature, similar to the speed of light in vacuum c and the Planck constant $\hbar$. Consequently, the Planck length $l_{\rm pl} = ct_{\rm pl}$ is the minimum distance in nature; therefore, a spacetime point has a finite minimum size.

Since a spacetime point has a finite minimum size, the number of spacetime points in a finite spacetime volume is also finite. Therefore, two integer indexes, n_s and n_t, can be used for all of the spacetime points in a spacetime volume. Here n_s and n_t denote the index number of space and time, respectively; Both n_s and n_t are natural numbers.

Let $|n_s, n_t\rangle$ denote the physical state at time n_t on spatial point n_s. In the QST model, the change of $|n_s, n_t\rangle$ to $|n_s, n_t + 1\rangle$ is given by:

$$|n_s, n_t + 1\rangle = \left(1 + \hat{\mathcal{L}}(n_s, n_t) dV_E\right) |n_s, n_t\rangle, \quad (1)$$

where dV_E is the minimum spacetime volume.

In the path integral formulation of the quantum field theory, the change of vaccuum state from t_i to t_f is given by:

$$|t_f\rangle = |t_i\rangle = \int \mathcal{D}\phi \exp\left(i \int \mathcal{L}[\phi] dx^3 dt\right) |t_i\rangle.$$

For a small spacetime volume, this equation becomes

$$|t + \delta t\rangle = \left(1 + i\mathcal{L}[\phi(x,t)]\delta x^3 \delta t\right) |t\rangle. \quad (2)$$

It can be observed that Eq. (1) corresponds to Eq. (2) and that $\hat{\mathcal{L}}(n_s, n_t)$ corresponds to the Lagrangian density $\mathcal{L}[\phi(x,t)]$.

In the QST model, $\hat{\mathcal{L}}(n_s, n_t)$ is given by:

$$\hat{\mathcal{L}}(n_s, n_t) = \sum \delta_p(n_s, n_t) \hat{\mathcal{L}}_p$$

Here, $\delta_p(n_s, n_t)$ is a function of spacetime point that takes only 0 or 1, and $\hat{\mathcal{L}}_p$ denotes operators named elementary action densities (EADs). An EAD corresponds to a term of Lagrangian density of the SM.

Table 1. Values of elementary action densities.

	$(6\pi)^2\epsilon_0 i\tau^3$	$(6\pi)^2\epsilon_0 i$	$(6\pi)\epsilon_0 i\tau^3$	$(6\pi\epsilon_0 i)$	$(6\pi)\epsilon_0$	$\epsilon_0 i\tau^3$	$\epsilon_0 i$	ϵ_0
$\hat{\mathcal{L}}_{g_{3D}}$								3_a^*
$\hat{\mathcal{L}}_{g_{2D}}$								2_a
$\hat{\mathcal{L}}_{GG}$								24_a^*
$\hat{\mathcal{L}}_{uG}$								8_a
$\hat{\mathcal{L}}_{cG}$								24_b^*
$\hat{\mathcal{L}}_{tG}$								8_b
$\hat{\mathcal{L}}_B^m$							18_b	
e	4_a					1		3_b^*
μ	4_a		-12_a			27_a		3_c^*
τ	4_a		-3		3_a^*	$1+4$		
ν_1		12_a		12				2_b
ν_2		-4_a		4				2_b
ν_3		12_a		12	2			
ν_3'		12_a		12	-2			
U_{15}	-12_a					2_a		
U_{17}	$3\times(-4)$		-12_b			2_b		
D	-12_a					1		
u	4_b							8_a
c	$4_b + 4_c$							24^*
t	4_c							8_b
d	-12_a		-12_a		-3^*			
s	-12_b							3_d^*
b	4_d		6		3_b^*	27_b	18_a	
Z		12_b^*		1			1	
H		-4		-6			18_c	
W		12_b^*		-18^*			-27	

In the QST model, an EAD is given by:

$$\hat{\mathcal{L}}_p = \hat{\partial}_{p_1} \vee \hat{\partial}_{p_2} \vee \cdots \vee \hat{\partial}_{p_{48}}$$

Here, $\hat{\partial}_{p_k} (k = 1, \cdots, 48)$ is one of the following 64 operators named normalized primordial action (NPA), and $\vee$ is the exterior product of the NPA space.

$$\left\{\frac{I^\mu \sigma^\nu \tau^a}{6\pi}, \frac{\tau^a}{3\pi}, \frac{i}{3\pi}, \frac{I^{[c-a]}\tau^a}{3\pi}, \frac{i\tau^3}{3\pi}, -\frac{I^c}{2\pi}, -\frac{i}{\pi}, -2, 2, i, 1\right\}.$$

The QST model contains 49 EADs which are summarized in Table 1. All 24 formulas of the parameters of the SM can be derived from the 49 EADs given in the table. The model also predicts that the CP violation in the neutrino sector to be 100%. Thus, all 25 free parameters of the SM are derived from the QST model. In additon, the model predicts that the product of the Hubble constant H_0 and the Planck time t_{pl} is $H_0 t_{pl} = 2 \times (6\pi)^{-48}$.

A paper describing the QST model is in preparation.

*1 RIKEN Nishina Center

References
1) Y. Akiba, RIKEN Accel. Prog. Rep. **54**, 69 (2021).
2) Y. Akiba, RIKEN Accel. Prog. Rep. **54**, 70 (2021).
3) Y. Akiba, RIKEN Accel. Prog. Rep. **54**, 71 (2021).

7. Astrophysics and Astro-Glaciology

Broad-band spectral analysis of the gamma-ray binary system LS 5039 and its strong MeV gamma-ray emission†

H. Yoneda,[*1] D. Khangulyan,[*2] K. Makishima,[*1,*3,*4] T. Enoto,[*5] K. Mine,[*3] T. Mizuno,[*6] and T. Takahashi[*4,*3]

With the development of GeV/TeV gamma-ray observation techniques, since the 2000 s it was established that several high-mass X-ray binary systems emit strong non-thermal emissions. They are called gamma-ray binary systems, and so far, approximately ten sources have been identified.[1)] Their spectral energy distributions (SEDs) have a peak typically beyond 1 MeV. Such non-thermal emissions indicate that efficient particle acceleration takes place in them, and they are considered a new particle accelerator in the Universe. However, the nature of compact objects and the acceleration mechanism in these systems are not well understood, and this has been a long-standing question.

LS 5039 is one of the brightest known gamma-ray binary systems in our galaxy.[2)] Its companion star is an O star with a mass of 23 $M_{\odot}$, but it is not known whether its compact object is a black hole or a neutron star. From X-ray and TeV gamma-ray observations, it is suggested that this object accelerates TeV electrons on the time scale of seconds, with an extremely high efficiency.[3)] Recently, by reanalysis of the COMPTEL data, strong MeV gamma-ray emission has been found from this source.[4)] These findings imply that it is essential to understand its broad-band spectrum from X-rays to TeV gamma-rays. In this report, we present our results of the spectral analysis using the latest data.[5)]

By using 11 years of Fermi-LAT GeV gamma-ray data and hard X-ray data of the NuSTAR observation, we updated the SED of LS 5039 with the highest available statistics (see Fig. 1). The obtained SED and its spectral modulation along the orbital phase suggest that LS 5039 has at least four spectral components from the X-ray to TeV band: (1) an X-ray component up to 100 keV, (2) a spectral component that is dominant above 100 keV up to a few tens of MeV, (3) a GeV gamma-ray component that is almost independent of the orbital motion, and (4) a TeV gamma-ray component. Existing theoretical models can interpret the first and fourth components, *e.g.*, particle acceleration at the pulsar wind termination shock. However, we found that the second and third components are not explained well. When the MeV emission is interpreted as synchrotron emission, we can constrain the acceleration efficiency parameter as $\eta < 10$. This result suggests that particle acceleration operating in LS 5039 is different from the diffusive shock acceleration (DSA) assumed in many models because DSA yields $\eta > 10$.

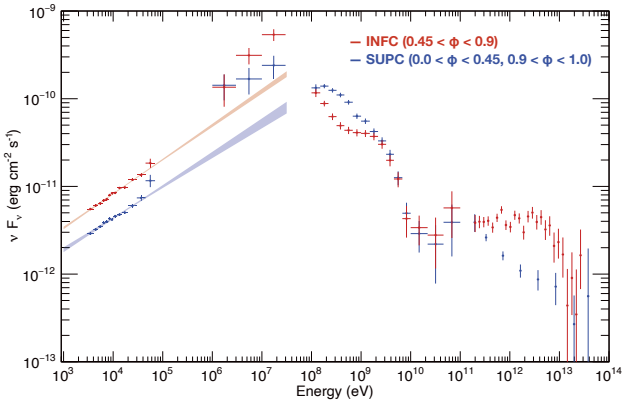

Fig. 1. The SED of LS 5039 with the NuSTAR and 11 years of Fermi LAT data. The red points represent the spectra in orbital phases around the inferior conjunction (INFC) when the compact star is in front of the companion star from the observer's perspective. The blue points denote the spectra around the superior conjunction (SUPC) when the compact star is behind the companion star. See Ref. 5) for details.

We have performed a broad-band spectrum analysis of the gamma-ray binary LS 5039 and summarized the features of the emission components in each band. The emission components from MeV to GeV remain uncertain, and further studies on this energy band are key to understanding this object's nature. The MeV gamma-ray satellite COSI will be launched in 2025.[6)] Moreover, towards MeV/subGeV gamma-ray observation in the 2030s, the GRAMS project with an unprecedentedly large effective area has been proposed.[7)] We expect that these future observations will further deepen our understanding of the mysterious gamma-ray binary systems.

† Condensed from the article in Astrophys. J. **917**, 90 (2021)
*1 RIKEN Nishina Center
*2 Department of Physics, Rikkyo University
*3 Department of Physics, University of Tokyo
*4 Kavli IPMU, University of Tokyo
*5 Extreme Natural Phenomena RIKEN Hakubi Research Team
*6 Hiroshima Astrophysical Science Center, Hiroshima University

References

1) G. Dubus, Astron. Astrophys. Rev. **21**, 64 (2013).
2) J. Casares *et al.*, Mon. Not. R. Astron. Soc. **364**, 899 (2005).
3) T. Takahashi *et al.*, Astrophys. J. **697**, 592 (2009).
4) W. Collmar, S. Zhang, Astron. Astrophys. **565**, A38 (2014).
5) H. Yoneda *et al.*, Astrophys. J. **90**, 917 (2021).
6) J. Tomsick *et al.*, Bull. Am. Astron. Soc. **51**, 7 (2019).
7) T. Aramaki *et al.*, Astrophys. J. **114**, 107 (2020).

8. Accelerator

Distributed control by EPICS for the SRILAC beam energy position monitoring system using LabVIEW†

T. Watanabe,[*1] A. Kamoshida,[*1,*2] A. Uchiyama,[*1] N. Fukunishi,[*1] R. Koyama,[*3] and K. Kaneko[*3]

For stable operation of the newly constructed Superconducting RIKEN Heavy-ion Linac (SRILAC), nondestructive and highly sensitive measurement using the beam energy and position monitor (BEPM) system is essential.[1,2] A great advantage of this system is that it can handle a time-chopped beam by synchronizing the measurement system with the beam chopping signal. Although the chopped beam intensity is of several electric nA, we can measure the beam position and energy to accuracies of ±0.1 mm and precision in the order of 10^{-4}, respectively.

These measurements and controls are programmed with LabVIEW. Further, by sharing these measured values, such as beam positions and beam energies, with a large-scale EPICS control system, it is easy to obtain the correlation of each relevant machine parameters in time series. A block diagram of the BEPMs and data-acquisition system is shown in Fig. 1. All the modules, including digitizers, multiplexers and a embedded controller, are integrated into a PXI express chassis. The signal process procedures are controlled using the LabVIEW 2020 graphical programming language, and the module drivers are supported by the National Instruments Corporation. The obtained data are shared using CA Lab, which is a user-friendly, lightweight, and high performance interface between

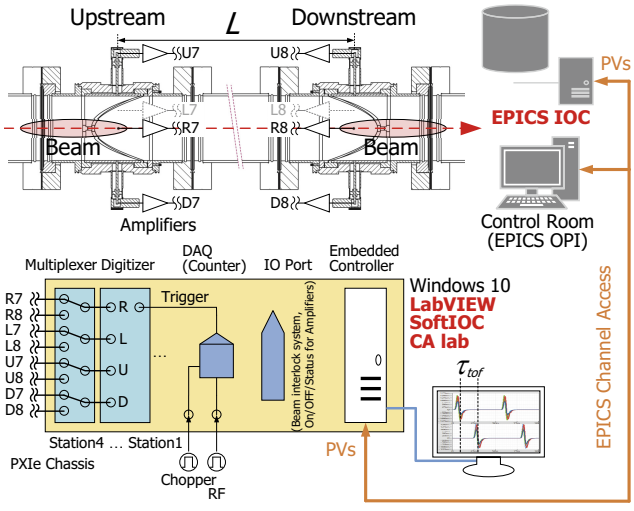

Fig. 1. Block diagram of the BEPMs and DAQ.

the LabVIEW program language and the EPICS-based control system. It allows easy reading and writing of EPICS process variables (PVs). The PVs used by the BEPM system include analog inputs, wave-forms, and analog and binary outputs. The measurement results are displayed on a local remote desktop. Furthermore, once these data are saved to PVs, the Control System Studio (CSS), which is an Eclipse-based tool to operate a large-scale control system, can display the results anywhere in the control room.

Figure 2 shows one example of the measured results, which presents the relationship between the beam position at BEPM 1 and the vacuum between the cryomodules of CM1 and CM2 when the $^{51}V^{13+}$ beam intensity is increased to 2.5 particle μA. Based on this measurement, we established that the vacuum rapidly became worse when the beam position shifted from −1 mm to −2 mm. Therefore, we changed the EPICS interlock system to start the beam attenuator automatically to prevent vacuum deterioration.

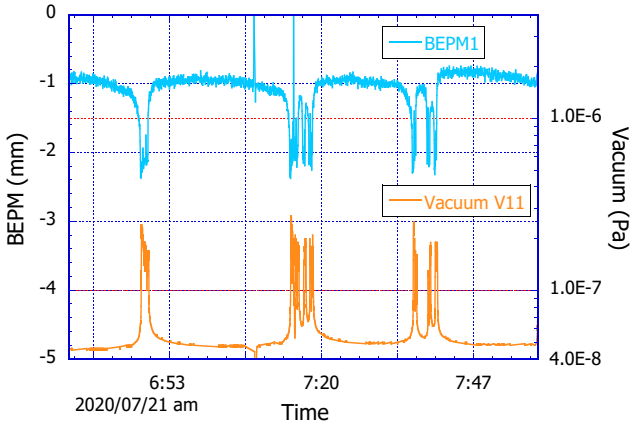

Fig. 2. Measured results showing the relationship between the beam position at BEPM 1 and the vacuum between cryomodules of CM1 and CM2.

We are currently working on measurement of the quadrupole moment to obtain the beam size, beam intensity from the bunched signal, and TOF using a lock-in amp technique.

References

1) T. Watanabe *et al.*, Proc. the 18th Annual Meeting of Particle Accelerator Society of Japan, (Online, Aug. 2021), pp. 683–686.
2) T. Watanabe *et al.*, Proc. 2020 Int. Beam Instrumentation Conf. (IBIC2020), (Santos Brazil, Online, Sept. 2020), pp. 295–302.

† Condensed from the article in Proceedings of the 18th Annual Meeting of Particle Accelerator Society of Japan, (2021) p. 683

*1 RIKEN Nishina Center
*2 National Instruments Japan Corporation
*3 SHI Accelerator Service Ltd.

Improvement of the transmission efficiency of RILAC

T. Nishi,[*1] T. Nagatomo,[*1] O. Kamigaito,[*1] N. Sakamoto,[*1] K. Yamada,[*1] and Y. Watanabe[*1]

The performance of the RIKEN heavy-ion linac (RILAC) has been upgraded[1] with a new superconducting electron cyclotron resonance ion source (SC-ECRIS)[2] and a superconducting linac booster (SRILAC).[3] Since July 2020, we have been successfully providing a high-intensity V^{13+} beam with an energy of 6 MeV/nucleon to the GARIS-III[4] experiment.

The RILAC facility leaves room for further improvement of the transmission efficiency to provide higher-intensity beams. The beam from SC-ECRIS is transported through the low-energy beam transport (LEBT) system, which is equipped with a slit triplet that controls the beam emittance in RILAC. The beam is then bunched and accelerated by a radio frequency quadrupole (RFQ) and injected to the RILAC cavities, booster cavities, and SRILAC. The transmission from the entrance of the RFQ to the entrance of SRILAC was inadequate at about 50%.

One of the causes of the low transmission efficiency was the mismatch of beam optics between the RFQ and the first acceleration cavity of RILAC. The beam line consists of two quadrupole doublets (QDL15 and QDL16) and a re-buncher, as shown in Fig. 1. The beam envelope should be narrowed inside the re-buncher because the duct radius in the re-buncher is 20 mm, which is smaller than the 32 mm duct radius in the rest of the beam line. The problem was that the QDL15 magnets were relatively far from an edge of the vane of RFQ (515 mm) and close to the re-buncher. The beam spreading in the long drift space after the RFQ should be suppressed in short drift space by a strong magnetic field for it to pass through the re-buncher. In contrast, the magnetic field of QDL15a, which is a horizontally focussing magnet, was limited to suppress the enhancement of the beam size in the vertical direction. Consequently, the optics lost flexibility and could not realize the emittance matching and good transmission efficiency simultaneously.

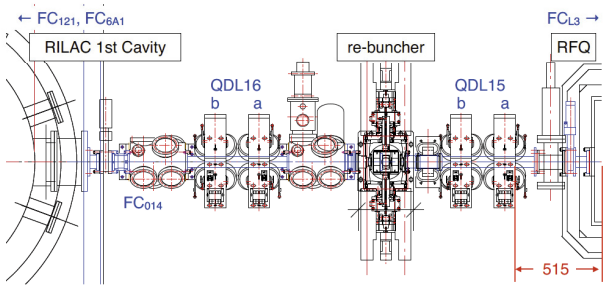

Fig. 1. Top view of the beam line from the RFQ to the 1st cavity of RILAC before the rearrangement.

*1 RIKEN Nishina Center

Therefore, we rearranged the QDL15 quadrupole magnets together with the other devices (a steerer, a gate valve, and a profile monitor) in September 2021. The cooling pipes of the RFQ were also relocated to avoid interference with the magnets. The improved transmission efficiency and the current applied to the magnets are summarized in Table 1. These values were measured when the beam was delivered to GARIS-III after the transmission optimization by RILAC operators. The transmission efficiency was measured by Faraday cups in the beam lines. L31, 014, 121, and 6A1 are the names of the locations where the Faraday cups are installed, representing the entrance to the RFQ, the entrance of the first cavity of RILAC, the middle point of 1st and 2nd cavities, and downstream of the last cavity of RILAC, respectively. As presented in Table 1, a larger current can be applied to QDL15a as expected. The transmission efficiency is improved by 5% upto 014 and 121 and by 10% upto 6A1. The simultaneous improvement in transmission from L31 to 014 and L31 to 121 is expected to be the result of increased flexibility of the optics downstream of the RFQ. For further increase in the transmission efficiency, we plan to measure the phase ellipse with the profile monitors installed between the RFQ and RILAC and to optimize the optics by realizing emittance matching to the acceptance of the first cavity of RILAC.

Table 1. Quadrupole magnet currents and transmission of RILAC after optimization.

		Jul. 2021	Dec. 2021
Current [A]	QDL15a (H)	38.0	46.8
	QDL15b (V)	36.8	40.8
	QDL16a (H)	21.5	29.2
	QDL16b (V)	13.0	30.1
Transmission efficiency from L31 [%]	014	80–85	90
	121	65	70
	6A1	50–55	60–65

In conclusion, the beam transmission from the RFQ was successfully improved. The upgrade of the aged beam line upstream of RILAC is essential to improve the transmission further.

References

1) RIKEN Accel. Prog. Rep. **54**, S1 (2021).
2) T. Nagatomo *et al.*, Rev. Sci. Instrum. **91**, 023318 (2020).
3) N. Sakamoto *et al.*, Proc. SRF2019, (Dresden, Germany, 2019), pp. 750–757.
4) H. Haba for RIKEN SHE Collaboration, Proc. EXON-2018, (Petrozavodsk, Russia, 2020) pp. 192–199.

Development of FPGA-based machine protection system for RIBF

M. Komiyama,[*1] M. Fujimaki,[*1] A. Uchiyama,[*1] and N. Fukunishi[*1]

We have been investigating a new machine protection system that will succeed the existing beam interlock system (BIS)[1] of RIBF since the latter half of 2020. The hardware configuration and the process flow in the BIS are shown in Fig. 1, where programmable logic controllers (PLCs) are used to process interlock signals. The typical response time of BIS is 18 ms, which will be insufficient for higher-intensity beams expected in the near future. Therefore, we plan to introduce a field-programmable gate array (FPGA) to process interlock signals, aiming at reducing the response time for digital input signals to less than 1 ms.

In the development of a BIS system using FPGAs (hereinafter, FPGA-BIS), the method of stopping a beam to protect the machine is basically the same as that of the BIS and AVF-BIS.[2] Each station that composes the FPGA-BIS will be installed at or near the existing BIS station to maximally reuse the existing signal wirings of the BIS. Therefore, the stations are widely distributed in the facility as well as in the BIS.

Based on the experience of operating BIS and AVF-BIS, we plan to use FPGAs and central processing units (CPUs) properly according to the signal processing time required. Various interlock conditions are imposed on the existing BIS and FPGA-BIS for each input signal. In essence, the process from the input of an alarm signal to the stopping of the beam through the evaluation of interlock conditions is performed on the FPGA, and the condition setting for and monitoring of each signal are performed from a host server via the CPU. As in the case of the AVF-BIS, the EPICS will be executed on the CPU.

In addition, since the BIS outputs a signal to the beam choppers, the FPGA-BIS implements not only the function of BIS, but also a function of controlling the beam intensity by using a beam chopper. Consequently, it can be expected that the system for sending signals to the beam choppers will be simplified relative to the current situation.

To achieve the performance required in FPGA-BIS, we compared two candidates: FA-M3 series PLC with the addition of input/output (I/O) modules with an FPGA (FPIO module, F3DF01-0N)[3] and CompactRIO, a product by National Instruments.[4] We concluded that both systems can meet the required performance as FPGA-BIS. Construction costs were also evaluated for both the systems with the same scale as the existing BIS, and we found that the construction cost using CompactRIO is about half of that using the FA-M3 PLCs. In a logic development of FPGA on the CompactRIO system, LabVIEW,[5] which has many useful functions and makes programming easier, can be used.

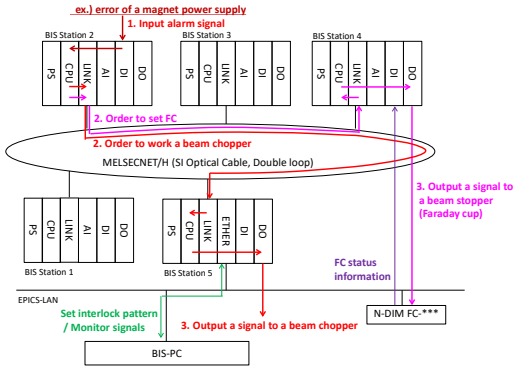

Fig. 1. Hardware configuration and process flow in BIS.

Therefore, CompactRIO is expected to shorten the software development time. Another merit of using CompactRIO is its maintainability when the FPGA used is updated, because LabVIEW is expected to absorb the difference between different FPGA versions.

Based on the above considerations, CompactRIO has greater merit for us. Therefore, we have been developing a prototype with a scale sufficient to conduct performance tests for the CompactRIO system, as shown in Fig. 2, since November 2021.

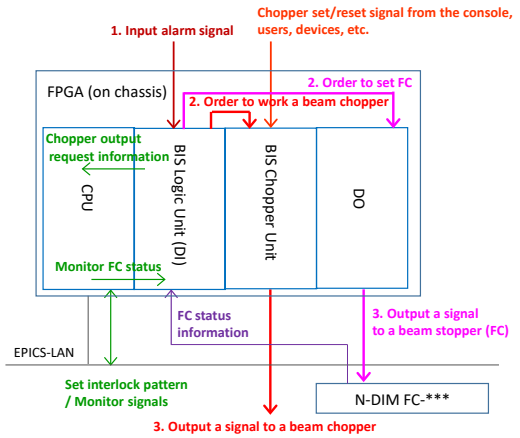

Fig. 2. Hardware constitution and process flow of the FPGA-BIS prototype using CompactRIO. FPGA is mounted on the chassis to which each module is installed.

References

1) M. Komiyama *et al.*, RIKEN Accel. Prog. Rep. **39**, 239 (2006).
2) M. Komiyama *et al.*, Proc. ICALEPCS2019, (2019), p. 384.
3) Yokogawa Electric Corporation, "Catalog of F3DF01-0N," unpublished.
4) CompactRIO, `https://www.ni.com/ja-jp/shop/compactrio.html`.
5) LabVIEW, `https://www.ni.com/ja-jp/shop/labview.html`.

*1 RIKEN Nishina Center

Deployment of a beam interlock system driven by changes in magnet current (Curs-BIS) at the RI Beam Factory

K. Kumagai[*1] and A. Uchiyama[*1]

The beam intensity has been gradually increasing at the RI Beam Factory. To prevent accidents such as melting of the vacuum chamber due to the beam orbit change, a system to detect the current change of the magnets due to unknown causes or noises during the beam operation and to stop the beam is required. The beam interlock system driven by changes in magnet current (Curs-BIS) was developed in 2019.[1)] The developed system could detect the current values of 24 magnet power supplies per unit, and now it can detect the current values of 48 power supplies. One unit of the Curs-BIS is shown in Fig. 1. Various improvements have been made to the sequence and web-based monitoring programs. The interlock signal is not erroneously when the power supply is set from 0 A, and the inactivity time of the interlock signal was adjusted according to the energizing characteristics of each power supply. It is now possible to directly link the monitoring screen to a table of power supply specifications and a graph of fluctuations in the current value of each power supply.

Three units of the system are currently installed in IRC and SRC, four units in the beam transport line of the RIBF, eight units in the RARF (the old facility) and fRC, three units in RILAC2 and AVF, three units in RILAC. The sequence program is the same for all units, and each unit can be operated independently by simply changing the parameter file for magnet power supply specifications, upper and lower limits of current values, *etc.*

Accelerators have various types and ages of magnet power supplies, and the current value of the magnet power supply is detected in three main ways. Power supplies with a very high current stability, such as cyclotron main power supplies, usually have a DCCT for monitoring in addition to the DCCT for power supply control; therefore, the monitor output is used for detection. For power supplies that do not have a high-precision DCCT for monitoring, an inexpensive external DCCT is installed to detect the current, although the output accuracy is poor at ±1% of full scale. For some power supplies, the signal from the feedback circuit is branched off and the signal through the isolation amplifier is detected. The Curs-BIS system is set to emit an interlock when the power supply current value fluctuates by more than ±1% of the rated current as the initial value, but it can be changed. For the power supply for steering magnets, the value is ±5% of the rated value.

The system is also used for the early detection of supply current oscillation in scenarios in which the feedback control of the power supply is not operating properly.

Fig. 1. Picture of a unit of the beam interlock system driven by changes in the magnet current (Curs-BIS).

A beam interlock system for detecting EIC and EDC discharges was also build using the same method as the Curs-BIS. The EIC and EDC are electric-field beam deflection channels used for beam injection and extraction of the cyclotron. The beam is deflected by applying a high voltage of approximately 100 kV to an electrode plate placed in the beam orbit. Because a high electric field is applied between the plates of ten and several millimeters, discharges often occur and the beam orbit is changed. Therefore, the beam should be stopped as soon as the discharge occurs.

Discharges were detected using only the actual voltage change with an analog type circuit. Now, a system similar to the Curs-BIS can stop the beam by detecting the change in the actual voltage and current replenishment due to the discharge. The system was installed in the cyclotrons of the SRC and IRC in parallel usage with the analog circuit. Since the RRC and fRC cyclotrons did not have a discharge detection system, this system was newly installed. With the system, the allowable value can be changed on the monitor screen, which was previously changed on site using the analog circuit. The system can also stop the beam under a sudden change in the set voltage and maintain a log of the number of discharges per hour, which can be monitored on the Web.

Most of the power supplies in the RIBF are now being monitored using Curs-BIS, but a few 10% of the power supplies on the RARF remain to be set. We are planning to increase the number of registered power supplies.

Reference

1) K. Kumagai *et al.*, RIKEN Accel. Prog. Rep. **52**, 115 (2019).

*1 RIKEN Nishina Center

2021 Operational report for the Nishina RIBF water-cooling system

T. Maie,[*1] K. Kusaka,[*1] E. Ikezawa,[*1] Y. Watanabe,[*1] M. Kidera,[*1] K. Kobayashi,[*2] J. Shibata,[*2] M. Oshima,[*3] and H. Shiraki[*3]

Operation condition

In 2021, the cooling systems of Nishina and RIBF were operated for a slightly longer period than the accelerators. Excluding the time for an installation that was performed continuously, RIBF's cooling systems were operated for approximately three months. Nishina's cooling systems as for AVF standalone, AVF+RRC, AVF+RRC+IRC, and RILAC2+RRC were operated for approximately five months. No significant troubles that might have caused the long-term interruption of accelerator operation occurred, and the cooling systems were operated stably, with the exception of some minor problems.

Trouble report

In troubleshooting during FY2021, trouble symptoms were fortunately minor. Therefore, instead of interrupting the machine time for repairs, while providing emergency measures, repairs were carried out during long-term accelerator outage periods such as those for switching beams or summer maintenance.

Typical examples of troubles that occurred in FY2021 are as follows: water leak from the cooling plumbing joint and deterioration of cooling-water purity due to the water leakage, bearing failure of the cooling water pump motor, inverter failure of the cooling water pump, and device outage caused by an instantaneous voltage drop due to a lightning strike (1–2 times a year).

Periodic maintenance

During the shutdown period of the accelerator, the following activities were carried out as part of regular maintenance.

(1) Cleaning of the cooling towers
(2) Inspection and overhauling of the cooling-water pumps
(3) Replacement of some superannuated hoses, joints, and valves used in the system
(4) Cleaning of the strainers and filters used in the deionized water production system
(5) Extension of the sensing wires of the water-leakage alarm to floors of new areas
(6) Flushing work of the cooling-water pipe that was blocked by dirt

Others

The accelerator facility at the Nishina Center has been operational in the Nishina Building for 35 years and the RIBF facility has been operational for more than 15 years. The same applies to the cooling equipment. With a limited budget, maintenance is performed every year, but the equipment is inevitably aging. Moreover, cooling-water consumables used for repairing pumps that have been used for more than 15 years are basically unobtainable or very difficult to obtain. Aging equipment is not only a cause of failure, but also one of the causes of unstable accelerator beams. However, anti-aging costs The budget for equipment maintenance is insufficient to cover the costs of anti-aging measures, and solving these problems will be a significant challenge in the future.

Reference

1) T. Maie *et al.*, RIKEN Accel. Prog. Rep. **54**, 78 (2021).

[*1] RIKEN Nishina Center
[*2] SHI Accelerator Service Ltd.
[*3] Nippon Air Conditioning Service Co., Ltd.

Development of a new indicator for the auto tuning system with high-intensity primary beams

T. Nishi,[*1] N. Fukuda,[*1] N. Fukunishi,[*1] E. Iwai,[*2,*3] H. Maesaka,[*2] Y. Shimizu,[*1] T. Sugimoto,[*2,*3] H. Suzuki,[*1] H. Takeda,[*1] A. Uchiyama,[*1] Y. Yanagisawa,[*1] and M. Yoshimoto[*1]

At the RIBF facility, more than 600 parameters, such as quadrupole magnets, steerers, rebunchers, and radio-frequency (RF) voltages/phases, are manually adjusted. After more than 10 years of operation, the local beam loss has been suppressed to a few percentage points. However, in order to control the beam beyond 1 particle μA, we need to optimize the parameters more precisely according to the beam state at the time while keeping the beam loss below 0.1%. Therefore, we decided to conduct research to introduce automatic parameter optimization using machine learning.

In this project, we adopt an auto tuning program using sequential learning based on Gaussian process regression, which is developed and already integrated in the regular operation at SACLA of SPring-8.[1)] We apply the program to RIBF via EPICS. As the first step to introduce the program to RIBF, we attempted to optimize the beam-line optics from the SRC to the first production target of BigRIPS, F0.

There are two approaches underway in this project: (A) the development of an auto tuning system for low-intensity beams using fluorescent targets and (B) the development of a new indicator for an auto tuning system with high-intensity beams using secondary beams. For (A), we conducted a 12-h experiment in October 2020 using a faint U^{86+} beam of about 0.001 electric nA (enA) and succeeded in increasing the transmission efficiency by 2% and reducing the spot width by 13% at F0 over the manually optimized optics.[2)]

For (B), we devised a method using different charge states as indicators for high-intensity primary beams. A primary U^{86+} beam is injected to a 1-mm-thick Be target at F0 to produce several charged-state particles. The primary beam width and intensity on the target are estimated from the trajectories and count rates of charge-converted particles at downstream focal planes with parallel-plate avalanche counters (PPACs) and a scintillator at the F3 focal plane. Figure 1 shows the distribution of different charged states at the slit position F1. As shown, the production rate of particles varies depending on each charge.[3)] One charge state is selected by adjusting the Bρ of the beam line and the F1 slit condition. The measurements of the beam spot size and intensity are realized for primary beams up to 10 enA by selecting charge states with lower production rates as the primary beam intensity increases.

We conducted an experiment to test this indicator in May 2021 with faint U^{86+} beams. The optimization program developed in approach (A) was utilized with the new indicator. The 1-mm-thick Be target was set behind the fluorescent viewer to compare the new indicator with the spot image obtained by the fluorescent target. We confirmed that the program optimized the 7 magnet currents simultaneously to increase value of the indicator. However, it was revealed that the transmission efficiency with optics "optimized" by our program was 10% worse than that with the manually optimized optics by comparing the beam current with upstream and downstream Faraday cups.

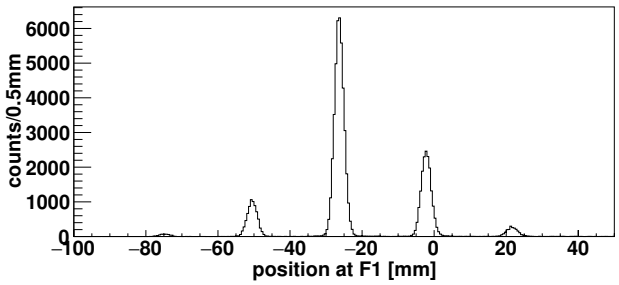

(a) Positions with a 1-mm-thick Be target

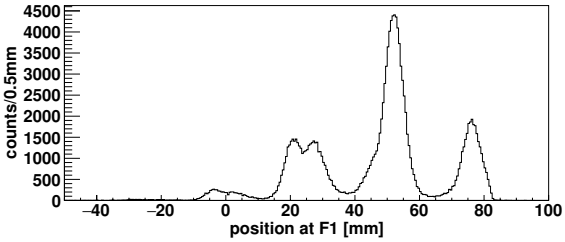

(b) Positions with a 1-mm-thick Be and fluorescent target

Fig. 1. Position distribution of U ions for different charge states at slit position F1.

After investigation, we found that this was due to the non-uniformity of the thickness of the fluorescent target, which increased the momentum spread and the beam size at the slit position as shown in Fig. 1(b). The distribution width was not small enough compared with the slit width of 23 mm, and the counts of the downstream scintillator strongly depended on the shape of the distribution at F1, rather than the primary beam intensity at F0. In order to solve the problem, we aim to adopt a 1-mm-thick Be solely to avoid enlarging the beam size at slit position F1.

*1 RIKEN Nishina Center
*2 RIKEN SPring-8 Center
*3 Japan Synchrotron Radiation Research Institute

References
1) E. Iwai *et al.*, Proc. PASJ2021, WEOB02 (2021).
2) T. Nishi *et al.*, Proc. PASJ2021, TUOA03 (2021).
3) D. S. Ahn *et al.*, RIKEN Accel. Prog. Rep. **52**, 133 (2019).

Status of vacuum pumping systems in accelerator facilities

Y. Watanabe,[*1] M. Fujimaki,[*1] E. Ikezawa,[*1] O. Kamigaito,[*1] M. Kidera,[*1] T. Nishi,[*1] S. Watanabe,[*1] K. Yamada,[*1] M. Nishida,[*2] K. Oyamada,[*2] J. Shibata,[*2] K. Yadomi,[*2] and A. Yusa[*2]

A vacuum pumping system in the RIBF accelerator facility comprises cryopump (CRP) systems, turbomolecular pump (TMP) systems, rough pumping systems (mechanical booster pump + rotary pump [RP]), additional chamber pumping systems (TMP + RP), and subpumping systems (TMP + RP) as subvacuum of a resonator.[1,2] In addition, module-type vacuum gauges (total pressure gauge [TPG] controller combined with two gauges) are used. In this paper, we report some malfunctions of vacuum pumping system encountered in 2021. Table 1 lists the malfunctions in the pumps, compressors, and gauges from 2018 to 2021. The vacuum pumping systems were relatively stable to maintain and manage in 2021. A malfunction of TMPs (including power supply) and RPs were less in 2021 compared to other years. Additionally, malfunctions of CRP and TPG increased in 2021.

Six cryopump compressors of the SRC malfunctioned around the G01 Faraday cup (SRC deflection beam line) in the uranium beam for the BigRIPS experiments during the months of April to May. The malfunctions of the cryopump compressors were caused mainly in the SRC room by a high environmental radiation dose. Therefore, we plan to relocate 13 compressors to a location far (SRC-north area) from the region of high environmental radiation (SRC-south area) within a few years. In addition, because the existing cryopump compressors (model; C30V, CRC-874) of the SRC and RRC have been discontinued by the manufacturer and cannot repaired in the future, a new cryopump compressor (model; C30VRT, P-875CA) for the SRC and RRC has been purchased as a spare unit in case of a malfunction.[3] Furthermore, because RRC cryopumps were manufactured in 1985 and the replacement of the cryopump to a new model should be realized early, one unused cryopump system set of the IRC-valley cavity was relocated to the RRC-valley cavity in 2020.[3]

We must update large TMP systems (5000 L/s) in the RILAC and RRC within a few years because they have been in operation for 35–43 years.[3] Therefore, in the fiscal year 2021, one 5000 L/s TMP is scheduled to be updated in the RILAC and another TMP is scheduled to be replaced by a set of smaller TMPs (800 L/s and 1100 L/s).

A large RP in the SRC-RES4 (Resonator 4) has malfunctioned owing to age-related deterioration, and a new spare large RP has been purchased, which has not been installed. In addition, some oil leaks in the small RPs were repaired by installing new O-rings and seals as usual.

Malfunctions in the TPG have increased year by year. The reason is unclear, but it is likely because of age-related deteriorations. Three of the five malfunctioned TPG controllers occurred when the power was restored after an electrical power outage in August and October. This is one common pattern in malfunctions in vacuum pumping systems. Furthermore, all malfunctioned gauges were replaced by spare units due to a contamination of the sensor head.

Regarding vacuum leaks at the RIBF, nearly all of the vacuum leaks were caused by age-related deterioration and repaired by installing new O-rings or applying a repair material. For example, water leaks in the water-cooling parts of the drift tubes in the RILAC cavities were repaired with a sealing agent, and multiple O-rings were replaced with new parts. A water leak from the water-cooling pipe of a small compensation board in the RILAC cavity #2 were also repaired with a sealing agent. A vacuum leak in the coupling of a lower feedthrough trim coil (C8) in the AVF was repaired with a sealing agent because it was difficult to replace the O-ring.

References

1) S. Yokouchi *et al.*, RIKEN Accel. Prog. Rep. **41**, 101 (2008).
2) Y. Watanabe *et al.*, RIKEN Accel. Prog. Rep. **50**, 154 (2016).
3) Y. Watanabe *et al.*, RIKEN Accel. Prog. Rep. **54**, 79 (2020).

Table 1. Number of malfunctions from 2018 to 2021.

	Number of units	2018	2019	2020	2021
CRP [a]	> 80	4	6	7	6 (Pump) 8 (Compressor)
TMP [b]	> 138	3	8	4	1 (Pump) 4 (Power supply)
RP [c]	> 146	5	3	7	1 (Pump)
TPG [d]	> 160	4	6	9	5 (Controller) 7 (Gauge)

a) Includes a compressor. b) Includes an attached power supply. c) Excludes an oil leak. d) Includes a controller, Pirani, and cold cathode gauge.

*1 RIKEN Nishina Center
*2 SHI Accelerator Service Ltd.

9. Instrumentation

Development of auto-focusing and auto-centering system for the BigRIPS separator (II)

Y. Shimizu,[*1] N. Fukuda,[*1] H. Takeda,[*1] H. Suzuki,[*1] M. Yoshimoto,[*1] T. Sumikama,[*1] T. Baba,[*1] and K. Yoshida[*1]

We are developing a fully-automatic system for radioactive-isotope (RI) beam production based on our technological developments and experiences to reduce the operation time. As the first step, an auto-focusing and auto-centering system[1,2] to tune the superconducting triplet quadrupole (STQ) and dipole magnets of the BigRIPS separator was developed. This is the second report on the auto-focusing and auto-centering system.

In a previous development,[2] auto-focusing or auto-centering, including data taking, analysis, and magnet adjustment, were performed for each focal plane. In the present development, we aimed to fully automate the focusing and centering at all the focal planes.

^{79}Ni-beam production using the auto-focusing and auto-centering system was conducted for the mass measurement around the ^{78}Ni region (NP2012-RIBF202-02). The ^{79}Ni yield was not high enough to perform centering and focusing quickly, and the ^{82}Ga beam was used instead. To center the ^{79}Ni-beam positions on the beamline, the goal of the ^{82}Ga positions were calculated as -2.7, -6.4, and -3.0 mm at F3, F5, and F7, respectively.

The STQ and dipole magnets were changed simultaneously to perform auto-focusing and auto-centering simultaneously at each focal plane. The focal plane for auto-tuning was automatically changed from upstream to downstream, *i.e.*, from F1 to F7. The position-detector PPACs installed at F2 were used only for RI-beam tuning at F2. The F2-PPACs were moved automatically on and off the beamline before and after the auto-tuning at F2. Figure 1 shows the positions and phase spaces at each focal plane after auto-focusing and auto-centering. For the auto-centering, the dipole magnet was tuned so that the center position of the distribution x_0 at the focal plane obtained from the result of Gaussian fitting became the goal of the ^{82}Ga position. For auto-focusing, the STQ magnets were tuned so that the first-order coefficient $p1$ obtained by fitting the phase space with the first-order polynomial function was greater than 10, which corresponds to $(x|a)$ less than 0.1. After confirming that auto-focusing and auto-centering were successful, the focal plane for these tunings was changed to the next one. A sequence of these procedures started by simply clicking an "AUTO TUNING" button on the web browser, after selecting the gate of the ^{82}Ga beam on an analysis program. The results shown in Fig. 1 demonstrate the success of focusing and centering.

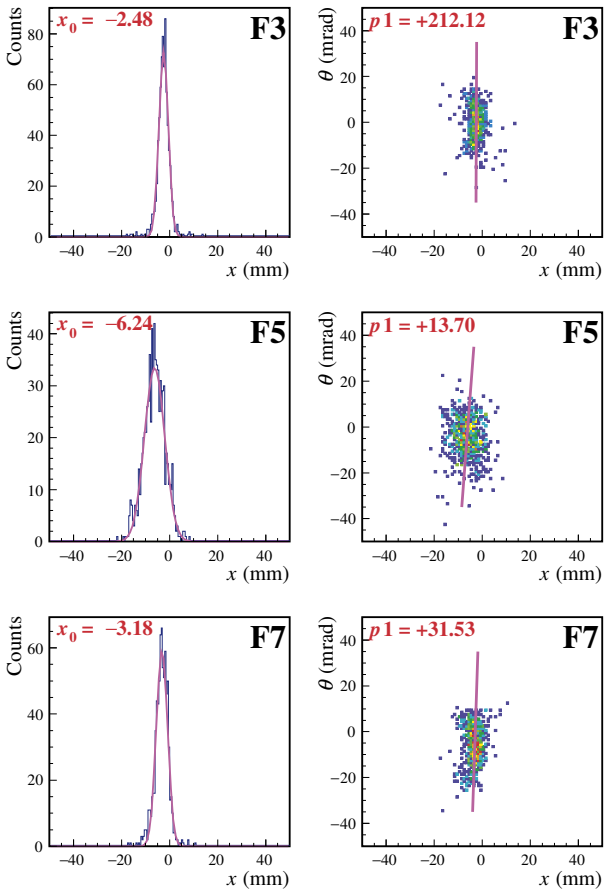

Fig. 1. Positions (left column) and phase spaces (right column) at each focal plane (F3, F5, and F7) after the auto-focusing and auto-centering. The pink curves and lines show the best-fit functions of the Gaussian and first-order polynomial, respectively. The x_0 and $p1$ values show the fit results.

Thus, the development of a novel auto-focusing and auto-centering system was completed. An operation test will be conducted by RI-beam physicists to confirm that this system is applicable to the regular operation of RI-beam production.

References

1) T. Sumikama *et al.*, RIKEN Accel. Prog. Rep. **54**, 82 (2021).
2) Y. Shimizu *et al.*, RIKEN Accel. Prog. Rep. **54**, 83 (2021).

*1 RIKEN Nishina Center

Development of new ionization chamber specialized in high-Z beam

M. Yoshimoto,[*1] N. Fukuda,[*1] R. Matsumura,[*1] D. Nishimura,[*2] H. Otsu,[*1] Y. Shimizu,[*1] T. Sumikama,[*1] H. Suzuki,[*1] H. Takahashi,[*2] H. Takeda,[*1] J. Tanaka,[*1] and K. Yoshida[*1]

An ionization chamber (IC) is an essential detector to identify particles in flight in the BigRIPS separator and ZeroDegree spectrometer.[1] Generally, the atomic number (Z) is deduced from the energy deposit (ΔE) in the IC. However, so far, the Z resolution of particles with $Z > 80$ emitted from the fragmentation of ^{238}U primary beam on a production target is insufficient for the clear particle identification. Here, we report on the construction and data acquisition of a new IC for high-Z beam with an effective diameter of 60 mm.

The deterioration in the Z resolution is caused by the δ-rays[2,3] and the fluctuation of the ionic charge state. The δ-rays bring about a long tail at the higher energy side of the ΔE distribution. The Z resolution can be enhanced if the IC does not collect the electron-ion pairs from the δ-rays. Accordingly, smaller electrodes were employed for the new IC. The outer diameter of the electrodes that form the electric fields was reduced from 280 mm for the conventional F7 IC to 80 mm for the new IC. Consequently, the change reduces the effective electrode diameter from 232 mm to 60 mm. The electrode size effects will be tested in the future.

The charge state fluctuation of heavy ions in matter is a well-known phenomenon.[4] The ΔE is proportional to the square of the charge state, instead of the Z of the particle. Therefore, the charge state fluctuation by the filled gas and other materials in the IC affects the ΔE distribution and the Z resolution. Accordingly, the materials in front of the first electrode should be reduced to measure the charge state incident on the F7 chamber with the IC. Therefore, the thickness of the upstream vacuum separation window was reduced from 150 μm to 77 μm, and the length of the dead gas from the vacuum separation window to the first electrode was reduced from 89 mm to 16 mm. Furthermore, we also adopted the methane gas with a smaller cross section of the charge state changing, compared to the P10 (argon 90% + methane 10%) gas. The P10 and methane pressures were 620 Torr. The distance between the electrodes is 20 mm and the effective gas thickness is 480 mm, as shown in Fig. 1. Six signals each from four gas cells were digitized.

The response of the new IC to the gas species was measured at F7 using $^{238}U^{90+}$ beam with 320 MeV/nucleon. The trigger rates at the F7 were approximately one kcps. The geometrical averages for the six ADC values of the P10 and the methane gas are shown in Fig. 2.

To understand these distributions, the charge state distributions in the IC were simulated with the GLOBAL code.[5] On the one hand, the charge states at the first→last electrode in the P10 is 76→37% for 90+ and 19→45% for 91+. On the other hand, those in methane are 79→68% for 90+ and 16→24% for 91+. The average number of charge state changes from 90+ to 91+ is 0.9 times for P10 and 0.2 times for methane. According to the simulation, the asymmetric energy distribution with the P10 was formed by the mixture of charge 90+ and 91+. In contrast to the P10, the energy distribution with methane has two peaks. The first narrow peak was formed by charge 90+ and the second peak was formed by 91+. Consequently, 0.9 times of the charge state changes in the P10 appears to be small to average different charge states and large for separating ΔE of each charge state. If a gas with a large cross section of the charge state changing is used, the distribution will be narrowed because the mixture of multiple charge states is well averaged.

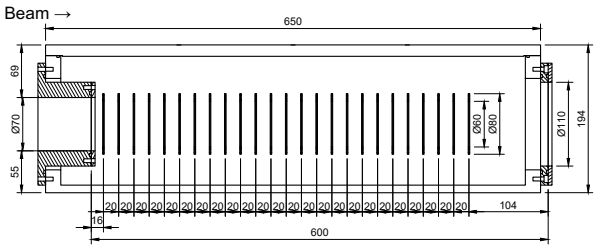

Fig. 1. Cross sectional view of the new IC. The electrode foil is aluminized (both sides) Mylar sheet with 2.5 μm thickness.

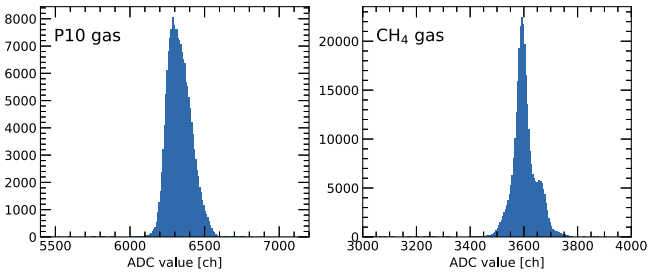

Fig. 2. Energy distributions for $^{238}U^{90+}$ beam at 320 MeV/nucleon directed onto the new IC with the P10 gas (left) and the methane gas (right).

References

1) K. Kimura *et al.*, Nucl. Instrum. Methods Phys. Res. A **538**, 608 (2005).
2) Y. Sato *et al.*, RIKEN Accel. Prog. Rep. **46**, 159 (2013).
3) M. Pfützner *et al.*, Nucl. Instrum. Methods Phys. Res. B **86**, 213 (1994).
4) H. Weick *et al.*, Phys. Rev. Lett. **85**, 2725 (2000).
5) C. Scheidenberger *et al.*, Nucl. Instrum. Methods Phys. Res. B **142**, 441 (1998).

*1 RIKEN Nishina Center
*2 Department of Natural Sciences, Tokyo City University

Radiation transport calculation of BigRIPS separator

K. Yoshida*1

Radiation transport calculations of the BigRIPS separator from the production target (F0) to the final focus (F7) have been conducted to investigate the origin of the neutron radiations in the BigRIPS room. During the BigRIPS operation, the power supplies and the control panel of the superconducting quadrupole magnets (STQs) in the BigRIPS room freeze occasionally owing to the neutron radiations. To prevent these problems, radiation shielding is necessary. In designing an efficient radiation shield, knowing the origin of neutrons is important.

Thus far, radiation transport calculations of the BigRIPS separator have been conducted from F0 to the first focus (F1) region[1–3] using the particle and heavy-ion transport code system (PHITS).[4] In the present study, we extended such a calculation to cover the entire BigRIPS region from F0 to F7. The previous geometry model was extended to include all magnets, beam ducts, chambers, and slits of the BigRIPS separator. The building walls and radiation shielding blocks in the BigRIPS room were also included in the model. Calculations were performed with PHITS ver. 3.24 code installed in the HOKUSAI BW supercomputer at RIKEN. Hybrid-parallel computing, with 128 parallel processes of 10 threads, was used to conduct the calculations. The calculations were performed under various conditions that replicated the experiments performed at the Radioactive Isotope Beam Factory. In a calculation, 100 million events were generated for all incident beams except ^{238}U. The event number was reduced to 30 million for the ^{238}U beam, because the calculations needed a longer CPU time. A total CPU time (CPU time summed over 1280 arithmetic cores) of 40–50 million seconds was used for one calculation.

Figure 1 shows the neutron dose distribution in the BigRIPS room for the ^{238}U beam at 345 MeV/nucleon impinging to a 5-millimeter-thick Be target. The BigRIPS separator was tuned for ^{79}Ni beam production. In this setting, the ^{238}U beam was stopped at the inner-side of the exit beam dump, which was located at the exit of the first dipole magnet. High doses were observed at the target (F0) and the beam dump (BD in Fig. 1) regions where the ^{238}U beam decreased their energies. The neutron dose gradually decreased with the distance from F2 in the F3-F7 region, whereas it was slightly high around F5.

The calculated neutron doses were compared with experimental measurements. Two neutron survey meter (TPS-451, manufactured by ALOKA Co., Ltd.) were placed at the power supply and the control panel of the STQs and used for neutron measurements. The observed doses were ∼1.8 μSv/h at the power supply and 0.8 μSv/h at the control panel with a 70-particle nA (pnA) ^{238}U beam; normalized to a 100-particle nA beam intensity, they were ∼2.5 μSv/h and ∼1.1 μSv/h, respectively. The calculated neutron doses were ∼8 μSv/h and ∼2 μSv/h for a 100-particle nA beam. Thus, the calculations reproduced the experimental observations by a factor 2–3. Based on the calculations, the design of the shielding blocks is undergoing.

References

1) T. Ohnishi *et al.*, RIKEN Accel. Prog. Rep. **44**, 129 (2011).
2) K. Tanaka *et al.*, RIKEN Accel. Prog. Rep. **44**, 132 (2011).
3) K. Tanaka *et al.*, Prog. Nucl. Sci. Technol. **4**, 201 (2014).
4) T. Sato *et al.*, J. Nucl. Sci. Technol. **55**, 684 (2018).

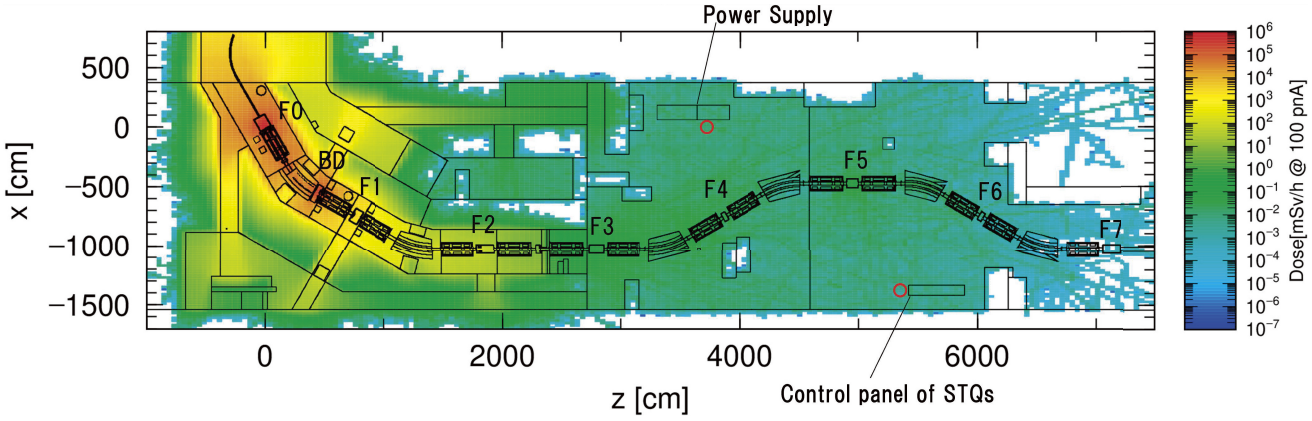

Fig. 1. Neutron dose distribution in BigRIPS room for ^{238}U beam impinged on 5-mm-thick Be target. Red circles represent positions of neutron survey meters that are used for neutron measurements.

*1 RIKEN Nishina Center

Present status of beam transport line from SRC to BigRIPS

K. Kusaka,[*1] K. Yoshida,[*1] M. Ohtake,[*1] and Y. Yanagisawa[*1]

A beam transport line delivering the primary beam extracted from the SRC to the BigRIPS target has been operated since 2007, and it is called the "T-course" beam line. The T-course beam line consists of 3 bending magnets and 17 quadrupoles.[1] Two identical 50° bending magnets DMT2 and DMT3 in the T-course are "2-Tesla" room-temperature dipoles, with a maximum current of 650 A. They are designed as resistive-type magnets with saddle-shaped correction coils in addition to main coils. The correction coils are installed in the gap of the magnet, and were originally excited with the main coils in series. Each main coil has 72 turns and consists of 6 double pancakes, in which a 13.5×13.5 mm hollow conductor is wound 6 times in each layer. In contrast, each correction coil is a 12-turn double pancake in which a 14×10 mm rectangular hollow conductor is wound 6 times in each layer.[1]

The layer isolation of the lower correction coil of the DMT3 magnet was damaged in an October 2017 incident,[2] and the upper correction coil was found to be short-circuited in November 2019.[3] Furthermore, the lower main coil of the DMT3 was damaged in a test excitation performed in March 2020.[4] When we energized only the main coils with a total current of 800 A by adding an auxiliary power supply to the original one, unstable behaviors were observed at the excitation voltages of the second and fourth pancakes of the lower main coil.[4] Although we considered that the upper main coil was not critically damaged, we decided to replace the main coils with new ones.

We designed the new main coils for the DMT3 magnet such that they are excited with the original DMT3 power supply using neither correction coils nor additional auxiliary DC power supply in its circuit. We increased the number of turns of each main coil from 72 to 84. Furthermore, the shape of each main coil was designed to fit in the original DMT3 iron pole and yoke without any modifications. As shown in Fig. 1, the 12-layer new main coil in the upper-half has a pentagonal-shaped cross-section. We choose the same 13.5×13.5 mm hollow conductor as in the original DMT3 main coils. Each new coil consists of three types of double pancake coils in which a hollow conductor is wound 4, 6, and 8 times in each layer, respectively. Each new pentagonal-shaped coil is formed by combining one 4-turn, one 6-turn, and four 8-turn pancakes with epoxy resin. Because the lengths of cooling water channels are different, we introduce valves and flow meters in each cooling channel at the cooling water header. The new coils were fabricated and tested by HANMI TECHWIN in Korea under the supervision of Toshiba and shipped to RIKEN in July 2021. The new coils were successfully installed in the DMT3 magnet on site, as shown in Fig. 2. Associated plumbing and wiring works were finished in August 2021. After a series of test excitations, the DMT3 magnet with the new main coils was excited, and a ^{238}U beam was successfully transported from the SRC to the BigRIPS target in the beam time from November to December 2021.

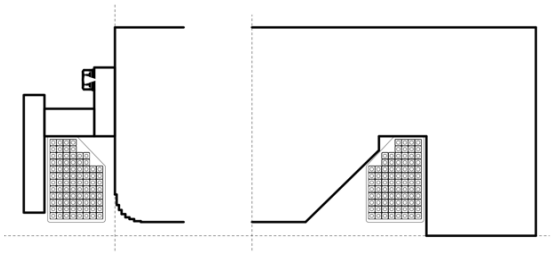

Fig. 1. Schematic of the upper-half cross section of DMT3 magnet with new main coil.

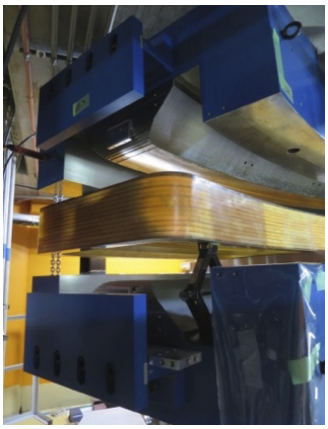

Fig. 2. Installation of new coil in DMT3 iron yokes.

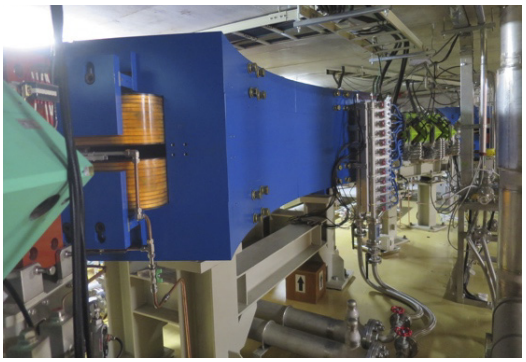

Fig. 3. DMT3 magnet with new coils in T-course beam line.

[*1] RIKEN Nishina Center

References
1) K. Kusaka *et al.*, IEEE Trans. Appl. Supercond. **18**, 318 (2008), and references therein.
2) K. Kusaka *et al.*, RIKEN Accel. Prog. Rep. **51**, 173 (2018).
3) K. Kusaka *et al.*, RIKEN Accel. Prog. Rep. **53**, 104 (2019).
4) K. Kusaka *et al.*, RIKEN Accel. Prog. Rep. **54**, 104 (2020).

Development of novel semiconductor detector towards high-rate heavy RI beam counting

T. Isobe,[*1] M. Togawa,[*2] M. Miyahara,[*2] J. Nishinaga,[*3] H. Okumura,[*4] M. Imura,[*5] and E. Takada[*6]

The precise measurement of heavy ion track and energy loss is important for the identification of projectile fragments with a fragment separator such as BigRIPS at RIBF. As the intensity of the primary beam increases, a stronger radiation-resistant detector is required to realize a high-rate ($\geq$1 MHz) RI beam experiment. A Si detector has the characteristics of high-resolution energy measurement, but it is weak in a high-radiation environment. In order to realize a radiation-resistant semiconductor detector, we have examined several types of novel semiconductors that were developed for other purposes. Table 1 lists the semiconductors we are testing. The chalcopyrite compound Cu(In,Ga)Se_2 (CIGS) is well investigated as it has potential for use as a semiconductor in thin-film photovoltaic devices, such as solar cells.[1)] CIGS can recover from radiation damage through the annealing of CIGS crystals. This characteristic is advantageous for a radiation detector since we often encountered the damage to semiconductor detectors by high-rate ion beams. GaN is one of the wide-bandgap semiconductors that are expected to be suitable for radiation detectors with long-term stability due to a small intrinsic carrier density and large threshold displacement energy.

We performed a detector test experiment at HIMAC in Chiba, where a highly intense 400 MeV/nucleon Xe beam was irradiated on semiconductor samples: CIGS and GaN. Figure 1 shows the sample of the CIGS detector, the thickness and effective area of which are 2 μm and 0.5 mm^2, respectively. This is thick enough to observe the signal with a 400 MeV/nucleon Xe ion, which loses an energy of 3.5 MeV in the semiconductor. This beam test was the first time a heavy-ion signal was observed from those semiconductors.

Table 1. Specifications of modern semiconductor candidates for radiation detection.

	Bandgap energy (eV)	Density (g/cm^3)	Normalized number of e-h pairs to Si
Si	1.1	2.33	1
CIGS	1.2	5.7	2.93
SiC	3.2	3.21	0.64
GaN	3.4	6.15	1.07
Diamond	5.5	3.50	0.45
AlN	6.1	3.26	0.33

*1 RIKEN Nishina Center
*2 Institute of Particle and Nuclear Studies, High Energy Accelerator Research Organization (KEK)
*3 Research Center for Photovoltaics, National Institute of Advanced Industrial Science and Technology (AIST)
*4 Faculty of Pure and Applied Sciences, University of Tsukuba
*5 Research Center for Functional Materials, National Institute for Materials Science (NIMS)
*6 Quantum Life and Medical Science Directorate, National Institutes for Quantum Science and Technology (QST)

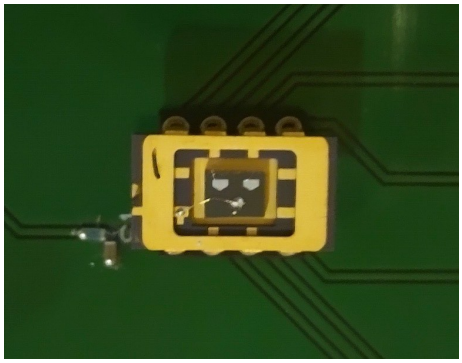

Fig. 1. CIGS samples (two pentagons shown at the center of the photograph) tested at HIMAC.

In addition to checking the signal from CIGS and GaN, we tested the hardness of each semiconductor against radiation damage by a Xe beam. Figure 2 shows the CIGS pulse height as a function of the irradiated Xe beam yield. During the irradiation of a high-rate (10^6 pps) Xe beam on CIGS, the pulse height decreased down to 60% of the original pulse height. After annealing the CIGS semiconductor (130°C, 5 h), we could observe the recovery of the pulse height to ~85% of the original pulse height.

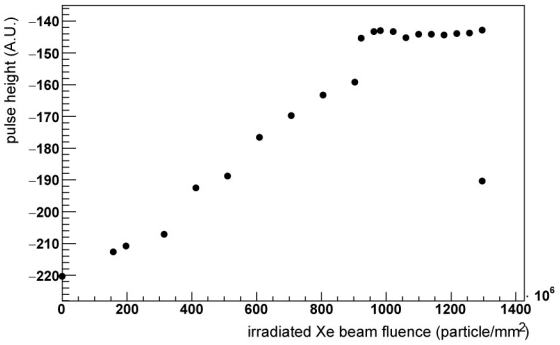

Fig. 2. CIGS negative pulse height as a function of irradiated Xe beam yield. A 400 MeV/nucleon 10^6 pps Xe beam was irradiated on a CIGS sample. After annealing the CIGS sample, the recovery of the pulse height was observed as shown by the rightmost point.

We will continue to develop the next generation of semiconductor detectors by employing a novel type of semiconductor.

Reference

1) J. Nishinaga *et al.*, Appl. Phys. Exp. **10**, 092301 (2017).

A pilot experiment for collective flow in heavy-ion collisions

S. Nishimura,[*1,*2] T. Isobe,[*1] V. H. Phong,[*1] H. Tanabe,[*2] S. Yamamura,[*3] S. Esumi,[*2] Y. Hijikata,[*4] R. Mizuno,[*3] Y. Nakai,[*1] M. Niikura,[*1,*3] and T. T. Yeung[*1,*3]

Asymmetric emissions of various particles in semi-central heavy-ion collisions are expected to be sensitive probe for the equation of state (EOS) of high-density nuclear matter.[1)] A pilot experiment was conducted by impinging 400 MeV/nucleon ^{132}Xe on a CsI target (500 mg/cm^2) at beam intensities of 10^5–10^6 particles/spill at the HIMAC SB2 beam line at NIRS. Our primary goal is to confirm asymmetric angular correlation of proton and neutrons at target rapidity with respect to the reaction plane determined by charged particles in forward rapidity.

A forward counter FC, 90 plastic scintillation detectors mounted in 3 rings centered along the beam axis, was developed to determine the reaction plane of heavy-ion collisions on an event by event basis. A cubic-shape plastic scintillator ($25 \times 25 \times 25$ cm^3) was coupled with a photomultiplier tube (Hamamatsu R3478S; used for the CERN-NA44 experiment). Figure 1 shows the experimental setup, where left detectors correspond to the NiGIRI[2)] to measure the particles at target rapidity region. The FC is installed at a distance of 43 cm, 46 cm, and 48 cm downstream from a target for inner-, middle-, and outer-rings, respectively. The signals of NiGIRI, FC, and beam counters are recorded using fast digitizers (CAEN V1730B, V1740) together with the TDC module (CAEN V1190A), where newly developed RCDAQ

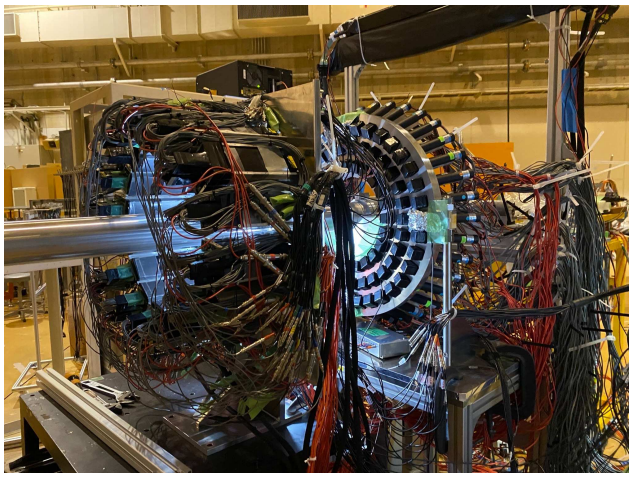

Fig. 1. Experimental setup for H447. Xe-beam is coming from left to right. CsI target is located at NiGIRI in left. The FC is installed after the target.

*1 RIKEN Nishina Center
*2 Department of Physics, University of Tsukuba
*3 Department of Physics, University of Tokyo
*4 Department of Physics, Kyoto University

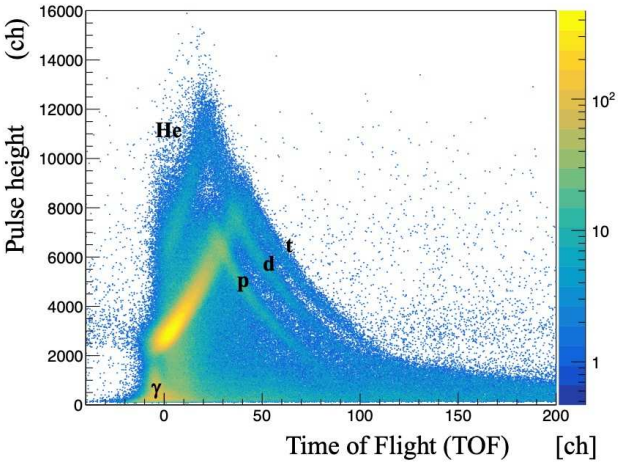

Fig. 2. Particle identification in FC. A plastic scintillator BC1 in the beam line is used for start timing of the FC. Charged particles (p, d, t, and He) are selected for reaction plane determination.

was employed to recode the waveform of signals at trigger rate of up to 1 kHz with bufferling mode.[3)] A plastic scintillator BC1 is installed as a start counter in the beam line.

Figure 2 shows a particle identification spectrum obtained by the FC, where the horizontal and vertical axes are the time-of-flight and the energy loss ΔE, respectively. The charged particles (p, d, t, He) in forward rapidity were identified from the background γ-rays. The collective flow of protons and neutrons was confirmed successfully as a function of the transverse momentum using the NiGIRI at target rapidity, where the reaction plane was determined by the FC using a sub-event sampling method.[4)]

In future, our experimental technique will be applied using the higher energy Xe-beam and high intensity radioactive beam at HIMAC and RIBF, respectively.

References

1) P. Danielewicz *et al.*, Science **298**, 1592 (2002).
2) H. Matsuzawa *et al.*, RIKEN Accel. Prog. Rep. **48**, 212 (2015).
3) M. L. Purschke, 2012 18th IEEE-NPSS Real Time Conference (IEEE, 2012), DOI: 10.1109/RTC.2012.6418184.
4) H. Tanabe, Master thesis, Univ. of Tsukuba (2022).
5) S. Yamamura, Master thesis, Univ. of Tokyo (2022).

Silicon trackers for cluster knockout reactions in ONOKORO

K. Higuchi,[*1,*2] J. Tanaka,[*1] T. Uesaka,[*1] R. Tusuji,[*3] J. Zenihiro,[*1,*3] S. Kawase,[*4] S. Kurosawa,[*5] S. Takeshige,[*1,*6] H. Baba,[*1] and Y. Hijikata[*1,*3] for the ONOKORO Collaboration

We developed silicon trackers for the cluster knockout reactions toward the ONOKORO[1,2] project at RIKEN, Nishina Center. Particle tracking with a good position resolution is necessary to measure the angle of the emitted particles from the cluster knockout reactions. The multi-channel signals from the silicon-strip detectors were pre-amplified and shaped (50 ns CR-RC circuit) using the ASIC integrated circuits APV25.[3] Each of these ASIC can treat 128 channels. The unit silicon wafers with 7.68 cm width (768 strips) require twelve chips (see Fig. 1), which actually operate 1536 channels. The half (odd) channels were connected to the strip electrodes of the silicon detector by wire bonding, and the other (even) half were used to measure the sync common-mode noises and subtract them from the odd channels. Skipping channels with no signal reduces the number of readout channel. As it does not generate a trigger signal by itself, the basic operation involves synchronizing with external triggers. The output of the shaping circuit was held at the timing of an external trigger and was converted into a serial signal using an analog multiplexer. The serial signal was digitized using an ADC module (ADCM) and the data was acquired by the DAQ based on the TRB3 (TDC Readout Board V3) system.

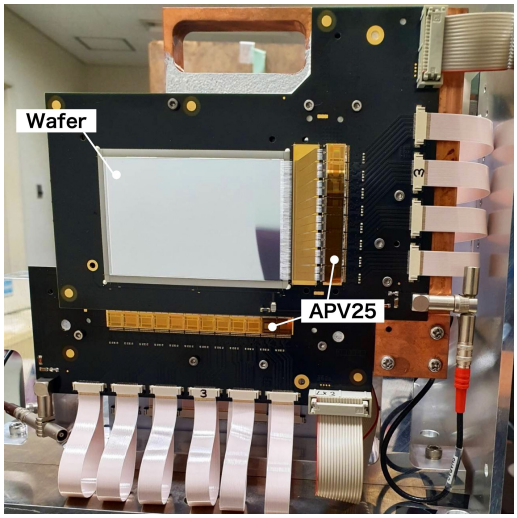

Fig. 1. Silicon detectors mounted for the text experiment at the HIMAC. A silicon wafer with vertical strips is placed in front of that with horizontal strips.

*1 RIKEN Nishina Center
*2 Department of Physics, Toho University
*3 Department of Physics, Kyoto University
*4 Department of Advanced Energy, Kyushu University
*5 Institute for Materials Research, Tohoku University
*6 Department of Physics, Rikkyo University

In August 2021 at HIMAC, we evaluated the responses of the silicon detectors to proton and α beams. Four silicon detectors, two each for measuring the positions in the X and Y directions with 100 μm strips, were installed in the beamline. Figure 2 shows the energy loss spectra of the proton 100 MeV beam and the α particle 230 MeV/nucleon beam in one silicon layer, respectively.

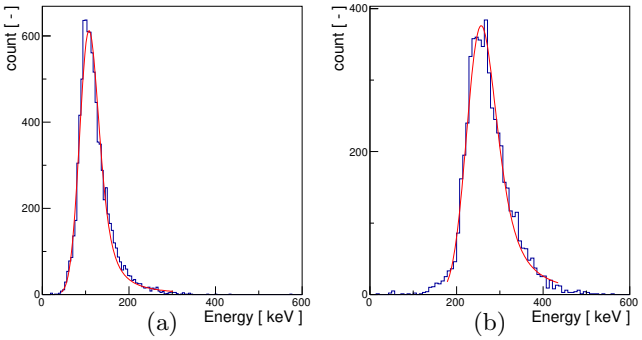

Fig. 2. Energy loss spectrum of (a) 100 MeV proton beam (b) 230 MeV/nucleon alpha-particle beam.

The distribution of small energy loss is known to be a Landau distribution. In (a) with proton beam, the fitting was performed using a Landau function convoluted by a Gaussian. It reproduced the pedestal widths (4.15 keV). In (b), the larger energy loss with the alpha-particle beam provides a rather symmetrical distribution. This result revealed that the responses of the silicon detectors, including the electric circuit, were under control. Moreover, we also evaluated the detection efficiencies. The particles were guaranteed to pass through the detector by detecting them in the same events in the front and back. In a low intensity (1 k cps) condition, 91.4% of the events had a single hit, and 8.10% were double hits. In the double hits, 75.7% were adjacent strips. Events with more than triple hits were 0.47%. Consequently, it was found that it is possible to uniquely determine the hit position with 97.5% in each silicon layer. The high detection efficiency under small energy loss conditions encouraged us to develop the full silicon detector array in the future.

References

1) T. Uesaka *et al.*, Grant-in-Aid for Specially Promoted Research, Grant Number 21H04975.
2) T. Uesaka *et al.*, RIBF Construction Proposal, "TOGAXSI: a new detector array for inverse-kinematics cluster and nucleon knock-out reaction experiments" (2021).
3) L. Jones, APV25-S1 User Guide V2.2 (2001).

Development of the GAGG(Ce) calorimeter for the cluster knockout reaction measurement

R. Tsuji,[*1] J. Zenihiro,[*1] T. Uesaka,[*2] J. Tanaka,[*2] K. Higuchi,[*2,*5] S. Kurosawa,[*3] H. Baba,[*2] S. Takeshige,[*4] and Y. Hijikata[*1,*2]

A new project named "ONOKORO" was recently launched to investigate the cluster formation phenomena in nuclei and nuclear matter with cluster knockout reactions.[1)] In this project, we plan to perform systematic measurements for various stable and unstable nuclei at the following accelerator facilities: RIBF, RIKEN, RCNP, Osaka University, and HIMAC at QST. At RCNP, we will measure the knockout reactions from fixed targets of stable nuclei with proton beams at 200–400 MeV. The expeirmental technique is already established with double-arm high-resolution magnetic spectrometers. At RIBF and HIMAC, the knock-out reactions with inverse kinematics will be measured with stable and unstable heavy-ion beams on liquid or solid hydrogen targets. For this measurement, we have proposed a new detector telescope, named TOGAXSI,[2)] consisting of silicon strip detectors (SSD) and GAGG(Ce) calorimeters. In this paper, we report the results of the performance test of the GAGG(Ce) calorimeters.

We chose the GAGG(Ce) scintillator to measure the kinetic energies of the recoil protons and knockout clusters (100–250 MeV/nucleon) because it has good scintillation properties compared to other standard scintillators such as NaI(Tl) and CsI(Tl). Figure 1 shows a photograph of the GAGG(Ce) crystal with a size of $40 \times 40 \times 120$ mm^3. In the ONOKORO experiments, high counting rates up to 100 kcps are expected; therefore, a good time response is required as well as a good energy resolution. To detect the scintillation photons, we prepared several photo sensors of PMT (R7600U, R11265U-20), APD (S8664-1010) and PD (S3584-08) produced by Hamamatsu. The PMT has a fast time response and a high gain, but low photo efficiency at ∼500 nm compared to APD and PD. Because APD and PD have small gains, we newly designed a fast amplifier circuit with a high-speed operational amplifier (Analog Devices, AD8000).

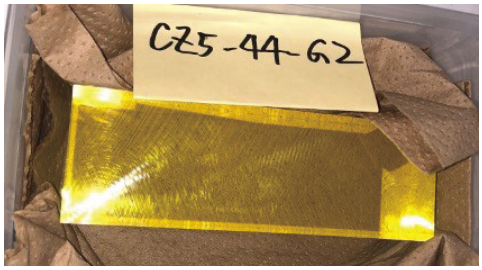

Fig. 1. The GAGG(Ce) crystal ($40 \times 40 \times 120$ mm^3).

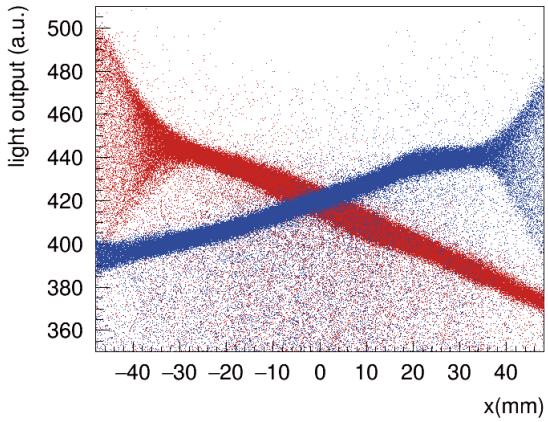

Fig. 2. Position dependence of the light outputs of the right (blue) and left (red) sensors located at $X = \pm 60$ mm.

To check the performance of the GAGG(Ce) calorimeter for high-energy charged particles, we performed a test experiment using p and α beams at 75–230 MeV/nucleon at HIMAC. We tested several detector configurations, but we briefly report the results of one setup: two photo sensors (PMT/APD/PD) were attached on both sides of the crystal, and p and α beams at 75 and 100 MeV/nucleon were impinged on the long side. The energy resolutions are <1% and <0.6% for the 100 MeV/nucleon proton and α beams focused on the center of the crystal, respectively. We also used defocused beams to check the position dependence by tracking the beam trajectories with SSDs. Figure 2 shows the correlation of the light outputs of the left and right sensors versus the horizontal position of the beam (X). On the far side from the sensor, attenuation effects can be clearly seen, but the signals are widely spread where the beam is close to the sensor. This is because the solid angle of the sensor drastically changes depending on the vertical (Y) positions as well as X. We applied a correction of the X and Y position dependences, and finally, a good energy resolution of 0.3–0.6% for 100 MeV/nucleon α beams was obtained in the wide range of the crystal. The result is good enough to achieve a separation energy resolution of ∼2 MeV in rms.

*1 Department of Physics, Kyoto University
*2 RIKEN Nishina Center
*3 NICHe, Tohoku University
*4 Department of Physics, Rikkyo University
*5 Department of Physics, Toho University

References

1) T. Uesaka *et al.*, Grant-in-Aid for Specially Promoted Research, Grant Number 21H04975.
2) T. Uesaka *et al.*, RIBF Construction Proposal, NP2112-SAMURAI72 (2021).

Development of a low-cost FPGA-Integrated TDC

H. Baba*1

The time-to-digital converter (TDC) is an indispensable instrument to measure timing information in physics experiments. In recent years, the TDC has been implemented in various methods using FPGAs and ASICs.[1] The tapped delay-line method is widely used to obtain an excellent timing resolution.[2,3] However, this method is disadvantageous in terms of cost because it consumes a large number of logic gates. In contract, the multi-phase clock method is suitable for many-channel systems with a moderate resolution.[4]

In RIBF experiments, many-channel detectors are being developed to increase the rate tolerance of beam detection. For example, SR-PPAC[5] requires 152 TDC channels per detector, which has the timing resolution of 250 ps (σ). We have began to develop a low-cost FPGA-integrated TDC based on the multi-phase clock method for many-channel gaseous detectors such as PPACs and drift chambers.

The prototype TDC board is shown in Fig. 1, and it operates under the MPV system.[6] We adopted Xilinx XC7A35T-2FTG256I which is a cost-optimized FPGA, to implement the TDC function. This board accepts a low voltage differential signaling (LVDS) level only. Thus, the production cost was significantly suppressed. The specifications of TDC are as follows: 64-ch hit input, 4-ch control I/O (1 ch for trigger), 125-ps LSB, 64-us full scale range, multi-hit, leading and trailing edge detection.

The TDC function consists of course timing (2-ns steps) by using 500-MHz clock counter and fine timing (125-ps LSB) using the dedicated circuit shown in Fig. 2. Eight clocks with different phases of 22.5 degrees each are distributed to the entire FPGA through the clock lines that has the almost equal length. Using an invert component, each clock can be shifted by 180 degrees. A total of 16 multi-phase clocks are connected to the clock input

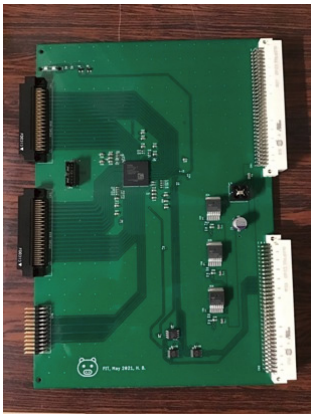

Fig. 1. Photo of the FPGA integrated TDC board.

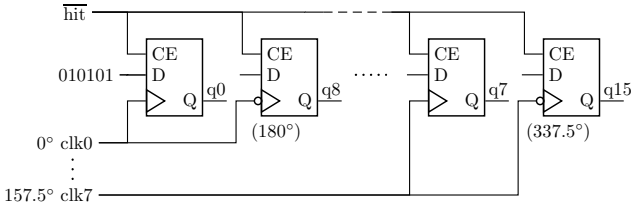

Fig. 2. Circuit diagram for fine timing.

ports of 16 flip-flops. To the D port (data), a signal that toggles 0→1→0→1 is input in sync with each clock. The inverted hit signals ($\overline{\text{hit}}$) are connected to the CE ports (clock enable). If CE is "1," output bits of q0–q15 are always toggling. When a hit occurs, *i.e.* CE is "0," these transitions are suspended. The bit pattern of q0–q15 determines the fine timing. For example, if the pattern is either "0000000000000111" or "1111111111110000," the fine timing is "4."

The multi-phase clocks are distributed to flip-flops through the clock lines with a small skew. Because the adopted FPGA has only 12 clock lines, wiring from the hit to each CE input should be manually configured to ensure that the propagation delay is as equal as possible. The variation of this delay determines the linearity of fine timing that affects the timing resolution. The differential non-linearity (DNL) and resolution for a typical channel was measured (Fig. 3). The timing resolution was 78.9 ps in σ, which is sufficient for many-channel gaseous detectors.

As shown in this report, we successfully confirmed the TDC functions. The implementation of the trigger processing is now in progress.

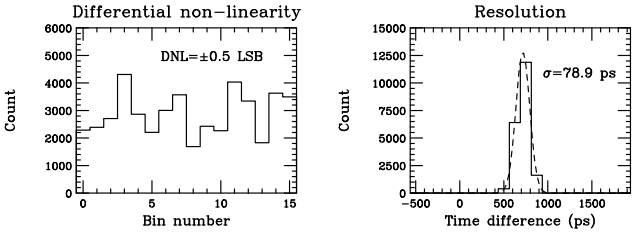

Fig. 3. Differential non-linearity and resolution.

*1 RIKEN Nishina Center

References

1) S. Tancock *et al.*, IEEE Trans. Instrum. Meas. **68**, 3406 (2019).
2) T. Yoshida, H. Baba, RIKEN Accel. Prog. Rep. **49**, 200 (2016).
3) T. N. Takahashi, RCNP Ann. Rep. **2017**, (2017).
4) Y. Kataoka, Y. Hayato, 2018 IEEE NSS/MIC Conf. Proc. **2018**, (2018)
5) S. Hanai *et al.*, CNS Ann. Rep. **2019**, 317 (2021).
6) H. Baba *et al.*, IEEE Trans. Nucl. Sci. **68**, 1841 (2021).

Development of a high-bandwidth waveform processing system using RFSoC

S. Takeshige,[*1,*2] H. Baba,[*2] K. Kurita,[*1] Y. Togano,[*1] J. Zenihiro,[*3] and Y. Hijikata[*2,*3]

We are developing a real-time digital waveform processing unit using a GHz-band flash-type analog-to-digital converter (FADC) to establish a next-generation data acquisition system at RIBF. Each particle needs to be identified in experiments using radioactive ion (RI) beams. Thus, detectors are installed along the beam line, and signals are acquired on an event-by-event basis. However, conventional CAMAC/VME ADC/TDC modules become a measurement bottleneck because of their slow processing rate with an increase in the amount of beams. For germanium detectors, real-time digital waveform analysis is applied using 100-MHz FADCs instead of conventional ADC/TDC modules.[1] However, the sampling rate of 100 MHz is insufficient for signals with high-frequency components such as those from plastic scintillators used as beam-line detectors. We started to develop a new system named as CALDERA using the Xilinx RFSoC ZCU111 evaluation kit[2] that has 8 channels of 4-GHz FADC since last year to apply waveform processing to a beam-line detector.[3]

First, we examined the performance of this device. We measured the resolution of CALDERA, and we compared it with those of the conventional CAEN V792 QDC[4] and V775 TDC.[5] The energy resolution was evaluated by measuring γ rays at 662 keV using a $LaBr_3$(Ce) scintillator, and the timing resolution was obtained from two NIM logic signals with a constant time difference.

The results of the CALDERA measurements are shown in Fig. 1. The energy and timing resolutions of CALDERA are 4.3% in FWHM and 15 ps in σ, respectively; those of QDC/TDC are 4.3% and σ = 27 ps, respectively. CALDERA achieves the same or better performance than that of the conventional QDC/TDC.

Next, this system was commissioned at the RIBF experiment (NP1712-RIBF141R1).[6] We acquired the waveforms of the plastic scintillators installed at F5 and

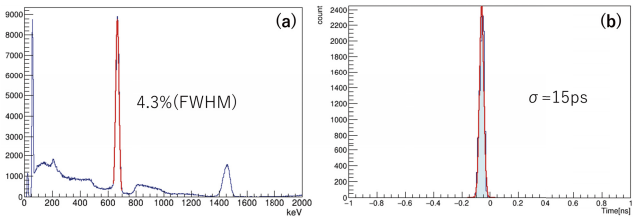

Fig. 1. Energy and timing resolutions with CALDERA. (a) ^{137}Cs energy spectrum using $LaBr_3$(Ce) scintillator. (b) Time difference obtained from two NIM logic signals.

*1 Rikkyo University
*2 RIKEN Nishina Center
*3 Kyoto University

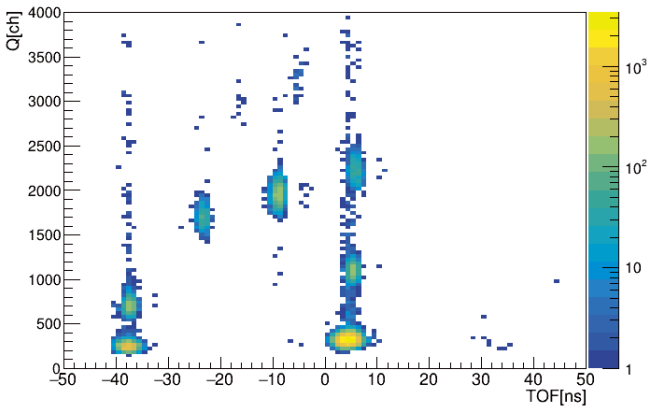

Fig. 2. Particle identification of ^{9}Li beam with CALDERA.

F7 in the ^{9}Li beam, and the charge and time information were obtained through waveform analysis. The particle identification plot is shown in Fig. 2. CALDERA can be used to acquire both charge and time information.

Further, we studied the algorithm to implement waveform processing in the FPGA. The timing information is determined by the centroid of the waveform as

$$G = \frac{\Sigma x_i y_i}{\Sigma y_i}. \tag{1}$$

This equation can be written as a recurrence formula

$$\begin{cases} q_n = q_{n-1} + v_n \\ g_n = g_{n-1} + q_n \end{cases}, \tag{2}$$

where v_n, q_n, and g_n represent the value of the n-th signal, denominator, and numerator, respectively.

The implementation of this waveform processing is now in progress.

References

1) J. -P. Martin *et al.*, IEEE Trans. Nucl. Sci. **55**, 84 (2008).
2) Xilinx, Zynq UltraScale+ RFSoC ZCU111 Evaluation Kit, `https://japan.xilinx.com/products/boards-and-kits/zcu111.html`.
3) S. Takeshige *et al.*, RIKEN Accel. Prog. Rep. **54**, 103 (2021).
4) CAEN, V792 - 32 Channel Multievent QDC, `https://www.caen.it/products/v792/`.
5) CAEN, V775 - 32 Channel Multievent TDC, `https://www.caen.it/products/v775/`.
6) A. Sakaue *et al.*, in this report.

Compensation for energy-spread growth in RUNBA

M. Wakasugi,[*1,*2] Y. Abe,[*2] R. Ogawara,[*1,*2] T. Ohnishi,[*2] H. Tongu,[*1] K. Tsukada,[*1] and Y. Yamaguchi[*2]

A small heavy-ion storage ring, RUNBA,[1] is under construction at E21. It will be used to develop a beam recycling technique, which will be a novel tool for the nuclear reaction study of rare radioactive isotopes (RIs). A few RIs, less than 10 in number, accumulate in RUNBA, which is equipped with an internal target, and hit the target many times until a nuclear reaction occurs. This is the beam recycling technique, which is established by compensating the energy loss U, energy straggling, and angular struggling given at a target. The energy loss can be compensated for by a radio-frequency (RF) cavity. Specially designed devices are, however, required to compensate for, turn by turn, the growth in energy spread and emittance due to the straggling. We will install an energy dispersion corrector (EDC) in RUNBA to compensate for energy-spread growth. Assuming a thin-foil internal target, we form a sinusoidal single-wave signal from the timing signal created when the beam passes through the target. This correction signal is applied to an acceleration gap in EDC in synchronization with the beam arrival. In this report, we analytically show the required characteristics of EDC.

The invariant of the longitudinal particle motion in $(\delta\phi, \delta\epsilon)$ phase space is given as

$$Q(\delta\phi,\delta\epsilon) = \frac{1}{2}\left(\frac{\eta\omega_{rf}}{\beta^2}\right)^2\delta\epsilon^2 + \frac{qV_{rf}\eta\omega_{rf}}{A\beta^2ET} \{\cos(\phi_s+\delta\phi)-\cos(\phi_s)+\delta\phi\sin(\phi_s)\}, \quad (1)$$

where E is the energy of ions, $\delta\epsilon = \delta E/E$, ϕ_s a synchronous phase; A the mass number, q the charge, β the velocity, T the revolution time, η the slipping factor, and V_{rf} and ω_{rf} are the amplitude and angular frequency of RF, respectively. The RF phase is shifted by $\Delta\phi_t$ and $\Delta\phi_e$ due to the energy straggling $\Delta\epsilon_t$ at the target and the energy correction $\Delta\epsilon_e$ given at EDC, respectively. Assuming $\Delta\epsilon_e$ is proportional to a time-of-flight difference in the design value from the target to EDC, it is expressed with a proportional coefficient λ_e as

$$\Delta\epsilon_e = K_{te}(\lambda_e)\big(\delta\epsilon + \Delta\epsilon_t\big) + K_\delta(\lambda_e)\delta_t, \quad (2)$$

where $K_{te}(\lambda_e) = \frac{q\lambda_e\eta_{te}T_{te}}{A\beta^2E}\big(1+\frac{\gamma^2+1}{\gamma^2-1}\frac{U}{E}\big)$; $K_\delta(\lambda_e) = \frac{q\lambda_e}{AE}$; η_{te} and T_{te} are the partial slipping factor and time of fight between the target and EDC, respectively; and δ_t is the uncertainty in timing measurement. Since $\Delta\epsilon_t$ and δ_t are stochastic variables, their probability density distributions are assumed to be Gaussian and denoted by $\psi(\Delta\epsilon_t)$ and $\theta(\delta_t)$, with standard deviations of σ_t and σ_τ, respectively. The averaged time derivative of $Q(\delta\phi,\delta\epsilon)$ is calculated as

$$\Big\langle\frac{dQ}{dt}\Big\rangle T = \int\{Q(\delta\phi+\Delta\phi_t+\Delta\phi_e,\delta\epsilon+\Delta\epsilon_t+\Delta\epsilon_e) - Q(\delta\phi,\delta\epsilon)\}\psi(\Delta\epsilon_t)d\Delta\epsilon_t\theta(\delta_t)d\delta_t. \quad (3)$$

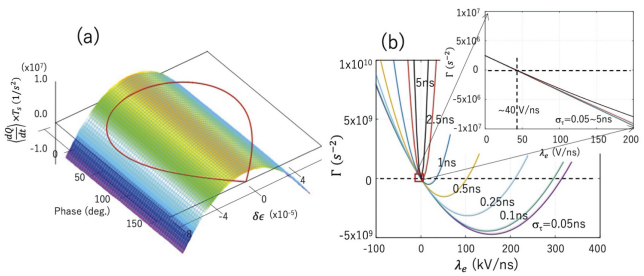

Fig. 1. (a) Time derivative of the invariant Q at $\lambda_e = 40$ V/ns calculated using Eq. (3) and (b) $\Gamma(\lambda_e)$ calculated using Eq. (4) for several cases of uncertainty σ_τ.

Since this is a function of the position in phase space $(\delta\phi, \delta\epsilon)$ and the coefficient λ_e, we take its average within a separatrix as

$$\Gamma(\lambda_e) = \frac{1}{S}\int_S\Big\langle\frac{dQ}{dt}\Big\rangle T d\delta\phi d\delta\epsilon. \quad (4)$$

Γ is a function of λ_e only. If Γ takes negative values, the invariant $Q(\delta\phi,\delta\epsilon)$ decreases with time on average and, consequently, the beam continues to circulate the ring. Here we omit the explicit expression of Eqs. (3) and (4) because of the limited text space.

We assume in the following calculation that the beam in RUNBA is a 10 MeV/nucleon $^{12}C^{6+}$ beam and the target is a thin ^{12}C foil with a thickness of $10^{18}/cm^2$. Figure 1(a) shows the time-derivative distribution in longitudinal phase space calculated using Eq. (3) at $\lambda_e =$ 40 V/ns. This has a quadric-like surface and is positive in the small $\delta\epsilon$ region but negative in the large $\delta\epsilon$ region. The averaged time derivative calculated using Eq. (4) is shown in Fig. 1(b) for several cases of the uncertainty σ_τ. λ_e has two solutions for each case: one indicates the minimum required correction, and the other indicates the maximum limit to avoid the invariant growth due to overcorrection. Although the λ_e value can be chosen in between the two solutions, the flexibility is reduced as uncertainty increases. Practically, the smallest possible value is the most convenient because we can reduce the signal power for EDC. The inset in Fig. 1(b) shows an expanded view around the lower limit of λ_e. We found that this is insensitive to the uncertainty and the minimum required correction coefficient is $\lambda_e \sim$40 V/ns.

*1 Institute for Chemical Research, Kyoto University
*2 RIKEN Nishina Center

Reference

1) M. Wakasugi *et al.*, RIKEN Accel. Prog. Rep. **54**, 87 (2021).

Compensation for emittance growth in RUNBA

M. Wakasugi,[*1,*2] Y. Abe,[*2] R. Ogawara,[*1,*2] T. Ohnishi,[*2] H. Tongu,[*1] K. Tsukada,[*1] and Y. Yamaguchi[*2]

RUNBA (Recycled-Unstable-Nuclear Beam Accumulator) is a small heavy-ion storage ring equipped with an internal target[1)] is under construction for development of a beam recycling technique, which is expected to serve as a novel tool for nuclear reaction based studies of rare radioactive isotopes (RIs). Beam recycling is established by compensating for disturbances in beam motion at targets, which are an energy loss, an energy-spread growth due to energy straggling and an emittance growth due to angular struggling. Since less than 10 RIs will be accumulated in RUNBA, timing and positioning signals can be obtained when individual ions hit the target. The signals are processed to appropriate wave forms and applied to specially designed devices, the energy dispersion corrector (EDC)[2)] and angular diffusion correctors (ADCh and ADCv). These devices correctly modulate the beam motion in 6-dimensional phase space turn by turn. In this report, we discuss the principle of ADC's for compensating the emittance growth, and show the required characteristic for ADC's.

The invariant of transverse particle motion in a storage ring is given by well-known Courant-Snyder invariant

$$W = \gamma x^2 + 2\alpha x x' + \beta x'^2, \tag{1}$$

where α, β, γ are twiss parameters at the target. The angle x' is irregularly modulated in one turn by $\Delta x'_t$ due to angular straggling at the target, a correction angle $\Delta x'_h$ at ADC, and an adiabatic damping effect $\Delta x'_c$ at the RF cavity. Assuming $\Delta x'_h$ is proportional to the position measured at the target, it is expressed as

$$\Delta x'_h = \kappa_h (x + \delta_x), \tag{2}$$

where κ_h is a proportional coefficient and δ_x is an uncertainty in position measurement. When net change in position in phase space including theses effects is expressed as $(\Delta x, \Delta x')$, the time derivative of an invariant is

$$\frac{dW}{dt} = \frac{1}{T}\{W(x_1+\Delta x, x'_1+\Delta x') - W(x_0, x'_0)\}, \tag{3}$$

where T is the revolution time, and $W(x_1, x'_1) = W(x_0, x'_0)$, as (x_0, x'_0) is transfered to (x_1, x'_1) in normal betatron motion in one turn. Since $\Delta x'_t$ and δ_x are stochastic variables and their probability density distributions are expressed as $\phi(\Delta x'_t)$ and $\psi(\delta_x)$, respectively, the time derivative must be averaged as

$$\left\langle \frac{dW}{dt} \right\rangle T = \int \{W(x_1 + \Delta x, x'_1 + \Delta x') - W(x_0, x'_0)\} \phi(\Delta x'_t)\psi(\delta_x) d\Delta x'_t d\delta_x. \tag{4}$$

*1 Institute for Chemical Research, Kyoto University
*2 RIKEN Nishina Center

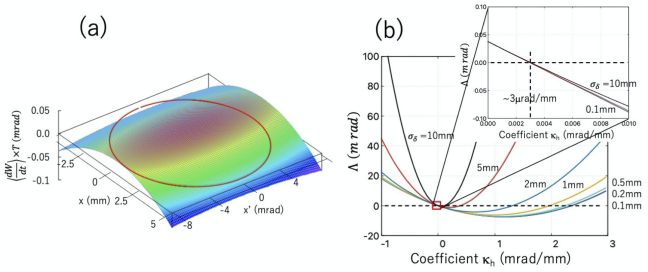

Fig. 1. (a) Time derivative of the invariant $\left\langle \frac{dW}{dt} \right\rangle T$ at $\kappa_h = 1$ μrad/mm calculated by Eq. (4) and (b) $\Lambda(\kappa_t)$ calculated by Eq. (5) for several cases of uncertainty δ_x.

Since this is a function of the position in transverse phase space (x, x') and the coefficient κ_h, we consider the average of Eq. (4) in the transverse acceptance as

$$\Lambda(\kappa_t) = \frac{1}{e}\int_e \left\langle \frac{dW}{dt} \right\rangle T dx dx', \tag{5}$$

where e is the volume of acceptance, and Λ is a function of κ_h only. When Λ is negative with appropriate κ_h setting, we can avoid growth in emittance, and consequently the beam continues to circulate in the ring.

We assume in the present calculation that the beam in RUNBA is of 10 MeV/nucleon $^{12}C^{6+}$, and the target is a thin ^{12}C foil of 10^{18}/cm^2 thickness. ADCh(v) is placed for effective correction at a position where the betatron phase advance from the target is 1.25 (0.75). Figure 1(a) shows the time-derivative distribution in transverse phase space calculated from Eq. (4) at $\kappa_h = 1$ μrad/mm. This is a quadric-like surface and positive in a small region, but negative in large x region. The averaged time derivative calculated by Eq. (5) is shown in Fig. 1(b) for several cases of uncertainty δ_x. There are two zero-cross points for each case, and κ_h can be in between these. The degree of freedom of κ_h decreases as the uncertainty increases. A smaller value of κ_h is convenient to reduce the load on ADCh(v). As seen in inset of Fig. 1(b), the minimum required value of κ_h is approximately independent of the uncertainty, and it is found to be $\kappa_h \sim 3$ μrad/mm. Since the largest beam position in the acceptance is $x \sim 5$ mm, the maximum kick angle at ADCh(v) is ~ 25 μrad. Assuming a strip-line-type electrode with a gap of 0.1 m, length of 0.5 m, and characteristic impedance of 50 Ω, the required transverse electric field is ~ 2 kV/m, and the supplied power is ~ 400 W.

References

1) M. Wakasugi *et al.*, RIKEN Accel. Prog. Rep. **54**, 87 (2021).
2) M. Wakasugi *et al.*, in this report.

Simulation study to compensate for growth in energy spread and emittance in RUNBA

M. Wakasugi,[*1,*2] Y. Abe,[*2] R. Ogawara,[*1,*2] T. Ohnishi,[*2] H. Tongu,[*1] K. Tsukada,[*1] and Y. Yamaguchi[*2]

A small heavy-ion storage ring called RUNBA,[1] equipped with an internal target, is under construction at the E21 room. This project aims at the development of a beam recycling technique, which will be a novel tool for nuclear reaction studies involving rare RI's. A few RIs, less than 10 in number, are accumulated in RUNBA, which is equipped with an internal target, and they hit the target many times until a nuclear reaction occurs. For establishing this technique, we will install an energy dispersion corrector (EDC) and angular diffusion correctors (ADCh and ADCv) to compensate for an energy-spread growth and an emittance growth, respectively (see Fig. 1). Their required characteristics, which were obtained analytically, are described in Refs. 2) and 3). In this report, we show the results of a particle simulation in RUNBA for supporting the analytical solutions.

When an ion passes through the target, its energy is modulated by an energy straggling, $\Delta\epsilon_t$ ($= \Delta E_t/E$), in addition to an energy loss, U, and the angle (traveling direction) is modulated by an angular straggling, $\Delta x'_t$. The energy loss is recovered in a radio frequency (RF) cavity. The energy difference is correctly modulated by $\Delta\epsilon_e$ at EDC, which is proportional to the difference in flight time from the design particle from the target and EDC. It is expressed as

$$\Delta\epsilon_e = \lambda_e \left\{ \frac{q\eta_{te}T_{te}}{A\beta^2}\left(1+\frac{\gamma^2+1}{\gamma^2-1}\frac{U}{E}\right)(\delta\epsilon+\Delta\epsilon_t) + \frac{q\delta_t}{AE}\right\}, \quad (1)$$

where λ_e is a proportional coefficient; A is the mass number; q is the charge numbers, E, γ, and β are the total energy (sum of mass and kinetic energy), Lorenz factor, and velocity of the design particle, respectively; η_{te} is the partial slipping factor between the target and EDC defined by the ring design; T_{te} is the flight time of the design particle from the target to EDC; $\delta\epsilon$ ($= \delta E/E$) is the energy difference from the design particle; and δ_t is the expected uncertainty in the timing acquired at the target. Due to $\Delta\epsilon_t$ and $\Delta\epsilon_e$, the RF phase is unusually shifted in one turn by $\Delta\phi_t$ and $\Delta\phi_e$, respectively. On the other hand, the angle of ion incidence is modulated in one turn by an angular straggling, $\Delta x'_t$, at the target; an angular correction, $\Delta x'_h$, at ADC; and an adiabatic damping effect, $\Delta x'_c$, at the RF cavity. $\Delta x'_h$ is proportional to the position, x, measured at the target and expressed as

$$\Delta x'_h = \kappa_h(x+\delta_x), \quad (2)$$

where δ_x is the uncertainty in the position measurement. In this simulation, $\Delta\epsilon_t$, δ_t, $\Delta x'_t$, and δ_x are given as random numbers with Gaussian statistical distributions.

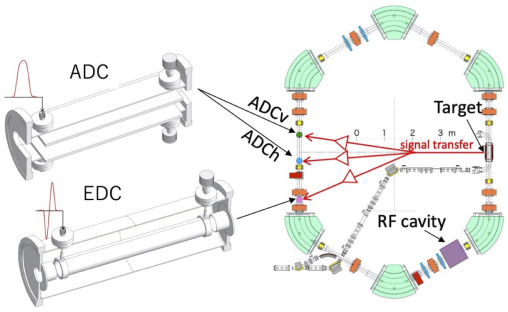

Fig. 1. RUNBA structure (right) and the designed ADC and EDC devices.

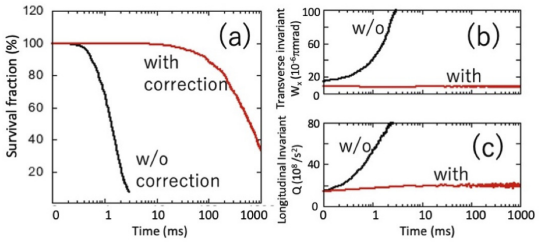

Fig. 2. Results of the present simulation. (a) Trends of the survival fraction and (b), (c) time evolution of the transverse invariant W and longitudinal invariant Q, respectively. The black and red curves show the simulation results without and with appropriate correction at the ADCs and EDC, respectively.

Using the RUNBA lattice structure designed in Ref. 1) and assuming that the beam is a 10 MeV/nucleon $^{12}C^{6+}$ beam and the target is ^{12}C with a thickness of $10^{18}/cm^2$, we performed a particle tracking simulation taking all the effects described above into account. As shown in Fig. 2(a), although the lifetime of the beam accumulation is less than 1 ms without corrections by the EDC and ADCs, it can be extended to ~1 s with the corrections. Appropriate corrections keep the invariants of transverse motion, W,[3] and longitudinal motion, Q,[2] almost constant, as shown in Figs. 2(b) and 2(c). The coefficients λ_e and κ_h in this case are 240 V/ns and 2.5 μrad/mm, respectively. They are consistent with the solutions obtained analytically in Refs. 2) and 3). On repeating this 1-s accumulation process for isotopes with a production rate of 1 Hz, the collisional luminosity reaches $10^{24}/(cm^2 s)$.

*1 Institute for Chemical Research, University
*2 RIKEN Nishina Center

References
1) M. Wakasugi *et al.*, RIKEN Accel. Prog. Rep. **54**, 87 (2021).
2) M. Wakasugi *et al.*, in this report.
3) M. Wakasugi *et al.*, in this report.

Improvements in the working environment for target handling at ERIS

T. Ohnishi,[*1] Y. Abe,[*1] S. Ichikawa,[*1] and M. Wakasugi[*1,*2]

The electron-beam-driven radioactive isotope separator for SCRIT (ERIS)[1] at the SCRIT electron scattering facility[2] is an online isotope-separator system used to produce low-energy radioactive isotope (RI) beams using the photofission of uranium. In this year, we transported a ^{137}Cs beam to the SCRIT system installed inside the electron storage ring[3] and performed the RI trap. Under these circumstances, ERIS has become a full-scale operation, around 4-month RI beam operation in a year. Therefore, it is important to maintain the working environment of target handling. In this paper, we introduce the working environment of the RI production target, as one of the recent developments of ERIS.

Uranium carbide is used as a RI production target using the fission reaction of uranium. It is more suitable for RI production target than uranium oxide because its vapor pressure and density are lower and higher than those of uranium oxide, respectively. Further, damages to materials of the ion source can be reduced using a small amount of oxygen.

The recent study shows that the porous structure with the nano material is important for fast diffusion inside the target and high-extraction efficiency of RI.[4] However, this porous structure causes high susceptibility to oxidation. Figure 1 shows the oxidation reaction of uranium carbide in the air. The uranium carbide disks shown in Fig. 1 are made with graphene. Oxidation started 1 min after the removal from the vacuum container, and it ended after almost 10 min. The temperature of uranium carbide disks reaches around 800°C, as shown in Fig. 1. After oxidation, these disks cannot hold their shape and turn into powder. The uranium oxide powder is planned to be cemented solid after sufficient cooling.

A glove box was installed in the draft chamber at the working area to handle uranium carbide targets safely. Figure 2(a) shows the setup with the glove box. Since this glove box has the capacity of vacuum gas replacement, the oxygen concentration becomes less than 0.001% vacuum gas replacement with nitrogen gas (less than 2% per one replacement is performed three times). In this situation, target handling can be performed without worrying about oxidation. One such example is shown in Fig. 2(b).

Fig. 1. Photograph of the oxidation reaction of uranium carbide disks in the graphite container. Diameter and thickness of a disk are 18 mm and 0.8 mm, respectively. The amount of uranium in a disk is about 0.7 g.

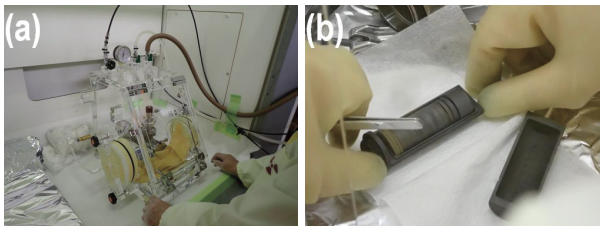

Fig. 2. (a) Photograph of the setup with the glove box inside the draft chamber. (b) Photograph of handling the uranium carbide disks inside the glove box.

The present size of the glove box is smaller than the target chamber, and therefore, we need to work in the air to install the target in the target chamber. A graphite-target container with keyway, as shown in Fig. 3, is used to reduce the installation time, and the target insertion practice is performed beforehand. It took almost 5 sec to remove the graphite-target container with the uranium target disks from the container filled with nitrogen gas, insert it into the target holder inside the target chamber, and start the vacuum pump. This short time was sufficient, as evidenced by the small amount of gas released during heating.

In the near future, the safety treatment of the production target will become an important issue because of the high radiation (a few mSv/h), which is two orders of magnitude higher than the present value (∼10 μSv/h), and active operation. Therefore, we plan to introduce a large glove box adapted to the target chamber and establish a remote handling system.

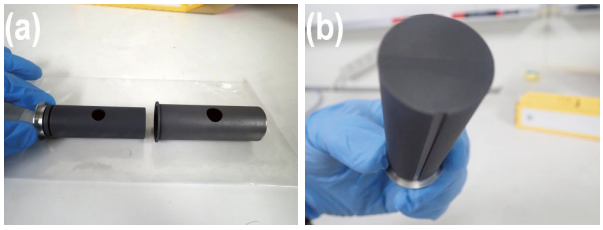

Fig. 3. (a) Photograph of the graphite-target container with keyway (left) and the target holder (right). (b) Photograph of keyway of the graphite-target container.

*1 RIKEN Nishina Center
*2 Institute for Chemical Research, Kyoto University

References

1) T. Ohnishi *et al.*, Nucl. Instrum. Methods Phys. Res. B **317**, 357 (2013).
2) M. Wakasugi *et al.*, Nucl. Instrum. Methods Phys. Res. B **317**, 668 (2013).
3) Y. Abe *et al.*, in this report.
4) A. Gottberg, Nucl. Instrum. Methods Phys. Res. B **376**, 8 (2016).

Compact position-sensitive detector for in-ring diagnostics at the Rare-RI Ring

S. Naimi,[*1] G. Hudson-Chang,[*1,*2] D. Nagae,[*3] N. Kaname,[*4] A. Yano,[*4] T. Moriguchi,[*4] Y. Yamaguchi,[*1] S. Suzuki,[*4] A. Ozawa,[*4] Y. Abe,[*1,*5] N. Sinozaki,[*6] and T. Yamaguchi[*6]

We have developed a large area position-sensitive detector for the Rare-RI Ring.[1,2] The position resolution achieved was less than 2 mm. A higher resolusion closer to that of the PPAC is needed for emittance matching confirmation at the injection of particles in the ring as well as for particle tracking inside the ring. To improve further the resolution we designed a compact version of the same detector. The horizontal size was kept the same (an opening of 200 mm), however the vertical size was reduced by 30%. We simulated the effect on the resolution of this size reduction for different acceleration potential applied to the secondary electrons (SEs) emitted from the foil (see Refs. 1) and 2) for the detector's principle). According to the simulation performed with SIMION,[3] the resolution of the detector should improve by about 25% in both horizontal and vertical direction, see Fig. 1. This is due to the reduction of the time-of-flight of SEs inside the detector. We built and tested the compact detector as shown in Fig. 2. The test experiment was conducted at HIMAC with a 200 MeV/nucleon ^{84}Kr beam. The experimental setup is the same as previous experiment.[1] A mask of 4 mm thick copper with rectangular openings of 12 × 17 mm separated with 3 mm in between was placed in front of the detector. The beam image captured by both detectors under the same conditions is shown in the bottom of Fig. 2. As it can be seen, the resolution of the compact detector is improved and the rectangular openings of the mask are more distinct compared to the original detector. Detailed analysis of the resolution showed an improvement of 24% in the horizontal direction and 20% in the vertical direction. The compact detector was placed inside the Rare-RI Ring during the last experiment.[4] The trajectory of the beam was confirmed. However, due to large noise further diagnostics was not possible. The source of the noise, as well as possible future improvements are under investigation. Further improvements of the detector design are under consideration to limit the outgassing, which will improve the vacuum in the detector chamber and lead to less discharge.

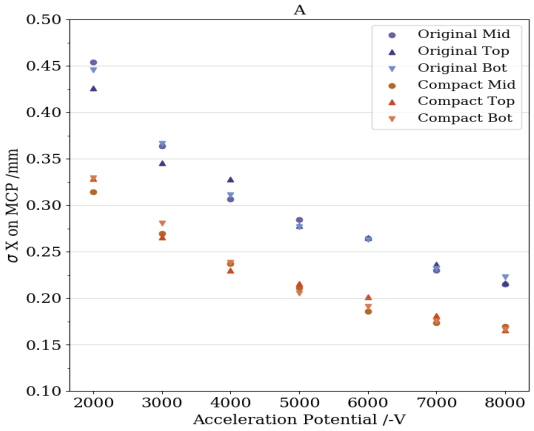

Fig. 1. Simulation results of position resolution for different SEs acceleration voltages in the original detector (blue) and compact detector (orange). Mid, Top, Bot correspond to different position in the detector, middle, top and bottom, respectively.

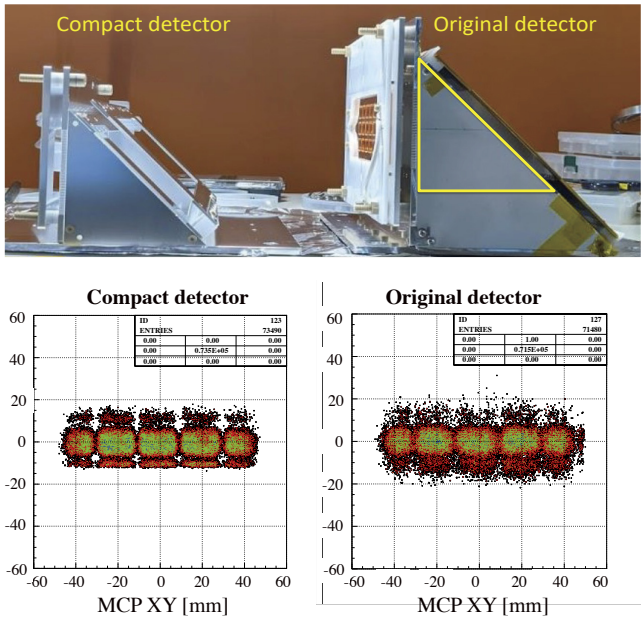

Fig. 2. (top) Picture of the compact and original size detectors with the size of the compact detector drawn in yellow on the original detector for reference. (bottom) Beam image modified with a copper mask placed in front of the detectors.

*1 RIKEN Nishina Center
*2 Department of Physics, University of Surrey
*3 Faculty of Sciences, Kyushu University
*4 Department of Physics, University of Tsukuba
*5 National Institute of Radiological Sciences (NIRS), National Institutes for Quantum Science and Technology
*6 Department of Physics, Saitama University

References
1) R. Crane, S. Naimi, RIKEN Accel. Prog. Rep. **53**, 117 (2020).
2) G. Hudson-Chang *et al.*, RIKEN Accel. Prog. Rep. **54**, 101 (2021).
3) SIMION, `https://simion.com/`.
4) S. Naimi *et al.*, in this report.

Extraction test of photo ionized Bi in PALIS gas cell

T. Sonoda,[*1] V. Sonnenschein,[*2] H. Tomita,[*2] K. Hattori,[*2] D. Hou,[*3] S. Iimura,[*3] H. Ishiyama,[*1] I. Katayama,[*1] T. M. Kojima,[*1] S. Nishimura,[*1] M. Rosenbusch,[*3] A. Takamine,[*1] M. Wada,[*3] Y. X. Watanabe,[*3] and W. Xian[*3] for the BigRIPS Collaboration

We are developing a scheme for parasitic low-energy radioactive isotope(RI) beam production (PALIS)[1] in the second focal chamber (F2) of the BigRIPS.

Our previous experiment,[2] confirmed the extraction of Bi isotopes after exiting the PALIS gas cell. As the next stage, we are aiming for laser photo ionization of Bi, which results in highly pure RI beam production. Figure 1 shows the present PALIS experimental setup. Bi atoms are irradiated by two colors of laser beam for multi-step resonance ionization. Photo ionized Bi species are emitted as a gas jet into differential pumping area, where the ions are confined by rf electric fields and move along an axial direction to the rf-carpet. The rf-carpet makes superimposed electric fields: one is dc-guidance sloping to the small exit hole whereas, the other is rf-barrier that prevents the ions from hitting the rf-carpet. For the fast evacuation, we utilized a large exit aperture for the gas cell (3.0 mm) compared to that for a conventional gas cell. Owing to the small exit aperture of the rf-carpet (0.4 mm), efficient differential pumping can be realized, even though several small vacuum dry pumps are arranged in the differential pumping area.

The extracted ions from the rf-carpet are detected by an ion counter in off-line experiments. In on-line beam experiment, the ion counter is replaced by a silicon detector to observe the alpha rays created by the decay of alpha-emitting Bi isotopes.

First, we examined the system performance by off-line experiments. Stable Bi atoms were produced in the gas cell via evaporation. The applied laser ionization scheme of Bi is shown in Fig. 2(1). For identification of Bi ionization, the first-step laser wavelength was scanned as a function of the ion intensity shown in Fig. 2(2). We also confirmed reasonable performance of the rf-carpet by scanning its rf-voltage, and the plot is shown in Fig. 2(3).

In November 2021, a 12-h on-line beam experiment was conducted for the extraction test of ^{191}Bi. The setting $B\rho$ at the BigRIPS provided the specific isotope region including ^{191}Bi in the order of 10^5 cps. We monitored the alpha rays after implantation of a catcher plate in front of the silicon detector, during the beam was stopped for avoiding background noise. Figure 3 shows the accumulated signals at the silicon detector. We considered that a few signals caused by alpha rays were observed in the expected area, >180 (MCA-ch) area. As the extraction efficiency was not achieved for expected value, some improvements are in progress.

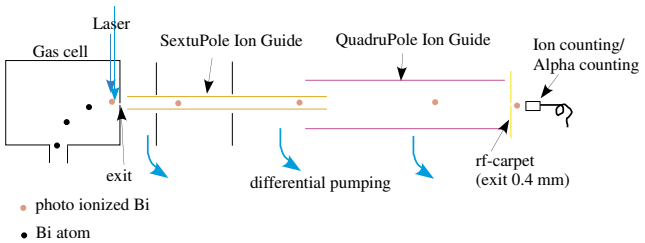

Fig. 1. Present experimental setup.

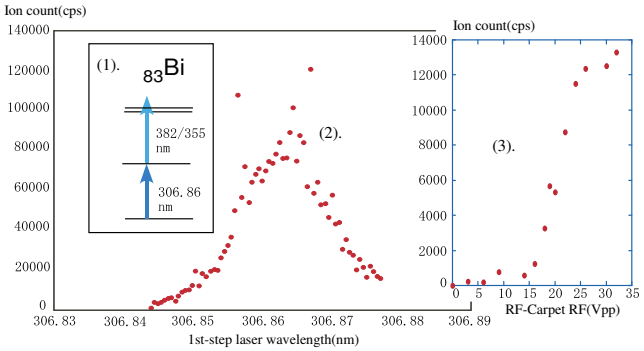

Fig. 2. (1): Bi-ionization scheme and number of ions per second versus (2): first-step wavelength, (3): rf voltage at the rf-carpet measured in off-line experiment.

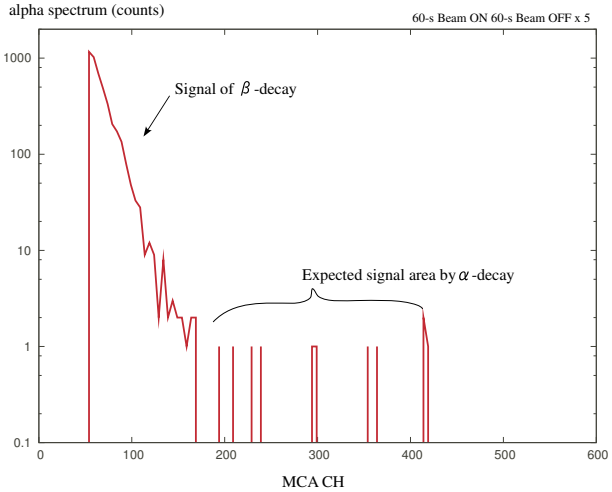

Fig. 3. Observed signals at silicon detector in online experiment.

*1 RIKEN Nishina Center
*2 Faculty of Engineering, Nagoya University
*3 Wako Nuclear Science Center, IPNS, KEK

References
1) T. Sonoda *et al.*, Prog. Theor. Exp. Phys. **113**, D02 (2019).
2) T. Sonoda *et al.*, RIKEN Accel. Prog. Rep. **54**, 91 (2020).

Development of a timing detector for decay spectroscopy in conjunction with MRTOF-MS

M. Mukai,[*1] Y. Hirayama,[*2] Y. X. Watanabe,[*2] P. Schury,[*2] S. C. Jeong,[*2] H. Miyatake,[*2] T. Niwase,[*2] M. Oyaizu,[*2] M. Rosenbusch,[*2] H. Ueno,[*1] and M. Wada[*2]

The KEK Isotope Separation System (KISS)[1] has been used to perform the β-γ decay and laser spectroscopy of heavy neutron-rich nuclei of refractory elements. In most scenarios, we had isobar and isomer (or ground state) contaminants owing to the limited mass resolution of a dipole magnet ($A/\Delta A \sim 900$). The isobar contaminants are the survival ions extracted from an argon gas cell, and isomer (or ground state) contaminants originate from the element-selective laser ionization at the exit of the Ar gas cell. The isobar and isomer contaminants often complicate[2] analyzing γ-ray energy spectra and decay half-lives. Therefore, for the spectroscopy of a single nuclide identified precisely using a multi-reflection time-of-flight mass spectrograph (MRTOF-MS), we will install a β-γ time-of-flight (TOF) detector that provides a stop signal of the MRTOF-MS for a time-correlated measurement between the MRTOF-MS and β-γ detectors.

The current β-γ detector station consists of an aluminized Mylar tape transport system placed at the center of the detector station, a proportional gas counter,[3] and germanium detectors. To perform the decay spectroscopy in conjunction with the MRTOF-MS, the decay station must be installed downstream of the MRTOF-MS, and the β-γ TOF detector must be installed at the front of the gas counter. The start timing of the TOF measurement is the timing of the ions injected into the MRTOF. The secondary electrons (SEs) emitted from the aluminized Mylar tape in the injection of mass-separated ions are detected by an annular-type MCP detector to supply the stop timing of the MRTOF-MS. We call the MCP detector the β-γ TOF detector. We report the simulation results of the SEs detection using the β-γ TOF detector.

Figure 1 shows the cross-sectional view of the setup for the detection of SEs. The setup consists of a solenoid coil with a length of approximately 54 mm, an electrode for the SEs transport to the MCP, and a metal plate with a thin pipe shielding the electric fields of the MCP for the ion transport. The mass-separated ions from the MRTOF-MS are accelerated up to 20 keV/q using a pulse drift tube and impinged on the tape, as shown at the bottom of Fig. 1. The SEs emitted from the surface of the tape (GND) are accelerated toward the solenoid coil by a potential of +370 V and transported upstream with a sufficiently small orbital radius by a magnetic field inside the solenoid coil and by the upstream electrode (+600 V). Subsequently, the SEs hit the front surface of the MCP, and the TOF stop signal

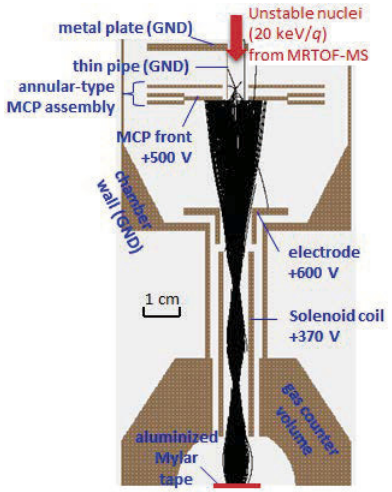

Fig. 1. Simulated trajectory (black line) of SEs emitted from the surface of an aluminized Mylar tape.

is obtained.

The SEs trajectories simulated using SIMION[4] are indicated by black lines in Fig. 1. In the simulation, SEs were generated at the tape position with the Gaussian distribution of 1 mm in standard deviation, and the initial emission angle was assumed to be uniform in 2π. The initial kinetic energy was assumed to be an order of 1 eV, which is the typical order of the energy for SEs. The simulated transport efficiency of a single electron from the tape position to the MCP surface was 77% and the time resolution was approximately 0.5 ns in FWHM. We expect the number of SEs of ~2.8 on average, which was the measured value in a previous study via a bombardment of W^+ ions (15 keV) on an Al_2O_3 target.[5] Therefore, we can expect a detection efficiency of as high as 90%. The simulated time resolution of the electron transportation, ~0.5 ns, is sufficiently small considering the typical TOF of approximately 15 ms and the contribution to the mass resolving power is smaller than 3%.

The offline study is ongoing. The setup will be installed early next fiscal year.

*1 RIKEN Nishina Center
*2 Wako Nuclear Science Center (WNSC), IPNS, KEK

References
1) Y. Hirayama *et al.*, Nucl. Instrum. Methods Phys. Res. B **412**, 11 (2017).
2) Y. Hirayama *et al.*, Phys. Rev. C **98**, 014321 (2018).
3) Y. Hirayama *et al.*, Nucl. Instrum. Methods Phys. Res. A **997**, 165152 (2021).
4) SIMION 8.1, `http://www.simion.com`.
5) G. Staudenmaier *et al.*, Int. J. Mass Spectrom. Ion Phys. **11**, 103 (1976).

New developments and progress of the ZD-MRTOF system in 2021

M. Rosenbusch,[*1] M. Wada,[*1] A. Takamine,[*2] W. Xian,[*3] D. Hou,[*4] S. Chen,[*3] S. Iimura,[*2,*5] P. Schury,[*1] T. Niwase,[*6,*1,*2] N. Fukuda,[*2] Y. Hirayama,[*1] H. Ishiyama,[*2] Y. Ito,[*7] S. Jeong,[*1] S. Kimura,[*2] T. Kojima,[*2] J. Liu,[*4] S. Michimasa,[*8] H. Miyatake,[*1] M. Mukai,[*2] S. Nishimura,[*2] Y. Shimizu,[*2] T. Sonoda,[*2] H. Suzuki,[*2] H. Takeda,[*2] Y. X. Watanabe,[*1] H. Wollnik,[*9] S. Yan,[*10] T. T. Yeung,[*11] and K. Yoshida[*2]

After the successful online commissioning in 2020,[1–3] in the year 2021 the ZD-MRTOF system[4] was subject to new upgrades, further optimization, and new on-line experiments. One of the new major modifications is a novel in-MRTOF deflector in the center region of the MRTOF-MS (see Fig. 1, and also Ref. 5)) and references therein), which allows for the dedicated ejection of contaminant ions at low electric fields of only about 40 V, so that the mass accuracy for the wanted ions is not affected in a measurement. The principle is that the ion deflector is always at 0 V if any ion of interest is crossing the deflection region, so that it can pass the region until a distance is reached beyond the electrically well-shielded area. By a newly developed timing system at the Wako Nuclear Science Center, an electric pulse pattern is programmed and applied to enable the selection of not only one preferred ion mass number, but several ion mass numbers can be selected and survive the separation process at the same time.

With the help of the new deflector system, molecular contaminations coming from the He filled gas cell[6] could be eliminated in online experiments and clean spectra have been observed.

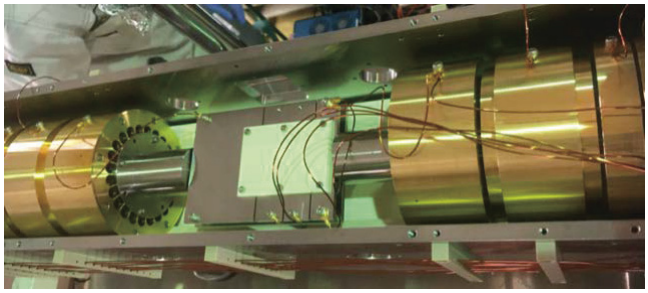

Fig. 1. Photo of the new in-MRTOF deflector at the time of assembly. At the center electrode (held by the white ceramics) the pulsed electric field is applied to deflect unwanted ions. Distances and sizes of the plated are chosen for optimal shielding of the deflection region.

*1 Wako Nuclear Science Center (WNSC), IPNS, KEK
*2 RIKEN Nishina Center
*3 Department of Physics, University of Hong Kong
*4 Institute of Modern Physics, Chinese Academy of Sciences
*5 Department of Physics, Osaka University
*6 Department of Physics, Kyushu University
*7 Advanced Science Research Center, Japan Atomic Energy Agency
*8 Center for Nuclear Study, University of Tokyo
*9 Department of Chemistry and Biochemistry, New Mexico State University
*10 Institute of Mass Spectrometer and Atmospheric Environment, Jinan University
*11 Department of Physics, University of Tokyo

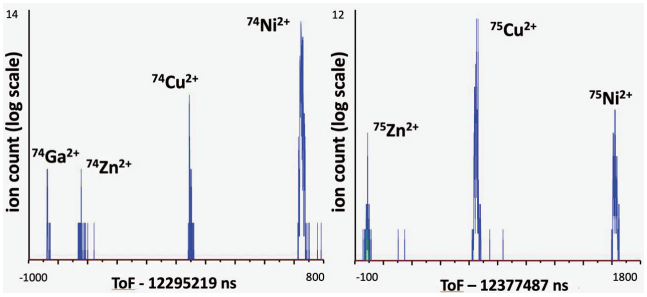

Fig. 2. New ion time-of-flight spectra of the $A = 74$ isobars Ga, Zn, Cu, and Ni in the left part, and $A = 75$ isobars Zn, Cu, and Ni produced from on-line beam centered on ^{79}Ni and also from in-trap decay.

In November and December 2021 the first part of the dedicated experiments for the ZD-MRTOF system have been performed using SRC and BigRIPS+ZeroDegree (NP2012-RIBF 199/202), where due to a high-quality beam from BigRIPS and the recent abilities of the ZD-MRTOF system, new spectra on Ni isotopes could be recorded (see Fig. 2). The preliminary results are under analysis and the experiment will continue after resolving the recent incident at the accelerator facility.

In off-line studies, new efforts for the mirror tuning of the MRTOF-MS have been spent by developing procedures for careful tuning. Together with an advanced algorithm for software drift correction, resolving powers of up to $R_m = 10^6$ have been reached enabling the identification of low-lying nuclear isomers in many isotopes (down to about 40 keV excitation energy for $A \approx 40$ and 190 keV for $A \approx 200$). An initial accuracy test using stable molecules ionized in the gas cell at ten different mass numbers could be performed using data from the online commissioning in 2020 and yielded an relative mean deviation of $\delta m/m = 2.80(99) \cdot 10^{-8}$ from the well known values of the Atomic Mass Evaluation (AME) 2016.[4] A further important development, providing proof of the radioactivity for rare events, is a combined detector for the ion's time-of-flight and their beta decay at the same time called β-ToF detector.[7]

References

1) S. Iimura *et al.*, in this report.
2) W. Xian *et al.*, in this report.
3) D. Hou *et al.*, in this report.
4) M. Rosenbusch *et al.*, arXiv:2110.11507, submitted to Nucl. Instrum. Methods Phys. Res. A (2021).
5) P. Fischer *et al.*, Rev. Sci. Instrum. **89**, 105114 (2018).
6) A. Takamine *et al.*, RIKEN Accel. Prog. Rep. **53**, 108 (2018).
7) T. Niwase *et al.*, in this report.

Fifth report on offline tests for RF carpet transportation in RF ion guide gas cell at the SLOWRI facility

A. Takamine,[*1] S. Iimura,[*1,*2,*3] D. Hou,[*3,*4,*5] M. Wada,[*3] M. Rosenbusch,[*3] W. Xian,[*3,*6] P. Schury,[*3] Y. Ito,[*1,*8] T. M. Kojima,[*1] T. Sonoda,[*1] Y. X. Watanabe,[*3] H. Ueno,[*1] and H. Ishiyama[*1]

We are developing an RF ion guide gas cell at the SLOWRI facility. The present gas cell has a gutter structure[1)] where the ions travel over a long distance on the 2nd RFC after they are first collected to the 1st RFC, travel over a short distance on the 1st RFC, and are pulled to the 2nd RFC (see Fig. 1 in Ref. 2)). We adopted the "ion surfing" method on the 2nd RFC by superimposing weak audio-frequency (AF) signals to form an ion traveling potential wave.[3)] We have so far reported offline tests with ions from surface-ionization ion sources in an "ion current" mode where the electrodes of the RF carpets and an ion beam guide were used as a Faraday cup.[1,2,4,5)] However the performance could be different from an online experiment because 1) ion currents contain many molecules and 2) ion currents of more than an order of pA could cause a space charge or a charging-up effects.

We conducted offline tests for $^{36}Ar^{+}$ and $^{86}Kr^{+}$ ions produced in the helium gas cell. We cannot evaluate the absolute transport efficiency in these measurements because the Ar and Kr contaminant rates in a helium gas are unknown. However, we can solely measure the count rates of $^{36}Ar^{+}$ or $^{86}Kr^{+}$ with the elimination of isobar impurities owing to the high resolving power of the MRTOF-MS, and we can investigate the transport performance in a similar condition as an online experiment.

We placed an ^{241}Am α-source behind the 6-μm-thick Mylar gas cell window at the downstream side. The emitted alpha particles enter the gas cell through the window and lose their energies in the helium gas to ionize the Ar and Kr atoms that are contained. Figure 1 shows the 2nd RFC AF voltage dependence of the transport performance in 200 mbar, in a room-temperature equivalent value, of 70 K helium gas. The RF voltage applied to the 2nd RFC was 103 Vpp at 11.8 MHz, and the push DC field onto the 2nd RFCs was 18 V/cm.

The present results for $^{36}Ar^{+}$ and $^{86}Kr^{+}$ clearly show different AF voltage dependence. This investigation has been coducted in clear conditions for the first time, *i.e.*, only focused on a separated mass instead of an ion current of mixed molecules as shown in the previous report.[2)] Contrary to the case when using a Cs ion source, a clearly different trend for light masses and heavier masses is now visible, showing a limited region of effective AF amplitudes for light masses of $A \approx 40$. For the $A \approx 80$ region, a stable transport is achieved for all tested amplitudes above 3 V. In both cases, the choice of the AF frequency seems to play a minor role for the transport efficiency, but has an impact on the transport time,[3)] which becomes important for short-lived isotopes. We plan to measure the transport time systematically in the gas cell for different AF conditions, producing a pulsed ion by placing a mechanical shutter in front of the α-source. We also plan to modify the 1st RFC configuration to achieve a faster ion collection. The transport time measurement results will be compared.

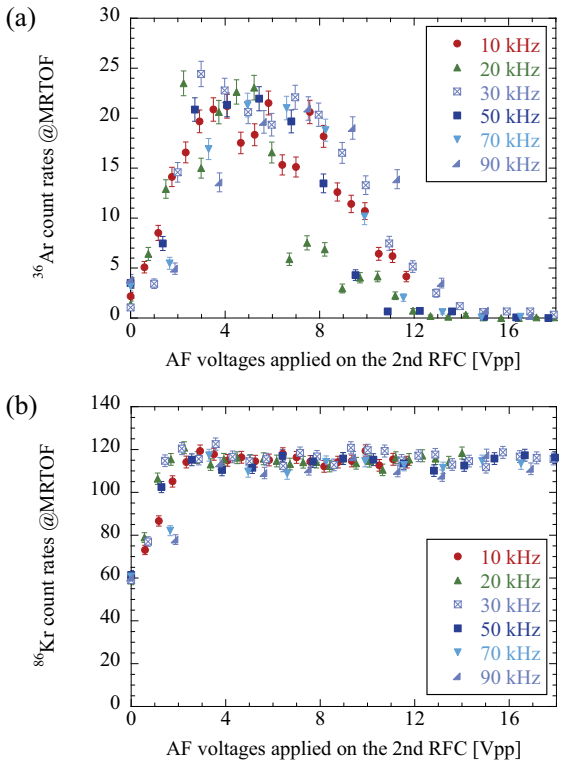

Fig. 1. Ion transportation count rates as a function of AF voltages at different AF frequencies for (a) $^{36}Ar^{+}$ and (b) $^{86}Kr^{+}$ in offline tests.

*1 RIKEN Nishina Center
*2 Department of Physics, Osaka University
*3 Wako Nuclear Science Center (WNSC), IPNS, KEK
*4 Institute of Modern Physics, Chinese Academy of Sciences
*5 School of Nuclear Science and Technology, Lanzhou University
*6 Department of Physics, University of Hong Kong
*7 Institute of Mass Spectrometry and Atmospheric Environment, Jinan University
*8 Advanced Science Research Center, Japan Atomic Energy Agency

References
1) A. Takamine *et al.*, RIKEN Accel. Prog. Rep. **52**, 139 (2019).
2) A. Takamine *et al.*, RIKEN Accel. Prog. Rep. **54**, 93 (2021).
3) G. Bollen, Int. J. Mass Spectrom. **299**, 131 (2011).
4) S. Iimura *et al.*, RIKEN Accel. Prog. Rep. **53**, 107 (2020).
5) A. Takamine *et al.*, RIKEN Accel. Prog. Rep. **53**, 108 (2020).

Development of β-TOF detector for decay-correlated mass measurement of β-decaying nuclides

T. Niwase,[*1] W. Xian,[*2,*1] M. Wada,[*1] M. Rosenbusch,[*1] S. D. Chen,[*2,*1] A. Takamine,[*3] J. Liu,[*2,*1] S. Iimura,[*4,*3,*1] D. S. Hou,[*5,*6] S. X. Yan,[*7] H. Ishiyama,[*3] S. Nishimura,[*3] Y. Hirayama,[*1] S. Kimura,[*3] D. Kaji,[*3] H. Miyatake,[*1] K. Morimoto,[*3] P. Schury,[*1] Y. X. Watanabe,[*1] and H. Wollnik[*8]

A novel "α-TOF" detector,[1] has been recently developed and installed on a multi-reflection time-of-flight mass spectrograph (MRTOF-MS). This detector can measure ion implantation to deduce the time-of-flight (TOF), along with subsequent α-decay and spontaneous fission (SF) events from the implanted ions. We recently succeeded in the direct mass measurement of superheavy nuclides, ^{257,258}Db,[2,3] wherein the count rate of ^{257}Db was as low as two events per day.[2] Furthermore, we have initiated a new field of nuclear spectroscopy using decay-correlated mass measurements.[4] The potential of this technique was initially demonstrated using decay properties to discriminate between the two states of ^{207}Ra, followed by mass analyses of each state; the two states could not be independently resolved by the MRTOF.

While the α-TOF detector is limited to α-decay and SF nuclides, it would be valuable to expand its performance to encompass β-decays. Here, we report the development of a new "β-TOF" detector, an extension of the α-TOF detector, that enables the decay-correlated mass spectroscopy of α/β/SF decaying nuclides.

The β-TOF detector uses double-layered SSDs with a thickness of 500 μm (Hamamatsu S-14605) to provide a ΔE-ΔE telescope for β-decay. In the first layer of the SSD, α-decay and SF are detected in the same manner as those in α-TOF. The basic characteristics—time resolution, α-particle energy resolution, implantation, and α-decay detection efficiency—of the β-TOF detector are the same as those of α-TOF. Owing to the solid angle coverage of the two SSDs, the telescope is geometrically limited to a detection efficiency of 33% for β-rays.

Online commissioning for the β-TOF detector was performed via MRTOF,[5] located at the end of the ZeroDegree spectrometer beamline.[6] The so-called ZD-MRTOF was coupled to a cryogenic helium gas cell that thermalized the relativistic beam delivered by BigRIPS. In the first online test of this new detector, we succeeded in measuring the correlation between the TOF of the neutron-rich ^{81}Ga isotope and subsequent β-decay. Figure 1 shows the histogram of TOF singles and decay-correlated TOF events. Accordingly, the detection efficiency for β-rays was found to be 27(7)%, which in good agreement with the geometric estimation. The half-life of ^{81}Ga was successfully extracted from the time between individual implantations and subsequent decay events. Figure 2 shows the decay time distribution with the expected decay curve. The half-life of ^{81}Ga was determined to be 1.44(31) s, which is in agreement with the value in literature, *i.e.*, 1.217(5) s.[7]

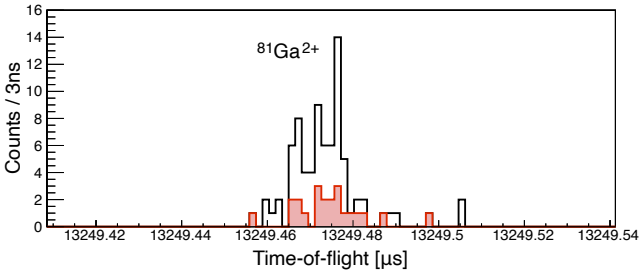

Fig. 1. TOF spectrum of ^{81}Ga^{2+}. The TOF singles spectra are drawn in black, while β-decay correlated events are shaded in red.

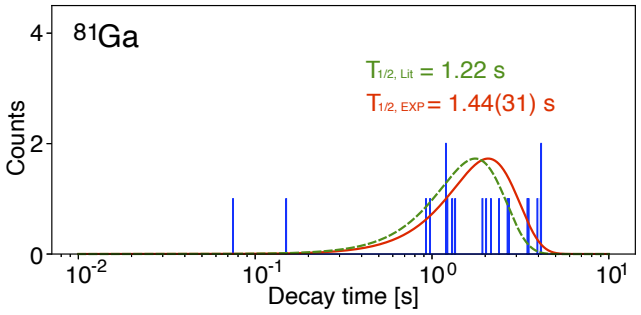

Fig. 2. Measured decay time distribution of ^{81}Ga. The red solid line and green dashed curve indicate the distribution curve drawn with the experimental and literature ($T_{1/2}$ = 1.22 s) values, respectively.

*1 Wako Nuclear Science Center (WNSC), IPNS, KEK
*2 Department of Physics, University of Hong Kong
*3 RIKEN Nishina Center
*4 Department of Physics, Osaka University
*5 Institute of Modern Physics, Chinese Academy of Sciences
*6 School of Nuclear Science and Technology, Lanzhou University
*7 Institute of Mass Spectrometer and Atmospheric Environment, Jinan University
*8 Department of Chemistry and Biochemistry, New Mexico State University

References
1) T. Niwase *et al.*, Nucl. Instrum. Methods Phys. Res. A, **953**, 163198 (2020).
2) P. Schury *et al.*, Phys. Rev. C **104**, L021304 (2021).
3) P. Schury *et al.*, in this report.
4) T. Niwase *et al.*, Phys. Rev. C **104**, 044617 (2021).
5) M. Rosenbusch *et al.*, arXiv:2110.11507.
6) T. Kubo *et al.*, Prog. Theo. Exp. Phys. **2012**, 03C003 (2012).
7) C. M. Baglin, Nucl. Data Sheets **109**, 2257 (2008).

Ion extraction from linear Paul trap via axially swinging field

K. Imamura,[*1] A. Takamine,[*1] S. Go,[*1] M. Tajima,[*1] A. Gladkov,[*1] and H. Ueno[*1]

Spin-polarized radioactive isotope (RI) beams have been used for the measurements of nuclear electromagnetic moments and spins to investigate nuclear structure. In many experiments, the polarization of nuclear spin is generated via projectile fragmentation reaction.[1] The reaction mechanism has been well studied so far. However, the achievable spin polarization is typically as low as several percentage points. Laser optical pumping can realize spin polarization of more than a few tens of percentage points but the method is element-limited. A highly efficient and universal method for producing spin-polarized RI beams is desired. For this purpose, we are developing a spin-polarized beam production apparatus using the atomic beam magnetic resonance (ABMR) method. In this method, the spin polarization of neutral atomic beams is generated by two-step spin selection using multi-pole magnets and one magnetic resonance.[2] The ABMR method itself has high spin selectivity. However, the efficient production of a neutral RI atomic beam using thermal energy is a significant technical challenge. We propose a new ion neutralization system based on a multi-segmented linear Paul trap.

In the proposed neutralization system, RI ions are simultaneously trapped with laser-cooled ions. The kinetic energy of trapped RI ions will decrease due to mutual Coulomb interaction between RI ions and laser cooled ions. After the cooling of RI ions, RI ions are neutralized using a neutralization gas. In a general linear Paul trap, an RF electric field is only used to confine the radial motion of trapped ions. However, neutralized ions are scattered around in the above situation because the axial component of the trapped ion motion is much smaller than the radial component of the motion. In order to extract neutral RIs from a linear Paul trap efficiently, we apply an additional alternating electric field in the axial direction (swinging field) to induce axial ion motion. We constructed a five-segmented linear Paul trap to demonstrate ion extraction using an axially swinging field. The setup of the experiment is shown in Fig. 1(a). Rubidium ions emitted from a surface ionization ion source were guided to the trap operated at a frequency of 1.18 MHz and 532 V_{pp} using a quadrupole mass separator. In order to trap Rb ions, helium buffer gas of the pressured at a 1×10^{-4} Torr was filled in the trap chamber. The kinetic energy of Rb ions decreased because of collision between the ions and the He buffer gas, following which Rb ions were confined in the center electrode of the trap, denoted as "C" in Fig. 1(a). After ion trapping, we superimposed sinusoidal voltages (frequency: 1 Hz, amplitude: 2 V) to each trap electrode as the swinging field. The phase difference of the each sinusoidal voltage was 45°. The time variation of the applied voltage of each trap electrode is schematically shown in Fig. 1(b). We turned off

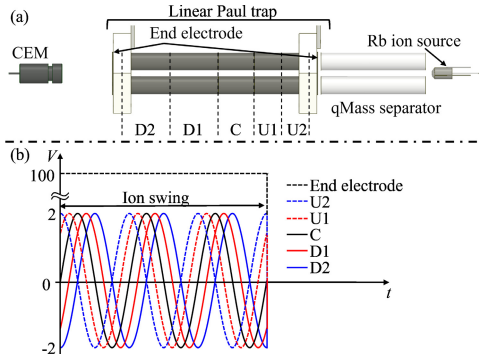

Fig. 1. (a) Schematic view of the experimental setup. The time variation of the applied voltages of each electrode during ion swinging is schematically shown in (b).

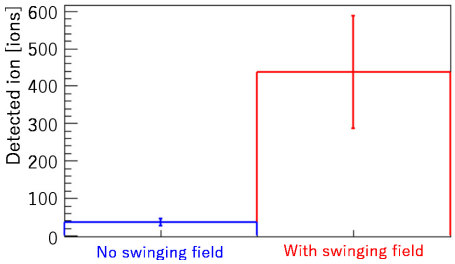

Fig. 2. Number of detected ions at the CEM position with/without an ion swinging field.

all the voltages including that of the end electrode at a given time after applying the swinging field. The ions extracted toward the downstream direction were detected using channel electron multiplier (CEM) detector.

The number of ions detected using the CEM detector with/without the swinging field is shown in Fig. 2. The detected ion number shown in Fig. 2 is the average value of 25 measurements. The error was calculated as the standard deviation of the number of detected ions in each measurement. As shown in Fig. 2, approximately 450 ions were detected at the CEM position when we applied a swinging field, while the signal rate decreased almost to the background level in the case of no swinging field. This result indicates that the trapped ions obtain an axial momentum component sufficient to eject in the axial direction using the swinging field before ion neutralization: that is ions neutralized using a gas are delivered to the downstream spin-selection magnet as a neutral atomic beam. In a rough estimation, the extraction efficiency of the trapped ions reached approximately 10% so far. Further investigation and development are in progress now.

*1 RIKEN Nishina Center

References
1) K. Asahi *et al.*, Phys. Lett. B **251**, 488 (1990).
2) N. F. Ramsey, *Molecular Beams* (Oxford University Press, New York, 1956).

Offline collinear laser spectroscopy of zirconium II

M. Tajima,[*1] A. Takamine,[*1] H. Iimura,[*2,*1] M. Wada,[*3] H. A. Schuessler,[*4,*1] Y. Matsuo,[*5,*1] and H. Ueno[*1]

The laser spectroscopy of atomic transitions is sensitive to nuclear structures in ground states. The measurement of isotope shifts and hyperfine splittings by collinear laser spectroscopy (CLS) is a powerful tool for studying radioactive isotopes (RIs) systematically along isotope chains. Charge radii, quadrupole deformation, electromagnetic moments, and spins have been extensively measured at ISOL-type facilities. We are preparing for the CLS of RIs at the gas-cell decelerator facility, SLOWRI. Our main targets include refractory elements near the $N = Z$ line in the intermediate mass region, where experimental data are not sufficient because of the experimental difficulties at ISOL-type facilities. Barium isotopes have been measured as a first offline demonstration of CLS.[1)] This report describes the next step wherein an offline measurement of zirconium ions was performed.

Zirconium ions were produced from a disk-shaped metal target by using pulsed-laser ablation. A Q-switched Nd:YAG laser (Coherent, Minilite II) was used with the time width of 5 ns at the repetition rate of 10 Hz at the maximum. Ion beams were extracted at ∼10 keV and mass separated so that a selected isotope could be transported to a photon detection region.[1)] We chose the transition $4d^2(^3F)5p\ z^4G^\circ_{5/2} \leftrightarrow 4d^2(^3F)5s\ a^4F_{3/2}$, which is at 357 nm, and the strongest transition from the atomic ground state.[2)] A continuous-wave Ti:Sapphire laser (M-square, SolsTis) pumped by a solid-state laser (Verdi, V10) was used to obtain the fundamental wavelength of 714 nm and a commercial second harmonics generator with a LBO crystal (M-square, ECD-X) was used. The fundamental wavelength was stabilized by a wavelength meter within 10 MHz (FWHM); the power was 0.5 mW at the detection region. The time-of-flight (TOF) of the ions was measured by a channeltron (Photonis, Magnum 5901) at the downstream of the beamline. We found that the TOF of the resonant ions were concentrated within 50 μs. Therefore, a time gate for the photon detection by a PMT was set to 50 μs for the timing of the pulsed laser irradiation to suppress background counts.

Figure 1 shows the observed spectra with Voigt fitting curves. Since $^{90,92,94}Zr^+$ and $^{91}Zr^+$ were measured at separate times and different wavelengths were available between them, the energy of ion beams was tuned to 13.6 keV for $^{90,92,94}Zr^+$ and 10.6 keV for $^{91}Zr^+$. The background count rates were suppressed by a factor of 1000 compared to that of the continuous measurement. In the future, we plan to suppress backgrounds further

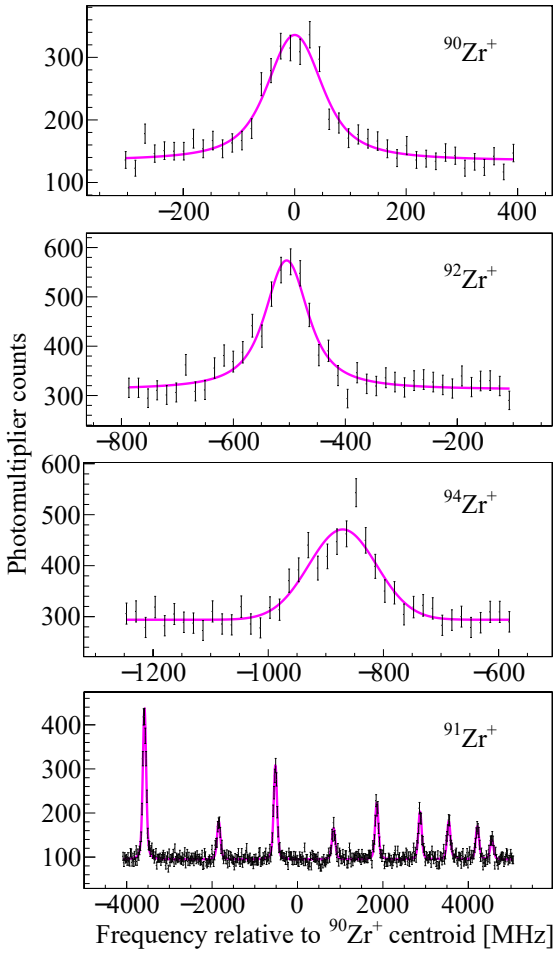

Fig. 1. Observed resonance spectra of Zr^+ at 357 nm with the time gate of 50 μs. Magenta lines represent the Voigt fitting curves.

with a shorter ion bunch by performing CLS with a multi reflection TOF mass spectrometer[3)] where the bunch length of 40 ns is possible. Although all 12 peaks were not fully resolved for $^{91}Zr^+$, hyperfine coefficients for both upper and lower levels were derived from five isolated peaks; these coefficients were consistent with those reported in previous measurements.[4,5)] In addition, this experiment is a benchmark for a new lifetime measurement of $^{93}Zr^+$,[6)] which is important to accurately evaluate the radioactivity of long lived fission products in nuclear wastes.

*1 RIKEN Nishina Center
*2 Nuclear Science and Engineering Center, JAEA
*3 Wako Nuclear Science Center (WNSC), IPNS, KEK
*4 Department of Physics and Astronomy, Texas A&M University
*5 Department of Advanced Science, Hosei University

References

1) M. Tajima *et al.*, RIKEN Accel. Prog. Rep. **53**, 15 (2020).
2) G. Ljung *et al.*, Astron. Astrophys. **456**, 1181 (2006).
3) P. Schury *et al.*, Phys. Rev. C **104**, L021304 (2021).
4) H. L. Thayer *et al.*, J. Phys. G **29**, 2247 (2003).
5) S. D. Rosner, R. A. Holt, J. Phys. B **49**, 11501 (2016).
6) A. Takamine *et al.*, in this report.

Fluorescence detection of the highly energetic radioactive Rb beams stopped in an optical cryostat at HIMAC

K. Tsubura,[*1,*2] K. Imamura,[*2] A. Takamine,[*2] S. Akimoto,[*1,*2] M. Ito,[*1,*2] K. Kikuchi,[*1,*2] R. Mitsuyasu,[*1,*2] A. Gladkov,[*2] M. Tajima,[*2] S. Go,[*2] M. Mukai,[*2] M. Doi,[*1,*2] M. Nishimura,[*1,*2] T. Yamamoto,[*1,*2] H. Endo,[*1,*2] M. Hase,[*3] K. Kawata,[*4] H. Nishibata,[*2,*5] Y. Ichikawa,[*2,*5] H. Ueno,[*2] and Y. Matsuo[*1,*2]

We are developing a laser spectroscopy technique called Optical RI-atom Observation in Condensed Helium as Ion- catcher (OROCHI) for the study of nuclear spins and moments. In the OROCHI experiment, we catch highly energetic ion beams in superfluid helium (He II) in our cryostat to neutralize them and conduct in-situ laser spectroscopy. We irradiate neutralized atoms with circularly polarized laser light to produce spin polarization and measure atomic Zeeman and hyperfine splitting energies using laser-radio frequency and laser-microwave double resonance method.

In a previous online experiment,[1] our group observed laser-rf double resonance spectra of $^{84-87}$Rb ion beams provided by the RIKEN RIPS at ∼60 MeV/nucleon. It is known that the hyperfine structure constants of atoms in superfluid helium are larger than those of free atoms by 1%.[2,3] Therefore, based on our interest in the hyperfine anomalies of atoms in superfluid helium, we plan to measure the hyperfine splitting of the radioactive Rb, Ag, Cs, and Au isotopes, to which this method has not yet been applied.

In FY2019, we measured the beam yields of a higher energy ^{84}Rb beam at the HIMAC SB2 beam line in order to estimate the number of stopped atoms in the laser-induced fluorescence (LIF) observation region (ϕ2 mm × 5 mm).[4]

Because the result of the FY2019 experiment showed that the diameter of the beam stopping area was over 15 mm, we decided to expand the laser diameter and the observation area to as large as possible (2 mm ×10 mm × 5 mm). We here report the result of an experiment conducted in FY2021 using laser irradiation at HIMAC.

The ^{84}Rb beam produced in proton pickup reactions by a ^{84}Kr beam with 350 MeV/nucleon on a Be target of 12 mm thickness was passed through a 2.1 mm-thick Al degrader and a plastic in the pre-cryochamber, and stopped in He II at the center of the optical cryostat. In the pre-cryostat chamber, the number of beams was counted using a trigger plastic scintillator and two photomultiplier tubes. A laser beam amplified by a taper amplifier (TA) was shaped to the above-mentioned size and introduced to the cryostat. The laser light wavelength was 780 nm with a bandwidth of 2.9 nm (FWHM), which corresponds to the Rb D1 excitation line in He II. The fluorescence from the stopped atoms was collected by a LIF detection system, passed through the optical fiber, the wavelength was selected by a monochromator with a resolution of 8 nm set to 794 nm, and detected using a photomultiplier tube.

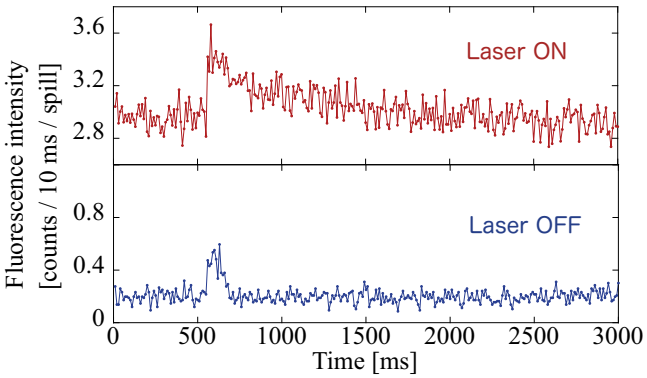

Fig. 1. Detected fluorescence intensity for laser on (upper) and off (lower).

Figure 1 shows the detected photon intensity for when the laser is turned on (upper) and off (lower). The incoming ^{84}Rb beam intensity was 3.7×10^4 particles per spill with a beam purity of 50% (the beam repetition cycle was 3.3 s). An evaluation revealed that 7% of the ^{84}Rb was stopped in the observation region from the previous experimental results[4] and a LISE^{++} calculation. The irradiated laser power was 200 mW. The upper plot clearly shows a long tail for the LIF based on remaining ^{84}Rb atoms compared with the beam-induced fluorescence in the lower plot. This tail stems from Rb atom diffusion caused by liquid helium flow and it shows a similar diffusion time of 1.77 s compared with the value (617 ms) that we measured in our previous experiment at RIPS.[5] The extended LIF decay time can be attributed to the expansion of the observation region being larger than that in the RIPS experiment.

We confirmed LIF detection of ^{84}Rb and conclude that OROCHI can be applied to the high energy beam from HIMAC SB2. Currently, we are in the process of analyzing the data.

*1 Department of Advanced Sciences, Hosei University
*2 RIKEN Nishina Center
*3 National Institute of Materials Science (NIMS)
*4 Center for Nuclear Study, University of Tokyo
*5 Department of Physics, Kyushu University

References

1) X. F. Yang *et al.*, Phys. Rev. A **90**, 052516 (2014).
2) Y. Takahashi *et al.*, Z. Phys. B **98**, 391 (1995).
3) T. Furukawa, Ph.D. thesis, Osaka University (2007).
4) K. Tsubura *et al.*, RIKEN Accel. Prog. Rep. **53**, 132 (2020).
5) K. Imamura *et al.*, Appl. Phys. Express **12**, 016502 (2019).

Development of dispersion matching optics in OEDO beamline

S. Hanai,[*1] S. Michimasa,[*1] T. Chillery,[*1] S. Ota,[*1] N. Imai,[*1] S. Shimoura,[*1] N. Fukuda,[*2] Y. Hijikata,[*3,*2] K. Kameya,[*4,*2] S. Kitayama,[*4,*2] K. Kishimoto,[*5,*2] K. Kusaka,[*2] J. Li,[*1] Y. Maeda,[*6,*2] Y. Maruta,[*4,*2] T. Matsui,[*4,*2] K. Miki,[*4,*2] D. Nagae,[*2] H. Nishibata,[*5,*2] D. Nishimura,[*7,*1,*2] M. Sasano,[*2] Y. Shimizu,[*2] S. Sugawara,[*2] T. Sumikama,[*2] H. Suzuki,[*2] H. Takahashi,[*7] H. Takeda,[*2] T. Uesaka,[*2] R. Urayama,[*4,*2] T. Wakasa,[*5] K. Yako,[*1] Y. Yamaguchi,[*2] Y. Yanagisawa,[*2] N. Yokota,[*5,*2] C. Yonemura,[*5,*2] and K. Yoshida[*2]

The Optimized Energy Degrading Optics (OEDO) beamline provides potential opportunities to perform nuclear physics experiments with spatially and achromatically well-forcused low-energy RI beams[1] or high momentum resolution by selecting a suitable ion transportation method. High-quality low-energy RI beam production has been achieved.[2] Recently, several beamline magnets in the OEDO beamline were rearranged aiming at the realizing a high momentum resolution. To conduct nuclear spectroscopy with a resolution greater than the energy width of the incident beam, lateral and angular momentum dispersion matching techniques are essential. Figure 1 shows a designed dispersion matching ion optics from BigRIPS F3 to SHARAQ S2 foci through the OEDO beamline. The S0 intermediate focus, where a target will be inserted in a future experiment, has the largest momentum dispersion in the beamline of 14.7 m, and this momentum dispersion vanishes at the final focus, S2. We report here a study showing dispersion matching optics of the OEDO beamline.

We performed the study using an 82 MeV/nucleon triton beam produced by the BigRIPS separator from the 200 MeV/nucleon ^{4}He primary beam. Position de-

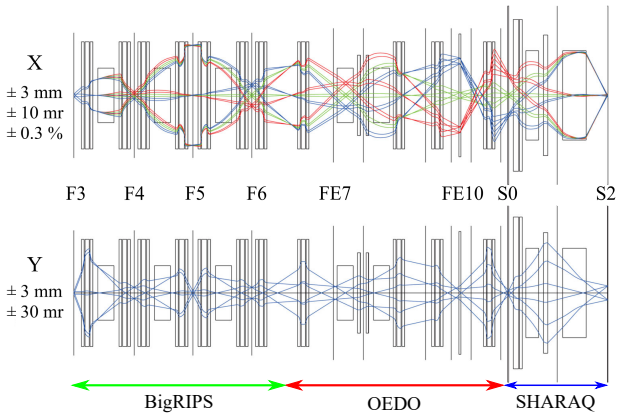

Fig. 1. Trajectories of ion beam with dispersion matching setting in BigRIPS-OEDO-SHARAQ beamline. Trajectories are calculated from first-order matrix elements.

*1 Center for Nuclear Study, University of Tokyo
*2 RIKEN Nishina Center
*3 Department of Physics, Kyoto University
*4 Department of Physics, Tohoku University
*5 Department of Physics, Kyushu University
*6 Faculty of Engineering, University of Miyazaki
*7 Department of Natural Sciences, Tokyo City University

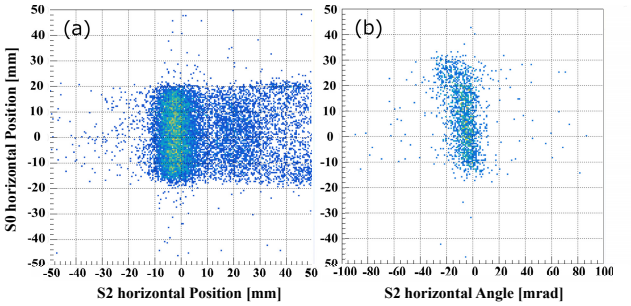

Fig. 2. (a) Correlation between S0 and S2 horizontal positions. (b) Correlation between S0 horizontal position and S2 horizontal angle. (a|δ) term is approximately 0.4 mrad/%.

tectors, a parallel-plate avalanche counter and a low-pressure multiwire drift chamber, were placed at the foci from F3 to S2, to measure the transfer matrix elements at each focal plane. We verified the consistency of the measured matrix elements by comparison with ion optics calculation results.

By evaluating the matrix elements, the momentum dispersion at S0 was deduced as 16.3 m, which corresponds to a dispersion of 0.025 mm/% and satisfies the lateral dispersion matching condition with the SHARAQ spectrometer. Figure 2(a) shows that there is no correlation between the horizontal position (momentum dispersion) at S0 and that at S2 and therefore, the condition of momentum dispersion matching is fulfilled. Figure 2(b) shows the correlation between the horizontal position (momentum dispersion) at S0 and the horizontal angle at S2, which suggests that angular dispersion matching is efficiently satisfied. We conclude that angular momentum dispersion matching is also achieved at S2.

Consequently, we achieved dispersion matching ion transportation through the OEDO beamline. Using this ion-optical mode, we plan to conduct an approved experimental program of direct mass measurements of very rare RI nuclei.

References

1) S. Michimasa *et al.*, Prog. Theor. Exp. Phys. **2019**, 043D01 (2019).
2) S. Michimasa *et al.*, CNS Ann. Rep. 2018, CNS-REP-**98**, 35 (2020).

Commissioning of the Si-CsI array TiNA for direct reactions at OEDO

B. Mauss,[*1] N. Ma,[*2] J. W. Hwang,[*2,*3] D. Suzuki,[*1] N. Imai,[*2] T. Teranishi,[*4,*1] S. Ota,[*2,*5] A. Kohda,[*5,*1] M. Dozono,[*2,*6] S. Michimasa,[*2] T. Sumikama,[*1] C. Iwamoto,[*7] and N. Iwasa[*8,*1]

The energy-degrading beamline OEDO is operating at RIBF to expand the scope of reaction studies for radioactive nuclei.[1] TiNA is an array of Si and CsI detectors for direct reaction studies at OEDO to address a wide range of objectives in nuclear structure and astrophysics.[2] The first version of the detector has been used in several transfer experiments.[3,4]

The TiNA detector was upgraded in 2020 to increase the solid angle and improve the resolution in angle and energy.[5] The upgraded TiNA consisted of two types of detector assemblies. Four square telescopes with a first stage of double-sided strip silicon detectors (DSSD) and a second stage of CsI detectors were arranged in a barrel configuration and placed just beyond the reaction target. The second detector assembly is a lampshade array consisting of six trapezoidal telescopes with a first stage of single-sided strip silicon detectors (SSSD) and a second stage of CsI detectors. The total angular coverage by the entire telescope ranges from 10° to 80° in the laboratory frame.

For the data taking, two different systems were unified. The DSSDs were connected to the General Electronics for TPCs (GET), an integrated system allowing the processing of a total of 1024 channels. The test of the GET electronics has been reported in a previous study.[5] The signals from the rest of the detectors, including the CsI crystals and SSSDs, were fed into standard analog amplifiers and digitized by VME-standard ADC modules. Triggers from both systems were merged in a trigger module. A common trigger is sent to both DAQs and synchronizes the event number.

The detector was commissioned in-beam at the tandem accelerator facility of the Center for Accelerator and Beam Applied Science, Kyushu University in January 2021. The aim of this commissioning was to measure the performances in terms of energy and angular resolutions, particle identification for light ions, and DAQ capabilities.

A 14 MeV deuteron beam impinged on a 1 mg/cm^2 thick ^{12}C target provided by the RCNP, Osaka University. At this beam energy, elastic scattering, inelastic scattering to excited states, and transfer (d, p) and (d, α) reactions are allowed. The preliminary results give an energy resolution of 125 keV FWHM for the elastic scattering events measured by the DSSDs. Figure 1 shows the excitation energy for the (d, p) transfer reaction. The protons were selected by the $E - \Delta E$ method using the CsI crystals and DSSDs. The excitation energy resolution is approximately 330 keV FWHM for proton energies around 14 MeV. Analysis is still ongoing to improve the resolution.

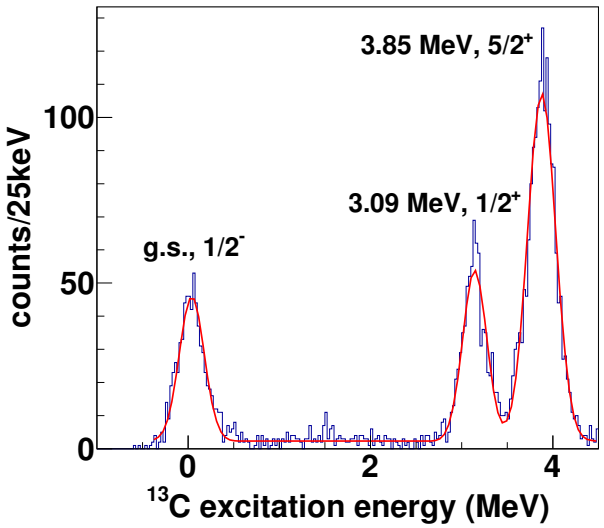

Fig. 1. Excitation energy spectrum for the ^{12}C$(d, p)^{13}$C transfer reaction using a 14 MeV deuteron beam.

In conclusion, the full setup of the TiNA detector was successfully commissioned at the tandem accelerator facility of the Kyushu University. The event correlation between the two independent data acquisition systems was validated; however, some DAQ capabilities should be improved in the future. The analysis is ongoing with encouraging preliminary results.

*1 RIKEN Nishina Center
*2 Center for Nuclear Study, University of Tokyo
*3 Center for Exotic Nuclear Studies, Institute for Basic Science
*4 Department of Physics, Kyushu University
*5 Research Center for Nuclear Physics, Osaka University
*6 Department of Physics, Kyoto University
*7 RIKEN Center for Advanced Photonics
*8 Department of Physics, Tohoku University

References

1) S. Michimasa *et al.*, Prog. Theor. Exp. Phys. **2019**, 043D01 (2019).
2) P. Schrock *et al.*, CNS Ann. Rep. 2016, CNS-REP-**96**, 7 (2017).
3) K. Wimmer *et al.*, CNS Ann. Rep. 2017, CNS-REP-**97**, 7 (2019).
4) N. Imai *et al.*, CNS Ann. Rep. 2018, CNS-REP-**98**, 1 (2020).
5) B. Mauss *et al.*, RIKEN Accel. Prog. Rep. **54**, 114 (2021).

First production of ^{6}He beam at CRIB

H. Yamaguchi,[*1] M. Sferrazza,[*2] S. Hayakawa,[*1] N. R. Ma,[*1] H. Shimizu,[*1] K. Okawa,[*1] T. Furuno,[*3] S. Okamoto,[*4] N. Imai,[*1] T. Chillery,[*1] J. T. Li,[*1] S. Ota,[*1,*3] N. Iwasa,[*5] and T. Kawabata[*3]

^{6}He is the second lightest unstable nuclide that could be used as a radioactive-isotope (RI) beam. In 2021, we performed a production test of ^{6}He beam at CRIB[1–4] for the first time, aiming to assess the feasibility of future experiments using this RI beam. The beam production was performed as a Machine Study beamtime in March, 2021. The primary beam was ^{7}Li^{3+}, accelerated with the AVF cyclotron up to an energy of 8.3 MeV/nucleon. The maximum beam current at the entrance of CRIB during the beamtime was 3 particle μA (= 9 electric μA (eμA)). The RI beam was produced with the ^{7}Li$(d,{}^3\mathrm{He})^6$He reaction, which was also used in other in-flight facilities, such as RESOLUT of Florida State University.[5] At RESOLUT, a ^{6}He beam was produced with an energy range of 18–29 MeV (3–5 MeV/nucleon), an intensity of 10^4 pps, and a purity of 40%. The target gas we used at CRIB was D_2 at 730 Torr, confined in a cell, and cooled with the cryogenic gas target system.[3]

We tested the beam production at two magnetic rigidity conditions: 1) $B\rho$ = 1.227 Tm (^{6}He^{2+}: 7.99 MeV/nucleon) with the original primary beam, and 2) $B\rho$ = 1.032 Tm (^{6}He^{2+}: 5.66 MeV/nucleon) by degrading the primary beam energy to 6.5 MeV/nucleon with a 48-μm-thick Havar foil. Particle identification (PI) was performed by measuring the time-of-flight and energy of the secondary beam with the PPACs and silicon detectors at the F2 and F3 focal planes. The identified particles are ^{6}He^{2+}, ^{3}H^{1+}, and a small number of ^{7}Li^{2+}.

After the optimization at F2 to maximize the ^{6}He beam intensity, the beam was transported to F3 with a transmission efficiency of 28%. ^{7}Li^{2+} disappeared from the PI diagram, while ^{3}H^{1+} remained due to its charge-to-mass ratio identical to ^{6}He. Table 1 summarizes the purities of secondary beam particles in each condition. The purity of ^{3}H^{1+} appeared to be higher at F3 compared to F2, however, this is supposed to be from the limited detection efficiency of the PPAC, which triggered the measurement at F2, against the light ^{3}H^{1+} ion. The ^{6}He energy after one PPAC (thickness equivalent to 9.5 μm Mylar) was measured as (47.80 ± 0.44) MeV or (7.943 ± 0.073) MeV/nucleon, where the energy loss in the PPAC (0.29 MeV) was in a good agreement with a calculated value (0.28 MeV).

We increased the primary beam current to confirm the highest intensity ^{6}He beam we can obtain. The ^{6}He rate increased almost proportional to the primary beam current with a ratio of 370 kcps/μA. The detection efficiency of the PPAC was 70–80% or better, when the secondary beam rate was 300–400 kcps. The intensity test was performed up to the primary beam current of 2 electric μA (eμA), at which the PPAC efficiency dropped down to 42% for the secondary-beam intensity of 630 kcps, even though we applied the possible maximum voltages on the PPAC electrodes.

Table 1. Summary of the secondary beam purity. Note that the F2 data were taken with the PPAC trigger, and F3 were with the SSD.

Ion	High $B\rho$ (1.227 Tm)		Low $B\rho$ (1.032 Tm)	
	F2	F3	F2	F3
^{6}He^{2+}	85%	73%	60%	61%
^{3}H^{1+}	15%	27%	17%	23%
^{7}Li^{2+}	0.2%	–	22%*	5.9%
^{4}He^{2+}	–	–		9.7%

* Summed purity of ^{7}Li^{2+} and ^{4}He^{2+}.

The beam production test in the low-energy condition was performed basically in the same procedure as the high-energy case. Due to the contamination ions of ^{7}Li^{3+} and ^{4}He^{2+}, we had a lower ^{6}He purity of about 60%, as shown in Table 1.

In conclusion, we succeeded in producing ^{6}He RI beams at 7.99 MeV/nucleon and 5.66 MeV/nucleon with an intensity of the order of 10^5 pps, superior to the beam at RESOLUT,[5] satisfying the requirement by the proposed ^{6}He+p experiment.[6] The practical beam intensity is presently limited to about 2×10^5 pps by the low detection efficiency of the PPAC for such a light-ion beam. To make the efficiency higher, we are planning to use wire chambers (MWDC) in the main experiment.

*1 Center for Nuclear Study, University of Tokyo
*2 Department of Physics, Université Libre de Bruxelles
*3 Department of Physics, Osaka University
*4 Department of Physics, Kyoto University
*5 Department of Physics, Tohoku University

References
1) S. Kubono *et al.*, Eur. Phys. J. A **13**, 217 (2002).
2) Y. Yanagisawa *et al.*, Nucl. Instrum. Methods Phys. Res. A **539**, 74 (2005).
3) H. Yamaguchi *et al.*, Nucl. Instrum. Methods Phys. Res. A **589**, 150 (2008).
4) H. Yamaguchi *et al.*, Nucl. Phys. News **30**(2), 21 (2020).
5) Web page of RESOLUT: `https://fsunuc.physics.fsu.edu/research/experimental_devices/#resolut`.
6) M. Sferrazza, *et al.*, proposal for RIBF NP-PAC-21, NP2021-AVF70 (2020, unpublished).

Long polarization-maintaining fiber link (440 m) for magneto-optical trapping of francium atoms

K. Nakamura,[*1] S. Nagase,[*2] T. Nakashita,[*3] T. Hayamizu,[*4] T. Aoki,[*3] H. Nagahama,[*1] N. Ozawa,[*2] M. Sato,[*3,*4] K. Yamane,[*3] M. Fukase,[*2] D. Uehara,[*2] A. Takamine,[*4] and Y. Sakemi[*1]

We are currently developing an optical lattice francium (Fr) atom interferometer to determine the permanent electric dipole moment of an electron (eEDM). Fr is the heaviest alkali atom with an eEDM enhancement factor of approximately 799.[1)] The trapping of such Fr atoms in the optical lattice leads to an ultra-sensitive eEDM measurement system with a long interaction time between the isolated atoms and electric field. To load the atoms into the optical lattice, they must be cooled and trapped beforehand by techniques such as magneto-optical trapping (MOT). We developed a MOT system and connected it to a ^{210}Fr production beamline, which consists of a surface ionizer[2)] and neutralizer, installed in the E7 vertical course. In addition, we linked the MOT system to laser devices in the laser spectroscopy room (referred to as L) on the first basement floor of the RIBF building with 440 m-long polarization-maintaining (PM) fibers. In this paper, we report the performance of the PM fiber link.

The fiber link consists of a polyvinyl chloride (PVC)-coated 400 m flexible stainless steel tube cable (Nippon Steel Welding & Engineering, Picoflec) from L to the E7 entrance and another 40 m tube cable from the E7 entrance to the MOT system (Fig. 1(a)). Seven PM fibers are housed in each cable; among these, four are Fujikura PM63 (cutoff wavelength is 520–620 nm, mode field diameter is 4.5 ± 0.5 μm at 630 nm), two are PM85 (650–800 nm, 5.5 ± 0.5 μm at 850 nm), and one is PM98 (870–950 nm, 6.6 ± 0.5 μm at 980 nm). Both cables are connected using fiber connectors inside the optical rack installed at the E7 entrance. The typical transmission loss due to the connector was 0.25. The optical rack was also expected to serve as a hub base for optical transmission to other laboratories. The lights of the trapping lasers (wavelength of 718 nm for ^{210}Fr, 780 nm for ^{87}Rb, used for offline test) and repumping lasers (817 nm for ^{210}Fr, 795 nm for ^{87}Rb), which were frequency-stabilized within the natural linewidth of relevant transitions (several MHz) using a wavelength meter (HighFinesse, WS8-2), were transmitted to the MOT system via fibers (PM63). In general, frequency instability due to a fiber is low (∼3 Hz for 6 km at 778 nm in Ref. 3)), and thus, negligible for our optical transmission.

In the case of a high-power CW laser beam transmitted along a long fiber, there are concerns related to the limit of transmitted power due to stimulated Brillouin scattering (SBS).[4)] To maximize the number of atoms to be captured, the trapping laser intensity (total of 6 axes of 3D MOT) should be several times (8 times in Ref. 5)) the saturation intensity of the cooling transition. The saturation intensity of ^{210}Fr (^{87}Rb) is ∼2.9 (∼1.6) mW/cm^2. When using our trapping laser (SolsTiS, CW, linewidth <50 kHz), the SBS threshold output power for the 400 m fiber (PM63) was 30 mW at 718 nm. This value is sufficient for our three-axis 3D MOT system (beam diameter of 1 cm) with opposing mirrors.

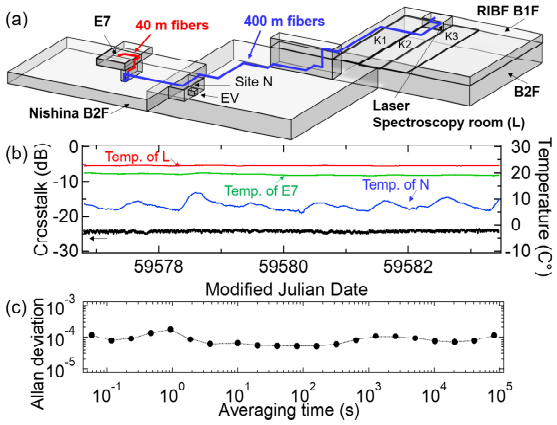

Fig. 1. (a) Overhead view showing the path of a fiber link. (b) Polarization crosstalk in the 400 m fiber and temperature measured at three sites. (c) Allan deviation of the crosstalk.

The stability of polarization of the 400 m PM fiber was investigated with a test laser (685 nm, 1 mW). The polarization crosstalk calculated from the optical power of the *p*- and *s*-polarized outputs split by the polarization beam splitter after launching from the 400 m PM fiber and the temperature measured at three sites (L, E7, and N) are shown in Fig. 2(b). Site N is near the elevator on the second basement floor of the Nishina Building (Fig. 1(a)). Figure 2(c) shows the Allan deviation calculated from the time series data of the polarization crosstalk. The PM fibers housed in the PVC-coated 400 m tube were robust against large diel temperature fluctuations along the fiber.

We achieved Rb MOT in July 2021 in an offline test. Online experiments are being conducted intermittently to achieve Fr MOT, and we are getting closer to achieving it.

*1 Center for Nuclear Study, University of Tokyo
*2 Department of Physics, University of Tokyo
*3 Graduate School of Arts and Sciences, University of Tokyo
*4 RIKEN Nishina Center

References

1) N. Shitara *et al.*, J. High Energy Phys. **2021**, 124 (2021).
2) N. Ozawa *et al.*, RIKEN Accel. Prog. Rep. **54**, 117 (2021).
3) B. deBeauvoir *et al.*, Phys. Rev. Lett. **78**, 440 (1997).
4) G. P. Agrawal, *Nonlinear Fiber Optics, 5th Edition* (Academic Press, Boston, 2013).
5) S. R. Muniz *et al.*, Phys. Rev. A **65**, 015402 (2001).

RI nuclides produced in stacked Si and Al plates by 135-MeV/nucleon ^{12}C beam

T. Kambara*1 and A. Yoshida*1

On the basis of a fee-based facility sharing program, private companies in Japan use heavy-ion beams to simulate single-event effects (SEE) on space-use semiconductor devices by cosmic rays.[1] The clients have utilized ion beams of Ar, Kr, and Xe from the RIKEN Ring Cyclotron (RRC) at the E5A beam line. The primary ion beam is spread with a scatterer foil and wobbler magnets and extracted to atmosphere. Then, it passes through transmission-type detectors for dose measurements and an energy degrader for linear energy transfer (LET) adjustments. The setup and irradiation procedures were described previously.[2]

The samples irradiated by the primary beam are also impinged on by various secondary particles produced by nuclear processes in the upstream materials. To evaluate the effects of the nuclear processes, we irradiate test samples in the same beam condition as the clients' irradiation and measure RI nuclides by radiochemical analyses. Similar studies have been reported for a Kr beam[3] and a Xe beam.[4]

Since clients expressed interest in the utilization of a C beam, we studied the characteristics of a 135 MeV/nucleon ^{12}C beam. During the beamtime, we irradiated a stack of two Si plates (100-mm diameter and 0.5-mm thick) and two Al plates (3-mm thick) for radiochemical analyses. The irradiation setup is shown in Fig. 1. The primary beam passed through a 51.2-μm-thick Kapton® window into the atmosphere and then entered an ionization chamber (IC). From measurement with the IC, the number of ions was estimated to be approximately 1.08×10^{12} during 5 min of irradiation. Then, the beam passed a 3-mm-thick plastic scintillator (not used) and an energy degrader of 18.42-mm-thick Al. Its thickness was selected so that the primary ions stopped in the second Si plate.

We measured the γ rays from each sample plate with a Ge detector from 13.4 min to 39.7 days after the irradiation for the Si plates and from 23.7 min to 6.49 days for the Al plates. Using the observed γ-ray spectra, we identified 10 radionuclides from ^{7}Be to ^{34m}Cl. We extrapolated the decay curve of the radioactivity of each nuclide to the end of the irradiation to obtain the number of the nuclei identified in the sample. Then, we divided it by the number of primary ions to obtain the production probability of the nuclide. The nuclides can be produced by nuclear reactions either in the sample or in the upstream materials followed by transport to the sample.

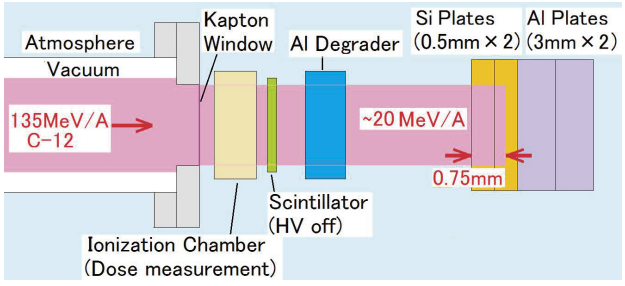

Fig. 1. Setup of the sample irradiation.

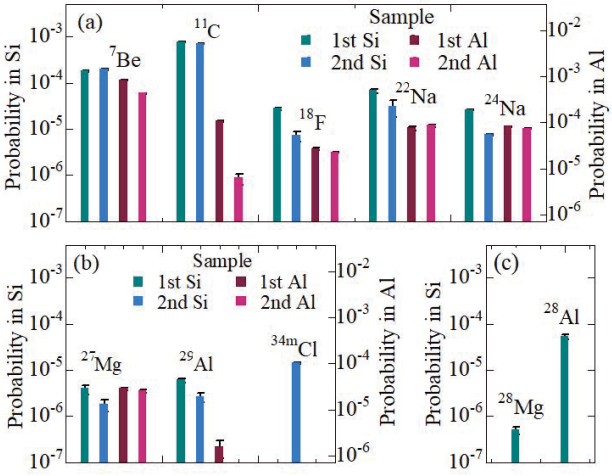

Fig. 2. Production probabilities of RI nuclides in the sample plates.

The results are shown in Fig. 2, where the colored bars indicate the probabilities in the sample plates. The values of the probabilities in the Si plates are shown on the left ordinate and those in the Al on the right so that the bar heights are scaled to the same number density of the sample atoms. Since the primary ^{12}C ions stopped in the second Si plate, the nuclides in the Al plates were either produced by secondary particles or transported from the upstream. The γ rays of ^{28}Mg and ^{28}Al shown in Fig. 2(c) were measured only in the first Si plate, and those of ^{34m}Cl in Fig. 2(b) were identified only in the second Si plate.

We are comparing the results with the simulation of nuclear processes using the Particle and Heavy Ion Transport System (PHITS) code.[5]

*1 RIKEN Nishina Center

References

1) http://ribf.riken.jp/sisetu-kyoyo/ (Japanese).
2) A. Yoshida, T. Kambara, RIKEN Accel. Prog. Rep. **51**, 185 (2018).
3) T. Kambara, A. Yoshida, Record of 2018 IEEE Radiation Effects Data Workshop (REDW), p. 94.
4) T. Kambara, A. Yoshida, RIKEN Accel. Prog. Rep. **52**, 158 (2019).
5) https://phits.jaea.go.jp/index.html .

Construction status of the INTT silicon tracker for sPHENIX at RHIC

I. Nakagawa,[*1] Y. Akiba,[*1] D. Cacace,[*2] K. Cheng,[*3] H. Enyo,[*1] T. Hachiya,[*1,*4] S. Hasegawa,[*1,*5] M. Hata,[*4] H. Imai,[*1,*6] T. Kondo,[*7] C. Kuo,[*3] H. -S. Li,[*8] R. -S. Lu,[*9] E. Mannel,[*2] C. Miraval,[*2] M. Morita,[*1,*4] Y. Nakamura,[*1,*6] G. Nakano,[*1,*6] Y. Namimoto,[*1,*4] R. Nouicer,[*2] G. Nukazuka,[*1] R. Pisani,[*2] M. Shibata,[*1,*4] C. Shih,[*3] M. Shimomura,[*4] M. Stojanovic,[*8] Y. Sugiyama,[*4] R. Takahama,[*1,*4] W. -C. Tang,[*3] K. Toho,[*10] K. Tsuruta,[*10] M. Watanabe,[*4] and X. Wei[*8]

The sPHENX experiment[1] at RHIC in Brookhaven National Laboratory (BNL) will be launched in January, 2023. The sPHENIX detector complex has been already in the construction phase in the experimental site at RHIC. The refurbished Barbar magnet was mounted on the outermost detector, *i.e.* hadron calorimeter in October, 2021 as shown in Fig. 1.

Japanese collaborators are in charge of development and construction of the silicon strip detector, namely INTermediate Tracker (INTT). Major components of the INTT detector have been developed and fabricated domestically, and the mass production of silicon ladder components (*i.e.* silicon sensors, high density interconnect (HDI) readout cables, and carbon fiber cooling plates) have been completed by the end of December, 2021. These components have been exported to the ladder assembly sites in BNL and Taiwan, and 70% of the ladder assembly have been completed by January, 2022. Shown in Fig. 2 is the mock-up of a quarter portion of the INTT inner layer barrel assembled in BNL. The construction of the INTT barrel will be started in Spring, 2022 and completed by early Summer, to be ready for the installation to the experimental site in September.

Fig. 1. The Babar magnet assembly on the bottom portion of the outermost detector, *i.e.* hadron calorimeters.

*1 RIKEN Nishina Center
*2 Physics Department, Brookhaven National Laboratory
*3 Department of Physics, National Central University
*4 Department of Mathematical and Physical Sciences, Nara Women's University
*5 Japan Atomic Energy Agency
*6 Department of Physics, Rikkyo University
*7 Tokyo Metropolitan Industrial Technology Research Institute
*8 Department of Physics and Astronomy, Purdue University
*9 Department of Physics, National Taiwan University
*10 Laboratory for Nuclear Science, Tohoku University

Fig. 2. The mock-up of a quarter portion of the INTT inner layer barrel assembled in BNL.

Fig. 3. The collaboration photo of the beam test at Tohoku University.

The readout cable chain of the INTT ladder consisted of the HDI, a bus extender,[2] and a conversion cable. While the bus extender is under mass production, the conversion cable under development employing the micro-coaxial cable technology. In December, 2021 we executed 3rd beam test[3] of the INTT ladder telescopes in Tohoku University.

References

1) Conceptual Design Report of sPHENIX (2018).
2) T. Hachiya *et al.*, in this report and references therein.
3) G. Nukazuka *et al.*, in this report and references therein.

Production of bus-extender for sPHENIX INTT detector

T. Hachiya,[*1,*2] Y. Akiba,[*1] D. Cacace,[*3] K. Cheng,[*4] H. En'yo,[*1] S. Hasegawa,[*1,*5] M. Hata,[*2] H. Imai,[*1,*6] T. Kondo,[*7] C. Kuo,[*4] H.-S. Li,[*8] R.-S. Lu,[*9] E. Mannel,[*3] C. Miraval,[*3] M. Morita,[*1,*2] I. Nakagawa,[*1] Y. Namimoto,[*1,*2] Y. Nakamura,[*1,*6] G. Nakano,[*1,*6] R. Nouicer,[*3] G. Nukazuka,[*1] R. Pisani,[*3] M. Shibata,[*1,*2] C. Shih,[*4] M. Shimomura,[*1] M. Stojanovic,[*8] Y. Sugiyama,[*2] R. Takahama,[*1,*2] W.-C. Tang,[*3] M. Watanabe,[*2] and X. Wei[*8]

sPHENIX is the second-generation heavy-ion collision experiment at the Relativistic Heavy-Ion Collider aimed at studying the properties of strongly coupled quark-gluon plasma. The intermediate tracker, INTT, is a silicon strip detector in sPHENIX that is used to perform precise tracking near the crossing point of colliding nuclei.[1)] A special cable for INTT called bus-extender is required to transmit large amounts of data from INTT to the readout electronics at high speed. The bus-extender is more than 1 m long and routed with a curving path. We developed the bus-extender based on flexible printed circuit (FPC) technology since no commercial cable is available.

The bus-extender is composed of four Cu layers including signal, power, and ground layers laminated with a liquid crystal polymer as a dielectric substrate. The signal layer contains 62 pairs of low-voltage differential signals within a 5 cm width of the cable, and their lines and spaces are both 130 μm.

We built prototype bus-extenders with a length of 1.3 m, as shown in Fig. 1, and evaluated their electrical and mechanical performance. The signal loss due to a long transmission line was 30%. The peel strength among the laminated layers was greater than 15 N/cm. These results are summarised elsewhere.[2)] From the results, the performance of the prototype is sufficient to satisfy the requirements. We completed the development and moved to the production stage.

The fabrication procedures are as follows: 1) the pattern of signal lines is printed by photolithography and etching, 2) all four layers are laminated by bonding sheets with pressure, and 3) through holes are opened and Cu-plated to connect the signal lines between the inner and outer layers. During the fabrication, we found that the yield rate was 30% because of short and open circuits of signal lines. Figure 2 shows two examples of short and open circuits found in the first fabrication procedure. This poor yield rate needs to be improved for the mass production since the yield rate directly impacts the production cost. We investigated

Fig. 1. Prototype bus-extender with a length of 1.3 m.

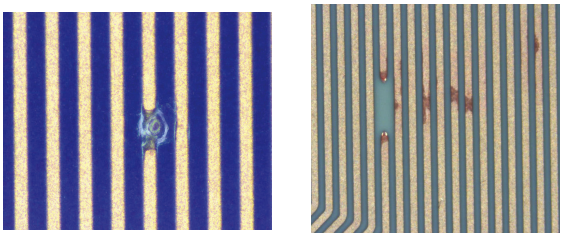

Fig. 2. Examples of short and open circuits after the photolithography (left) and etching (right).

why the short and open circuits were produced and found that the major cause of the problem is the contamination of tiny dust particles, which can interrupt light exposure and the flow of the etching solution. To solve the problem, we added two steps to the first procedure. One is to remove dust particles as much as possible using a silicon rubber roller. The other is to check the open/short lines after etching and to remove the bad signal layer in the later lamination process if found. With these new steps, the yield rate was improved to 75%. The visual inspection of signal lines after etching is useful to improve the yield rate further. An inspection system to search the bad lines semi-automatically is under development.[3)]

In summary, the development of the bus-extender was completed, and new steps added to the fabrication procedure successfully improved the the yield rate. The mass production of the bus-extender will be started in January 2022 with the semi-automated inspection system.

[*1] RIKEN Nishina Center
[*2] Nara Women's University
[*3] Brookhaven National Laboratory
[*4] National Central University
[*5] Japan Atomic Energy Agency
[*6] Rikkyo University
[*7] Tokyo Metropolitan Industrial Technology Research Institute
[*8] Purdue University
[*9] National Taiwan University

References

1) I. Nakagawa *et al.*, in this report.
2) T. Kondo *et al.*, submitted to IEICE Electron. Expr.
3) H. Imai *et al.*, in this report.

Detection efficiency of the RHIC-sPHENIX-INTT detector

M. Morita,[*1,*4] Y. Akiba,[*1] D. Cacace,[*2] K. Cheng,[*3] H. En'yo,[*1] T. Hachiya,[*1,*4] S. Hasegawa,[*1,*5] M. Hata,[*4] H. Imai,[*1,*6] T. Kondo,[*7] C. Kuo,[*3] H. -S. Li,[*8] R. -S. Lu,[*9] E. Mannel,[*2] C. Miraval,[*2] I. Nakagawa,[*1] Y. Nakamura,[*1,*6] G. Nakano,[*1,*6] Y. Namimoto,[*1,*4] R. Nouicer,[*2] G. Nukazuka,[*1] R. Pisani,[*2] M. Shibata,[*1,*4] C. Shih,[*3] M. Shimomura,[*4] M. Stojanovic,[*8] Y. Sugiyama,[*4] R. Takahama,[*1,*4] W. -C. Tang,[*3] K. Toho,[*10] K. Tsuruta,[*10] M. Watanabe,[*4] and X. Wei[*8]

The intermediate tracker (INTT), consisting of 56 ladders of silicon strip detectors, is a tracking detector of charged particles for the sPHENIX experiment[1] at the Relativistic Heavy Ion Collider. So far, by using test pulses, radiation sources, cosmic rays, and proton test beams at Fermilab, we have confirmed that the performance required of the INTT ladders is mostly fulfilled. After the completion of the research and development of INTT, mass production and detector construction are now in progress.[2]

A silicon detector is expected to have a detection efficiency of almost 100%; however, we obtained an efficiency of 96.5 ± 0.5% from a previous test beam experiment.[3] This low efficiency may have been caused by the missing beam clock information in the experimental data because one cannot confirm whether each hit in the detectors originated from one beam particle without the beam clock information. Thus, the INTT data acquisition (DAQ) system was modified to save the beam clock information and accept an external trigger.

In December 2021, at Research Center for Electron Photon Science, Tohoku University, we performed a new test beam experiment[4] with the mass-produced ladders and the new INTT DAQ system. Three ladders were collinearly placed along the beamline and sandwiched by trigger plastic scintillators. A positron beam with an energy of 1 GeV impinged on these detectors.[3]

The detection efficiency $\epsilon(L_i)$ of the i-th ladder L_i is calculated as

$$\epsilon(L_i) = \frac{N(L_i \cap L_j \cap L_k)}{N(L_j \cap L_k)}, \quad (i,j,k = 0,1,2)(i \neq j \neq k) \tag{1}$$

where $N(x)$ is the number of hits under a condition x.

The events from noisy strips are excluded from the analysis. Hit clusters are formed by merging adjacent hits in a ladder before the calculation of detection efficiency. The strip ID of the hit clusters are determined by the weighted mean of the merged hits with their analog-to-digital conversion (ADC) value. The events in which the beam penetrates all ladders almost perpendicularly are used to evaluate the detection efficiency. The fired strip-ID difference between two ladders are utilized to select such events, as shown in Fig. 1. A smaller absolute value of the difference between the fired strip IDs corresponds to a smaller position difference in the plane perpendicular to the beam axis. The events inside the 2σ region in the fired strip-ID distribution (the region enclosed by dashed lines in Fig. 1) are treated as the coincidence condition in Eq. (1). The mean of the fired strip-ID difference is approximately 4, implying that the position difference between ladders is approximately 320 µm. The width of the distribution is governed by the angular spread of the beam. With the coincidence condition described above, the detection efficiencies of the three ladders are determined to be 99.53 ± 0.02%, 99.39 ± 0.03%, and 99.56 ± 0.02%, respectively. The high detection efficiency of the INTT detector is confirmed, implying that the detector is ready for the day-one experiment of sPHENIX.

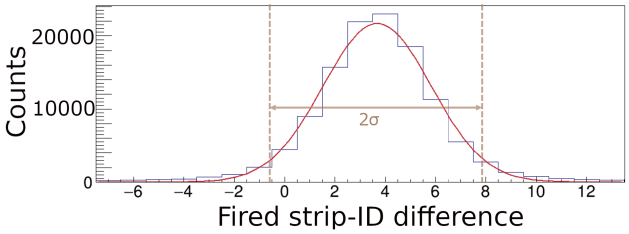

Fig. 1. Fired strip-ID difference between two ladders. The events in the 2σ region (enclosed by dashed lines) are used to evaluate the detection efficiency of each ladder.

*1 RIKEN Nishina Center
*2 Brookhaven National Laboratory
*3 Department of Physics, National Central University
*4 Department of Physics, Nara Women's University
*5 Japan Atomic Energy Agency
*6 Department of Physics, Rikkyo University
*7 Tokyo Metropolitan Industrial Technology Research Institute
*8 Department of Physics, Purdue University
*9 Department of Physics, National Taiwan University
*10 Department of Physics, Tohoku University

References

1) Conceptual Design Report of sPHENIX (2018).
2) I. Nakagawa *et al.*, in this report.
3) A. Suzuki, Master thesis, Nara Women's University (2019).
4) G. Nukazuka *et al.*, in this report.

Test beam experiment at ELPH in Tohoku University for sPHENIX INTT

G. Nukazuka,[*1] Y. Akiba,[*1] D. Cacace,[*2] H. En'yo,[*1] K. Cheng,[*3] T. Hachiya,[*1,*4] S. Hasegawa,[*1,*5] M. Hata,[*4] H. Imai,[*1,*6] T. Kondo,[*7] C. Kuo,[*3] H. -S. Li,[*8] R. -S. Lu,[*9] E. Mannel,[*2] C. Miraval,[*2] M. Morita,[*1,*4] I. Nakagawa,[*1] Y. Nakamura,[*1,6] G. Nakano,[*1,*6] Y. Namimoto,[*1,*4] R. Nouicer,[*2] R. Pisani,[*2] M. Shibata,[*1,*4] M. Shimomura,[*4] C. Shih,[*3] M. Stojanovic,[*7] Y. Sugiyama,[*4] R. Takahama,[*1,*4] W. -C. Tang,[*3] K. Toho,[*10] K. Tsuruta,[*10] M. Watanabe,[*4] and X. Wei[*8]

The sPHENIX[1] collaboration will start data acquisition from 2023 to study quark-gluon plasma and cold quantum chromodynamics at the Relativistic Heavy Ion Collider (RHIC) in Brookhaven National Laboratory. The intermediate silicon tracker (INTT),[2] one of the tracking detectors in the sPHENIX detector complex, plays a crucial role in tracking and jet flavor tagging with high precision and low background. Fifty-six INTT ladders with about 370 thousand silicon strips in total form a double-layer barrel to surround the interaction point. The position and timing resolutions of the prototype showed satisfactory performance in the previous experiment at Fermilab in 2019. Although a detection efficiency of 100% is expected owing to its high sensitivity to ionizing radiation, a detection efficiency about 96% was obtained in the experiment.[3] An internal clock of 9.4 MHz (beam clock, BCO) in the system drove the INTT while the signals synchronized with the beam collision drove at RHIC. The timing mismatch of the BCO and the beam may explain the insufficient detection efficiency. The insufficient detection efficiency in the experiment may be due to the unsynchronized operation of INTT with the test beam.

We performed a test beam experiment in December 2021 to test the hypothesis and perform the following:

- Tests and performance evaluation of the mass-production ladders
- Tests of the long readout extension cable of 1.2 m[4]
- Analog-digital converter distribution measurements with various beam injection angles with respect to the INTT ladders
- Performance evaluation of the ladders in a multi-track condition similar to that in RHIC by installing a lead plate the upstream of the setup

We measured hits on INTT ladders with a positron beam of 1 GeV at the Research Center for Electron Photon Science (ELPH) in Tohoku University. A dark box containing four INTT ladders, which have 6656 strips in the active area of about 465.5×20.0 mm^2, was set on the beamline, and two plastic scintillators were placed upstream and downstream as external triggers (Fig. 1). Depending on the trigger and veto configurations, the trigger rate was up to 100 Hz. Three of the ladders could take hit data successfully. A readout card acquires hit information from the ladders, and the DAQ stores hit coincidences with the external trigger signal. A fingertip scintillator was installed additionally to restrict the position of the hits in analysis.

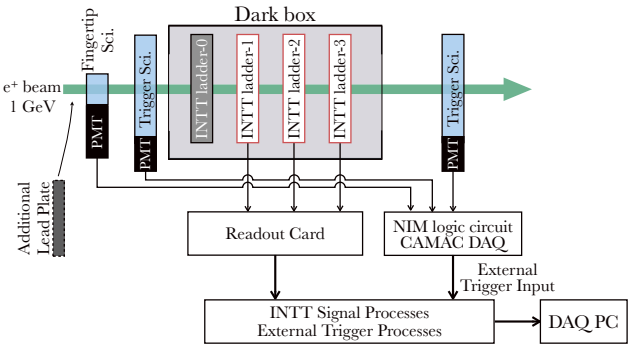

Fig. 1. Schematic diagram of the setup.

Data acquisition for about 50 h, divided into 65 runs, collected about 4×10^7 hits (Fig. 2). A hit map of ladder-1 with a typical setup (Fig. 3) shows the beam profile clearly. Data analysis is currently ongoing, and preliminary results for the detection efficiency are discussed in this report.[5]

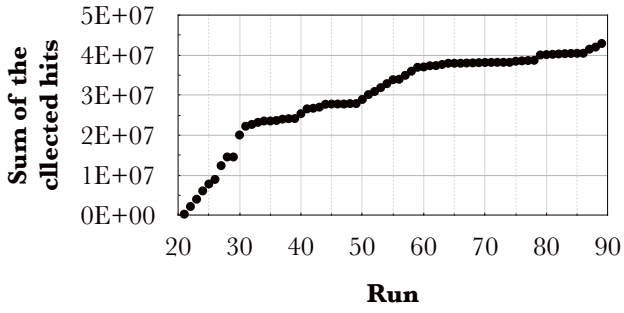

Fig. 2. Sum of the collected hits on the INTT ladders.

*1 RIKEN Nishina Center
*2 Physics Department, Brookhaven National Laboratory
*3 Department of Physics, National Central University
*4 Department of Mathematical and Physical Sciences, Nara Women's University
*5 Japan Atomic Energy Agency
*6 Department of Physics, Rikkyo University
*7 Tokyo Metropolitan Industrial Technology Research Institute
*8 Department of Physics and Astronomy, Purdue University
*9 Department of Physics, National Taiwan University
*10 Laboratory for Nuclear Science, Tohoku University

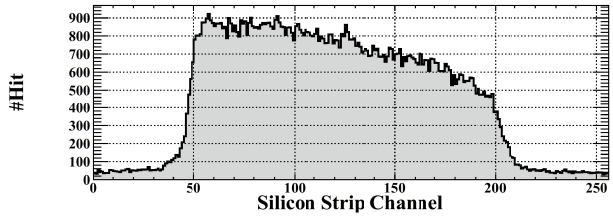

Fig. 3. Hit map of ladder-1.

References

1) A. Adare *et al.*, sPHENIX proposal (2015).
2) I. Nakagawa *et al.*, in this report.
3) A. Suzuki, Master thesis, Nara Women's University (2020).
4) T. Hachiya *et al.*, in this report.
5) M. Morita *et al.*, in this report.

Computing and network environment at the RIKEN Nishina Center

T. Ichihara,[*1] Y. Watanabe,[*1] and H. Baba[*1]

We operate the Linux cluster systems[1] at the RIKEN Nishina Center (RNC).

Figure 1 shows the current configuration of the Linux servers at the RNC. Scientific Linux (SL) 7 and CentOS 8 have been installed in these systems.

CentOS 8 was released in September 2019, and it was announced that support will be planned until 2029. However, in December 2020, there was a sudden announcement that support would end at the end of 2021. Therefore, we need to replace CentOS 8. In the high-energy and nuclear physics community, it has been proposed to migrate from CentOS 8 to CentOS stream 8.[2] Therefore, we have migrated CentOS 8 to CentOS stream 8 in December 2021.

The host *RIBF.RIKEN.JP* is used as the mail server, NFS server of the user home directory, and NIS master server.

The hosts *RIBFSMTP1/2* are the mail gateways used for tagging spam mails and isolating virus-infected mails. The latest version of Sophos Email Protection-Advanced (PMX 6.4.9) was installed. The support for Sophos PMX is scheduled to end in July 2023. Figure 2 shows the mail trends in 2021. Approximately 33% of the incoming mails were blocked by the PMX ip-blocker.

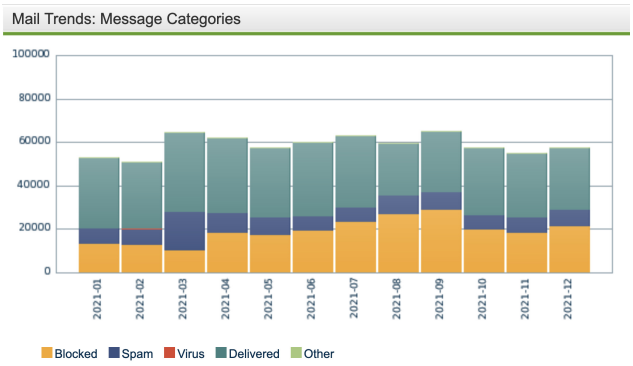

Fig. 2. Mail trends: message categories in 2021.

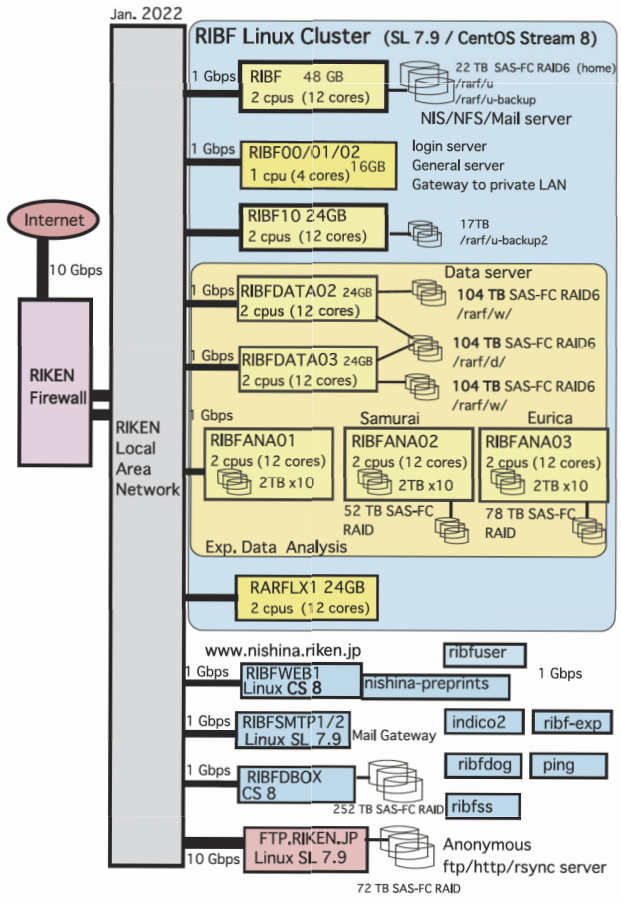

Fig. 1. Configuration of the RIBF Linux cluster.

A new TeX software, TeX Live 2021 was installed in the *RIBF00* and *RIBF01* servers. The Japanese font in TeX was changed from IPAex font to HaranoAji-Fonts.[3]

Temperature control in the computer server room is important to prevent failure. The latest Cacti software[4] was installed in the server *RIBFSS*, which monitors the temperature of the server rooms and some experimental rooms.

An anonymous ftp server, *FTP.RIKEN.JP*, is managed and operated at the RNC. Major Linux distributions are mirrored daily for the convenience of the users, and for facilitating high-speed access. Linux distributions Alma Linux, Rocky Linux, and Springdale Linux, which are binary compatible to the Red Hat Enterprise Linux, were newly archived in the server in 2021.

We have been operating approximately 70 units of wireless LAN access points in RNC for the convenience of experiments and daily work. Two units of new wireless LAN access points (WAPM1266R) were installed in the experimental hole of the Linac Bldg. in 2021.[5]

References

1) T. Ichihara *et al.*, RIKEN Accel. Prog. Rep. **54**, 120 (2021).
2) `https://linux.web.cern.ch/`.
3) `https://github.com/trueroad/HaranoAjiFonts`.
4) `https://www.cacti.net/`.
5) `https://ribf.riken.jp/comp/net/wireless.html`.

*1 RIKEN Nishina Center

CCJ operations in 2021

S. Yokkaichi,[*1] H. En'yo,[*1] T. Ichihara,[*1] W. Nakai,[*1] and Y. Watanabe[*1]

Overview

The RIKEN Computing Center in Japan (CCJ)[1] commenced operations in June 2000 as the largest offsite computing center for the PHENIX[2] experiment being conducted at RHIC. Since then, CCJ has been providing numerous services as a regional computing center in Asia. We have transferred several hundred terabytes of raw data files and nDST [a] files from the USA.

Many analysis and simulation projects are being conducted at CCJ, which are listed on the web page `http://ccjsun.riken.jp/ccj/proposals/`. As of December 2021, CCJ has contributed to 46 published papers and 45 doctoral theses.

Computing hardware and software

The network configuration and computing hardware (nodes) and software (OS, batch queuing systems, database engine, *etc.*) are almost the same as described in the previous APR[3] and the number of servers are summarized in the Table 1. One of disk servers, which had a 13-TB built-in RAID, was replaced by one with 39 TB in November. The main server (users' home directory, NIS, DNS, and NTP) and SAS RAID will be replaced in March 2022. In 4Q 2021, Hewlett-Packerd hardware was in short supply, owing to the "semiconductor crisis." Thus, we gave up to purchase built-in RAID as the previous server had. In addition, we operate two dedicated servers for the RHICf group[4] and two servers for the J-PARC E16 group[5] in order to maintain their dedicated compilation and library environments along with some data.

Table 1. Number of servers and disk sizes.

	number	disk (TB)	(type)
main server	1	21 + 13	DL380eG8
login server	2	-	DL145G3/DL20G9
interactive server	3	-	-/DL320G6/DL160G9
calculation server 1	16	10	DL180G6
calculation server 2	8	20	DL180G6
work disk server (replaced in Nov.)	2	26 / 13 →39	DL180G9/DL180G6 →DL385G10
DB server	1	1	DL145G3
library(AFS) server	1	9	DL180G6
transfer server	2	12 / 39	DL180G9/DL380G10
docker test server	1	-	DL20G9

We operate 25 computing nodes, and 328 (= 8 × 17 nodes + 24 × 8 nodes) jobs can be processed simultaneously by these computing nodes using a batch queuing system, LSF 9.1.3.[6] Table 2 lists the number of malfunctioning SATA or SAS disks in the HP servers, namely, computing nodes and NFS/AFS servers. The OS of nine calculation nodes and of one interactive server were upgraded to SL7.9 from SL5.3[7] in October, and the remainder will be upgraded in March 2022.

Three 10-KVA UPSs are operated as power supplies for these CCJ nodes and their batteries were replaced in March.

Table 2. Number of malfunctioning HDDs in HP servers during 2011–2021.

Type (TB)	total	21	20	19	18	17	16	15	14	13	12	11
SATA (1.0)	192	10	9	8	16	18	8	14	11	16	20	9
SATA (2.0)	120	9	5	10	2	10	2	10	0	2	5	4
SATA (4.0)	26	2	0	0	0	-	-	-	-	-	-	-
SATA (6.0)	20	0	0	0	0	-	-	-	-	-	-	-
SAS (0.15)	38	5	3	6	3	1	5	3	2	0	1	1
SAS (0.3)	26	2	1	2	0	1	0	1	1	0	0	1

Joint operation with ACCC/HOKUSAI

CCJ and the RIKEN Integrated Cluster of Clusters (RICC) have been jointly operated since July 2009. In April 2015, a new system named "HOKUSAI Greatwave"[8] was launched by RIKEN Advanced Center for Computing and Communication (ACCC), and the joint operation with CCJ continued, with the inclusion of a new hierarchical archive system in which approximately 1060 TB of CCJ data were stored as of December 2021. A breakdown of the data is presented in Table 3. Data transfer from J-PARC was performed in February and June during an experiment of over 18 and 12 days, and 28 and 46 TB of raw data were transferred to CCJ, respectively. The data were archived in a tape device in Hokusai.[8]

Table 3. Tape usage in Hokusai as of December 2021.

user	total	PHENIX official	KEK/ J-PARC	RHICf	user-level archive
size (TB)	1059	749	171	8	130

References
1) `http://ccjsun.riken.jp/ccj/`.
2) `http://www.phenix.bnl.gov/`.
3) S. Yokkaichi *et al.*, RIKEN Accel. Prog. Rep. **54**, 121 (2021).
4) Y. Itow *et al.*, arXiv:1409.4860 (Proposal).
5) S. Yokkaichi, in this report.
6) `https://www.ibm.com/docs/en/spectrum-lsf/`.
7) `http://www.scientificlinux.org/`.
8) `https://i.riken.jp/en/supercom/`.

[*1] RIKEN Nishina Center

[a] term for a type of summary data files in PHENIX

III. RESEARCH ACTIVITIES II
(Material Science and Biology)

1. Atomic and Solid State Physics (Ion)

Crystal growth and β-NMR studies of the simplest copper oxide (CuO)

H. Yamazaki,[*1] A. Gladkov,[*1] X. G. Zheng,[*2] A. Yamamoto,[*3] Y. Ichikawa,[*1] A. Takamine,[*1] H. Nishibata,[*4] K. Asahi,[*1] K. Kawata,[*1,*5] K. Imamura,[*1] M. Tajima,[*1] K. Tsubura,[*1] and H. Ueno[*1]

The significance of oxide-based systems both in technology and basic science has been strongly emphasized. Particularly, the strong electronic correlation caused by Coulomb repulsion in the Cu-O framework is recognized to play a key role in describing many unconventional experimental observations. Even now, however, the origin of the high-T_c superconductivity in copper oxides remains unclear. Meanwhile, another novel function of copper oxide was found about twenty years ago. The simplest copper oxide, CuO (cupric oxide, tenorite), which crystallizes in a monoclinic structure with the space group C2/c, was found to show a cross-correlation effect in one of its magnetically ordered states in the temperature range between 213 K and 230 K.[1)] In this so-called "multiferroic" phase, unconventional ferroelectricity emerges with the emergence of specific magnetic ordering.[2)] The theoretical proposal by Katsura-Nagaosa-Baratzky argues the microscopic polarization of electrons at oxygen sites in association with a noncollinear magnetic structure;[3)] however, no microscopic evidence of the polarization has been demonstrated so far.

CuO single crystals were grown in quartz tubes using the chemical vapor transport method (Fig. 1).[4)] Using ^{17}O-rich oxygen gas, single crystals of CuO with the oxygen sites substituted with ^{17}O nuclei ($S = 5/2$) were also prepared for comparative ^{17}O-NMR experiments. A large plate-like crystal was typically ∼10 mm in diameter. SEM images indicate that each crystal is composed of twinned single crystals, in which we can in many cases identify two different rotated images of structural domains with their c-axes nearly perpendicular to the sample plane. X-ray diffraction measurements were carried out to check the quality of the samples in detail. Magnetic susceptibility measurements showed that the magnetic phase transition temperatures and sharpness of the transitions were in good agreement with the literature data for high-quality CuO single crystals.

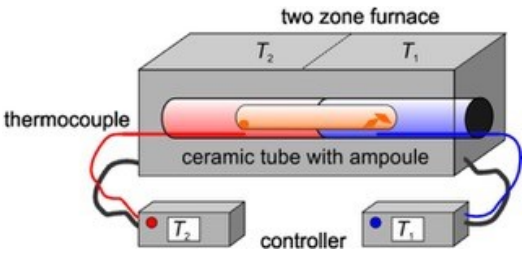

Fig. 1. Conceptual diagram of the chemical vapor transport method for the growth of CuO crystals.

We performed β-NMR/NQR experiments using a ^{21}O ($S = 5/2$) beam, where we used the nuclear reaction ^{22}Ne + ^{9}Be → ^{21}O + X for a ^{22}Ne energy of 70 MeV/nucleon with 250 particle nA. The β-rays emitted from the implanted ^{21}O nuclei were detected with plastic scintillator telescopes located above and below the sample crystal. The resonance frequency can be derived from the peak or dip observed in the spectrum of the up/down ratio of the β-ray count. We were allocated the following accelerator beamtime at the E6 (RIPS) beam port in the RIBF facility: (1) 114 h [2–7 September, 2016] and (2) 111 h [10–14 March, 2020]. The former was mainly used to evaluate the nuclear magnetic moment μ and the nuclear quadrupole moment Q inherent to ^{21}O. Typical NQR spectra are shown in Fig. 2. The following results were obtained: $\mu = 1.5118 \pm 0.0012$ and $Q = 17.4 \pm 2.4$ emb. Based on this achievement, during the latter beamtime, we attempted to obtain the β-NMR spectra for the ^{21}O nuclei implanted in CuO crystals at room temperature. This time, we could not observe a clear NMR signal of ^{21}O in CuO, although our experiments were performed for CuO in the paramagnetic phase ($T > 230$ K). It is considered that the magnetic low-dimensional correlations, which remain up to ∼550 K,[5)] possibly affected the polarization of the implanted ^{21}O, leading to a reduction of the polarization. At the next beam time allocated in FY2022, we will also have to check some technical issues such as the degree of beam collimation and the thickness of the CuO crystal.

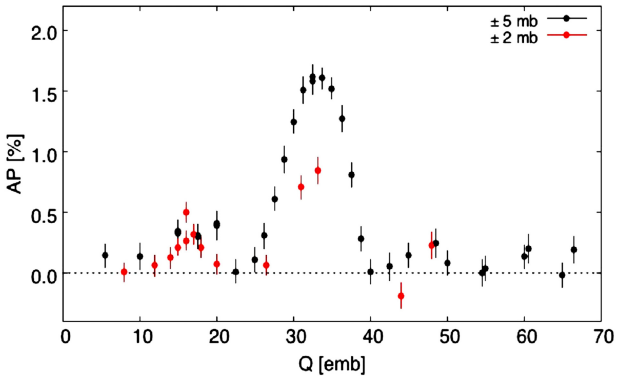

Fig. 2. NQR spectra of ^{21}O in TiO_2 reference crystals.

*1 RIKEN Nishina Center
*2 Department of Physics, Saga University
*3 Graduate School of Engineering and Science, Shibaura Institute of Technology
*4 Department of Physics, Kyushu University
*5 Center for Nuclear Study, University of Tokyo

References

1) X. G. Zheng *et al.*, J. Phys. Soc. Jpn. **70**, 1054 (2001).
2) T. Kimura *et al.*, Nat. Mater. **7**, 291 (2008).
3) H. Katsura *et al.*, Phys. Rev. Lett. **98**, 027203 (2007).
4) X. G. Zheng *et al.*, J. Appl. Phys. **92**, 2703 (2002).
5) T. Shimizu *et al.*, J. Phys. Soc. Jpn. **72**, 2165 (2003).

Single-event damages on SiC junction barrier Schottky diodes

M. Iwata,[*1] M. Takahashi,[*1] and H. Shindou[*1]

Silicon carbide (SiC) power devices are being applied to various fields because of their excellent properties such as high breakdown voltage and high frequency. Although Si power devices have been used for space applications, there is an urgent demand for SiC power devices for realizing future advanced missions. The mechanisms of single-event effects (SEEs) on SiC devices caused by heavy ions are yet to be well understood, and there is no product that is sufficiently resistant against space radiation. In this study, irradiation test results for SiC diodes that use a junction barrier Schottky (JBS) structure, as shown in Fig. 1 are reported. This structure is widely used in commercial products because of its lower off-state leakage current.[1)]

In this study, the charge collection characteristics of the 1200 V commercial SiC JBS diodes were measured by the EPICS system[2)] during irradiation. This system enabled measurements of higher signal levels of ∼50 nC, which is sufficient for detecting the sign of the single-event burnout (SEB). Irradiation tests were performed by bombarding ^{136}Xe ions (544 MeV) perpendicularly at the test device surface at room temperature in air using RIKEN RILAC2 in combination with the RIKEN Ring Cyclotron (RRC). The range of ions was calculated as 30.0 μm in SiC by the SRIM code;[3)] this range is sufficient to reach the active layer of the samples.

Figure 2 shows the collected charge spectra at different reverse voltages, V_R. The cross marks represent the maximum collected charge for each spectrum. The total counts of the spectra at V_R = 240 V increased significantly, especially at lower charges, and therefore, it did not show the accurate number of the ion-induced charge. This result indicates that a permanent leakage path was created at this voltage. The maximum collected charge did not reach the order of nanocoulombs, which is observed as the sign of the SEB in Si power metal-oxide-semiconductor field-effect transistors (MOSFETs). This

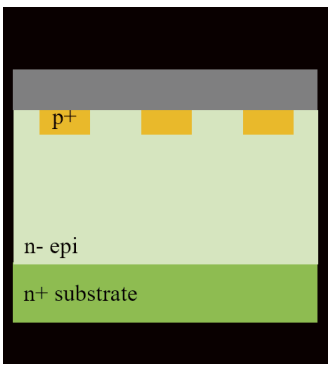

Fig. 1. Cross-sectional structure of JBS diodes.

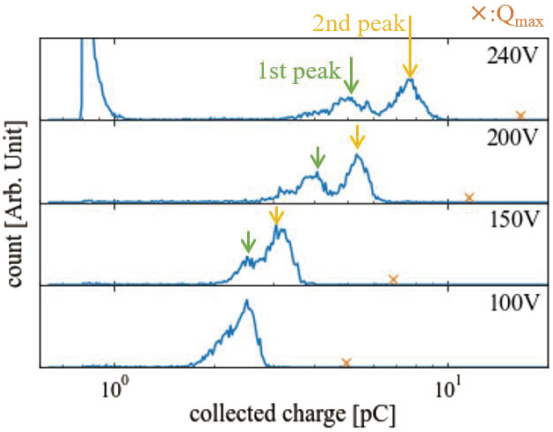

Fig. 2. Collected charge spectra taken by the EPICS system.

is attributed to the higher electron-hole pair creation energy of SiC compared to that of Si and the lack of a charge amplification mechanism like the parasitic bipolar transistor in MOSFETs in the JBS diodes. If a leakage path was created by local heating, a considerably large current would flow instantaneously in a tiny area. Transient current measurement is required to clarify the failure mechanism because charge collection measurements cannot check the time distribution of the collection process.

The peaks of the spectra shifted to the higher charge level, and the charge distribution was gradually divided into two with an increase in V_R. It is assumed that these two peaks appear based on whether the heavy ions pass through the Schottky interface or the p+ region because only one peak is observed in our previous experiment of the planar type SiC-SBD devices.[4)] The ratio of these peak levels indicate that the charge level of the first peak corresponds to the case wherein the incident ion passes through the p+ region, while the second peak level corresponds to the one wherein the incident ion passes through the Schottky region. Further, it is assumed that the charge generated by ions passing through the Schottky region is amplified further by impact ionization because the fluctuation in the positions of the second peaks are larger than those of the first peaks. Therefore, it might be possible to increase the voltage at which the leakage path is formed by adjusting the size, pitch, and doping concentration of the p+ region such that the electric field applied to the Schottky region is relaxed.

*1 Research and Development Directorate, Japan Aerospace Exploration Agency

References
1) X. She *et al.*, IEEE Trans. Ind. Electron. **64**, 10 (2017).
2) S. Kuboyama *et al.*, IEEE Trans. Nucl. Sci. **39**, 6 (1992).
3) J. F. Ziegler *et al.*, SRIM: the Stopping and Range of Ions in Matter, `http://www.srim.org/`.
4) S. Kuboyama *et al.*, IEEE Trans. Nucl. Sci. **53**, 6 (2006).

Analysis of diffraction patterns of laser spots in dual-microbeams generated by glass capillary optics for future biological use

K. Inayoshi,[*2,*1] T. Ikeda,[*1,*2] K. Ono,[*2,*1] Y. Kozu,[*2] K. Sangu,[*2,*1] Y. Hikima,[*2,*1] and W. -G. Jin[*2]

We have developed an ion microbeam irradiation system employing tapered glass capillary optics for biological use in the RIKEN Pelletron accelerator facility in the Nishina R&D Building. Glass capillary optics is a simple and reliable tool to generate ion/laser microbeams,[1–3] where both the ion and laser can be extracted from the capillary outlet simultaneously. When an end window is installed at the outlet, the microbeams can be applied to targets in the liquid/gas phase. At the microbeam irradiation port, cultivated living cells in a liquid medium or parts of small living insects in air are targets.[4] The corresponding irradiation lengths are expected to be a few micrometers or submillimeters for liquid and air, respectively. The ion species are H and He ions with energies of a few MeV so that the range in water (approximately 100 and 30 μm for H and He ions, respectively) approximately corresponds to the sizes of the biological targets. The maximum linear energy transfer (LET) is selected to be 80 or 240 keV/μm for H or He ions, respectively, which is sufficiently high to cause serious damage to DNA. In this ion irradiation, any mishits should be avoided because such a single ion hit may cause an undesirable effect on the living target. To realize precise ion targeting, a laser microbeam extracted from the same capillary is used as a laser sight of a μm-order scale. The laser microspot on the target consists of a center spot and higher order rings of diffraction, which are different from those of Fraunhofer diffraction. The higher order rings deteriorate the sharpness of the laser spot, which then reduces the accuracy of the laser sight. In this study, to understand the mechanism of ring generation, the brightness of each ring was measured according to the distance from the capillary outlet so that the results could be discussed based on ray tracing simulations. For this purpose, the distance range was selected to be in the order of 100 mm because larger ring images can provide detailed information of light trajectories. The end window was not introduced to obtain clear ring images.

Figure 1 shows the setup at Toho University. A visible light laser with a wavelength $\lambda = 488$ nm from a source (Photochemical Research Associates Inc. LA15R) entered a glass capillary with an outlet diameter of 62 μm, as shown in Figs. 2(a)–(c). The width of the input beam was approximately 570 μm at the full width at half maximum (FWHM).[2] Laser spots on a transparent screen were recorded by a digital camera for a distance L ranging from 120 to 300 mm, where L was defined as the distance between the capillary outlet and the screen. An ND filter was used to reduce the intensity of the input beam so that rings of a lower brightness were clearly

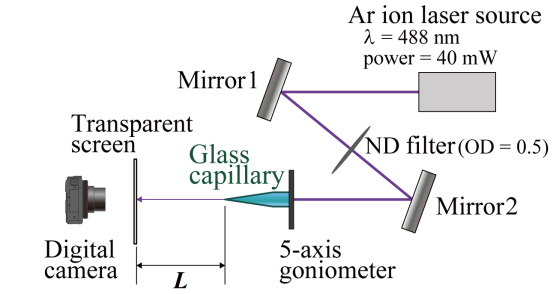

Fig. 1. Experimental setup to obtain diffraction patterns of laser spots. The distance L ranged from 120 to 300 mm.

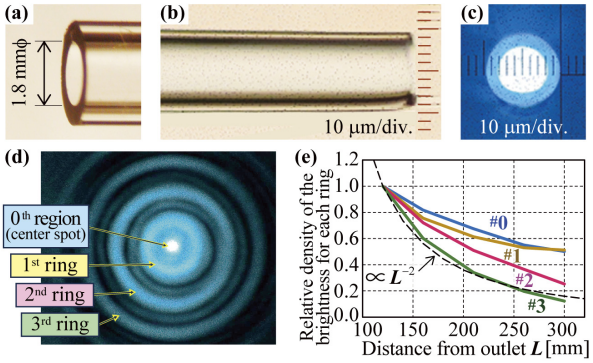

Fig. 2. (a) Capillary inlet, (b) capillary outlet with a diameter of 62 μm, (c) the downstream view of the outlet, (d) a typical laser spot on the screen, and (e) relative density of the brightness as a function of L.

recorded with an 8-bit dynamic range of the image files. A typical laser spot image is shown in Fig. 2(d) along with the definition of the center spot (0th region) and higher order rings (1st, 2nd, and 3rd rings). The total brightness of each component (0–3) was obtained by integrating over the area, and the brightness density was calculated by dividing by the area. To compare the L-dependence of each density, the density was normalized by that at $L = 120$ mm, as shown in Fig. 2(e) with a dashed line corresponding to L^{-2}. The density for the 3rd ring (#3) was found to follow the L^{-2} curve; that is, #3 was emitted from a point-like source, which may be owing to reflection at the inner surface around the outlet. Although curve #0 was expected to be constant because it was the component without any reflection inside the capillary, the curve was found to depend on L. The obtained behaviors of the curves will be compared with ray tracing simulation results.

References
1) T. Ikeda, Quantum Beam Sci. **4**(2), 22 (2020).
2) W.-G. Jin *et al.*, J. Phys. Soc. Jpn. **84**, 114301 (2015).
3) S. Kawamura *et al.*, J. Phys. Soc. Jpn. **89**, 055002 (2020).
4) T. Ikeda *et al.*, Nucl. Instrum. Methods Phys. Res. B **470**, 42 (2020).

*1 RIKEN Nishina Center
*2 Department of Physics, Toho University

2. Atomic and Solid State Physics (Muon)

μSR study on the low-temperature anomaly in triangular-lattice antiferromagnet CuOHCl

I. Yamauchi,[*1] X. G. Zheng,[*1] and I. Watanabe[*2]

Recently we found a new magnetodielectric triangular-lattice compound CuOHCl. It showed geometric frustration and antiferromagnetic transition at $T_N = 11$ K. Then we observed an anomaly below ~5 K, with magnetic susceptibility and specific heat change, as well as an increase in the dielectric constant.[1)]

Our μSR experiments on powder sample showed additional precession frequency for $T < 5$ K with an increase in its value. Considering the observed results of i) the small specific heat anomaly at 5 K; ii) the apparently stable antiferromagnetic spin arrangement revealed by neutron diffraction experiments; iii) the continuity of the other muon precession frequencies, and iv) the dielectric increase below 5 K, it is reasonable to assume a multiferroic transition occurring in CuOHCl.[1)] However, the mechanism for this multiferroic-like state is unclear and further study is demanded. Since we succeeded in growing single crystals, we proposed the use of single crystals for μSR experiments. Related experiments along three crystal-axis directions were planned, but unfortunately due to limited beam time, only a part of them were performed.

As shown in Fig. 1, we observed an additional muon spin precession frequency below $T \sim 5$ K, which suggests that the low-temperature change is an intrinsic property in CuOHCl and further detailed experiments using the single crystals should be planned.

A new result has been obtained from the present experiment. LF-μSR measurements as shown in Fig. 2 suggested a dynamical nature for the low-temperature state below ~5 K.

In summary, we performed ZF-μSR and LF-μSR on a newly found magnetodielectric compound CuOHCl using high-quality single crystals. The intrinsic nature of the low-temperature phase below $T <$ ~5 K has been verified. Further, persisting spin fluctuations have been found to exist in the low-temperature phase. There are only few experimental realizations of triangular-lattice, in special, multiferroic systems in slightly nonstoichiometric oxides, *i.e.*, $CuFeO_2$ ($S = 5/2$), $CuCrO_2/AgCrO_2$ ($S = 3/2$) and $RbFe(MoO_4)_2$($S = 5/2$).[2)] The present system provides a precious structurally two-dimensional triangular lattice showing quantum spin-related properties with perfect chemical stoichiometry.

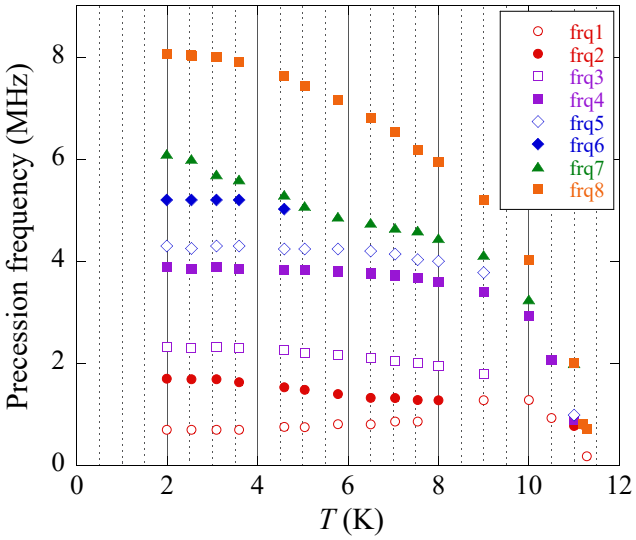

Fig. 1. Muon spin precession frequencies in single crystal CuOHCl.

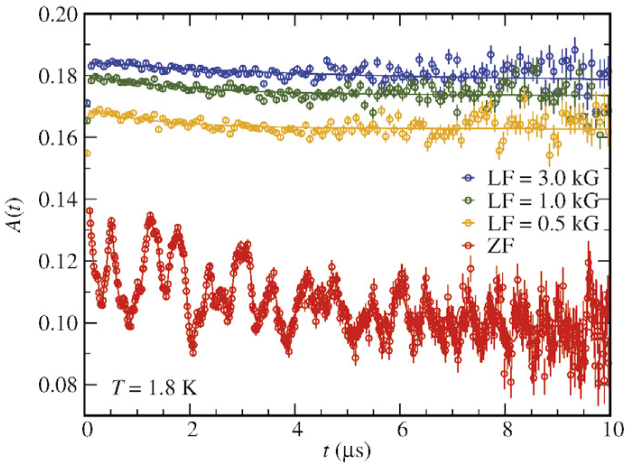

Fig. 2. μSR asymmetries in longitudinal external fields for single crystal CuOHCl.

References

1) X. -G. Zheng *et al.*, Phys. Rev. Mater. **2**, 104401 (2008).
2) Y. Tokura, Rep. Prog. Phys. **77**, 076501 (2014).

*1 Department of Physics, Saga University
*2 RIKEN Nishina Center

Zero-field μSR measurements to investigate the magnetic ordering of $Nd_2Ru_2O_7$

U. Widyaiswari,[*1,*2] H. Sakai,[*3] H. Hanasaki,[*3] D. P. Sari,[*4] B. Kurniawan,[*2] and I. Watanabe[*1,*2]

Pyrochlore oxides have a general formula $A_2B_2O_7$, where A and B represent trivalent rare-earth and tetravalent transition metal ions, respectively. The pyrochlore oxides are constructed from the interpenetrating corner-sharing tetrahedral lattices of A and B sites.[1] The spins at vertices of the tetrahedral lattice are magnetically frustrated and can lead to various novel physical properties.[1] The magnetic frustration, competition between the exchange and dipolar interactions, and crystal electric field effect control the nature of the ground state of pyrochlore oxide.[2]

Pyrochlore ruthenate, $A_2Ru_2O_7$, has Ru $4d^4$ electrons in the low-spin state with $S = 1$. In $Nd_2Ru_2O_7$, both Nd and Ru are magnetic ions. The magnetic ground state of $Nd_2Ru_2O_7$ is an interesting research topic because we can investigate the coupling between Nd and Ru spins by comparing it with that of $Nd_2Ir_2O_7$ known to have Ir^{4+} ions with $5d$ electrons, and they show ferromagnetic coupling between Nd and Ir spins.[3] $Nd_2Ru_2O_7$ showed magnetic anomalies around 1.8 K, 21 K, and 146 K.[4,5] At 1.8 K and 146 K, the magnetic transition were attributed to the ordering of Nd and Ru spins, respectively.[4] The origin of the anomaly at 21 K remains debatable.[4,5] Accordingly, we investigated the magnetic properties of $Nd_2Ru_2O_7$ using various measurement techniques such as muon spin relaxation (μ^+SR) measurement.

The polycrystalline $Nd_2Ru_2O_7$ was prepared using a solid-state reaction method. μ^+SR experiments were carried out on an HiFi spectrometer at the ISIS, Rutherford Appleton Laboratory in the UK and on the ARTEMIS spectrometer at Material and Life Science Experiment Facility (MLF), J-PARC in Japan. We measured the μ^+SR time spectra in the zero-field (ZF) condition at a temperature range of 2–150 K on HiFi, whereas the time spectra below 5 K down to 0.3 K were obtained by using Heliox cryostat on ARTEMIS.

The oscillations do not occur in the ZF-μ^+SR time spectra of $Nd_2Ru_2O_7$, as shown in Fig. 1(a). However, the decreases in the initial asymmetry at $t = 0$ was observed by decreasing the temperature indicating the appearance of a magnetic ordered state. The time spectra were analyzed using two exponential functions as

$$A(t) = A_1 \exp(-\lambda_1 t) + A_2 \exp(-\lambda_2 t) \quad (1)$$

The first and second components of Eq. (1) correspond to the slow and fast components of muon spin relaxation, respectively, and λ represents the muon-spin relaxation rates.

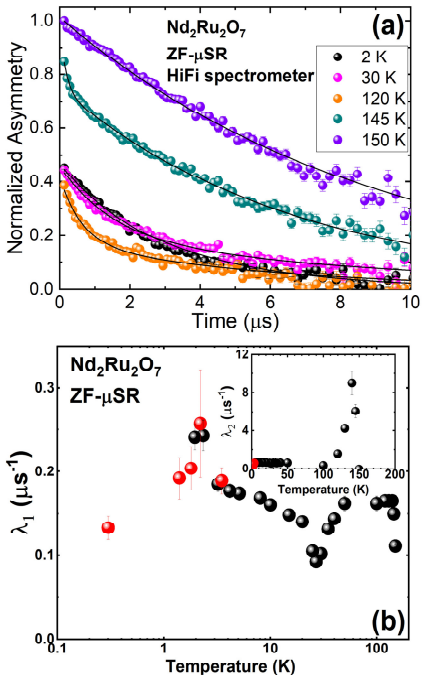

Fig. 1. (a) ZF-μ^+SR time spectra of $Nd_2Ru_2O_7$. (b) Temperature dependence of λ_1; the inset shows the temperature dependence of λ_2.

The appearance of Ru ordering at 146 K is confirmed from a sharp peak observed in $\lambda_2(T)$, as shown in the inset of Fig. 1(b). λ_1 decreases below 50 K with decreasing temperature and shows a dip around 30 K; this anomaly is not related to the anomaly at 21 K observed from the DC susceptibility measurement, which was expected from the magnetic property of Nd_3RuO_7.[6] Therefore, the anomaly around 30 K in the temperature dependence of λ_1 could be related to the short-range magnetic interaction of Nd spins. The long-range ordering of Nd spins was expected to appear around 2 K, as indicated by a peak in the temperature dependence of λ_1. Currently, we cannot determine the magnetic interaction between Nd and Ru spins. Further investigation using continuous muon beam is required to determine the internal field as a function of temperature that occurred in this system.

*1 RIKEN Nishina Center
*2 Department of Physics, Universitas Indonesia
*3 Department of Physics, Graduate School of Science, Osaka University
*4 Innovative Global Program, Shibaura Institute of Technology

References
1) J. S. Gardner *et al.*, Rev. Mod. Phys. **82**, 53 (2010).
2) B. C. D. Hertog *et al.*, Phys. Rev. Lett. **84**, 3430 (2000).
3) R. Asih *et al.*, J. Phys. Soc. Jpn. **86**, 024705 (2017).
4) S. T. Ku *et al.*, J. Phys. Condens. Matter **30**, 155601 (2018).
5) M. W. Gaultois *et al.*, J. Phys. Condens. Matter **25**, 186004 (2013).
6) U. Widyaiswari *et al.*, Mater. Sci. Forum **1028**, 3 (2021).

Spin dynamics of $Nd_2Pt_2O_7$ at 0.3 K observed by longitudinal-field μSR measurements

U. Widyaiswari,[*1,*2] Y. S. Chen,[*3] J. Kung,[*4] B. Kurniawan,[*2] L. J. Cheng,[*3] and I. Watanabe[*1,*2]

Pyrochlore oxides, $A_2B_2O_7$ (A = trivalent rare-earth ion and B = tetravalent transition metal ion), are constructed from the interpenetrating corner-sharing tetrahedra units of A and B sites.[1] The spins at the vertices of the tetrahedra units are magnetically frustrated and lead to various novel physical properties, such as spin-glass, spin-ice, and spin-liquid states.[1] In Nd-based pyrochlores, $Nd_2B_2O_7$, an Ising-type magnetic interaction occurs among the Nd spins with an easy local axis in the $\langle 111 \rangle$ direction; therefore, the spins point either in to or out from the center of the tetrahedra units.[2–4]

In $Nd_2B_2O_7$ with a nonmagnetic B ion, such as Zr, Hf, and Sn, an Nd spin static ordered state is accompanied by spin fluctuations.[2–4] This phenomenon can be explained by a spin fragmentation model based on the spin-wave theory.[5,6] Compared to $Nd_2B_2O_7$ (B = Zr, Hf, Sn) pyrochlores that have either full or empty d orbitals, $Nd_2Pt_2O_7$ has a nonmagnetic Pt^{4+} ion with a $5d^6$ orbital in a low-spin state, with a configuration of ${t_{2g}}^6$ ${e_g}^0$. The empty e_g orbital can affect the exchange interaction among the Nd spins and change the spin dynamics of $Nd_2Pt_2O_7$.

Previous muon spin relaxation (μSR) measurements on $Nd_2Pt_2O_7$ conducted at the Paul Scherrer Institute showed that the initial asymmetry at $t = 0$ neither oscillated not decreased in the time spectra.[7] It was inferred that the spin fluctuations smeared out the signal from the static ordered state, suggesting the occurrence of spin fragmentation. We observed an ordered state indicated by a sharp peak at approximately 1.5 K in the temperature dependence of the muon-spin relaxation rate, λ.[7] Persistent spin fluctuations were expected to occur from the observation of the remaining λ down to 0.3 K.[7] Accordingly, we conducted measurements by using a pulsed muon beam suitable for observing long-time relaxation and investigating the spin dynamics of Nd.

Polycrystalline $Nd_2Ru_2O_7$ was prepared by mixing the oxides precursors at 4 GPa and 1200°C, following the conditions obtained in a previous study,[8] using a high-pressure apparatus at the Department of Earth Sciences, National Cheng Kung University, Taiwan.[9] μSR experiments were carried out on ARGUS spectrometer at the ISIS, Rutherford Appleton Laboratory, UK. We measured the μSR time spectra in the longitudinal-field (LF) condition at 0.3 K.

The LF-μSR time spectra are shown in Fig. 1(a). At

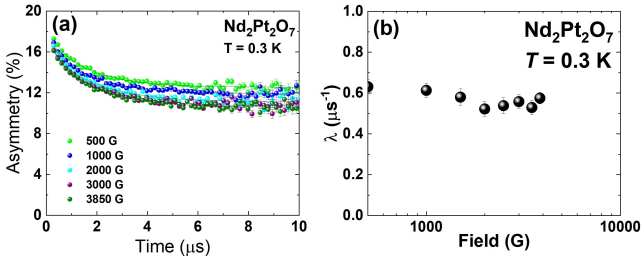

Fig. 1. (a) LF-μSR time spectra of $Nd_2Pt_2O_7$ at 0.3 K. (b) Field dependence of muon-spin relaxation rate at 0.3 K.

3850 G, the time spectrum shows a relaxation, indicating the persistent spin fluctuation at 0.3 K. The baseline shifting in the time spectra is attributed to the background signal when applying an external magnetic field because it also occurs in the paramagnetic state.

The time spectra were analyzed using two exponential functions:

$$A(t) = A_G \exp(-(\sigma t)^2/2) + A_E \exp(-\lambda t) \quad (1)$$

The first and second components of Eq. (1) are Gaussian-type and exponential-type components, respectively. This analysis function has been used to analyze the time spectra in the zero-field condition, where the Gaussian-type component occurs at early time spectra. For consistency, we kept the analysis functions to treat the time spectra. The Gaussian-type component was related to the static ordered state of Nd spins, whereas the exponential one corresponded to the spin dynamics of Nd. Fig. 1(b) shows that no significant change in λ occurs by applying an external field up to 3850 G. This suggests that the muon spin is depolarized by a strong spin fluctuation that occurs even at 0.3 K. Accordingly, from the previous and current μSR measurements, we suggest that the Nd spins are fragmented into two parts: a static ordered state and fluctuating spins.

*1 RIKEN Nishina Center
*2 Department of Physics, Universitas Indonesia
*3 Department of Physics, National Cheng Kung University
*4 Department of Earth Sciences, National Cheng Kung University

References
1) J. S. Gardner *et al.*, Rev. Mod. Phys. **82**, 53 (2010).
2) J. Xu *et al.*, Phys. Rev. B **94**, 064425 (2016).
3) V. K. Anand *et al.*, Phys. Rev. B **95**, 224420 (2017).
4) A. Bertin *et al.*, Phys. Rev. B **92**, 144423 (2015).
5) S. Petit *et al.*, Nat. Phys. **12**, 746 (2016).
6) O. Benton, Phys. Rev. B **94**, 104430 (2016).
7) U. Widyaiswari *et al.*, submitted.
8) H. R. Hoekstra, F. Gallagher, Inorg. Chem. **7**, 2553 (1968).
9) F. B. Hua *et al.*, Terr. Atmos. Ocean. Sci. **23**, 647 (2012).

Novel quantum spin liquid state in $Ba_3ZnRu_2O_9$

Y. Yasui,[*1] D. P. Sari,[*2] I. Watanabe,[*3] and I. Terasaki[*4]

We discovered a novel type of quantum spin liquid in $Ba_3ZnRu_2O_9$, which has a hexagonal lattice of Ru^{5+} dimers.[1,2] In the temperature (T) dependence of the magnetic susceptibility (χ) of $Ba_3ZnRu_2O_9$, no trace of the Curie tail or glassy behavior has been detected down to 50 mK. We studied the magnetic behavior of the Nb-doped system, $Ba_3Zn(Ru_{1-y}Nb_y)_2O_9$, where Nb^{5+} $(4d)^0$ is a non-magnetic ion that disturbs the formation of the Ru^{5+} dimer. The χ-T curves of the Nb-doped system also show no trace of the Curie tail at low temperatures, indicating that the local Ru^{5+} spin induced by Nb-doping does not act like a free spin. The spin liquid state of $Ba_3ZnRu_2O_9$ has been found to be robust by impurity doping.

To study magnetic dynamics at low temperatures, we attempted to perform ZF-μSR and LF-μSR measurements on three samples of $Ba_3Zn(Ru_{1-y}Nb_y)_2O_9$ ($y = 0$, 0.06, and 0.12), down to 0.3 K. First, we performed ZF-μSR and LF-μSR measurements on $Ba_3ZnRu_2O_9$ using ARGUS. Figure 1 shows the ZF-μSR time spectra obtained at various temperatures for $Ba_3ZnRu_2O_9$. The muon-precession behavior with small amplitude was observed below ~35 K. The initial asymmetry began dropping below ~100 K and the relaxation rate λ_2 rapidly increased at ~100 K with decreasing T. In contrast, the internal field started developing from 80 K and saturated below 3 K at 450 G. These results simply indicate the appearance of long-range magnetic ordering with a tiny long-range ordered moment; however, a spin-liquid state is expected in this sample, as suggested from other studies. Nevertheless, the results of LF-μSR measurements suggest that the internal field is 500 G with a 40% volume fraction. These results indicate that the spin is still dynamic at 2 K and slows at 0.3 K. The spin system coexists with an antiferromagnetic long-range state with tiny ordered moments and dynamical spin liquid state.

Next, we performed similar measurements on $Ba_3Zn(Ru_{1-y}Nb_y)_2O_9$ with $y = 0.06$ and 0.12. However, owing to issues with the dilution refrigerator, we performed ZF-μSR and LF-μSR measurements at temperatures above 2 K on the sample with $y = 0.06$ using ARGUS. Moreover, we performed ZF-μSR measurements above 10 K on the sample with $y = 0.12$ using EMU. Although the temperature range was limited, we observed similar decreasing behavior in the initial asymmetry at ~100 K with decreasing T for $y = 0.06$ and 0.12. However, the muon-spin precession behavior was not observed in the measured temperature region for $y =$ 0.06 and 0.12, which may be due to the randomness effect by Nb-doping. Then, the overall scheme of the magnetic behavior was found to be similar for all samples with y = 0, 0.06 and 0.12.

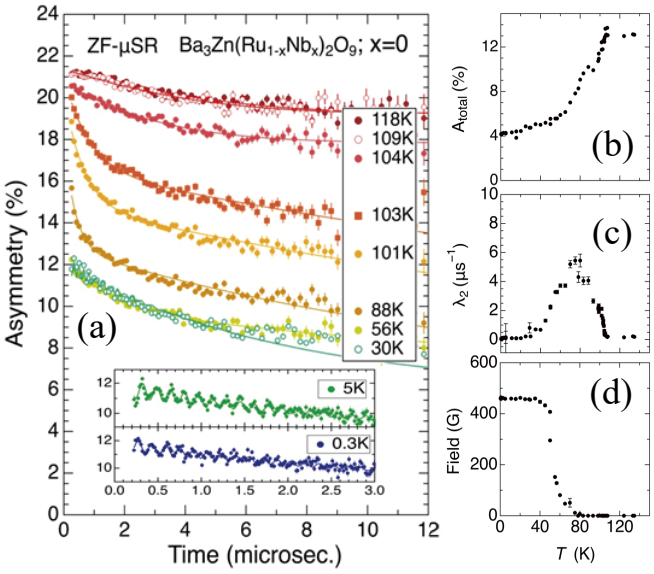

Fig. 1. (a) ZF-μSR time spectra of $Ba_3ZnRu_2O_9$ measured at various temperatures. Temperature dependence of (b) the initial asymmetry Atotal, (c) relaxation rate λ_2, and (d) internal field of $Ba_3ZnRu_2O_9$ deduced from the analysis of ZF-μSR time spectra.

Using these results, we consider a novel scenario in this system wherein a spin liquid state accommodates long-range magnetic ordering with a tiny ordered moment. When Nb substitution is increasing, the coexistence of a spin-liquid state with long-range magnetic ordering is suppressed by the random disconnection of the frustrated magnetic path, and magnetic ordering becomes smeared. Thus, detailed ZF-μSR and LF-μSR measurements are required, along with other measurements, for $Ba_3ZnRu_2O_9$ ($y = 0$, 0.06, and 0.12).

Recently, Tanaka and Hotta reported a theoretical study based on the intriguingly characteristics of the $Ba_3MRu_2O_9$ family.[3] They adopted Heisenberg exchange interactions, J, J', J'', and biquadratic interaction, B. Using a phase diagram with reasonable J, J', J'', and B parameters, they proposed the parameter regions of novel magnetic states such as the nonmagnetic singlet, Ferroquadrupolar nematic Bose-Einstein condensation (FQ-p-BEC), AFM-solid, AFM-BEC-coexistence, *etc.* states. It is significantly interesting in the correspondence between the theoretically proposed novel magnetic states and the experimental results of present materials.

*1 Department of Physics, Meiji University
*2 College of Engineering, Shibaura Institute of Technology
*3 Meson Science Laboratory, RIKEN
*4 Department of Physics, Nagoya University

References
1) I. Terasaki *et al.*, J. Phys. Soc. Jpn. **86**, 033702 (2017).
2) T. D. Yamamoto *et al.*, J. Phys. Condens. Matter **30**, 355801 (2018).
3) K. Tanaka, C. Hotta, Phys. Rev. B **101**, 094422 (2020).

μ^+SR Knight shift of the Mott insulator κ-$(ET)_4Hg_{2.78}Cl_8$

D. P. Sari,[*1,*2] Y. Cai,[*3,*4] M. -V. deToro Sanchez,[*5,*4] K. Kojima,[*3,*4] I. Watanabe,[*2] Y. Ishii,[*1] and H. Taniguchi[*6]

The hole-doped organic superconductor κ-$(ET)_4Hg_{3-\delta}Br_8$, (κ-HgBr), where $\delta = 11\%$ and ET = bis (ethylenedithio) tetrathiafulvalene, has been the key to bridge the knowledge gap between half-filled organics and doped cuprate systems, as the well-known Mott-Hubbard model in the laboratory. Usually, organic superconductivity appears under pressure when the ratio of Hubbard interaction and bandwidth, U/W, is larger than 1. Nonetheless, the triangular lattice of organics, unlike the square lattice in cuprates, provides extensive geometrically control through nearest, t, and next-nearest, t', transfer integrals between sites. In the case of geometrically triangular frustration ($t \sim t'$), the Mott insulating state cannot be magnetically ordered down to the miliKelvin (mK) order, becoming a Mott quantum spin liquid.[1)] Specifically, both hole-doped superconductors have a region corresponding to a strange metallic state at which resistivity exhibits a linear temperature dependence, $\rho \propto T$, which is not a Fermi-liquid (FL) behavior.[1–3)]

In 2015, an important model to study strange metal was developed by Sachdev-Ye-Kitaev (SYK).[4,5)] It consists of Majorana fermions with random all-to-all interactions, leading to quantum information science and quantum many-body physics. Although the realization of the SYK-strange metal remains complex, Tsuji-Werner theoretically found an SYK-strange metal region after an out-of-time-order correlation treatment of a multi-band Hubbard model.[6)] In the strange metal region, the electron behaves as a system having a non-FL electronic scattering rate with $\rho \propto T$. In this region, the spin fluctuates strongly while adjusting the competition between the localized spin in the Mott insulating state and the itinerant one in the FL state, and U/W should be close to unity, which is known as a quantum critical point (QCP).[6)] Cha *et al.* further showed that when the itinerant spin-1/2 fermions interact via onsite U and random infinite-ranged spin-spin interaction, the QCP appears with quantum spin liquid dynamics, identical to that of SYK-local spin dynamics.[7)] On the other hand, the growth of antiferromagnetic spin fluctuations (AFSFs) towards low temperature without any long-range order can lead to the QCP at which a non-FL behavior is observed, like in the heavy fermion system.[1)]

Our experiment[8)] showed that the time-reversal symmetry is preserved in the superconducting state of κ-HgBr down to 0.3 K, narrowing the similarity down to that of cuprates despite the triangular lattice. To seek evidence of strong AFSFs towards the Mott spin-liquid ground state, we also study the sister insulating compound, which has a different doping content yet slightly higher U/W than that of κ-HgBr, κ-$(ET)_4Hg_{3-\delta}Cl_8$ (κ-HgCl), with $\delta = 22\%$. It shows a metal-insulator transition at $T_{MI} = 20$ K and ambient pressure.

The signature of strong AFSFs has been observed in κ-HgBr, in which the temperature dependence of μ^+ Knight shift, $K(T)$, is not proportional to that of susceptibility, $\chi(T)$ in the low-temperature region below 50 K, unlike in other κ-type organic superconductors; this signature is often found in heavy-fermion system.[1)] One possible reason is that μ^+ probes a hyperfine coupling constant different from itinerant electrons in the high-T region and localized electrons. From the linear part of the K-χ plot from 50 to 300 K, the hyperfine coupling constant, A_{hf}, in κ-HgBr was reported to be 166 Oe/μ_B. If this deviation is a signature of such a different hyperfine coupling constant, we naively expect a larger A_{hf} in κ-HgCl.

We have followed the same experimental condition to measure the μ^+ Knight shift in κ-HgCl with that of κ-HgBr.[9)] The measurement was performed using DC muon beam on the NuTime spectrometer in M15 beamline, TRIUMF Canada, in a field of 6 T. Figure 1 shows the measured μ^+SR time spectra after Fourier transforming. From 300 down to 2 K, the central peak is gradually shifted to the positive side, and a prominent shift was detected below T_{MI}. $K(T)$ follows Curie-

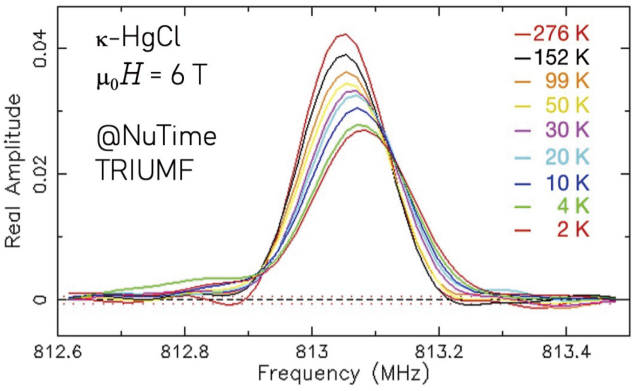

Fig. 1. Fourier transform of μ^+SR time spectra in the field of 6 T in κ-$(ET)_4Hg_{2.78}Cl_8$ measured at several temperatures, represented by colorful lines, from 276–2 K.

*1 College of Engineering, Shibaura Institute of Technology
*2 RIKEN Nishina Center
*3 SBQM Institute, University British Columbia
*4 CMMS, TRIUMF
*5 School of Physics and Astronomy, University of Edinburg
*6 Department of Physics, Saitama University

Weiss paramagnetic behavior well while $\chi(T)$ has a broad peak at 70 K. From the linear region of the K-χ plot above 100 K, our preliminary analysis obtained $A_{\rm hf} = 230(20)$ Oe/$\mu_{\rm B}$. The value is about 40% larger than that of κ-HgBr. Next, we are going to study the spin dynamics of κ-HgCl down to the mK order.

References

1) H. Oike *et al.*, Nat. Commun. **8**, 756 (2017).
2) B. Keimer *et al.*, Nature **518**, 179 (2015).
3) H. Taniguchi *et al.*, J. Phys. Soc. Jpn. **76**, 113709 (2007).
4) S. Sachdev, J. Ye, Phys. Rev. Lett. **70**, 3339 (1993).
5) A. Kitaev, J. Suh, J. High Energy Phys. **183** (2018).
6) N. Tsuji, P. Werner, Phys. Rev. B **99**, 115132 (2019).
7) P. Cha *et al.*, Proc. Natl. Acad. Sci. U.S.A. **31**, 18341 (2020).
8) D. P. Sari, RIKEN Accel. Prog. Rep. **54**, S30 (2021).
9) K. Satoh *et al.*, Physica B **404**, 597 (2009).

μSR study of the stabilization mechanism of antiferromagnetic state in molecular π-d system λ-(BEDT-STF)$_2$Fe$_x$Ga$_{1-x}$Cl$_4$

S. Fukuoka,[*1] Y. Ito,[*1] A. Kawamoto,[*1] D. P. Sari,[*2] and I. Watanabe[*3]

In some molecular conductors, the coexistence of strongly correlated π electrons and localized 3d spins is realized by introducing magnetic molecules, such as $FeCl_4^-$ and $FeBr_4^-$, as anion molecules. Such coexistent systems are known as π-d systems. In π-d systems, the magnetic interactions between strongly correlated π electrons and localized 3d spins (π-d interaction) give rise to interesting magnetic and conducting properties.

λ-(BEDT-STF)$_2$FeCl$_4$, where BEDT-STF denotes bis(ethylenedithio)dithiadiselenafulvalene, exhibits an antiferromagnetic ordering at 16 K.[1,2] In the alloy compound of λ-(BEDT-STF)$_2$Fe$_{0.2}$Ga$_{0.8}$Cl$_4$, an antiferromagnetic ordering is observed at 8 K. In contrast, λ-(BEDT-STF)$_2$GaCl$_4$ shows no magnetic ordering down to 300 mK. These results indicate that the introduction of π-d interaction stabilizes the antiferromagnetic ground state. However, the stabilization mechanism has not yet been demonstrated. This study aims to clarify the stabilization mechanism of the antiferromagnetic ground state induced by π-d interaction.

In this study, we performed zero field (ZF) μSR measurements below 10 K and longitudinal field (LF) μSR measurements at base temperature and 10 K for λ-(BEDT-STF)$_2$Fe$_{0.1}$Ga$_{0.9}$Cl$_4$ (Fe-0.1) and λ-(BEDT-STF)$_2$Fe$_{0.05}$Ga$_{0.95}$Cl$_4$ (Fe-0.05), respectively.

Figure 1 shows the temperature dependence of the ZF time spectra of Fe-0.1 and Fe-0.05. In this analysis, we fitted the time spectra by the following functions.

$$A(t) = A_0\exp(-\lambda_0 t) + G_{\mathrm{KT}}(t) + A_{\mathrm{bg}}, \quad (1)$$

$$A(t) = A_1\exp(-\lambda_1 t) + A_2\cos(\omega t + \phi)\exp(-\lambda_2 t) + A_{\mathrm{bg}}, \quad (2)$$

$$A(t) = A_3\exp(-\lambda_3 t) + A_4\exp(-\lambda_4 t) + A_{\mathrm{bg}}. \quad (3)$$

Here, A_i and λ_i denote the initial asymmetries and relaxation rates, respectively. A_{bg} is the background contribution derived from the muons stopped in the sample holder. $G_{\mathrm{KT}}(t)$ is the Kubo-Toyabe function. ω and ϕ are the precession frequency and phase of muon spin precession, respectively. The time spectra measured at high temperatures were fitted using Eq. (1), and those of Fe-0.1 and Fe-0.05 measured below 7 K were fitted using Eqs. (2) and (3), respectively.

We confirmed that the shape of the ZF time spectra of Fe-0.1 changes below 7 K, suggesting that an antiferromagnetic transition occurs around 7 K. In contrast, no clear change was observed in the shape of the ZF time spectra down to 1.5 K for Fe-0.05. As complementary experiments, we performed ^{13}C NMR measurements for λ-(BEDT-STF)$_2$Fe$_{0.05}$Ga$_{0.95}$Cl$_4$ and confirmed that no peak was observed in the temperature dependence of the spin-lattice relaxation rate ($1/T_1$) down to 4 K. These suggest that T_{N} of Fe-0.05 is lower than 4 K or does not exist and antiferromagnetic ordering is drastically stabilized in the small Fe content region below $x = 0.1$. These results are consistent with theoretical studies suggesting that the antiferromagnetic ground state is stabilized even for small π-d interactions.[3] However, our results indicate that there exists a phase boundary between the no- and antiferromagnetic-ordered states in the low Fe content region between $x = 0$ and 0.1, which is different from the theoretical prediction. Detailed analysis regarding the development of internal fields from the results of μSR time spectra and comparison with the results of theoretical studies are in progress.

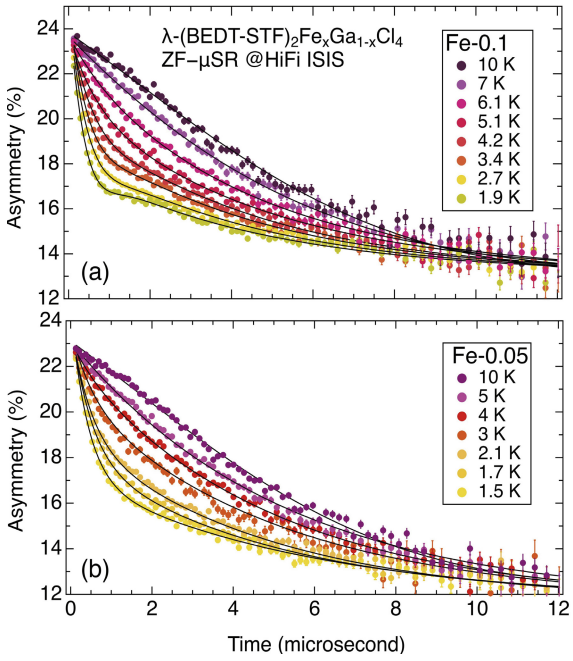

Fig. 1. Temperature dependence of the ZF time spectra of (a) Fe-0.1 and (b) Fe-0.05.

*1 Graduate School of Science, Hokkaido University
*2 College of Engineering, Shibaura Institute of Technology
*3 Meson Science Laboratory, RIKEN

References
1) S. Fukuoka *et al.*, Phys. Rev. B **101**, 184402 (2020).
2) S. Fukuoka *et al.*, J. Phys. Soc. Jpn. **87**, 093705 (2018).
3) H. Shimahara, K. Ito, J. Phys. Soc. Jpn. **83**, 114702 (2014).

μSR study of Fe-substitution effects on ferromagnetic fluctuations in nonsuperconducting heavily overdoped Bi-2201 cuprates

T. Adachi,[*1,*2] Y. Komiyama,[*2] D. P. Sari,[*1,*3] and I. Watanabe[*1]

Hole-doped high-T_c cuprate superconductivity arises by hole doping into a parent antiferromagnetic (AF) Mott insulator, suggesting that superconductivity is mediated by AF spin fluctuations in the underdoped and optimally doped regimes. For the overdoped regime, where superconductivity weakens and eventually disappears with hole doping, it has been theoretically suggested that a ferromagnetic (FM) phase exists in the nonsuperconducting heavily overdoped regime and competes with superconductivity.[1] In fact, zero-field (ZF) μSR and transport measurements have revealed an FM order/FM fluctuations in nonsuperconducting heavily overdoped $La_{2-x}Sr_xCuO_4$[2] and Bi-2201.[3] To understand the details of the FM fluctuations, we previously performed ZF-μSR at RIKEN-RAL in 5% Fe-substituted Bi-2201 single crystals of $Bi_{1.74}Pb_{0.38}Sr_{1.88}Cu_{1-y}Fe_yO_{6+\delta}$. It was found that the relaxation rate of the muon spins was significantly enhanced at low temperatures and a peak was observed at approximately 6 K, which coincided with the onset temperature of the hysteresis between the ZF-cooled and field-cooled magnetic susceptibility, T_{SG}.[4] These results suggest the occurrence of an FM cluster spin-glass state in which FM spin clusters are formed around Fe and the random orientation of the spins between the clusters results in the formation of a spin-glass state.[4] However, the details have not yet been clarified.

To further understand the Fe-substitution effects on FM fluctuations, we performed ZF and longitudinal-field μSR of 9.6% Fe-substituted single crystals of $Bi_{1.74}Pb_{0.38}Sr_{1.88}Cu_{1-y}Fe_yO_{6+\delta}$ with $y = 0.096$ using the HELIOX and VARIOX cryostats at the RIKEN-RAL.

Figure 1 shows ZF-μSR time spectra of the 9.6% Fe-substituted single crystals of $Bi_{1.74}Pb_{0.38}Sr_{1.86}Cu_{1-y}Fe_yO_{6+\delta}$ with $y = 0.096$. At high temperatures above 57 K, the spectra show Gaussian-like relaxations due to nuclear dipole fields randomly oriented at the muon site. Below 57 K, the muon spin relaxation becomes fast and an exponential-like behavior is caused by the development of spin correlation. At 4.1 K, a muon spin precession in a short-time region and slow relaxation in a long-time region are observed, suggesting the coexistence of a long-range magnetic order and slowly fluctuating spins in a sample.

The spectra were analyzed using the following function: $A(t) = A_0 \exp(-\lambda_0 t) G_Z(\Delta, t) + A_1 \exp(-\lambda_1 t) \cos(\omega_t + \phi) + A_{BG}$. The first, second, and third terms represent slowly fluctuating component, muon spin precession component, and background asymmetry, respectively. λ_0 was found to exhibit a peak at approximately 12 K, which almost coincides with T_{SG} determined from magnetic susceptibility.[4] The internal field at the muon site, B_{int}, was estimated from ω as ~92 G, which is comparable to Bint ~100 G obtained for overdoped Bi-2201, in which an incommensurate AF order is formed.[5] The magnetic volume fraction was estimated from the A_0 at the base temperature as ~33%, suggesting the coexistence of long-range ordered and slowly fluctuating regions.

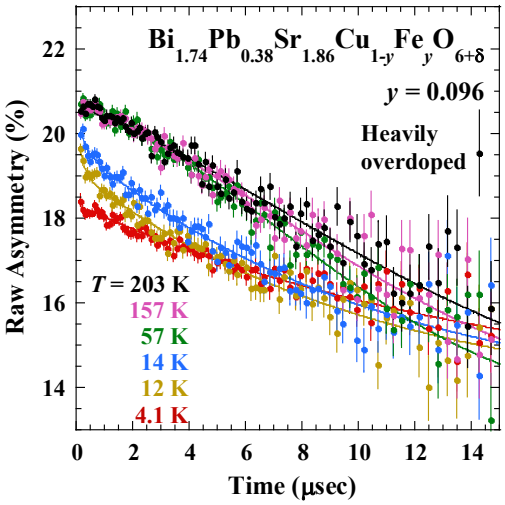

Fig. 1. ZF μSR time spectra of 9.6% Fe-substituted single crystals of $Bi_{1.74}Pb_{0.38}Sr_{1.86}Cu_{1-y}Fe_yO_{6+\delta}$ with $y = 0.096$.

The present results suggest that 9.6% Fe substitution forms a long-rage magnetic order, which is not observed in a 5% Fe-substituted sample. Accordingly, the FM fluctuations are probably stabilized by the Fe substitution. Concurrently, considering the similar values of B_{int} of the heavily overdoped and overdoped[5] samples, an incommensurate AF order might also occur in the heavily overdoped Bi-2201. How the AF and FM order/fluctuations coexist in the heavily overdoped Bi-2201 is to be clarified in future.

*1 RIKEN Nishina Center
*2 Department of Engineering and Applied Sciences, Sophia University
*3 College of Engineering, Shibaura Institute of Technology

References
1) A. Kopp *et al.*, Proc. Natl. Acad. Sci. U.S.A. **104**, 6123 (2007).
2) J. E. Sonier *et al.*, Proc. Natl. Acad. Sci. U.S.A. **107**, 17131 (2010).
3) K. Kurashima *et al.*, Phys. Rev. Lett. **121**, 057002 (2018).
4) Y. Komiyama *et al.*, J. Phys. Soc. Jpn. **90**, 084701 (2021).
5) H. Hiraka *et al.*, Phys. Rev. B **81**, 144501 (2010).

Hole-doping effect on the magnetic correlation in the undoped (Ce-free) superconductor T'-$La_{1.8}Eu_{0.2}CuO_4$ studied by μSR

T. Kawamata,[*1,*2] T. Sunohara,[*2] K. Shiosaka,[*2] T. Nagaoka,[*2] T. Adachi,[*1,*3] M. Kato,[*2] I. Watanabe,[*1] and Y. Koike[*1,*2]

The electronic state of the high-T_c cuprate Ln_2CuO_4 (Ln: lanthanide elements) with the Nd_2CuO_4-type (so-called T'-type) structure has attracted great interest, because adequately oxygen-reduced samples of T'-Ln_2CuO_4 have been reported to show superconductivity without electron-carrier doping.[1,2] Regarding the electron-doped (Ce-doped) high-T_c superconductors T'-$Ln_{2-x}Ce_xCuO_4$, it has been believed since their discovery that superconductivity appears at $x > 0.14$, while an antiferromagnetic (AF) long-range order is developed in oxygen-reduced samples with $x < 0.14$.[3] Hence, the reason why superconductivity emerges without carrier doping in the undoped (Ce-free) superconductor T'-Ln_2CuO_4 has yet to be clarified.

Two reasons have been suggested for the electronic state of the undoped superconductivity in T'-Ln_2CuO_4. One is a strongly correlated metallic state without a charge-transfer (CT) gap between the upper Hubbard band (UHB) of Cu3$d_{x^2-y^2}$ and the O2p band.[4] In this case, the half-filled Fermi surface with a good nesting condition is formed from UHB of Cu3$d_{x^2-y^2}$ and the O2p band, indicating a strong AF correlation. Therefore, the AF correlation is expected to be weakened by electron- and hole-carrier doping, leading to a bad nesting condition. The other is a strongly correlated metallic state with a finite CT gap and the UHB of Cu3$d_{x^2-y^2}$ having been doped with electron carriers due to oxygen defects induced by reduction annealing.[5] That is, superconductivity appears due to electron-carrier doping of the Mott insulator. In this case, the AF correlation is expected to arise due to hole doping corresponding to a decrease in the electron-carrier concentration. Accordingly, an investigation of changes in the AF correlation caused by hole doping of the undoped superconductor T'-Ln_2CuO_4 is expected to reveal why superconductivity emerges without carrier doping.

We performed muon spin relaxation (μSR) experiments on the polycrystalline samples of T'-$La_{1.8-x}Eu_{0.2}Sr_xCuO_4$ ($x = 0.01, 0.02, 0.03$), whereby the undoped (Ce-free) superconductor T'-$La_{1.8}Eu_{0.2}CuO_4$ was doped with hole carriers.

It is found that the μSR spectra at high temperatures above 100 K show a Gaussian-type slow depolarization of the muon spins and that the μSR spectra change to Lorentzian-type fast depolarization gradually with decreasing temperature for all x. The depolarization at low temperatures is the slowest for $x = 0.03$ in all samples, indicating that the AF correlation becomes weak at $x = 0.03$. The AF transition temperature, T_N, is estimated from the analysis of the μSR spectra and is plotted together with T_N of the electron-doped and undoped superconductors T'-$La_{1.8}Eu_{0.2}CuO_{4-y}F_y$[6] in Fig. 1. It is found that T_N has a maximum for $x = 0.01$ and it decreases by both hole and electron doping. These results are incompatible with a finite CT-gap model in which T_N increases with Sr substitution of the AF Mott insulator. Therefore, the present results suggest that the electronic state of the undoped superconductor T'-$La_{1.8}Eu_{0.2}CuO_4$ is a strongly correlated metallic state without a CT gap.[4]

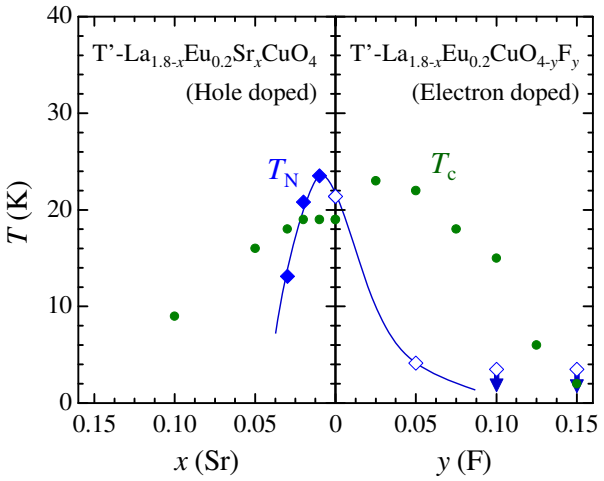

Fig. 1. Doped-carrier concentration dependence of the magnetic transition temperature, T_N, of T'-$La_{1.8-x}Eu_{0.2}Sr_xCuO_4$ and T'-$La_{1.8}Eu_{0.2}CuO_{4-y}F_y$.[6] Green solid circles indicate the critical temperature, T_c, of T'-$La_{1.8-x}Eu_{0.2}Sr_xCuO_4$[2] and T'-$La_{1.8}Eu_{0.2}CuO_{4-y}F_y$.[7] Solid line is guide for the eyes. Arrows indicate that samples are not antiferromagnetic above ~3.8 K.

*1 RIKEN Nishina Center
*2 Department of Applied Physics, Tohoku University
*3 Department of Engineering and Applied Sciences, Sophia University

References
1) O. Matsumoto *et al.*, Physica C **469**, 924 (2009).
2) T. Takamatsu *et al.*, Phys. Procedia **58**, 46 (2014).
3) Y. Tokura *et al.*, Nature **337**, 345 (1989).
4) T. Adachi *et al.*, J. Phys. Soc. Jpn. **82**, 063713 (2013).
5) M. Horio *et al.*, Nat. Commun. **7**, 10567 (2016).
6) T. Kawamata *et al.* (unpublished).
7) T. Sunohara *et al.*, J. Phys. Soc. Jpn. **89**, 014701 (2020).

3. Radiochemistry and Nuclear Chemistry

Isothermal gas chromatography study of Zr and Hf tetrachlorides using radiotracers of ^{88}Zr and ^{175}Hf—Towards investigation of gas-phase chemistry of Rf—†

K. Shirai,[*1] S. Goto,[*1,*2] K. Ooe,[*3] and H. Kudo[*4,*2]

The gas-phase chemical study of Rf, $Z = 104$, has been carried out for its tetrachloride together with $ZrCl_4$ and $HfCl_4$, which are homologues of Rf in the periodic table.[1] Zvára pointed out that the reported values of adsorption enthalpy ($\Delta_{ads}H$) were quite different between experiments and attributed this to the differences in the modification of the surface of the quartz glass column by different chlorinating reagents.[2] To overcome this problem, the present study aimed at obtaining reliable $\Delta_{ads}H$ values of $ZrCl_4$ and $HfCl_4$ by using isothermal gas chromatography.

The apparatus consisted of four components: (i) a reaction part; (ii) a chloride collection part; (iii) an isothermal part; and (iv) a measurement part. Parts (i)–(iii) were heated individually using an electric tube furnace, and part (iv) was cooled with water to collect the chloride passed through the isothermal column. A straight quartz glass tube passed through the four parts. The inner diameter of the isothermal part was 4 mm, and its length was 30 cm.

The radioactive tracers of ^{88}Zr and ^{175}Hf were produced via ^{89}Y$(d,3n)$ and ^{nat}Lu(d,xn) reactions, respectively, by a 24 MeV deuteron beam supplied by the RIKEN K70 AVF cyclotron. Zr and Hf tracers were reacted with CCl_4 at 600°C for 90 min, and the formed chloride was collected on carbon filter put upstream of the isothermal part. Then, the chloride was evaporated at 400°C, and cumulative yields of the chloride were obtained with γ-ray measurement.

The surface-chlorinated quartz column was examined to study the effect of the surface state of the column on the behaviors of $ZrCl_4$ and $HfCl_4$ in the isothermal chromatography. The column was chlorinated with CCl_4 at 600°C for 2 h. After the chlorination, the $ZrCl_4$ and $HfCl_4$ chromatography was carried out. Chromatography experiments were performed at column tempetatures of 135–160°C for the non-treated column and at 100–140°C for the chlorinated column.

In the column-migration model applied to isothermal chromatography,[3] the average retention time ($\bar{t}_r$) is expressed as the following eqation:

$$\ln\left(\bar{t}_r\sqrt{T_{iso}}\right) = -\frac{\Delta_{ads}H}{R}\frac{1}{T_{iso}} + k$$

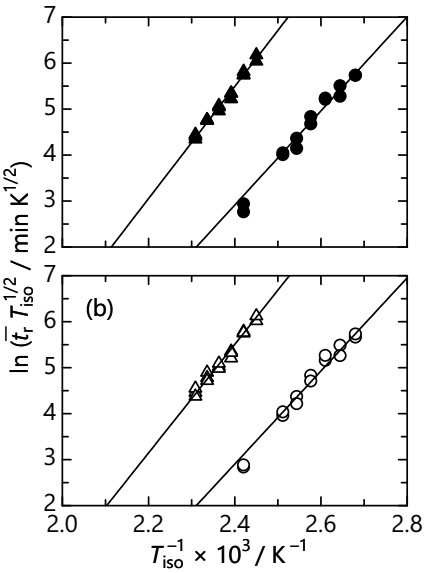

Fig. 1. Plot of $\ln\left(\bar{t}_r\sqrt{T_{iso}}\right)$ versus $1/T_{iso}$ for $ZrCl_4$ (a) and $HfCl_4$ (b). Triangles and circles indicate the type of the column, non-treated and chlorinated, respectively. The solid lines are the results of a least-square fitting.

where k is a constat value including the experimental parameters. Therefore, a plot of $\ln\left(\bar{t}_r\sqrt{T_{iso}}\right)$ against $1/T_{iso}$ is expected to yield a straight line and from its slope, $\Delta_{ads}H$ can be obtained independent of the ambiguous experimental parameters.

Figure 1 plots the results of $\ln\left(\bar{t}_r\sqrt{T_{iso}}\right)$ against $1/T_{iso}$. From the slopes of the fitted lines, the values of $\Delta_{ads}H$ free from parameters were obtained for the first time and those of $ZrCl_4$ and $HfCl_4$ for the non-treated column were -101.3 ± 4.0 kJ mol^{-1} and -98.1 ± 3.1 kJ mol^{-1}, respectively. For the chlorinated column, $\Delta_{ads}H$ of $ZrCl_4$ was -85.1 ± 4.5 kJ mol^{-1} and that of $HfCl_4$ was -84.2 ± 3.3 kJ mol^{-1}.

Comparing with the theoritical calculation by Pershina *et al.*,[4] in both types of column, this is more likely to include a physisorption of MCl_4. If this adsorption mechanism is adopted, $RfCl_4$ is expected to have an enthalpy close to that of the homologues.[4]

† Condensed from the article in J. Nucl. Radiochem. Sci. **21**, 7 (2021)

*1 Graduate School of Science and Technology, Niigata University
*2 RIKEN Nishina Center
*3 Graduate School of Medicine, Osaka University
*4 Faculty of Science, Niigata University

References

1) A. Türler, V. Pershina, Chem. Rev. **113**, 1237 (2013).
2) I. Zvára, *The Inorganic Radiochemistry of Heavy Elements* (Springer, Switzerland, 2008).
3) I. Zvára, Radiochim. Acta **38**, 95 (1985).
4) V. Pershina *et al.*, J. Chem. Phys. **141**, 064315 (2014).

Online anion-exchange experiment of ^{89m}Zr in the Adogen 464/HNO_3 system for the chemical research of Rf

E. Watanabe,[*1] T. Yokokita,[*2] Y. Kasamatsu,[*1] S. Hayami,[*1] K. Tonai,[*1] Y. Shigekawa,[*2] H. Haba,[*2] and A. Shinohara[*1]

Chemical elements with $Z \geq 104$ are called superheavy elements (SHEs) and synthesized by heavy-ion-induced nuclear reactions using accelerators. The chemical properties of SHEs are almost entirely unknown because of the very low cross sections of their nuclides and short half-lives ($T_{1/2} \leq 1$ min). Some chemical experiments on $_{104}$Rf in an aqueous solution were reported; however, its chemical properties are not sufficiently understood owing to limited experimental methods. We previously developed an automated batch-type solid-liquid extraction apparatus (AMBER) and investigated the anion-exchange behavior of Rf in HCl and H_2SO_4 to obtain the distribution coefficients (K_d) of Rf under chemical equilibrium conditions.[1,2)]

In this study, we focus on the formation of the Rf nitrate complexes. The clear difference between the complexation of Th (pseudo homologue of Rf) and those of Zr and Hf (homologues) in HNO_3 is known; Th forms an anionic complex with large coordination numbers of 10 and/or 12, while Zr and Hf do not. We found in a previous study that anion-exchange reactions using the Adogen 464 resin in HNO_3 reach chemical equilibrium in 60 s. This suggests that this resin is suitable for ^{261}Rf ($T_{1/2} = 68$ s) experiments. We also optimized the experimental condition for ^{261}Rf with long-lived radiotracers, ^{88}Zr, ^{175}Hf, and ^{234}Th.[3)] To check the stability of AMBER in the accelerator-online situation, we performed the online anion-exchange experiments of ^{89m}Zr in the Adogen 464/HNO_3 system as a model experiment of ^{261}Rf.

^{89m}Zr ($T_{1/2} = 4.16$ min) was produced in the ^{89}Y$(d, 2n)^{89m}$Zr reaction. A d beam with 24-MeV energy was extracted from the K70 AVF cyclotron at RIKEN. The nuclear-reaction products were transported to the chemistry laboratory by using a He/KCl gas-jet system and deposited on AMBER for 60 s. Then, ^{89m}Zr was dissolved in 270 μL of 8.1 M HNO_3. The solution was loaded into a chemical reaction container containing 32 mg of the Adogen 464 resin. After shaking the container with a vortex mixer for 30–120 s, only the liquid phase was pushed out of the container by compressed air. Then, the solution samples were collected in a 0.5 mL PP tube, and the 587.8-keV γ rays of ^{89m}Zr were counted with a Ge detector. The residual ^{89m}Zr adsorbed on the resin was stripped by washing the resin four times with about 150 μL of 0.1 M HCl. Subsequently, the resin was conditioned with 8.1 M HNO_3 twice. This procedures was repeated 30 times. The distribution coefficient (K_d) was determined by the equation

$$K_d = (A_{STD} - \alpha A_s)V/\alpha A_s w,$$

where A_s and A_{STD} are the radioactivities of ^{89m}Zr in the resin and the control solution, respectively; V is the volume of the aqueous phase (mL); and w is the mass of the dry resin (g). Note that α is a correction factor that accounts for the adsorption of some ^{89m}Zr in the reaction container.

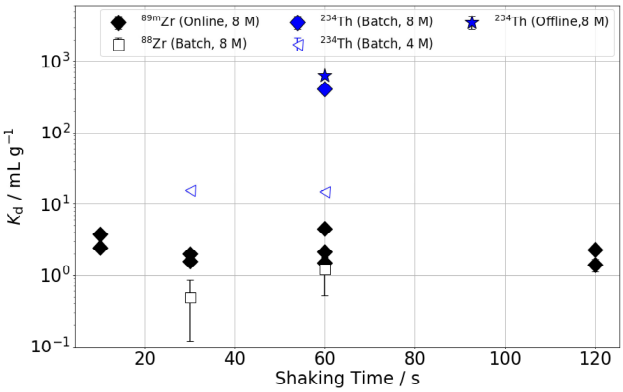

Fig. 1. K_d values of Zr and Th in the Adogen 464/HNO_3 system.

Figure 1 shows the K_d values of ^{89m}Zr using accelerator-online AMBER ("Online" in the figure) as a function of shaking time, along with those of ^{88}Zr and ^{234}Th previously obtained by AMBER in the offline condition and PP tube ("Offline" and "Batch" in the figure, respectively). The K_d of ^{89m}Zr for all shaking times are consistent with the values obtained under equilibrium conditions (60 s) in the batch experiments. This result indicates that the distribution coefficient can be obtained under the conditions of online experiments for the short-lived ^{261}Rf.

In 30 consecutive anion-exchange experiments, the K_d values of ^{89m}Zr are obtained reproducibly. We have previously confirmed good reproducibility for the K_d values of ^{234}Th by AMBER under the offline condition.[3)] Therefore, a wide range of K_d values of anion exchange in HNO_3 can be obtained in consecutive experiments by AMBER. Irrespective of the behavior of Rf in the system, we should be able to obtain reliable K_d values for Rf.

In this study, the applicability of the anion-exchange experiment to Rf in the Adogen 464/HNO_3 system us-

*1 Graduate School of Science, Osaka University
*2 RIKEN Nishina Center

ing AMBER was demonstrated by the success of the model experiment with the short-lived nuclei ^{89m}Zr. In addition to the ^{261}Rf experiment, we plan to conduct theoretical studies on Rf nitrate complexes using DFT calculations.

References

1) T. Yokokita *et al.*, Dalton Trans. **45**, 18827 (2016).
2) T. Yokokita *et al.*, RIKEN Accel. Prog. Rep. **54**, 148 (2021).
3) E. Watanabe *et al.*, RIKEN Accel. Prog. Rep. **53**, 166 (2020).

Solvent extraction of Zr and Hf in trioctylamine/H_2SO_4 system

T. Yokokita*1 and H. Haba*2

The chemical properties of superheavy elements (SHEs) with atomic number $Z \geq 104$ are expected to deviate from the periodicity of their lighter homologues in the periodic table. Thus, chemical studies on SHEs are interesting. SHEs are produced at accelerators using heavy-ion-induced nuclear reactions. The production rates of SHEs are low, and their half-lives are short ($T_{1/2} \leq 1$ min). Thus, the chemical studies of SHEs are conducted on a single-atom basis, which makes it difficult to perform chemical experiments with SHEs. Thus far, the chemical properties of SHEs have been discussed by comparing their behavior with those of homologous elemenets.[1)]

We performed anion-exchange experiments of Rf and its homologous elements, Zr and Hf, to study its sulfate complexation.[2)] From the previous study, we obtained the distribution coefficients of Rf, Zr and Hf in 0.060–0.46 M H_2SO_4.[2)] We need to identify the chemical species of the sulfate complexes of Zr and Hf under the studied conditions to discuss the sulfate complexation of Rf based on the comparison of the anion-exchange behavior of Rf and its homologous elements. In this work, we performed solvent extraction with an anion exchanger, trioctylamine (TOA), from H_2SO_4 and ESI-MS spectroscopy to deduce the anionic sulfate complexes of Zr and Hf under the experimental condition of Rf.

Radiotracers ^{88}Zr and ^{175}Hf were produced in ^{89}Y$(d, 3n)^{88}$Zr and $^{\mathrm{nat}}$Lu$(d, xn)^{175}$Hf reactions, respectively, using the RIKEN AVF cyclotron. Then, these tracers were purified by an anion-exchange method. The solvent extractions of Zr and Hf were performed by employing the batch method with 1.6–20 mM trioctylamine in CH_2Cl_2 from 0.11 M H_2SO_4. The distribution ratios (D) were obtained according to $D = [\mathrm{M}]_{\mathrm{org}}/[\mathrm{M}]_{\mathrm{aq}}$; here, $[\mathrm{M}]_{\mathrm{org}}$ and $[\mathrm{M}]_{\mathrm{aq}}$ denote the metal concentration in the organic and aqueous phases, respectively.

For ESI-MS spectroscopy, Zr and Hf samples in the organic phases were obtained in the solvent extraction of 9.4 mM Zr and 7.6 mM of Hf, respectively, from 0.15 M H_2SO_4 into 3.6 mM TOA-CH_2Cl_2 solutions. Further, we made blank samples, *i.e.*, TOA-CH_2Cl_2 solutions without Zr and Hf. They were the organic phases obtained in the solvent extraction of 0.15 M H_2SO_4 without the metal ions and 3.6 mM TOA-CH_2Cl_2 solutions. All samples were diluted with CH_2Cl_2 before ESI-MS measurement using LTQ Orbitrap XL mass spectrometer (Thermo Fisher Scientific).

The slopes of log D and log [TOA] of Zr and Hf were obtained: the slope is related to the number of the protonated TOA cation ($HTOA^+$) of the extracted species. The slope values of both Zr and Hf were 1.9 ± 0.1, which implies two $HTOA^+$ cations are paired with the anionic sulfate complexes of Zr and Hf with a net charge −2 to be extracted into the organic phase from the aqueous phase.

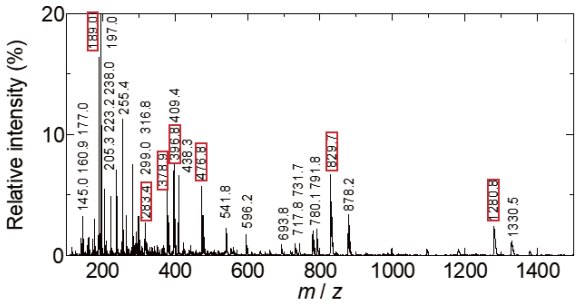

Fig. 1. ESI-MS spectrum (negative mode) of the Zr sample. The m/z values marked by the squares are the distinguishable peaks of the Zr sample.

In ESI-MS spectroscopy, the peaks of the ionized Zr and Hf species in the organic phase were assigned by comparing the mass spectra of Zr and Hf samples in the organic phase with those of the blank samples. The mass spectrum of the Zr samples is shown in Fig. 1. 7 distinguishable peaks were observed at m/z = 189.0, 238.0, 378.9, 396.8, 476.7, 830.0, and 1280.8, which corresponded to $[Zr(SO_4)_3]^{2-}$, $[Zr(HSO_4)_2(SO_4)_2]^{2-}$, $[Zr(HSO_4)(SO_4)_2]^{-}$, $[Zr(OH)(HSO_4)_2(SO_4)]^{-}$, $[Zr(HSO_4)_3(SO_4)]^{-}$, $(HTOA)[Zr(HSO_4)_2(SO_4)_2]^{-}$, and $(HTOA)_2[Zr(HSO_4)_3(SO_4)_2]^{-}$, respectively. The extracted Zr species in organic phase contains the two $HTOA^+$ cations, and therefore, the Zr species before ionization are $(HTOA)_2[Zr(SO_4)_3]$, $(HTOA)_2[Zr(HSO_4)_2(SO_4)_2]$, $(HTOA)_2[Zr(OH)(HSO_4)(SO_4)_2]$, and $(HTOA)_2[Zr(OH)(HSO_4)_3(SO_4)]$.

For the Hf sample, 4 distinguishable peaks were observed at m/z = 234.0, 486.8, 919.6, and 1371.2, which correspond to $[Hf(SO_4)_3]^{2-}$, $[Hf(OH)(HSO_4)_2(SO_4)]^{-}$, $(HTOA)[Hf(HSO_4)_2(SO_4)_2]^{-}$, and $(HTOA)_2Hf(HSO_4)_3(SO_4)_2]^{-}$, respectively. The extracted Hf species in organic phase contains the two $HTOA^+$ cations, and therefore, the Hf species before ionization are $(HTOA)_2[Hf(SO_4)_3]$, $(HTOA)_2$ $[Hf(OH)(HSO_4)(SO_4)_2]$, $(HTOA)_2[Hf(OH)(HSO_4)_3(SO_4)]$, and $(HTOA)_2[Hf(HSO_4)_2(SO_4)_2]$.

These results indicate that the proposed Zr and Hf species at 0.1 M H_2SO_4 are $[M(SO_4)_3]^{2-}$, $[M(HSO_4)_2(SO_4)_2]^{2-}$, $[M(OH)(HSO_4)(SO_4)_2]^{2-}$, and $[M(OH)(HSO_4)_3(SO_4)]^{2-}$ (M = Zr and Hf). However, the main species of Zr and Hf in this studied condition cannot be determined from the present study. A combination of other analytical methods must be performed to identify the main chemical species.

References

1) A. Türler, V. Pershina, Chem. Rev. **113**, 1273 (2013).
2) T. Yokokita *et al.*, RIKEN Accel. Prog. Rep. **54**, 148 (2021).

*1 Department of General Education, Salesian Polytechnic
*2 RIKEN Nishina Center

Determination of ^{236}U in a Th target irradiated with Li ions by ICP mass spectrometry

A. Nagai,[*1,*2] K. Teranishi,[*1,*2] R. Morita,[*1,*2] H. Hosokawa,[*1,*3] A. Yokoyama,[*1,*3] A. Nakajima,[*1,*4] A. Sakaguchi,[*1,*5] Y. Shigekawa,[*1] A. Nambu,[*1] T. Yokokita,[*1] and H. Haba[*1]

Neptunium-237 ($T_{1/2} = 2.1\times10^6$ y) released from nuclear facilities is an important radioactive target nuclide that contaminates the environment.[1] The nuclide can be analyzed by accelerator mass spectrometry; however, a spike material of neptunium for the measurement has not been obtained, thus far. We previously proposed the production of neptunium-236 ($T_{1/2} = 1.5 \times 10^5$ y) in a Th + Li reaction as a candidate for the material.[2,3] However, the material prepared from the irradiated target may be contaminated with long-lived isobars of ^{236}Pu and ^{236}U, which are the decay products from ^{236m}Np, or a byproduct in the reaction. In addition, ^{235}U contained in Th as an impurity, may also absorb neutrons and produce ^{236}U. In this study, we aimed to determine U isotopes contained originally in the Th target as well as those produced in the nuclear reaction by High Resolution ICP-MS (HR-ICP-MS). The amount of ^{236}U produced in the reaction can be estimated by measuring a neutron flux during irradiation through the use of a monitoring foil of Au.

We irradiated a ^{232}Th target with 43 MeV ^{7}Li ions at the RIKEN AVF cyclotron. Au metal foils (ca. 200 mg each) and electrodeposited U samples (ca. 1 mg each) were placed at the end of the beam course to function as a neutron monitor and a reference, respectively, as illustrated in Fig. 1.

After irradiation, the neutron flux was obtained from activation of the Au foil measured by γ-ray spectroscopy using a Ge semiconductor detector. The U-electrodeposited sample was dissolved in a concentrated

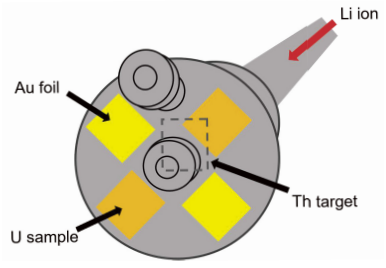

Fig. 1. Experimental setup of neutron monitor foils (Au) and U targets attached to the end of a target holder of an irradiation beam course at RIKEN.

*1 RIKEN Nishina Center
*2 Graduate School of Natural Science and Technology, Kanazawa University
*3 Institute and College of Science and Engineering, Kanazawa University
*4 Master's Program in Chemistry, University of Tsukuba
*5 Center for Research in Isotopes and Environmental Dynamics, University of Tsukuba

Table 1. U isotopic ratios in U-electrodeposited samples by ICP-MS.

	Irradiated		Unirradiated
	U-1	U2	U-3
	Ratio%		Ratio%
235/238	0.62~0.82	0.61~0.84	0.63~0.85
236/238	0.5×0.82^{-4}	$(1–7)\times0.82^{-4}$	N.D

nitrate solution. Subsequently, the solution was diluted so that the U concentration was 0.1 or 1 ng/g, as measured by HR-ICP-MS with a reference solution of XSTC-13 supplied by SPEX Industries, Inc. for calibration.

From the measurements of photopeak intensities due to ^{198}Au and ^{196}Au in the Au foils, the thermal neutron flux and fast neutron flux were 6.5×10^5 s^{-1} and 1.6×10^7 s^{-1}, respectively. These values were calculated from induced radioactivities and the cross section data[4] of (n,γ) and $(n,2n)$ reactions. The isotope measurement results of the U-electrodeposited sample by HR-ICP-MS are shown in Table 1, where the ratios denote the range of observation due to the large dispersion of the data depending on the sample. The abundance ratios of ^{235}U to ^{238}U for all the samples are approximately 0.7%, corresponding to the natural abundance of U. Some events due to ^{236}U were observed for the samples attached to the target holder. However, the events due to the unirradiated sample was less than the detection limit. It was confirmed that ^{236}U was produced in the U-electrodeposited samples. The amount of ^{236}U produced agrees with the amount estimated from the thermal neutron flux by the monitor within some uncertainty of the data. Based on the measured concentration of U and the measured thermal flux, the number of ^{236}U atoms produced in the target sample was $(0.9 - 2.0) \times 10^2$, much less than the number of ^{236g}Np atoms estimated from the measured cross section,[2] that is, approximately 1 mb. Thus, the amount of U was concluded to be negligible to contaminate a Np tracer prepared from the irradiated target.

References

1) W. Rund, G. S. Goff, in *Radionuclide in the Environment*, edited by D. A. Atwood (Wiley, 2013).
2) Y. Hayakawa *et al.*, RIKEN Accel. Prog. Rep. **53**, 179 (2020).
3) A. Nakajima *et al.*, RIKEN Accel. Prog. Rep. **54**, 142 (2021).
4) Japanese Evaluated Nuclear Data Library, JENDL-4.0, (2010), `https://wwwndc.jaea.go.jp/jendl/Jendl_J.html` .

Development of a photon measurement apparatus for observing the radiative decay of ^{229m}Th produced from ^{229}Pa

Y. Shigekawa,[*1] Y. Wang,[*1] X. Yin,[*1] A. Nambu,[*1] T. Yokokita,[*1] and H. Haba[*1]

The first excited state in the ^{229}Th nucleus (^{229m}Th) has an excitation energy of ∼8.3 eV (150 nm),[1] which potentially enables an ultraprecise nuclear clock. We have been aiming to observe the radiative decay (γ rays) of ^{229m}Th and to determine its radiative half-life, which is an essential parameter to develop the nuclear clock, by doping a CaF_2 crystal with ^{229}Pa, which decays to ^{229m}Th with negligibly small recoil energy.[2] In this study, we developed a photon measurement apparatus for observing the γ rays of ^{229m}Th. We also investigated the background photons originating from the decay of ^{229}Pa ($T_{1/2}$ = 1.5 d) and other impurities such as ^{232}Pa ($T_{1/2}$ = 1.31 d) and ^{230}Pa ($T_{1/2}$ = 17.4 d).

Figure 1 shows a schematic view of the developed apparatus. Two photomultipliers are placed inside a vacuum chamber: one is for measuring the γ rays of ^{229m}Th in the vacuum ultraviolet (VUV) range (PMT1, Hamamatsu R10454), and the other is for measuring scintillation photons produced from ^{229}Pa and other isotopes in a CaF_2 crystal (PMT2, Hamamatsu R7154). The events of PMT1 that coincided with those of PMT2 correspond to high-energy radiation that can produce scintillation photons, and thus, such events can be excluded from the analysis of the γ-ray events of ^{229m}Th. Band-pass (BP) filters for photons of 151 ± 20 and 171 ± 20 nm (eSource Optics) are placed between PMT1 and the CaF_2 sample. The filters can be switched using a linear drive driven by a stepper motor; the γ rays of ^{229m}Th are expected to be detected only for the 151-nm BP filter. PMT1 and PMT2 can be cooled to −25°C using a Peltier cooler, reducing the dark count rate to 0.09 s^{-1} for PMT1 and 0.25 s^{-1} for PMT2. Considering the half-life of ^{229m}Th (10^3–10^4 s), the ^{229}Pa-doped CaF_2 can be rapidly introduced to the measurement position (∼10 min) as follows without the leakage of the large vacuum chamber (Fig. 1). First, the sample fixed on a linear drive is

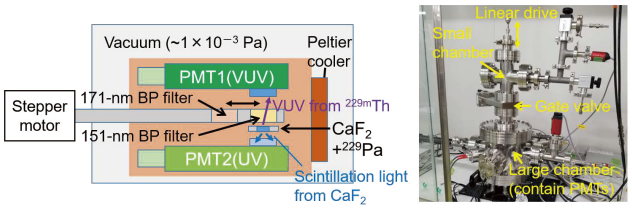

Fig. 1. Schematic view of the developed apparatus (left) and a photograph of the sample loading system (right).

*1 RIKEN Nishina Center

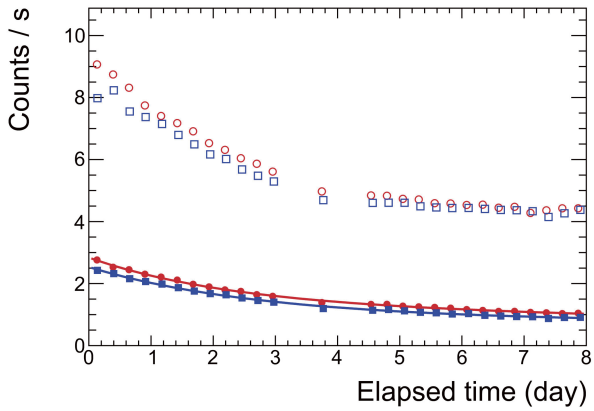

Fig. 2. Count rate of photons measured using PMT1 for the 151-nm (circle) and 171-nm (square) BP filters with (closed) and without (open) anticoincidence using the events measured by PMT2. The sum of the exponential decay functions of ^{229}Pa and ^{230}Pa is fitted to the count rate with anticoincidence for each filter (solid lines).

placed inside a small vacuum chamber, which is then rapidly evacuated. Next, a gate valve is opened, and the sample is moved to the large chamber for photon measurement.

We investigated the background photons originating from ^{229}Pa and other isotopes, which may interfere with the observation of the γ rays of ^{229m}Th. The production and chemical separation of ^{229}Pa were performed similarly to those in a previous study.[2] First, two ^{232}Th metallic foils (total 138 mg/cm^2) were irradiated with 1 μA of a 30-MeV proton beam for 10 h at the RIKEN AVF cyclotron. Next, the foils were dissolved with concentrated HCl and fed onto an anion-exchange column (Muromac 1X8, 100–200 mesh, ∼1.0 mL). After pouring concentrated HCl, 6 M HCl, and 8 M HNO_3 to the column, Pa isotopes were eluted with 9 M HCl/0.1 M HF. In this study, we performed an additional anion-exchange process to reduce radioactive impurities such as ^{97}Zr as follows. First, Pa isotopes were dissolved in 0.1 M HCl/0.1 M HF and fed onto an anion-exchange column (Muromac 1X8, 100–200 mesh, ∼0.5 mL). After pouring 0.1 M HCl/0.1 M HF, Pa isotopes were eluted with 0.4 M HCl/0.1 M HF. The ratio of radioactivity of ^{229}Pa isotopes to that of other radioactive elements was ∼10^5 after the chemical separation. Thereafter, we dropped the ^{229}Pa solution on a CaF_2 crystal, annealed it, and started a photon measurement four days after the proton irradiation. Compared with the previous measurement,[2]

the amount of ^{229}Pa was dominant over other isotopes (^{229}Pa 48(3) kBq, ^{232}Pa 2.51(6) kBq, and ^{230}Pa 6.6(4) kBq); thus, we could evaluate the background photons produced by high-energy radiation from ^{229}Pa more precisely.

As shown in Fig. 2, the count rate of photons detected by PMT1 for the 151-nm BP filter was $\sim$9 s^{-1} at the start of the measurement. Anticoincidence using PMT2 reduced the count rate to $\sim$1/3. For each BP filter, the sum of the exponential decay functions of ^{229}Pa and ^{230}Pa was well fitted to the data, indicating that the photons originate from ^{229}Pa and ^{230}Pa. The ratio of photons from ^{229}Pa to those from ^{230}Pa was $\sim$1. In the presence of these background photons, if we use a CaF_2 sample doped with 100 kBq of ^{229}Pa, our simulation indicated that we can observe the γ rays of ^{229m}Th without the mass separation of ^{229}Pa and determine its half-life with a relative error of $\sim$25%; the development of the apparatus for measuring the γ rays of ^{229m}Th is nearly complete.

References

1) B. Seiferle *et al.*, Nature **573**, 243 (2019).
2) Y. Shigekawa *et al.*, RIKEN Accel. Prog. Rep. **54**, 143 (2021).

Surface ionization of protactinium toward implanting ^{229}Pa into a CaF_2 crystal

Y. Shigekawa*1 and H. Haba*1

The first excited state in the ^{229}Th nucleus (^{229m}Th) has an excitation energy of ∼8.3 eV,[1] which may allow an ultraprecise nuclear clock. We aim to observe the γ rays of ^{229m}Th and to determine its half-life, which is an essential parameter to develop the nuclear clock, by doping a CaF_2 crystal with ^{229}Pa, which decays to ^{229m}Th with a negligibly small recoil energy.[2] The doping with ^{229}Pa will be achieved by ionizing ^{229}Pa, implanting ^{229}Pa ions with high energy (>10 keV) into a CaF_2 crystal, and annealing the crystal. Ionizing ^{229}Pa with high efficiency and implanting ∼100 kBq of ^{229}Pa are important to clearly observe the γ rays of ^{229m}Th. Surface ionization, which is the ionization of atoms on the surface of a metal at a high temperature, is one of the methods that can realize a high ionization efficiency (0.1–100%); however, the ionization efficiency for Pa is as low as 0.001–0.01%[3] because of the high stability of Pa compounds such as Pa_2O_5. To overcome this difficulty, Pickett *et al.* developed a method to bring Pa compounds into contact with colloidal graphite on the surface of a Re filament, realizing an ionization efficiency of 0.3–0.7%.[4,5] Following this method, we performed experiments for ionizing ^{233}Pa ($T_{1/2}$ = 26.975 d) in this study toward the ionization of ^{229}Pa ($T_{1/2}$ = 1.5 d).

^{233}Pa was separated from its mother nuclide ^{237}Np in the following procedure. First, 9 M HCl solution containing ^{237}Np and ^{233}Pa was fed onto a TK400 resin's column (TrisKem). Next, ^{237}Np was eluted by pouring 9 M HCl, following which ^{233}Pa was eluted by pouring 1 M HCl. The eluate contacting ^{233}Pa was evaporated, dissolved with 0.1 M HCl/0.1 M HF, and fed onto an anion-exchange column (Muromac 1X8). After pouring 0.1 M HCl/0.1 M HF, ^{233}Pa was eluted with 0.4 M HCl/0.1 M HF. Finally, we prepared a stock solution of ^{233}Pa in 50 μL of 1 M HNO_3/0.4 M HF.

Figure 1 shows a schematic view of the setup for the surface ionization and implantation of Pa, performed in a high vacuum (10^{-4}–10^{-5} Pa). A Re filament (0.0254 × 0.762 × 10 mm) was fixed by spot welding to two SUS316 wires (φ1.0 mm), which were connected to a vacuum feedthrough to apply a current for heating the filament. The temperature of the filament was measured using an infrared thermometer. An Al electrode, where −15 kV was applied, was placed 86.4 mm below the filament. We fixed a CaF_2 crystal (φ12 mm, 0.5 mm thickness) or a Cu foil (φ12 mm, 0.05 mm thickness) to the Al electrode. The Cu foil was used for optimizing the setup and conditions of surface ionization. According to our simulation, the collection efficiency of ions in the CaF_2 crystal or the Cu foil is ∼100%; therefore, the collection efficiency of Pa corresponds to the ionization efficiency.

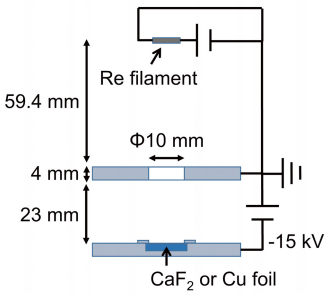

Fig. 1. Schematic view of the setup for the surface ionization and implantation of Pa.

The surface ionization and implantation of ^{233}Pa were performed for the Cu foil (Run A) and the CaF_2 crystal (Run B) as follows. First, the Re filament was heated with a current of ∼5.5 A for 10 min to remove impurities on the filament. Next, 1 μL of water containing colloidal graphite (EM Science 12650) was dropped on the filament and evaporated by applying a current of 0.7 A to the filament. Then, 1 μL of the stock solution containing 19.1(2) kBq of ^{233}Pa was dropped on the Re filament and evaporated with a current of 0.7 A. After the filament was placed in a vacuum chamber, the current applied to the filament was gradually increased. At a filament current of 2.5 A, we applied a voltage of −15 kV to the Al electrode (Fig. 1). The temperature of the filament exceeded 1960°C with a current of ∼5.5 A and increased to 2000°C in ∼20 min. The heating at ∼2000°C lasted until the filament was broken (79 and 127 min for Runs A and B, respectively).

The radioactivity of ^{233}Pa collected in the Cu foil (Run A) was measured to be 121(2) Bq. Considering the solid angle between the filament and the foil, the radioactivity of ^{229}Pa atoms deposited on the foil was calculated to be 15.8(2) Bq. Hence, the ionization efficiency was 0.55(1)%. The radioactivity of ^{233}Pa remaining on the filament after heating was 4.3(1)% of that before heating, implying that highly stable ^{233}Pa compounds were efficiently reduced and evaporated. For the case of the implantation into the CaF_2 crystal (Run B), the ionization efficiency was 0.53(1)%, which is close to the value for the Cu foil, although CaF_2 is a non-conducting material. We will be able to implant 100 kBq of ^{229}Pa, which is expected to sufficient to clearly observe the γ rays of ^{229m}Th, by using a solution containing 19 MBq of ^{229}Pa.

*1 RIKEN Nishina Center

References
1) B. Seiferle *et al.*, Nature **573**, 243 (2019).
2) Y. Shigekawa *et al.*, RIKEN Accel. Prog. Rep. **54**, 143 (2021).
3) J. Fietzke *et al.*, Nucl. Instrum. Methods Phys. Res. B **149**, 353 (1999).
4) D. A. Pickett *et al.*, Anal. Chem. **66**, 1044 (1994).
5) C. -C. Shen *et al.*, Anal. Chem. **75**, 1075 (2003).

Development of RF carpet gas cell for extracting ^{229m}Th ions

Y. Shigekawa,[*1] K. Tokoi,[*2] A. Yamaguchi,[*3,*4] N. Sato,[*1] M. Wada,[*5] and H. Haba[*1]

The first excited state of a ^{229}Th nucleus (^{229m}Th) has an excitation energy of ∼8.3 eV.[1,2] Because this is close to the binding energy of the valence electrons, decay modes of ^{229m}Th [internal conversion (IC), electronic bridge (EB) transitions, and γ-ray emission] may vary depending on the chemical environment. However, EB transitions and γ-ray emission of ^{229m}Th have never been observed, because the IC process dominantly occurs in most chemical environments in which electron biding energies are below 8 eV. Examples in which the IC process is inhibited are ^{229m}Th ions trapped in vacuum. The trapping of $^{229m}Th^{2+}$ and $^{229m}Th^{3+}$, which have high ionization energies (18.3 and 28.65 eV, respectively), may lead to γ-ray emission. Moreover, because the electron transition energies in a Th^{+} ion are close to 8 eV, the trapping of $^{229m}Th^{+}$ may allow occurrence of an EB transition, which is an unknown high-order decay mode along with the transition of an occupied orbital electron to an unoccupied orbital and the emission of a photon. Observing such decay modes requires the extraction of numerous ^{229m}Th ions to an ion trap. In this study, we fabricated a radiofrequency (RF) carpet gas cell to efficiently extract ^{229m}Th ions recoiling out of a ^{233}U source. Moreover, we optimized and evaluated the device by extracting ^{220}Rn ($T_{1/2}$ = 55.6 s) and ^{216}Po ($T_{1/2}$ = 0.144 s) ions emitted from a ^{224}Ra source under the recoil energy of an α decay.

Figure 1 shows a photograph and schematic of the developed gas cell. The ions emitted from a source placed inside the gas cell are decelerated by He gas, pushed toward an RF carpet by a positive (push) voltage, and transported to the central hole of the RF carpet using the RF surfing technique.[3] Subsequently, the ions are guided to high vacuum by a quadrupole ion guide (QPIG). The ions with a specific mass-to-charge ratio (m/z) are separated by a quadrupole mass separator (QMS) and guided to a channeltron detector. The vacuum chamber consists of conflat flanges, and it is baked to reach a base pressure of $\sim 1 \times 10^{-7}$ Pa, to ensure that the amount of impurities emitted from the gas cell is small. Thus, the neutralization or molecularization of ions by impurities is minimized. Because of the relatively small recoil energy of an α decay (∼100 keV), we shortened the length of the gas cell to 10 cm compared to that of the gas cell we developed for the study of superheavy elements (26 cm).[3]

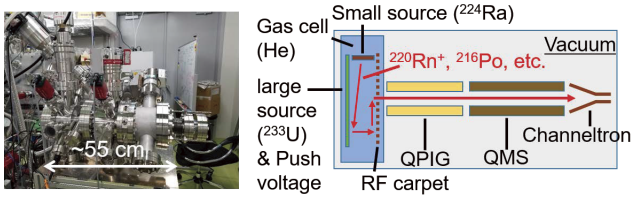

Fig. 1. Photograph (left) and schematic (right) of developed RF carpet gas cell.

We investigated the conditions under which the extraction efficiency is maximum, by extracting $^{216}Po^{+}$ ions emitted from a thin ^{224}Ra source[3,4] (∼400 Bq) placed inside the gas cell. The counts of $^{216}Po^{+}$ ions measured by the channeltron detector reached maximum when the push voltage of the RF carpet was from +5 V to +90 V, the offset voltage of the RF carpet was +4 V (He 10 mbar) and +10 V (He 15 mbar), the RF voltage of the RF carpet was 217 Vpp (15.43 MHz), the audiofrequency voltage of the RF carpet was 2.6 Vpp (200 kHz), the DC voltage of the QPIG was +1 V, and the RF voltage of the QPIG exceeded 106 Vpp.

We measured the mass spectrum of the ions emitted from the ^{224}Ra source under the above-mentioned conditions. In Fig. 2, the peaks of $^{220}Rn^{+}$, $^{216}Po^{+}$, $^{212}Pb^{+}$, $^{208}Pb^{+}$, and $^{208}Tl^{+}$ are noticeable. Only when He gas introduced in the gas cell is purified using purifiers (SAES PS3-MT3-R-1 and MC1-902F), the peaks of $^{216}Po^{2+}$, $^{212}Pb^{2+}$, $^{208}Pb^{2+}$, and $^{208}Tl^{2+}$ are observed. Thus, when $^{229m}Th^{2+}$ and $^{229m}Th^{3+}$ ions are needed, gas purification should be conducted.

We measured the absolute maximum extraction efficiency of $^{220}Rn^{+}$ as the ratio of the number of extracted $^{220}Rn^{+}$ to that of $^{220}Rn^{+}$ emitted from the ^{224}Ra source.[3] The former was determined from the alpha-decay events of ^{220}Rn detected by the channeltron (the counts increased during extraction and decayed after stopping the extraction with a half-life of 55.6 s). The extraction efficiency was 16(2)% at He 10 mbar and 20(1)% at He 15 mbar with purified He

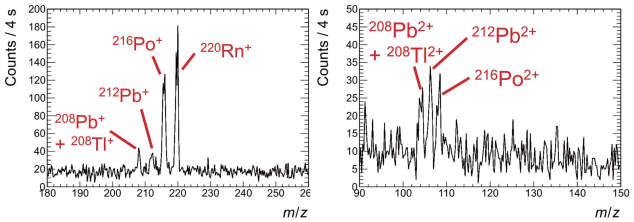

Fig. 2. Mass spectra of ions extracted from ^{224}Ra source without (left) and with (right) He gas purification.

*1 RIKEN Nishina Center
*2 Graduate School of Science, Osaka University
*3 Quantum Metrology Laboratory, RIKEN
*4 PRESTO, Japan Science and Technology Agency
*5 Wako Nuclear Science Center (WNSC), IPNS, KEK

gas. Hence, using a ^{233}U source with a diameter of 90 mm and a radioactivity of 100 kBq would enable extracting ^{229m}Th ions at a rate of $\sim$400 s^{-1}, which is sufficiently high to observe γ-ray emission and EB transitions using photomultipliers.

References

1) B. Seiferle *et al.*, Nature **573**, 243 (2019).
2) A. Yamaguchi *et al.*, Phys. Rev. Lett. **123**, 222501 (2019).
3) Y. Shigekawa *et al.*, RIKEN Accel. Prog. Rep. **53**, 168 (2020).
4) Y. Shigekawa *et al.*, Rev. Sci. Instrum. **87**, 053508 (2016).

Preparation of an ^{225}Ac source for ^{221}Fr EDM measurement

M. Sato,[*1,*2] K. Yamane,[*2] H. Haba,[*1] A. Nambu,[*1] N. Ozawa,[*3] S. Nagase,[*3] T. Nakashita,[*2] M. Fukase,[*3] D. Uehara,[*3] T. Hayamizu,[*1] K. Nakamura,[*4] H. Nagahama,[*4] Y. Sakemi,[*4] and Y. Matsuda[*2]

The origin of the matter-dominant universe is one of the greatest mysteries in modern physics. It is considered that the violation of the charge conjugate and parity symmetry (CP violation) is needed to explain the mystery.[1] The existence of the electric dipole moment (EDM) of elementary particles could lead to the discovery of the source of CP violation and the prospects of new physics beyond the standard model of particle physics.

Francium (Fr), which is the heaviest alkali element, has a large enhancement factor of about 10^3 for the electron EDM.[2] In addition, ^{221}Fr is sensitive to the nuclear EDM. We aim to extract the nuclear EDM by comparing it with the ^{210}Fr EDM, which is sensitive to the electron EDM.

In this paper, we report the preparation of an ^{225}Ac source to obtain the ^{221}Fr recoiling from it. ^{221}Fr, which is produced from the alpha decay of ^{225}Ac with a half-life of 10 days, is convenient to conduct the EDM experiment without accelerator operation. We used an electrodeposition method to fix ^{225}Ac firmly on a plate. To obtain sufficient statistics for EDM measurements, we aimed to develop a source of 10 MBq or higher.

Figure 1 shows an overview of the cell used for the electrodeposition experiment. A Pt plate ($0.1 \times 15 \times 15$ mm^3) on a water-cooled Ti block is used as a cathode, and a Pt rod (1-mm diameter) stuck into the solution is used as an anode applied with +1 kV. Silicon rubber with a hole of 5 mm diameter functions as an electrode seal, and we can obtain an active target area as we arranged.

Before preparing the Ac source, the best condition of the electrodeposition was determined using Y, which is chemically similar to Ac. The Y sample we prepared included ^{88}Y, which has a long half-life of 106.6 days and emits γ rays with energies of 898 and 1836 keV that can be detected using a germanium semiconductor detector. By dividing the amount of Y electrodeposited on the Pt plate by that used for electrodeposition, we could determine the electrodeposition yields. ^{88}Y was produced by irradiating a ^{nat}SrO target with a 24-MeV deuteron beam for 4 h at the AVF cyclotron. The beam current was 3 μA. The target included 157.9 mg of ^{nat}SrO and was pressed into a disc of 10-mm diameter at 1.6 t for 5 min. After the irradiation, ^{88}Y was chemically isolated from the target by extraction chromatography using an Ln resin (particle size: 100–150 μm) filled in a column (internal diameter: φ5 mm, height: 50 mm).

This purified ^{88}Y was mixed with stable ^{89}Y and dissolved in 1 mL of 0.01 M HNO_3. 10 μL of the solution was mixed with 2 mL 2-propanol for electrodeposition. The number of Y atoms in the mixed solution was the same as that of 1-MBq ^{225}Ac.

Figure 2 shows the time dependence of the electrodeposition yield. At an applied voltage of +1 kV and at room temperature, the yields increased with time from ~15% at 10 min to ~100% at 40 min. We could visually observe the target layer on the Pt plate.

We purchased ^{225}Ac and attempted the electrodeposition with the optimized condition which achieved the highest yield. As a result, a maximum yield of 77.9% was achieved for the ^{225}Ac source of 20.4(6) MBq. A sufficient dose was achieved, but the difference in yields between Y and Ac may be due to subtle differences in chemical properties. The ^{225}Ac used in this research was supplied by the U.S. Department of Energy Isotope Program managed by the Office of Isotope R&D and Production.

The development of the experimental apparatus to trap ^{221}Fr from the ^{225}Ac source and measure the EDM is now in progress.

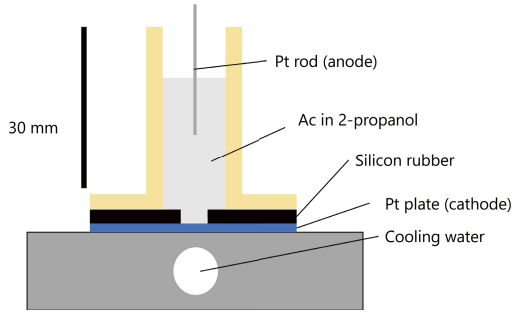

Fig. 1. Overview of the cell for Ac electrodeposition.

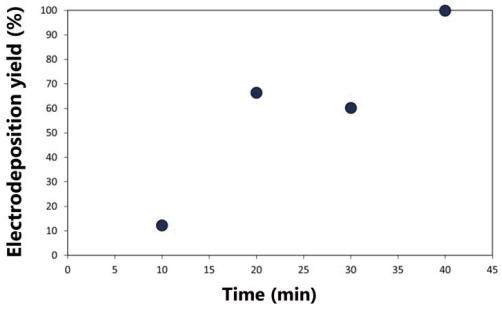

Fig. 2. Time dependence of the electrodeposition yields of Y at an applied voltage of +1 kV.

*1 RIKEN Nishina Center
*2 Graduate School of Arts and Sciences, University of Tokyo
*3 Department of Physics, University of Tokyo
*4 Center for Nuclear Study, University of Tokyo

References

1) A. D. Sakharov, Sov. Phys. Usp. **34**, 392 (1991).
2) N. Shitara *et al.*, J. High Energy Phys. **2**, 124 (2021).

Accelerator production and chemical separation of theranostic radionuclide ^{141}Ce

K. Ooe,[*1,*2] T. Watabe,[*1,*2] Y. Shirakami,[*2] A. Nambu,[*3] H. Haba,[*3] and J. Hatazawa[*4]

Because all of the therapeutic radionuclides used in clinical practice in Japan are imported from other countries, domestic production using accelerators is desirable for the stable supply of therapeutic nuclides.

Cerium-141 (^{141}Ce, $T_{1/2}$ = 32.5 d) is a candidate radionuclide for theranostics (therapeutics + diagnosis) and can be produced in the ^{138}Ba$(\alpha, n)^{141}$Ce reaction using accelerators. This nuclide emits β-particles (maximum β energy: 580.7 keV), which can be applied to the therapy of tumors, as well as a γ-ray with an energy of 145.4 keV (branching ratio: 48.2%), which can be used for imaging by single photon emission computed tomography (SPECT). In particular, ^{141}Ce is expected to be useful for SPECT imaging because the energy of the γ-ray of ^{141}Ce is similar to that of ^{99m}Tc (140 keV), which is the most widely used SPECT nuclide in clinical application. However, ^{141}Ce has been rarely applied to nuclear medicine. In this study, a suitable target material of ^{nat}Ba for the accelerator production of ^{141}Ce was investigated. A chemical separation method for ^{141}Ce from the irradiated ^{nat}Ba target was also investigated through column chromatography with a Ln resin (extraction chromatographic resin with di(2-ethylhexyl) phosphoric acid).

For the determination of a suitable target material of ^{nat}Ba, $BaCl_2$ and BaO pellets (both approximately 100 mg) were irradiated with a 29-MeV alpha beam (beam intensity: 1.3 particle μA, irradiation time: 10 min) using the RIKEN K70 AVF cyclotron. The irradiated ^{nat}Ba targets were subjected to γ-ray spectrometry with a Ge semiconductor detector. In the chemical separation of ^{141}Ce from the ^{nat}Ba target, the irradiated ^{nat}Ba target (approximately 100 mg) was dissolved in 3 mL of 1 M HCl. After evaporation to dryness, the residue was dissolved in 3 mL of 0.01 M HCl solution and then fed into a Ln resin column (5-mm diameter × 50-mm height). ^{nat}Ba was eluted by 0.01 M HCl, following which ^{141}Ce was eluted by 1 M HCl solution by referring to the literature.[1] Each eluted sample (1 mL) was subjected to γ-ray spectrometry with the Ge detector for the determination of ^{141}Ce radioactivity. After measurement with the Ge detector, the concentration of ^{nat}Ba in each eluted sample was measured by inductively coupled plasma mass spectrometry (ICP-MS).

In the production of ^{141}Ce from the $BaCl_2$ target, high radioactivities of short-lived 38 K ($T_{1/2}$ = 7.636 min) and ^{34m}Cl ($T_{1/2}$ = 31.99 min) were observed. These by-products are considered to be produced from ^{nat}Cl in the $BaCl_2$ target and α beam. Because of these by-products, the radiation dose from the irradiated $BaCl_2$ target was quite high, and the γ-ray of ^{141}Ce was only observed after the decay of these by-products. On the other hand, in the γ-ray spectrum of ^{141}Ce produced with BaO, no such interference nuclides were observed, and the γ-ray of ^{141}Ce was observed soon after the end of irradiation. Therefore, BaO is considered to be a suitable target material for the production of ^{141}Ce by the α beam.

The elution curves for ^{nat}Ba and ^{141}Ce from the Ln resin are shown in Fig. 1 (BaO was used as the target material). ^{nat}Ba was eluted before ^{141}Ce with 0.01 M HCl. After the elution of ^{nat}Ba, ^{141}Ce was recovered by elution with 1 M HCl. The recovery yield for ^{141}Ce was greater than 99%. The contamination of ^{nat}Ba into ^{141}Ce fraction was calculated as less than 3 μg in the ICP-MS measurement: the separation factor of ^{141}Ce for ^{nat}Ba is greater than 10^4.

In the next study, the radiopharmaceutical labeling of ^{141}Ce will be investigated.

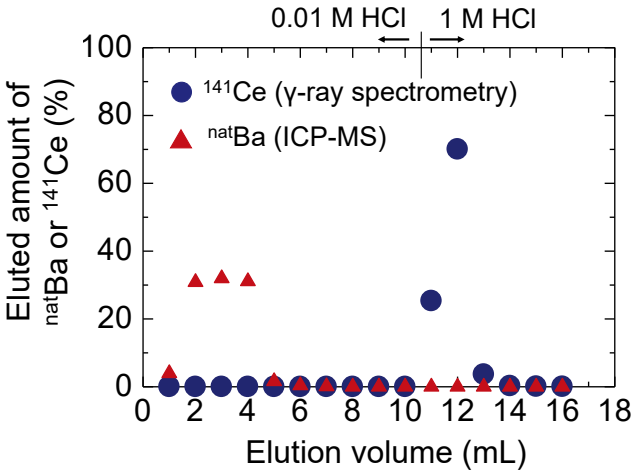

Fig. 1. Elution curves of ^{nat}Ba and ^{141}Ce in chromatographic separation with Ln resin.

Reference

1) E. P. Horwitz, C. A. A. Bloomquist, J. Inorg. Nucl. Chem. **37**, 425 (1975).

*1 Department of Nuclear Medicine and Tracer Kinetics, Graduate School of Medicine, Osaka University
*2 Institute for Radiation Sciences, Osaka University
*3 RIKEN Nishina Center
*4 Research Center for Nuclear Physics, Osaka University

Production of no-carrier-added Cr radiotracers in α-particle-induced reactions on Ti target

T. Yokokita*1 and H. Haba*2

^{48}Cr is a promising radioisotope for a double photon emission computed tomography.[1] The proposed method can achieve high spatial resolution and high signal-to-noise ratio.[2] As ^{48}Cr, a pair of 112- and 308-keV photons can be used for coincidence imaging.[1] We plan to produce ^{48}Cr in the ^{46}Ti$(\alpha, 2n)^{48}$Cr reaction. In nuclear medicine, ^{48}Cr must be chemically separated from the target material and byproducts. In this study, we investigated a production method of no-carrier-added Cr radiotracers from an α-particle-irradiated ^{nat}Ti (nat = natural isotopic abundance) target using ^{51}Cr ($T_{1/2}$ = 27.7 d) produced in the ^{nat}Ti$(\alpha, xn)^{51}$Cr reaction. In the future, ^{48}Cr can be produced using expensive enriched $^{46}TiO_2$ as the target material. Therefore, we also investigated the recovery of the target material after the production of the Cr radiotracers.

^{48,51}Cr were produced in the ^{nat}Ti$(\alpha, xn)^{48,51}$Cr reactions using the RIKEN AVF cyclotron. A metallic ^{nat}Ti plate of thickness 45 mg/cm^2 was irradiated for 1.69 h with a 28.9-MeV α beam of intensity 3.1 particle μA. Upon irradiating the target, ^{48}V ($T_{1/2}$ = 16.0 d) was also produced in the ^{nat}Ti$(\alpha, x)^{48}$V reaction and as the electron-capture and β^+-decay daughter of ^{48}Cr ($T_{1/2}$ = 21.6 h). It is desirable to remove the long-lived ^{48}V just before the imaging experiment with ^{48}Cr to increase the signal-to-noise ratio.

The irradiated ^{nat}Ti plate (63.4 mg) was dissolved in a mixture of 1 mL of concentrated HF (c. HF) and 0.3 mL of c. HNO_3 by heating, and the solution was evaporated to dryness. The residue was dissolved with 1 mL of c. HF by heating, and the solution was evaporated to dryness. The residue was dissolved in 6 mL of 4.5 M HF by heating. Subsequently, the solution was fed into an anion-exchange column (Muromac 1X8, 100–200 mesh, 10 mm *i.d.* × 110 mm height). The resin was washed with 9 mL (1 mL × 9) of 4.5 M HF and 35 mL (5 mL × 7) of c. HF. The 4.5 M HF fractions were combined, and 3 mL of it was used for the ICP-MS measurement to confirm the contamination of ^{nat}Ti.

The remainder of the 4.5 M HF was evaporated to dryness and further purified to remove ^{48}V using cation-exchange chromatography. The residue was dissolved in 3 mL of 0.5 M HNO_3. The solution (1 mL × 3) was fed into a cation-exchange column (Muromac 50WX8, 100–200 mesh, 5 mm *i.d.* × 50 mm height). The resin was washed with 3 mL (1 mL × 3) of 0.5 M HNO_3 and 5 mL (1 mL × 5) of 6 M HNO_3.

Each eluent from the anion- and cation-exchange columns were subjected to γ-ray spectrometry with a Ge detector to obtain the elution curves of ^{51}Cr and ^{48}V. To evaluate the elution curve of ^{nat}Ti, each c. HF fraction was evaporated to dryness, and the residue was weighted.

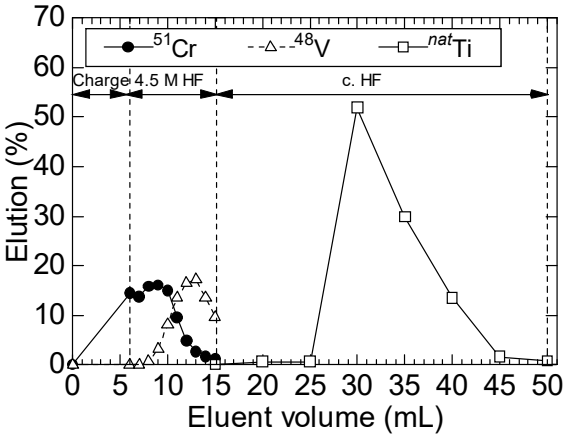

Fig. 1. Elution curves of ^{51}Cr, ^{48}V, and ^{nat}Ti for the anion-exchange chromatography.

The elution curves for the anion-exchange chromatography of ^{51}Cr, ^{48}V, and ^{nat}Ti are shown in Fig. 1. 95% of ^{51}Cr were eluted with 15 mL of 4.5 M HF. The decontamination factor of the ^{nat}Ti for ^{51}Cr was 4.9×10^{-4}, indicating that the anion-exchange separation was useful in the separation of the Cr radiotracers from the target material Ti. However, the decontamination factor of ^{48}V for ^{51}Cr was not satisfied (0.83). In regards to ^{nat}Ti, 99% was eluted with 35 mL of c. HF. This high recovery yield of ^{nat}Ti is promising for recycling of the enriched ^{46}Ti target material.

The elution curves in the cation-exchange chromatography of ^{51}Cr and ^{48}V are shown in Fig. 2. 94% of ^{51}Cr

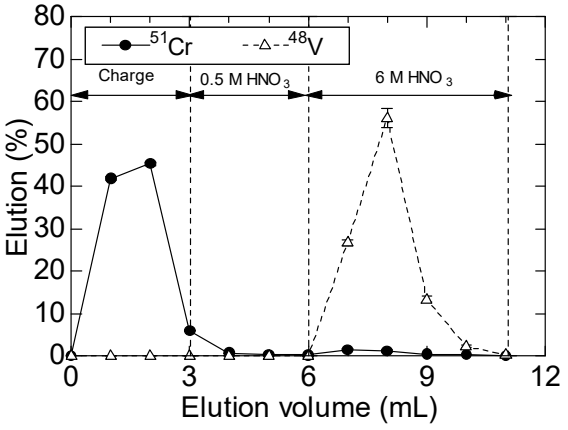

Fig. 2. Elution curves of ^{51}Cr and ^{48}V for the cation-exchange chromatography.

*1 Department of General Education, Salesian Polytechnic
*2 RIKEN Nishina Center

was eluted with 6 mL of 0.5 M HNO_3. The decontamination factor of ^{48}V for ^{51}Cr was improved from 0.83 to 1.1×10^{-3}. The chemical yield of ^{51}Cr was 90% after both the anion- and cation-exchange separations.

We propose a method for the production no-carrier-added Cr radiotracers from an α-particle-irradiated Ti target. The ^{48}Cr produced using the proposed method using enriched $^{46}TiO_2$ as the target material can be used for double photon coincidence imaging experiments.

References

1) M. A. Choghadi *et al.*, Radioisotopes **70**, 271 (2021).
2) Y. Yoshihara *et al.*, Nucl. Instrum. Methods Phys. Res. A **873**, 51 (2017).

Production of ^{44}Ti via the ^{45}Sc$(p, 2n)^{44}$Ti reaction for ^{44}Ti/^{44g}Sc generator development

X. Yin,[*1] T. Fukuchi,[*2] Y. Watanabe,[*2] and H. Haba[*1]

^{44g}Sc is a promising radionuclide for PET imaging applications. Its direct production via the ^{44}Ca$(p, n)^{44m, g}$Sc and ^{44}Ca$(d, 2n)^{44m, g}$Sc reactions were investigated by several groups.[1–4] Owing to the short half-life of ^{44g}Sc ($T_{1/2}$ = 3.9 h), daily irradiations close to the site where it is used are required to maintain a constant supply of ^{44g}Sc. An alternative approach to obtain ^{44g}Sc is the production by the ^{44}Ti ($T_{1/2}$ = 59.1 y)/^{44g}Sc generator.[5] In this work, we investigated the production of ^{44}Ti via the ^{45}Sc$(p, 2n)^{44}$Ti reaction to develop the ^{44}Ti/^{44g}Sc generator.

A metallic ^{45}Sc (99.99%) disk target with a diameter and thickness of 10 mm and 0.90 g/cm^2, respectively, was placed in an irradiation chamber with helium gas and water cooling.[6] The target was irradiated for 1.25 h with a 0.25-μA proton beam from the RIKEN AVF cyclotron. The incoming and outgoing proton beam energies were 30 MeV and 15 MeV, respectively.

Large amounts of ^{44m}Sc ($T_{1/2}$ = 58.6 h) and ^{44g}Sc were also produced in the ^{45}Sc$(p, x)^{44m, g}$Sc reactions. The short-lived ^{44g}Sc fully decays in several days. Thus, the activities of ^{44m}Sc and ^{44}Ti at the end of bombardment (EOB) were determined by fitting the decay curve of the 1157-keV gamma line of ^{44g}Sc after radioactive equilibrium. The yields of ^{44}Ti and ^{44m}Sc with the beam energy range of 30–15 MeV were calculated based on the cross-section data reported by L. Daraban.[7] The calculated results agree well with the experimental results. In addition, ^{46}Sc ($T_{1/2}$ = 83.8 d) was co-produced via the secondary-neutron-induced reaction of ^{45}Sc$(n, \gamma)^{46}$Sc. The activity of ^{46}Sc was determined by the 889-keV and 1121-keV gamma lines after 76 days of cooling. The results from the two gamma lines agree well with each other and are listed in Table 1.

^{44}Ti was separated from the target with ZR resin. Firstly, the irradiated ^{45}Sc target (0.71 g) was dissolved in 20 mL of 6 M HCl and heated to dryness. Subsequently, the residue was dissolved in 5 mL of 6 M HCl and fed into a column filled with conditioned ZR resin (100–150 μm, 5 mm *i.d.* × 5 mm). Scandium passed through the column while titanium was adsorbed on the resin. Finally, ^{44}Ti was eluted with 6 mL of 3 M HCl/0.325 M H_2O_2 solution.[8] The Ti/Sc separation factor was determined by the activity ratio of ^{44}Ti and ^{46}Sc before and after separation. The recovery yield of ^{44}Ti was 95%, and the Ti/Sc separation factor was >10^3 in this scheme. The gamma-ray spectrum of ^{44}Ti after the chemical separation is shown in Fig. 1. Small amounts of long-lived ^{56}Co ($T_{1/2}$ = 77.3 d) and ^{54}Mn ($T_{1/2}$ = 312.3 d) found in the irradiated target were successfully removed by the chemical separation. Only gamma lines from ^{44}Ti and its daughter, ^{44g}Sc, were identified in the gamma-ray spectrum. The radionnuclidic purity of ^{44}Ti after chemical separation was evaluated to be >99%.

Table 1. Activities of ^{44}Ti, $^{44m, 46}$Sc at EOB.

Nuclide	γ-ray energy (keV)	Calc. yield (Bq/μAh)	Activity at EOB (Bq)	
			Calc.	Exp.
^{44}Ti	1157	3338	1043	1114 ± 55
^{44m}Sc	1157	1.3×10^8	4.2×10^7	4.1×10^7 ± 2.5×10^5
^{46}Sc	889		-	454 ± 15
	1121			459 ± 15

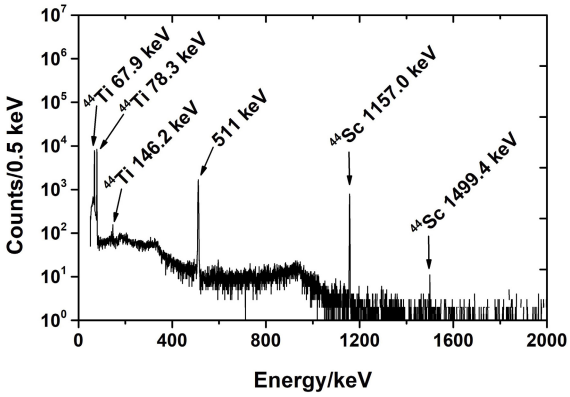

Fig. 1. Gamma-ray spectrum of ^{44}Ti after separation.

By assuming experimental conditions (incident beam energy: 30 MeV; beam intensity: 10 μA; target thickness: 0.9 g/cm^2; irradiation time: 10 d), 8 MBq of ^{44}Ti can be produced at the EOB.

In the future, we will develop a prototype of the ^{44}Ti/^{44g}Sc generator with long-term stability, high yield of ^{44g}Sc, and no ^{44}Ti breakthrough.

References
1) C. Alliot *et al.*, Nucl. Med. Biol. **42**, 524 (2015).
2) G. W. Severin *et al.*, Appl. Radiat. Isot. **70**, 1526 (2012).
3) C. Müller *et al.*, J. Nucl. Med. **54**, 2168 (2013).
4) R. Hernandez *et al.*, Mol. Pharm. **11**, 2954 (2014).
5) D. Filosofov *et al.*, Radiochim. Acta **98**, 149 (2010).
6) S. Yano *et al.*, RIKEN Accel. Prog. Rep. **50**, 261 (2017).
7) L. Daraban *et al.*, Nucl. Instrum. Methods Phys. Res. B **267**, 755 (2009).
8) V. Radchenko *et al.*, J. Chromatogr. A **1477**, 39 (2016).

*1 RIKEN Nishina Center
*2 RIKEN Center for Biosystems Dynamics Research

HPLC elution behavior of heavy lanthanide metallofullerene: Ln@C_{82} (Tb, Dy, Ho, Er, Lu) on pyrenyl stationary phase

K. Akiyama,[*1,*2] K. Amekura,[*1] H. Haba,[*2] and S. Kubuki[*1]

Metallofullerene (MF) is a clathrate compound encapsulating metal atoms in a fullerene molecule. Lanthanide (Ln) EMF, Ln@C_{82}, have two or three charge transferred electrons on the C_{82} cage from the encapsulated Ln atom, and their electronic states reflect the number of charge transfer electrons.[1] From the view point of inorgnic chemistry, it is interesting to probe the effect of the electronic state for the series of the ten lanthanide elements (La, Ce, Pr, Nd, Gd, Tb, Dy, Ho, Er, Lu) with the electronic states of $(Ln^{3+})@({C_{82}}^{3-})$ on the electronic state of the Ln@C_{82} molecule from the difference in interaction with pylenyl stationary phase. To this end, we have determined the retention time in the pyrenyl stationary phase for five types of Ln@C_{82} from La to Gd by using radio chromatography with ten Ln metal atoms activated by the thermal neutron activation method. Moreover, the retention times in the High Performance Liquid Chromatography (HPLC) of Ln@C_{82} with heavy lanthanide elements have not been obtained, because the half-lives of the radionuclides produced by thermal neutron irradiation such as ^{165}Dy and ^{171}Er are very short. Moreover, the production of Ln_2@C_{82} and Ln_2C_2@C_{80}, whose production rate increase competitive products, inteferes with the detection of Ln@C_{82} with increasing atomic number of Ln. In this paper, we report the HPLC retention time of Ln@C_{82} encapsulating heavy lanthanides evaluated from HPLC data of already purified Ln@C_{82} and ^{139}Ce@C_{82}, where ^{139}Ce was produced using the RIKEN AVF cyclotron as a comparative standard of HPLC analysis.

Cerium-139 produced by ^{139}La$(d, 2n)^{139}$Ce reaction using a ^{nat}La target irradiated with 5 μA of 24 MeV deuterons for 5 h at the RIKEN AVF cyclotron was purified from the target material of La by a solvent extraction method. The studied heavy Ln@C_{82} in this work were produced and separated by a previously reported method.[2] The separated metallofullerene solutions were purified by HPLC with a Buckyprep-M column (flow rate: 3.2 mL min^{-1}, developing solvent: toluene) from other interfering metallofullerenes such as Ln_2@C_{82}. These purified Ln@C_{82} with ^{139}Ce@C_{82} were injected into a buckyprep column, whose stationary phase is silicate modified with propylpylenylsilyl (flow rate: 3.2 mL min^{-1}, developing solvent: toluene), monitored by UV absorption. Then, the elution components were fractionated every 20 seconds. The HPLC retention times of ^{139}Ce@C_{82} and Ln@C_{82} were evaluated from the gamma-ray measurement of each sample with a Ge detector and HPLC chromatogram monitored by the UV absorption, respectively.

Here, we define the HPLC retention time of Ln@C_{82} obtained in this study and the void retention time corresponding to the void volume of column as t_{Ln} and t_0, respectively, and the retention ratio of k_{Ln} of Ln@C_{82} is given by $k_{Ln} = (t_{Ln} - t_0)/t_0$. The separation coefficient (α) can be expressed as the ratio of the retention ratio for Ln@C_{82} (k_{Ln}) to that for ^{139}Ce@C_{82} (k_{Ce}). The HPLC retention time t_{Ln} and the evaluated separation coefficient of the studied Ln@C_{82} are shown in Table 1. Figure 1 shows the separation coefficient for each heavy lanthanide Ln@C_{82} as a function of the spin multiplicity of Ln, together with those for previously reported α of light lanthanide Ln@C_{82}. Since a very good correlation can be seen between $2S + 1$ and α of Ln@C_{82} (Ln: La to Er), it is presumed that the small difference in the interaction between the pyrenyl stationary phase and Ln@C_{82} is caused by the 4f electronic state of the encapsulated lanthanide atom. For Lu@C_{82}, the large separation coefficient cannot be explained. In the near future, it is necessary to investigate the properties of Lu@C_{82} in detail.

Table 1. HPLC retention time and separation coefficient α of studied Ln@C_{82}.

	Tb	Dy	Ho	Er	Lu
k_{Ce}	10.17	10.16	10.11	9.196	9.303
k_{Ln}	10.38	10.20	10.19	9.307	9.453
α	1.021	1.004	1.008	1.012	1.016

Error of t and α is estimated to be less than 0.3%

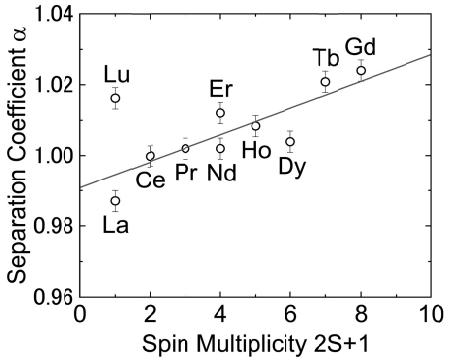

Fig. 1. Relation between spin multiplicity of Ln and separation coefficient α.

*1 Department of Chemistry, Tokyo Metropolitan University
*2 RIKEN Nishina Center

References

1) H. Shinohara, Rep. Prog. Phys. **63**, 843 (2000).
2) K. Akiyama *et al.*, RIKEN Accel. Prog. Rep. **53**, 194 (2019).

Ionic liquid extraction of astatine for a nuclear medical utilization

Y. Nagai,[*1] K. Aoi,[*1] S. Maruyama,[*1] A. Yokoyama,[*2,*3] K. Washiyama,[*4] I. Nishinaka,[*5] Y. Wang,[*3] X. Yin,[*3] A. Nambu,[*3] Y. Shigekawa,[*3] and H. Haba[*3]

Astatine-211 is a nuclide with potential applications in α-ray internal therapy. Solvent extraction with an organic solvent has been used as a conventional method for separating ^{211}At from the ^{209}Bi target irradiated with an α beam from an accelerator. Although organic solvents are inexpensive and readily available, they are volatile and flammable, and therefore, they raise concerns about environmental pollution and handling of dangerous substances.

In recent years, ionic liquids have attracted attention as an alternative to organic solvents from the viewpoint of green chemistry. Ionic liquids are in the liquid phase at room temperature, have low volatility, and are flame-retardant: therefore, there is little environmental load or risk of accidents. Further, the amount of radioactive waste can be reduced compared to that using organic solvents because they can be used repeatedly. In addition, ionic liquids are considered promising solvents for extracting ^{211}At given the reports on radiation resistance.[1] However, few studies on the extraction of ^{211}At with ionic liquids have been reported in the literature.[2] Therefore, in this study, we investigated the suitability of the HCl system, which has been reported to show excellent performance for ^{211}At solvent extraction,[2] depending on the type of ionic liquid.

The nuclide of ^{211}At was produced via the ^{209}Bi$(\alpha, 2n)$ reaction at the RIKEN AVF cyclotron and delivered to Kanazawa University. The irradiated Bi target was dissolved in 3 mL of 6 M HNO_3 and mixed with an appropriate amount of H_2O to prepare a 1 M HNO_3 solution, 7 mL of which was used to extract the ^{211}At nuclide into 7 mL of dodecane solvent. After extracting ^{211}At to dodecane from HNO_3 solution, it was further extracted to 0.1 M, 1 M, and 3 M HCl solutions. Then, ^{211}At was extracted into five kinds of ionic liquids: $[C_8\ \mathrm{mim}]^+$ $[PF_6]^-$, $[C_8\ \mathrm{mim}]^+$ $[BF_4]^-$, and $[C_{4,6,8}\ \mathrm{mim}]^+$ $[Tf_2N]^-$, where $[C_n\ \mathrm{mim}]^+$ and $[Tf_2N]^-$ stand for alkylimidazolium ion and bis(trifluoromethanesulfonyl)imide ion, respectively. Finally, it was back extracted into 0.1, 1, and 3 M NaOH solutions. The radioactivity of ^{211}At was measured with a liquid scintillation counter for the HCl solution samples before and after extraction and the NaOH solution samples after back extraction. The extraction rate of ^{211}At from the HCl solution to the ionic liquid and the back extraction rate from the ionic liquid to the NaOH solution were determined. Further, the At chemical species in the HCl solution were inferred by the TLC analysis of dodecane before and after extraction.

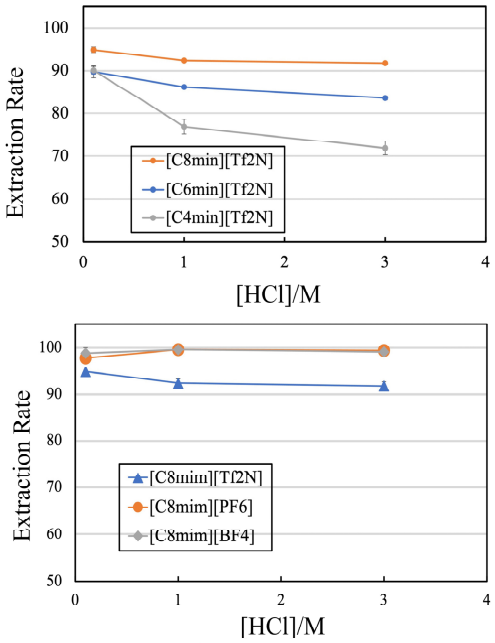

Fig. 1. At extraction rates of ionic liquids from HCl solutions.

Figure 1 shows the extraction rates of ^{211}At from the HCl solutions for five ionic liquids of ion pairs from three cations and three anions. When comparing cations, the larger the carbon chain, the higher is the extraction rate. When comparing anions, the larger the hydrophobicity, the smaller is the extraction rate. The hydrophobicity of cations and anions in the ionic liquid affects the ion exchange with At ions in the aqueous phase. In addition, the rates for $[C_8\ \mathrm{mim}]$ $[Tf_2N]$ have values exceeding 90% for both extraction and back extraction while $[C_8\ \mathrm{mim}]$ $[PF_6]$ and $[C_8\ \mathrm{mim}]$ $[BF_4]$ exhibit back extraction rates of less than 20%. Therefore, one of the ion liquids studied is considered promising for ^{211}At solvent extraction in practical applications.

*1 Graduate School of Natural Science and Technology, Kanazawa University
*2 Institute of Science and Engineering, Kanazawa University
*3 RIKEN Nishina Center
*4 Fukushima Global Medical Science Center, Fukushima Medical University
*5 Quantum Beam Science Research Directorate, National Institutes for Quantum Science and Technology

References

1) L. Yuan *et al.*, J. Phys. Chem. B **113**, 8948 (2009).
2) K. Kawasaki, Master thesis, Graduate School of Natural Science and Technology, Kanazawa University (2020).

Synthesis of [^{211}At]4-astato-L-phenylalanine by dihydroxyboryl-astatine substitution reaction in aqueous solution†

Y. Shirakami,[*1] T. Watabe,[*2] H. Obata,[*3] K. Kaneda,[*1] K. Ooe,[*2] Y. Liu,[*2] T. Teramoto,[*1] A. Toyoshima,[*1] A. Shinohara,[*1] E. Shimosegawa,[*2] J. Hatazawa,[*1] and K. Fukase[*3]

Radiopharmaceutical therapy, including targeted alpha-particle therapy (TAT), has recently emerged as a novel therapeutic modality for the treatment of tumor. We previously demonstrated the utility of [^{211}At]4-astato-L-phenylalanine ([^{211}At]APA) for the treatment of glioma in tumor-bearing mice by means of TAT.[1] [^{211}At]APA specifically accumulates in tumor cells and are transported by the LAT1 transporters, which are predominantly expressed on the surface of various tumor cells including the glioma cells. In a mouse model xenografted with rat glioma cells, [^{211}At]APA significantly decreased the tumor volume after a single injection of the agent (dose range: 0.1–1.0 MBq/mouse) in the mouse.

Phenylalanine has been previously labeled with ^{211}At using different methods.[2,3] However, most of the existing reactions for the synthesis of radiolabeled compounds either require the use of toxic and hazardous chemicals or are unable to yield a carrier-free final product.

We have developed a new and improved method for the preparation of [^{211}At]APA using 4-borono-L-phenylalanine (BPA) as the starting molecule. [^{211}At]APA was synthesized by the electrophilic substitution of ^{211}At for a dihydroxyboryl (or borono) group on an aromatic ring of the corresponding precursor molecule BPA using N-bromosuccinimde (NBS; NBS method) as an oxidant or KI (KI method) as shown in Fig. 1. The radiochemical yield (RCY) and radiochemical purity (RCP) were better with the latter method. The reagents and compounds used for the synthesis of [^{211}At]APA were commercially approved drugs and physiologically relevant for clinical use. The entire synthesis could be accomplished in aqueous media; no organic solvents or toxic metals were required, suggesting that this method is relevant for practical applications. We also elucidated the differences between the chemical properties of iodine and astatine for the labeling reactions.

Based on our findings, the reaction scheme for the ^{211}At labeling of arylboronic acids is depicted in Fig. 2. In the NBS method, ^{211}At initially reacts with NBS to form the [^{211}At]astatosuccinimide intermediate (Fig. 2, top). Then, [^{211}At]astatosuccinimide reacts with the arylboronic acid to produce [^{211}At]arylastatide. In the KI method, ^{211}At reacts with KI to form the [^{211}At]AtI and/or AtI_2^- intermediate (Fig. 2, bottom). Several

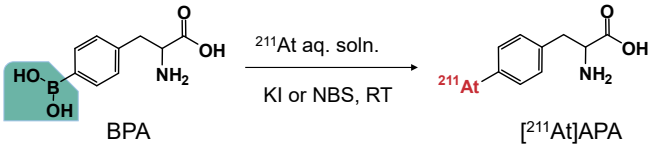

Fig. 1. Radioastatination reaction of boronophenylalanine.

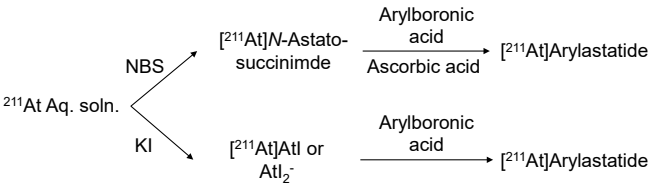

Fig. 2. Mechanism of astatination of arylboronic acids.

studies have suggested that astatine can react with iodide and produce inter-halogen compounds such as AtI and AtI_2^-.[4] The AtI and/or AtI_2^- intermediate reacts with the arylboronic acid to give [^{211}At]arylastatide. Compared to NBS, KI was found to be more efficient for the substitution of the dihydroxyboryl group by astatine in the aqueous media. KI can probably reduce the hypervalent ^{211}At species present in the aqueous solution (∼10%), forming the reactive [^{211}At]AtI and/or AtI_2^- intermediate that allows higher RCYs compared to that obtained using the NBS method.

KI was originally intended to be used as the carrier atom of ^{211}At since there are no natural stable isotopes of astatine. Unexpectedly, the radiolabeling yield of [^{211}At]APA using KI was much higher than 95%, due to the formation of [^{211}At]AtI and/or AtI_2^- as a reaction intermediate in the aqueous solution.

It is well known that tyrosine can be labeled with radioactive iodine via an electrophilic substitution reaction in the presence of an oxidant, such as chloramine T, Iodogen, *N*-chlorosuccinimde, NBS, or H_2O_2. Astatination of tyrosine, however, gave a low yield of [^{211}At] astatotyrosine (<15%) with H_2O_2, and the product was unstable under neutral and basic conditions. Additionally, the labeling yield was low. These results were suggestive of the different chemical properties of astatine and iodine.

In summary, we developed a novel method for the synthesis and purification of [^{211}At]APA, which has potential clinical uses.

† Condensed from the article in Sci. Rep. **11**, 12982 (2021)
*1 Institute for Radiation Sciences, Osaka University
*2 Department of Tracer Kinetics and Nuclear Medicine, Graduate school of Medicine, Osaka University
*3 Department of Chemistry, Graduate School of Science, Osaka University

References

1) T. Watabe *et al.*, Oncotarget **11**, 1388 (2020).
2) G. J. Meyer *et al.*, Appl. Radiat. Isot. **68**, 1060 (2010).
3) N. Borrmann *et al.*, Nuklearmedizin **52**, 212 (2013).
4) G. W. Visser *et al.*, Int. J. Appl. Radiat. Isot. **32**, 905 (1981).

Neopentyl glycol as a scaffold to provide radiohalogenated theranostic pairs of high *in vivo* stability†

H. Suzuki,[*1] Y. Kaizuka,[*1] M. Tatsuta,[*2] H. Tanaka,[*2] N. Washiya,[*1] Y. Shirakami,[*3] K. Ooe,[*4] A. Toyoshima,[*3] T. Watabe,[*4] T. Teramoto,[*3] I. Sasaki,[*5] S. Watanabe,[*5] N. S. Ishioka,[*5] J. Hatazawa,[*6] T. Uehara,[*1] and Y. Arano[*1]

^{211}At is one of the most promising α-emitting radionuclides applicable to targeted α-therapy. Low-molecular-weight targeting molecules are suitable for delivering ^{211}At to target tissues because of its short half-life (7.2 h). Benzoate derivatives have been widely used to prepare radioiodinated low-molecular-weight targeting molecules of high stability against *in vivo* deiodination.[1] Although astatine shares some chemical properties similar to those of iodine, ^{211}At-labeled benzoate derivatives are unstable against *in vivo* deastatination.[2] Therefore, a new scaffold applicable to a radiotheranostic system with ^{211}At and radioiodine needs to be developed.

We focus on a neopentyl glycol structure used for 2-dihydroxymethyl-3-[^{18}F]fluoropropyl-2-nitroimidazole ([^{18}F]DiFA, Fig. 1) that shows high stability against *in vivo* defluorination.[3] In this study, the neopentyl glycol structure was applied for heavier radiohalogens such as radioiodine and ^{211}At; however, the dissociation energy of sp^3 carbon-halogen bonds in alkyl halides is low and decreases with an increase in the atomic number of halogen.[4] Three neopentyl iodide compounds with or without hydroxyl groups ([^{125}I]**1a**, [^{125}I]**2**, and [^{125}I]**3**, Fig. 1) were synthesized to investigate the role played by the hydroxyl groups before studying with ^{211}At-labeled compounds.

All three neopentyl iodides remained stable against the nucleophilic attack. While [^{125}I]**2** and [^{125}I]**3** were deiodinated by cytochrome P450 (CYP)-mediated metabolism, [^{125}I]**1a** remained stable against CYP-mediated metabolism. The biodistribution study was correlated with the *in vitro* study of CYP-mediated metabolism; [^{125}I]**1a** showed the lowest accumulation in the stomach and neck where free [^{125}I]I$^-$ accumulates. The liberation of [^{125}I]I$^-$ was observed via the urine analyses of [^{125}I]**2** and [^{125}I]**3** but it was not observed for [^{125}I]**1a**, which indicates that the C-I bond of [^{125}I]**1a** was stable against in vivo deiodination.

The structure of [^{125}I]**1a** was applied for ^{211}At to prepare [^{211}At]**1b**. ^{211}At used in this work was produced in the ^{209}Bi(α, 2n)^{211}At reaction using the RIKEN AVF cyclotron. [^{211}At]**1b** showed high *in vitro* stability against nucleophilic attack and the CYP-mediated metabolism.

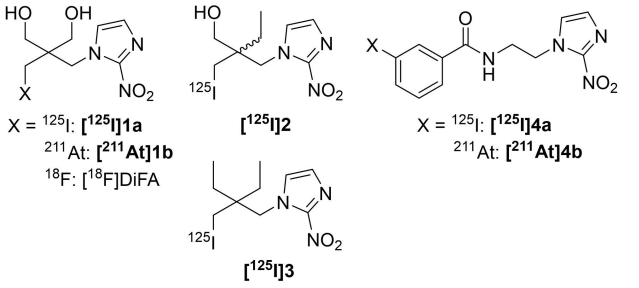

Fig. 1. Chemical structures of neopentyl and benzoate derivatives evaluated in this study.

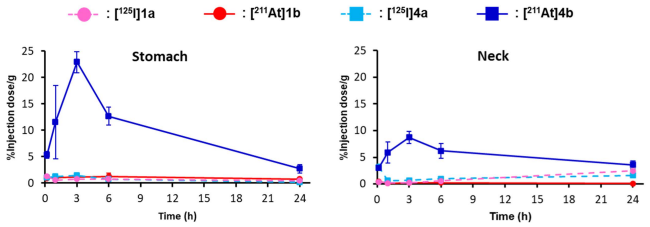

Fig. 2. Biodistribution in selected organs after the injection of [^{125}I]**1a**, [^{211}At]**1b**, [^{125}I]**4a**, and [^{211}At]**4b**.

When injected into normal mice, the radioactivity levels in the stomach and the neck registered low levels. The biodistribution profiles of [^{211}At]**1b** were similar to those of [^{125}I]**1a** (Fig. 2). However, the reference compound [^{211}At]**4b** (Fig. 1) exhibited pharmacokinetics different from [^{125}I]**4a**, with high radioactivity levels observed in the stomach and the neck. Further, the urine analysis showed that [^{211}At]At$^-$ was liberated from [^{211}At]**4b** but not from [^{211}At]**1b**, which implies that the C-At bond of [^{211}At]**1b** was stable against *in vivo* deastatination.

In this study, a neopentyl structure with two hydroxyl groups (neopentyl glycol) provided ^{125}I- and ^{211}At-labeled compounds with high stability against nucleophilic attack and the CYP-mediated metabolism. Furthermore, both compounds registered similar biodistribution profiles and metabolic fate. These findings indicate that neopentyl glycol would constitute a useful scaffold for developing a radiotheranostic system with radioiodine and astatine as radiolabels for further applications.

† Condensed from the article in J. Med. Chem. **64**, 15846 (2021)
*1 Graduate School of Pharmaceutical Sciences, Chiba University
*2 Department of Chemical Science and Engineering, Tokyo Institute of Technology
*3 Institute for Radiation Sciences, Osaka University
*4 Graduate School of Medicine, Osaka University
*5 Takasaki Advanced Radiation Research Institute, National Institutes for Quantum Science and Technology
*6 Research Center for Nuclear Physics, Osaka University

References
1) M. R. Zalutsky *et al.*, Cancer. Res. **49**, 5543 (1989).
2) G. Vaidyanathan, M. R. Zalutsky, Curr. Radiopharm. **1**, 177 (2008).
3) N. Nakata *et al.*, Nucl. Med. Biol. **70**, 39 (2019).
4) H. H. Coenen *et al.*, Radiochim. Acta **34**, 47 (1983).

Treatment for peritoneal dissemination of gastric cancer using ^{211}At

S. Nomura,[*1] A. Sugiyama,[*2] H. Haba,[*3] Y. Wang,[*3] Y. Kumakura,[*4] N. Akimitsu,[*2] and Y. Wada[*]

Peritoneal dissemination is one of the miserable patterns of recurrence of cancer. This recurrence pattern is the most common in gastric cancer. There is no way to cure it and there are only treatment methods to decelerate the cancer growing by chemotherapy or immunotherapy. External irradiation is also difficult for avoiding intestinal irradiation. We developed murine gastric cancer cell lines, YTN that can be transplanted into C57BL/6, immunocompetent mouse.[1] YTN16 can develop peritoneal dissemination in C57BL/6 mice with 100% rate, when 1×10^7 cells are injected into the peritoneal cavity. We also have less aggressive subline YTN2. Comparing mRNA expression between YTN16 and YTN2, using microarray, Fibroblast Growth Factor Receptor 4 (FGFR4) was highly expressed in YTN16. Since α-emitting ^{211}At is reported to be an effective therapy for peritoneal dissemination,[2] we sought to develop the treatment for YTN16 peritoneal dissemination using ^{211}At-FGFR4 Ab.

YTN16 peritoneal dissemination mouse model was made as we reported and 3 weeks later, ^{211}At was administered and the accumulation of ^{211}At into peritoneum was measured using a gamma-counter after 4.5 hours, 16 hours, and 23 hours after administration. The 1 MBq of free ^{211}At was administered through intra venous (0.2 mL), intra peritoneum (1.0 mL), and intra gastric (0.5 mL). The ^{211}At-FGFR4 Ab (1 MBq-16.4 μg Ab) was administered through intra venous (0.2 mL) and intra peritoneum (1.0 mL). As shown in Fig. 1, ^{211}At conjugated with Ab accumulated in peritoneum 16 hours and 23 hours after administration.

Next, to confirm the treatment effect of ^{211}At, we sacrificed the mice 5 weeks after transplantation of YTN16, through ^{211}At treatment 10 days before sacrifying. The severity of peritoneal dissemination could be diagnosed macroscopically. As shown in Fig. 2, intraperitoneal

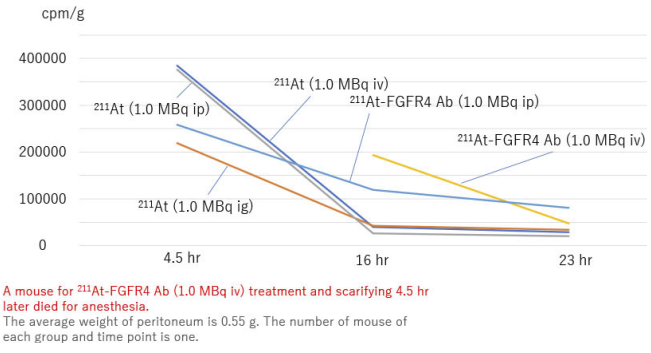

Fig. 1. ^{211}At accumulation in peritoneum.

*1 Department of Gastrointestinal Surgery, University of Tokyo
*2 Isotope Science Center, University of Tokyo
*3 RIKEN Nishina Center
*4 Department of Radiology, Saitama Medical University

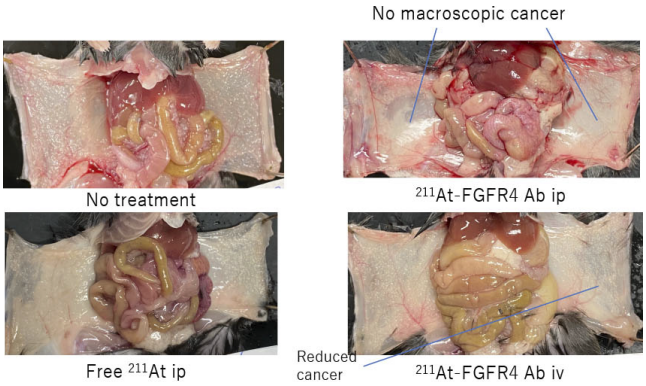

Fig. 2. Treatment effect of ^{211}At for peritoneal dissemination.

administration of ^{211}At-FGFR4 Ab was most effective followed by intravenous administration of ^{211}At-FGFR4 Ab, and intraperitoneal administration of free ^{211}At.

Finally, the effect for overall survival of mice was analyzed by Kaplan-Mayer curves. As shown in Fig. 3, ^{211}At-FGFR4 Ab significantly prolonged the overall survival of mice with gastric cancer peritoneal dissemination.

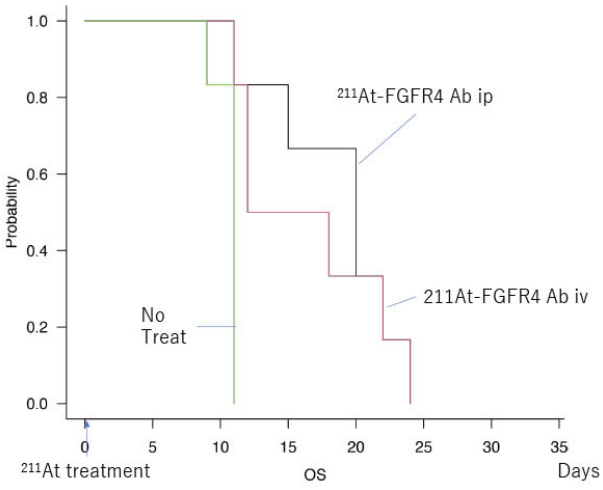

Fig. 3. Kaplan-Mayer analysis for treated mice.

The ^{211}At-Ab treatment for peritoneal dissemination was effective for reducing the cancer and elongating overall survival. More improvement is needed for prolonging the survival. Especially effective methods for gathering ^{211}At to cancer faster are needed.

References

1) M. Yamamoto *et al.*, Cancer Sci. **109**, 1480 (2018).
2) H. K. Li *et al.*, Cancer Sci. **108**, 1648 (2017).

Analysis of complex formation between rhenium and various hydrophilic ligands using HPLC and preparation of ^{186}Re-carrying liposomes

I. O. Umeda,[*1] Y. Hamane,[*1] M. Nagata,[*1] A. Tenzaki,[*1] H. Haba,[*2] A. Nambu,[*2] X. Yin,[*2] H. Fujii,[*3] and T. Takahashi[*1]

Theranostics is an emerging and expanding medical field based on therapeutic interventions after imaging to verify the presence of a biological target. Radioisotope-based therapeutics, *i.e.*, radiotheranostics, is perhaps the most clinically advanced application of theranostics, with many developments and emerging opportunities. A key aspect of radiotheranostics is that the selection of patients for radiotargeted treatments is based on imaging of the same target area. Therefore, imaging and therapeutic intervention are closely linked.[1)] Technetium-99m is the most widely used nuclide in diagnostic nuclear medical imaging, because the energy of the corresponding gamma-ray emission (140 keV) is ideal for imaging using gamma cameras, and it can be generated on demand at medical facilities using ^{99}Mo/^{99m}Tc generators. Rhenium, a group 7 homologous element of technetium, is assumed to have chemical properties similar to those of Tc. ^{186}Re (half-life $T_{1/2} = 3.72$ days) emits beta rays of 1.07 MeV, appropriate for radionuclide therapy. Thus, ^{186}Re and ^{99m}Tc should be an ideal "theranostics pair." To this end, ^{186}Re has been produced by neutron irradiation in nuclear reactors, which is difficult to realize in Japan. At the RIKEN RI beam factory (RIBF), we succeeded in producing no-carrier-added, high-purity ^{186}Re using an accelerator-based ion beam irradiation. We are aiming to develop new radiotheranostics using ^{186}Re.

For radiotheranostics, a common platform for diagnostic and therapeutic nuclides is important. We have been investigating the application of liposomes, well-known drug carriers, as a radiotheranostics platform. Liposomes are promising tools for radiotheranostics, because they can in principle encapsulate any radionuclides, and deliver them to the target lesion. In this study, we conducted a basic investigation for efficient encapsulation of ^{186}Re into liposomes.

We encapsulated various radionuclides in liposomes with high efficiency using the remote loading method, *i.e.*, a ligand exchange reaction across the liposomal membrane using lipophilic and hydrophilic ligands.[2)] In this method, the complex formation between the nuclide and ligand and their stability are important factors. There are few data on the complex formation of ^{186}Re. We first developed an analytical method to evaluate their formation and stability using high performance liquid chromatography (HPLC) and a stable isotope of rhenium.

Rhenium-186 was produced in the ^{186}W$(d, 2n)^{186}$Re reaction. A 24-MeV deuteron beam delivered from the AVF cyclotron was irradiated onto a $^{186}WO_3$ pellet target (isotope enrichment of ^{186}W: 99.79%; thickness: 580 mg/cm^2). After irradiation, ^{186}Re was purified by chemical separation.[3)] An aqueous solution of ^{186}Re-perrhenate in 0.01 M HCl (radioactivity concentration: 83.0 MBq/mL) was supplied. Ammonium perrhenate was used as a stable isotope of rhenium. Diethylenetriamine-$N, N, N', N,'' N''$-pentaacetic acid (DTPA), dimercaptosuccinic acid (DMSA), hydrazinonicotinamide (HYNIC), and ethylenedicysteine (EC) were examined as hydrophilic ligands. HPLC analysis was conducted using Shimazu Prominence LC-20 equipped with aerosol-based detector NQAD and gamma-ray radiodetector. Liposomes comprised DSPC and cholesterol, or PEGylated, and preloaded hydrophilic ligands.

The formation of complexes between metal ions and ligands is difficult to analyze using conventional HPLC systems, because these samples have no UV absorption, and are highly water-soluble. We realized this using unique columns, combination of cation exchange column (CapcelPak CR) and unique ODS column (Capcell Core ADME), and a unique detector, NQAD. Using this system, we were able to detect metal ions, ligands, and the metal ion-ligand complexes as separate peaks. Figure 1 shows HPLC profiles of rhenium, technetium, EC, and their complexes.

Using this system, the formation of complexes between rhenium and various hydrophilic ligands was investigated. All the ligands used formed complexes with ^{99m}Tc. Under the conditions studied, DTPA and HYNIC did not form complexes with rhenium. In case of DMSA and EC, complex formation with rhenium was observed. However, unlike ^{99m}Tc, the complexes were formed only under acidic conditions, high temperature, and required approximately ten times more reducing agent than in the case of ^{99m}Tc.

Next, we preloaded EC into liposomes and attempted to encapsulate ^{186}Re and ^{99m}Tc into liposomes using the remote loading method. Incubation at 40°C allowed only ^{99m}Tc to be encapsulated, but heating to 90°C allowed ^{186}Re to be encapsulated into liposomes. Since ^{186}Re radioactivity was present in the water-soluble fraction of liposomes, it was assumed

*1 Kavli IPMU, University of Tokyo
*2 RIKEN Nishina Center
*3 EPOC, National Cancer Center

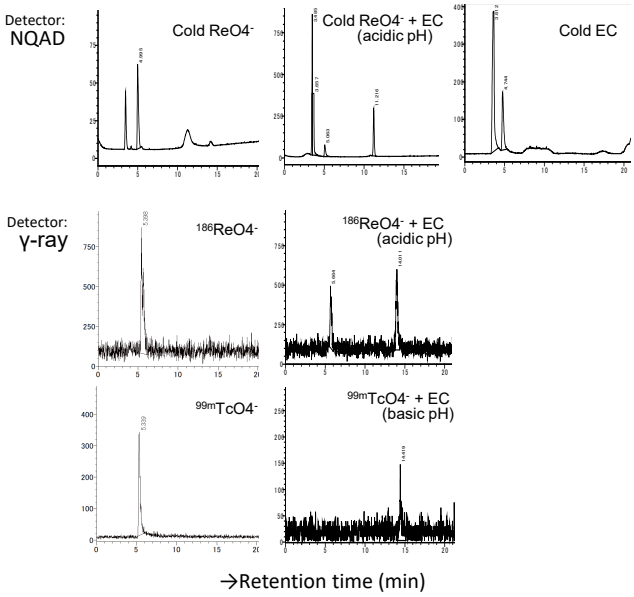

Fig. 1. HPLC separation of metal ions, ligands and metal-ligand complexes. Stable rhenium was used to determine the analytical conditions. NQAD was used for detection. ^{99m}Tc and ^{186}Re were then used to confirm the peaks.

that the ^{186}Re-EC complex was formed.

In this study, we have established a means to analyze complex formation between hydrophilic ligands and rhenium, and evaluated optimal conditions for stable rhenium complex formation. Based on the results, we have successfully prepared ^{186}Re-EC/^{99m}Tc-EC-encapsulated liposomes. These are expected to be useful radiopharmaceuticals for radiotheranostics. We are further investigating the quality control of the drugs and their pharmacokinetics and tumor accumulation.

References

1) K. Herrmann *et al.*, Lancet Oncol. **21**, e146 (2020).
2) I. Ogihara-Umeda *et al.*, J. Nucl. Med. **37**, 326 (1996).
3) N. Shigeta *et al.*, J. Radioanal. Nucl. Chem. **205**, 85 (1996).

Effect of tumor size on the therapeutic effect of ^{67}Cu-labeled compounds targeting the somatostatin receptor

Y. Fujisawa,[*1] H. Haba,[*2] A. Nambu,[*2] Y. Shigekawa,[*2] Y. Wang,[*2] X. Yin,[*2] Y. Magata,[*3] and Y. Iida[*1]

Nuclear medicine therapy, wherein a radiopharmaceutical is administered to patients for treatment, is an effective medical treatment that targets cancer cells in the body; it has garnered significant attention in recent years as an effective treatment process that places less burden on patients. Four nuclides are available in Japan, namely, ^{131}I, ^{90}Y, and ^{177}Lu, which are β-particle emitting nuclides, and ^{223}Ra, which is an α-particle emitting nuclide. ^{90}Y has a high energy β-particle of 2.28 MeV and exhibits good therapeutic effect; however, it has a significant impact on the surrounding tissues and the injected dose is limited by exposure to other organs.[1] Several other nuclides can be potentially used for nuclear medicine therapy. For example, ^{67}Cu has a low energy β-particle of 0.392 MeV; it can be administered in large doses but its effectiveness has not yet been sufficiently analyzed. Therefore, depending on the property of cancer tissue, effective and efficient treatment can be realized. It should be noted that the effectiveness of nuclear medicine therapy is affected by the properties and size of target cancer tissue, radiation quality, and energy, suggesting that the most efficient radiation energy may exist for each target.[2] In other words, although the range of therapeutic effect is limited owing to low energy, sufficient effects can be obtained with low-energy β-particles for small tumors, thus leading to effective treatment.[3] We previously synthesized ^{67}Cu-ToDBTTATE targeting the somatostatin receptor and demonstrated that this compound constricts tumor growth in model mice bearing AR42J rat pancreatic tumor cells.[4] Further investigations regarding the characteristics of ^{67}Cu may contribute to effective and efficient treatment and/or customized medicine according to patient conditions.

In this study, we prepared model mice with tumors of various sizes and attempted to investigate the differences in the therapeutic effect of ^{67}Cu-ToDBTTATE on the tumor size to clarify the relationship between tumor size and the therapeutic effects of ^{67}Cu-ToDBTTATE.

Tumor-bearing mice were prepared by implanting AR42J tumor cells (5×10^6 cells), in 0.1 mL PBS, into the flanks of nude mice (BALB/c-nu/nu, male). After the tumor grew to various sizes, 16.0–25.2 MBq of ^{67}Cu-ToDBTTATE was injected into the mice from the tail vein. Saline or non-labeled ToDBTTATE-administered mice were used as the control. All mice were weighed and the tumor diameters were regularly measured using a caliper; the tumor volumes were determined using the following formula: (longer diameter) × (shorter diameter)^2/2. This study was performed in accordance with the recommendations by the Guide for the Care and Use of Laboratory Animals of Suzuka University of Medical Science.

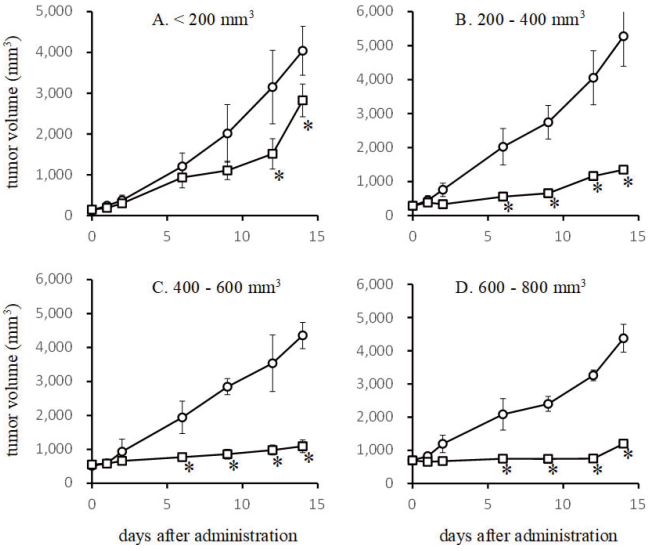

Fig. 1. Relationship between tumor size and the therapeutic effect of ^{67}Cu-ToDBTTATE (○: control, □: ^{67}Cu-ToDBTTATE). *: $p < 0.05$ (2-way ANOVA, sidack-test).

The mice were divided into four groups according to the tumor size, *i.e.*, less than 200, 200 to 400, 400 to 600, and 600 to 800 mm^3; then, the ^{67}Cu-ToDBTTATE-administered mice were compared with the control in each group. A tumor growth constricting effect was observed in the ^{67}Cu-ToDBTTATE-administered mice in all groups compared with the control (Fig. 1). Some tumor growth was observed in the group with a tumor size of less than 200 mm^3, which may be because the days after cell implantation were short and the targeted somatostatin receptor was not well expressed. No difference in the therapeutic effect of ^{67}Cu-ToDBTTATE on the tumor size was observed in this study. In future works, we plan to conduct comparative studies using model mice with larger tumors.

*1 Faculty of Pharmaceutical Sciences, Suzuka University of Medical Science
*2 RIKEN Nishina Center
*3 Department of Molecular Imaging, Hamamatsu University School of Medicine

References
1) G. A. Wiseman *et al.*, Eur. J. Nucl. Med. **27**, 766 (2000).
2) K. Fujimori *et al.*, Kaku Igaku **31**, 241 (1994).
3) E. B. van Dieren *et al.*, Int. J. Radiat. Oncol. Biol. Phys. **36**, 197 (1996).
4) Y. Fujisawa *et al.*, RIKEN Accel. Prog. Rep. **53**, 175 (2019).

Synthesis of ^{44m}Sc-DOTA-TATE for multiple-isotope PET imaging

T. Fukuchi,[*1] Y. Kanayama,[*1] A. Nambu,[*2] S. Usuda,[*2] Y. Shigekawa,[*2] Y. Wang,[*2] X. Yin,[*2] T. Yokokita,[*2] H. Haba,[*2] and Y. Watanabe[*1]

Positron emission tomography (PET) is a useful tool for radio-tracer imaging in a living organism. However, conventional PET can only be adapted for a single tracer because of the energy constancy of annihilation photons, which are utilized for PET imaging. To overcome this disadvantage, we have developed a new PET system that can be used for multiple-tracer simultaneous imaging. Our PET system, named multiple-isotope PET (MI-PET), detects not only annihilation photons but also prompt γ-rays, which are emitted successively after positrons. We have succeeded in proving the basic principle of MI-PET using a prototype system.[1)]

The MI-PET system uses a positron-γ emitter, which emits a de-excitation γ-ray after the positron emission in β^+-decay, as a tracer, and identifies the tracer by detecting the prompt γ-ray. For the MI-PET tracer, a proper half-life, prompt γ-ray energy, and emission ratio are required by the positron-γ emitter to ensure future clinical use. One promising candidates for this type of positron-γ emitter is ^{44}Sc (^{44m}Sc), which emits 1157 keV prompt γ-rays (99.9%) with a half-life of 3.97 h (^{44m}Sc: 58.6 h). The imaging ability of MI-PET for ^{44}Sc (^{44m}Sc) has been already evaluated by several experiments using phantoms and animals.[2,3)] Therefore, as a next step, we have begun to develop a useful drug, such as a cancer diagnosing reagent labeled by ^{44}Sc (^{44m}Sc). In our first attempt, we synthesized a ^{44m}Sc labelled DOTA-TATE, which is a compound containing tyrosine3-octreotate and a somatostatin receptor for numerous malignancies.

^{44m}Sc was produced *via* the reaction of ^{44}Ca(d, $2n$)^{44m}Sc with a 24 MeV deuterium beam and was purified by chemical processes at the RIKEN AVF cyclotron. The produced ^{44m}Sc was transported to the RIKEN Kobe campus for the drug synthesis.

The labelling protocol was based on a method developed by Huclier-Markai *et al.*[4)] The protocol scheme is shown in Fig. 1. DOTA-TATE (DOTA-[Tyr3]-octreotide) was purchased from BACHEM (Switzerland). A total of 2.1 nmol of DOTA-TATE and 7.7 MBq of ^{44m}Sc were resolved into 55 μL of NaOH (0.1 M) and 200 μL of ammonium acetate (pH 4.0, 0.25 M) and incubated at 95°C for 30 min with shaking. After incubation, 5.7 MBq of ^{44m}Sc labeled DOTA-TATE was washed out using an ion-exchange column (Sep-Pak C18 1cc Vac cartridge) by 500 μL of ethanol.

To evaluate the radio-labeling yield, TLC analyses

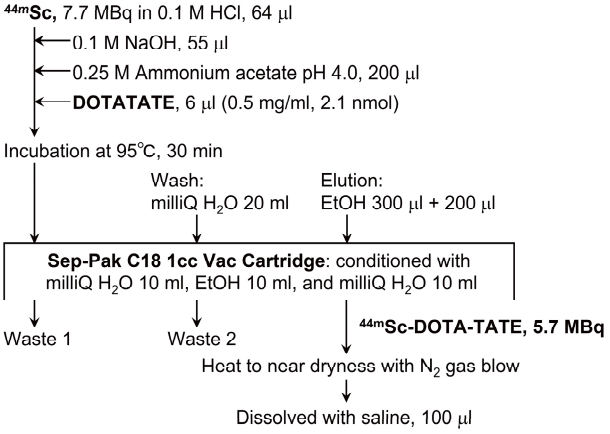

Fig. 1. Scheme for synthesis of ^{44m}Sc labeled DOTA-TATE.

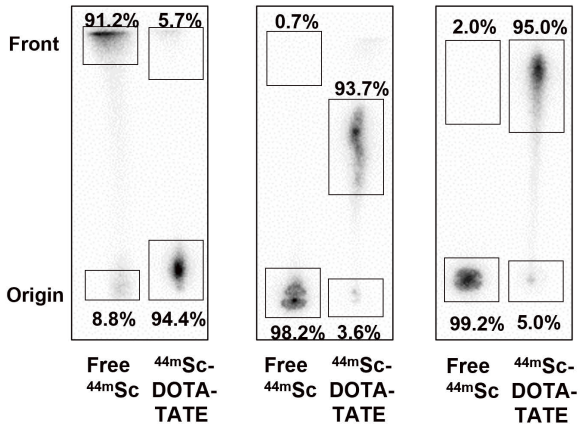

Fig. 2. TLC profiles of the free ^{44m}Sc and ^{44m}Sc-DOTA-TATE with developing solutions of citric acid (left), NaCl/MeOH (center), and NaCl/MeOH/NH_3 (right). An imaging plate was used for analysis.

were performed by spotting onto TLC plates (silica gel 60 F_{254}) with developing solutions of citric acid (pH 4.0), NaCl/MeOH (3 : 1), and NaCl/MeOH/NH_3 (3 : 1 : 1). The TLC results obtained through an analysis of an imaging plate are shown in Fig. 2. These results indicate that the labeling ratio for ^{44m}Sc-DOTA-TATE was above 90%.

*1 RIKEN Center for Biosystems Dynamics Research
*2 RIKEN Nishina Center

References
1) T. Fukuchi *et al.*, Med. Phys. **4**, 2257 (2017).
2) T. Fukuchi *et al.*, RIKEN Accel. Prog. Rep. **53**, 21 (2020).
3) T. Fukuchi *et al.*, J. Instrum. **16**, P01035 (2021).
4) S. Huclier-Markai *et al.*, Nucl. Med. Bio. **41**, e36 (2014).

Investigation of the usability of RIKEN ^{44m}Sc for radiolabeling on chelate-compounds

S. Oshikiri,[*1,*2] S. Kubota,[*1,*2] H. Kato,[*1,*2] T. Yokokita,[*1] K. Suzuki,[*1,*2] A. Hino,[*2] and H. Haba[*1]

Scandium-44m (^{44m}Sc) with a half-life of 58.61 h decays to scandium-44 (^{44}Sc) with a half-life of 3.97 h by emitting gamma rays. ^{44}Sc has been reported to be a promising radioisotope (RI) in positron emission tomography imaging, while ^{47}Sc, which emits a beta particle, is proposed as a promising therapeutic nuclide.[1] Furthermore, ^{44m}Sc appears to be useful as an imaging RI[2] and a surrogate nuclide for other Sc isotopes in basic science research because of a relatively long half-life. A study on the optimization of ^{44m}Sc radiolabeling of macrocyclics-functionalized biomolecules has been published.[3]

We have been developing a production method of ^{44m}Sc via the nuclear reaction ^{44}Ca$(d, 2n)^{44m}$Sc at the RIKEN AVF cyclotron and distributing purified ^{44m}Sc (RIKEN ^{44m}Sc) to users.[4] To confirm the quality of the RIKEN ^{44m}Sc for research on radiolabeling, we performed ^{44m}Sc radiolabeling on chelate-compounds in this study. To investigate the structural effect of chemical-compounds on ^{44m}Sc radiolabeling, four commercially available compounds were selected: DOTA-Substance P (DOTA-SP), DOTA-RGD$_2$, NOTA-RGD$_2$ and NODAGA-RGD$_2$. The operations for ^{44m}Sc radiolabeling are as described below.

Step 1: RIKEN ^{44m}Sc (9.1 MBq) was dissolved in 0.05 M hydrochloric acid to prepare a ^{44m}Sc solution (79 MBq/mL). The radioactivity of ^{44m}Sc was determined using a germanium semiconductor detector.

Step 2: Each chelate-compound was dissolved in 0.75 M sodium acetate buffer at pH3.0, 4.0, 5.0, and 6.0 to prepare 1.4×10^{-4} M sample solutions.

Step 3: 1.5 μL of the ^{44m}Sc solution was added to 3 μL of each sample solution: the specific radioactivity of each sample solution was 0.29 MBq/nmol.

Step 4: The mixtures in Step 3 were heated at 97°C for 10 min and kept at 20°C for 5 min.

Step 5: Radiolabeling yields of ^{44m}Sc-labeled compounds were determined using thin-layer chromatography (TLC) with a C18 reverse phase TLC plate (NAGEL RP-18W/UV254), which was eluted with a mixture of acetonitrile, 0.5 M ammonium acetate, methanol, and tetrahydrofuran in a volume ratio of 4 : 3 : 2 : 1 using an image analyzer.

Consequently, the radiolabeling yields of each compound were over 90% at pH 5.0–6.0, although they were different from each other at lower pH values. In case of compounds with the same affinity moiety, DOTA-RGD$_2$ was radiolabeled over 70% at pH 3.0 which was higher than that of NODAGA-RGD$_2$ and NOTA-RGD$_2$.

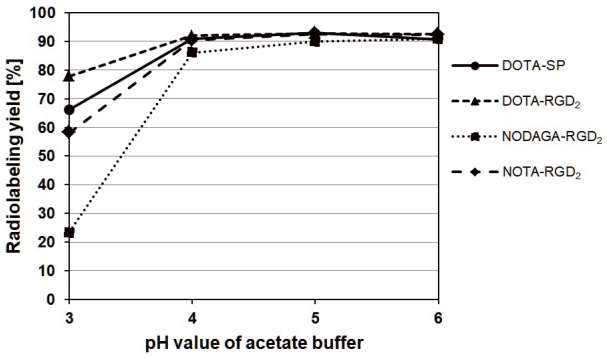

Fig. 1. Relation between pH value of acetate buffer and radiolabeling yield (%) of ^{44m}Sc-labeled compounds at 0.29 MBq/nmol ($n = 1$).

It has been reported that the suitable pH range for ^{44m}Sc labeling with DOTA-based ligands is from 4 to 5.5.[3] The result obtained in our study was consistent with the result of the previous study. Moreover, regarding the difference in reactivity among chelators, one report shows that DOTA is a better chelator than NODAGA because NODAGA is more susceptible to contamination metals than DOTA.[5] Another report shows that the thermodynamic stability of Sc-DOTA is high compared to that of Sc-NOTA.[6] These reports are consistent with our radiolabeled result at pH 3.0. Hence, these results support the possibility of further radiolabeling studies using RIKEN ^{44m}Sc.

We investigated the possibility of RIKEN ^{44m}Sc for radiolabeling studies and compared our results with those of previous reports of Sc radioisotopes. In addition, the pH responsiveness of the ^{44m}Sc radiolabeling yield to compounds having different chelating sites was confirmed. In future, we plan to optimize the radiolabeling condition of Sc isotopes, such as ^{44}Sc, which is eluted from the ^{44}Ti/^{44}Sc generator, and conduct a feasibility study for imaging tracer with ^{44m}Sc.

*1 RIKEN Nishina Center
*2 RI Research Department, FUJIFILM Toyama Chemical Co., Ltd.

References
1) C. Müller *et al.*, J. Nucl. Med. **55**, 1658 (2014).
2) T. Fukuchi *et al.*, RIKEN Accel. Prog. Rep. **53**, 21 (2020).
3) S. Huclier-Markai *et al.*, Nucl. Med. Biol. **41**, e36 (2014).
4) H. Haba, Drug Deliv. Syst. **35**, 114 (2020).
5) K. A. Domnanich *et al.*, EJNMMI Radiopharm. Chem. **1**, 8 (2016).
6) S. Huclier-Markai *et al.*, Radiochim. Acta **99**, 653 (2011).

Progress of double-photon coincidence imaging with ^{28}Mg

M. Uenomachi,[*1] F. Sensui,[*1,*2] Z. Zhong,[*1,*2] K. Shimazoe,[*1,*2] H. Takahashi,[*1,*2] Y. Shigekawa,[*1] A. Nambu,[*1] Y. Wang,[*1] X. Yin,[*1] and H. Haba[*1]

In nuclear medicine, positron emission tomography (PET) and single photon emission computed tomography (SPECT) have been widely used for diagnosis. However, the principles of these imaging technologies constrain the type of radioisotopes that can be used. Clinically available radioisotopes are positron emitters or single photon emitters with low energies (typically up to 400 keV). Recently, Compton imaging[1] has been studied as a promising gamma-ray imaging technology because it can offer image capture for a wide range of energy (100 keV to a few MeV) without mechanical collimators. Therefore, this capability provides an opportunity for the exploitation of new radionuclides in nuclear medicine.

In conventional Compton imaging, the source position can be estimated only on the surface of a cone with an opening angle θ, which is calculated from the recoil electron and scattered photon energies by following the equation of Compton scattering kinematics. However, this results in low signal-to-background ratio (SBR) in the Compton image. For improvement in the SBR, we have demonstrated the double-photon coincidence imaging technology.[2–5] Some nuclides emitting two or more successive gamma-rays with an intermediate state can be applied for the double-photon coincidence imaging (*e.g.* ^{60}Co,[3] ^{43}K,[4] and ^{111}In[5]). Thus, one can specify the position at the intersection of two (or more) Compton cones by coincidence detection. In this study, we focused on a radionuclide of ^{28}Mg. ^{28}Mg is a promising radionuclide for bio-imaging owing to its suitable half life of 21 hours. Moreover, because it emits cascade photons with energies of 400.6 keV (Intensity: 35.9%), 941.7 keV (36.3%), and 30.6 keV (89%) via short duration, coincidence imaging can be applied.

We produced ^{28}Mg via the ^{27}Al$(\alpha, 3p)^{28}$Mg reaction at the RIKEN AVF cyclotron. After chemical separation, 0.5 MBq in 37 μL HCl was dispensed in a 0.5 mL micro tube. Figure 1(a) shows the experimental setup. Eight Compton cameras surrounded the ^{28}Mg source. The distance between the source and camera was approximately 42 mm. A Compton camera consists of a scatterer and an absorber, which are 8 × 8 arrays of $Gd_3(Al, Ga)_5O_{12}$(Ce) (GAGG) scintillators (C&A Co.) coupled to an 8 × 8 array of silicon photomultipliers (SiPM, Hamamatsu MPPC S13361-3050). The GAGG crystal size is 2.5 mm × 2.5 mm, and the pitch size is 3.2 mm × 3.2 mm. The thicknesses of the scatterer and absorber are 4 mm and 9 mm, respectively.

*1 RIKEN Nishina Center
*2 School of Engineering, University of Tokyo

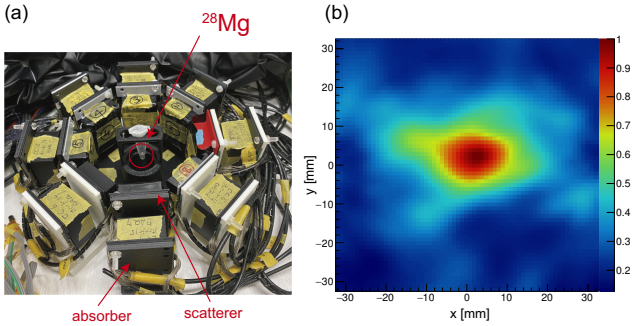

Fig. 1. (a) Photograph of the experimental setup. (b) Double-photon coincidence imaging of ^{28}Mg.

The 64 channel signals from the SiPM array are processed by the dynamic time over threshold method[6] and are then converted to digital signals of a time width. The 128 channel digital signals from the scatterer and absorber are acquired using 125 ps sampling by a field-programmable gate array-based data acquisition system. The data is recorded as list-mode data. In analysis, coincidence events between the scatterer and absorber were extracted as single-photon Compton events. For double-photon coincidence imaging, coincidence events between two different Compton camera events were selected as double Compton events.

Figure 1(b) shows the preliminary double-photon coincidence imaging of ^{28}Mg. In image reconstruction, double Compton events with energies of 400.6 keV and 941.7 keV were used. Although we succeeded the double-photon coincidence imaging, the detection efficiency is a disadvantage of this method. While the absolute efficiency of the single-photon Compton imaging with our imaging system was 0.029% @ 400.6 keV gamma-ray, and 0.014% @ 941.7 keV gamma-ray, that of the double-photon coincidence imaging was 8.2×10^{-6}%. Unlike the annihilation gamma-rays emitted at opposite directions, cascade gamma-rays are emitted without collinearity. We must improve the imaging system geometry, such that it covers a wider range of solid angles to increase the detection efficiency.

References

1) R. W. Todd *et al.*, Nature **251**, 5471 (1974).
2) Y. Yoshihara *et al.*, Nucl. Instrum. Methods Phys. Res. A **837**, (2017).
3) M. Uenomachi *et al.*, Nucl. Instrum. Methods Phys. Res. A **954**, (2020) .
4) H. Takahashi *et al.*, RIKEN Accel. Prog. Rep. **54**, (2020).
5) T. Orita *et al.*, IEEE Trans. Nucl. Sci. (in press).
6) K. Shimazoe *et al.*, IEEE Trans. Nucl. Sci. **59**, 6 (2012).

Source preparation technique of astatine-211 without electroplating for alpha spectroscopy

S. Fujino,[*1] K. Mori,[*1] S. Hamagami,[*1] T. Yamada,[*1,*2] Y. Wang,[*3] X. Yin,[*3] and H. Haba[*3]

^{211}At has attracted much interest because of its potential advantages in targeted alpha therapy. The high-resolution alpha spectrometry is one of the most important techniques in radiochemical analyses and precise radioactivity measurements. The electroplating method is widely used as a conventional technique to prepare α sources. However, some difficulties are encountered in applying this method to ^{211}At owing to its short half-life and high volatility. There difficulties were overcome by employing another practical approach using a silver plate, which is one of the major procedures of preparing solid radio-iodine sources,[1)] to prepare ^{211}At α sources. In addition, a coprecipitation technique using $AgNO_3$ was studied.

In this study, carrier-free ^{211}At produced via the ^{209}Bi$(\alpha, 2n)^{211}$At reaction at the RIKEN AVF cyclotron was used.[2)] Approximately 1 MBq of dried elemental ^{211}At was dissolved in 10 mL of ion-exchanged water. Silver plates with a thickness of 0.1 mm were used to fix ^{211}At. In this study, approximately 10 μL of the ^{211}At solution was directly dropped onto silver plates. As another approach, an ^{211}At source was also prepared with ascorbic acid (AA) to avoid ^{211}At loss due to volatilization.[3)] In this case, a 180 μL of ^{211}At solution was mixed with 20 μL of AA solution with a concentration of 0.01 mg/mL, and the mixed solution was dropped onto silver plates. All sources were dried in the atmosphere at room temperature. To investigate the time dependence of the deposition yield of ^{211}At, ^{211}At deposited on the plate was washed off with ion-exchanged water in 15, 30, 45, 60, or 75 min for the sources prepared without AA.

A 0.1 mg/g $AgNO_3$ solution was used to prepare the source using the coprecipitation technique. Here, 30 μL of the ^{211}At solution was directly dropped on the plastic plate and 10 μL of the $AgNO_3$ solution was added. These sources were dried in a desiccator with silica gel. All the sources prepared were measured using a ZnS(Ag) scintillation detector with 2π geometry and/or an ion-implanted Si detector (MIRRION PD 300-16-100 AM) with the defined source-detector geometry in a vacuum.

Figure 1 shows the time dependence of the deposition yield of ^{211}At on the silver plates. The deposition yield was determined as a ratio of the ^{211}At α count rate measured for each silver plate to that estimated from the radioactivity concentration of the ^{211}At solution and a weight of its drop on each plate. As shown in this figure, the deposition yield was saturated at approximately 75% in 30 min. For the sample dried with AA, the deposition yield reached 98% in this study. However, the deposition yield of the sample coprecipitated with silver nitrate was 70%. The method with silver nitrate is one of reliable methods for the standardization of the radio-iodine activity. These results suggest that the methods applicable to the radio-iodine cannot always be applied to the same halogen elemental astatine source without volatilization.

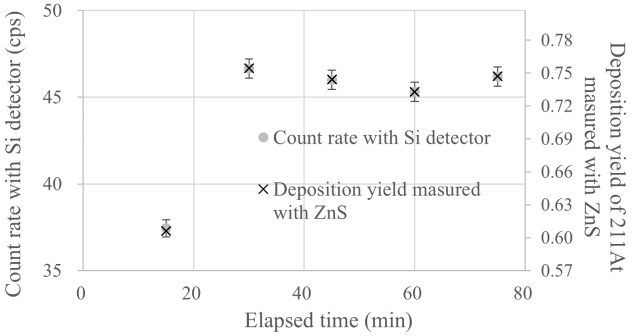

Fig. 1. Time dependence of the deposition yield.

Alpha spectra were measured using the Si detector for the sources prepared above. Two alpha-peaks of ^{211}At (E_α = 5.87 MeV) and ^{211}Po (E_α = 7.45 MeV) were observed in each spectrum. As shown in Fig. 2,

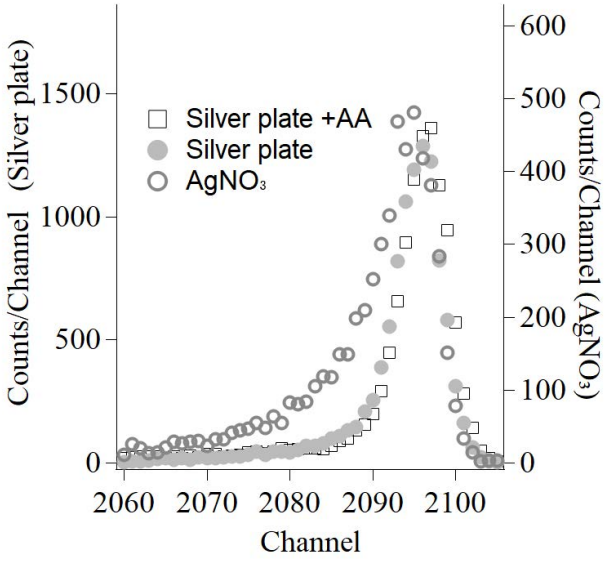

Fig. 2. Measured α-spectra of ^{211}At (E_α = 5.87 MeV).

*1 Graduate School of Science and Engineering, Kindai University
*2 Atomic Energy Research Institute, Kindai University
*3 RIKEN Nishina Center

the FWHMs of the 5.87 MeV peak in the measured spectra for the source prepared on a silver plate with and without AA were approximately 20 keV or less. For the source prepared using the coprecipitation technique, significant broadenings were observed, resulting in a FWHM of 23.9 keV at 5.87 MeV.

Among three types of sources, the sources prepared on a silver plate with and without AA exhibited better FWHM, and the source prepared on a silver plate with AA had the best deposition yield, while an additional study using more samples is required. Therefore, the method to prepare the source on a silver plate with AA can have potential advantage to be employed as a source preparation technique for radioactivity measurement using the solid angle α counting technique with a small correction for loss of radioactivity during the drying process owing to its volatility.

Acknowledgement: The authors would like to thank to Dr. Y. Komori and Dr. T. Yokokita.for their technical assistance.

References

1) I. Cieszykowska *et al.*, Nukleonika **50**, 17 (2005).
2) Y. Wang *et al.*, RIKEN Accel. Prog. Rep. **53**, 192 (2019).
3) A. Toyoshima *et al.*, Radiat. Safe. Manage. **18**, 13 (2019).

Production cross sections of ^{225}Ac and ^{225}Ra in the ^{232}Th(^{14}N, $xnyp$) reactions at 56, 79, and 98 MeV/nucleon

X. Yin,[*1] A. Nambu,[*1] S. Oshikiri,[*1,*2] K. Suzuki,[*1,*2] A. Hino,[*2] and H. Haba[*1]

^{225}Ac ($T_{1/2}$ = 10.0 d) is one of the most promising alpha-particle-emitting radionuclides for targeted radionuclide therapy.[1] Its precursor, ^{225}Ra ($T_{1/2}$ = 14.9 d), is useful to generate high-purity ^{225}Ac. Thus, proton-induced reactions on ^{232}Th to form ^{225}Ac and ^{225}Ra have been well investigated.[2] Proton beams up to 210 MeV are available for ^{225}Ac production from RRC.

In 1991, Ambe *et al.*[3] proposed the production of radionuclides of a large number of elements (multitracer) by the spallation of metallic targets such as ^{nat}Cu, ^{nat}Ag, and ^{197}Au irradiated with a 135-MeV/nucleon ^{14}N (or ^{12}C, ^{16}O) beam from RRC. With this ^{14}N beam, ^{225}Ac and ^{225}Ra can be produced in the ^{232}Th(^{14}N, $xnyp$)^{225}Ac, ^{225}Ra reactions.[4] The cross sections are essential to verify the feasibility of the ^{232}Th(^{14}N, $xnyp$)^{225}Ac, ^{225}Ra reactions for practical productions of ^{225}Ac and ^{225}Ra with RRC. In our previous paper,[4] we reported the cross sections of the ^{232}Th(^{14}N, $xnyp$)^{225}Ac, ^{225}Ra reactions at 116 and 132 MeV/nucleon. In this work, the cross sections at lower energies of 56, 79, and 98 MeV/nucleon were measured to evaluate the production yields of ^{225}Ac and ^{225}Ra more reliably.

The target consisted of three assemblies of three metallic ^{232}Th foils, each with a thickness of 69 mg/cm^2 and size of 12.5 × 12.5 mm^2. Two aluminum disks, each with a thickness of 370 mg/cm^2 and diameter of 15 mm, were interleaved between the thorium assemblies as beam energy degraders. The target was placed in a multitracer production chamber.[5] A 100.1-MeV/nucleon ^{14}N^{7+} beam was extracted from RRC. The target was irradiated for 2 h with an 18-particle nA intensity. After irradiation, the middle ^{232}Th foils in every assembly were subjected to γ-ray spectrometry to determine the cross sections of ^{225}Ac and ^{225}Ra. The beam energies on the measured ^{232}Th targets were calculated to be 98, 79, and 56 MeV/nucleon using the stopping power model in the LISE^{++} program.[6] The cross sections of ^{225}Ac and ^{225}Ra were determined by fitting the 440-keV γ-ray intensity of ^{213}Bi ($T_{1/2}$ = 45.59 min) in their radioactive decay chain.[4]

The cross sections of ^{225}Ac and ^{225}Ra obtained in this work are shown in Fig. 1, together with those at 116 and 132 MeV/nucleon in our previous work.[4] The cross sections of ^{225}Ac are larger than those of ^{225}Ra by factors of 4.2–5.3 at 56–132 MeV/nucleon, respectively. The experimental results are compared with those calculated by the Particle and Heavy Ion Transport code System (PHITS).[7] The PHITS code reproduces the cross sections of ^{225}Ac above 98 MeV/nucleon, while it underestimates those at the lower energies. The cross sections calculated for ^{225}Ra by the PHITS code are larger than the experimental ones. The calculated values increase with the beam energy, while the experimental ones are independent of the beam energy. In Fig. 2, production yields of ^{225}Ac by 135-MeV/nucleon ^{14}N beams are compared with those by 210-MeV proton beams.[2] The yields of both reactions are comparable if we use a target with the same thickness in the range of 0.5–5 g/cm^2.

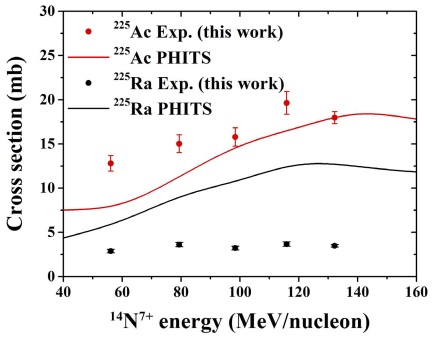

Fig. 1. Experimental and calculated excitation functions for the ^{232}Th(^{14}N, $xnyp$)^{225}Ac, ^{225}Ra reactions.

By assuming experimental conditions (incident beam energy: 132 MeV/nucleon; beam intensity: 1 particle μA; target thickness: 4.5 g/cm^2; irradiation time: 2 d), 165 MBq of ^{225}Ac can be produced at the end of bombardment via the ^{232}Th(^{14}N, $xnyp$)^{225}Ac reaction.

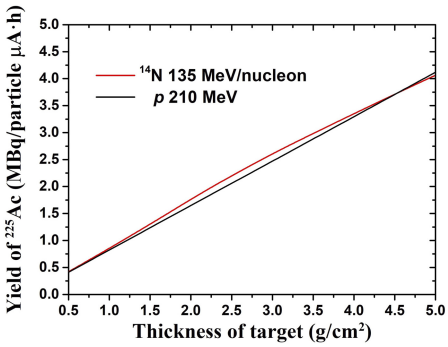

Fig. 2. Yields of 135-MeV/nucleon ^{14}N and 210-MeV proton beams on ^{232}Th targets with different thicknesses.

*1 RIKEN Nishina Center
*2 RI Research Department, FUJIFILM Toyama Chemical Co., Ltd.

References
1) M. Ferrier *et al.*, Radiochim. Acta **107**, 1065 (2019).
2) J. Weidner *et al.*, Appl. Radiat. Isot. **70**, 2602 (2012).
3) S. Ambe *et al.*, Anal. Sci. **7**, 317 (1991).
4) X. Yin *et al.*, RIKEN Accel. Prog. Rep. **54**, 162 (2021).
5) H. Haba *et al.*, Radiochim. Acta **93**, 539 (2005).
6) O. B. Tarasov, D. Bazin, LISE^{++} site, `https://lise.nscl.msu.edu/lise.html` .
7) Y. Iwamoto *et al.*, J. Nucl. Sci. Technol. **54**, 617 (2017).

Production cross sections of ^{28}Mg via the α-particle-induced reaction on aluminum

M. Aikawa,[*1,*2] G. Damdinsuren,[*3,*2] H. Huang,[*3,*2] and H. Haba[*2]

The radionuclide ^{28}Mg has a half-life of $T_{1/2}$ = 20.915 h and decays with the emission of a β^- particle and γ rays. These nuclear properties are appropriate for radiotracers in a wide range of applications.[1] One of its promising production reactions is the α-particle-induced reaction on aluminum. We found ten experimental studies in the production cross sections of ^{28}Mg in a literature survey in the EXFOR library.[2] However, the cross sections of the previous studies are largely scattered. Therefore, we conducted an experiment to determine reliable cross sections of the ^{27}Al$(\alpha, 3p)^{28}$Mg reaction.

The experiment to measure the activation cross sections of the reaction was performed at the RIKEN AVF cyclotron. The stacked-foil activation technique and high-resolution γ-ray spectrometry were used. Pure metal foils of ^{27}Al (>99% purity) and $^{\rm nat}$Ti (99.6% purity) were purchased from Nilaco Corp., Japan. The Ti foil was used for the $^{\rm nat}$Ti$(\alpha, x)^{51}$Cr monitor reaction. The average thicknesses of the Al and Ti foils were 13.7 and 2.23 mg/cm^2, respectively, which were derived from the measured size and weight of each foil. After the thickness measurement, the foils were cut into small pieces of 10 × 10 mm^2 to fit a target holder that served as a Faraday cup. The stacked target consisted of ten Al foils upstream and seven sets of Ti-Ti-Ti-Al foils downstream of the beam line. The upstream Al foils were used to derive activation cross sections of the ^{27}Al$(\alpha, 3p)^{28}$Mg reaction, the threshold energy of which is 24.8 MeV. The following Ti-Ti-Ti-Al foils were stacked for the $^{\rm nat}$Ti$(\alpha, x)^{51}$Cr monitor reaction in a lower-energy region. The stacked target was irradiated for 30 min with an α-particle beam. The initial energy of the α-particle beam was determined using the time-of-flight method.[3] The average beam intensity was measured using the Faraday cup and found to be 216 nA. The energy degradation of the α-particle beam in the target foils was calculated using stopping powers obtained from the SRIM code.[4] The γ-ray spectrometry was performed using a high-purity germanium detector (ORTEC GEM30P4-70) and dedicated analysis software (SEIKO EG&G Gamma Studio). γ rays emitted from each irradiated foil were measured without chemical separation three times (Ser. 1: 2.7–7.5 h, Ser. 2: 8.0–32 h, Ser. 3: 1.9–3.6 d). The dead time was kept below 1.4% throughout the measurements. Nuclear data used for cross-section derivation were retrieved from the online database, NuDat 3.0.[5]

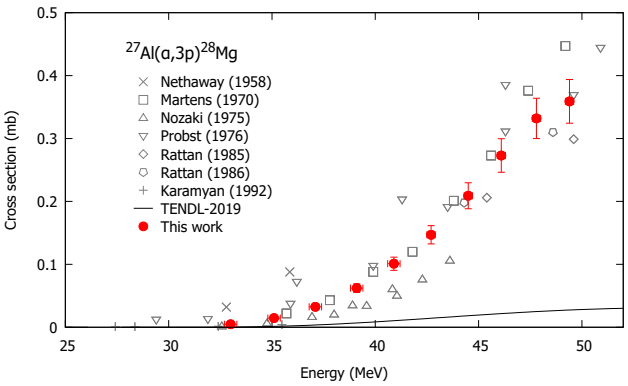

Fig. 1. Excitation function of the ^{27}Al$(\alpha, 3p)^{28}$Mg reaction in comparison with the previous studies found in the EXFOR library[2] and the TENDL-2019 values.[6]

The γ line at 1342.2 keV (I_γ = 54%) emitted with the decay of ^{28}Mg ($T_{1/2}$ = 20.915 h) was measured during the cooling time of 8.0–32 h (Ser. 2). The cross sections of the ^{27}Al$(\alpha, 3p)^{28}$Mg reaction were determined using the measured spectra. Figure 1 compares our preliminary result with the experimental data in the EXFOR library[2] and the TENDL-2019 values.[6] The cross section at the highest energy may be affected by the recoil effect and slightly decreased. The previous data of Martens *et al.* [7] and Rattan *et al.* [8] are consistent with our data, although their data deviate from each other in the higher-energy region. The other previous data are systematically larger or smaller than our data. The TENDL-2019 values are fairly smaller than all the experimental data. We will finish analyses of the measured γ-ray spectra and determine the production cross sections of radioactive products in the reaction.

*1 Faculty of Science, Hokkaido University
*2 RIKEN Nishina Center
*3 Graduate School of Biomedical Science and Engineering, Hokkaido University

References

1) N. P. van der Meulen *et al.*, Appl. Radiat. Isot. **115**, 125 (2016) and references therein.
2) N. Otuka *et al.*, Nucl. Data Sheets **120**, 272 (2014).
3) T. Watanabe *et al.*, Proc. 5th Int. Part. Accel. Conf. (IPAC2014), (2014), p. 3566.
4) J. F. Ziegler *et al.*, SRIM: the Stopping and Range of Ions in Matter (2008), `http://www.srim.org/` .
5) National Nuclear Data Center, The NuDat 3.0 database, `http://www.nndc.bnl.gov/nudat3/` .
6) A. J. Koning *et al.*, Nucl. Data Sheets **155**, 1 (2019).
7) U. Martens *et al.*, Z. Phys. **233**, 170 (1970).
8) S. S. Rattan *et al.*, Radiochim. Acta **39**, 61 (1986).

Production cross sections of titanium radionuclides via proton-induced reactions on scandium

M. Aikawa,[*1,*2,*3] H. Huang,[*2,*3] H. Haba,[*2] S. Takács,[*4] F. Ditrói,[*4] and Z. Szücs[*4]

Titanium radionuclides can be used in nuclear medicine. ^{45}Ti ($T_{1/2}$ = 3.08 h, $I_{\beta+}$ = 84.8%) and ^{44g}Sc ($T_{1/2}$ = 3.89 h, $I_{\beta+}$ = 94.3%), which is the daughter of ^{44}Ti ($T_{1/2}$ = 59.1 y), are positron emitters and suitable for positron emission tomography (PET).[1] The two titanium radionuclides ^{44}Ti and ^{45}Ti can be produced via charged-particle-induced reactions, such as α-particle-induced reactions on calcium and proton- and deuteron-induced reactions on scandium in a no-carrier-added form. The former reaction on calcium requires enriched ^{42}Ca targets. However, the composition of this isotope in natural calcium is only 0.647%. For proton- and deuteron-induced reactions, the monoisotopic element scandium ^{45}Sc can be used as a target material. The proton- and deuteron-induced reactions on ^{45}Sc are thus promising for the production of both titanium radionuclides. We have previously studied the deuteron-induced reaction on ^{45}Sc.[2] Subsequently, we focused on the proton-induced reaction on ^{45}Sc. In a literature survey and in the EXFOR library,[3] we found four and ten experimental studies on the production cross sections of ^{44}Ti and ^{45}Ti isotopes, respectively. The cross sections reported in these previous studies are largely scattered. Therefore, additional and reliable cross sections of the proton-induced reactions on ^{45}Sc are required.

We performed an experiment at the RIKEN AVF cyclotron using well-established methods, namely, the stacked-foil activation technique and high-resolution γ-ray spectrometry. Pure metal foils of ^{45}Sc (99.0% purity, Goodfellow Co., Ltd., UK), ^{nat}Ti (99.6% purity, Nilaco Corp., Japan), and ^{27}Al (>99% purity, Nilaco Corp., Japan) were purchased and used for the stacked target. The ^{nat}Ti and ^{27}Al foils were used for the ^{nat}Ti$(p,x)^{48}$V monitor reaction and for catching recoiled products, respectively. The lateral size and weight of each foil were measured. The derived average thicknesses of the ^{45}Sc, ^{nat}Ti, and ^{27}Al foils were 30.5, 2.25, and 13.7 mg/cm^2, respectively. The foils were then cut into 10 × 10 mm pieces to fit a target holder that served as a Faraday cup. Twenty sets of Sc-Al-Ti-Ti-Al foils were stacked in the target holder. The stacked target was irradiated with a 30.1 ± 0.1MeV proton beam for 60 min. The initial beam energy was determined by the time-of-flight method.[4] The average beam intensity measured by the Faraday cup was 203 nA. The energy degradation of the beam in the stacked target was calculated using stopping powers derived from the SRIM code.[5] The γ-ray spectra from each irradiated foil were measured three times using a high-purity germanium detector (ORTEC GEM30P4-70). Nuclear decay data were obtained from the online database NuDat 3.0.[6]

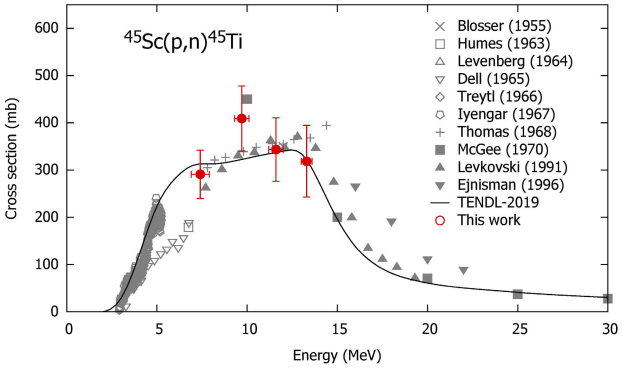

Fig. 1. Excitation function of the ^{45}Sc$(p,n)^{45}$Ti reaction in comparison with the previous data found in the EXFOR library[3] and the TENDL-2019 values.[7]

The weak γ line at 719.6 keV (I_γ = 0.154%) emitted with the decay of ^{45}Ti was measured. Due to its low intensity, only four cross sections of the ^{45}Sc$(p,n)^{45}$Ti reaction, with large statistical uncertainties, at around the peak were determined. Our preliminary result in comparison with the earlier experimental data found in the EXFOR library[3] and the TENDL-2019 values[7] is shown in Fig. 1. The peak position and amplitude of our result are similar to the data obtained by McGee *et al.*[8] The TENDL data are slightly smaller than our data at the peak.

Additional measurement after several months will be performed for the long-lived radioisotope ^{44}Ti. Production cross sections of scandium radioisotopes in the reaction will be also determined.

This work was supported by Japan-Hungary Research Cooperative Program between JSPS and HUS, Grant numbers JPJSBP120193808 and NKM-43/2019.

References

1) I. F. Chaple *et al.*, J. Nucl. Med. **59**, 1655 (2018).
2) Z. Tsoodol *et al.*, Appl. Radiat. Isot. **168**, 109448 (2021).
3) N. Otuka *et al.*, Nucl. Data Sheets **120**, 272 (2014).
4) T. Watanabe *et al.*, Proc. 5th Int. Part. Accel. Conf. (IPAC2014), (2014), p. 3566.
5) J. F. Ziegler *et al.*, SRIM: the Stopping and Range of Ions in Matter (2008), `http://www.srim.org/` .
6) National Nuclear Data Center, The NuDat 3.0, database, `http://www.nndc.bnl.gov/nudat3/` .
7) A. J. Koning *et al.*, Nucl. Data Sheets **155**, 1 (2019).
8) T. McGee *et al.*, Nucl. Phys. A **150**, 11 (1970).

*1 Faculty of Science, Hokkaido University
*2 RIKEN Nishina Center
*3 Graduate School of Biomedical Science and Engineering, Hokkaido University
*4 Institute for Nuclear Research (ATOMKI)

Production cross sections of ^{45}Ti via deuteron-induced reaction on ^{45}Sc†

Ts. Zolbadral,[*1,*2] M. Aikawa,[*2,*3,*4] D. Ichinkhorloo,[*1,*2] Kh. Tegshjargal,[*5] N. Erdene,[*5] Y. Komori,[*3] H. Haba,[*3] S. Takács,[*6] F. Ditrói,[*6] and Z. Szücs[*6]

^{45}Ti ($T_{1/2}$ = 184.8 min) is an appropriate positron emitter isotope ($E_{\beta+}$ = 439 keV, $I_{\beta+}$ = 84.8%) for positron emission tomography (PET). This radioisotope can be produced in the deuteron-induced reaction on a scandium-45 target at cyclotrons. However, the quality of experimental data on the cross sections of the ^{45}Sc$(d,2n)^{45}$Ti reaction is not satisfactory. Therefore, we aim to measure the cross sections of the ^{45}Sc$(d,2n)^{45}$Ti reaction and to investigate a route for ^{45}Ti production.

The stacked-foil activation technique and γ-ray spectrometry were adopted to determine the cross sections. The stacked target included metallic foils of ^{45}Sc (thicknesses of 25.8 and 250 μm with a purity of 99.0%), ^{27}Al (18.5 μm, 99.6%), and $^{\rm nat}$Ti (20.2 μm, 99.6%). The target was irradiated for 30 min with a 24-MeV deuteron beam from the RIKEN AVF cyclotron. The incident beam energy was measured using the time-of-flight method. The energy degradation in the stacked target was calculated using the SRIM code.[1)] The beam intensity was measured using a Faraday cup and double-checked with the $^{\rm nat}$Ti$(d,x)^{48}$V monitor reaction.[2)] By comparing the monitor reaction, the measured intensity (180 ± 9 nA) was corrected by decreasing it by 2% to 176 ± 9 nA. The γ-ray spectra of the irradiated foils were measured using a high-resolution and a high-purity germanium (HPGe) detector. The detector was calibrated using a mixed γ-ray point source. In the measurements, the dead time was kept below 7%.

Subsequently, the activation cross sections of ^{44,45}Ti and ^{44g,44m,46}Sc were determined. The measurements of the 719.6-keV γ-ray (I_γ = 0.154%) from the ^{45}Ti decay were used to derive the cross sections of the ^{45}Sc$(d,2n)^{45}$Ti reaction. Figure 1 shows our measured excitation function of the ^{45}Sc$(d,2n)^{45}$Ti reaction in comparison with previous experimental data[3)] and the theoretical estimation retrieved from TENDL-2019.[4)] The derived excitation function is consistent with the data reported by Hermanne *et al.*;[3)] however, it is less scattered. The peak position of the TENDL-2019 data is slightly shifted to a lower energy.

The physical yield of ^{45}Ti was deduced from the measured excitation function and is shown in Fig. 2. The

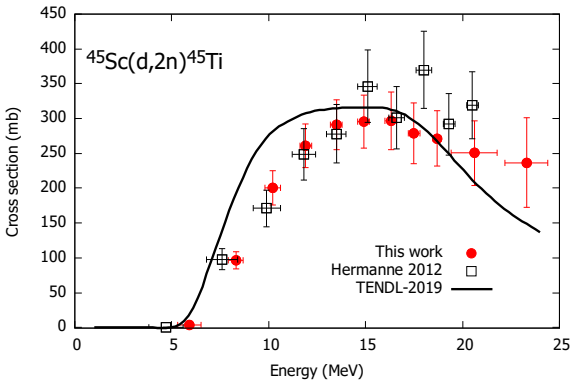

Fig. 1. Excitation function of the ^{45}Sc$(d,2n)^{45}$Ti reaction.

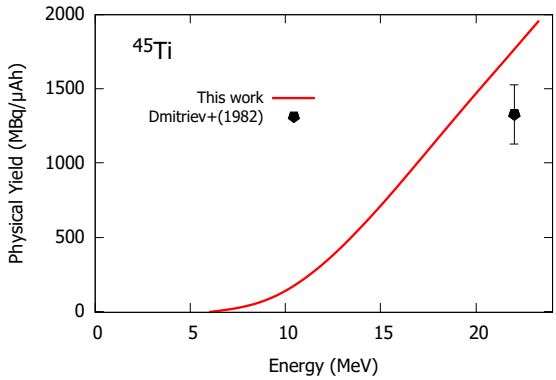

Fig. 2. Physical yield of ^{45}Ti.

present yield curve of ^{45}Ti is slightly higher than the experimental data obtained by Dmitriev *et al.*[5)] at 22 MeV. ^{44}Ti is the only one co-produced radioactive isotope of titanium in our experiment and can be formed by $(d,3n)$ reaction on ^{45}Sc above 15 MeV. Therefore, isotopically pure ^{45}Ti production is possible in $(d,2n)$ reaction on ^{45}Sc in an energy range of 8–15 MeV.

This work is supported by JSPS KAKENHI Grant Number 17K07004 and partly supported by the research program between the JSPS and HAS Contract No: JPJSBP120193808 and NKM-43/2019. Ts.Z was granted a scholarship by the M-JEED project (Mongolian-Japan Engineering Education Development Program, J11B16).

References
1) J. F. Ziegler *et al.*, Nucl. Instrum. Methods Phys. Res. B **268**, 1818 (2010).
2) A. Hermanne *et al.*, Nucl. Data Sheets **148**, 338 (2018).
3) A. Hermanne *et al.*, Nucl. Instrum. Methods Phys. Res. B **270**, 106 (2012).
4) A. J. Koning *et al.*, Nucl. Data Sheets **155**, 1 (2019).
5) P. P. Dmitriev *et al.*, INDC(CCP)-210, 1 (1983).

† Condensed from the article in Appl. Radiat. Isot. **168**, 109448 (2021)

*1 Nuclear Research Center, National University of Mongolia
*2 Graduate School of Biomedical Science and Engineering, Hokkaido University
*3 RIKEN Nishina Center
*4 Faculty of Science, Hokkaido University
*5 School of Engineering and Applied Sciences, National University of Mongolia
*6 Institute for Nuclear Research (ATOMKI)

Production cross sections of ^{47}Sc via proton-induced reactions on calcium

M. Aikawa,[*1,*2,*3] Y. Hanada,[*2,*3] H. Huang,[*2,*3] H. Haba,[*3] S. Takács,[*4] F. Ditrói,[*4] and Z. Szücs[*4]

Scandium radionuclides can be used for theranostics, a combination of therapeutics and diagnosis.[1] ^{43}Sc ($T_{1/2}$ = 3.89 h) and ^{44g}Sc ($T_{1/2}$ = 3.97 h) are positron emitters that are used in positron emission tomography (PET). ^{47}Sc ($T_{1/2}$ = 3.35 d) decays with beta particle emissions that can be used for therapy. These radionuclides can be produced via charged-particle-induced reactions on calcium. Only a few experimental studies of each reaction were found with scattered cross sections in a literature survey. Therefore, we performed experiments to measure reliable cross sections of proton-, deuteron-[2] and alpha-particle-induced reactions on natural calcium.[3] The abundance of natural calcium is ^{40}Ca: 96.941%, ^{42}Ca: 0.647%, ^{43}Ca: 0.135%, ^{44}Ca: 2.086%, ^{46}Ca: 0.004%, and ^{48}Ca: 0.187%. In this report, we present the preliminary results of the proton-induced reactions on natural calcium for ^{47}Sc production. ^{47}Sc can be directly produced in the proton-induced reactions on ^{46,48}Ca. However, the contribution of the (p,γ) reaction on ^{46}Ca is expected to be negligibly small owing to the extremely low abundance of ^{46}Ca and tiny cross sections of the (p,γ) reaction. Thus, the measured cross sections of the $^{\mathrm{nat}}$Ca$(p,x)^{47}$Sc reaction can be converted to those on ^{48}Ca enriched targets and vice versa.

We performed an experiment using a 30-MeV proton beam at the RIKEN AVF cyclotron. The stacked-foil activation technique and high-resolution gamma-ray spectrometry were employed.

Calcium targets were prepared from a calcium-fluoride (CaF_2) layer deposited on a high-purity ^{27}Al backing foil (99.999% purity, Goodfellow Co. Ltd., UK). Additional foils of $^{\mathrm{nat}}$Ti (99.5% purity, Nilaco Corp., Japan) and ^{27}Al (>99% purity, Nilaco Corp., Japan) were used for the $^{\mathrm{nat}}$Ti$(p,x)^{48}$V monitor reaction and beam-energy degradation, respectively. Based on size and weight measurements of each foil, average thicknesses of the CaF_2 layer, its ^{27}Al backing, the ^{27}Al degrader, and the $^{\mathrm{nat}}$Ti monitor foils were derived as 0.148, 5.26, 27.3, and 2.30 mg/cm^2, respectively. The foils were then cut into a size of 8 × 8 mm to fit a target holder served as a Faraday cup. Each calcium target was composed of two CaF_2 layers sandwiched between the ^{27}Al backing foils followed by a set of Ti-Ti-Al-Al foils. Eighteen calcium targets were stacked together in the target holder.

The stacked target was irradiated for 60 min with a 30.2 ± 0.1-MeV proton beam. The average beam intensity measured by the Faraday cup was 199 nA. The energy degradation of the beam in the stacked target was calculated using stopping powers derived from the SRIM code.[4] The irradiated foils without chemical separation were subjected to gamma-ray spectrometry using a high-purity germanium detector. Nuclear data for determining the cross section were obtained from an online database, NuDat 3.0.[5]

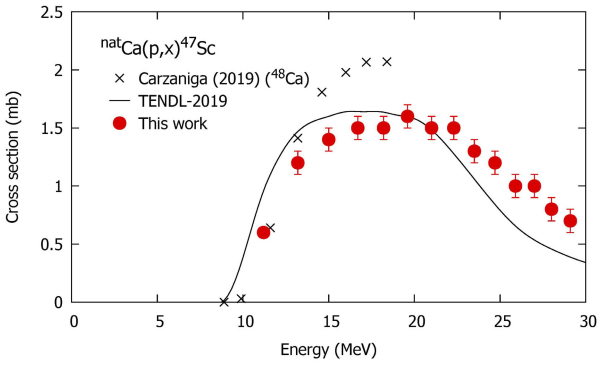

Fig. 1. Excitation function of the $^{\mathrm{nat}}$Ca$(p,x)^{47}$Sc reaction in comparison with previously reported experimental data for ^{48}Ca[3] normalized to $^{\mathrm{nat}}$Ca and TENDL-2019 values.[7]

We derived cross sections of the $^{\mathrm{nat}}$Ca$(p,x)^{47}$Sc reaction using a specific gamma line at 159.381 keV (I_γ = 68.3%) emitted after the decay of ^{47}Sc. The co-produced ^{47}Ca ($T_{1/2}$ = 4.536 d) can also contribute to the production of ^{47}Sc. Our preliminary result on ^{47}Sc including the partial contribution from the ^{47}Ca decay is shown in Fig. 1 in comparison with previous experimental data[6] and TENDL-2019 values.[7] The previously reported experimental data were normalized to those of $^{\mathrm{nat}}$Ca for the comparison. Previous data are larger than our data around the peak. The TENDL-2019 values show a peak amplitude that is consistent with our data, while the peak position shifts to the lower energy region.

We continue to analyze the measured spectra in more details and to determine production cross sections of other scandium radioisotopes as well.

This work was partly supported by the Japan-Hungary Research Cooperative Program between JSPS and HAS, Grant number JPJSBP120193808 and NKM-43/2019.

References

1) R. Mikolajczak *et al.*, EJNMMI Radiopharm. Chem. **6**, 19 (2021).
2) M. Aikawa *et al.*, in this report.
3) M. Aikawa *et al.*, in this report.
4) J. F. Ziegler *et al.*, SRIM: the Stopping and Range of Ions in Matter (2008), `http://www.srim.org/`.
5) National Nuclear Data Center, The NuDat 3.0 database, `http://www.nndc.bnl.gov/nudat3/`.
6) T. S. Carzaniga *et al.*, Appl. Radiat. Isot. **143**, 18 (2019).
7) A. J. Koning *et al.*, Nucl. Data Sheets **155**, 1 (2019).

*1 Faculty of Science, Hokkaido University
*2 Graduate School of Biomedical Science and Engineering, Hokkaido University
*3 RIKEN Nishina Center
*4 Institute for Nuclear Research (ATOMKI)

Production cross sections of ^{47}Sc via deuteron-induced reactions on natural calcium

M. Aikawa,[*1,*2,*3] Y. Hanada,[*2,*3] H. Huang,[*2,*3] H. Haba,[*3] S. Takács,[*4] F. Ditrói,[*4] and Z. Szücs[*4]

Production of scandium radionuclides is of interest for practical use in nuclear medicine owing to the applicability of ^{43,44g}Sc in positron emission tomography (PET) and ^{47}Sc in therapy.[1] We systematically study production cross sections of the radionuclides via charged-particle-induced reactions on natural calcium. Preliminary results of the proton- and alpha-particle-induced reactions have been reported in previous studies.[2] In this study, we focus on the deuteron-induced reactions on natural calcium, in which the isotopic ratio is ^{40}Ca: 96.941%, ^{42}Ca: 0.647%, ^{43}Ca: 0.135%, ^{44}Ca: 2.086%, ^{46}Ca: 0.004%, and ^{48}Ca: 0.187%. In our survey, we found only two experimental cross sections of the reaction below 25 MeV.[3,4] In previous studies, however, cross sections for ^{47}Sc production were not presented. Therefore, we conducted an experiment to measure the production cross sections of scandium radionuclides with a special focus on ^{47}Sc.

The experiment was performed at the RIKEN AVF cyclotron. The stacked-foil activation technique and high-resolution gamma-ray spectrometry were employed.

The stacked target was prepared using ^{nat}Ca targets and ^{nat}Ti and ^{27}Al foils. Each ^{nat}Ca target was composed of two calcium-fluoride (CaF_2) layers (0.148 mg/cm^2 per layer) sandwiched between high-purity ^{27}Al backing foils (5.26 mg/cm^2, 99.999% purity, Goodfellow Co. Ltd., UK). The ^{nat}Ti (2.30 mg/cm^2, 99.6% purity, Nilaco Corp., Japan) and ^{27}Al foils (13.7 mg/cm^2, >99% purity, Nilaco Corp., Japan) were interleaved for monitoring the beam via the ^{nat}Ti$(d,x)^{48}$V monitor reaction and energy degradation of a deuteron beam, respectively. The average thicknesses were determined from the measured sizes and weights of the original foils. Once the thicknesses were determined, the original foils were cut into small pieces of 8 × 8 mm. Seventeen sets of a ^{nat}Ca target with Ti-Ti-Al foils were stacked in a target holder served as a Faraday cup.

The stacked target was irradiated for 60 min with a 24.2 ± 0.1-MeV deuteron beam. The average beam intensity measured by the Faraday cup was 105 nA. The energy degradation of the beam in the stacked target was calculated using stopping powers obtained from the SRIM code.[6] Gamma rays emitted from the irradiated foils were measured without chemical separation using a high-purity germanium detector. Nuclear data required to determine activation cross sections were obtained from the online database, NuDat 3.0.[7]

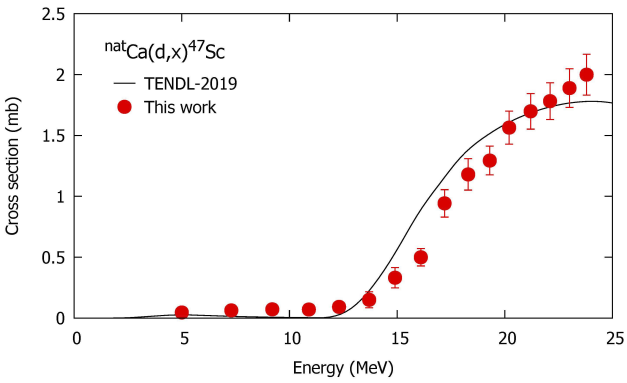

Fig. 1. Measured excitation function of the ^{nat}Ca$(d,x)^{47}$Sc reaction with a theoretical prediction of the TENDL-2019 values.[7]

We determined the production cross sections of ^{47}Sc ($T_{1/2}$ = 3.35 d) via the deuteron-induced reactions on ^{nat}Ca. The cross sections were derived using the measured gamma line at 159.381 keV (I_γ = 68.3%) emitted with the decay of ^{47}Sc. The co-produced parent ^{47}Ca ($T_{1/2}$ = 4.54 d) also contributed to the production of ^{47}Sc. Our preliminary result, including the partial contribution of ^{47}Ca, is shown in Fig. 1. Below the threshold energy of the ^{48}Ca$(d,3n)^{47}$Sc reaction (E_{th} = 11.4 MeV), ^{47}Sc was dominantly formed from the reaction on ^{46}Ca. The result is compared with the cross sections of the ^{47}Sc direct production obtained from the TENDL-2019 library.[7] The TENDL-2019 values show a slightly different shape from that of our result. Previously published experimental studies on this subject could not be found.

The measured spectra are analyzed in more detail, and the production cross sections of other scandium radioisotopes are determined. The results have potential implications for application in nuclear medicine.

This work was partly supported by Japan-Hungary Research Cooperative Program between JSPS and HAS, Grant number JPJSBP120193808 and NKM-43/2019.

References

1) R. Mikolajczak *et al.*, EJNMMI Radiopharm. Chem. **6**, 19 (2021).
2) M. Aikawa *et al.*, in this report.
3) T. J. de Waal *et al.*, Radiochim. Acta **15**, 123 (1971).
4) M. Alabyad *et al.*, J. Radioanal. Nucl. Chem. **316**, 119 (2018).
5) J. F. Ziegler *et al.*, SRIM: the Stopping and Range of Ions in Matter (2008), `http://www.srim.org/` .
6) National Nuclear Data Center, The NuDat 3.0 database, `http://www.nndc.bnl.gov/nudat3/` .
7) A. J. Koning *et al.*, Nucl. Data Sheets **155**, 1 (2019).

*1 Faculty of Science, Hokkaido University
*2 Graduate School of Biomedical Science and Engineering, Hokkaido University
*3 RIKEN Nishina Center
*4 Institute for Nuclear Research (ATOMKI)

Activation cross sections of alpha-particle-induced reactions on natural calcium

M. Aikawa,[*1,*2] Y. Hanada,[*3,*2] D. Ichinkhorloo,[*4,*2] H. Haba,[*2] S. Takács,[*5] F. Ditrói,[*5] and Z. Szűcs[*5]

We focused on the production of the therapeutic radionuclide ^{47}Sc ($T_{1/2}$ = 3.3492 d) via alpha-particle-induced reactions on calcium. Owing to the relatively small abundance of ^{46}Ca (0.004%) and ^{48}Ca (0.187%) in natural calcium, the dominant route for ^{47}Sc production is the reaction on ^{44}Ca (2.086%). Only one experimental study was found in a literature survey,[1] and therefore, we performed an experiment to obtain the cross sections of the ^{nat}Ca$(\alpha, x)^{47}$Sc reaction. The production cross sections of $^{46, 44m, 44g, 43}$Sc and ^{47}Ca were also determined.

The experiment was conducted with a 29-MeV alpha-particle beam at the RIKEN AVF cyclotron. Stacked-foil activation technique and high-resolution gamma-ray spectrometry were used in the experiment. Calcium-fluoride (CaF_2) deposited on a high-purity ^{27}Al backing foil (99.999% purity, Goodfellow Co. Ltd., UK) was used as the calcium target. In addition, two metallic foils of ^{nat}Ti (99.5% purity) for the ^{nat}Ti$(\alpha, x)^{51}$Cr monitor reaction and ^{27}Al (>99% purity) to catch recoiled products were purchased from Nilaco Corp., Japan. The measured average thicknesses of the ^{27}Al backing, ^{27}Al catcher and ^{nat}Ti monitor foils were 2.57, 1.50 and 2.30 mg/cm^2, respectively. The thickness of the CaF_2 layer was 0.135 mg/cm^2, as derived from the measured deposited area and net weight of CaF_2. Thickness uncertainties were estimated to be 5% for the CaF_2 layer and 1% for the other foils. All foils were cut into a size of 10 × 10 mm^2 to fit a target holder. Each calcium target consisted of two CaF_2 layers sandwiched with the ^{27}Al backing foils. Twelve calcium targets and seven sets of the ^{nat}Ti monitor and ^{27}Al catcher foils were stacked together in the target holder.

The stacked target was irradiated for 30 min with an alpha-particle beam. The measured average beam intensity and energy were 175 nA and 29.0 ± 0.2 MeV, respectively. The energy degradation in the stacked target was calculated using stopping powers obtained from the SRIM code.[2]

The high-resolution gamma-ray spectrometry using a high-purity germanium detector was performed without chemical separation. The calcium targets were measured five times with cooling times from 3.2 h to 77.0 d and dead times below 2.1%.

The derived cross sections of the ^{nat}Ti$(\alpha, x)^{51}$Cr monitor reaction were compared with the IAEA recommended values.[3] The comparison results indicated that the beam intensity and thicknesses of both ^{27}Al backing and catcher foils were corrected within the uncertainties by +5.6% and −1%, respectively. The measured thicknesses of the ^{nat}Ti monitor foil and the CaF_2 layer were adopted without any correction.

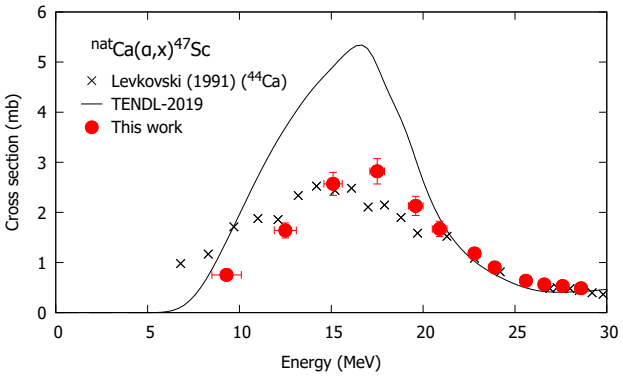

Fig. 1. Excitation function of the ^{nat}Ca$(\alpha, x)^{47}$Sc reaction in comparison with normalized data from the previous study[1] and TENDL-2019 values.[4]

^{47}Sc can be produced directly from the ^{44}Ca$(\alpha, p)^{47}$Sc reaction and indirectly from the decay of the co-produced parents, ^{47}Ca and ^{47}K. The indirect contribution was negligible because the co-produced parents can be formed only from the lower-abundant isotopes, ^{46}Ca and ^{48}Ca. The gamma line at 159.381 keV (I_γ = 68.3%) from the ^{47}Sc decay was measured after cooling times of 1.2–2.8 d. The derived cross sections of the ^{nat}Ca$(\alpha, x)^{47}$Sc reaction are shown in Fig. 1 in comparison with the experimental data studied earlier[3] and the theoretical values provided in the TENDL-2019 library.[4] The previous data of the ^{44}Ca$(\alpha, x)^{47}$Sc reaction are normalized to those using natural calcium targets. The peak of the previous data shifts to the low-energy region. The TENDL-2019 calculation largely overestimates the excitation function.

This work was supported by the Japan-Hungary Research Cooperative Program between JSPS and HUS, Grant number JPJSBP120193808 and NKM-43/2019.

References

1) V. N. Levkovski, *Cross Sections of Medium Mass Nuclide Activation (A = 40–100) by medium energy protons and alpha particles (E = 10–50 MeV)* (Inter-Vesi, Moscow, USSR, 1991).
2) J. F. Ziegler *et al.*, Nucl. Instrum. Methods Phys. Res. B **268**, 1818 (2010).
3) A. Hermanne *et al.*, Nucl. Data Sheets **148**, 338 (2018).
4) A. J. Koning *et al.*, Nucl. Data Sheets **155**, 1 (2019).

*1 Faculty of Science, Hokkaido University
*2 RIKEN Nishina Center
*3 Graduate School of Biomedical Science and Engineering, Hokkaido University
*4 Nuclear Research Center, National University of Mongolia
*5 Institute for Nuclear Research (ATOMKI)

Activation cross sections of proton-induced reactions on manganese up to 30 MeV

H. Huang,[*1,*2] M. Aikawa,[*1,*2,*3] and H. Haba[*2]

^{51}Cr ($T_{1/2}$ = 27.8 d) decays through electron capture. It has been used to label the ethylenediaminetetraacetic acid (^{51}Cr-EDTA), whose blood clearance counting responds to the glomerular filtration rate.[1] It has also been used to label red blood cells as a tracer for measuring the of mass and volume of living systems.[2] This medical radionuclide is expected to be produced via charged-particle-induced reactions on neighbor elements. In this research, we focused on the proton-induced reaction on manganese. Manganese has only one stable isotope: ^{55}Mn. We found four former experimental data on the cross sections of the ^{55}Mn$(p,x)^{51}$Cr reaction in the literature survey.[3–6] However, they are scattered and not consistent with each other. Therefore, we performed an experiment to measure the cross sections of this reaction.

We conducted the experiment using a 30-MeV proton beam at the AVF cyclotron at RIKEN. We adopted the well-established stacked-foil activation technique, followed by high-resolution gamma-ray spectrometry to determine the excitation functions. The target consisted of manganin (Nilaco Corp., Japan), ^{nat}Ti (99.6% purity, Nilaco Corp., Japan) and ^{27}Al (>99% purity, Nilaco Corp., Japan) foils. Manganin is an alloy consisting of copper, manganese, and nickel. We analyzed the elemental ratio of the manganin foil using scanning electron microscopy with energy dispersive spectroscopy (Hitachi TM4000 Plus II). The measured mass ratios were 12.5%, 85.2% and 2.24% for Mn, Cu and Ni, respectively. The ^{nat}Ti foil was used for the ^{nat}Ti$(p,x)^{48}$V monitor reaction to assess beam parameters and target thicknesses. The ^{27}Al foil was interleaved to collect recoiled products. We measured the weight and size of these foils to obtain their average thicknesses. The foils were then cut into squares of 8 × 8 mm^2 to fit the size of a target holder, which also served as a Faraday cup. Seventeen sets of Mn-Mn-Ti-Ti-Al foils were stacked as the target.

The stacked target was irradiated for 20 min. The average intensity and primary energy of the beam were measured to be 182 nA and 30.1 MeV, respectively. Energy degradation in the stacked target was calculated using the stopping powers obtained using the SRIM code.[7] The gamma-ray spectrometry was performed using a high-purity germanium detector (ORTEC GEM30P4-70) and analyzed using the analysis software (SEIKO EG&G Gamma Studio). We assumed that the recoiled nuclides from the first foils compensate for the loss of the second foils. Only gamma spectra from second manganin and Ti foils were measured, The cooling times were from 18.4 to 52.8 h. The dead time was maintained below 3.6%. The cross sections of the ^{nat}Ti$(p,x)^{48}$V monitor reaction were derived and then compared with the recommended values of IAEA.[8] According to the comparison, the thicknesses of all the foils were corrected by +1%. The other parameters were adopted without any correction.

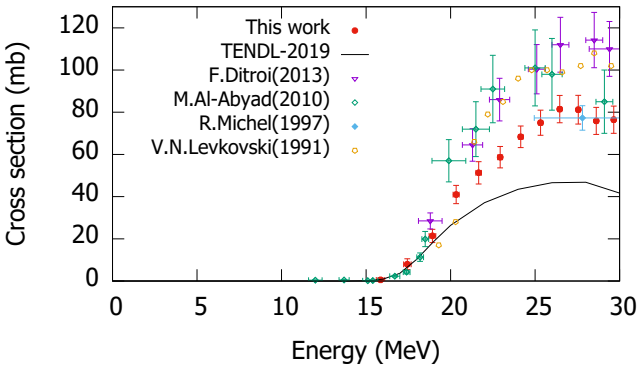

Fig. 1. Cross sections of the ^{55}Mn$(p,x)^{51}$Cr reaction with previous data[3–6] and TENDL-2019 values.[8]

The gamma line emitted from the decay of ^{51}Cr with an energy of 320.08 keV (I_γ = 9.91%) was measured to derive the cross sections of the ^{55}Mn$(p,x)^{51}$Cr reaction. We compared our data with previous experimental studies[3–6] and the theoretical values of TENDL-2019[9] in Fig. 1. Our data had fewer total uncertainties than former studies because the partial uncertainties of target thickness and beam intensity were smaller. The peak positions of previous experimental data were consistent with ours, whereas the amplitudes of some data were larger. The theoretical values of TENDL-2019 underestimated the experimental data.

*1 Graduate School of Biomedical Science and Engineering, Hokkaido University
*2 RIKEN Nishina Center
*3 Faculty of Science, Hokkaido University

References
1) S. J. Gray *et al.*, J. Clin. Investig. **29**, 1604 (1950).
2) A. A. Chaves *et al.*, Clinics (Sao Paulo) **65**, 607 (2010).
3) F. Ditroi *et al.*, Nucl. Instrum. Methods Phys. Res. B. **308**, 34 (2013).
4) M. Al-Abyad *et al.*, Appl. Radiat. Isot. **68**, 2393 (2010).
5) R. Michel *et al.*, Nucl. Instrum. Methods Phys. Res. B **129**, 153 (1997).
6) V. N. Levkovskii *et al.*, Radiat. Eff. **80**, 223 (1984).
7) J. F. Ziegler *et al.*, SRIM: the Stopping and Range of Ions in Matter (2008), `http://www.srim.org/` .
8) F. Tárkányi *et al.*, IAEA-TECDOC-1211 (2007).
9) A. J. Koning *et al.*, Nucl. Data Sheets **113**, 2841 (2012).

Activation cross sections of deuteron-induced reactions on natural chromium up to 24 MeV

H. Huang,[*1,*2] M. Aikawa,[*1,*2,*3] Y. Hanada,[*1,*2] and H. Haba[*2]

^{52g}Mn ($T_{1/2}$ = 5.591 d) that decays by electron capture and positron emission can be used in positron emission tomography (PET).[1] ^{51}Cr ($T_{1/2}$ = 27.8 d) that decays by the same mode was used to label red blood cells as a tracer in the measurement of the mass and volume of living systems.[2] These medical radionuclides can be produced via charged-particle-induced reactions on neighbor elements. We focused on the deuteron-induced reaction on natural chromium. Experimental literature data regarding the cross sections of the reaction are inconsistent,[3–5] and therefore, we performed the experiment to measure the production cross sections of ^{52g}Mn and ^{51}Cr. In addition, the cross sections of the by-products ^{48}V and ^{52m,54}Mn were determined.

We adopted the well-established stacked-foil activation technique followed by high-resolution gamma-ray spectrometry to determine excitation functions. The target comprised nickel-chromium (NiCr) alloy (99.9% purity, Goodfellow Co., Ltd., UK), ^{nat}Ti (99.6% purity, Nilaco Corp., Japan), and ^{27}Al (>99% purity, Nilaco Corp., Japan) foils. The ^{nat}Ti foil was used for the ^{nat}Ti$(d,x)^{48}$V monitor reaction to assess the beam parameters. The ^{27}Al foil was interleaved to collect recoiled products. The average thickness of each foil was derived from their measured weight and size. We analyzed the elemental ratio of the NiCr alloy foil by a scanning electron microscope with an energy dispersive X-ray spectrometer (Hitachi TM4000 Plus II). The measured mass ratios were Cr 21.5%, Ni 76.7%, and Mn 1.7%, respectively. All foils were then cut into squares of 8 × 8 mm^2 to fit the size of a target holder that served as a Faraday cup. Thirteen sets of NiCr-NiCr-Al-Ti-Ti-Al foils were stacked as the target.

The stacked target was irradiated for 15 min by a 24-MeV deuteron beam from the AVF cyclotron at RIKEN. The average intensity and primary energy of the beam were measured to be 105 nA and 24.0 ± 0.1 MeV. Energy degradation in the stacked target was calculated using stopping powers obtained by the SRIM code.[6] Gamma-ray spectrometry was performed using a high-purity germanium detector (ORTEC GEM30P4-70) and analyzed by the analysis software (SEIKO EG&G Gamma Studio). Only gamma spectra from each second NiCr alloy and Ti foil were measured assuming that recoiled nuclides from the second foils were compensated by those from the first.

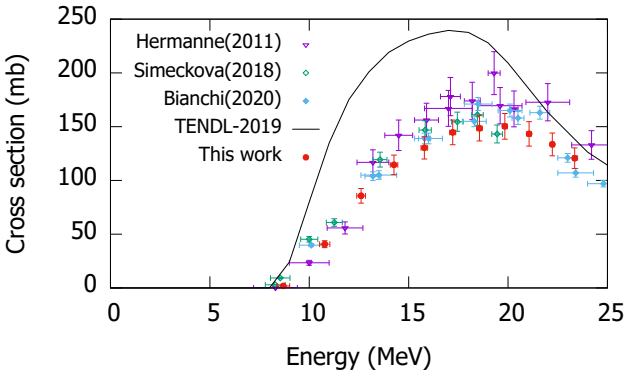

Fig. 1. Cross sections of the ^{nat}Cr$(d,x)^{52g}$Mn reaction with previous data[3–5] and the TENDL-2019 values.[8]

During 1 h–32 d cooling, NiCr alloy foils were measured 7 times to assess the radionuclides with different half-lives. The measurement distances were 3–50 cm. The dead time was kept below 5.2%.

The cross sections of the ^{nat}Ti$(d,x)^{48}$V monitor reaction were derived and compared with the recommended values of IAEA.[7] The comparison results indicated that, the beam intensity was corrected by −1.1% within the uncertainty (5%). The other parameters were adopted without any correction.

We derived the cross sections using the measurement of the 935.544-keV gamma line (I_γ = 94.5%) emitted with the decay of ^{52g}Mn. A short-lived metastable isomer ^{52m}Mn ($T_{1/2}$ = 21.1 min) decayed to the ground state ^{52g}Mn by isomeric transition with a branching ratio of 1.78%. Thus, we determined the cumulative cross section of ^{52g}Mn. We compare our data with the previous studies[3–5] and the TENDL-2019 values[8] in Fig. 1; our data are less scattered and in agreement with the recently published data.[4,5] The theoretical values of TENDL-2019 obviously overestimate the experimental data.

*1 Graduate School of Biomedical Science and Engineering, Hokkaido University
*2 RIKEN Nishina Center
*3 Faculty of Science, Hokkaido University

References
1) I. F. Chaple *et al.*, J. Nucl. Med. **59**, 1655 (2018).
2) S. J. Gray *et al.*, J. Clin. Investig. **29**, 1604 (1950).
3) A. Hermanne *et al.*, Nucl. Instrum. Methods Phys. Res. B **269**, 2563 (2011).
4) E. Šimečková *et al.*, Phys. Rev. C **3**, 034606 (2018).
5) F. Bianchi *et al.*, Appl. Radiat. Isot. **166**, 109329 (2020).
6) J. F. Ziegler *et al.*, SRIM: the Stopping and Range of Ions in Matter (2008), `http://www.srim.org/` .
7) F. Tárkányi *et al.*, IAEA-TECDOC-1211 (2007).
8) A. J. Koning *et al.*, Nucl. Data Sheets **113**, 2841 (2012).

Production cross-sections of ^{52m}Mn in alpha-particle-induced reactions in natural vanadium

G. Damdinsuren,[*1,*2] M. Aikawa,[*1,*2,*3] Kh. Tegshjargal,[*4] N. Erdene,[*4] S. Ebata,[*5,*2] and H. Haba[*2]

The ground state of the ^{52m}Mn radioisotope has a half-life of $T_{1/2}$ = 5.6 days and decays via electron capture (70.6%) and positron emission processes (29.4%, $\langle E_{\beta+}\rangle$ = 242 keV). ^{52m}Mn can be used in positron emission tomography (PET) imaging to study biological and physiological processes with a time scale similar to its decay.[1] The routes for ^{52m}Mn production include charged-particle-induced reactions. Among the possible reactions, we focused on the α-particle-induced reaction on natural vanadium targets. Eleven previous experimental studies were found in the EXFOR library.[2] However, their data exhibited show large uncertainties and discrepancies. Therefore, we measured the excitation function of the ^{nat}V$(\alpha, x)^{52m}$Mn reaction. The experimental result was compared with the literature data obtained from the EXFOR database and TENDL-2019 data.[3]

The stacked-foil activation technique and high-resolution γ-ray spectrometry were used for cross-section measurements. The experiment target consisted of pure metal foils of ^{nat}V (25-μm thick, 99% purity), ^{nat}Ti (5-μm thick, 99.6% purity), and ^{27}Al (5-μm thick, 99.9% purity) from Nilaco Corp., Japan. ^{27}Al foils were inserted to sandwich ^{nat}V foils to separate the recoiled reaction products from ^{nat}V and ^{nat}Ti foils. ^{nat}Ti foils were used in the ^{nat}Ti$(\alpha, x)^{51}$Cr monitor reaction to assess beam parameters and energy loss in the particles in the stack.

The target thickness was derived using the measured size and weight of the foils. The derived thickness of ^{nat}V, ^{nat}Ti, and ^{27}Al foils was 20.4, 2.24, and 1.22 mg/cm^2, respectively. These foils were then cut into 8 × 8 mm pieces to fit a target holder that served as a Faraday cup. Eleven sets of V-Al-Ti-Ti-Al foils were stacked into the target holder.

The stacked target was irradiated with a 50.6 ± 0.2 MeV alpha-particle beam for 30 min. The primary energy was measured by the time-of-flight method.[4] Energy degradation in the stacked target was calculated using the SRIM code.[5] The average beam intensity measured by the Faraday cup was 194 nA.

The γ-ray spectra of each irradiated foil were measured by a high-resolution HPGe detector (ORTEC GEM-25185-P) and analyzed using dedicated software (SEIKO EG&G Gamma Studio). Each ^{nat}V foil was measured with the following ^{27}Al catcher foil for the recoiled products. The distance between the detector and foils was arranged to ensure a dead time of less than 3%.

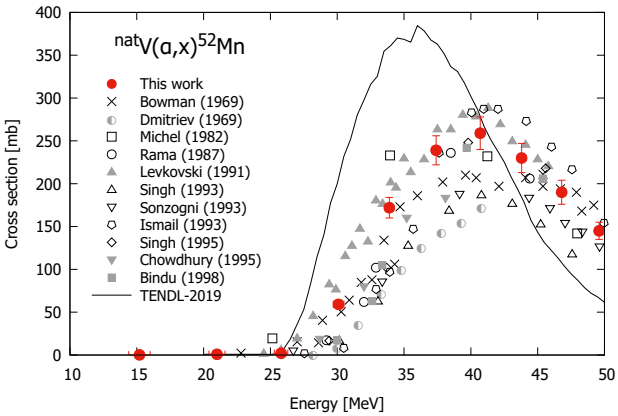

Fig. 1. Excitation function of the ^{nat}V$(\alpha, x)^{52m}$Mn reaction.

The cross-sections of the ^{nat}Ti$(\alpha, x)^{51}$Cr monitor reaction were derived to assess the beam parameters and target thickness. The γ line at 320.08 keV (I_γ = 9.91%) from the decay of ^{51}Cr ($T_{1/2}$ = 27.7025 d) in each low-energy foil of Ti-Ti pairs were measured. The derived cross-sections were compared with the IAEA recommended values.[6] Our result was consistent with the recommended values and no corrections were adopted for data analysis.

Further, the cumulative cross-sections of the ^{nat}V$(\alpha, x)^{52m}$Mn reaction were derived. The shorter-lived metastable state of the ^{52m}Mn ($T_{1/2}$ = 21.1 min) radionuclide decayed to the ground state ^{52m}Mn ($T_{1/2}$ = 5.591 d) and ^{52}Cr (stable) soon after the end of the bombardment. The γ line at 935.544 keV (I_γ = 94.5%) from the decay of ^{52m}Mn was measured after cooling for 17 days. The cumulative cross-sections were obtained from the net count of the γ line. Figure 1 shows the derived cross-sections in comparison to previous experimental studies and TENDL-2019 data.[3] The present cross-section data exhibited a smooth curve and they were consistent with a part of previous experimental data. The peak position and amplitude of TENDL-2019 data were different from the experimental data.

G. Damdinsuren was granted a scholarship by the M-JEED project (Mongolian-Japan Engineering Education Development Program, J11B16).

*1 Graduate School of Biomedical Science and Engineering, Hokkaido University
*2 RIKEN Nishina Center
*3 Faculty of Science, Hokkaido University
*4 School of Engineering and Applied Sciences, National University of Mongolia
*5 Graduate School of Science and Engineering, Saitama University

References
1) F. Bianchi *et al.*, Appl. Radiat. Isot. **166** (2020).
2) N. Otuka *et al.*, Nucl. Data Sheets **120**, 272 (2014).
3) A. J. Koning *et al.*, Nucl. Data Sheets **155**, 1 (2019).
4) T. Watanabe *et al.*, Proc. 5th Int. Part. Accel. Conf. (2014), p. 3566.
5) J. F. Ziegler *et al.*, Nucl. Instrum. Methods Phys. Res. B **268**, 1818 (2010).
6) F. Tárkányi *et al.*, IAEA-TECDOC-1211 (2007).

Measurement of production cross sections of medical isotope ^{110m}In in alpha-particle-induced reaction on natural silver up to 50 MeV

Ts. Zolbadral,[*1,*2,*3] M. Aikawa,[*3,*4,*5] D. Ichinkhorloo,[*1,*4] G. Damdinsuren,[*3,*4] H. Huang,[*3,*4] and H. Haba[*4]

The metastable state of indium-110 (^{110m}In) has a half-life of 69.1 min and emits positrons ($E_{\beta+}$ = 1011 keV, $I_{\beta+}$ = 61.3%). This radionuclide can be used to label proteins and peptides for application in positron emission tomography (PET) imaging.[1,2] Furthermore, ^{110m}In emits a medium-energy and high-intensity γ line that is useful for $\beta + \gamma$ coincidence PET.[3]

A suitable route for direct production of ^{110m}In is the α-particle-induced reaction on a silver target (^{107}Ag 51.839%, ^{109}Ag 48.161%). ^{110m}In can be produced by the (α, n) reaction ($E_{\rm thr}$ = 7.87 MeV) on ^{107}Ag and the $(\alpha, 3n)$ reaction ($E_{\rm thr}$ = 24.92 MeV) on ^{109}Ag. Because most radioactive impurities can be eliminated, the ^{107}Ag$(\alpha, n)^{110m}$In reaction is a promising candidate for the production of ^{110m}In;[4] however an isotopically enriched ^{107}Ag target is required for the reaction. The longer-lived ground state, ^{110g}In ($T_{1/2}$ = 4.92 h), is co-produced in the energy region in addition to ^{110m}In. To investigate the production route of ^{110m}In, reliable data on the cross sections of the α-induced reaction on a natural silver target are required.

Thus, the main aim of this study is to measure the cross sections of the $^{\rm nat}$Ag$(\alpha, x)^{110m}$In reaction and to investigate a route for ^{110m}In production.

The cross sections were determined using the stacked-foil activation technique and γ-ray spectrometry. Pure metallic foils of $^{\rm nat}$Ag (thickness of 10.1 mg/cm^2 with a purity of 99.9%) and $^{\rm nat}$Ti (thickness of 2.2 mg/cm^2 with a purity of 99.5%) were stacked to form the target.

The stacked target was irradiated for 30 min with a 50.2-MeV α-particle beam from the RIKEN AVF cyclotron. The energy of the incident beam was measured using the time-of-flight method. The SRIM code[5] was used to calculate the energy degradation in the stacked target. The beam intensity was 213 nA measured with a Faraday cup.

A high-resolution high-purity germanium (HPGe) detector was used to measure the γ-ray spectra of the irradiated foils. The detector was calibrated by a mixed γ-ray point source. In the measurements, the dead time was less than 10%.

The cross sections of the $^{\rm nat}$Ag$(\alpha, x)^{110m}$In reaction were derived from the measurements of the 657.75-keV γ line (I_γ = 97.74%) from the ^{110m}In decay.

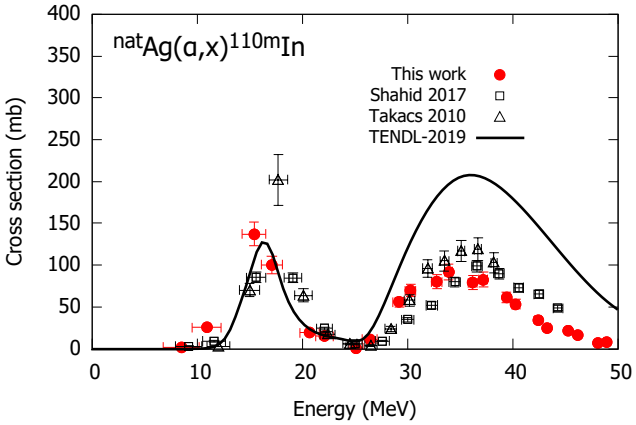

Fig. 1. Excitation function of the $^{\rm nat}$Ag$(\alpha, x)^{110m}$In reaction with previous experimental data[6,7] and the TENDL-2019 values.[8]

Figure 1 shows the preliminary results of the measured excitation function of the $^{\rm nat}$Ag$(\alpha, x)^{110m}$In reaction in comparison with recent experimental data reported by Shahid *et al.*,[6] Takács *et al.*,[7] and the theoretical estimation from TENDL-2019.[8]

Our measured excitation function of the $^{\rm nat}$Ag$(\alpha, x)^{110m}$In reaction is consistent with those of the previous experimental data sets[6,7] within uncertainties, however, the peak position of our result shifts slightly to lower energy.

The TENDL-2019 data show partial agreement with the experimental data sets. The second peak in the higher-energy region is much larger than the experimental data.

*1 Nuclear Research Center, National University of Mongolia
*2 New Mongolia College of Technology
*3 Graduate School of Biomedical Science and Engineering, Hokkaido University
*4 RIKEN Nishina Center
*5 Faculty of Science, Hokkaido University

References

1) M. Lubberink *et al.*, J. Nucl. Med. **43**, 1391 (2002).
2) V. Tolmachev *et al.*, Biochim. Biophys. Acta, Gen. Subj. **1800**, 487 (2010).
3) M. Sitarz *et al.*, Appl. Radiat. Isot. **155**, 108898 (2020).
4) F. Tárkányi *et al.*, Nucl. Instrum. Methods Phys. Res. B **351**, 6 (2015).
5) J. F. Ziegler *et al.*, Nucl. Instrum. Methods Phys. Res. B **268**, 1818 (2010).
6) M. Shahid *et al.*, J. Radioanal. Nucl. Chem. **311**, 1971 (2017).
7) S. Takács *et al.*, Nucl. Instrum. Methods Phys. Res. B **268**, 2 (2010).
8) A. J. Koning *et al.*, Nucl. Data Sheets **155**, 1 (2019).

Cross sections of alpha-particle-induced reactions on ^{nat}Sb†

S. Takács,[*1] F. Ditrói,[*1] Z. Szücs,[*1] K. Brezovcsik,[*1] H. Haba,[*2] Y. Komori,[*2] M. Aikawa,[*3,*2] M. Saito,[*4,*2] T. Murata,[*4,*2] M. Sakaguchi,[*4,*2] and N. Ukon[*5,*2]

Cross sections of alpha-particle-induced reactions on natural antimony targets were investigated up to 51 MeV. Some produced iodine isotopes are frequently used in nuclear medicine; therefore, their cross sections can be interesting as alternative production routes. For most of these reactions, the available experimental data in the literature are not sufficiently consistent; therefore, additional experimental cross sections of these reactions are required. The experiment was performed at the RIKEN AVF cyclotron. The stacked-foil activation technique and high-resolution γ-ray spectrometry were used. Thin Sb targets were prepared by vacuum evaporation onto Kapton (polyimide) (24.5 ± 0.25 μm, Goodfellow, Co., Ltd., UK). Kapton backings with a diameter of 13 mm were cut, numbered, and measured by weight before the evaporation process. Small grains of Sb (approximately 5 mg) were placed in a resistive heated tantalum boat to evaporate it in vacuum and deposit a thin layer of Sb onto the Kapton backings with a 10 mm in diameter mask placed approximately 15 cm from the source of evaporating Sb. This geometry provided relatively even Sb layers on the Kapton backings. The thickness of the evaporated Sb layer was determined from the measured weight and known surface of the evaporated spot. Each sandwiched Sb target was composed of two Sb layers enclosed between two Kapton backings with an average thickness of $\sim$1 mg/cm^2. Pure ^{nat}Ti foils (99.9% Nilaco Corp., Japan) with an average thickness of 5.3 ± 0.05 μm were inserted into the stack to monitor the irradiation parameters. To address the recoil effect, an additional Kapton catcher foil was used behind every Ti foil. The irradiations lasted for 2 h with an alpha-particle beam of 50.42 ± 0.2 MeV and 50 nA. The incident beam energy was measured using the time-of-flight method.[1)] The energy loss of the alpha particles was calculated using the semi-empirical formula proposed by Andersen and Ziegler.[2)] The average beam intensity measured using a Faraday cup was cross checked with the ^{nat}Ti$(\alpha,x)^{51}$Cr monitor reaction.[3)] After applying a +5% correction of the measured beam intensity, the re-measured cross sections for the ^{nat}Ti$(\alpha,x)^{51}$Cr monitor reaction agreed perfectly with their recommended values[3)] indicating that a proper beam and target parameters were used. Three series of γ-ray spectra were recorded for every irradiated foil by using a high-resolution HPGe detector-based γ-spectrometer without chemical separation with average cooling times of 25, 75, and 180 h to follow the decay of the reaction products. Q-values and decay data were obtained using the Q-value calculator[4)] and NuDat 2.7 database[5)] of National Nuclear Data Center, respectively.

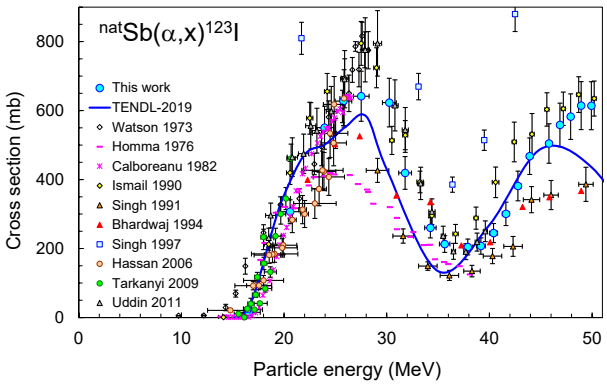

Fig. 1. Excitation function of the ^{nat}Sb$(\alpha,x)^{123}$I reaction in comparison with previously reported experimental data and results of the model calculation from the TENDL-2019 database.[5)]

Direct or cumulative cross sections for the formation of ^{121,123,124,125,126}I, ^{121m,g,123m,125m}Te, and ^{118m,120m,122g}Sb were determined. The obtained experimental data were compared with the experimental data available in the literature and the results of the TALYS theoretical model calculation taken from the TENDL-2019[6)] data library.

A comparison with the theoretical estimation revealed that the TALYS prediction provided an acceptable agreement with the experimental data except for the ^{125m}Te isotope, for which the prediction was far too conservative.

Cross section data were reported for the first time for the ^{nat}Sb$(\alpha,x)^{121m}$Te, ^{nat}Sb$(\alpha,x)^{123m}$Te, ^{nat}Sb$(\alpha,x)^{125m}$Te, ^{nat}Sb$(\alpha,x)^{118m}$Sb, and ^{nat}Sb$(\alpha,x)^{122g}$Sb reactions.

This work was conducted in the framework of a common research program between the JSPS and HAS (Contract No: JPJSBP120193808 and NKM-43/2019).

References

1) T. Watanabe *et al.*, Proc. 5th Int. Part. Accel. Conf. (IPAC2014), (2014), p. 3566.
2) H. H. Andersen, J. F. Ziegler, *Helium Stopping Powers and Ranges in all Elements* (Pergamon, Oxford, 1997).
3) A. Hermanne *et al.*, Nucl. Data Sheets **148**, 338 (2018).
4) NNDC, Q-calc, `https://www.nndc.bnl.gov/qcalc/`.
5) NNDC, NuDat 2.7 database, `http://www.nndc.bnl.gov/nudat2/`.
6) A. J. Koning *et al.*, Nucl. Data Sheets **155**, 1 (2019).

† Condensed from the article in Nucl. Instrum. Methods Phys. Res. B **505**, 24 (2021)

*1 Institute for Nuclear Research (ATOMKI)
*2 RIKEN Nishina Center
*3 Faculty of Science, Hokkaido University
*4 Graduate School of Biomedical Science and Engineering, Hokkaido University
*1 Advanced Clinical Research Center, Fukushima Medical University

Activation cross sections of deuteron-induced reactions on praseodymium up to 24 MeV†

M. Aikawa,[*1,*2] T. Maehashi,[*3] D. Ichinkhorloo,[*1,*2] S. Ebata,[*4,*2] Y. Komori,[*2] and H. Haba[*2]

The ^{140}Nd ($T_{1/2}$ = 3.37 d) and ^{142}Pr ($T_{1/2}$ = 19.12 h) radionuclides can be used for a ^{140}Nd/^{140}Pr in-vivo generator for positron emission tomography (PET)[1] and for the treatment for arteriovenous malformations,[2] respectively. We focused on the deuteron-induced reaction on the monoisotopic element ^{141}Pr among possible production reactions. In a literature survey, we found only two experimental studies on the ^{141}Pr$(d,3n)^{140}$Nd reaction, the experimental cross sections of which are scattered.[3,4] Therefore, we conducted two experiments to measure the cross sections of this reaction. The production cross sections of ^{141,140}Nd, ^{142}Pr, and ^{141}Ce were determined up to 24 MeV.

Two independent experiments were conducted using 24-MeV deuteron beams at the RIKEN AVF cyclotron. The stacked-foil activation technique and high-resolution gamma-ray spectrometry were adopted for the experiments. For the stacked targets, two ^{141}Pr (99% purity), two ^{nat}Ti (99.6% purity), and one ^{27}Al (>99% purity) metal foils were purchased from Nilaco Corp., Japan. The measured thicknesses of the foils were 67.6 and 72.3 mg/cm^2 (^{141}Pr), 2.34 and 2.30 mg/cm^2 (^{nat}Ti), and 1.50 mg/cm^2 (^{27}Al). The first (#1) and second stacked targets (#2) were composed of ^{141}Pr and ^{nat}Ti and ^{141}Pr, ^{nat}Ti, and ^{27}Al, respectively. The ^{nat}Ti foils were interleaved for the ^{nat}Ti$(d,x)^{48}$V monitor reaction to assess beam parameters and target thicknesses. The ^{27}Al foils were used as catchers of the recoiled products and to address the variation in energy degradation. Nine sets of Pr-Ti-Ti (#1) and Pr-Al-Ti-Ti-Al foils (#2), which were cut into a size of 8 × 8 mm^2, were stacked into target folders served as Faraday cups.

Both stacked targets were irradiated with deuteron beams for 30 min. The average beam intensities measured by the Faraday cups were 107 (#1) and 110 nA (#2). The measured primary beam energies were 24.1 (#1) and 24.3 MeV (#2). The energy degradation of the beams in the stacked targets was calculated using stopping powers obtained from the SRIM code.[5]

Gamma rays emitted from the irradiated foils were measured without chemical separation using a high-purity germanium detector. The ^{141}Pr foils with the following ^{27}Al foils were measured several times with a dead time below 5.2%.

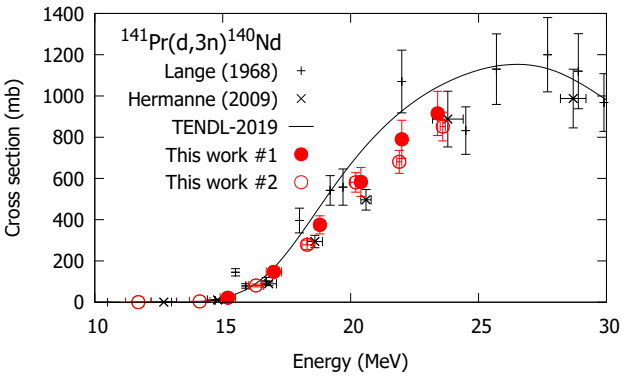

Fig. 1. Cross sections of the ^{141}Pr$(d,3n)^{140}$Nd reaction with the previous data[3,4] and the TENDL-2019 values.[7]

Cross sections of the ^{nat}Ti$(d,x)^{48}$V monitor reaction were derived to assess beam parameters and target thicknesses. A comparison with the IAEA recommended values[6] indicated that the thicknesses of the ^{141}Pr foils were corrected by +1% within the uncertainties (2%). The other target thicknesses and beam parameters were adopted without any correction.

There are no gamma lines with the decay of ^{140}Nd ($T_{1/2}$ = 3.37 d). Considering the secular equilibrium, the gamma lines at 1596.1 keV (I_γ = 0.49%) and 511 keV (I_γ = 102%) emitted with the decay of ^{140}Pr ($T_{1/2}$ = 3.39 min) were measured instead. The directly produced ^{140}Pr decayed during the cooling times. The cross sections of the ^{141}Pr$(d,3n)^{140}$Nd reaction in the first experiment (#1) were deduced from the gamma line at 1596.1 keV, and those in the second experiment (#2) were determined from the gamma line at 511 keV. A comparison of the results with previous studies[3,4] and TENDL-2019 values[7] is shown in Fig. 1. Previous experimental data are scattered, but almost consistent with ours within the uncertainties. The TENDL-2019 values are slightly larger than our data.

References
1) K. P. Zhernosekov *et al.*, Radiochim. Acta **95**, 319 (2007).
2) S. W. Lee *et al.*, Phys. Med. Biol. **50**, 151 (2005).
3) V. J. Lange *et al.*, Radiochim. Acta **9**, 66 (1968).
4) A. Hermanne *et al.*, Nucl. Instrum. Methods Phys. Res. B **383**, 81 (2016).
5) J. F. Ziegler *et al.*, Nucl. Instrum. Methods Phys. Res. B **268**, 1818 (2010).
6) F. Tárkányi *et al.*, IAEA-TECDOC-1211 (2007).
7) A. J. Koning *et al.*, Nucl. Data Sheets **155**, 1 (2019).

† Condensed from the article in Nucl. Instrum. Methods Phys. Res. B **498**, 23 (2021)

*1 Faculty of Science, Hokkaido University
*2 RIKEN Nishina Center
*3 School of Science, Hokkaido University
*4 Graduate School of Science and Engineering, Saitama University

Production cross sections for α-particle-induced reactions on ^{nat}La

S. Ebata,[*1,*2] M. Aikawa,[*3,*2] G. Damdinsuren,[*4,*2] and H. Haba[*2]

The application of radionuclides was started several decades ago. Given its widespread use, it is important for the nuclear medicine field to generate new medical isotopes using more safe and effective methods. To this end, radionuclides suitable for both therapy and diagnosis have been investigated in recent years. The radionuclide ^{142}Pr ($T_{1/2}$ = 19.12 h) is one of the applicable candidates because of its β decay ($\langle E_{\beta^-} \rangle$ = 810 keV, 96.3%) and low-intensity specific γ emission with E_γ = 1575 keV (3.7%).[1] Among the possible ways to generate ^{142}Pr, the proton-, deuteron-, and alpha-particle induced reactions on cerium and lanthanum can be considered for on-site production at small light-ion accelerators used in hospitals. In the literature survey, only two experimental studies were found for the ^{nat}La$(\alpha, x)^{142}$Pr reaction,[2,3] and they did not provide consistent results (See Fig. 1.). Therefore, we focus on the α-particle-induced reaction on natural lanthanum and measure the production cross sections for the reaction using an activation method.

Two independent experiments were performed using 50-(#1) and 29-MeV (#2) α beams at the RIKEN AVF cyclotron. The stacked-foil technique was adopted in the activation method, and high-resolution germanium-detector based γ-spectrometry was used to measure γ rays from the generated radionuclides. The stacked targets comprised ^{nat}La (99% purity), ^{27}Al (> 99% purity), and ^{nat}Ti (99.6% purity) metal foils purchased from Nilaco Corp., Japan. The natural abundances of ^{138}La and ^{139}La are 0.09% and 99.91%, respectively. The measured thicknesses of the foils were 15.4 mg/cm^2 (^{nat}La), 2.25 mg/cm^2 (^{nat}Ti), and 1.22 mg/cm^2 (^{27}Al). The ^{nat}Ti foils were interleaved for the ^{nat}Ti$(\alpha, x)^{51}$Cr monitor reaction to assess beam parameters and target thicknesses. The ^{27}Al foils were used as catchers for recoiled products and for energy degradation. Eighteen sets of La-Al-Ti-Ti (#1) and eight La-Al-Ti foils (#2), which were cut into a size of 8 × 8 mm^2, were stacked into target holders served as Faraday cups.

Both stacked targets were irradiated with α beams for 30 min. The average beam intensities were 196 (#1) and 210 nA (#2), which were measured on the Faraday cups. The measured primary beam energies were 50.6 (#1) and 29.0 MeV (#2). The energy degradation of the beams in the stacked targets was calculated using stopping powers by the SRIM code.[4]

The emitted γ rays from the irradiated foils were measured using a high-purity germanium detector.

*1 Department of Physics, Saitama University
*2 RIKEN Nishina Center
*3 Faculty of Science, Hokkaido University
*4 Graduate School of Biomedical Science and Engineering, Hokkaido University

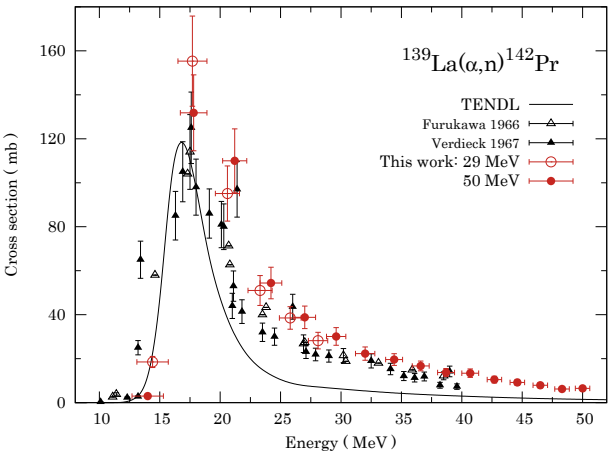

Fig. 1. Cross sections of the ^{139}La$(\alpha, n)^{142}$Pr reaction. The previous studies[2,3] and the TENDL-2019 values[5] are shown.

Each ^{nat}La foil with its following ^{27}Al catcher foil was measured several times with a dead time less than 2.8%. The ^{nat}Ti$(\alpha, x)^{51}$Cr monitor reaction was used to assess beam parameters and target thicknesses by comparing the measured cross sections for the reaction with the IAEA recommended values.[5] Only the thickness of the ^{nat}La foils was corrected by +1% within uncertainties to ensure consistency with the recommended values.

The γ line at 1575 keV with the decay of ^{142}Pr was analyzed to derive the cross sections of the ^{nat}La$(\alpha, x)^{142}$Pr reaction. The cross sections are practically the same as those of the ^{139}La$(\alpha, n)^{142}$Pr reaction because the contribution of the capture reaction on the less-abundant ^{138}La is negligible. The results with 50 and 29 MeV α beams are shown in Fig. 1 and are compared to those reported in previous studies[2,3] and the TENDL-2019 values.[6] Our independent data for 50 and 29 MeV agree well with each other. The present cross sections are slightly larger than those reported in the literature above 20 MeV, whereas the TENDL values underestimate all experimental data. Moreover, the peak widths of the experimental data were broader than those of the TENDL values.

References

1) M. Sadeghi *et al.*, J. Radioanal. Nucl. Chem. **288**, 937 (2011).
2) M. Furukawa, Nucl. Phys. **77**, 565 (1966).
3) E. V. Verdiegk, J. M. Miller, Phys. Rev. **153**, 1253 (1967).
4) J. F. Ziegler *et al.*, Nucl. Instrum. Methods Phys. Res. B **268**, 1818 (2010).
5) F. Tárkányi *et al.*, IAEA-TECDOC-1211 (2007).
6) A. J. Koning *et al.*, Nucl. Data. Sheets **155**, 1 (2019).

Production cross sections of ^{153}Sm via alpha-particle-induced reactions on natural neodymium

M. Aikawa,[*1,*2,*3] M. Sakaguchi,[*2,*3] N. Ukon,[*4,*3] Y. Komori,[*3] H. Haba,[*3] N. Otsuka,[*5] and S. Takács[*6]

Samarium radionuclides ^{153}Sm ($T_{1/2}$ = 46.3 h) and ^{145}Sm ($T_{1/2}$ = 340 d) can be used to treat bone metastases[1] and for brachytherapy,[2] respectively. We investigated the production of the radionuclides via alpha-particle-induced reactions on natural neodymium.[3] However, the measured cross sections of the ^{nat}Nd$(\alpha, x)^{153}$Sm reaction exhibit significant deviations from a previously published experimental study.[4] More specifically, the peak amplitude of the cross sections was different from each other by a factor of more than two. Therefore, we performed additional experiments to measure the activation cross sections of the reactions with an emphasis on the peak amplitude of the ^{nat}Nd$(\alpha, x)^{153}$Sm reaction.

Accordingly, two experiments (#1 and #2) were performed at the RIKEN AVF cyclotron using the stacked-foil activation technique and high-resolution gamma-ray spectrometry. Two targets of the experiments were composed of pure metallic foils of ^{nat}Nd (99% purity, Goodfellow Co., Ltd., UK) and ^{nat}Ti (99.6% purity, Nilaco Corp., Japan). The ^{nat}Ti foils were utilized for monitoring the beam via the ^{nat}Ti$(\alpha, x)^{51}$Cr monitor reaction and for beam-energy degradation. The average foil thicknesses, derived from the size and weight of the original ^{nat}Nd and ^{nat}Ti foils, were 16.7 and 2.25 mg/cm^2, respectively. The original foils were cut into a size of 10×10 mm. The two stacked targets with different configurations of six ^{nat}Nd and fourteen ^{nat}Ti target foils were placed in target holders that served as Faraday cups.

Both stacked targets were irradiated for 33 min with 28.9 ± 0.2-MeV alpha-particle beams. The energy degradation of the beams in the stacked targets were computed using stopping powers obtained from the SRIM code.[5] The average beam intensities measured by the Faraday cups were 103 nA (#1) and 104 nA (#2), respectively. Gamma rays emitted from the irradiated foils were measured without chemical separation using high-purity germanium detectors. To deduce activation cross sections, nuclear data were retrieved from the online database, NuDat 3.0.[6]

Cumulative cross sections of ^{153}Sm including contribution form decay of ^{153}Pm ($T_{1/2}$ = 5.25 min) via the alpha-particle-induced reactions on natural neodymium were determined. The cross sections were derived from measured net counts of the gamma line at 103.18 keV (I_γ = 29.25%), which was emitted from the decay of ^{153}Sm. The attenuation of the low-energy gamma rays in the ^{nat}Nd foil was calculated using the X-ray mass attenuation coefficients[7] and estimated to be 2.1%. The cross sections were determined using the corrected counts. The preliminary results are depicted in Fig. 1 along with the experimental data published earlier[3,4] and the TENDL-2019 values.[7] The present results conform with each other and also with our previous study,[3] however the other literature data[4] are inconsistent. Based on our new results, the smaller cross sections would be more reliable. The TENDL-2019 values are even smaller than the experimental data.

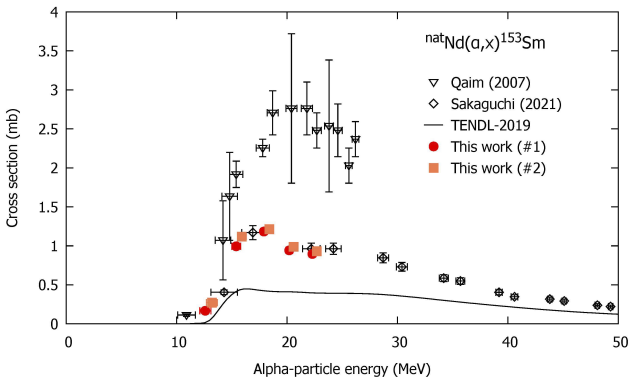

Fig. 1. Cross sections of the ^{nat}Nd$(\alpha, x)^{153}$Sm reaction with previous experimental data[3,4] and a theoretical prediction of the TENDL-2019 values.[7]

In addition to the cross sections of the ^{nat}Nd$(\alpha, x)^{153}$Sm reaction, those of the ^{nat}Nd$(\alpha, x)^{145}$Sm reaction will also be determined. There are no experimental data on the ^{nat}Nd$(\alpha, x)^{145}$Sm reaction other than our previous study. The cross sections derived in this work will increase the reliability of the cross sections.

*1 Faculty of Science, Hokkaido University
*2 Graduate School of Biomedical Science and Engineering, Hokkaido University
*3 RIKEN Nishina Center
*4 Advanced Clinical Research Center, Fukushima Medical University
*5 Nuclear Data Section, IAEA
*6 Institute for Nuclear Research (ATOMKI)

References
1) I. G. Finlay *et al.*, Lancet Oncol. **6**, 392 (2005).
2) R. G. Fairchild *et al.*, Phys. Med. Biol. **32**, 847 (1987).
3) M. Sakaguchi *et al.*, Appl. Radiat. Isot. **176**, 109826 (2021); M. Sakaguchi *et al.*, in this report.
4) S. M. Qaim *et al.*, Radiochim. Acta **95**, 313 (2007).
5) J. F. Ziegler *et al.*, SRIM: the Stopping and Range of Ions in Matter (2008), `http://www.srim.org/` .
6) National Nuclear Data Center, The NuDat 3.0 database, `http://www.nndc.bnl.gov/nudat3/` .
7) A. J. Koning *et al.*, Nucl. Data Sheets **155**, 1 (2019).
8) J. H. Hubble *et al.*, X-Ray Mass Attenuation Coefficients, NIST Standard Reference Database 126, `https://dx.doi.org/10.18434/T4D01F` .

Production cross-sections of dysprosium-159 radioisotope obtained by α-particle-induced reactions of natural gadolinium up to 50 MeV†

D. Ichinkhorloo,[*1,*2,*3] M. Aikawa,[*1,*4,*3] Ts. Zolbadral,[*4,*2,*3] T. Murata,[*4,*3] M. Sakaguchi,[*4,*3] Y. Komori,[*3] T. Yokokita,[*3] and H. Haba[*3]

Dysprosium and terbium radioisotopes are of interest for diagnosis and therapy in nuclear medicine. Dysprosium-157 ($T_{1/2}$ = 8.14 h), dysprosium-159 ($T_{1/2}$ = 144.4 d), and terbium-155 ($T_{1/2}$ = 5.32 d) can be used for bone scanning (skeletal imaging),[1] determination of bone mineral,[2] and single-photon emission computerized tomography imaging,[3] respectively.

Radionuclides can be produced in natural gadolinium by charged-particle-induced reactions. In this study, the activation cross-sections of α-particle-induced reactions in natural gadolinium were investigated. Production cross-sections of ^{155,157,159}Dy, ^{153,155,156g,160,161}Tb, and ^{153}Gd were determined. The results were compared with TENDL-2019 data based on TALYS code calculation.[4]

Experiments were conducted at the RIKEN AVF cyclotron, which in the stacked foil technique, the activation method and the high-resolution γ-ray spectrometry to determine the activation cross-sections.

A stacked target was formed of 8 × 8 mm^2 foils cut from large Gd (25 μm, 50×50 mm^2, 99.9% purity, Nilaco Corp., Japan) and Ti foils (5 μm, 50 × 100 mm^2, 99.6% purity, Nilaco Corp., Japan). The isotopic composition of the natural Gd target was ^{152}Gd (0.2%), ^{154}Gd (2.2%), ^{155}Gd (14.8%), ^{156}Gd (20.5%), ^{157}Gd (15.6%), ^{158}Gd (24.8%), and ^{160}Gd (21.9%).

The sizes and weights of the large foils were measured to derive the thicknesses of the Gd and Ti foils, which were found to be 25.4 and 2.29 mg/cm^2, respectively. The Ti foils were used in the ^{nat}Ti$(\alpha,x)^{51}$Cr monitor reaction to assess beam parameters and target thicknesses. The cut foils were stacked into the target holder, which was used as a Faraday cup.

An α-particle beam was accelerated to 51.1 MeV by the RIKEN AVF cyclotron. The beam energy was obtained using the time-of-flight method.[5] The stacked target was irradiated by the beam for 60 min with an average intensity of 257.6 nA. The beam intensity was measured using the Faraday cup. Energy degradation in the stacked target was calculated using the SRIM code.[6]

The γ rays emitted from the irradiated foils were measured by a high-resolution high-purity germanium detector.

The γ-ray spectra were analyzed with the Gamma Studio (SEIKO EG&G) software.

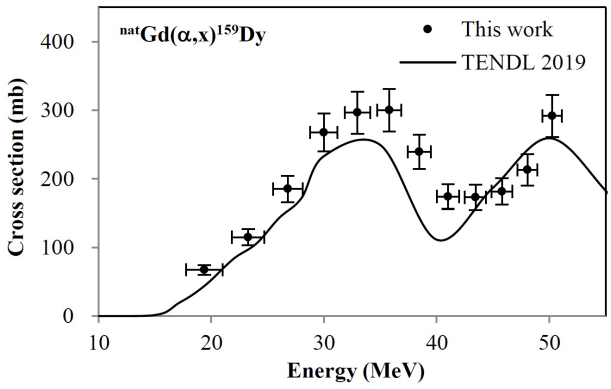

Fig. 1. Excitation function of the ^{nat}Gd$(\alpha,x)^{159}$Dy reaction compared to TENDL-2019 data.[4]

The cross-sections of the ^{nat}Gd$(\alpha,x)^{159}$Dy reaction were determined using the γ-ray line at 58.0 keV (I_γ = 2.27%) from the ^{159}Dy decay ($T_{1/2}$ = 144.4 d). To reduce the γ-ray background from the short-lived radionuclides, the measurements were executed after cooling times of 25.4–28.8 d. The mass attenuation coefficient adopted for the γ-ray line at 58.0 keV was 12.8 cm^2/g.[7] The correction factor using Eq. (1) of Ref. 8) is 1.17. The cross-sections of the ^{159}Dy production derived from the corrected activities are presented with the TENDL-2019 data[4] in Fig. 1. Our experimental data show peaks at approximately 35 and above 50 MeV. The peak amplitudes and positions in the TENDL-2019 data agree with our results. Reported experimental data were no found in our literature survey.

Production cross-sections of ^{155,157}Dy, ^{153,155,156g,160,161}Tb, and ^{153}Gd were also determined. The results of this study are expected to contribute to the research and development of nuclear medicine.

References
1) G. Subramanian *et al.*, J. Nucl. Med. **12**, 558 (1971).
2) D. V. Rao *et al.*, Med. Phys. **4**, 109 (1977).
3) C. Müller *et al.*, J. Nucl. Med. **53**, 1951 (2012).
4) A. J. Koning *et al.*, Nucl. Data Sheets **155**, 1 (2019).
5) T. Watanabe *et al.*, Proc. 5th Int. Part. Accel. Conf. (2014), p. 3566.
6) J. F. Ziegler *et al.*, SRIM: the Stopping and Range of Ions in Matter, `http://www.srim.org`.
7) Photon Interaction Database, National Institute of Standards and Technology (2004), `https://physics.nist.gov/PhysRefData/XrayMassCoef/tab3.html`.
8) Z. B. Alfassi *et al.*, Appl. Radiat. Isot. **67**, 240 (2009).

† Condensed from the article in Nucl. Instrum. Methods Phys. Res. B **499**, 46 (2021)

*1 Faculty of Science, Hokkaido University
*2 Nuclear Research Center, National University of Mongolia
*3 RIKEN Nishina Center
*4 Graduate School of Biomedical Science and Engineering, Hokkaido University
*5 School of Science, Hokkaido University

Production cross-sections of holmium-161 radioisotope from alpha-particle-induced reaction on terbium-159 up to 29 MeV

D. Ichinkhorloo,[*1,*2,*3] M. Aikawa,[*1,*4,*3] Ts. Zolbadral,[*4,*2,*3] Y. Hanada,[*4,*3] G. Damdinsuren,[*4,*3] and H. Haba[*3]

Terbium and holmium radioisotopes are of interest in medical applications.[1,2] These radioisotopes can be produced by charged-particle-induced reactions on neighbor elements, such as gadolinium and terbium. Among such reactions, we focused on alpha-particle-induced reactions on the monoisotopic element terbium-159 to produce the possible medical radioisotope, holmium-161. In a literature using the EXFOR library, only two relevant experimental studies were found.[3,4] Therefore, we performed an experiment to measure the activation cross-sections of the reaction. In this work, the production cross-sections of ^{160,161}Tb and ^{160g,160m,161,162m}Ho were studied. The results were compared with previous experimental data and TENDL-2019 data based on calculations using the TALYS code.[5]

The experiment was performed the RIKEN AVF cyclotron. In the experiment, we used the stacked foil technique, activation method, and high-resolution γ-ray spectrometry to determine the activation cross-sections.

The stacked target consisted of 8 × 8 mm^2 foils cut from large ^{159}Tb (nominal thickness: 25 μm, size: 50 × 50 mm^2, 99.9% purity, Nilaco Corp., Japan), ^{27}Al (5 μm, 100 × 100 mm^2, 99.9% purity, Nilaco Corp., Japan), and ^{nat}Ti foils (5 μm, 50 × 100 mm^2, 99.6% purity, Nilaco Corp., Japan).

The thickneses of Tb, Al and Ti foils were determined using the measured size and weight; they were found to be 19.1, 1.50, and 2.29 mg/cm^2, respectively. Ti foils were interleaved to check the beam parameters using the ^{nat}Ti$(\alpha,x)^{51}$Cr monitor reaction. The cut foils were stacked in a target holder, which also served as a Faraday cup.

The alpha-particle beam was accelerated to 29.1 MeV by the RIKEN AVF cyclotron. The beam energy was measured by the time-of-flight method.[6] The stacked target was irradiated by the beam for 30 min with an average intensity of 201 nA. The beam intensity was measured by the Faraday cup. Energy degradation in the stacked target was calculated using the SRIM code.[7]

The γ-rays emitted from irradiated foils were measured by a high-resolution high-purity germanium (HPGe) detector. The detector efficiency was calibrated using a multiple γ-ray emitting point source. The γ-ray spectra were analyzed by the software Gamma Studio software (SEIKO EG&G).

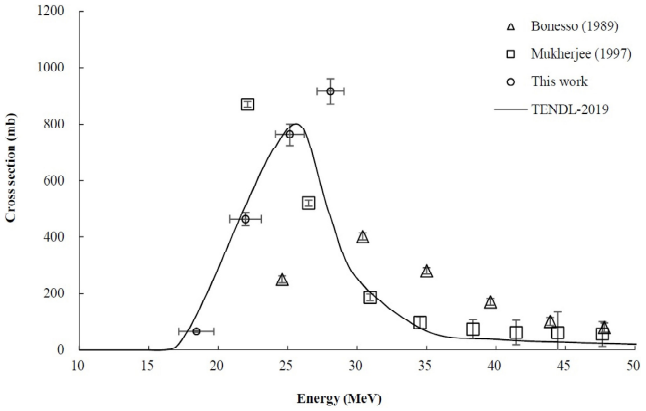

Fig. 1. Excitation function of the ^{159}Tb$(\alpha,2n)^{161}$Ho reaction with previous experimental data[3,4] and TENDL-2019 values.[5]

The cross-sections of the ^{159}Tb$(\alpha,2n)^{161}$Ho reaction were determined using measurements of the γ line at 103.05 keV (I_γ = 3.9%) from ^{161}Ho decay ($T_{1/2}$ = 2.48 h). To reduce γ-ray backgrounds from shorter-lived radionuclides, measurements were executed after cooling for 3.7–8.5 h. The cross-sections of ^{161}Ho production derived from the measured activities are presented with previous experimental data[3,4] and TENDL-2019 data[5] in Fig. 1. Previous experimental data demonstrated different tendencies in comparison to the present result. Our experimental data exhibited peaks above 28 MeV. The peak position and amplitude of TENDL-2019 data were also substantially different.

In summary, we performed an experiment to measure the excitation functions of alpha-particle-induced reactions on ^{159}Tb up to 29.1 MeV in the RIKEN AVF cyclotron. The production cross-sections of ^{160,161}Tb and ^{160g,160m,161,162m}Ho were determined. Subsequently, results were compared with previous experimental data and TENDL data.

References

1) C. Müller *et al.*, J. Nucl. Med. **53**, 1951 (2012).
2) F. Tárkányi *et al.*, J. Radioanal. Nucl. Chem. **298**, 277 (2013).
3) O. Bonesso *et al.*, J. Radioanal. Nucl. Chem. Lett. **137**, 29 (1989).
4) S. Mukherjee *et al.*, Phys. Rev. C **55**, 2556 (1997).
5) A. J. Koning *et al.*, Nucl. Data Sheets **155**, 1 (2019).
6) T. Watanabe *et al.*, Proc. 5th Int. Part. Accel. Conf. (IPAC 2014), (2014), p 3566.
7) J. F. Ziegler *et al.*, SRIM: the Stopping and Range of Ions in Matter, `http://www.srim.org`.

*1 Faculty of Science, Hokkaido University
*2 Nuclear Research Center, National University of Mongolia
*3 RIKEN Nishina Center
*4 Graduate School of Biomedical Science and Engineering, Hokkaido University

4. Radiation Chemistry and Biology

Responsible gene analysis of phenotypic mutants revealed the linear energy transfer (LET)-dependent mutation spectrum in rice†

R. Morita,[*1] H. Ichida,[*1] Y. Hayashi,[*1] K. Ishii,[*1] Y. Shirakawa,[*1] S. Usuda-Kogure,[*1] K. Ichinose,[*1] M. Hatashita,[*2] K. Takagi,[*2] K. Miura,[*3] M. Kusajima,[*3] H. Nakashita,[*3] T. Endo,[*4] Y. Tojo,[*5] Y. Okumoto,[*6] T. Sato,[*1,*7] K. Toriyama,[*7] and T. Abe[*1]

Linear energy transfer (LET), which refers to the amount of energy deposited per unit length of a particle's path (keV/μm), is an important parameter for ion beam mutagenesis. We previously demonstrated that the C ion irradiation (30 keV/μm) of Arabidopsis results in single nucleotide variants (SNVs), small indels (<100 bp), and translocations in the responsible genes for mutant phenotypes, with SNVs and small indels representing more than 80% of the mutations.[1)] Although the mutation frequencies induced by C ions (290 keV/μm) and Ar ions (290 keV/μm) are relatively low, both irradiations frequently result in large deletions (≧100 bp) in the responsible genes for mutant phenotypes.[2)] During an earlier whole-genome sequencing (WGS) analysis of Arabidopsis mutant lines conducted to compare the effects of Ar and C ions, the Ar ion (290 keV/μm) caused chromosomal rearrangements and large deletions more frequently than the C ions (30 keV/μm), whereas the C ions induced more SNVs and small indels in the genomes.[3)] These results indicated that the LETs of ion beams clearly affected DNA mutations in Arabidopsis. However, the effects of LETs of ion beams for mutation induction in plants other than Arabidopsis are largely unknown.

In this study, we irradiated rice seeds (dry or imbibed seeds) with C, Ne, or Ar ions with various LETs. The resulting mutant plants were isolated and the mutations in the responsible genes for the mutant phenotypes were examined using Sanger sequencing, whole-exome sequencing, or whole-genome sequencing to determine whether the mutation types differed among the LETs. We classified the mutations into the following four types: SNVs, small deletions (<100 bp), large deletions (≥100 bp), and chromosomal rearrangements (CRs; inversions or translocations). We complied the mutations according to the ion beam LETs and compared the tendencies of each irradiation. For the C ion (23, 30, 50, or 57 keV/μm) and Ne ion (63 or 70 keV/μm) irradiations, small deletions were the most frequent DNA mutations (Fig. 1). In contrast, the most frequent mutations induced by the Ar ion (290 keV/μm) irradiation were large deletions. Thus, we compared the proportions of the four types of mutations between the

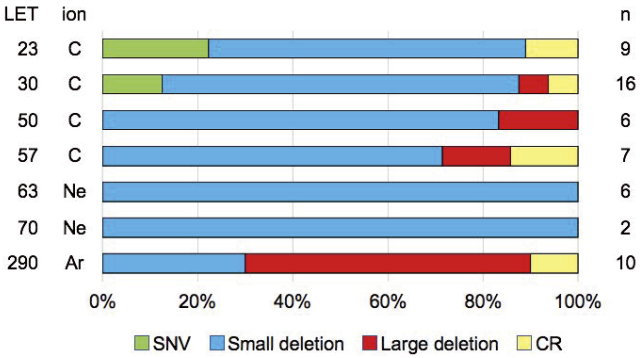

Fig. 1. Mutations on responsible genes classified on the basis of the LET.

Ar ion and C ion irradiations, which revealed significant differences ($p < 0.01$; Fisher's exact test). The differences were also significant when we compared the proportions of the mutations between the Ar and Ne ion irradiations ($p < 0.01$; Fisher's exact test). However, the differences in the proportions of the mutations between the C and Ne ion irradiations were not significant ($p > 0.05$; Fisher's exact test). Our data indicated ion beams with LETs of 23, 30, 50, 57, 63, and 70 keV/μm tended to cause small deletions, whereas the Ar ion irradiation tended to induce large deletions. These observations were consistent with the results of our previous studies on Arabidopsis mutants irradiated with C ions (23 or 30 keV/μm[1)]) or Ar ions (290 keV/μm[2,3)]). Thus, C ions (23 or 30 keV/μm) tend to induce small deletions, whereas Ar ions (290 keV/μm) tend to induce large deletions in the responsible genes for mutant phenotypes in rice and Arabidopsis. Therefore, we inferred that in rice and Arabidopsis, C ion (23 or 30 keV/μm) irradiations are suitable for efficiently inducing null mutants, whereas an Ar ion (290 keV/μm) irradiation is suitable for producing mutants with large deletions that can disrupt tandemly arrayed genes. Future investigations should clarify whether plant species other than rice and Arabidopsis exhibit similar tendencies regarding genetic mutations induced by ion beam irradiations. If these tendencies are common among plant species, ion beams with specific LETs may be used to induce particular mutation types, with important implications for research and plant breeding.

† Condensed from the article in Cytologia **86**, 303 (2021)
*1 RIKEN Nishina Center
*2 The Wakasa Wan Energy Research Center
*3 Fukui Prefectural University
*4 Miyagi Prefectural Furukawa Agricultural Experiment Station
*5 FUJICCO Co., Ltd.
*6 Setsunan University
*7 Tohoku University

References

1) Y. Kazama *et al.*, BMC Plant Biol. **11**, 161 (2011).
2) T. Hirano *et al.*, Mutat. Res. **735**, 19 (2012).
3) Y. Kazama *et al.*, Plant J. **92**, 1020 (2017).

Genetic characterization of large flower mutant *ohbana1* induced by heavy-ion beam irradiation in *Arabidopsis thaliana*†

V. Q. Nhat,[*1] Y. Kazama,[*2,*3] K. Ishii,[3,*4] S. Ohbu,[*3] H. Kunitake,[*1] T. Abe,[*3] and T. Hirano[*1,*3]

Flower size is an important trait that influences the economic value of ornamental plants, and most cultivars have relatively larger floral organs than their corresponding wild species. Thus, the genetic control of floral organ size is a principal target for ornamental plant breeding. The development of floral organs is based on two distinct processes: cell proliferation and cell expansion, which increase the cell number and cell size, respectively. Positive and negative regulatory genes corresponding to each developmental process have been identified in *Arabidopsis thaliana*. In this study, an Arabidopsis large flower mutant, *ohbana1* (*ohb1*), was isolated from a mutant library induced by heavy-ion beam irradiation.[1–3] We characterized the flower phenotypes of *ohb1* and revealed the gene responsible for the mutant phenotype by the resequencing of the mutant genome to gain more insight on the regulatory network for floral organ size.

Flowers at stage 14, which had fully expanded petals but had not been pollinated, were fixed with a fixative solution containing 86% ethanol and 14% acetic acid. After fixation, the flowers were dissected using a stereoscopic microscope, and abaxial epidermal cells in the distal region of the petals were observed and photographed. The genomic DNA for whole-genome resequencing was isolated from the leaves of 40 M_3 generation mutants. Library construction was performed according to the method reported by Hirano *et al.*[4] The obtained reads were input into the automated mutation analysis pipeline.[5] The mutations in the mutant induced by heavy-ion beam irradiation were selected by removing pre-existent polymorphisms in the wild type (WT) and false-positive mutations.

The sepal and petal sizes in the mutant were compared to those in the WT to evaluate the phenotypic characteristics of the *ohb1* mutant; the *ohb1* mutant formed large petals and sepals. The petal area in the *ohb1* mutant was approximately 1.4 times larger than that in the WT (Fig. 1A). Furthermore, cell sizes in the petal of the *ohb1* mutant were also 1.4 times larger than those of WT (Fig. 1B). We concluded that the large petal formation in *ohb1* is mainly caused by cell-size increment because the increasing rates in whole petals and its organizing cells are almost the same in *ohb1* petals.

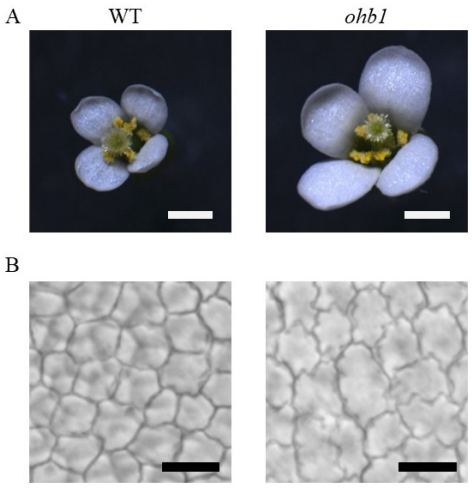

Fig. 1. Flower phenotypes of the *ohb1* mutant. Whole flower (A) and epidermal cells in the petal (B). Bars = 1 mm (A) and 20 μm (B).

In the M_3 generation, five homogenous mutations in three loci, which had been predicted to affect gene function, were detected in the mutant genome. The results of the linkage analyses and complementation test indicated that the mutated gene in AT4G04920 is responsible for the large flower phenotype. The gene in AT4G04920 encodes one mediator subunit, *MEDIATOR* (*MED*) *16*, and it has been identified as a multifunctional regulator. MED16 restricted post-mitotic cell expansion to control the final flower size in Arabidopsis, and these results agree with a previous study.[6]

Interestingly, MED16 also contributed to seed-size regulation. In double mutants crossed between *ohb1* and the representative large flower mutants, some of them formed larger and heavier seeds than each parental single mutant. Therefore, size-regulation pathways are believed to be partly different between floral organs and seeds. The *ohb* mutants derived from heavy-ion irradiation are valuable genetic resources for investigating the size-regulation pathways, and they can lead to further understanding of plant size control.

† Condensed from the article in Plants **10**, 1881 (2021)
*1 Faculty of Agriculture, University of Miyazaki
*2 Faculty of Bioscience and Biotechnology, Fukui Prefectural University
*3 RIKEN Nishina Center
*4 National Institutes for Quantum and Radiological Science and Technology

References

1) Y. Kazama *et al.*, Plant Biotechnol. **25**, 113 (2008).
2) Y. Kazama *et al.*, BMC Plant Biol. **11**, 161 (2011).
3) T. Hirano *et al.*, Mutat. Res. **735**, 19 (2012).
4) T. Hirano *et al.*, Plant J. **82**, 93 (2015).
5) K. Ishii *et al.*, Genes Genet. Syst. **91**, 229 (2016).
6) Z. Liu *et al.*, Plant Cell **31**, 1899 (2019).

$^{40}Ar^{17+}$ beam-induced mutants of the mycorrhizal mushroom *Tricholoma matsutake* defective in β-1,4 endoglucanase activity better promote the *Pinus densiflora* seedling growth in vitro than the wild-type strain†

H. Murata,[*1] S. Nakano,[*1] T. Yamanaka,[*1] T. Shimokawa,[*1] T. Abe,[*2] H. Ichida,[*2] Y. Hayashi,[*2] and K. Tahara[*1]

Unlike wood-decaying fungi, ectomycorrhizal fungi have limited plant biomass degrading enzymes, which are mostly hydrolytic enzymes.[1)] The model ectomycorrhizal fungus *Laccaria bicolor* requires its sole cellulolytic enzyme β-1,4 endoglucanase as an effector for cell-wall remodeling during the ectomycorrhizal association with *Populus tremula* × *P. alba*.[1)] Unlike *L. bicolor, Tricholoma matsutake*, which is another ectomycorrhizal fungus that produces "*matsutake*" in association with live pine trees, has many degrading enzymes such as β-1,4 endoglucanase, β-glucosidase, α-gluculonidase, xylanse and β-xylosidase.[2)] In the present study, we examined how *T. matsutake* mutants defective in β-1,4 endoglucanase activity behave in association with the natural symbiotic partner *Pinus densiflora* in vitro.

T. matsutake mutants Ar 5002 and Ar 5012 were generated by the argon-ion beam ($^{40}Ar^{17+}$, 160 MeV/nucleon) irradiation of *T. matsutake* NBRC 33136. Both mutants were defective in β-1,4 endoglucanase activity as per an agar plate assay that uses potato dextrose agar containing 0.1% azurin-crosslinked (AZCL)-hydroxyethyl (HE)-cellulose (Fig. 1). *T. matsutake* has 11 potential cellulase genes, at least one of which is predicted to encode β-1,4 endoglucanase; the rest are classified in the same carbohydrate-active enzyme database (CAZy) family based on the JGI whole genome information, which indicates a mutation could have occurred in a regulatory region.

The wild-type strain NBRC 33136 significantly promoted *P. densiflora* growth in vitro compared with the no inocula control (Fig. 2). Both *T. matsutake* mutants Ar 5002 and Ar 5012 significantly promoted *P. densiflora* growth compared to the growth achieved with the wild-type. The former confers a significantly higher above-ground plant biomass, as well as total biomass, than that with the wild-type strain, whereas the latter confers a significantly higher above- and below-ground plant biomasses, as well as the total biomass, as shown in Fig. 2. No differences in the numbers of lateral roots or mycorrhizal root tips were noted between the mutant and the wild-type strains. No significant differences in the shoot/root (S/R) biomass ratios were noted between the wild-type and mutant strains, as well. The Hartig nets, a hallmark structure of ectomycorrhizal association, was observed among seedlings associated with the wild-type and mutant strains (Fig. 3).

The data suggest that *T. matsutake* without its own β-1,4 endoglucanase activity exerts improved beneficial effects on *P. densiflora* growth in vitro. However, further clarification is required about whether the symbiotic relationship can be strengthened by such a mutated fungal trait.

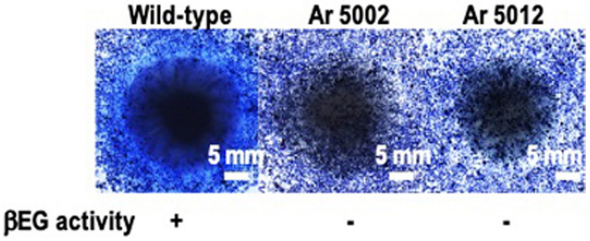

Fig. 1. β-1,4 Endoglucanase (βEG) activities of *T. matsutake*.

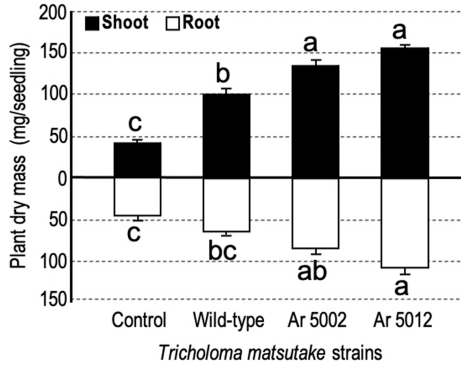

Fig. 2. *P. densiflora* seedling growth after co-culturing with *T. matsutake* strains for 140 d. Bars represent mean ±SEs. The same letters indicate treatments that should be classified as same based on the results of Tukey-Kramer tests.

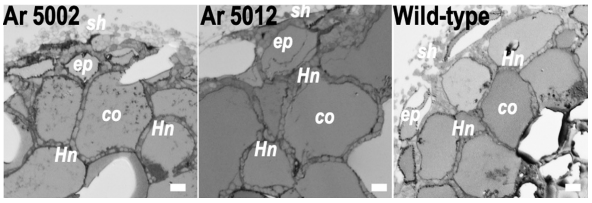

Fig. 3. Cross-section micrographs of the root tissues of *P. densiflora* seedlings associated with *T. matsutake* strains. Abbreviations: co, cortical cell; ep, epidermal cell; Hn, Hartig net; sh, mycelial sheath. *Bars*: 10 μM.

† Condensed from the article in Botany **99**, 139 (2021)

*1 Forest Research and Management Organization
*2 RIKEN Nishina Center

References
1) F. Zhang *et al.*, New Phytol. **220**, 1309 (2018).
2) T. Shimokawa *et al.*, Mycoscience **58**, 35 (2017).

Highly efficient and comprehensive identification of ethyl methanesulfonate-induced mutations in *Nicotiana tabacum* L. by whole-genome and whole-exome sequencing†

H. Ichida,[*1] H. Udagawa,[*2] T. Takeuchi,[*2] T. Abe,[*1] and Y. Takakura[*2]

Tobacco (*Nicotiana tabacum* L.) is one of the most widely cultivated non-food crops. It is a complex allotetraploid ($2n = 4x = 48$) species with a large genome of 4.5 Gb, which possesses a high repetitive element content.[1] Tobacco carries a pair of duplicated genes (referred to as homeologs) from the S- and T-genomes, and owing to this redundancy, loss-of-function mutations in any single homeolog are typically masked by the correspondent, thereby limiting the use of forward genetic phenotypic screens. Owing to its large genome size, whole-genome sequencing is not readily applicable, as it requires a large amount of sequencing reads and computational power and storage. Whole-exome sequencing (WES) is an approach to primarily sequence on genomic regions that encode proteins. Because the protein-coding sequences only considers approximately 1.3% of the tobacco genome, this technique is particularly effective in organisms with large genomes. In the present study, we developed a set of whole-exon capturing probes for tobacco and tested the set by analyzing 19 independent mutant lines produced by ethyl methanesulfonate (EMS) mutagenesis.[2,3] We also investigated the optimum conditions to detect mutations in tobacco.

We employed 19 individual EMS-treated tobacco lines, designated NtEMS-01–19, and a technical replicate of NtEMS-19, called NtEMS-19-rep2, for the sequencing analyses. A commercial target enrichment platform (SureSelect XT Custom kit, Agilent Technologies) was used to establish a whole-exon enrichment method for tobacco. The custom-designed capturing kit contained 517,835 oligonucleotide probes of 120 bases, and it was expected to capture coding sequences with a size of 50.3 Mb spanning 41,038 genes that had at least one coding sequence (CDS) defined in the target genes. After we produced the whole-exome capturing probes, a new version of the K326 reference genome sequence, Nitab-v4.5, which significantly improves coverage and contiguity, was published.[4] Therefore, we translated the target locations to the Nitab-v4.5 sequences and performed all subsequent analysis based on the new reference genome sequence.

The number of read bases varied from 11.6 to 18.9 Gb per sample, which corresponded to 165.3× to 270.8× of the total CDS length and indicated that, as expected, sufficient sequencing data were obtained. More than 98% of the reads were mapped to the reference sequences, resulting in an average read depth of 93.7× in the CDS regions that commonly existed in the new and previous reference genome assemblies. An average of 97.1% of the target CDS bases in the 19 NtEMS lines were covered by at least 30 reads. Among all the mapped read bases, approximately 75% were located on or were adjacent to the target regions, indicating that the whole-exome capturing was successfully accomplished here. In the variant calling, we used two different programs, GATK and BcfTools. Each program detected 60,884 and 50,260 mutations and resulted in a total of 61,146 non-redundant mutations. Almost all (98.8%) of the detected mutations in the 19 NtEMS lines were single-nucleotide variations, while 95.6% of them were C/G to T/A transitions, which is consistent with the known properties of EMS mutagenesis.The numbers of detected mutations varied from 1987 to 4966 in the 19 NtEMS lines. The average numbers of detected mutations in each line were 2715.7 (1987–3857) and 3511.3 (2415–4966) in 0.6% and 0.8% EMS treatments, respectively. The mutation density was largely proportional to the target CDS density in the genome, indicating that the EMS-induced mutations were sufficiently random, at least practically, despite base preferences resulting from the chemical nature of EMS mutagenesis. A computational experiment using down-sampled sequencing reads demonstrated that approximately 80% of the mutations located in the target regions could be detected with 60× sequencing reads.

At 160× of the total CDS length equivalent, a total of 20,960 out of the 35,667 genes located within the targets harbored at least one mutation in the CDS regions of the 19 NtEMS lines defined by WES. This indicates that an average of 1103 genes could be expected to have mutated within their CDS regions in the mutagenized NtEMS population that was partly analyzed in the present study. Based on the probability formula,[5] one can expect at least one mutation from 95 lines (at 95% confidence level) in the NtEMS library, for all of the 35,667 genes in the target regions.

References
1) N. Sierro *et al.*, Nat. Commun. **5**, 3833 (2014).
2) T. Tajima *et al.*, Ann. Phytopathol. Soc. Jpn. **77**, 258 (2011).
3) Y. Takakura *et al.*, Mol. Plant Pathol. **19**, 2124 (2018).
4) K. D. Edwards *et al.*, BMC Genom. **18**, 448 (2017).
5) L. Clarke, J. Carbon, Cell **9**, 91 (1976).

† Condensed from the article in Front. Plant Sci. **12**, 671598 (2021)

*1 RIKEN Nishina Center
*2 Leaf Tobacco Research Center, Japan Tobacco Inc.

Method of chromosome observation in the dioecious plant *Silene latifolia*†

T. Kobayashi,[*1] M. Takahashi,[*2] R. Nishijima,[*1] R. Sugiyama,[*3] K. Ishii,[*4] T. Abe,[*4] S. Kawano,[*2,*5] and Y. Kazama[*1,*4]

Silene latifolia is a dioecious plants, which is considered to be evolved from monoecious plants to develop heteromorphic sex chromosomes.[1)] The sizes of X and Y chromosomes are approximately 400 Mb and 570 Mb, respectively, such that they can be observed under a microscope. The architecture of these sex chromosomes has been investigated by using cytological techniques, *e.g.* fluorescence *in situ* hybridization analysis.[2)]

We previously irradiated heavy-ion beams to seeds and pollens of *S. latifolia* and obtained hermaphroditic and asexual mutants, which possessed deletions on the Y chromosome.[3)] Subsequently, a Y-chromosome map was constructed by conducting PCR-based deletion mapping. To further investigate the size of the deletions after the heavy-ion irradiation and confirm the accuracy of the deletion map, observation of chromosomes in *S. latifolia* is required. However, an efficient method for the chromosome specimen preparation has not been fully developed so far.

In many plants, root tip portions are typically used for preparing chromosome specimens because they are highly enriched in rapidly cycling cells with a steady state of growth. Synchronization of cell cycle is typically achieved by using DNA synthesis inhibitors. In *Silene latifolia*, these methods were applied to prepare the chromosome specimens. However, the timing for chromosome preparation after initiating root tip growth was not to be optimized. We hypothesized that the cell cycle was roughly synchronized during the first few days after rooting. Therefore, we investigated an appropriate incubation period after germination, during which the roots possessed many metaphase chromosomes. Moreover, we investigated variations of telocentric chromosomes by changing the duration of the ice-cold treatment (8, 16, and 32 h).

Every six hours after the germination, root lengths of thegerminating seeds were measured. The percentage of roots with a length of 2 mm that were amenable to enzyme treatment reached a maximum after 60 h of incubation starting (HAIS) at 23°C. The rough observation of metaphase cells in root tips from 48 to 60 HAIS by the Feulgen method[4)] showed a high frequency of metaphase cells during 51 to 56 HAIS. Therefore, root tip samples collected every hour from 51 to 56 HAIS were closely examined. The number of metaphase cells in the root tips reached a peak at 54 HAIS (Fig. 1).

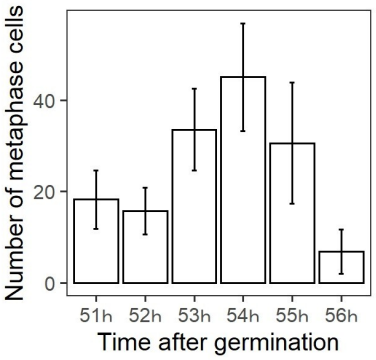

Fig. 1. Number of metaphase cells 51–56 hours after germination. Bars represent standard deviations.

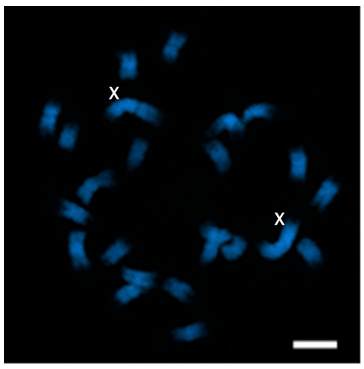

Fig. 2. Photograph of metaphase chromosomes in a female plant (Bar = 5 μm).

DNA synthesis inhibition for metaphase chromosome preparation is typically achieved by using aphidicolin. The aphidicolin treatment was initiated 24 h before 51–56 HAIS and was terminated 9 h before 51–56 HAIS. Consequently, a peak in the number of metaphase cells was observed at 54 HAIS. The mean value of the metaphase cells at 54 HAIS with aphidicolin was fourteen times higher than that at 56 HAIS without aphidicolin (Wilcoxon rank sun test, $p < 0.01$). This result indicates that DNA synthesis inhibition at the appropriate time helps increase the number of metaphase cells, which facilitates an effective chromosome observation. With this sample, *S. latifolia* chromosomes were easily observed using confocal microscopy (Fig. 2). These techniques can be applied to observe the chromosomes of heavy-ion induced partial Y-deletion mutants.

References
1) S. Matsunaga, S. Kawano, Plant Biol. **3**, 481 (2001).
2) Y. Kazama *et al.*, Genome **49**, 520 (2006).
3) Y. Kazama *et al.*, Sci. Rep. **6**, 18917 (2016).
4) R. Feulgen *et al.*, Physiol. Chem. **135**, 203 (1924).

† Condensed from the article in Cytologia **86**, 323 (2021)

*1 Department of Bioscience and Biotechnology, Fukui Prefectural University
*2 Department of Integrated Biosciences, Graduate School of Frontier Sciences, University of Tokyo
*3 Botanical Garden, Faculty of Agriculture, Tokyo University of Agriculture
*4 RIKEN Nishina Center
*5 Future Center Initiative, University of Tokyo

Producing high brix content of the sweet potato Anno-Beni by mutation induced using ion-beam irradiation

T. Hashiguchi,[*1] K. Yamane,[*1] J. Nagai,[*1] K. Fujikawa,[*1] K. Ishii,[*2] Y. Hayashi,[*2] and T. Abe[*2]

Ion-beam irradiation effectively induces plant mutations and is used for plant breeding.[1] The sweet potato cultivar Anno-Beni, which has a high sugar content, is an important and exquisite product in the Tanegashima island area. There has been a high demand for Anno-Beni with a high brix content that remains stable. The dry-matter contents and brix contents in the sweet potato are correlated.[2] Therefore, by inducing mutations through ion-beam irradiation, lines with higher dry-matter contents and higher brix contents can be selected. In a previous report, we described 31 lines selected from the population of the Anno-Beni B1 line irradiated with a C-ion-beam.[3] This report describes the results of the continued selection.

In 2017, five lines with better growth and higher dry-matter contents than those of the control were selected from 31 lines.

In 2018, the five selected lines were cultured at the shoot apex to produce 20 lines. The 20 lines were grown by vegetative propagation, and five individual plants per line were cultivated in the field. We selected four lines that grew better and had higher dry-matter contents and higher brix contents (0.8–3.2 and 2.0–2.9, respectively) than the control (Table 1).

In 2019, the four lines were grown by vegetative propagation, and 30 individual plants per line were cultivated in the field. The four lines that grew better and had higher dry-matter contents and brix contents (2.4–4.1 and 1.1–2.4, respectively) than the control (Table 1).

The four lines had 22–35% lower yield contents than the control. The shapes of the tuberous roots were spindle to cylindrical for the control and No.36-2, whereas it was long-spindle to cylindrical for No.19-1, No.19-4, and No.20-2 (Fig. 1).

Table 1. Dry-matter and brix contents of four mutant lines of sweet potato.

Line name	Dose (Gy)	Mean of dry matter ratio (%)		Mean of brix(%)		2019 Mean of yield	
		2018	2019	2018	2019	(Kg/a)	Control ratio
NO. 19-1	5	33. 6	37. 8	14. 0	14. 1	278	(78)
No. 19-4	5	36. 0	38. 6	14. 7	14. 7	271	(76)
No. 20-2	5	35. 0	39. 5	14. 4	13. 4	274	(77)
No. 36-2	15	34. 9	38. 2	13. 8	14. 1	232	(65)
Control (B1)	–	32. 8	35. 4	11. 8	12. 3	356	(100)

1) The tuberous roots of the four lines were steamed and diluted with water in a 1:1 ratio. Subsequently, their brix contents were measured.

*1 Kagoshima Prefectural Institute for Agricultural Development (KIAD)
*2 RIKEN Nishina Center

Fig. 1. Tuberous roots of the four lines and control.
1) Control (upper), No.19-1(lower left end), No.19-4 (lower left center), No.20-2 (lower right center), No.36-2 (lower right end).
2) Harvested on September 17, 2019 (planting period:132 days).

Table 2. Evaluation results of four mutant lines of sweet potato.

Line name	Dose (Gy)	Mean of sweetness		Mean of flesh color		Mean of aroma		Mean of stickiness	
		3 days later	1 month later	3 days later	1 month later	3 days later	1 month later	3 days later	1 month later
NO. 19-1	5	0. 4	0. 9	-0. 6	-0. 4	-0. 4	0. 2	-0. 7	0. 1
No. 19-4	5	0. 2	0. 5	-1. 1	0. 5	-0. 2	0. 0	-1. 0	0. 2
No. 20-2	5	0. 5	0. 4	-0. 5	-1. 0	-0. 1	0. 1	-0. 7	-0. 6
No. 36-2	15	0. 2	1. 1	-0. 5	-0. 1	0. 0	0. 3	-0. 6	0. 2
Control (B1)	–	0. 0	0. 0	0. 0	0. 0	0. 0	0. 0	0. 0	0. 0

1) The evaluation scores were in the order of -3,-2,-1, 0, 1, 2, 3 from the lowest score.
2) Mean of 13 evaluations after three days and 10 evaluations after one month.

The four lines were examined for taste survey after three days and after one month of storage (Table 2). The sweetness of the four lines was higher than that of the control after one month. The flesh color of No.19-1, No.20-2, and No.36-2 was lighter than that of the control after one month. The aroma of the four lines after storage for one month were almost equal to that of the control. The stickiness of No.19-1, No.19-4, and No.36-2 were equal to that of the control after storage for one month. The sweetness, flesh color, aroma, and stickiness tended to increase after storage for one month. By selecting the dry matter rate from ion-beam irradiated postgrowth, we were able to select lines with high brix contents and a sweet taste.

References

1) T. Abe *et al.*, Breed. Res. **16**, 67 (2014).
2) M. Ouchida, K. Ueno, Rep. Kyushu Br. Crop Sci. Soc. Jpn. **80**, 22 (2014).
3) T. Hashiguchi *et al.*, RIKEN Accel. Prog. Rep. **53**, 207 (2019).

Isolation method of marine red alga *Agardhiella subulate*

K. Tsuneizumi,[*1] M. Yamada,[*1] M. Mogamiya,[*2] Y. Sato,[*2] and T. Abe[*1]

Agardhiella subulate, a red macroalga, is commonly known as seaweed and it is consumed as aquatic food. This sea vegetable is attracting increasing attention as an emerging source of bioactive natural products.[1] Breeding new cultivars with properties such as high yield, high environmental adaptability, or high concentrations of constituents with human health benefits is desirable to enhance its value. In this study, we attempted to establish mutagenesis in *A. subulate* using an argon (Ar) ion beam as mutagen to meet future demands. First, we observed the growing point of the red algae.

The *A. subulate* were cultured with NORI SEED (Daiichi Seimo Co., Ltd.), a highly enriched culture solution. A culture medium was prepared using 80 μL of NORI SEED diluted with 300 mL of autoclaved sea water. Microplantlets were cultivated for a month in a stirred 300 mL marine flask with the culture medium. The flask was placed at 25°C under a 12 h photoperiod, with light intensity of 50 μmol photons $\cdot$ m^{-2}s^{-1} and the culture medium in the flask was replaced every week. Each microplantlet was inoculated into a well of a 12-well plate containing 2 mL of fresh culture medium.

For a morphometrical evaluation, we took photographs of growing tips of the algal thalli every day. From the comparison of the branching patterns in each image, the curved structure was observed in the same position (Fig. 1c, arrow head), whereas a difference was found in the newly elongated tissue (Fig. 1c, white bar). This result indicates that cell division and cell elongation occurred in this region and there were growing points in the tips of the algal thallus.

To develop an isolation method for the mutant line, we applied a heavy-ion-beam irradiation system to *A. subulate*. The microplantlets were replaced into 15 mL conical tubes with fresh 2 mL of culture medium at each irradiation condition. The tubes containing microplantlets were placed in the automatic sample irradiation apparatus[2] and each of them was irradiated with a heavy-ion beam. Heavy-ion-beam irradiation was performed using Ar (LET = 188 keV/μm) at 6 irradiation doses of 1, 2, 4, 8, 16, and 32 Gy generated via RIKEN RI Beam Factory.[3] Four hours after irradiation, each microplantlet was inoculated into a well of the 12-well plate containing 2 mL of fresh culture medium for each irradiation condition. The plates were placed at 25°C under a 12 h photoperiod with light intensity of 50 μmol photons $\cdot$ m^{-2}s^{-1} and the culture medium in the dishes was replaced every week. After monthly culture, the morphological mutants were selected with microscopic observation. The most front edge of the algal thallus was cut off with 5 mm length and replaced into a well of a 6-well plate containing 5 mL of fresh culture medium. Mutant lines were established by repeating these processes four times (Fig. 2a). According to the comparison between control and mutant lines, significant differences were observed in shape and growth ratio (Figs. 2b and 2c). These phenotypes were stably observed at each isolation process. These results suggest that the possibility of chimericalness in the apical meristem has been excluded. This method will be useful in the future to screen valuable mutants with human benefits.

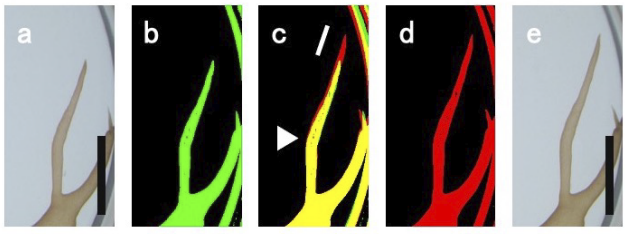

Fig. 1. Photographs of growing front edges of algal thalli. (a) Control branching pattern of red alga. (b) Binarized image of (a). (c) Merged data. The arrow head represents the bended structure of thalli. The white bar represents the difference in the length. (d) Binarized image of (e). (e) One day after branching pattern of red alga. Scale bars represent 2.5 mm.

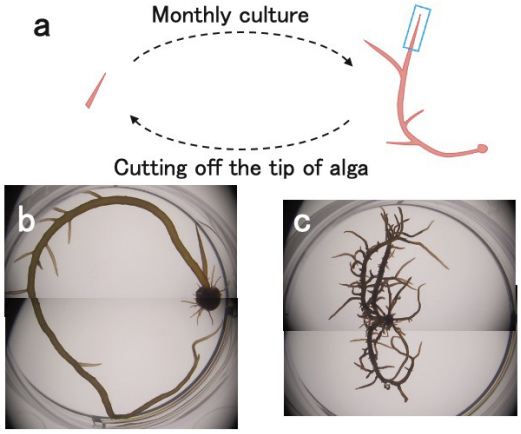

Fig. 2. Mutant isolation method and isolated mutant alga. (a) Diagram of the mutant isolation method. (b) A whole-body figure of the control alga. (c) A whole-body figure of the mutant alga.

*1 RIKEN Nishina Center
*2 Riken Food Co., Ltd.

References
1) M. Witvrouw *et al.*, Antivir. Chem. Chemother. **5**, 297 (1994).
2) H. Ryuto *et al.*, J. Biomed. Nanotechnol. **2**, 88 (2006).
3) T. Abe *et al.*, in *Plant Mutation Breeding and Biotechnology*, edited by Q. Y. Shu *et al.* (CABI, Oxfordshire, 2012), p. 99.

Survival rate of yeast cells in different storage media

Y. Nishimiya*1 and H. Ichida*1

Yeast fermentation has played a vital role in food production throughout the millennia of human history. Notable examples of its applications include alcoholic beverages, such as wine and beer, as well as breads found globally.[1] Besides its extensive industrial applications, yeast is an extensively used model organism in studies on ageing,[2] population genetics and other topics.[3] It is a highly common target organism in irradiation experiments and ensuing mutation breeding at the Beam Mutagenesis Group. It typically takes 3–5 days from the preparation of the target samples for irradiation until they arrive at the partner institution for post-experiment examination. During this time, including that for irradiation itself, yeast cells are suspended in a liquid medium, for which phosphate-buffered saline (PBS) is commonly used. However, its effect on cell viability, including the possibility of using alternative media, has not been fully elucidated. Therefore, we tested the survival of yeast cells in three different storage media over time, simulating the time frame of common irradiation experiments.

A wild-type bakers' yeast, *Saccharomyces cerevisiae* BY4743, was chosen as the model. Three storage media including ultrapure water (Milli-Q water), PBS (8.1 mM disodium hydrogen phosphate, 1.47 mM potassium dihydrogen phosphate, 2.68 mM potassium chloride, 137 mM sodium chloride) and 10 mM magnesium sulfate ($MgSO_4$) were tested.

First, a well-isolated colony was inoculated into a test tube filled with 5 mL YPD broth (10 g yeast extract, 20 g meat peptone and 20 g D-glucose, per litre). A portion of this pre-culture was transferred to 20 mL YPD in a 125-mL baffled flask. The culture was incubated at 30°C, shaking at a rate of 225 rpm.

Second, *S. cerevisiae* cells were harvested by centrifugation of 12 mL of the above culture and washed thrice with one of the three tested storage media. The cell concentration was adjusted to $OD_{600} \approx 1.0$ (equivalent to $\approx 10^7$ cells/mL) to replicate a typical irradiation target. After a given time at 4°C, 100 μL of the solution was diluted with 10 mM $MgSO_4$ and 30 μL of the diluted solution was spread on five YPD plates.

Finally, after approximately two days of incubation at 30°C, we recorded the number of colonies in each plate. The survival rate was calculated based on the mean colony count of three plates, eliminating the two plates with maximum and minimum colony counts, respectively.

We repeated the above experiment thrice. The most representative result from the three trials is shown here.

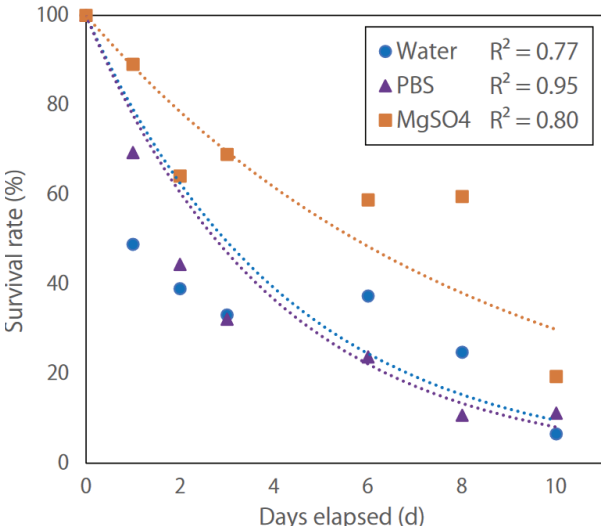

Fig. 1. Survival rate of BY4743 expressed relative to Day 0 control value set as 100%.

Figure 1 shows the survival rate of *S. cerevisiae* over ten days, in which the dotted lines represent the exponential regression models applied to the data of the three tested storage media.

For all of them, the coefficients of determination, R^2, between the days elapsed and the survival rate, are greater than 0.7. Storage in PBS and water resulted in similar trends wherein approximately 40% cells die after only two days. In contrast, 10 mM $MgSO_4$ allows for a relatively higher rate at which approximately a half of the viable cells survives for six days.

The above results show that the viability of the yeast cells significantly differs between the tested storage media. Despite the prominent use of PBS as a storage medium, our results indicate that the survival rate of the yeast cells therein is similar to that in water and hence, PBS is a non-ideal medium for long-term storage. In contrast, based on the higher survival rate, 10 mM $MgSO_4$ is more recommendable for its use as a yeast storage medium.

References

1) S. Maicas, Microorganisms **8**, 1142 (2020).
2) A. D. Lippuner, T. Julou, Y. Barral, FEMS Microbiol. Rev. **38**, 300 (2014).
3) C. Zeyl, Yeast **16**, 773 (2000).

*1 RIKEN Nishina Center

Effect of irradiation ions and doses on the survival rate of yeast

N. Lei,[*1] T. Abe,[*1] and H. Ichida[*1]

Yeast has been playing an important role in many human activities, such as winemaking, baking, and brewing for a long period.[1] The budding yeast, *Saccharomyces cerevisiae*, has been considered as the most fundamental eukaryotic model organism. Its small genome size (around 12 Mb), fast growth character, and DNA repair system that is similar to that of plants and animals make it a useful model for gene function and mutation analyses.[2,3]

Heavy ion beams cause mutations in the genome, such as deletions, insertions, and base substitutions. Therefore, it has been used as a physical mutagen and to develop new cultivars in the last two decades. Carbon ions have been used frequently because of the high mutation rates and long penetration range, and heavier ions, such as argon and iron, are more suitable for microbial mutagenesis, as they induce larger deletions and insertions, and are more stable than base substitutions.[4]

In the present study, we investigated the dose-survival relationship of a diploid baker's yeast strain Hi1060 (*MATa/α his3Δ1 leu2Δ0ura3Δ0*). It is genetically equivalent to BY4743 and is established by a cross between BY4741 and BY4742; It is more than three times the size of single-colony isolations on a selective medium. The strain and its parents are all derivatives of the widely used and genome-sequenced laboratory strain S288C. This strain is fully functional for DNA repair by homologous recombination and non-homologous end-joining.

For heavy-ion beam irradiations, Hi1060 was grown in a liquid YPD medium, harvested by centrifugation at 3000 × g, and washed three times with 10 mM $MgSO_4$. The cell concentration was adjusted to 1 OD_{600} unit per mL, which is equivalent ∼10^7 cells per mL, with 10 mM $MgSO_4$, and was kept at 4°C before and after irradiation. We irradiated $^{12}C^{6+}$ (135 MeV/nucleon, LET: 23 keV/μm; 0–1000 Gy), $^{40}Ar^{18+}$ (160 MeV/nucleon, 189 keV/μm; 0–800 Gy), and $^{56}Fe^{24+}$ (90 MeV/nucleon, 647 keV/μm; 0–800 Gy). After irradiation, the cells were diluted to different concentrations and spread on YPD plates, and the survival rates were calculated as follows:

Survival rate (%) = num. of the colonies in each dose/non-irradiated control × 100

The determined survival rates and their fitting results by exponential functions are shown in Fig. 1. The results showed that carbon-, argon- and iron-ion irradiations all decreased the survived cell ratio in a dose-dependent manner. The survival curves were well represented by exponential functions with determination coefficients (R^2) of 0.9793, 0.7691, and 0.9509 in carbon, argon, and iron ions, respectively. Ar showed unexpectedly higher and lower survival rates compared with the other two ions. We are interested in further investigating Ar irradiations soon.

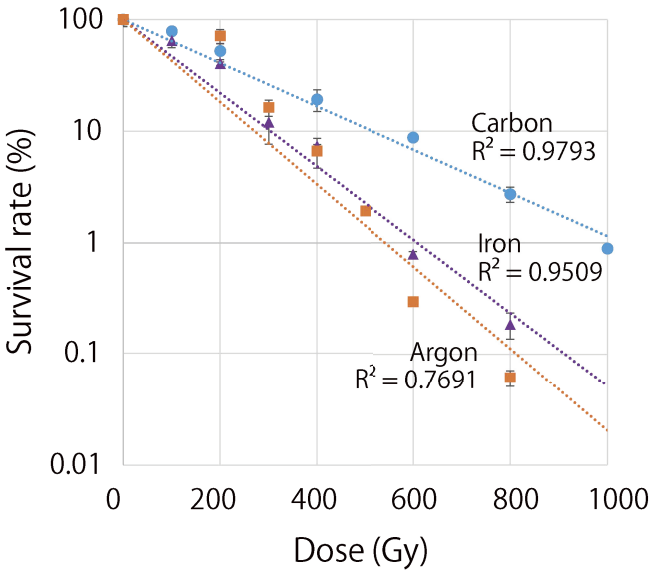

Fig. 1. Dose-survival responses of *S. cerevisiae* Hi1060 (equivalent to BY4743) cells after irradiation by carbon, argon, and iron ions with different doses. The error bars represent standard deviation in technical replicates.

The lethal effects were more obvious in heavier argon and iron ions than the lighter carbon ions. This is consistent with the previous observations that the relative biological effect of a radiation is higher in heavier ions than the lighter ones. This may reflect that heavier ions, which have higher LETs, induce more deleterious types of mutations to the genome. The doses for 10% survival (D_{10}) were 600 Gy for carbon- and 400 Gy for argon- and iron-ions, respectively. These D_{10} values were in a comparable range to a previous yeast breeding project, where 400 Gy irradiations with carbon and iron ions were used to select high aromatic compound-producing sake yeasts.[5] Currently, we have been preparing to perform whole-genome sequencing of these irradiated yeast cells. This will quantitatively describe the mutagenic effect of different ions on yeast genomes. At the same time, it would help to understand the relationship between irradiation conditions, survival rate, and the resulting genomic mutations in a base-pair resolution in a genome-wide manner.

*1 RIKEN Nishina Center

References
1) R. K. Mortimer, Genome Res. **10**, 403 (2000).
2) M. J. Harsch *et al.*, FEMS Yeast Res. **10**, 72 (2009).
3) H. Mewes *et al.*, Nature **387**, 7 (1997).
4) H. Ichida *et al.*, Mutat. Res. **639**, 101 (2008).
5) M. Yokobori *et al.*, RIKEN Accel. Prog. Rep. **45**, xxiii (2011).

Recruitment of Rad51 onto chromatin is suppressed by high dose heavy-ion irradiation in mammalian cells

M. Izumi*1 and T. Abe*1

Among the DNA damages caused by an ionizing radiation, DNA double strand breaks (DSBs) are the most lethal because accumulation of misrepaired or unrepaired DSBs can lead to a loss of genetic information and cell death. Mammalian cells have four pathways to repair DSBs: canonical non-homologous end joining (NHEJ), homologous recombination (HR), alternative NHEJ (alt-NHEJ), and single-strand annealing (SSA). Recently, DNA repair pathways are considered as targets for cancer therapy, because their inhibitors increase the efficacy of radiotherapy. It is also important to know whether error-prone pathways such as SSA and alt-NHEJ are involved in DSB repair, to estimate the risk of secondary carcinogenesis in radiotherapy.

After exposure to low-linear energy transfer (LET) radiation such as X-ray, NHEJ is the dominant repair pathway throughout the cell cycle in mammalian cells, whereas HR can only repair DSBs in the late S/G2 phase. Additionally, alt-NHEJ or SSA is effective when both NHEJ and HR are impaired, and it contributes to genome rearrangements and oncogenic transformations. Previous studies have suggested that the end-resection of DSBs is stimulated after heavy-ion irradiation throughout the cell cycle,[1,2] which can promote HR, SSA, or alt-NHEJ. However, the repair mechanism after heavy-ion irradiation has not been fully understood.

Our previous study using mammalian cells and specific inhibitors against NHEJ or HR suggested that NHEJ is the major repair pathway after 2 Gy heavy-ion irradiation.[3] We also showed that HR is favored after heavy-ion irradiation in the G2-phase; however, the DSB repair by HR is less efficiently than that after X-ray irradiation.[4]

Recent studies revealed that the number of DSBs is an additional key parameter of pathway selection because several repair proteins limit HR at high doses in mammalian cells.[5,6] In this study, we examined the amount of Rad51 on chromatin after irradiation, to investigate the effect of irradiation dose on the repair pathway selection. Rad51 is an essential core component of HR and recruited around DSBs after irradiation. Exponentially growing HeLa cells were irradiated with argon ions (LET = 300 keV/μm) of different doses (0.5–15 Gy), and chromatin fractions were obtained and subjected to immunoblot analysis (Fig. 1(A)). The amount of Rad51 in the chromatin fraction increased up to 5 Gy in a dose-dependent manner (Fig. 1(B)). However, the amount of Rad51 decreased following 15 Gy irradiation. We performed the same experiment using a carbon-ion beam (LET = 80 keV/μm), which yielded similar results (data not shown). These results suggest that HR is suppressed after high dose irradiation (∼15 Gy) of high-LET radiations (80–300 keV/μm). In contrast, the amount of chromatin-bound Rad51 increased up to 15 Gy and decreased at 30 Gy after X-ray irradiation (data not shown).

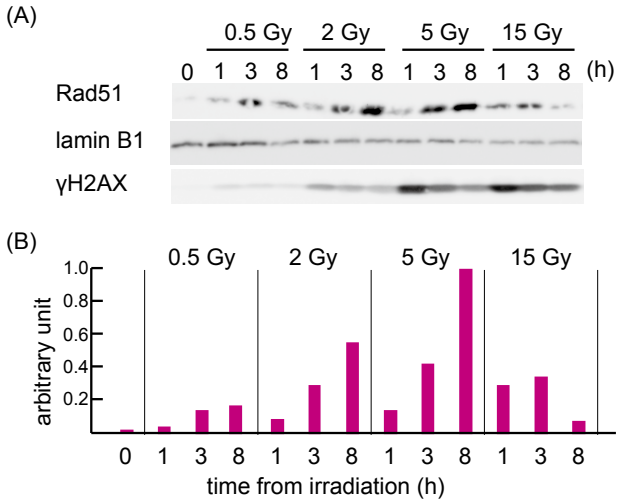

Fig. 1. Immunoblot analysis of chromatin-bound Rad51 after heavy-ion irradiation. (A) HeLa cells were irradiated with indicated doses of Ar ions, and 0.1% Triton-insoluble fractions (chromatin franctions) were prepared at indicated time points and subjected to immunoblot analysis. Phosphorylated histone H2AX (γH2AX) and lamin B1 were detected as an indicator of DSB and a loading control, respectively. (B) The relative intensity of Rad51 band was measured using luminoimage analyzer and normalized against the amount of lamin B1.

We previously reported that trichostatin A (TSA), a histone deacetylase inhibitor, enhanced radiosensitivity at low doses, whereas TSA suppressed it at high doses of heavy-ion irradiation by an unknown mechanism.[7] This finding also suggests that DNA damage response induced by heavy-ion irradiation depends on the dose. Currently, we are investigating the localization of several repair proteins involved in NHEJ and SSA after irradiation of different doses.

*1 RIKEN Nishina Center

References
1) H. Yajima *et al.*, DNA Repair **12**, 936 (2013).
2) N. B. Averbeck *et al.*, Cell Cycle **13**, 2509 (2014).
3) M. Izumi, T. Abe, RIKEN Accel. Prog. Rep. **53**, 24 (2020).
4) M. Izumi, T. Abe, RIKEN Accel. Prog. Rep. **54**, 33 (2021).
5) F. Ochs *et al.*, Nat. Str. Mol. Biol. **23**, 714 (2016).
6) E. Mladenov *et al.*, Nucl. Acid. Res. **48**, 1905 (2020).
7) M. Izumi, T. Abe, RIKEN Accel. Prog. Rep. **48**, 301 (2015).

IV. OPERATION RECORDS

Program advisory committee meetings for nuclear physics and for materials and life experiments

K. Yoneda,[*1] K. Ishida,[*1] H. Yamazaki,[*1] N. Imai,[*2] Y. X. Watanabe,[*3] K. Yako,[*2] Y. Hirayama,[*3] and H. Ueno[*1]

The Program Advisory Committees (PAC) are in charge of reviewing the scientific proposals submitted for the use of the accelerator facility in the RIKEN Nishina Center (RNC). Two PAC meetings were held in fiscal year 2021; one for proposals in the field of nuclear physics (NP-PAC), and one for proposals in the field of materials and life sciences (ML-PAC).

NP-PAC

The 22nd NP-PAC meeting was held from December 1 to December 3, 2021,[1)] with the attendance of 16 PAC members. As oversea travels were difficult due to COVID-19, the meeting was held online via Zoom. Before this NP-PAC meeting, seven PAC members were replaced. The new members are: S. Grevy (CENBG), M. Dasgupta (The Australian National University), J. Dilling (Oak Ridge National Laboratory), M. Gorska (GSI), T. Kawabata (Osaka University), M. Matsuo (Niigata University), R. Zegers (Michigan State University). M. J. G. Borge from CSIC, Madrid, had newly taken on the role of chairperson of the meeting. 31 proposals were reviewed, and 1 proposal and 13 proposals were approved as grade S and A, respectively. The outcome of the NP-PAC meeting is summarized in Table 1.

Table 1. Summary of the outcome of the 22nd NP-PAC meeting. The proposals ranked as S and A are treated as "approved" proposals.

22nd NP-PAC (December 1–3, 2021)	requested proposals (days)	approved proposals (days)
GARIS	3 (39)	1 (25)
CRIB (AVF)	2 (19)	0 (0)
RRC	1 (8)	1 (8)
KISS	1 (5)	1 (5)
BigRIPS/ZD	12 (97.5)	7 (55.5, inc. 11 of "S")
SHARAQ/OEDO	1 (9.5)	1 (2)
Rare RI Ring	2 (36)	0 (0)
SAMURAI	10 (92)	3 (22.5)
LOI	1 (-)	- (-)
Total	31 (306)	14 (93)

The members of 22nd NP-PAC are as follows: M. J. G. Borge (CSIC, Madrid, the chair), N. Aoi (RCNP, Osaka University), R. Charity (Washington University in St. Louis), G. Martinez-Pinedo (TU Darmstadt/GSI), I. Moore (University of Jyvaskyla), T. Saito (RIKEN), P. J. Woods (University of Edingurgh), A. Vitturi (University of Padova), X. Zhou (Chinese Academy of Science), J. Dilling (Oak Ridge National Laboratory), M. Dasgupta (The Australian National University), M. Gorska (GSI), S. Grevy (CENBG), T. Kawabata (Osaka University), M. Matsuo (Niigata University), R. Zegers (Michigan State University).

ML-PAC The 21st ML-PAC meeting was held via email review, from December 9, 2021 to January 4, 2022.[2)] At that time there was no call for proposals for RIKEN-RAL due to the planned long shutdown of ISIS. Three proposals for the RIBF facility were reviewed, and two proposals were approved as grade A. The outcome of this meeting is summarized in Table 2.

Table 2. Summary of the outcome of the 21st ML-PAC meetings. The RIBF proposals ranked as A are treated as "approved" proposals.

21st ML-PAC (December 2021–January 2022)	requested proposals (days)	approved proposals (days)
RAL	no call	-
RIBF	3 (10)	2 (7)

The members of the 21st ML-PAC are as follows: A. Hillier (ISIS, RAL, the chair), Y. Kobayashi (The University of Electro-Communications), Y. Miyazawa (Yamagata University), T. Takayanagi (Saitama University), and Z. Qin (Chinese Academy of Sciences).

References

1) https://www.nishina.riken.jp/RIBF/NP-PAC/index.html.
2) https://www.nishina.riken.jp/RIBF/ML-PAC/index.html.

[*1] RIKEN Nishina Center
[*2] Center for Nuclear Study, University of Tokyo
[*3] Wako Nulcear Science Center, Institute of Particle and Nuclear Studies, KEK

Electric power consumption of RIKEN Nishina Center in 2021

M. Kidera,[*1] T. Maie,[*1] S. Watanabe,[*1] E. Ikezawa,[*1] and O. Kamigaito[*1]

An electricity consumption of RIKEN Nishina Center (RNC) for each month in 2021 compared to 2019 and 2020 is shown in Fig. 1. The reason for the large increase in power consumption from April to June compared to last year is mainly due to a fact that no RI Beam Factory (RIBF) experiments were conducted last year due to the pandemic and failure of the RRC cavities.

In 2021, a total annual power consumption of the RNC was 63,746 MWh, an increase of 13% compared to 2020. The increase in the total annual power consumption is mainly due to the RIBF experiment in the previous period, as mentioned earlier. The total power of the RNC reached a maximum of 17.5 MW on November 18 when the RIBF experiment with a uranium (^{238}U) beam was being tuned.

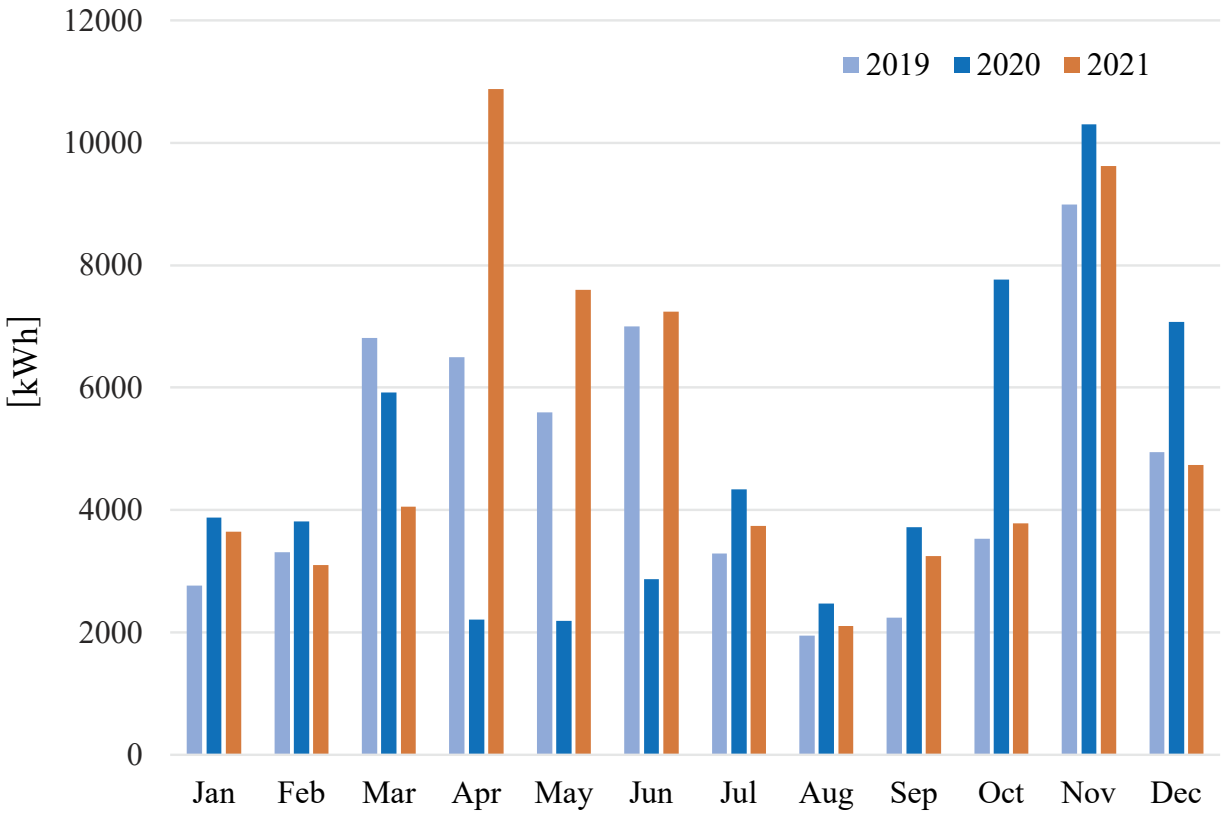

Fig. 1. Electricity consumption of RNC for each month in 2021 compared to 2019 and 2020.

[*1] RIKEN Nishina Center

Operation report on ring cyclotrons in the RIBF accelerator complex

T. Nakamura,[*1] K. Ozeki,[*2] T. Dantsuka,[*2] M. Fujimaki,[*2] T. Fujinawa,[*2] N. Fukunishi,[*2] S. Fukuzawa,[*1] M. Hamanaka,[*1] H. Hasebe,[*2] Y. Higurashi,[*2] E. Ikezawa,[*2] H. Imao,[*2] S. Ishikawa,[*1] O. Kamigaito,[*2] Y. Kanai,[*2] M. Kidera,[*2] K. Kobayashi,[*1] M. Komiyama,[*2] R. Koyama,[*1] K. Kumagai,[*2] T. Maie,[*2] T. Nagatomo,[*2] T. Nakagawa,[*2] M. Nakamura,[*2] M. Nishida,[*1] M. Nishimura,[*1] J. Ohnishi,[*2] H. Okuno,[*2] N. Sakamoto,[*2] J. Shibata,[*1] K. Suda,[*2] N. Tsukiori,[*1] A. Uchiyama,[*2] S. Watanabe,[*2] T. Watanabe,[*2] Y. Watanabe,[*2] K. Yadomi,[*1] K. Yamada,[*2] and H. Yamasawa[*2]

This paper presents an operation report on the ring cyclotrons in the RIBF accelerator complex from January to December 2021. Table 1 presents a summary of the beams accelerated by these cyclotrons. Availability can be defined as the ratio of the actual beam service time to the scheduled beam service time, which is an index of stable operation of accelerators. When calculating each availability for the beam service times completed earlier than scheduled, the scheduled times were identified with the actual times. Further, multiple experiments performed with identical beams were treated as one and presented in a row. The total actual beam service time was 2198.3 h. The ratio of beam service time between the experiments conducted in the old (RARF) and new (RIBF) facilities was 32 : 68.

In the RARF, the actual beam service time was 702.5 h, with an availability of 113.8%.

In the RIBF, five beam services were conducted; the actual beam service time was 1495.8 h with an availability of 98.3%. Accelerations in the light-ion mode were conducted using the AVF as an injector for the first time in three years. Three types of beams of ^{2}H, ^{4}He, and ^{12}C were supplied. A ^{4}He beam with an energy of 200 MeV/nucleon was delivered for the first time; the ^{12}C beam was delivered for the first time as well. Despite the difficulties in transporting the first beams (new ions or energies), higher transport efficiencies were achieved from the RRC to SRC in comparison to those of similar light ions or energies, and high-quality single-turn-extracted beams could be supplied. In ^{4}He beam supply, we recorded the highest ever beam intensity of 1000 particle nA. In the final phase of the experiment, the apparatus malfunctioned, which can be attributed to radiation. The availability of ^{2}H and ^{4}He was 100.7% and 104.7%, respectively, because the beam services could be started ahead of schedule owing to smooth beam tuning. The beam service of ^{12}C was interrupted for approximately 26 h owing to issues in the SRC helium refrigerator. However, it exhibited an availability of 102.3% because the beam service began ahead of schedule and the beam service time was extended by 8 h.

The beam services of ^{238}U 345 MeV/nucleon were conducted twice. In the first U-beam service held in April 2021, discharges were frequently observed in SRC resonator 3 (SRC-RES3). An internal inspection was performed on SRC-RES3 and the burned-out RF contact fingers were replaced. In addition, the steering electromagnets installed at the exit of fRC (fRC-SH3, SV3) tripped owing to thermal anomaly. In the aftermath, a beam changed its trajectory to hit a bellow upstream a gas stripper installed in the E1 hall, thus leading to vacuum leakage; the availability was 94.2%. In the second U-beam service held in November 2021, no serious issues were observed in the accelerators. However, the beam supply was suspended earlier than scheduled owing to issues in the compressor of the BigRIPS helium refrigerator; the availability was 98.9%.

The total availability in the RARF and RIBF reached a record high of 102.8%.

Table 1. Summary of accelerated beams in 2021.

	Beam particle	Energy (MeV/nucleon)	Acceleration mode	Beam course	Beam intensity (particle nA)		Beam service time (h)		Availability (%)
					Requested	Actual	Scheduled	Actual	
RARF	^{12}C	135	AVF-RRC	E5B (Biology)	2	541.7	33.0	13.0	100.0
				E5A (Industry)	2	183.3	10.0	10.9	109.2
	^{14}N	100		E3B (RI Production)	200	320.0	6.0	6.5	108.3
	^{20}Ne	135		E5B (Biology)	2	120.0	3.0	1.9	100.0
	^{40}Ar	95		E5A (Industry)	1	82.4	48.0	80.6	167.8
	^{56}Fe	90		E5B (Biology)	2	9.2	9.0	2.8	100.0
	^{84}Kr	70		E5A (Industry)	2	10.5	161.0	212.4	131.9
				E3A (JAXA)	2	8.1	18.0	18.5	103.0
	^{51}V	6	RILAC2-RRC	E6 (KEK/MRTOF)	2000	3576.9	126.0	125.8	99.8
	^{86}Kr	10.75		E2B (KEK/KISS)	500	555.6	48.0	47.4	98.8
	^{136}Xe	10.75		E2B (KEK/KISS)	100	140.0	120.0	120.4	100.3
				E3A (JAXA)	1	100.0	18.0	17.3	100.0
	^{238}U	10.75		E5A (Material)	2	214.3	48.0	37.4	100.0
	^{40}Ar	160	AVF-RRC-IRC	E5B (Biology)	2	30.3	18.0	7.7	100.0
RIBF	^{2}H	250	AVF-RRC-SRC	BigRIPS	200	220.0	180.0	181.3	100.7
	^{4}He	250		BigRIPS/SHARAQ	> 500	1000.0	197.0	206.2	104.7
	^{12}C	200		BigRIPS/ZDS	500	500.0	192.0	196.5	102.3
	^{238}U (1st)	345	RILAC2-RRC-fRC-IRC-SRC	BigRIPS/ZDS/Rare RI Ring	70	89.5	648.0	610.6	94.2
	^{238}U (2nd)			BigRIPS/ZDS/Rare RI Ring/PALIS	120	73.0	304.5	301.2	98.9
						Total	2187.5	2198.3	102.8

*1 SHI Accelerator Service Ltd.
*2 RIKEN Nishina Center

RILAC operation

T. Ohki,[*1] M. Fujimaki,[*2] N. Fukunishi,[*2] H. Hasebe,[*2] Y. Higurashi,[*2] E. Ikezawa,[*2] H. Imao,[*2] O. Kamigaito,[*2] K. Kaneko,[*1] M. Kidera,[*2] M. Komiyama,[*2] R. Koyama,[*1] K. Kumagai,[*2] T. Maie,[*2] T. Nagatomo,[*2] T. Nakagawa,[*2] T. Nishi,[*2] J. Ohnishi,[*2] H. Okuno,[*2] K. Oyamada,[*1] K. Ozeki,[*2] N. Sakamoto,[*2] K. Suda,[*2] M. Tamura,[*1] A. Uchiyama,[*2] S. Watanabe,[*2] T. Watanabe,[*2] Y. Watanabe,[*2] K. Yamada,[*2] H. Yamauchi,[*1] and A. Yusa[*1]

Originally, beam service was scheduled to start in January 2021. However, because of a failure owing to the aging of radio-frequency (RF) tanks of RILAC, repair of the breakdown and preventive measures were performed from January to March. In April, the external vacuum windows and the vacuum ports were added to the RF transmission line to energize the superconducting (SC) cavities, which were not used because of a vacuum leakage through the coupler ceramic windows. It operated well and ten SC-cavities became available. A user beam service started in May.

Some statistics regarding the RILAC operation from January 1 to December 31, 2021 are provided in Table 1.

Table 1. Statistics of RILAC operation from January 1 to December 31, 2021.

Operation time of RILAC	3294.0 h
Mechanical problems	185.4 h
Standalone RILAC	2141.5 h
Injection into RRC	0.0 h
Total beam service time of RILAC	2141.5 h

We performed the following maintenance works during the reporting period.

(1) Replacement of the leaky flowmeters for the cooling channels of the drift-tube quadrupole magnets in RILAC tanks and the quadrupole singlet magnets of the beam-transport-line.
(2) Rearrangement of the quadrupole magnets of the injection transport line to the tank #1 to enhance the transmission efficiency from the exit of the RFQ to the exit of tank #1.
(3) Renewal of the control and driving system of the coarse frequency tuners of RILAC tank #3 and tank #4.
(4) Removal of the fine frequency tuner of RILAC tank #2 because of the vacuum problem.
(5) Development of the beam interlock system (BIS) against the failure of the magnet power supplies.
(6) Construction of the quick BIS which instantly chops the beam when there is an error of the RF control system.
(7) Improvement of the rough evacuation ducts of the RILAC tanks by adding an automatic evacuation system.
(8) Introduction of automatic operation system of the cooling fans of the cooling towers for the ion source and the RFQ.
(9) Introduction of the automatic operation system of the cooling fans of the cooling towers for SRILAC and RILAC tanks with a function of alternating operation control.
(10) Renewal of the GPIB control system of the magnet power supplies.
(11) Feasibility test of the gyrotron for newly constructed SC-ECRIS (R28G-K).
(12) Installation of the external vacuum windows and the vacuum ports to the RF transmission lines of the SC-cavities.

We encountered several machine troubles during the reporting beam service period, which are listed as follows.

(1) Significant amount of coolant leakage from the drift-tubes of the RILAC tanks.
(2) RF power shortage of the RF power source for RILAC tank #1 due to the aging of a power tetrode.
(3) RF power shortage of the 1st-stage RF amplifier for the RILAC tank #6.
(4) Abnormal RF field error caused by the malfunctioning of the 1st-stage RF amplifier.
(5) Leakage of the cooling water from the final stage amplifier for RILAC tank #4.
(6) Burn out of the RF contacts for the shorting plate of the RFQ cavity due to a lack of cooling water.
(7) Leakage of the cooling water from the cooling pipe of the RFQ cavity.
(8) Leakage of the cooling water from the cooling pipe adopted to the end drift-tube of the tank A1.
(9) Malfunction of the power source for the solenoid coil (SoL11ab).
(10) Vacuum leakage from the bellows of the drive shaft of a mesh-beam-attenuator.
(11) Serious damage of the water pumps for the cooling system of the SRILAC RF amplifiers.

All the troubles were successfully fixed, and beam service was recovered instantly. The license of radiation safety to use heavy-ion beams with an intensity of 10 particle μA was updated after an inspection by the Secretariat of the Nuclear Regulation Authority.

[*1] SHI Accelerator Service Ltd.
[*2] RIKEN Nishina Center

Operation report on the RIKEN AVF cyclotron for 2021

S. Fukuzawa,[*1] K. Suda,[*2] M. Fujimaki,[*2] N. Fukunishi,[*2] A. Goto,[*2] M. Hamanaka,[*1] H. Hasebe,[*2] Y. Higurashi,[*2] E. Ikezawa,[*2] H. Imao,[*2] S. Ishikawa,[*1] K. Kamakura,[*3] O. Kamigaito,[*2] M. Kase,[*2] M. Kidera,[*2] K. Kobayashi,[*1] M. Komiyama,[*2] Y. Kotaka,[*3] R. Koyama,[*1] K. Kumagai,[*2] T. Maie,[*2] T. Nagatomo,[*2] T. Nakagawa,[*2] T. Nakamura,[*1] M. Nishida,[*1] M. Nishimura,[*1] J. Ohnishi,[*2] H. Okuno,[*2] K. Ozeki,[*2] N. Sakamoto,[*2] J. Shibata,[*1] N. Tsukiori,[*1] A. Uchiyama,[*2] S. Watanabe,[*2] T. Watanabe,[*2] Y. Watanabe,[*2] K. Yadomi,[*1] and K. Yamada[*2]

The annual report on the operation of the RIKEN AVF cyclotron (hereafter denoted as AVF) for the period January–December 2021 is presented. The beams accelerated using AVF in the period are listed in Table 1, where beam currents are the maximum values measured by the Faraday cup FC-C01 at the exit of AVF. The operation statistics are summarized in Table 2. The operation time for stand-alone operation was increased to 2100 h from 1520 h, which was reduced because of the COVID-19 outbreak in 2020. Moreover, the operation time for injection to RRC was also increased to 1816 h from 1182 h because the acceleration in the AVF-RRC-SRC mode was performed for the first time in three years from May to June, and ^{2}H, ^{4}He, and ^{12}C beams were supplied to experiments for 28 days.

To supply high-quality beams required for the experiments and to reduce beam losses in two cyclotrons (RRC and SRC) downstream of AVF, AVF was tuned to extract single turn beams so that components of different turns were minimized in the extracted beams. The minimum mixing rate for ^{2}H beam was 2.3% ± 1.3%.

In the stand-alone operation which supplied $^{7}Li^{3+}$ at 8.3 MeV/nucleon, the highest beam current of 5670 particle nA was achieved at FC-C01, which was increased by 2.4 times compared with that recorded at a slightly different energy of 8.6 MeV/nucleon in an acceleration test performed in 2011. The increase was because of a high beam current of 70000 particle nA extracted from the Hyper ECR ion source owing to a modification of an extraction electrode, as well as a research for supporting gases.

A main trouble occurred at each compensator for two Dees, which was used to tune a resonant frequency by changing the capacitance. When compensator #2 was rotated, a vacuum was leaked through a driving shaft, so that a vacuum degree of the main chamber deteriorated from 10^{-5} Pa to 10^{-3} Pa. In the repair process, the other leakage was found from compensator #1. The vacuum was recovered by replacing the X-rings.

As a recent improvement, we started monitoring temperatures at the tips of septum electrodes for the electrostatic deflector using a pair of thermocouples. The monitor signals are fed into the beam interlock system (AVF-BIS), so that beams are stopped automatically by a chopper and a Faraday cup, which are located before injection to AVF, if an increase of the temperature caused by beam loss exceeds a certain value. Currently, the preset value is 45°C.

Table 1. AVF beam list in 2021.

Particle	Energy [MeV/nucleon]	Acceleration Mode	Experimental Course	Beam Current at C01 [particle nA]
$^{1}H^{+}$	19	AVF	E7V/RI production	10000
	30		C03/RI production	10000
$^{2}H^{+}$	4.93	→RRC→SRC	BigRIPS	7000
	12	AVF	C03/RI production	19800
	15		C03/RI production	13000
$^{4}He^{2+}$	4.17	→RRC→SRC	BigRIPS	1670
	6.5	AVF	E7B/Student	6000
	7.25		C03/RI production	25000
			E7B/RI Production	
	12.5		C03/RI production	3850
$^{7}Li^{2+}$	6		C03/RI production	8000
$^{7}Li^{3+}$	8.3		E7A/CRIB	5670
$^{12}C^{4+}$	4.93	→RRC→SRC	BigRIPS	1130
	7	→RRC	E5B/Biology	880
			E5A/Industry	
$^{14}N^{5+}$	5.54		E3B/Industry	450
$^{16}O^{6+}$	6.8	AVF	E7A/CNS	4080
$^{18}O^{6+}$	7		E7V/CNS	4580
$^{20}Ne^{7+}$	7	→RRC	E5B/Biology	540
$^{40}Ar^{11+}$	3.8	→RRC→IRC	E5B/Biology	390
	5.2	→RRC	E5A/Industry	520
$^{56}Fe^{15+}$	5.01		E5B/Biology	110
$^{84}Kr^{20+}$	3.97		E5A/Industry	230

Table 2. Comparison of AVF operation statistics with that in the previous years.

AVF stand-alone operation	Year 2019	2020	2021
Tuning of AVF [h]	1314	744	1149
Trouble of AVF [h]	0	1	5
C01 MS [h]	0	12	35
C03 Exp [h]	873	631	672
E7V Exp [h]	36	18	95
E7A Exp [h]	790	12	48
E7B Exp [h]	153	101	96
Sub total [h]	3166	1519	2100
AVF operation as injector of RRC	Year 2019	2020	2021
Tuning of AVF [h]	118	178	214
Trouble of AVF [h]	0	5	1
RRC-Exp (-IRC-Exp) [h]	320	999	834
RRC-SRC-Exp [h]	0	0	767
Sub total [h]	438	1182	1816
Total [h]	3604	2702	3916

*1 SHI Accelerator Service Ltd.
*2 RIKEN Nishina Center
*3 Center for Nuclear Study, University of Tokyo

Present status of liquid-helium supply and recovery system

T. Dantsuka,[*1] H. Okuno,[*1] M. Nakamura,[*1] S. Tsuruma,[*1] M. Takahashi,[*1] M. Kuroiwa,[*1] M. Ohshima,[*2] H. Shiraki,[*2] H. Hirai,[*2] K. Kimura,[*2] S. Okada,[*2] A. Mikami,[*2] M. Nagano,[*2] H. Shiba,[*2] and H. Hazama[*2]

A liquid-helium supply and recovery system,[1)] which can produce liquid helium at a liquefaction rate of 200 L/h from pure helium gas, has been under stable operation since the beginning of April 2001. However, because operation failures due to deterioration over time have increased recently, the liquefier was duplicated in 2017. The new liquefier can produce liquid helium at a liquefaction rate of 220 L/h from pure helium gas. Although the older helium liquefier has been failing since the summer of 2018, the new helium liquefier provides a constant supply of liquid helium. The older helium liquefier was repaired in February 2020.

The volumes of liquid helium supplied each year from 2001 to 2020 are illustrated in Fig. 1. From 2001 to 2013, there was a gradual increase in the supplied volume, with two decrements in 2009 and 2011. In 2014, the supplied volume decreased owing to a system malfunction. However, in 2015, it returned to its original value. In 2016, the supplied volume decreased, whereas it increased slightly in 2017 and significantly in 2018. In 2019, approximately 140,000 L liquid helium was supplied despite the high price of helium gas. In 2020, a supply volume decreases of approximately 15,000 L was caused by the influence of the new coronavirus.

However, the purity of helium gas recovered from the laboratories has gradually deteriorated. At present, the impurity concentration in the recovered gas is approximately 1700 ppm, which affects the liquefaction process and makes continuous operation difficult. Therefore, improving the purity of the recovered helium gas is necessary.

Furthermore, the volume of helium gas recovered from each building in the Wako campus as well as the volume transported to the liquid-helium supply and recovery system were measured. The recovery efficiency was calculated as the ratio of the amount of recovered helium gas to the amount of supplied liquid helium. The recovery efficiency for the buildings on the south side of the Wako campus, *i.e.*, the Cooperation Center building of the Advanced Device Laboratory, Chemistry and Material Physics building, and Nanoscience Joint Laboratory building, increased to approximately 96%.

Reference

1) K. Ikegami *et al.*, RIKEN Accel. Prog. Rep. **34**, 349 (2001).

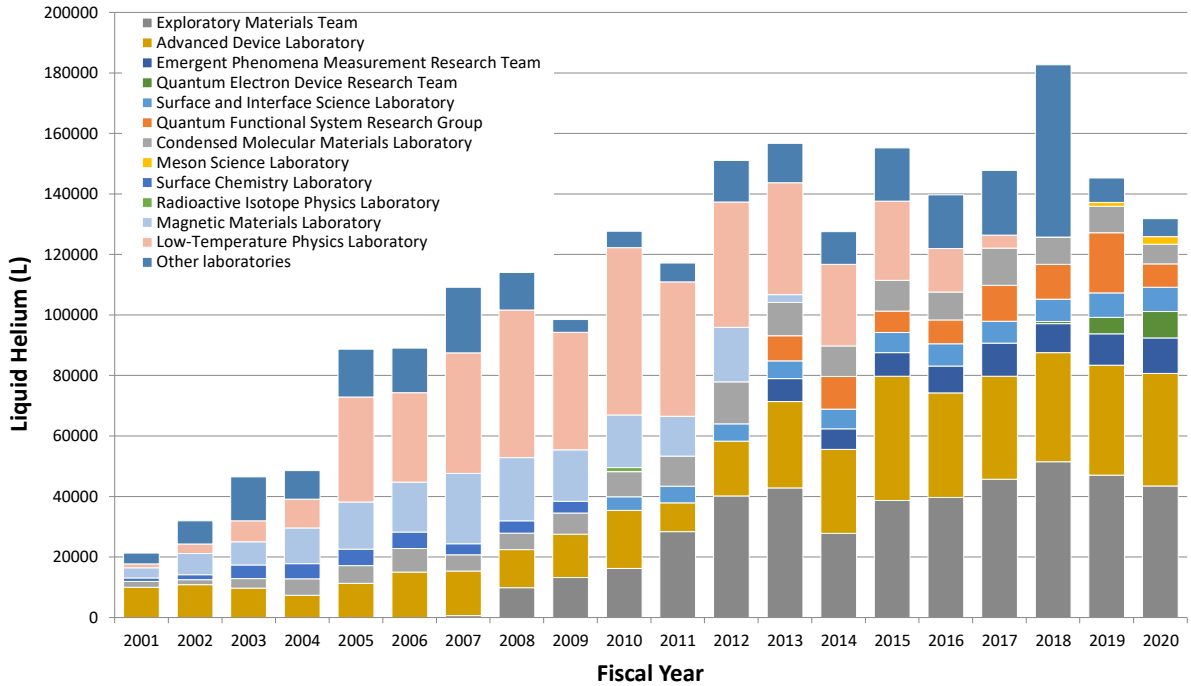

Fig. 1. Volumes of liquid helium supplied to various laboratories for each fiscal year from 2001 to 2020.

*1 RIKEN Nishina Center
*2 Nippon Air Conditioning Service K.K

Impurity concentration in recovered helium gas of liquid-helium supply and recovery system

M. Nakamura,[*1] T. Dantsuka,[*1] H. Okuno,[*1] S. Turuma,[*1] M. Kuroiwa,[*1] M. Ohshima,[*2] H. Hirai,[*2] H. Shiraki,[*2] H. Shiba,[*2] K. Kimura,[*2] S. Okada,[*2] A. Mikami,[*2] H. Hazama,[*2] M. Nagano,[*2] and M. Nakayama[*2]

We use recovered helium gas for a liquid-helium supply system. However 1–2 ppm hydrogen gas, for example, was intermixed with the recovered helium gas, and we had to stop the operation of our system for a few month in 2004.[1] To cope with such serious troubles, we introduced gas chromatography equipment and have been analyzing the recovered helium gas. Then, we could observe the concentration of impurity gas and the condition of the recovered helium gas for effective operation. In this paper, we report the change in concentration of impurity gases in 2021.

The recovered helium was analyzed using SHIMADZ 2014 every day except Saturdays and holidays. The results from January 4 to December 28 in 2021 are shown in Fig. 1. The left axis shows the concentration of N_2 and O_2, and the right axis shows that of H_2, CO_2, and CO. The results for CO_2 and CO are presented in a bar chart because we could rarely observe these gases and the results are difficult to plot using polygonal lines. The black, gray, and red lines show the N_2, O_2, and H_2 concentration, respectively. The blue and green bars show the CO_2 and CO concentration, respectively.

The concentration changes of N_2 and O_2 were almost in exact correspondence. The N_2 and O_2 concentrations changed from 1300 to 2000 ppm and from 900 to 1300 ppm, respectively. From April to September, the N_2 and O_2 concentrations reduced to approximately 1300 and 900 ppm, respectively. We presume that N_2 and O_2 from air intermixed into the helium gas when helium was recovered. However, the ratio of N_2 and O_2 of our result is approximately 0.7 and not the same as that of the air (0.25). The cause of this difference cannot be explicated at present.

The fluctuation of the H_2 concentration was fairly radical. Ordinarily, the H_2 concentration settled around 0.1 ppm. However, the concentration suddenly increased to 0.3–0.7 ppm at several instances. The correlation of H_2 concentration change with that of N_2 and O_2 is not so clear. We presume that the H_2 impurity intermixed into the recovered helium gas through a mechanism different from that of N_2 and O_2.

We cannot estimate the CO_2 and CO impurity concentrations because these gases were observed only a few times in this year.

In January, some parts included in the helium liquefier were blocked, and we could not operate the helium liquefier. In the term of this trouble, we could observe CO_2 and CO several times, and H_2 concentration increased to 0.7 ppm. The N_2 and O_2 concentrations also increased. Hence, we can presume that this serious trouble was caused by impurity gases. However, the cause of this trouble could not be clarified.

To keep the purity of liquid helium, we have to analyze the impurity gases in the recovered helium gas.

Reference

1) K. Ikegami *et al.*, RIKEN Accel. Prog. Rep. **38**, 286 (2005).

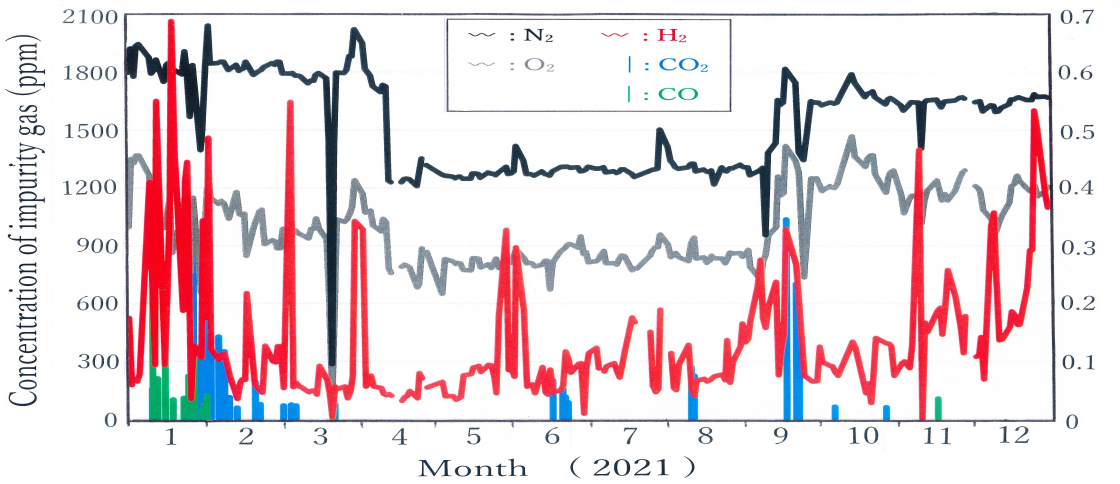

Fig. 1. Impurity concentration in the recovered helium gas in 2021.

*1 RIKEN Nishina Center
*2 Nippon Air Conditioning Service Co., Ltd.

Operation of the BigRIPS cryogenic plant

K. Kusaka,[*1] M. Ohtake,[*1] K. Yoshida,[*1] M. Ohshima,[*2] A. Mikami,[*2] H. Hazama,[*2] H. Shiraki,[*2] H. Hirai,[*2] K. Kimura,[*2] M. Nagano,[*2] H. Shiba,[*2] and S. Okada[*2]

Since the total operation time of the helium compressor unit has reached to 77,680 h in August 2021, the main compressor was shipped to the manufacturer's factory for maintenance. The compressor unit was disassembled, and its interior was cleaned. All the components were checked carefully, and no significant mechanical damage was found.

In addition to maintaining the mechanical components of the compressor unit, we replaced the activated charcoal and molecular sieves in the adsorbent vessel in August 2021. We measured the operation interval of the drain valves of the coalescer vessels in the compressor unit, to evaluate the oil contamination level. We replaced coalescer filter elements five times since 2008. The operation periods of replaced filter elements are from Aug. 2008 to July 2010, Sept. 2010 to July 2012, Sept. 2012 to July 2014, Sept. 2014 to July 2016, and Sept. 2016 to June 2019. Figure 1 shows an estimate of the oil contamination level at the entrance of the third coalescer vessel as a function of the coalescer filter operation time. The navy blue, green, and yellow diamonds represent the estimates for the first, the second, and the third elements, respectively. The fourth, the fifth and the sixth elements are shown with pink, red, and purple diamonds, respectively. The oil contamination values measured using the oil check kit are also shown. The open triangles, squares, and circles represent the results for the first, the second, and the third elements. The results for the fourth and the fifth elements are indicated by the open diamonds and circles, respectively. The cross represents the results of the sixth elements. Both estimations of the oil contamination level are consistent with each other, and the performance efficiency of the sixth filter element is apparently better than that of the others.

At the end of October 2021, we started continuous operation of the BigRIPS cryogenic plant after summer maintenance. This operation was terminated by an incident in the 2021 winter beam time. At 7:35 on December 3, the fire alarm of the RI-Beam Factory (RIBF) building rang, and the cryogenic plant operator found smoke emanating from the compressor unit of the BigRIPS cryogenic plant. After having made necessary emergency contacts, the plant operator stopped the compressor unit safely at 7:50. Evaporated helium gas from the STQ cryostats was transferred to the RIKEN liquid-helium supply and recovery system using a temporary recovery line. We inferred that the smoke was emitted from the coupling side baring unit of the main motor of the compressor unit, since burnt grease was found around the coupling. A sudden increase in the operation current of the motor unit from 30.6 A to 33.6 A, which was measured at 7:28, also indicates a breakdown of the main motor.

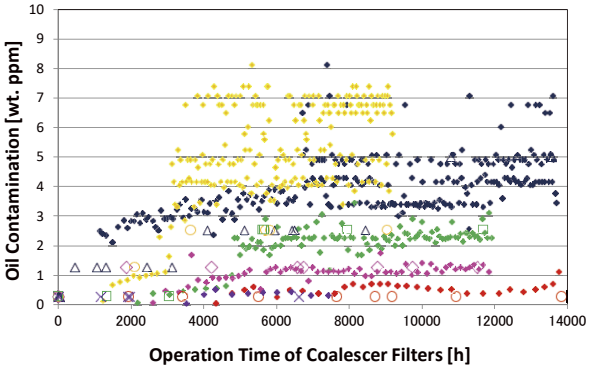

Fig. 1. Oil contamination at the entrance of the third coalescer vessel.

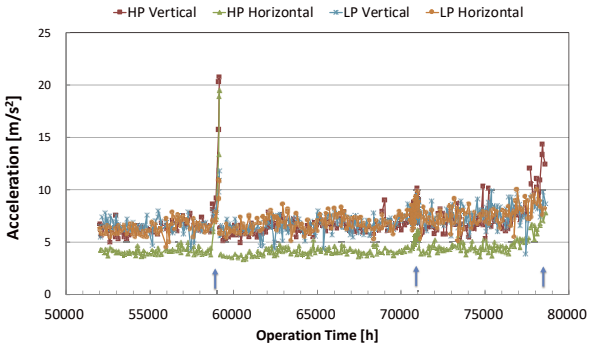

Fig. 2. Vibration acceleration of the compressor unit.

We noticed an unusual noise produced by the main motor of the compressor unit since November 2021. We measured the vibrations of the compressor at the high-pressure and low-pressure sides since 2015. Figure 2 shows the vibration acceleration in the vertical and horizontal directions as a function of the total operation time. Continuous operation started with a total operation time of 77,683 h and the acceleration increased rapidly. The final measurement of the vibrations was performed on Dec. 1. Two additional rapid increases in the vibration acceleration at operation times of 59,000 h and 71,000 h were caused by damage to the bearing unit occurred in Dec. 2016[1] and in June 2019.[2]

The main motor unit was dismounted from the compressor unit and shipped to the manufacturer's factory for repairs in January 2022. The origin of the unusual vibrations is under investigation.

*1 RIKEN Nishina Center
*2 Nippon Air Conditioning Services Co., Ltd.

References

1) K. Kusaka *et al.*, RIKEN Accel. Prog. Rep. **50**, 285 (2017).
2) K. Kusaka *et al.*, RIKEN Accel. Prog. Rep. **53**, 222 (2019).

Radiation safety management at RIBF

K. Tanaka,[*1] Y. Uwamino,[*1,*2] H. Sakamoto,[*1] R. Hirunuma-Higurashi,[*1] H. Mukai,[*3] A. Akashio,[*1] T. Okayasu,[*1] R. Suzuki,[*4] M. Takekoshi,[*4] T. Sato,[*4] K. Igarashi,[*1] S. Iizuka,[*1] N. Usudate,[*1] Y. Shioda,[*1] and K. Sugihara[*1,*5]

The results of radiation monitoring at the RIBF, performed at the border of the facility and the radiation-controlled area are reported. The residual doses along the accelerator setups are also presented. In 2021, a ^{238}U beam of about 345 MeV/nucleon was provided at an intensity of 70 particle nA in April, May, and November. Subsequently, light-ion beams such as ^{12}C beam of about 200 MeV/nucleon of 500 particle nA, ^{2}H beam of about 250 MeV/nucleon, and ^{4}He beam of about 200 MeV/nucleon were used in May and June.

The dose rates at the boundary of the radiation-controlled area were monitored. Neutron and γ-ray monitors were used at three locations: roofs of the RRC, IRC, and BigRIPS. Figure 1 shows the annual neutron dose at these positions. In 2021, even the highest annual dose of 18 μSv/y at the IRC roof was lower than the legal limit of 5.2 mSv/y. The dose at the IRC roof at 2021 is sensitive to IRC and SRC operation time. In 2021, these were operated only four months. Therefore, the annual dose of IRC roof was small.

The dose rates at the site boundary, where the legal limit is 1 mSv/y, were monitored using neutron and γ-ray monitors. The detection limit of the neutron monitor is 2 μSv/y. The annual dose in 2021 was 3.6 μSv of neutrons after the background correction. The detection limit of the γ-ray monitor is 8 μSv/y. The annual dose of the γ-ray was lower than the limit. Therefore, we inferred that the annual dose at the boundary was less than 10 μSv/y, which is considerably lower than the legal limit.

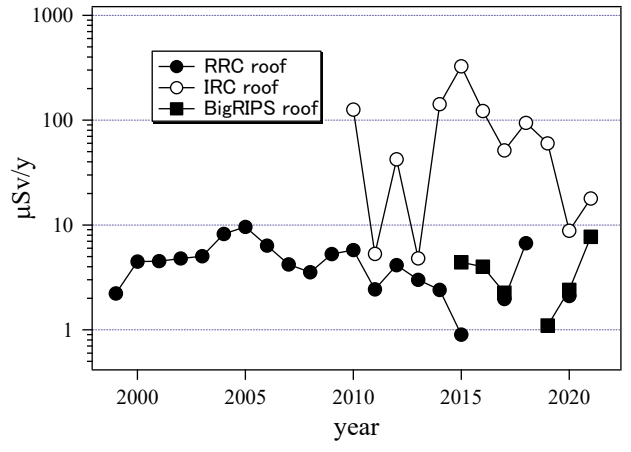

Fig. 1. Radiation dose at the boundary of the radiation-controlled area.

The residual radioactivity at the deflectors of the cyclotrons was measured immediately before the maintenance work. The residual dose depends on factors such as the beam intensity, accelerator operation time, and cooling time. The data were captured at the cyclotrons maintenance works, when the deflectors were able to accessible. Therefore, the cooling times have not been constant. The dose rates from 1986 are shown in Fig. 2. The dose rates for FRC, IRC, and SRC are shown for years after 2006, when the RIBF operation started. For the AVF, the dose rate increased in 2006 because the radioisotope production started and the beam intensity increased.

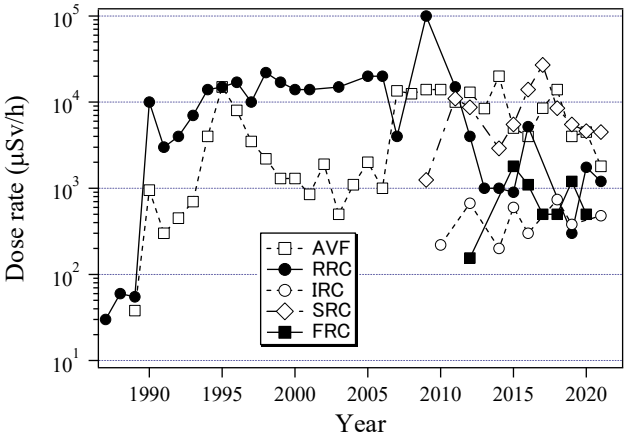

Fig. 2. Dose rates of residual radioactivity at the deflectors of five cyclotrons. Except for measurements, numbers below 10 are preferably spelled out and those above indicated numerically.

The residual radioactivity along the beam lines was measured after almost every experiment. Figure 3 shows the locations of measurement points where high residual doses were observed. Table 1 lists the dose rates, beam conditions, and cooling time at the measurement points. The maximum dose was 13 mSv/h at point 19, which is in the vicinity of the beam dump of BigRIPS.

Although the radioactivity in the closed cooling system at BigRIPS have been reported annually, it is omitted because the radioactivity was not measured in 2021.

The E-learning module, which can be accessed any-

*1 RIKEN Nishina Center
*2 Japan Radioisotope Association
*3 Japan Environment Research Corporation
*4 Daiwa Atomic Engineering Corporation
*5 Kyushu University

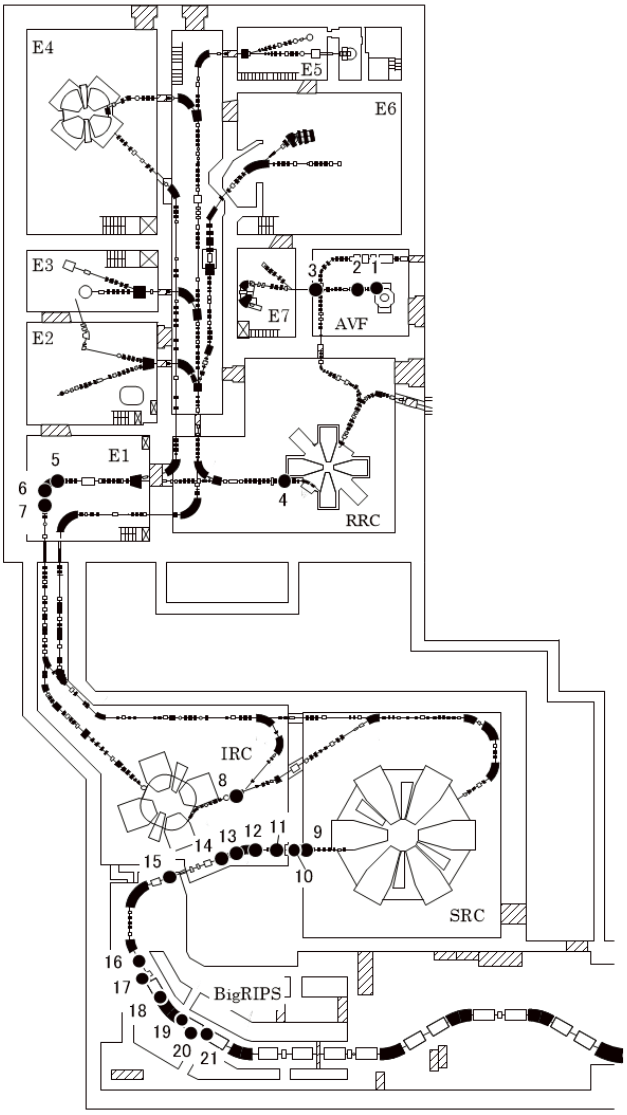

Fig. 3. Layout of the beam lines at RIBF. The measurement locations listed in Table 1 are indicated.

time and from anywhere (even from outside RIKEN), has been used for the re-training of radiation workers at the RIBF. A total of 595 radiation workers completed the training in 2021. It is lower than that in recent years because of COVID-19 restriction on immigration, *etc.*

As described above, radiation management to comply with lows and to maintain radiation level as low as usual has been performed successfully.

Table 1. Dose rates measured at beam lines in 2021. Points 1–21 indicate the locations where measurements were performed as shown in Fig. 3.

Point	Dose rate (μSv/h)	Date (M/D)	Particle	Energy (MeV/u)	Intensity (pnA)	Decay period (h)
1	130	7/30	Li-7	6	1000	313
2	150	7/30	Li-7	6	1000	313
3	650	7/30	Li-7	6	1000	313
4	400	7/30	N-14	100	200	476
5	2400	7/20	α	74	1200	694
6	2200	7/20	α	74	1200	694
7	450	7/20	α	74	1200	694
8	100	7/20	α	200	1000	708
9	5100	7/20	α	200	1000	708
10	8000	7/20	α	200	1000	708
11	350	7/20	α	200	1000	708
12	130	7/20	α	200	1000	708
13	350	7/20	α	200	1000	708
14	380	7/20	α	200	1000	708
15	250	7/20	α	200	1000	708
16	240	12/14	U-238	345	72	269
17	1570	12/14	U-238	345	72	269
18	2300	12/14	U-238	345	72	269
19	13000	12/14	U-238	345	72	269
20	200	12/14	U-238	345	72	269
21	180	12/14	U-238	345	72	269

Operation of Pelletron tandem accelerator

T. Ikeda,[*1] K. Inayoshi,[*2,*1] and H. Sato[*1]

The Pelletron tandem accelerator (5SDH-2) managed by the Detector Team of RNC provides ion beams accelerated by up to 1.7 MV. This accelerator is also registered as a joint-use equipment at the Wako campus for material analysis. As shown in the configuration of the accelerator and the beam lines (Fig. 1), two ion sources are available. One is the RF charge-exchange ion source, called Alphatross, which is employed for experiments using He ion beams. The other is the Source of Negative Ions by Cesium Sputtering (SNICS), which can generate almost all other ions. Thus far, ion species of H, He, B, C, O, and Au have been mainly accelerated in the range of 0.5–1.7 MV.

The maximum energies of different accelerated ions are listed in Table 1. Since 2019, the regulation of the maximum energy of carbon ions was changed from 7.2 MeV to 11.9 MeV, where $^{12}C^{6+}$ is accelerated with the full voltage of 1.7 MV. However, owing to aged deterioration (more than 30 years), acceleration voltages of less than 1.4 MV have been used in recent years.

A unique feature of this facility is the ability to irradiate samples in liquid with a microbeam produced by glass capillary optics at some beam lines.[1] There are four beam lines named BL-E/W*nn* (*nn* denotes the bending angle of the east or west beam line). BL-E45 is dedicated to microbeam irradiation for samples in liquid.[2] BL-E15 is used by user groups in the field of material science to perform Rutherford backscattering (RBS) spectrometry analysis.[3] The RBS apparatus (Charles Evans and Associates Model RBS-400) consists of a goniometer to rotate a sample and a particle detector at 165° to the incident beam direction to measure the back scattered ion energies. Both are inside a vacuum chamber with a vacuum level of the order of 10^{-4} Pa. The intensity of the input He^{2+} beam of 2.28 MeV is approximately 10 nA when the beam size is collimated to 5 mm in diameter. On the west side, BL-W15 was previously used for channeling experiments;[4] however, since 2016, it is employed as a multipurpose line for various equipment. Some examples are a profile measurement system

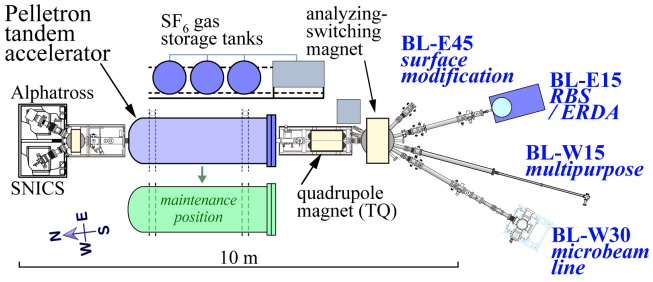

Fig. 1. Pelletron tandem accelerator and beam lines at Nishina R&D Building.

Table 1. Approved conditions at RIKEN Pelletron.

Ion	Maximum Energy	Ion	Maximum Energy
H	3.4 MeV	B	10.2 MeV
He	5.1 MeV	C	12 MeV
Li / Be	6.8 MeV	other	0.6 MeV/u

* Z: 1–83 excluding deuterons

* Maximum intensity: 6.3×10^{12} ions / s (1 pμA)

for an ion microbeam produced by glass capillary,[5] microbeam irradiation tool to induce damage in DNA of mammalian cells,[6] cross-section measurement setup for an international summer school, Nishina School, and detector calibration system based on proton-induced resonance reactions to produce γ rays of up to 10.8 MeV[7] BL-W30 was previously used for detector calibration;[8] however, since 2020, it is dedicated to a new microbeam irradiation port equipped with an Olympus research microscope.

The total machine time (MT) from January 1 to December 31, 2021, was 27 days, which can be seen from Table 2. The MT included a machine study on acceleration, whereas excluded the conditioning of the ion sources. One team used both H and He ion beams in one MT.

Table 2. Beam conditions employed in accelerator.

Ion	Energy [MeV]	Beam current [pnA]	Experiment	Operation time [days]
$^{1}H^{+}$	1.0–2.8	0.3–450	Irradiation	20
$^{4}He^{2+}$	2.28	0.015–12.5	RBS	7

Points 1–5 below list the studies that used the beam lines, along with the number of days of MT. The Nishina School experiment was not performed in 2021.

(1) Microbeam performance study with H ions using glass capillaries at BL-W15 (10 days)
(2) Microbeam (H/He ion) irradiation for single cells at BL-W30 (4 days without samples)
(3) RBS experiments (8 days)
(4) Educational experiment of proton capture by carbon/boron-nucleus for the Nishina School (0 days)
(5) Development of a charged-particle/γ-ray detector to be used for RIBF experiments (5 days)

References

1) T. Ikeda, Quantum Beam Sci. **4**, 22 (2020).
2) T. Kobayashi *et al.*, Surf. Coat. Technol. **331**, 206 (2017).
3) L. Jianjun *et al.*, Chem. Sci. **12**, 10354 (2021).
4) E. Yagi *et al.*, J. Phys. Soc. Jpn. **85**, 124601 (2016).
5) T. Ikeda *et al.*, Nucl. Instrum. Methods Phys. Res. B **470**, 42 (2020).
6) T. Ikeda *et al.*, RIKEN Accel. Prog. Rep. **53**, 215 (2020).
7) R. Mizuno *et al.*, in this report.
8) F. P. Gustafsson *et al.*, RIKEN Accel. Prog. Rep. **50**, 209 (2017).

*1 RIKEN Nishina Center
*2 Department of Physics, Toho University

Fee-based activities performed by the RI Application Research Group

A. Nambu,[*1] H. Haba,[*1] A. Yoshida,[*1] and T. Kambara[*1]

This article summarizes the fee-based activities performed by the RI Application Research Group in 2021, which include the distribution of radioisotopes (RIs) and utilization of heavy-ion beams in the industry.

Since 2007, RIKEN has distributed RIs to users in Japan for a fee in collaboration with the Japan Radioisotope Association[1] (JRIA). The nuclides include ^{65}Zn ($T_{1/2}$ = 244 days), ^{109}Cd ($T_{1/2}$ = 463 days), ^{88}Y ($T_{1/2}$ = 107 days), ^{85}Sr ($T_{1/2}$ = 65 days), and ^{67}Cu ($T_{1/2}$ = 61.8 hours) produced in the RIKEN AVF cyclotron by the Nuclear Chemistry Research Team of the RI Application Research Group.

According to a material transfer agreement (MTA) drawn between the JRIA and RIKEN, JRIA mediates the transaction of RIs and distributes them to users. ^{65}Zn and ^{109}Cd are delivered approximately two weeks after the acceptance of an order.

^{85}Sr, ^{88}Y, and ^{67}Cu, which have short half-lives, are not stocked like ^{65}Zn and ^{109}Cd; instead, they are produced in a scheduled beamtime after an order is accepted. Therefore, they are delivered after two or more months.

Details regarding RIKEN RIs can be found on the online ordering system, J-RAM,[2] of JRIA.

In 2021, we delivered 4, 2, and 10 shipments of ^{65}Zn, ^{88}Y, and ^{85}Sr with a total activity of 31, 2, and 36.4 MBq, respectively, and no shipment of ^{67}Cu and ^{109}Cd. The final recipients of RIs included 11 universities, two research institutes, one private company, and one medical research center.

Figure 1 shows the yearly trends in the number of orders and amount of distributed RIs.

Compared with 2020, the amount of distributed ^{65}Zn and ^{85}Sr increased, that of ^{109}Cd decreased, and that of ^{88}Y remained the same. The amount of ^{85}Sr distributed in 2021 was the highest since the beginning of its distribution. The number of orders for ^{65}Zn in 2021 was the highest in the last seven years; however, it was significantly less than that in 2010.

The Industrial Application Research Team of the RI Application Research Group promotes the utilization of heavy-ion beams in the industry. The RIKEN Nishina Center allows the use of the AVF cyclotron, RILAC, and RIKEN Ring Cyclotron (RRC) by private companies in Japan for a fee.[3] Currently, the main users include semiconductor companies that irradiate space-use semiconductor devices with ^{40}Ar, ^{84}Kr, or ^{136}Xe ions from the RRC to simulate single-event effects due to the heavy-ion components of cosmic radiation.

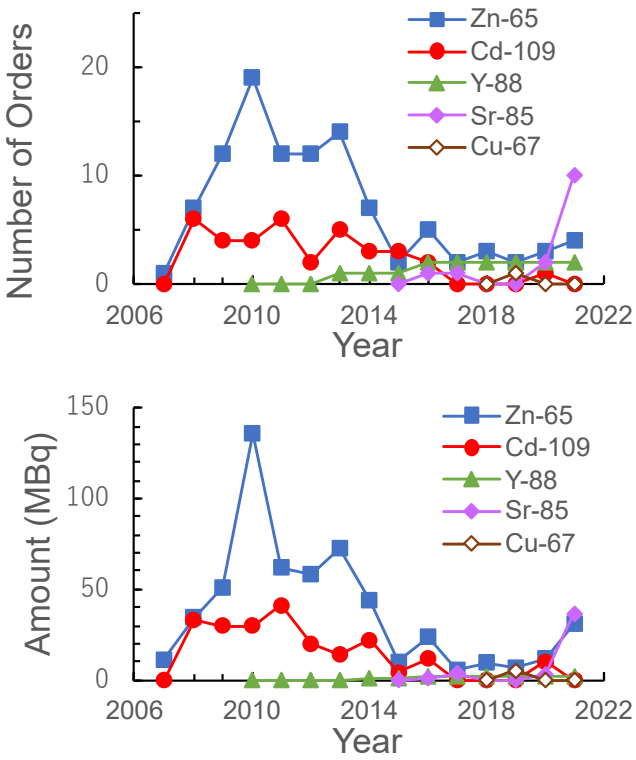

Fig. 1. Number of orders (upper) and amount (lower) of RIs distributed yearly from 2007 to 2021. The distribution of ^{88}Y, ^{85}Sr, and ^{67}Cu started in 2010, 2015, and 2018, respectively.

The proposals for beam utilization are reviewed by a program advisory committee dedicated to industrial use (InPAC).

In January 2021, In-PAC reviewed and approved three proposals via e-mail. In July, In-PAC held its 17th meeting, where it reviewed and approved seven proposals, including two new proposals.

In 2021, four companies executed 13 fee-based beamtimes, nine of which used a ^{84}Kr beam with a total beamtime of 161 h and four utilized an ^{40}Ar beam with a total beamtime of 48 h. In response to user demand, we are prepared to supply ^{12}C beam; furth details are provided elsewhere in this progress report.

References

1) http://www.jrias.or.jp/ (Japanese), http://www.jrias.or.jp/e/ (English).
2) https://j-ram.org/ (Japanese).
3) http://ribf.riken.jp/sisetu-kyoyo/ (Japanese).

*1 RIKEN Nishina Center

V. EVENTS

International workshops on the extension project for the J-PARC hadron experimental facility (J-PARC HEF-ex WSs)

F. Sakuma*1 for the J-PARC HEF-ex WS Local Organizing Committee

International Workshops on the Extension Project for the J-PARC Hadron Experimental Facility (J-PARC HEF-ex WSs) were held online on [first] June 7–9, 2021, and [second] February 16–18, 2022. The workshops were organized by Hadron Hall Users' Association (HUA) and supported by J-PARC Center, KEK Theory Center, RCNP, and RIKEN Nishina Center.

We have been extensively discussing a new plan for the J-PARC Hadron Experimental Facility to extend the existing experimental facility. The idea is to extend the Hadron Hall to include another production target downstream of the current production target and build multiple new beamlines. Four new beamlines are being planned to be constructed with the highest priority.

- A "high-intensity and high-energy-resolution beamline (HIHR)" and "high-purity and high-intensity low-momentum charged K beamline (K1.1)" to solve the so-called hyperon puzzle through the super-precision spectroscopy of Λ-hypernuclei and precise hyperon-nucleon scattering measurement, respectively
- A "high-intensity neutral KL beamline (KL2)" to explore new physics beyond the Standard Model by dramatically increasing the sensitivities of the kaon rare decay
- A "high-momentum particle-separated beamline (K10)" to resolve the conundrum of the strong interaction based on the investigation of Xi and Omega baryons

We will develop new physics programs in particle and nuclear physics that cannot be implemented at the existing facilities.

The J-PARC HEF-ex WSs were part of a series of workshops to discuss and detail the physics case at the Hadron Experimental Facility. In the first half of 2021, several workshops were held focusing on the future physics case at the extended Hadron Experimental Facility; their outputs were summarized as the third white paper.[1] The extension project was reviewed by an international committee formed under J-PARC PAC in August 2021 and was highly evaluated toward the early realization of the facility extension. Detailed information on the extension project can be found on HUA's home page.[2]

[First J-PARC HEF-ex WS on 7–9 June 2021]
The first workshop was dedicated to discussions on important physics features at the extended J-PARC Hadron Experimental Facility. This workshop included plenary sessions by invited speakers, and the physics case for the new beamlines was discussed.

✓ Project overview
✓ Strangeness nuclear physics at the HIHR and K1.1 beamlines
✓ Flavor physics at the KL2 beamline
✓ Hadron physics at the K10 beamline

The workshop included 138 participants from 12 countries (42 participants from abroad). There were 12 plenary talks. The full program and presentation files are available online at the workshop website.[3]

Fig. 1. The Second J-PARC HEF-ex WS.

[Second J-PARC HEF-ex WS on 16–18 February 2022]
In the second workshop, discussions were dedicated to the physics case connecting the "present" and "future" Hadron Experimental Facility of J-PARC. For that purpose, this workshop covered wide-ranging topics related to experimental and theoretical activities conducted at the Hadron Experimental Facility.

✓ S = −1 and −2 hypernuclei
✓ Meson in nuclei
✓ Baryon spectroscopy
✓ Kaon rare decays
✓ μ-e conversion
✓ Future facilities and instrumentation

The scientific program comprised plenary sessions by invited speakers and parallel sessions by invited and contributed speakers. The workshop included 250 participants from 15 countries (94 participants from abroad). There were 19 plenary talks and 86 parallel talks (including 23 invited keynote talks). The full program and presentation files are available online at the workshop website.[4] A group photo is shown in Fig. 1.

Following the success of the workshops, we are planning to conduct the third workshop in FY2022 to continuously discuss physics at the J-PARC Hadron Experimental Facility and its extension.

References

1) Taskforce on the extension of the Hadron Experimental Facility, arXiv:2110.04462.
2) http://www.rcnp.osaka-u.ac.jp/~jparchua/en/index.html .
3) https://indico2.riken.jp/event/3773/ .
4) https://kds.kek.jp/event/40010/ (An access key is required.).

*1 RIKEN Nishina Center

SPIN2021 international spin symposium

Y. Goto*1 and T. Uesaka*1 for the SPIN2021 Local Organizing Committee

The 24th International Symposium on Spin Physics (SPIN2021) was held at the Kunibiki Messe Convention Center in Matsue, Shimane Prefecture, Japan in October 18–22, 2021. We aimed to cover a wide range of topics related to particle and nuclear spin physics from low energy to high energy, including experimental, theoretical, computational and technological aspects and applications.

This symposium was originally scheduled to be held in 2020 as SPIN 2020; however, it was postponed because of the COVID-19 pandemic. This symposium series has been held jointly since 2000, combining the High Energy Spin Symposia and Nuclear Polarization Conferences. The most recent symposia took place in Dubna, Russia (2012); Beijing, China (2014); Urbana Champaign, USA (2016); and Ferrara, Italy (2018).

The symposium was held in a hybrid style, *i.e.*, in-person and online participation were possible. As a result, in-person on-site participation was limited to the symposium organizers, which was 20 people, while online participation included about 160 presenters and 150 audience participants. The total number of participants was about 330, which is a larger number for this symposium series.

The hybrid style was useful to invigorate our scientific discussions under the present situation of the pandemic. We had successfully tested the hybrid style with a domestic workshop on spin physics.[1)] In the hybrid style of the SPIN2021 symposium, the structure of the plenary and parallel sessions was set up to be convenient for online participants residing outside Asia. In the first two days, the symposium started at 3 p.m. to facilitate online participation from Europe, and in the last two days, it started at 7 a.m. to facilitate online participation from the United States.

The scientific program of SPIN 2021 included topics related to spin phenomena in particle and nuclear physics and related fields. The following symposium topics were covered:

- Nucleon helicity structure
- 3D structure of the nucleon: transverse-momentum dependent distribution
- 3D structure of the nucleon: general parton distribution
- Fundamental symmetries and spin physics beyond the Standard Model
- Spin physics in nuclear reactions and nuclei
- Low energy spin physics with lepton, proton and hadron probes
- Future facilities and experiments
- Acceleration, storage and polarimetry of polarized beams
- Polarized ion and lepton sources and targets
- Applications of nuclear polarization techniques to other fields

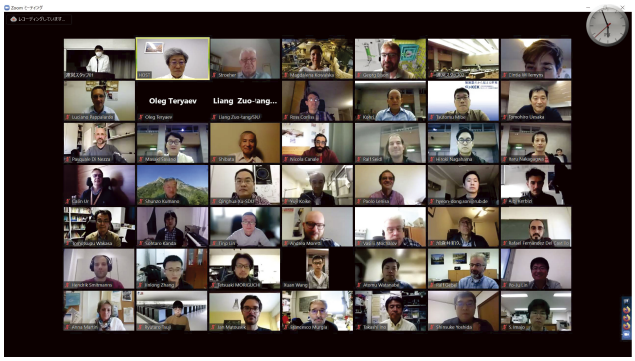

Fig. 1. Online participants of the SPIN2021 symposium.

The symposium format comprised discussions in plenary and parallel sessions. The plenary session began with a discussion on the recent major topic of muon g-2 measurements, and two more special discussions on spintronics and polarization measurements of the cosmic microwave background took place. In total, 29 plenary talks were given. Parallel sessions were held for the aforementioned listed topics, with up to five sessions running in parallel. Few sessions were conducted as joint sessions for multiple topics.

The symposium is hosted by RIKEN Nishina Center and co-hosted by KEK, J-PARC, RCNP Osaka University, CNS University of Tokyo, and Yamagata University. Moreover, it is supported by RIKEN as a part of the RIKEN Symposium Series, and subsidy system for international conferences in Matsue and Shimane Prefecture.

A screenshot of online participants (not all the participants) is shown in Fig. 1. The full program and presentation slides presented in the sypmposim are available at the symposium website (`https://indico2.riken.jp/event/3082/`), and the proceedings of the SPIN2021 symposium will be pulished in the JPS Conference Proceedings.

Reference

1) Y. Goto, RIKEN Accel. Prog. Rep. **54**, 197 (2021).

*1 RIKEN Nishina Center

Small-x physics in the electron-ion collider era

Y. Hatta,[*1,*2] A. Morreale,[*3] F. Salazar,[*4] B. Schenke,[*2] and R. Venugopalan[*2]

Understanding the high energy limit of hadronic and nuclear collisions is at the forefront of nuclear and particle physics. When boosted to ultrahigh energies, all hadrons and nuclei eventually transform into a universal form of matter called the Color Glass Condensate (CGC). The CGC is characterized by the high density (saturation) of small-x gluons which leads to distinct experimental signatures. Tantalizing hints of the CGC have been observed at HERA, RHIC and the LHC, but the prospects for the discovery of the CGC are more promising at future experiments such as the Electron-Ion Collider (EIC) at Brookhaven National Laboratory Indeed, according to the National Science Academy report published in 2019, one of the three major goals of the EIC is to address the nature of the gluon saturation. (The other two are the mass and spin structure of the nucleons.)

With this in mind, the small-x community is gearing up to meet the challenges of the EIC era. Over the past several years, there has been impressive progress in the next-to-leading order (NLO) calculations in the CGC framework of various observables such as single hadron production in proton-nucleus collisions, inclusive and exclusive dijet and trijet production in Deep Inelastic Scattering (DIS), jet-plus-photon production in DIS, *etc.* We expect that NLO calculations will be the standard tool to confront future experimental data at the EIC.

Another emerging trend of the community is the interplay between small-x physics and spin physics. The RHIC result for the gluon helicity ΔG has underscored the necessity to understand the longitudinal spin structure of the proton at small-x. There have been theoretical indications that a significant fraction of spin and orbital angular momentum is stored in the small-x region. As for the transversely polarized proton, a surprising new connection between the gluon Sivers function at small-x and the QCD Odderon has been pointed out and its implications at the EIC has been discussed.

On 15–17, December 2021, we have held a 3-day virtual workshop dedicated to small-x physics in order to summarize the present status of the field described above and to discuss future directions. A major focus of this workshop was to identify outstanding problems that could significantly benefit from collaborative efforts amongst scientists working on formal, phenomenological, and computational aspects of small-x physics. The topics covered include:

What are the best observables of gluon saturation at the EIC?

- NLO calculations in the CGC
- Interplay between spin and small-x
- TMD, GPD and Wigner distributions at small-x
- Initial conditions (momentum space, coordinate space, nonperturbative input, ...)
- Hadronization (MC implementation, coupling to existing event generators, ...)
- Outstanding open problems at small-x requiring a topical theory collaboration

We have had 102 registered participants and 31 invited talks including 6 experimental talks in a very interactive atmosphere. The most important outcome of the workshop is that, after this workshop, the participants have decided to apply for a topical collaboration of the U.S. Department of Energy (DOE). One of the organizers, B. Schenke (BNL) is taking a lead in this initiative and many other workshop participants who have faculty positions in the U.S. are serving as co-PIs. The workshop can be therefore regarded as a great success.

*1 RIKEN BNL Research Center
*2 Physics Department, Brookhaven National Laboratory
*3 Los Alamos National Laboratory
*4 University of California, Los Angeles

RIKEN open day 2021

K. Tanaka,[*1] M. Shishido,[*1] Y. Watanabe,[*1] N. Miyauchi,[*1] and A. Akashio[*1]

RIKEN open day was held on April 17, 2021. Because of the COVID-19 pandemic, open day 2020 was canceled. In 2021, the open day was held but limited to online only. Figure 1 shows framework of contents. It was operated by using Zoom video conference software.[1] A breakout room was assigned to a virtual laboratory which could relay an experimental room in RIKEN to the open day visitors. Nishina Center had two virtual laboratory rooms. One offers a virtual accelerator tour. The other provides an introduction of RIBF research and collaborated with the Center for Nuclear Study at the university of Tokyo (CNS) and the KEK Wako Nuclear Science Center.

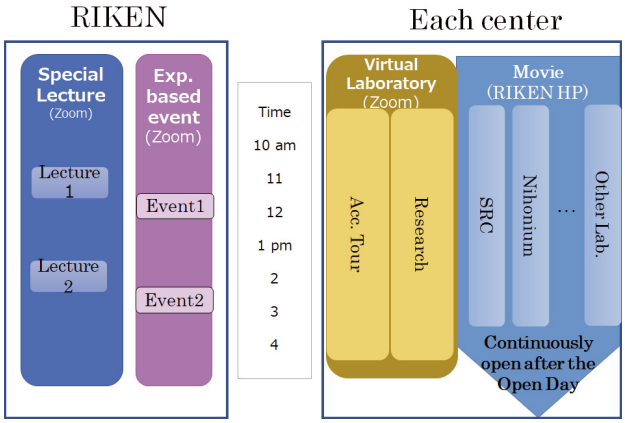

Fig. 1. Contents for the RIKEN open day.

For the virtual accelerator tour, RIBF movie taken along to the accelerator and downstream beamline was shared to visitors. Figure 2 shows the movie shared for the RIBF tour. SRC, BigRIPS, and SAMURAI were contained in the movie. Researchers described about RIBF accelerators and experimental instruments with the RIBF movie. Six time of tours were performed.

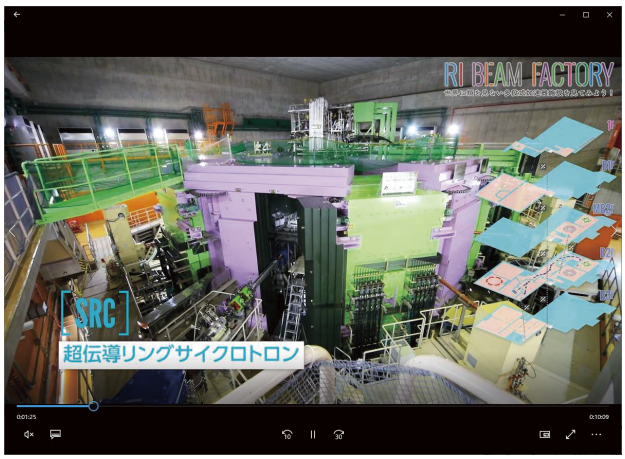

Fig. 2. Movie for the RIBF virtual tour.

To present an introduction to RIBF research, experiments and researches about ZDS with HIKARI detector, SAMURAI, SHARAQ by CNS, KISS by KEK, and nuclear chemistry were introduced. Six different exhibition tours were performed. Figure 3 shows a screen shot of the introduction to the nuclear chemistry presentation.

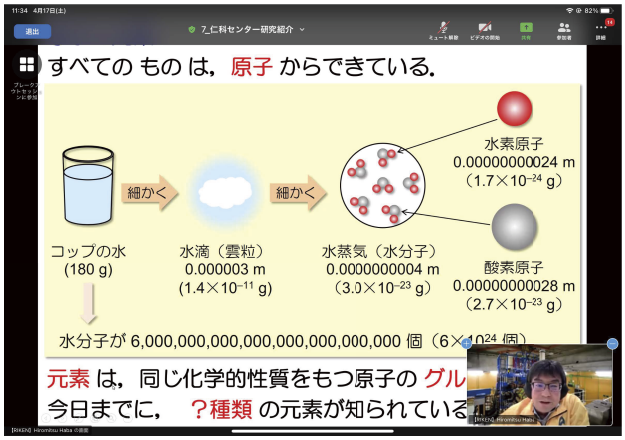

Fig. 3. Screen shot of an introduction of research of virtual laboratory.

Movies for RIKEN laboratories were also exhibited on the RIKEN web page. Nishina Center released two, five-minute movies. One was introduction to SRC and the other was about the discovery of the 113th element, Nihonium. These videos were shared for a month after the open day.

RIKEN organized a special lecture and an experience-based event. Dr. Tomoko Abe gave a special lecture, “Creating novel plants of your dreams using heavy-ion beams.”

She introduced studies about various biological effects of fast heavy-ions. Ion beams have been used to create over 35 new varieties in RIKEN in the last two decades and beneficial mutants have been identified in various species.

Nishina Center also presented at the experience-based event. During a hands-on event for children, participants made their own handmade spectrometers and used them during the interactive online class to learn in a fun way that light is composed of various colors, like a rainbow. Spectroscope kits were distributed to registered participants in advance.

About 800 participants visited RIKEN open day. The approximate numbers of visitors in the breakout rooms for the virtual laboratory of Nishina Center were 200. Twenty four staff from Nishina Center participated in the open day.

*1 RIKEN Nishina Center

Reference

1) https://zoom.us .

VI. ORGANIZATION AND ACTIVITIES OF RIKEN NISHINA CENTER

(Activities, Members, Publications & Presentations)

1. Organization

1.1 Organization Chart as of March 31, 2022 （End of FY2021）

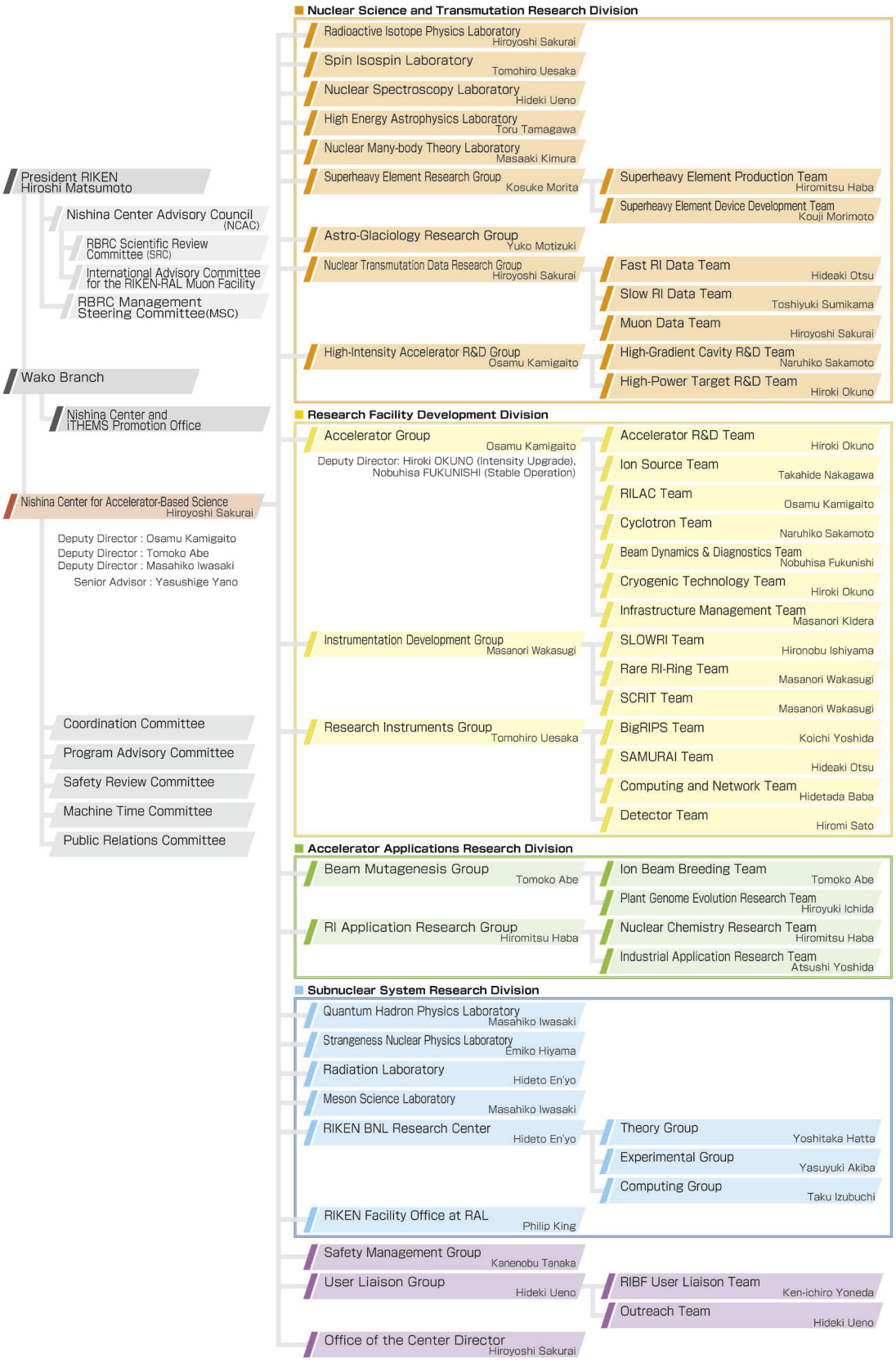

1.2 Topics in FY2021

Year	Date	Topics in Management
2021	Apr. 1	Newly appointed: Team Leader of RILAC Team: Osamu KAMIGAITO
2021	May 1	Newly appointed: Group Leader of Theory Gtoup: Yoshitaka HATTA
2021	Oct. 1	Newly appointed: Director of Nuclear Many-body Theory Laboratory: Masaaki KIMURA

2. Finances

A transition of the RNC budget for the past four years is shown in following graph.

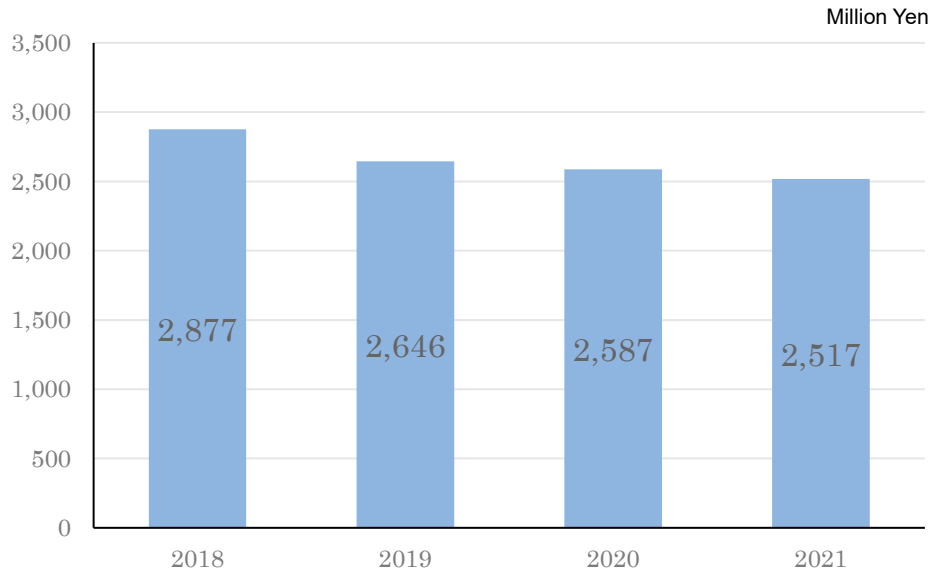

3. Staffing

At the start of FY 2021, there were 142 personnel affiliated with RNC and 418 researchers visiting RNC for research purpose. The following graphs show a breakdown of personnel into six categories as of April 1, 2021, and a transition of the number of each category.

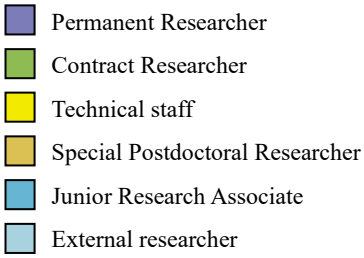

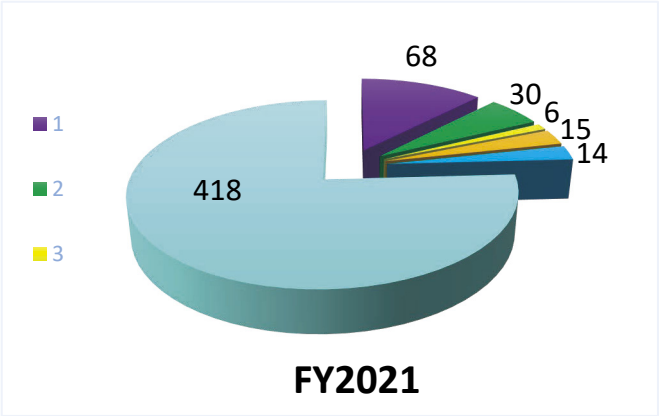

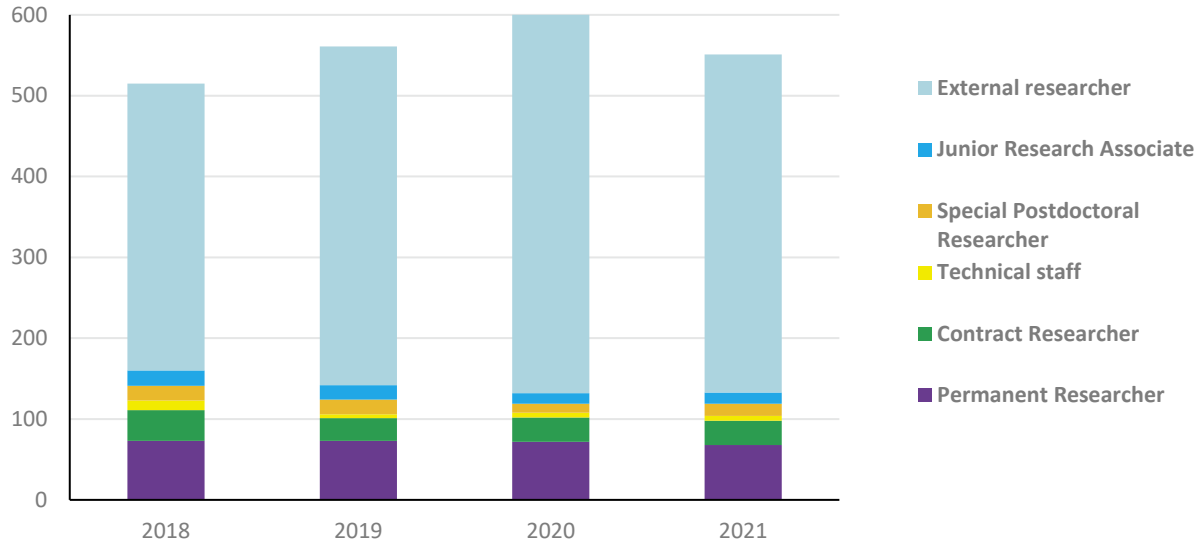

4. Research publication

The number of papers published annually from RNC is shown graphically using the data obtained from Clarivate Analytics' Web of Science Documents.

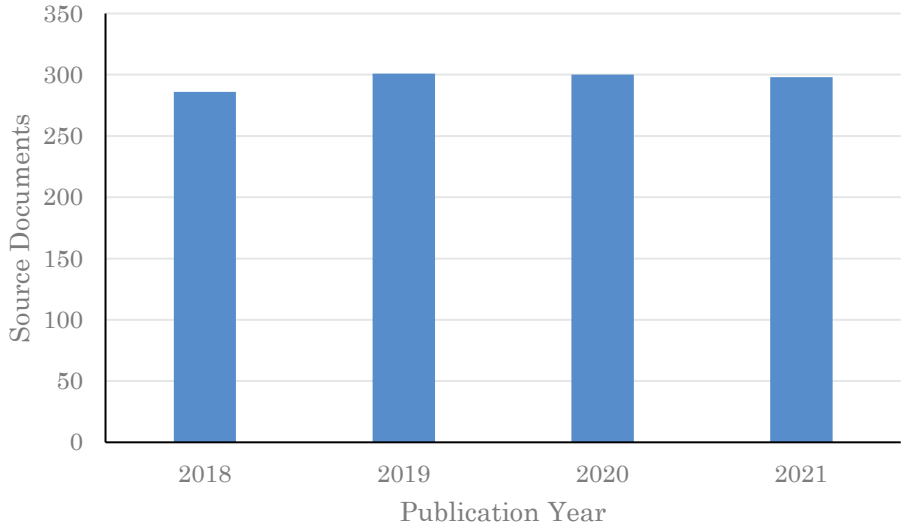

Citation analysis for the past four years

As of April 2022

Indicators \ Year	2018	2019	2020	2021
Total number of papers	286	301	300	298
Percentage of papers in top 10%	20.63	9.63	12.67	14.1
Percentage of papers in top 1%	4.20	1.00	1.33	3.4

5. Management

Headed by the RNC Director Hiroyoshi SAKURAI, the RIKEN Nishina Center for Accelerator-Based Science (RNC) consists of:

- 9 Laboratories
- 11 Groups with 27 Teams
- 2 overseas research centers with 3 Groups

as of the end of FY2021. There are also two 'Partner Institutes' which conduct research in the laboratories set up in RNC. RNC is managed by its Director who takes into consideration the majority decision of the RNC Coordination Committee. The management of RNC is supported by the following committees:

- Program Advisory Committee
- Safety Review Committee
- RIBF Machine Time Committee
- Public Relations Committee

There are also committees to support the President of RIKEN and/or the Director of RNC such as:

- Nishina Center Advisory Council with three subcommittees:
  - ・RBRC Scientific Review Committee (SRC)
  - ・International Advisory Committee for the RIKEN-RAL Muon Facility
  - ・RBRC Management Steering Committee (MSC)

Nishina Center for Accelerator-based Science

Executive Members (as of March 31, 2022)

Hiroyoshi SAKURAI	Director
Osamu KAMIGAITO	Deputy Director (Research Facility Development Division)
Tomoko ABE	Deputy Director (Accelerator Applications Research Division)
Masahiro IWASAKI	Deputy Director (Subnuclear System Research Division)
Yasushige YANO	Senior Advisor

RNC Coordination Committee

The following subjects relevant to the RNC management are deliberated under the chairmanship of the RNC Director:

- Establishment of the new organization or reorganization in RNC
- Personnel management of RNC researchers
- Research themes and research budget
- Approval of the Partner Institutes
- Evaluation of the management of RNC and the response to the recommendations by external evaluation

The RNC Coordination Committee is held monthly.

Members (as of March 31, 2022)

Hiroyoshi SAKURAI	Director, RNC; Director, Radioactive Isotope Physics Laboratory and Nuclear Transmutation Data Research Group; Team Leader, Muon Date Team
Osamu KAMIGAITO	Deputy Director, RNC; Director, Accelerator Group and High-Intensity Accelerator R&D Group; Team Leader, RILAC Team
Tomoko ABE	Deputy Director, RNC; Director, Beam Mutagenesis Group; Team Leader, Ion Beam Breeding Team
Masahiko IWASAKI	Deputy Director, RNC; Director, Meson Science Laboratory and Quantum Hadron Physics Laboratory
Yasushige YANO	Senior Advisor, RNC
Tomohiro UESAKA	Director, Spin Isospin Laboratory and Research Instruments Group
Hideki UENO	Director, Nuclear Spectroscopy Laboratory and User Liaison Group; Team Leader, Outreach Team
Toru TAMAGAWA	Director, High Energy Astrophysics Laboratory
Emiko HIYAMA	Director, Strangeness Nuclear Physics Laboratory
Masaaki KIMURA	Director, Nuclear Many-body Theory Laboratory
Yuko MOTIZUKI	Director, Astro-Glaciology Research Group
Kosuke MORITA	Director, Superheavy Element Research Group
Hiroki OKUNO	Deputy Group Director, Accelerator Group; Team Leader, Accelerator R&D Team, Cryogenic Technology Team, and High-Power Target R&D Team
Nobuhisa FUKUNISHI	Deputy Group Director, Accelerator Group; Team Leader, Beam Dynamics & Diagnostics Team
Masanori WAKASUGI	Director, Instrumentation Development Group; Team Leader, Rare RI-Ring Team and SCRIT Team
Hiromitsu HABA	Director, RI Application Research Group; Team Leader, Nuclear Chemistry Research Team and Superheavy Element Production Team

Kanenobu TANAKA	Director, Safety Management Group
Hideaki OTSU	Team Leader, SAMURAI Team and Fast RI Data Team
Naruhiko SAKAMOTO	Team Leader, Cyclotron Team and High-Gradient Cavity R&D Team
Hiromi SATO	Team Leader, Detector Team
Toshiyuki SUMIKAMA	Team Leader, Slow RI Data Team
Takahide NAKAGAWA	Team Leader, Ion Source Team
Koji MORIMOTO	Team Leader, Superheavy Element Device Development Team
Atsushi YOSHIDA	Team Leader, Industrial Application Research Team
Koichi YOSHIDA	Team Leader, BigRIPS Team
Ken-ichiro YONEDA	Team Leader, RIBF User Liaison Team
Hironobu ISHIYAMA	Team Leader, SLOWRI Team
Hidetada BABA	Team Leader, Computing and Network Team
Hiroyuki Ichida	Team Leader, Plant Genome Evolution Research Team
Masanori Kidera	Team Leader, Infrastructure Management Team
Tsukasa TADA	Vice Chief Scientist, Quantum Hadron Physics Laboratory
Hideto EN'YO	Director, RIKEN BNL Research Center; Director, Radiation Laboratory
Yoshitaka HATTA	Group Leader, Theory Group, RIKEN BNL Research Center
Yasuyuki AKIBA	Group Leader, Experimental Group, RIKEN BNL Research Center
Taku IZUBUCHI	Group Leader, Computing Group, RIKEN BNL Research Center
Toshiyuki HASHIMOTO	Director, Nishina Center and iTHEMS Promotion Office

Program Advisory Committee

The Program Advisory Committee reviews experimental proposals submitted by researchers and reports the approval/disapproval of the proposals to the RNC Director. The Committee also reports to the RNC Director the available days of operation at RIBF or the Muon Facility at RAL allocated to researchers. The Committee is divided into three categories according to the research field.

- Nuclear Physics Experiments at RIBF (NP-PAC): academic research in nuclear physics
- Materials and Life Science Researches at RNC (ML-PAC): academic research in materials science and life science
- Industrial Program Advisory Committee (In-PAC): non-academic research

Program Advisory Committee for Nuclear Physics Experiments at RI Beam Factory (NP-PAC)

The 22nd NP-PAC was held on December 1−3, 2021 via Web meeting.

Members (as of March 31, 2022)

Maria J.G. BORGE (Chair)	Consejo Superior de Investigaciones Científicas
Stéphane GREVY	Centre d'Etudes Nucléaires de Bordeaux Gradignan
Mahananda DASGUPTA	The Australian National University
Jens DILLING	Ork Ridge National Laboratory
Magdalena GORSKA	GSI Darmstadt
Takahiro KAWABATA	Osaka University
Masayuki MATSUO	Niigata University
Remco ZEGERS	Michigan State University
Nori AOI	RCNP, Osaka University
Robert CHARITY	Washington University in St. Louis
Gabriel MARTINEZ-PINEDO	Technische Universität Darmstadt, GSI Helmholtzzentrum für Schwerionenforschung
Iain MOORE	University of Jyväskylä
Takehiko SAITO	RIKEN
Philip J. WOODS	University of Edinburgh
Andrea VITTURI	Universita' di Padova
Xiaohong ZHOU	Chinese Academy of Sciences

Program Advisory Committee for Materials and Life Science Researches at RIKEN Nishina Center (ML-PAC)

The ML-PAC of FY2021 was held between December 13, 2021 and January 20, 2022 via e-mail.

Members (as of March 31, 2022)

Adrian HILLIER (Chair)	ISIS, RAL (UK)
Zhi QIN	Chinese Academy of Sciences (China)
Toshiyuki TAKAYANAGI	Saitama University
Yoshio KOBAYASHI	The University of Electro-Communications
Yutaka MIYAZAWA	Yamagata University

Industrial Program Advisory Committee (In-PAC)

The 17th In-PAC was held on July 7, 2021 via Web meeting.
The 18th In-PAC was held between December 8 and 27, 2021 via e-mail.

Safety Review Committee

The Safety Review Committee is composed of two sub committees, the Safety Review Committee for Accelerator Experiments and the Hot-Lab Safety Review Committee. These Committees review the safety regarding the usage of radiation generating equipment based on the proposal submitted to the RNC Director from the spokesperson of the approved experiment.

Safety Review Committee for Accelerator Experiments

Members (as of March 31, 2022)

Hiromi SATO (Chair)	Team Leader, Detector Team
Kouji MORIMOTO	Team Leader, Superheavy Element Device Development Team
Takashi NAGATOMO	Senior Technical Scientist, Ion Source Team
Hiromitsu HABA	Team Leader, Nuclear Chemistry Reaserach Team
Atsushi YOSHIDA	Team Leader, Industrial Application Research Team
Koichi YOSHIDA	Team Leader, BigRIPS Team
Naoki FUKUDA	Technical Scientis, BigRIPS Team
Naruhiko SAKAMOTO	Team Leader, Cyclotron Team
Daisuke SUZUKI	Research Scientist, Radioactive Isotope Physics Laboratory
Masaki SASANO	Senior Research Scientist, Spin Isospin Laboratory
Shunji NISHIMURA	Senior Research Scientist, Radioactive Isotope Physics Laboratory

External members

Shinichiro MICHIMASA	Assistant Professor, Center for Nuclear Study, University of Tokyo
Hidetoshi YAMAGUCHI	Lecturer, Center for Nuclear Study, University of Tokyo
Yutaka WATANABE	Associate Professor, High Energy Accelerator Research Organization, KEK

Ex officio members

Kanenobu TANAKA	Director, Safety Management Group
Hisao SAKAMOTO	Technical Scientist, Safety Management Group

Hot-Lab Safety Review Committee

Members (as of March 31, 2022)

Tetsuya OHNISHI (Chair)	Senior Research Scientist, SCRIT Team
Kanenobu TANAKA	Director, Safety Management Group
Hisao SAKAMOTO	Technical Scientist, Safety Management Group
Hiroki MUKAI	Technical Staff I, Safety Management Group
Rieko HIGURASHI	Technical Scientist, Safety Management Group
Hiromitsu HABA	Team Leader, Nuclear Chemistry Research Team
Kazuya TAKAHASHI	Special Temporary Research Scientist, Nuclear Chemistry Research Team

RIBF Machine Time Committee

Upon request of the RNC Director, the RIBF Machine Time Committee deliberates on the machine time schedule of RIBF and reports the results to the Director.

Members (as of March 31, 2022)

Hideki UENO (Chair)	Director, User Liaison Group and Nuclear Spectroscopy Laboratory
Osamu KAMIGAITO	Director, High-Intensity Accelerator R&D Group and Accelerator Group
Masanori WAKASUGI	Director, Instrumentation Development Group
Tomohiro UESAKA	Director, Research Instruments Group and Spin Isospin Laboratory
Nobuhisa FUKUNISHI	Deputy Group Director, Accelerator Group
Hiroki OKUNO	Deputy Group Director, Accelerator Group
Shunji NISHIMURA	Senior Research Scientist, Radioactive Isotope Physics Laboratory
Tomoko ABE	Director, Beam Mutagenesis Group
Hiromitsu HABA	Director, RI Application Research Group
Kanenobu TANAKA	Director, Safety Management Group
Ken-ichiro YONEDA	Team Leader, RIBF User Liaison Team
Kouji MORIMOTO	Team Leader, Superheavy Element Device Development Team
Koichi YOSHIDA	Team Leader, BigRIPS Team

External members

Kentaro YAKO	Associate Professor, Center for Nuclear Study, University of Tokyo
Hidetoshi YAMAGUCHI	Lecturer, Center for Nuclear Study, University of Tokyo
Yutaka WATANABE	Associate Professor, High Energy Accelerator Research Organization, KEK

Observers

Hiroyoshi SAKURAI	Director, RNC; Director, Radioactive Isotope Physics Laboratory and Nuclear Transmutation Data Research Group; Team Leader, Muon Data Team
Susumu SHIMOURA	Director, Center for Nuclear Study, University of Tokyo
Michiharu WADA	Director, KEK Wako Nuclear Science Center
Hiroari MIYATAKE	Professor, High Energy Accelerator Research Organization, KEK
Daisuke SUZUKI	Chair, The RIBF Users Executive Committee (RIBF-UEC), Research Scientist, Radioactive Isotope Physics Laboratory
Kosuke MORITA	Director, Superheavy Element Research Group
Tohru MOTOBAYASHI	Senior Advisor, RNC
Hideyuki SAKAI	Senior Advisor, RNC
Yasuhiro SAKEMI	Professor, Center for Nuclear Study, University of Tokyo
Hideaki OTSU	Team Leader, Fast RI Data Team and SAMURAI Team
Atsushi YOSHIDA	Team Leader, Industrial Application Research Team
Hironobu ISHIYAMA	Team Leader, SLOWRI Team
Toshiyuki HASHIMOTO	Director, Nishina Center and iTHEMS Promotion Office
Soh OSUKA	Manager, Nishina Center and iTHEMS Promotion Office

Public Relations Committee

Upon request of the RNC Director, the Public Relations Committee deliberates and coordinates the following matters:

- Creating public relations system for RNC
- Prioritization of the public relations activities for RNC
- Other general and important matters concerning the public relations of RNC

Members (as of March 31, 2022)

Toshiyuki HASHIMOTO (Chair)	Director, Nishina Center and iTHEMS Promotion Office
Osamu KAMIGAITO	Deputy Director, RNC; Director, Accelerator Group
Tomoko ABE	Deputy Director, RNC; Director, Beam Mutagenesis Group
Masahiko IWASAKI	Deputy Director, RNC; Director, Meson Science Laboratory
Tomohiro UESAKA	Director, Spin Isospin Laboratory and Research Instruments Group
Hideki UENO	Director, Nuclear Spectroscopy Laboratory and User Liaison Group
Yuko MOTIZUKI	Director, Astro-Glaciology Research Group
Narumasa MIYAUCHI	Technical Staff I, Outreach Team
Yasushi WATANABE	Special Temporary Research Scientist, Outreach Team
Motohide YOKOTA	Coordinator, Office of the Center Director

RBRC Management Steering Committee (MSC)

RBRC MSC is set up according to the Memorandum of Understanding between RIKEN and BNL concerning the collaboration on the Spin Physics Program at the Relativistic Heavy Ion Collider (RHIC). The 28th MSC was held on May 26, 2021.

Members (as of March 31, 2022)

Shigeo KOYASU	Executive Director, RIKEN
Hiroyoshi SAKURAI	Director, RNC; Director, Radioactive Isotope Physics Laboratory and Nuclear Transmutation Data Research Group; Team Leader, Muon Data Team
Shoji NAGAMIYA	Senior Visiting Scientist, RNC
Robert TRIBBLE	Deputy Director for Science and Technology, BNL
Dmitori DENISOV	Deputy Associate Laboratory Director for High Energy Physics, BNL
Haiyan GAO	Associate Laboratory Director for Nuclear and Particle Physics, BNL

6. International Collaboration (as of March 31, 2022)

Country	Partner Institute	Objects	RNC contact person
Austria	Stefan Meyer Institute for Subatomic Physics	Framework	Masahiko IWASAKI, Director, Meson Science Laboratory
China	China Nuclear Physics Society	Creation of the council for China -Japan research collaboration on nuclear physics	Hiroyoshi SAKURAI, Director, Radioactive Isotope Physics Laboratory
	Peking University	Nuclear Science	Hiroyoshi SAKURAI, Director, Radioactive Isotope Physics Laboratory
	Institute of Modern Physics, Chinese Academy of Science	Physics of heavy ions	Hiroyoshi SAKURAI, Director, Radioactive Isotope Physics Laboratory
	School of Nuclear Science and Technology, Lanzhou University	Framework	Masahiko IWASAKI, Director, Meson Science Laboratory
	School of Physics, Nanjing University	Framework	Emiko HIYAMA, Director, Strangeness Nuclear Physics Laboratory
	Department of Physics, Faculty of Science, The University of Hong Kong	Experimental and educational research collaboration in experimental nuclear physics	Hiroyoshi SAKURAI, Director, Radioactive Isotope Physics Laboratory
	School of physics, Nankai University	Framework	Emiko HIYAMA, Director, Strangeness Nuclear Physics Laboratory
	School of Physical Sciences, USTC	Framework	Masahiko IWASAKI, Director, Meson Science Laboratory
Finland	University of Jyvaskyla	Basic nuclear physics and related instrumentation	Hironobu ISHIYAMA, Team Leader, SLOWRI Team
France	National Institute of Nuclear Physics and Particle Physics (IN2P3)	Physics of heavy ions	Tomohiro UESAKA, Director, Spin Isospin Laboratory
	Normandy University	Framework	Tomohiro UESAKA, Director, Spin Isospin Laboratory
	Commissariat à l'énergie atomique et aux énergies alternatives (CEA, French Alternative Energies and Atomic Energy Commission)•Direction des Sciences de la Matière (DSM)		Tomohiro UESAKA, Director, Spin Isospin Laboratory
	The Institut National de Physique Nucléaire et de Physique des Particules CNRS (CNRS/IN2P3)	Experiments with NEBULA-Plus array	Tomohiro UESAKA, Director, Spin Isospin Laboratory
Germany	GSI	Physics of heavy ions and accelerator	Hiroyoshi SAKURAI, Director, Radioactive Isotope Physics Laboratory
	Department of Physics, Technische Universität Darmstadt	Framework	Emiko HIYAMA, Director, Strangeness Nuclear Physics Laboratory
Hungary	The Institute of Nuclear Research of the Hungarian Academy of Sciences (ATOMKI)	Nuclear physics, Atomic Physics	Tomohiro UESAKA, Director, Spin Isospin Laboratory
Indonesia	ITB, UNPAD, ITS, UGM, UI	Material science using muons at the RIKEN-RAL muon facility	Masahiko IWASAKI, Director, Meson Science Laboratory
	Hasanuddin University	Agricultural science and related fields involving heavy-ion beam mutagenesis using Indonesian crops	Tomoko ABE, Director, Beam Mutagenesis Group
Italy	National Agency for New Technologies, Energy and the Environment (ENEA)	Framework	Hiroyoshi SAKURAI, Director, Radioactive Isotope Physics Laboratory
	European Center for Theoretical Studies in Nuclear Physics and Related Areas (ECT*)	Theoretical physics	Masaaki KIMURA Director, Nuclear Many-body Theory Laboratory

Country	Partner Institute	Objects	RNC contact person
Italy	Istituto Nazionale di Fisica Nucleare (INFN)	Physics of heavy ions	Hiroyoshi SAKURAI, Director, Radioactive Isotope Physics Laboratory
Korea	College of Natural Science, Seoul National University	Nishina School	Hiroyoshi SAKURAI, Director, Radioactive Isotope Physics Laboratory
	College of Natural Science, Ewha Women's University	Framework	Tomohiro UESAKA, Director, Spin Isospin Laboratory
	College of Natural Sciences, INHA University	Framework	Emiko HIYAMA, Director, Strangeness Nuclear Physics Laboratory
Malaysia	Universiti Sains Malaysia	Muon Science	Masahiko IWASAKI, Director, Meson Science Laboratory
Norway	Faculty of Mathematics and Natural Science, University of Oslo（UiO MN）	Framework	Hiroyoshi SAKURAI, Director, Radioactive Isotope Physics Laboratory
Poland	The Henryk Niewodniczanski Institute of Nuclear Physics, Polish Academy of Sciences (IFPAN)	Framework	Hiroyoshi SAKURAI, Director, Radioactive Isotope Physics Laboratory
Romania	"Horia Hulubei" National Institute of Physics and Nuclear Engineering Bucharest-Magurele, Romania	Framework	Tomohiro UESAKA, Director, Spin Isospin Laboratory
	University of Bucharest	Framework	Tomohiro UESAKA, Director, Spin Isospin Laboratory
Russia	Joint Institute for Nuclear Research (JINR)	Framework	Tomohiro UESAKA, Director, Spin Isospin Laboratory
	Russian Research Center "Kurchatov Institute"	Framework	Hiroyoshi SAKURAI, Director, Radioactive Isotope Physics Laboratory
Switzerland	Paul Scherrer Institute	Improve the performance and reliability of accelerator systems	Osamu KAMIGAITO, Director, Accelerator Group
Taiwan	Taiwan Instrumentation Detector Consortium（TIDC）	Framework	Itaru Nakagawa, Senior Research Scientist, Radiation Laboratory
USA	Brookhaven National Laboratory	Framework	Hideto EN'YO, Director, Radiation Laboratory
	Columbia University	The development of QCDCQ	Hideto EN'YO, Director, Radiation Laboratory
	Michigan State University	Comprehensive The use of TPC (Time Projection Chamber)	Tomohiro UESAKA, Director, Spin Isospin Laboratory
UK	UK Research Innovation	Framework	Masahiko IWASAKI, Director, Meson Science Laboratory
Vietnam	Vietnam Atomic Energy Commission	Framework	
Europe	The European Organization for Nuclear Research (CERN)	R&D and application of micro-pattern gas detectors (MPGD) technology (RD51 Collaboration)	Hideto EN'YO, Director, Radiation Laboratory
	The European Organization for Nuclear Research (CERN)	Collaboration in the ALICE Experiment	Hideto EN'YO, Director, Radiation Laboratory

7. Awards

Awardee, Laboratory / Team	Award	Organization	Date
Masaomi TANAKA, Special Postdoctoral Researcher at the Radioactive Isotope Physics Laboratory	RIBF Users Group Thesis Awards 2021	RIBF USER GROUP	Aug. 6

Tomoko ABE, Director of the Beam Mutagenesis Group	Outstanding Presentation Award	Carbon Recycling Fund Institute (CRF)	Sep. 7
Tomoko ABE, Director of the Beam Mutagenesis Group	Women in PlantMutation Breeding Award	International Atomic Energy Agency (IAEA)	Sep. 20
Akira HIRAYAMA, Student Trainee at the Quantum Hadron Physics Laboratory	The Student Presentation Award	The Physical Society of Japan (JPS)	Oct. 9
Junki TANAKA, Postdoctoral Researcher at the Spin Isospin Laboratory	The 16th Young Scientist Award of the Physical Society of Japan for 2022 (the 28th KAKUDAN Best Newcomer Award)	The Physical Society of Japan (JPS)	Oct. 21
Kenta SUGIHARA, Junior Research Associate at the Safety Management Group	The Poster Presentation Award at the 2021 Symposium on Nuclear Data	Nuclear Data Division Atomic Energy Society of Japan	Nov. 18
Kanenobu TANAKA, Director of the Safety Management Group	The Poster Presentation Award at the 2021 Symposium on Nuclear Data	Nuclear Data Division Atomic Energy Society of Japan	Nov. 18
Nobuhiro SHIGYO，Visiting Scientist at the Safety Management Group	The Poster Presentation Award at the 2021 Symposium on Nuclear Data	Nuclear Data Division Atomic Energy Society of Japan	Nov. 18
Toshiya SANAMI, Visiting Scientist at the Safety Management Group	The Poster Presentation Award at the 2021 Symposium on Nuclear Data	Nuclear Data Division Atomic Energy Society of Japan	Nov. 18
Ryo TANIUCHI, Visiting Scientist at the Radioactive Isotope Physics Laboratory	The 38th Inoue Research Award for Young Scientist (2022)	Inoue Foundation for Science	Dec. 13
Tokuro FUKUI, Special Postdoctoral Researcher at the Strangeness Nuclear Physics Laboratory	The 16th Young Scientist Award of the Physical Society of Japan for 2022 (the 23rd Best Paper Award in Nuclear Theory)	The Physical Society of Japan (JPS)	Mar.15

8. RIKEN Awards

Awardee	Award	Laboratory	Date
Momo MUKAI	Ohbu Award（桜舞賞） The 13th RIKEN Researcher Incentive Awards（研究奨励賞）	Nuclear Spectroscopy Laboratory	Mar. 23
Minori TAJIMA	Ohbu Award（桜舞賞） The 13th RIKEN Technician Incentive Awards（技術奨励賞）	Nuclear Spectroscopy Laboratory	Mar. 23
Tsuneizumi KAZUHIDE, Mieko YAMADA, Katsunori ICHINOSE, and Tomoko ABE	Eiho Award（栄峰賞）	Ion Beam Breeding Team	Mar. 23
Junki TANAKA	Baiho Award（梅峰賞）	Spin isospin Laboratory	Mar. 23
Tadaaki ISOBE	Baiho Award（梅峰賞）	Radioactive Isotope Physics Laboratory	Mar. 23

9. Brief overview of the RI Beam Factory

Intensity of Primary Beams

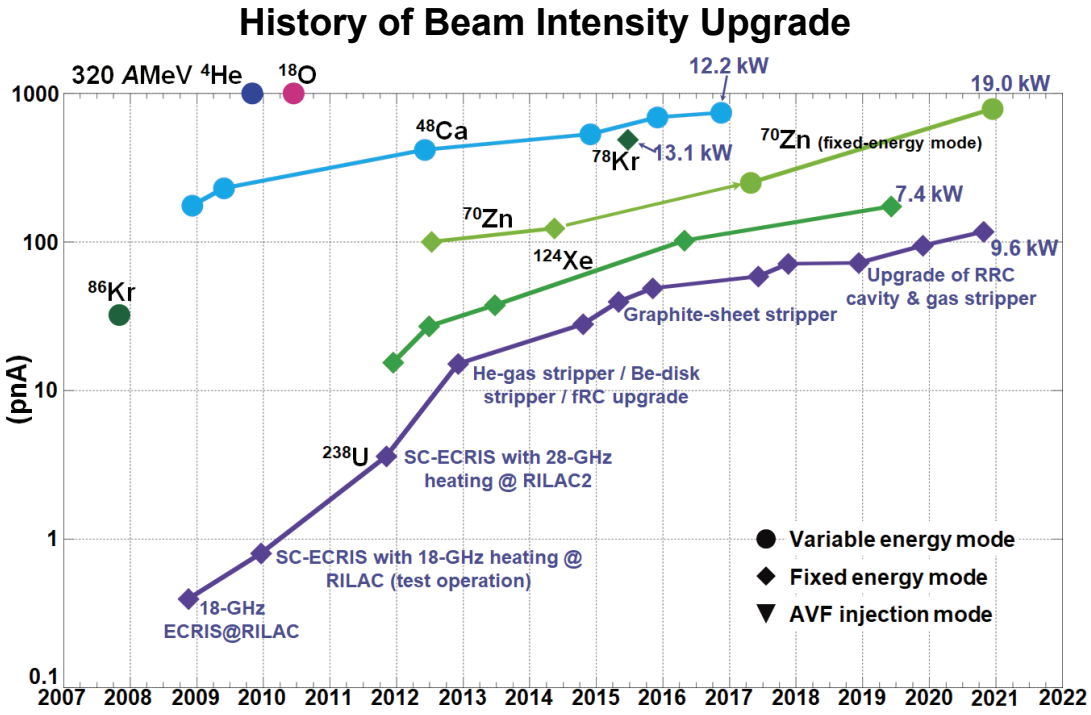

Beam energies of the beams without explicitly indicated are 345 AMeV.

Beamtime for experiments

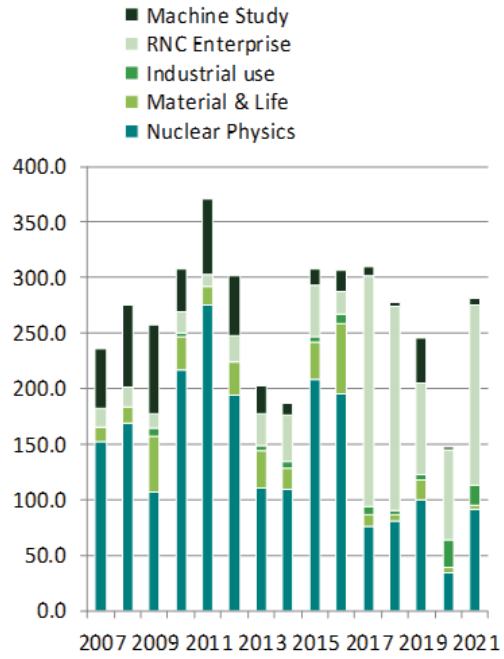

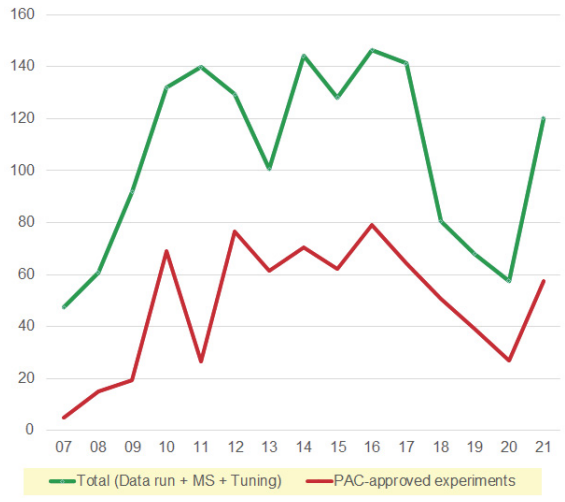

Activities of The Center Director

Meeting Attendance as Ex Officio

International Meetings

[NuPECC associate member]

∗ September 17–18, 2021, online.
∗ January 14–15, 2022, online, Belgium, hybrid.

[IUPAP WG9]

∗ June 10–11, 2021 on-line.

Domestic Meetings

[核物理委員会]

仁科センター報告，オンライン，2021 年 6 月 9 日.
仁科センター報告，オンライン，2021 年 9 月 15 日.
仁科センター報告，オンライン，2021 年 12 月 23 日.
仁科センター報告，オンライン，2022 年 3 月 16 日.

List of Publications & Presentations

Presentations

[International Conferences/Workshops]

H. Sakurai (invited), “RIKEN Nishina Center,” IEEE Nuclear Science Symposium, Online, October 22, 2021.

H. Sakurai (invited), “Research activities in nuclear physics and engineering with RIBF,” 14th Vietnam Conference on Nuclear Science and Technology (VINANST-14), Hanoi, Vietnam, Hybrid, December 9–10, 2021.

H. Sakurai (invited), “RI Beam Factory,” RIKEN-Europe Symposium 2022 “Sustainable research infrastructure for a sustainable world,” Online, Feburary 22, 2022.

H. Sakurai (invited), “Rare isotope science,” 15th Canada-Japan Joint committee on Science and Technology, Online, March 14–15, 2022.

[Domestic Conferences/Workshops]

櫻井博儀（招待講演），「理研 RIBF 高度化計画の最新情報」, 先端加速器科学技術推進協議会第 67 回技術部会, 2021 年 10 月 7 日.

櫻井博儀（招待講演），「元素を自在に変換する重イオンビームと関連技術」, 第 9 回理研イノベーションセミナー, 2022 年 1 月 21 日.

櫻井博儀（招待講演），「重イオン加速器を利用して世界人類の問題に挑む」, 第 35 回理化学研究所と産業界との交流会, 2022 年 3 月 10 日.

Nuclear Science and Transmutation Research Division
Radioactive Isotope Physics Laboratory

1. Abstract

This Laboratory works as one of core research groups conducting programs at the world-premiere heavy-ion accelerator facility of RIKEN "RI Beam Factory (RIBF)." The Laboratory explores exotic nuclear structures and dynamics in exotic nuclei that have never been investigated before, such as those with largely imbalanced proton and neutron numbers. Our aim is to develop new experimental techniques utilizing fast radioactive isotope (RI) beams at RIBF, to discover new phenomena and properties in exotic nuclei. The Laboratory is focusing three major subjects; shell evolution of very neutron-rich nuclei, the *r*-process path and equation-of-state in asymmetric nuclear matter. The Laboratory has initiated international collaborations for in-beam gamma spectroscopy, decay spectroscopy and heavy-ion induced reactions, and has formed a discussion forum for next generation gamma-ray detectors.

2. Major Research Subjects

(1) Study of structure and dynamics of exotic nuclei through developments of new tools in terms of reaction- and technique-based methodology
(2) Research on EOS in asymmetric nuclear matter via heavy-ion induced reactions
(3) Detector developments for spectroscopy and reaction studies

3. Summary of Research Activity

(1) In-beam gamma spectroscopy

In the medium and heavy mass region explored at RIBF, collective natures of nuclei are one of important subjects, which are obtained through production and observation of high excited and high spin states. To populate such states, heavy-ion induced reactions such as fragmentation, fission are useful. So far, we have developed two-step fragmentation method as an efficient method to identify and populate excited states, and lifetime measurements to deduce transition strength.

Devices utilized for the in-beam gamma spectroscopy are ZeroDegree Spectrometer (ZDS) and a NaI array DALI2. Since the end of 2008, the first spectroscopy on nuclei island-of-inversion region was performed, we have explored step-by-step new and unknown regions in the nuclear chart. The second campaign in 2009 was organized to study background components originating from atomic processes in a heavy target. Neutron-rich nuclei at $N = 20$ to 28 were studied in 2010. In 2011–2013, we conducted experiment programs for Ca-54, Ni-78, neutron-rich nuclei at $N = 82$ and neutron-deficient nuclei at $Z = 50$.

A multitude of data obtained with inelastic, nucleon knock-out, fragmentation channels have been analyzed and published. In 2011–2013, collective natures of Mg-36, 38 and Si-42 were both published in PRL. Excited states firstly observed in Ca-54 were reported in Nature to demonstrate a new nuclear magic number of 34. Fragmentation reaction has been found efficient for nuclei with $A > 100$ and low-lying excited state in Pd-126 has been successfully observed and reported in PRC. In 2019, results of the first spectrosocpy of ^{40}Mg was published in PRL, to demonstrate the exotic structure which is very different from in other neutron-rich Mg isotopes.

To further strengthen the in-beam gamma spectroscopy at RIBF, we have proposed a new setup of MINOS + DALI2 to search for the 1st excited states in even-even neutron-rich nuclei with $Z \sim 20$ to 40. The program was submitted to the PAC 2013 as a new category of proposal, "proposal for scientific program" and was S-ranked. A dedicated collaboration "SEASTAR" has been established as a subset of in-beam gamma collaboration "SUNFLOWER." The three campaigns were organized in 2014, 2015 and 2017 to study very neutron-rich isotopes, and were very productive to access very neutron-rich nuclei such as Ar-52, Ca-56, Ni-78, Kr-100, Zr-110. In 2019, the result of the first spectroscopy of Ni-78 was published in Nature.

A new project of high resolution gamma spectroscopy with fast beams "HiCARI" has been proposed at PAC 2018. MINIBALL and several Ge tracking detectors from Japan, Europe, the USA and Korea are being combined to form an array of germanium detectors. The new setup aims to accelerate researches of the nuclear structure by observing gamma-lines in even-odd nuclei and measuring lifetimes of excited states. The two workshops were organized in 2019, and the machine time of 43.5 days in total was approved at PAC 2019. A part of the HiCARI programs was successfully conducted in 2020 and 2021.

Concerning a next generation detector, a discussion forum has been established to write up a white paper on tracking germanium detectors and high-efficient crystal detectors such $LaBr_3$ and GAGG.

(2) Decay spectroscopy

Beta- and isomer-spectroscopy is an efficient method for studying nuclear structure, especially for non-yrast levels. We had accumulated experimental techniques at the RIPS facility to investigate nuclear structure in light mass region via beta-gamma and beta-*p* coincidence. Concerning the medium and heavy mass region available at RIBF, we have developed two position-sensitive active-stoppers, strip-silicon detectors and a cylindrical active stopper called CAITEN, to achieve a low-background measurement by taking correlation between heavy ion stop position and beta-ray emission position. A site of decay-spectroscopy at the new facility of RIBF is the final focal plane of ZDS, where high precision of TOF in particle identification is obtained due to a long flight path from BigRIPS to ZDS.

At the end of 2009, the first decay spectroscopy was organized with a minimum setup of four clover gamma detectors and silicon strip detectors, to study neutron-rich nuclei with $A \sim 110$. The first campaign was found successful and efficient to publish four letter articles in 2011, two PRL's and two PLB's. One of the PRL papers is associated to the *r*-process path where half-lives for 18

neutron-rich nuclei were determined for the first time. The other PRL paper reported a finding of deformed magic number 64 in the Zr isotopes.

The success of the first decay-spectroscopy campaign stimulated to form a new large-scale collaboration "EURICA," where a twelve Euroball cluster array is coupled with the silicon-strip detectors to enhance gamma efficiency by a factor of 10. A construction proposal of "EURICA" was approved in the PAC 2011, and the commissioning was successfully organized in spring 2012. Since then, physics runs had been conducted for programs approved to survey nuclei of interest as many as possible, such as Ni-78, Pd-128, Sn-100. The EURICA collaboration finished its physics programs in summer 2016. So far, 54 papers including 14 PRL's and 13 PLB's were published. One of the highlights is discovery of a seniority isomer in Pd-128, of which cascade gamma decay gives the energy of first excited state and robustness of $N = 82$ magic number, and the other is a half-life measurement for 110 neutron-rich nuclei across the $N = 82$ shell gap, which shows implications for the mechanism and universality of the *r*-process path.

Beta-delayed neutron emission probability of medium and heavy neutron-rich nuclei is important to understand nuclear structure and the *r*-process path. In 2013, a new collaboration "BRIKEN" has been established to form a He-3 detector array. A present design of the array has neutron efficiency as high as 70% up to 3 MeV. The array was coupled with the AIDA silicon strip system. A construction proposal was approved at the PAC 2013 and three physics proposals have been approved. The commissioning run was conducted in autumn 2016. The major physics runs were conducted in 2017–2021.

A new project "IDATEN" has been launched in 2021 to measure lifetime of excited states with a large size $LaBr_3$ array, which is formed by combination of FATIMA and Khala arrays. The construction proposal was submitted to PAC, 2021, and proposals with IDATEN will be evaluated at PAC, 2022.

The CAITEN detector was successfully tested with fragments produced with a Ca-48 beam in 2010.

(3) Equation-of-state via heavy-ion central collisions

Equation-of-state in asymmetric nuclear matter is one of major subjects in physics of exotic nuclei. Pi-plus and pi-minus yields in central heavy ion collisions at the RIBF energy are considered as one of EOS sensitive observables at the RIBF energy. To observe charged pions, a TPC for the SAMURAI spectrometer is being constructed under an international collaboration "SπRIT," Construction proposal was submitted at the PAC 2012, and physics proposals were approved at the PAC 2012 and 2013. The physics runs were successfully conducted in spring 2016. The first three papers were published in 2020 and 2021. One of them has been ranked as the TOP 1% paper by WoS in 2021.

An international symposium "NuSYM" on nuclear symmetry energy was organized at RIKEN July 2010 to invite researchers in three sub-fields, nuclear structure, nuclear reaction and nuclear astrophysics, and to discuss nuclear symmetry energy together. Since then, the symposium series have been held every year and been useful to encourage theoretical works and to strengthen the collaboration.

(4) Nucleon correlation and cluster in nuclei

Nucleon correlation and cluster in nuclei are matters of central focus in a "beyond mean-field" picture. The relevant programs with in-beam gamma and missing-mass techniques are to depict nucleon condensations and correlations in nuclear media as a function of density as well as temperature. Neutron-halo and -skin nuclei are objects to study dilute neutron matter at the surface. By changing excitation energies in neutron-rich nuclei, clustering phenomena and role of neutrons are to be investigated.

In 2013, two programs were conducted at the SAMURAI spectrometer. One is related to proton-neutron correlation in the C-12 nucleus via *p*-*n* knockout reaction with a carbon target. The other is to search for a cluster state in C-16, which was populated via inelastic alpha scattering. The data is being analyzed.

In 2018, a new project based on missing mass spectroscopy was launched to investigate an exotic cluster state in a very proton-rich nucleus. The experiment was organized at GANIL with combination of RIKEN liquid hydrogen target CRYPTA and the MUST2 detector array in 2018.

Members

Director

Hiroyoshi SAKURAI

Research/Technical Scientists

Pieter Christiaan DOORNENBAL (Senior Research Scientist)
Tadaaki ISOBE (Senior Research Scientist)
Akihisa KOHAMA (Senior Research Scientist)
Yoichi NAKAI (Senior Research Scientist)
Shunji NISHIMURA (Senior Research Scientist)
Daisuke SUZUKI (Research Scientist)

Contract Researcher

Nobuya NISHIMURA

Special Postdoctoral Researchers

Frank BROWNE
Masaomi TANAKA

Postdoctoral Researchers

Phong VI
Zuxing YANG

Junior Research Associate

Takuma KOIWAI (Univ. of Tokyo)

International Program Associate

Jinn Ming YAP (Univ. of Hong Kong)

Special Temporary Research Scientist

Takashi ICHIHARA

Research Consultants

Masayasu ISHIHARA
Hiroyuki MURAKAMI
Kenichi MATSUYANAGI

Senior Visiting Scientists

Koichiro ASAHI (Tokyo Tech)
Tetsuya MURAKAMI
Shigeru KUBONO (Univ. of Tokyo)

Visiting Scientists

Nori AOI (Osaka Univ.)
Megumi NIIKURA (Univ. of Tokyo)
Frank BROWNE (CERN)
Evgueni NIKOLSKI (Kurchatov Inst.)
Hue BUI (Vietnam Academy of Sci. and Tech.)
Daiki NISHIMURA (Tokyo City Univ.)
Giordano CERIZZA (Michigan State Univ.)
Takashi OHTSUBO (Niigata Univ.)
Silvio CHERUBINI (Univ. of Catania)
Akira ONO (Tohoku Univ.)
Martha Liliana CORTES SUA (TU Darmstadt)
Naohiko OTSUKA (IAEA)
Mitsunori FUKUDA (Osaka Univ.)
Kazuhiro OYAMATSU (Aichi Shukutoku Univ.)
Byungsik HONG (Korea Univ.)
Clementine Angelique Marie-Th SANTAMARIA (Berkeley Lab)
Kei IIDA (Kochi Univ.)
Natsumi IKENO (Tottori Univ.)
Paer-Anders SOEDERSTROEM (IFIN-HH)
Takuji IZUMIKAWA (Niigata Univ.)
Ryo TANIUCHI (Univ. of York)
Takashi KISHIDA (Aoyama Gakuin Univ.)
Rensheng WANG (Soochow Univ.)
Gabor KISS (ATOMKI)
Hiroshi WATANABE (Beihang Univ.)
Khiem LE (Vietnam Academy of Sci. and Tech.)
Kathrin WIMMER (GSI)
Giuseppe LORUSSO (Nat'l Phys. Lab.)
Jin WU (Argonne Nat'l Lab.)
Byul MOON (IBS)
Yasutaka YAMAMOTO (Osaka Univ.)
Yoshiharu MORI (Kyoto Univ.)

Visiting Technicians

Hilde DE WITTE (KU Leuven)
Herbert E. HESS (Univ. of Cologne)

Student Trainees

Takamichi AOKI (Univ. of Tokyo)
Nurhafiza MOHAMAD NOR (Osaka Univ.)
Linh BUI (Vietnam Atomic Energy Inst.)
Norihide NOGUCHI (Niigata Univ.)
Richard CRANE (Univ. of York)
Thomas PARRY (Univ. of Surrey)
Miki FUKUTOME (Osaka Univ.)
Takeshi SAITO (Univ. of Tokyo)
Yumo INADA (Univ. of Tokyo))
Sora SUGAWARA (Tokyo City Univ.)
Satoko IWAZAKI (Osaka Univ.)
Ryo TAGUCHI (Osaka Univ.)
Jiseok KIM (Korea Univ.)
Hiroyuki TAKAHASHI (Tokyo City Univ.)
Asahi KOHDA (Osaka Univ.)
Gen TAKAYAMA (Osaka Univ.)
Takuma KOIWAI (Univ. of Tokyo)
Hidaka TANABE (Tsukuba Univ.)
Kei KOKUBUN (Univ. of Tokyo)
Chun Yuen TSANG (Michigan State Univ.)
Haruo KONDO (Univ. of Tokyo)
Chiaki UNE (Tokyo City Univ.)
Jung Woo LEE (Korea Univ.)
Shu YAMAMURA (Univ. of Tokyo)
Rurie MIZUNO (Univ. of Tokyo)
Tik Tsun YEUNG (Univ. of Tokyo)

Part-time Workers

Kiyomi ARAI (Research Part-time Worker I)
Noriko OKAYASU (Research Part-time Worker I)
Mie DOI (Research Part-time Worker I)
Tsuneyo SUZUKI (Research Part-time Worker I)
Masanori KANEKO (Research Part-time Worker I)
Mayumi SAITO (Research Part-time Worker II)
Miki KANOU (Research Part-time Worker I)
Miyuki TAMABAYASHI (Research Part-time Worker II)
Eiko MIZUMOTO (Research Part-time Worker I)

List of Publications & Presentations

Publications

[Original Papers]

R. -B. Gerst, A. Blazhev, K. Moschner, P. Doornenbal, A. Obertelli, K. Nomura, J. -P. Ebran, S. Hilaire, J. Libert, G. Authelet, H. Baba, D. Calvet, F. Chateau, S. Chen, A. Corsi, A. Delbart, J. -M. Gheller, A. Giganon, A. Gillibert, V. Lapoux, T. Motobayashi, M. Niikura, N. Paul, J. -Y. Rousse, H. Sakurai, C. Santamaria, D. Steppenbeck, R. Taniuchi, T. Uesaka, T. Ando, T. Arici, F. Browne, A. M. Bruce, R. Caroll, L. X. Chung, M. L. Cortes, M. Dewald, B. Ding, F. Flavigny, S. Franchoo, M. Gorska, A. Gottardo, J. Jolie, A. Jungclaus, J. Lee, M. Lettmann, B. D. Linh, J. Liu, Z. Liu, C. Lizarazo, S. Momiyama, S. Nagamine, N. Nakatsuka, C. R. Nita, C. Nobs, L. Olivier, R. Orlandi, Z. Patel, Zs. Podolyak, M. Rudigier, T. Saito, C. Shand, P. -A. Soderstrom, I. Stefan, V. Vaquero, V. Werner, K. Wimmer, and Z. Xu, "γ-ray spectroscopy of low-lying yrast and non-yrast states in neutron-rich ^{94,95,96}Kr," Phys. Rev. C **105**, 024302 (2022).

S. Kim, J. Hwang, Y. Satou, N. A. Orr, T. Nakamura, Y. Kondo, J. Gibelin, N. L. Achouri, T. Aumann, H. Baba, F. Delaunay, P. Doornenbal, N. Fukuda, N. Inabe, T. Isobe, D. Kameda, D. Kanno, N. Kobayashi, T. Kobayashi, T. Kubo, S. Leblond, J. Lee, F. M. Marques, R. Minakata, T. Motobayashi, D. Murai, T. Murakami, K. Muto, T. Nakashima, N. Nakatsuka, A. Navin, S. Nishi, S. Ogoshi, H. Otsu, H. Sato, Y. Shimizu, H. Suzuki, K. Takahashi, H. Takeda, S. Takeuchi, R. Tanaka, Y. Togano, A. G. Tuff, M. Vandebrouck, and K. -I. Yoneda, "Spectroscopy of ^{17}C above the neutron separation energy," Few-Body Syst. **63**, 21 (2022).

T. Koiwai, K. Wimmer, P. Doornenbal, A. Obertelli, C. Barbieri, T. Duguet, J. D. Holt, T. Miyagi, P. Navratil, K. Ogata, N. Shimizu, V. Soma, Y. Utsuno, K. Yoshida, N. L. Achouri, H. Baba, F. Browne, D. Calvet, F. Chateau, S. Chen, N. Chiga, A. Corsi, M. L. Cortes, A. Delbart, J. -M. Gheller, A. Giganon, A. Gillibert, C. Hilaire, T. Isobe, T. Kobayashi, Y. Kubota, V. Lapoux, H. N. Liu, T. Motobayashi, I. Murray, H. Otsu, V. Panin, N. Paul, W. Rodriguez, H. Sakurai, M. Sasano, D. Steppenbeck, L. Stuhl, Y. L. Sun, Y. Togano, T. Uesaka, K. Yoneda, O. Aktas, T. Aumann, L. X. Chung, F. Flavigny, S. Franchoo, I. Gasparic, R. -B. Gerst, J. Gibelin, K. I. Hahn, D. Kim, Y. Kondo, P. Koseoglou, J. Lee, C. Lehr, B. D. Linh, T. Lokotko, M. MacCormick, K. Moschner, T. Nakamura, S. Y. Park, D. Rossi, E. Sahin, P. -A. Soderstrom, D. Sohler, S. Takeuchi, H. Toernqvist, V. Vaquero, V. Wagner, S. Wang, V. Werner, X. Xu, H. Yamada, D. Yan, Z. Yang, M. Yasuda, and L. Zanetti, "A first glimpse at the shell structure beyond ^{54}Ca: Spectroscopy of ^{55}K, ^{55}Ca, and ^{57}Ca," Phys. Lett. B **827**, 136953 (2022).

B. Le Crom, M. Assie, Y. Blumenfeld, J. Guillot, H. Sagawa, T. Suzuki, M. Honma, N. L. Achouri, B. Bastin, R. Borcea, W. N. Catford, E. Clement, L. Caceres, M. Caamano, A. Corsi, G. De France, F. Delaunay, N. De Sereville, B. Fernandez-Dominguez, M. Fisichella, S. Franchoo, A. Georgiadou, J. Gibelin, A. Gillibert, F. Hammache, O. Kamalou, A. Knapton, V. Lapoux, S. Leblond, A. O. Macchiavelli, F. M. Marques, A. Matta, L. Menager, P. Morfouace, N. A. Orr, J. Pancin, X. Pereira-Lopez, L. Perrot, J. Piot, E. Pollacco, D. Ramos, T. Roger, F. Rotaru, A. M. Sanchez-Benitez, M. Senoville, O. Sorlin, M. Stanoiu, I. Stefan, C. Stodel, D. Suzuki, J. -C. Thomas, and M. Vandebrouck, "Neutron-proton pairing in the $N = Z$ radioactive *fp*-shell nuclei ^{56}Ni and ^{52}Fe probed by pair transfer," Phys. Lett. B **829**, 137057 (2022).

W. P. Liu, Z. H. Li, J. J. He, X. D. Tang, G. Lian, J. Su, Y. P. Shen, Z. An, F. Q. Chao, J. J. Chang, L. H. Chen, H. Chen, X. J. Chen, Y. H. Chen, Z. J. Chen, B. Q. Cui, X. C. Du, X. Fang, C. B. Fu, L. Gan, B. Guo, Z. Y. Han, X. Y. Guo, G. Z. He, J. R. He, A. Heger, S. Q. Hou, H. X. Huang, N. Huang, B. L. Jia, L. Y. Jiang, S. Kubono, J. M. Li, M. C. Li, K. A. Li, E. T. Li, T. Li, Y. J. Li, M. Lugaro, X. B. Luo, H. Y. Ma, S. B. Ma, D. M. Mei, W. Nan, W. K. Nan, N. C. Qi, Y. Z. Qian, J. C. Qin, J. Ren, C. S. Shang, L. T. Sun, W. L. Sun, W. P. Tan, I. Tanihata, S. Wang, P. Wang, Y. B. Wang, Q. Wu, S. W. Xu, S. Q. Yan, L. T. Yang, Y. Yang, X. Q. Yu, Q. Yue, S. Zeng, L. Zhang, H. Zhang, H. Y. Zhang, L. Y. Zhang, N. T. Zhang, P. Zhang, Q. W. Zhang, T. Zhang, X. P. Zhang, X. Z. Zhang, W. Zhao, J. F. Zhou, and Y. Zho, "Progress of underground nuclear astrophysics experiment JUNA in China," Few-Body Syst. **63**, 43 (2022).

B. Moon, A. Gargano, H. Naidja, C. -B. Moon, A. Odahara, R. Lozeva, S. Nishimura, C. Yuan, F. Browne, P. Doornenbal, G. Lorusso, Z. Patel, S. Rice, M. Si, L. Sinclair, P. -A. Soderstrom, T. Sumikama, H. Watanabe, J. Wu, Z. Y. Xu, A. Yagi, D. S. Ahn, H. Baba, F. L. Bello Garrote, R. Daido, J. M. Daugas, F. Didierjean, Y. Fang, N. Fukuda, B. Hong, E. Ideguchi, N. Inabe, T. Ishigaki, T. Isobe, H. S. Jung, D. Kameda, I. Kojouharov, T. Komatsubara, T. Kubo, Y. K. Kwon, C. S. Lee, P. Lee, S. Morimoto, D. Murai, M. Niikura, H. Nishibata, I. Nishizuka, H. Sakurai, Y. Shimizu, H. Suzuki, H. Takeda, K. Tshoo, and R. Yokoyama, "First observation of the $\pi 0h_{11/2} \otimes \nu 0h_{9/2}$ partner orbital configuration in the odd-odd ^{138}I nucleus," Phys. Rev. C **105**, 034334 (2022).

A. Vitez-Sveiczer, A. Algora, A. I. Morales, B. Rubio, G. G. Kiss, P. Sarriguren, P. Van Isacker, G. de Angelis, F. Recchia, S. Nishimura, J. Agramunt, V. Guadilla, A. Montaner-Piza, S. E. A. Orrigo, A. Horvath, D. Napoli, S. Lenzi, A. Boso, V. H. Phong, J. Wu, P. -A. Soderstrom, T. Sumikama, H. Suzuki, H. Takeda, D. S. Ahn, H. Baba, P. Doornebal, N. Fukuda, N. Inabe, T. Isobe, T. Kubo, S. Kubono, H. Sakurai, Y. Shimizu, C. Sidong, B. Blank, P. Ascher, M. Gerbaux, T. Goigoux, J. Giovinazzo, S. Grevy, T. Kurtukian Nieto, C. Magron, W. Gelletly, Zs. Dombradi, Y. Fujita, M. Tanaka, P. Aguilera, F. Molina, J. Eberth, F. Diel, D. Lubos, C. Borcea, E. Ganioglu, D. Nishimura, H. Oikawa, Y. Takei, S. Yagi, W. Korten, G. de France, P. Davies, J. Liu, J. Lee, T. Lokotko, I. Kojouharov, N. Kurz, H. Shaffner, and A. Petrovici, "The β-decay of ^{70}Kr into ^{70}Br: Restoration of the pseudo-SU(4) symmetry," Phys. Lett. B **830**, 137123 (2022).

A. Yagi, A. Odahara, H. Nishibata, R. Lozeva, C. -B. Moon, S. Nishimura, K. Yoshida, N. Yoshinaga, C. Watanabe, K. Higashiyama, T. Shimoda, R. Daido, Y. Fang, P. S. Lee, B. Moon, P. Doornenbal, G. Lorusso, P. -A. Soderstrom, T. Sumikama, H. Watanabe, T. Isobe, H. Baba, H. Sakurai, F. Browne, Z. Patel, S. Rice, L. Sinclair, J. Wu, Z. Y. Xu, R. Yokoyama, T. Kubo, N. Inabe, H. Suzuki, N. Fukuda, D. Kameda, H. Takeda, D. S. Ahn, Y. Shimizu, D. Murai, F. L. Bello Garrote, J. -M. Daugas, F. Didierjean, E. Ideguchi, S. Iimura, T. Ishigaki, H. S. Jung, T. Komatsubara, Y. K. Kwon, C. S. Lee, S. Morimoto, M. Niikura, I. Nishizuka, and K. Tshoo, "Various nuclear structures in ^{140}Xe studied by β decay of ground and isomeric states in ^{140}I," Phys. Rev. C **105**, 044325 (2022).

D. Bazin, N. Aoi, H. Baba, J. Chen, H. Crawford, P. Doornenbal, P. Fallon, K. Li, J. Lee, M. Matsushita, T. Motobayashi, H. Sakurai, H. Scheit, D. Steppenbeck, R. Stroberg, S. Takeuchi, H. Wang, K. Yoneda, and C. X. Yuan, "Spectroscopy of ^{33}Mg with knockout reactions," Phys. Rev. C **103**, 064318 (2021).

F. Browne, S. Chen, P. Doornenbal, A. Obertelli, K. Ogata, Y. Utsuno, K. Yoshida, N. L. Achouri, H. Baba, D. Calvet, F. Chateau, N. Chiga, A. Corsi, M. L. Cortes, A. Delbart, J. -M. Gheller, A. Giganon, A. Gillibert, C. Hilaire, T. Isobe, T. Kobayashi, Y. Kubota, V. Lapoux, H. N. Liu, T. Motobayashi, I. Murray, H. Otsu, V. Panin, N. Paul, W. Rodriguez, H. Sakurai, M. Sasano, D. Steppenbeck, L. Stuhl, Y. L. Sun, Y. Togano, T. Uesaka, K. Wimmer, K. Yoneda, O. Aktas, T. Aumann, K. Boretzky, C. Caesar, L. X. Chung, F. Flavigny, S. Franchoo, I. Gasparic, R. -B. Gerst, J. Gibelin, K. I. Hahn, M. Holl, J. Kahlbow, D. Kim, D. Korper, T. Koiwai, Y. Kondo, P. Koseoglou, J. Lee, C. Lehr, B. D. Linh, T. Lokotko, M. MacCormick, K. Miki, K. Moschner, T. Nakamura, S. Y. Park, D. Rossi, E. Sahin, F. Schindler, H. Simon, P. -A. Soderstrom, D. Sohler, S. Takeuchi, H. Tornqvist, J. Tscheuschner, V. Vaquero, V. Wagner, S. Wang, V. Werner, X. Xu, H. Yamada, D. Yan, Z. Yang, M. Yasuda, and L. Zanetti, "Pairing forces govern population of doubly magic ^{54}Ca from direct reactions," Phys. Rev. Lett **126**, 252501 (2021).

S. Escrig, A. I. Morales, S. Nishimura, M. Niikura, A. Poves, Z. Y. Xu, G. Lorusso, F. Browne, P. Doornenbal, G. Gey, H. -S. Jung, Z. Li, P. -A. Soderstrom, T. Sumikama, J. Taprogge, Zs. Vajta, H. Watanabe, J. Wu, A. Yagi, K. Yoshinaga, H. Baba, S. Franchoo, T. Isobe, P. R. John, I. Kojouharov, S. Kubono, N. Kurz, I. Matea, K. Matsui, D. Mengoni, P. Morfouace, D. R. Napoli, F. Naqvi, H. Nishibata, A. Odahara, E. Sahin, H. Sakurai, H. Schaffner, I. G. Stefan, D. Suzuki, R. Taniuchi, V. Werner, and D. Sohler, "Persistence of the $Z = 28$ shell gap in $A = 75$ isobars: Identification of a possible $(1/2^-)\mu$s isomer in ^{75}Co and β decay to ^{75}Ni," Phys. Rev. C **103**, 064328 (2021).

A. Fernandez, A. Jungclaus, P. Doornenbal, M. A. Bentley, S. M. Lenzi, D. Rudolph, F. Browne, M. L. Cortes, T. Koiwai, R. Taniuchi, V. Vaquero, K. Wimmer, T. Arici, N. Imai, N. Kitamura, B. Longfellow, R. Lozeva, B. Mauss, D. R. Napoli, M. Niikura, X. Pereira-Lopez, S. Pigliapoco, A. Poves, F. Recchia, P. Ruotsalainen, H. Sakurai, S. Uthayakumaar, R. Wadsworth, and R. Yajzey, "Mirror energy differences above the $0f_{7/2}$ shell: First γ-ray spectroscopy of the $T_z = -2$ nucleus ^{56}Zn," Phys. Lett. B **823**, 136784 (2021).

V. Girard Alcindor, I. Stefan, F. de Oliveira Santos, O. Sorlin, D. Ackermann, P. Adsley, J. C. Angelique, M. Assie, M. Assuncao, D. Beaumel, E. Berthoumieux, R. Borcea, L. Caceres, I. Celikovic, M. Ciemala, V. Chudoba, G. D'Agata, F. de Grancey, G. Dumitru, F. Flavigny, C. Fougeres, S. Franchoo, A. Georgiadou, N. Goyal, S. Grevy, J. Guillot, V. Guimaraes, F. Hammache, O. Kamalou, J. Kiener, S. Koyama, L. Lalanne, V. Lapoux, I. Matea, A. Matta, A. Meyer, N. Michel, P. Morfouace, J. Mrazek, F. Negoita, M. Niikura, D. Pantelica, L. Perrot, C. Petrone, J. Piot, C. Portail, T. Roger, F. Rotaru, A. M. Sanchez-Benitez, N. de Sereville, M. Stanoiu, C. Stodel, K. Subotic, D. Suzuki, V. Tatischeff, J. C. Thomas, P. Ujic, and D. Verney, "Probing nuclear forces beyond the nuclear drip line: the cases of ^{16}F and ^{15}F." Eur. Phys. J. A **57**, 93 (2021).

O. Hall, T. Davinson, A. Estrade, J. Liu, G. Lorusso, F. Montes, S. Nishimura, V. H. Phong, P. J. Woods, J. Agramunt, D. S. Ahn, A. Algora, J. M. Allmond, H. Baba, S. Bae, N. T. Brewer, C. G. Bruno, R. Caballero-Folch, F. Calvino, P. J. Coleman-Smith, G. Cortes, I. Dillmann, C. Domingo-Pardo, A. Fijalkowska, N. Fukuda, S. Go, C. J. Griffin, R. Grzywacz, J. Ha, L. J. Harkness-Brennan, T. Isobe, D. Kahl, L. H. Khiem, G. G. Kiss, A. Korgul, S. Kubono, M. Labiche, I. Lazarus, J. Liang, Z. Liu, K. Matsui, K. Miernik, B. Moon, A. I. Morales, P. Morrall, M. R. Mumpower, N. Nepal, R. D. Page, M. Piersa, V. F. E. Pucknell, B. C. Rasco, B. Rubio, K. P. Rykaczewski, H. Sakurai, Y. Shimizu, D. W. Stracener, T. Sumikama, H. Suzuki, J. L. Tain, H. Takeda, A. Tarifeno-Saldivia, A. Tolosa-Delgado, M. Wolinska-Cichocka, and R. Yokoyama, "β-delayed neutron emission of r-process nuclei at the $N = 82$ shell closure," Phys. Lett. B **816**, 136266 (2021).

J. Hu, H. Yamaguchi, Y. H. Lam, A. Heger, D. Kahl, A. M. Jacobs, Z. Johnston, S. W. Xu, N. T. Zhang, S. B. Ma, L. H. Ru, E. Q. Liu, T. Liu, S. Hayakawa, L. Yang, H. Shimizu, C. B. Hamill, A. St J. Murphy, J. Su, X. Fang, K. Y. Chae, M. S. Kwag, S. M. Cha, N. N. Duy, N. K. Uyen, D. H. Kim, R. G. Pizzone, M. La Cognata, S. Cherubini, S. Romano, A. Tumino, J. Liang, A. Psaltis, M. Sferrazza, D. Kim, Y. Y. Li, and S. Kubono, "Advancement of photospheric radius expansion and clocked type-I X-ray burst models with the new ^{22}Mg$(\alpha, p)^{25}$Al reaction rate determined at the Gamow energy," Phys. Rev. Lett. **127**, 172701 (2021).

S. W. Huang, Z. H. Yang, F. M. Marques, N. L. Achouri, D. S. Ahn, T. Aumann, H. Baba, D. Beaumel, M. Bohmer, K. Boretzky, M. Caamano, S. Chen, N. Chiga, M. L. Cortes, D. Cortina, P. Doornenbal, C. A. Douma, F. Dufter, J. Feng, B. Fernandez-Dominguez, Z. Elekes, U. Forsberg, T. Fujino, N. Fukuda, I. Gasparic, Z. Ge, R. Gernhauser, J. M. Gheller, J. Gibelin, A. Gillibert, Z. Halasz, T. Harada, M. N. Harakeh, A. Hirayama, N. Inabe, T. Isobe, J. Kahlbow, N. Kalantar-Nayestanaki, D. Kim, S. Kim, S. Kiyotake, T. Kobayashi, Y. Kondo, P. Koseoglou, Y. Kubota, I. Kuti, C. Lehr, C. Lenain, P. J. Li, Y. Liu, Y. Maeda, S. Masuoka, M. Matsumoto, A. Matta, J. Mayer, H. Miki, M. Miwa, B. Monteagudo, I. Murray, T. Nakamura, A. Obertelli, N. A. Orr, H. Otsu, V. Panin, S. Park, M. Parlog, S. Paschalis, M. Potlog, S. Reichert, A. Revel, D. Rossi, A. Saito, M. Sasano, H. Sato, H. Scheit, F. Schindler, T. Shimada, Y. Shimizu, S. Shimoura, H. Simon, I. Stefan, S. Storck, L. Stuhl, H. Suzuki, D. Symochko, H. Takeda, S. Takeuchi, J. Tanaka, Y. Togano, T. Tomai, H. T. Tornqvist, E. Tronchin, J. Tscheuschner, T. Uesaka, V. Wagner, K. Wimmer, H. Yamada, B. Yang, L. Yang, Y. Yasuda, K. Yoneda, L. Zanetti, and J. Zenihiro, "Experimental study of ^4n by directly detecting the decay neutrons," Few-Body Syst. **62**, 102 (2021).

S. Y. Jin, S. T. Wang, J. Lee, A. Corsi, K. Wimmer, F. Browne, S. Chen, M. L. Cortes, P. Doornenbal, T. Koiwai, C. X. Yuan, A. Algora, D. Brugnara, J. Cederkall, J. Gerl, M. Gorska, G. Hafner, K. Kokubun, P. Koseoglou, S. Kubono, P. Li, P. Liang, J. Liu, Z. Liu, T. Lokotko, J. Park, H. Sakurai, L. G. Sarmiento, Z. Y. Sun, R. Taniuchi, W. Xian, and I. Zanon, "Spectroscopy of ^{98}Cd by two-nucleon removal from ^{100}In," Phys. Rev. C **104**, 024302 (2021).

M. M. Juhasz, Z. Elekes, D. Sohler, K. Sieja, K. Yoshida, K. Ogata, P. Doornenbal, A. Obertelli, H. Baba, F. Browne, D. Calvet, F. Chateau, S. Chen, N. Chiga, A. Corsi, M. L. Cortes, A. Delbart, J. -M. Gheller, A. Giganon, A. Gillibert, C. Hilaire, T. Isobe, T. Kobayashi, Y. Kubota, V. Lapoux, T. Motobayashi, I. Murray, H. Otsu, V. Panin, N. Paul, W. Rodriguez, H. Sakurai, M. Sasano, D. Steppenbeck, L. Stuhl, Y. L. Sun, Y. Togano, T. Uesaka, K. Wimmer, K. Yoneda, N. L. Achouri, O. Aktas, T. Aumann, L. X. Chung, Zs. Dombradi, F. Flavigny, S. Franchoo, I. Gasparic, R. -B. Gerst, J. Gibelin, K. I. Hahn, D. Kim, T. Koiwai, Y. Kondo, P. Koseoglou, J. Lee, C. Lehr, B. D. Linh, H. N. Liu, T. Lokotko, M. MacCormick, K. Moschner, T. Nakamura, S. Y. Park, D. Rossi, E. Sahin, P. -A. Soderstrom, S. Takeuchi, H. Tornqvist, V. Vaquero, V. Wagner, S. Wang, V. Werner, X. Xu, H. Yamada, D. Yan, Z. Yang, M. Yasuda, and L. Zanetti, "First spectroscopic study of ^{63}V at the $N = 40$ island of inversion," Phys. Rev. C **103**, 064308 (2021).

M. Kaneko, T. Murakami, T. Isobe, M. Kurata-Nishimura, A. Ono, N. Ikeno, J. Barney, G. Cerizza, J. Estee, G. Jhang, J. W. Lee, W. G. Lynch, C. Santamaria, C. Y. Tsang, M. B. Tsang, R. Wang, D. S. Ahn, L. Atar, T. Aumann, H. Baba, K. Boretzky, J. Brzychczyk,

N. Chiga, N. Fukuda, I. Gasparic, B. Hong, A. Horvat, T. Ichihara, K. Ieki, N. Inabe, Y. J. Kim, T. Kobayashi, Y. Kondo, P. Lasko, H. S. Lee, Y. Leifels, J. Lukasik, J. Manfredi, A. B. McIntosh, P. Morfouace, T. Nakamura, N. Nakatsuka, S. Nishimura, R. Olsen, H. Otsu, P. Pawlowski, K. Pelczar, D. Rossi, H. Sakurai, H. Sato, H. Scheit, R. Shane, Y. Shimizu, H. Simon, T. Sumikama, D. Suzuki, H. Suzuki, H. Takeda, S. Tangwancharoen, Y. Togano, H. Tornqvist, Z. Xiao, S. J. Yennello, J. Yurkon, and Y. Zhang, "Rapidity distributions of $Z = 1$ isotopes and the nuclear symmetry energy from Sn+Sn collisions with radioactive beams at 270 MeV/nucleon," Phys. Lett. B **822**, 136681 (2021).

A. Kubiela, H. Suzuki, O. B. Tarasov, M. Pfutzner, D. -S. Ahn, H. Baba, A. Bezbakh, A. A. Ciemny, W. Dominik, N. Fukuda, A. Giska, R. Grzywacz, Y. Ichikawa, Z. Janas, L. Janiak, G. Kaminski, K. Kawata, T. Kubo, M. Madurga, C. Mazzocchi, H. Nishibata, M. Pomorski, Y. Shimizu, N. Sokolowska, D. Suzuki, P. Szymkiewicz, A. Swiercz, M. Tajima, A. Takamine, H. Takeda, Y. Takeuchi, C. R. Thornsberry, H. Ueno, H. Yamazaki, R. Yokoyama, and K. Yoshida, "Production of the most neutron-deficient Zn isotopes by projectile fragmentation of ^{78}Kr," Phys. Rev. C **104**, 064610 (2021).

L. Lalanne, O. Sorlin, M. Assie, F. Hammache, N. de Sereville, S. Koyama, D. Suzuki, F. Flavigny, D. Beaumel, Y. Blumenfeld, B. A. Brown, F. De Oliveira Santos, F. Delaunay, S. Franchoo, J. Gibelin, V. Girard Alcindor, J. Guillot, O. Kamalou, N. Kitamura, V. Lapoux, A. Lemasson, A. Matta, B. Mauss, P. Morfouace, M. Niikura, J. Pancin, A. Poves, T. Roger, T. Saito, C. Stodel, and J. -C. Thomas, "Evaluation of the ^{35}K$(p,\gamma)^{36}$Ca reaction rate using the ^{37}Ca$(p,d)^{36}$Ca transfer reaction," Phys. Rev. C **103**, 055809 (2021).

B. D. Linh, A. Corsi, A. Gillibert, A. Obertelli, P. Doornenbal, C. Barbieri, S. Chen, L. X. Chung, T. Duguet, M. Gomez-Ramos, J. D. Holt, A. Moro, P. Navratil, K. Ogata, N. T. T. Phuc, N. Shimizu, V. Soma, Y. Utsuno, N. L. Achouri, H. Baba, F. Browne, D. Calvet, F. Chateau, N. Chiga, M. L. Cortes, A. Delbart, J. -M. Gheller, A. Giganon, C. Hilaire, T. Isobe, T. Kobayashi, Y. Kubota, V. Lapoux, H. N. Liu, T. Motobayashi, I. Murray, H. Otsu, V. Panin, N. Paul, W. Rodriguez, H. Sakurai, M. Sasano, D. Steppenbeck, L. Stuhl, Y. L. Sun, Y. Togano, T. Uesaka, K. Wimmer, K. Yoneda, O. Aktas, T. Aumann, F. Flavigny, S. Franchoo, I. Gasparic, R. -B. Gerst, J. Gibelin, K. I. Hahn, N. T. Khai, D. Kim, T. Koiwai, Y. Kondo, P. Koseoglou, J. Lee, C. Lehr, T. Lokotko, M. MacCormick, K. Moschner, T. Nakamura, S. Y. Park, D. Rossi, E. Sahin, D. Sohler, P. -A. Soderstrom, S. Takeuchi, N. D. Ton, H. Tornqvist, V. Vaquero, V. Wagner, H. Wang, V. Werner, X. Xu, Y. Yamada, D. Yan, Z. Yang, M. Yasuda, and L. Zanetti, "Investigation of the ground-state spin inversion in the neutron-rich ^{47,49}Cl isotopes," Phys. Rev. C **104**, 044331 (2021).

J. E. Riley, A. M. Laird, N. de Sereville, A. Parikh, S. P. Fox, F. Hammache, I. Stefan, P. Adsley, M. Assie, B. Bastin, F. Boulay, A. Coc, S. Franchoo, R. Garg, S. A. Gillespie, V. Guimaraes, C. Hamadache, N. Hubbard, J. Kiener, A. Lefebvre-Schuhl, F. de Oliveira Santos, A. Remadi, L. Perrot, D. Suzuki, G. Verde, V. Tatischeff, and M. Williams, "Sub-threshold states in ^{19}Ne relevant to ^{18}F$(p,\alpha)^{15}$O," Phys. Rev. C **103**, 015807 (2021).

Y. Shigekawa, A. Yamaguchi, K. Suzuki, H. Haba, T. Hiraki, H. Kikunaga, T. Masuda, S. Nishimura, N. Sasao, A. Yoshimi, and K. Yoshimura, "Estimation of radiative half-life of ^{229m}Th by half-life measurement of other nuclear excited states in ^{229}Th," Phys. Rev. C **104**, 024306 (2021).

M. Tsumura, T. Kawabata, Y. Takahashi, S. Adachi, H. Akimune, S. Ashikaga, T. Baba, Y. Fujikawa, H. Fujimura, H. Fujioka, T. Furuno, T. Hashimoto, T. Harada, M. Ichikawa, K. Inaba, Y. Ishii, N. Itagaki, M. Itoh, C. Iwamoto, N. Kobayashi, A. Koshikawa, S. Kubono, Y. Maeda, Y. Matsuda, S. Matsumoto, K. Miki, T. Morimoto, M. Murata, T. Nanamura, I. Ou, S. Sakaguchi, A. Sakaue, M. Sferrazza, K. N. Suzuki, T. Takeda, A. Tamii, K. Watanabe, Y. N. Watanabe, H. P. Yoshida, and J. Zenihiro, "First experimental determination of the radiative-decay probability of the 3^-_1 state in ^{12}C for estimating the triple alpha reaction rate in high temperature environments," Phys. Lett. B **817**, 136283 (2021).

H. Watanabe, C. X. Yuan, G. Lorusso, S. Nishimura, Z. Y. Xu, T. Sumikama, P. -A. Soderstrom, P. Doornenbal, F. Browne, G. Gey, H. S. Jung, J. Taprogge, Zs. Vajta, H. K. Wang, J. Wu, A. Yagi, H. Baba, G. Benzoni, K. Y. Chae, F. C. L. Crespi, N. Fukuda, R. Gernhauser, N. Inabe, T. Isobe, A. Jungclaus, D. Kameda, G. D. Kim, Y. K. Kim, I. Kojouharov, F. G. Kondev, T. Kubo, N. Kurz, Y. K. Kwon, G. J. Lane, Z. Li, C. -B. Moon, A. Montaner-Piza, K. Moschner, F. Naqvi, M. Niikura, H. Nishibata, D. Nishimura, A. Odahara, R. Orlandi, Z. Patel, Zs. Podolyak, H. Sakurai, H. Schaffner, G. S. Simpson, K. Steiger, H. Suzuki, H. Takeda, A. Wendt, and K. Yoshinaga, "Impact of shell evolution on Gamow-Teller β decay from a high-spin long-lived isomer in ^{127}Ag," Phys. Lett. B **823**, 136766 (2021).

K. Wimmer, F. Recchia, S. M. Lenzi, S. Riccetto, T. Davinson, A. Estrade, C. J. Griffin, S. Nishimura, V. Phong, P. -A. Soderstrom, O. Aktas, M. Al-Aqeel, T. Ando, H. Baba, S. Bae, S. Choi, P. Doornenbal, J. Ha, L. Harkness-Brennan, T. Isobe, P. R. John, D. Kahl, G. Kiss, I. Kojouharov, N. Kurz, M. Labiche, K. Matsui, S. Momiyama, D. R. Napoli, M. Niikura, C. Nita, Y. Saito, H. Sakurai, H. Schaffner, P. Schrock, C. Stahl, T. Sumikama, V. Werner, W. Witt, and P. J. Woods, "Isomeric states in neutron-rich nuclei near $N = 40$," Phys. Rev. C **104**, 014304 (2021).

D. Wu, C. L. Bai, H. Sagawa, S. Nishimura, and H. Q. Zhang, "β-delayed one-neutron emission probabilities within a neural network model," Phys. Rev. C **104**, 054303 (2021).

R. Yokoyama, E. Ideguchi, G. S. Simpson, M. Tanaka, Y. Sun, C. -J. Lv, Y. -X. Liu, L. -J. Wang, S. Nishimura, P. Doornenbal, G. Lorusso, P. -A. Soderstrom, T. Sumikama, J. Wu, Z. Y. Xu, N. Aoi, H. Baba, F. L. Bello Garrote, G. Benzoni, F. Browne, R. Daido, Y. Fang, N. Fukuda, A. Gottardo, G. Gey, S. Go, S. Inabe, T. Isobe, D. Kameda, K. Kobayashi, M. Kobayashi, I. Kojouharov, T. Komatsubara, T. Kubo, N. Kurz, I. Kuti, Z. Li, M. Matsushita, S. Michimasa, C. B. Moon, H. Nishibata, I. Nishizuka, A. Odahara, Z. Patel, S. Rice, E. Sahin, H. Sakurai, H. Schaffner, L. Sinclair, H. Suzuki, H. Takeda, J. Taprogge, Zs. Vajta, H. Watanabe, and A. Yagi, "Three-quasiparticle isomers in odd-even ^{159,161}Pm: Calling for modified spin-orbit interaction for the neutron-rich region," Phys. Rev. C **104**, L021303 (2021).

S. Hayakawa, M. La Cognata, L. Lamia, H. Yamaguchi, D. Kahl, K. Abe, H. Shimizu, L. Yang, O. Beliuskina, S. M. Cha, K. Y. Chae, S. Cherubini, P. Figuera, Z. Ge, M. Gulino, J. Hu, A. Inoue, N. Iwasa, A. Kim, D. Kim, G. Kiss, S. Kubono, M. La Commara, M. Lattuada, E. J. Lee, J. Y. Moon, S. Palmerini, C. Parascandolo, S. Y. Park, V. H. Phong, D. Pierroutsakou, R. G. Pizzone, G. G. Rapisarda, S. Romano, C. Spitaleri, X. D. Tang, O. Trippella, A. Tumino, and N. T. Zhang, "Constraining the primordial lithium abundance: New cross section measurement of the ^{7}Be + n reactions updates the total ^{7}Be destruction rate," Astrophys. J. Lett. **915**, L13 (2021).

J. Estee, W. G. Lynch, C. Y. Tsang, J. Barney, G. Jhang, M. B. Tsang, R. Wang, M. Kaneko, J. W. Lee, T. Isobe, M. Kurata-Nishimura, T. Murakami, D. S. Ahn, L. Atar, T. Aumann, H. Baba, K. Boretzky, J. Brzychczyk, G. Cerizza, N. Chiga, N. Fukuda, I. Gasparic, B. Hong, A. Horvat, K. Ieki, N. Inabe, Y. J. Kim, T. Kobayashi, Y. Kondo, P. Lasko, H. S. Lee, Y. Leifels, J. Lukasik, J. Manfredi, A. B. McIntosh, P. Morfouace, T. Nakamura, N. Nakatsuka, S. Nishimura, H. Otsu, P. Pawlowski, K. Pelczar, D. Rossi, H. Sakurai, C. Santamaria, H. Sato, H. Scheit, R. Shane, Y. Shimizu, H. Simon, K. Snoch, A. Sochocka, T. Sumikama, H. Suzuki, D. Suzuki, H. Takeda, S. Tangwancharoen, Y. Togano, H. Tornqvist, Z. Xiao, S. J. Yennello, Y. Zhang, and M. D. Cozma, "Probing the symmetry energy with the spectral pion ratio," Phys. Rev. Lett **126**, 162701 (2021).

J. Barney, J. Estee, W. G. Lynch, T. Isobe, G. Jhang, M. Kurata-Nishimura, A. B. McIntosh, T. Murakami, R. Shane, S. Tangwancharoen, M. B. Tsang, G. Cerizza, M. Kaneko, J. W. Lee, C. Y. Tsang, R. Wang, C. Anderson, H. Baba, Z. Chajecki,M. Famiano, R. Hodges-Showalter, B. Hong, T. Kobayashi, P. Lasko, J. Lukasik, N. Nakatsuka, R. Olsen, H. Otsu, P. Pawlowski, K. Pelczar, H. Sakurai, C. Santamaria, H. Setiawan, A. Taketani,J. R. Winkelbauer, Z. Xiao, S. J. Yennello, J. Yurkon, and Y. Zhang, "The SπRIT time projection chamber," Rev. Sci. Instrum. **92**, 063302 (2021).

S. Koyama, D. Suzuki, M. Assie, N. Kitamura, L. Lalanne, M. Niikura, H. Otsu, T. Y. Saito, and O. Sorlin, "A liquid hydrogen target for radioactive beam experiments using the missing mass method," Nucl. Instrum. Methods Phys. Res. A **1010**, 165477 (2021).

H. Baba, T. Ichihara, T. Isobe, T. Ohnishi, K. Yoshida, Y. Watanabe, S. Ota, H. Shimizu, S. Shimoura, S. Takeuchi, D. Nishimura, J. Zenihiro, A. O. Tokiyasu, and R. Yokoyama, "MPV-parallel readout architecture for the VME data acquisition system," IEEE Trans. Nucl. Sci. **68**, 1841 (2021).

T. Okumura, T. Azuma, D. A. Bennett, P. Caradonna,I. H. Chiu, W. B Doriese, M. S. Durkin, J. W. Fowler, J. D. Gard, T. Hashimoto, R. Hayakawa, G. C. Hilton, Y. Ichinohe, P. Indelicato, T. Isobe, S. Kanda, M. Katsuragawa, N. Kawamura, Y. Kino, K. Mine, Y. Miyake, K. M. Morgan, K. Ninomiya, H. Noda, G. C. O'Neil, S. Okada, K. Okutsu, T. Osawa, N. Paul, C. D. Reintsema, D. R. Schmidt, K. Shimomura, P. Strasser, H. Suda, D. S. Swetz, T. Takahashi, S. Takeda, S. Takeshita, H. Tatsuno, Y. Ueno, J. N., Ullom, S. Watanabe, and S. Yamada, "Dynamical response of transition-edge sensor microcalorimeters to a pulsed charged-particle beam," IEEE Trans. Appl. Supercond. **31**, 2101704 (2021).

M. Holl *et al*. (SAMURAI21 Collaboration), "Border of the island of inversion: Unbound states in ^{29}Ne," Phys. Rev. C **105**, 034301 (2021).

H. Grawe, K. Straub, T. Faestermann, M. Górska, C. Hinke, R. Krücken, F. Nowacki, M. Böhmer, P. Boutachkov, H. Geissel, R. Gernhäuser, A. Gottardo, J. Grebosz, N. Kurz, Z. Liu, L. Maier, S. Pietri, Zs. Podolyák, K. Steiger, H. Weick, H. J. Wollersheim, P. J. Woods, N. Al-Dahan, N. Alkhomashi, A. Ataç, A. Blazhev, N. Braun, T. Davinson, I. Dillmann, C. Domingo-Pardo, P. Doornenbal, G. Farrelly, F. Farinon, G.de France, J. Gerl, N. Goel, T. Habermann, R. Hoischen, R. Janik, M. Karny, A. Kaskas, I. Kojouharov, Th. Kröll, M. Lewitowicz, Yu.A. Litvinov, S. Myalski, F. Nebel, S. Nishimura, C. Nociforo, J. Nyberg, A. Parikh, A. Procházka, P. H. Regan, C. Rigollet, H. Schaffner, C. Scheidenberger, S. Schwertel, P. -A. Söderström, S. Steer, A. Stolz, P. Strmeň, and the RISING Collaboration, "The (6^+) isomer in ^{102}Sn revisited: Neutron and proton effective charges close to the double shell closure," Phys. Lett. B **820**, 136591 (2021).

[Review Article]

A. A. Aziz, N. S. Ahmad, S. Ahn, W. Aoki, M. Bhuyan, K. J. Chen, G. Guo, K. I. Hahn, T. Kajino, H. Abu Kassim, D. Kim, S. Kubono, M. Kusakabe, A. Li, H. N. Li, Z. H. Li, W. P. Liu, Z. W. Liu, T. Motobayashi, K. C. Pan, T. -S. Park, J. R. Shi, X. D. Tang, W. Wang, L. J. Wen, M. R. Wu H. L. Yan, and N. Yusof, "Progress in nuclear astrophysics of east and southeast Asia," AAPPS Bulletin **31**, 18 (2021).

Presentations

[Seminars]

R. Taniuchi, "Gamma-ray spectroscopy in the vicinity of double-magic ^{78}Ni," NUSTAR Seminar, Online/GSI, Germany, June 2, 2021.

櫻井博儀, 「現代の錬金術による元素変換科学—元素合成, 魔法数から核変換まで—」, 日本物理学会第 5 回オンライン物理講話, 2021 年 10 月 23 日.

Award

谷内稜, 第 38 回 井上研究奨励賞（Inoue Research Award for Young Scientists）, 公益財団法人 井上科学振興財団, 2022 年 2 月 4 日.

Press Releases

「高密度な中性子物質の硬さの測定に初めて成功—中性子星内の状態を実験室で再現—」, 2021 年 5 月 11 日.

「荷電対称性の破れを発見—クリプトン-70 とセレン-70 の形状は大きく異なっていた—」, 2021 年 5 月 19 日.

Outreach Activity

櫻井博儀, 2021 年度「はかる！」, 埼玉県立不動岡高等学校.

Nuclear Science and Transmutation Research Division
Spin isospin Laboratory

1. Abstract

The Spin Isospin Laboratory pursues research activities putting primary focus on interplay of spin and isospin in exotic nuclei. Understanding nucleosyntheses in the universe, especially those in *r*- and *rp*-processes is another big goal of our laboratory.

Investigations on isospin dependences of nuclear equation of state, spin-isospin responses of exotic nuclei, occurrence of various correlations at low-densities, evolution of spin-orbit coupling are main subjects along the line. We are leading a mass measurement project with the Rare RI Ring project, too. Through the experimental studies, we will be able to elucidate a variety of nuclear phenomena in terms of interplay of spin and isospin, which will in turn, lead us to better understanding of our universe.

2. Major Research Subjects

(1) Direct reaction studies of neutron-matter equation of state
(2) Study of spin-isospin responses with RI-beams
(3) *r*-process nucleosynthesis study with heavy-ion storage ring
(4) Application of spin-polarization technique to RI-beam experiments and other fields
(5) Development of special targets for RI-beam experiments

3. Summary of Research Activity

(1) Direct reaction studies of neutron matter equation of state

Direct reactions induced by light-ions serve as powerful tools to investigate various aspects of nuclei. We are advancing experimental programs to explore equation of state of neutron matter, via light-ion induced reactions with RI-beams.

(1-1) Determination of a neutron skin thickness by proton elastic scattering

A neutron skin thickness is known to have strong relevance to asymmetry terms of nuclear equation of state, especially to a term proportional to density. The ESPRI project aims at determining density distributions in exotic nuclei precisely by proton elastic scattering at 200–300 MeV/nucleon. An experiment for ^{132}Sn that is a flagship in this project has been successfully performed.

(1-2) Asymmetry terms in nuclear incompressibility

Nuclear incompressibility represents stiffness of nuclear matter. Incompressibility of symmetric nuclear matter is determined to be 230 ± 20 MeV, but its isospin dependence still has a large uncertainty at present. A direct approach to the incompressibility of asymmetric nuclear matter is an experimental determination of energies of isoscalar giant monopole resonances (GMR) in heavy nuclei. We have developed, in close collaboration with Center for Nuclear Study (CNS) of University of Tokyo, an active gas target for deuteron inelastic scattering experiments to determine GMR energies. The active gas target has been already tested with oxygen and xenon beams at HIMAC and finally has been applied to a ^{132}Sn experiment at RIBF.

(1-3) Multi-neutron and α-cluster correlations at low densities

Occurrences of multi-neutron and α-cluster correlations are other interesting aspects of nuclear matter and define its low-density behavior. The multi-neutron and α-cluster correlations can be investigated with the large-acceptance SAMURAI spectrometer. The SAMURAI has been already applied to experiments to explore light neutron-rich nuclei close to the dripline. We plan to reinforce experimental capabilities of the SAMURAI by introducing advanced devices such as MINOS (Saclay) and NeuLAND (GSI).

(1-4) Fission barrier heights in neutron-rich heavy nuclei

The symmetry energy has a strong influence on fission barrier heights in neutron-rich nuclei. Knowledge on the fission barrier heights, which is quite poor at present, is quite important for our proper understanding on termination of the *r*-process. We are planning to perform, in collaboration with the TU Munich group, $(p, 2p)$-delayed fission experiments at the SAMURAI to determine the fission barrier heights in neutron-rich nuclei in Pb region.

(2) Study of spin-isospin responses with RI-beams

The study of spin-isospin responses in nuclei forms one of the important cores of nuclear physics. A variety of collective states, for example isovector giant dipole resonances, isobaric analogue states, Gamow-Teller resonances, have been extensively studied by use of electromagnetic and hadronic reactions from stable targets.

The research opportunities can be largely enhanced with light of availabilities of radioactive isotope (RI) beams and of physics of unstable nuclei. There are three possible directions to proceed. The first direction is studies of spin-isospin responses of unstable nuclei via inverse-kinematics charge exchange reactions. A neutron-detector array WINDS has been constructed, under a collaboration of CNS, Tokyo and RIKEN, for inverse kinematics (p, n) experiments at the RI Beam Factory. We have already applied WINDS to the (p, n) experiments for ^{12}Be, ^{132}Sn and plan to extend this kind of study to other exotic nuclei.

The second direction is studies with RI-beam induced charge exchange reaction. RI-beam induced reactions have unique properties which are missing in stable-beam induced reactions and can be used to reach the yet-to-be-discovered states. We have constructed the SHARAQ spectrometer and the high-resolution beam-line at the RI Beam Factory to pursue the capabilities of RI-beam induced reactions as new probes to nuclei. One of the highlights is an observation of β^+ type isovector spin monopole resonances (IVSMR) in ^{208}Pb and ^{90}Zr via the $(t, {}^3\mathrm{He})$ reaction at 300 MeV/nucleon.

The third direction is studies of neutron- and proton-rich nuclei via stable-beam induced charge exchange reactions, which is conducted under collaboration with Research Center for Nuclear Physics (RCNP), Osaka University. We have performed the double

charge exchange ^{12}C(^{18}O, ^{18}Ne)^{12}Be reaction at 80 MeV/nucleon to investigate structure of a neutron-rich ^{12}Be nucleus. Peaks corresponding to ground and excited levels in ^{12}Be have been clearly observed. Another double charge exchange reaction, (^{12}C, ^{12}Be(0_2^+)) are being used to search for double Gamow-Teller resonances.

(3) *r*-process nucleosynthesis study with heavy-ion storage ring

Most of the *r*-process nuclei become within reach of experimental studies for the first time at RI Beam Factory at RIKEN. The Rare RI Ring at RIBF is the unique facility with which we can perform mass measurements of *r*-process nuclei. Construction of the Rare RI Ring started in FY2012 in collaboration with Tsukuba and Saitama Universities. A major part of the ring has been completed and the commissioning run is planned in FY2014.

We are planning to start precise mass measurements of *r*-process nuclei soon. A series of experiments will start with nuclei in the $A = 80$ region and will be extended to heavier region.

(4) Application of spin-polarization technique to RI-beam experiments and other fields

A technique to produce nuclear polarization by means of electron polarization in photo-excited triplet states of aromatic molecules can open new applications. The technique is called "Tripletd-DNP." A distinguished feature of Triplet-DNP is that it works under a low magnetic field of 0.1–0.7 T and temperature higher than 100 K, which exhibits a striking contrast to standard dynamic nuclear polarization (DNP) techniques working in extreme conditions of several Tesla and sub-Kelvin.

We have constructed a polarized proton target system for use in RI-beam experiments. Recent experimental and theoretical studies have revealed that spin degrees of freedom play a vital role in exotic nuclei. Tensor force effects on the evolution of shell and possible occurrence of *p*-*n* pairing in the proton-rich region are good examples of manifestations of spin degrees of freedom. Experiments with the target system allow us to explore the spin effects in exotic nuclei. It should be noted that we have recently achieved a proton polarization of 40% at room temperature in a pentacene-d_{14} doped *p*-terphenyl crystal.

Another interesting application of Triplet-DNP is sensitivity enhancement in NMR spectroscopy of biomolecules. We started a new project to apply the Triplet-DNP technique to study protein-protein interaction via two-dimensional NMR spectroscopy, in close collaboration with biologists and chemists.

(5) Development of special targets for RI-beam experiments

For the research activities shown above, we are developing and hosting special targets for RI-beam experiments listed below:

(a) Polarized proton target (described in (4))
(b) Thin solid hydrogen target
(c) MINOS (developed at Saclay and hosted by the Spin Isospin Laboratory)

Members

Director
Tomohiro UESAKA

Senior Research Scientists
Masaki SASANO
Juzo ZENIHIRO
Ken-ichiro YONEDA

Research Scientists
Sarah NAIMI
Kenichiro TATEISHI

Research & Development Scientist
Yohei SHIMIZU

Postdoctoral Researcher
Junki TANAKA

Junior Research Associates
Shutaro HANAI
Tomoya HARADA

International Program Associates
Siwei HUANG
Yutian LI

Research Consultants
Harutaka SAKAGUCHI (Osaka Univ.)
Kazuko TANABE
Yasuyuki SUZUKI

Senior Visiting Scientist

Hiroyuki SAGAWA (Univ. of Aizu)

Visiting Scientists

Satoshi ADACHI (Osaka Univ.)
Hidetoshi AKIMUNE (Konan Univ.)
Didier BEAUMEL (Inst. de Phys.Nucl.)
Konstanze BORETZKY (GSI)
Anna CORSI (CEA Saclay)
Masanori DOZONO (Kyoto Univ.)
Zoltan ELEKES (ATOMKI)
Zsolt FULOP (ATOMKI)
Tatsuya FURUNO (Osaka Univ.)
Igor GASPARIC (Rudjer Boskovic Inst.)
Valdir GUIMARAES (Inst.o de Fisica da Univ. de Sao Paulo)
Zoltan HALASZ (ATOMKI)
Kaori KAKI (Shizuoka Univ.)
Takahiro KAWABATA (Osaka Univ.)
Yuma KIKUCHI (NIT, Tokuyama College)
Yosuke KONDO (Tokyo Tech)
Zeren KORKULU (Inst. for Basic Sci. (IBS))
Attila KRASZNAHORKAY (ATOMKI)
Dorottya KUNNE SOHLER (ATOMKI)
Istvan KUTI (ATOMKI)
Valerie LAPOUX (Inst.ion CEA-Saclay)
Yury LITVINOV (GSI)
Hongna LIU (TU Darmstadt)
Yohei MATSUDA (Konan Univ.)
Kenjiro MIKI (Tohoku Univ.)
Tetsuaki MORIGUCHI (Tsukuba Univ.)
Sarah NAIMI (IJCLab (Laboratoire de physique des 2 infinis - Irene Joliot-Curie))
Takashi NAKAMURA (Tokyo Tech)
Noritsugu NAKATSUKA (Tokyo Tech)
Alexandre OBERTELLI (TU Darmstadt)
Kazuyuki OGATA (Osaka Univ.)
Valerii PANIN (GSI)
Aldric REVEL (CEA Saclay)
Kimiko SEKIGUCHI (Tokyo Tech)
Laszlo STUHL (Inst. for Basic Sci. (IBS))
Baohua SUN (Beihang Univ.)
Yelei SUN (TU Darmstadt)
Shinji SUZUKI (Chinese Academy of Sci.)
Satoru TERASHIMA (Beihang Univ.)
Yasuhiro TOGANO (Rikkyo Univ.)
Takashi WAKUI (QST)
Atomu WATANABE (JSPS)
Takayuki YAMAGUCHI (Saitama Univ.)
Zaihong YANG (Osaka Univ.)
Juzo ZENIHIRO (Kyoto Univ.)
Yuhu ZHANG (IMP, CAS)

Visiting Technicians

Denis CALVET (CEA)
Alain DELBART (CEA/CE Saclay)
Clement HILAIRE (CEA Saclay)
Shoji SUZUKI (KEK)
Olivier TELLIER (CEA Saclay)

Student Trainees

Tomoki ADACHI (Kyushu Univ.)
Sota ANDO (Kyushu Univ.)
Paul ANDRE (CEA Saclay)
Naoki EBINA (Tokyo Tech)
Shiyo EN'YO (Kyoto Univ.)
Yuki FUJIKAWA (Kyoto Univ.)
Saiya FUJIWARA (Kyushu Univ.)
Jian GAO (Peking Univ.)
Shutaro HANAI (Univ. of Tokyo)
Sakumi HARAYAMA (Saitama Univ.)
Koshi HIGUCHI (Saitama Univ.)
Kouta HORIKAWA (Tokyo Tech)
Kento INABA (Kyoto Univ.)
Kakeru ISOBE (Tokyo Tech)
Koki KAMEYA (Tohoku Univ.)
Naoto KANAME (Tsukuba Univ.)
Masanori KANDA (Saitama Univ.)
Fumiya KAWAGUCHI (Tokyo Tech)
Yusuke KAWASHIMA (Kyushu Univ.)
Kanki KISHIMOTO (Kyushu Univ.)
Sho KITAYAMA (Tohoku Univ.)
Yukari KOIZUMI (Saitama Univ.)
Hyeji LEE (Tokyo Tech)
Hongfu LI (IMP, CAS)
Yoshiki MARUTA (Tohoku Univ.)
Takaya MATSUI (Tohoku Univ.)
Tomoki MATSUI (Tokyo Tech)
Riku MATSUMURA (Saitama Univ.)
Atsuyuki MORIYAMA (Tsukuba Univ.)
Shintaro OKAMOTO (Kyoto Univ.)
Kengo OKUBO (Saitama Univ.)
Misaki OTSU (Saitama Univ.)
Yuko SAITO (Tohoku Univ.)
Kosuke SAKANASHI (Osaka Univ.)
Kenta SASAKI (Saitama Univ.)
Hibiki SEKI (Saitama Univ.)
Yusuke SHINOHARA (Kyushu Univ.)
Naru SHINOZAKI (Saitama Univ.)
Kohei TAKAHASHI (Tokyo Tech)
Ryotaro TSUJI (Kyoto Univ.)
Ren URAYAMA (Tohoku Univ.)
Kanta YAHIRO (Kyoto Univ.)
Kohei YAMAMOTO (Tohoku Univ.)
Wataru YAMASHITA (Kyushu Univ.)
Asahi YANO (Tsukuba Univ.)
Nozomi YOKOTA (Kyushu Univ.)
Chieko YONEMURA (Kyushu Univ.)
Ryohsuke YOSHIDA (Kyoto Univ.)

Assistants

Emiko ISOGAI Yuri TSUBURAI

List of Publications & Presentations

Publications

[Original Papers]

M. Holl, S. Lindberg, A. Heinz, Y. Kondo, T. Nakamura, J. A. Tostevin, H. Wang, T. Nilsson, N. L. Achouri, H. Al Falou, L. Atar, T. Aumann, H. Baba, K. Boretzky, C. Caesar, D. Calvet, H. Chae, N. Chiga, A. Corsi, H. L. Crawford, F. Delaunay, A. Delbart, Q. Deshayes, P. Díaz Fernández, Z. Dombrádi, C. A. Douma, Z. Elekes, P. Fallon, I. Gašparic, J. -M. Gheller, J. Gibelin, A. Gillibert, M. N. Harakeh, A. Hirayama, C. R. Hoffman, A. Horvat, Á. Horváth, J. W. Hwang, T. Isobe, J. Kahlbow, N. Kalantar-Nayestanaki, S. Kawase, S. Kim, K. Kisamori, T. Kobayashi, D. Körper, S. Koyama, I. Kuti, V. Lapoux, F. M. Marqués, S. Masuoka, J. Mayer, K. Miki, T. Murakami, M. Najafi, K. Nakano, N. Nakatsuka, A. Obertelli, F. de Oliveira Santos, N. A. Orr, H. Otsu, T. Ozaki, V. Panin, S. Paschalis, A. Revel, D. Rossi, A. T. Saito, T. Y. Saito, M. Sasano, H. Sato, Y. Satou, H. Scheit, F. Schindler, P. Schrock, M. Shikata, Y. Shimizu, H. Simon, D. Sohler, O. Sorlin, L. Stuhl, S. Takeuchi, M. Tanaka, M. Thoennessen, H. Törnqvist, Y. Togano, T. Tomai, J. Tscheuschner, J. Tsubota, T. Uesaka, Z. Yang, M. Yasuda, and K. Yoneda, "Border of the island of inversion: Unbound states in ^{29}Ne," Phys. Rev. C **105**, 034301 (2022).

L. Olivier, R. Orlandi, Z. Patel, Zs. Podolyák, M. Rudigier, T. Saito, C. Shand, P. -A. Söderström, I. Stefan, V. Vaquero, V. Werner, K. Wimmer, and Z. Xu, "γ-ray spectroscopy of low-lying yrast and non-yrast states in neutron-rich ^{94,95,96}Kr," Phys. Rev. C **105**, 024302 (2022).

M. Janek, V. P. Ladygin, A. V. Averyanov, E. V. Chernykh, D. D. Enache, Y. V. Gurchin, A. Yu. Isupov, J. -T. Karachuk, A. N. Khrenov, D. O. Krivenkov, P. K. Kurilkin, N. B. Ladygina, A. N. Livanov, O. Mezhenska, S. M. Piyadin, S. G. Reznikov, Y. T. Skhomenko, A. A. Terekhin, A. V. Tishevsky, T. Uesaka, and I. S. Volkov, "Study of the dp elastic and dp breakup complementary processes using polarized and unpolarized beam of nuclotron," Few-Body Syst. **63**, 3 (2022).

A. Watanabe, S. Nakai, Y. Wada, K. Sekiguchi, T. Akieda, D. Etoh, M. Inoue, Y. Inoue, K. Kawahara, H. Kon, K. Miki, T. Mukai, D. Sakai, S. Shibuya, Y. Shiokawa, T. Taguchi, H. Umetsu, Y. Utsuki, M. Watanabe, S. Goto, K. Hatanaka, Y. Hirai, Y. Ikeda, T. Ino, D. Inomoto, S. Ishikawa, M. Itoh, H. Kanda, H. Kasahara, Y. Maeda, S. Mitsumoto, K. Nonaka, H. J. Ong, H. Oshiro, Y. Otake, H. Sakai, A. Taketani, D. T. Tran, T. Uesaka, T. Wakasa, Y. Wakabayashi, and T. Wakui, "Analyzing power measurement for p-^{3}He elastic scattering at intermediate energies," Few-Body Syst. **62**, 112 (2021).

S. W. Huang, Z. H. Yang, F. M. Marqués, N. L. Achouri, D. S. Ahn, T. Aumann, H. Baba, D. Beaumel, M. Böhmer, K. Boretzky, M. Caamaño, S. Chen, N. Chiga, M. L. Cortés, D. Cortina, P. Doornenbal, C. A. Douma, F. Dufter, J. Feng, B. Fernández-Domínguez, Z. Elekes, U. Forsberg, T. Fujino, N. Fukuda, I. Gašparić, Z. Ge, R. Gernhäuser, J. M. Gheller, J. Gibelin, A. Gillibert, Z. Halász, T. Harada, M. N. Harakeh, A. Hirayama, N. Inabe, T. Isobe, J. Kahlbow, N. Kalantar-Nayestanaki, D. Kim, S. Kim, S. Kiyotake, T. Kobayashi, Y. Kondo, P. Koseoglou, Y. Kubota, I. Kuti, C. Lehr, C. Lenain, P. J. Li, Y. Liu, Y. Maeda, S. Masuoka, M. Matsumoto, A. Matta, J. Mayer, H. Miki, M. Miwa, B. Monteagudo, I. Murray, T. Nakamura, A. Obertelli, N. A. Orr, H. Otsu, V. Panin, S. Park, M. Parlog, S. Paschalis, M. Potlog, S. Reichert, A. Revel, D. Rossi, A. Saito, M. Sasano, H. Sato, H. Scheit, F. Schindler, T. Shimada, Y. Shimizu, S. Shimoura, H. Simon, I. Stefan, S. Storck, L. Stuhl, H. Suzuki, D. Symochko, H. Takeda, S. Takeuchi, J. Tanaka, Y. Togano, T. Tomai, H. T. Törnqvist, E. Tronchin, J. Tscheuschner, T. Uesaka, V. Wagner, K. Wimmer, H. Yamada, B. Yang, L. Yang, Y. Yasuda, K. Yoneda, L. Zanetti, and J. Zenihiro, "Experimental study of ^4n by directly detecting the decay neutrons," Few-Body Syst. **62**, 102 (2021).

B. D. Linh, A. Corsi, A. Gillibert, A. Obertelli, P. Doornenbal, C. Barbieri, S. Chen, L. X. Chung, T. Duguet, M. Gómez-Ramos, J. D. Holt, A. Moro, P. Navrátil, K. Ogata, N. T. T. Phuc, N. Shimizu, V. Somà, Y. Utsuno, N. L. Achouri, H. Baba, F. Browne, D. Calvet, F. Château, N. Chiga, M. L. Cortés, A. Delbart, J. -M. Gheller, A. Giganon, C. Hilaire, T. Isobe, T. Kobayashi, Y. Kubota, V. Lapoux, H. N. Liu, T. Motobayashi, I. Murray, H. Otsu, V. Panin, N. Paul, W. Rodriguez, H. Sakurai, M. Sasano, D. Steppenbeck, L. Stuhl, Y. L. Sun, Y. Togano, T. Uesaka, K. Wimmer, K. Yoneda, O. Aktas, T. Aumann, F. Flavigny, S. Franchoo, I. Gašparić, R. -B. Gerst, J. Gibelin, K. I. Hahn, N. T. Khai, D. Kim, T. Koiwai, Y. Kondo, P. Koseoglou, J. Lee, C. Lehr, T. Lokotko, M. MacCormick, K. Moschner, T. Nakamura, S. Y. Park, D. Rossi, E. Sahin, D. Sohler, P. -A. Söderström, S. Takeuchi, N. D. Ton, H. Törnqvist, V. Vaquero, V. Wagner, H. Wang, V. Werner, X. Xu, Y. Yamada, D. Yan, Z. Yang, M. Yasuda, and L. Zanetti, "Investigation of the ground-state spin inversion in the neutron-rich ^{47,49}Cl isotopes," Phys. Rev. C **104**, 044331 (2021).

K. Inaba, Y. Sasamoto, T. Kawabata, M. Fujiwara, Y. Funaki, K. Hatanaka, K. Itoh, M. Itoh, K. Kawase, H. Matsubara, Y. Maeda, K. Suda, S. Sakaguchi, Y. Shimizu, A. Tamii, Y. Tameshige, M. Uchida, T. Uesaka, T. Yamada, and H. P. Yoshida, "Search for α condensed states in ^{13}C using α inelastic scattering," Prog. Theor. Exp. Phys. **9**, 093D01 (2021).

F. Browne, S. Chen, P. Doornenbal, A. Obertelli, K. Ogata, Y. Utsuno, K. Yoshida, N. L. Achouri, H. Baba, D. Calvet, F. Château, N. Chiga, A. Corsi, M. L. Cortes, A. Delbart, J. -M. Gheller, A. Giganon, A. Gillibert, C. Hilaire, T. Isobe, T. Kobayashi, Y. Kubota, V. Lapoux, H. N. Liu, T. Motobayashi, I. Murray, H. Otsu, V. Panin, N. Paul, W. Rodriguez, H. Sakurai, M. Sasano, D. Steppenbeck, L. Stuhl, Y. L. Sun, Y. Togano, T. Uesaka, K. Wimmer, K. Yoneda, O. Aktas, T. Aumann, K. Boretzky, C. Caesar, L. X. Chung, F. Flavigny, S. Franchoo, I. Gasparic, R. -B. Gerst, J. Gibelin, K. I. Hahn, M. Holl, J. Kahlbow, D. Kim, D. Körper, T. Koiwai, Y. Kondo, P. Koseoglou, J. Lee, C. Lehr, B. D. Linh, T. Lokotko, M. MacCormick, K. Miki, K. Moschner, T. Nakamura, S. Y. Park, D. Rossi, E. Sahin, F. Schindler, H. Simon, P. -A. Söderström, D. Sohler, S. Takeuchi, H. Törnqvist, J. Tscheuschner, V. Vaquero, V. Wagner, S. Wang, V. Werner, X. Xu, H. Yamada, D. Yan, Z. Yang, M. Yasuda, and L. Zanetti, "Pairing forces govern population of doubly magic ^{54}Ca from direct reactions," Phys. Rev. Lett. **126**, 252501 (2021).

M. M. Juhász, Z. Elekes, D. Sohler, K. Sieja, K. Yoshida, K. Ogata, P. Doornenbal, A. Obertelli, H. Baba, F. Browne, D. Calvet, F. Château, S. Chen, N. Chiga, A. Corsi, M. L. Cortés, A. Delbart, J. -M. Gheller, A. Giganon, A. Gillibert, C. Hilaire, T. Isobe, T. Kobayashi,

Y. Kubota, V. Lapoux, T. Motobayashi, I. Murray, H. Otsu, V. Panin, N. Paul, W. Rodriguez, H. Sakurai, M. Sasano, D. Steppenbeck, L. Stuhl, Y. L. Sun, Y. Togano, T. Uesaka, K. Wimmer, K. Yoneda, N. L Achouri, O. Aktas, T. Aumann, L. X. Chung, Zs. Dombrádi, F. Flavigny, S. Franchoo, I. Gašparic, R. -B. Gerst, J. Gibelin, K. I. Hahn, D. Kim, T. Koiwai, Y. Kondo, P. Koseoglou, J. Lee, C. Lehr, B. D. Linh, H. N. Liu, T. Lokotko, M. MacCormick, K. Moschner, T. Nakamura, S. Y. Park, D. Rossi, E. Sahin, P. -A. Söderström, S. Takeuchi, H. Törnqvist, V. Vaquero, V. Wagner, S. Wang, V. Werner, X. Xu, H. Yamada, D. Yan, Z. Yang, M. Yasuda, and L. Zanetti, "First spectroscopic study of ^{63}V at the $N = 40$ island of inversion," Phys. Rev. C **103**, 064308 (2021).

M. M. Juhász, Z. Elekesa, D. Sohlera, Y. Utsuno, K. Yoshida, T. Otsuka, K. Ogatagh, P. Doornenbal, A. Obertelli, H. Baba, F. Browne, D. Calvet, F. Château, S. Chen, N. Chiga, A. Corsi, M. L. Cortés, A. Delbart, J. -M. Gheller, A. Giganon, A. Gillibert, C. Hilaire, T. Isobe, T. Kobayashi, Y. Kubota, V. Lapoux, T. Motobayashi, I. Murray, H. Otsu, V. Panin, N. Paul, W. Rodriguez, H. Sakurai, M. Sasano, D. Steppenbeck, L. Stuhl, Y. L. Sun, Y. Togano, T. Uesaka, K. Wimmers, K. Yoneda, N. L. Achouri, O. Aktas,T. Aumann, L. X. Chung, Zs. Dombrádi, F. Flavigny, S. Franchoo, I. Gašparić, R. -B. Gerst, J. Gibelin, K. I. Hahn, D. Kim, T. Koiwai, Y. Kondo, P. Koseoglou, J. Lee, C. Lehr, B. D. Linh, H. N. Liu, T. Lokotko. M. MacCormick, K. Moschner, T. Nakamura, S. Y. Park, D. Rossi, E. Sahin, P. -A. Söderström, S. Takeuchi, H. Törnqvist, V. Vaquero, V. Wagner, S. Wang, V. Werner, X. Xu, H. Yamada, D. Yan, Z. Yang, M. Yasuda, and L. Zanetti, "First spectroscopic study of ^{51}Ar by the $(p, 2p)$ reaction," Phys. Lett. B **814**, 136108 (2021).

T. Aumann, C. Barbieri, D. Bazin, C. A. Bertulani, A. Bonaccorso, W. H. Dickhoff, A. Gade, M. Gómez-Ramos, B. P. Kay, A. M. Moro, T. Nakamura, A. Obertelli, K. Ogata, S. Paschalis, and T. Uesaka, "Quenching of single-particle strength from direct reactions with stable and rare-isotope beams," Prog. Part. Nucl. Phys. **118**, 103847 (2021).

P. Ascher, L. Daudin, M. Flayol, M. Gerbaux, S. Grévya, M. Hukkanen, A. Husson, A. de Roubin, P. Alfaurt, B. Blank, K. Blaum, B. Lachacinski, D. Lunney, E. Minaya Ramirezd, S. Naimi, S. Perard, and B. Thomas, "PIPERADE: A double Penning trap for mass separation and mass spectrometry at DESIR/SPIRAL2," Nucl. Instrum. Methods Phys. Res. A **1019**, 165857 (2021).

J. Tanaka, Z. Yang, S. Typel, S. Adachi. S. Bai, P. van Beek, D. Beaumel, Y. Fujikawa, J. Han, S. Heil, S. Huang, A. Inoue, Y. Jiang, M. Knösel, N. Kobayashi, Y. Kubota, W. Liu, J. Lou, Y. Maeda, Y. Matsuda, K. Miki, S. Nakamura, K. Ogata, V. Panin, H. Scheit, F. Schindler, P. Schrock, D. Symochko, A. Tamii, T. Uesaka, V. Wagner, K. Yoshida, J. Zenihiro, and T. Aumann, "Formation of α clusters in dilute neutron-rich matter," Science **371**, 260 (2021).

J. Zenihiro, T. Uesaka, H. Sagawa, and S. Yoshida, "Proton density polarization of the doubly magic ^{40}Ca core in ^{48}Ca and EoS parameters," Prog. Theor. Exp. Phys. **4**, 049301 (2021).

[Book]

A. Obertelli and H. Sagawa, "Modern Nuclear Physics: From Fundamentals to Frontiers," Springer Nature Singapore, 2022.

Presentations

[International Conference/Workshop]

T. Uesaka, "Knock-out reaction studies of clustering in heavy nuclei—ONOKORO project—", C2R2 Seminar, Online & IBS CENS, Korea, July 8, 2021.

[Domestic Conference/Workshop]

佐川弘幸 (口頭発表), 「IV density and Isospin Symmetry Breaking (ISB) forces in $N = Z$ nuclei」, 第 7 回クラスター階層領域研究会, 大阪大学核物理研究センター, 2021 年 12 月 27 日.

[Seminar]

上坂友洋, 久保田祐樹, 「ノックアウト反応による大ニュートロンの空間構造抽出」, 物質階層を横断する会, オンライン, 2021 年 7 月 30 日.

Outreach Activity

上坂友洋, 「元素をつくる『巨大地下工場』～工学が支える研究の現場に潜入!～」, IEEE ウェビナーシリーズ第 24 回 Engineering Spotlight, 2022 年 2 月 20 日.

Nuclear Science and Transmutation Research Division
Nuclear Spectroscopy Laborarory

1. Abstract

The research group has conducted nuclear-physics studies utilizing stopped/slowed-down radioactive-isotope (RI) beams mainly at the RIBF facility. These studies are based on the technique of nuclear spectroscopy such as β-ray-detected NMR (β-NMR), γ-PAD (Perturbed Angular Distribution), laser, and Mössbauer among other methods that takes advantage of intrinsic nuclear properties such as nuclear spins, electromagnetic moments, and decay modes. In particular, techniques and devices for the production of spin-controlled RI beams have been developed and combined to the spectroscopic studies, which enable high-sensitivity measurements of spin precessions/resonances through a change in the angular distribution of radiations. Anomalous nuclear structures and properties of far unstable nuclei are investigated from thus determined spin-related observables. The group also conducts nuclear-structure studies based on large-scale numerical calculations such as *ab initio* calculations and large-scale shell-model calculations. The group also aims to apply such techniques to interdisciplinary fields such as fundamental physics and materials science by exploiting nuclear probes.

2. Major Research Subjects

(1) Nuclear spectroscopy utilizing spin-oriented fast RI beams
(2) Nuclear/Atomic laser spectroscopy & SLOWRI R&D
(3) Application of RI probes to materials science

3. Summary of Research Activity

(1) Nuclear spectroscopy utilizing spin-oriented fast RI beams

Measurements of static electromagnetic nuclear moments over a substantial region of the nuclear chart have been conducted for structure studies on the nuclei far from the β-decay stability. Utilizing nuclear spin orientation phenomena of RIs created in the projectile-fragmentation reaction, ground- and excited-state electromagnetic nuclear moments been determined by means of the β-ray-detected nuclear magnetic resonance (β-NMR) and the γ-ray time differential perturbed angular distribution (γ-TDPAD) methods. In particular, a new method developed for controlling spin in a system of rare RIs, taking advantage of the mechanism of the two-step projectile fragmentation reaction combined with the momentum-dispersion matching technique, has been developed and employed making fully use of world's highest intensity rare RIBs delivered from BigRIPS for rare isotopes.

(2) Nuclear/Atomic laser spectroscopy & SLOWRI R&D

The group has been conducting system development for nuclear laser spectroscopy from the following two approaches in order to realize experiments for rare isotopes at RIBF. One is collinear laser spectroscopy for a large variety of elements using slowed-down RI beams produced via a projectile-fragmentation reaction, which can be achieved only by the universal low-energy RI-beam delivery system, SLOWRI, under installation in collaboration with the SLOWRI Team. This slowed-down RI-beam scheme enables to perform high-precision laser spectroscopy even with fast-fragmentation-based RIBs without the elemental limitation problematic in the ISOL-based RIBs.

The other approach is a new method utilizing superfluid helium (He II) as a stopping medium of energetic RI beams, in which the characteristic atomic properties of ions surrounded by superfluid helium enables us to perform unique nuclear laser spectroscopy. RI ions trapped in He II are known to exhibit a characteristic excitation spectrum significantly blue-shifted compared with the emission one. Consequently, the background derived from the excitation-laser stray light, which often causes serious problems in measurements, can be drastically reduced.

(3) Application of RI probes to materials science

The application of RI and heavy ion beams as a probe for condensed matter studies is also conducted by the group. The microscopic material dynamics and properties have been investigated through the deduced internal local fields and the spin relaxation of RI probes based on various spectroscopies utilizing RI probes such as β-NMR/NQR spectroscopy, Mössbauer spectroscopy, the γ-ray time differential perturbed angular correlation (γ-TDPAC) spectroscopy. Furthermore, studies on the control of electrical conductivity of diamond by boron and nitrogen implantation are ongoing.

Provided that highly spin-polarized RI probes are produced independently of their element properties and doped into a substance as an impurity, the constituent particle of the substance can be substituted by the same element RI probe without changing the material structure. This scheme provides a new opportunity for materials-science researches, but a key technology, production of element-independent highly spin-polarized RI beams, has not yet been achieved. In this subject, the group has conducted R&D studies to realize an ultra-slow & highly-spin-polarized RI beams, based on the technique of the atomic beam resonance.

Members

Director

Hideki UENO

Research/Technical Scientists

Hiroki YAMAZAKI (Senior Research Scientist)
Isao WATANABE (Senior Research Scientist)
Aiko TAKAMINE (Research Scientist)
Shintaro GO (Research Scientist)

Research & Development Scientist

Tetsu SONODA

Contract Researcher

Takashi ABE

Special Postdoctoral Researcher

Momo MUKAI

Postdoctoral Researchers

Minori TAJIMA
Kei IMAMURA (CPR)

Research Associate

Aleksey GLADKOV

Senior Visiting Scientists

Yukari MATSUO (Hosei Univ.)
Takaharu OTSUKA (Univ. of Tokyo)

Visiting Scientists

Dimiter L. BALABANSKI (IFIN-HH)
Jean-Michel DAUGAS (CNRS)
Georgi GEORGIEV (CNRS-IN2P3)
Yuichi ICHIKAWA (Kyushu Univ.)
Yoshio KOBAYASHI (Univ. of Electro-Commun.)
Kenya M. KUBO (Int'l Christian Univ.)
Kensaku MATSUTA (Osaka Univ.)
Jun MIYAZAKI (Tokyo Denki Univ.)
Takamasa MOMOSE (The Univ. of British Columbia)
Jin NAKAMURA (Univ. of Electro-Commun.)
Hiroki NISHIBATA (Kyushu Univ.)
Tomoya SATO (Tokyo Tech)
Wataru SATO (Kanazawa Univ.)
Shinichiro TAKEDA (Univ. of Tokyo)
Andrew E. STUCHBERY (The Australian Nat'l Univ.)
Satoshi TSUTSUI (Japan Synchrotron Radiation Res. Inst.)
Shin WATANABE (JAXA)
Yasuhiro YAMADA (Tokyo Univ. Sci)
Deyan T. YORDANOV (CNRS-IN2P3)
Akihiro YOSHIMI (Okayama Univ.)

Student Trainees

Sai AKIMOTO (Hosei Univ.)
Miru DOI (Hosei Univ.)
Hiroki ENDO (Hosei Univ.)
Manami ITO (Hosei Univ.)
Kai KIKUCHI (Hosei Univ.)
Yoko KIMURA (Osaka Univ.)
Rikuta MITSUYASU (Hosei Univ.)
Yusuke NAKASHIMA (Univ. of Electro-Commun.)
Masaki NISHIMURA (Hosei Univ.)
Yurika OTANI (Osaka Univ.)
Takato SUGISAKI (Osaka Univ.)
Satoshi TANAKA (Hosei Univ.)
Kenta TSUBURA (Hosei Univ.)
Takumi YAMAMOTO (Hosei Univ.)
Mio YOSHIDA (Univ. of Electro-Commun.)

Temporary Staffing

Emiko SUGISAKI

Assistants

Yuri TSUBURAI
Izumi YOSHIDA

List of Publications & Presentations

Publications

[Original Papers]

Y. Hirayama, P. Schury, M. Mukai, H. Choi, S. Imamura, X. Y. Watanabe, M. Wada, H. Watanabe, and H. Miyatake, "Three-dimensional tracking multi-segmented proportional gas counter for β-decay spectroscopy of unstable nuclei," Nucl. Instrum. Methods Phys. Res. A **997**, 165152-1–10 (2021). DOI: 10.1016/j.nima.2021.165152 .

T. Aoki, R. Sreekantham, B. K. Sahoo, Bindiya Arora, A. Kastberg, T. Sato, H. Ikeda, N. Okamoto, Y. Torii, T. Hayamizu, K. Nakamura, S. Nagase, M. Ohtsuka, H. Nagahama, N. Ozawa, M. Sato, T. Nakashita, K. Yamane, K. S. Tanaka, K. Harada, H. Kawamura, T. Inoue, A. Uchiyama, A. Hatakeyama, A. Takamine, H. Ueno, Y. Ichikawa, Y. Matsuda, H. Haba, and Y. Sakemi, "Quantum sensing of the electron electric dipole moment using ultracold entangled Fr atoms," Quantum Sci. Technol. **6**, 044008-1–17 (2021). DOI: 10.1088/2058-9565/ac1b6a .

S. Kimura, Y. Ito, D. Kaji, P. Schury, M. Wada, H. Haba, T. Hashimoto, Y. Hirayama, M. MacCormick, H. Miyatake, J. Y. Moon, K. Morimoto, M. Mukai, I. Murray, A. Ozawa, M. Rosenbusch, H. Schatz, A. Takamine, T. Tanaka, Y. X. Watanabe, and H. Wollnik, "High precision mass measurements of intermediate-mass neutron-deficient nuclei via MRTOF-MS," JPS Conf. Proc. **35**, 011005-1–6 (2021). DOI: 10.7566/JPSCP.35.011005 .

P. Schury, T. Niwase, M. Wada, P. Brionnet, S. Chen, T. Hashimoto, H. Haba, Y. Hirayama, D. S. Hou, S. Iimura, H. Ishiyama, S. Ishizawa, Y. Ito, D. Kaji, S. Kimura, H. Koura, J. J. Liu, H. Miyatake, J. -Y. Moon, K. Morimoto, K. Morita, D. Nagae, M. Rosenbusch, A. Takamine, Y. X. Watanabe, H. Wollnik, W. Xian, and S. X. Yan, "First high-precision direct determination of the atomic mass of a superheavy nuclide," Phys. Rev. C **104**, L021304-1–7 (2021). DOI: 10.1103/PhysRevC.104.L021304 .

T. Niwase, M. Wada, P. Schury, P. Brionnet, S. D. Chen, T. Hashimoto, H. Haba, Y. Hirayama, D. S. Hou, S. Iimura, H. Ishiyama, S. Ishizawa, Y. Ito, D. Kaji, S. Kimura, J. Liu, H. Miyatake, J. Y. Moon, K. Morimoto, K. Morita, D. Nagae, M. Rosenbusch, A. Takamine, T. Tanaka, Y. X. Watanabe, H. Wollnik, W. Xian, and S. X. Yan, "α-decay-correlated mass measurement of ^{206,207g,m}Ra using an α-TOF detector equipped multireflection time-of-flight mass spectrograph system," Phys. Rev. C **103**, 054312-1–8 (2021). DOI: 10.1103/PhysRevC.104.044617 .

M. Ahmed, Y. X. Watanabe, Y. Hirayama, M. Mukai, J. H. Park, P. Schury, Y. Kakiguchi, A. Ozawa, M. Oyaizu, M. Wada, and H. Miyatake, "β-γ Spectroscopy of the ^{195}Os nucleus," Phys. Rev. C **104**, 044617-1–9 (2021). DOI: 10.1103/PhysRevC.103.054312 .

Y. X. Watanabe, P. M. Walker, Y. Hirayama, M. Mukai, H. Watanabe, G. J. Lane, M. Ahmed, M. Brunet, T. Hashimoto, S. Ishizawa, S. Kimura, F. G. Kondev, Yu. A. Litvinov, H. Miyatake, J. Y. Moon, T. Niwase, M. Oyaizu, J. H. Park, Zs. Podolyák, M. Rosenbusch, P. Schury, and M. Wada, "First direct observation of isomeric decay in neutron-rich odd-odd ^{186}Ta," Phys. Rev. C **104**, 024330-1–6. DOI: 10.1103/PhysRevC.104.024330 .

A. Kubiela, H. Suzuki, O. B. Tarasov, M. Pfützner, D. -S. Ahn, H. Baba, A. Bezbakh, A. A. Ciemny, W. Dominik, N. Fukuda, A. Giska, R. Grzywacz, Y. Ichikawa, Z. Janas, Ł. Janiak, G. Kamiński, K. Kawata, T. Kubo, M. Madurga, C. Mazzocchi, H. Nishibata, M. Pomorski, Y. Shimizu, N. Sokołowska, D. Suzuki, P. Szymkiewicz, A. Świercz, M. Tajima, A. Takamine, H. Takeda, Y. Takeuchi, C. R. Thornsberry, H. Ueno, H. Yamazaki, R. Yokoyama, and K. Yoshida, "Production of the most neutron-deficient Zn isotopes by projectile fragmentation of ^{78}Kr," Phys. Rev. C **104**, 064610-1–7 (2021). DOI: 10.1103/PhysRevC.104.064610 .

B. Kolbinger, C. Amsler, S. Arguedas Cuendis, H. Breuker, A. Capon, G. Costantini, P. Dupré, M. Fleck, A. Gligorova, H. Higaki, Y. Kanai, V. Kletzl, N. Kuroda, A. Lanz, M. Leali, V. Mäckel, C. Malbrunot, V. Mascagna, O. Massiczek, Y. Matsuda, D. J. Murtagh, Y. Nagata, A. Nanda, L. Nowak, B. Radics, C. Sauerzopf, M. C. Simon, M. Tajima, H. A. Torii, U. Uggerhøj, S. Ulmer, L. Venturelli, A. Weiser, M. Wiesinger, E. Widmann, T. Wolz, Y. Yamazaki, and J. Zmeskal, "Measurement of the principal quantum number distribution in a beam of antihydrogen atoms," Eur. Phys. J. D **75**, 91-1–14 (2021). DOI: 10.1140/epjd/s10053-021-00101-y .

Y. Sato, Y. Yamada, Y. Kobayashi, K. M. Kubo, M. Mihara, W. Sato, J. Miyazaki, T. Nagatomo, T. Ando, N. Takahama, K. Some, M. Sato, S. Sato, and A. Kitagawa, "In-beam Mössbauer spectra of ^{57}Mn implanted into lithium aluminium hydride," Appl. Radiat. Isot. **170**, 109582-1–7 (2021). DOI: 10.1016/j.apradiso.2020.109582 .

Y. Kobayashi, M. Sato, Y. Yamada, K. M. Kubo, M. Mihara, W. Sato, J. Miyazaki, T. Nagatomo, A. Okazawa, S. Sato, and A. Kitagawa, "Chemical species of localized Fe atoms in solid hydrogen using in-beam Mössbauer spectroscopy," Hyperfine Interact. **243**, 13-1–8 (2022). DOI: 10.1007/s10751-022-01793-3 .

S. Tsutsui, R. Higashinaka, R. Nakamura, K. Fujiwara, J. Nakamura, Y. Kobayashi, T. U. Ito, Y. Yoda, K. Kato, K. Nitta, N. Kawamura, M. Mizumaki, T. D. Matsuda, and Y. Aoki, "Sm valence determination of Sm-based Intermetallics using ^{149}Sm Mössbauer and Sm LIII-edge X-ray absorption spectroscopies," Hyperfine Interact. **242**, 32-1–10 (2021). DOI: 10.1007/s10751-021-01759-x .

O. Hall, T. Davinson, A. Estrade, J. Liu, G. Lorusso, F. Montes, S. Nishimura, V. H. Phong, P. J. Woods, J. Agramunt, D. S. Ahn, A. Algora, J. M. Allmond, H. Baba, S. Bae, N. T. Brewer, C. G. Bruno, R. Caballero-Folch, F. Calviño, P. J. Coleman-Smith, G. Cortes, I. Dillmann, C. Domingo-Pardo, A. Fijalkowska, N. Fukuda, S. Go, C. J. Griffin, R. Grzywacz, J. Ha, L. J. Harkness-Brennan, T. Isobe, D. Kahl, L. H. Khiem, G. G. Kiss, A. Korgul, S. Kubono, M. Labiche, I. Lazarus, J. Liang, Z. Liu, K. Matsui, K. Miernik, B. Moon, A. I. Morales, P. Morrall, M. R. Mumpower, N. Nepal, R. D. Page, M. Piersa, V. F. E. Pucknell, B. C. Rasco, B. Rubio, K. P. Rykaczewski, H. Sakurai, Y. Shimizu, D. W. Stracener, T. Sumikama, H. Suzuki, J. L. Tain, H. Takeda, A. Tarifeño-Saldivia, A. Tolosa-Delgado, M. Wolińska-Cichocka, and R. Yokoyama, "β-delayed neutron emission of r-process nuclei at the $N = 82$ shell closure," Phys. Lett. B **816**, 136266-1–7 (2021). DOI: 10.1016/j.physletb.2021.136266 .

T. Abe, P. Maris, T. Otsuka, N. Shimizu, Y. Utsuno, and J. P. Vary, "Ground-state properties of light 4n self-conjugate nuclei in *ab initio* no-core Monte Carlo shell model calculations with nonlocal *NN* interactions," Phys. Rev. C **104**, 054315-1–22 (2021). DOI: 10.1103/PhysRevC.104.054315 .

M. M. Juhász, Z. Elekes, D. Sohler, Y. Utsuno, K. Yoshida, T. Otsuka, K. Ogata, P. Doornenbal, A. Obertelli, H. Baba, F. Browne, D. Calvet, F. Château, S. Chen, N. Chiga, A. Corsi, M. L. Cortés, A. Delbart, and L. Zanetti, "First spectroscopic study of ^{51}Ar by the

(p, 2p) reaction," Phys. Lett. B **814**, 136108-1–8 (2021). DOI: 10.1016/j.physletb.2021.136108 .

T. Suzuki and T. Otsuka, "Structure of two-neutron halo in light exotic nuclei," Few-Body Syst. **62**, 32-1–5 (2021). DOI: 10.1007/s00601-021-01612-5 .

N. Shimizu, Y. Tsunoda, Y. Utsuno, and T. Otsuka, "Variational approach with the superposition of the symmetry-restored quasiparticle vacua for nuclear shell-model calculations," Phys. Rev. C **103**, 014312-1–11 (2021). DOI: 10.1103/PhysRevC.103.014312 .

T. Otsuka, N. Shimizu, and Y. Tsunoda, "Moments and radii of exotic Na and Mg isotopes," Phys. Rev. C **105**, 014319-1–8 (2021). DOI: 10.1103/PhysRevC.105.014319 .

[Review Article]

T. Otsuka, "Emerging concepts in nuclear structure based on the shell models," Physics **4**, 258–285 (2022). DOI: 10.3390/physics4010018 .

Presentations

[International Conferences/Workshops]

H. A. Schuessler (oral), A. Takamine, M. Wada, H. Iimura, and J. Lassen, "Nuclei at extreme deformations and configurations: Touching horizon with on-line laser spectroscopy," 29th Annual International Laser Physics Workshop (LPHYS'21), Online, July 19–23, 2021.

T. Abe (oral), "*Ab initio* description of nuclear structure in no-core Monte Carlo shell model," XXXII IUPAP Conference on Computational Physics (CCP2021), Online, August 1–5, 2021.

M. Mukai (oral), "Isotope shift measurement of ^{182,184}Hf and ^{185,187,188,190}W," SSRI-PNS Collaboration Meeting 2021, Online, September 2–3, 2021.

T. Otsuka (invited), "Spin contents of Na isotopes towards dripline," 24th International Spin Symposium (SPIN2021), Online & Matsue, Japan, Ocober, 18–22, 2021.

[Domestic Conferences/Workshops]

上野秀樹 (依頼講演), 「計画研究 B03 班 高偏極 RI ビームの生成と核・物質科学研究への応用」, 新学術領域研究「宇宙観測検出器と量子ビームの出会い. 新た応用の架け橋.」, 領域研究会 (第 3 回領域全体会議), オンライン, 2021 年 6 月 14–15 日.

今村慧 (依頼講演), 「RI 原子ビーム共鳴装置の開発」, 新学術領域研究「宇宙観測検出器と量子ビームの出会い. 新た応用の架け橋. 」, 領域研究会 (第 3 回領域全体会議), オンライン, 2021 年 6 月 14–15 日.

田島美典 (ポスター発表), 高峰愛子, 飯村秀紀, 「不安定原子核の同位体シフト測定に向けた開発」, 第 17 回原子・分子・光科学（AMO）討論会, オンライン, 2021 年 6 月 18–19 日.

山本匠 (ポスター発表), 「超流動ヘリウム中 ^{107,109}Ag 原子の超微細構造間隔測定へ向けた DPSS レーザーの導入」, 第 17 回原子・分子・光科学（AMO）討論会, オンライン, 2021 年 6 月 18–19 日.

土居三瑠 (ポスター発表), 「観測原子数補正システムを用いた 超流動ヘリウム中の Rb 原子の超微細構造間隔の測定」, 第 17 回原子・分子・光科学（AMO）討論会, オンライン, 2021 年 6 月 18–19 日.

伊藤愛美 (ポスター発表), 「加速器実験に向けた二重共鳴法による外部磁場補正コイルの開発」, 第 17 回原子・分子・光科学（AMO）討論会, オンライン, 2021 年 6 月 18–19 日.

郷慎太郎 (依頼講演), 「原子核物理学実験における偏光ガンマ線観測実験の将来」, 新学術領域研究「宇宙観測検出器と量子ビームの出会い. 新たな応用への架け橋. 」, 高精度硬 X 線・ガンマ線偏光計を用いた原子物理・原子核物理実験の検討小研究会, オンライン, 2021 年 8 月 19 日.

飯村俊, M. Rosenbusch, 高峰愛子, 和田道治, S. Chen, D. Hou, J. Liu, W. Xian, S. Yan, P. Schury, 木村創大, 庭瀬暁隆, 伊藤由太, 園田哲, 小島隆夫, 渡辺裕, 平山賀一, 宮武宇也, S. Naimi, 道正新一郎, 西村俊二, 小田原厚子, 石山博恒, 「新規開発された ZD-MRTOF 装置を用いた中性子過剰 Sc, Ti, V 核の系統的質量測定」, 日本物理学会 2021 年 秋季大会, オンライン, 2021 年 9 月 14–17 日.

庭瀬暁隆, P. Schury, 和田道治, P. Brionnet, S. Chen, 橋本尚志, 羽場宏光, 平山賀一, D. S. Hou, 飯村俊, 石山博恒, 石澤倫, 伊藤由太, 加治大哉, 木村創大, 小浦寛之, 宮武宇也, J. Y. Moon, 森本幸司, 森田浩介, 長江大輔, M. Rosenbusch, 高峰愛子, 渡辺裕, H. Wollnik, W. Xian, S. X. Yan, 「超重核 ^{257}Db の直接質量測定」, 日本物理学会 2021 年 秋季大会, オンライン, 2021 年 9 月 14–17 日.

M. Rosenbusch, S. Chen, W. Xian, S. Yan, A. Takamine, D. Hou, S. Iimura, M. Wada, P. Schury, Y. Hirayama, H. Ishiyama, Y. Ito, S. Kimura, T. M. Kojima, J. Liu, S. Michimasa, H. Miyatake, S. Naimi, S. Nishimura, T. Niwase, T. Sonoda, Y. X. Watanabe, H. Wollnik, "New technologies for multi-reflection time-of-flight mass spectrometry at BigRIPS," 日本物理学会 2021 年 秋季大会, オンライン, 2021 年 9 月 14–17 日.

W. Xian, S. Chen, M. Rosenbusch, S. Yan, D. Hou, S. Iimura, A. Takamine, M. Wada, P. Schury, H. Ishiyama, Y. Hirayama, S. Kimura, T. Niwase, J. Liu, Y. Ito, T. M. Kojima, S. Naimi, S. Michimasa, H. Miyatake, S. Nishimura, T. Sonoda, Y. X. Watanabe, H. Wollnik, "New mass measurements of neutron-rich nuclei of Ge, As, and Se, and an accuracy study of the new ZD-MRTOF system," 日本物理学会 2021 年 秋季大会, オンライン, 2021 年 9 月 14–17 日.

D. Hou, A. Takamine, S. Iimura, M. Rosenbusch, S. Chen, W. Xian, S. Yan, M. Wada, P. Schury, Y. Hirayama, H. Ishiyama, Y. Ito, S. Kimura, J. Liu, S. Michimasa, H. Miyatake, S. Naimi, S. Nishimura, T. Niwase, Y. X. Watanabe, H. Wollnik, "Mass measurement in the neutron-rich Mo region using the new ZD-MRTOF system," 日本物理学会 2021 年 秋季大会, オンライン, 2021 年 9 月 14–17 日.

向井もも, 平山賀一, 渡辺裕, 渡邉寛, S. C. Jeong, 宮武宇也, M. Brunet, 石澤倫, F. G. Kondev, G. J. Lane, Yu. A. Litvinov, 庭瀬暁隆, Zs. Podolyák, M. Rosenbusch, P. Schury, 和田道治, P. M. Walker, 「^{187}Ta のベータ崩壊核分光」, 日本物理学会 2021 年 秋季大会, オンライン, 2021 年 9 月 14–17 日.

平山賀一, H. Choi, P. Schury, 渡辺裕, 向井もも, J. Y. Moon, T. Hashimoto, S. C. Jeong, M. Rosenbusch, 小柳津充広, 庭瀬暁隆, 谷口秋洋, 和田道治, 宮武宇也, 「KISS での核分光: MRTOF-MS を用いた不安定核のレーザー共鳴イオン化核分光」, 日本物

理学会 2021 年 秋季大会, オンライン, 2021 年 9 月 14–17 日.

川田敬太, 大田晋輔, 堂園昌伯, 銭廣十三, 岩本ちひろ, 北村徳隆, 酒井英行, 増岡翔一朗, 道正新一郎, 横山輪, 矢向謙太郎, 原田知也, 西畑洸希, 角田理恵子, 今井伸明, N. Zhang, J. Hwang, 遠藤史隆, 「核破砕反応における核運動量移行」, 日本物理学会 2021 年 秋季大会, オンライン, 2021 年 9 月 14–17 日.

大谷優里花, 三原基嗣, 松多健策, 福田光順, 若林諒, 沖本直哉, 福留美樹, 木村容子, 高山元, 泉川卓司, 野口法秀, 生越瑞揮, 佐藤弥紗, 高津和哉, 大坪隆, 西村太樹, 髙橋弘幸, 菅原奏来, A. Gladkov, 石山博恒, 北川敦志, 佐藤眞二, 百田佐多生, 奥村寛之, 森口哲朗, 小沢顕, 冨田啓介, 矢野朝陽, 「酸素イオン伝導体 YSZ 中における短寿命核 ^{19}O のスピン格子緩和時間」, 日本物理学会 2021 年 秋季大会, オンライン, 2021 年 9 月 20–23 日.

郷慎太郎 (依頼講演), 「アルファ・ベータ・ガンマ線核分光測定から探る原子核構造研究」, 理研新領域開拓課題「物質階層原理研究」&「ヘテロ界面研究」合同冬研究会, 埼玉県和光市 (理研) & オンライン, 2021 年 12 月 5–6 日.

阿部喬 (パネリスト), 「コロナ禍が研究生活にもたらしたもの」, 理研新領域開拓課題「物質階層原理研究」&「ヘテロ界面研究」合同冬研究会, 埼玉県和光市 (理研) & オンライン, 2021 年 12 月 5–6 日.

阿部喬 (口頭発表), 「モンテカルロ殻模型による第一原理計算の進展」, 京大基研研究会「核力に基づいた原子核の構造と反応」, 京都府京都市 (京大基研) & オンライン, 2021 年 12 月 7–10 日.

螺良健太 (口頭発表), 「核モーメント測定法開発のための 光学用クライオスタットにおける超流動ヘリウム中 Rb 原子の収量測定」, 日本量子医科学会第 1 回学術大会, オンライン, 2021 年 12 月 10–11 日.

大塚孝治 (招待講演), "Novel crossover between alpha clustering and quantum liquid in ^{12}C described by First Principles calculation," 第 7 回クラスター階層領域研究会, オンライン & 宮城県仙台市 (東北大学電子光理学研究センター), 2021 年 12 月 27–28 日.

中下輝士, 松田恭幸, 酒見泰寛, 長濱弘季, 中村圭佑, 早水友洋, 青木貴稔, 永瀬慎太郎, 山根風樹, 小澤直也, 佐藤幹, 深瀬実来, 上原大祐, 高峰愛子, 「フランシウムの電気双極子能率探索に向けた冷却原子制御系の開発」, 日本物理学会第 77 回年次大会, オンライン, 2022 年 3 月 15–19 日.

永瀬慎太郎, 酒見泰寛, 長濱弘季, 中村圭佑, 早水友洋, 青木貴稔, 中下輝士, 山根風樹, 小澤直也, 佐藤幹, 深瀬実来, 上原大祐, 高峰愛子, 「原子の電気双極子能率探索に向けたレーザー冷却フランシウム源の開発」, 日本物理学会第 77 回年次大会, オンライン, 2022 年 3 月 15–19 日.

安藤蒼太, 市川雄一, 佐藤智哉, 篠原悠介, 西畑洸希, 岸本侃己, 山下渉, 横田望海, 郷慎太郎, 高峰愛子, 上野秀樹, 旭耕一郎, 「EDM 測定に向けたガラスセル中 Xe 原子のスピン緩和機構の評価」, 日本物理学会第 77 回年次大会, オンライン, 2022 年 3 月 15–19 日.

庭瀬暁隆, P. Schury, 和田道治, P. Brionnet, S. Chen, 羽場宏光, 平山賀一, D. S. Hou, 飯村俊, 石山博恒, 伊藤由太, 加治大哉, 木村創大, 小浦寛之, 宮武宇也, 森本幸司, 森田浩介, 長江大輔, M. Rosenbusch, 高峰愛子, 渡辺裕, H. Wollnik, W. Xian, S. X. Yan, 「MRTOF + α-TOF による ^{257,258}Db の精密質量測定」, 日本物理学会第 77 回年次大会, オンライン, 2022 年 3 月 15–19 日.

今村慧, 高峰愛子, 郷慎太郎, 田島美典, Aleksey Gladkov, 上野秀樹, 「原子ビーム共鳴法による高スピン偏極 RI ビーム生成装置の開発」, 日本物理学会第 77 回年次大会, オンライン, 2022 年 3 月 15–19 日.

西畑洸希, Gladkov Aleksey, 上野秀樹, 市川雄一, 高峰愛子, 山崎展樹, 佐藤智哉, 田島美典, 今村彗, 川田敬太, 竹内由衣花, 螺良健一, 田中聡, 土居三瑠, 伊藤愛美, 秋元彩, 西村昌輝, 旭耕一郎, 三原基嗣, 足立智輝, 河本彩帆, 北川敦志, 佐藤眞二, 「スピン整列不安定原子核を用いたベータ核磁気共鳴法の開発」, 日本物理学会第 77 回年次大会, オンライン, 2022 年 3 月 15–19 日.

高峰愛子, 「高偏極 RI 原子ビーム生成へ向けた低速 RI ビーム生成装置と中性化装置の開発」, 日本物理学会第 77 回年次大会 共催シンポジウム, オンライン, 2022 年 3 月 15–19 日.

水野るり惠, 池田時浩, 郷慎太郎, 齋藤岳志, 櫻井博儀, 新倉潤, 松崎禎市郎, 道正新一郎, 「ミューオン原子 X 線分光のための Ge 検出器を用いた広ダイナミックレンジ光子検出システムの性能評価」, 日本物理学会第 77 回年次大会, オンライン, 2022 年 3 月 15–19 日.

Nuclear Science and Transmutation Research Division
High Energy Astrophysics Laborarory

1. Abstract

In the immediate aftermath of the Big Bang, the beginning of our universe, only hydrogen and helium existed. However, nuclear fusion in the interior of stars and the explosion of supernovae in the universe over 13.8 billion years led to the evolution of a world brimming with the many different elements we have today. By using scientific satellites or balloons to observe X-rays and gamma-rays emitted from celestial objects, we are observing the synthesis of the elements at their actual source. Our goal is to comprehensively elucidate the scenarios for the formation of the elements in the universe, together with our research on sub-atomic physics through the use of an accelerator.

2. Major Research Subjects

(1) History of nucleosynthesis in the universe
(2) Physics in extreme conditions in the universe
(3) Research and development of innovative radiation detectors
(4) Apply radiation technology for human to live in space

3. Summary of Research Activity

High Energy Astrophysics Laboratory started in April 2010. The goal of our research is to reveal the mechanism of nucleosynthesis and the evolution of elements in the universe, and to observe/discover exotic physical phenomena in extremely strong magnetic and/or gravitational fields. We have observed supernova remnants, strongly magnetized neutron stars, pulsars, black holes and galaxies with X-ray astronomical satellites, balloons and ground-based telescopes.

(1) Nucleosynthesis in the universe

(1-1) XRISM

X-Ray Imaging and Spectroscopy Mission (XRISM) is a new X-ray astrophysics observatory developed by a joint effort between Japan and US with participation of Europe. It is aimed at recovering the high-resolution X-ray spectroscopy of hot plasma in the Universe initiated by the short-lived Hitomi satellite. The spacecraft, payload instruments, and science observation program are currently under development. In FY2021, the development and subsystem-level tests of the two payload instruments, Resolve and Xtend, have been completed successfully. The two instruments are now on the spacecraft and ready for the spacecraft tests. The major milestone was achieved also in the science observation program. The observation targets for the Performance Verification (PV) phase have been selected and released to public and a new program called the XRISM Guest Scientist has started to offer researchers in the astrophysics community an opportunity to participate in scientific activities with the observations in the PV phase.

(1-2) MAXI

From April 2018, High Energy Astrophysics Laboratory hosts MAXI (Monitor of All-sky X-ray Image) onboard International Space Station (ISS), which was attached on ISS in 2009. MAXI is a RIKEN-lead project collaborating with JAXA and other universities. In FY2021, MAXI discovered the 14th blackhole binary MAXI J1803-298, and two Be X-ray binary pulsars MAXI J0903-531 and MAXI J0709-159. The former was followed up by Swift and NICER, while the latter was by NuSTAR and NICER. We reported 28 ATELs (Astronomer's Telegrams) on transient objects, and 8 GCNs (Gamma-ray Burst Coordinate Network) of gamma-ray bursts.

A new project OHMAN, which is automatic MAXI-NICER coordinate observations on ISS for quick follow-up of transient events such as gamma-ray bursts and gravitational events, was begun in earnest since 2020 November. We cooperated to equip OHMAN to ISS, and finally OHMAN has started on 2022 May 26. Immediate follow-up observations of X-ray transient objects detected by MAXI are possible with a high-sensitivity X-ray telescope.

(2) Extremely strong magnetism and gravity

(2-1) IXPE

We have contributed to the NASA's world-first X-ray polarimeter mission IXPE (Imaging X-ray Polarimeter Explorer). High Energy Astrophysics Laboratory is responsible for providing the gas electron multipliers (GEMs) to the IXPE mission: the GEM is a key device of the X-ray polarimeter and produced based on our patent for space use. The IXPE satellite was successfully launched on December 9, 2021 from Florida. After one month commissioning in orbit, IXPE started science observations of X-ray stellar objects from January 11, 2022.

By using the IXPE satellite, we aim to proof the strong magnetism of Magnetars, which are one of the species of neutron stars which have ultra-strong magnetic field $B > 10^{11}$ T. In such ultra-strong magnetic field, higher-order diagrams, $O(eB/m^2)$, $O(eB/m^2)^2$ *etc.*, never ignored in the QED perturbation theory. As the results, we observe newly-emerging phenomenon such as vacuum polarization, vacuum birefringence, *etc.* If such exotic phenomena are detected, we sure that Magnetars have really ultra-strong magnetic field. We have performed quick-analysis of a Magnetar, which is a neutron star with ultra-strong magnetic fields, observed by IXPE in the very early stage of the scientific observations.

(2-2) Astrophysical data analysis

In parallel with the mission development/operations, we are studying gamma-ray binary systems, which are one of the most important astrophysical targets in the MeV gamma-ray band. We analyzed the broad-band emission of gamma-ray binary LS 5039,

a bright gamma-ray object in the MeV band, using NuSTAR and Fermi. The obtained spectrum with the highest available statistics shows that the emission from MeV to sub-GeV bands is difficult to explain with current theoretical models, suggesting particle acceleration there is much more efficient than well-known standard diffusive shock acceleration.

(3) Innovative breakthrough in astrophysics with a small satellite

We are developing technology and acquiring know-how to make space observation, which requires a lot of money, possible with small satellites at low cost. NASA and other space agencies around the world have realized the importance of this opportunities and have started space observation activities using small satellites. NinjaSat is a micro-satellite mission (6U CubeSat; $30 \times 20 \times 10$ cm^3) led by RIKEN in collaboration with universities. NinjaSat will be deployed from the ISS in 2022. Although several science missions have recently been conducted using micro-satellites, NinjaSat is the world's first general purpose CubeSat mission to observe X-ray sources. NinjaSat carries two Xe-filled gas detectors with 2-degree-wide collimators and performs spectroscopy between 2–50 keV and timing obervation with a timing resolution of about 120 μs. Since the effective area is not large (~40 cm^2 at 6 keV), the target of the NinjaSat is a long-term monitoring of bright X-ray sources which are discovered by MAXI *etc.* In general, bright objects are difficult to observe and a continuous observations for long period is impossible with large satellite missions. The aim of NinjaSat is to perform observations that are difficult to perform on larger missions. For example, NinjaSat observes the time variability of binary neutron stars and binary black holes in conjunction with the ground-based optical, radio and gravitational telescopes. We fabricated and tested X-ray detectors for flight in FY2021.

(4) Future X-ray and gamma-ray detectors

In collaboration with NASA Goddard Space Flight Center, we have developed and tested a hard X-ray polarimeter with a Time Projection Chamber technique. This TPC polarimeter is one of candidates of the future satellite XPP (X-ray polarimeter Probe mission) planned with an international consortium.

As an successor of the MAXI mission, we are also verifying the principle of a new concept, multiplexing lobster-eye (MuLE) optics, to monitor the entire sky with a wide field-of-view for detecting and immediate reporting transient objects such as a neutron star merger. We published a paper on the conceptual design of MuLE, and proved the concept by a simple experiment.

To explore the MeV gamma-ray sky in the Universe, we are working on the technical development of the GRAMS (Gamma-Ray and AntiMatter Survey) project, which aims at future MeV gamma-ray observations with a Compton telescope using a liquid argon time projection chamber. We developed two types of event reconstruction algorithms for multiple Compton scattering events using probabilistic and neural network methods. Based on them, we confirmed that the advantage of the GRAMS project, which is an observation with an effective area larger than previous by 1-2 orders magnitudes, can be achievable with a current mission concept.

Members

Director

Toru TAMAGAWA

Research/Technical Scientist

Tatehiro MIHARA (Senior Research Scientist)

Special Postdoctoral Researcher

Hiroki YONEDA

Visiting Scientists

Aya BAMBA (Univ. of Tokyo)
Naohisa INADA (NIT, Nara College)
Satoru KATSUDA (Saitama Univ.)
Tomoki KIMURA (Tohoku Univ.)
Kazuki KOMIYA (Tokyo Metropolitan Industrial Tech. Res. Inst.)
Toru MISAWA (Shinshu Univ.)
Ikuyuki MITSUISHI (Nagoya Univ.)
Yujin NAKAGAWA (JAMSTEC)
Hirofumi NODA (Osaka Univ.)
Hirokazu ODAKA (Univ. of Tokyo)
Yuki OKURA (NAOJ/Nat'l Inst. of Natural Sci.)
Rohta TAKAHASHI (NIT, Tomakomai College)
Yoko TAKEUCHI (Tokyo Metropolitan Industrial Tech. Res. Inst.)
Yukikatsu TERADA (Saitama Univ.)
Masaki WAKABAYASHI (Jakulin Commercial Company LC)
Shinya YAMADA (Rikkyo Univ.)

Student Trainees

Syoki HAYASHI (Tokyo Univ. Sci)
Naoyuki OTA (Tokyo Univ. Sci)
Tomoshi TAKEDA (Tokyo Univ. Sci)
Keisuke UCHIYAMA (Tokyo Univ. Sci)
Yuto YOSHIDA (Tokyo Univ. Sci)

List of Publications & Presentations

Publications

[Original Papers]

L. Baldini, M. Barbanera, R. Bellazzini, R. Bonino, F. Borotto, A. Brez, C. Caporale, C. Cardelli, S. Castellano, M. Ceccanti, S. Citraro, N. D. Lalla, L. Latronico, L. Lucchesi, C. Magazzù, G. Magazzù, S. Maldera, A. Manfreda, M. Marengo, A. Marrocchesi, P. Mereu, M. Minuti, F. Mosti, H. Nasimi, A. Nuti, C. Oppedisano, L. Orsini, M. Pesce-Rollins, M. Pinchera, A. Profeti, C. Sgrò, G. Spandre, M. Tardiola, D. Zanetti, F. Amici, H. Andersson, P. Attinà, M. Bachetti, W. Baumgartner, D. Brienza, R. Carpentiero, M. Castronuovo, L. Cavalli, E. Cavazzuti, M. Centrone, E. Costa, E. D'Alba, F. D'Amico, E. D. Monte, S. D. Cosimo, A. D. Marco, G. D. Persio, I. Donnarumma, Y. Evangelista, S. Fabiani, R. Ferrazzoli, T. Kitaguchi, F. L. Monaca, C. Lefevre, P. Loffredo, P. Lorenzi, E. Mangraviti, G. Matt, T. Meilahti, A. Morbidini, F. Muleri, T. Nakano, B. Negri, S. Nenonen, S. L. O'Dell, M. Perri, R. Piazzolla, S. Pieraccini, M. Pilia, S. Puccetti, B. D. Ramsey, J. Rankin, A. Ratheesh, A. Rubini, F. Santoli, P. Sarra, E. Scalise, A. Sciortino, P. Soffitta, T. Tamagawa, A. F. Tennant, A. Tobia, A. Trois, K. Uchiyama, M. Vimercati, M. C. Weisskopf, F. Xie, F. Zanetti, and Y. Zhou, "Design, construction, and test of the gas pixel detectors for the IXPE mission," Astropart. Phys. **133**, 102628 (2021).

P. Soffitta, L. Baldini, R. Bellazzini, E. Costa, L. Latronico, F. Muleri, E. D. Monte, S. Fabiani, M. Minuti, M. Pinchera, C. Sgro', G. Spandre, A. Trois, F. Amici, H. Andersson, P. Attina', M. Bachetti, M. Barbanera, F. Borotto, A. Brez, D. Brienza, C. Caporale, C. Cardelli, R. Carpentiero, S. Castellano, M. Castronuovo, L. Cavalli, E. Cavazzuti, M. Ceccanti, M. Centrone, S. Ciprini, S. Citraro, F. D'Amico, E. D'Alba, S. D. Cosimo, N. D. Lalla, A. D. Marco, G. D. Persio, I. Donnarumma, Y. Evangelista, R. Ferrazzoli, A. Hayato, T. Kitaguchi, F. L. Monaca, C. Lefevre, P. Loffredo, P. Lorenzi, L. Lucchesi, C. Magazzu, S. Maldera, A. Manfreda, E. Mangraviti, M. Marengo, G. Matt, P. Mereu, A. Morbidini, F. Mosti, T. Nakano, H. Nasimi, B. Negri, S. Nenonen, A. Nuti, L. Orsini, M. Perri, M. Pesce-Rollins, R. Piazzolla, M. Pilia, A. Profeti, S. Puccetti, J. Rankin, A. Ratheesh, A. Rubini, F. Santoli, P. Sarra, E. Scalise, A. Sciortino, T. Tamagawa, M. Tardiola, A. Tobia, M. Vimercati, and F. Xie, "The instrument of the imaging X-ray polarimetry explorer," Astron. J. **162**, 208 (2021).

Q. Abarr, H. Awaki, M. G. Baring, R. Bose, G. D. Geronimo, P. Dowkontt, M. Errando, V. Guarino, K. Hattori, K. Hayashida, F. Imazato, M. Ishida, N. K. Iyer, F. Kislat, M. Kiss, T. Kitaguchi, H. Krawczynski, L. Lisalda, H. Matake, Y. Maeda, H. Matsumoto, T. Mineta, T. Miyazawa, T. Mizuno, T. Okajima, M. Pearce, B. F. Rauch, F. Ryde, C. Shreves, S. Spooner, T. -A. Stana, H. Takahashi, M. Takeo, T. Tamagawa, K. Tamura, H. Tsunemi, N. Uchida, Y. Uchida, A. T. West, E. A. Wulf, and R. Yamamoto, "XL-calibur – A second-generation balloon-borne hard X-ray polarimetry mission," Astropart. Phys. **126**, 102529 (2021).

W. B. Iwakiri, M. Serino, T. Mihara, L. Gu, H. Yamaguchi, M. Shidatsu, and K. Makishima, "Discovery of a strong 6.6 keV emission feature from EXO 1745-248 after the superburst in 2011 October," Publ. Astron. Soc. Jpn. **73**, 108 (2021).

M. Kimura, S. Yamada, N. Nakaniwa, Y. Makita, H. Negoro, M. Shidatsu, T. Kato, T. Enoto, K. Isogai, T. Mihara, H. Akazawa, K. C. Gendreau, F. -J. Hambsch, P. A. Dubovsky, I. Kudzej, K. Kasai, Tamás Tordai, E. Pavlenko, A. A. Sosnovskij, J. V. Babina, O. I. Antonyuk, H. Itoh, and H. Maehara, "On the nature of the anomalous event in 2021 in the dwarf nova SS Cygni and its multi-wavelength transition," Publ. Astron. Soc. Jpn. **73**, 1262 (2021).

Y. Yao, S. R. Kulkarni, K. C. Gendreau, G. K. Jaisawal, T. Enoto, B. W. Grefenstette, H. L. Marshall, J. A. García, R. M. Ludlam, S. N. Pike, M. Ng, L. Zhang, D. Altamirano, A. Jaodand, S. B. Cenko, R. A. Remillard, J. F. Steiner, H. Negoro, M. Brightman, A. Lien, M. T. Wolff, P. S. Ray, K. Mukai, Z. Wadiasingh, Z. Arzoumanian, N. Kawai, T. Mihara, and T. E. Strohmayer, "A comprehensive X-ray report on AT2019wey," Astrophys. J. **920**, 121 (2021).

M. Shidatsu, W. Iwakiri, H. Negoro, T. Mihara, Y. Ueda, N. Kawai, S. Nakahira, J. A. Kennea, P. A. Evans, K. C. Gendreau, T. Enoto, and F. Tombesi, "The peculiar X-ray transient swift J0840.7-3516: An unusual low-mass X-ray binary or a tidal disruption event?," Astrophys. J. **910**, 144 (2021).

R. Sasaki, Y. Tsuboi, W. Iwakiri, S. Nakahira, Y. Maeda, K. C. Gendreau, M. F. Corcoran, K. Hamaguchi, Z. Arzoumanian, C. Markwardt, T. Enoto, T. Sato, H. Kawai, T. Mihara, M. Shidatsu, H. Negoro, and M. Serino, "The RS CVn-type Star GT mus shows most energetic X-ray flares throughout the 2010s," Astrophys. J. **910**, 25 (2021).

K. Makishima, T. Tamba, Y. Aizawa, H. Odaka, H. Yoneda, T. Enoto, and H. Suzuki, "Discovery of 40.5 ks hard X-ray pulse-phase modulations from SGR 1900+14," Astrophys. J. **923**, 63 (2021).

T. Orita, G. Yabu, H. Yoneda, S. I. Takeda, P. Caradonna, T. Takahashi, S. Watanabe, Y. Uchida, F. Moriyama, H. Sugawara, M. Ueno-machi, and K. Shimazoe, "Double-photon emission imaging with high-resolution Si/CdTe compton cameras," IEEE Trans. Nucl. Sci. **68**, 2279 (2021).

H. Yoneda, D. Khangulyan, T. Enoto, K. Makishima, K. Mine, T. Mizuno, and T. Takahashi, "Broadband high-energy emission of the gamma-ray binary system LS 5039: Spectral and temporal features using NuSTAR and Fermi observations," Astrophys. J. **917**, 90 (2021).

N. Tsuji, H. Yoneda, Y. Inoue, T. Aramaki, G. Karagiorgi, R. Mukherjee, and H. Odaka, "Cross-match between the Latest Swift-BAT and Fermi-LAT catalogs," Astrophys. J. **916**, 28 (2021).

Y. Tsuzuki, S. Watanabe, S. Oishi, N. Nakamura, N. Numadate, H. Odaka, Y. Uchida, H. Yoneda, and T. Takahashi, "An application of a Si/CdTe Compton camera for the polarization measurement of hard X rays from highly charged heavy ions," Rev. Sci. Instrum. **92**, 063101 (2021).

K. Makishima, T. Enoto, H. Yoneda, and H. Odaka, "A NuSTAR confirmation of the 36 ks hard X-ray pulse-phase modulation in the magnetar 1E 1547.0-5408," Mon. Notices Royal Astron. Soc. **502**, 2266 (2021).

S. N. Pike, H. Negoro, J. A. Tomsick, M. Bachetti, McK. Brumback, R. M T. Connors, J. A. García, B. Grefenstette, J. Hare, F. A. Harrison, A. Jaodand, R. M. Ludlam, G. Mastroserio, T. Mihara, M. Shidatsu, M. Sugizaki, and R. Takagi, "MAXI and NuSTAR observations of the faint X-ray transient MAXI J1848-015 in the GLIMPSE-C01 cluster," Astrophys. J. **927**, 190 (2022).

M. Shidatsu, K. Kobayashi, H. Negoro, W. Iwakiri, S. Nakahira, Y. Ueda, T. Mihara, T. Enoto, K. Gendreau, Z. Arzoumanian, J. Pope, B. Trout, T. Okajima, and Y. Soong, "Discovery and long-term broadband X-ray monitoring of galactic black hole candidate MAXI J1803-298," Astrophys. J. **927**, 151 (2022).

N. Numadate, S. Oishi, H. Odaka, M. Sakurai, T. Takahashi, Y. Tsuzuki, Y. Uchida, H. Watanabe, S. Watanabe, H. Yoneda, and N. Nakamura, "Polarization measurement of *L*-shell radiative recombination X rays from highly charged bismuth ions," Phys. Rev. A **105**, 023109 (2022).

[Proceeding]

B. D. Ramsey, P. Attina, L. Baldini, M. Barbanera, W. H. Baumgartner, R. Bellazzini, J. Bladt, S. D. Bongiorno, A. Brez, S. Castellano, R. Carpentiero, M. Castronuovo, L. Cavalli, E. Cavazutti, F. D'Amico, S. Citraro, E. Costa, W. D. Deininger, E. D'Alba, E. Delmonte, K. L. Dietz, N. D. Lalla, A. D. Marco, G. D. Persio, I. Donnarumma, S. Fabiani, R. Ferrazzoli, J. Footdale, M. Head, W. Kalinowski, J. J. Kolodziejczak, L. Latronico, C. Lefevre, P. Lorenzi, L. Lucchesi, S. Maldera, A. Manfreda, E. Mangravati, H. L. Marshall, G. Matt, M. Minuti, R. Mize, F. Muleri, H. Nasimi, B. Negri, A. Nuti, S. O'Dell, L. Orsini, D. Osborne, C. Pentz, M. Pilia, M. Perri, M. Pesce-Rollins, C. Peterson, M. Pinchera, S. Puccetti, J. Rankin, A. Ratheesh, R. W. Romani, P. Sarra, F. Santoli, A. Sciortino, C. Schroeder, C. Sgro, P. Soffitta, G. Spandre, A. Tennant, A. Tobia, N. E. Thomas, A. Trois, M. Vimercati, J. Wedmore, M. C. Weisskopf, F. Xie, F. Zanetti, C. Alexander, D. Z. Allen, F. Amici, J. Andersen, A. Antonelli, S. Antoniak, M. Bachetti, R. M. Baggett, R. Bonino, C. Boree, F. Borotto, S. Breeding, D. Brienza, H. K. Byggott, C. Caporale, C. Cardelli, M. Ceccanti, M. Centrone, D. Dolan, Y. Evangelista, K. Ferrant, M. Ferrie, B. Forsyth, M. Foster, B. Garelick, S. Gunji, E. Gurnee, G. Hibbard, S. Johnson, E. Kelly, K. Kilaru, F. L. Monaca, S. L. Roy, P. Lofredo, T. Maddox, G. Magazzu, M. Marengo, A. Marrocchesi, F. Massaro, D. Mauger, J. McCracken, M. McEachen, P. Mereu, S. Mitchell, I. Mitsuishi, A. Morbidini, F. Mosti, T. Nguyen, M. Negro, I. Nitschke, M. Onizuka, C. Oppedisano, R. Pacheco, A. Paggi, W. Painter, S. D. Pavelitz, R. Piazzolla, A. Profeti, J. Ranganathan, L. Reedy, N. Root, A. Rubini, S. Ruswick, J. Sanchez, E. Scalise, T. Seek, K. Sosdian, C. O. Speegle, T. Tamagawa, M. Tardiola, R. Valerie, A. L. Walden, B. Weddendorf, and D. Welch, "The imaging X-ray polarimetry explorer (IXPE): Technical overview IV," Proc. SPIE **11821**, 118210M (2021).

Presentations

[Domestic Conferences/Workshops]

玉川徹, 北口貴雄, 榎戸輝揚, 内山慶祐, 武田朋志, 三石郁之, 柏倉一斗, 田原譲, 郡司修一, 渡邉瑛里, 寺島政伸, 斎藤耀, 管佑真, 深沢泰司, 水野恒史, 高橋弘充, 内田和海, S. Zhang, 岩切渉, 林田清, 朝倉一統, M. Weisskopf, B. Ramsey, S. O'Dell, P. Soffitta, L. Baldini, ほか IXPE 衛星チーム, 「X 線偏光観測衛星 IXPE への参加現状 (7)」, 日本天文学会 2021 年秋季年会, オンライン, 2021 年 9 月.

三原建弘, 根来均, 岩切渉, 海老沢研, ほか MAXI チーム, 「OHMAN (MAXI-NICER ISS 上連携) の準備状況」, 日本天文学会 2021 年秋季年会, オンライン, 2021 年 9 月.

武田朋志, 玉川徹, 榎戸輝揚, 北口貴雄, 加藤陽, 沼澤正樹, 三原建弘, 岩切渉, 内山慶祐, 吉田勇登, 大田尚享, 林昇輝, 佐藤宏樹, C. -P. Hu, 高橋弘充, 小高裕和, 丹波翼, 谷口絢太郎, 「明るい X 線天体を狙う 6U キューブサット NinjaSat の進捗」, 日本天文学会 2021 年秋季年会, オンライン, 2021 年 9 月.

吉田勇登, 玉川徹, 榎戸輝揚, 北口貴雄, 加藤陽, 沼澤正樹, 三原建弘, 岩切渉, 内山慶祐, 武田朋志, 大田尚享, 林昇輝, 佐藤宏樹, C. -P. Hu, 高橋弘充, 小高裕和, 丹波翼, 谷口絢太郎, 「NinjaSat における信号波形による X 線と荷電粒子の弁別方法の開発」, 日本天文学会 2021 年秋季年会, オンライン, 2021 年 9 月.

沼澤正樹, 玉川徹, 榎戸輝揚, 北口貴雄, 加藤陽, 三原建弘, 岩切渉, 内山慶祐, 武田朋志, 大田尚享, 吉田勇登, 林昇輝, 佐藤宏樹, C. -P. Hu, 高橋弘充, 小高裕和, 丹波翼, 谷口絢太郎, 「NinjaSat に搭載する観測機器のコンポーネント環境試験」, 日本天文学会 2021 年秋季年会, オンライン, 2021 年 9 月.

大田尚享, 玉川徹, 榎戸輝揚, 北口貴雄, 加藤陽, 沼澤正樹, 三原建弘, 岩切渉, 内山慶祐, 武田朋志, 吉田勇登, 林昇輝, 佐藤宏樹, C. -P. Hu, 高橋弘充, 小高裕和, 丹波翼, 谷口絢太郎, 「NinjaSat に搭載するアナログ信号処理基板の開発」, 日本天文学会 2021 年秋季年会, オンライン, 2021 年 9 月.

内山慶祐, 玉川徹, 三原建弘, 榎戸輝揚, 沼澤正樹, 周圓輝, 江副祐一郎, 伊師大貴, 福島碧都, 内野友樹, 作田紗恵, 石川久美, 森下弘海, 関口るな, 辻雪音, 村川貴俊, 稲垣綾太, 上田陽功, 坂本貴紀, 「広視野を少数の撮像素子でカバーする多重化ロブスターアイ X 線光学系」, 日本天文学会 2021 年秋季年会, オンライン, 2021 年 9 月.

Y. Ishisaki, R. L. Kelley, H. Akamatsu, H. Awaki, T. G. Bialas, G. V. Brown, M. P. Chiao, E. Costantini, J. -W. den Herder, M. J. Dipirro, M. E. Eckart, Y. Ezoe, C. Ferrigno, R. Fujimoto, A. Furuzawa, S. M. Graham, M. Grim, T. Hayashi, A. Hoshino, Y. Ichinohe, R. Iizuka, M. Ishida, K. Ishikawa, C. A. Kilbourne, S. Kitamoto, M. A. Leutenegger, Y. Maeda, D. McCammon, I. Mitsuishi, M. Mizumoto, T. Okajima, S. Paltani, F. S. Porter, K. Sato, T. Sato, M. Sawada, H. Seta, P. J. Shirron, G. A. Sneiderman, Y. Soong, A. E. Szymkowiak, Y. Takei, T. Tamagawa, M. Tsujimoto, Y. Uchida, C. P. de Vries, S. Yamada, N. Y. Yamasaki, S. Yasuda, and N. Yoshioka, 「X 線分光撮像衛星 XRISM 搭載 Resolve の開発の現状 VII」, 日本天文学会 2021 年秋季年会, オンライン, 2021 年 9 月.

寺島政伸, 郡司修一, 渡邉瑛里, 管佑真, 斎藤耀, 玉川徹, 北口貴雄, 榎戸輝揚, 内山慶祐, 武田朋志, 三石郁之, 柏倉一斗, 田原譲, 深沢泰司, 水野恒史, 高橋弘充, 内田和海, Z. Sixuan, 岩切渉, 林田清, 朝倉一統, M. Weisskopf, B. Ramsey, S. O'Dell, P. Soffitta, L. Baldini, ほか IXPE 衛星チーム, 「IXPE におけるガンマ線バースト残光の観測クライテリア」, 日本物理学会 2021 年秋季大会, オンライン, 2021 年 9 月.

高橋弘充, Q. Abarr, 青柳美緒, 朝倉一統, 粟木久光, M. G. Baring, R. Bose, D. Braun, Gianluigi de Geronimo, P. Dowkontt, J. Elliot, 榎戸輝揚, M. Errando, 深沢泰司, 古澤彰浩, T. Gadson, E. Gau, V. Guarino, 郡司修一, 袴田知宏, 萩原涼太, K. Hall, 花岡真帆, K. Harmon, 服部憲吾, 林田清, L, S. Heatwole, A. Hossen, 井出峻太郎, 今村竜太, 今里郁弥, 今澤遼, 石橋和紀, 石田学, 石倉彩美, 石渡幸太, N. K. Iyer, F. Kislat, M. Kiss, 亀谷紀香, 鴨川航, 北口貴 G, D. Kotsifakis, H. Krawczynski, J. Lanzi, L. Lisalda, 前田良知, 松下友亮, 眞武寛人, 松本浩典, 峯田大晴, 宮本明日香, 宮澤拓也, 水野恒史, 中庭望, 野田博文, 大出優一, 岡島崇, 岡崎貴樹, I. Pastrani, M. Pearce, N, Z. Peterson, H. Poon, C. Purdy, B. Rauch, F. Ryde, 斎藤芳隆, 佐久間翔太郎, 佐藤淳矢, 澤上拳明, C. Shreeves, G. Simburger, C. Snow, S. Spooner, Theodor-A. Stana, D. Stuchlik, 鈴木瞳, 武田朋志, 武尾舞, 玉川徹, 田村啓輔, 常深

博, 内田和海, 内田悠介, 内山慶祐, B. Vincent, A. West, E. Wulf, 山本龍哉, 楊冲, 米山友景, 吉田勇登, 善本真梨那, ほか XL-Calibur チーム, 「硬 X 線偏光観測 XL-Calibur 気球実験の 2022 年フライトへ向けた準備状況」, 日本物理学会 2021 年秋季大会, オンライン, 2021 年 9 月.

小高裕和, 高嶋聡, 南木宙斗, 馬場彩, 青山一天, 岩澤広大, 木村眞人, 櫻井真由, 田中雅士, 中曽根太地, 寄田浩平, 一戸悠人, 井上芳幸, 辻直美, 米田浩基, T. Aramaki, G. Karagiorgi, R. Mukherjee, ほか GRAMS コラボレーション「GRAMS 実験 5：全体報告」, 日本物理学会 2021 年秋季大会, オンライン, 2021 年 9 月.

高嶋聡, 小高裕和, 南木宙斗, 馬場彩, 青山一天, 岩澤広大, 木村眞人, 櫻井真由, 田中雅士, 中曽根太地, 寄田浩平, 一戸悠人, 井上芳幸, 辻直美, 米田浩基, T. Aramaki, G. Karagiorgi, R. Mukherjee, ほか GRAMS コラボレーション, 「GRAMS 実験 6：マルチタスク深層学習によるイベント再構成手法の開発」, 日本物理学会 2021 年秋季大会, オンライン, 2021 年 9 月.

青山一天, 岩澤広大, 木村眞人, 櫻井真由, 田中雅士, 中曽根太地, 寄田浩平, 小高裕和, 高嶋聡, 南木宙斗, 馬場彩, 一戸悠人, 井上芳幸, 辻直美, 米田浩基, T. Aramaki, G. Karagiorgi, R. Mukherjee, ほか GRAMS コラボレーション, 「GRAMS 実験 7：液体アルゴン TPC における光子・電子信号のエネルギー分解能測定」, 日本物理学会 2021 年秋季大会, オンライン, 2021 年 9 月.

櫻井真由, 青山一天, 岩澤広大, 木村眞人, 田中雅士, 中曽根太地, 寄田浩平, 小高裕和, 高嶋聡, 米田浩基, 一戸悠人, ほか GRAMS コラボレーション, 「宇宙線反重陽子探索に向けた液体アルゴン検出器による宇宙線荷電粒子の識別」, 日本物理学会 2021 年秋季大会, オンライン, 2021 年 9 月.

中曽根太地, 青山一天, 岩澤広大, 木村眞人, 櫻井真由, 田中雅士, 寄田浩平, 小高裕和, 高嶋聡, 米田浩基, 一戸悠人, ほか GRAMS コラボレーション「宇宙反重陽子探索に向けた液体アルゴン検出器における原子核捕獲事象の検証」, 日本物理学会 2021 年秋季大会, オンライン, 2021 年 9 月.

玉川徹, 北口貴雄, 榎戸輝揚, 内山慶祐, 武田朋志, 三石郁之, 柏倉一斗, 田原譲, 郡司修一, 渡邉瑛里, 寺島政伸, 斎藤耀, 管佑真, 深沢泰司, 水野恒史, 高橋弘充, 内田和海, S. Zhang, 岩切渉, 林田清, 朝倉一統, M. Weisskopf, B. Ramsey, S. O'Dell, P. Soffitta, L. Baldini, ほか IXPE 衛星チーム, 「X 線偏光観測衛星 IXPE」, 第 22 回宇宙科学シンポジウム, 相模原 (宇宙科学研究所), 2022 年 1 月.

玉川徹, 北口貴雄, 榎戸輝揚, 内山慶祐, 武田朋志, 三石郁之, 柏倉一斗, 田原譲, 郡司修一, 渡邉瑛里, 寺島政伸, 斎藤耀, 管佑真, 深沢泰司, 水野恒史, 高橋弘充, 内田和海, Z. Sixuan, 岩切渉, 林田清, 朝倉一統, M. Weisskopf, B. Ramsey, S. O'Dell, P. Soffitta, L. Baldini, ほか IXPE 衛星チーム, 「X 線偏光観測衛星 IXPE の現状 (1)」, 日本天文学会 2022 年春季年会, オンライン, 2022 年 3 月.

林昇輝, 玉川徹, 榎戸輝揚, 北口貴雄, 加藤陽, 三原建弘, 岩切渉, 沼澤正樹, 武田朋志, 吉田勇登, 大田尚享, 内山慶祐, 佐藤宏樹, C. -P. Hu, 高橋弘充, 小高裕和, 丹波翼, 谷口絢太郎, 「超小型 X 線衛星 NinjaSat に搭載するガス X 線検出器の開発 (3)」, 日本天文学会 2022 年春季年会, オンライン, 2022 年 3 月.

大田尚享, 玉川徹, 榎戸輝揚, 北口貴雄, 加藤陽, 三原建弘, 岩切渉, 沼澤正樹, 武田朋志, 吉田勇登, 林昇輝, 内山慶祐, 佐藤宏樹, C. -P. Hu, 高橋弘充, 小高裕和, 丹波翼, 谷口絢太郎, 「超小型 X 線衛星 NinjaSat に搭載するガス検出器用の電子回路基板の開発」, 日本天文学会 2022 年春季年会, オンライン, 2022 年 3 月.

加藤陽, 玉川徹, 榎戸輝揚, 北口貴雄, 三原建弘, 岩切渉, 沼澤正樹, 武田朋志, 吉田勇登, 大田尚享, 林昇輝, 内山慶祐, 佐藤宏樹, C. -P. Hu, 高橋弘充, 小高裕和, 丹波翼, 谷口絢太郎, 「超小型 X 線衛星 NinjaSat に搭載する放射線帯モニターの開発」, 日本天文学会 2022 年春季年会, オンライン, 2022 年 3 月.

米田浩基, 辻直美, 小高裕和, 高嶋聡, 丹波翼, 南木宙斗, 馬場彩, 八幡和志, 青山一天, 岩澤広大, 櫻井真由, 田中雅士, 中曽根太地, 寄田浩平, 一戸悠人, D. Khangulyan, 井上芳幸, 内田悠介, 須田祐介, 高橋弘允, 深沢泰司, 大野雅功, 広島渚, T. Aramaki, G. Karagiorgi, R. Mukherjee, ほか GRAMS コラボレーション, 「GRAMS 計画 4:MeV ガンマ線観測・ダークマター探索気球実験」, 日本天文学会 2022 年春季年会, オンライン, 2022 年 3 月.

Y. Ishisaki, R. L. Kelley, H. Akamatsu, H. Awaki, T. G. Bialas, G. V. Brown, M. P. Chiao, E. Costantini, J. -W. den Herder, M. J. Dipirro, M. E. Eckart, Y. Ezoe, C. Ferrigno, R. Fujimoto, A. Furuzawa, S. M. Graham, M. Grim, T. Hayashi, A. Hoshino, Y. Ichinohe, R. Iizuka, M. Ishida, K. Ishikawa, C. A. Kilbourne, S. Kitamoto, M. A. Leutenegger, Y. Maeda, D. McCammon, I. Mitsuishi, M. Mizumoto, T. Okajima, S. Paltani, F. S. Porter, K. Sato, T. Sato, M. Sawada, H. Seta, P. J. Shirron, G. A. Sneiderman, Y. Soong, A. E. Szymkowiak, Y. Takei, T. Tamagawa, M. Tsujimoto, Y. Uchida, C. P. de Vries, S. Yamada, N. Y. Yamasaki, S. Yasuda, N. Yoshioka, 「X 線分光撮像衛星 XRISM 搭載 Resolve の開発の現状 VIII」, 日本天文学会 2022 年春季年会, オンライン, 2022 年 3 月.

郡司修一, 渡邉瑛里, 寺島政伸, 管佑真, 斎藤耀, 玉川徹, 北口貴雄, 榎戸輝揚, 内山慶祐, 武田朋志, 三石郁之, 柏倉一斗, 田原譲, 深沢泰司, 水野恒史, 高橋弘充, 内田和海, Z. Sixuan, 岩切渉, 林田清, 朝倉一統, M. Weisskopf, B. Ramsey, S. O'Dell, P. Soffitta, L. Baldini, ほか IXPE 衛星チーム, 「IXPE 衛星によって開かれるイメージング X 線偏光観測」, 日本物理学会第 77 回年次大会, オンライン, 2022 年 3 月.

渡邉瑛里, 郡司修一, 寺島政伸, 管佑真, 斎藤耀, 玉川徹, 北口貴雄, 榎戸輝揚, 内山慶祐, 武田朋志, 三石郁之, 柏倉一斗, 田原譲, 深沢泰司, 水野恒史, 高橋弘充, 内田和海, Z. Sixuan, 岩切渉, 林田清, 朝倉一統, M. Weisskopf, B. Ramsey, S. O'Dell, P. Soffitta, L. Baldini, ほか IXPE 衛星チーム, 「カニ星雲を用いた Chandra と IXPE のジョイント解析による偏光解析手法の開発」, 日本物理学会第 77 回年次大会, オンライン, 2022 年 3 月.

高橋弘充, Q. Abarr, 青柳美緒, 朝倉一統, 粟木久光, M. G. Baring, R. Bose, D. Braun, Gianluigi de Geronimo, P. Dowkontt, J. Elliot, 榎戸輝揚, M. Errando, 深沢泰司, 古澤彰浩, T. Gadson, E. Gau, V. Guarino, 郡司修一, 袴田知宏, 萩原涼太, K. Hall, 花岡真帆, K. Harmon, 服部憲吾, 林田清, S. Heatwole, A. Hossen, 井出峻太郎, 今村竜太, 今里郁弥, 今澤遼, 石橋和紀, 石田学, 石倉彩美, 石渡幸太, N. K. Iyer, F. Kislat, M. Kiss, 亀谷紀香, 鴨川航, 北口貴雄, D. Kotsifakis, H. Krawczynski, J. Lanzi, L. Lisalda, 前田良知, 松下友亮, 眞武寛人, 松本浩典, 峯田大晴, 宮本明日香, 宮澤拓也, 水野恒史, 中庭望, 野田博文, 大出優一, 岡島崇, 岡崎貴樹, I. Pastrani, M. Pearce, Z. Peterson, H. Poon, C. Purdy, B. Rauch, F. Ryde, 斎藤芳隆, 佐久間翔太郎, 佐藤淳矢, 澤上拳明, C. Shreeves, G. Simburger, C. Snow, S. Spooner, Theodor-A. Stana, D. Stuchlik, 鈴木瞳, 武田朋志, 武尾舞, 玉川徹, 田村啓輔, 常深博, 内田和海, 内田悠介, 内山慶祐, B. Vincent, A. West, E. Wulf, 山本龍哉, 楊冲, 米山友景, 吉田勇登, 善本真梨那, ほか XL-Calibur チーム, 「硬 X 線偏光観測 XL-Calibur 気球実験の 2022 年フライトへ向けた準備状況」, 日本物理学会第 77 回年次大会, オンライン, 2022 年 3 月.

武田朋志, 玉川徹, 榎戸輝揚, 北口貴雄, 加藤陽, 三原建弘, 岩切渉, 沼澤正樹, 内山慶祐, 吉田勇登, 大田尚享, 林昇輝, 佐藤宏樹, C. -P. Hu, 高橋弘充, 小高裕和, 丹波翼, 谷口絢太郎, 「超小型 X 線衛星 NinjaSat 搭載のガス X 線検出器の開発進捗」, 日本物理学

会第 77 回年次大会, オンライン, 2022 年 3 月.

吉田勇登, 玉川徹, 榎戸輝揚, 北口貴雄, 加藤陽, 三原建弘, 岩切渉, 沼澤正樹, 内山慶祐, 武田朋志, 大田尚享, 林昇輝, 佐藤宏樹, C. -P. Hu, 高橋弘充, 小高裕和, 丹波翼, 谷口絢太郎, 「超小型 X 線衛星 NinjaSat における X 線と宇宙線の波形弁別方法の開発」, 日本物理学会第 77 回年次大会, オンライン, 2022 年 3 月.

北口貴雄, 玉川徹, 榎戸輝揚, 加藤陽, 三原建弘, 岩切渉, 沼澤正樹, 内山慶祐, 武田朋志, 吉田勇登, 大田尚享, 林昇輝, 佐藤宏樹, C. -P. Hu, 高橋弘充, 小高裕和, 丹波翼, 谷口絢太郎, 「超小型 X 線衛星 NinjaSat に搭載するデータ取得ボードの開発」, 日本物理学会第 77 回年次大会, オンライン, 2022 年 3 月.

後藤初音, 米徳大輔, 荻野直樹, 有元誠, 澤野達哉, 三原建弘, 「軟 X 線ビームラインによる Lobster Eye Optics の結像性能評価」, 日本物理学会第 77 回年次大会, オンライン, 2022 年 3 月.

Nuclear Science and Transmutation Research Division
Nuclear Many-Body Theory Laborarory

1. Abstract

The nuclear many-body theory laboratory aims to understand various aspects of nuclear structure and reactions due to the assembly and disassembly of protons and neutrons in the nuclear many-body systems. For this purpose, we construct theoretical models and conduct numerical calculations to describe them. Our research topics include nuclear structure issues such as nuclear deformation, shell structure, and clustering of unstable nuclei, and nuclear reactions in the Universe where elements originate. In addition to fundamental research, we are also developing nuclear reaction database by combining the nuclear models and machine learning. The database will be used for various scientific and technological applications such as nuclear reactors, medicine and industry.

2. Major Research Subjects

(1) Structure and reactions of unstable nuclei
(2) Nuclear clustering and related nuclear reactions
(3) Nuclear reactions in the universe
(4) Research and development of the nuclear reaction database for applications

3. Summary of Research Activity

(1) Structure and reactions of unstable nuclei

The study of the structure and reactions of unstable nuclei is an important subject of the Nishina Center, as well as one of the core issues in modern nuclear physics. Our group approaches this problem by performing numerical calculations using theoretical models such as antisymmetrized molecular dynamics and density functional theory.

In this fiscal year, we mainly discussed the nuclear deformation and shape coexistence phenomena induced by the disappearance of the magic numbers in neutron-rich nuclei. One of the research highlights is the study of ^{44}S, in which we have found the onset of the large amplitude collective motion due to the disappearance of the magic number $N = 28$. We have shown that this nucleus does not have definite shape but is always fluctuating. We have also pointed out that the monopole transition strength is an experimental probe to this shape fluctuation. By using the obtained density distribution of unstable nuclei as an input to the Glauber model, we also investigated how the disappearance of magic number and the shape of the nuclei affect the reaction cross section and the angular distribution of elastic scattering.

(2) Nuclear clustering and related nuclear reactions

The nuclear clustering, in which nucleons are confined into into several subunits (clusters), is an eligible research subject for understanding the correlation of nucleons interacting with strong force. Since the clusters are linked to the nuclear reaction channels, they also appear as the intermediate states of various nuclear reaction dynamics.

In this year, we have studied the $3\alpha + n$ cluster structure in order to understand how the 3α cluster state (the 0_2^+ state of ^{12}C), known as the Bose-Einstein condensate (BEC) of α clusters, is influenced by the addition of a neutron as impurity. Using the real-time evolution method, we have identified the $3\alpha + n$ cluster state as an excited state of ^{13}C, and have shown that its matter radius is considerably reduced than that of the 3α BEC due to the attraction of the additional neutron. In addition, by using the antisymmetrized molecular dynamics model, we have investigated how the α cluster formation probability in unstable Be and C isotopes changes as function of neutron skin thickness. We have demonstrated that the α cluster formation is hindered by the growth of the neutron skin, which is consistent with the experimental data reported for the Sn isotopes.

(3) Nuclear reactions in the universe

Fusion reactions that occur in stellar and explosive astronomical events are key to understanding the origin of the elements. However, many reactions have extremely small cross sections, making direct experimental measurement difficult, and estimating reaction rates by theoretical calculation is critically important.

In this fiscal year, using the antisymmetrized molecular dynamics, we have obtained an estimate of the reaction rate of ^{12}C +^{12} C fusion. It must be emphasized that this is a well-known key reaction which affects the steller evolution and superburst of neutron star, and that our result is the first estimates from a full-microscopic nuclear model. We have shown that there are many resonances within the Gamow window, and hence, the reaction rate at steller temperatures are not hindered but are enhanced in contradiction to the estimation by a phenomenological model.

(4) Research and development of the nuclear reaction database for applications

Evaluated nuclear data are indispensable in the field of nuclear science and technology, and the demand of nuclear data is altering year by year with technical developments of nuclear science and technology. To catch up with the demands, an effective method that can regularly generate evaluated nuclear data has been highly desired.

The machine learning technologies can be an answer to this demand, and we are training nuclear reaction models by adopting the Bayesian optimization (BO) to effectively produce the nuclear data. In this fiscal year, we have developed a prototype system which combines the assembly of the nuclear reaction codes CCONE and BO with Gaussian regression. It is found that the optimization of the reaction model parameter works well to reproduce the observed angular distributions of neutron and proton elastic scatterings at various incident energies.

Members

Director

Masaaki KIMURA

Visiting Scientists

Kenichi YOSHIDA (Kyoto Univ.)
Kazuyuki SEKIZAWA (TITECH)
Futoshi MINATO (JAEA)
Koichi SATO (Kochi Univ.)

Assistant

Izumi YOSHIDA

List of Publications & Presentations

Publications

[Original Papers]

V. Choudhary, W. Horiuchi, M. Kimura, and R. Chatterjee, "Enormous nuclear surface diffuseness of Ne and Mg isotopes in the island of inversion," Phys. Rev. C **104**, 054313 (2021).

S. Shin, B. Zhou, and M. Kimura, "Shape of ^{13}C studied by the real-time evolution method," Phys. Rev. C **103**, 054313 (2021).

S. Shin, B. Zhou, and M. Kimura, "The isoscalar monopole strength of ^{13}C," Few-Body Syst. **62**, 93 (2021).

Q. Zhao, Y. Suzuki, J. He, B. Zhou, and M. Kimura, "α clustering and neutron-skin thickness of carbon isotopes," Eur. Phys. J. A **57**, 157 (2021).

Y. Suzuki and M. Kimura, "Triaxial deformation and the disappearance of the $N = 28$ shell gap," Phys. Rev. C **104**, 024327 (2021).

Y. Taniguchi and M. Kimura, "^{12}C +^{12} C fusion S^*-factor from a full-microscopic nuclear model," Phys. Lett. B **823**, 136790 (2021).

M. Dan, R. Chatterjee, and M. Kimura, "A description of the structure and electromagnetic breakup of Be with microscopic inputs," Eur. Phys. J. A **57**, 203 (2021).

P. Adsley, V. O. Nesterenko, M. Kimura, L. M. Donaldson, R. Neveling, J. W. Brümmer, D. G. Jenkins, N. Y. Kheswa, J. Kvasil, K. C. W. Li, D. J. Marín-Lámbarri, Z. Mabika, P. Papka, L. Pellegri, V. Pesudo, B. Rebeiro, P. -G. Reinhard, F. D. Smit, and W. Yahia-Cherif, "Isoscalar monopole and dipole transitions in ^{24}Mg, ^{26}Mg, and ^{28}Si," Phys. Rev. C **103**, 044315 (2021).

Y. Taniguchi, K. Yoshida, Y. Chiba, Y. Kanada-En'yo, M. Kimura, and K. Ogata, "Unexpectedly enhanced alpha-particle preformation in ^{48}Ti probed by the (p, $p\alpha$) reaction," Phys. Rev. C **103**, L031305 (2021).

Z. H. Yang, Y. Kubota, A. Corsi, K. Yoshida, X. -X. Sun, J. G. i, M. Kimura, N. Michel, K. Ogata, C. X. Yuan, Q. Yuan, G. Authelet, H. Baba, C. Caesar, D. Calvet, A. Delbart, M. Dozono, J. Feng, F. Flavigny, J. -M. Gheller, J. Gibelin, A. Giganon, A. Gillibert, K. Hasegawa, T. Isobe, Y. Kanaya, S. Kawakami, D. Kim, Y. Kiyokawa, M. Kobayashi, N. Kobayashi, T. Kobayashi, Y. Kondo, Z. Korkulu, S. Koyama, V. Lapoux, Y. Maeda, F. M. Marqués, T. Motobayashi, T. Miyazaki, T. Nakamura, N. Nakatsuka, Y. Nishio, A. Obertelli, A. Ohkura, N. A. Orr, S. Ota, H. Otsu, T. Ozaki, V. Panin, S. Paschalis, E. C. Pollacco, S. Reichert, J. -Y. Roussé, A. T. Saito, S. Sakaguchi, M. Sako, C. Santamaria, M. Sasano, H. Sato, M. Shikata, Y. Shimizu, Y. Shindo, L. Stuhl, T. Sumikama, Y. L. Sun, M. Tabata, Y. Togano, J. Tsubota, F. R. Xu, J. Yasuda, K. Yoneda, J. Zenihiro, S. -G. Zhou, W. Zuo, and T. Uesaka, "Quasifree neutron knockout reaction reveals a small s-orbital component in the Borromean nucleus ^{17}B," Phys. Rev. Lett. **126**, 082501 (2021).

M. Kimura, Y. Suzuki, T. Baba, and Y. Taniguchi, "Description of isospin mixing by a generator coordinate method," Phys. Rev. C **105**, 014311 (2021).

K. Yoshida, "Isovector giant monopole and quadrupole resonances in a Skyrme energy density functional approach with axial symmetry," Phys. Rev. C **104**, 044309 (2021).

K. Uzawa, K. Hagino, and K. Yoshida, "Microscopic description of cluster decays based on the generator coordinate method," Phys. Rev. C **105**, 034326 (2022).

K. Yoshida, "Super- and hyperdeformation in ^{60}Zn, ^{62}Zn, and ^{64}Ge at high spins," Phys. Rev. C **105**, 024318 (2022).

K. Hossain, K. Kobuszewski, M. M. Forbes, P. Magierski, K. Sekizawa, and G. Wlazłowski, "Rotating quantum turbulence in the unitary fermi gas," Phys. Rev. A **105**, 013304 (2022).

[Review Article]

関澤一之, 「時間依存密度汎関数法で探る原子核ダイナミクス : 原子核反応から超流動現象, 中性子星まで」, 2021 年度原子核三者若手夏の学校 原子核パート講義録, 原子核研究, Vol. 66, Suppl. 3, pp. 5–12 (2022).

Presentations

[International Conferences/Workshops]

H. Masui (oral), W. Horiuchi, and M. Kimura, "Two-neutron halo structure and anti-halo effect in ^{31}F," Yamada Conference LXXII: The 8th Asia-Pacific Conference on Few-Body Problems in Physics (APFB2020), Kanazawa bunka hall, Kanazawa, Japan, May 1–5, 2021.

S. Shin (oral), B. Zhou, and M. Kimura, "The shape of ^{13}C studied by the real-time evolution method," Yamada Conference LXXII: The 8th Asia-Pacific Conference on Few-Body Problems in Physics (APFB2020), Kanazawa bunka hall, Kanazawa, Japan, May 1–5, 2021.

H. Motoki (oral) and M. Kimura, "Research on the α condensate in ^{16}O using real time evolution method," Yamada Conference LXXII: The 8th Asia-Pacific Conference on Few-Body Problems in Physics (APFB2020), Kanazawa bunka hall, Kanazawa, Japan, May 1–5, 2021.

M. Kimura (oral), "Shape of $N = 28$ isotonesand monopole transitions," RIBF Users Meeting 2021, September 7–9, 2021.

H. Motoki (oral) and M. Kimura, "The structure of 0^+ states in ^{16}O using real-time evolution method," The 16th International Symposium on Nuclei in the Cosmos (NIC-XVI), Online, September 21–25 2021.

V. Choudhary (oral), W. Horiuchi, M. Kimura, and R. Chatterjee, "Exploring the bubble structure in ^{22}O," 65th DAE Symposium on Nuclear Physics, Bhabha Atomic Research Centre, Mumbai, India, December 1–5, 2021.

T. Baba (oral), Y. Taniguchi, and M. Kimura, "^{9}Be + ^{9}Be correlation in the 4α linear chain of ^{18}O," RCNP International Workshop on Cluster Phenomena in Knockout and Astrophysical Reactions, Online, October 14–15, 2021.

K. Sekizawa (invited), "Entrainment effects in neutron stars: Overview and progress," JSPS/NRF/NSFC A3 Foresight Program, "Nuclear physics in the 21st century," Joint Annual Meeting, Online, Feburary 17–18, 2022.

[Domestic Conferences/Workshops]

木村真明, 「光核反応からのクラスター崩壊の理論研究と最高エネルギー宇宙線への応用」, 新学術領域「量子クラスターで読み解く物質の階層構造」ワークショップ, オンライン, 2021 年 6 月 14, 19 日.

渡辺証斗, 湊太志, 木村真明, 岩本信之, 「チャネル結合光学模型を用いた核子–原子核散乱に対するポテンシャルの最適化 (2)」, 日本原子力学会 2021 年秋の大会, オンライン, 2021 年 9 月 8–10 日.

谷口億宇, 木村真明「天体において共鳴状態により誘発される ^{12}C +^{12} C 核融合反応」, 日本物理学会 2021 年秋季大会, オンライン, 2021 年 9 月 14–17 日.

本木英陽, 鈴木祥輝, 川合毅, 木村真明「中性子過剰核でのクラスター形成と中性子スキンの相関」, 日本物理学会 2021 年秋季大会, オンライン, 2021 年 9 月 14–17 日.

木村真明, 鈴木祥輝, 馬場智之「生成座標法によるアイソバリックアナログ状態とアイソスピン混合の記述」, 日本物理学会 2021 年秋季大会, オンライン, 2021 年 9 月 14–17 日.

Vishal Choudhary, 堀内渉, 木村真明, Rajdeep Chatterjee, 「陽子弾性散乱でみる中性子過剰 Ne, Mg 同位体の核表面変化」, 日本物理学会 2021 年秋季大会, オンライン, 2021 年 9 月 14–17 日.

鈴木祥輝, 木村真明, 堀内渉, 「中性子過剰 $N = 28$ 核での変形共存現象の研究」, 日本物理学会 2021 年秋季大会, オンライン, 2021 年 9 月 14–17 日.

木戸英治, 稲倉恒法, 宇都野穣, 木村真明, 清水則孝, 民井淳, 長瀧重博, 「光核反応の超高エネルギー宇宙線伝播への影響 II」, 日本物理学会 2021 年秋季大会, オンライン, 2021 年 9 月 14–17 日.

S. Shin, B. Zhou, and M. Kimura, "α cluster resonances studied by analytic continuation in the coupling constant," 日本物理学会 2021 年秋季大会, オンライン, 2021 年 9 月 14–17 日.

S. Shin, B. Zhou, and M. Kimura, "α cluster resonances studied by analytic continuation in the coupling constant," 「大規模シミュレーションと機械学習による原子核反応研究」, 北海道大学, 2021 年 11 月 17–19 日.

鈴木祥輝, 堀内渉, 木村真明, 「$N = 28$ 核における変形共存現象」, 「大規模シミュレーションと機械学習による原子核反応研究」, 北海道大学, 2021 年 11 月 17–19 日.

本木英陽, 鈴木祥輝, 川合毅, 木村真明, 「軽い中性子過剰核におけるクラスター形成」, 「大規模シミュレーションと機械学習による原子核反応研究」, 北海道大学, 2021 年 11 月 17–19 日.

吉田賢市, "Anomalous quadrupole collectivity of neutron-rich Mg isotopes near the drip line," 基研研究会「核力に基づいた原子核の構造と反応」, 京都大学/オンライン, 2021 年 12 月 7–10 日.

本木英陽, 木村真明, 「4α 微視的模型による ^{16}O の幾何学的構造の理解」, 第 7 回クラスター階層領域研究会, 東北大学電子光理学研究センター, 2021 年 12 月 27–28 日.

木村真明, 「核データの取り組みについて」, 原子核物理学実験におけるデータ利活用による研究戦略会議, 理研神戸・融合連携イノベーション推進棟, 2022 年 3 月 7 日.

湊太志, 「これまでの核データ研究活動と最新の取り組み」, 原子核物理学実験におけるデータ利活用による研究戦略会議, 理研神戸・融合連携イノベーション推進棟, 2022 年 3 月 7 日.

馬場智之, 谷口億宇, 木村真明, 「^{9}Be + ^{9}Be 衝突による 4α 直鎖状態の生成可能性について」, 日本物理学会 第 77 回年次大会, オンライン, 2022 年 3 月 15–19 日.

高津隆苑, 木村真明, 堀内渉, 「^{31}Ne の変形ハローと共鳴の研究」, 日本物理学会 第 77 回年次大会, オンライン, 2022 年 3 月 15–19 日.

鈴木祥輝, 木村真明, 堀内渉, 「中性子数 28 近傍核における魔法数消失に伴う変形共存現象」, 日本物理学会 第 77 回年次大会, オンライン, 2022 年 3 月 15–19 日.

谷口億宇, 木村真明「低エネルギー ^{12}C +^{13} C 核融合の微視的模型による評価」, 日本物理学会 第 77 回年次大会, オンライン, 2022 年 3 月 15–19 日.

吉田賢市, "Anomalous quadrupole collectivity of Mg isotopes near the neutron drip line," 日本物理学会第 77 回年次大会, オンライン, 2022 年 3 月 15–19 日.

関澤一之, P. Magierski, A. Makowski, M. C. Barton, G. Wlazłowski, 「低エネルギー重イオン反応における新奇な超流動ダイナミクス」, 日本物理学会第 77 回年次大会, オンライン, 2022 年 3 月 15–19 日.

佐々木哲平, 関澤一之, 松尾正之, 「時間依存 Gross-Pitaevskii 方程式による量子渦のピン留め・ピン外れ機構の研究」, 日本物理学会第 77 回年次大会, オンライン, 2022 年 3 月 15–19 日.

佐藤弘一, 「日本物理学会第 77 回年次大会「2 次の集団演算子を入れた Adiabatic SCC 理論による集団経路の抽出」, 日本物理学会第 77 回年次大会, オンライン, 2022 年 3 月 15–19 日.

陳敬徳, 小野章, 木村真明, 石塚知香子, 千葉 敏, 「AMD による核分裂片のスピン, 相対軌道角運動量及びそれらの相関の研究」, 日本原子力学会 2022 年春の年会, オンライン, 2022 年 3 月 16–18 日.

[Seminars]

M. Kimura, Y. Suzuki, and W. Horiuchi, "Erosion of $N = 28$ shell gap: shape coexistence and monopole transitionsin the vicinity of ^{44}S," RIKEN RIBF Nuclear Physics Seminar, Online, January 8, 2022.

M. Kimura and Y. Taniguch, "Astrophysical S-factor for ^{12}C+^{12}C fusion reaction from a full-microscopic nuclear model," CINA/COSNAP Colloquium, October 19, 2022.

Nuclear Science and Transmutation Research Division
Superheavy Element Research Group

1. Abstract

The heavy elements with atomic numbers exceeding 103 are called superheavy elements (SHEs). In Superheavy Element Research Group, Superheavy Element Production Team and Superheavy Element Devise Development Team work together to investigate synthesis of SHEs, nuclear properties of SHE nuclei, and chemical properties of SHEs. We also develop and maintain SHE production and separation devices, detectors, and chemistry apparatuses.

2. Major Research Subjects

(1) Search for new superheavy elements
(2) Decay spectroscopy of the heaviest nuclei
(3) Study of reaction mechanisms for production of the heaviest nuclei
(4) Study of chemical properties of the heaviest elements
(5) Development, maintenance, and operation of GARIS, GARIS-II, and GARIS-III
(6) Development and maintenance of detector and DAQ system of GARIS, GARIS-II, and GARIS-III
(7) Development and maintenance of target system of GARIS, GARIS-II, and GARIS-III

3. Summary of Research Activity

See the subsections of Superheavy Element Production Team and Superheavy Element Device Development Team.

Members

Director

Kosuke MORITA

List of Publications & Presentations

See the subsections of Superheavy Element Production Team and Superheavy Element Device Development Team.

Nuclear Science and Transmutation Research Division
Superheavy Element Research Group
Superheavy Element Production Team

1. Abstract

The elements with atomic number $Z \geq 104$ are called as trans-actinide or superheavy elements (SHEs). Superheavy Element Production Team synthesizes SHE nuclei including new elements and investigates synthesis mechanisms of SHE nuclei, nuclear properties of SHE nuclei, and chemical properties of SHEs in collaboration with Superheavy Element Devise Development Team and Nuclear Chemistry Research Team of RIKEN Nishina Center.

2. Major Research Subjects

(1) Search for new superheavy elements
(2) Decay spectroscopy of the heaviest nuclei
(3) Study of reaction mechanisms for production of the heaviest nuclei
(4) Study of chemical properties of the heaviest elements

3. Summary of Research Activity

(1) Search for new superheavy elements

In November 2016, the 7th period of the periodic table was completed with the official approval of four new elements, nihonium (Nh, atomic number $Z = 113$), moscovium (Mc, $Z = 115$), tennessine (Ts, $Z = 117$), and oganesson (Og, $Z = 118$) by International Union of Pure and Applied Chemistry. We have started to search for new elements to expand the chart of the nuclides toward to the island of stability and the periodic table of the elements toward the 8th period. In January 2020, RIKEN heavy-ion Linear ACcelerator (RILAC) was upgraded as Superconducting RIKEN heavy-ion Linear ACcelerator (SRILAC). We developed the new gas-filled recoil ion separator GARIS-III on the beam line of SRILAC. In June–July 2020, we conducted the commissioning of SRILAC and GARIS-III using the ^{169}Tm + ^{40}Ar, ^{208}Pb + ^{40}Ar, and ^{208}Pb + ^{51}V reactions. Since October 2020, we have been conducting a synthesis experiment of isotopes of new element 119 in the ^{248}Cm + ^{51}V reaction under the nSHE collaboration.

(2) Decay spectroscopy of the heaviest nuclei

In collaboration with KEK, we developed a multi-refection time-of-fight mass spectrograph (MRTOF-MS) equipped with an α-TOF detector on the focal plane of GARIS-II at RRC for decay-correlated mass measurements of low-yield and short-lived SHE isotopes. In 2021, the first high-precision direct determination of the atomic mass of a superheavy nuclide was successfully conducted for ^{257}Db ($Z = 105$) produced in the ^{208}Pb(^{51}V, $2n$)^{257}Db reaction. The atomic masses of $^{206,\,207g,\,m}$Ra were also measured in the ^{159}Tb(^{51}V, 4;$3n$)$^{206,\,207g,\,m}$Ra reactions.

(3) Study of reaction mechanisms for production of the heaviest nuclei

SHE nuclei have been produced by complete fusion reactions of two heavy nuclei. However, the reaction mechanism of the fusion process is still not well understood both theoretically and experimentally. We measured excitation functions for the quasielastic scattering of the ^{248}Cm + ^{51}V reaction using GARIS III at SRILAC. The result was utilized to estimate the optimal incident beam energy for production of isotopes of new element 119.

(4) Study of chemical properties of the heaviest elements

Chemical characterization of newly-discovered SHEs is an extremely interesting and challenging subject in modern nuclear and radiochemistry. In collaboration with Nuclear Chemistry Research Team of RIKEN Nishina Center, we are developing SHE production systems as well as rapid single-atom chemistry apparatuses for chemistry studies of SHEs. We installed a gas-jet transport system to the focal plane of GARIS at RILAC. This system is a promising approach for exploring new frontiers in SHE chemistry: the background radiations from unwanted products are strongly suppressed, the intense primary heavy-ion beam is absent in the gas-jet chamber, and hence the high gas-jet extraction yield is attained. Furthermore, the beam-free conditions make it possible to investigate new chemical systems. In 2021, we continued to develop an ultra-rapid gas-chromatograph apparatus, which consists of an RF carpet gas cell and a cryo-gas-chromatograph column with a Si detector array, at the focal plane of GARIS for the gas chemistry of SHEs. To realize aqueous chemistry studies of Sg ($Z = 106$) and Bh ($Z = 107$), we have been developing a continuous and rapid solvent extraction apparatus which consists of a continuous dissolution apparatus Membrane DeGasser (MDG), a Flow Solvent Extractor (FSE), and a liquid scintillation detector for α/SF-spectrometry. In 2021, we also conducted model experiments for ion-exchange studies of Rf ($Z = 104$) in HNO_3 and H_2SO_4 using long-lived radiotracers of ^{88}Zr and ^{175}Hf.

Members

Team Leader

Hiromitsu HABA

Research & Development Scientist

Daiya KAJI

Special Postdoctoral Researcher

Tomohiro HAYAMIZU

Visiting Scientists

Marc ASFARI (IPHC/Strasbourg Univ.)
Mahananda DASGUPTA (Australian Nat'l Univ.)
Olivier DORVAUX (Strasbourg Univ.)
Benoit Jean-Paul GALL (Strasbourg Univ.)
Zaiguo GAN (Chinese Academy of Sci.)
Shintaro GO (Kyushu Univ.)
David HINDE (The Australian Nat'l Univ.)
Minghui HUANG (IMP, CAS)
Hiroyuki KOURA (JAEA)
Daisuke NAGAE (Kyushu Univ.)
Satoshi SAKAGUCHI (Kyushu Univ.)
Mirei TAKEYAMA (Yamagata Univ.)
Taiki TANAKA (The Australian Nat'l Univ.)
Huabin YANG (IMP, CAS)
Zhiyuan ZHANG (IMP, CAS)

Student Trainees

Yuichi ISHIBASHI (Kyushu Univ.)
Tamito KAI (Kyushu Univ.)
Kieran KESSACI (IPHC/Strasbourg Univ.)
Raiden LEMON (The Australian Nat'l Univ.)
Milan LEONARD (The Australian Nat'l Univ.)
Sotaro MATSUNAGA (Kyushu Univ.)
Ikuto MURAKAMI (Kyushu Univ.)
Taiga MUTO (Kyushu Univ.)
Yuto NAGATA (Kyushu Univ.)
Koichi SUGIYAMA (Kyushu Univ.)
Taro TOMIMATSU (Kyushu Univ.)

List of Publications & Presentations

Publications

[Original Papers]

P. Schury, T. Niwase, M. Wada, P. Brionnet, S. Chen, T. Hashimoto, H. Haba, Y. Hirayama, D. S. Hou, S. Iimura, H. Ishiyama, S. Ishizawa, Y. Ito, D. Kaji, S. Kimura, H. Koura, J. J. Liu, H. Miyatake, J. -Y. Moon, K. Morimoto, K. Morita, D. Nagae, M. Rosenbusch, A. Takamine, Y. X. Watanabe, H. Wollnik, W. Xian, and S. X. Yan, "First high-precision direct determination of the atomic mass of a superheavy nuclide," Phys. Rev. C **104**, L021304 (2021).

T. Niwase, M. Wada, P. Schury, P. Brionnet, S. D. Chen, T. Hashimoto, H. Haba, Y. Hirayama, D. S. Hou, S. Iimura, H. Ishiyama, S. Ishizawa, Y. Ito, D. Kaji, S. Kimura, J. Liu, H. Miyatake, J. Y. Moon, K. Morimoto, K. Morita, D. Nagae, M. Rosenbusch, A. Takamine, T. Tanaka, Y. X. Watanabe, H. Wollnik, W. Xian, and S. X. Yan, "α-decay-correlated mass measurement of ^{206,207g,m}Ra using an α-TOF detector equipped multireflection time-of-flight mass spectrographs system," Phys. Rev. C **104**, 044617 (2021).

T. Aoki, R. Sreekantham, B. K. Sahoo, B. Arora, A. Kastberg, T. Sato, H. Ikeda, N. Okamoto, Y. Torii, T. Hayamizu, K. Nakamura., S. Nagase, M. Ohtsuka, H. Nagahama, N. Ozawa, M. Sato, T. Nakashita, K. Yamane, K. S. Tanaka, K. Harada, H. Kawamura, T. Inoue, A. Uchiyama, A. Hatakeyama, A. Takamine, H. Ueno, Y. Ichikawa, Y. Matsuda, H. Haba, and Y. Sakemi, "Quantum sensing of the electron electric dipole moment using ultracold entangled Fr atoms," Quantum Sci. Technol. **6**, 044008 (2021).

A. Yakushev, L. Lens, C. E. Düllmann, M. Block, H. Brand, M. Dasgupta, T. Calverley, A. D. Nitto, M. Götz, S. Götz, H. Haba, L. Harkness-Brennan, R-D. Herzberg, F. P. Heßberger, D. Hinde, A. Hübner, E. Jäger, D. Judson, J. Khuyagbaatar, B. Kindler, Y. Komori, J. Konki, J. V. Kratz, J. Krier, N. Kurz, M. Laatiaoui, B. Lommel, C. Lorenz, M. Maiti, A. K. Mistry, C. Mokry, Y. Nagame, P. Papadakis, A. Såmark-Roth, D. Rudolph, J. Runke, L. G. Sarmiento, T. K. Sato, M. Schädel, P. Scharrer, B. Schausten, J. Steiner, P. Thörle-Pospiech, A. Toyoshima, N. Trautmann, J. Uusitalo, A. Ward, M. Wegrzecki, and V. Yakusheva, "First study on nihonium (Nh, element 113) chemistry at TASCA," Front. Chem. **9**, 753738 (2021).

E. Watanabe, Y. Kasamatsu, T. Yokokita, S. Hayami, K. Tonai, H. Ninomiya, N. Kondo, Y. Shigekawa, H. Haba, Y. Kitagawa, M. Nakano, and A. Shinohara, "Anion-exchange experiment of Zr, Hf, and Th in HNO_3 and quantum chemical study on the nitrate complexes toward chemical research on element 104, Rf," Solvent Extr. Ion Exch. published online (December 31, 2021). DOI: 10.1080/07366299.2021.2020956 .

T. Hayamizu, H. Haba, K. Nakamura, T. Aoki, H. Nagahama, K. S. Tanaka, N. Ozawa, M. Ohtsuka, and Y. Sakemi, "Development of ultracold francium atomic sources towards the permanent EDM search," Few-Body Syst. **63**, 11 (2022).

T. Yokokita, S. Yano, Y. Komori, and H. Haba, "Anion- and cation-exchange studies of Zr, Hf, and Th using ion-exchange resin and fiber in H_2SO_4 media for chemical characterization of sulfate complex of Rf," J. Radioanal. Nucl. Chem. **331**, 1127 (2022).

[Book]

羽場宏光, 「新元素ニホニウムはいかにして創られたか」, 東京化学同人, 176 ページ, 2021 年 12 月 17 日.

Presentations

[International Conferences/Workshops]

H. Haba (invited), "Production and applications of radioisotopes at RIKEN RI Beam Factory," International Discussion Meeting on Future of Accelerator Applications and Radiotracers Research (FAAARR2021), Online, July 26–27, 2021.

H. Haba (invited), "Production of radioisotopes for application studies at RIKEN RI Beam Factory," Snowmass'21 Workshop on High Power Cyclotrons/FFAs, Online, September 7–9, 2021.

H. Haba (invited), "Production and applications of radioisotopes at RIKEN RI Beam Factory—Search for new elements through diagnosis and therapy of cancer—," RIKEN-KFU (Kazan Federal University) 3rd Joint Symposium, Online, November 5–6, 2021.

T. Aoki (poster), R. Sreekantham, B. K. Sahoo, B. Arora, A. Kastberg, T. Sato, H. Ikeda, N. Okamoto, Y. Torii, T. Hayamizu, K. Nakamura, S. Nagase, M. Ohtsuka, H. Nagahama, N. Ozawa, M. Sato, T. Nakashita, K. Yamane, K. S. Tanaka, K. Harada, H. Kawamura, T. Inoue, A. Uchiyama, A. Hatakeyama, A. Takamine, H. Ueno, Y. Ichikawa, Y. Matsuda, H. Haba, and Y. Sakemi, "Quantum sensing of the electron electric dipole moment using quantum entangled atoms," International Symposium on Novel Materials and Quantum Technologies (ISNTT2021), Online, December 16, 2021.

[Domestic Conferences/Workshops]

羽場宏光 (口頭発表), 「理研 RI ビームファクトリーにおける RI 製造供給」, 第 58 回アイソトープ・放射線研究発表会, オンライン, 2021 年 7 月 7–9 日.

羽場宏光 (口頭発表), 「RIBF 施設紹介」, 新学術領域研究（研究領域提案型）『学術研究支援基盤形成』短寿命 RI 供給プラットフォーム成果報告会 兼 RI 利用研究会, オンライン, 2021 年 7 月 19–20 日.

羽場宏光 (依頼講演), 「核化学ロードマップについて」, 第 59 回核化学夏の学校, オンライン, 2021 年 8 月 26–27 日.

庭瀬暁隆 (口頭発表), P. Schury, 和田道治, P. Brionnet, S. Chen, 橋本尚志, 羽場宏光, 平山賀一, D. S. Hou, 飯村俊, 石山博恒, 石澤倫, 伊藤由太, 加治大哉, 木村創大, 小浦寛之, 宮武宇也, J. Y. Moon, 森本幸司, 森田浩介, 長江大輔, M. Rosenbusch, 高峰愛子, 渡辺裕, H. Wollnik, W. Xian, S. X. Yan, 「超重核 ^{257}Db の直接質量測定」, 日本物理学会 2021 年秋季大会, オンライン, 2021 年 9 月 14–17 日.

庭瀬暁隆 (口頭発表), 和田道治, P. Schury, P. Brionnet, S. D. Chen, 橋本尚志, 羽場宏光, 平山賀一, D. S. Hou, 飯村俊, 石山博恒, 石澤倫, 伊藤由太, 加治大哉, 木村創大, J. Liu, 宮武宇也, J. Y. Moon, 森本幸司, 森田浩介, 長江大輔, M. Rosenbusch, 高峰愛子, 田中泰貴, 渡辺裕, H. Wollnik, W. Xian, S. X. Yan, 「MRTOF と α-TOF 検出器による, α 崩壊に相関した精密質量測定法の開拓」, 日本放射化学会第 65 回討論会 (2021), オンライン, 2021 年 9 月 22–24 日.

武藤大河 (口頭発表), P. Brionnet, 浅井雅人, 郷慎太郎, R. Grzywacz, 羽場宏光, 加治大哉, 木村創太, T. King, 森本幸司, K. Rykaczewski, 坂口聡志, 酒井英行, 森田浩介, 庭瀬暁隆, 田中聖臣, 「Si 検出器の波形解析による軽粒子識別」, 第 127 回日本物理学会九州支部例会, オンライン, 2021 年 12 月 4 日.

木村創大 (口頭発表), 和田道治, 羽場宏光, 石澤倫, 森本幸司, 庭瀬暁隆, Marco Rosenbusch, Peter Schury for the SHE-Mass Collaboration, 「MRTOF-MS を用いた ^{252}Cf 自発核分裂片の網羅的精密質量測定」, 日本物理学会第 77 回年次大会 (2022 年), オンライン, 2022 年 3 月 15–19 日.

庭瀬暁隆 (口頭発表), P. Schury, 和田道治, P. Brionnet, S. Chen, 羽場宏光, 平山賀一, D. S. Hou, 飯村俊, 石山博恒, 伊藤由太, 加治大哉, 木村創大, 小浦寛之, 宮武宇也, 森本幸司, 森田浩介, 長江大輔, M. Rosenbusch, 高峰愛子, 渡辺裕, H. Wollnik, W. Xian, S. X. Yan, 「MRTOF+α-TOF による ^{257,258}Db の精密質量測定」, 日本物理学会第 77 回年次大会 (2022 年), オンライン, 2022 年 3 月 15–19 日.

横北卓也 (口頭発表), 羽場宏光, 「Zr 及び Hf のスルファト錯体推定に向けた TOA/H_2SO_4 系の溶媒抽出」, 日本化学会第 102 春季年会 (2022), オンライン, 2022 年 3 月 23–26 日.

Outreach Activities

羽場宏光 (依頼講演), 「ニホニウム発見への道のり」, 大宮北高校 SSH 特別講演会, 大宮市, 2021 年 10 月 4 日.

羽場宏光（依頼講演）, 「新元素でがん治療〜RIBF がつくるラジオアイソトープ〜」, 第 9 回理研イノベーションセミナー, オンライン, 2022 年 1 月 21 日.

羽場宏光（依頼講演）, 「ニホニウム発見への道のり」, 早稲田大学本庄高等学院課外講義, オンライン, 2022 年 3 月 12 日.

Nuclear Science and Transmutation Research Division
Superheavy Element Research Group
Superheavy Element Device Development Team

1. Abstract

A gas-filled recoil ion separator has been used as a main experimental device for the study of superheavy elements. This team is in charge of maintaining, improving, developing, and operating the separators and related devices. In the RIBF facility, three gas-filled recoil ion separators are installed at RILAC and RRC facility. One is GARIS that is designed for a symmetric reaction such as coldfusion reaction, and the other two are developed for an asymmetric reaction such as hot-fusion reaction, GARIS-II and GARIS-III. New elements ^{278}113 were produced by ^{70}Zn + ^{209}Bi reaction using GARIS. Further the new element search is currently in progress by using GARIS-II and GARIS-III.

2. Major Research Subjects

(1) Maintenance of GARIS, GARIS-II and development of new separator GARIS-III
(2) Maintenance and development of detector and DAQ system for superheavy element research
(3) Maintenance and development of target system for GARIS, GARIS-II and GARIS-III

3. Summary of Research Activity

The GARIS-II and III are newly developed which has an acceptance twice as large as existing GARIS, in order to realize higher transmission. A new element search program aiming to element 119 was started using GARIS-II. And new separator GARIS-III was developed and installed into the RILAC experimental hall. After the some commissioning works of GARIS-III, new 119th element search has been started. We will also offer user-support if a researcher wishes to use the devices for his/her own research program.

Members

Team Leader
Kouji MORIMOTO

Senior Technical Scientists
Masaki FUJIMAKI
Daiya KAJI

Postdoctoral Researchers
Pierre BRIONNET
Sota KIMURA

Visiting Scientists
Shin-ichi GOTO (Niigata Univ.)
Eiji IDEGUCHI (Osaka Univ.)
Yuta ITO (JAEA)
Katsuhisa NISHIO (JAEA)
Toshitaka NIWASE (KEK)
Fuyuki TOKANAI (Yamagata Univ.)

Student Trainee
Kosaku KURAMOTO (Yamagata Univ.)

List of Publications & Presentations

Publications

[Original Papers]

T. Niwase, M. Wada, P. Schury, P. Brionnet, S. D. Chen, T. Hashimoto, H. Haba, Y. Hirayama, D. S. Hou, S. Iimura, H. Ishiyama, S. Ishizawa, Y. Ito, D. Kaji, S. Kimura, J. Liu, H. Miyatake, J. Y. Moon, K. Morimoto, K. Morita, D. Nagae, M. Rosenbusch, A. Takamine, T. Tanaka, Y. X. Watanabe, H. Wollnik, W. Xian, and S. X. Yan, "α-decay-correlated mass measurement of ^{206,207g,m}Ra using an α-TOF detector equipped multireflection time-of-flight mass spectrograph system," Phys. Rev. C **104**, 044617 (2021).

P. Schury, T. Niwase, M. Wada, P. Brionnet, S. Chen, T. Hashimoto, H. Haba, Y. Hirayama, D. S. Hou, S. Iimura, H. Ishiyama, S. Ishizawa, Y. Ito, D. Kaji, S. Kimura, H. Koura, J. J. Liu, H. Miyatake, J. -Y. Moon, K. Morimoto, K. Morita, D. Nagae, M. Rosenbusch, A. Takamine, Y. X. Watanabe, H. Wollnik, W. Xian, and S. X. Yan, "First high-precision direct determination of the atomic mass of a superheavy nuclide," Phys. Rev. C **104**, L021304 (2021).

Presentations

[International Conference/Workshop]

T. Niwase (invited), "Recent results of GARIS-II + MRTOF experiment," TASCA21 workshop, Online, June 21, 2021.

[Domestic Conferences/Workshops]

庭瀬暁隆 (口頭発表), 「MRTOF+α-TOF による ^{257,258}Db の精密質量測定」, 日本物理学会第 77 回年次大会, オンライン, 2022 年 3 月 15–19 日.

庭瀬暁隆 (口頭発表), 「MRTOF と α-TOF 検出器による, α 崩壊に相関した精密質量測定法の開拓」, 日本放射化学会第 65 回討論会 (2021), オンライン, 2021 年 9 月 22–24 日.

庭瀬暁隆 (口頭発表), 「超重核 ^{257}Db の直接質量測定」, 日本物理学会 2021 年度秋季大会, オンライン, 2021 年 9 月 14 日–17 日.

[Seminars]

T. Niwase, "Direct mass measurement of superheavy nuclides via MRTOF mass spectrograph equipped with an α-TOF detector," RIBF Nuclear Physics Seminar, Online, February 22, 2022.

庭瀬暁隆, 「超重元素の質量測定」, 2021 年度核化学夏の学校, オンライン, 2021 年 8 月 26–27 日.

Nuclear Science and Transmutation Research Division
Astro-Glaciology Research Group
Summary of Research Activities

1. Abstract

Our Astro-Glaciology Research Group promotes both experimental and theoretical studies to open up the new interdisciplinary research field of astro-glaciology, which combines astrophysics, astrochemistry, glaciology, and climate science.

On the experimental side, we measure isotopic and ionic concentrations in ice cores drilled at Dome Fuji station, Antarctica, in collaboration with the National Institute of Polar Research (NIPR, Tokyo). Here, the ice cores are time capsules which preserve atmospheric information of the past. In particular, the ice cores obtained around the Dome Fuji site are very unique, because they contain much more information on the stratosphere than any other ice cores obtained from elsewhere on Earth. This means that we have significant advantages in using Dome Fuji ice cores if we wish to study the Universe, since UV photons, gamma-rays, and highenergy protons emitted by astronomical phenomena affect the stratosphere. Our principal aim is thus to acquire and interpret information preserved in ice cores regarding:

- Signatures of past volcanic eruptions and solar cycles;
- Relationships between climate change and volcanic activity, and climate change and solar activity as well;
- Traces of past supernovae in our galaxy, in order to understand better the rate of galactic supernova explosions.

Moreover, we are promoting experimental projects on:

- Development of an automated laser melting sampler for analyzing ice cores with high depth resolution;
- Development of precise analytical techniques of high sensitivity for analyzing ice cores;
- The evolution of molecules in space;
- The application of analytical methods for measuring isotopes in ice cores to archaeological artifacts.

On the theoretical side, we are simulating numerically:

- Chemical effects of giant solar flares and supernovae on the Earth's atmosphere;
- The explosive and the *r*-process nucleosynthesis in core-collapse supernovae.

Combining our experimental evidence and theoretical simulations, we are promoting the researches mentioned above. These all will contribute to understanding relationships between the Universe and Earth. In particular, climate change is the most critical issue facing the world in the 21st century. It is also emphasized that the frequency of supernova explosions in our galaxy has not yet been fully understood, and it is the key to understand the *r*-process nucleosynthesis.

Members

Director
Yuko MOTIZUKI

Senior Research Scientist
Yoichi NAKAI

Special Temporary Research Scientist
Kazuya TAKAHASHI

Technical Staff
Yu Vin SAHOO

Senior Visiting Scientists
Yasushige YANO (Nishina Memorial Foundation)
Kunihiko KODERA (Meteorological Res. Inst.)

Visiting Scientists
Hideharu AKIYOSHI (Nat'l Inst. for Environmental Studies)
Hisashi HAYAKAWA (Nagoya Univ.)
Akira HORI (Kitami Inst. of Tech.)
Kazuho HORIUCHI (Hirosaki Univ.)
Yoshinori IIZUKA (Hokkaido Univ.)
Naoyuki KURITA (Nagoya Univ.)
Hideki MADOKORO (Mitsubushi Heavy Industries, Ltd.)
Hideaki MOTOYAMA (Nat'l Inst. of Polar Res.)

Visiting Technicians
Junya HIROSE (Fusion Tech. Co., Ltd.)
Yuma HASEBE (Denryoku Comp. Ctr., Ltd.)

Administrative Part-time Worker
Kanako FUJITA (Administrative Part-time Worker I)

Assistant
Keiko SUZUKI

List of Publications & Presentations

Publications

[Original Papers]

K. Takahashi, Y. V. Sahoo, Y. Nakai, H. Motoyama, and Y. Motizuki, "Annually resolved profiles of δ^{34}S and sulfate in shallow ice core DF01 (Dome Fuji, Antarctica) spanning the nineteenth century and their geochemical implications," J. Geophys. Res. Atmos. **127**, 2021JD036137 (2022).

Y. Miyake, N. Ikoma, K. Takahashi, Y. V. Sahoo, and H. Okuno, "Test of ^{107}Pd transmutation with macroscopic quantities," J. Nucl. Sci. Technol., published online (May 11, 2022). DOI: 10.1080/00223131.2022.2072012 .

K. Kanzawa, F. Miyake, K. Horiuchi, K. Sasa, K. Takano, M. Matsumura, T. Takahashi, Y. Motizuki, K. Takahashi, Y. Nakai, K. Ohtani, Y. Tada, Y. Ochiai, H. Motoyama, H. Matsuzaki, A. Yamazaki, Y. Muramatsu, and T. Yamagata, "High-resolution ^{10}Be and ^{36}Cl data from the antarctic dome Fuji Ice core (100 years around 5480 BCE): An unusual grand solar minimum occurrenc?," J. Geophys. Res. Space Phys. **126**, e2021JA029378 (2021).

S. Katsuda, H. Fujiwara, Y. Ishisaki, Y. Maeda, K. Mori, Y. Motizuki, K. Sato, M. S. Tashiro, and Y. Terada, "New measurement of the vertical atmospheric density profile from occultations of the crab nebula with X-ray astronomy satellites Suzaku and Hitomi," J. Geophys. Res. Space Phys. **126**, e2020JA028886, (2021).

K. Kitajima, Y. Nakai, W. M. C. Sameera, M. Tsuge, A. Miyazaki, H. Hidaka, A. Kouchi, and N. Watanabe, "Delivery of electrons by proton-hole transfer in ice at 10 K: Role of surface OH radicals," J. Phys. Chem. Lett. **12**, 704 (2021).

[Books]

望月優子, 「シリース現代の天文学第 1 巻人類の住む宇宙第 2 版」(第 3 刷新規業績), pp. 147–149（「第 4 章太陽系 4.1.2 節太陽の現在」), 岡村定矩他編, 日本評論社, 2021 年 11 月, ISBN 978-4-535-60751-4.

望月優子, 佐藤勝彦, 「シリース現代の天文学第 1 巻人類の住む宇宙第 2 版」（第 3 刷改訂), pp. 99–144（「第 3 章元素の起源」), 岡村定矩他編, 日本評論社, 2021 年 11 月, ISBN 978-4-535-60751-4.

Presentations

[International Conferences/Workshops]

Y. Motizuki (iPoster paper), Y. Nakai, K. Takahashi, J. Hirose, Y. V. Sahoo, Y. Yano, M. Yumoto, M. Maruyama, M. Sakasita, K. Kase, S. Wada, and H. Motoyama, "A novel, ultra-high-resolution laser-melting sampler with resolution controllability for discrete analyses of ion concentrations and stable water isotopic compositions in ice cores," AGU Fall Meeting 2021, New Orleans & Online, December 13–17, 2021.

K. Kitajima (poster), Y. Nakai, W. M. C. Sameera, M. Tsuge, A. Miyazaki, H. Hidaka, A. Kouchi, and N. Watanabe, "A new electrochemical property of ice: negative charge transport triggered by reactions of surface OH radicals with electrons," Workshop on Interstellar Matter 2021, Sapporo, November 17–19, 2021.

Y. Nakai (poster), H. Hidaka, and N. Watanabe, "Methanol production via interactions of low-energy CH_3^+ ions with ASW surface: experimental investigation of ion-surface reaction," Workshop on Interstellar Matter 2021, Sapporo, November 17–19, 2021.

Y. Motizuki, Y. Nakai, K. Takahashi, T. Imamura, and H. Motoyama, "A proxy for decadal solar cycles from AD 1600 to 1900 based on nitrate concentrations in a Dome Fuji (Antarctica) ice core," The 6th Workshop of the Astronomy & Astrophysics from Antarctica (SCAR AAA 2021), Virtual meeting, September 8–10, 2021.

K. Kitajima, Y. Nakai, M. Tsuge, A. Miyazaki, H. Hidaka, A. Kouchi, and N. Watanabe, "Verification of proton-hole transfer in ice at 10 K via detection of surface OH radicals," 36th Symposium on Chemical Kinetics and Dynamics, Online, Jun 2–4, 2021.

Y. Motizuki, Y. Nakai, K. Takahashi, J. Hirose, Y. V. Sahoo, Y. Yano, M. Yumoto, M. Maruyama, M. Sakasita, K. Kase, S. Wada, and H. Motoyama, "A novel high-resolution laser-melting sampler for discrete analyses of ion concentrations and stable water isotopic compositions in firn and ice cores," virtual EGU General Assembly 2021 (vEGU21), April 19–30, 2021.

Y. Motizuki (invited), "Astro-glaciology sciences using antarctic ice cores—A key project of RNC for the origin of elements and climate change," Workshop3 on Climate Change and Geoscience, OIST-RIKEN Joint Symposium, Series 1: Green and blue planet—How can ecological research shape our future?, Onna-Son, Okinawa, April 6–7, 2021. (With organizing and serving as a Discussion Leader of Workshop3)

Y. Motizuki (invited), "Some topics on gender issues related to nuclear astrophysics calendar - based on a keynote talk at the IAU symposium on equality, equity, and inclusion in astronomy, celebrating the 100-year of IAU," UKAKUREN Seminar, Online, March 7, 2022.

[Domestic Conferences/Workshops]

望月優子 (招待講演), 「地球アーカイブからさぐる, 宇宙と地球の歴史」, 朝日カルチャーセンター中之島教室 「宇宙と地球と元素」シリーズ講座, オンライン, 2022 年 3 月 26 日.

勝田哲, 藤原均, 石﨑欣尚, 前田良知, 森浩二, 望月優子, 佐藤浩介, 田代信, 寺田幸功, 安井良輔, 「X 線天文衛星を用いた地球超高層大気および太陽コロナの観測的研究」, 第 21 回高宇連研究会, 豊中, オンライン, 2022 年 3 月 9–11 日.

望月優子, 中井陽一, 高橋和也, 今村隆史, 本山秀明, 「南極ドームふじアイスコアを用いた 10 年スケール太陽周期の同時検出」, 日本天文学会 2022 年春季年会, オンライン, 2022 年 3 月 2–5 日.

渡部直樹 (ポスター), 北島謙生, 中井陽一, 柘植雅士, 日高宏, 香内晃, 「極低温の氷と NH_3, H_2S 固体の界面における負電荷移動機構」, 原子衝突学会第 46 回年会, オンライン, 2021 年 10 月 26–28 日.

勝田哲, 藤原均, 石﨑欣尚, 前田良知, 森浩二, 望月優子, 佐藤浩介, 田代信, 寺田幸功, 「X線天文衛星『すざく』と『ひとみ』が捉えたカニ星雲の地球大気遮蔽による大気密度鉛直プロファイルの測定」, 令和 3 年 (2021 年) 度・第 1 回 STE (太陽地球環境) 現象報告会 (合同研究集会), 2021 年 9 月 28–30 日.

望月優子 (招待トーク), “A new-type, innovative automated ice-core sampler using laser melting method”, Online seminar “How to give an impressive pitch presentation in global situation”, JST 世界で活躍できる研究者育成プログラム総合支援事業, オンライン, 2021 年 8 月 13 日.

望月優子 (招待講演), 「南極の氷からひもとく宇宙と地球の歴史」, 早稲田大学高等学院理工学特論, オンライン, 2021 年 4 月 20 日.

Nuclear Science and Transmutation Research Division
Nuclear Transmutation Data Research Group

1. Abstract

The nuclear waste problem is an inevitable subject in nuclear physics and nuclear engineering communities. Since the Chicago Pile was established in 1942, nuclear energy has become one of major sources of energy. However, nowadays the nuclear waste produced at nuclear power plants has caused social problems. Minor actinide components of the waste have been studied well as a fuel in fast breeder reactors or ADS. Long-lived fission products (LLFP) in waste, on the other hand, have not been studied extensively. A deep geological disposal has been a policy of several governments, but it is difficult to find out location of the disposal station in terms of security, sociology and politics. To solve the social problem, a scientific effort is necessary for nuclear physics community to find out efficient methods for reduction of nuclear waste radioactivity. In the world-wide situation above, our Group aims to obtain reaction data of LLFP at RIBF and other muon facilities for muon capture data. These data are necessary to design an accelerator-based system for transmutation, and also may lead to a new discovery and invention for peaceful use of nuclear power and the welfare of humanity.

2. Major Research Subjects

The Group is formed by three research teams. The first two Teams, "Fast RI Data Team" and "Slow RI Data Team," are in charge of proton- and deuteron-induced reaction data of LLFP in inverse kinematics at RIBF. The third Team "Muon Data Team" is to obtain muon capture data of LLFP at muon facilities. All of the teams are focusing to obtain high-quality data which are essentially necessary to establish reliable reaction models. Each team has its own subjects and promotes LLFP reaction programs based on their large experiences, techniques and skills.

3. Summary of Research Activity

In 2014, all the teams polished up experimental strategies, formed collaboration and prepared experiments. Physics runs for spallation reaction were successfully organized at RIBF in 2015–2017. The muon program started at RCNP, Osaka University in spring 2016 and the data for Pd isotopes were successfully obtained in 2017–2019 via in-beam method with DC beams at RCNP, and via activation method with pulsed beams at J-PARC and ISIS-RAL/RIKEN facilities.

The reaction data obtained with both fast and energy-degraded beams at RIBF encouraged the nuclear data group of JAEA, and a new database called "JENDLE/ImPACT-2018" has been released. The new database has been generated by a newly developed reaction model "DEURACS" which treats deuteron-induced reactions. DEURACS reproduces very well cross section data, and much better than other reaction models. A simulation code "PHITS" has been re-coordianted to use the database information.

In December 2018, the Team leader, Hideaki Otsu, was invited to join Technical Meeting of IAEA, entitled "Novel Multidisciplinary Applications with Unstable Ion Beams and Complementary Techniques." Our activity has been demonstrated and recognized internationally. In November 2020, Hideaki Otsu organized a domestic conference entitled "RIKEN Sympoium on Nuclear Data 2020."

At the end of fiscal year 2021, the spallation reaction data with ^{99}Tc beam was obtained and a secondary beam test for ^{237}Np production was conducted.

Member

Director

Hiroyoshi SAKURAI

List of Publication & Presentation

Publication

[Review Article]

H. Sakurai, "ImPACT under RIKEN Nishina Center," Nucl. Phys. News **31**, 26–29 (2021).

Presentation

[International Conference/Workshop]

H. Sakurai (invited), "A challenge to solve the nuclear waste problem," International Round Table on Applied Research and Innovations at NICA, Dubna, Russia & Online, September 15–16, 2021.

Nuclear Science and Transmutation Research Division
Nuclear Transmutation Data Research Group
Fast RI Data Team

1. Abstract

Fast RI team aims at obtaining and accumulating the cross section data for long lived fission products (LLFPs) in order to explore the possibility of using accelerator for nuclear transmutation.

LLFPs as nuclear waste have been generated continuously in nuclear power plants for wealth for human lives, while people noticed the way of disposal has not necessarily been established, especially after the Fukushima Daiichi power plant disaster. One of the ways to reduce the amount of LLFP or to recover them as recycled resources is nuclear transmutation technique.

RIBF facility has a property to generate such LLFP as a secondary beam and the beam species are identified by event by event. Utilizing the property, absolute values of the cross section of various reactions on LLFPs are measured and accumulated as a database.

2. Major Research Subjects

(1) Measurement of reaction products by the interaction of LLFPs with proton, deuteron, and photon to explore candidate reactions for the transmutation of LLFPs
(2) Evaluation of the cross section data for the neutron induced reactions from the obtained data

3. Summary of Research Activity

(1) Acting as a collaboration hub on many groups which plan to take data using fast RI beams in RIBF facility
(2) Concentrating on taking data for proton and deuteron induced spallation reactions with inverse kinematics
(3) Accumulating the cross section data and evaluating them as evaluated nuclear data
(4) Evaluating cross section of neutron induced reaction on LLFP by collaborating with the nuclear model calculation and evaluation group

Members

Team Leader

Hideaki OTSU (Concurrent: Team Leader, SAMURAI Team)

Visiting Scientist

Takashi TERANISHI (Kyushu Univ.)

Student Trainee

Koichi GOTO (Kyushu Univ.)

List of Publications & Presentations

Publication

[Proceeding]

R. Matsumura, H. Otsu, and H. Wang *et al.*, "Research for nuclear transmutation of high-radiotoxic nuclide ^{90}Sr via proton- and deuteron-induced reactions," JAEA-Conf 2021-001, pp. 225–230 (2022).

Presentations

[Domestic Conferences/Workshops]

松村理久, 大津秀暁, 王赫, 千賀信幸, 他 ImPACT-RIBF Collaboration, 「高放射性核種 ^{90}Sr の陽子及び重陽子誘起反応による同位体生成」, 日本物理学会 第 76 回年次大会, オンライン, 2021 年 3 月.

松村理久, 大津秀暁, 王赫, 炭竈聡之, 千賀信幸, 他, 「中性子入射断面積の評価に向けた安定核 ^{95}Mo の陽子・重陽子入射反応による同位体生成断面積の測定」, 日本物理学会 第 77 回年次大会, オンライン, 2022 年 3 月.

Others

[Master Theses]

松村理久, 修士論文, 「陽子・重陽子入射反応による ^{90}Sr, ^{95}Mo の同位体生成断面積の測定」, 埼玉大学, 2022 年 3 月.

西津美咲, 修士論文, 「^{79}Se に対する 200 MeV/u 陽子及び重陽子入射核破砕反応による同位体生成断面積測定」, 九州大学, 2022 年 3 月.

Nuclear Science and Transmutation Research Division
Nuclear Transmutation Data Research Group
Slow RI Data Team

1. Abstract

This team is in charge of the development of low-energy RI beams of long-lived fission fragments (LLFP) or minor actinides (MA) from the ^{238}U by means of degrading the energy of beams produced by the BigRIPS fragment separator.

2. Major Research Subjects

Studies of the slowing down and purification of RI beams are the main subjects of the team. Developments of devices used for the slowing down of RI beams are also an important subject.

(1) Study and development of the slowed-down methods for LLFP
(2) Operation of the BigRIPS separator and supply the low energy LLFP beam to the experiment in which the cross sections of LLFP are measured at the low energy
(3) Development of MA (such as Np) beams for the nuclear data
(4) Development of the framework to seamlessly handle device, detector, DAQ, and analysis for the easy control of the complicate slowed-down RI beam production and its development

3. Summary of Research Activity

A new OEDO beam line, designed for the slowed-down RI beams, was constructed under the collaboration with CNS, the University of Tokyo. Our group was responsible for the construction of the infrastructure such as the cooling water and the electrical equipment, and the movement and alignment of existing vacuum chambers, quadrupole magnets. The power supply for the Superconducting Triplet Quadrupoles (STQ) was made, which had a stability also under the low current condition.

Slowed-down ^{93}Zr beams with 20 or 50 MeV/nucleon were successfully developed at June 2016 for the first time. The methods to obtain the narrow energy, position, and angle distribution were developed. The methods of the energy adjustment and the particle identification at 50 MeV/nucleon were developed. The ^{93}Zr and ^{107}Pd beams with 50 MeV/nucleon were produced for the nuclear-transmutation experiments using proton or deuteron targets in October 2016. The commissioning experiment of the OEDO beam line was successfully performed at June 2017. The first transmutation experiments using OEDO beam line were performed with ^{93}Zr, ^{107}Pd, and ^{79}Se around 20 MeV/nucleon.

With our developments, the slowed-down RI beams became ready for the transmutation experiments. On the other hand, the procedure to make the slowed-down RI beams became highly specialized. In order to easily produce the slowed-down RI beam, the framework, called BYACO, is being developed to seamlessly handle the device, detector, DAQ, and analysis. The procedure of the RI-beam energy control was implemented in the web application. The BYACO system was used also for an RI-beam automatic tuning project by the BigRIPS team.

The extension of the RI-beam separation using the $B\rho$-ΔE-$B\rho$ method by the charge state of RI beam was found to be essential to produce the heavy RI beams. The simulation tool of this extended separation, called Q+ separation, was developed and implemented into BYACO in 2021. With this tool, we succeeded to produce a ^{237}Np beam as a secondary beam by collaborating mainly with the fast RI data team and the BigRIPS team.

Members

Team Leader

Toshiyuki SUMIKAMA

Visiting Scientist

SungHan BAE (Inst. for Basic Sci.)

Student Trainees

Hiroya FUKUDA (Kyushu Univ.)
Misaki SAITSU (Kyushu Univ.)
Masaya OISHI (Kyushu Univ.)

Nuclear Science and Transmutation Research Division
Nuclear Transmutation Data Research Group
Muon Data Team

1. Abstract

Dr. Yoshio Nishina observed muons in cosmic rays in 1937. The muon is an elementary particle similar to electron and classified to lepton group. The muon has positive or negative electric charge, and the lifetime is 2.2 μsec. The negative muon (μ^-) is 207 times heavier than the electron and behaves as a "heavy electron" in materials. The negative muon is captured by atomic orbits of nuclei to form a muonic atom and cascades down to the $1s$ orbit to make muon nuclear capture. The muon is combined with a proton in the nucleus to convert to a neutron and a neutrino. The muon nuclear capture reaction on a nucleus ($^A_Z N$) with the atomic number Z and mass number A generates the isotopes of $^{A-x}_{Z-1}N$ ($x = 0, 1, 2, 3, 4$) by emitting some neutrons in the reaction. The phenomenon is called "muon nuclear transmutation." The reaction branching ratio of $^A_Z N(\mu^-, x n\nu)^{A-x}_{Z-1}N$ reactions ($x = 0, 1, 2, 3, 4$) is one of important factors toward various applications with nuclear transmutation technique. From a viewpoint of the nuclear physic, the muon nuclear capture reaction is very unique and interesting. A high-energy compound nuclear state is suddenly generated in the nuclei associated with a weak conversion process of proton to neutron and neutrino. Many experimental results have been so far reported, however, the reaction mechanism itself is not well clarified. The research team aims at obtaining the experimental data to investigate the reaction mechanism of muon nuclear capture, and also at theoretical understanding on the nuclear capture reaction.

2. Major Research Subjects

(1) Experimental clarification on the mechanism of nuclear muon capture reaction
(2) Theoretical understanding on the nuclear muon capture reaction
(3) Interdisciplinary applications with the nuclear transmutation technique

3. Summary of Research Activity

There are two experimental methods to study the muon nuclear capture reaction. The first one is "muon in-beam spectroscopy method." The neutron and γ-ray emissions from the excited states of $^{A-x}_{Z-1}N$ nuclei are prompt events and are observed by the "muon in-beam spectroscopy method" with a DC muon beam. The reaction branching ratio is directly determined by measuring the neutron multiplicity in the reaction. The DC muon beam is available at the MuSIC (Muon Science Innovative Channel) muon facility in the Research Center for Nuclear Physics (RCNP) at Osaka University. The second one is "muon activation method" with the pulsed muon beam. The produced unstable nuclei $^{A-x}_{Z-1}N$ make $\beta^{+/-}$ decays. The γ-rays associated with $\beta^{+/-}$ decays to the daughter nuclei are observed in the experiment. The build-up curve of γ-ray yield at muon beam-on and the decay curve at beam-off are measured. Since the half-lives and decay branching ratios of $\beta^{+/-}$-γ decays are known, the reaction branching ratios to the $^{A-x}_{Z-1}N$ nuclei are determined by the γ-ray yield curves. The pulsed muon beam is available at the RIKEN-RAL Muon Facility in the UK and J-PARC muon facility.

Muon nuclear capture reactions are studied on five isotope-enriched palladium targets ($^{104, 105, 106, 108, 110}$Pd) and five isotope-enriched zirconium targets ($^{90, 91, 92, 94, 96}$Zr) employing two experimental methods. By obtaining the experimental data on the Pd and Zr targets, the reaction mechanism is investigated experimentally, and the results are compared with appropriate theoretical calculations. The ^{107}Pd is classified to a long-lived fission product (LLFP) and is contained in a spent nuclear fuel. The study of muon nuclear capture on the Pd and Zr targets is aiming at exploring a possible reaction path to make the nuclear transmutation of the Pd and Zr metal extracted from the spent nuclear fuel without an isotope separation process. This research was funded by the ImPACT Program of Council for Science, Technology and Innovation (Cabinet Office, Government of Japan).

(1) Experiments with "muon in-beam spectroscopy method"

Muon nuclear capture reactions were investigated on five palladium targets ($^{104, 105, 106, 108, 110}$Pd) by employing the DC muon beam at MuSIC. The γ-ray and neutron in the muon nuclear capture reaction were measured with the time information relative to muon beam arrival. The measured neutron multiplicity gives the reaction branching ratio of $^A_{46}\mathrm{Pd}(\mu^-, x n\nu)^{A-x}_{45}\mathrm{Rh}$ reactions, where $A = 104, 105, 106, 108, 110$ and $x = 0, 1, 2, 3, 4$.

Employing a newly built neutron spectrometer, the neutron was measured to obtain the reaction branching ratios of muon capture reactions on the Pd targets. We have constructed a neutron spectrometer named "Seamine": **S**cintillator **E**nclosure **A**rray for **M**uon **I**nduced **N**eutron **E**mission. The spectrometer consists of 21 liquid scintillation counters, 2 Ge γ-ray detectors, 7 BaF_2 counters. The Pd target, muon beam counters and muon degraders are placed at the center of spectrometer. The neutron counter is a BC-501A liquid scintillation counter with 20 cm diameter and 5 cm depth and is connected to a 5" photo multiplication tube (H4144-01). The total neuron detection efficiency is estimated 5%, where the distance is 4 cm from the target to neutron counters. The Ge γ-ray detectors are placed at 10 cm form the target, and the typical detection efficiency is 0.5% for 200 keV γ-ray. The BaF_2 counters are located beneath the target to detect fast γ-rays emitted from the compound nucleus formed in the reactions. Signals from the liquid scintillation counters are processed in a CAEN V1730B waveform digitizer (16 channel, 14 bit, 500 M samplings/sec.). The neuron-γ discrimination is performed on-line during the experiment, and the detailed data analysis is conducted off-line after the experiment. The neutron energy spectrum is constructed in the digitizer. Signals from Ge detectors are also processed in the digitizer to obtain the energy and time spectrum of γ-rays associated with the reaction. Signals from the BaF_2 counters and muon beam counters are sent to the digitizer to make the fast timing signals.

We have established the muon in-beam spectroscopy method employing the "Seamine" spectrometer. The neutron data analysis

is in progress to obtain the multiplicity, the energy and the TOF spectrum using start signals given by γ-rays detected in the BaF_2 counters. The γ-ray data gives the energy spectrum of prompt γ-rays and muonic X-rays originated from the ^{104,105,106,108,110}Pd targets.

(2) Experiments with "muon activation method" at the RIKEN-RAL Muon Facility

We conducted the experiments on the muon nuclear capture employing the muon activation method at the RIKEN-RAL Muon Facility in the UK. The pulsed muon beam was irradiated on the ^{104,105,106,108,110}Pd targets. The γ-rays were detected by a Ge detector located at the downstream of the Pd targets to maximize the detection efficiency. The build-up and decay curves of γ-ray intensities were measured associated with $\beta^{+/-}$ decays of produced unstable nuclei to daughter nuclei. The γ-ray-yield curves give the absolute radiation activity produced by the reaction, and the reaction branching ratios are determined for ${}^{A}_{46}\mathrm{Pd}(\mu^-, xn\nu)^{A-x}_{45}\mathrm{Rh}$ reactions. The decay curves of γ-rays from the produced nuclei with long half-lives were measured under low γ-ray background at an experimental apparatus built in a separated room. The detailed off-line data analysis is in progress.

(3) Experiments with "muon activation method" at J-PARC muon facility

The experiments employing the muon activation method were performed at J-PARC muon facility. The five isotope-enriched Pd targets (^{104,105,106,108,110}Pd) were irradiated by the pulsed muon beam, and the build-up and decay curves of γ-ray intensities were measured.

In addition to the Pd targets, the experiments on five isotope-enriched Zr target (^{90,91,92,94,96}Zr) were conducted to obtain the reaction branching ratios of ${}^{A}_{40}\mathrm{Zr}(\mu^-, xn\nu)^{A-x}_{39}\mathrm{Y}$ reactions, where $A = 90, 91, 92, 94, 96$. The obtained reaction branching ratios on the Pd and Zr targets are important to understand the reaction mechanism of muon nuclear capture. The ^{93}Zr is one of the LLFP and is contained in a spent nuclear fuel. The experiment on the Zr targets is to explore a possibility to realize the nuclear transmutation of the Zr metal extracted from the spent nuclear fuel.

In order to obtain the reaction branching ratio of ${}^{107}_{46}\mathrm{Pd}(\mu^-, xn\nu)^{107-x}_{45}\mathrm{Rh}$ reactions, the muon activation experiment was performed employing a Pd target containing ^{107}Pd of 15.3%. The γ-ray intensities associated with $\beta^{+/-}$ decays of produced unstable nuclei were measured to obtain the build-up and decay curves. Once the branching ratios of the reactions on the ^{104,105,106,108,110}Pd targets are obtained, these contributions are extracted from the branching-ratio data obtained for the Pd target with ^{107}Pd. The reaction branching ratio of ${}^{107}_{46}\mathrm{Pd}(\mu^-, xn\nu)^{107-x}_{45}\mathrm{Rh}$ reactions is finally determined. The detailed off-line data analysis is in progress.

(4) Comparison with theory

The muon activation method gives the reaction branching ratios. The muon in-beam spectroscopy method gives the neutron multiplicity and the neutron energy spectrum. These experimental results are important to understand the compound nuclear state and neutron emission mechanism. The reaction branching ratios obtained by the muon activation method are compared with the results of neutron multiplicity measurements. The neutron energy spectrum is considered to be reflected by the energy distribution of compound nuclear state and neutron emission mechanism. The experimental results are compared with the appropriate calculations employing the neutron emission mechanisms due to an evaporation, a cascade and a direct emission processes with assuming the energy distribution at compound nuclear state.

Members

Team Leader
Hiroyoshi SAKURAI

Contract Researcher
Teiichiro MATSUZAKI

Part-time Worker
Takeshi SAITO (Research Part-time Worker I)

List of Publications & Presentations

Presentations

[Domestic Conferences/Workshops]

水野るり惠, 他, 「ミューオン原子 X 線分光のためのコンプトンサプレッサー付き Ge 検出器開発」, 日本物理学会 2021 年秋季大会, オンライン, 2021 年 9 月 14–17 日.

水野るり惠, 他, 「Ge 検出器を用いたミューオン原子 X 線分光のための光子検出システムの性能評価」, Muon 科学と加速器研究, 大阪府豊中市 (大阪大学), 2022 年 1 月 6–8 日.

水野るり惠, 他, 「ミューオン原子 X 線分光のための Ge 検出器を用いた広ダイナミックレンジ光子検出システムの性能評価」, 日本物理学会第 77 回年次大会, オンライン, 2022 年 3 月 15–19 日.

齋藤岳志, 「原子核ミューオン捕獲に伴う放出中性子の測定」, RCNP 研究会「ミューオン原子核捕獲反応による原子核関連研究の可能性」, 大阪府茨木市（大阪大学核物理研究センター), 2022 年 3 月 24–25 日.

新倉潤, 他, 「ミューオン原子 X 線測定のための検出器開発」, RCNP 研究会「ミューオン X 線 γ 線分光」, 大阪府茨木市（大阪大学核物理研究センター), 2022 年 3 月 24–25 日.

齋藤岳志, 「ミューオン原子 X 線分光とその将来について」, ソフトエラー研究会, 山口県大島郡（ゲストハウス HOSHI-KAZE）, 2022 年 3 月 28 日.

水野るり惠, 他, 「Si ミューオン原子由来の生成原子核分岐比の絶対値測定実験」, ソフトエラー研究会, 山口県大島郡（ゲストハウス HOSHI-KAZE）, 2022 年 3 月 28 日.

Others

[Master Thesis]

水野るり惠,「ミューオン原子 X 線分光のためのコンプトンサプレッサー付きゲルマニウム検出器の開発」, 東京大学, 2022 年 3 月.

[PhD. Thesis]

T. Saito, “Study of muonic X-ray spectroscopy and nuclear muon capture reaction”, University of Tokyo, March 2022.

Nuclear Science and Transmutation Research Division
High-Intensity Accelerator R&D Group

1. Abstract

The High-Intensity Accelerator R&D group, consisting of two teams, develops elemental technology of high-power accelerators and high-power targets, aiming at future applications to nuclear transmutations of long-lived fission product into short-lived nuclides. The research subjects are superconducting rf cavities for low-velocity ions, design of high-power accelerators, high-power target systems and related technologies.

Nuclear transmutation with high-intensity accelerators is expected to reduce the high-level radioactive wastes and to recycle the precious resources such as rare-earth materials in future. This method is one of the important applications of the ion-accelerator technologies that have been developed at RIKEN for a long time. Under the framework of ImPACT Fujita Program, we have conducted R&D of elemental technology related to the high-power accelerators and high-power targets, from FY2014 to FY2018. We gained a lot of experiences in these R&Ds. Among them, the development of a superconducting rf cavity has become the basis of the upgrade program of the RILAC facility which started in 2016.

2. Major Research Subject

R&D of elemental technology of high-power accelerators and high-power targets.

3. Summary of Research Activity

(1) A high-gradient rf cavity has been constructed and tested based on the superconducting rf technology.
(2) Several candidates for the high-power target have been proposed and their prototypes have been tested.
(3) A high-current deuteron RFQ has been designed.

Members

Director

Osamu KAMIGAITO
(concurrent: Group Director, Accelerator Group)

Nuclear Science and Transmutation Research Division
High-Intensity Accelerator R&D Group
High-Gradient Cavity R&D Team

1. Abstract

We develop new components for accelerators dedicated for low-beta-ions with very high intensity. Specifically, we are designing and constructing a cryomodule for superconducting linac efficient for acceleration of low-beta-ions. In parallel, we try to optimize an rf acceleration system by making computer simulations for acceleration of very high intensity beams.

2. Major Research Subjects

(1) Development of high-gradient cavites for low beta ions
(2) Development of power saving cryomodules

3. Summary of Research Activity

Development of highly efficient superconducting accelerator modules

Members

Team Leader

Naruhiko SAKAMOTO

Research/Technical Scientists

Yutaka WATANABE
Kazutaka OZEKI

Research & Development Scientist

Kenji SUDA

Nuclear Science and Transmutation Research Division
High-Intensity Accelerator R&D Group
High-Power Target R&D Team

1. Abstract

The subjects of this team cover R&D studies with respect to target technology for the transmutation of the LLFPs.

2. Major Research Subjects

(1) Liquid lithium target for production of neutron or muon
(2) Beam window without solid structure

3. Summary of Research Activity

(1) Liquid lithium target for production of neutron or muon (H. Okuno)
(2) Beam window with solid structure (H. Okuno)

Members

Team Leader
Hiroki OKUNO

Special Postdoctoral Researcher
Yasuto MIYAKE

Visiting Scientist
Katsuyoshi TSUMORI (Nat'l Inst. Fusion Science)

Research Facility Development Division
Accelerator Group

1. Abstract

The Accelerator Group, consisting of seven teams, pursues various upgrade programs on the world-leading heavy-ion accelerator facility, RI Beam Factory (RIBF), to enhance the accelerator performance and operation efficiency. The programs include the R&D of superconducting ECR ion source, charge stripping systems, beam diagnostic devices, radio-frequency systems, control systems, and beam simulation studies. We are also maintaining the large infrastructure to realize effective operation of the RIBF. Moreover, we are actively promoting the applications of the facility to various research fields.

Our primary mission is to supply intense, stable heavy-ion beams for the users through effective operation, maintenance, and upgrade of the RIBF accelerators and related infrastructure. The director members govern the development programs that are not dealt with by a single team, such as intensity upgrade and effective operation. We also discuss the future plans of RIBF along with other laboratories belonging to the RIBF research division.

Various improvements and developments have been carried out for the RIBF accelerators in order to upgrade the beam intensities and stability. Owing to the efforts, for example, we succeeded in accelerating the uranium beam of 117 particle nA through SRC in October 2020. This surpassed the long-standing target of 100 particle nA, and also means that one of goals of the current mid-term plan of RNC has been achieved. Moreover, the beam availability for the RIBF experiments has increased to 98.3% in 2021, which is the highest value since RIBF started operation.

At the RILAC facility, upgraded with a superconducting ECR ion source and superconducting booster linac, synthesis experiments of new elements has been conducted since 2020. In the first half of 2021, major repairs were made to the normal-conducting cavities. The coupler part of the superconducting cavities, which had a vacuum leak problem, were modified during the summer shutdown. As a result, a high intensity beam of ^{51}V is now being supplied stably. Moreover, construction of a new beam line for the R&D of mass production method of ^{211}At has been almost completed, in cooperation with the Safety Management Group under the leadership of the RI Application Research Group.

An upgrade plan of RIBF for further increasing uranium beam has been continuously discussed. Based on the basic design of the "charge-stripper ring (CSR)," which will be used to increase the overall stripping efficiency of the uranium beam, a pair of quadrupole magnets was fabricated as a prototype. The measured magnetic field was in good agreement with the simulations, including the magnetic field leaking around the magnets. Design study of the extraction bending magnet was also performed.

2. Major Research Subjects

(1) Intensity upgrade of RIBF accelerators (Okuno)
(2) Effective and stable operation of RIBF accelerators (Fukunishi)
(3) Stable operation of the upgraded RILAC facility
(4) Promotion of the upgrade plan of RIBF

3. Summary of Research Activity

(1) The beams were provided for the RIBF experiments at the intensities requested by the users.
(2) The beam availability for the RIBF experiments was 98.3% in 2021. This is the highest value since RIBF started operation.
(3) A high intensity beam of ^{51}V was supplied stably to the synthesis experiments of new elements at the upgraded RILAC facility.
(4) An intensity-upgrade plan of the RIBF has been further investigated. Elemental R&D of the first charge-stripper ring (CSR1) is under progress.

Members

Director

Osamu KAMIGAITO

Deputy Directors

Hiroki OKUNO (for intensity upgrade)
Nobuhisa FUKUNISHI (for stable and efficient operation)

Junior Research Associate

Kaori NAKAMURA

Research Consultants

Tadashi FUJINAWA
Masayuki KASE

Visiting Scientists

Eiji KAKO (KEK)
Hirotaka NAKAI (KEK)
Kensei UMEMORI (KEK)
Hiroshi SAKAI (KEK)
Taro KONOMI (KEK)
Masahiro OKAMURA (BNL)
Noboru SASAO (Okayama Univ.)
Yasutaka IMAI (Okayama Univ.)

Assistant
Karen SAKUMA

Administrative Part-time Worker II
Ryoko UMEZAKI

List of Publications & Presentations

Publication

[Original Paper]

O. Kamigaito, “Scale invariance of electrodynamics in radio-frequency linear accelerators,” arXiv:2109.14273.

Research Facility Development Division
Accelerator Group
Accelerator R&D Team

1. Abstract

We are developing the key hardware in upgrading the RIBF accelerator complex. Our primary focus and research is charge stripper which plays an essential role in the RIBF accelerator complex. Charge strippers remove many electrons in ions and realize efficient acceleration of heavy ions by greatly enhancing charge state. The intensity of uranium beams is limited by the lifetime of the carbon foil stripper conventionally installed in the acceleration chain. The improvement of stripper lifetimes is essential to increase beam power towards the final goal of RIBF in the future. We are developing the low-Z gas stripper. In general gas stripper is free from the lifetime related problems but gives low equilibrium charge state because of the lack of density effect. Low-Z gas stripper, however, can give as high equilibrium charge state as that in carbon foil because of the suppression of the electron capture process. Another our focus is the upgrade of the world's first superconducting ring cyclotron.

2. Major Research Subjects

(1) Development of charge strippers for high power beams (highly oriented graphene film, low-Z gas)
(2) Upgrade of the superconducting ring cyclotron
(3) Maintenance and R&D of the electrostatic deflection/inflection channels for the beam extraction/injection

3. Summary of Research Activity

(1) Development of charge strippers for high power beams (foil, low-Z gas)

(H. Hasebe, H. Imao, H. Okuno)

We are developing the charge strippers for high intensity heavy ion beams. We are focusing on the developments on highly oriented carbon graphite films and gas strippers including He gas stripper.

(2) Upgrade of the superconducting ring cyclotron

(J. Ohnishi, H. Okuno)

We are focusing on the upgrade of the superconducting ring cyclotron.

(3) Maintenance and R&D of the electrostatic deflection/inflection channels for the beam extraction/injection

(J. Ohnishi, H. Okuno)

We are developing high-performance electrostatic channels for high power beam injection and extraction.

Members

Team Leader
Hiroki OKUNO

Senior Research Scientist
Hiroshi IMAO

Technical Scientist
Hiroo HASEBE

Special Temporary Technical Scientist
Jun-ichi OHNISHI

Visiting Scientist
Noriyosu HAYASHIZAKI (Tokyo Tech)

List of Publications & Presentations

Publication

[Original Paper]

H. Imao, "Charge stripper ring for RIKEN RI Beam Factory," J. Instrum. **15**, P12036 (2020).

Research Facility Development Division
Accelerator Group
Ion Source Team

1. Abstract

Our aim is to operate and develop the ECR ion sources for the accelerator-complex system of the RI Beam Factory. We focus on further upgrading the performance of the RI Beam Factory through the design and fabrication of a superconducting ECR ion source for production of high-intensity heavy ions.

2. Major Research Subjects

(1) Operation and development of the ECR ion sources
(2) Development of a superconducting ECR heavy-ion source for production of high-intensity heavy ion beams

3. Summary of Research Activity

(1) Operation and development of ECR ion sources

(T. Nakagawa, M. Kidera, Y. Higurashi, T. Nagatomo, Y. Kanai, and H. Haba)

We routinely produce and supply various kinds of heavy ions such as zinc and calcium ions for the super-heavy element search experiment as well as uranium ions for RIBF experiments. We also perform R&D's to meet the requirements for stable supply of high-intensity heavy ion beams.

(2) Development of a superconducting ECR ion source for use in production of a high-intensity heavy ion beam

(T. Nakagawa, J. Ohnishi, M. Kidera, Y. Higurashi, and T. Nagatomo)

The RIBF is required to supply heavy ion beams with very high intensity so as to produce RI's and for super-heavy element search experiment. We have designed and are fabricating an ECR ion source with high magnetic field and high microwave- frequency, since the existing ECR ion sources have their limits in beam intensity. The coils of this ion source are designed to be superconducting for the production of high magnetic field. We are also designing the low-energy beam transport line of the superconducting ECR ion source.

Members

Team Leader

Takahide NAKAGAWA

Senior Technical Scientists

Yoshihide HIGURASHI
Takashi NAGATOMO

Special Temporary Research Scientist

Yasuyuki KANAI

Research Facility Development Division
Accelerator Group
RILAC Team

1. Abstract

Our team is responsible for the operation, maintenance, and upgrade of the RIKEN heavy-ion linear accelerator (RILAC), a unique variable-frequency linac that has been in operation since 1980. RILAC was upgraded in the 1990s as part of the RI Beam Factory (RIBF) project, and made a significant contribution to the synthesis and discovery of the element 113, nihonium. In 2019, a superconducting linac booster, SRILAC, was installed, and it will play a major role in the synthesis of heavier new elements, development of the technologies for production of medical radioisotopes, and as a powerful injector to RIBF.

2. Major Research Subjects

(1) Development of technology to operate RILAC with high intensity and high stability
(2) Construction and maintenance of the RILAC beamlines
(3) Efficient operation, maintenance and management of the vacuum equipment in the RIBF accelerators

3. Summary of Research Activity

In 2021, we have made various improvements of the whole RILAC with the cooperation of other teams of the Accelerator Group, in order to provide high-intensity beams more stably to the new element synthesis experiments being conducted at GARIS III. For example, leak of refrigerant in the normal conducting cavities was thoroughly investigated and repaired. In addition, vacuum leak at the couplers of the superconducting cavities, which had been a problem since its start, was repaired. With these efforts, the beam availability has been improved significantly.

A beamline is being prepared at the RILAC facility for mass production of ^{211}At, which has potential medical applications. Under the leadership of the RI Application Research Group and with the help of other teams of the Accelerator Group, the optical calculations, electromagnet design, radiation shielding design, and overall beamline installation were undertaken and the beamline is almost complete.

As in the past, we maintained the vacuum system of the whole accelerators at RIBF. While taking into consideration the aging of the vacuum pumps, an efficient maintenance plan was established and cost-conscious maintenance was executed.

Members

Team Leader
Osamu KAMIGAITO

Deputy Team Leader
Naruhiko SAKAMOTO

Research/Technical Scientists
Yutaka WATANABE (Senior Technical Scientist)
Takahiro NISHI (Research Scientist)

Research Consultant
Eiji IKEZAWA

List of Publications & Presentations

[Proceedings]

T. Nishi, E. Iwai, A. Uchiyama, Y. Shimizu, T. Sugimoto, H. Suzuki, H. Takeda, N. Fukuda, N. Fukunishi, H. Fujii, H. Maesaka, and M. Yoshimoto, "Development of auto tuning system of ion optics for high intensity primary beam using machine learning," Proceedings of the 18th Annual Meeting of Particle Accelerator Society of Japan, QST-Takasaki Online, Japan, August 9–12, 2021, TUOA03, 71–74 (2021). https://www.pasj.jp/web_publish/pasj2021/proceedings/PDF/TUOA/TUOA03.pdf.

T. Nakamura, K. Ozeki, S. Fukuzawa, M. Hamanaka, S. Ishikawa, K. Kobayashi, R. Koyama, M. Nishida, M. Nishimura, J. Shibata, N. Tsukiori, K. Yadomi, T. Dantsuka, M. Fujimaki, T. Fujinawa, N. Fukunishi, H. Hasebe, Y. Higurashi, E. Ikezawa, H. Imao, O. Kamigaito, Y. Kanai, M. Kidera, M. Komiyama, K. Kumagai, T. Maie, T. Nagatomo, T. Nakagawa, M. Nakamura, J. Ohnishi, H. Okuno, N. Sakamoto, S. Kenji, A. Uchiyama, W. Shu, W. Tamaki, Y. Watanabe, K. Yamada, and H. Yamasawa, "Status report on the operation of RIKEN AVF cyclotron," Proceedings of the 18th Annual Meeting of Particle Accelerator Society of Japan, QST-Takasaki Online, Japan, August 9–12, 2021, TUP052, 575–579 (2021). https://www.pasj.jp/web_publish/pasj2021/proceedings/PDF/TUP0/TUP052.pdf.

S. Fukuzawa, K. Suda, A. Goto, J. Ohnishi, M. Hamanaka, S. Ishikawa, K. Kobayashi, R. Koyama, T. Nakamura, M. Nishida, M. Nishimura, J. Shibata, N. Tsukiori, K. Yadomi, M. Fujimaki, N. Fukunishi, H. Hasebe, Y. Higurashi, H. Imao, O. Kamigaito, M. Kase, M. Kidera, M. Komiyama, K. Kumagai, T. Maie, T. Nagatomo, T. Nakagawa, H. Okuno, K. Ozeki, N. Sakamoto,

A. Uchiyama, S. Watanabe, T. Watanabe, Y. Watanabe, K. Yamada, K. Kamakura, and Y. Kotaka, "Status report on the operation of RIKEN AVF cyclotron," Proceedings of the 18th Annual Meeting of Particle Accelerator Society of Japan, QST-Takasaki Online, Japan, August 9–12, 2021, WEP052, 760–764 (2021). https://www.pasj.jp/web_publish/pasj2021/proceedings/PDF/WEP0/WEP052.pdf.

T. Ohki, H. Yamauchi, K. Oyamada M. Tamura, A. Yusa, K. Kaneko, N. Sakamoto, M. Fujimaki, E. Ikezawa, H. Imao, M. Kidera, T. Nagatomo, T. Nishi, K. Ozeki, K. Suda, A. Uchiyama, T. Watanabe, Y. Watanabe, K. Yamada, and O. Kamigaito, "Present status of RILAC," Proceedings of the 18th Annual Meeting of Particle Accelerator Society of Japan, QST-Takasaki Online, Japan, August 9–12, 2021, THP059, 983–985 (2021). https://www.pasj.jp/web_publish/pasj2021/proceedings/PDF/THP0/THP059.pdf.

Presentations

[International Conferences/Workshops]

T. Yanagisawa (invited), K. Yamada, T. Dantsuka, M. Fujimaki, E. Ikezawa, H. Imao, O. Kamigaito, M. Komiyama, K. Kumagai, T. Nagatomo, T. Nishi, H. Okuno, K. Ozeki, N. Sakamoto, K. Suda, A. Uchiyama, T. Watanabe, Y. Watanabe, E. Kako, H. Nakai, H. Sakai, K. Umemori, H. Hara, A. Miyamoto, and K. Sennyu, "Successful beam commissioning of heavy-ion superconducting linac at RIKEN," 2021 International Conference on RF Superconductivity (SRF2021), East Lansing, MI, USA, Online, June 28–July 2, 2021.

K. Yamada (invited), T. Nishi, M. Fujimaki, N. Fukunishi, H. Imao, O. Kamigaito, T. Nagatomo, N. Sakamoto, A. Uchiyama, T. Watanabe, and Y. Watanabe, "Beam acceleration with the upgraded RIKEN heavy-ion linac," 64th ICFA Advanced Beam Dynamics Workshop on High-Intensity and High-Brightness Hadron Beams (HB2021), Batavia, IL, USA, Online, October 4–8, 2021.

A. Yusa (poster), A. Uchiyama, M. Fujimaki, N. Fukunishi, Y. Higurashi, E. Ikezawa, H. Imao, O. Kamigaito, M. Kidera, K. Kumagai, T. Nagatomo, T. Nishi, J. Ohnishi, K. Ozeki, N. Sakamoto, K. Suda, T. Watanabe, Y. Watanabe, K. Yamada, M. Komiyama, A. Kamoshida, K. Kaneko, R. Koyama, T. Ohki, K. Oyamada, M. Tamura, and H. Yamauchi, "Control system of the SRILAC project at RIBF," 18th International Conference on Accelerator and Large Experimental Physics Control Systems (ICALEPCS 2021), China, Shanghai, October 14–22, 2021.

[Domestic Conferences/Workshops]

西隆博 (招待講演), 「理化学研究所におけるガウシアンプロセスを用いた一次重イオンビームトランスポートの自動調整の開発」, 日本物理学会 第 77 回年次大会, オンライン, 2022 年 3 月 15 日–19 日.

吉本雅浩 (口頭発表), 西隆博, 岩井瑛人, 内山暁仁, 清水陽平, 杉本崇, 鈴木宏, 竹田浩之, 福田直樹, 藤井洋樹, 前坂比呂和, 「機械学習を用いた高強度一次ビームのイオン光学系の自動調整の開発」, 第 18 回日本加速器学会年会, オンライン, 2021 年 8 月 9–12 日.

上垣外修一 (ポスター発表), 大木智則, 小山田和幸, 山内啓資, 田村匡史, 遊佐陽, 金子健太, 坂本成彦, 藤巻正樹, 池沢英二, 今尾浩士, 木寺正憲, 長友傑, 大関和貴, 須田健嗣, 内山暁仁, 渡邉環, 渡邉裕, 山田一成, 「理研重イオンリニアックの現状報告」, 第 18 回日本加速器学会年会, オンライン, 2021 年 8 月 9–12 日.

小高康照 (ポスター発表), 福澤聖児, 須田健嗣, 後藤彰, 大西純一, 濱仲誠, 石川盛, 小林清志, 小山亮, 仲村武志, 西田稔, 柴田順翔, 月居憲俊, 矢冨一慎, 藤巻正樹, 福西暢尚, 長谷部裕雄, 日暮祥英, 今尾浩士, 上垣外修一, 加瀬昌之, 木寺正憲, 込山美咲, 熊谷桂子, 眞家武士, 長友傑, 中川孝秀, 奥野広樹, 大関和貴, 坂本成彦, 内山暁仁, 渡部秀, 渡邉環, 渡邉裕, 山田一成, 鎌倉恵太, 「理研 AVF サイクロトロン運転の現状報告」, 第 18 回日本加速器学会年会, オンライン, 2021 年 8 月 9–12 日.

山澤秀行 (ポスター発表), 仲村武志, 福澤聖児, 濱仲誠, 石川盛, 小林清志, 小山亮, 西田稔, 西村誠, 柴田順翔, 月居憲俊, 矢冨一慎, 大関和貴, 段塚知志, 藤巻正樹, 藤縄雅, 福西暢尚, 長谷部裕雄, 日暮祥英, 池沢英二, 今尾浩士, 上垣外修一, 金井保之, 加瀬昌之, 木寺正憲, 込山美咲, 熊谷桂子, 眞家武士, 長友傑, 中川孝秀, 中村仁音, 大西純一, 奥野広樹, 坂本成彦, 須田健嗣, 内山暁仁, 渡部秀, 渡邉環, 渡邉裕, 山田一成, 「理研 RIBF におけるリングサイクロトロンの運転報告」, 第 18 回日本加速器学会年会, オンライン, 2021 年 8 月 9–12 日.

Outreach Activity

熊谷洸希, 渋谷遥斗, 森内厚佑, 水谷凜都, 登藤成琉, 丸田京華, 秋山翔希, 西隆博, 田中香津生, 遠藤金吾, 「秋田県における地上でのμ粒子検出頻度と天気ごとの地上気温、湿度、気圧との偏相関」, J. Sci. EGGS, **4**, 2110004, 1–6 (2021). https://www3.e-kenkyu.com/j-sci-eggs/uploads/manuscript/file/21/Vol.4-2110004_2021.pdf.

Research Facility Development Division
Accelerator Group
Cyclotron Team

1. Abstract

Together with other teams of Nishina Center accelerator division, maintaining and improving the RIBF cyclotron complex. The accelerator provides high intensity heavy ions. Our mission is to have stable operation of cyclotrons for high power beam operation. Recently stabilization of the rf system is a key issue to provide 10 kW heavy ion beam.

2. Major Research Subjects

(1) RF technology for Cyclotrons
(2) Operation of RIBF cyclotron complex
(3) Maintenance and improvement of RIBF cyclotrons
(4) Single turn operation for polarized deuteron beams
(5) Development of superconducting linac

3. Summary of Research Activity

- Development of the rf system for a reliable operation
- Development of highly stabilized low level rf system
- Development of superconducting linac
- Development of the intermediate-energy polarized deuteron beams

Members

Team Leader
Naruhiko SAKAMOTO

Research/Technical Scientists
Kazutaka OZEKI (Senior Technical Scientist)
Kenji SUDA (Technical Scientist)

List of Publications & Presentations

Publications

[Proceedings]

T. Nakamura, K. Ozeki, S. Fukuzawa, M. Hamanaka, S. Ishikawa, K. Kobayashi, R. Koyama, M. Nishida, M. Nishimura, J. Shibata, N. Tsukiori, K. Yadomi, T. Dantsuka, M. Fujimaki, T. Fujinawa, N. Fukunishi, H. Hasebe, Y. Higurashi, E. Ikezawa, H. Imao, O. Kamigaito, Y. Kanai, M. Kidera, M. Komiyama, K. Kumagai, T. Maie, T. Nagatomo, T. Nakagawa, M. Nakamura, J. Ohnishi, H. Okuno, N. Sakamoto, S. Kenji, A. Uchiyama, W. Shu, W. Tamaki, Y. Watanabe, K. Yamada, and H. Yamasawa, "Status report on the operation of RIKEN AVF cyclotron," Proceedings of the 18th Annual Meeting of Particle Accelerator Society of Japan, QST-Takasaki Online, Japan, August 9–12, 2021, TUP052, 575–579 (2021). https://www.pasj.jp/web_publish/pasj2021/proceedings/PDF/TUP0/TUP052.pdf.

S. Fukuzawa, K. Suda, A. Goto, J. Ohnishi, M. Hamanaka, S. Ishikawa, K. Kobayashi, R. Koyama, T. Nakamura, M. Nishida, M. Nishimura, J. Shibata, N. Tsukiori, K. Yadomi, M. Fujimaki, N. Fukunishi, H. Hasebe, Y. Higurashi, H. Imao, O. Kamigaito, M. Kase, M. Kidera, M. Komiyama, K. Kumagai, T. Maie, T. Nagatomo, T. Nakagawa, H. Okuno, K. Ozeki, N. Sakamoto, A. Uchiyama, S. Watanabe, T. Watanabe, Y. Watanabe, K. Yamada, K. Kamakura, and Y. Kotaka, "Status report on the operation of RIKEN AVF cyclotron," Proceedings of the 18th Annual Meeting of Particle Accelerator Society of Japan, QST-Takasaki Online, Japan, August 9–12, 2021, WEP052, 760–764 (2021). https://www.pasj.jp/web_publish/pasj2021/proceedings/PDF/WEP0/WEP052.pdf.

T. Ohki, H. Yamauchi, K. Oyamada M. Tamura, A. Yusa, K. Kaneko, N. Sakamoto, M. Fujimaki, E. Ikezawa, H. Imao, M. Kidera, T. Nagatomo, T. Nishi, K. Ozeki, K. Suda, A. Uchiyama, T. Watanabe, Y. Watanabe, K. Yamada, and O. Kamigaito, "Present status of RILAC," Proceedings of the 18th Annual Meeting of Particle Accelerator Society of Japan, QST-Takasaki Online, Japan, August 9–12, 2021, THP059, 983–985 (2021). https://www.pasj.jp/web_publish/pasj2021/proceedings/PDF/THP0/THP059.pdf.

Presentations

[International Conference/Workshops]

K. Yamada (invited), T. Dantsuka, M. Fujimaki, E. Ikezawa, H. Imao, O. Kamigaito, M. Komiyama, K. Kumagai, T. Nagatomo, T. Nishi, H. Okuno, K. Ozeki, N. Sakamoto, K. Suda, A. Uchiyama, T. Watanabe, Y. Watanabe, E. Kako, H. Nakai, H. Sakai, K. Umemori, H. Hara, A. Miyamoto, K. Sennyu, and T. Yanagisawa, "Successful beam commissioning of heavy-ion superconducting linac at RIKEN," 2021 International Conference on RF Superconductivity (SRF2021), East Lansing, MI, USA, Online, June 28–July 2, 2021.

K. Ozeki (poster), O. Kamigaito, N. Sakamoto, K. Suda, and K. Yamada, "FPC for RIKEN QWR," 2021 International Conference on RF Superconductivity (SRF2021), East Lansing, MI, USA, Online, June 28–July 2, 2021.

K. Suda (poster), O. Kamigaito, K. Ozeki, N. Sakamoto, K. Yamada, E. Kako, H. Nakai, H. Sakai, K. Umemori, H. Hara, A. Miyamoto, K. Sennyu, and T. Yanagisawa, "New frequency-tuning system and digital LLRF for stable and reliable operation of SRILAC," 2021 International Conference on RF Superconductivity (SRF2021), East Lansing, MI, USA, Online, June 28–July 2, 2021.

N. Sakamoto (poster), H. Imao, O. Kamigaito, T. Nagatomo, T. Nishi, K. Ozeki, K. Suda, A. Uchiyama, and K. Yamada, "Operation experience of the superconducting linac at RIKEN RIBF," 2021 International Conference on RF Superconductivity (SRF2021), East Lansing, MI, USA, Online, June 28–July 2, 2021.

[Domestic Conferences/Workshops]

仲村武志（ポスター発表）, 福澤聖児, 濱仲誠, 石川盛, 小林清志, 小山亮, 西田稔, 西村誠, 柴田順翔, 月居憲俊, 矢冨一慎, 大関和貴, 段塚知志, 藤巻正樹, 藤縄雅, 福西暢尚, 長谷部裕雄, 日暮祥英, 池沢英二, 今尾浩士, 上垣外修一, 金井保之, 木寺正憲, 込山美咲, 熊谷桂子, 真家武士, 長友傑, 中川孝秀, 中村仁音, 大西純一, 奥野広樹, 坂本成彦, 須田健嗣, 内山暁仁, 渡部秀, 渡邉環, 渡邉裕, 山田一成, 山澤秀行, 「理研 RIBF におけるリングサイクロトロンの運転報告」, 第 18 回日本加速器学会年会, オンライン, 2021 年 8 月 9–12 日.

福澤聖児, 須田健嗣, 後藤彰, 大西純一, 濱仲誠, 石川盛, 小林清志, 小山亮, 仲村武志, 西田稔, 西村誠, 柴田順翔, 月居憲俊, 矢冨一慎, 藤巻正樹, 福西暢尚, 長谷部裕雄, 日暮祥英, 今尾浩士, 上垣外修一, 加瀬昌之, 木寺正憲, 込山美咲, 熊谷桂子, 真家武士, 長友傑, 中川孝秀, 奥野広樹, 大関和貴, 坂本成彦, 内山暁仁, 渡部秀, 渡邉環, 渡邉裕, 山田一成, 鎌倉恵太, 小高康照, 「理研 AVF サイクロトロン運転の現状報告」, 第 18 回日本加速器学会年会, オンライン, 2021 年 8 月 9–12 日.

大木智則, 小山田和幸, 山内啓資, 田村匡史, 遊佐陽, 金子健太, 坂本成彦, 藤巻正樹, 池沢英二, 今尾浩士, 木寺正憲, 長友傑, 大関和貴, 須田健嗣, 内山暁仁, 渡邉環, 渡邉裕, 山田一成, 上垣外修一, 「理研重イオンリニアックの現状報告」, 第 18 回日本加速器学会年会, オンライン, 2021 年 8 月 9–12 日.

Outreach Activity

坂本成彦, 私立武蔵越生高校講演会, 「加速器入門」, オンライン, 2021 年 12 月 13 日.

Research Facility Development Division
Accelerator Group
Beam Dynamics & Diagnostics Team

1. Abstract

Aiming at stable and efficient operation of the RIBF cascaded cyclotron system, Beam Dynamics and Diagnostics Team developes power supplies, beam instrumentation, computer control and beam dynamic studies. We have successfully increased the beam availability for user experiments to more than 98%. We have also established small-beam-loss operations. The latter strongly contributes to recent high-power operations at RIBF.

2. Major Research Subjects

(1) More efficient and stable operations of the RIBF cascaded cyclotron system
(2) Maintenance and developments of the beam instrumentation
(3) Developments of computer control system for more intelligent and efficient operations
(4) Maintenance and improvements of the magnet power supplies for more stable operations
(5) Upgrade of the existing beam interlock system for high-power beams with few tens of kW

3. Summary of Research Activity

(1) High-intensity heavy-ion beams such as 117-particle-nA (pnA) uranium, 173-pnA xenon, 486-pnA krypton, 788-pnA Zinc and 740-pnA calcium beams have been obtained.
(2) The world-first high-Tc SQUID beam current monitor has been developed.
(3) The bending power of the fixed-frequency Ring Cyclotron has been upgraded to 700 MeV.
(4) The world-most-intense V beams are stably supplied to super-heavy-element-search experiments.
(5) The RIBF control system has been operated stably by replacing legacy hardware controllers carried over from our old facility with new ones. Several useful operation tools are also developed.
(6) The dated power supplies exciting the main coils of RIKEN Ring Cyclotron has been upgraded to a new one having a better long-term stability than the old ones.
(7) Developments of automatic beam tuning methods based on recent machine-learning technology and adaptive control are in progress.

Members

Team Leader
Nobuhisa FUKUNISHI

Senior Technical Scientists
Masaki FUJIMAKI
Keiko KUMAGAI
Akito UCHIYAMA
Tamaki WATANABE
Kazunari YAMADA

Expert Technician
Misaki KOMIYAMA

Postdoctoral Researcher
Takahiro NISHI

Research Associate
Hiroki FUJII

Visiting Scientists
Shin-ichiro HAYASHI (Hiroshima Int'l Univ.)
Atsushi KAMOSHIDA (Nat'l Instruments Japan Corporation)
Takuya MAEYAMA (Kitasato Univ.)

List of Publications & Presentations

Publication

[Review Article]

K. Yamada, K. Ozeki, and K. Suda, "Helium cryogenic system for the RIKEN superconducting heavy-ion linear accelerator—System overview and operation," Teion Kogaku (J. Cryo. Super. Soc. Jpn.) **56**, 201–208 (2021).

[Proceedings]

A. Uchiyama, M. Komiyama, M. Kidera, and N. Fukunishi, "Data archive system for superconducting RIKEN linear accelerator at RIBF," 12th International Particle Accelerator Conference (IPAC'21), Campinas, Brazil (virtual format), 2178–2181 (2021).

K. Yamada, T. Dantsuka, M. Fujimaki, E. Ikezawa, H. Imao, O. Kamigaito, M. Komiyama, K. Kumagai, T. Nagatomo, T. Nishi, H. Okuno, K. Ozeki, N. Sakamoto, K. Suda, A. Uchiyama, T. Watanabe, Y. Watanabe, H. Hara, A. Miyamoto, K. Sennyu, T. Yanagisawa, E. Kako, H. Nakai, H. Sakai, and K. Umemori, "Successful beam commissioning of heavy-ion superconducting linac at RIKEN," Proceedings of 20th International Conference on RF Superconductivity (SRF2021), 167–174 (2021).

A. Uchiyama, M. Komiyama, M. Fujimaki, K. Kumagai, H. Yamaychi, and K. Kaneko, "Development of machine protection system for SRILAC," Proceedings of the 18th Particle Accelerator Society of Japan, TUP042, 532–535 (2021).

T. Watanabe, A. Kamoshida, A. Uchiyama, T. Nishi, R. Koyama, and K. Kaneko, "Distributed control by EPICS for the SRILAC beam energy position monitoring system using LabVIEW," Proceedings of the 18th Particle Accelerator Society of Japan, WEP026, 683–686 (2021).

A. Uchiyama, M. Fujimaki, N. Fukunishi, Y. Higurashi, E. Ikezawa, H. Imao, O. Kamigaito, M. Kidera, M. Komiyama, K. Kumagai, T. Nagatomo, T. Nakagawa, T. Nishi, J. Ohnishi, K. Ozeki, N. Sakamoto, K. Suda, T. Watanabe, Y. Watanabe, K. Yamada, A. Kamoshida, K. Kaneko, R. Koyama, T. Ohki, K. Oyamada, M. Tamura, H. Yamauchi, and A. Yusa, "Control system of the SRILAC project at RIBF," 18th International Conference on Accelerator and Large Experimental Physics Control Systems (ICALEPCS2021), Shanghai, China (virtual format), 147–152 (2021).

M. Komiyama, A. Uchiyama, M. Fujimaki, K. Kumagai, N. Fukunishi, T. Nakamura, and M. Hamanaka, "Performance verification of new machine protection system prototype for RIKEN RI Beam Factory," 18th International Conference on Accelerator and Large Experimental Physics Control Systems (ICALEPCS2021), Shanghai, China (virtual format), 742–745 (2021).

Presentations

[International Conferences/Workshops]

N. Fukunishi (poster), A. Uchiyama, M. Komiyama, and M. Kidera, "Data archive system for superconducting RIKEN linear accelerator at RIBF," 12th International Particle Accelerator Conference (IPAC'21), Campinas, Brazil (virtual format), May 24–28, 2021.

K. Yamada (invited), T. Dantsuka, M. Fujimaki, E. Ikezawa, H. Imao, O. Kamigaito, M. Komiyama, K. Kumagai, T. Nagatomo, T. Nishi, H. Okuno, K. Ozeki, N. Sakamoto, K. Suda, A. Uchiyama, T. Watanabe, Y. Watanabe, H. Hara, A. Miyamoto, K. Sennyu, T. Yanagisawa, E. Kako, H. Nakai, H. Sakai, and K. Umemori, "Successful beam commissioning of heavy-ion superconducting linac at RIKEN," 20th International Conference on RF Superconductivity (SRF2021), MOOFAV01, East Lansing, USA, Online, June 28–July 2, 2021.

M. Hamanaka (poster), M. Komiyama, A. Uchiyama, M. Fujimaki, K. Kumagai, N. Fukunishi, and T. Nakamura, "Performance verification of new machine protection system prototype for RIKEN RI Beam Factory," 18th International Conference on Accelerator and Large Experimental Physics Control Systems (ICALEPCS2021), Shanghai, China (virtual format), October 14–22, 2021.

A. Yusa (poster), A. Uchiyama, M. Fujimaki, N. Fukunishi, Y. Higurashi, E. Ikezawa, H. Imao, O. Kamigaito, M. Kidera, M. Komiyama, K. Kumagai, T. Nagatomo, T. Nakagawa, T. Nishi, J. Ohnishi, K. Ozeki, N. Sakamoto, K. Suda, T. Watanabe, Y. Watanabe, K. Yamada, A. Kamoshida, K. Kaneko, R. Koyama, T. Ohki, K. Oyamada, M. Tamura, and H. Yamauchi, "Control system of the SRILAC project at RIBF," 18th International Conference on Accelerator and Large Experimental Physics Control Systems (ICALEPCS2021), Shanghai, China (virtual format), October 14–22, 2021.

M. Hamanaka (poster), M. Komiyama, A. Uchiyama, M. Fujimaki, K. Kumagai, N. Fukunishi, and T. Nakamura, "Performance verification of new machine protection system prototype for RIKEN RI Beam Factory," 18th International Conference on Accelerator and Large Experimental Physics Control Systems (ICALEPCS2021), Shanghai, China (virtual format), October 14–22, 2021.

[Domestic Conferences/Workshops]

金子健太 (ポスター発表), 内山暁仁, 込山美咲, 藤巻正樹, 熊谷桂子, 山内啓資, 「SRILAC 用マシンプロテクションシステムの構築」, 日本物理学会第 18 回年次大会, QST 高崎-オンライン, 2021 年 8 月 9–12 日.

金子健太 (ポスター発表), 渡邉環, 鴨志田敦史, 内山暁仁, 福西暢尚, 西隆博, 小山亮, 「LabVIEW を用いた SRILAC ビームエネルギー・位置モニターシステムの EPICS による分散制御」, 第 18 回日本加速器学会年会, QST 高崎-オンライン, 2021 年 8 月 9–12 日.

仲村武志 (ポスター発表), 込山美咲, 他 37 名, 「理研 RIBF におけるリングサイクロトロンの運転報告」, 日本物理学会第 18 回年次大会, QST 高崎-オンライン, 2021 年 8 月 9–12 日.

福澤聖児 (ポスター発表), 込山美咲, 他 35 名, 「理研 AVF サイクロトロン運転の現状報告」, 日本物理学会第 18 回年次大会, QST 高崎-オンライン, 2021 年 8 月 9–12 日.

渡邉環 (招待講演), 「理研超伝導加速空洞用ビームエネルギー・位置モニター」, 第 7 回 IFMIF 研究会 〜ビーム診断・ビーム制御〜, 量子科学技術研究開発機構六ヶ所研（北郡六ヶ所村）, オンライン, 2022 年 3 月 7 日.

Patents

T. Watanabe and N. Fukunishi, "Charged particle beam current measurement apparatus（日本語: 荷電粒子ビームの電流測定装置）," 2021, 6843903, JY Patent.

T. Watanabe and N. Fukunishi, "Charged particle beam current measurement apparatus," 2021, 17836891.6, FR, DE Patent.

Research Facility Development Division
Accelerator Group
Cryogenic Technology Team

1. Abstract

We are operating the cryogenic system for the superconducting ring cyclotron in RIBF. We are operating the helium cryogenic system in the south area of RIKEN Wako campus and delivering the liquid helium to users in RIKEN. We are trying to collect efficiently gas helium after usage of liquid helium.

2. Major Research Subjects

(1) Operation of the cryogenic system for the superconducting ring cyclotron in RIBF
(2) Operation of the helium cryogenic plant in the south area of Wako campus and delivering the liquid helium to users in Wako campus

3. Summary of Research Activity

(1) Operation of the cryogenic system for the superconducting ring cyclotron in RIBF (H. Okuno, T. Dantsuka, M. Nakamura)
(2) Operation of the helium cryogenic plant in the south area of Wako campus and delivering the liquid helium to users in Wako campus
(T. Dantsuka, S. Tsuruma, M. Kuroiwa, M. Takahashi, H. Okuno).

Members

Team Leader
Hiroki OKUNO

Senior Technical Scientist
Masato NAKAMURA

Technical Scientist
Tomoyuki DANTSUKA

Expert Technician
Takeshi MAIE

Research Part-time Worker
Mamoru TAKAHASHI (Research Part-time Worker I)

Administrative Part-time Workers
Shizuho TSURUMA (Administrative Part-time Worker I)
Mayumi KUROIWA (Administrative Part-time Worker II)

Research Facility Development Division
Accelerator Group
Infrastructure Management Team

1. Abstract

Our team is in charge of the design, operation, and maintenance of the large-scale infrastructure for the entire RI Beam Factory (RIBF), including cooling water, air conditioning, and electrical equipment, as well as the research and development of their advanced management. In order to operate the RIBF efficiently, it is very important to ensure the sound operation of these infrastructures that lead to the stable functioning of various devices. Another important mission is to coordinate the scheduling of major construction and repair work related to the RIBF so that beamtime runs smoothly.

The recent issue is the aging of infrastructure equipment. In line with these measures, we are making modifications that contribute to the stability of accelerator equipment and energy saving. In addition, infrastructure equipment has many sensors for management, and a huge amount of measurement data from these sensors is archived. We are planning to use this data to build a more advanced management system.

2. Major Research Subjects

(1) Operation, maintenance and monitoring of infrastructure of RI Beam Factory
(2) Development of advanced management of infrastructure that contributes to accelerator and beam stability
(3) Coordination of large construction work and modification related to RI Beam Factory

Members

Team Leader
Masanori KIDERA

Technical Scientist
Takeshi MAIE

Special Temporary Technical Scientist
Shu WATANABE

List of Publications & Presentations

Publications

[Proceedings]

仲村武志, 福澤聖児, 濱仲誠, 石川盛, 小林清志, 小山亮, 西田稔, 西村誠, 柴田順翔, 月居憲俊, 矢冨一慎, 大関和貴, 段塚知志, 藤巻正樹, 藤縄雅, 福西暢尚, 長谷部裕雄, 日暮祥英, 池沢英二, 今尾浩士, 上垣外修一, 金井保之, 木寺正憲, 込山美咲, 熊谷桂子, 真家武士, 長友傑, 中川孝秀, 中村仁音, 大西純一, 奥野広樹, 坂本成彦, 須田健嗣, 内山暁仁, 渡部秀, 渡邉環, 渡邉裕, 山田一成, 山澤秀行, 「理研 RIBF におけるリングサイクロトロンの運転報告」, “Status report on the operation of RIKEN RING Cyclotron,” Proceedings of the 18th Annual Meeting of Particle Accelerator Society of Japan, QST-Takasaki Online, Japan, August 9–12, 2021, p. 575.

福澤聖児, 須田健嗣, 後藤彰, 大西純一, 濱仲誠, 石川盛, 小林清志, 小山亮, 仲村武志, 西田稔, 西村誠, 柴田順翔, 月居憲俊, 矢冨一慎, 藤巻正樹, 福西暢尚, 長谷部裕雄, 日暮祥英, 今尾浩士, 上垣外修一, 加瀬昌之, 木寺正憲, 込山美咲, 熊谷桂子, 真家武士, 長友傑, 中川孝秀, 奥野広樹, 大関和貴, 坂本成彦, 内山暁仁, 渡部秀, 渡邉環, 渡邉裕, 山田一成, 鎌倉, 恵太, 小高康照, 「理研 AVF サイクロトロン運転の現状報告」, “Status report on the operation of RIKEN AVF Cyclotron,” Proceedings of the 18th Annual Meeting of Particle Accelerator Society of Japan, QST-Takasaki Online, Japan, August 9–12, 2021, p. 760.

大木智則, 小山田和幸, 山内啓資, 田村匡史, 遊佐陽, 金子健太, 坂本成彦, 藤巻正樹, 池沢英二, 今尾浩士, 木寺正憲, 長友傑, 大関和貴, 須田健嗣, 内山暁仁, 渡邉環, 渡邉裕, 山田一成, 上垣外修一, 「理研重イオンリニアックの現状報告」, “Present status of RILAC,” Proceedings of the 18th Annual Meeting of Particle Accelerator Society of Japan, QST-Takasaki Online, Japan, August 9–12, 2021, p. 983.

Research Facility Development Division
Instrumentation Development Group

1. Abstract

This group develops the core-experimental instruments at the RI Beam Factory. Four projects are currently going on. SLOWRI is an experimental instrument to provide low and cold ion beam. The high energy RI beam is stopped by a gas catcher system and re-accelerated to several tens of keV to deliver a high-quality cold RI beam to the user. SCRIT is the world's first experimental facility for electron scattering of unstable nuclei and was constructed off the main beamline of RIBF. The first physic result was demonstrated in 2017, and the electron scattering experiment for radioactive isotopes has been started in this year. An upgrade of the electron beam power that drives RI beam production is currently underway. The Rare-RI Ring is an event-by-event-operated heavy ion storage ring for precise mass measurement of extremely rare exotic nuclei. It is currently accepting applications for experimental proposals and has already conducted PAC-approved experiments and published its first physics results. Improvements are currently underway to achieve more precise mass measurements. The compact heavy-ion storage ring RUNBA is an R&D machine for the development of beam recycling techniques for nuclear reaction research on rare elements. This is currently under construction and some of the critical components of the ring are currently undergoing technical development. All instrumentations is designed to maximize the research potential of the world's most intense RI beams, and dedicated RI Beam Factory equipment makes the experimental challenge possible. The experimental technique and experience accumulated in this group provide opportunities for new experimental challenges and form the basis for the future development of the RIBF.

2. Major Research Subjects

(1) SCRIT Project
(2) SLOWRI Project
(3) Rear RI Ring Project
(4) RUNBA project (Beam recycling development)

3. Summary of Research Activity

We are developing beam manipulation techniques to carry out the above projects. These are high-quality slow RI beam generation technology (SCRIT, SLOWRI), beam cooling and stopping technology (SCRIT, SLOWRI) and beam accumulation technology in a storage ring (Rare RI Ring, RUNBA). The technical know-how accumulated in the project will play a major role in the next generation of RIBF. The current status and future plans for each project are described in the respective sections. We have successfully measured electron elastic scattering from ^{132}Xe isotopes and obtained nuclear charge density distributions in SCRIT. Recently, we have started electron scattering experiment for unstable nuclei. That will be the world's first electron-RI collision experiment. We are in the process of power upgrading of the electron beam from the RTM, which is the driving for RI production, and expanding the nuclei that can be accessed. The Rare RI Ring is an event-by-event based mass measurement system, designed specifically for extremely low-producing isotopes. We carried out PAC-approved experiments and successfully measured the masses of ^{74,76}Ni, ^{122}Rh, ^{123,124}Pd and ^{125}Ag for the first time. To improve mass resolution and efficiency, the first-response kicker system and optical tuning system are being improved. Test experiments are currently underway at SLOWRI to establish slow RI beam generation using two different type of gas cells. PALIS has been commissioned from 2015, and basic functions such as, the RI-beam stopping in Ar gas cell, the extraction from the gas cell and laser ionization have beam evaluated. Movable mass spectrometer combining RF carpet gas cells (RPGC) and multiple reflection time-of-flight (MRTOF) are in operation at facilities such as Zero Degree and GARIS. The combination of RFGC and MRTOF has been used successfully to measure the mass of ^{74,75}Ni isotopes.

According to the future plans of Nishina center, a beam re-cycling technique is under development. Beam recycling technology allows the circulation of RI beams to be maintained in a storage ring with a thin internal target until a nuclear reaction occurs. In order to establish beam recirculation, the increase in energy width and emittance needs to be compensated for using a fast feedback system. We have demonstrated the possibility of compensation in an analytical way and found the properties of EDC and ADC devices necessary for compensation. To develop these new technologies, a compact heavy ion storage ring (RUNBA) connected to ISOL (ERIS) is under construction at the SCRIT facility. Under a research cooperation agreement with ICR in Kyoto University, technical development of the main components required for RUNBA *i.e.* the charge breeder, energy dispersion corrector, angular diffusion corrector and internal target system are underway.

Members

Director
Masanori WAKASUGI

Contract Researcher
Ryo OGAWARA

Visiting Scientists
Akira OZAWA (Tsukuba Univ.)
Kyo TSUKADA (Kyoto Univ.)
Fumi SUZAKI (JAEA)

Student Trainee
Yoshiki MAEHARA (Kyoto Univ.)

Part-time Worker
Midori TAKEMON (Administrative Part-time Worker I)

List of Publications & Presentations

Publications and presentations for each project team are listed in subsections.

Research Facility Development Division
Instrumentation Development Group
SLOWRI Team

1. Abstract

SLOWRI is a universal low-energy RI-beam facility at RIBF that provides a wide variety of short-lived nuclei as high-purity and low-emittance ion beams or stored ions in a trap, including a parasitic operation mode. The SLOWRI team develops and manages the facility and performs high-precision spectroscopy experiments. The construction of the SLOWRI facility began in FY2013 and commissioning work is ongoing. From FY2019, SLOWRI has been started to be co-operated under RNC and WNSC/KEK collaboration.

High-energy radioactive ion beams from the projectile fragment separator BigRIPS are thermalized in a large He gas catcher cell (RFGC) or in a small Ar gas catcher cell (PALIS cell). From these gas cells, the low-energy ion beams will be delivered via mass separators and switchyards to various devices: such as an ion trap, a collinear fast beam apparatus, and a multi-reflection time of flight mass spectrograph. A multi-reflection time-of-flight mass spectrograph (MRTOF) has been also developed.

Two mass measurement projects using MRTOF mass spectrographs have been started: one is for trans uranium elements at the GARIS facility and the other is for *r*-process nuclides at SLOWRI facility. At GARIS-II, we installed second prototype RFCG combined with MRTOF, which is a medium-sized cryogenic RF-carpet He gas cell. Using second prototype RFGC, more than 80 nuclear masses have been measured including first mass measurements of Md and Es isotopes. In FY2021, masses on more than 100 radioactive isotopes from the fission source have been measured and the analysis is going on. At SLOWRI facility, third prototype RFGC has been installed at F11, the downstream of ZeroDegree spectrometer, which is a 50-cm-long RF-carpet-type He gas cell combined with MRTOF. In FY2020, we have successfully performed the on-line commissioning, symbiotically by using RIs provided for HiCARI campaign. The extraction efficiency in total has been achieved at 1% in maximum and the masses on more than 70 nuclei have been measured using RIs provided with BigRIPS. In FY2021, Mass measurement in the vicinity of double magic nucleus of ^{78}Ni was successfully performed, which was approved at NP-PAC. As the result, masses of ^{74}Ni and ^{75}Ni have been measured for the first time. The analysis is going on.

Parallelly, the on-line commissioning for PALIS has been continuously performed at F2 of BigRIPS. In FY2021, the extraction of α-emitter Ac Isotopes without a laser ionization has been confirmed after the ion guide from PALIS gas cell. We will try to the laser ionization in FY2022.

2. Major Research Subjects

(1) Construction of the stopped and low-energy RI-beam facility, SLOWRI
(2) Development of a multi-reflection time-of-flight mass spectrograph for precision mass measurements of short-lived nuclei
(3) Development of collinear laser spectroscopy apparatus
(4) Development of a parasitic slow RI-beam production method using resonance laser ionization

3. Summary of Research Activity

(1) Construction of stopped and low-energy RI-beam facility (SLOWRI)

SLOWRI consists of two gas catchers (RF carpet gas cell and PALIS gas cell), mass separators a 50-m-long beam transport line, a beam cooler-buncher, an isobar separator, and a laser system. The RF carpet gas cell (RFGC) will be installed at the exit of the D5 dipole magnet of BigRIPS. The gas catcher contains a large cryogenic He gas cell with a large traveling wave rf-carpet. The PALIS gas cell is installed in the vicinity of the second focal plane slit of BigRIPS. It will provide parasitic RI-beams from those ions lost in the slits during other experiments. In this gas catcher, thermalized RI ions quickly become neutral and will be re-ionized by resonant laser radiations. Off- and on-line commissioning is underway.

Based on test experiments with the prototype setups, the RF-carpet gas cell contains a three stage rf-carpet structure: a gutter rf carpet (1st carpet) for the collection thermal ions in the cell into a small slit, a narrow (about 10 mm) traveling-wave rf-carpet (2nd carpet) for collection of ions from the gutter carpet and for transporting the ions towards the exit, and a small rf carpet for extraction from the gas cell. The off-line test has been completed in FY2019.

A 50-cm-long RFGC, which is a prototype for final version RFGC with 1.5 m length, has been installed at F11 of ZeroDegreee spectrometer of BigRIPS in FY2020, and the on-line commissioning has been successfully performed symbiotically using RIs provided with BigRIPS during HiCARI campaign. The extraction efficiency in total has been achieved at 1% in maximum. In FY2021, first experiment approved in NP-PAC has been performed, which has aimed the mass measurement in the vicinity of the double magic nucleus of ^{78}Ni. As the result, masses of ^{74}Ni and ^{75}Ni have been measured with high precision less than 20 keV for the first time.

(2) Development of a multi-reflection TOF mass spectrograph for short-lived nuclei

The atomic mass is one of the most important quantities of a nucleus and has been studied in various methods since the early days of modern physics. From among many methods we have chosen a multi-reflection time-of-flight (MRTOF) mass spectrometer. Slow RI beams extracted from the RF ion-guide are bunched and injected into the spectrometer with a repetition rate of ~100 Hz. A mass-resolving power of 170,000 has been obtained with a 2 ms flight time for ^{40}K and ^{40}Ca isobaric doublet. This mass-resolving power should allow us to determine ion masses with an accuracy of $\leq 10^{-7}$. A new MRTOF has been assembled in FY2019 to be coupled with the third prototype of RFGC and has been installed at F11 of BigRIPS in FY2020. Mass measurements using RIs provided with BigRIPS during HiCARI campaign have been symbiotically performed. As the result, atomic masses on more than 70 nuclei have

been successfully measured. Among them, 11 isotope masses improve the present uncertainty significantly and 3 isotope masses have been measured for the first time. In FY2021, thanks to the fine tuning and the improved data analysis, the mass resolving power has reached up to ~1 M in maximum for A/q ~ 80/1+. Also, to eliminate contaminant ions, a TOF mass filter has been installed inside the MRTOF, which has been working well.

(3) Development of collinear fast beam apparatus for nuclear charge radii measurements

The root-mean-square charge radii of unstable nuclei have been determined exclusively by isotope shift measurements of the optical transitions of singly charged ions or neutral atoms by laser spectroscopy. Many isotopes of alkali, alkali-earth, and noble-gas elements in addition to several other elements have been measured by collinear laser spectroscopy since these ions all have good optical transitions and are available at conventional ISOL facilities. However, isotopes of other elements, especially refractory and short-lived ones, have not been investigated so far.

In SLOWRI, isotopes of all atomic elements will be provided as well collimated, mono-energetic ion beams. This should expand the range of nuclides available for laser spectroscopy. An off-line mass separator and a collinear fast beam apparatus with a large solid-angle fluorescence detector was built previously. A 617-nm transition of the metastable Ar^+ ion at 20 keV was measured with both collinear and anti-collinear geometry, which allowed determination of the absolute resonant frequency of the transition at rest with a relative accuracy better than 10^{-8}. A new setup is under preparation at the SLOWRI experiment area in collaboration with the Nuclear Spectroscopy Laboratory.

(4) Development of parasitic slow RI-beam production scheme using resonance laser ionization

More than 99.9% of RI ions produced in projectile fission or fragmentation are simply dumped in the first dipole magnet and the slits. A new scheme, named PALIS, meant to rescue such precious RI using a compact gas catcher cell and resonance laser ionization, was proposed as a part of SLOWRI. The thermalized RI ions in a cell filled with Ar gas can be quickly neutralized and transported to the exit of the cell by gas flow. Irradiation of resonance lasers at the exit ionizes neutral RI atoms efficiently and selectively. PALIS has been installed at F2 at the downstream of BigRIPS and off- and on-line commissioning is under progress.

At F2, due to high radiation from a beam dump, it is not easy to handle ions using electric ion guides. Therefore, a 70-cm-long gas pipe from the Ar gas cell was newly installed to transport RIs to relatively low radiation area thanks for the Ar gas flow. In FY2021, we have confirmed the transportation of ions of interest at the downstream of an ion guide behind the gas pipe using α-emitting Ac isotopes provided with BigRIPS. Also, we have found a lot of contaminant ions from the gas cell, which are originated from impurities in the gas. To reduce the influence of such contaminant, a quadrupole mass filter will be installed at the downstream of the ion guide. In FY2022, an on-line test for resonant laser ionization is planned.

Members

Team Leader

Hironobu ISHIYAMA

Senior Research Scientist

Takao KOJIMA

Research Scientist

Aiko TAKAMINE

Technical Scientist

Tetsu SONODA

Expert Technician

Takeshi MAIE

Junior Research Associate

Shun IIMURA

Visiting Scientists

Hideki IIMURA (JAEA)
Minoru TANIGAKI (Kyoto Univ.)
Hideki TOMITA (Nagoya Univ.)

Student Trainee

Shun IIMURA

List of Publications & Presentations

Publications

[Original Papers]

M. Tajima, A. Takamine, M. Wada, and H. Ueno, "Offline ion source for laser spectroscopy of RI at the SLOWRI," Nucl. Instrum. Methods Phys. Res. B **486**, 48–54 (2021).

T. Niwase, M. Wada, P. Schury, P. Brionnet, S. D. Chen, T. Hashimoto, H. Haba, Y. Hirayama, D. S. Hou, S. Iimura, H. Ishiyama, S. Ishizawa, Y. Ito, D. Kaji, S. Kimura, J. Liu, H. Miyatake, J. Y. Moon, K. Morimoto, K. Morita, D. Nagae, M. Rosenbusch, A. Takamine, T. Tanaka, Y. X. Watanabe, H. Wollnik, W. Xian, and S. X. Yan, "α-decay-correlated mass measurement of ^{206,207g,m}Ra using an α-TOF detector equipped multireflection time-of-flight mass spectrograph system," Phys. Rev. C **104**, 044617 (2021).

P. Schury, T. Niwase, M. Wada, P. Brionnet, S. Chen, T. Hashimoto, H. Haba, Y. Hirayama, D. S. Hou, S. Iimura, H. Ishiyama, S. Ishizawa, Y. Ito, D. Kaji, S. Kimura, H. Koura, J. J. Liu, H. Miyatake, J. -Y. Moon, K. Morimoto, K. Morita, D. Nagae, M. Rosenbusch, A. Takamine, Y. X. Watanabe, H. Wollnik, W. Xian, and S. X. Yan, "First high-precision direct determination of the atomic mass of a superheavy nuclide," Phys. Rev. C **104**, L021304 (2021).

[Proceeding]

S. Kimura, Y. Ito, D. Kaji, P. Schury, M. Wada, H. Haba, T. Hashimoto, Y. Hirayama, M. MacCormick, H. Miyatake, J. Y. Moon, K. Morimoto, M. Mukai, I. Murray, A. Ozawa, M. Rosenbusch, H. Schatz, A. Takamine, T. Tanaka, Y. X. Watanabe, and H. Wollnik, "High precision mass measurements of intermediate-mass neutron-deficient nuclei via MRTOF-MS," JPS Conf. Proc. **35**, 011005 (2021).

Presentations

[International Conferences/Workshops]

S. Iimura (poster), A. Takamine, M. Rosenbusch, M. Wada, S. Chen, D. Hou, J. Liu, W. Xian, S. Yan, P. Schury, S. Kimura, A. Niwase, Y. Ito, S. Sonoda, T. Kojima, Y. Watanabe, S. Naimi, S. Michimasa, S. Nishimura, A. Odahara, and H. Ishiyama, "Mass measurement of neutron rich nuclei of Sc, Ti, and V region using the new ZD-MRTOF system," The 16th International Symposium on Nuclei in the Cosmos (NIC-XVI), Online, China, September 21–25, 2021.

M. Rosenbusch (oral), S. Chen, W. Xian, S. Yan, A. Takamine, D. Hou, S. Iimura, M. Wada, P. Schury, Y. Hirayama, H. Ishiyama, Y. Ito, S. Kimura, T. M. Kojima, J. Liu, S. Michimasa, H. Miyatake, S. Naimi, S. Nishimura, T. Niwase, T. Sonoda, Y. X. Watanabe, and H. Wollnik, "The new high-precision MR-TOF mass spectrograph at the ZeroDegree spectrometer of BigRIPS," The 16th International Symposium on Nuclei in the Cosmos (NIC-XVI), Online, China, September 21–25, 2021.

M. Rosenbusch (invited), "The new high-precision MR-TOF mass spectrograph at the ZeroDegree spectrometer of BigRIPS," RIBF Users Meeting 2021, Wako, Japan, Online, September 7–9, 2021.

H. Ishiyama (invited), "Present status of SLOWRI," SSRI-PNS Collaboration Meeting 2021, Online, September 2–3, 2021.

[Domestic Conferences/Workshops]

富田英生 (口頭発表), V. Sonnenschein, 服部浩也, 山口穂乃花, 井坪暁, 寺林稜平, 島添健次, 園田哲, 石山博恒, K. Wendt, 「理研 RI ビームファクトリー—低速 RI ビーム施設におけるレーザー共鳴イオン化イオン源の開発」, 日本原子力学会 2022 年春季大会, オンライン, 2022 年 3 月 16–18 日.

飯村俊 (口頭発表), 高峰愛子, M. Rosenbusch, 和田道治, S. Chen, D. Hou, J. Liu, W. Xian, S. Yan, P. Schury, 木村創大, 庭瀬暁隆, 伊藤由太, 園田哲, 小島隆夫, 渡辺裕, S. Naimi, 道正新一郎, 西村俊二, 小田原厚子, 石山博恒, "Mass measurement of neutron rich nuclei of Sc, Ti, and V region using the new ZD-MRTOF system," 日本物理学会 2021 年度秋季大会, オンライン, 2021 年 9 月 14–17 日.

W. Xian (口頭発表), S. Chen, M. Rosenbusch, S. Yan, D. Hou, S. Iimura, A. Takamine, M. Wada, J. Liu, P. Schur, S. Kimura, T. Niwase, Y. Ito, T. Sonoda, T. M. Kojima, Y. X. Watanabe, S. Naimi, S. Michimasa, S. Nishimura, H. Ishiyama, and H. Wollnik, "New mass measurements of neutron-rich nuclei of Ge, As, and Se, and an accuracy study of the new ZD-MRTOF system," 日本物理学会 2021 年度秋季大会, オンライン, 2021 年 9 月 14–17 日.

D. Hou (口頭発表), A. Takamine, S. Iimura, M. Rosenbusch, S. Chen, W. Xian, S. Yan, M. Wada, P. Schury, Y. Hirayama, H. Ishiyama, Y. Ito, S. Kimura, J. Liu, S. Michimasa, H. Miyatake, S. Naimi, S. Nishimura, T. Niwase, Y. X. Watanabe, and H. Wollnik, "Mass measurement in the neutron-rich Mo region using the new ZD-MRTOF system," 日本物理学会 2021 年度秋季大会, オンライン, 2021 年 9 月 14–17 日.

M. Rosenbusch (口頭発表), S. Chen, W. Xian, S. Yan, A. Takamine, D. Hou, S. Iimura, M. Wada, P. Schury, Y. Hirayama, H. Ishiyama, Y. Ito, S. Kimura, T. M. Kojima, J. Liu, S. Michimasa, H. Miyatake, S. Naimi, S. Nishimura, T. Niwase, T. Sonoda, Y. X. Watanabe, and H. Wollnik, "New technologies for multi-reflection time-of-flight mass spectrometry at BigRIPS," 日本物理学会 2021 年度秋季大会, オンライン, 2021 年 9 月 14–17 日.

庭瀬暁隆 (口頭発表), P. Schury, 和田道治, P. Brionnet, S. Chen, 橋本尚志, 羽場宏光, 平山賀一, D. S. Hou, 飯村俊, 石山博恒, 石澤倫, 伊藤由太, 加治大哉, 木村創大, 小浦寛之, 宮武宇也, J. Y. Moon, 森本幸司, 森田浩介, 長江大輔, M. Rosenbusch, 高峰愛子, 渡辺裕, H. Wollnik, W. Xian, and S. X. Yan, 「超重核 ^{257}Db の直接質量測定」, 日本物理学会 2021 年度秋季大会, オンライン, 2021 年 9 月 14–17 日.

服部浩也 (口頭発表), V. Sonnenschein, 山口穂乃花, 井坪暁, 寺林稜平, 島添健次, 園田哲, 石山博恒, K. Wendt, 富田英生, 「半導体レーザー直接励起 Ti:Sapphire レーザーを用いた高分解能共鳴イオン化分光法の開発」, 日本物理学会 2021 年度秋季大会, オンライン, 2021 年 9 月 14–17 日.

Research Facility Development Division
Instrumentation Development Group
Rare RI-ring Team

1. Abstract

The aim of Rare-RI Ring (R3) is to measure the masses of short-lived unstable nuclei far from the beta-stability line. In particular, a high-precision mass measurement for nuclei located around the *r*-process pass (rare-RI) is required in nucleosynthesis point of view. Through the commissioning experiments by 2017, we confirmed the high ability of R3 as a storage ring capable of handling one event, and demonstrated that it is possible to perform the time-of-flight Isochronous Mass Spectrometry (IMS) in shorter than 1 millisecond. In 2018, we performed mass measurement experiments for the first time. In 2020, the kicker system was modified to flatten the magnetic field distribution, and the performance study using unstable nuclei was successfully conducted. In this fiscal year, we performed mass measurement experiments using the upgraded kicker system. The preliminary results of the experiment dispelled concerns about the results of the previous experiment that the injection angle might greatly affected the accuracy of the mass determination. On the other hand, through the experiments of this fiscal year, a problem was found in the kicker power supply. We are currently taking measures to the problem.

2. Major Research Subjects

(1) Further improvement of experimental efficiency and mass measurement precision
(2) Precision mass measurement for rarely produced isotopes related to *r*-process

3. Summary of Research Activity

In the commissioning experiments up to 2017, we confirmed the unique performances of R3 and demonstrated the time-of-flight isochronous mass measurement method. The ring structure of R3 was designed with a similar concept of a separate-sector ring cyclotron. It consists of six sectors and straight sections, and each sector consists of four rectangular bending magnets. Two magnets at both ends of each sector are additionally equipped with ten trim coils to form a precise isochronous field. We have realized in forming the precise isochronous field of less than 5 ppm with wide momentum range of $\Delta p/p = \pm 0.5\%$. Another performance required for R3 is to efficiently seize hold of an opportunity of the mass measurement for rare-RIs produced unpredictably. It was realized by constructing the Isotope-Selectable Self-trigger Injection (ISSI) scheme which pre-identified rare-RI itself triggers the injection kicker magnets. Key device was a fast response kicker system that has been successfully developed. Full activation of the kicker magnetic field can be completed within the flight time of the rare-RI from an originating point (F3 focal point in BigRIPS) of the trigger signal to the kicker position in R3.

Since R3 accumulates, in principle, only one event, we fabricated high-sensitive beam diagnostic devices in the ring. One of them is a cavity type of Schottky pick-up installed in a straight section of R3. The Schottky pick-up successfully monitored a single $^{78}Kr^{36+}$ ion circulation with the measurement time of less than 10 milliseconds in the first commissioning experiment. We also confirmed that it is useful for fine tuning of the isochronous field. Another is a timing monitor called E-MCP, which detects secondary electrons emitted from thin carbon foil placed on the circulation orbit. The thickness of the foil is 60 μg/cm^2. This timing monitor is working well to observe first several tens turns for injected event.

We performed mass measurement in the third commissioning experiment by using unstable nuclei which masses are well-known. The masses of ^{79}As, ^{77}Ga, ^{76}Zn, and ^{75}Cu relative to ^{78}Ge were deduced with the accuracy of several ppm. In addition, we have improved the extraction efficiency to 2% by considering the matching condition between the emittance of injection events and the acceptance of R3 in the fourth commissioning experiment. This extraction efficiency was sufficient to conduct the accepted two proposals: mass measurements of Ni isotopes and Sn region.

In November 2018, we conducted the first experiment using R3 to measure the masses for ^{74,76}Ni in 4 days. After that, we also measured the masses for ^{122}Rh, ^{123,124}Pd, and ^{125}Ag in 4.5 days. These nuclei were successfully extracted from R3 with the efficiency of 1–2%. However, unexpected deviation from the evaluated values of literature remained in the masses obtained by detailed analysis. This was thought to be due to the following two reasons. One is that due to the kicker field distribution is not flattened, the injection angle is different between the reference and target nucleus, and therefore the relative value of TOF is incorrect. The other is that the absolute value of beta or magnetic rigidity determined for each extracted event is incorrect.

In 2020, we modified the kicker system to flatten the magnetic field distribution as well as to dispel the concerns of the results of first experiment. As a result of performance study using unstable nuclei, we succeeded in forming the kicker field with 100 ns flat-top for injection and long flat-top of 350 ns or more for extraction. The experimental efficiency had been improved by a factor of two or more than previous condition because all nuclides can be extracted at once thanks to the long flat-top.

Using this upgraded kicker system, we measured the mass for ^{74}Ni again in April 2021. Although the kicker field distribution was flattened, the results of masses were the same as those of the first experiment. In other words, concerns about the effects of differences in injection angles have been dispelled. As a subsequent analysis, it was clarified that the reason is the second concern described above. The final mass values will be determined soon. On the other hand, the ceramic capacitor of the kicker power supply broken several times due to insulation breakdown. We are currently working on measures to prevent insulation breakdown of ceramic capacitors, since this problem defects reliable mass measurement experiments.

Members

Team Leader
Masanori WAKASUGI

Technical Scientist
Yoshitaka YAMAGUCHI

Expert Technician
Takeshi MAIE

Student Trainee
Yuto NAGATA (Kyushu Univ.)

List of Publications & Presentations

Publications

[Review Article]

T. Yamaguchi, H. Koura, Yu. A. Litvinov, and M. Wang, "Masses of exotic nuclei," Prog. Part. Nucl. Phys. **120**, 103882-1–98 (2021).

[Proceedings]

A. Ozawa for Rare-RI Ring Collaboration, "Past and future for Rare-RI Ring," JPS Conf. Proc. **35**, 011011-1–5 (2021).

D. Nagae, S. Omika, Y. Abe, Y. Yamaguchi, F. Suzaki, K. Wakayama, N. Tadano, R. Igosawa, K. Inomata, H. Arakawa, K. Nishimuro, T. Fujii, T. Mitsui, T. Yamaguchi, T. Suzuki, S. Suzuki, T. Moriguchi, M. Amano, D. Kamioka, A. Ozawa, S. Naimi, Z. Ge, Y. Yanagisawa, H. Baba, S. Michimasa, S. Ota, G. Lorusso, Yu. A. Litvinov, M. Wakasugi, T. Uesaka, and Y. Yano, "First demonstration of mass measurements for exotic nuclei using Rare-RI Ring", JPS Conf. Proc. **35**, 011014-1–8 (2021).

S. Suzuki, A. Ozawa, T. Moriguchi, M. Amano, D. Kamioka, Y. Ichikawa, Y. Tajiri, K. Hiraishi, T. Matsumoto, D. Nagae, Y. Abe, S. Naimi, H. Li, T. Yamaguchi, S. Omika, Z. Ge, K. Wakayama, N. Tadano, H. Arakawa, K. Inomata, T. Kobayashi, A. Kitagawa, and S. Sato, "Performance of a Time-Of-Flight detector and demonstration of a novel position-sensitive detector for mass measurements with Rare-RI Ring", JPS Conf. Proc. **35**, 011017-1–6 (2021).

K. Inomata, T. Yamaguchi, Y. Abe, M. Amano, H. Arakawa, T. Fujii, D. Kamioka, A. Kitagawa, H. Li, T. Moriguchi, D. Nagae, S. Omika, A. Ozawa, S. Sato, S. Suzuki, T. Suzuki, and K. Wakayama, "Basic study on delta ray detection for the determination of in-ring revolution time", JPS Conf. Proc. **35**, 011020-1–4 (2021).

K. Inomata, T. Yamaguchi, H. Arakawa, A. Kitagawa, D. Nagae, K. Nishimuro, S. Omika, S. Sato, T. Suzuki, N. Tadano, and K. Wakayama, "Best test on a long scintillating fiber as a position sensor in a storage ring facility", JPS Conf. Proc. **35**, 011021-1–5 (2021).

H. Arakawa, T. Yamaguchi, Y. Abe, M. Amano, K. Inomata, D. Kamioka, A. Kitagawa, H. Li, T. Moriguchi, D. Nagae, S. Omika, A. Ozawa, S. Sato, S. Suzuki, T. Suzuki, and K. Wakayama, "Properties of a thin YAP(Ce) scintillation counter for heavy ions", JPS Conf. Proc. **35**, 011022-1–5 (2021).

Z. Ge, S. Naimi, D. Nagae, Y. Abe, S. Omika, T. Uesaka, F. Suzaki, H. Li, Y. Yamaguchi, M. Wakasugi, K. Wakayama, T. Yamaguchi, A. Ozawa, H. Arakawa, K. Inomata, T. Kobayashi, K. Nishimuro, S. Suzuki, T. Moriguchi, D. Kamioka, M. Mukai, M. Amano, A. Kitagawa, S. Sato, G. Lorusso, and Y. Yano, "Development of mirror-type MCP detectors for mass measurements at the Rare-RI Ring", JPS Conf. Proc. **35**, 011023-1–4 (2021).

K. Wakayama, T. Yamaguchi, Y. Abe, M. Amano, H. Arakawa, Z. Ge, K. Inomata, D. Kamioka, A. Kitagawa, T. Kobayashi, H. Li, T. Moriguchi, D. Nagae, S. Omika, A. Ozawa, S. Sato, S. Suzuki, T. Suzuki, and N. Tadano, "A simple readout method for a position-sensitive detector using plastic scintillator bars", JPS Conf. Proc. **35**, 011024-1–5 (2021).

H. Li, Z. Ge, S. Naimi, D. Nagae, Y. Abe, T. Uesaka, F. Suzaki, M. Wakasugi, S. Omika, Y. Yamaguchi, T. Yamaguchi, K. Wakayama, H. Arakawa, K. Inomata, A. Ozawa, S. Suzuki, and T. Moriguchi, "MCP with delay-line anode used for position sensitive detector at Rare RI-Ring", JPS Conf. Proc. **35**, 011025-1–4 (2021).

S. Omika, T. Yamaguchi, Y. Abe, M. Amano, H. Arakawa, Z. Ge, K. Inomata, D. Kamioka, H. Li, H. Miura, T. Moriguchi, D. Nagae, S. Naimi, K. Nishimuro, A. Ozawa, F. Suzaki, S. Suzuki, and T. Suzuki, "Development of experimental devices for precise mass measurements at the Rare-RI Ring", JPS Conf. Proc. **35**, 011026-1–5 (2021).

Presentations

[International Conference/Workshop]

T. Yamaguchi (invited), "Precision experiments of exotic nuclei at the storage rings," Tsukuba Global Science Week 2021, Online, Tsukuba, Japan, September 6–11, 2018.

[Domestic Conferences/Workshops]

森口哲明 (口頭発表), 「RI ビーム飛行時間検出器の開発. —理研稀少 RI リングのための検出器—」, 2020 年度 HIMAC 共同利用研究成果発表会, オンライン, 2021 年 6 月 7–10 日.

山口貴之 (口頭発表), 「多価イオンビームによる 2 光子稀崩壊の観測」, 新学術領域研究「宇宙観測検出器と量子ビームの出会い. 新たな応用への架け橋」領域研究会, オンライン, 2021 年 6 月 14–15 日.

要直登 (ポスター発表), 「薄膜からの二次電子放出を利用した RI ビーム位置敏感型検出器の開発」, 第一回日本量子医学学会学術大会, オンライン, 2021 年 12 月 10–11 日.

Research Facility Development Division
Instrumentation Development Group
SCRIT Team

1. Abstract

The SCRIT Electron Scattering Facility has been constructed at RIKEN RIBF. This aims at investigation of internal nuclear structure for short-lived unstable nuclei by means of electron scattering. SCRIT (Self-Confining RI Ion Target) is a novel method to form internal targets in an electron storage ring. This is a unique method for making electron scattering experiments for unstable nuclei possible. Construction of the facility has been started in 2009. This facility consists of an electron accelerator (RTM), a SCRITequipped electron storage ring (SR2), an electron-beam-driven RI separator (ERIS), and a window-frame spectrometer for electron scattering (WiSES) which consists of a large window-frame dipole magnet, drift chambers and trigger scintillators. Installation of all components in the facility was completed in 2015. After the comprehensive test and tuning, the luminosity was reached to $3 \times 10^{27}/(\mathrm{cm}^2\mathrm{s})$ with the number of injected ions of 3×10^8. In 2016, we successfully completed a measurement of diffraction of scattered electrons from ^{132}Xe nuclei and determined the charge density distribution for the first time. In 2021, we have been trying to obtain the world first electron scattering data of unstable nuclei.

2. Major Research Subjects

Development of SCRIT electron scattering technique and measurement of the nuclear charge density distributions of unstable nuclei.

3. Summary of Research Activity

SCRIT is a novel technique to form internal target in an electron storage ring. Positive ions are three dimensionally confined in the electron beam axis by transverse focusing force given by the circulating electron beam and applied electrostatic longitudinal mirror potential. The created ion cloud composed of RI ions injected from outside works as a target for electron scattering. Construction of the SCRIT electron scattering facility has been started in 2009. The electron accelerators RTM and the storage ring SR2 were successfully commissioned in 2010. Typical accumulation current in SR2 is 250–300 mA at the energy range of 120–300 MeV that is required energy range in electron scattering experiment. The SCRIT device was inserted in the straight section of SR2 and connected to an ISOL named ERIS (Electron-beam-driven RI separator for SCRIT) by 20-m long low energy ion transport line. A buncher system based on RFQ linear trap named FRAC (Fringing-RF-field-Activated dc-to-pulse converter) was inserted in the transport line to convert the continuous beam from ERIS to pulsed beam, which is acceptable for SCRIT. The detector system WiSES consisting of a high-resolution magnetic spectrometer, drift chambers and trigger scintillators, was constructed, and it has a solid angle of 100 msr, energy resolution of 10^{-3}, and the scattering angle coverage of 25–55 degrees. A wide range of momentum transfer, 80–300 MeV/c, is covered by changing the electron beam energy from 150 to 300 MeV.

We successfully measured a diffraction pattern in the angular distribution of scattered electron from ^{132}Xe isotope at the electron beam energy of 150 MeV, 200 MeV, and 300 MeV, and derived the nuclear charge distribution by assuming two-parameters Fermi model for the first time. At this time, luminosity was reached to $3 \times 10^{27}/(\mathrm{cm}^2\mathrm{s})$ at maximum and the averaged value was $1.2 \times 10^{27}/(\mathrm{cm}^2\mathrm{s})$ with the number of injected target ions of 3×10^8.

We are now under preparation for going to the experiments for unstable nuclei. There are some key issues for that. They are increasing the intensity of the RI beams from ERIS, efficient DC-to-pulse conversion at FRAC, improving the transmission efficiency from FRAC to SCRIT, and effective suppression of the background in measurement of scattered electrons. RI beam intensity will be improved by upgrading the electron beam power from 10 W to 60 W, increasing the contained amount of U in the target ion source, and some modifications in mechanical structure in the ion source. For upgrading the electron beam power, the RF system of RTM has been maintained intensively, and we will continue the development of RTM. For efficient DC-to-pulse conversion, we established the two-step bunching method, which is time compression at FRAC in combination with pre-bunching at the ion source using grid action. Furthermore, we will improve the conversion efficiency and the transmission efficiency from FRAC to the SCRIT device by cooling the trapped ions using minuscule amounts of a buffer gas. These improvements on FRAC were already confirmed in off-line test. Since one of significant contribution to the background for scattered electron is scattering from massive structural objects around the trapping region originated from halo components of the electron beam, we remodeled the SCRIT electrodes. The vacuum pump system at the SCRIT device has been upgraded to reduce the contribution of residual gases. Luminosity for radioactive Xe isotopes is expected to be more than $10^{26}/(\mathrm{cm}^2\mathrm{s})$ after these improvements. Then, we will be able to start experiments for unstable nuclei. When further upgrading in the RTM power planed to be 3 kW will be achieved, we can extend the measurements to more exotic nuclei.

In 2018, we developed several instruments. One is the introduction of the surface-ionization type ion source at ERIS in order to increase kinds of radioactive beam and to produce high intensity beam. Another development is the upgrading of the drift chamber located in front of the magnetic spectrometer of WiSES to improve the momentum resolution and angular acceptance. These developments help us to realize experiments for unstable nuclei.

In 2019, we installed a newly designed SCRIT electrodes. The main purpose of the replacement was to lower the background during the measurement due to the electron scattering from the SCRIT electrodes itself but not from the ion targets for the experiment. For that purpose, we employed thin metal wires to construct the electrodes rather than metal plates nor blocks. In addition, we modified the inside structure of the SCRIT chamber to symmetrize the electric ground potential affecting the potential curve inside the electrodes.

In 2020, we tested accelerators RTM and SR2 if they bear for long term experiment for 24 hours. Currently, we are adjusting the SR2 accelerator and ion source ERIS to be ready for the real electron scattering measurement of unstable nuclei.

In 2021, ERIS became ready to provide enough ions for the experiment of unstable nuclei. We have been trying to measure electron scattering of unstable nuclei. Hopefully, we can publish those data very soon.

Members

Team Leader
Masanori WAKASUGI

Senior Research Scientist
Masamitsu WATANABE

Senior Technical Scientist
Tetsuya OHNISHI

Expert Technician
Takeshi MAIE

Contract Researcher
Yasushi ABE

Junior Research Associate
Hikari WAUKE

Research Consultants
Takashi EMOTO
Masahiro HARA
Toshitada HORI (Hiroshima Univ.)
Shinichi ICHIKAWA

Visiting Scientists
Akitomo ENOKIZONO (Rikkyo Univ.)
Yuki HONDA (Tohoku Univ.)
Toshimi SUDA (Tohoku Univ.)
Shuo WANG (Shandong Univ. (Weihai))

Student Trainees
Taiga GOKE (Tohoku Univ.)
Yuma ISHIKURA (Tohoku Univ.)
Kazushi ISHIZAKI (Tohoku Univ.)
Clement V. LEGRIS (Tohoku Univ.)
Hikari WAUKE (Tohoku Univ.)

List of Publications & Presentations

Publications

[Original Papers]

須田利美, 本多佑記, 瀧大祐, 郷家大雅, C. Legris, 石崎一志, 三浦禎雄, 武藤俊哉, 玉江忠明, 前田幸重, Z. Hang, 塚田暁, 「Proton radius」, 原子核研究 **66**, 2–11 (2021).

須田利美, 本多佑記, 前田幸重, 塚田暁, 「陽子半径」, 高エネルギーニュース **40**, 107–116 (2022).

[Proceeding]

T. Ohnishi, K. Adachi, A. Enokizono, T. Fujita, M. Hara, M. Hori, T. Hori, S. Ichikawa, K. Kurita, T. Suda, T. Tamae, K. Tsukada, M. Togasaki, N. Uchida, M. Wakasugi, M. Watanabe, and K. Yamada, "The SCRIT electron scattering facility at RIKEN RI Beam Factory," JPS Conf. Proc. **35**, 011027 (2021).

Presentations

[International Conferences/Workshops]

T. Suda (oral), "Study of radii of proton and exotic nuclei by electron scattering," 2021 Symposium on Nuclear Data, Online, November 18–19, 2021.

C. Legris (oral), "Commissioning results for the ULQ2 experiment towards the proton charge radius determination," The Nineth International School for Strangeness Nuclear Physics, RCNP, Osaka University, Online, December 13–16, 2021.

T. Goke (oral), "New type scattering chamber optimized for proton radius measurement by low-energy electron scattering," The Nineth International School for Strangeness Nuclear Physics, RCNP, Osaka University, Online, December 13–16, 2021.

[Domestic Conferences/Workshops]

大西哲哉 (招待講演), 「The SCRIT e-RI scattering facility at RIKEN」, RCNP での次期計画検討会, 大阪府茨木市 (大阪大学核物理研究センター), 2021 年 9 月 27–29 日.

H. Wauke (oral), "Study of internal structure of unstable nuclei by electron scattering," The RIBF Users Meeting 2021, RIKEN, Japan, Online, September 7–9, 2021.

T. Goke (poster), "Development of new vacuum scattering target chamber optimized for proton radius measurement by low-energy electron scattering," ELPH Symposium 2022, Sendai, March 11, 2022.

T. Goke (oral), "Future plans for proton radius measurement by low-energy electron scattering," JPS 2021 Autumn Meeting, Kobe, Online, September 14–17, 2021.

C. Legris (oral), "First test results for the ULQ2 experiment towards the proton charge radius determination," JPS 2021 Autumn Meeting, Kobe, Online, September 14–17, 2021.

H. Wauke (oral), "Isotope and isotone dependence of nuclear charge density distribution at SCRIT electron scattering facility," 2022 Annual (77th) Meeting of The Physical Society of Japan, Okayama, Online, March 15–19, 2022.

T. Goke (oral), "Development of new vacuum scattering target chamber for proton radius measurement by low-energy electron scattering," 2022 Annual (77th) Meeting of The Physical Society of Japan, Okayama, Online, March 15–19, 2022.

Y. Ishikura (oral), "Commissioning of the twin spectrometers for proton radius measurement by low-energy electron scattering," 2022 Annual (77th) Meeting of The Physical Society of Japan, Okayama, Online, March 15–19, 2022.

[Seminar]

須田利美（招待講演),「陽子のサイズがおかしい？」, 千葉大学先進科学プログラム・オムニバスセミナー, 千葉県千葉市（千葉大学), 2021 年 10 月 15 日.

Outreach Activities

須田利美 (インタービュー記事), 「陽子の半径の正確な値を突き止めよ—半世紀前の古い加速器だからこそできること」, 国立大学附置研・センター会議, http://shochou-kaigi.org/interview/interview_93/ .

須田利美（特別講義),「陽子などの物の大きさはどう測る？」, 埼玉県立熊谷高等学校, 埼玉県熊谷市 (埼玉県立熊谷高等学校), 2022 年 1 月 14 日.

須田利美 (集中講義), 「電子散乱による原子核研究」, 北海道札幌市 (北海道大学物理学科), 2021 年 12 月 13–15 日.

Research Facility Development Division
Research Instruments Group

1. Abstract

The Research Instruments Group is the driving force at RI Beam Factory (RIBF) for continuous enhancement of activities and competitiveness of experimental research. Consisting of four teams, we are in charge of the operation, maintenance, and improvement of the core research instruments at RIBF, such as the BigRIPS in-flight RI separator, ZeroDegree spectrometer and SAMURAI spectrometer, and the related infrastructure and equipment. We are also in charge of the production and delivery of RI beams using the BigRIPS separator. The group also conducts related experimental research as well as R&D studies on the research instruments.

2. Major Research Subjects

Design, construction, operation, maintenance, and improvement of the core research instruments at RIBF and related R&D studies. Experimental studies on exotic nuclei.

3. Summary of Research Activity

The current research subjects are summarized as follows:

(1) Production and delivery of RI beams and related research;
(2) Design, construction, operation, maintenance, and improvement of the core research instruments at RIBF and their related infrastructure and equipment;
(3) R&D studies on the core research instruments and their related equipment at RIBF;
(4) Experimental research on exotic nuclei using the core research instruments at RIBF.

Members

Director

Tomohiro UESAKA

Contract Researcher

Toshiyuki KUBO

Junior Research Associate

Rieko TSUNODA

Senior Visiting Scientist

Toshio KOBAYASHI (Tohoku Univ.)

Student Trainees

Fumitaka ENDO (Tohoku Univ.)
Kosuke ICHIMURA (Tohoku Univ.)
Rieko TSUNODA

Research Facility Development Division
Research Instruments Group
BigRIPS Team

1. Abstract

This team is in charge of design, construction, development and operation of BigRIPS in-flight separator and its related research instruments at RI beam factory (RIBF). They are employed not only for the production of RI beams but also the experimental studies using RI beams.

2. Major Research Subjects

Design, construction, development and operation of BigRIPS in-flight separator, RI-beam transport lines, and their related research instruments.

3. Summary of Research Activity

This team is in charge of design, construction, development and operation of BigRIPS in-flight separator, RI-beam transport lines, and their related research instruments such as ZeroDegree spectrometer at RI beam factory (RIBF). They are employed not only for the production of RI beams but also various kinds of experimental studies using RI beams. The research subjects may be summarized as follows:

(1) General studies on RI-beam production using in-flight scheme;
(2) Studies on ion-optics of in-flight separators, including particle identification of RI beams;
(3) Simulation and optimization of RI-beam production;
(4) Development of beam-line detectors and their data acquisition system;
(5) Experimental studies on production reactions and unstable nuclei;
(6) Experimental studies of the limits of nuclear binding;
(7) Development of superconducting magnets and their helium cryogenic systems;
(8) Development of a high-power production target system;
(9) Development of a high-power beam dump system;
(10) Development of a remote maintenance and remote handling systems;
(11) Operation, maintenance and improvement of BigRIPS separator system, RI-beam transport lines, and their related research instruments such as ZeroDegree spectrometer and so on;
(12) Experimental research using RI beams.

Members

Team Leader

Koichi YOSHIDA

Senior Research Scientist

Yoshiyuki YANAGISAWA

Senior Technical Scientists

Naohito INABE
Masao OHTAKE
Kensuke KUSAKA

Technical Scientists

Naoki FUKUDA
Hiroshi SUZUKI
Yohei SHIMIZU
Hiroyuki TAKEDA)

Postdoctoral Researcher

Masahiro YOSHIMOTO

Visiting Scientists

Deuk Soon AHN (Korea Basic Sci. Inst.)
Yutaka MIZOI (Univ. of Electro-Commun.)
Daniel P. BAZIN (Michigan State Univ.)
Sadao MOMOTA (Kochi Univ. Tech.)
Hans GEISSEL (GSI)
David MORRISSEY (Michigan State Univ.)
Naohito IWASA (Tohoku Univ.)
Oleg TARASOV (Michigan State Univ.)

Student Trainees

Mika EGETA (Tohoku Univ.)
Shunki ISHIKAWA (Tohoku Univ.)
Taiga HAGINOUCHI (Tohoku Univ.)

List of Publications & Presentations

Publications

[Original Papers]

J. Estee, W. G. Lynch, C. Y. Tsang, J. Barney, G. Jhang, M. B. Tsang, R. Wang, M. Kaneko, J. W. Lee, T. Isobe, M. Kurata-Nishimura, T. Murakami, D. S. Ahn, L. Atar, T. Aumann, H. Baba, K. Boretzky, J. Brzychczyk, G. Cerizza, N. Chiga, N. Fukuda, I. Gasparic, B. Hong, A. Horvat, K. Ieki, N. Inabe, Y. J. Kim, T. Kobayashi, Y. Kondo, P. Lasko, H. S. Lee, Y. Leifels, J. Łukasik, J. Manfredi, A. B. McIntoshl, P. Morfouace, T. Nakamural, N. Nakatsuka, S. Nishimura, H. Otsu, P. Pawłowski, K. Pelczar, D. Rossi, H. Sakurai, C. Santamaria, H. Sato, H. Scheit, R. Shane, Y. Shimizu, H. Simon, A. Snoch, A. Sochocka, T. Sumikama, H. Suzuki, D. Suzuki, H. Takeda, S. Tangwancharoen, H. Toernqvist, Y. Togano, Z. G. Xiao, S. J. Yennello, and Y. Zhang (SπRIT Collaboration) and M. D. Cozma, "Probing the symmetry energy with the spectral pion ratio," Phys. Rev. Lett. **126**, 162701 (2021).

G. Jhang, J. Estee, J. Barney, G. Cerizza, M. Kaneko, J. W. Lee, W. G. Lynch, T. Isobe, M. Kurata-Nishimura, T. Murakami, C. Y. Tsang, M. B. Tsang, R. Wang, D. S. Ahn, L. Atar, T. Aumann, H. Baba, K. Boretzky, J. Brzychczyk, N. Chiga, N. Fukuda, I. Gasparici, B. Hong, A. Horvat, K. Ieki, N. Inabe, Y. J. Kim, T. Kobayashi, Y. Kondo, P. Lasko, H. S. Lee, Y. Leifels, J. Łukasik, J. Manfredi, A. B. McIntosh, P. Morfouace, T. Nakamura, N. Nakatsuka, S. Nishimura, R. Olsen, H. Otsu, P. Pawłowski, K. Pelczar, D. Rossi, H. Sakurai, C. Santamaria, H. Sato, H. Scheit, R. Shane, Y. Shimizu, H. Simon, A. Snoch, A. Sochocka, Z. Sosin, T. Sumikama, H. Suzuki, D. Suzuki, H. Takeda, S. Tangwancharoen, H. Toernqvist, Y. Togano, Z. G. Xiao, S. J. Yennello, J. Yurkon, Y. Zhang, the SπRIT Collaboration, M. Colonna, D. Cozma, PawełDanielewicz, H. Elfner, N. Ikeno, C. M. Ko, J. Mohs, D. Oliinychenko, A. Ono, J. Su, Y. J. Wang, H. Wolter, J. Xu, Y. -X. Zhang, and Z. Zhang, the TMEP Collaboration, "Symmetry energy investigation with pion production from Sn+Sn systems," Phys. Lett. B **813**, 136016 (2021).

O. Hall, T. Davinson, A. Estrade, J. Liu, G. Lorusso, F. Montes, S. Nishimura, V. H. Phong, P. J. Woods, J. Agramunt, D. S. Ahn, A. Algora, J. M. Allmond, H. Baba, S. Bae, N. T. Brewer, C. G. Bruno, R. Caballero-Folch, F. Calviño, P. J. Coleman-Smith, G. Cortes, I. Dillmann, C. Domingo-Pardo, A. Fijalkowska, N. Fukuda, S. Go, C. J. Griffin, R. Grzywacz, J. Ha, L. J. Harkness-Brennan, T. Isobe, D. Kahl, L. H. Khiem, G. G. Kiss, A. Korgul, S. Kubono, M. Labiche, I. Lazarus, J. Liang, Z. Liu, K. Matsui, K. Miernik, B. Moon, A. I. Morales, P. Morrall, M. R. Mumpower, N. Nepal, R. D. Page, M. Piersa, V. F. E. Pucknell, B. C. Rasco, B. Rubio, K. P. Rykaczewski, H. Sakurai, Y. Shimizu, D. W. Stracener, T. Sumikama, H. Suzuki, J. L. Tain, H. Takeda, A. Tarifeño-Saldivia, A. Tolosa-Delgado, M. Wolińska-Cichocka, and R. Yokoyama, "β-delayed neutron emission of r-process nuclei at the $N = 82$ shell closure," Phys. Lett. B **816**, 136266 (2021).

M. Kaneko, T. Murakami, T. Isobe, M. Kurata-Nishimura, A. Ono, N. Ikeno, J. Barney, G. Cerizza, J. Estee, G. Jhang, J. W. Lee, W. G. Lynch, C. Santamaria, C. Y. Tsang, M. B. Tsang, R. Wang, D. S. Ahn, L. Atar, T. Aumann, H. Baba, K. Boretzky, J. Brzychczyk, N. Chiga, N. Fukuda, I. Gašparić, B. Hong, A. Horvati, T. Ichihara, K. Ieki, N. Inabe, Y. J. Kim, T. Kobayashi, Y. Kondo, P. Lasko, H. S. Lee, Y. Leifels, J. Łukasik, J. Manfredi, A. B. McIntosh, P. Morfouace, T. Nakamura, N. Nakatsuka, S. Nishimura, R. Olsen, H. Otsu, P. Pawłowski, K. Pelczar, D. Rossi, H. Sakurai, H. Sato, H. Scheit, R. Shane, Y. Shimizu, H. Simon, T. Sumikama, D. Suzuki, H. Suzuki, H. Takeda, S. Tangwancharoen, Y. Togano, H. Törnqvist, Z. Xiao, S. J. Yennellor, J. Yurkon, and Y. Zhang, SπRIT Collaboration, "Rapidity distributions of $Z = 1$ isotopes and the nuclear symmetry energy from Sn+Sn collisions with radioactive beams at 270 MeV/nucleon," Phys. Lett. B **822**, 136681 (2021).

H. Watanabe, C. X. Yuan, G. Lorusso, S. Nishimura, Z. Y. Xu, T. Sumikama, P. -A. Söderström, P. Doornenbal, F. Browne, G. Gey, H. S. Jung, J. Taprogge, Zs. Vajta, H. K. Wang, J. Wu, A. Yagi, H. Baba, G. Benzoni, K. Y. Chae, F. C. L. Crespi, N. Fukuda, R. Gernhäuser, N. Inabe, T. Isobe, A. Jungclaus, D. Kameda, G. D. Kim, Y. K. Kim, I. Kojouharov, F. G. Kondev, T. Kubo, N. Kurz, Y. K. Kwon, G. J. Lane, Z. Li, C. -B. Moon, A. Montaner-Pizá, K. Moschner, F. Naqvi, M. Niikura, H. Nishibata, D. Nishimura, A. Odahara, R. Orlandi, Z. Patel, Zs. Podolyák, H. Sakurai, H. Schaffner, G. S. Simpson, K. Steiger, H. Suzuki, H. Takeda, A. Wendt, and K. Yoshinaga, "Impact of shell evolution on Gamow-Teller β decay from a high-spin long-lived isomer in ^{127}Ag," Phys. Lett. B **823**, 136766 (2021).

S. E. A. Orrigo, B. Rubio, W. Gelletly, P. Aguilera, A. Algora, A. I. Morales, J. Agramunt, D. S. Ahn, P. Ascher, B. Blank, C. Borcea, A. Boso, R. B. Cakirli, J. Chiba, G. de Angelis, G. de France, F. Diel, P. Doornenbal, Y. Fujita, N. Fukuda, E. Ganioğlu, M. Gerbaux, J. Giovinazzo, S. Go, T. Goigoux, S. Grévy, V. Guadilla, N. Inabe, G. G. Kiss, T. Kubo, S. Kubono, T. Kurtukian-Nieto, D. Lubos, C. Magron, F. Molina, A. Montaner-Pizá, D. Napoli, D. Nishimura, S. Nishimura, H. Oikawa, V. H. Phong, H. Sakurai, Y. Shimizu, C. Sidong, P. -A. Söderström, T. Sumikama, H. Suzuki, H. Takeda, Y. Takei, M. Tanaka, J. Wu, and S. Yagi, "β decay of the very neutron-deficient ^{60}Ge and ^{62}Ge nuclei," Phys. Rev. C **103**, 014324 (2021).

T. Sumikama, N. Fukuda, N. Inabe, D. Kameda, T. Kubo, Y. Shimizu, H. Suzuki, H. Takeda, K. Yoshida, H. Baba, F. Browne, A. M. Bruce, R. Carrol, N. Chiga, R. Daido, F. Didierjean, P. Doornenbal, Y. Fang, G. Gey, E. Ideguchi, T. Isobe, S. Lalkovski, Z. Li, G. Lorusso R. Lozeva, H. Nishibata, S. Nishimura, I. Nishizuka, A. Odahara, Z. Pate, Zs. Podolyák, P. H. Regan, S. Rice, O. J. Roberts, H. Sakurai, G. S. Simpson, L. Sinclair, P. -A. Söderström, M. Tanaka, J. Taprogge, H. Watanabe, V. Werner, O. Wieland, J. Wu, Z. Y. Xu, and A. Yagi, "Observation of new neutron-rich isotopes in the vicinity of ^{110}Zr," Phys. Rev. C **130**, 014614 (2021).

B. Moon, A. Jungclaus, H. Naïdja, A. Gargano, R. Lozeva, C. -B. Moon, A. Odahara, G. S. Simpson, S. Nishimura, F. Browne, P. Doornenbal, G. Gey, J. Keatings, G. Lorusso, Z. Patel, S. Rice, M. Si, L. Sinclair, P. -A. Söderström, T. Sumikama, J. Taprogge, H. Watanabe, J. Wu, Z. Y. Xu, A. Yagi, D. S. Ahn, H. Baba, F. L. Bello Garrote, S. Bönig, R. Daido, J. M. Daugas, F. Didierjean, F. Drouet, Y. Fang, N. Fukuda, R. Gernhäuser, B. Hong, E. Ideguchi, S. Ilieva, N. Inabe, T. Ishigaki, T. Isobe, H. S. Jung, D. Kameda, I. Kojouharov, T. Komatsubara, T. Kröll, T. Kubo, N. Kurz, Y. K. Kwon, C. S. Lee, P. Lee, Z. Li, A. Montaner-Pizá, S. Morimoto, K. Moschner, D. Mücher, D. Murai, M. Niikura, H. Nishibata, I. Nishizuka, R. Orlandi, H. Sakurai, H. Schaffner, Y. Shimizu, K. Steiger, H. Suzuki, H. Takeda, K. Tshoo, Zs. Vajta, A. Wendt, R. Yokoyama, and K. Yoshinaga, "Nuclear structure of Te isotopes beyond neutron magic number $N = 82$," Phys. Rev. C **103**, 034320 (2021).

R. Yokoyama, E. Ideguchi, G. S. Simpson, Mn. Tanaka, Y. Sun, C. -J. Lv, Y. -X. Liu, L. -J. Wang, S. Nishimura, P. Doornenbal, G. Lorusso, P. -A. Söderström, T. Sumikama, J. Wu, Z. Y. Xu, N. Aoi, H. Baba, F. L. Bello Garrotel, G. Benzonil, F. Browne, R. Daido, Y. Fang,

N. Fukuda, A. Gottardo, G. Gey, S. Go, S. Inabe, T. Isobe, D. Kameda, K. Kobayashi, M. Kobayashi, I. Kojouharov, T. Komatsubara, T. Kubo, N. Kurz, I. Kuti, Z. Li, M. Matsushita, S. Michimasa, C. B. Moon, H. Nishibata, I. Nishizuka, A. Odahara, Z. Patel, S. Rice, E. Sahin, H. Sakurai, H. Schaffner, L. Sinclair, H. Suzuki, H. Takeda, J. Taprogge, Zs. Vajta, H. Watanabe, and A. Yagi, "Three-quasiparticle isomers in odd-even ^{159,161}Pm: Calling for modified spin-orbit interaction for the neutron-rich region," Phys. Rev. C **104**, L021303 (2021).

A. Kubiela, H. Suzuki, O. B. Tarasov, M. Pfützner, D. -S. Ahn, H. Baba, A. Bezbakh, A. A. Ciemny, W. Dominik, N. Fukuda, A. Giska, R. Grzywacz, Y. Ichikawa, Z. Janas, Ł. Janiak, G. Kamiński, K. Kawata, T. Kubo, M. Madurga, C. Mazzocchi, H. Nishibata, M. Pomorski, Y. Shimizu, N. Sokołowska, D. Suzuki, P. Szymkiewicz, A. Świercz, M. Tajima, A. Takamine, H. Takeda, Y. Takeuchi, C. R. Thornsberry, H. Ueno, H. Yamazaki, R. Yokoyama, and K. Yoshida, "Production of the most neutron-deficient Zn isotopes by projectile fragmentation of ^{78}Kr," Phys. Rev. C **104**, 064610 (2021).

T. Sumikama, D. S. Ahn, N. Fukuda, Y. Shimizu, H. Suzuki, H. Takeda, H. Wang, K. Yoshida, J. Amano, N. Chiga, K. Chikaato, A. Hirayama, N. Inabe, S. Kawase, S. Kubono, M. Matsushita, S. Michimasa, K. Nakano, H. Otsu, H. Sakurai, A. Saito, S. Shimoura, J. Suwa, M. Takechi, S. Takeuchi, Y. Togano, T. Tomai, and Y. Watanabe, "Energy-control and novel particle-identification methods combined with range in a multi-sampling ionization chamber for experiments using slowed-down RI beams," Nucl. Instrum. Methods Phys. Res. A **986**, 164687 (2021).

Presentations

[Domestic Conferences/Workshops]

福田直樹, 「大強度不安定核ビームの生成〜理研超伝導 RI ビーム生成分離装置 BigRIPS の現在とこれから〜」, 日本物理学会 第 76 回年次大会（2021 年）, オンライン, 2021 年 3 月 12–15 日.

吉留勇起, 近藤洋介, 中村隆司, N. L. Achouri, T. Aumann, 馬場秀忠, F. Delaunay, P. Doornenbal, 福田直樹, J. Gibelin, J. Hwang, 稲辺尚人, 磯部忠昭, 亀田大輔, 簡野大輝, S. Kim, 小林信之, 小林俊雄, 久保敏幸, S. Leblond, J. Lee, M. Marques, 本林透, 村井大地, 村上哲也, 武藤琴美, 中嶋丈嘉, 中塚徳継, A. Navin, 西征爾郎, N. A. Orr, 大津秀暁, 佐藤広海, 佐藤義輝, 清水陽平, 鈴木宏, 高橋賢人, 竹田浩之, 栂野泰宏, A. G. Tuff, M. Vandebrouck, 米田健一郎, 「^{25}O の不変質量核分光」, 日本物理学会 第 76 回年次大会, オンライン, 2021 年 3 月 12 日.

N. M. Nor, A. Odahara, A. Yagi, R. Lozeva, C. B. Moon, S. Nishimura, H. Nishibata, P. Doornenbal, G. Lorusso, T. Sumikama, H. Watanabe, F. Brown, Z. Y. Xu, J. Wu, R. Yokoyama, T. Isobe, H. Baba, H. Sakurai, H. Suzuki, N. Inabe, D. Kameda, N. Fukuda, H. Takeda, D. S. Ahn, Y. Shimizu, H. Sato, T. Kubo, S. Iimura, Y. Fang, R. Daido, T. Ishigaki, S. Morimoto, E. Ideguchi, T. Komatsubara, M. Niikura, I. Nishizuka and the EURICA Collaborators, "Nuclear structure study of neutron-rich Xe nuclei by beta decay of ^{141}I," 日本物理学会 第 76 回年次大会（2021 年）, オンライン, 2021 年 3 月 12–15 日.

道正新一郎, 小林幹, 清川裕, 大田晋輔, 横山輪, 西村太樹, D. S. Ahn, 馬場秀忠, G. P. A. Berg, 堂園昌伯, 福田直樹, 古野達也, 井手口栄治, 稲辺尚人, 川畑貴裕, 川瀬頌一郎, 木佐森慶一, 小林和馬, 久保敏幸, 久保田悠樹, C. S. Lee, 松下昌史, 宮裕之, 水上敦, 永倉弘康, 笈川浩之, 酒井英行, 清水陽平, C A. Stolz, 鈴木宏, 高木基伸, 竹田浩之, 武内聡, 時枝紘史, 上坂友洋, 矢向謙太郎, 山口勇貴, 柳澤善行, 吉田光一, 下浦享, 「中性子過剰 ^{62}Ti 核および近傍核の質量測定」, 日本物理学会 第 76 回年次大会（2021 年）, オンライン, 2021 年 3 月 12–15 日.

生越瑞揮, 本間彰, 武智麻耶, 大坪隆, 田中聖臣, 福田光順, 鈴木健, 西村太樹, 森口哲朗, 安得順, A. S. Aimaganbetov, 天野将道, 荒川裕樹, S. Bagchi, K. -H. Behr, N. Burtebayev, 親跡和弥, 杜航, 藤井朋也, 福田直樹, H. Geissel, 堀太地, 星野寿春, 伊五澤涼, 池田彩夏, 稲辺尚人, 猪股玖美, 板橋健太, 泉川卓司, 上岡大起, 神田直人, 加藤郁磨, I. Kenzhina, Z. Korkulu, Ye. Kuk, 日下健祐, 三原基嗣, 宮田恵理, 長江大輔, 中村翔健, M. Nassurlla, 西室国光, 西塚賢治, 大饗舜一朗, 大西康介, 大竹政雄, 王恵仁, 小沢顕, A. Prochazka, 櫻井博儀, C. Scheidenberger, 清水陽平, 杉原貴信, 炭竈聡之, 鈴木伸司, 鈴木宏, 竹田浩之, 田中悠太郎, 田中良樹, 和田太郎, 若山清志, 八木翔一, 山口貴之, 柳原陸斗, 柳澤善行, 吉田光一, T. K. Zholdybayev, 「Ni 同位体の陽子標的荷電変化断面積」, 日本物理学会 第 76 回年次大会（2021 年）, オンライン, 2021 年 3 月 12–15 日.

髙橋弘幸, 西村太樹, 菅原奏来, 延與紫世, 福田直樹, 原田知也, 土方佑斗, 松村理久, 佐藤広海, 清水陽平, 鈴木宏, 竹田浩之, 田中純貴, 上坂友洋, 宇根千晶, 吉田光一, 銭廣十三, 「Th ビームの開発に向けたイオンチェンバーの性能評価」, 日本物理学会 第 76 回年次大会（2021 年）, オンライン, 2021 年 3 月 12–15 日.

阪上朱音, A. D. Soon, 板橋健太, 日下健祐, 清水陽平, 炭竈聡之, 鈴木宏, 竹田浩之, 上坂友洋, 西隆博, 馬場秀忠, 福田直樹, 福西暢尚, 稲辺尚人, 矢向謙太郎, 柳澤善行, 吉田光一, 松本翔汰, 関屋涼平, G. Hans, 田中良樹, 「BigRIPS における二重ガモフ・テラー巨大共鳴探索実験のための光学系の開発」, 日本物理学会 第 76 回年次大会（2021 年）, オンライン, 2021 年 3 月 12–15 日.

土方佑斗, 銭廣十三, 上坂友洋, 延與紫世, 大田晋輔, 坂口治隆, 佐藤広海, 清水陽平, 菅原奏来, 鈴木宏, 髙橋弘幸, 武重祥子, 竹田浩之, 田中純貴, 辻崚太朗, 寺嶋知, 堂園昌伯, 西村俊二, 西村太樹, 馬場秀忠, 原田知也, 福田直樹, 松田洋平, 道正新一郎, 山村周, 吉田光一, 「大強度かつ極めて重い不安定核ビームの粒子識別に向けた Xe ガスシンチレータの開発」, 日本物理学会 第 76 回年次大会（2021 年）, オンライン, 2021 年 3 月 12–15 日.

Research Facility Development Division
Research Instruments Group
SAMURAI Team

1. Abstract

In collaboration with research groups in and outside RIKEN, the team designs, develops and constructs the SAMURAI spectrometer and relevant equipment that are and will be used for reaction experiments using RI beams at RI Beam Factory. The SAMURAI spectrometer consists of a large superconducting dipole magnet and a variety of detectors to measure charged particles and neutrons. After the commissioning experiment in March 2012, the team prepared and conducted, in collaboration with researchers in individual experimental groups, the first series of experiments with SAMURAI in May 2012. Then, several numbers of experiments were well performed until now utilizing the property of SAMURAI. The team also provides a basis for research activities by, for example, organizing collaboration workshops by researchers who are interested in studies or plan to perform experiments with the SAMURAI spectrometer.

2. Summary of Research Activity

The current research subjects are summarized as follows:

(1) Operation, maintenance and improvement of a large superconducting dipole magnet that is the main component of the SAMURAI spectrometer;
(2) Design, development and construction of various detectors that are used for nuclear reaction experiments using the SAMURAI spectrometer;
(3) Preparation for planning experiments using SAMURAI spectrometer;
(4) Maintenance and improvement of the SAMURAI beam lines;
(5) Formation of a collaboration platform called SAMURAI collaborations;
(6) Preparation for next generation spectrometer for nuclear reaction studies.

Members

Team Leader
Hideaki OTSU

Research & Development Scientist
Mizuki NISHIMURA

List of Publications & Presentations

Publications

[Original Papers]

M. M. Juhasz *et al.*, "First spectroscopic study of ^{63}V at the $N = 40$ island of inversion," Phys. Rev. C **103**, 064308 (2021).

B. D. Linh *et al.*, "Investigation of the ground-state spin inversion in the neutron-rich ^{47,49}Cl isotopes," Phys. Rev. C **104**, 044331 (2021).

F. Browne *et al.*, "Pairing forces govern population of doubly magic ^{54}Ca from direct reactions," Phys. Rev. Lett. **126**, 252501 (2021).

J. Estee *et al.*, "Probing the symmetry energy with the spectral pion ratio," Phys. Rev. Lett. **126**, 162701 (2021).

M. Kaneko *et al.*, "Rapidity distributions of $Z = 1$ isotopes and the nuclear symmetry energy from Sn+Sn collisions with radioactive beams at 270 MeV/nucleon," Phys. Lett. B **822**, 136681 (2021).

G. Jhang *et al.*, "Symmetry energy investigation with pion production from Sn+Sn systems," Phys. Lett. B **813**, 136016 (2021).

[Proceeding]

S. W. Huang *et al.*, "Experimental study of ^{4}n by directly detecting the decay neutrons," Few-Body System **62**, 102 (2021).

Presentations

[International Conference/Workshop]

SAMURAI International Collaboration Workshop 2021, Online, August 30–September 1, 2021,
`https://indico2.riken.jp/e/SAMURAIICW2021`.

[Domestic Conferences/Workshops]

磯部忠昭, 「重 RI ビーム衝突からの荷電パイ中間子測定による高密度核物質対称エネルギーの研究」, 日本物理学会 2021 年秋季大会, オンライン, 2021 年 9 月 14–17 日.

倉田（西村）美月, 「重 RI ビームを用いた生成粒子の集団運動の観測と対称エネルギー依存性の研究」, 日本物理学会 2021 年秋季大会, オンライン, 2021 年 9 月 14–17 日.

斗米貴人, 「直接反応による ^{31}Ne の非束縛励起状態のスペクトロスコピー」, 日本物理学会 2021 年秋季大会, オンライン, 2021 年 9 月 14–17 日.

中塚徳継, 「中性子過剰核の準弾性散乱実験で用いる反跳陽子検出器の開発」, 日本物理学会 2021 年秋季大会, オンライン, 2021 年 9 月 14–17 日.

堀川晃太, 「中性子過剰核における短距離相関探索実験のための前方散乱粒子検出器の開発」, 日本物理学会 2021 年秋季大会, オンライン, 2021 年 9 月 14–17 日.

海老名直樹, 「多中性子クラスター探索実験のための陽子飛跡検出シミュレーション」, 日本物理学会 2021 年秋季大会, オンライン, 2021 年 9 月 14–17 日.

松井智輝, 「多中性子クラスター探索実験のための陽子全エネルギー検出器の開発 II」, 日本物理学会 2021 年秋季大会, オンライン, 2021 年 9 月 14–17 日.

金子雅紀, 「RI ビームを用いた重イオン衝突における水素同位体生成と高密度核物質の対称エネルギー」, 日本物理学会第 77 回年次大会, オンライン, 2022 年 3 月 15–18 日.

磯部忠昭, 「中性子過剰な原子核を用いた中性子星状態方程式の実験的研究」, 日本物理学会第 77 回年次大会, シンポジウム「宇宙観測, 加速器実験と理論の協奏で探る高密度核物質」, オンライン, 2022 年 3 月 15–18 日.

Master Thesis

西津美咲, 修士論文, 「^{79}Se に対する 200 MeV/u 陽子及び重陽子入射核破砕反応による同位体生成断面積測定」, 九州大学, 2022 年 3 月.

Research Facility Development Division
Research Instruments Group
Computing and Network Team

1. Abstract

This team is in charge of development, management and operation of the computing and network environment, mail and information servers and data acquisition system and management of the information security of the RIKEN Nishina Center.

2. Major Research Subjects

(1) Development, management and operation of the general computing servers
(2) Development, management and operation of the mail and information servers
(3) Development, management and operation of the data acquisition system
(4) Development, management and operation of the network environment
(5) Management of the information security

3. Summary of Research Activity

This team is in charge of development, management and operation of the computing and network environment, mail and information servers and data acquisition system and management of the information security. The details are described elsewhere in this progress report.

(1) Development, management and operation of the general computing servers

We are operating Linux/Unix NIS/NFS cluster system for the data analysis of the experiments and general computing. This cluster system consists of eight computing servers with 64 CPU cores and totally 200 TB RAID of highly-reliable Fibre-channel interconnection. There are approximately 300 active user accounts on this cluster system (a total of about 800 accounts were registered so far). We are adopting the latest version of the Scientific Linux (X86 64) as the primary operating system, which is widely used in the accelerator research facilities, nuclear physics and high-energy physics communities in the world.

(2) Development, management and operation of the mail and information servers

We are operating RIBF.RIKEN.JP server as a mail/NFS/NIS server. This server is a core server of RIBF Linux cluster system. Postfix has been used for mail transport software and dovecot has been used for imap and pop services. These software packages enable secure and reliable mail delivery. Sophos Email Security and Control (PMX) installed on the mail front-end servers which tags spam mails and isolates virus-infected mails. The probability to identify the spam is approximately 95–99%. We are operating several information servers such as Web servers, Integrated Digital Conference (INDICO) server, Wiki servers, Groupware servers, Wowza streaming servers. We have been operating approximately 70 units of wireless LAN access points in RNC. Almost the entire radiation-controlled area of the East Area of RIKEN Wako campus is covered by wireless LAN for the convenience of experiments and daily work.

(3) Development, management and operation of the data acquisition system

We have developed the standard data-acquisition system named as RIBFDAQ. This system can process up to 40 MB/s data. By using crate-parallel readout from front-end systems such as CAMAC and VME, the dead time could be minimized. To synchronize the independent DAQ systems, the time stamping system has been developed. The resolution and depth of the time stamp are 10 ns and 48 bits, respectively. This time stamping system is very useful for beta decay experiments such as EURICA, BRIKEN and VANDLE projects. One of the important tasks is the DAQ coupling, because detector systems with dedicated DAQ systems are transported to RIBF from foreign facilities. In case of SAMURAI Silicon (NSCL/TUM/WUSTL), the readout system is integrated into RIBFDAQ. The projects of MUST2 (GANIL), MINOS (CEA Saclay), NeuLAND (GSI) and TRB3 (TUM) cases, data from their DAQ systems are transferred to RIBFDAQ and merged online. For SPIRIT (RIKEN/GANIL/CEA Saclay/NSCL), RIBFDAQ is controlled from the NARVAL-GET system that is a large-scale signal processing system for the time projection chamber. EURICA (GSI), BRIKEN (GSI/Univ. Liverpool/IFIC), VANDLE (UTK) and OTPC (U. Warsaw) projects, we adopt the time stamping system to apply individual trigger for each detector system. In this case, data are merged in offline. In addition, we are developing intelligent circuits based on FPGA. General Trigger Operator (GTO) is an intelligent triggering NIM module. The trigger system in BigRIPS DAQ is managed by 5 GTO modules. To improve the data readout speed of VME system, we have successfully developed the MPV system which is a parallel readout extension of the VME system. Data readout sequence is completely parallelized that helps to improve the DAQ deadtime. Thanks to the MPV system, now the DAQ system in RIBF is 10 times faster than in 2007. Toward to the next generation DAQ system, we have started to develop a real-time data processing unit based on Xilinx RFSoC that includes FPGA and 4 GHz FADC for TOF measurements of plastic scintillators. For gaseous detectors like PPAC and drift chamber, the development of FPGA-based dead-time free TDC is now in progress.

(4) Development, management and operation of the network environment

We have been managing the network environment collaborating with Information Systems Division in RIKEN. All the Ethernet ports of the information wall sockets are capable of the Gigabit Ethernet connection (10/100/1000 bps). In addition, some 10 Gbps networks port has been introduced to RIBF experimental area. Approximately 100 units of wireless LAN access points have been

installed to cover the almost entire area of Nishina Center.

(5) Management of the information security

It is essential to take proper information security measures for information assets. We are managing the information security of Nishina Center collaborating with Information Systems Division in RIKEN.

Members

Team Leader

Hidetada BABA

Special Temporary Research Scientists

Takashi ICHIHARA

Yasushi WATANABE

Visiting Scientists

Kazuo IEKI (Rikkyo Univ.)

Shoichiro KAWASE (Kyushu Univ.)

Student Trainee

Shoko TAKESHIGE (Rikkyo Univ.)

List of Publications & Presentations

Publication

[Original Paper]

H. Baba, T. Ichihara, T. Isobe, T. Ohnishi, K. Yoshida, Y. Watanabe, S. Ota, H. Shimizu, S. Shimoura, S. Takeuchi, D. Nishimura, J. Zenihiro, A. O. Tokiyasu, and R. Yokoyama, "MPV—Parallel readout architecture for the VME data acquisition system," IEEE Trans. Nucl. Sci. **68**, 1841 (2021).

Presentations

[Domestic Conferences/Workshops]

馬場秀忠 (口頭発表), 「RIBFDAQ のアップグレード計画」, 日本物理学会第 77 回年次大会, オンライン, 2022 年 3 月 15–19 日.

武重祥子 (口頭発表), 馬場秀忠, 栗田和好, 栂野泰宏, 銭廣十三, 土方佑斗, 「RFSoC 波形処理システムの RI ビーム実験への実装」, 日本物理学会第 77 回年次大会, オンライン, 2022 年 3 月 15–19 日.

Research Facility Development Division
Research Instruments Group
Detector Team

1. Abstract

This team is in charge of maintenance and improvement of detectors which are used at BigRIPS separator and its succeeding beam lines for beam diagnosis and particle identification of RI beams. We are also engaged in R&D of new detectors that can be used for higher-intensity RI beams. In addition, we are doing the R&D which uses the pelletron accelerator together with other groups.

2. Major Research Subjects

Development, fabrication, and operation of beam-line detectors which are used for the production and delivery of RI beams (beam diagnosis and particle identification). R&D which uses the pelletron accelerator.

3. Summary of Research Activity

The current research subjects are summarized as follows:

(1) Maintenance and improvement of the beam-line detectors which are used at BigRIPS separator and its succeeding beam lines
(2) Development of new beam-line detectors with radiation hardness and tolerance for higher counting rates
(3) Management of the pelletron accelerator and R&D which uses the pelletron

Members

Team Leader
Hiromi SATO

Research/Technical Scientist
Tokihiro IKEDA (Senior Research Scientist)

Visiting Scientist
Takeshi KOIKE (Tohoku University)

Student Trainees
Yuka HIKIMA (Toho University)
Kotoko INAYOSHI (Toho University)
Keisuke ONO (Toho University)
Keito SANGU (Toho University)

List of Publications & Presentations

Publications

[Original Papers]

J. Estee, W. G. Lynch, C. Y. Tsang, J. Barney, G. Jhang, M. B. Tsang, R. Wang, M. Kaneko, J. W. Lee, T. Isobe, M. Kurata-Nishimura, T. Murakami, D. S. Ahn, L. Atar, T. Aumann, H. Baba, K. Boretzky, J. Brzychczyk, G. Cerizza, N. Chiga, N. Fukuda, I. Gasparic, B. Hong, A. Horvat, K. Ieki, N. Inabe, Y. J. Kim, T. Kobayashi, Y. Kondo, P. Lasko, H. S. Lee, Y. Leifels, J. Łukasik, J. Manfredi, A. B. McIntosh, P. Morfouace, T. Nakamura, N. Nakatsuka, S. Nishimura, H. Otsu, P. Pawłowski, K. Pelczar, D. Rossi, H. Sakurai, C. Santamaria, H. Sato, H. Scheit, R. Shane, Y. Shimizu, H. Simon, A. Snoch, A. Sochocka, T. Sumikama, H. Suzuki, D. Suzuki, H. Takeda, S. Tangwancharoen, H. Toernqvist, Y. Togano, Z. G. Xiao, S. J. Yennello, and Y. Zhang, "Probing the symmetry energy with the spectral pion ratio," Phys. Rev. Lett. **126**, 162701 (2021).

M. Kaneko, T. Murakami, T. Isobe, M. Kurata-Nishimura, A. Ono, N. Ikeno, J. Barney, G. Cerizza, J. Estee, G. Jhang, J. W. Lee, W. G. Lynch, C. Santamaria, C. Y. Tsang, M. B. Tsang, R. Wang, D. S. Ahn, L. Atar, T. Aumann, H. Baba, K. Boretzky, J. Brzychczyk, N. Chiga, N. Fukuda, I. Gašparić, B. Hong, A. Horvat, T. Ichihara, K. Ieki, N. Inabe, Y. J. Kim, T. Kobayashi, Y. Kondo, P. Lasko, H. S. Lee, Y. Leifels, J. Łukasik, J. Manfredi, A. B. McIntosh, P. Morfouace, T. Nakamura, N. Nakatsuka, S. Nishimura, R. Olsen, H. Otsu, P. Pawłowski, K. Pelczar, D. Rossi, H. Sakurai, H. Sato, H. Scheit, R. Shane, Y. Shimizu, H. Simon, T. Sumikama, D. Suzuki, H. Suzuki, H. Takeda, S. Tangwancharoen, Y. Togano, H. Tornqvist, Z. Xiao, S. J. Yennello, J. Yurkon, and Y. Zhang, "Rapidity distributions of $Z = 1$ isotopes and the nuclear symmetry energy from Sn+Sn collisions with radioactive beams at 270 MeV/nucleon," Phys. Lett. B **822**, 136681 (2021).

M. Holl S. Lindberg, A. Heinz, Y. Kondo, T. Nakamura, J. A. Tostevin, H. Wang, T. Nilsson, N. L. Achouri, H. Al Falou, L. Atar, T. Aumann, H. Baba, K. Boretzky, C. Caesar, D. Calvet, H. Chae, N. Chiga, A. Corsi, H. L. Crawford, F. Delaunay, A. Delbart, Q. Deshayes, P. Díaz Fernández, Z. Dombrádi, C. A. Douma, Z. Elekes, P. Fallon, I. Gašparić, J. -M. Gheller, J. Gibelin, A. Gillibert, M. N. Harakeh, A. Hirayama, C. R. Hoffman, A. Horvat, Á. Horváth, J. W. Hwang, T. Isobe, J. Kahlbow, N. Kalantar-Nayestanaki, S. Kawase, S. Kim, K. Kisamori, T. Kobayashi, D. Körper, S. Koyama, I. Kuti, V. Lapoux, F. M. Marqués, S. Masuoka, J. Mayer, K. Miki, T. Murakami, M. Najafi, K. Nakano, N. Nakatsuka, A. Obertelli, F. de Oliveira Santos, N. A. Orr, H. Otsu, T. Ozaki, V. Panin, S. Paschalis, A. Revel, D. Rossi, A. T. Saito, T. Y. Saito, M. Sasano, H. Sato, Y. Satou, H. Scheit, F. Schindler, P. Schrock, M. Shikata, Y. Shimizu, H. Simon, D. Sohler, O. Sorlin, L. Stuhl, S. Takeuchi, M. Tanaka, M. Thoennessen, H. Törnqvist, Y. Togano, T. Tomai, J. Tscheuschner, J. Tsubota, T. Uesaka, Z. Yang, M. Yasuda, and K. Yoneda, "Border of the island of inversion: Unbound states in ^{29}Ne," Phys. Rev. C **105**, 034301 (2022).

Presentations

[Domestic Conferences/Workshops]

金衛国 (口頭発表), 小野敬祐, 池田時浩, 稲吉琴子, 神津雄哉, 三宮圭人, 引間宥花, 「ガラスキャピラリーによるレーザーマイクロビームのスポット構造の解析: 高次リング成分の消失距離の測定」, 第 64 回放射線化学討論会, オンライン, 2021 年 9 月 6–8 日.

金衛国 (口頭発表), 稲吉琴子, 池田時浩, 小野敬祐, 神津雄哉, 三宮圭人, 引間宥花, 「ガラスキャピラリーによるレーザーマイクロビームのスポット構造の解析: 各高次リング輝度の距離依存性」, 第 64 回放射線化学討論会, オンライン, 2021 年 9 月 6–8 日.

金衛国 (ポスター発表), 稲吉琴子, 池田時浩, 小野敬祐, 神津雄哉, 三宮圭人, 引間宥花, 「ガラスキャピラリーで生成されたレーザーマイクロビームの各スポットリング輝度の距離依存性」, 第 41 回原子衝突若手の会 秋の学校, オンライン, 2021 年 11 月 27 日.

Y. Zhang (口頭発表), 金子雅紀, 村上哲也, 磯部忠昭, 倉田 (西村) 美月, 小野章, 池野なつ美, J. Barney, G. Cerizza, J. Estee, G. Jhang, J. W. Lee, W. G. Lynch, C. Santamaria, C. Y. Tsang, M. B. Tsang, R. Wang, D. S. Ahn, L. Atar, T. Aumann, 馬場秀忠, K. Boretzky, J. Brzychczyk, 千賀信幸, 福田直樹, I. Gašparić, B. Hong, A. Horvat, 市原卓, 家城和夫, 稲辺尚人, Y. J. Kim, 小林俊雄, 近藤洋介, P. Lasko, H. S. Lee, Y. Leifels, J. Łukasik, J. Manfredi, A. B. McIntosh, P. Morfouace, 中村隆司, 中塚徳継, 西村俊二, R. Olsen, 大津秀暁, P. Pawłowski, K. Pelczar, D. Rossi, 櫻井博儀, 佐藤広海, H. Scheit, R. Shane, 清水陽平, H. Simon, 炭竈聡之, 鈴木大介, 鈴木宏, 竹田浩之, S. Tangwancharoen, 栂野康宏, H. Tornqvist, Z. Xiao, S. J. Yennello, J. Yurkon, 「RI ビームを用いた重イオン衝突における水素同位体生成と高密度核物質の対称エネルギー」, 日本物理学会第 77 回年次大会, オンライン, 2022 年 3 月 15–19 日.

金衛国 (口頭発表), 稲吉琴子, 池田時浩, 小野敬祐, 神津雄哉, 三宮圭人, 引間宥花, 「レーザーマイクロビーム生成のためのガラスキャピラリー内輸送特性の研究: スポット構造の距離依存性測定」, 日本物理学会第 77 回年次大会, オンライン, 2022 年 3 月 15–19 日.

道正新一郎 (口頭発表), 水野るり惠, 池田時浩, 郷慎太郎, 齋藤岳志, 櫻井博儀, 新倉潤, 松崎禎市郎, 「ミューオン原子 X 線分光のための Ge 検出器を用いた広ダイナミックレンジ光子検出システムの性能評価」, 日本物理学会第 77 回年次大会, オンライン, 2022 年 3 月 15–19 日.

Accelerator Applications Research Division
Beam Mutagenesis Group

1. Abstract

This group promotes biological applications of ion beams from RI Beam Factory (RIBF). Ion Beam Breeding Team studies various biological effects of fast heavy ions and develops new technology to breed plants and microbes by heavy-ion irradiations. Plant Genome Evolution Research Team choose baker's yeast and the legume *Lotus japonicus* as model systems to characterize genomic mutations using the population genomics approach with robust molecular biology and bioinformatics techniques.

2. Major Research Subjects

(1) Biological effects of fast heavy ions
(2) Molecular nature of DNA alterations induced by heavy-ion irradiation
(3) Research and development of heavy-ion breeding
(4) Genomics-based approach to revolutionize the mutagenesis in plants and microbes

3. Summary of Research Activity

Summary of research activities of the two teams are given in the sections of each team.

Members

Director
Tomoko ABE

Senior Visiting Scientist
Yutaka ARIMOTO

Visiting Scientist
Yoko AIDA (Univ. of Tokyo)

Accelerator Applications Research Division
Beam Mutagenesis Group
Ion Beam Breeding Team

1. Abstract

Ion beam breeding team studies various biological effects of fast heavy ions. It also develops new technique to breed plants and microbes by heavy-ion irradiations. Fast heavy ions can produce dense and localized ionizations in matters along their tracks, in contrast to photons (X rays and gamma rays) which produce randomly distributed isolated ionizations. These localized and dense ionization can cause double-strand breaks of DNA which are not easily repaired and result in mutation more effectively than single-strand breaks. A unique feature of our experimental facility at the RIKEN Ring Cyclotron (RRC) is that we can irradiate living tissues in atmosphere since the delivered heavy-ion beams have energies high enough to penetrate deep in matter. This team utilizes a dedicated beam line (E5B) of the RRC to irradiate microbes, plants and animals with beams ranging from carbon to iron. Its research subjects cover study of ion-beam radiation mutagenesis, genome-wide analyses of mutation, and development of new plants and microbial varieties by heavy-ion irradiation. Thirty-nine new varieties have already been brought to the market.

2. Major Research Subjects

(1) Study on the biological effects by heavy-ion irradiation
(2) Study on the molecular nature of DNA alterations induced by heavy-ion irradiation
(3) Innovative applications of heavy-ion irradiation

3. Summary of Research Activity

We study biological effects of fast heavy ions from the RRC using 135 MeV/nucleon C, N, Ne ions, 95 MeV/nucleon Ar ions, 90 MeV/nucleon Fe ions and from the IRC using 160 MeV/nucleon Ar ions. We also develop breeding technology of microbes and plants. Main subjects are:

(1) Study on the biological effects by heavy-ion irradiation

Heavy-ion beam deposits a concentrated amount of dose at just before stop with severely changing the linear energy transfer (LET). The peak of LET is achieved at the stopping point and known at the Bragg peak (BP). Adjusting the BP to target malignant cells is well known to be effective for cancer therapy. On the other hand, a uniform dose distribution is a key to the systematic study for heavy-ion mutagenesis, thus to the improvement of the mutation efficiency. Plants and microbes therefore, are irradiated using ions with stable LET. We investigated the effect of LET ranging from 23 to 640 keV/μm, on mutation induction using dry seeds of the model plants Arabidopsis thaliana and rice (*Oryza sativa* L.). The most effective LET (LETmax) was 30 keV/μm in *Arabidopsis*. LETmax irradiations showed the same mutation rate as that by chemical mutagens, which typically cause high mutation rate. The LETmax was 23–39 keV/μm in buckwheat, 23–50 keV/m in rice and 50–70 keV/μm in wheat. By contrast, when LET was 290 keV/μm, the mutation rate was low and the survival rate was greatly reduced in plants. In the case of microbe, filamentous fungus (*Neurospora crassa*), the Ar ions at 290 keV/μm demonstrated higher mutagenic activity than the Fe-ions at 640 keV/μm. Thus, the LET is an important factor to be considered in heavy-ion mutagenesis.

(2) Study on the molecular nature of DNA alterations induced by heavy-ion irradiation

A whole-genome analysis with high-throughput sequencing is a powerful tool used to characterize the nature of induced mutations. We have been using whole genome sequencing to analyze DNA mutations in *Arabidopsis* and rice genomes. C ions with LETmax mainly induced single nucleotide variants (SNVs) and small insertions and deletions (InDels), while the number of large deletions and chromosomal rearrangements was low in *Arabidopsis*. However, 290 keV/μm Ar ions showed a different mutation spectrum: SNVs and number of small InDels was low, while the number of large deletions ($\geqq$100 bp) and chromosomal rearrangements was high. Number of mutated gene induced by C-ion and Ar-ion irradiation is less than 10, relatively small, and often only 1 mutation is found near the mapped location. Thus, irradiation with these ions can efficiently generate knockout mutants of a target gene and can be applied to reverse genetics. Rice mutants of the causative gene induced by ion-beam irradiation were compared at 23–50 keV/μm and 290 keV/μm with typical LETs. The most mutations irradiated with C ion at 23–50 keV/μm were small deletions ($<$ 100 bp). Irradiation with 290 keV/μm Ar-ion resulted in the highest number of large deletions and decreased small deletions. In rice, as in *Arabidopsis*, the LETmax with high mutagenic effects was dominated by SNVs and small deletion mutations, while large deletions and chromosomal rearrangement mutations dominated LETs with high lethal effects.

(3) Innovative application of heavy-ion irradiation

In 1999, we formed a consortium for ion-beam breeding consisting of 24 groups. In 2020, the consortium grew to 183 groups from Japan and 20 from overseas. Previously, the ion-beam breeding procedures were carried out using mainly flowers and ornamental plants. We have recently put a new non-pungent and tearless onion, 'Smile Ball,' on the market along with 'Kiku Meigetsu,' an edible late flowering chrysanthemum. In addition, a new project was launched to expand the cultivation area of this variety of chrysanthemum in Yamagata prefecture. Beneficial variants have been grown for various plant species, such as high yield sea weeds, lipids hyperaccumulating unicellular alga, medicinal plant with high productivity of medicinal ingredient, peanuts without major allergens, oranges with delayed coloring and one-month late harvest, and lettuce with a low browning property as a cut vegetable. As

a result of a collaborative study with Shizuoka prefecture, we have created a new variety of 'Haru Shizuka,' which is late coloring. The harvest time of the Satsuma mandarin has tended to come earlier due to global warming, 'Haru Shizuka' is harvested about a month later than the original variety, but the fruits are sour when harvested. 'Haru Shizuka' is suitable for long-term storage and the fruits turn into good quality sweet oranges during storage till April. By broadening the target of heavy-ion breeding extending from flowers to crops, the technology will contribute to solving the global problems of food shortage and environmental destruction.

Members

Team Leader

Tomoko ABE

Research/Technical Scientists

Tokihiro IKEDA (Senior Research Scientist)
Masako IZUMI (Senior Research Scientist)
Ryouhei MORITA (Technical Scientist)
Teruyo TSUKADA (Senior Research Scientist)
Kazuhide TSUNEIZUMI (Senior Research Scientist)

Technical Staffs

Yoriko HAYASHI
Yuki SHIRAKAWA
Sumie OHBU
Mieko YAMADA

Special Temporary Technical Scientists

Hiroshi ABE
Katsunori ICHINOSE

Research Consultant

Masahiro MII (Chiba Univ.)

Visiting Scientists

Ayumi DEGUCHI (Chiba Univ.)
Makoto FUJIWARA (Sophia Univ.)
Eitaro FUKATSU (Forestry and Forest Products Res. Inst.)
Tomonari HIRANO (Univ. of Miyazaki)
Akiko HOKURA (Tokyo Denki Univ.)
Kotaro ISHII (QST)
Yutaka MIYAZAWA (Yamagata Univ.)
Kazumitsu MIYOSHI (Chiba Univ.)
Koji MURAI (Fukui Prefectural Univ.)
Kyosuke NIWA (Tokyo Univ. of Marine Sci. and Tech.)
Tadashi SATO (Tohoku Univ.)
Yoichi SATO (Riken Food Co., Ltd.)
Kenichi SUZUKI (Suntory Flowers Co., Ltd.)
Hinako TAKEHISA (Nat'l Agriculture and Food Res. Org.)
Masao WATANABE (Tohoku Univ.)

Visiting Technicians

Yukiko KANAZAWA (Nippon Beet Sugar Manufacturing Co., Ltd.)
Norihide KISHINO (Sanwa Norin Co. Ltd.)
Miho MOGAMIYA (Riken Food Co., Ltd.)
Daisuke SAITO (Riken Food Co., Ltd.)

Research Fellow

Hironari UCHIDA (Saitama Agricultural Tech. Res. Center)

Student Trainee

Yuzo MARUYAMA (Tokyo Denki Univ.)

List of Publications & Presentations

Publications

[Original Papers]

R. Tabassum, T. Dosaka, H. Ichida, Y. Ding, T. Abe, and T. Katsube-Tanaka, "The conditional chalky grain mutant '*flo11-2*' of rice (*Oryza sativa* L.) is sensitive to high temperature and useful for studies on chalkiness," Plant Prod. Sci. **24**, 230–243 (2020).

S. Muramatsu, K. Atsuji, K. Yamada, K. Ozawa, H. Suzuki, T. Takeuchi, Y. Hashimoto-Marukawa, Y. Kazama, T. Abe, K. Suzuki, and O. Iwata, "Isolation and characterization of a motility-defective mutant of *Euglena gracilis*," PeerJ **8**, e10002 (2020).

K. Tsuneizumi, M. Yamada, H. J. Kim, H. Ichida, K. Ichinose, Y. Sakakura, K. Suga, A. Hagiwara, M. Kawata, T. Katayama, N. Tezuka, T. Kobayashi, M. Koiso, and T. Abe, "Application of heavy-ion-beam irradiation to breeding large rotifer," Biosci. Biotechnol. Biochem. **85**, 703–713 (2021).

H. Tojo, A. Nakamura, A. Ferjani, Y. Kazama, T. Abe, and H. Iida, "A method enabling comprehensive isolation of arabidopsis mutants exhibiting unusual root mechanical behavior," Front. Plant Sci. **12**, 646404 (2021).

T. Kashiwabara, N. Kitajima, R. Onuma, N. Fukuda, S. Endo, Y. Terada, T. Abe, A. Hokura, and I. Nakai, "Synchrotron micro-X-ray fluorescence imaging of arsenic in frozen-hydrated sections of a root of *Pteris vittate*," Metallomics **13**, mfab009 (2021).

A. Sanjaya, Y. Kazama, K. Ishii, R. Muramatsu, K. Kanamaru, S. Ohbu, T. Abe, and M. T. Fujiwara, "An argon-ion-induced pale green mutant of arabidopsis exhibiting rapid disassembly of mesophyll chloroplast grana," Plants **10**, 848 (2021).

H. Udagawa, H. Ichida, T. Takeuchi, T. Abe, and Y. Takakura, "Highly efficient and comprehensive identification of ethyl methanesulfonate-induced mutations in *Nicotiana tabacum L.* by whole-genome and whole-exome sequencing," Front. Plant Sci. **12**, 671598 (2021).

Y. Sato, H. Nagae, G. N. Nishihara, and R. Terada, "The photosynthetic response of cultivated juvenile and mature *Undaria pinnatifida* (Laminariales) sporophytes to light," J. Appl. Phycol. **33**, 3437–3448 (2021).

A. Sanjaya, R. Muramatsu, S. Sato, M. Suzuki, S. Sasaki, H. Ishikawa, Y. Fujii, M. Asano, R. D. Itoh, K. Kanamaru, S. Ohbu, T. Abe, Y. Kazama, and M. T. Fujiwara, "Arabidopsis EGY1 is critical for chloroplast development in leaf epidermal guard cells," Plants **10**, 1254 (2021).

R. D. Itoh, K. P. Nakajima, S. Sasaki, H. Ishikawa, Y. Kazama, T. Abe, and M. T. Fujiwara, "TGD5 is required for normal morphogenesis of non-mesophyll plastids, but not mesophyll chloroplasts, in arabidopsis," Plant J. **107**, 237–255 (2021).

A. M. Okasa, R. Sjahril, M. Riadi, M. Mahendradatta, T. Sato, K. Toriyama, K. Ishii, Y. Hayashi, and T. Abe, "Evaluation of Toraja (Indonesia) local aromatic rice mutant developed using heavy-ion beam irradiation," Biodiversitas **22**, 3474–3481 (2021).

V. Q. Nhat, Y. Kazama, K. Ishii, S. Ohbu, H. Kunitake, T. Abe, and T. Hirano, "Double mutant analysis with the large flower mutant, ohbana1, to explore the regulatory network controlling the flower and seed sizes in *Arabidopsis thaliana*," Plants **10**, 1881 (2021).

Y. Sato, T. Hirano, H. Ichida, N. Fukunishi, T. Abe, and S. Kawano, Extending the cultivation period of *Undaria pinnatifida* by using regional strains with phenotypic differentiation along the Sanriku coast in northern Japan, Phycology **1**, 129–142 (2021).

K. Ishii, S. Kawano, and T. Abe, "Creation of green innovation and functional gene analyses using heavy-ion beam breeding," Cytologia (Tokyo) **84**, 273–274 (2021).

T. Takesita, K. Takita, K. Ishii, Y. Kazama, T. Abe, and S. Kawano, "Robust mutants isolated through heavy-ion beam irradiation and endurance screening in the green *Alga Haematococcus pluvialis*," Cytologia (Tokyo) **84**, 283–289 (2021).

Y. Sato, T. Hirano, Y. Hayashi, N. Fukunishi, T. Abe, and S. Kawano, "Screening for high-growth mutants in sporophytes of *Undaria pinnatifida* using heavy-ion beam irradiation," Cytologia (Tokyo), **84**, 291–295 (2021).

K. Hashimoto, Y. Kazama, H. Ichida, T. Abe, and K. Murai, "Eincorn wheat (*Triticum monococcum*) mutant *extra-early flowering 4*, generated by heavy-ion beam irradiation, has a deletion of the *LIGHT-REGULATED WD1* homolog," Cytologia (Tokyo) **84**, 297–302 (2021).

R. Morita, H. Ichida, Y. Hayashi, K. Ishii, Y. Shirakawa, S. Usuda-Kogure, K. Ichinose, M. Hatashita, K. Takagi, K. Miura, M. Kusajima, H. Nakashita, T. Endo, Y. Tojo, Y. Okumoto, T. Sato, K. Toriyama, and T. Abe, "Responsible gene analysis of phenotypic mutants revealed the linear energy transfer (LET)-dependent mutation spectrum in rice," Cytologia (Tokyo) **84**, 303–309 (2021).

T. Hirano, Y. Matsuyama, A. Hanada, Y. Hayashi, T. Abe, and H. Kunitake, "DNA damage response of *Cyrtanthus mackenii* male gametes following argon ion beam irradiation," Cytologia (Tokyo) **84**, 311–315 (2021).

A. Matsuta, T. Mayuzumi, H. Katano, M. Hatashita, K. Takagi, Y. Hayashi, T. Abe, K. Murai, and Y. Kazama, "The effect of heavy-ion beams with high linear energy transfer on mutant production in M_1 generation of *Torenia Fournieri*," Cytologia (Tokyo) **84**, 317–322 (2021).

T. Kobayashi, M. Takahashi, R. Nishijima, R. Sugiyama, K. Ishii, S. Kawano, and Y. Kazama, "Effective chromosomal preparation protocol for the dioecious plant *Silene Latifolia*," Cytologia (Tokyo) **84**, 323–328 (2021).

W. Aonuma, H. Kawamoto, Y. Kazama, K. Ishii, T. Abe, and S. Kawano, "Male/female trade-Off in hermaphroditic Y-chromosome deletion mutants of the dioecious plant *Silene Latifolia*," Cytologia (Tokyo) **84**, 329–338 (2021).

[Review Articles]

常泉和秀, 阿部知子, 「重イオンビームで魚養殖餌料に適した大型ワムシを創る」, バイオサイエンスとインダストリー **79**, 284–287 (2021).

T. Abe, "Ion beam mutagenesis for crop improvement," Plant Breeding & Genetics Newsletter **47**, 17–19 (2021).

K. Murai and T. Abe, "Development of early-flowering durum wheat suitable for the climate conditions of the Hokuriku region of Japan through conventional breeding aided by heavy ion beam mutagenesis," Plant Breeding & Genetics Newsletter **47**, 20–22 (2021).

[Book]

T. Abe, H. Ichida, Y. Hayashi, R. Morita, Y. Shirakawa, K. Ishii, T. Sato, H. Saito, and Y. Okumoto, "Ion beam mutagenesis—An innovative and effective method for plant breeding and gene discovery," in S. Sivasankar, N. Ellis, L. Jankuloski, and I. Ngelbrecht (eds.), Mutation Breeding, Genetic Diversity and Crop Adaptation to Climate Change, The Joint FAO/IAEA Programme, CABI, Oxfordshire UK, pp. 411–423 (2021).

Presentations

[International Conferences/Workshops]

T. Abe (invited), "New varieties developed in various crops using ion-beam irradiation in Japan," The Contribution of Innovative Nuclear Technology to Sustainable Agriculture, VCDNP (Vienna Center for Disarmament and Non-proliferation), Online, April 1, 2021.

T. Abe (invited), "New mutagen-ion beam-development for ion-beam breeding technology over the last two decades in Japan," Consultants meeting on radiation-induced crop genetic diversity and functional genomics to accelerate variety development for tolerance to climate extremes, Joint FAO/IAEA Center of Nuclear Techniques in Food and Agriculture, Online, August 2–6, 2021.

J. G. Pablo, M. Lindley, A. Isozaki, K. Hiramatsu, W. Peterson, K. Ishii, T. Abe, and K. Goda, "High-throughput Raman flow cytometry

for directed evolution," The Great Scientific Exchange 2021, Providence RI, USA, September 26–October 1, 2021.

H. Park, Y. Narasako, T. Abe, H. Kunitake, and T. Hirano, "Construction of mutant library by heavy-ion beam irradiation: toward efficient sweet potato breeding," JKTC Extra Edition 2021 International Student Online Seminar, "The future of plant, environment, and human with/after COVID-19," Online, November 22, 2021.

[Domestic Conferences/Workshops]

T. Abe (口頭発表), K. Tsuneizumi, M. Yamada, H. J. Kim, H. Ichida, K. Ichinose, Y. Sakakura, K. Suga, A. Hagiwara, M. Kawata, T. Katayama, N. Tezuka, T. Kobayashi, and M. Koiso, "Application of heavy-ion-beam irradiation to breeding large rotifer," 第一回沖縄科学技術大学院大学—理研連携シンポジウム, 沖縄県国頭郡恩納村 (沖縄科学技術大学院大学), 2021 年 4 月 6–7 日.

T. Abe (口頭発表) and H. Ichida, "Heavy-ion beam mutagenesis and its molecular characteristics in plants," ibid.

T. Abe (ポスター発表), R. Morita, H. Ichida, Y. Hayashi, Y. Shirakawa, and K. Ichinose, "Heavy ion mutagenesis in rice (*Oryza sativa* L.)," ibid.

常泉和秀 (口頭発表), 「重イオンビーム照射による有用系統の作出」, 理化学研究所—水産研究・教育機構連携ワークショップ, オンライン, 2021 年 4 月 27 日.

阿部知子（招待講演), 「イオンビーム育種技術による特産品の創成」, 先端技術セミナー兼福井イオンビーム育種研究会高エネルギービーム利活用に向けた展望〜イオンビームを用いた育種と社会実装に向けた研究〜, オンライン, 2021 年 9 月 15 日.

鳥山欽哉 (口頭発表), 武田信哉, 市田裕之, 阿部知子, 有村慎一, 風間智彦, 陳孫禄, 金岡義高, 貴島祐治, 「台中 65 号の細胞質を持つ *Oryza glaberrima* の CMS 関連遺伝子の解析」, 日本育種学会第 140 回講演会, オンライン, 2021 年 9 月 23–25 日.

阿部知子 (口頭発表), 森田竜平, 市田裕之, 林依子, 石井公太郎, 白川侑希, 臼田祥子, 一瀬勝紀, 畑下昌範, 高城啓一, 三浦孝太郎, 草島美幸, 仲下英雄, 遠藤貴司, 奥本裕, 佐藤雅志, 鳥山欽哉, 「重イオンビームの LET がイネ変異体の原因遺伝子に与える影響」, 同上.

高倉由光 (口頭発表), 市田裕之, 宇田川久史, 竹内貴規, 阿部知子, 「Whole-exome sequencing を用いたタバコの EMS 変異体における網羅的変異検出法の開発」, 同上.

風間裕介 (ポスター発表), 黛隆宏, 松田彩花, 畑下昌範, 高城啓一, 阿部知子, 村井耕二, 「重イオンビームを用いたトレニア変異系統の作出」, 同上.

村井耕二 (ポスター発表), 橋本佳澄, 風間裕介, 阿部知子, 「CO-like 遺伝子の日周期発現パターンシフトが超極早生コムギ変異体 extra early-flowering 4 (EXE4) における早生性」, 同上.

阿部知子 (ポスター発表), 田中朋之, 小林麻子, 「地球温暖化とお米の未来/福井のいろいろなお米」, ふるさと環境フェア 2021, 福井県福井市 (福井県産業会館), 2021 年 11 月 23 日.

阿部知子 (口頭発表), 橋口太亮, 飯山光太郎, 長井純一, 藤川和博, 「サツマイモ『シロユタカ』と外観識別可能な『こなみずき』欠刻葉系統の作出」, 第 84 回（令和 3 年度）九州農業研究発表会, 作物部会, オンライン, 2021 年 12 月 7–8 日.

村井耕二 (ポスター発表), 橋本佳澄, 風間裕介, 阿部知子, 「WD リピートタンパク質遺伝子（WWDR1）を欠失した変異体 exe4 はどうしてこんなに早生なのか？」, 第 16 回ムギ類研究会, オンライン, 2021 年 12 月 25 日.

Award

T. Abe, Women in plant mutation breeding award, Joint FAO/IAEA Center, September 20, 2021.

Press Release

「赤ちゃんマグロの餌, ワムシの大型化に成功—重イオンビームで 『メガワムシ』が誕生—」, 理化学研究所, 水産研究・教育機構, 長崎大学, 2021 年 1 月 15 日.

Patents

久村麻子, 諸岡淳司, 阿部知子, 林依子, 平野智也, 石井公太郎, キク 「長崎 SYC1」, 品種登録出願番号 35321, 出願日 2021 年 3 月 26 日.

中村茂和, 中嶌輝子, 平井実季, 小林康志, 加々美裕, 澤野郁夫, 稲葉元良, 小野章子, 寺岡毅, 馬場明子, 荒木勇二, 青島加奈子, 吉川公規, 土田友香, 阿部知子, 福西暢尚, 龍頭啓充, ウンシュウミカン 「春しずか」, 品種登録出願番号 35533, 出願日 2021 年 6 月 28 日.

Outreach Activity

We established the "Asagao (morning glory) club" to deepen the understanding of our technology of mutation breeding. The club distributes the morning glory seeds irradiated with C-ion on request, and collects and compiles the observation reports of their growth.

Accelerator Applications Research Division
Beam Mutagenesis Group
Plant Genome Evolution Research Team

1. Abstract

Established in May 2018 and succeed in October 2020, the plant genome evolution research team studies the effect of heavy-ion induced mutations on plant and microbial phenotypes. Chromosome rearrangements including translocations, inversions, and deletions are thought to play an important role in evolution and have a greater potential to achieve large phenotypic changes. However, this potential has not been fully investigated due to the lack of an effective method to induce and analyze complexed mutations. We employ the population genomics approach with robust molecular biology and bioinformatics techniques to characterize genomic mutations in model and non-model plant and microbial species, and create the future of mutation breeding.

2. Major Research Subjects

(1) Genomics-based approach to revolutionize the mutagenesis in model and non-model plants and microbes
(2) De novo genome sequencing and assembly of cultivars and isolates, and its application to evolution and breeding studies

3. Summary of Research Activity

(1) Genomics-based approach to revolutionize the mutagenesis in model and non-model plants and microbes

Recent advances in genome sequencing and bioinformatics technology enabled us to obtain a genome-wide view of the induced mutations in unselected populations. We chose baker's yeast and a legume *Lotus japonicus* as model systems, irradiated different doses of carbon-ion beams to these organisms, and determined the dose-survival correlation. We isolated a semi-dwarf *L. japonicus* mutant, identified the responsible mutation by whole-genome sequencing, and started to characterize the phenotypic traits of this mutant. Phenotyping analysis indicated that the isolated semi-dwarf mutant shows significantly shortened internode length while still maintaining good seed production equivalent to the wild-type plants. The semi-dwarf *L. japonicus* mutant is suitable for high-density cultivation in the laboratory environment and may serve as an efficient model platform for legume-*Rhizobium* symbiosis.

(2) *De novo* genome sequencing and assembly of new cultivars and isolates, and its application to evolution and breeding studies

We apply the latest *de novo* genome sequencing technology to elucidate genome sequences in different cultivars and isolates and successfully created some high-quality draft genome sequences. The determined and assembled draft genome sequences are subjected to gene predictions and functional annotations, then shared in a searchable data visualization and analysis system accessible through the internet. With these fundamental genome information resources, we and our collaborators work together to achieve new findings that will achieve major advances in both science and practical applications. These resources as well as the overall experimental techniques and the analysis pipeline are essential to further expand our genome-wide mutation and evolution approach to previously uncharacterized non-model species.

Members

Team Leader
Hiroyuki ICHIDA

Postdoctoral Researcher
Ni LEI

Visiting Scientist
Yusuke KAZAMA (Fukui Prefectural Univ.)

Student Trainee
Alvin SANJAYA (Sophia Univ.)

Administrative Part-time Workers
Yusaku NISHIMIYA (Administrative Part-time Worker II) Chiharu HINO (Administrative Part-time Worker II)

List of Publications & Presentations

Publications

[Original Papers]

Y. Sato, T. Hirano, H. Ichida, N. Fukunishi, T. Abe, and S. Kawano, "Extending the cultivation period of *Undaria pinnatifida* by using regional strains with phenotypic differentiation along the Sanriku coast in northern Japan," Phycology **1**, 129–142 (2021).

K. Hashimoto, Y. Kazama, H. Ichida, T. Abe, and K. Murai, "Einkorn wheat (*Triticum monococcum*) mutant *extra-early flowering 4*, generated by heavy-ion beam irradiation, has a deletion of the *LIGHT-REGULATED WD1* homolog," Cytologia **86**, 297–302 (2021).

R. Morita, H. Ichida, Y. Hayashi, K. Ishii, Y. Shirakawa, S. Usuda-Kogure, K. Ichinose, M. Hatashita, K. Takagi, K. Miura, M. Kusajima, H. Nakashita, T. Endo, Y. Tojo, Y. Okumoto, T. Sato, K. Toriyama, and T. Abe, "Responsible gene analysis of phenotypic mutants revealed the linear energy transfer (LET)-dependent mutation spectrum in rice," Cytologia **86**, 303–309 (2021).

H. Udagawa, H. Ichida, T. Takeuchi, T. Abe, and Y. Takakura, "Highly efficient and comprehensive identification of ethyl methanesulfonate-induced mutations in *Nicotiana tabacum* L. by whole-genome and whole-exome sequencing," Front. Plant Sci. **12**, 671598 (2021).

H. Murata, S. Nakano, T. Yamanaka, T. Shimokawa, T. Abe, H. Ichida, Y. Hayashi, and K. Tahara, "Argon-ion beam induced mutants of the ectomycorrhizal agaricomycete *Tricholoma matsutake* defective in β-1,4 endoglucanase activity promote the seedling growth of *Pinus densiflora* in vitro," Botany **99**, 139–149 (2021).

R. Tabassum, T. Dosaka, R. Morita, H. Ichida, Y. Ding, T. Abe, and T. Katsube-Tanaka, "The conditional chalky grain mutant '*flo11-2*' of rice (*Oryza sativa* L.) is sensitive to high temperature and useful for studies on chalkiness," Plant Prod. Sci. **24**, 230–243 (2021).

K. Tsuneizumi, M. Yamada, H. J. Kim, H. Ichida, K. Ichinose, Y. Sakakura, K. Suga, A. Hagiwara, M. Kawata, T. Katayama, N. Tezuka, T. Kobayashi, M. Koiso, and T. Abe, "Application of heavy-ion-beam irradiation to breeding large rotifer," Biosci. Biotechnol. Biochem. **85**, 703–713 (2021).

Presentations

[International Conference/Workshop]

T. Abe (invited), Y. Hayashi, R. Morita, Y. Shirakawa, and H. Ichida, "Ion-beam mutagenesis for creation of new varieties and discovery of genes", Bangabandhu International Conference on Sustainable Agriculture through Nuclear and Frontier Research, Online, January 2022.

[Domestic Conferences/Workshops]

H. Ichida (invited), "Heavy-ion beam mutagenesis and its molecular characteristics in plants", RIKEN-OIST Joint Symposium, Series 1: Green and Blue Planet How Can Ecological Research Shape Our Future?, Okinawa (OIST), April 2021.

森田竜平, 市田裕之, 林依子, 石井公太郎, 白川侑希, 臼田祥子, 一瀬勝紀, 畑下昌範, 高城啓一, 三浦孝太郎, 草島美幸, 仲下英雄, 遠藤貴司, 奥本裕, 佐藤雅志, 鳥山欽哉, 阿部知子, 「重イオンビームの LET がイネ変異体の原因遺伝子に与える影響」, 日本育種学会 第 140 回講演会, オンライン, 2021 年 9 月 24 日.

市田裕之, 宇田川久史, 竹内貴規, 阿部知子, 高倉由光, 「Whole-exome sequencing を用いたタバコ EMS 変異体における網羅的変異検出法の開発」, 日本育種学会 第 140 回講演会, オンライン, 2021 年 9 月 25 日.

武田信哉, 市田裕之, 阿部知子, 有村慎一, 陳孫禄, 金岡義高, 貴島祐治, 鳥山欽哉, 「台中 65 号の細胞質を持つ *Oryza glaberrima* の CMS 関連遺伝子の解析」, 日本育種学会 第 140 回講演会, オンライン, 2021 年 9 月 25 日.

N. Lei, T. Abe, and H. Ichida, "Massive genome sequencing analysis of accelerated carbon-ion-induced mutations in *Saccharomyces cerevisiae*", RIKEN-OIST Joint Symposium, Series 2: Kinds of Minds—what is thinking?, Online, October 2021.

Accelerator Applications Research Division
RI Application Research Group

1. Abstract

RI Application Research Group promotes industrial applications of radioisotopes (RIs) and ion beams at RIKEN RI Beam Factory (RIBF). Nuclear Chemistry Research Team develops production technologies of useful RIs for application studies in nuclear and radiochemistry. The team also develops technologies of mass spectrometry for trace-element and isotope analyses and apply them to the research fields such as cosmochemistry, environmental science, archaeology, and so on. Industrial Application Research Team promotes industrial applications of the accelerator facility and its related technologies.

2. Major Research Subjects

(1) Research and development of RI production technologies at RIBF
(2) RI application research
(3) Distribution of RIs produced at RIBF
(4) Development of radioactive targets and sources
(5) Development of trace element analyses using accelerator techniques and their applications to geoscience and archaeological research fields
(6) Development of chemical materials for ECR ion sources of the RIBF accelerators
(7) Development of technologies on industrial utilization and novel industrial applications of RIBF
(8) Support of industrial utilization of the heavy-ion beams at RIBF
(9) Support of materials science experiments

3. Summary of Research Activity

See the subsections of Nuclear Chemistry Research Team and Industrial Application Research Team.

Members

Director

Hiromitsu HABA

List of Publications & Presentations

See the subsections of Nuclear Chemistry Research Team and Industrial Application Research Team.

Accelerator Applications Research Division
RI Application Research Group
Nuclear Chemistry Research Team

1. Abstract

The Nuclear Chemistry Research Team develops production technologies of unique radioisotopes (RIs) at RIKEN RI Beam Factory (RIBF) and applies them in the research fields of physics, chemistry, biology, engineering, medicine, pharmaceutical and environmental sciences. The purified RIs such as ^{65}Zn, ^{67}Cu, ^{85}Sr, ^{88}Y, and ^{109}Cd are delivered to universities and institutes through Japan Radioisotope Association. We also develop new technologies of mass spectrometry for the trace-element analyses using accelerator techniques and apply them to the research fields such as cosmochemistry, environmental science, archaeology, and so on. We perform various isotopic analyses on the elements such as S, Pd, and Pb using ICP-MS, TIMS, and IRMS. We also develop radioactive targets and sources, and chemical materials such as metallic ^{238}U, $^{238}UO_2$, and ^{48}CaO for ECR ion sources of the heavy-ion accelerators at RIBF.

2. Major Research Subjects

(1) Research and development of RI production technologies at RIBF
(2) RI application research
(3) Development of trace element analyses using accelerator techniques and their applications to geoscience and archaeological research fields
(4) Development of radioactive targets and sources, and chemical materials for ECR ion sources of the heavy-ion accelerators at RIBF

3. Summary of Research Activity

(1) Research and development of RI production technologies at RIBF and RI application research

Due to its high sensitivity, the radioactive tracer technique has been successfully applied for investigations of the behavior of elements in the fields of chemistry, biology, engineering, medicine, pharmaceutical and environmental sciences. We have been developing production technologies of useful radioisotopes (RIs) at RIBF and conducting their application studies in collaboration with many researchers in various fields. With 30-MeV proton, 24-MeV deuteron, and 50-MeV alpha beams from the AVF cyclotron, we presently produce about 100 RIs from ^{7}Be to ^{211}At. Among them, ^{65}Zn, ^{67}Cu, ^{85}Sr, ^{88}Y, and ^{109}Cd are delivered to Japan Radioisotope Association for fee-based distribution to the general public in Japan. Our RIs are also distributed to researchers under the Supply Platform of Short-lived Radioisotopes for Fundamental Research, supported by MEXT KAKENHI in FY2016-2027. On the other hand, RIs of a large number of elements are simultaneously produced from metallic targets such as ^{nat}Ti, ^{nat}Ag, ^{nat}Hf, ^{197}Au, and ^{232}Th irradiated with a 135 MeV/nucleon ^{14}N beam from the RIKEN Ring Cyclotron. These multitracers are also supplied to universities and institutes as collaborative research.

In 2021, we developed production technologies of RIs such as ^{28}Mg, ^{44m}Sc, ^{44}Ti, ^{67}Cu, ^{111}Ag, ^{141}Ce, ^{186}Re, ^{196}Au, ^{211}At, ^{212}Pb, ^{224}Ra, ^{225}Ac, and ^{229}Pa which were strongly demanded but lack supply sources in Japan. We also investigated the excitation functions for the ^{27}Al(α, x), ^{nat}Ca(p, x), ^{nat}Ca(d, x), ^{nat}Ca(α, x), ^{nat}Cr(d, x), ^{45}Sc(p, x), ^{55}Mn(p, x), ^{nat}La(α, x), ^{159}Tb(α, x), and ^{141}Pr(p, x) reactions to effectively and quantitatively produce useful RIs. We used radiotracers of ^{44}Ti, ^{211}At, ^{212}Pb, ^{224}Ra, and ^{229}Pa for application studies in chemistry, ^{44m}Sc, ^{67}Cu, ^{111}Ag, ^{141}Ce, ^{186}Re, ^{211}At, and ^{225}Ac in nuclear medicine, and ^{28}Mg, ^{44m}Sc, ^{67}Cu, ^{186}Re, ^{196}Au, and ^{211}At in engineering. We also produced ^{65}Zn, ^{67}Cu, ^{85}Sr, ^{88}Y, and ^{109}Cd for our scientific research on a regular schedule and supplied the surpluses through Japan Radioisotope Association to the general public. In 2021, we accepted 2 orders of ^{65}Zn with a total activity of 15 MBq, 1 order of ^{67}Cu with 10 MBq, 8 orders of ^{85}Sr with 34.7 MBq, 2 orders of ^{88}Y with 2 MBq, and 1 order of ^{109}Cd with 5 MBq. We also distributed ^{28}Mg (2 MBq × 1), ^{67}Cu (100 MBq × 1), ^{88}Zr (1 MBq × 2), ^{95}Nb (1 MBq × 1), ^{111}Ag (1 MBq × 1), ^{141}Ce (0.24 MBq × 1, 0.5 MBq × 1), ^{175}Hf (1 MBq × 2), ^{179}Ta (0.5 MBq × 1), and ^{211}At (5 MBq × 3, 10 MBq × 1, 50 MBq × 6, 80 MBq × 2, and 100 MBq × 3) under the Supply Platform of Short-lived Radioisotopes for Fundamental Research.

(2) Superheavy element chemistry

Chemical characterization of newly-discovered superheavy elements (SHEs, atomic number $Z \geq 104$) is an extremely interesting and challenging subject in modern nuclear and radiochemistry. We are developing SHE production systems as well as rapid single-atom chemistry apparatuses at RIBF. Using heavy-ion beams from RILAC and AVF, ^{261}Rf ($Z = 104$), ^{262}Db ($Z = 105$), ^{265}Sg ($Z = 106$), and ^{266}Bh ($Z = 107$) are produced in the ^{248}Cm(^{18}O, $5n$)^{261}Rf, ^{248}Cm(^{19}F, $5n$)^{262}Db, ^{248}Cm(^{22}Ne, $5n$)^{265}Sg, and ^{248}Cm(^{23}Na, $5n$)^{266}Bh reactions, respectively, and their chemical properties are investigated.

We installed a gas-jet transport system to the focal plane of the gas-filled recoil ion separator GARIS at SRILAC. This system is a promising approach for exploring new frontiers in SHE chemistry: the background radiations from unwanted products are strongly suppressed, the intense primary heavy-ion beam is absent in the gas-jet chamber, and hence the high gas-jet extraction yield is attained. Furthermore, the beam-free condition makes it possible to investigate new chemical systems. To realize aqueous chemistry studies of Sg and Bh, we have been developing a continuous and rapid solvent extraction apparatus which consists of a continuous dissolution apparatus Membrane DeGasser (MDG), a Flow Solvent Extractor (FSE), and a liquid scintillation detector for α/SF-spectrometry. On the other hand, we produced radiotracers of ^{88}Zr, ^{95}Nb, ^{175}Hf, and ^{179}Ta at the AVF cyclotron and conducted model experiments for aqueous chemistry studies on Rf and Db. We also developed a cryogenic RF-carpet gas cell, which will be placed on the focal

plane of GARIS and connected to a gas-chromatograph apparatus, for the future gas-phase chemistry of the short-lived SHEs (half-life $T_{1/2} < 1$ s).

(3) Development of trace element analyses using accelerator techniques and their applications to geoscience and archaeological research fields

We have been developing the ECR Ion Source Mass Spectrometer (ECRIS-MS) for trace element analyses. We renovated the detection system of ECRIS-MS and evaluated its sensitivity and mass resolution power. We equipped a laser-ablation system with an ion source and a pre-concentration system to achieve high-resolution analyses for noble gases such as Kr and Xe.

Using the conventional ICP-MS, TIMS, IRMS, and so on, we studied Pb and S isotope ratios on cinnabar and asphalt samples from ancient ruins in Japan to elucidate the distribution of goods in the archaic society and to reveal the establishment of the Yamato dynasty in the period from Jomon to Tumulus. We established a sampling technique for pigment without any damages on the artifacts or wall paintings, using a S-free adhesive tape. Then, we applied the technique to the analyses of vermilion used in three representative tombs from Kofun period in Japan. We also applied the technique to the analyses of the red pigment from Roman ruins (Badalona, Spain). Furthermore, we started to develop a method for the analyses of 3 isotopic abundance ratios (^{32}S, ^{33}S, and ^{34}S) of sulfur as a new parameter for identification of source mine. By analyzing these isotope ratios, it is possible to analyze the MIF (mass-independent-fractionation) effect. This is also expected to provide a new parameter for the analysis of environmental dynamics.

In FY2021, we operated ICP-MS as a shared-use instrument and analyzed a total of 179 samples from five laboratories.

(4) Development of chemical materials for ECR ion sources of the heavy-ion accelerators at RIBF

In 2021, we prepared $^{238}UO_2$ on a regular schedule for ^{238}U-ion accelerations with the 28-GHz ECR of RILAC II.

Members

Team Leader
Hiromitsu HABA

Research & Development Scientist
Hiroo HASEBE

Special Postdoctoral Researcher
Yudai SHIGEKAWA

Postdoctoral Researchers
Yang WANG
Xiaojie YIN

Technical Staff
Akihiro NAMBU

Junior Research Associate
Motoki SATO

Special Temporary Research Scientist
Kazuya TAKAHASHI

Visiting Researcher
Mizuki UENOMACHI

Research Part-time Workers
Michiko KITAGAWA (Research Part-time Worker I)
Nozomi SATO (Research Part-time Worker I)
Sachiko USUDA (Research Part-time Worker I)
Minako OSANAI (Research Part-time Worker II)

Research Consultant
Hisaaki KUDO (Niigata Univ.)

Visiting Scientists
Msayuki AIKAWA (Hokkaido Univ.)
Kazuhiko AKIYAMA (Tokyo Metropolitan Univ.)
Takatoshi AOKI (Univ. of Tokyo)
Masato ASAI (JAEA)
Ferenc DITROI (ATOMKI)
Shuichiro EBATA (Saitama Univ.)
Osuke FUJIMOTO (Fujifilm Toyama Chemical Co., Ltd.)
Yuichi FUNASE (Fujifilm Toyama Chemical Co., Ltd.)
Takahiro HIRAKI (Okayama Univ.)
Hayato IKEDA (Tohoku Univ.)
Masamichi KAJITA (Fujifilm Toyama Chemical Co., Ltd.)
Yoshitaka KASAMATSU (Osaka Univ.)
Hiroshi KATO (Fujifilm Toyama Chemical Co., Ltd.)
Mayeen U. KHANDAKER (Sunway Univ.)
Hidetoshi KIKUNAGA (Tohoku Univ.)
Yoshikatsu KOGA (Nat'l Cancer Center)
Shoko KUBOTA (Fujifilm Toyama Chemical Co., Ltd.)
Takumi KUBOTA (Kyoto Univ.)

Takahiko MASUDA (Okayama Univ.)
Toshimitsu MOMOSE (Int'l Univ. of Health and Welfare)
Eri NAKAMURA (Fujifilm Toyama Chemical Co., Ltd.)
Kenichiro OGANE (Int'l Univ. of Health and Welfare)
Miki OHTSUKA (Waseda Univ.)
Kazuhiro OOE (Osaka Univ.)
Kai ORIHARA (Fujifilm Toyama Chemical Co., Ltd.)
Shinobu OSHIKIRI (Fujifilm Toyama Chemical Co., Ltd.)
Yasutaka SAITO (Fujifilm Toyama Chemical Co., Ltd.)
Aya SAKAGUCHI (Tsukuba Univ.)
Miho SATAKE (Fujifilm Toyama Chemical Co., Ltd.)
Tetsuya SATO (JAEA)
Yuki SATO (Fujifilm Toyama Chemical Co., Ltd.)
Kenji SHIMAZOE (Univ. of Tokyo)
Keisuke SUEKI (Tsukuba Univ.)
Kentaro SUZUKI (Fujifilm Toyama Chemical Co., Ltd.)
Zoltan SZUCS (ATOMKI)
Sandor TAKACS (ATOMKI)
Hiroyuki TAKAHASHI (Univ. of Tokyo)
Miho TAKAHASHI (Tokyo Univ. of Marine Sci. and Tech.)
Miwako TAKAHASHI (QST)
Hiroki TAKASHIMA (Nat'l Cancer Center)
Atsushi TOYOSHIMA (Osaka Univ.)
Kazuaki TSUKADA (JAEA)
Naoyuki UKON (Fukushima Medical Univ.)
Ahmed R. USMAN (Umaru Musa Yar'adua Univ.)
Takahiro YAMADA (Kindai Univ.)
Chunli YANG (Inst. of Modern Phys./Chinese Academy of Sci.)
Akihiko YOKOYAMA (Kanazawa Univ.)
Zenko YOSHIDA (ATOX Co., Ltd.)
Koji YOSHIMURA (Okayama Univ.)

Visiting Technicians

Hideyuki ARAI (Metal Tech. Co., Ltd.)
Hiroshi ARATA (Metal Tech. Co., Ltd.)
Mai FUKUMORI (ATOX Co., Ltd.)
Hidehiro HASHIMOTO (Metal Tech. Co., Ltd.)
Yoshiyuki IIZUKA (ATOX Co., Ltd.)
Masataka IMAMURA (Japan Radioisotope Association)
Shota KIMURA (Japan Radioisotope Association)
Yukiyoshi KON (Osaka Univ.)
Takashi KURIHARA (Metal Tech. Co., Ltd.)
Takahiro MIKAMOTO (Japan Radioisotope Association)
Daiki MORI (Japan Radioisotope Association)
Shingo NAKAMURA (Metal Tech. Co., Ltd.)
Hiroki SHIBAHARA (ATOX Co., Ltd.)
Yuki TAKEMURA (ATOX Co., Ltd.)
Yasutaka TAKEUCHI (ATOX Co., Ltd.)
Shusaku TAZAWA (ATOX Co., Ltd.)
Sho TOMITA (ATOX Co., Ltd.)
Yuichirou WAKITANI (Japan Radioisotope Association)
Mami YUKI (ATOX Co., Ltd.)

Student Trainees

Kjeld A.A.G. BEEKS (Vienna Univ. of Tech.)
Desheng CHEN (Univ. of Chinese Academy of Sci.)
Gantumur DAMDINSUREN (Hokkaido Univ.)
Shunsuke FUJINO (Kindai Univ.)
Saki GOTO (Hokkaido Univ.)
Ming GUAN (Okayama Univ.)
Sena HAMAGAMI (Kindai Univ.)
Yukina HANADA (Hokkaido Univ.)
Mariko HISAMATSU (Osaka Univ.)
Hiroyuki HOSOKAWA (Kanazawa Univ.)
Xuan HOU (Univ. of Tokyo)
He HUANG (Hokkaido Univ.)
Mizuho KATO (Tsukuba Univ.)
Cheonghun KIM (Univ. of Tokyo)
Hongchang LIN (Univ. of Tokyo)
Kenichi MORI (Kindai Univ.)
Ayumu NAGAI (Kanazawa Univ.)
Akihisa NAKAJIMA (Tsukuba Univ.)
Ryohei NAKANISHI (Osaka Univ.)
Teruhito NAKASHITA (Univ. of Tokyo)
Koichi OKAI (Okayama Univ.)
Motoki SATO (Univ. of Tokyo)
Kei SAWAMURA (Osaka Univ.)
Fumiki SENSUI (Univ. of Tokyo)
Katsuyuki TOKOI (Osaka Univ.)
Eisuke WATANABE (Osaka Univ.)
Kazeki YAMANE (Univ. of Tokyo)
Zihan ZHANG (Rikkyo Univ.)
Zhihong ZHONG (Univ. of Tokyo)

List of Publications & Presentations

Publications

[Original Papers]

M. Aikawa, T. Maehashi, D. Ichinkhorloo, S. Ebata, Y. Komori, and H. Haba, "Activation cross sections of deuteron-induced reactions on praseodymium up to 24 MeV," Nucl. Instrum. Methods Phys. Res. B **498**, 23 (2021).

D. Ichinkhorloo, M. Aikawa, Z. Tsoodol, T. Murata, M. Sakaguchi, Y. Komori, T. Yokokita, and H. Haba, "Production cross sections of dysprosium, terbium and gadolinium radioisotopes from the alpha-induced reactions on natural gadolinium up to 50 MeV," Nucl. Instrum. Methods Phys. Res. B **499**, 46 (2021).

S. Manabe, H. Takashima, K. Ohnuki, Y. Koga, R. Tsumura, N. Iwata, Y. Wang, T. Yokokita, Y. Komori, S. Usuda, D. Mori, H. Haba, H. Fujii, M. Yasunaga, and Y. Matsumura, "Stabilization of an ^{211}At-labeled antibody with sodium ascorbate," ACS Omega **6**, 14887 (2021).

M. Sakaguchi, M. Aikawa, N. Ukon, Y. Komori, H. Haba, N. Otuka, and S. Takács, "Activation cross section measurement of the alpha-particle induced reaction on natural neodymium," Appl. Radiat. Isot. **176**, 109826 (2021).

Y. Shigekawa, A. Yamaguchi, K. Suzuki, H. Haba, T. Hiraki, H. Kikunaga, T. Masuda, S. Nishimura, N. Sasao, A. Yoshimi, and K. Yoshimura, "Estimation of radiative half-life of ^{229m}Th by half-life measurement of other nuclear excited states in ^{229}Th," Phys. Rev. C **104**, 024306 (2021).

P. Schury, T. Niwase, M. Wada, P. Brionnet, S. Chen, T. Hashimoto, H. Haba, Y. Hirayama, D. S. Hou, S. Iimura, H. Ishiyama, S. Ishizawa, Y. Ito, D. Kaji, S. Kimura, H. Koura, J. J. Liu, H. Miyatake, J. -Y. Moon, K. Morimoto, K. Morita, D. Nagae, M. Rosenbusch, A. Takamine, Y. X. Watanabe, H. Wollnik, W. Xian, and S. X. Yan, "First high-precision direct determination of the atomic mass of a superheavy nuclide," Phys. Rev. C **104**, L021304 (2021).

S. Takács, F. Ditrói, Z. Szűcs, K. Brezovcsik, H. Haba, Y. Komori, M. Aikawa, M. Saito, T. Murata, M. Sakaguchi, and N. Ukon, "Cross section measurement of alpha-particle-induced reactions on ^{nat}Sb," Nucl. Instrum. Methods Phys. Res. B **505**, 24 (2021).

N. Kitamura, N. Imai, H. Haba, S. Michimasa, S. Shimoura, and Y. Yamaguchi, "Production of ^{178}Hf^{m2} and a simple chemical separation method for Hf recovery," J. Radioanal. Nucl. Chem. **330**, 721 (2021).

T. Niwase, M. Wada, P. Schury, P. Brionnet, S. D. Chen, T. Hashimoto, H. Haba, Y. Hirayama, D. S. Hou, S. Iimura, H. Ishiyama, S. Ishizawa, Y. Ito, D. Kaji, S. Kimura, J. Liu, H. Miyatake, J. Y. Moon, K. Morimoto, K. Morita, D. Nagae, M. Rosenbusch, A. Takamine, T. Tanaka, Y. X. Watanabe, H. Wollnik, W. Xian, and S. X. Yan, "α-decay-correlated mass measurement of $^{206,\,207g,\,m}$Ra using an α-TOF detector equipped multireflection time-of-flight mass spectrographs system," Phys. Rev. C **104**, 044617 (2021).

T. Aoki, R. Sreekantham, B. K. Sahoo, B. Arora, A. Kastberg, T. Sato, H. Ikeda, N. Okamoto, Y. Torii, T. Hayamizu, K. Nakamura, S. Nagase, M. Ohtsuka, H. Nagahama, N. Ozawa, M. Sato, T. Nakashita, K. Yamane, K. S. Tanaka, K. Harada, H. Kawamura, T. Inoue, A. Uchiyama, A. Hatakeyama, A. Takamine, H. Ueno, Y. Ichikawa, Y. Matsuda, H. Haba, and Y. Sakemi, "Quantum sensing of the electron electric dipole moment using ultracold entangled Fr atoms," Quantum Sci. Technol. **6**, 044008 (2021).

M. Aikawa, Y. Hanada, H. Huang, and H. Haba, "Activation cross sections of proton-induced reactions on praseodymium up to 30 MeV," Nucl. Instrum. Methods Phys. Res. B **508**, 29 (2021).

A. Yakushev, L. Lens, C. E. Düllmann, M. Block, H. Brand, M. Dasgupta, T. Calverley, A. D. Nitto, M. Götz, S. Götz, H. Haba, L. Harkness-Brennan, R-D. Herzberg, F. P. Heßberger, D. Hinde, A. Hübner, E. Jäger, D. Judson, J. Khuyagbaatar, B. Kindler, Y. Komori, J. Konki, J. V. Kratz, J. Krier, N. Kurz, M. Laatiaoui, B. Lommel, C. Lorenz, M. Maiti, A. K. Mistry, C. Mokry, Y. Nagame, P. Papadakis, A. Såmark-Roth, D. Rudolph, J. Runke, L. G. Sarmiento, T. K. Sato, M. Schädel, P. Scharrer, B. Schausten, J. Steiner, P. Thörle-Pospiech, A. Toyoshima, N. Trautmann, J. Uusitalo, A. Ward, M. Wegrzecki, and V. Yakusheva, "First study on nihonium (Nh, element 113) chemistry at TASCA," Front. Chem. **9**, 753738 (2021).

E. Watanabe, Y. Kasamatsu, T. Yokokita, S. Hayami, K. Tonai, H. Ninomiya, N. Kondo, Y. Shigekawa, H. Haba, Y. Kitagawa, M. Nakano, and A. Shinohara, "Anion-exchange experiment of Zr, Hf, and Th in HNO_3 and quantum chemical study on the nitrate complexes toward chemical research on element 104, Rf," Solvent Extr. Ion Exch., published online (December 31, 2021). DOI: 10.1080/07366299.2021.2020956 .

T. Minami, A. Takeuchi, S. Imazu, M. Okuyama, Y. Higashikage, T. Mizuno, K. Okabayashi, and K. Takahashi, "Identification of source mine using sulfur, mercury, and lead isotope analyses of vermilion used in three representative tombs from Kofun period in Japan," J. Archaeol. Sci. **37**, 102970 (2021).

D. Kim, M. Uenomachi, K. Shimazoe, and H. Takahashi, "Evaluation of single scattering correction method in Compton imaging system," Nucl. Instrum. Methods Phys. Res. A **1010**, 165568 (2021).

羽場宏光, 「理研における At-211 の製造分離状況と将来計画」, 放射線科学フロンティア〜孟宗竹〜, 第 3 号, p. 9 (2021).

島添健次, 上ノ町水紀, 吉野将生, 「コンプトン PET ハイブリッドカメラによる PET/SPECT 診断・治療における多核種撮像技術の開発」, Med. Imag. Tech. **39**, 206 (2021).

T. Hayamizu, H. Haba, K. Nakamura, T. Aoki, H. Nagahama, K. S. Tanaka, N. Ozawa, M. Ohtsuka, and Y. Sakemi, "Development of ultracold francium atomic sources towards the permanent EDM search," Few-Body Syst. **63**, 11 (2022).

T. Yokokita, S. Yano, Y. Komori, and H. Haba, "Anion- and cation-exchange studies of Zr, Hf, and Th using ion-exchange resin and fiber in H_2SO_4 media for chemical characterization of sulfate complex of Rf," J. Radioanal. Nucl. Chem. **331**, 1127 (2022).

M. Aikawa, Y. Hanada, D. Ichinkhorloo, H. Haba, S. Takács, F. Ditrói, and Z. Szűcs, "Production cross sections of ^{47}Sc via alpha-particle-induced reactions on natural calcium up to 29 MeV," Nucl. Instrum. Methods Phys. Res. B **515**, 1 (2022).

M. Uenomachi, K. Shimazoe, and H. Takahashi, "Double photon coincidence crosstalk reduction method for multi-nuclide Compton imaging," J. Instrum. **17**, P04001 (2022).

[Review Article]

羽場宏光, 小林奈通子, 永津弘太郎, 西弘大, 簱野健太郎, 福田光宏, 間賀田泰寛, 山田崇裕, 鷲山幸信, 渡部浩司, 「2019 年度 RI 製造・利用調査報告書」, Radioisotopes **70**, 251 (2021).

[Books]

羽場宏光, 「新元素ニホニウムはいかにして創られたか」, 東京化学同人, 176 ページ, 2021 年 12 月 17 日.

南武志, 高橋和也, 「旧練兵場遺跡出土赤色顔料（朱）の硫黄同位体比分析」, 香川県立善通寺養護学校移転に伴う埋蔵文化財発掘調査報告書「旧練兵場遺跡 (第 26 次調査)」, 香川県教育委員会, pp. 391–403, 2022 年 3 月.

[Proceedings]

羽場宏光, 「モニタリングポスト 第 58 回アイソトープ・放射線研究発表会印象記 パネル討論 我が国の RI 製造供給の現状と将来」, Isotope News, **778**, 12 月号, 58 (2021).

南武志, 高橋和也, 「みやき町大塚遺跡出土朱の産地推定」, みやき町文化財調査報告書第 28 集みやき町内遺跡 確認・試掘調査報告書, 佐賀県みやき町教育委員会, pp. 391–413 (2021).

A. Mukai, S. Hara, K. Yamagishi, R. Terabayashi, K. Shimazoe, Y. Tamura, H. Woo, T. Kishimoto, H. Kogami, Z. Zhihong, M. Ueno-

machi, A. Naurrachman, H. Takahashi, H. Asama, F. Ishida, H. Ebi, E. Takada, J. Kawarabayashi, K. Tanave, K. Kamada, and H. Tomita, "Optimization of detector movement algorithm using decision trees analysis for radiation source identification based on 4π gamma imaging," in 2022 IEEE/SICE International Symposium on System Integration (SII), IEEE, pp. 1026–1029 (2022).

Presentations

[International Conferences/Workshops]

M. Uenomachi (poster), K. Shimazoe, and H. Takahashi, "Double photon coincidence crosstalk reduction method for multi-nuclide Compton imaging," 22nd International Workshop on Radiation Imaging Detectors (22nd iWoRiD), Online, June 27–July 1, 2021.

K. Tanaka (poster), K. Hirano, A. Yamaguchi, H. Muramatsu, T. Hayashi, N. Yuasa, K. Nakamura, M. Takimoto, H. Haba, K. Shirasaki, H. Kikunaga, K. Maehata, N. Y. Yamasaki, and K. Mitsuda, "Challenge to improve the ^{229}Th isomer energy measurement with TES calorimeters," 19th International Workshop on Low Temperature Detectors (LTD19), Online, July 19–29, 2021.

A. Yamaguchi (oral), Y. Shigekawa, H. Haba, and M. Wada, "Development of an RF-carpet gas cell to obtain an ion beam of thorium-229," 32nd International Conference on Photonic, Electronic and Atomic Collisions (ViCPEAC 2021), Online, July 20–23, 2021.

H. Haba (invited), "Production and applications of radioisotopes at RIKEN RI Beam Factory," International Discussion Meeting on Future of Accelerator Applications and Radiotracers Research (FAAARR2021), Online, July 26–27, 2021.

M. Sato (oral), "Search for permanent EDM by using Fr atoms," CNS Summer School, Wako, Japan, August 16–20, 2021.

H. Haba (invited), "Production of radioisotopes for application studies at RIKEN RI Beam Factory," Snowmass'21 Workshop on High Power Cyclotrons/FFAs, Online, September 7–9, 2021.

M. Uenomachi (oral), K. Shimazoe, K. Kamada, T. Orita, M. Takahashi, and H. Takahashi, "Development of Compton-PET hybrid imaging system with $CeBr_3$-SiPM arrays," The 12th International Conference on Position Sensitive Detectors (PSD12), Online, September 12–17, 2021.

H. Takashima (oral), Y. Koga, S. Manabe, K. Ohnuki, R. Tsumura, T. Anzai, Y. Wang, X. Yin, A. Nambu, N. Sato, S. Usuda, H. Haba, H. Fujii, Y. Matsumura, and M. Yasunaga, "Antitumor effect of astatine-211-labeled anti-tissue factor antibody stabilized with sodium ascorbate," The 80th Annual Meeting of the Japanese Cancer Association, Yokohama, Japan, September 30–October 2, 2021.

T. Fukuchi (oral), H. Kikunaga, H. Haba, S. Yamamoto, and Y. Watanabe, "Titanium-44 phantom production and PET imaging for photon activation analysis," 2021 IEEE Nuclear Science Symposium and Medical Imaging Conference, Online, October 16–23, 2021.

M. Uenomachi (oral/poster), K. Ogane, Z. Zhong, K. Shimazoe, K. Kamada, H. Takahashi, Y. Wang, and H. Haba, "Simultaneous PET, SPECT and therapeutic nuclides imaging with Compton-PET hybrid camera," 2021 Virtual IEEE Nuclear Science Symposium and Medical Imaging Conference (2021 IEEE NSS/MIC), Online, October 16–23, 2021.

M. Sato (oral), "Search for permanent EDM by using Fr atoms," SPIN 2021, Online, October 18–21, 2021.

H. Haba (invited), "Production and applications of radioisotopes at RIKEN RI Beam Factory -Search for new elements through diagnosis and therapy of cancer-," RIKEN-KFU (Kazan Federal University) 3rd Joint Symposium, Online, November 5–6, 2021.

T. Aoki (poster), R. Sreekantham, B. K. Sahoo, B. Arora, A. Kastberg, T. Sato, H. Ikeda, N. Okamoto, Y. Torii, T. Hayamizu, K. Nakamura, S. Nagase, M. Ohtsuka, H. Nagahama, N. Ozawa, M. Sato, T. Nakashita, K. Yamane, K. S. Tanaka, K. Harada, H. Kawamura, T. Inoue, A. Uchiyama, A. Hatakeyama, A. Takamine, H. Ueno, Y. Ichikawa, Y. Matsuda, H. Haba, and Y. Sakemi, "Quantum sensing of the electron electric dipole moment using quantum entangled atoms," International Symposium on Novel maTerials and quantum Technologies (ISNTT2021), Online, December 16, 2021.

A. Yamaguchi (oral), Y. Shigekawa, H. Haba, M. Wada, and H. Katori, "Development of an RF-carpet gas cell to obtain a low-energy thorium ion beam," Second Workshop of the Center for Time, Constants and Fundamental Symmetries, Online, March 23, 2022.

[Domestic Conferences/Workshops]

福地知則 (口頭発表/ポスター発表), 金山洋介, 蔵地理代, 中谷友香, 羽場宏光, 森大輝, 横北卓也, 小森有希子, 山本誠一, 渡辺恭良, 「複数トレーサー PET を用いた異なるがん診断薬の直接比較」, 第 15 回日本分子イメージング学会総会・学術集会, 熊本市, 2021 年 5 月 26–27 日.

髙島大輝 (口頭発表), 眞鍋史乃, 大貫和信, 古賀宣勝, 津村遼, 安西高廣, Wang Yang, Ying Xiaojie, 南部明弘, 佐藤望, 臼田祥子, 羽場宏光, 藤井博史, 松村保広, 安永正浩, 「アルファ線放出核種アスタチン-211 結合抗組織因子抗体の前臨床試験」, 第 37 回日本 DDS 学会学術集会, 千葉市, 2021 年 6 月 29–30 日.

羽場宏光 (口頭発表), 「理研 RI ビームファクトリーにおける RI 製造供給」, 第 58 回アイソトープ・放射線研究発表会, オンライン, 2021 月 7 月 7–9 日.

南部明弘 (口頭発表), Y. Xiaojie, 羽場宏光, 押切忍, 加藤寛, 日野明弘, 「^{232}Th + ^{14}N 反応による ^{225}Ac の製造」, 第 58 回アイソトープ・放射線研究発表会, オンライン, 2021 月 7 月 7–9 日.

羽場宏光 (口頭発表), 「RIBF 施設紹介」, 新学術領域研究（研究領域提案型）『学術研究支援基盤形成』短寿命 RI 供給プラットフォーム成果報告会 兼 RI 利用研究会, オンライン, 2021 年 7 月 19–20 日.

井上貴之 (口頭発表), 羽場宏光 (口頭発表), 「2019 年度 RI 製造・利用調査概要報告」, 新学術領域研究（研究領域提案型）『学術研究支援基盤形成』短寿命 RI 供給プラットフォーム成果報告会 兼 RI 利用研究会, オンライン, 2021 年 7 月 19–20 日.

上ノ町水紀 (招待講演), 「二光子同時計測法を用いたマルチ RI トレーサーイメージング技術の開発」, 電気学会調査専門委員会「放射線技術を利用した微量分析およびイメージング技術」, オンライン, 2021 年 8 月 6 日.

羽場宏光 (口頭発表), 「核化学ロードマップについて」, 第 59 回核化学夏の学校, オンライン, 2021 月 8 月 26–27 日.

中島朗久 (口頭発表), 坂口綾, 早川優太, 羽場宏光, 塚田和明, K. Hain, J. Zheng, 瀬古典明, 保科宏行, 山崎信哉, 末木啓介, 横山明彦, 「質量分析による環境中 ^{237}Np 定量法確立に向けて」, 日本地球化学会第 68 回年会, 弘前市/オンライン, 2021 年 9 月 6–10 日.

合川正幸 (口頭発表), 前橋拓斗, ダグワドルジ イチンホルロー, 江幡修一郎, 小森有希子, 羽場宏光, 「^{141}Pr 標的への重陽子入射反

応による ^{140}Nd 生成反応断面積の測定」, 日本原子力学会 2021 年秋の大会, オンライン, 2021 年 9 月 8–10 日.

上ノ町水紀 (口頭発表), 島添健次, 織田忠, 鎌田圭, 高橋浩之, 「$CeBr_3$ ピクエル検出器を用いた Compton-PET hybrid camera の開発」, 日本原子力学会 2021 年秋の大会, オンライン, 2021 年 9 月 8–10 日.

庭瀬暁隆 (口頭発表), P. Schury, 和田道治, P. Brionnet, S. Chen, 橋本尚志, 羽場宏光, 平山賀一, D. S. Hou, 飯村俊, 石山博恒, 石澤倫, 伊藤由太, 加治大哉, 木村創大, 小浦寛之, 宮武宇也, J. Y. Moon, 森本幸司, 森田浩介, 長江大輔, M. Rosenbusch, 高峰愛子, 渡辺裕, H. Wollnik, W. Xian, S. X. Yan, 「超重核 ^{257}Db の直接質量測定」, 日本物理学会 2021 年秋季大会, オンライン, 2021 年 9 月 14–17 日.

岡井晃一 (口頭発表), K. Beeks, 藤本弘之, M. Guan, 羽場宏光, 原秀明, 海野弘之, 笠松良崇, 北尾真司, 小早川大貴, 小無健司, 増田孝彦, 宮本祐樹, 平木貴宏, 笹尾登, T. Schumm, 瀬戸誠, 重河優大, 玉作賢治, 植竹智, J. Wang, 渡部信, 渡部司, 山口敦史, 安田勇輝, 依田芳卓, 吉見彰洋, 吉村浩司, 吉村太彦, 「トリウム 229 アイソマー状態からの真空紫外光探索」, 日本物理学会 2021 年秋季大会, オンライン, 2021 年 9 月 14–17 日.

庭瀬暁隆 (口頭発表), 和田道治, P. Schury, P. Brionnet, S. D. Chen, 橋本尚志, 羽場宏光, 平山賀一, D. S. Hou, 飯村俊, 石山博恒, 石澤倫, 伊藤由太, 加治大哉, 木村創大, J. Liu, 宮武宇也, J. Y. Moon, 森本幸司, 森田浩介, 長江大輔, M. Rosenbusch, 高峰愛子, 田中泰貴, 渡辺裕, H. Wollnik, W. Xian, S. X. Yan, 「MRTOF と α-TOF 検出器による, α 崩壊に相関した精密質量測定法の開拓」, 日本放射化学会第 65 回討論会 (2021), オンライン, 2021 年 9 月 22–24 日.

床井健運 (ポスター発表), 豊嶋厚史, 大江一弘, 角永悠一郎, 寺本高啓, 中川創太, 吉村崇, 笠松良崇, 羽場宏光, 王洋, 篠原厚, 「At が形成するハロゲン結合の解離エネルギー測定に向けた AtI の生成条件と揮発性の分析」, 日本放射化学会第 65 回討論会 (2021), オンライン, 2021 年 9 月 22–24 日.

永井歩夢 (ポスター発表), 寺西翔, 坂口綾, 中島朗久, 羽場宏光, 横北卓也, 南部明弘, 横山明彦, 「トリウム標的への Li イオン照射によって生じる ^{236}U の ICP-MS による定量」, 日本放射化学会第 65 回討論会 (2021), オンライン, 2021 年 9 月 22–24 日.

永井雄太 (ポスター発表), 青井景都, 丸山俊平, 西中一朗, 鷲山幸信, 羽場宏光, 横山明彦, 「核医学用アスタチン抽出に利用できるイオン液体の研究」, 日本放射化学会第 65 回討論会 (2021), オンライン, 2021 年 9 月 22–24 日.

中川創太 (口頭発表), 豊嶋厚史, 角永悠一郎, 大江一弘, 寺本高啓, 床井健運, 神田晃充, 吉村崇, 永田光知郎, 笠松良崇, 羽場宏光, 王洋, 篠原厚, 「電解酸化反応を用いた分子標的薬への ^{211}At 標識化法の開発」, 日本放射化学会第 65 回討論会 (2021), オンライン, 2021 年 9 月 22–24 日.

黄栩昊 (口頭発表), 加藤弘樹, 角永悠一郎, 下山敦史, 樺山一哉, 片山大輔, 大江一弘, 豊嶋厚史, 羽場宏光, 王洋, 篠原厚, 深瀬浩一, 「新規アルファ線ブラキセラピー開発に向けた At-211 標識金ナノ粒子の合成と機能評価」, 日本放射化学会第 65 回討論会 (2021), オンライン, 2021 年 9 月 22–24 日.

寺本高啓 (ポスター発表), 大江一弘, 王洋, 羽場宏光, 豊嶋厚史, 「アスタチン化合物の分光・可視化にむけた新規手法の提案」, 日本放射化学会第 65 回討論会 (2021), オンライン, 2021 年 9 月 22–24 日.

重河優大 (ポスター発表), 床井健運, 山口敦史, W. Yang, Y. Xiaojie, 南部明弘, 佐藤望, 和田道治, 羽場宏光, 「Th-229m の壊変特性の解明に向けた高周波イオン収集・質量分離装置の開発」, 日本放射化学会第 65 回討論会 (2021), オンライン, 2021 年 9 月 22–24 日.

西村峻 (ポスター発表), 雨倉啓, 秋山和彦, 羽場宏光, 高宮幸一, 久冨木志郎, 「HPLC 分析によるランタノイド内包フラーレン（$Ln^{3+}@C_{82}{}^{3-}$）の電子状態に関する研究」, 日本放射化学会第 65 回討論会 (2021), オンライン, 2021 年 9 月 22–24 日.

澤村慶 (ポスター発表), 笠松良崇, 重河優大, 篠原厚, 「低エネルギー励起核種 U-235m のハロゲン化物の半減期変化」, 日本放射化学会第 65 回討論会 (2021), オンライン, 2021 年 9 月 22–24 日.

梅田泉 (口頭発表), 永田みどり, 天﨑茜, 大貫和信, 柳下淳, 桂川美穂, 織田忠, 武田伸一郎, 羽場宏光, 藤井博史, 高橋忠幸,「Rhenium-186 の錯体形成に関する諸検討」, 第 61 回日本核医学会学術総会, 名古屋市, 2021 年 11 月 4–6 日.

芝原裕規 (口頭発表), 竹村友紀, 福森麻衣, 殷小杰, 南部明弘, 結城真美, 田沢周作, 羽場宏光, 「TAT のための ^{228}Th/^{224}Ra/^{212}Pb ジェネレータシステム開発（2）—高比放射能 ^{212}Pb の製造—」, 第 61 回日本核医学会学術総会, 名古屋市, 2021 年 11 月 4–6 日.

武藤大河 (口頭発表), P. Brionnet, 浅井雅人, 郷慎太郎, R. Grzywacz, 羽場宏光, 加治大哉, 木村創太, T. King, 森本幸司, K. Rykaczewski, 坂口聡志, 酒井英行, 森田浩介, 庭瀬暁隆, 田中聖臣, 「Si 検出器の波形解析による軽粒子識別」, 第 127 回日本物理学会九州支部例会, オンライン, 2021 年 12 月 4 日.

大島康宏 (ポスター発表), 鈴木博元, 花岡宏史, 佐々木一郎, 渡辺茂樹, 羽場宏光, 荒野泰, 対馬義人, 石岡典子, 「LAT1 を標的とした新規 α 線標的アイソトープ治療薬: 2-[^{211}At]astato-α-methyl-L-phenylalanine の非臨床評価」, QST 高崎サイエンスフェスタ 2021, 高崎市/オンライン, 2021 年 12 月 7–8 日.

羽場宏光 (招待講演), 「短寿命 RI の製造・分離」, QiSS シンポジウム, 大阪市/オンライン, 2022 年 2 月 19 日.

山口敦史 (ポスター発表), 重河優大, 羽場宏光, 和田道治, 香取秀俊, 「原子核時計実現にむけたトリウムイオンのトラップ」, 第 9 回「光量子工学研究」—エクストリームフォトニクスが拓く未来の光科学—, オンライン, 2022 年 2 月 28 日–3 月 1 日.

羽場宏光 (口頭発表),「ケミカルプローブ用ラジオアイソトープの製造開発」, Chemical Probe（生命現象探索分子）最終報告会（第 4 回）, 和光市, 2022 年 3 月 1 日.

木村創大 (口頭発表), 和田道治, 羽場宏光, 石澤倫, 森本幸司, 庭瀬暁隆, M. Rosenbusch, Peter Schury for the SHE-Mass Collaboration, 「MRTOF-MS を用いた ^{252}Cf 自発核分裂片の網羅的精密質量測定」, 日本物理学会第 77 回年次大会 (2022 年), オンライン, 2022 年 3 月 15–19 日.

平木貴宏 (口頭発表), Kjeld Beeks, 藤本弘之, 福永優太, 管明, 羽場宏光, 原秀明, 稲垣新, 小早川大貴, 笠松良崇, 北尾真司, 小無健司, 増田孝彦, 宮本祐樹, 岡井晃一, 笹尾登, T. Schumm, 瀬戸誠, 重河優大, 玉作賢治, 植竹智, 渡部司, 渡部信, 山口敦史, 安田勇輝, 依田芳卓, 吉見彰洋, 吉村浩司, 吉村太彦, 「トリウム 229 アイソマー状態からの脱励起真空紫外光探索」, 日本物理学会第 77 回年次大会 (2022 年), オンライン, 2022 年 3 月 15–19 日.

庭瀬暁隆 (口頭発表), P. Schury, 和田道治, P. Brionnet, S. Chen, 羽場宏光, 平山賀一, D. S. Hou, 飯村俊, 石山博恒, 伊藤由太, 加治大哉, 木村創大, 小浦寛之, 宮武宇也, 森本幸司, 森田浩介, 長江大輔, M. Rosenbusch, 高峰愛子, 渡辺裕, H. Wollnik, W. Xian, S. X. Yan,

「MRTOF+α-TOF による ^{257,258}Db の精密質量測定」, 日本物理学会第 77 回年次大会 (2022 年), オンライン, 2022 年 3 月 15–19 日.

亀谷晃毅 (口頭発表), 三木謙二郎, 今井伸明, 上坂友洋, 大田晋輔, 笹野匡紀, 竹田浩之, 波多野雄治, 羽場宏光, 早水友洋, 原正憲, 道正新一郎他, RIBF-SHARAQ11 Collaboration, 「^{3}H(t, ^{3}He)^{3}n 反応による三中性子系質量欠損測定の遂行」, 日本物理学会第 77 回年次大会 (2022 年), オンライン, 2022 年 3 月 15–19 日.

高橋浩之 (口頭発表), 島添健次, 鎌田圭, 羽場宏光, 百瀬敏光, 「多光子ガンマ線時間・空間相関型イメージング法の研究 1(全体概要)」, 2022 年第 69 回応用物理学会春季学術講演会, 相模原市/オンライン, 2022 年 3 月 22–26 日.

島添健次 (口頭発表), 高橋浩之, 鎌田圭, 羽場宏光, 上ノ町水紀, 百瀬敏光, 大鐘健一朗, 「多光子ガンマ線時間・空間相関型イメージング法の研究 2 (システム開発)」, 2022 年第 69 回応用物理学会春季学術講演会, 相模原市/オンライン, 2022 年 3 月 22–26 日.

横北卓也 (口頭発表), 羽場宏光, 「Zr 及び Hf のスルファト錯体推定に向けた TOA/H_2SO_4 系の溶媒抽出」, 日本化学会第 102 春季年会 (2022), オンライン, 2022 年 3 月 23–26 日.

中川創太 (口頭発表), 角永悠一郎, 大江一弘, 寺本高啓, 床井健運, 神田晃充, 笠松良崇, 永田光知郎, 羽場宏光, 王洋, 吉村崇, 豊嶋厚史, 篠原厚, 「電解酸化反応を利用したアミノ酸へのアスタチン標識法の開発」, 日本化学会第 102 春季年会 (2022), オンライン, 2022 年 3 月 23–26 日.

麻生彩佳 (口頭発表), 兼田加珠子, 下山敦史, 角永悠一郎, 白神宜史, 渡部直史, 豊嶋厚史, 羽場宏光, 王洋, 篠原厚, 深瀬浩一, 「新規アルファ線核医学治療薬剤開発を目指した ^{211}At-FAPI の合成と評価」, 日本化学会第 102 春季年会 (2022), オンライン, 2022 年 3 月 23–26 日.

床井健運 (口頭発表), 豊嶋厚史, 大江一弘, 角永悠一郎, 寺本高啓, 中川創太, 今田彩香, 吉村崇, 笠松良崇, 羽場宏光, 王洋, 篠原厚, 「アスタチンのハロゲン結合エネルギー測定に向けた条件検討」, 日本化学会第 102 春季年会 (2022), オンライン, 2022 年 3 月 23–26 日.

合川正幸 (口頭発表), 花田幸奈, ダグワドルジ イチンホルロー, 羽場宏光, タカッチ サンドール, ディトロイ フェレンチ, ズーチ ゾルタン, 「カルシウム標的へのアルファ粒子入射反応による Sc 生成反応断面積測定」, 日本原子力学会 2022 年春の年会, オンライン, 2022 年 3 月 16–18 日.

上ノ町水紀 (口頭発表), 大鐘健一朗, Zhihong Zhong, 島添健次, 鎌田圭, 高橋浩之, Yang Wang, 羽場宏光, 「Compton-PET ハイブリッドカメラを用いた診断治療核種同時撮像検証」, 日本原子力学会 2022 年春の年会, オンライン, 2022 年 3 月 16–18 日.

Award

上ノ町水紀, "Double photon emission coincidence imaging with GAGG-SiPM Compton camera," 日本原子力学会放射線工学部会賞奨励賞, 2021 年 9 月.

Press Release

難治性甲状腺がんに対する医師主導治験を開始—アスタチンを用いた新しい標的アルファ線治療—, 大阪大学, 理化学研究所, 2021 年 11 月 29 日. https://www.riken.jp/pr/news/2021/20211129_1.

Patent

安良田寛, 中村伸悟, 栗原嵩司, 羽場宏光, 「量子線照射のための標的保持装置, システム, 標的, および方法」, 特願 2021-190640.

Outreach Activities

羽場宏光 (依頼講演), 「ニホニウム発見への道のり」, 大宮北高校 SSH 特別講演会, 大宮市, 2021 年 10 月 4 日.

羽場宏光（依頼講演）, 「新元素でがん治療 〜RIBF がつくるラジオアイソトープ〜」, 第 9 回理研イノベーションセミナー, オンライン, 2022 年 1 月 21 日.

羽場宏光（依頼講演）, 「ニホニウム発見への道のり」, 早稲田大学本庄高等学院課外講義, オンライン, 2022 年 3 月 12 日.

Others

小川美香子, 渡部直史, 上原知也, 清野泰, 永津弘太郎, 藤井博史, 小川数馬, 羽場宏光, 「短飛程放射線を活用した核医学治療薬剤の現状と将来」, 第 2 回日本アイソトープ協会シンポジウムパネル討論, オンライン, 2021 年 11 月 29 日.

出光一哉, 大越実, 羽場宏光, 福谷哲, 坂井章浩, 「研究施設等廃棄物の埋設事業へ向けた取り組みについて」, 日本原子力学会 2022 年春の年会バックエンド部会企画セッション, オンライン, 2022 年 3 月 17 日.

Accelerator Applications Research Division
RI Application Research Group
Industrial Application Research Team

1. Abstract

Industrial application research team handles non-academic activities at RIBF corresponding mainly to industries.

2. Major Research Subjects

Support of industrial utilization of the RIBF accelerator beam.

3. Summary of Research Activity

RNC promote facility-sharing program "Promotion of applications of high-energy heavy ions and RI beams." In this program, RNC opens a part of the RIBF facility, which includes the AVF cyclotron, RILAC, RIKEN Ring Cyclotron and experimental instruments, to non-academic proposals from users including private companies. The proposals are reviewed by a program advisory committee, industrial PAC (IN-PAC). The proposals which have been approved by the IN-PAC are allocated with beam times and the users pay RIKEN the beam time fee. The intellectual properties obtained by the use of RIBF belong to the users. In order to encourage the use of RIBF by those who are not familiar with utilization of ion beams, the first two beam times of each proposal can be assigned to trial uses which are free of beam time fee.

In July 2021, the IN-PAC met and approved fee-based proposals from private companies; two proposals from new companies and five proposals from continuously using companies. In January 2022, the IN-PAC held a mail review and approved two fee-based proposals from continuous users. In 2020, four companies executed 23 fee-based beamtimes, twelve of which utilized a Kr beam with a total beam time of 221 h, nine utilized an Ar beam with a total beam time of 120 h and two of which utilized a Xe beam with a total beam time of 20 h.

Members

Team Leader

Atsushi YOSHIDA

Research Consultant

Tadashi KAMBARA

List of Publications & Presentations

Other

Fee-based beamtimes for private companies: Kr beam 221 h, Ar beam 120 h, Xe beam 20 h.

Subnuclear System Research Division
Quantum Hadron Physics Laboratory

1. Abstract

Atomic nuclei are made of protons and neutrons bound by the exchange of pion and other mesons. Also, protons and neutrons are made of quarks bound by the exchange of gluons. These strong interactions are governed by the non-Abelian gauge theory called the quantum chromodynamics (QCD). On the basis of theoretical and numerical analyses of QCD, we study the interactions between the nucleons, properties of the dense quark matter realized at the center of neutron stars, and properties of the hot quark-gluon plasma realized in the early Universe. Strong correlations common in QCD and cold atoms are also studied theoretically to unravel the universal features of the strongly interacting many-body systems. Developing perturbative and non-perturbative techniques in quantum field theory and string theory are of great importance not only to solve gauge theories such as QED and QCD, but also to find the theories beyond the standard model of elementary particles. Various theoretical approaches along this line have been attempted.

2. Major Research Subjects

(1) Perturbative and non-perturbative methods in quantum field theories
(2) Quantum computing
(3) Lattice gauge theory
(4) QCD under extreme conditions
(5) Nuclear and atomic many-body problems

3. Summary of Research Activity

(1) Perturbative and non-perturbative methods in quantum field theories

(1-1) Theory of the anomalous magnetic moment of the electron

The anomalous magnetic moment of the electron ae measured in a Penning trap occupies a unique position among high precision measurements of physical constants in the sense that it can be compared directly with the theoretical calculation based on the renormalized quantum electrodynamics (QED) to high orders of perturbation expansion in the fine structure constant α, with an effective parameter α/π. Both numerical and analytic evaluations of ae up to $(\alpha/\pi)^4$ were firmly established. The coefficient of $(\alpha/\pi)^5$ has been obtained recently by an extensive numerical integration. The contributions of hadronic and weak interactions have also been estimated. The sum of all these terms leads to a_e (theory) = 1 159 652 181.606 (11)(12)(229) $\times 10^{-12}$, where the first two uncertainties are from the tenth-order QED term and the hadronic term, respectively. The third and largest uncertainty comes from the current best value of the fine-structure constant derived from the cesium recoil measurement: α^{-1} (Cs) = 137.035 999 046 (27). The discrepancy between a_e (theory) and a_e (experiment) is 2.4σ. Assuming that the standard model is valid so that a_e (theory) = a_e (experiment) holds, we obtained $\alpha^{-1}(a_e)$ = 137.035 999 1496 (13)(14)(330), which is nearly as accurate as α^{-1} (Cs). The uncertainties are from the tenth-order QED term, hadronic term, and the best measurement of a_e, in this order.

(1-2) Transport theory of chiral fermions under external gravity and fluid field

We formulated the kinetic theory of chiral matter in external gravitational fields, based on quantum field theory. The resulting kinetic theory reveals that the Riemann curvature induces non-dissipative transport phenomena of chiral fermions. In particular, we found that the spin-gravity coupling results in the antiparallel flow of the charge current and energy current of fermions, which is never explained in the classical picture. These novel framework and phenomena takes place not only in cosmological systems involving neutrinos but also in chiral matter affected by background fluid, such as quark-gluon plasma, graphene and Dirac/Weyl semimetals. We demonstrated that a temperature gradient and fluid vorticity induce a pressure correction and charge and energy flow in Dirac/Weyl semimetals.

(1-3) Spin transport of massive fermion

We derived the spin kinetic theory under external electromagnetic and gravitational fields. We derived the global equilibrium conditions from the kinetic equations and find that the finite Riemann curvature or an external electromagnetic field is necessary to determine the spin-thermal vorticity coupling. Solving the equation of motion of axial vector part of the Wigner transformed fermion propagator, we evaluated the Pauli-Lubanski vector, which expresses the spin polarization of massive fermions, at the local equilibrium and out of equilibrium. This formula is potentially important of the Λ polarization puzzle found in heavy-ion collisions, which cannot be understood in the calculations based on global equilibrium assumption.

(1-4) Chiral vortical effect in condensed matter systems

We revisited the chiral vortical effect in condensed matter physics, by using the semiclassical wave-packet theory. In high-energy physics, the chiral vortical current is conventionally defined as the Noether current. Such a definition is however improper in the context of condensed matter systems since there potentially exists the contributions of the magnetization current. Indeed we showed that the chiral vortical current is compensated by the magnetization current. Hence the chiral vortical effect cannot be observed in pseudo-relativistic condensed matter systems, such as Dirac/Weyl semimetals. Instead, we demonstrated that the chiral vortical effect is an observable in several nonrelativistic matter, and suggested possible table-top experimental setups.

(1-5) Conformal field theories and time-developments in higher dimensions

In quantum field theories, symmetry plays an essential and exceptional role. Focusing on some proper symmetry and delving into its meaning have been proven to be one of the most fruitful strategies. We try to extend the result obtained in two-dimensional conformal field theory using the formalism developed in a study of sine-square deformation of Euclidean conformal field theory to

higher dimensional conformal field theory with both Euclidean and Lorentzian metric. Here the time developments of the system are chosen to honor the conformal symmetry of the system, yet they are classified into three distinct categories, each corresponds the cases found in the study of two-dimensional conformal field theory.

(2) Quantum computing

(2-1) Hybrid quantum annealing via molecular dynamics

A novel quantum-classical hybrid scheme was proposed to efficiently solve large-scale combinatorial optimization problems. The key concept is to introduce a Hamiltonian dynamics of the classical flux variables associated with the quantum spins of the transverse-field Ising model. Molecular dynamics of the classical fluxes can be used as a powerful preconditioner to sort out the frozen and ambivalent spins for quantum annealers. It was demonstrated that the performance and accuracy of our smooth hybridization are better in comparison to the standard classical algorithms (the tabu search and the simulated annealing) by employing the MAX-CUT and Ising spin-glass problems.

(3) Lattice gauge theory

(3-1) Dibaryon with highest charm number near unitarity from lattice QCD

A pair of triply charmed baryons, $\Omega_{ccc}\Omega_{ccc}$, is studied as an ideal dibaryon system by (2+1)-flavor lattice QCD with nearly physical light-quark masses and the relativistic heavy quark action with the physical charm quark mass. The spatial baryon-baryon correlation is related to their scattering parameters on the basis of the HAL QCD method. The $\Omega_{ccc}\Omega_{ccc}$ in the $^1S_0^0$ channel taking into account the Coulomb repulsion with the charge form factor of Ω_{ccc} leads to the scattering length $a_0^C \simeq -19$ fm and the effective range $r_{\rm eff}^C \simeq 0.45$ fm. The ratio $r_{\rm eff}^C/a_0^C \simeq -0.024$, whose magnitude is considerably smaller than that of the dineutron (-0.149), indicates that $\Omega_{ccc}\Omega_{ccc}$ is located in the unitary regime.

(3-2) Emergence of the ρ resonance from the HAL QCD potential in lattice QCD

We investigate the $I = 1$ $\pi\pi$ interaction using the HAL QCD method in lattice QCD. We employ the (2+1)-flavor gauge configurations at $m_\pi \approx 411$ MeV, in which the ρ meson appears as a resonance state. We find that all-to-all propagators necessary in this calculation can be obtained with reasonable precision by a combination of three techniques, the one-end trick, the sequential propagator, and the covariant approximation averaging (CAA). The non-local $I = 1$ $\pi\pi$ potential is determined at the next-to-next-to-leading order (N2LO) of the derivative expansion for the first time, and the resonance parameters of the ρ meson are extracted. The obtained ρ meson mass is found to be consistent with the value in the literature. This opens up new possibilities for the study of resonances in lattice QCD.

(3-3) Stress tensor around static quark-anti-quark from Yang-Mills gradient flow

The spatial distribution of the stress tensor around the quark-anti-quark pair in SU(3) lattice gauge theory was studied. The YangMills gradient flow plays a crucial role to make the stress tensor well-defined and derivable from the numerical simulations on the lattice. The resultant stress tensor with a decomposition into local principal axes shows, for the first time, the detailed structure of the flux tube along the longitudinal and transverse directions in a gauge invariant manner. The linear confining behavior of the potential at long distances is derived directly from the integral of the local stress tensor.

(4) QCD under extreme conditions

(4-1) Finite density QCD based on complex Langevin method

The complex Langevin method (CLM) is one of a promising approach to overcome the sign problem. The central idea of this approach is that the stochastic quantization does not require the probabilistic interpretation of the Boltzmann weight e^{-S} even when the action takes complex values. Although the equivalence between CLM and the familiar path integral quantization is quite nontrivial, it is pointed out that the probability distribution of the drift term can judge the correctness of the CLM. This enable us to perform lattice simulation of QCD based on CLM in the finite density region in a self-contained manner. We discussed the applicability of the CLM with four-flavor staggered fermions on a $8^3 \times 16$ lattice with quark mass $m = 0.01$. In particular, we focus on the behavior of the eigenvalue distribution of the fermion mass matrix which is closely related to the appearance of the singular drift problem.

(4-2) Non-equilibrium quantum transport of chiral fluids from kinetic theory

We introduced the quantum-field-theory (QFT) derivation of chiral kinetic theory (CKT) from the Wigner-function approach, which manifests side jumps and non-scalar distribution functions associated with Lorentz covariance and incorporates both background fields and collisions. The formalism is utilized to investigate second-order responses of chiral fluids near local equilibrium. Such nonequilibrium anomalous transport is dissipative and affected by interactions. Contributions from both quantum corrections in anomalous hydrodynamic equations (EOM) of motion and those from the CKT and Wigner functions (WF) are considered in a relaxation-time approximation (RTA). Anomalous charged Hall currents engendered by background electric fields and temperature/chemical-potential gradients are obtained. Furthermore, chiral magnetic/vortical effects (CME/CVE) receive viscous corrections as non-equilibrium modifications stemming from the interplay between side jumps, magnetic-moment coupling, and chiral anomaly.

(4-3) Hadron-quark crossover in cold and hot neutron stars

We presented a much improved equation of state for neutron star matter, QHC19, with a smooth crossover from the hadronic regime at lower densities to the quark regime at higher densities. We now use the Togashi *et al*. equation of state, a generalization of the Akmal-Pandharipande-Ravenhall equation of state of uniform nuclear matter, in the entire hadronic regime; the Togashi equation of state consistently describes nonuniform as well as uniform matter, and matter at beta equilibrium without the need for an interpolation between pure neutron and symmetric nuclear matter. We describe the quark matter regime at higher densities with the Nambu-JonaLasinio model, now identifying tight constraints on the phenomenological universal vector repulsion between quarks and the

pairing interaction between quarks arising from the requirements of thermodynamic stability and causal propagation of sound. The resultant neutron star properties agree very well with the inferences of the LIGO/Virgo collaboration, from GW170817, of the pressure versus baryon density, neutron star radii, and tidal deformabilities. The maximum neutron star mass allowed by QHC19 is 2.35 MS, consistent with all neutron star mass determinations.

(4-4) Gluonic energy and momentum distribution at finite temperature

We studied the energy-momentum distribution of the gluons around a static quark at finite temperature on the basis of the effective field theory (EFT) of thermal QCD. Spatial correlations between the Polyakov loop and the energy-momentum tensor were calculated up to the next-to-leading order in EFT. The results were compared with the recent quenched lattice QCD calculation obtained by using the gradient flow formalism. The EFT results and the lattice QCD data agree quite well without any fitting parameters at high temperature above deconfinement. On the other hand, there is a substantial difference near the critical temperature especially in the distribution of the energy density, which indicates some non-perturbative effect.

(5) Nuclear and atomic many-body problems

(5-1) Density functional theory for nuclear structure

The atomic nuclei are composed of protons and neutrons interacting via the nuclear and Coulomb interactions. The density functional theory (DFT) is widely used to calculate the ground-state properties. Nevertheless, because of the lack of knowledge of nuclear interaction in medium (effective interaction), the effective interaction is fitted to experimental data, and it has been attained to develop a high-accuracy one. As the first step, the effective interaction of the charge symmetry breaking term, a part of the nuclear interaction, is proposed.

(5-2) Fundamental problems of density functional theory

The density functional theory (DFT) is one of the powerful methods to calculate ground-state properties of the quantum many-body problems, including atomic nuclei, atoms, molecules, and solids. The accuracy of the DFT depends on the energy density functional (EDF), which contains information on the interaction. We develop a method to calculate EDF for electronic systems purely microscopically using the functional renormalization group. In this method, energy density for so many various densities can be calculated, and eventually, DFT calculation can be performed without fitting energy density to some functional forms. We also develop the relativistic DFT in which the finite-light-speed correction to the Coulomb interaction is also considered to calculate the ground-state properties of super-heavy elements.

Members

Director

Masahiko IWASAKI

Vice Chief Scientist

Tsukasa TADA

Research/Technical Scientist

Takumi DOI (Senior Research Scientist)

Senior Scientist

Makiko NIO

Contract Researcher

Dang NGUYEN DINH

Special Postdoctoral Researchers

Matthias W.G. BERWEIN
Kazuya MAMEDA
Shoichiro TSUTSUI

Research Consultant

Takeo INAMI (Vietnam Academy of Sci. and Tech.)

Visiting Scientists

Shinya AOKI (Kyoto Univ.)
Tatsumi AOYAMA (KEK)
Gergely P. FEJOS (Eotvos Lorand Univ.)
Kenji FUKUSHIMA (Univ. of Tokyo)
Hideki HAMAGAKI (Nagasaki Inst. of Applied Sci.)
Koji HASHIMOTO (Osaka Univ.)
Masashi HAYAKAWA (Nagoya Univ.)
Tomoya HAYATA (Keio Univ.)
Takashi INOUE (Nihon Univ.)
Noriyoshi ISHII (Osaka Univ.)
Yuki KAMIYA (Helmholtz-Inst. fuer Strahlen- und Kernphysik Rheinische Friedrich-Wilhelms-Universitaet Bonn)
Phuc T. LE (Inst. of Fundamental and Applied Sci. Duy Tan Univ.)
Haozhao LIANG (Univ. of Tokyo)
Takaya MIYAMOTO (NEC Corporation)
Kenji MORITA (QST)
Masaki MURATA (Japan Univ. of Economics)
Atsushi NAKAMURA (Osaka Univ.)
Takashi NAKATSUKASA (Tsukuba Univ.)

Hung NGUYEN (Duy Tan Univ.)
Yoji OHASHI (Keio Univ.)
RHINE KUMAR ARAYAKKANDI KEECH (Cochin Univ. of Sci. and Tech.)
Shoichi SASAKI (Tohoku Univ.)
Kenji SASAKI (Kyoto Univ.)
Hiroshi SUZUKI (Kyushu Univ.)
Motoi TACHIBANA (Saga Univ.)

Student Trainees

Yutaro AKAHOSHI (Kyoto Univ.)
Asahi CHIKAOKA (Univ. of Tokyo)
Yixin GUO (Univ. of Tokyo)
Akira HIRAYAMA (Saitama Univ.)
Xun LIU (Univ. of Tokyo)
Yan LYU (Peking Univ.)
Kotaro MURAKAMI (Kyoto Univ.)
Tomoya NAITO (Univ. of Tokyo)

List of Publications & Presentations

Publications

[Original Papers]

T. Naito, G. Colò, H. Liang, X. Roca-Maza, and H. Sagawa, "Toward ab initio charge symmetry breaking in nuclear energy density functionals," Phys. Rev. C **105**, L021304 (2022).

Z. Wang, T. Naito, H. Liang, and W. H. Long, "Exploring effects of tensor force and its strength via neutron drops," Chin. Phys. C **45**, 064103 (2021).

G. Accorto, T. Naito, H. Liang, T. Nikšić, and D. Vretenar, "Nuclear energy density functionals from empirical ground-state densities," Phys. Rev. C **103**, 044304 (2021).

Y. Sekino, H. Tajima, and S. Uchino, "Optical spin transport in ultracold quantum gases," arXiv:2103.02418.

K. Mameda, N. Yamamoto, and D. -L. Yang, "Photonic quantum kinetic theory in curved spacetime and the spin Hall effect," Phys. Rev. D **105**, 096019 (2022).

T. M. Doi, H. Tajima, and S. Tsutsui, "Complex Langevin study for polarons in an attractively interacting one-dimensional two-component Fermi gas", Phys. Rev. Res. **3**, 033180 (2021).

Y. Akahoshi, S. Aoki, and T. Doi, "Emergence of the rho resonance from the HAL QCD potential in lattice QCD," arXiv:2111.15138.

S. Tsutsui, M. Hongo, S. Sato, and T. Sagawa, "Quantum hydrodynamics from local thermal pure states," arXiv:2106.12777.

H. Tajima, S. Tsutsui, T. M. Doi, and K. Iida, "Unitary p-wave Fermi gas in one dimension," Phys. Rev. A **104**, 023319 (2021).

T. Naito, "Effects of finite-light-speed correction for the Coulomb interaction on nuclear binding energies and radii in spherical nuclei," arXiv:2106.14270.

H. Tajima, S. Tsutsui, T. M. Doi, and K. Iida, "Three-body crossover from a Cooper triple to bound trimer statein three-component Fermi gases near a triatomic resonance," Phys. Rev. A **104**, 053328 (2021).

T. Yokota and T. Naito, "Construction of energy density functional for arbitrary spin polarization using functional renormalization group," Phys. Rev. B **105**, 035105 (2022).

H. Sotani, N. Nishimura, and T. Naito, "New constraints on the neutron-star mass and radius relation from terrestrial nuclear experiments," Prog. Theor. Exp. Phys. **2022**, 041D01 (2022).

N. Itagaki, T. Naito, and Y. Hirata, "Persistence of cluster structure in the ground state of ^{11}B," Phys. Rev. C **105**, 024304 (2022).

H. Tajima, Y. Sekino, and S. Uchino, "Optical spin transport theory of spin-1/2 topological Fermi superfluids," Phys. Rev. B **105**, 064508 (2022).

T. Yokota, Y. Asano, Y. Ito, H. Matsufuru, Y. Namekawa, J. Nishimura, A. Tsuchiya, and S. Tsutsui, "Perturbative predictions for color superconductivity on the lattice," arXiv:2111.14578.

S. Tsutsui, Y. Asano, Y. Ito, H. Matsufuru, Y. Namekawa, J. Nishimura, A. Tsuchiya, and T. Yokota, "Color superconductivity in a small box: a complex," arXiv:2111.15095.

H. Sagawa, S. Yoshida, T. Naito, T. Uesaka, J. Zenihiro, J. Tanaka, and T. Suzuki, "Isovector density and isospin impurity in ^{40}Ca," Phys. Lett. B **829**, 137072 (2022).

K. Murakami, Y. Akahoshi, S. Aoki, and K. Sasaki for HAL QCD Collaboration, "Investigations of decuplet baryons from meson-baryon interactions in the HAL QCD method," arXiv:2111.15563.

Y. Namekawa, S. Tsutsui, Y. Ito, H. Matsufuru, J. Nishimura, S. Shimasaki, and A. Tsuchiya, "Flavor number dependence of QCD at finite density by the complex Langevin method," arXiv:2112.00150.

Y. Akahoshi, S. Aoki, and T. Doi, "Emergence of the rho resonance from the HAL QCD potential," arXiv:2111.15138.

Y. Lyu, H. Tong, T. Sugiura, S. Aoki, T. Doi, T. Hatsuda, J. Meng, and T. Miyamoto, "Most charming dibaryon near unitarity," arXiv:2112.01682.

T. Doi, Y. Lyu, H. Tong, T. Sugiura, S. Aoki, T. Hatsuda, J. Meng, and T. Miyamoto, "Finite volume analysis on systematics of the derivative expansion in HAL QCD method," arXiv:2112.04997.

Y. Lyu, H. Tong, T. Sugiura, S. Aoki, T. Doi, T. Hatsuda, J. Meng, and T. Miyamoto, "Optimized two-baryon operators in lattice QCD," Phys. Rev. D **105**, 074512 (2022).

T. Naito, X. Roca-Maza, G. Colò, H. Liang, and H, Sagawa, "Isospin symmetry breaking in the charge radius difference of mirror nuclei," arXiv:2202.05035.

N. Itagaki and T. Naito, "Consistent description for cluster dynamics and single-particle correlation," Phys. Rev. C **103**, 044303 (2021).

Z. Wang, T. Naito, and H. Liang, "Tensor-force effects on shell-structure evolution in $N = 82$ isotones and $Z = 50$ isotopes in the relativistic Hartree-Fock theory," Phys. Rev. C **103**, 064326 (2021).

T. Naito, G. Colò, H. Liang, and X. Roca-Maza, "Second and fourth moments of the charge density and neutron-skin thickness of atomic nuclei," Phys. Rev. C **104**, 024316 (2021).

T. Naito, S. Endo, K. Hagino, and Y. Tanimura, "On deformability of atoms—comparative study between atoms and atomic nuclei," J. Phys. B **54**, 165201 (2021).

[Review Article]

内藤智也, 萩野浩一, 小林良彦, 「アイソスピンの符号の慣習をめぐって」, 日本物理学会誌 **77**, 99 (2022).

Presentations

[Domestic Conferences/Workshops]

内藤智也 (招待講演), 「原子核構造で探る中性子星」～中性子星の観測と理論～研究活性化ワークショップ 2021, 埼玉県和光市 (理化学研究所), 2021 年 8 月 10 日.

内藤智也 (招待講演), 「ミュオン波動関数計算コードの開発」, RCNP 研究会 「ミューオン X 線 γ 線分光—非破壊分析, 化学, 原子核物理への新展開・ミューオン原子核捕獲反応による原子核関連研究の可能性」, 大阪府茨木市 (大阪大学 核物理研究センター), 2022 年 3 月 25 日.

T. Naito, "Isospin symmetry breaking in ground-state properties," 85th DFT Meeting, 北海道札幌市 (北海道大学大学院理学研究院物理部門), 2022 年 1 月 25 日.

板垣直之, 内藤智也, 平田雄一, 「^{11}B のクラスター構造とその応用」, 日本物理学会 第 77 回年次大会, オンライン, 2022 年 3 月 15 日.

[Seminar]

内藤智也, 「Ab initio エネルギー密度汎関数に向けて」, 酒見グループセミナー (東京大学大学院理学系研究科附属原子核科学研究センター), オンライン, 2021 年 7 月 16 日.

Award

A. Hirayama, Student Presentation Award of the Physical Society of Japan, 2021 Autumn meeting.

Subnuclear System Research Division
Strangeness Nuclear Physics Laboratory

1. Abstract

We proposed accurate calculation method called 'Gaussian Expansion Method using infinitesimally shifted Gaussian lobe basis function.' When one proceeds to four-body systems, calculation of the Hamiltonian matrix elements becomes much laborious. In order to make the four-body calculation tractable even for complicated interactions, the infinitesimally-shifted Gaussian lobe basis function has been proposed. The GEM with the technique of infinitesimally-shifted Gaussians has been applied to various three-, four- and five-body calculations in hypernuclei, the four-nucleon systems, and cold-atom systems. As results, we succeeded in extracting new understandings in various fields.

2. Major Research Subjects

(1) Structure of Hypernuclei and neutron-rich nuclei from the view point of few-body problem
(2) Structure of exotic hadron system
(3) Quantum atomic systems and ultra-cold atomic systems
(4) Equation of state for neutron star

3. Summary of Research Activity

Motivaed by observation of Ξ hyperuclei, IBUKI, KINKA and IRRAWADDY events, to study Ξ N interaction, we study ^{14}N+Ξ hypernucleus withing the framework of relativistic mean field theory. We found that the *s*-wave interaction deduced from the HAL LQCD results is rather weak to obtain the energy difference between IRRAWADDY and KINKA events. The *p*-wave interaction is added and fitted to reproduce the energy difference. The resulting interaction together with the *s*-wave one gives a reasonable energy simultaneously for the IBUKI event as an excited Ξ *p* state.

(1) We investigate the role of interaction in the *p*-wave channel in a mixture of two kinds of fermions. We find that three-body bound states of 2+1 fermions which were known to exist only when the two kinds of fermions have very different masses, can in fact exist for any mass of the fermions when their interaction is taken into account in the *p*-wave channel.
(2) We predict a possible bound state of exotic titanium isotopes using the nuclear shell model based on the modern nuclear force. In addition, we study nucleon-Ξ interaction in nucleon-Ξ scattering and deuteron-Ξ scattering. For the former, we find that nucleon-Ξ interaction induces small coupling to deuteron continuum states, while, for the latter, the system shows small contribution of the coupling between nucleon-Ξ and Λ-Λ channels.

Members

Director
Emiko HIYAMA

Senior Research Scientists
Takumi DOI
Pascal NAIDON

Contract Researchers
Etsuko ITOU
Daisuke INOTANI

Special Postdoctoral Researcher
Tokuro FUKUI

Research Consultants
Shoji SHINMURA
Wolfram WEISE (TU Munich)

Senior Visiting Scientist
Makoto OKA (JAEA)

Visiting Scientists
Masayuki ASAKAWA (Osaka Univ.)
Kadir Utku CAN (The Univ. of Adelaide)
Jaume CARBONELL (Irène Joliot-Curie Lab.)
Akinobu DOTE (KEK)
Shimpei ENDO (Tohoku Univ.)
Tomokazu FUKUDA (Osaka Elec.-Com. Univ.)
Yasuro FUNAKI (Kanto Gakuin Univ.)
Takenori FURUMOTO (Yokohama Nat'l Univ.)
Philipp GUBLER (JAEA)
Satoru HIRENZAKI (Nara Women's Univ.)
Atsushi HOSAKA (Osaka Univ.)
Jinniu HU (Nankai Univ.)
Tetsuo HYODO (Tokyo Metropolitan Univ.)
Yoichi IKEDA (Kyushu Univ.)
Masahiro ISAKA (Hosei Univ.)
Souichi ISHIKAWA (Hosei Univ.)
Daisuke JIDO (Tokyo Tech.)
Hyun-Chul KIM (Inha Univ.)
Toshio MOTOBA (Osaka Elec.-Com. Univ.)
Takayuki MYO (Osaka Inst. of Tech.)

Sho NAGAO (Tohoku Univ.)
Satoshi NAKAMURA (Tohoku Univ.)
Kazuma NAKAZAWA (Gifu Univ.)
Hidekatsu NEMURA (Kyoto Univ.)
Jean-Marc RICHARD (Lyon Univ.)
Thomas RIJKEN (Univ. Of Nijmegen)
Shoichi SASAKI (Tohoku Univ.)
Hans-Josef SCHULZE (INFN)
Jirina STONE (Univ. of Tennessee)
Tingting SUN (Zhengzhou Univ.)
Hiroyuki TAJIMA (Univ. of Tokyo)
Hajime TOGASHI (Tohoku Univ.)
Masaaki TOKIEDA (INRIA)
Hui TONG (Tianjin Normal Univ.)
Atsushi UMEYA (Nippon Inst. of Tech.)
Shin WATANABE (NIT, Gifu College)
Chengjun XIA (Zhejiang Univ.)
Masanobu YAHIRO (Kyushu Univ.)
Ulugbek YAKHSHIEV (Inha Univ.)
Taiichi YAMADA (Kanto Gakuin Univ.)
Yasuo YAMAMOTO (Tsuru Univ.)
Nodoka YAMANAKA (Nagoya Univ.)
Takuma YAMASHITA (Tohoku Univ.)
Ying ZHANG (Tianjin Univ.)
Xian-Rong ZHOU (East China Normal Univ.)

Student Trainees

Naoto HASEGAWA (Tohoku Univ.)
Dongwook LEE (Kyushu Univ.)
Jie LIU (Nanjing Univ.)
Moemi MATSUMOTO (Tohoku Univ.)
Qi MENG (Nanjing Univ.)

Research Part-time Worker

Daisuke INOTANI (Research Part-time Worker I)

Administrative Part-time Worker

Yoko FUJITA (Administrative Part-time Worker I)

List of Publications & Presentations

Publications

[Original Papers]

Y. Tanimura, H. Sagawa, T. Sun, and E. Hiyama, "Ξ hypernuclei ($^{15}_{\Xi}$C and and $^{12}_{\Xi}$Be, and the Ξ*N* two-body interaction," Phys. Rev. C **105**, 044324 (2022).

Y. Zhang, H. Sagawa, and E. Hiyama, "Prediction of exotic hyperon halos in neutron-rich Zr hypernuclei," Prog. Theor. Exp. Phys. **2022**, 023D01 (2022).

Q. Meng, M. Harada, E. Hiyama, A. Hosaka, and M. Oka, "Doubly heavy tetraquark resonant states," Phys. Lett. B **824**, 136800 (2022).

M. Honda, E. Itou, Y. Kikuchi, and Y. Tanizaki, "Negative string tension of higher-charge Schwinger model via digital quantum simulation," PTEP **2022**, 033B01 (2022).

M. Honda, E. Itou, Y. Kikuchi, L. Nagano, and T. Okuda, "Classically emulated digital quantum simulation for screening and confinement in the Schwinger model with a topological term," Phys. Rev. D **105**, 014504 (2022).

T. Fukui, "Towards modeling cluster structure of ^{8}Be with chiral interaction," J. Phys. G **49**, 055102 (2022).

Y. Kamiya, K. Sasaki, T. Fukui, T. Hyodo, K. Morita, K. Ogata, A. Ohnishi, and T. Hatsuda, "Femtoscopic study of coupled-channel N-Ξ and ΛΛ interactions", Phys. Rev. C **105**, 014915 (2022).

L. Coraggio, G. D. Gregorio, A. Gargano, N. Itaco, T. Fukui, Y. Z. Ma, and F. R. Xu, "Shell-model study of titanium isotopic chain with chiral two- and three-body forces," Phys. Rev. C **104**, 054304 (2021).

J. Singh, T. Matsumoto, T. Fukui, and K. Ogata, "Three-body description of ^{9}C: Role of low-lying resonances in breakup reactions," Phys. Rev. C **104**, 034612 (2021).

K. Ogata, T. Fukui, Y. Kamiya, and A. Ohnishi, "Effect of deuteron breakup on the deuteron-Ξ correlation function," Phys. Rev. C **103**, 065205 (2021).

M. Tokieda and S. Endo, "Equivalence of dissipative and dissipationless dynamics of interacting quantum systems with its application to the unitary Fermi gas," Front. Phys. **9**, 730761 (2021).

[Proceedings]

E. Itou and Y. Nagai, "QCD viscosity by combining the gradient flow and sparse modeling methods," Proc. Sci. **LATTICE2021**, 214 (2021).

K. Ishiguro, K. Iida, and E. Itou, "Flux tube profiles in two-color QCD at low temperature and high density," Proc. Sci. **LATTICE2021**, 063 (2021).

T. Fukui, L. Coraggio, G. D. Gregorio, A. Gargano, N. Itaco, Y. Z. Ma, and F. R. Xu, "Realistic shell model with chiral interaction and its application to drip-line predictions," Few-Body Syst. **62**, 64 (2021).

A. Ohnishi, Y. Kamiya, K. Sasaki, T. Fukui, T. Hatsuda, T. Hyodo, K. Morita, and K. Ogata, "Femtoscopic study of NΞ interaction and search for the H dibaryon state around the NΞ threshold," Few-Body Syst. **62**, 42 (2021).

Presentations

[International Conferences/Workshops]

E. Hiyama (invited), "Recent progress of hypernuclear physics," International Conference on Light Cone 2021—Physics of Hadron on the Light Front, Online, November 29–December 4, 2021.

E. Hiyama (invited), "Few-body aspect of hypernuclear physics," JPS Symposium on Intersection of Nuclear Physics in Japan and the United States, Online, September 17, 2021.

E. Hiyama (invited), "Four-body structure of tetra-neutron system," Workshop on Neutron Unbound Systems Around the dripline, Online, July 13–14, 2021.

P. Naidon (invited), "Efimov physics and universality in few-body systems," Lecture at the School on Critical Stability of Few-body Quantum Systems, São Paulo, ICTP-SAIFR Brazil, Online, October 4–8, 2021.

E. Itou (oral), "Sparse modeling approach to obtaining the shear viscosity from smeared correlation functions," The 38th International Symposium on Lattice Field Theory (LATTICE 2021), Online, July 26–30, 2021.

E. Itou (invited), "Sparse modeling approach to obtaining the QCD shear viscosity from smeared correlation functions," ECT* online workshop "Tackling The Real-Time Challenge In Strongly Correlated Systems: Spectral Properties From Euclidean Path Integrals," Online, September 13–17, 2021.

E. Itou (invited), "Digital quantum simulation for screening and confinement in gauge theory with a topological term," RIKEN-Vancouver Joint Workshop on Quantum Computing, August 24–25, 2021.

T. Fukui (oral), "Cluster-model calculations with chiral interaction," Newcomers Seminar I, RIBF Nuclear Physics Seminar, Online, June 8, 2021.

[Domestic Conferences/Workshops]

肥山詠美子 (招待講演), 「ハイパー核の構造とハイペロン－核子間相互作用」, ELPH 研究会 C031 「多彩なビーム実験と多様な理論的手法で迫るハドロン間相互作用」, オンライン, 2021 年 11 月 4–5 日.

伊藤悦子 (招待講演), 「量子計算の場の理論への応用」, 金沢大学研究会「2022 計算物理学の発展」, オンライン, 2022 年 3 月 9 日.

伊藤悦子 (口頭発表), 「物理点におけるハドロン間力の計算に向けて—格子 QCD の配位生成」, 「富岳で加速する素粒子・原子核・宇宙・惑星」シンポジウム, オンライン, 2022 年 1 月 17–18 日.

伊藤悦子 (口頭発表), 「2 カラー QCD の低温高密度相における状態方程式」, 日本物理学会 2021 年秋季大会, オンライン, 2021 年 9 月 14–17 日.

伊藤悦子 (口頭発表), 「量子計算でみる負のストリングテンションの出現」, 日本物理学会 2021 年秋季大会, オンライン, 2021 年 9 月 14–17 日.

福井徳朗 (口頭発表), L. Coraggio, G. D. Gregorio, A. Gargano, N. Itaco, Y. Z. Ma, F. R. Xu, 「現実的殻模型で探る Ca および Ti のドリップライン」, 日本物理学会第 77 回年次大会, オンライン, 2022 年 3 月 15–17 日.

福井徳朗 (招待講演), 「『日本物理学会若手奨励賞受賞記念講演』3 体力の適正な取扱いに基づく第一原理殻模型計算の発展」, 日本物理学会第 77 回年次大会, オンライン, 2022 年 3 月 15–17 日.

福井徳朗 (口頭発表), 「カイラル相互作用に基づく現実的殻模型の進展」, 基研研究会「核力に基づいた原子核の構造と反応」, 京都市, 2021 年 12 月 7–10 日.

福井徳朗 (招待講演), "Frontiers of many-body calculations with chiral interaction," ELPH 研究会 C031 「多彩なビーム実験と多様な理論的手法で迫るハドロン間相互作用」, オンライン, 2021 年 11 月 4–5 日.

福井徳朗 (口頭発表), "Perspectives of many-body calculations with realistic nuclear force," RCNP での次期計画検討会, オンライン, 2021 年 9 月 27–29 日.

猪谷太輔 (招待講演), 「量子計算を用いた (1+1) 次元 Schwinger 模型における実時間ダイナミクスの解析」, 国内モレキュール型研究会「場の理論の量子計算 2022」, 京都市, 2022 年 2 月 24–25 日.

[Seminars]

P. Naidon, "Physics of ultra-cold atoms," Lecture at Tohoku University GPPU seminars, Decembeer 8, 2021.

P. Naidon, "Prediction of a "mixed bubble," quantum phase", RIBF Nuclear Physics Seminar, Online, September 7, 2021.

E. Itou, "Digital quantum simulation for screening and confinement in gauge theory with a topological term," RCNP Nuclear Physics Theory Seminar, July 16, 2021.

T. Fukui,「現実的殻模型の進展—カイラル 3 体力と諸現象—」, Seminar at CNS, University of Tokyo, Online, Japan, February 4, 2022.

Awards

E. Itou, "Editors' Choice" of Progress of Theoretical and Experimental Physics **2022**, Issue 3, March 2022.

福井徳朗, 第 16 回 (2022 年) 日本物理学会若手奨励賞 理論核物理領域 (第 23 回核理論新人論文賞).

Press Release

E. Itou, "Negative string tension of a higher-charge Schwinger model via digital quantum simulation," RIKEN Interdisciplinary Theoretical and Mathematical Sciences Program, March 9, 2022. https://ithems.riken.jp/ja/news/negative-string-tension-of-a-higher-charge-schwinger-model-via-digital-quantum-simulation.

Subnuclear System Research Division
Radiation Laboratory

1. Abstract

When Yoshio Nishina passed away in 1951, the research activities in Nishina's Laboratory in RIKEN were inherited by three laboratories, and Radiation Laboratory is the one of them. The Radiation Laboratory, whose legacy has been kept for 64 years, lead by F. Yamazaki, T. Hamada, M. Ishihara and last 21 years by H. En'yo, is closed in March 2022. In the last 28 years, we have proposed and built a polarized proton collider at RHIC, Relativistic Heavy Ion Collider at Brookhaven National Laboratory in the USA, and discovered that gluons in the proton carry a sizable portion of the proton spin which is 1/2. We also identified W bosons in the electron/positron decay channel and in the muon decay channel, with which we showed how much anti-quarks carry the proton spin. We were successful at RHIC to create Quark Gluon Plasma, the state of Universe just after the Big Bang. Such creation was confirmed through the many interesting discoveries such as "Jet Quenching," "Elliptic Particle Flows," "Thermal Photon Radiation" and so on. The RIKEN-CCJ, Linux-based Computer Cluster in Japan, was firstly built in Japan and is still operational in our laboratory and lead many analyses towards those discoveries. We have discovered the first hint of the restoration of Chiral Symmetry Breaking, the mechanism to create 99% of our weight, through the observation of phi meson mass-modification in nuclear matter at the 12-GeV Proton Synchrotron in KEK. This program is now acceded by the E16 experiment in J-PARC.

On the course of those experiments, we have conducted handful of technical developments, which include laser-induced novel ion sources, helical snake magnets for RHIC and AGS, fine-pitch silicon pixel detectors for PHENIX and sPHENIX experiments, high-performance trigger electronics, gas-electron-multipliers for hadron-blind detectors and trackers. With some of those new developments, we are preparing and starting new experiments at J-PARC and Fermilab to study the nature of hadron and preparing for the electron-ion collider (EIC) yet to be built at BNL in near future.

The legacy of our laboratory is taken over by RIKEN-BNL Research Center (RBRC) in BNL and by the new laboratory "RHIC Physics Research Group" headed by Y. Akiba in RIKEN Nishina Center for Accelerator-Based Science.

2. Major Research Subjects

(1) Spin physics with relativistic polarized-proton collisions at RHIC
(2) Study of nuclear matter at high temperature and/or at high density
(3) Technical developments on radiation detectors and accelerators

3. Summary of Research Activity

(1) Experimental study of spin structure of proton using RHIC polarized proton collider

[See also RIKEN-BNL Research Center Experimental Group for the activities at BNL]

After the previously published central-rapidity neutral and charged pion double-spin asymmetries at the highest collision energies at RHIC of 510 GeV now also the world's first direct photon results have been brought to publication. The direct photon probe also restricts the initial, hard interaction to be predominantly between a quark and a gluon thus further increasing the sensitivity to the gluon spin. It has therefore been considered the golden channel to access the gluon spin since the inception of the RHIC spin program more than two decades ago. Because of the electromagnetic interaction involved in the direct photon process the statistics are limited, compared to hadronic final states. Therefore, it took the largest polarized data set to finally be able to extract these double spin asymmetries. The results are found to be consistent with global fits of the previous hadron and jet measurements from RHIC as well as semi-inclusive DIS. All these results will be included in future global fits of all the existing experimental data in the world and will improve the sensitivity of quark and gluon spin contributions to the total spin of the nucleon.

While orbital angular momentum cannot be directly accessed at RHIC, several transverse spin phenomena have been observed which relate to orbital angular momentum and the three-dimensional structure of the nucleon. These phenomena by themselves have become a major field of research as the dynamics of the strong interaction can be studies with these functions. Various single spin asymmetry measurements have been obtained for various rapidities. When moving to central rapidities, these left-right asymmetries are known to be expectingly small for neutral pions. Since then, they have been confirmed to be small also for eta mesons. A substantially improved data set with significantly reduced uncertainties has been recently published in PRD for both final states. A recently published measurement by PHENIX for charged pions at mid-rapidity shows also small asymmetries but at the same time also a hint of a charge separation. Such a charge separation could originate from a flavor dependence and could also explain the smallness of the neutral meson asymmetries where the effects from up and down quark flavors could cancel each other out.

For the first time also direct photon single spin asymmetries have been extracted at RHIC. The direct photon asymmetries are again important here as they are only sensitive to the transverse spin effects in the initial state and not the fragmentation-related effects. Furthermore, it provides sensitivity to a gluon correlation function that is not accessible in other processes. The direct photon results have been published in PRL.

In June of 2017, an electro-magnetic calorimeter, RHICf, was installed in the most forward area of the STAR experiment and took polarized proton collision data for neutral particle production (neutron, photon, neutral pion). The cross-section measurement will give us new inputs to develop high-energy particle-collision models which are essential to understand air-shower from ultra-high energy cosmic rays. The first photon cross section measurements at very forward rapidities have recently been submitted for publication.

At similar rapidities also neutron asymmetries have been observed in the past. While previously only their general magnitude was obtained, using unfolding techniques it was possible to extract the first asymmetries as a function of the neutron transverse moment

for proton-proton collisions. The RHICf results have followed up these PHENIX results and, after confirming the consistency at small transverse momenta, extended the transverse momentum range significantly. These results are currently being prepared for publication. Similar PHENIX neutron asymmetries in proton-nucleus collisions have been analyzed as a function of both transverse and longitudinal momenta, as well as in (anti)correlation with hadronic detector activity elsewhere. These results have been published in PRD and clearly show the interplay between hadronic interactions that predominantly produce negative asymmetries and ultra-peripheral collisions that produce positive asymmetries and gain in relevance with heavier nuclei.

Some of us are participating in the Fermilab SeaQuest experiment as a pilot measurement of muon pairs from Drell-Yan process using a 120-GeV unpolarized proton at Fermilab. After finishing unpolarized measurements in 2017 to study the quark spin-orbit effect, a new measurement with a polarized proton target will start in 2022 to study the sea-quark orbit effect of the polarized proton in the target. The first result from the SeaQuest experiment on the asymmetry of the antimatter in the proton has been published in Nature.

For many jet related measurements fragmentation functions are necessary to gain spin and or flavor sensitivity. Those are currently extracted by some of us using the KEK-Belle data. In addition to using the fragmentation results with RHIC measurements, they will also provide the basis for most of the key measurements to be performed at the electron-ion collider. In 2021, a new fragmentation analysis of predominantly vector mesons and D mesons decaying into two or three light hadrons has been prepared and is in the process of being finalized. All these measurements are essential to nearly all nucleon structure measurements at RHIC, semi-inclusive DIS and the EIC.

As the Electron-Ion Collider is becoming a reality, many of us are participating in the various community efforts to define the physics goals of the EIC and how they inform on the choices of collisions energies, luminosities, and detector components. While the accelerator efforts are naturally led by the two main nuclear physics laboratories in the US, BNL and JLAB, a large EIC user group of more than 1200 members from all around the world is working on making the EIC a reality. During 2021, the first detector proposals were prepared with the selection of the first EIC detector by an external committee. The first detector is part of the DOE based EIC project. Given the participation in the sPHENIX experiment, we participated heavily in the ECCE proposal that also revolves around reusing the BABAR/sPHENIX magnet. We were leading the inclusive and semi-inclusive physics studies that showed the feasibility of the main EIC goals with such a detector. Others participated strongly in the detector considerations for an ECCE zero-degree calorimeter. At the end of 2021 the ECCE proposal was unanimously selected as the first EIC detector and is currently being prepared to form an actual collaboration.

(2) Experimental study of quark-gluon plasma using RHIC heavy ion collider

[See also RIKEN-BNL Research Center Experimental Group for the activities at BNL]

We have completed several key measurements in the study of quark-gluon plasma at RHIC. As the top of them, we lead the analysis of the first thermal photon measurement in heavy ion collisions. The measurement indicates that the initial temperature reached in the central Au + Au collision at 200 GeV is about 350 MeV, far above the expected transition temperature $T_c \sim 170$ MeV, from hadronic phase to quark-gluon plasma. This work was rewarded by Nishina Memorial Prize given to Y. Akiba in 2011. We also measured direct photons in d + Au and direct photon flow strength v_2 and v_3 in Au + Au.

We led measurement of heavy quark (charm and bottom) using VTX, a 4-layer silicon vertex tracker which we jointly constructed with US DOE. The detector was installed in PHENIX in 2011. PHENIX recorded approximately 10 times more data of Au+Au collisions in the 2014 run than the 2011 run. PHENIX recorded high statistics $p + p$ and $p + A$ data in 2015, and the doubled the Au + Au in 2016. PHENIX concluded its data taking in the 2016 run.

The results of the 2011 run were published in Physical Review C (Phys. Rev. C **93**, 034904 (2016)). This is the first publication from VTX. The result showed that the electrons from bottom quark decay is suppressed for $p_T > 4$ GeV/c, but the suppression factor is smaller than that of charm decay electrons for $3 < p_T < 4$ GeV/c. This is the first observation of bottom electron suppression in heavy ion collisions, and the first result that shows the bottom and charm suppression is different. A paper reporting the results of $b \to e$ and $c \to e$ measurement in the 2015 $p + p$ run has been published in Phys. Rev. D **99**, 092003 (2019). The centrality dependence of the suppression $b \to e$ and $c \to e$ from the 2014 Au+Au data has been submitted for publication. The results show clear quark mass dependence of energy loss in the QGP produced at RHIC. The 2016 run is the final data taking run of PHENIX, and this run doubled the dataset for heavy-flavor measurement with VTX. The production of nDSTs of the 2016 VTX data is completed and they are ready for physics analysis.

PHENIX published measurements of flow strength in p + Au, d + Au, and ^{3}He+Au (Nature Physics **15**, 214 (2019)). The results provide strong evidence for formation of small droplet of quark gluon plasma in collisions of small systems at RHIC.

In Wako we are operating a cluster computer system (CCJ) specialized to analyze huge data sets taken with the PHENIX detector. It consists of 25 nodes (17 old nodes and 8 new nodes) each of which has two CPUs and 10 sets of local disks for data repository (old node: quad-core CPU, 1 TB disk, new node: six-core CPU, 2 TB disk). There are 264 CPU cores and 380 TB disks in total. This configuration ensures the fastest disk I/O when each job is assigned to the node where the required data sets are stored. It is also important that this scheme does not require an expensive RAID system and network. Through this development we have established a fast and cost-effective solution in analyzing massive data.

The data of 1.1 PByte obtained by the PHENIX experiment is stored in a hierarchical storage system which is a part of HOKUSAI BigWaterfall/SailingShip supercomputer systems operated by the Head Office for Information Systems and Cybersecurity. In addition, we operate a dedicated server for the RHICf group and two servers for the J-PARC E16 group, to keep their dedicated compilation and library environments, and some data.

(3) Study of properties of mesons and exotic hadrons with domestic accelerators

Preparation of the experiment E16 at J-PARC Hadron experimental facility is underway with several Grant-in-Aids. This experiment aims to perform a systematic study of the spectral modification of low-mass vector mesons in nuclei to explore the physics of chiral symmetry breaking and restoration in dense nuclear matter, namely, the mechanism proposed by Nambu to generate most of hadron masses.

The Gas Electron Multiplier (GEM) technology is adopted for the two key detectors, GEM Tracker (GTR) and Hadron-blind Cherenkov detector (HBD). To improve electron-identification performance, lead-glass calorimeters (LG) are used in combination with HBD. We are in the production phase. Read-out electronics and trigger logic modules are also installed and tested. We have been a member of the CERN-RD51 collaboration to acquire the read-out technology for GEM. The MoU for RD51 was extended for the period of 2019–2023.

Due to the budgetary limitation, we aim to install a part of the detectors at the beginning of the experiment, eight modules of a set of GTR, HBD and LG, out of 26 modules in the full installation. J-PARC PAC (Program Advisory Committee) gave us a stage-2 approval in July 2017 to perform commissioning runs (Run 0). Although there is a significant delay from the originally planned date of March 2016, the construction of the beam line by KEK was completed finally in early 2020 to perform this experiment.

After the successful commissioning runs held in JFY 2020, we performed the second commissioning run in June 2021. Two-electron trigger to accumulate the data of vector meson decays were tested. The micro beam structures were newly found which deteriorates DAQ and trigger performances. Countermeasures for the structures were already discussed in cooperation with the accelerator group and Beam line group in J-PARC, and will be adopted in the coming beam time in the first quarter of 2023. On the other hand, detector performances were almost satisfied. In our plan, physics run will be performed in 2023–24, after the beam study. Approval of physics run will be discussed in PAC held in Summer 2022.

This activity is moved to Meson Science Laboratory after the closing of Radiation Laboratory.

(4) Detector development for PHENIX/sPHENIX experiment

The PHENIX experiment proposes substantial detector upgrades to go along the expected accelerator improvements, including the future electron-ion collider "EIC." The present PHENIX detector is repurposed to the sPHENIX (super PHENIX) detector which reuses the Babar solenoid magnet at SLAC and is covered by the hadronic calorimeter which was not available in the previous RHIC experiments. The sPHENIX was approved for the Project Decision-2/3 (corresponds to DOE's Critical Decision-2/3) in May 2019. We RIKEN group have been developing the one of the tracking devices of sPHENIX detector, so called intermediate tracker (INTT) since 2015. The INTT provides the best timing resolution among the sPHENIX tracking system, in conjunction with a time projection chamber and a MAPS based vertex detectors. The INTT silicon ladders have been demonstrated the satisfactory performance as designed through the three beam tests in 2018, 2019, and 2021 in Fermilab Test Beam Facility (FTBF) and Research Center for Electron Photon Science, Tohoku University. The production of silicon-ladder assembly was completed by Spring 2022 in the Taiwan Silicon Detector Facility (TSiDF) and in BNL. And the INTT barrel assembly has been started since June 2022 in BNL. The INTT barrel is scheduled to be installed to the beam line at the sPHENIX site in January 2023 followed by the sPHENIX commissioning in February 2023.

As the further investigation of the neutral pion production asymmetry discovered in the RHICf experiment, we started preparation for the next phase of the experiment, namely RHICf-II. Since physics data taking at RHIC in 2024, which is required for RHICf-II, will not be implemented, we are considering other possibilities to achieve its physics goal. The highlight of the upgraded experiment is to adopt a larger acceptance with higher position resolution for the zero-degree calorimeter (ZDC). The detector technology developed for the FoCAL upgrade project of the ALICE experiment at LHC well satisfies the RHICf-II performance requirement. We thus resumed the associated membership of the ALICE collaboration, and the RHICf-II detectors are to be developed together with the ALICE FoCAL collaboration. This new detector technology development is also a part of an essential R&D programs for a ZDC detector for EIC.

Members

Director

Hideto EN'YO

Senior Research Scientists

Yuji GOTO
Itaru NAKAGAWA
Ralf SEIDL
Satoshi YOKKAICHI

Contract Researcher

Tomonori TAKAHASHI

Special Postdoctoral Researcher

Koki KANNO

Research Associate
Wataru NAKAI

Junior Research Associate
Tomoki MURAKAMI

Special Temporary Research Scientist
Yasushi WATANABE

Senior Visiting Scientist
Toshiaki SHIBATA (Nihon Univ.)

Visiting Scientists
Kazuya AOKI (KEK)
Wen-Chen CHANG (Inst. of Phys., Academia Sinica)
Tatsuya CHUJO (Tsukuba Univ.)
Shoichi HASEGAWA (JAEA)
Motoi INABA (Tsukuba Univ. of Tech.)
Shunzo KUMANO (KEK)
Tsutomu MIBE (KEK)
Yuhei MORINO (KEK)
Ken-ichi NAKANO (Tokyo Tech)
Megumi NARUKI
Kyoichiro OZAWA (KEK)
Susumu SATO (JAEA)
Kenta SHIGAKI (Hiroshima Univ.)
Maya SHIMOMURA (Nara Women's Univ.)
Kiyoshi TANIDA (JAEA)

Visiting Technician
Che-Sheng LIN (Academia Sinica)

Student Trainees
Daichi ARIMIZU (Kyoto Univ.)
Shunsuke KAJIKAWA (Tohoku Univ.)
Natsuki KURODA (Nara Women's Univ.)
Shono KYAN (Tsukuba Univ.)
Miu MORITA (Nara Women's Univ.)
Tomoki MURAKAMI (Univ. of Tokyo)
Satomi NAKASUGA (Kyoto Univ.)
Yumika NAMIMOTO (Nara Women's Univ.)
Naoki OGATA (Kyoto Univ.)
Mika SHIBATA (Nara Women's Univ.)
Runa TAKAHAMA (Nara Women's Univ.)
Po-Hung WANG (Nat'l Central Univ.)

Interns
Hikaru IMAI (Rikkyo Univ.)
Miu MORITA (Nara Women's Univ.)
Yusuke NAKAMURA (Rikkyo Univ.)
Genta NAKANO (Rikkyo Univ.)
Yumika NAMIMOTO (Nara Women's Univ.)
Mika SHIBATA (Nara Women's Univ.)
Runa TAKAHAMA (Nara Women's Univ.)

Assistant
Keiko SUZUKI

List of Publications & Presentations

Publications

[Original Papers]

U. A. Acharya *et al*. (PHENIX Collaboration), "Improving constraints on gluon spin-momentum correlations in transversely polarized protons via midrapidity open-heavy-flavor electrons in $p \uparrow + p$ collisions at $\sqrt{s}$ = 200 GeV," e-Print: 2204.12899 [hep-ex], April 27, (2022).

U. A. Acharya *et al*. (PHENIX Collaboration), "Measurements of second-harmonic Fourier coefficients from azimuthal anisotropies in p+p, p+Au d+Au, and ^{3}He + Au collisions at $\sqrt{s_{NN}}$ = 200 GeV," e-Print: 2203.09894 [nucl-ex], March 18, (2022).

U. A. Acharya *et al*. (PHENIX Collaboration), "Study of ϕ-meson production in p+Al, p+Au, d+Au, and ^{3}He+Au collisions at $\sqrt{s_{NN}}$ = 200 GeV," Contribution to 2022 Snowmass Summer Study, e-Print:2203.06087 [nucl-ex], March 11, (2022).

U. A. Acharya *et al*. (PHENIX Collaboration), "Measurement of direct-photon cross section and double-helicity asymmetry at $\sqrt{s}$ = 510 GeV in $\vec{p} + \vec{p}$ collisions," e-Print: 2202.08158 [hep-ex], February 16, (2022).

U. A. Acharya *et al*. (PHENIX Collaboration), "Measurement of ψ (2S) nuclear modification at backward and forward rapidity in p+p, p+Al, and p+Au collisions at $\sqrt{s}$ = 200 GeV," e-Print: 2202.03863 [nucl-ex], February 8, (2022).

U. A. Acharya *et al*. (PHENIX Collaboration), "Transverse-single-spin asymmetries of charged pions at midrapidity in transversely polarized p+p collisions at $\sqrt{s}$ = 200 GeV," Phys. Rev. D **105**, 032003 (2022).

U. A. Acharya *et al*. (PHENIX Collaboration), "Systematic study of nuclear effects in p+Al, p+Au, d+Au, and ^{3}He+Au collisions at $\sqrt{s_{NN}}$ = 200 GeV using π^0 production," Phys. Rev. C **105**, 064902 (2022).

U. A. Acharya *et al*. (PHENIX Collaboration), "Transverse single spin asymmetries of forward neutrons in p+p, p+Al and p+Au collisions at $\sqrt{s_{NN}}$ = 200 GeV as a function of transverse and longitudinal momenta," Phys. Rev. D **105**, 032004 (2022).

U. A. Acharya *et al*. (PHENIX Collaboration), "Kinematic dependence of azimuthal anisotropies in p+Au, d+Au, and ^{3}He+Au at $\sqrt{s_{NN}}$ = 200 GeV, Phys. Rev. C **105**, 024901 (2022).

U. A. Acharya *et al*. (PHENIX Collaboration), "Probing gluon spin-momentum correlations in transversely polarized protons through midrapidity isolated direct photons in $p\uparrow + p$ collisions at $\sqrt{s}$ = 200 GeV," Phys. Rev. Lett. **127**, 162001 (2021).

U. A. Acharya *et al*. (PHENIX Collaboration), "Transverse single-spin asymmetries of midrapidity π^0 and η mesons in polarized p+p collisions at $\sqrt{s}$ = 200 GeV," Phys. Rev. D **103**, 052009 (2021).

U. A. Acharya *et al*. (PHENIX Collaboration), "Transverse momentum dependent forward neutron single spin asymmetries in transversely polarized p+p collisions at $\sqrt{s}$ = 200 GeV," Phys. Rev. D **103**, 032007 (2021).

O. Adriani *et al*. (RHICf Collaboration), "Performance of RHICf detector during operation in 2017," J. Instrum. **16**, P10027 (2021).

T. N. Takahashi *et al*., "Data acquisition system in the first commissioning run of the J-PARC E16 experiment," IEEE Trans. Nucl. Sci. **68**, 1907 (2021).

Presentations

[International Conferences/Workshops]

Y. Goto (invited), "Prospective physics study at EIC," 8th Asian Triangle Heavy-Ion Conference (ATHIC2021), Incheon, South Korea, Online, Novermber 9, 2021.

T. N. Murakami (poster), "Construction and operation of gas electron multiplier tracker for the J-PARC E16 experiment in run0," 2021 Virtual IEEE Nuclear Science Symposium, Online, October 16–23, 2021.

K. Kanno (invited), "Study of spectral change of vector mesons in nuclear medium at J-PARC," 2nd International Workshop on the Extension Project for the J-PARC Hadron Experimental Facility, Online, February 16–18, 2022.

S. Yokkaichi (invited), "J-PARC E16 has started—spectral change of vector mesons in nuclei—," Reimei Workshop, "Hadrons in dense matter at J-PARC", Tokai, Japan, Hybrid, February 21–23, 2022.

S. Nakasuga (poster), "Commissioning of the electron identification system for dilepton measurement in pA collisions at J-PARC," VCI2022 (The 16th Vienna Conference on Instrumentation), Online, February 21–25, 2022.

[Domestic Conferences/Workshops]

後藤雄二（招待講演), 「RHIC Spin Physics」, 日本物理学会 2021 年秋季大会, オンライン, 2021 年 9 月 17 日.

後藤雄二（口頭発表), 「PHENIX 実験での $\sqrt{s_{NN}}$ = 200 GeV 偏極陽子＋原子核衝突による超前方中性子のシングルスピン非対称度の横運動量依存性」, 日本物理学会 2021 年秋季大会, オンライン, 2021 年 9 月 16 日.

高橋智則 (招待講演), 「有限密度媒質中でのクォーク相関の解明に向けたレプトン対精密測定」, 第 6 回クラスター階層領域研究会, オンライン, 2021 年 6 月 14 日, 6 月 19 日.

高橋智則 (招待講演), 「J-PARC E16 実験の計測システムの現状と課題」, 計測システム研究会 2021, 九州大学 (福岡市), ハイブリッド, 2021 年 10 月 28–29 日.

村上智紀, 「J-PARC E16 実験 Run0 における GEM 飛跡検出器実機の性能評価」, 日本物理学会 第 77 回 年会, オンライン, 2022 年 3 月 15–19 日.

村上智紀, 「J-PARC 高運動量ビームラインを用いた原子核密度中における ϕ 中間子質量スペクトルの測定」, J-PARC ハドロン研究会, オンライン, 2022 年 3 月 22–24 日.

[Seminars]

H. En'yo, "Forty academic years with physics of high density nuclear matter (in Japanese)," Heavy Ion Pub, Nagoya University, Online, November 12, 2021.

H. En'yo, "My 40 years seeking for the new phase of nuclear matter (in Japanese)," ELPH Seminar, Research Center for Electron Photon Science (ELPH), Tohoku University, Sendai, Japan, Hybrid, December 23, 2021.

Press Release

"Direct Photons Offer Glimpse of Gluons' Dynamic Motion—PHENIX data validate approach for future studies of proton spin and structure—," October 12, 2011. https://www.bnl.gov/newsroom/news.php?a=119077,https://www.riken.jp/press/2021/20211015_1/index.html .

Subnuclear System Research Division
Meson Science Laboratory

1. Abstract

Particles like muons, pions, and kaons have finite lifetimes, so they do not exist in natural nuclei or matters. By implanting these particles into nuclei/matters, exotic phenomena in various objects can be studied from new point of view.

For example, kaon is the second lightest meson, which has strange quark as a constituent quark. It is expected that if one embeds mesons into nuclei, the sizes of the nuclei become smaller, and one can form a high-density object beyond the normal nuclear density. Study of this object could lead to better understanding of the origin of the mass of the matter and may reveal the quark degree of freedom beyond the quark-confinement. The other example is the weak interaction in nuclear matter. It can only be studied by the weak decay of hypernuclei, which have Lambda particle in the nuclei.

Muon provides even wider scope of studies, covering condensed matter physics as well as nuclear and atomic physics, and we are trying to extend the application field further into chemical and biological studies. For instance, stopping positively charged muon in a material, we obtain information on the magnetic properties or the local field at the muon trapped site (μSR). Injecting negatively charged muon to hydrogen gas, muonic hydrogen atom (μp) is formed. We use muonic atoms for proton magnetic radius measurement, muon catalyzed fusion and elemental analysis with muonic X-rays. We are also interested in precision measurement of muon property itself, such as muon anomalous magnetic moment ($g-2$).

In our research, we introduce different kind of impurities into nuclei/matters, and study new states of matter, new phenomena, or the object properties.

2. Major Research Subjects

(1) Study of meson property and interaction in nuclei
(2) Origin of matter mass/quark degree of freedom in nuclei
(3) Condensed matter and material studies with muon
(4) Nuclear and particle physics studies via muonic hydrogen
(5) Development of ultra cold muon beam, and its application from material science to particle physics

3. Summary of Research Activity

(1) Hadron physics at J-PARC, RIKEN-RIBF, GSI and SPring-8

Kaon and pion will shed a new insight to the nuclear physics. The recent discovery of deeply bound pionic atom enables us to investigate the properties of mesons in nuclear matter. At RIKEN-RIBF, we are preparing precise experimental study of the pionic atom. Very lately, we succeeded to discover kaonic nuclear bound state, "*K-pp*," at J-PARC. The yield dependence on momentum-transfer shows that observed system is unexpectedly small. We extended our study on $\Lambda(1405)$ that could be *K-p* bound state. By these experiments, we are studying the KN^- interaction, and clarify the nature of kaon in nuclei. At Spring-8 and at GSI, we are planning to study omega and η' nuclei. By these experiments, we aim to be a world-leading scientific research group using these light meta-stable particles.

(1-1) Deeply bound kaonic nuclei

J-PARC E15 experiment had been performed to explore the simplest kaonic nuclear bound state, "K^-pp". Because of the strong attraction between KN^-, the K^- in nuclei may attract surrounding nucleons, resulting in forming a deeply bound and extremely dense object. Measurement of the kaon properties at such a high-density medium will provide precious information on the origin of hadron masses, if the standard scenario of the hadron-mass-generation mechanism, in which the hadron masses are depends on matter density and energy, is correct. Namely, one may study the chiral symmetry breaking of the universe and its partial restoration in nuclear medium.

The E15 experiment was completed to observe the "K^-pp" bound state by the in-flight ^{3}He(K^-, n) reaction, which allows us the formation via the invariant-mass spectroscopy by detecting decay particles from "K^-pp". For the experiment, we constructed a dedicated spectrometer system at the secondary beam-line, K1.8BR, in the hadron hall of J-PARC.

With the Λpn final states obtained in the first stage experiment, we observed a kinematic anomaly in the Λp invariant mass near the mass threshold of M(K^--pp) (total mass of kaon and two protons) at the lower momentum transfer q region. We conducted a successive experiment to examine the nature of the observed kinematical anomaly in the Λpn final state, and we confirmed the existence of the bound state below the mass threshold of M(K^-pp) at as deep as the binding energy of 40 MeV. The momentum transfer q naturally prefers lower momentum for the bound state formation, but the observed event concentration extended having the form-factor parameter ~400 MeV/c. Based on the PWIA calculation, the data indicated that the "K^-pp" system could be as small as ~0.6 fm. It is astonishingly compact in contrast to the mean nucleon distance ~1.8 fm.

This observed signal shows that ***a meson (qq^-) forms a quantum state where baryons (qqq) exist as nuclear medium***, *i.e.*, a highly excited novel form of nucleus with a kaon, in which ***the mesonic degree-of-freedom still holds***. This is totally new form of nuclear system, which never been observed before.

(1-2) Precision X-ray measurement of kaonic atom

To study the KN^- interaction at zero energy from the atomic state level shift and width of kaon, we have performed an X-ray spectroscopy of atomic $3d \rightarrow 2p$ transition of negatively charged K-mesons captured by helium atoms. However, our first experiment is insufficient in energy resolution to see the K^--nucleus potential. Aiming to provide a breakthrough from atomic level observation,

we introduce a novel X-ray detector, namely superconducting transition-edge-sensor (TES) microcalorimeter offering unprecedented high energy resolution, being more than one order of magnitude better than that achieved in the past experiments using conventional semiconductor detectors. The experiment J-PARC E62 aims to determine $2p$-level strong interaction shifts of kaonic ^{3}He and ^{4}He atoms by measuring the atomic $3d \rightarrow 2p$ transition X-rays using TES detector with 240 pixels having about 23 mm^2 effective area and the average energy resolution of 7 eV (FWHM) at 6 keV. We carried out the experiment at J-PARC in June 2018 and successfully observed distinct X-ray peaks from both atoms. The energies were determined to be 6224.5 +/− 0.4 (stat) +/− 0.2 (syst) eV and 6463.7 +/− 0.3 (stat) +/− 0.1 (syst) eV, and widths to be 2.5 +/− 1.0 (stat) +/− 0.4 (syst) eV and 1.0 +/− 0.6 (stat) +/− 0.3 (syst) eV, for kaonic ^{3}He and ^{4}He, respectively. These values are nearly 10 times more precise than in previous measurements. The results exclude the large strong-interaction shifts and widths that are suggested by a coupled-channel approach and agree with calculations based on optical-potential models.

Another important X-ray measurement of kaonic atom would be $2p \rightarrow 1$ stransition of kaonic deuteron (K^--d). We have measured same transition of kaonic hydrogen (K^--p), but the width and shift from electro-magnetic (EM) value reflect only isospin average of the $K^{\rm bar}N$ interaction. We can resolve isospin dependence of the strong interaction by the measurements both for K^--p and K^--d. The experiment J-PARC E57 aims at pioneering measurement of the X-rays from K^--d atoms. Prior to full (stage-2) approval of the E57 proposal, we performed a pilot run with hydrogen target in March 2019.

(1-3) Deeply bound pionic atoms and η' mesonic nuclei

We have been working on precision spectroscopy of pionic atoms systematically, which leads to understanding of the non-trivial structure of the vacuum and the origin of hadron masses. The precision data set stringent constraints on the chiral condensate at nuclear medium. We are presently preparing for the precision systematic measurements at RIBF. A pilot experiment performed in 2010 showed a unprecedented results of pionic atom formation spectra with finite reaction angles. The measurement of pionic ^{121}Sn performed in 2014 provided high-precision data and set constraints on the pion-nucleus strong interaction, which led to deduction of the chiral condensate at the normal nuclear density. In 2021, systematic high precision spectroscopy of pionic Sn atoms were performed and the analysis is ongoing.

We are also working on spectroscopy of η' mesonic nuclei in GSI/FAIR. Theoretically, peculiarly large mass of η' is attributed to UA(1) symmetry and chiral symmetry breaking. As a result, large binding energy is expected for η' meson bound states in nuclei (η'-mesonic nuclei). From the measurement, we can access information about gluon dynamics in the vacuum via the binding energy and decay width of η'-nuclear bound state. In 2022, we performed a new experiment using a large solid angle detector of WASA at GSI to search for the η'-nucleus bound state with an enhanced signal-to-noise ratio.

(1-4) $^3_\Lambda$H lifetime puzzle and our approach

Three recent heavy ion experiments (HypHI, STAR, and ALICE) announced surprisingly short lifetime for $^3_\Lambda$H hyper-nucleus's *Mesonic Weak Decay* (MWD), which seems to be inconsistent with the fact that the $^3_\Lambda$H is a very loosely bound system. It is very interesting to study this with a different experimental approach. We proposed a direct measurement of $^3_\Lambda$H MWD lifetime with ~20% resolution at J-PARC hadron facility by using K-meson beam at 1 GeV/c. As for the feasibility test, we also measure $^4_\Lambda$H lifetime.

A Cylindrical Detector System (CDS) used in J-PARC E15/E31 experiment is employed to capture the delayed π^- as a weak decay product from $^{3,4}_\Lambda$H a calorimeter is installed in the very forward region to tag fast π^0 meson emission at ~0 degree, which ensures that the Λ hyperon production with small recoil momentum. By this selection, we can improve the ratio between $^{3,4}_\Lambda$H and quasi-free Λ and Σ background. A test beam for feasibility study with ^{4}He target has been conditionally approved by J-PARC PAC. We will conduct the experiment and to present the data in short.

(2) Muon science at RIKEN-RAL branch

The research area ranges over particle physics, condensed matter studies, chemistry and life science. Our core activities are based on the RIKEN-RAL Muon Facility located at the Rutherford-Appleton Laboratory (UK), which provides intense pulsed-muon beams. We have variety of important research activities such as particle/nuclear physics studies with muon's spin and condensed matter physics by muon spin rotation/relaxation/resonance (μSR).

(3) Condensed matter/materials studies with μSR

We share experimental equipment with those of RAL in order to make organization of RIKEN beam time schedules easier and to enhance the efficiency to carry out RIKEN's experiments. We use shared cryostats and manpower supports available from RAL as well we other experimental areas. Both two μSR spectrometers, ARGUS (Port-2) and CHRNUS (Port-4), are working well with maintenance supports provide from RAL. Among our scientific activities on μSR studies from year 2017 to 2021, following studies are most important subjects of material sciences at the RIKEN-RAL muon facility:

(1) Multi magnetic transitions in the Ru-based pyrochlore systems, $R_2Ru_2O_7$;
(2) Magnetic properties of the nano-cluster gold in the border of macro- and micro- scale;
(3) Novel magnetic and superconducting properties of nano-size La-based high-TC superconducting curates;
(4) Determination of muon positions estimated from density functional theory (DFT) and dipole-field calculations;
(5) Chemical muonic states in DNA molecules.

(3-1) Nuclear and particle physics studies via ultra-cold muon beam and muonic atoms

If we can improve muon beam emittance, timing and energy dispersion (so-called "ultra-cold muon"), then the capability of μSR studies will be drastically improved. The ultra-cold muon beam can stop in a thin foil, multi-layered materials and artificial lattices, so one can apply the μSR techniques to surface and interface science. The development of ultra-cold muon beam is also very important as the source of pencil-like small emittance muon beam for muon $g-2$ measurement.

Ultra-cold muon beam has been produced by laser ionization of muoniums in vacuum (bound system of μ^+ and electron). We developed a very promising materials for muonium production, laser ablated silica aerogel. We also developed a high power Lyman-α laser in collaboration with laser group at RIKEN. In this laser development, we succeeded to synthesize novel laser crystals Nd:YGAG and Nd:YSAG, which has an ideal wavelength property for laser amplification to generate Lyman-α by four-wave mixing in Kr gas cell. We are now building the actual muon source to be used for muon $g-2$. Basic design has been completed and the manufacture is in progress.

We are planning a precise measurement of proton Zemach radius (with charge and magnetic distributions combined) using the laser spectroscopy of hyperfine splitting energy in the muonic hydrogen atom. As a key parameter for designing the experiment, we need to know the quench rate of the muonic proton polarization. We are analyzing data on muonic deuterium and muonic proton polarization obtained in low pressure hydrogen gas.

Members

Director

Masahiko IWASAKI

Senior Research Scientists

Kenta ITAHASHI
Yue MA
Haruhiko OUTA
Fuminori SAKUMA
Isao WATANABE

Contract Researcher

Katsuhiko ISHIDA

Postdoctoral Researcher

Rie MURAYAMA

Junior Research Associates

Shun SEO
Muhamad UMAR

International Program Associates

Supparat CHAROENPHON
Muhammad CHE LAH
Li DENG
Anita PUTRI
Utami WIDYAISWARI

Research Consultant

Masayasu KAMIMURA

Senior Visiting Scientists

Hiroyuki NOUMI (Osaka Univ.)
Kazuhiro TANAKA (KEK)

Visiting Scientists

Tadashi ADACHI (Sophia Univ.)
Retno ASIH (Inst. Teknologi Sepuluh Nopember)
Fahmi ASTUTI (Inst. Teknologi Sepuluh Nopember)
Catalina Oana CURCEANU (INFN)
Zyun EZAWA (Tohoku Univ.)
Hiroyuki FUJIOKA (Tokyo Tech)
Masaki FUJITA (Tohoku Univ.)
Shuhei FUKUOKA (Hokkaido Univ.)
Takayuki GOTO (Sophia Univ.)
Maryam HASSANVAND (Isfahan Univ. of Tech.)
Wataru HIGEMOTO (JAEA)
Taichi HINOKIHARA (Univ. of Tokyo)
Ko-ichi HIRAKI (Fukushima Medical Univ.)
Satoru HIRENZAKI (Nara Women's Univ.)
Koichi ICHIMURA (Hokkaido Univ.)
Yasuyuki ISHII (Shibaura Inst. of Tech.)
Ryosuke KADONO (KEK)
Takayuki KAWAMATA (Tohoku Univ.)
Seiko KAWAMURA (JAEA)
Hikomitsu KIKUCHI (Univ. of Fukui)
Takuya KOBAYASHI (Saitama Univ.)
Yoji KOIKE (Tohoku Univ.)
Kenji MATSUDA (Univ. of Toyama)
Hiroyasu MATSUURA (Univ. of Tokyo)
Mototsugu MIHARA (Osaka Univ.)
Takaaki MINAMIDATE (Tokyo Univ. Sci)
Yasuhiro MIYAKE (KEK)
Takehito NAKANO (Ibaraki Univ.)
Takahiro NAMIKI (Univ. of Toyama)
Katsuhiko NISHIMURA (Univ. of Toyama)
Agustinus NUGROHO (Inst. Teknologi Bandung)
Kazuki OHISHI (Comprehensive Res. Org. for Sci. and Soc.)
Yu OISHI (KEK)
Dita PUSPITA SARI (Shibaura Inst. of Tech.)
Muhammad RAMADHAN (Univ. Pertahanan Republik Indonesia)
Irwan RAMLI (Univ. Cokroaminoto Palopo)
RISDIANA (Padjadjaran Univ.)
Lusi SAFRIANI (Padjadjaran Univ.)
Naohito SAITO (KEK)
Shinichi SHAMOTO (Comprehensive Res. Org. for Sci. and Soc.)

Ichiro SHIRAKI (Univ. of Yamanashi)
Shukri SULAIMAN (Univ. Sains Malaysia)
Takao SUZUKI (Shibaura Inst. of Tech.)
Takanori TANIGUCHI (Tohoku Univ.)
Andrea VACCHI (Udine Univ. (Italy))
Eberhard WIDMANN (Stefan Meyer Inst.)
Yasuhiro YAMAGUCHI (JAEA)
Ichihiro YAMAUCHI (Saga Univ.)
Yukio YASUI (Meiji Univ.)
Masaru YOSOI (Osaka Univ.)
Wan Nurfadhilah ZAHARIM (UNIVERSITI SAINS MALAYSIA)
Xu-Guang ZHENG (Saga Univ.)
Johann ZMESKAL (Austrian Academy of Sci.)

Research Fellow

Harison ROZAK (Shibaura Inst. of Tech.)

Student Trainees

Kanato HIGUCHI (Tokyo Tech)
Harison ROZAK (Shibaura Inst. of Tech.)
Manaka YOSHIDA (Tokyo Univ. Sci)

Assistants

Kumiko TAKAHASHI
Mitsue YAMAMOTO

List of Publications & Presentations

Publications

[Original Papers]

T. Hashimoto *et al*. (J-PARC E62 Collaboration), "Measurements of strong-interaction effects in kaonic-helium isotopes at sub-eV precision with X-ray microcalorimeters," Phys. Rev. Lett. **128**, 112503 (2022).

F. Sakuma *et al*. (J-PARC E15/E80 Collaboration), "Recent results and future prospects of kaonic nuclei at J-PARC," Few-Body Sys. **62**, 103 (2021).

C. Pizzolottoa, A. Sbrizzia, A. Adamczak, D. Bakalov, G. Baldazzie, M. Baruzzoa, R. Benoccih, R. Bertoni, M. Bonesinih, H. Cabrera, D. Cirrincione, M. Clemenza, L. Colace, M. Danailov, P. Danev, A. deBari, C. DeVecchi, M. DeVincenzik, E. Fasci, F. Fuschino, K. S. Gadedjisso-Tossou, L .Gianfrani, K. I shida, C. Labanti, V. Maggi, R. Mazza, A. Menegolli, E. Mocchiutti, S. Monzani, L. Moretti, G. Morgante, J. Niemela, A. Pullia, R. Ramponi, L. P. Rignanese, M. Rossella, M. Stoilov, L. Stoychev, J. J. Suárez-Vargas, L. Tortora, E. Vallazza, and A. Vacchi, "Measurement of the muon transfer rate from muonic hydrogen to oxygen in the range 70–336 K," Phys. Lett. A **403**, 127401 (2021).

T. Yamashita, K. Okutsu, Y. Kino, R. Nakashima, K. Miyashita, K. Yasuda, S. Okada, M. Sato, T. Oka, N. Kawamura, S. Kanda, K. Shimomura, P. Strasser, S. Takeshita, M. Tampo, S. Doiuchi, Y. Nagatani, H. Natori, S. Nishimura, A. D. Pant, Y. Miyake, and K. Ishida, "Time evolution calculation of muon catalysed fusion: Emission of recycling muons from a two-layer hydrogen film," Fusion Eng. Des. **169**, 112580 (2021).

A. D. Pant, K. Nagamine, E. Torikai, I. Shiraki, K. Shimomura, F. L. Pratt, H. Ariga-Miwa, K. Ishida, and J. S. Schultz, "Muonium response to low oxygen levels in haemoglobin and other biological aqueous solutions and potential application towards monitoring hypoxia," Nucl. Instrum. Methods Phys. Res. A **1010**, 165561 (2021).

M. D. Umar, K. Ishida, R. Murayama, D. P. Sari, U. Widyaiswari, M. Fronzi, I. Watanabe, and M. Iwasaki, "Muon-spin motion at the crossover regime between Gaussian and lorentzian distribution of magnetic fields," Prog. Theor. Exp. Phys. **2021**, 083101 (2021).

K. Okutsu, T. Yamashita, Y. Kino, R. Nakashima, K. Miyashita, K. Yasuda, S. Okada, M. Sato, T. Oka, N. Kawamura, S. Kanda, K. Shimomura, P. Strasser, S. Takeshita, M. Tampo, S. Doiuchi, Y. Nagatani, H. Natori, S. Nishimura, A. D. Pant, Y. Miyake, and K. Ishida, "Design for detecting recycling muon after muon-catalyzed fusion reaction in solid hydrogen isotope target," Fusion Eng. Des. **170**, 112712 (2021).

A. Green, K. Ishida, B. V. Hampshire, K. Butcher, M. Pollard, and A. D. Hillier, "Understanding roman gold coinage inside out," J. Archaeol. Sci. **134**, 105470 (2021).

J. Sugiyama, K. Ohishi, O. K. Forslund, M. Månsson, S. P. Cottrell, A. D. Hillier, and K. Ishida, "How Li diffusion in spinel $Li[Ni_{1/2}Mn_{3/2}]O_4$ is seen with $\mu^{\pm}$SR," Z. Phys. Chem. **236**, 799 (2022).

W. N. Zaharim, S. N. A. Ahmad, S. Sulaiman, H. Rozak, D. F. H. Baseri, N. A. M. Rosli, S. S. Mohd-Tajudin, L. S. Ang, and I. Watanabe, "Density functional theory study of 12mer single-strand Guanine oligomer and associated muon hyperfine interaction," ACS Omega **6**, 29641–29650 (2021).

A. Jamaludin, W. N. Zaharim, S. Sulaiman, H. Rozak, A. L. Sin, and I. Watanabe, "Density functional theory investigation of muon hyperfine interaction in guanine-cytosine double-strand DNA," J. Phys. Soc. Jpn. **91**, 024301 (2022).

S. Yoon, W. Lee, S. Lee, J. Park, H. Lee, Y. S. Choi, S.-H. Do, W. -J. Choi, W. -T. Chen, F. Chou, D. I. Gorbunov, Y. Oshima, A. Ali, Y. Singh, A. Berlie, I. Watanabe, and K. -Y. Choi1, "Quantum disordered state in the J_1-J_2 square-lattice antiferromagnet $Sr_2Cu(Te_{0.95}W_{0.05})O_6$," Phys. Rev. Res. **5**, 014441 (2021).

M. Miyajima, F. Astuti, T. Fukuda, M. Kodani, S. Iida, S. Asai, A. Matsuo, T. Masuda, K. Kindo, T. Hasegawa, Tatsuo C. Kobayashi, T. Nakano, I. Watanabe, and T. Kambe, "Spin-gap formation due to spin-peierls instability in π-orbital-ordered NaO_2," Phy. Rev. B **104**, L140402 (2021).

[Review Articles]

M. Cataldo, M. Clemenza, K. Ishida, and A. D. Hillier, "A novel non-destructive technique for cultural heritage: Depth profiling and elemental analysis underneath the surface with negative muons," Appl. Sci. **12**, 4237 (2022).

A.D. Hillier, S. J. Blundell, I. McKenzie, I. Umegaki, L. Shu, J. A. Wright, T. Prokscha, F. B. K. Shimomura, A. Berlie, H. Alberto, and I. Watanabe, "Muon spin spectroscopy," Nat. Rev. Meths. Primers **2**, 4 (2022).

I. Watanabe, D. P. Sari, R. Ramadhan, B. Adiperdana, and S. Sulaiman, "Muon-site determination in materials by using computational methods," J. Comput. Chem. Jpn. **19**, 115–123 (2020).

[Book]

A. D. Hillier, B. Hampshire, and K. Ishida, "Depth-dependent bulk elemental analysis using negative muons," in "Handbook of Cultural Heritage Analysis," S. D'Amico and V. Venuti (Eds.), Springer, 2022, pp. 23–44.

Presentations

[International Conferences/Workshops]

F. Sakuma (invited), "Light kaonic nuclei at J-PARC," Strangeness Nuclear Physics Workshop 2021, Online, December 18–19, 2021.

F. Sakuma (invited), "Summary of the *K-pp* bound-state observation in E15 and future prospects," International Conference on Exotic Atoms and Related Topics (EXA 2021), Online, September 13–17, 2021.

M. Iwasaki (invited), "Experimental study toward spin-parity assignment of the first Kaonic nuclear bound state, *K-pp*," STRANU: Hot Topics in STRANgeness NUclear and Atomic Physics, ECT*, Online, May 24–28, 2021.

T. Akaishi, "Experimental status toward the direct lifetime measurement of Hypertriton using the (K^-, π^0) reaction at J-PARC," Particles and Nuclei International Conference (PANIC), Online, September 5–10, 2021.

Y. Ma, "Towards solving the hypertriton lifetime puzzle with direct lifetime measurement: Update from J-PARC E73 experiment," 19th International Conference on Hadron Spectroscopy and Structure in memoriam Simon Eidelman (HADRON 2021), Online, July 26–31, 2021.

K. Ishida, "Muon *g*-2 experiment at J-PARC," 14th European Research Conference on Electromagnetic Interactions with Nucleons and Nuclei (EINN2021), Online, November 2–6, 2021.

[Domestic Conferences/Workshops]

石田勝彦,「ミュオン原子分子とスピン状態」, 新学術領域「宇宙観測検出器と量子ビームの出会い. 新たな応用への架け橋. 」, 第 1 回超低速負ミュオンビーム研究会, オンライン, 2021 年 12 月 20 日.

石田勝彦,「RIKEN-RAL 施設」, 第 12 回「Muon 科学と加速器研究」, 第 6 回「文理融合シンポジウム 量子ビームで歴史を探る—加速器が紡ぐ文理融合の地平—」,「ミュオンで見る磁性・超伝導物質研究の最前線」, 合同研究会, 豊中市（大阪大学）, 2022 年 1 月 6–8 日.

石田勝彦,「パルスミュオン施設でのミュオン科学研究」,「ミューオン X 線 γ 線分光 非破壊分析, 化学, 原子核物理への新展開」,「ミューオン原子核捕獲反応による原子核関連研究の可能性」, 合同研究会, 豊中市（大阪大学 RNCP）&オンライン, 2022 年 3 月 24 日.

Press Release

神田聡太郎, 下村浩一郎, 他「『理想の水素原子』で未知の物理現象を探索する, ミュオニウムのマイクロ波分光実験がスタート」, 高エネルギー加速器研究機構, J-PARC センター, 理化学研究所, 東京大学大学院理学系研究科, 東京大学大学院総合文化研究科, 2021 年 4 月 16 日.

Subnuclear System Research Division
RIKEN BNL Research Center

1. Abstract

The RIKEN BNL Research Center was established in April 1997 at Brookhaven National Laboratory with Professor T. D. Lee of Columbia University as its initial Director. The Center is dedicated to the study of strong interactions, including spin physics, lattice QCD and RHIC physics through the nurturing of a new generation of young physicists. Professor Lee was succeeded by BNL Distinguished Scientist, the former BNL director, N. P. Samios, who served until 2013. The other former BNL director, S. H. Aronson led the Center from 2013. Hideto En'yo succeeded the director position starting from JFY 2017. Support for RBRC was initially for five years and has been renewed four times, and presently extends to March 2023. The five year extension from April 2023 is agreed between BNL and RIKEN in order to cover the era of sPHENIX experiment which is the upgraded of the PHENIX experiment. Theoretical activities in the RBRC Theory and Computing Groups are closely and intimately related to those of the Nuclear Theory, High Energy Theory and Lattice Gauge Theory Groups at BNL. The RBRC Experimental Group jointly works with Radiation Laboratory at Wako RIKEN, the RHIC Spin Group at BNL, the RHIC Spin Physics community, and the PHENIX/sPHENIX collaboration. Radiation Laboratory at Wako is closed in March 2022, and its functions are taken over by the new laboratory "RHIC Physics Research Group" headed by Y. Akiba. BNL provides office space, management, computing and administrative support. The Deputy Director of RBRC is D. Morrison (BNL). In May 2021 Y. Hatta (BNL) becomes Theory Group leader, succeeding D. Kharzeev. Y. Akiba (RIKEN) is Experimental Group leader and T. Izubuchi (BNL) is Computing Group leader.

2. Major Research Subjects

Major research subjects of the theory group are
(1) Spin structure of proton;
(2) Gluon saturation at small-x;
(3) Physics of quark gluon plasma.

Major research subjects of the computing group are
(1) Search for new law of physics through tests for Standard Model of particle and nuclear physics;
(2) Dynamics of QCD and related theories;
(3) Theoretical and algorithmic development for lattice field theories, QCD machine design.

Major research subject of the experimental group are
(1) Experimental Studies of the Spin Structure of the Nucleon;
(2) Study of Quark-Gluon Plasma at RHIC;
(3) sPHENIX detector construction.

3. Summary of Research Activity

Summary of Research Activities of the three groups of the Center are given in the sections of each group.

Members

Director

Hideto EN'YO

Deputy Director

David P. MORRISON

Administrative Staff

Keiko IWANO (Administration Manager)
Pamela ESPOSITO (Administrative Assistant)
Maureen MCNEIL-SHEA (Administrative Assistant)

List of Publications & Presentations

Publications

[Original Papers]

See the lists of each group.

Presentations

[Seminars]

H. En'yo, "Forty academic years with physics of high density nuclear matter (in Japanese)", Heavy Ion Pub, Nagoya University, Online, November 12, 2021.

H. En'yo, "My 40 years seeking for the new phase of nuclear matter (in Japanese)", ELPH Seminar, Research Center for Electron Photon Science (ELPH), Tohoku University, Sendai, Japan, Hybrid, December 23, 2021.

Press Release

Direct Photons Offer Glimpse of Gluons' Dynamic Motion—PHENIX data validate approach for future studies of proton spin and structure—, October 12, 2011.
https://www.bnl.gov/newsroom/news.php?a=119077,
https://www.riken.jp/press/2021/20211015_1/index.html .

Subnuclear System Research Division
RIKEN BNL Research Center
Theory Group

1. Abstract

The efforts of the RBRC theory group are concentrated on the major topics of interest in High Energy Nuclear Physics, in particular, the physics explored by the RHIC experiment at Brookhaven National Laboratory (BNL). This includes: understanding of the Quark-Gluon Plasma (QGP); the nature of dense quark matter; the initial state in high energy collisions, the Color Glass Condensate and its evolution to QGP through a Glasma; QCD spin physics; physics relevant to the future Electron-Ion Collider at BNL.

2. Major Research Subjects

(1) Heavy Ion Collisions, QCD phase diagram
(2) Perturbative Quantum Chromo-Dynamics (QCD)
(3) Nucleon structure, mass and spin

3. Summary of Research Activity

(1) Phase diagram of QCD

The major goal of RHIC heavy-ion program is to map out the QCD phase diagram at finite temperature and density. Together with a collaborator, V. Skokov has determined the precise location of the Yang-Lee edge singularity for the Ising universality class using the functional renormalization group method and the epsilon expansion. This can be applied to the QCD phase diagram to determine the location of the QCD critical point (which belongs to the Ising universality class) at finite chemical potential.

(2) QCD at small x

The initial condition of heavy-ion collisions at RHIC is governed by the Color Glass Condensate (CGC) which is the universal form of matter in the high energy (small-x) limit of QCD. The RBRC scientists have made major contributions to this field, and the efforts continue to date. V. Skokov and collaborators showed that the Bose-Einstein correlation between two small-x gluons in the saturated environment can be experimentally probed via three-jet production in Deep Inelastic scattering. He also continued a project with M. Li on the first saturation corrections in pA collisions. Y. Mehtar-Tani and R. Boussarie further developed their proposal for a new semi-classical approach to gluon-mediated DIS processes. They derived a factorization formula that involves a novel gluon transverse momentum dependent (TMD) distribution function and showed that both the DGLAP and Regge limits are recovered.

(3) Jet quenching

Jets have become an important tool to uncover the transport properties of matter created in heavy-ion collisions and the nontrivial parton structure in the nucleon. These are important goals of the sPHENIX and EIC experiments. Y. Mehtar-Tani and collaborators showed that transverse momentum broadening of emergetic partons in QCD media can be formulated as a super-diffusive process due to non-local quantum corrections. This yields anomalous system size dependence of momentum broadening. They also showed that the momentum broadening exhibits geometric scaling and heavy tails akin to Levy random walks.

(4) Resummation for jet angular distribution

Y. Hatta and collaborators continued to study the impact of soft gluon resummation on the azimuthal angular correlation of jets. They calculated various types of angular correlation in lepton-jet production and inclusive dijet production in DIS, dijet production in pp collisions and lepton pair production in ultraperipheral collisions. They also studied the relative strengths of angular correlations from soft gluon resummation and the linearly polarized gluon distribution. It is shown that the former can overshadow the signal from the latter.

(5) $gT(x)$ contribution to single spin asymmetry

Y. Hatta and collaborators calculated the purely perturbative contribution to transverse single spin asymmetry which first arises in two-loop perturbation theory. It has been believed for more than 40 years that such a contribution is negligible. However, they have demonstrated that at the future Electron-Ion Collider, it can be comparable to other sources of single spin asymmetry such as three-parton correlation functions.

(6) Hydrodynamical simulation of heavy-ion collisions

C. Shen has developed a full 3+1-dimensiional dynamical framework based on Glauber geometry with string deceleration + hydrodynamics + hadronic transport model. This model provides good predictions for particle production in pp, pA and AA collisions from GeV to TeV energy regions. It is an essential tool to quantify baryon stopping at the RHIC BES phas II and study the origin of collectivity in ultra-peripheral collisions at RHIC and LHC.

(7) Signature of the gluon orbital angular momentum

Y. Hatta and collaborators proposed a novel observable for the experimental detection of the gluon orbital angular momentum that constitutes the proton spin sum rule. They proposed to study double spin asymmetry in diffractive dijet production in DIS. A concrete

numerical prediction is given for the kinematics of the Electron-Ion Collider.

Members

Group Leaders

Hideto EN'YO
Yoshitaka HATTA

RBRC Researchers

Yacine MEHTAR-TANI
Vladimir SKOKOV
Chun SHEN

Visiting Scientists

Hiromichi NISHIMURA (Keio Univ.)
Yuya TANIZAKI (North Carolina State Univ.)

List of Publications & Presentations

Publications

[Original Papers]

Y. Hatta, B. Xiao, F. Yuan, and J. Zhou, "Azimuthal angular asymmetry of soft gluon radiation in jet production," Phys. Rev. D **104**, 054037 (2021).

S. Benic, Y. Hatta, A. Kaushik, and H. Li, "$gT(x)$ contribution to single spin asymmetries in SIDIS," Phys. Rev. D **104**, 094027 (2021).

S. Bhattacharya, R. Boussarie, and Y. Hatta, "Signature of the gluon orbital angular momentum," Phys. Rev. Lett. **128**, 182002 (2022).

S. Alzhrani, S. Ryu, and C. Shen, "Lambda spin polarization in event-by-event relativistic heavy-ion collisions," arXiv:2203.15718.

D. Everett *et al*. [JETSCAPE Collaboration], "Role of bulk viscosity in deuteron production in ultrarelativistic nuclear collisions," arXiv:2203.08286.

W. Zhao, C. Shen, and B. Schenke, "Collectivity in ultra-peripheral Pb+Pb collisions at the large hadron collider," arXiv:2203.06094.

C. Shen and B. Schenke, "Longitudinal dynamics and particle production in relativistic nuclear collisions," arXiv:2203.04685.

A. De, C. Shen, and J. Kapusta, "Stochastic hydrodynamics meets hydro-kinetics," arXiv:2203.02134.

H. Mantysaari, B. Schenke, C. Shen, and W. Zhao, "Bayesian inference of the fluctuating proton shape," arXiv:2202.01998.

K. J. Sun, R. Wang, C. M. Ko, Y. G. Ma, and C. Shen, "Relativistic kinetic approach to light nuclei production in high-energy nuclear collisions," arXiv:2106.12742.

D. Oliinychenko and C. Shen, "Resonance production in PbPb collisions at 5.02 TeV via hydrodynamics and hadronic afterburner," arXiv:2105.07539.

G. Giacalone, B. Schenke, and C. Shen, "Constraining the nucleon size with relativistic nuclear collisions," Phys. Rev. Lett. **128**, 042301 (2022).

X. An *et al*., "The BEST framework for the search for the QCD critical point and the chiral magnetic effect," Nucl. Phys. A **1017**, 122343 (2022).

V. Vovchenko, V. Koch, and C. Shen, "Proton number cumulants and correlation functions in Au-Au collisions at $\sqrt{s_{NN}}$ = 7.7-200 GeV from hydrodynamics," Phys. Rev. C **105**, 014904 (2022).

C. Gale, J. F. Paquet, B. Schenke, and C. Shen, "Multimessenger heavy-ion collision physics," Phys. Rev. C **105**, 014909 (2022).

S. Ryu, V. Jupic, and C. Shen, "Probing early-time longitudinal dynamics with the Lambda hyperon's spin polarization in relativistic heavy-ion collisions," Phys. Rev. C **104**, 054908 (2021).

S. Wu, C. Shen, and H. Song, "Dynamically exploring the QCD matter at finite temperatures and densities: A short review," Chin. Phys. Lett. **38**, 081201 (2021).

G. Giacalone and C. Shen, "Manipulating strong electromagnetic fields with the average transverse momentum of relativistic nuclear collisions," Eur. Phys. J. A **57**, 230 (2021).

C. Chiu and C. Shen, "Exploring theoretical uncertainties in the hydrodynamic description of relativistic heavy-ion collisions," Phys. Rev. C **103**, 064901 (2021).

W. M. Serenone, J. G. P. Barbon, D. D. Chinellato, M. A. Lisa, C. Shen, J. Takahashi, and G. Torrieri, "Lambda polarization from thermalized jet energy," Phys. Lett. B **820**, 136500 (2021).

S. Cao *et al*. [JETSCAPE], "Determining the jet transport coefficient $\hat{q}$ from inclusive hadron suppression measurements using Bayesian parameter estimation," Phys. Rev. C **104**, 024905 (2021).

M. A. Lisa, J. G. P. Barbon, D. D. Chinellato, W. M. Serenone, C. Shen, J. Takahashi, and G. Torrieri, "Vortex rings from high energy central p+A collisions," Phys. Rev. C **104**, 011901 (2021).

P. Caucal and Y. Mehtar-Tani, "Universality aspects of quantum corrections to transverse momentum broadening in QCD media," arXiv:2203.09407.

R. Boussarie and Y. Mehtar-Tani, "Gluon-mediated inclusive deep inelastic scattering from regge to bjorken kinematics," arXiv:2112.01412.

P. Caucal and Y. Mehtar-Tani, "Anomalous diffusion in QCD matter," arXiv:2109.12041.

J. Barata, Y. Mehtar-Tani, A. Soto-Ontoso, and K. Tywoniuk, "Medium-induced radiative kernel with the Improved opacity expansion," J. High Energy Phys. **09**, 153 (2021).

Y. Mehtar-Tani, D. Pablos, and K. Tywoniuk, "Cone size dependence of jet suppression in heavy-ion collisions," Phys. Rev. Lett. **127**, 252301 (2021).

F. Rennecke and V. V. Skokov, "Universal location of Yang Lee edge singularity for a one-component field theory in $1 \leq d \leq 4$," arXiv:2203.16651.

H. Duan, A. Kovner, and V. V. Skokov, "Gluon quasiparticles and the CGC density matrix," Phys. Rev. D **105**, 056009 (2022).

M. Li and V. V. Skokov, "First saturation correction in high energy proton-nucleus collisions. Part III. Ensemble averaging," J. High Energy Phys. **01**, 160 (2022).

S. Mukherjee, F. Rennecke, and V. V. Skokov, "Analytical structure of the equation of state at finite density: Resummation versus expansion in a low energy model," Phys. Rev. D **105**, 014026 (2022).

A. Kovner, M. Li, and V. V. Skokov, "Probing gluon bose correlations in deep inelastic scattering," Phys. Rev. Lett. **128**, 182003 (2022).

M. Li and V. V. Skokov, "First saturation correction in high energy proton-nucleus collisions. Part II. Single inclusive semi-hard gluon production," J. High Energy Phys. **06**, 141 (2021).

M. Li and V. V. Skokov, "First saturation correction in high energy proton-nucleus collisions. Part I. Time evolution of classical Yang-Mills fields beyond leading order," J. High Energy Phys. **06**, 140 (2021).

T. Altinoluk, N. Armesto, A. Kovner, M. Lublinsky, and V. V. Skokov, "Angular correlations in pA collisions from CGC: multiplicity and mean transverse momentum dependence of v_2," Eur. Phys. J. C **81**, 583 (2021).

F. Oosterhof, J. de Vries, R. Timmermans, and U. van Kolck, "Nucleon decay in the deuteron," Phys. Lett. B **820**, 136525 (2021).

[Proceedings]

D. Oliinychenko and C. Shen, "Resonance production in Pb+Pb collisions at 5.02 TeV," EPJ Web Conf. **259**, 10008 (2022).

V. Vovchenko, V. Koch, and C. Shen, "Net-particle number fluctuations in a hydrodynamic description of heavy-ion collisions," EPJ Web Conf. **259**, 10011 (2022).

S. Ryu, S. McDonald, C. Shen, S. Jeon, and C. Gale, "Medium response from mini-jets and in-medium hadronization in relativistic heavy ion collisions," Proc. Sci. **HardProbes2020**, 160 (2021).

C. Shen, "Dynamic modeling for heavy-ion collisions," EPJ Web Conf. **259**, 02001 (2022).

Y. Mehtar-Tani, "A novel formulation of the unintegrated gluon distribution for DIS," Contribution to: DIS2021, arXiv:2110.02105.

R. Boussarie and Y. Mehtar-Tani, "On gauge invariance of transverse momentum dependent distributions at small x," Proc. Sci. **HardProbes2020**, 182 (2021).

Presentations

[International Conferences/Workshops]

Y. Hatta (invited), "Quarkonium production near threshold," CFNS Workshop on Open Questions in Photon-Induced Interactions, Stony Brook, USA, April 26–28, 2021.

Y. Hatta (invited), "Odderon measurements at the EIC," Saturation and Diffraction at the LHC and the EIC, ECT*, Italy, June 29–July 1, 2021.

Y. Hatta (invited), "Connection observables with different terms contributing to the proton mass," EICUG Summer Meeting, Remote Workshop, August 2–7, 2021.

Y. Hatta (invited), "Parton orbital angular momentum," QCD Structure of the Nucleon, University of Alcala, Spain, October 4–8, 2021.

Y. Hatta (invited), "Resummation of nonglobal logarithms," Simons Center Workshop on Particle Jets in Quantum Field Theory, Stony Brook, USA, March 21–25, 2022.

C. Shen (invited), "Computational challenges and opportunities in multi-messenger heavy-ion physics," OSG All-Hands Meeting 2022, March 14, 2022.

C. Shen (invited), "Challenges of hydrodynamic modeling at FAIR and NICA energies," The 3rd Workshop on Physics Performance Studies at FAIR and NICA, December 1, 2021.

C. Shen (invited), "Dynamical modeling of high energy nuclear collisions," The 8th Asian Triangle Heavy-Ion Conference, November 6, 2021.

C. Shen (invited), "Local polarization from hydrodynamics," The 6th International Conference on Chirality, Vorticity, and Magnetic Field in Heavy-Ion Collisions, November 2, 2021.

C. Shen (invited), "Dynamical modeling for heavy-ion collisions," Strangeness in Quark Matter 2021, May 18, 2021.

Y. Mehtar-Tani (invited), "Universality aspects of quantum corrections to transverse momentum broadening," Simons Center Workshop on Particle Jets in Quantum Field Theory, Stony Brook, USA, March 21–25, 2022.

Y. Mehtar-Tani (invited), "Jet quenching and quantum applications," MITP for the Youngst@rs event on "The Quantumness of Hard Probes," Online, January 17–21, 2022.

V. Skokov (invited), "Entropies and multiplicity distribution in DIS," RBRC Workshop: Small-x Physics in the EIC Era, Brookhaven National Laboratory, December 15–18, 2021.

V. Skokov (invited), "Universality driven analytic structure of QCD crossover," International Workshop, "FunQCD: from first principles to effective theories," Online, March 29–April1, 2021.

[Domestic Conference/Workshop]

Y. Hatta (invited), "Physics at EIC: Nucleon structure," J. Polym. Sci. Symposium, Online, September 17, 2021.

[Seminars]

Y. Hatta, "Gravitational form factors of the proton," Temple University, USA, November 15, 2021.

Y. Hatta, "Gravitational form factors of the proton," Sun Yat-sen University, China, November 18, 2021.

Y. Hatta, "Two topics in QCD spin," National Center for Nuclear Research, Poland, May 26, 2021.

Y. Hatta, "Azimuthal angular asymmetry of soft gluons in jet production," University of Bergen, Norway, March 1, 2022.

C. Shen, "Longitudinal dynamics and particle production in relativistic nuclear collisions," Wayne State PAN Seminar, February 4, 2022.

C. Shen, "Progress in dynamical modeling of heavy-ion collisions at high energy," NBI Heavy-ion Seminar, September 16, 2021.

C. Shen, "Going with the flow—Explore the nuclear phase diagram at the highest temperatures and densities," The Ohio State University, August 31, 2021.

C. Shen, "Probing early-time longitudinal dynamics with Lambda's spin polarization," Invited Nuclear Seminar, The BESTea Seminar, July 30, 2021.

Y. Mehtar-Tani, "Anomalous diffusion in QCD matter," Nuclear Theory Group Seminar, McGill University, Canada, Online, December 7, 2021.

Y. Mehtar-Tani, "Wave Turbulence and anomalous diffusion in QCD matter," Physics Colloquium, Tata Institute of Fundamental Research, India, Online, November 16, 2021.

Y. Mehtar-Tani, "Anomalous diffusion in QCD matter," Heavy Ion Tea Seminar, LBNL, USA, Online, Septetmber 7, 2021.

Y. Mehtar-Tani, "Wave turbulence and anomalous diffusion of jets in the QGP," ASU Theoretical Physics Colloquium, USA, Online, July 7, 2021.

Y. Mehtar-Tani, "The anatomy of jets in heavy ion collisions," BNL Physics Colloquium, Online, June 22, 2021.

V. Skokov, "Analytic structure of QCD crossover," Physics Department, Ben-Gurion University of the Negev, Israel, April 19, 2021.

Award

C. Shen, DOE early career award.

Subnuclear System Research Division
RIKEN BNL Research Center
Experimental Group

1. Abstract

RIKEN BNL Research Center (RBRC) Experimental Group studies the strong interactions (QCD) using RHIC accelerator at Brookhaven National Laboratory, the world first heavy ion collider and polarized $p + p$ collider. We have three major activities: Spin Physics at RHIC, Heavy ion physics at RHIC, and detector upgrades of PHENIX experiment at RHIC.

We study the spin structure of the proton using the polarized proton-proton collisions at RHIC. This program has been promoted by RIKEN's leadership. The first focus of the research is to measure the gluon spin contribution to the proton spin. Results from PHENIX π^0 measurement and STAR jet measurement has shown that gluons in the proton carry about 30% of the proton spin. This is a major milestone of the RHIC spin program. The second goal of the spin program is to measure the polarization of anti-quarks in the proton using $W \to e$ and $W \to \mu$ decays. The results of $W \to e$ measurement was published in 2016. The final results of $W \to \mu$ was published in 2018. The focus of the RHIC spin program is moved to study of transverse spin measurement.

The aim of Heavy ion physics at RHIC is to re-create Quark Gluon Plasma (QGP), the state of Universe just after the Big Bang. Two important discoveries, jet quenching effect and strong elliptic flows, have established that new state of dense matter is indeed produced in heavy ion collisions at RHIC. We are now studying the property of the QGP. We measured direct photons in Au + Au collisions for $1 < p_{\mathrm{T}} < 3$ GeV/c, where thermal radiation from hot QGP is expected to dominate. The comparison between the data and theory calculations indicates that the initial temperature of 300 MeV to 600 MeV is achieved. These values are well above the transition temperature to QGP, which is calculated to be approximately 160 MeV by lattice QCD calculations.

We had major roles in detector upgrades of PHENIX experiment, namely, the silicon vertex tracker (VTX) and muon trigger upgrades. The VTX is the main device to measure heavy quark (charm and bottom) production and the muon trigger is essential for $W \to \mu$ measurement. The results from the first run with VTX detector in 2011 was published. The results show that electrons from bottom quark decay is strongly suppressed at high p_{T}, but the suppression is weaker than that of charm decay electron for $3 < p_{\mathrm{T}} < 4$ GeV/c. PHENIX recorded 10 times as much Au + Au collisions data in each of the 2014 run and 2016 run. A paper on the suppression of electrons from charm and bottom decays in the 2014 run has been submitted for publication this year. The data shows clear different of the suppression of $b \to e$ and $c \to e$.

PHENIX completed its data taking in 2016. We are now working on construction of intermediate-silicon tracker INTT for sPHENIX, a new experiment at RHIC that will be installed in the PHENIX IR and to start taking data in 2023. Production of all ladders of INTT was complete, and the INTT detector is now being assembled at BNL. The INTT will be installed in sPHENIX in early 2023.

2. Major Research Subjects

(1) Experimental Studies of the Spin Structure of the Nucleon
(2) Study of Quark-Gluon Plasma at RHIC
(3) sPHENIX INTT detector

3. Summary of Research Activity

We study the strong interactions (QCD) using the RHIC accelerator at Brookhaven National Laboratory, the world first heavy ion collider and polarized $p + p$ collider. We have three major activities: Spin Physics at RHIC, Heavy ion physics at RHIC, and detector upgrades of PHENIX experiment. Y. Akiba (Experimental Group Leader) is the Spokesperson of PHENIX experiment since 2016.

(1) Experimental study of spin structure of proton using RHIC polarized proton collider

How is the spin of proton formed with 3 quarks and gluons? This is a very fundamental question in Quantum Chromodynamics (QCD), the theory of the strong nuclear forces. The RHIC Spin Project has been established as an international collaboration between RIKEN and Brookhaven National Laboratory (BNL) to solve this problem by colliding two polarized protons for the first time in history. This project also has extended the physics capabilities of RHIC.

The first goal of the Spin Physics program at RHIC is to determine the gluon contribution to proton spin. It is known that the spin of quark accounts for only 25% of proton spin. The remaining 75% should be carried either by the spin of gluons or the orbital angular momentum of quarks and gluons. One of the main goals of the RHIC spin program has been to determine the gluon spin contribution. Before the start of RHIC, there was little experimental constraint on the gluon polarization, ΔG.

PHENIX measures the double helicity asymmetry (A_{LL}) of π^0 production to determine the gluon polarization. Our most recent publication of π^0 A_{LL} measurement at 510 GeV shows non-zero value of A_{LL}, indicating that gluons in the proton is polarized. Global analysis shows that approximately 30% of proton spin is carried by gluon spin. PHENIX measured the parity-violating single spin asymmetry A_L of the W boson production in $p + p$ in wide rapidity range. The results of the W boson measurements were published in 2016 and 2018, and these results give constraints on the anti-quark polarization in the proton. The focus of the spin physics is now moved to the measurements of the single spin asymmetry A_N.

Figure 1 show the A_N of isolated direct photons in polarized $p + p$ collisions at $\sqrt{s} = 200$ GeV at midrapidity. This is the first precise measurement of the A_N of direct photons. The uncertainties of the results are a 50-fold improvement with respect to those of the only prior measurement. Direct photons are clean probe of proton structure with no contribution from final-state strong interactions.

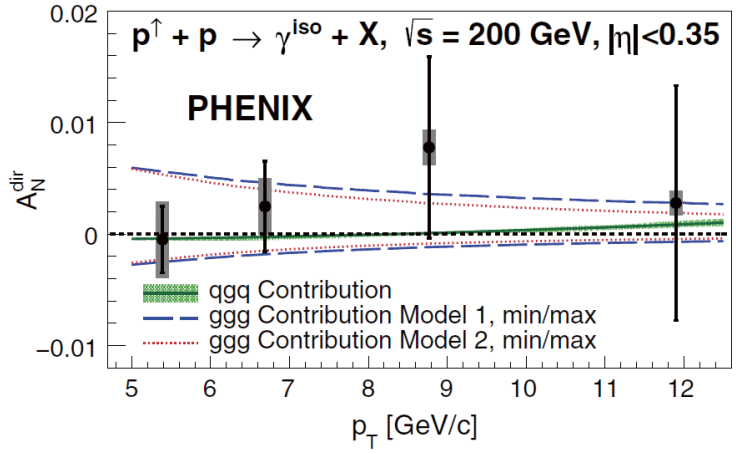

Fig. 1. Single spin asymmetry A_N of isolated direct photons in midrapidity in $p + p$ collisions at $\sqrt{s} = 200$ GeV compared with theoretical predictions of perturbative QCD. Published in Phys. Rev. Lett. **127**, 162001 (2021).

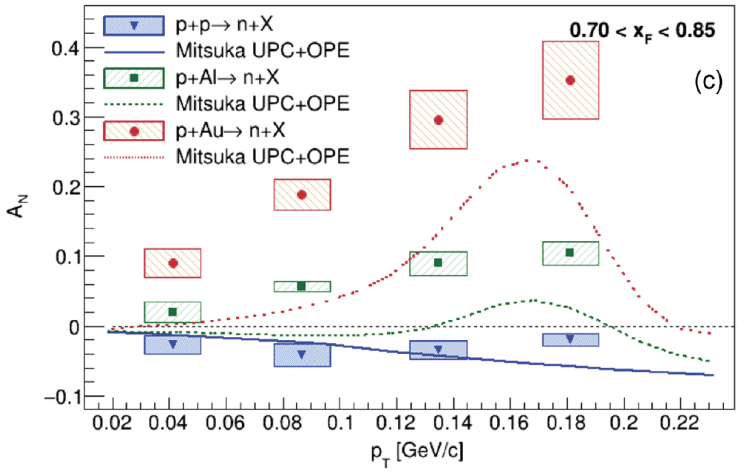

Fig. 2. Pt dependence of single spin asymmetry A_N of very forward neutron in $p + p$, p + Al, and p + Au. Published in Phys. Rev. D **105**, 032004 (2022).

These results constrain gluon spin-momentum correlations in transversely polarized protons. A paper of these results is published in Physical Review Letters.

Figure 2 shows $A_N(p_T)$ of very forward neutron in $p + p$, p + Al and p + Au collisions. A model based on hadronic interaction (OPE) and electromagnetic interaction (UPC) qualitatively describe the data. A paper reporting these results is published in Physical Review D.

Figure 3 shows $A_N(p_T)$ of charged pions in $p + p$ collisions at $\sqrt{s} = 200$ GeV at midrapidity. A paper reporting these results is published in Physical Review D.

Members of our group also participate in RHICf experiment, a small experiment at RHIC to measure particle production and single spin asymmetry of particles produced at very forward direction. Figure 3 shows $A_N(x_F)$ of very forward π^0 measured by RHICf compared with other experiments, published in Physical Review Letters. This is the first published results of RHICf experiment.

(2) Experimental study of Quark-Gluon Plasma using RHIC heavy-ion collider

The goal of high energy heavy ion physics at RHIC is study of QCD in extreme conditions *i.e.* at very high temperature and at very high energy density. Experimental results from RHIC have established that dense partonic matter is formed in Au + Au collisions at RHIC. The matter is very dense and opaque, and it has almost no viscosity and behaves like a perfect fluid. These conclusions are primarily based on the following two discoveries:

- Strong suppression of high transverse momentum hadrons in central Au + Au collisions (jet quenching);
- Strong elliptic flow.

These results are summarized in PHENIX White paper, which has more than 3000 citations to date. The focus of the research in heavy ion physics at RHIC is now to investigate the properties of the matter. RBRC have played the leading roles in some of the most important results from PHENIX in the study of the matter properties. These include (1) measurements of heavy quark production

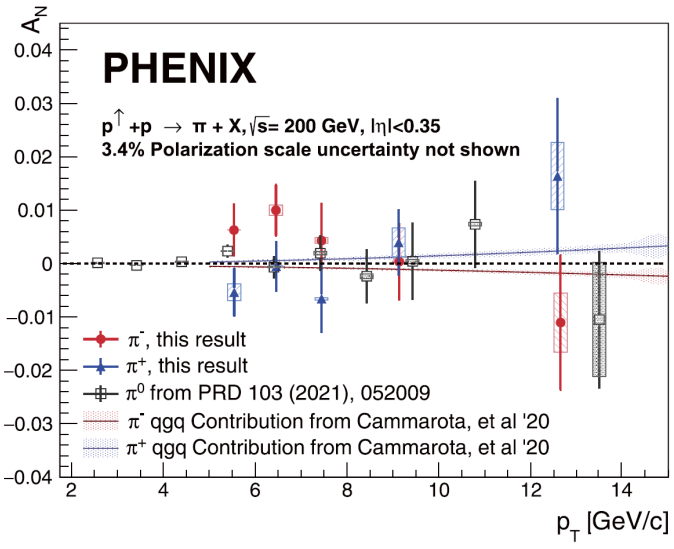

Fig. 3. $A_N(p_T)$ of charged pions measured by PHENIX. Published in Phys. Rev. D **105**, 032003 (2022).

from the single electrons from heavy flavor decay (2) measurements of J/Ψ production (3) measurements of di-electron continuum and (4) measurements of direct photons.

Our most important result is the measurement of direct photons for $1 < p_{\rm T} < 5$ GeV/c in $p+p$ and Au + Au through their internal conversion to $e+e^-$ pairs. If the dense partonic matter formed at RHIC is thermalized, it should emit thermal photons. Observation of thermal photon is direct evidence of early thermalization, and we can determine the initial temperature of the matter. It is predicted that thermal photons from QGP phase is the dominant source of direct photons for $1 < p_{\rm T} < 3$ GeV/c at the RHIC energy. We measured the direct photon in this $p_{\rm T}$ region from measurements of quasi-real virtual photons that decays into low-mass $e+e^-$ pairs. Strong enhancement of direct photon yield in Au + Au over the scaled $p+p$ data has been observed. Several hydrodynamical models can reproduce the central Au + A data within a factor of two. These models assume formation of a hot system with initial temperature of $T_{\rm init}$ = 300 MeV to 600 MeV. This is the first measurement of initial temperature of quark gluon plasma formed at RHIC. Y. Akiba received 2011 Nishina memorial Prize mainly based on this work.

PHENIX experiment recently measured the flow in small collision systems (p + Au, d + Au, and ^{3}He + Au), and observed strong flow in all of these systems. Theoretical models that assume formation of small QGP droplets best describe the data. These results are published in Nature Physics in 2019.

We constructed VTX detector of PHENIX. VTX is a 4-layer silicon tracker and it is the main device for measurement of charm and bottom quark production in PHENIX. VTX took data from the 2011 to 2016 when PHENIX completed data taking. PHENIX recorded high statistics Au+Au data, approximately 20 billion events with VTX in each of the 2014 run and the 2016 run. Figure 4 shows the nuclear modification factor R_{AA} of electron from the charm and the bottom decays in Au+Au collisions relative to the $p+p$ collisions. The left panel shows the results of the most central 0–10% Au+Au collisions, and the right panel shows that of 40–60% centrality. One can clearly see that the charm decay electrons (dashed curve) is more suppressed than the bottom decay electrons (solid curve). This clearly indicates the quark mass dependence of the energy loss of quark in the QGP produced at RHIC. These results are final results of R_{AA} measurement of charm and bottom decay electron from the 2014 data. A paper reporting these results is submitted to Physical Review C.

(3) sPHENIX INTT detector

The group had major roles in several PHENIX detector upgrades, namely, the silicon vertex tracker (VTX) and muon trigger upgrades. VTX is a high precision charged particle tracker made of 4 layers of silicon detectors. It is jointly funded by RIKEN and the US DOE. The inner two layers are silicon pixel detectors and the outer two layers are silicon strip detectors. Y. Akiba is the project manager. The VTX detector was completed in November 2010 and subsequently installed in PHENIX. The detector started taking data in the 2011 run. With the new detector, we measure heavy quark (charm and bottom) production in $p+p$, A + A collisions to study the properties of quark-gluon plasma. The final result of the 2011 run was published. The result show that single electrons from bottom quark decay is suppressed, but not as strong as that from charm decay in low $p_{\rm T}$ region ($3 < p_{\rm T} < 4$ GeV/c). This is the first measurement of suppression of bottom decay electrons at RHIC and the first observation that bottom suppression is smaller than charm. We have recorded 10 times as much Au + Au collisions data in each of the 2014 run and 2016 run. The results of bottom/charm ratios in $p+p$ collisions at 200 GeV from the 2015 run was published (Phys. Rev. D **99** 092003 (2019)). A paper reporting measurements of the nuclear suppression factor R_{AA} of charm and bottom in Au + Au collisions from the 2014 data has been submitted for publication to Physical Review C.

PHENIX completed its data taking in 2016. We are now working on construction of intermediate silicon tracker INTT for sPHENIX, a new experiment at RHIC that will start taking data in 2023. INTT consists of 56 ladders of silicon detector, and production

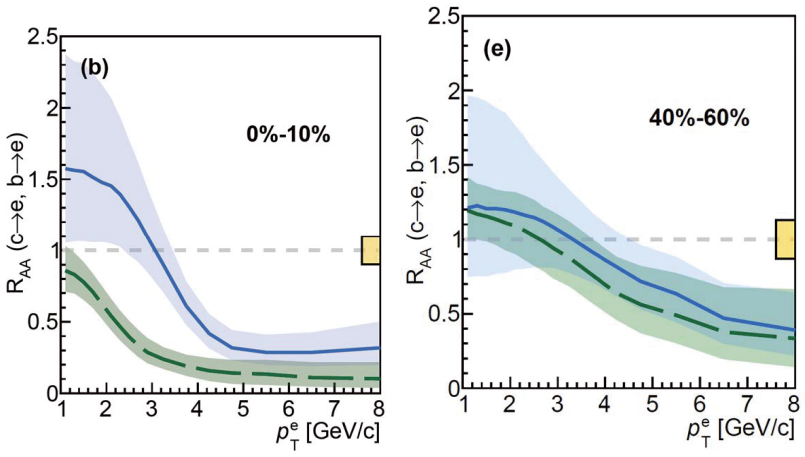

Fig. 4. The nuclear modification factor, R_{AA}, of charm and bottom decay electrons by PHENIX. Submitted to PRC.

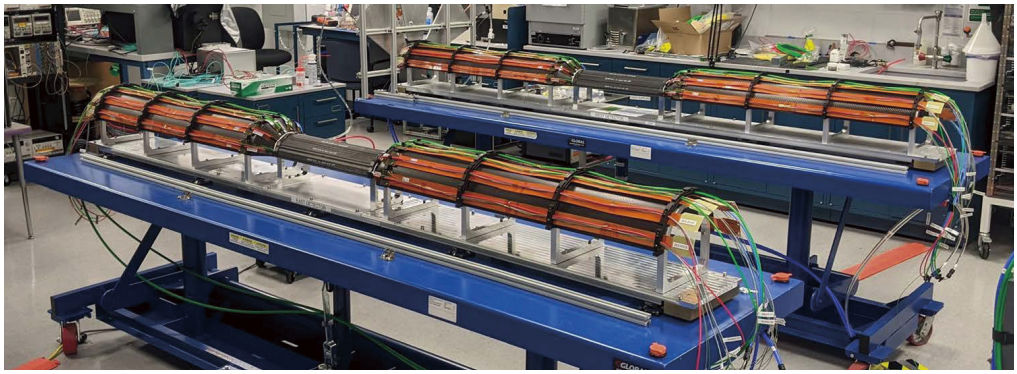

Fig. 5. Two INTT half barrels being assembled at BNL. In both of the half INTT, the B0L0 barrels are assembled.

of all ladders are complete. We are now assembling the INTT. Figure 5 shows two half INTT barrels being assembled in the silicon lab in BNL. The INTT will be installed in sPHENIX in January 2023.

Members

Group Leader

Yasuyuki AKIBA

RBRC Researchers

Jan C. BERNAUER
Yuji GOTO
Takashi HACHIYA
Itaru NAKAGAWA
Genki NUKAZUKA
Ralf SEIDL
Atsushi TAKETANI
Satoshi YOKKAICHI

Special Postdoctoral Researcher

Minho KIM

Junior Research Associate

Takuya KUMAOKA

Special Temporary Research Scientists

Takashi ICHIHARA
Yasushi WATANABE

Senior Visiting Scientist
Rachid NOUICER (BNL)

Visiting Scientists
Stefan BATHE (City Univ. of New York)
Gaku MITSUKA (KEK)
Masahiro OKAMURA (BNL)
Takao SAKAGUCHI (BNL)
Takashi SAKO (Univ. of Tokyo)
Milan STOJANOVIC (Purdue Univ.)

Visiting Technician
Li-Hsin HSU (Nat'l Central Univ.)

Visiting Researcher
Shima SHIMIZU (JSPS)

Student Trainees
Kai-Yu CHENG (Nat'l Central Univ.)
Takuya KUMAOKA (Tsukuba Univ.)
Han-Sheng LI (Purdue Univ.)
Xiao RUI (Purdue Univ.)

List of Publications & Presentations

Publications

[Original Papers]

U. A. Acharya *et al*., "Systematic study of nuclear effects in p+Al, p+Au, d+Au, and ^{3}He+Au collisions at $\sqrt{s_{NN}}$ = 200 GeV using π^0 production," Phys. Rev. C **105**, 064902 (2022).

U. A. Acharya *et al*., "Transverse-single-spin asymmetries of charged pions at midrapidity in transversely polarized p + p collisions at $\sqrt{s}$ = 200 GeV," Phys. Rev. D **105**, 032003 (2022).

U. A. Acharya *et al*., "Transverse-single-spin asymmetries of forward neutron in p+p, p+Al, p+Au collisions at $\sqrt{s_{NN}}$ = 200 GeV," Phys. Rev. D **105**, 032004 (2022).

U. A. Acharya *et al*., "Kinematic dependence of azimuthal anisotropies in p+Au, d+Au, and He+Au at $\sqrt{s_{NN}}$ = 200 GeV," Phys. Rev. C **105**, 024901 (2022).

U. A. Acharya *et al*., "Probing gluon spin-momentum correlations in transversely polarized protons through midrapidity isolated direct photons in p+p collisions at $\sqrt{s}$ = 200 GeV," Phys. Rev. Lett. **127**, 162001 (2021).

U. A. Acharya *et al*., "Transverse sngle-spn asymmetries of midrapidty π^0 and η mesons in polarized p + p collisions at $\sqrt{s}$ = 200 GeV", Phys. Rev. D **103**, 052009 (2021).

U. A. Acharya *et al*., "Transverse momentum dependent forward neutron ssingle spin asymmetries in transversely polarized p+ collisions at $\sqrt{s}$ = 200 GeV", Phys. Rev. D **103**, 032007 (2021).

[Proceedings]

T. Todoroki, "Quark flavor dependence of particle flow in nucleus-nucleus collisions measured by PHENIX," Nucl. Phys. A **1005**, 121960 (2021).

M. Connors, "Highlights from the PHENIX collaboration," Nucl. Phys. A **1005**, 121925 (2021).

Press Release

「直接光子による陽子内グルーオンの運動の観測に成功—グルーオンの回転運動はあまり大きくなかった—」, 2021 年 10 月 15 日 理化学研究所. https://www.riken.jp/press/2021/20211015_1/ .

Subnuclear System Research Division
RIKEN BNL Research Center
Computing Group

1. Abstract

The computing group founded in 2011 as a part of the RIKEN BNL Research Center established at Brookhaven National Laboratory in New York, USA, and dedicated to conduct researches and developments for large-scale physics computations important for particle and nuclear physics. The group was forked from the RBRC Theory Group.

The main mission of the group is to provide important numerical information that is indispensable for theoretical interpretation of experimental data from the first principle theories of particle and nuclear physics. Their primary area of research is lattice quantum chromodynamics (QCD), which describes the sub-atomic structures of hadrons, which allow us the ab-initio investigation for strongly interacting quantum field theories beyond perturbative analysis.

The RBRC group and its collaborators have emphasized the necessity and importance of precision calculations, which will precisely check the current understandings of nature, and will have a potential to find a physics beyond the current standard model of fundamental physics. We have therefore adopted techniques that aim to control and reduce any systematic errors. This approach has yielded many reliable results.

The areas of the major activities are R&D for high performance computers, developments for computing algorithms, and researches of particle, nuclear, and lattice theories. Since the inception of RBRC, many breakthroughs and pioneering works has carried out in computational forefronts. These are the use of the domain-wall fermions, which preserve chiral symmetry, a key symmetry for understanding nature of particle nuclear physics, the three generations of QCD devoted supercomputers, pioneering works for QCD calculation for Cabibbo-Kobayashi-Maskawa theory, QCD + QED simulation for isospin breaking, novel algorithm for error reduction in general lattice calculation. Now the chiral quark simulation is performed at the physical up, down quark mass, the precision for many basic quantities reached to accuracy of sub-percent, and the group is aiming for further important and challenging calculations, such as the full and complete calculation of CP violating $K \to \pi\pi$ decay and ε'/ε, or hadronic contributions to muon's anomalous magnetic moment $g-2$. Another focus area is the nucleon's shape, structures, and the motion of quarks and gluon inside nucleon called parton distribution, which provide theoretical guidance to physics for sPHENIX and future Electron Ion Collider (EIC), Hyper Kamiokande, DUNE, or the origin of the current matter rich universe (rather than anti-matter). Towards finite density QCD, they also explore Quantum Computing to overcome the sign problem. The Machine Learning (ML) and Artificial Intelligence (AI) are the new topics some of members are enthusiastically studying lately.

2. Major Research Subjects

(1) Search for new law of physics through tests for Standard Model of particle and nuclear physics, especially in the framework of the Cabibbo-Kobayashi-Maskawa (CKM), hadronic contributions to the muon's anomalous magnetic moment $(g-2)$ for FNAL and J-PARC's experiments, as well as B physics at Belle II and LHCb

(2) Nuclear Physics and dynamics of QCD or related theories, including study for the structures of nucleons related to physics for Electron Ion Collider (EIC or eRHIC), Hyper Kamiokande, T2K, DUNE

(3) Theoretical and algorithmic development for lattice field theories, QCD machine (co-)design and code optimization

3. Summary of Research Activity

In 2011, QCD with Chiral Quarks (QCDCQ), a third-generation lattice QCD computer that is a pre-commercial version of IBM's Blue Gene/Q, was installed as an in-house computing resource at the RBRC. The computer was developed by collaboration among RBRC, Columbia University, the University of Edinburgh, and IBM. Two racks of QCDCQ having a peak computing power of 2×200 TFLOPS are in operation at the RBRC. In addition to the RBRC machine, one rack of QCDCQ is owned by BNL for wider use for scientific computing. In 2013, 1/2 rack of Blue Gene/Q is also installed by US-wide lattice QCD collaboration, USQCD. The group has also used the IBM Blue Gene supercomputers located at Argonne National Laboratory and BNL (NY Blue), and Hokusai and RICC, the super computers at RIKEN (Japan), Fermi National Accelerator Laboratory, the Jefferson Lab, and others. From 2016, the group started to use the institutional cluster both GPU and Intel Knight Landing (KNL) clusters installed at BNL and University of Tokyo extensively.

Such computing power enables the group to perform precise calculations using up, down, and strange quark flavors with proper handling of the important symmetry, called chiral symmetry, that quarks have. The group and its collaborators carried out the first calculation for the direct breaking of CP (Charge Parity) symmetry in the hadronic K meson decay ($K \to \pi\pi$) amplitudes, ε'/ε, which provide a new information to CKM paradigm and its beyond. They also provide the hadronic contribution in muon's anomalous magnetic moment $(g-2)_\mu$. These calculation for ε'/ε, hadronic light-by-light of $(g-2)$, are long waited calculation in theoretical physics delivered for the first time by the group. The $K \to \pi\pi$ result in terms of ε'/ε currently has a large error, and deviates from experimental results by 2.1σ. To collect more information to decide whether this deviation is from the unknown new physics or not, the group continues to improve the calculation in various way to reduce their error. Hadronic light-by-light contribution to $(g-2)_\mu$ is improved by more than two order of magnitudes compared to our previous results. As of 2019 summer, their calculation is among the most precise determination for the $g-2$ hadronic vacuum polarization (HVP), and only one calculation in the world for the hadronic light-by-light (HLbL) contribution at physical point. These $(g-2)_\mu$ calculations provide the first principle theoretical prediction for on-going new experiment at FNAL and also for the planned experiment at J-PARC. Other projects including flavor physics in the framework of the

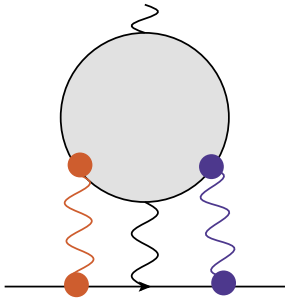

Fig. 1. Feynman diagrams for Lattice QCD computations of Muon's anomalous magnetic moment $(g-2)_\mu$ to take into account for the effects of quark's electric charges. Each diagram, in which the black dots connecting the quark propagators (solid curves) are the electric current emmitting or absorbing photons (wave curves), represents a part of the isospin breaking effects to hadronic vacuum polarization contribution to $(g-2)_\mu$ (top plot).

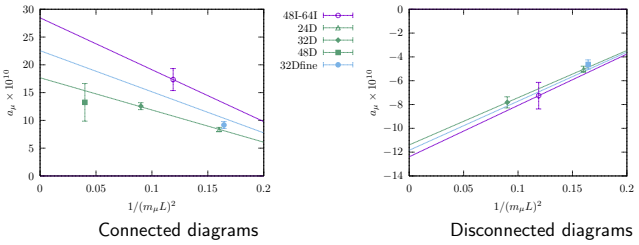

Fig. 2. Current summary of the Hadronic Vacuum Polarization (HVP) contribution for Muon's anomalous magnetic moment $(g-2)_\mu$. Above the upper horizontal line shows various Lattice QCD determinations of HVP while the red results from hadronic decay of electron positron scattering (R-ratio), the green bands is the experimental results of $(g-2)_\mu$ showing a 3–4σ discrepancies.

CKM theory for kaons and B mesons that include the new calculation of b-baryon decay, $\Lambda_b \to p$; the electromagnetic properties of hadrons; the proton's and neutron's form factors and structure function including electric dipole moments; proton decay; nucleon form factors, which are related to the proton spin problem or neutrino-nucleon interaction; Neutron-antineutron oscillations; inclusive hadronic decay of τ leptons; nonperturbative studies for beyond standard model such composite Higgs or dark matter models from strong strongly interacting gauge theories; a few-body nuclear physics and their electromagnetic properties; QCD thermodynamics in finite temperature/density systems such as those produced in heavy-ion collisions at the Relativistic Heavy Ion Collider; Quantum Information, Quantum Computing; and applications of Machine Learning (ML) in field theories.

The RBRC group and its collaborators have emphasized the necessity and importance of precision calculations, which will provide stringent checks for the current understandings of nature, and will have a potential to find physics beyond the current standard model of fundamental physics. We have therefore adopted techniques that aim to control and reduce any systematic errors. This approach has yielded many reliable results, many of basic quantities are now computed within sub-percent accuracies.

The group also delivers several algorithmic breakthroughs, which speed up generic lattice gauge theory computation. These novel technique divides the whole calculation into frequent approximated calculations, and infrequent expensive and accurate calculation using lattice symmetries called All Mode Averaging (AMA), or a compression for memory needs by exploiting the local-coherence of QCD dynamics. Together with another formalism, zMobius fermion, which approximate chiral lattice quark action efficiently, the typical calculation is now improved by a couple of orders of magnitudes, and more than an order of magnitude less memory needs compared to the traditional methods. RBRC group and its collaborators also provide very efficient and generic code optimized to the state-of-arts CPU or GPU, and also improve how to efficiently generate QCD ensemble.

Members

Group Leader

Taku IZUBUCHI

RBRC Researchers

Luchang JIN

Sergey SYRITSYN

Special Postdoctoral Researchers

Nobuyuki MATSUMOTO

Akio TOMIYA

Visiting Scientists

Thomas BLUM (Univ. of Connecticut)

Hiroshi OKI (Nara Women's Univ.)

List of Publications & Presentations

Publications

[Original Papers]

M. Abramczyk, T. Blum, T. Izubuchi, C. Jung, M. Lin, A. Lytle, S. Ohta, and E. Shintani, "Nucleon mass and isovector couplings in 2+1-flavor dynamical domain-wall lattice QCD near physical mass," Phys. Rev. D **101**, 034510 (2020).

T. Izubuchi, L. Jin, C. Kallidonis, N. Karthik, S. Mukherjee, P. Petreczky, C. Shugert, and S. Syritsyn, "Valence parton distribution function of pion from fine lattice," Phys. Rev. D **100**, 034516 (2019).

N. H. Christ, X. Feng, L. C. Jin, and C. T. Sachrajda, "Finite-volume effects in long-distance processes with massless leptonic propagators," Phys. Rev. D **103**, 014507 (2021).

Y. Li, S. C. Xia, X. Feng, L. C. Jin, and C. Liu, "Field sparsening for the construction of the correlation functions in lattice QCD," Phys. Rev. D **103**, 014514 (2021).

C. Y. Seng, X. Feng, M. Gorchtein, L. C. Jin, and U. G. Meißner, "New method for calculating electromagnetic effects in semileptonic beta-decays of mesons," J. High Energy Phys. **10**, 179 (2020).

X. Gao, L. Jin, C. Kallidonis, N. Karthik, S. Mukherjee, P. Petreczky, C. Shugert, S. Syritsyn, and Y. Zhao, "Valence parton distribution of the pion from lattice QCD: Approaching the continuum limit," Phys. Rev. D **102**, 094513 (2020).

X. Feng, L. C. Jin, Z. Y. Wang, and Z. Zhang, "Finite-volume formalism in the $2 \xrightarrow{H_I+H_I} 2$ transition: An application to the lattice QCD calculation of double beta decays," Phys. Rev. D **103**, 034508 (2021).

R. Abdul Khalek *et al*., "Science requirements and detector concepts for the electron-ion collider: EIC yellow report," arXiv:2103.05419.

X. Gao, N. Karthik, S. Mukherjee, P. Petreczky, S. Syritsyn, and Y. Zhao, "Pion form factor and charge radius from Lattice QCD at physical point," arXiv:2102.06047.

X. Gao, N. Karthik, S. Mukherjee, P. Petreczky, S. Syritsyn, and Y. Zhao, "Towards studying the structural differences between the pion and its radial excitation," Phys. Rev. D **103**, 094510 (2021).

G. Silvi, S. Paul, C. Alexandrou, S. Krieg, L. Leskovec *et al*., "P-wave nucleon-pion scattering amplitude in the $\Delta(1232)$ channel from lattice QCD," Phys. Rev. D **103**, 094508 (2021).

M. Yu. Barabanov, M. A. Bedolla, W. K. Brooks, G. D Cates, C. Chen *et al*., "Diquark correlations in hadron physics: Origin, impact and evidence," Prog. Part. Nucl. Phys. **116**, 103835 (2021).

M. Engelhardt, J. R. Green, N. Hasan, S. Krieg, S. Meinel, J. Negele, A. Pochinsky, and S. Syritsyn, "From Ji to Jaffe-Manohar orbital angular momentum in lattice QCD using a direct derivative method," Phys. Rev. D **102**, 074505 (2020).

G. Rendon, L. Leskovec, S. Meinel, J. Negele, S. Paul *et al*., "$I = 1/2$ S-wave and P-wave $K\pi$ scattering and the κ and K^* resonances from lattice QCD," Phys. Rev. D **102**, 114520 (2020).

Z. Fan, X. Gao, R. Li, H. -W. Lin, N. Karthik *et al*., "Isovector parton distribution functions of the proton on a superfine lattice," Phys. Rev. D **102**, 074504 (2020).

H. T. Ding, S. T. Li, Swagato Mukherjee, A. Tomiya, X. D. Wang, and Y. Zhang, "Correlated Dirac eigenvalues and axial anomaly in chiral symmetric QCD," Phys. Rev. Lett. **126**, 082001 (2021).

M. Kawaguchi, S. Matsuzaki, and A. Tomiya, "Nonperturbative flavor breaking in topological susceptibility at HotQCD criticality," Phys. Lett. B **813**, 136044 (2021).

H. -T. Ding, C. Schmidt, A. Tomiya, and X. -D. Wang, "Chiral phase structure of three flavor QCD in a background magneticfield," Phys. Rev. D **102**, 054505 (2020).

B. Chakraborty, M. Honda, T. Izubuchi, Y. Kikuchi, and A. Tomiya, "Digital quantum simulation of the Schwinger model with topological term via adiabatic state preparation," arXiv:2001.00485.

[Review Article]

T. Aoyama, N. Asmussen, M. Benayoun, J. Bijnens, T. Blum, M. Bruno, I. Caprini, C. M. Carloni Calame, M. Cè, G. Colangelo *et al.*, "The anomalous magnetic moment of the muon in the standard model," Phys. Rept. **887**, 1–166 (2020).

[Books]

A. Tomiya, "An introduction to machine learning in physics," (in Japanese), Kodansha, March 2021.

K. Hashimoto, A. Tanaka, and A. Tomiya, "Deep learning and physics," Springer, February 2021.

[Proceedings]

T. Izubuchi, H. Ohki, and S. Syritsyn, "Computing nucleon electric dipole moment from lattice QCD," Proc. Sci. **LATTICE2019**, 290 (2020).

M. Bruno, T. Izubuchi, C. Lehner, and A. S. Meyer, "Exclusive channel study of the muon HVP," Proc. Sci. **LATTICE2019**, 239 (2019).

M. Kawaguchi, S. Matsuzaki, and A. Tomiya, "Analysis on nonperturbative flavor violation at chiral crossovercriticality in QCD," arXiv:2005.07003.

A. Tomiya and Y. Nagai, "Gauge covariant neural network for 4 dimensional non-abelian gaugetheory," arXiv:2103.11965.

M. Kawaguchi, S. Matsuzaki, and A. Tomiya, "A new critical endpoint in thermomagnetic QCD," arXiv:2102.05294.

Y. Nagai, A. Tanaka, and A. Tomiya, "Self-learning Monte-Carlo for non-abelian gauge theory withdynamical fermions," arXiv:2010.11900.

H. -T. Ding, S. -T. Li, A. Tomiya, X. -D. Wang, and Y. Zhang, "Chiral properties of (2+1)-flavor QCD in strong magnetic fields at zerotemperature," arXiv:2008.00493.

H. -T. Ding, S. -T. Li, S. Mukherjee, A. Tomiya, and X. -D. Wang, "Meson masses in external magnetic fields with HISQ fermions," arXiv:2001.05322.

Presentations

[International Conferences/Workshops]

L. Jin (invited), "Lattice calculations in muon g − 2.," The Hadron Mass and Structure Forum, Online, April 2021.

L. Jin (invited), "Muon g − 2: hadronic light-by-light contribution and lattice QCD," The Muon g-2 Discussion Forum, Peking University, Online, April 2021.

L. Jin (invited), "Pion electric polarizability," the χ QCD Collaboration Meeting, Online, January 2021.

L. Jin (invited), "Lattice calculation of the hadronic light-by-light contribution to the muon magnetic moment," The Hadron Physics Online Forum, Online, August 2020.

S. Syritsyn (invited), "Nucleon form factors at high momentum transfer from lattice QCD," Nuclear & Particle Theory Seminar, MIT/CTP, March 9, 2020.

A. Tomiya (oral), "Self-learning Monte-Carlo for non-abelian gauge theory withdynamical fermions," APS April Meeting, Virtual, April 20, 2020.

A. Tomiya (invited), "Self-learning Monte-Carlo for non-abelian gauge theory with dynamical fermions," Workshop on Non-equilibrium Systems and Machine Learning, Virtual, March 30, 2020.

A. Tomiya (oral), "Quantum computing for QCD phase diagram? Finite chemicalpotential and temperature?," Kickoff Meeting of C2QA Center, Virtual, BNL, October 30, 2020.

A. Tomiya (invited), "Machine learning and theoretical physics," Progress of Particle Physics 2020, Virtual, Yukawa Institute for Theoretical Physics, Japan, Sepember 4, 2020.

A. Tomiya (oral), "Thermal field theory with pure states," Asia-Pacific Symposium for Lattice Field Theory (APLAT 2020), Virtual, KEK, August 6, 2020.

A. Tomiya (invited), "Applications of machine learning to computational physics," A.I. for Nuclear Physics, JeffersonLaboratory, Virginia, USA, March 3, 2020.

[Domestic Conferences/Workshops]

A. Tomiya (oral), "Gauge covariant neural network for 4 dimensional non-abelian gaugetheory," Deep Learning and Physics, Virtual, April 7, 2020.

A. Tomiya (oral), "Self-learning Monte-Carlo for QCD," JPS, Virtual, March 13, 2020.

A. Tomiya (invited), "Machine learning for physics," 5th Symposium on Statistical Machine Learning, Virtual, Nagoya University, December 5, 2020.

A. Tomiya (oral), "A lecture on usage of neural nets in physics," DLAP 2020 Lecture, Virtual, Osaka University, November 26, 2020.

[Seminars]

L. Jin (invited), "Lattice calculations in muon g − 2.," The Theory Seminar at the Department of Physics and Astronomy, University of California, Davis, Online, May 2021.

L. Jin (invited), "Lattice calculations in muon g − 2.," The Lunch Seminar at the Institute of Theoretical Physics, Chinese Academy of Sciences, Online, April 2021.

L. Jin (invited), "First-principles calculation of electroweak box diagrams from lattice QCD," The Physics Seminar in Hunan University, Online, December 2020.

L. Jin (invited), "First-principles calculation of electroweak box diagrams from lattice QCD," The Theory Seminar at the Institute of Modern Physics, Chinese Academy of Sciences, July 2020.

L. Jin (invited), "First-principles calculation of electroweak box diagrams from lattice QCD," The BNL Nuclear Theory Seminar, Online, May 2020.

L. Jin (invited), "Lattice calculation of the hadronic light-by-light contribution to the muon magnetic moment," The QCD Seminar, Online, May 2020.

S. Syritsyn (invited), "From quarks and gluons to nucleons and nuclei," Seminar at IACS (Inst. Adv. Comp. Sci), Stony Brook, October 8, 2020.

A. Tomiya (oral), "Gauge covariant neural network for 4 dimensional non-abelian gaugetheory," Virtual, MIT, April 29, 2020.

A. Tomiya (oral), "Applications of machine learning on theoretical physics," Virtual, Ochanomizu University, Japan, May 19, 2020.

A. Tomiya (oral), "Gauge covariant neural network for 4 dimensional non-abelian gaugetheory," Virtual, RIKEN Center for Computational Science, Japan, April 28, 2020.

A. Tomiya (oral), "Applications of machine learning for theoretical physics," Virtual, JPARC, Japan, March 18, 2020.

A. Tomiya (oral), "Self-learning Monte-Carlo for non-abelian gauge theory withdynamical fermions," Virtual, Yukawa Institute for Theoretical Physics, Japan, December 7, 2020.

A. Tomiya (oral), "Applications of machine learning on theoretical physics," Virtual, Shimane University, Japan, October 29, 2020.

A. Tomiya (oral), "Lattice gauge theory with quantum computers," Virtual, RIKEN Center for Computational Science, Japan, June 3, 2020.

A. Tomiya (oral), "Lattice gauge theory with quantum computers," Virtual, Osaka University, Japan, May 12, 2020.

Award

A. Tomiya "Best presentation award," SPDR program, RIKEN, 2021.

Press Releases

Brookhaven National Laboratory, "Background on Brookhaven Lab's Involvement in the Muon g-2 Experiment," April 7, 2021. https://www.bnl.gov/newsroom/news.php?a=218814 .

CERN Courier, "An anomalous moment for the muon," April 14, 2021. https://cerncourier.com/a/an-anomalous-moment-for-the-muon/ .

UConn Today, "UConn Physicists Focus on a Law-Breaking Particle," May 20, 2021. https://today.uconn.edu/2021/05/uconn-physicists-focus-on-a-law-breaking-particle/ .

Subnuclear System Research Division
RIKEN Facility Office at RAL

1. Abstract

Our core activities are based on the RIKEN-RAL Muon Facility located at the ISIS Neutron & Muon Source at the Rutherford Appleton Laboratory (UK), which provides intense pulsed-muon beams. The RIKEN-RAL Muon Facility is a significant and long-standing collaboration between RIKEN and RAL in muon science—with 2020 being the 30th years of continuous agreements between RIKEN and RAL. The Facility enables muon science throughout Japan and other field—it continues to attract proposals from a wide variety of Japanese universities and institutions (with over 80 groups having now used the facility), and including industrial users such at Toyota, and has been instrumental in establishing scientific links with other Asian universities.

Muons have their own spins with 100% polarization, and can detect local magnetic fields and their fluctuations at muon stopping sites very precisely. The method to study the characteristics of materials by observing time dependent changes of muon spin polarization is called "Muon Spin Rotation, Relaxation and Resonance" (μSR method), and is applied to study electro-magnetic properties of insulating, metallic, magnetic and superconducting systems. Muons reveal static and dynamic properties of the electronic state of materials in the zero-field condition, which is the ideal magnetic condition for research into magnetism. For example, we have carried out μSR investigations on a wide range of materials including frustrated pyrochlore systems, which have variety of exotic ground states of magnetic spins, so the magnetism study of this system using muon is quite unique.

The ultra-cold muon beam can be stopped in thin foil, multi-layered materials and artificial lattices, which enables us to apply the aSR techniques to surface and interface science. The development of an ultra-cold muon beam is also very important as a source of pencil-like small emittance muon beam for muon g-2/EDM measurement. We have been developing muonium generators to create more muonium atoms in vacuum even at room temperature to improve beam quality compared with the conventional hot-tungsten muonium generator. We have demonstrated a strong increase in the muonium emission efficiency by fabricating fine laser drill-holes on the surface of silica aerogel. We are also developing a high power Lyman-alpha laser in collaboration with the Advanced Photonics group at RIKEN. The new laser will ionize muoniums 100 times more efficiently for slow muon beam generation.

Over the past 2–3 years, a significant development activity in muon elemental analysis has taken place, proton radius experiments have continued and been developed, and chip irradiation experiments have also continued.

2. Major Research Subjects

(1) Materials science by muon-spin-relaxation method and muon site calculation
(2) Development of elemental analysis using pulsed negative muons
(3) Nuclear and particle physics studies via muonic atoms and ultra-cold muon beam
(4) Other muon applications

3. Summary of Research Activity

(1) Material science at the RIKEN-RAL muon facility

Muons have their own spins with 100% polarization, and can detect local magnetic fields and their fluctuations at muon stopping sites very precisely. The μSR method is applied to studies of newly fabricated materials. Muons enable us to conduct (1) material studies under external zero-field condition, (2) magnetism studies with samples without nuclear spins, and (3) measurements of muon spin relaxation changes at wide temperature range with same detection sensitivity. The detection time range of local field fluctuations by μSR is 10^{-6} to 10^{-11} second, which is an intermediate region between neutron scattering method (10^{-10}–10^{-12} second) and Nuclear Magnetic Resonance (NMR) (longer than 10^{-6} second). At Port-2 and 4 of the RIKEN-RAL Muon Facility, we have been performing μSR researches on strong correlated-electron systems, organic molecules, energy related materials and biological samples to study electron structures, superconductivity, magnetism, molecular structures and crystal structures.

Among our scientific activities on μSR studies from year 2018 to 2021, following subjects of material sciences are most important achievements at the RIKEN-RAL muon facility:

(1) Quasi magnetic monopole state in the Ru-based pyrochlore systems, $R_2Ru_2O_7$;
(2) Novel magnetic and superconducting properties of nano-size La-based high-T_C superconducting cuprates;
(3) Determination of muon positions estimated from density functional theory (DFT) and dipole-field calculations;
(4) Chemical muonic states in DNA molecules.

Result-1) Quasi magnetic monopole state in pyrochlore systems gave us new interpretations to understand exotic phenomena, like the quantum spin liquid and spin fragmentation states. Result-2) The same nano-size effect was examined on the La-based high-T_C superconducting oxide changing the electronic state from insulating to superconducting. We confirmed the reduction in the magnetic interaction and the disappearance of the superconducting state leading the increase in the ferromagnetic interaction within the wide-range of the hole concentration. Result-3) Well known and deeply investigated La_2CuO_4 has opened a new scheme of the Cu spin. Taking into account quantum effects to expand the Cu-spin orbital and muon positions, we have succeeded to explain newly found muon sites and hyperfine fields at those sites. Result-4) Chemical states of the muon which attaches to DNA molecules were investigated by the avoided level-crossing muon-spin resonance experiments. In conjunction with DFT calculations, we are trying to reveal the electron motion though the DNA molecule.

We have been continuing to develop muon-science activities in Asian countries. We enhanced international collaborations to organize new μSR experimental groups and to develop muon-site calculation groups using computational method. We are creating

new collaborations with new teams in different countries and also continuing collaborations in μSR experiments on strongly correlated systems with researchers from Taiwan, Indonesia, China, Thailand and Malaysia including graduate students. We are starting to collaborate with the new Chinese muon group who are developing the Chinese Muon Facility and trying to develop more muon activities in the Asian area.

(2) Development of elemental analysis using pulsed negative muons

There has been significant development of elemental analysis using negative muons on Port 4 and Port 1 over the past couple of years. Currently, elemental analysis commonly uses X-ray and electron beams, which accurately measure surfaces. However, a significant advantage of muonic X-rays over those of electronic X-rays is their higher energy due to the mass of the muon. These high energy muonic X-rays are emitted from the bulk of the samples without significant photon self-absorption. The penetration depth of the muons can be varied by controlling the muon momentum, providing data from a thin slice of sample at a given depth. This can be over a centimeter in iron, silver and gold or over 4 cm in less dense materials such as carbon.

Some techniques for elemental analysis are destructive or require the material under investigation to undergo significant treatment and some of the techniques are only sensitive to the surface. Therefore, negative muons offer a unique service in which they can measure inside, beyond the surface layer and completely non-destructively.

The areas of science that have used negative muons for elemental analysis have been very diverse. The largest area is the cultural heritage community as the non-destructive ability is particularly important and will become more so. This community have investigated swords from different eras, coins (Roman gold and silver, Islamic silver and from the Tudor Warship Mary Rose), miniature boats from Sardinia, reliefs on Baptist church gate, Bronze Age tools and cannon balls. In addition, energy materials (Li composition for hydrogen storage), bio-materials (search for iron to potentially help understand Alzheimer's), engineering alloys (manufacturing processes for new materials for jet engines), and functional materials (surface effects in piezo electrics) have also been investigated.

The study was extended to see the difference by isotopes of silver and lead, which may give hint on the source of the material.

(3) Ultra-cold (low energy) muon beam generation and applications

Positive muon beam with thermal energy has been produced by laser ionization of muonium (bound system of μ^+ and electron) emitted from a hot tungsten surface with stopping surface muon beam at Port-3. The method generates a positive muon beam with acceleration energy from several 100 eV to several 10 keV, small beam size (a few mm) and good time resolution (less than 8 nsec). By stopping the ultra-cold muon beam in thin foil, multi-layered materials and artificial lattices, we can precisely measure local magnetic field in the materials, and apply the μSR techniques to surface and interface science. In addition, the ultra-cold muon is very important as the source of pencil-like small emittance muon beam for muon $g-2$/EDM measurement. It is essential to increase the slow muon beam production efficiency by 100 times for these applications. There are three key techniques in ultra-cold muon generation: production of thermal muonium, high intensity Lyman-alpha laser and the ultra-cold muon beam line.

A high-power Lyman-alpha laser was developed in collaboration with the Advanced Photonics group at RIKEN. The new laser system is used at J-PARC U-line and, upon completion, will ionize muoniums 100 times more efficiently for slow muon beam generation. In this development, we succeeded to synthesize novel ceramic-based Nd:YGAG and Nd:YSAG crystals, which realized a highly efficient and stable laser system. We are working hard to improve the homogeneity of large size crystals in order to achieve full design power.

We also succeeded in developing an efficient muonium generator, laser ablated silica aerogel, which emits more muoniums into vacuum even at room temperature. Study has been done at TRIUMF utilizing positron tracking method of muon decay position. We demonstrated in 2013 at least 10 times increase of the muonium emission efficiency by fabricating fine laser drill-holes on the surface of silica aerogel. Further study was carried out in 2017 to find the optimum fabrication that will maximize the muonium emission. From the analysis, we found the emission has large positive correlation with the laser ablated area rather than with any other parameters. We also confirmed the muon polarization in vacuum. An alternative detection method for muonium emission using muonium spin rotation, which will be sensitive even to muoniums near the surface, was tested at RIKEN-RAL in 2018 and was found successful. The study was further applied to the measurement of the temperature dependence.

In RIKEN-RAL Port 3, the ultra-cold muon beam line, which had been designed with hot tungsten, was completely rebuilt to use advantage of the new room temperature silica aerogel target. The equipment was tested with surface muon beam and basic data such as muon stopping in aerogel were taken. Based on the design, an ultimate cold muon source is under preparation for muon $g-2$/EDM at J-PARC.

(4) Other fundamental physics studies

We proposed the measurement of the proton radius by using the hyperfine splitting of the muonic hydrogen ground state. This hyperfine splitting is sensitive to the Zemach radius, which is a convolution of charge and magnetic-dipole distributions inside proton. We are planning to re-polarize the muonic hydrogen by a circularly polarized excitation laser (excites one of the $F = 1$ states and regenerates the muon spin polarization), and detect the recovery of the muon decay-asymmetry along the laser.

Preparation using muon beam is in progress. We measured the muon stopping distribution in low-density hydrogen-gas cell, which gave us consistent results with beam simulation. Another key is the lifetime of the upper hyperfine state of the muonic hydrogen that will contribute the polarization. We successfully observed the clear muon spin precession of muonic deuterium atom in 2018 for the first time in the world. The measurement with muonic protium was carried out in 2019 and the data is being analyzed.

(5) Facility operation and refurbishment

The research activity at RIKEN-RAL had severe restriction in FY2021 also since the COVID-19 pandemic continued. It was impossible for users from outside RAL to carry out the experiment. Even though, we managed to carry out several μSR experiments with mailed samples. Since July 2021, RIKEN-RAL muon facility is undergoing major refurbishment, first time since its operation in 1994. The work covers many important components, such as the cooling water circuit, vacuum system, radiation shielding, magnet power supplies and power cables, detectors and beamline control system.

Members

Director

Philip KING

Senior Research Scientist

Isao WATANABE

Contract Researcher

Katsuhiko ISHIDA

List of Publications & Presentations

Publications

[Original Papers]

C. Pizzolottoa, A. Sbrizzia, A. Adamczak, D. Bakalov, G. Baldazzie, M. Baruzzoa, R. Benoccih, R. Bertoni, M. Bonesinih, H. Cabrera, D. Cirrincione, M. Clemenza, L. Colace, M. Danailov, P. Danev, A. deBari, C. DeVecchi, M. DeVincenzik, E. Fasci, F. Fuschino, K. S. Gadedjisso-Tossou, L .Gianfrani, K. I shida, C. Labanti, V. Maggi, R. Mazza, A. Menegolli, E. Mocchiutti, S. Monzani, L. Moretti, G. Morgante, J. Niemela, A. Pullia, R. Ramponi, L. P. Rignanese, M. Rossella, M. Stoilov, L. Stoychev, J. J. Suárez-Vargas, L. Tortora, E. Vallazza, and A. Vacchi, "Measurement of the muon transfer rate from muonic hydrogen to oxygen in the range 70–336 K," Phys. Lett. A **403**, 127401 (2021).

T. Yamashita, K. Okutsu, Y. Kino, R. Nakashima, K. Miyashita, K. Yasuda, S. Okada, M. Sato, T. Oka, N. Kawamura, S. Kanda, K. Shimomura, P. Strasser, S. Takeshita, M. Tampo, S. Doiuchi, Y. Nagatani, H. Natori, S. Nishimura, A. D. Pant, Y. Miyake, and K. Ishida, "Time evolution calculation of muon catalysed fusion: Emission of recycling muons from a two-layer hydrogen film," Fusion Eng. Des. **169**, 112580 (2021).

A. D. Pant, K. Nagamine, E. Torikai, I. Shiraki, K. Shimomura, Francis L. Pratt, H. Ariga-Miwa, K. Ishida, and J. S. Schultz, "Muonium response to low oxygen levels in haemoglobin and other biological aqueous solutions and potential application towards monitoring hypoxia," Nucl. Instrum. Methods Phys. Res. A **1010**, 165561 (2021).

M. D. Umar, K. Ishida, R. Murayama, D. P. Sari, U. Widyaiswari, M. Fronzi, I. Watanabe, and M. Iwasaki, "Muon-spin motion at the crossover regime between gaussian and lorentzian distribution of magnetic fields," Prog. Theor. Exp. Phys. **2021**, 083101 (2021).

K. Okutsu, T. Yamashita, Y. Kino, R. Nakashima, K. Miyashita, K. Yasuda, S. Okada, M. Sato, T. Oka, N. Kawamura, S. Kanda, K. Shimomura, P. Strasser, S. Takeshita, M. Tampo, S. Doiuchi, Y. Nagatani, H. Natori, S. Nishimura, A. D. Pant, Y. Miyake, and K. Ishida, "Design for detecting recycling muon after muon-catalyzed fusion reaction in solid hydrogen isotope target," Fusion Eng. Des. **170**, 112712 (2021).

A. Green, K. Ishida, Bethany V. Hampshire, K. Butcher, M. Pollard, and A. D. Hillier, "Understanding roman gold coinage inside out," J. Archaeol. Sci. **134**, 105470 (2021).

J. Sugiyama, K. Ohishi, O. K. Forslund, M. Månsson, S. P. Cottrell, A. D. Hillier, and K. Ishida, "How Li diffusion in spinel $Li[Ni_{1/2}Mn_{3/2}]O_4$ is seen with $\mu^{\pm}$SR," Z. Phys. Chem. **236**, 799 (2022).

W. N. Zaharim, S. N. A. Ahmad, S. Sulaiman, H. Rozak, D. F. H. Baseri, N. A. M. Rosli, S. S. Mohd-Tajudin, L. S. Ang, and I. Watanabe, "Density functional theory study of 12mer single-strand guanine oligomer and associated muon hyperfine interaction," ACS Omega **6**, 29641–29650 (2021).

A. Jamaludin, W. N. Zaharim, S. Sulaiman, H. Rozak, A. L. Sin, and I. Watanabe, "Density functional theory investigation of muon hyperfine interaction in guanine-cytosine double-strand DNA," J. Phys. Soc. Jpn. **91**, 024301 (2022).

S. Yoon, W. Lee, S. Lee, J. Park, H. Lee, Y. S. Choi, S. -H. Do, W. -J. Choi, W. -T. Chen, F. Chou, D. I. Gorbunov, Y. Oshima, A. Ali, Y. Singh, A. Berlie, I. Watanabe, and K. -Y. Choi1, "Quantum disordered state in the J_1-J_2 square-lattice antiferromagnet $Sr_2Cu(Te_{0.95}W_{0.05})O_6$," Phys. Rev. Res. **5**, 014411 (2021).

M. Miyajima, F. Astuti, T. Fukuda, M. Kodani, S. Iida, S. Asai, A. Matsuo, T. Masuda, K. Kindo, T. Hasegawa, T. C. Kobayashi, T. Nakano, I. Watanabe, and T. Kambe, "Spin-gap formation due to spin-Peierls instability in π-orbital-ordered NaO_2," Phys. Rev. B **104**, L140402 (2021).

[Review Articles]

M. Cataldo, M. Clemenza, K. Ishida, and A. D. Hillier, "A novel non-destructive technique for cultural heritage: Depth profiling and elemental analysis underneath the surface with negative muons," Appl. Sci. **12**, 4237 (2022).

A. D. Hillier, S. J. Blundell, I. McKenzie, I. Umegaki, L. Shu, J. A. Wright, T. Prokscha, F. B. K. Shimomura, A. Berlie, H. Alberto, and I. Watanabe, "Muon spin spectroscopy," Nat. Rev. Meth. Primers **2**, 4 (2022).

I. Watanabe, D. P. Sari, R. Ramadhan, B. Adiperdana, and S. Sulaiman, "Muon-site determination in materials by using computational methods," J. Comput. Chem. Jpn. **19**, 115–123 (2020).

[Book]

A. D. Hillier, B. Hampshire, and K. Ishida, "Depth-dependent bulk elemental analysis using negative muons," in "Handbook of Cultural Heritage Analysis," S. D'Amico and V. Venuti (Eds.), Springer, 2022, pp. 23–44.

Presentations

[International Conference/Workshop]

K. Ishida, "Muon g-2 experiment at J-PARC," 14th European Research Conference on Electromagnetic Interactions with Nucleons and Nuclei (EINN2021), Online, November 2–6, 2021.

[Domestic Conferences/Workshops]

石田勝彦,「ミュオン原子分子とスピン状態」, 新学術領域「宇宙観測検出器と量子ビームの出会い. 新たな応用への架け橋. 」, 第 1 回超低速負ミュオンビーム研究会, オンライン, 2021 年 12 月 20 日.

石田勝彦,「RIKEN-RAL 施設」, 第 12 回「Muon 科学と加速器研究」, 第 6 回「文理融合シンポジウム 量子ビームで歴史を探る—加速器が紡ぐ文理融合の地平—」,「ミュオンで見る磁性・超伝導物質研究の最前線」合同研究会, 豊中市（大阪大学), 2022 年 1 月 6–8 日.

石田勝彦,「パルスミュオン施設でのミュオン科学研究」,「ミューオン X 線 γ 線分光 非破壊分析, 化学, 原子核物理への新展開」,「ミューオン原子核捕獲反応による原子核関連研究の可能性」, 合同研究会, 豊中市（大阪大学 RNCP）&オンライン, 2022 年 3 月 24 日.

Press Release

神田聡太郎, 下村浩一郎他,「『理想の水素原子』で未知の物理現象を探索する, ミュオニウムのマイクロ波分光実験がスタート」, 高エネルギー加速器研究機構, J-PARC センター, 理化学研究所, 東京大学大学院理学系研究科, 東京大学大学院総合文化研究科, 2021 年 4 月 16 日. https://www.riken.jp/press/2021/20210416_1/index.html .

Safety Management Group

1. Abstract

The RIKEN Nishina Center for Accelerator-Based Science possesses one of the largest accelerator facilities in the world, which consists of two heavy-ion linear accelerators and five cyclotrons. This is the only site in Japan where uranium ions are accelerated. The center also has electron accelerators of microtron and synchrotron storage ring. Our function is to keep the radiation level in and around the facility below the allowable limit and to keep the exposure of workers as low as reasonably achievable. We are also involved in the safety management of the Radioisotope Center, where many types of experiments are performed with sealed and unsealed radioisotopes.

2. Major Research Subjects

(1) Safety management at radiation facilities of Nishina Center for Accelerator-Based Science
(2) Safety management at Radioisotope Center
(3) Radiation shielding design and development of accelerator safety systems

3. Summary of Research Activity

Our most important task is to keep the personnel exposure as low as reasonably achievable, and to prevent an accident. Therefore, we daily patrol the facility, measure the ambient dose rates, maintain the survey meters, shield doors and facilities of exhaust air and wastewater, replenish the protective supplies, and manage the radioactive waste. Advice, supervision and assistance at major accelerator maintenance works are also our task.

Minor improvements of the radiation safety systems were also done. The old exhaust equipment for the radiation-controlled area in the RIBF experimental building was replaced. A small and fully effective shielding for the RI production beamline in the Linac building was designed by using a Monte-Calo radiation transport calculation code.

Members

Director
Kanenobu TANAKA

Technical Scientists
Rieko HIGURASHI
Hisao SAKAMOTO

Expert Technician
Atsuko AKASHIO

Technical Staff
Hiroki MUKAI

Junior Research Associate
Kenta SUGIHARA

Visiting Scientists
Masayuki HAGIWARA (KEK)
Toshiya SANAMI (KEK)
Nobuhiro SHIGYO (Kyushu Univ.)
Hiroshi YASHIMA (Kyoto Univ.)

Administrative Part-time Workers
Kimie IGARASHI (Administrative Part-time Worker I)
Satomi IIZUKA (Administrative Part-time Worker I)
Tokie KUDO (Administrative Part-time Worker II)
Yukiko SHIODA (Administrative Part-time Worker II)
Naoko USUDATE (Administrative Part-time Worker II)

Temporary Staffing
Ryuji SUZUKI

Assistant
Tomomi OKAYASU

List of Publications & Presentations

Publication

[Original Paper]

K. Sugihara, N. Shigyo, A. Akashio, and K. Tanaka, "Measurement of neutron energy spectra of 345 MeV/u ^{238}U incidence on a copper target," Nucl. Instrum. Methods Phys. Res. B **512**, 102 (2022).

Presentations

[International Conference/Workshop]

K. Sugihara (poster), N. Shigyo, E. Lee, T. Sanami, and K. Tanaka, "Study on JQMD and INCL models for α particle incident neutron production," 2021 Symposium on Nuclear Data (SN2021), Online, November 18–19, 2021.

[Domestic Conferences/Workshops]

田中鐘信 (招待講演), 「理研 RIBF における感染症対策と最近の安全管理状況」, 第 8 回加速器施設安全シンポジウム, オンライン, 2021 年 8 月 27 日.

杉原健太 (口頭発表), 池田裕二郎, 小林知洋, 池田翔太, 藤田訓裕, 大竹淑恵, 「RANS-II の *p*-Li 中性子線源特性の実験的研究」, RANS シンポジウム, 和光市 (理化学研究所), 2021 年 5 月 13 日.

User Liaison Group

1. Abstract

The User Liaison Group is a group that provides user support, including various procedures required for accelerator use, in order to promote collaborative-use of the RIBF facilities. The group will provide user support on matters necessary for RIBF experiments, from application to completion. The group will also provide technical support for the dissemination of information on the research results of the RIBF.

The group consists of two teams. The RIBF User Liaison Team provides various supports to visiting RIBF users through the RIBF Users Office. Managing RIBF beam time and organizing the Program Advisory Committee Meetings to review RIBF experimental proposals are also important mission of the Team in order to enhance collaborative-use of the RIBF. The Outreach Team has created various information materials, such as pamphlets, posters, and homepages, to introduce the research activities in the RNC. On the homepage, we provide information on usage of the RIBF facility. The team also participate in science introduction events hosted by public institutions. In addition, the User Liaison Group also takes care of laboratory tours for RIBF visitors from public. The numbers of visitors usually amounts to 2,300 per year.

Members

Director

Hideki UENO

Assistants

Yu NAYA
Asako TAKAHASHI
Tomomi OKAYASU

User Liaison Group
RIBF User Liaison Team

1. Abstract

To enhance synergetic common use of the world-class accelerator facility, the Radioisotope Beam Factory (RIBF), it is necessary to promote a broad range of applications and to maximize the facility's importance. The facilitation and promotion of the RIBF are important missions charged to the team. Important operational activities of the team include: i) the organization of international Program Advisory Committee (PAC) meetings to review experimental proposals submitted by RIBF users, ii) RIBF beam-time operation management, and iii) promotion of facility use by hosting outside users through the RIBF Independent Users program, which is a new-user registration program begun in FY2010 at the RIKEN Nishina Center (RNC) to enhance the synergetic common use of the RIBF. The team opened the RIBF Users Office in the RIBF building in 2010, which is the main point of contact for Independent Users and provides a wide range of services and information.

2. Major Research Subjects

(1) Facilitation of the use of the RIBF
(2) Promotion of the RIBF to interested researchers

3. Summary of Research Activity

(1) Facilitation of the use of the RIBF

The RIBF Users Office, formed by the team in 2010, is a point of contact for user registration through the RIBF Independent User program. This activity includes:

- registration of users as RIBF Independent Users,
- registration of radiation workers at the RIKEN Wako Institute,
- provision of an RIBF User Card (a regular entry permit) and an optically stimulated luminescence dosimeter for each RIBF Independent User, and
- provision of safety training for new registrants regarding working around radiation, accelerator use at the RIBF facility, and information security, which must be completed before they begin RIBF research. The RIBF Users Office is also a point of contact for users regarding RIBF beam-time-related paperwork, which includes:
- contact for beam-time scheduling and safety review of experiments by the In-House Safety Committee, and
- maintaining the above information in a beam-time record database.

In addition, the RIBF Users Office assists RIBF Independent Users with matters related to their visit, such as invitation procedures, visa applications, and the reservation of on-campus accommodation.

(2) Promotion of the RIBF to interested researchers

- The team has organized an international PAC for RIBF experiments; it consists of leading scientists worldwide and reviews proposals in the field of nuclear physics (NP) purely on the basis of their scientific merit and feasibility. The team also assists another PAC meeting for material and life sciences (ML) organized by the RNC Advanced Meson Laboratory. The NP PAC meeting is organized once a year regularly, and the ML PAC meetings are organized once or twice a year.
- The team coordinates beam times for PAC-approved experiments and other development activities. It manages the operating schedule of the RIBF accelerator complex according to the decisions arrived at by the RIBF Machine Time Committee.
- To promote research activities at RIBF, proposals for User Liaison and Industrial Cooperation Group symposia/mini-workshops are solicited broadly both inside and outside of the RNC. The RIBF Users Office assists in the related paperwork.
- The team is the point of contact for the RIBF users' association. It arranges meetings at RNC headquarters for the RIBF User Executive Committee of the users' association.
- The Team conducts publicity activities, such as arranging for RIBF tours, development and improvement of the RNC official web site, and delivery of RNC news via email and the web.

Member

Team Leader

Ken-ichiro YONEDA

User Liaison Group
Outreach Team

1. Abstract

The mission of the Outreach Team is to provide various "intangible" technical support for the dissemination of information on the research in RNC. For instance, the team creates brochures introducing the RNC and the RIBF accelerator facility, posters of symposia and the summer school hosted by RNC, the center homepage containing information such as details of RNC and the procedure for the use of the RIBF facility, and images of equipment and facilities available for researchers inside and outside RIKEN, among the others. Furthermore, the team also participates in science introduction events hosted by public institutions.

2. Major Work Contents

The major work contents of the Outreach Team is to promote the publicity of RNC, through the creation of various materials such as brochures, websites, posters, and videos, among the others. The arrangement of tours of the RIBF facility and the exhibition and introduction of the RIBF facility at science events are also conducted independently or in cooperation with RIKEN Public Relations Office.

3. Summary of Work Activity

The specific work contents performed by the team are as follows:

- [Website] The Team creates/manages the RNC official website (`http://www.nishina.riken.jp`), which introduces the organization and its research activities. This website plays an important role in providing information to researchers who visit RNC to conduct his/her own research.
- [Brochures] The Team has produced various brochures introducing the organization and the studies performed at RNC. The brochures named "Your body is made of star scraps" explaining element synthesis in the universe and "Introduction of RIBF Facility" in a cartoon style for children are among them.
- [Posters] Conference/Symposium posters connected with RNC were prepared on the request of organizers. For general purpose, a special poster featuring the nuclear chart has been prepared for distribution. In commemoration of the discovery of nihonium, brochures and posters dedicated to the ceremony were made.
- [RIBF Cyclopedia] In April 2012, the permanent exhibition hall (RIBF Cyclopedia) located at the entrance hall of the RIBF building was set up in cooperation with RIKEN Public Relations Office. Explanatory illustrations on nuclear science, research at RIBF, RIBF history, a 3D nuclear chart built with LEGO blocks, and a 1/6-size GARIS model are displayed to help understanding through visual means. The Team is also working on updating the exhibits.
- [RIBF facility tour] The Team arranges RIBF facility tour for over 2000 visitors per year. The tour is guided by a researcher.
- [Science event participation] In 2010, 2012, 2013, 2015, and 2016, the sub-team opened an exhibition booth of RNC to introduce the latest research activities on the occasion of the "Science Agora" organized by Japan Science and Technology Agency (JST). From time to time, the sub-team was invited to participate in scientific events by MEXT, Wako city, and Nissan global foundation. One attraction targeting children is the hands-on work of assembling "Iron-beads" to create a nuclear chart or a shape of nihonium.

In addition to the above-noted work contents, the Team conducts a variety of works, such as taking pictures of meetings organized by RNC, cooperation in the production of a 3D video to explain the accelerators and the research at RIBF, among the others.

Members

Team Leader
Hideki UENO

Deputy Team Leader
Yasushi WATANABE

Technical Staff
Narumasa MIYAUCHI

Office of the Center Director

1. Abstract

This office is in place from JFY2018 to conduct works that the Center Director deems necessary for the operation of the research center and the secretarial work related to the research center in general.

2. Major Work Contents

- Nishina Center Monthly Meeting
  The pupose of the meeting is to share information on activities within the Nishina Center with all of the members. The meeting covers introduction of new comers, press-released achievements, announcement of events organized by or related to the Nishina Center, safety issues, and others to be informed to all members. The meeting agenda is distributed to all of the members via mailing-list.
- Conference Support
  Assistant staff members support coherently a large-size conference hosted by the Nishina Center.
- Orientation for new comers to the Nishina Center
  The Orientation is organized once a year to the new comers to give instructions for emergency response, safety in research, computer and network resources and security, and research misconduct prevention.

3. Summary of Work Activity

- Nishina Center Monthly Meeting
  Noriko Asakawa arranged the agenda and Hidetada Baba supported the on-line video system for the meeting.
  - The 168th April 14, 2021
    (1) Greetings from the RNC director to kick off new fiscal year
    (2) Award
    RIKEN Ohbu Award, RIKEN Baiho Award
    (3) Introduction of newcomers
    (4) Announcement of RIKEN Information Systems FY2021
  - The 169th May 12, 2021
    (1) Introduction of newcomers:
    (2) Press release
    “Mixed bubbles in Bose-Bose mixtures” (P. Naidon)
    Not officially announced yet (Isobe)
    (3) Report on RIKEN Open Day (Tanaka)
    (4) Report from the RNC Director
  - The 170th June 9, 2021
    (1) Broadcast on Thai PBS program (Abe)
    (2) Moving of the Promotion Office to the new HQ bldg (Hashimoto)
    (3) Information on the Newcomers Seminar (Kohama)
    (4) Report from the RNC Director
  - The 171st July 14, 2021
    (1) Machine learning and theoretical physics (A. Tomiya, SPDR, BNL)
    (2) Report from the RNC Director
    VIP visit to RIBF, COVID-19, Tokyo 2020 traffic regulations
    (3) Others
  - The 172nd September 8, 2021
    (1) Article on “3 nucleon force” in Nikkei newspaper (Sekiguchi)
    (2) Diversity working group (Nio)
    (3) Report from the RNC Director
  - The 173rd October 13, 2021
    (1) Introduction of newcomers
    Masaaki Kimura (Director, Nuclear Many-body Theory Lab)
    Phong Vi (PD Researcher, Radioactive Isotope Physics Lab)
    Zuxing Yang (PD Researcher, Radioactive Isotope Physics Lab)
    Kenichiro Tateishi (Research Scientist, Spin Isospin Lab)
    (2) Awards
    IAEA Women in Plant Mutation Breeding Award, Tomoko Abe (Director, Beam Mutagenesis Group)
    RIBF Thesis Award, Masaomi Tanaka (SPD Researcher, Radioactive Isotope Physics Lab)
    (3) Report from the RNC director
    (4) Other

- The 174th November 10, 2021
  (1) Young Scientist Award of the Physical Society of Japan, 2022
  Tokuro Fukui (SPDR, Strangeness Nuclear Physics Lab), Junki Tanaka (PD, Spin Isospin Lab), Takumi Yamaga (PD, Meson Science Lab),
  (2) Direct photons probe Gluon's dynamic motion in the proton.
  Yasuyuki Akiba (Group Leader, RBRC Beam Mutagenesis Group)
  (3) Introduction of a new textbook "Modern Nuclear Physics" (H. Sagawa)
  (4) Report from the RNC director
  (5) Other
- The 175th December 8, 2021
  (1) Introduction of a newcomer
  Daisuke Inotani (Contract Researcher, Strangeness Nuclear Physics Laboratory)
  (2) Press release
  Start of investigator-initiated clinical trial to treat refractory thyroid cancer - New targeted alpha particle therapy using astatine - (Haba)
  (3) Report from the RNC director
  Visit of the MEXT vice minister
  COVID-19
  (4) Other
- The 176th January 12, 2022
  (1) New Year's Greetings from the RNC Director
  (2) Introduction of a newcomer
  Li, Yutian (IPA, Spin Isospin Laboratory), Yap, Jinn Ming (IPA, Radioactive Isotope Physics Laboratory)
  (3) Awards
  Student Presentation Award of the Physical Society of Japan: A. Hirayama, Inoue Research Award for Young Scientist: R. Taniuchi
  (4) Press Release
  "Breeding a new Satsuma mandarin variety suitable for long-term storage" (T. Abe)
  (5) New book
  "How was the new element nihonium created?" (H. Haba)
  (6) TV broadcast
  Program on TV Saitama: "Shibusawa Kaitai Shinsho" (December 23, 2021) (Y. Watanabe)
  (7) Feature article
  2022 February Issue of "Nikkei Science" (K. Sekiguchi)
  (8) Report from the RNC director
  (9) Other
- The 177th February 9, 2022
  (1) Award
  2021 Symposium on Nuclear Data Poster Presentation Award
  (2) Special issue of "CYTOLOGIA" featuring heavy ion breeding (Abe)
  (3) Journal of the Particle of Accelerator Society of Japan: "Relocation and restoration of the third RIKEN cyclotron" (Okuno)
  (4) Fire drill (Tanaka)
  (5) Report from the RNC director
  (6) Other
- The 178th March 9, 2022
  (1) 2022 Calendar featuring "Women Scientists Who Made Nuclear Astrophysics" (Motizuki)
  (2) RIKEN Open Day on Apr. 23, recruiting explainers (Abe, Ikeda)
  (3) Report on the fire drill on Feb. 25 (Tanaka)
  (4) Report from the RNC director
  (5) Greeting from the closing of the Radiation Laboratory (En'yo)

- Conference Support
  No large size conferences hosted by the Nishina Center were organized.

- Orientation for new comers to the Nishina Center
  The Orientation was organized on May 20, 2021.

Members

Director

Hiroyoshi SAKURAI

Research Administrator

Narumasa MIYAUCHI

Assistants

Noriko ASAKAWA
Yu NAYA
Asako SAKIHAMA
Karen SAKUMA
Asako TAKAHASHI
Mitsue YAMAMOTO
Izumi YOSHIDA

Partner Institutions

The RIKEN Nishina Center for Accelerator-Based Science (RNC) has collaborated with universities and research institutes since 2008 under the research partnership agreement. This collaboration framework permits an external institute to develop its own projects at the RIKEN Wako Campus in equal partnership with the RNC. At present, two institutes—the Center for Nuclear Study (CNS), the University of Tokyo and the Wako Nuclear Science Center (WNSC), Institute of Particle and Nuclear Studies (IPNS), High Energy Accelerator Research Organization (KEK)—are conducting joint research under the research partnership agreement.

The CNS and RNC signed the research partnership agreement in 2008. Until then, the CNS had collaborated in joint programs with RIKEN under the "Research Collaboration Agreement on Heavy Ion Physics" (collaboration agreement) signed in 1998. The partnership agreement redefines procedures related to the joint programs while keeping the spirit of the collaboration agreement. The joint programs include experimental nuclear-physics activities using CRIB, SHARAQ, and GRAPE at the RI Beam Factory (RIBF), accelerator development; and activities at RHIC PHENIX.

The KEK-WNSC and RNC signed a research partnership agreement on "Low-Energy Unstable Nuclear Beam Science" in 2011. The joint experimental programs are based on the KEK Isotope Separation System (KISS). The KISS has been available for RIBF users since 2015. The research collaboration agreement for the SLOWRI facility and the multi-reflection time-of-flight (MRTOF) mass spectrograph was then signed in 2019, based on which the SLOWRI Joint Operation Committee has been established for the collaborative use and operation of the SLOWRI facility.

Experimental proposals that request the use of the above-noted devices of the CNS and KEK, together with other key devices at the RIBF, are screened by the Program Advisory Committee for Nuclear Physics experiments at the RIBF (NP-PAC). The NP-PAC meetings are co-hosted by the CNS and KEK.

Matters necessary for the smooth promotion of joint research based on the research partner agreement are determined at the Collaboration Liaison Council. More specific matters related to the execution of collaborative research are discussed at the Collaboration Liaison Committee established under the Liaison Council. In order to enhance the effectiveness of coordination and information sharing on joint research programs, the Joint Researchers Meeting was established in 2020 under the Collaboration Liaison Committee.

Several members of both institutes have also been invited to participate as external members in RNC committees related to the operation of the RIBF, such as the Machine-Time Committee and the Safety Review Committee.

The activities of the CNS and KEK are reported in the succeeding pages.

Partner Institution
Center for Nuclear Study, Graduate School of Science
The University of Tokyo

1. Abstract

The Center for Nuclear Study (CNS) aims to elucidate the nature of nuclear system by producing the characteristic states where the Isospin, Spin and Quark degrees of freedom play central roles. These researches in CNS lead to the understanding of the matter based on common natures of many-body systems in various phases. We also aim at elucidating the explosion phenomena and the evolution of the universe by the direct measurements simulating nuclear reactions in the universe. In order to advance the nuclear science with heavy-ion reactions, we develop AVF upgrade, CRIB and SHARAQ facilities in the large-scale accelerators laboratories RIBF. The OEDO facility has been developed as an upgrade of the SHARAQ, where a RF deflector system has been introduced to obtain a good quality of low-energy beam. A new project for fundamental symmetry using heavy RIs has been starting to install new experimental devices in the RIBF. We promote collaboration programs at RIBF as well as RHIC-PHENIX and ALICE-LHC with scientists in the world, and host international meetings and conferences. We also provide educational opportunities to young scientists in the heavy-ion science through the graduate course as a member of the department of physics in the University of Tokyo and through hosting the international summer school.

2. Major Research Subjects

(1) Accelerator Physics
(2) Nuclear Astrophysics
(3) NUSPEQ/Low Energy Nuclear Reaction group
(4) Quark physics
(5) Nuclear Theory
(6) OEDO/SHARAQ project
(7) Exotic Nuclear Reaction
(8) Active Target Development
(9) Fundamental Physics

3. Summary of Research Activity

(1) Accelerator physics

One of the major tasks of the accelerator group is the development of ion sources and the optimization of the beam transport system to CRIB, E7B, and C12 in the E7 experiment room. In 2021, the operating time of HyperECR ion source was 1773 hours. The beam production methods for metallic ions such as Li, Mg, and Fe have matured. High brightness metallic ion beams to match the requirement for the experiments can now be achieved stably and sustainably. Together with undergoing studies on ECR plasma, further improvements in beam qualities are expected. For the development of the 4-dimensional emittance monitor for the extracted beam from AVF cyclotron, the design of an optical system with a digital camera equipped with a tele lens was completed. Then, it is expected that the monitor can be kept away from the beamline which was the radiation source caused by the ion beam.

(2) Nuclear astrophysics

The main activity of the nuclear astrophysics group is to study astrophysical reactions and special nuclear structure, such as clusters, using the low-energy RI beam separator CRIB. In 2021, two major experimental projects at CRIB were completed and final publications were made; One was on the study of the ^{7}Be destruction process in the Big-bang nucleosynthesis, to solve the cosmological ^{7}Li abundance problem. The other is on the precise determination of the ^{22}Mg(α, p) astrophysical reaction, relevant in X-ray bursts. In January 2022, we performed the first physics experiment at CRIB after the pandemic, which was to simultaneously study the ^{26}Si(α, α) scattering and the (α, p) reaction, relevant to the astrophysics.

(3) NUSPEQ/Low Energy Nuclear Reaction group

The NUSPEQ (NUclear SPectroscopy for Extreme Quantum system) and Low Energy Nuclear Reaction group study exotic structures in high-isospin and/or high-spin states in nuclei. The groups play a major role in the OEDO/SHARAQ project described below. In 2021, analysis of a new measurement of the ^{4}He(^{8}He, ^{8}Be)4n reaction for better statistics and better accuracy has been proceeding. A recoil particle detector for missing mass spectroscopy, named TiNA, at OEDO had been upgraded under the collaboration with RIKEN and RCNP. The original TiNA consisted of 6 sector telescopes and 12 CsI (Tl) crystals. Four TTT-type (1024 channels) doubly-sided silicon detectors and twenty-two CsI(Tl) were added to make a TiNA2 array. The production cross sections of ^{178m2}Hf were evaluated for the mass production in the future with a new and simple chemical separation method. The inelastic decays from the isobaric analog resonances of ^{97}Zr were studied for the single particle wave functions coupled to the second 0^{+} state in ^{96}Zr. The nature of the different shape of the second 0^{+} state from the ground state was revealed. The systematic studies of neutron-rich Zr isotopes are planned. The CNS GRAPE (Gamma-Ray detector Array with Position and Energy sensitivity) is also a major apparatus for high-resolution in-beam gamma-ray spectroscopy. The digital signal processing devices for the GRAPE are under development.

(4) Quark physics

Main goal of the quark physics group is to understand the properties of hot and dense nuclear matter created by colliding heavy nuclei at relativistic energies. The group has been involved in the ALICE experiment at Large Hadron Collider (LHC) at CERN. The group has led the global commissioning of the ALICE upgrades in 2021. The group has involved in the data analyses, which include the measurement of low-mass lepton pairs in Pb-Pb collisions, the measurement of long range two particle correlations in *p*-Pb collisions, searches for thermal photons in high multiplicity *pp* and *p*-Pb collisions. The group has involved in the ALICE-TPC upgrade using a Gas Electron Multiplier (GEM), where the group is very active in the development and benchmarking of the online space-charge distortion corrections using machine learning techniques running on the Graphical Processing Unit (GPU).

(5) Nuclear theory

The nuclear theory group participates in a project, "Program for Promoting Researches on the Supercomputer Fugaku," and has been promoting computational nuclear physics utilizing the Fugaku supercomputer. In FY2021, we performed large-scale shell-model calculations employing the Monte Carlo shell model and quasi-particle vacua shell model to investigate various exotic structures of unstable nuclei. By using the no-core Monte Carlo shell model, we successfully describe the Hoyle state of ^{12}C from the first principle without assuming any cluster structure. In the medium-heavy mass region, we successfully described the shape phase transition of Nd and Sm isotopes based on shell-model calculations and evaluated the nuclear matrix element of the neutrinoless double-beta decay of ^{150}Nd. The nuclear Schiff moment of ^{129}Xe was also investigated based on the shell model and we found an approximately linear correlation between the Schiff moment and the magnetic moment. In parallel, we promoted many research collaborations with experimental groups for investigating the structure of various nuclei such as ^{40}Ca, ^{32}Mg, ^{47,49}Cl, and ^{55}Cr.

(6) OEDO/SHARAQ project

The OEDO/SHARAQ group pursues experimental studies of RI beams by using the high-resolution beamline and the SHARAQ spectrometer, and the OEDO for the decelerated RI beams. SHARAQ11 experiment with a tritium-doped titanium target, which has been developed by Tohoku Univ., was successfully conducted. For SHARAQ13, a mass measurement by the TOF-Brho technique for very proton-rich nuclei, an active stopper detector has been developed. The optics study of OEDO is under way to improve the transmission of the ion beams. For the high intensity RIBs, the delay-line PPACs have been replaced with the strip-readout PPACs. The experimental study of 0^- strength in nuclei using the parity-transfer charge exchange (^{16}O, ^{16}F) will be reported soon. As for The OEDO beamline, the results of the first and second experiments for LLFPs will be finalised and reported soon. The profile of X ray from the RFD had been measured comprehensively, which finalised the design of the lead shield to enable us to conduct the in-beam gamma experiment at OEDO.

(7) Exotic nuclear reaction

The Exotic Nuclear Reaction group studies various exotic reactions induced by heavy-ion beams. We conducted a search of double Gamow-Teller resonance by a double charge exchange reaction (^{12}C, ^{12}Be) at BigRIPS.

(8) Active target development

Three gaseous active target TPCs called CAT-S, CAT-M and GEM-MSTPC are developed and used for the missing mass spectroscopies. The CAT's are employed for the study of equation of state of nuclear matter. The measurement of giant monopole resonance in ^{132}Sn at RIBF with CAT-S and the data analysis is ongoing. The CAT-M was employed for the systematic measurement of the deuteron inelastic scattering of the Xe and Kr isotopes. Newly developed permanent dipole magnet system was installed to reduce the background due to the delta rays. The GEM-MSTPC is employed for the nuclear astrophysics study. The data analysis of (α, p) reaction on ^{18}Ne and ^{22}Mg and the β-decay of ^{16}Ne followed by α emission are ongoing.

(9) Fundamental physics

The development of an optical lattice interferometer to search for a permanent electric dipole moment (EDM) with Francium (Fr) atoms is now in progress at RIKEN. The lattice-like potential with a standing wave of laser light, the so-called optical lattice, can realize a long interaction time of the trapped Fr atoms with external fields, which allows to measure the EDM with high precision. The experimental apparatus to produce the cold Fr atoms trapped in the magneto-optical trap (MOT) is ready at present. We have confirmed that the newly developed surface ionizer can produce approximately 10^6 Fr^+/s as a secondary beam via nuclear fusion reaction. We are now optimizing the experimental parameters to realize the high intensity cold Fr sources with 10^6 atoms to measure the EDM.

Members

Director

Susumu SHIMOURA

Scientific Staff

Susumu SHIMOURA (Professor)
Yasuhiro SAKEMI (Professor)
Kentaro YAKO (Associate Professor)
Nobuaki IMAI (Associate Professor)
Taku GUNJI (Associate Professor)
Noritaka SHIMIZU (Project Associate Professor)
Hidetoshi YAMAGUCHI (Lecturer)
Shin'ichiro MICHIMASA (Assistant Professor)
Shinsuke OTA (Assistant Professor)
Hiroki NAGAHAMA (Assistant Professor)

Guest Scientists

Yutaka UTSUNO (Guest Professor)
Daiki NISHIMURA (Guest Associate Professor)
Toshitaka KAJINO (Guest Post Doctoral Associate)
Ikuko HAMAMOTO (Guest Post Doctoral Associate)
Jongwon HWANG (Guest Post Doctoral Associate)

Academic Specialist

Reiko KOJIMA

Technical Specialist

Yasuteru KOTAKA

Techinical Assistant

Masayoshi YAGYU

Project Research Associates

Masanori DOZONO
Seiya HAYAKAWA
Daiki SEKIHATA
Rin YOKOYAMA

Post Doctoral Associates

Keisuke NAKAMURA
Keita KAMAKURA
Nanru MA
Yusuke TSUNODA
Kota YANASE
Thomas William CHILLERY

Assistant Teaching Staff

Yuko SEKIGUCHI
Keita KAWATA
Akane SAKAUE
Shoichiro MASUOKA

Graduate Students

Hideki SHIMIZU
Rieko TSUNODA
Naoya OZAWA
Shutaro HANAI
Shintaro NAGASE
Ryotaro KOHARA
Jiatai LI
Daisuke UEHARA
Kodai OKAWA
Hitoshi BABA
Mirai FUKASE

Administration Staff

Noriko SHIMANE
Ikuko YAMAMOTO
Yukino KISHI
Aki KOTAKA

List of Publications & Presentations

Publications

[Original Papers]

S. Go, E. Ideguchi, R. Yokoyama, N. Aoi, F. Azaiez, K. Furutaka, Y. Hatsukawa, A. Kimura, K. Kisamori, M. Kobayashi, F. Kitatani, M. Koizumi, H. Harada, I. Matea, S. Michimasa, H. Miya, S. Nakamura, M. Niikura, H. Nishibata, N. Shimizu, S. Shimoura, T. Shizuma, M. Sugawara, D. Suzuki, M. Takaki, Y. Toh, Y. Utsuno, D. Verney, and A. Yagi, "High-spin states in ^{35}S," Phys. Rev. C **103**, 034327 (2021).

H. Baba, T. Ichihara, T. Isobe, T. Ohnishi, K. Yoshida, Y. Watanabe, S. Ota, H. Shimizu, S. Shimoura, S. Takeuchi, D. Nishimura, J. Zenihiro, A. O. Tokiyasu, and R. Yokoyama, "MPV-parallel readout architecture for the VME data acquisition system," IEEE Trans. Nucl. Sci. **68**, 1841–1848 (2021).

R. Nakamoto, M. Ito, A. Saito, and S. Shimoura, "Extended Migdal-Watson formula to evaluate background strength in binary breakup reactions," Phys. Rev. C **104**, 034602 (2021).

N. Kitamura, N. Imai, H. Haba, S. Michimasa, S. Shimoura, and Y. Yamaguchi, "Production of ^{178}Hf^{m2} and a simple chemical separation method for Hf recovery," J. Radioanal. Nucl. Chem. **330**, 721–725 (2021).

S. W. Huang, Z. H. Yang, F. M. Marqués, N. L. Achouri, D. S. Ahn, T. Aumann, H. Baba, D. Beaumel, M. Böhmer, K. Boretzky, M. Caamaño, S. Chen, N. Chiga, M. L. Cortés, D. Cortina, P. Doornenbal, CA. Douma, F. Dufter, J. Feng, B. Fernandez-dominguez, Z. Elekes, U. Forsberg, T. Fujino, N. Fukuda, I. Gašparić, Z. Ge, R. Gernhäuser, J. M. Gheller, J. Gibelin, A. Gillibert, Z. Halász, T. Harada, M. N. Harakeh, A. Hirayama, N. Inabe, T. Isobe, J. Kahlbow, N. Kalantar-Nayestanaki, D. Kim, S. Kim, S. Kiyotake, T. Kobayashi, Y. Kondo, P. Koseoglou, Y. Kubota, I. Kuti, C. Lehr, C. Lenain, P. J. Li, Y. Liu, Y. Maeda, S. Masuoka, M. Matsumoto, A. Matta, J. Mayer, H. Miki, M. Miwa, B. Monteagudo, I. Murray, T. Nakamura, A. Obertelli, N. A. Orr, H. Otsu, V. Panin, S. Park, M. Parlog, S. Paschalis, M. Potlog, S. Reichert, A. Revel, D. Rossi, A. Saito, M. Sasano, H. Sato, H. Scheit, F. Schindler, T. Shimada, Y. Shimizu, S. Shimoura, H. Simon, I. Stefan, S. Storck, L. Stuhl, H. Suzuki, D. Symochko, H. Takeda, S. Takeuchi, J. Tanaka, Y. Togano, T. Tomai, H. T. Törnqvist, E. Tronchin, J. Tscheuschner, T. Uesaka, V. Wagner, K. Wimmer, H. Yamada, B. Yang, L. Yang, Y. Yasuda, K. Yoneda, L. Zanetti, and J. Zenihiro, "Experimental study of ^{4}n by directly detecting the decay neutrons," Few-Body Systems **62**, 102 (2021).

R. Nakamoto, M. Ito, A. Saito, and S. Shimoura, "Continuum strength of direct breakup induced by external isoscalar field," Few-Body Systems **62**, 107 (2021).

W. Horiuchi, T. Inakura, and S. Michimasa, "Large enhancement of total reaction cross sections at the edge of the island of inversion in Ti, Cr, and Fe isotopes," Phys. Rev. C **105**, 014316 (2022).

R. Yokoyama, E. Ideguchi, G. S. Simpson, Mn. Tanaka, Y. Sun, C. -J. Lv, Y. -X. Liu, L. -J. Wang, S. Nishimura, P. Doornenbal, G. Lorusso, P. A. Soderstrom, T. Sumikama, J. Wu, Z. Y. Xu, N. Aoi, H. Baba, F. L. B. Garrote, G. Benzoni, F. Browne, R. Daido, Y. Fang, N. Fukuda, A. Gottardo, G. Gey, S. Go, S. Inabe, T. Isobe, D. Kameda, K. Kobayashi, M. Kobayashi, I. Kojouharov, T. Komatsubara, T. Kubo, N. Kurz, I. Kuti, Z. Li, M. Matsushita, S. Michimasa, C. B. Moon, H. Nishibata, I. Nishizuka, A. Odahara, Z. Patel, S. Rice, E. Sahin, H. Sakurai, H. Schaffner, L. Sinclair, H. Suzuki, H. Takeda, J. Taprogge, Z. Vajta, H. Watanabe, and A. Yagi, "Three-quasiparticle isomers in odd-even ^{159,161}Pm: Calling for modified spin-orbit interaction for the neutron-rich region," Phys. Rev. C **104**, L021303 (2021).

R. D. Harding, A. N. Andreyev, A. E. Barzakh, J. G. Cubiss1, P. Van Duppen, M. Al Monthery, N. A. Althubiti, B. Andel, S. Antalic, T. E. Cocolios, T. Day Goodacre, K. Dockx, G. J. Farooq-Smith, D. V. Fedorov, V. N. Fedosseev, D. A. Fink, L. P. Gaffney, L. Ghys, J. D. Johnson, D. T. Joss, M. Huyse, N. Imai, K. M. Lynch, B. A. Marsh, Y. Martinez Palenzuel, P. L. Molkanov, G. G. O'Neill, R. D. Page, R. E. Rossel, S. Rothe, M. D. Seliverstov, S. Sels, C. Van Beveren, and E. Verstraelen, "Laser-assisted nuclear decay spectroscopy of ^{176,177,179}Au," Phys. Rev. C **104**, 024326 (2022).

N. Kitamura, K. Wimmer, T. Miyagi, A. Poves, N. Shimizu, J. A. Tostevin, V. M. Bader, C. Bancroft, D. Barofsky, T. Baugher, D. Bazin, J. S. Berryman, V. Bildstein, A. Gade, N. Imai, T. Kröll, C. Langer, J. Lloyd, E. Lunderberg, F. Nowacki, G. Perdikakis, F. Recchia, T. Redpath, S. Saenz, D. Smalley, S. R. Stroberg, Y. Utsuno, D. Weisshaar, and A. Westerberg, "In-beam γ-ray spectroscopy of ^{32}Mg via direct reactions," Phys. Rev. C **105**, 034318 (2022).

A. Fernández, A. Jungclaus, P. Doornenbal, M. A. Bentley, S. M. Lenzi, D. Rudolph, F. Browne, M. L. Cortés, T. Koiwai, R. Taniuchi, V. Vaquero, K. Wimmer, T. Arici, N. Imai, N. Kitamura, B. Longfellow, R. Lozeva, B. Mauss, D. R. Napoli, M. Niikura, X. Pereira-Lopez, S Pigliapoco, A. Poves, F. Recchia, P. Ruotsalainen, H. Sakurai, S. Uthayakumaar, R. Wadsworth, and R. Yajzey, "Mirror energy differences above the $0f(7/2)$ shell: First gamma-ray spectroscopy of the $T_z = -2$ nucleus ^{56}Zn," Phys. Lett. **823**, 136784 (2021).

S. Hayakawa, M. La Cognata, L. Lamia, H. Yamaguchi, D. Kahl, K. Abe, H. Shimizu, L. Yang, O. Beliuskina, S. M. Cha, K. Y. Chae, S. Cherubini, P. Figuera, Z. Ge, M. Gulino, J. Hu, A. Inoue, N. Iwasa, A. Kim, D. Kim, G. Kiss, S. Kubono, M. La Commara, M. Lattuada, E. J. Lee, J. Y. Moon, S. Palmerini, C. Parascandolo, S. Y. Park, V. H. Phong, D. Pierroutsakou, R. G. Pizzone, G. G. Rapisarda, S. Romano, C. Spitaleri, X. D. Tang, O. Trippella, A. Tumino, and N. T. Zhang, "Constraining the primordial lithium abundance: New cross section measurement of the ^{7}Be+n reactions updates the total ^{7}Be destruction rate," Astrophys. J. Lett. **915**, L13 (2021).

S. Palmerini, M. La Cognata, F. Hammache, L. Acosta, R. Alba, V. Burjan, E. Chávez, S. Cherubini, A. Cvetinović, G. D'Agata, N. de Séréville, A. Di Pietro, P. Figuera, Z. Fülöp, K. Gaitán De Los Rios, G. L. Guardo, M. Gulino, S. Hayakawa, G. G. Kiss, M. La Commara, L. Lamia, C. Maiolino, G. Manicó, C. Matei, M. Mazzocco, J. Mrazek, T. Parascandolo, T. Petruse, D. Pierroutsakou, R. G. Pizzone, G. G. Rapisarda, S. Romano, D. Santonocito, M. L. Sergi, R. Spartà, A. Tumino, and H. Yamaguchi, "The ^{27}Al$(p,\alpha)^{24}$Mg reaction at astrophysical energies studied by means of the trojan horse method applied to the ^{2}H(^{27}Al, α ^{24}Mg)n reaction," Eur. Phys. J. Plus **136**, 898 (2021).

J. Hu, H. Yamaguchi, Y. H. Lam, A. Heger, D. Kahl, A. M. Jacobs, Z. Johnston, S. W. Xu, N. T. Zhang, S. B. Ma, L. H. Ru, E. Q. Liu, T. Liu, S. Hayakawa, L. Yang, H. Shimizu, C. B. Hamill, A. St J. Murphy, J. Su, X. Fang, K. Y. Chae, M. S. Kwag, S. M. Cha, N. N. Duy, N. K. Uyen, D. H. Kim, R. G. Pizzone, M. La Cognata, S. Cherubini, S. Romano, A. Tumino, J. Liang, A. Psaltis, M. Sferrazza, D. Kim, Y. Y. Li, and S. Kubono, "Advancement of photospheric radius expansion and clocked type-I X-ray burst models with the new ^{22}Mg$(\alpha, p)^{25}$Al reaction rate determined at the Gamow energy," Phys. Rev. Lett. **127**, 172701 (2021).

G. G. Kiss, M. La Cognata, R. Yarmukhamedov, K. I. Tursunmakhatov, I. Wiedenhöver, L. T. Baby, S. Cherubini, A. Cvetinović, G. D'Agata, P. Figuera, G. L. Guardo, M. Gulino, S. Hayakawa, I. Indelicato, L. Lamia, M. Lattuada, F. Mudò, S. Palmerini, R. G. Pizzone, G. G. Rapisarda, S. Romano, M. L. Sergi, R. Spartà, C. Spitaleri, O. Trippella, A. Tumino, M. Anastasiou, S. A. Kuvin, N. Rijal, B. Schmidt, S. B. Igamov, S. B. Sakuta, Zs. Fülöp, Gs. Gyürky, T. Szücs, Z. Halász, E. Somorjai, Z. Hons, J. Mrázek, R. E. Tribble, and A. M. Mukhamedzhanov, "Indirect determination of the astrophysical S factor for the ^{6}Li(p, γ)^{7}Be reaction using the asymptotic normalization coefficient method," Phys. Rev. C **104**, 015807 (2021).

U. A. Acharya *et al.* [PHENIX], "Transverse-single-spin asymmetries of charged pions at midrapidity in transversely polarized p+p collisions at $\sqrt{s}$ = 200 GeV," Phys. Rev. D **105**, 032003 (2022).

S. Acharya *et al.* [ALICE], "Production of light (anti)nuclei in pp collisions at $\sqrt{s}$ = 5.02 TeV," Eur. Phys. J. C **82**, 289 (2022).

S. Acharya *et al.* [ALICE], "Observation of a multiplicity dependence in the p_T-differential charm baryon-to-meson ratios in proton–proton collisions at $\sqrt{s}$ = 13 TeV," Phys. Lett. B **829**, 137065 (2022).

S. Acharya *et al.* [ALICE], "Investigating charm production and fragmentation via azimuthal correlations of prompt D mesons with

charged particles in pp collisions at $\sqrt{s}$ = **13** TeV," Eur. Phys. J. C **82**, 335 (2022).

S. Acharya *et al.* [ALICE], "Measurement of prompt D_s^+-meson production and azimuthal anisotropy in Pb–Pb collisions at $\sqrt{s_{NN}}$=5.02 TeV," Phys. Lett. B **827**, 136986 (2022).

S. Acharya *et al*. [ALICE], "Prompt D^0, D^+, and D^{*+} production in Pb–Pb collisions at $\sqrt{s_{\rm NN}}$ = 5.02 TeV," J. High Energy Phys. **01**, 174 (2022).

U. A. Acharya *et al.* [PHENIX], "Transverse single spin asymmetries of forward neutrons in p + p, p+Al and p+Au collisions at $\sqrt{s_{NN}}$ = 200 GeV as a function of transverse and longitudinal momenta," Phys. Rev. D **105**, 032004 (2022).

S. Acharya *et al.* [ALICE], "Measurement of inclusive charged-particle b-jet production in pp and p-Pb collisions at $\sqrt{s_{\rm NN}}$ = 5.02 TeV," J. High Energy Phys. **01**, 178 (2022).

S. Acharya *et al.* [ALICE], "Production of light (anti)nuclei in pp collisions at $\sqrt{s}$ = 13 TeV," J. High Energy Phys. **01**, 106 (2022).

S. Acharya *et al.* [ALICE], "Prompt and non-prompt J/ψ production cross sections at midrapidity in proton-proton collisions at $\sqrt{s}$ = 5.02 and 13 TeV," J. High Energy Phys. **03**, 190 (2022).

S. Acharya *et al.* [ALICE], "Inclusive J/ψ production at midrapidity in pp collisions at $\sqrt{s}$ = 13 TeV," Eur. Phys. J. C **81**, 1121 (2021).

S. Acharya *et al.* [A Large Ion Collider Experiment and ALICE], "Measurement of the groomed jet radius and momentum splitting fraction in *pp* and Pb−Pb collisions at $\sqrt{s_{NN}}$ = 5.02 TeV," Phys. Rev. Lett. **128**, 102001 (2022).

S. Acharya *et al.* [ALICE], "Measurements of the groomed and ungroomed jet angularities in pp collisions at $\sqrt{s}$ = 5.02 TeV," J. High Energy Phys. **05**, 061 (2022).

S. Acharya *et al.* [ALICE], "Polarization of Λ and $\bar{\Lambda}$ hyperons along the beam direction in Pb-Pb collisions at $\sqrt{s_{NN}}$=5.02 TeV," Phys. Rev. Lett. **128**, 172005 (2022).

S. Acharya *et al*. [ALICE], "$K_S{}^0$- and (anti-)Λ-hadron correlations in pp collisions at $\sqrt{s}$ = 13 TeV," Eur. Phys. J. C **81**, 945 (2021).

S. Acharya *et al.* [ALICE], "Anisotropic flow of identified hadrons in Xe-Xe collisions at $\sqrt{s_{\rm NN}}$ = 5.44 TeV," J. High Energy Phys. **10**, 152 (2021).

U. A. Acharya *et al*. [PHENIX], "Kinematic dependence of azimuthal anisotropies in p+Au, d+Au, and ^{3}He+Au at $\sqrt{s_{NN}}$ = 200 GeV," Phys. Rev. C **105**, 024901 (2022).

S. Acharya *et al*. [ALICE], "Direct observation of the dead-cone effect in quantum chromodynamics," Nature **605**, 440 (2022).

S. Acharya *et al*. [ALICE], "Measurement of prompt D^0, Λ_c^+, and $\Sigma_c^{0,++}$(2455) production in proton–proton collisions at $\sqrt{s}$ = 13 TeV," Phys. Rev. Lett. **128**, 012001 (2022).

S. Acharya *et al*. [ALICE], "Charm-quark fragmentation fractions and production cross section at midrapidity in pp collisions at the LHC," Phys. Rev. D **105**, L011103 (2022).

S. Acharya *et al*. [ALICE], "Measurement of the production cross section of prompt Ξ_c^0 baryons at midrapidity in pp collisions at $\sqrt{s}$ = 5.02 TeV," J. High Energy Phys. **10**, 159 (2021).

S. Acharya *et al*. [ALICE], "Experimental evidence for an attractive p-ϕ interaction," Phys. Rev. Lett. **127**, 172301 (2021).

S. Acharya *et al*. [ALICE], "Kaon–proton strong interaction at low relative momentum via femtoscopy in Pb–Pb collisions at the LHC," Phys. Lett. B **822**, 136708 (2021).

S. Acharya *et al*. [ALICE], "Charged-particle multiplicity fluctuations in Pb–Pb collisions at $\sqrt{s_{\rm NN}}$ = 2.76 TeV," Eur. Phys. J. C **81**, 1012 (2021).

S. Acharya *et al*. [ALICE], "Measurement of $K^*(892)^\pm$ production in inelastic pp collisions at the LHC," Phys. Lett. B **828**, 137013 (2022).

S. Acharya *et al*. [ALICE], "First measurements of N-subjettiness in central Pb-Pb collisions at $\sqrt{s_{\rm NN}}$ = 2.76 TeV," J. High Energy Phys. **10**, 003 (2021).

S. Acharya *et al*. [ALICE], "Measurement of the cross sections of Ξ_c^0 and Ξ_c^+ baryons and of the branching-fraction ratio BR($\Xi_c^0 \rightarrow \Xi^- e^+ \nu_e$)/BR($\Xi_c^0 \rightarrow \Xi^- \pi^+$) in *pp* collisions at 13 TeV," Phys. Rev. Lett. **127**, 272001 (2021).

S. Acharya *et al*. [ALICE], "Investigating the role of strangeness in baryon–antibaryon annihilation at the LHC," Phys. Lett. B **829**, 137060 (2022).

S. Acharya *et al*. [ALICE], "Production of Λ and K_s^0 in jets in p–Pb collisions at $\sqrt{s_{NN}}$=5.02 TeV and pp collisions at $\sqrt{s}$=7 TeV," Phys. Lett. B **827**, 136984 (2022).

S. Acharya *et al*. [ALICE], "Energy dependence of ϕ meson production at forward rapidity in pp collisions at the LHC," Eur. Phys. J. C **81**, 772 (2021).

S. Acharya *et al*. [ALICE], "Nuclear modification factor of light neutral-meson spectra up to high transverse momentum in p–Pb collisions at $\sqrt{s_{\rm NN}}$ = 8.16 TeV," Phys. Lett. B **827**, 136943 (2022).

U. A. Acharya *et al*. [PHENIX], "Probing gluon spin-momentum correlations in transversely polarized protons through midrapidity isolated direct photons in $p^\uparrow + p$ collisions at $\sqrt{s}$=200 GeV," Phys. Rev. Lett. **127**, 162001 (2021).

S. Acharya *et al*. [ALICE], "Measurement of beauty and charm production in pp collisions at $\sqrt{s}$ = 5.02 TeV via non-prompt and prompt D mesons," J. High Energy Phys. **05**, 220 (2021).

S. Acharya *et al*. [ALICE], "Measurements of mixed harmonic cumulants in Pb–Pb collisions at $\sqrt{s_{NN}}$ = 5.02 TeV," Phys. Lett. B **818**, 136354 (2021).

S. Acharya *et al*. [ALICE], "First measurement of the $|t|$-dependence of coherent J/ψ photonuclear production," Phys. Lett. B **817**, 136280 (2021).

S. Acharya *et al*. [ALICE], "Coherent J/ψ and ψ' photoproduction at midrapidity in ultra-peripheral Pb-Pb collisions at $\sqrt{s_{\rm NN}}$ = 5.02 TeV," Eur. Phys. J. C **81**, 712 (2021).

S. Acharya *et al*. [ALICE], "Long- and short-range correlations and their event-scale dependence in high-multiplicity pp collisions at $\sqrt{s}$ = 13 TeV," J. High Energy Phys. **05**, 290 (2021).

S. Acharya *et al*. [ALICE], "Production of pions, kaons, (anti-)protons and ϕ mesons in Xe–Xe collisions at $\sqrt{s_{\rm NN}}$ = 5.44 TeV," Eur. Phys. J. C **81**, 584 (2021).

S. Acharya *et al*. [ALICE], "First measurement of coherent ρ^0 photoproduction in ultra-peripheral Xe–Xe collisions at $\sqrt{s_{\rm NN}}$ = 5.44 TeV," Phys. Lett. B **820**, 136481 (2021).

S. Acharya *et al*. [ALICE], "Multiharmonic correlations of different flow amplitudes in Pb-Pb collisions at $\sqrt{s_{NN}}$ = 2.76 TeV," Phys. Rev. Lett. **127**, 092302 (2021).

K. S. Tanaka, K. Harada, T. Hayamizu, R. Kita, R. Kono, K. Maruta, H. Nagahama, N. Ozawa, Y. Sakemi, and R. Sugimori, "The accelerator experiment for junior and senior high school students to improve students' involvement in fundamental physics," Phys. Edu. **57**, 045013 (2022).

R. Mitra, V. S. Prasannaa, R. F. Garcia Ruiz, T. K. Sato, M. Abe, Y. Sakemi, B. P. Das, and B. K. Sahoo, "Towards CP violation studies on superheavy molecules: Theoretical and experimental perspectives," Phys. Rev. A **104**, 062801 (2021).

T. Aoki, R. Sreekantham, B. K. Sahoo, Bindiya Arora, A. Kastberg, T. Sato, H. Ikeda, N. Okamoto, Y. Torii, T. Hayamizu, K. Nakamura, S. Nagase, M. Ohtsuka, H. Nagahama, N. Ozawa, M. Sato, T. Nakashita, K. Yamane, K. S. Tanaka, K. Harada, H. Kawamura, T. Inoue, A. Uchiyama, A. Hatakeyama, A. Takamine, H. Ueno, Y. Ichikawa, Y. Matsuda, H. Haba, and Y. Sakemi, "Quantum sensing of the electron electric dipole moment using ultracold entangled Fr atoms," Quantum Sci. Technol. **6**, 044008 (2021).

K. S. Tanaka, U. Dammalapati, K. Harada, T. Hayamizu, M. Itoh, H. Kawamura, H. Nagahama, K. Nakamura, N. Ozawa, and Y. Sakemi, "Two-dimensional beam profile monitor for the detection of alpha-emitting radioactive isotope beam," Nucl. Instrum. Methods Phys. Res. A **1017**, 165803 (2021).

E. Ideguchi, T. Kibedi, J. Dowie, H. T. Hoang, Kumar Raju M., G. Lane, L. Bignell, T. K. Eriksen, A. J. Mitchell, A. Akber, B. Combes, B. McCormik, T. Gray, A. Stuchbery, N. Shimizu, and Y. Utsuno, "Electric monopole transition from the superdeformed band in ^{40}Ca," Phys. Rev. Lett. **2022**, 053D02 (2022).

S. Yoshida and N. Shimizu, "A new workflow of shell-model calculations with the emulator and preprocessing using eigenvector continuation," Prog. Theor. Exp. Phys. **128**, 252501 (2022).

T. Otsuka, T. Abe, T. Yoshida, Y. Tsunoda, N. Shimizu, N. Itagaki, Y. Utsuno, J. Vary, P. Maris, and H. Ueno, "α-Clustering in atomic nuclei from first principles with statistical learning and the hoyle state character," Nat. Commun. **13**, 2234 (2022).

N. Kitamura, K. Wimmer, T. Miyagi, A. Poves, N. Shimizu, J. A. Tostevin, V. M. Bader, C. Bancroft, D. Barofsky, T. Baugher, D. Bazin, J. S. Berryman, V. Bildstein, A. Gade, N. Imai, T. Kröll, C. Langer, J. Lloyd, E. Lunderberg, F. Nowacki, G. Perdikakis, F. Recchia, T. Redpath, S. Saenz, D. Smalley, S. R. Stroberg, Y. Utsuno, D. Weisshaar, and A. Westerberg, "In-beam γ-ray spectroscopy of ^{32}Mg via direct reactions," Phys. Rev. C **105**, 034318 (2022).

T. Koiwai, K. Wimmer, P. Doornenbal, A. Obertellid, T. Miyagi, J. D. Holt, N. Shimizu, V. Soma, Y. Utsuno, K. Ogata, K. Yoshida, N. Achouri, H. Baba, F. Browne, D. Calvet, F. Chateaue, S. Chen, N. Chiga, A. Corsi, M. L. Cortes, A. Delbart, J-M. Gheller, A. Giganon, A. Gillibert, C. Hilaire, T. Isobe, T. Kobayashi, Y. Kubota, V. Lapoux, H. N. Liue, T. Motobayashi, I. Murray, H. Otsu, V. Panin, N. Paul, W. Rodriguez, H. Sakurai, M. Sasano, D. Steppenbeck, L. Stuhl, Y. L. Sun, Y. Togano, T. Uesaka,K. Yoneda, O. Aktas, T. Aumann, L. X. Chung, F. Flavigny, S. Franchoo, I. Gasparic, R. -B. Gerst, J. Gibelin, K. I. Hahn, D. Kim, Y. Kondo, P. Koseoglou, J. Lee, C. Lehr, B. D. Linh, T. Lokotko, M. MacCormick, K. Moschner, T. Nakamura, S. Y. Park, D. Rossi, E. Sahina, P. -A. Soderstrom, D. Sohlera, S. Takeuchi, H. Toernqvist, V. Vaquero, V. Wagner, S. Wanga, V. Werner, X. Xu, H. Yamada, D. Yana, Z. Yang, M. Yasuda, and L. Zanetti, "A first glimpse at the shell structure beyond ^{54}Ca: spectroscopy of ^{55}K, ^{55}Ca and ^{57}Ca," Phys. Lett. B **827**, 136953 (2022).

T. Otsuka, N. Shimizu, and Y. Tsunoda, "Moments and radii of exotic Na and Mg isotopes," Phys. Rev. C **105**, 014319 (2022).

B. D. Linh, A. Corsi, A. Gillibert, A. Obertelli, P. Doornenbal, C. Barbieri, S. Chen, L. X. Chung, T. Duguet, M. Gomez-Ramos, J. D. Holt, A. Moro, P. Navratil, K. Ogata, N. T. T. Phuc, N. Shimizu, V. Soma, Y. Utsuno, N. Achouri, H. Baba, F. Browne, D. Calvet, F. Chateau, N. Chiga, M. L. Cortes, A. Delbart, J. -M. Gheller, A. Giganon, C. Hilaire, T. Isobe, T. Kobayashi, Y. Kubota, V. Lapoux, H. N. Liu, T. Motobayashi, I. Murray, H. Otsu, V. Panin, N. Paul, W. Rodriguez, H. Sakurai, M. Sasano, D. Steppenbeck, L. Stuhl, Y. L. Sun, Y. Togano, T. Uesaka, K. Wimmer, K. Yoneda, O. Aktas, T. Aumann, F. Flavigny, S. Franchoo, I. Gasparic, R. B. Gerst, J. Gibelin, K. I. Hahn, N. T. Khai, D. Kim, T. Koiwai, Y. Kondo, P. Koseoglou, J. Lee, C. Lehr, T. Lokotko, M. Maccormick, K. Moschner, T. Nakamura, S. Y. Park, D. Rossi, E. Sahin, D. Sohler, P. -A. Soderstrom, S. Takeuchi, H. Tornqvist, V. Vaquero, V. Wagner, H. Wang, V. Werner, X. Xu, N. D. Ton, Y. Yamada, D. Yan, Z. Yang, M. Yasuda, and L. Zanetti, "Investigation of the ground-state spin inversion in the neutron-rich ^{47,49}Cl isotopes," Phys. Rev. C **104**, 044331 (2021).

N. Kitamura, K. Wimmer, A. Poves, N. Shimizu, J. Tostevin, V. M. Bader, C. Bancroft, D. Barofsky, T. Baugher, D. Bazin, J. S. Berryman, V. Bildstein, A. Gade, N. Imai, T. Kroll, C. Langer, J. Lloyd, E. Lunderberg, G. Perdikakis, F. Recchia, T. Redpath, S. Saenz, D. Smalley, S. R. Stroberg, Y. Utsuno, D. Weisshaar, and A. Westerberg, "Coexisting normal and intruder configurations in ^{32}Mg," Phys. Lett. B **822**, 136682 (2021).

T. Abe, P. Maris, T. Otsuka, N. Shimizu, Y. Utsuno, and J. P. Vary, "Ground-state properties of light 4*n* self-conjugate nuclei in no-core Monte Carlo shell model with nonlogcal *NN* interactions," Phys. Rev. C **104**, 054315 (2021).

R. Nakamoto, E. Ueda, M. Ito, and N. Shimizu, "Formulation of shell-cluster overlap integral with Gaussian expansion method," Prog. Theor. Exp. Phys. **2021**, 113D01 (2021).

H. Kleis, M. Seidlitz, A. Blazhev, L. Kaya, P. Reiter, K. Arnswald, A. Dewald, M. Droste, C. Fransen, O. Möller, N. Shimizu, Y. Utsuno, P. von Brentano, and K. O. Zell, "Lifetime measurements of excited states in ^{55}Cr," Phys. Rev. C **104**, 034310 (2021).

N. Shimizu, T. Mizusaki, K. Kaneko, and Y. Tsunoda, "Generator-coordinate methods with symmetry-restored Hartree-Fock-Bogoliubov wave functions for large-scale shell-model calculations," Phys. Rev. C **103**, 064302 (2021).

K. Kaneko, N. Shimizu, T. Mizusaki, and Y. Sun, "Triple enhancement of quasi-SU(3) quadrupole collectivity in strontium-zirconium $N \approx Z$ isotopes," Phys. Lett. B **817**, 136286 (2021).

[Review Article]

Y. Utsuno, "Probing different characteristics of shell evolution driven by central, spin-orbit, and tensor forces," Physics **4**, 185–201 (2022).

[Proceedings]

S. Michimasa, "Development of energy-degraded RI beam and expansion of nuclear reaction studies—Recent results obtained by the OEDO-SHARAQ system," Proceedings of the 2020 Symposium on Nuclear Data, November 26–27, 2020, RIKEN Nishina Center, Wako, Japan, JAEA-Conf 2021-001, pp.59–64.

S. Gorbunov, E. Hellbar, G. M. Innocenti, M. Ivanov, M. Kabus, M. Kleiner, H. Riaz, D. Rohr, R. Sadikin, K. Schweda *et al*., "Deep neural network techniques in the calibration of space-charge distortion fluctuations for the ALICE TPC," EPJ Web Conf. **251**, 03020 (2021).

D. Sekihata for the ALICE Collaboration, "Low-mass dielectron measurements in pp, p-Pb and Pb-Pb collisions with ALICE at the LHC," Proc. Sci. **HardProbes2020**, 047 (2021).

T. Hayamizu, H. Haba, K. Nakamura, T. Aoki, H. Nagahama, K. Tanaka, N. Ozawa, M. Ohtsuka, and Y. Sakemi, "Development of ultracold francium atomic sources towards the permanent EDM search," Few-Body Syst. **63**, 11 (2022).

N. Shimizu, Y. Utsuno, and T. Togashi, "β-decay half-lives of neutron-rich $N = 82, 81$ isotones by shell-model calculations," EPJ Web Conf. **260**, 11049 (2022).

Presentations

[International Conferences/Workshops]

H. Yamaguchi (oral), "Nuclear astrophysics at the low-energy RI beam separator CRIB," RIBF Users Meeting 2021, Web meeting hosted by RIKEN, Wako, Saitama, Japan, September 7–9, 2021.

H. Yamaguchi (oral), "Experimental studies on astrophysical reactions at the low-energy RI beam separator CRIB," The 16th International Symposium on Nuclei in the Cosmos (NIC-XVI), Web symposium hosted by JUNA, China, September 21–25, 2021.

H. Yamaguchi (oral), "Cluster states and astrophysical (α, p) reactionss," RCNP Workshop, "Cluster phenomena in knockout and astrophysical reactions," Web workshop hosted by RCNP, Osaka University, October 14–15, 2021.

T. Gunji (invited) for the ALICE collaboration, "Future measurements from ALICE Run3 and Run4," The 8th Asian Triangle Heavy-Ion Conference (ATHIC2021), Inha Univ. Incheon, South Korea, Hybrid, November 5–9, 2021.

D. Sekihata for the ALICE Collaboration, "Low-mass dielectron measurement in ALICE at the LHC," The 8th Asian Triangle Heavy-Ion Conference, Inha Univ. Incheon, South Korea, Hybrid, November 5–9, 2021.

K. Nakamura (oral), "Development of a laser frequency stabilization and an optical transmission system for the francium electric dipole moment search," 29th Annual International Laser Physics Workshop (LPHYS'21), Online, Jul 23, 2021.

N. Ozawa (oral), "Current status of the electron EDM search using laser-cooled francium atoms," 13th International Workshop on Fundamental Physics Using Atoms (FPUA2021), Online, August 4–5, 2021.

M. Sato (keynote talk), "Search for permanent EDM by using Fr atoms," SPIN2021, Kunibiki Messe, Shimane, Japan, Hybrid, October 18–22, 2021.

Y. Utsuno (oral), "Present status of large-scale shell-model calculations for photonuclear reactions," Second PANDORA Workshop, September 10, 2021.

N. Shimizu (oral), "Microscopic description of the collective motions of medium-heavy nuclei based on shell-model calculations," 13th symposium on Discovery, Fusion, Creation of New Knowledge by Multidisciplinary Computational Sciences, Online, October 8, 2021.

Y. Tsunoda (oral), "Nuclear shapes and collective motions in the region of Sm," 13th symposium on Discovery, Fusion, Creation of New Knowledge by Multidisciplinary Computational Sciences, Online, October 8, 2021.

N. Shimizu (poster), "Gamow-Teller transition of neutron-rich $N = 82, 81$ nuclei by shell-model calculations," 16th International Symposium on Nuclei in the Cosmos (NIC-XVI), Online, September 25, 2021.

[Domestic Conferences/Workshops]

S. Shimoura (invited): "High-resolution spectroscopy with SHARAQ and advice on HIHR," the 2nd J-PARC HEF-ex workshop, Online, February 16–18, 2022.

T. Chillery (oral): "Measurement of deuteron-induced pre-equilibrium reactions on ^{93}Zr at 30 MeV/u for the Treatment of Radioactive Waste," 2022 Annual (77th) Meeting of The Physical Society of Japan, Online, March 15–19, 2022.

R. Tsunoda (oral): "Observation of the isobaric analog resonances coupled to the excited state in Zr isotope," 2022 Annual (77th) Meeting of The Physical Society of Japan, Online, March 15–19, 2022.

J. T. Li (oral): "New project to explore neutron-deficient actinide nuclei," 2022 Annual (77th) Meeting of The Physical Society of Japan, Online, March 15–19, 2022.

S. Hanai (oral): "A fast-response tracking detector for high-intensity heavy ion beams," Workshop for radiation detector and their uses, KEK, January 24–26, 2022.

N. Imai (invited): "Nuclear Structure study with decelerated RI beams," RCNP future workshop, October 27–29, 2021.

川田敬太 (口頭発表), 「核破砕反応における角運動量移行」, 日本物理学会 2021 年秋季大会, オンライン, 2021 年 9 月 14–17 日.

早川勢也（口頭発表）:「^{7}Be+n ビッグバン元素合成反応の測定と原始 ^{7}Li 生成量の検証」, 日本物理学会 秋季大会, オンライン,

2021 年 9 月 14–17 日.

郡司卓 (招待講演), “Status of ALICE upgrade and commissioning for run3,” 第 7 回クラスター階層領域研究会, 東北大学, 2021 年 12 月 27–28 日.

郡司卓 (招待講演), 「高密度クォーク物質探索の展望」, シンポジウム「宇宙観測, 加速器実験と理論の協奏で探る高密度核物質」, 日本物理学会第 77 回年次大会, オンライン, 2022 年 3 月 15–19 日.

関畑大貴 (招待講演), 「光子・レプトン対・ハード測定」, 重イオン衝突の時空発展の理解に向けた理論・実験合同研究会, オンライン, 2021 年 9 月 24 日.

D. Sekihata for the ALICE Collaboration, 「$\sqrt{\mathrm{sNN}}$ = 5.02 TeV 鉛+鉛原子核衝突における ALICE 実験の電子対測定」, 日本物理学会 2021 年秋季大会, オンライン, 2021 年 9 月 14–17 日.

関畑大貴, 「ALICE 実験での電子対の結果と展望」, Heavy Ion Pub 研究会, オンライン, 2021 年 5 月 28 日.

関口裕子 for the ALICE Collaboration, 「LHC-ALICE 実験を用いた長距離 2 粒子相関のシステムサイズ依存性測定」, 日本物理学会第 77 回年次大会, オンライン, 2022 年 3 月 15–19 日.

関口裕子 for the ALICE Collaboration, 「LHC-ALICE 実験を用いた小さな衝突系における 2 粒子相関測定」, 日本物理学会 2021 年秋季大会, オンライン, 2021 年 9 月 14–17 日.

中村 圭佑（口頭発表）:「波長計による光周波数安定化、光ファイバー伝送システム」, 第 82 回応用物理学会秋季学術講演会, オンライン, 2021 年 9 月 11–13 日.

永瀬慎太郎（口頭発表）:「原子の電気双極子能率探索に向けたレーザー冷却フランシウム源の開発」, 日本物理学会 2021 年秋季大会, オンライン, 2021 年 9 月 14–17 日.

中下輝士（口頭発表）:「フランシウムの電気双極子能率探索に向けた冷却原子制御系開発」, 日本物理学会 2021 年秋季大会, オンライン, 2021 年 9 月 14–17 日.

山根風樹（口頭発表）:「永久電気双極子能率探索に向けたアクチニウム-225 電着基板を用いたフランシウム-221 原子線源の開発」, 日本物理学会 2021 年秋季大会, オンライン, 2021 年 9 月 14–17 日.

鎌倉恵太 (ポスター発表), 「東京大学 CNS 14 GHz Hyper ECR イオン源の現状」, 第 18 回日本加速器学会年会, オンライン, 2021 年 8 月 9–12 日.

清水則孝（口頭発表）, 「CI 計算とその発展的手法による大規模原子核構造計算」, 2021 年度第 2 回 HPCIC 計算科学フォーラム, オンライン, 2022 年 3 月 28 日.

大塚孝治（口頭発表）, 清水則孝, 吉田聡太, 角田直文, 角田佑介, 「殻模型計算による中性子過剰 pf 殻核の構造」, 日本物理学会第 76 回年次大会, オンライン, 2022 年 3 月 17 日.

清水則孝（口頭発表）, 「CI 計算とその発展的手法による大規模原子核構造計算」, 「富岳」成果創出加速プログラム シンポジウム・研究交流会「富岳百景」2021 年度第 2 回 HPCIC 計算科学フォーラム, オンライン, 2022 年 3 月 14 日.

清水則孝（口頭発表）, 「大規模殻模型計算による中重核構造研究の進展」, 「富岳で加速する素粒子・原子核・宇宙・惑星」シンポジウム, オンライン, 2022 年 1 月 17 日.

富樫智章（口頭発表）, 清水則孝, 宇都野穣, 「殻模型計算による $N = 82, 81$ 中性子過剰核のガモフテラー遷移」, 日本物理学会 2021 年秋の分科会, オンライン, 2021 年 9 月 14 日.

大塚孝治（口頭発表）, 角田佑介, 清水則孝, 「準粒子真空殻模型計算による中重核の構造の研究」, 日本物理学会 2021 年秋季大会, オンライン, 2021 年 9 月 15 日.

大塚孝治（口頭発表）, 角田佑介, 清水則孝, 「準粒子真空殻模型計算による Sm 領域の構造の研究」, 日本物理学会第 77 回年次大会, オンライン, 2022 年 3 月 17 日.

吉永尚孝（口頭発表）, 柳瀬宏太, 清水則孝, 東山幸司, 「キセノン原子核のシッフモーメントと中性子 EDM 探索」, 日本物理学会第 77 回年次大会, 2022 年 3 月 17 日.

清水則孝（口頭発表）, 宇都野穣, 角田佑介, 「大規模殻模型計算による M1 バンドの解析」, 日本物理学会 2021 年秋季大会, オンライン, 2021 年 9 月 15 日.

宇都野穣（口頭発表）, 「非イラスト領域における原子核の秩序の探求」, RCNP での次期計画検討会, 2021 年 9 月 27 日.

宇都野穣（口頭発表）, “Cluster formation in nuclei from first-principles Monte Carlo shell model,” 第 7 回クラスター階層領域研究会, 2021 年 12 月 27 日.

[Seminar]

T. Otsuka, “What determines the driplines of atomic nuclei?,” CNS+RIBF NP seminar, Online, November 5, 2021.

Press Releases

山口英斉, 早川勢也, Hu Jun, 「X 線バースト天体における不安定マグネシウム燃焼の解明」, 2021 年 10 月 20 日.

早川勢也, 山口英斉, 「ビッグバンで生成されるリチウム量の矛盾、解決へ一歩前進」, 2021 年 7 月 1 日.

Partner Institution
Wako Nuclear Science Center, IPNS (Institute of Particle and Nuclear Studies)
KEK (High Energy Accelerator Research Organization)

1. Abstract

The Wako Nuclear Science Center (WNSC) of KEK aims to promote low-energy nuclear physics and nuclear astrophysics research as well as interdisciplinary studies using short-lived radioactive nuclei. WNSC operates the KEK Isotope Separation System (KISS), an electromagnetic isotope separator featuring elemental selectivity from resonance laser ionization in a gas catcher. The KISS facility uniquely provides various neutron-rich isotopes of refractory elements via multinucleon transfer reactions to the users from universities. Its provision of nuclei in the vicinity of the neutron magic number $N = 126$. Optical and β-γ spectroscopy have been applied to these neutron-rich nuclear beams for nuclear structure and nuclear astrophysical studies. Several new developments—a rotating target, a donut-shaped gas cell, and an in-jet laser ionization scheme—have been performed to improve the performance of the KISS facility. The WNSC also leads comprehensive mass measurements of all-available nuclides at RIBF using multi-reflection time of flight mass spectrographs (MRTOF-MS). Three MRTOF setups were placed at the GARIS-II, the beam dump of the ZeroDegree Spectrometer, and the KISS. The masses of more ore than 400 nuclides, including superheavy elements, were measured so far. KISS-II is being considered a future project of WNSC. Combining KISS and MRTOF technologies, 10,000 times more performance than conventional methods are expected. It aims to study the origin of uranium for the first time.

2. Major Research Subjects

(1) Production and manipulation of radioactive isotope beams for nuclear experiments
(2) Explosive nucleosynthesis (r- and rp-process)
(3) Heavy ion reaction mechanism for producing heavy neutron-rich nuclei
(4) Development of MRTOF mass spectrographs for short-lived nuclei
(5) Comprehensive mass measurements of short-lived nuclei including superheavy elements
(6) Development of KISS-II

3. Summary of Research Activity

The Wako Nuclear Science Center (WNSC) provides low-energy short-lived radioactive ion beams of neutron-rich refractory elements to researchers from universities using the KEK isotope separator system (KISS). In FY2021, five experiments with a total of 69 participants from 3 domestic institutes were executed. Due to the restrictions of COVID-19, the participation of foreign collaborators was limited, and no experiment with foreign spokesperson was conducted. A highlight at the KISS facility was the discovery of a new uranium isotope by means of mass spectrometry, described in a different article of this report.

The team of WNSC leads comprehensive mass measurements of all available nuclides at RIKEN RIBF using multiple MRTOF mass spectrographs. KEK announced a press release for the first mass measurement of superheavy elements performed at the GARIS-MRTOF facility. It claims a new method for identifying new elements via a high precision mass measurement. Mass measurement of dubnium isotopes continued with a new sulfide target, allowing the use of much higher primary beam intensity. A newly installed In-MRTOF mass filter eliminates molecular contaminants in a mass spectrum, making possible accurate mass determinations without a need for decay correlation. Mass measurements at the BigRIPS-SLOWRI facility of RIBF continued for more exotic isotopes of nickel. In total, more than 400 nuclides were measured in the campaigns led by WNSC.

The WNSC plans to extend the present KISS facility to investigate the nuclides in the neutron-rich region of uranium using the multi-nucleon transfer reactions of actinide targets to study the origin of uranium. The IPNS organized review committee meetings for the design report of KISS-II and received high marks and helpful suggestions.

Members

Group Leader
Michiharu WADA

Researchers
Yutaka WATANABE
Peter SCHURY
Sunchan JEONG
Yoshikazu HIRAYAMA
Hiroari MIYATAKE
Marco ROSENBUSCH

Technical Staff
Yutaka KAKIGUCHI
Michihiro OYAIZU

Visiting Researchers
Hermann WOLLNIK (NMSU)
Sidong CHEN (HKU)
Wenduo XIAN (HKU)
Hiroshi WATANABE (Beihan University)
Dongsheng HOU (IMP)
Toshitaka NIWASE (JPS PD)

Student Trainee

Shun IIMURA (PhD. Student, Osaka Univ.)

Assistant

Machiko IZAWA

List of Publications & Presentations

Publications

[Original Papers]

M. Mukai, Y. Hirayama, Y. X. Watanabe, H. Watanabe, H. Koura, S. C. Jeong, H. Miyatake, M. Brunet, S. Ishizawa, F. G. Kondev, G. J. Lane, Yu. A. Litvinov, T. Niwase, M. Oyaizu, Zs. Podolyák, M. Rosenbusch, P. Schury, M. Wada, and P. M. Walker, "Ground-state β-decay spectroscopy of ^{187}Ta," Phys. Rev. C **105**, 034331 (2022).

T. Niwase, M. Wada, P. Schury, P. Brionnet, S. D. Chen, T. Hashimoto, H. Haba, Y. Hirayama, D. S. Hou, S. Iimura, H. Ishiyama, S. Ishizawa, Y. Ito, D. Kaji, S. Kimura, J. Liu, H. Miyatake, J. Y. Moon, K. Morimoto, K. Morita, D. Nagae, M. Rosenbusch, A. Takamine, T. Tanaka, Y. X. Watanabe, H. Wollnik, W. Xian, and S. X. Yan, "α-decay-correlated mass measurement of ^{206,207g,m}Ra using an α-TOF detector equipped multireflection time-of-flight mass spectrograph system," Phys. Rev. C **104**, 044617 (2021).

P. Schury, T. Niwase, M. Wada, P. Brionnet, S. Chen, T. Hashimoto, H. Haba, Y. Hirayama, D. S. Hou, S. Iimura, H. Ishiyama, S. Ishizawa, Y. Ito, D. Kaji, S. Kimura, H. Koura, J. J. Liu, H. Miyatake, J. Y. Moon, K. Morimoto, K. Morita, D. Nagae, M. Rosenbusch, A. Takamine, Y. X. Watanabe, H. Wollnik, W. Xian, and S. X. Yan, "First high-precision direct determination of the atomic mass of a superheavy nuclide," Phys. Rev. C **104**, L021304 (2021).

Y. X. Watanabe, P. M. Walker, Y. Hirayama, M. Mukai, H. Watanabe, G. J. Lane, M. Ahmed, M. Brunet, T. Hashimoto, S. Ishizawa, S. Kimura, F. G. Kondev, Yu. A. Litvinov, H. Miyatake, J. Y. Moon, T. Niwase, M. Oyaizu, J. H. Park, Zs. Podolyák, M. Rosenbusch, P. Schury, and M. Wada, "First direct observation of isomeric decay in neutron-rich odd-odd ^{186}Ta," Phys. Rev. C **104**, 024330 (2021).

M. Ahmed, Y. X. Watanabe, Y. Hirayama, M. Mukai, J. H. Park, P. Schury, Y. Kakiguchi, A. Ozawa, M. Oyaizu, M. Wada, and H. Miyatake, "β-γ Spectroscopy of the ^{195}Os nucleus," Phys. Rev. C **103**, 054312 (2021).

S. Kimura, D. Kaji, Y. Ito, H. Miyatake, K. Morimoto, P. Schury, and M. Wada, "Reduction of contaminants originating from primary beam by improving the beam stoppers in GARIS-II," Nucl. Instrum. Method Phys. Res. A **992**, 164996 (2021).

Y. Hirayama, P. Schury, M. Mukai, H. Choi, S. Iimura, Y. X. Watanabe, M. Wada, H. Watanabe, and H. Miyatake, "Three-dimensional tracking multi-segmented proportional gas counter for β-decay spectroscopy of unstable nuclei," Nucl. Instrum. Methods Phys. Res. A **997**, 165152 (2021).

M. Tajima, A. Takamine, M. Wada, and H. Ueno, "Offline ion source for laser spectroscopy of RI at the SLOWRI," Nucl. Instrum. Methods Phys. Res. B **486**, 48–54 (2021).

T. Day Goodacre, A. V. Afanasjev, A. E. Barzakh, B. A. Marsh, S. Sels, P. Ring, H. Nakada, A. N. Andreyev, P. Van Duppen, N. A. Althubiti, B. Andel, D. Atanasov, J. Billowes, K. Blaum, T. E. Cocolios, J. G. Cubiss, G. J. Farooq-Smith, D. V. Fedorov, V. N. Fedosseev, K. T. Flanagan, L. P. Gaffney, L. Ghys, M. Huyse, S. Kreim, D. Lunney, K. M. Lynch, V. Manea, Y. Martinez Palenzuela, P. L. Molkanov, M. Rosenbusch, R. E. Rossel, S. Rothe, L. Schweikhard, M. D. Seliverstov, P. Spagnoletti, C. Van Beveren, M. Veinhard, E. Verstraelen, A. Welker, K. Wendt, F. Wienholtz, R. N. Wolf, A. Zadvornaya, and K. Zuber, "Laser spectroscopy of neutron-rich ^{207,208}Hg isotopes: Illuminating the kink and odd-even staggering in charge radii across the $N = 126$ shell closure," Phys. Rev. Lett. **126**, 032502 (2021).

[Book]

和田道治, 「重元素の起源と短寿命核原子の質量」, in 「物理科学, この 1 年 2022」, パリティ編集委員会編, 丸善, 2022 年 01 月, pp. 109–113.

[Proceeding]

H. Miyatake, "KISS project," AIP Conf. Proc. **2319**, 080006 (2021).

Presentations

[International Conferences/Workshops]

M. Wada (invited), "KISS to KISS-II—exploring the origins of uranium," JSPS/NRF/NSFC A3 Foresight Program, "Nuclear physics in the 21st century" Joint Annual Meeting, Online, February 18, 2022.

M. Rosenbusch (oral), "The new high-precision MRTOF mass spectrograph at the ZeroDegree spectrometer of BigRIPS," The 16th International Symposium on Nuclei in the Cosmos 2021 (NIC-XVI), Chengdu, Online, September 21–25, 2021.

M. Rosenbusch (oral), "The new MRTOF mass spectrograph at the ZeroDegree spectrometer," RIBF Users Meeting 2021, Online, September 7–9, 2021.

Y. Hirayama (oral), "Nuclear spectroscopy at KISS," RIBF Users Meeting 2021, Online, September 7–9, 2021.

[Domestic Conferences/Workshops]

庭瀬暁隆 (口頭発表), 「MRTOF+α-TOF による ^{257,258}Db の精密質量測定」, 日本物理学会第 77 回年次大会, オンライン, 2022 年 3 月 15–19 日.

平山賀一 (招待講演), 「KISS でのレーザー核分光」, 令和 3 年度専門研究会「短寿命 RI を用いた核分光と核物性研究 (VIII)」, オンライン, 2022 年 1 月 28 日.

庭瀬暁隆 (口頭発表), 「MRTOF と α-TOF 検出器による, α 崩壊に相関した精密質量測定法の開拓」, 日本放射化学会第 65 回討論会（2021）, オンライン, 2021 年 9 月 22–24 日.

庭瀬暁隆 (口頭発表), 「超重核 ^{257}Db の直接質量測定」, 日本物理学会 2021 年秋季大会, オンライン, 2021 年 9 月 14–17 日.

平山賀一 (口頭発表), 「KISS での核分光: MRTOF-MS を用いた不安定核のレーザー共鳴イオン化核分光」, 日本物理学会 2021 年秋季大会, オンライン, 2021 年 9 月 14–17 日.

D. Hou (口頭発表), "Mass measurement in the neutron-rich Mo region using the new ZD-MRTOF system," 日本物理学会 2021 年秋季大会, オンライン, 2021 年 9 月 14–17 日.

W. Xian (口頭発表), "New mass measurements of neutron-rich nuclei of Ge, As, and Se, and an accuracy study of the new ZD-MRTOF system," 日本物理学会 2021 年秋季大会, オンライン, 2021 年 9 月 14–17 日.

飯村俊 (口頭発表), 「新規開発された ZD-MRTOF 装置を用いた中性子過剰 Sc, Ti, V 核の系統的質量測定」, 日本物理学会 2021 年秋季大会, オンライン, 2021 年 9 月 14–17 日.

M. Rosenbusch (口頭発表), "New technologies for multi-reflection time-of-flight mass spectrometry at BigRIPS," 日本物理学会 2021 年秋季大会, オンライン, 2021 年 9 月 14–17 日.

[Seminars]

T. Niwase, "Direct mass measurement of superheavy nuclides via MRTOF mass spectrograph equipped with an α-TOF detector," RIBF Nuclear Physics Seminar, Online, February 12, 2022.

M. Wada, "KISS to KISS-II—An expedition to the origin of uranium—," Nuclear Astrophysics Seminar, Online, November 19, 2021.

Y. Watanabe, "Production of neutron-rich nuclei around $N = 126$ and beyond using multinucleon transfer reactions at KISS project," Virtual SHE seminars, Online, October 12, 2021.

Award

向井もも, 「^{196,197,198}Ir のガスセル内レーザー共鳴イオン化分光」, 2021 年度理化学研究所桜舞賞 (研究奨励賞), 2022 年 3 月.

Press Release

超重元素の初めての精密質量測定に成功〜新元素の新しい原子番号決定法の証明〜, KEK, RIKEN, Kyushu University, 2021 年 8 月 31 日, https://www.kek.jp/ja/press/202109010000/.

VII. APPENDICES

List of Symposia & Workshops (April 2021—March 2022)

RNC

1	International Workshop on the Extension Project for the J-PARC Hadron Experimental Facility (J-PARC HEF-ex WS) https://indico2.riken.jp/event/3773/	online	Jul. 7–9
2	RIBF Users Meeting 2021 https://indico2.riken.jp/event/3821/	online	Sep. 7–9
3	高エネルギービーム利活用に向けた展望～イオンビームを用いた育種と社会実装に向けた研究～ http://www.werc.or.jp/newsdetail/img/R030806press2.pdf	online	Sep. 15
4	24th International SPIN Symposium http://spin2021.riken.jp	Kunibiki Messe, Shimane	Oct. 18–22
5	BNL-HET & RBRC Joint Workshop "DWQ@25": The event marks the passage of twenty-five years since the first numerical simulations with Domain Wall Quarks (DWQ) https://indico.bnl.gov/event/13576/	online	Dec. 13–17
6	RBRC Workshop: Small-x Physics in the EIC Era https://www.bnl.gov/smallxphysicsworkshop/	online	Dec. 15–17
7	原子核物理学実験におけるデータ利活用による研究戦略（研究 DX 化推進ファンド） https://indico2.riken.jp/event/4016/	RIKEN Integrated Innovation Building/online	Mar. 7

KEK

1	SSRI-PNS Collaboration Meeting 2021 https://indico2.riken.jp/event/3807/overview	online	Sep. 2–3

List of Seminars (April 2021—March 2022)

Nuclear Physics Monthly Colloquium

	Not held in 2021		

RIBF Nuclear Physics Seminar

1	Emiko Hiyama (Tohoku U.)	Structure of light ¥Xi hypernuclei and Hyperon-Hyperon interaction (virtual) https://indico2.riken.jp/event/3701/	Apr. 13
2	Minho Kim (Korea Univ./RIKEN)	Transverse single-spin asymmetry for very forward neutral particle production in high-energy polarized p + p collisions (virtual) https://indico2.riken.jp/event/3719/	May 11
3	Leung Tsz Tang (Argonne National Laboratory)	Study the role of the valence proton in ^{23,25}F using the (p,2p) quasi-free knockout reaction (virtual) https://indico2.riken.jp/event/3761/	Jul. 6
4	Pascal Naidon (RIKEN)	Prediction of a "mixed bubble" quantum phase (virtual) https://indico2.riken.jp/event/3849/	Sep. 7
5	Tadaaki Isobe (RNC)	Measurement of spectral pion ratio in Sn+Sn collisions for the constraint of density dependent nuclear symmetry energy (virtual) https://indico2.riken.jp/event/3846/	Sep. 28
6	Rituparna Kanungo (Saint Mary's U.)	Exploring nuclear shell structure in the neutron-rich landscape (virtual) https://indico2.riken.jp/event/3867/	Oct. 5
7	Takaharu Otsuka (UT and RNC)	What determines the driplines of atomic nuclei? (Let's look back to basic concepts of nuclear physics.) (Hybrid: Zoom + RIBF Hall) https://indico2.riken.jp/event/3912/	Nov. 5
8	Masaaki Kimura (RNC)	Erosion of N = 28 shell gap, shape coexistence and monopole transitions in the vicinity of ^{44}S (virtual) https://indico2.riken.jp/event/3997/	Jan. 18
9	Ralf Seidl (RNC)	Direct photon single spin asymmetries and gluon dynamics (virtual) https://indico2.riken.jp/event/4019/	Feb. 8
10	Toshitaka Niwase (KEK)	Direct mass measurement of superheavy nuclides via MRTOF mass spectrograph equipped with an α-TOF detector (virtual) https://indico2.riken.jp/event/4042/	Feb. 22
11	Takehiko Saito (RIKEN)	New directions in hypernuclear physics (virtual) https://indico2.riken.jp/event/4079/	Mar. 29

Seminar by Each Laboratory

High Energy Astrophysics Laboratory

1	Yuuki Wada (RIKEN)	実験装置開発のすすめ (virtual)	Apr. 14
2	Shoda Munehiro (NAOJ)	Stellar wind from Sun-like stars: Implications for solar wind evolution (virtual)	May 19
3	Satoru Katsuda (Saitama U.)	Density profile of the earth's upper atmosphere from its occultations of the Crab Nebula with X-ray astronomy satellites) (virtual)	Jun. 22
4	Tatsuki Washimi (NAOJ)	Gravitational wave detector KAGRA and background events induced by lightning (virtual)	Jul. 12
5	Toshiki SATO (Rikkyo U.)	超新星最深部での元素合成: X 線観測による超新星残骸内の高エントロピー上昇流の発見 (virtual)	Aug. 17

6	Ting Wu (Gifu U.)	Strong lightning discharges associated with terrestrial gamma-ray flashes in winter thunderstorms (virtual)	Sep. 29
7	Shintaro Yoshiura (NAOJ)	新時代の低周波電波観測-宇宙再電離から暗黒時代の 21cm 線探査 (virtual)	Oct. 12
8	Yousuke Sato (Hokkaido U.)	Development of a lightning model for the meteorological simulation (virtual)	Nov. 18
9	Yuko Ikkatai (Kanazawa U.)	日本における科学への市民参加 (virtual)	Dec. 20

High Energy Astrophysics Lab. Seminar → http://astro.riken.jp/wordpress/?page_id=65

Subnuclear System Research Division

1	Yoni Kahn (U. Illinois)	High-Energy Physics & RIKEN Theory Seminar Discovering the new physics of g-2 with a muon collider (virtual)	Apr. 1
2	Cédric Lorcé (CPHT)	Nuclear Physics & RIKEN Theory Seminar Revisiting the concept of relativistic charge distribution (virtual)	Apr. 2
3	Florentin Jaffredo (IJCLab Orsay)	High-Energy Physics & RIKEN Theory Seminar Single Leptoquark Solutions to the B-physics anomalies (virtual)	Apr. 8
4	Brendan Reed (Indiana U.)	RBRC Seminar The neutron skin of Pb-208 and the structure of neutron stars (virtual)	Apr. 8
5	Chirilli Giovanni (Regensburg)	Nuclear Physics & RIKEN Theory Seminar High-energy OPE for polarized DIS (virtual)	Apr. 9
6	Dalibor Djukanovic (Mainz U.)	RBRC Seminar Nucleon form factors from lattice QCD (virtual)	Apr. 15
7	Kallia Petraki (Sorbonne U.)	High-Energy Physics & RIKEN Theory Seminar Dark matter goes nuclear: The role of bound states in thermal decoupling (virtual)	Apr. 15
8	David Kaplan (Johns Hopkins U.)	High-Energy Physics & RIKEN Theory Seminar Relaxing the cosmological constant and dark energy radiation (virtual)	Apr. 22
9	Abhay Deshpande (Stony Brook U.)	RBRC Seminar EIC: Science, status and prospects (virtual)	Apr. 22
10	Alexei Bazavov (Michigan State U.)	Nuclear Physics & RIKEN Theory Seminar Efficient integration of gradient flow in lattice gauge theory and properties of low-storage commutator-free Lie group methods (virtual)	Apr. 23
11	Xiaoling Cui (Chinese Academy of Science)	SNP Seminar Stability of quantum droplet against confinement and multi-component (virtual)	Apr. 28
12	Alexander Huss (CERN)	High-Energy Physics & RIKEN Theory Seminar Precision predictions for Higgs boson production (virtual)	Apr. 29
13	Julia Gehrlein and Peter Boyle (BNL)	High-Energy Physics & RIKEN Theory Seminar Muon magnetic moment: New physics or not (virtual)	May 6
14	Alexander Kovner (UConn)	RBRC Seminar High energy evolution and S-channel unitarity: An interesting problem that bothers no one (virtual)	May 6
15	Emilie Passemar (LANL)	RBRC Seminar Precision tests of fundamental physics with η and η′ mesons (virtual)	May 13
16	Matthias Neubert (U. Mainz)	High-Energy Physics & RIKEN Theory Seminar Adventures in the ALPs — Effective Lagrangians, flavor observables and indirect searches for axion-like particles (virtual)	May 13
17	Koji Hashimoto (Kyoto U.)	RBRC Seminar An attempt for deriving nuclear physics by holography (virtual)	May 14

18	Li Sheng Geng (Beihang U.)	SNP Seminar Understanding of the LHCb pentaquark states as hadronic molecules, from masses, spin-parities to production yields (virtual)	May 14
19	Koji Hashimoto (Kyoto U.)	Nuclear Physics & RIKEN Theory Seminar An attempt for deriving nuclear physics by holography (virtual)	May 14
20	Soebur Razzaque (U. Johannesburg)	High-Energy Physics & RIKEN Theory Seminar Non-unitary neutrino oscillations to reduce tension between the NOvA and T2K data (virtual)	May 20
21	Constantia Alexandrou (U. Cyprus)	RBRC Seminar Parton distributions using lattice QCD (virtual)	May 20
22	Jacopo Ghiglieri (SUBATECH)	Nuclear Physics & RIKEN Theory Seminar Thermal gravitational wave production in the early universe (virtual)	May 21
23	Radja Boughezal (Argonne)	RBRC Seminar Proton structure, new physics and more: The EIC potential for probing the unknown (virtual)	May 27
24	Hiro Ejiri (RCNP Osaka U.)	SNP Seminar Delta isobar (Δ) contribution to neutrino nuclear response for double beta decay (virtual)	May 28
25	Feng Yuan (Lawrence Berkeley National Lab)	Nuclear Physics & RIKEN Theory Seminar Single transverse-spin asymmetry and Sivers Function on lattice (virtual)	May 28
26	Andreas Crivellin (CERN)	High-Energy Physics & RIKEN Theory Seminar Discovering lepton flavour universality violating new physics (virtual)	Jun. 3
27	Jamie Stafford (U. Houston)	RBRC Seminar First-principles-based equations of state for QCD at finite temperature and density (virtual)	Jun. 3
28	Kenji Fukushima (U. Tokyo)	Nuclear Physics & RIKEN Theory Seminar Toward understanding the high-baryon state of matter (virtual)	Jun. 4
29	Naoyuki Itagaki (Kyoto U.)	SNP Seminar Cluster structure comprised of shell model states (virtual)	Jun. 4
30	Silas Beane (U. Washington)	Nuclear Physics & RIKEN Theory Seminar Entanglement minimization in hadronic scattering (virtual)	Jun. 11
31	Kazuyuki SEKIZAWA (Tokyo Institute of Technology)	SNP Seminar Dynamics of quantized vortices in superfluid fermionic systems: From cold atoms to neutron stars (virtual)	Jun. 24
32	Jan Pawlowski (Heidelberg U.)	RBRC Seminar On the phase structure of QCD (virtual)	Jun. 25
33	Patrick Barry (Jefferson Lab)	RBRC Seminar Tagged deep inelastic scattering and its relation to pion parton distributions (virtual)	Jul. 1
34	Lucas PLATTER (U. Tennessee)	SNP Seminar Few-body systems with a van der Waals interaction (virtual)	Jul. 2
35	Anna Stasto (Penn State U.)	RBRC Seminar A new Wilson line-based action for gluodynamics (virtual)	Jul. 2
36	Yi Chen (CERN)	RBRC Seminar Extraction of qhat in heavy-ion collisions with a Bayesian analysis (virtual)	Jul. 8
37	Son Dam Thanh (U. Chicago)	RBRC Seminar Nonrelativistic conformal field theory and unnuclear physics	Jul. 9
38	Marlene Nahrgang (Subatech)	RBRC Seminar Discovering the QCD critical point with dynamical fluctuations (virtual)	Jul. 15
39	Andrey Sadofyev (U. Santiago de Compostela)	RBRC Seminar Ab initio coupling of jets to collective flow in the opacity expansion approach (virtual)	Jul. 16
40	Veronica Dexheimer (Kent State U.)	RBRC Seminar Equation of state from heavy-ion collisions to neutron stars (virtual)	Jul. 22

41	Miguel Escobedo (Santiago de Compostela U.)	RBRC Seminar Phenomenological study of quarkonium suppression and the impact of the energy gap between singlets and octets (virtual)	Jul. 23
42	Claudia Ratti (U. Houston)	RBRC Seminar Equation of state from lattice QCD (virtual)	Jul. 29
43	Prasad Hegde (Indian Institute of Science)	RBRC Seminar A new way to resum the finite-density lattice QCD Taylor series (virtual)	Aug. 19
44	Kazuhiro Watanabe (SUBATECH)	RBRC Seminar Hadronic quarkonium production at high pT in QCD factorization approach (virtual)	Aug. 20
45	Martin Hentschinski (BNL)	RBRC Seminar TMD gluon distributions at NLO within high energy factorization (virtual)	Aug. 26
46	Adrien Florio (Stony Brook U.)	RBRC Seminar Gibbs entropy from entanglement in electric quenches (virtual)	Aug. 27
47	Prithwish Tribedy (BNL)	RBRC Seminar Blind analysis of isobar data for the CME search by the STAR collaboration (virtual)	Sep. 2
48	Xu-Guang Huang (Fudan U.)	RBRC Seminar Phenomenology of spin polarization and vorticity (virtual)	Sep. 3
49	Ted Rogers (Old Dominion U.)	RBRC Seminar Transverse momentum integrals and the properties of collinear PDFs (virtual)	Sep. 10
50	Lex Kemper (North Carolina State U.)	RBRC Seminar Examining topology and thermodynamics using quantum computers (virtual)	Sep. 16
51	Colin Morningstar (Carnegie Mellon U.)	RBRC Seminar Multi-hadron physics in lattice QCD (virtual)	Sep. 17
52	Dimitra Anastasia Pefkou (MIT)	RBRC Seminar Gravitational form factors of hadrons from lattice QCD (virtual)	Sep. 23
53	Chihiro Sasaki (Wroclaw)	RBRC Seminar Chiral mixing in dense matter (virtual)	Sep. 24
54	Niklas Mueller (U. Maryland)	RBRC Seminar Thermalization of gauge theories from their entanglement spectrum (virtual)	Sep. 30
55	Antonio Pineda (IFAE Barcelona)	RBRC Seminar Theoretical description of the plaquette with exponential accuracy (virtual)	Oct. 1
56	Muneto Nitta (Keio U.)	SNP Seminar $^3P_2$ superfluids and pulsar glitches from quantum vortex networks (virtual)	Oct. 6
57	Yuuka Kanakubo (Sophia U.)	RBRC Seminar Interplay between core and corona components in high-energy nuclear collisions (virtual)	Oct. 7
58	Yukari Yamauchi (Maryland U.)	RBRC Seminar Quantum algorithms for transport coefficients in gauge theories (virtual)	Oct. 8
59	Yasuki Tachibana (Akita International U.)	RBRC Seminar Description of medium response to jet propagation in quark-gluon plasma fluid (virtual)	Oct. 14
60	Guang Juan Wang (ASRC, JAEA)	SNP Seminar Novel coupled channel framework connecting quark model and lattice QCD: An investigation on near-threshold Ds states (virtual)	Oct. 15
61	Peter Arnold (U. Virginia)	RBRC Seminar Universality (beyond leading log) of soft radiative corrections to momentum broadening and energy loss of high-energy partons in QCD matter (virtual)	Oct. 15
62	Yasushi Nara (Akita International U.)	RBRC Seminar Transport theoretical approach for heavy-ion collision at high baryon densities (virtual)	Oct. 21
63	Jianhui Zhang (Beijing Normal U.)	RBRC Seminar Recent updates on meson distribution amplitudes from lattice QCD (virtual)	Oct. 22

64	Daniel Boer (U. Groningen)	RBRC Seminar GTMD studies at small x (virtual)	Oct. 28
65	Dimitrios Bachtis (Swansea U.)	RBRC Seminar Inverse renormalization group: Evading the critical slowing down effect (virtual)	Oct. 29
66	Frédéric Chevy (LKB, ENS)	SNP Seminar Impurity physics with cold atoms: Fermi polaron, Bose polaron and beyond (virtual)	Nov. 10
67	Tuomas Lappi (U. Jyvaskyla)	RBRC Seminar Loops in light cone perturbation theory (virtual)	Nov. 12
68	Neha Shah (Indian Institute of Technology Patna)	SNP Seminar Understanding hypernuclear interactions with heavy-ion collisions (virtual)	Nov. 17
69	Nobuyuki Matsumoto (Gakushuin U.)	RBRC Seminar Worldvolume tempered Lefschetz thimble method as an algorithm towards solving the sign problem (virtual)	Nov. 18
70	Pieter Taels (U. Antwerp)	RBRC Seminar Quarkonium production at the EIC as a probe of gluon TMDs (virtual)	Nov. 19
71	Daisuke Inotani (RIKEN)	SNP Seminar Strong-coupling effects of pairing fluctuations, and Anderson-Bogoliubov mode in neutron superfluids in neutron stars (virtual)	Nov. 24
72	Andrey Tarasov (Ohio State U.)	RBRC Seminar The role of the chiral anomaly in polarized deep inelastic scattering: Topological screening and transitions from emergent axion-like dynamics. (virtual)	Dec. 2
73	Jorge Noronha (U. Illinois)	RBRC Seminar Hydrodynamic frames: The good, the bad, and the ugly (virtual)	Dec. 3
74	Filip Bergabo (City U. of New York)	RBRC Seminar Coherent energy loss effects in dihadron azimuthal angular correlations in deep inelastic scattering at small x (virtual)	Dec. 9
75	Michal P. Heller (Max Planck Institute for Gravitational Physics)	RBRC Seminar The hydrodynamic gradient expansion diverges beyond Bjorken flow (virtual)	Dec. 10
76	Yuki Kamiya (Bonn U.)	SNP Seminar Femtoscopic study on the hadron-hadron interaction (virtual)	Dec. 17
77	Gabriel Santiago (Ohio State U.)	RBRC Seminar Quark sivers function at small x: Spin-dependent odderon and the sub-eikonal evolution (virtual)	Jan. 7
78	Lorenzo Contessi (IRFU)	SNP Seminar Universality in multi-fermion systems (virtual)	Jan. 12
79	Raju Venugopalan (BNL)	RBRC Seminar Classicalization and unitarization of wee partons in QCD and gravity: The CGC-black hole correspondence (virtual)	Jan. 13
80	Jean-Paul Blaizot (IPhT U.)	RBRC Seminar Attractor and fixed points in Bjorken flows (virtual)	Jan. 14
81	Lájer Márton (Eötvös Loránd U.)	RBRC Seminar When cold, dense quarks are not a Fermi liquid (virtual)	Jan. 20
82	Ismail Zahed (Stony Brook U.)	RBRC Seminar On the topological origin of hadronic mass and spin (virtual)	Jan. 21
83	Luigi Coraggio (U. Campania)	SNP Seminar Microscopic approaches to the calculation of the nuclear matrix element for the neutrinoless double-beta decay (virtual)	Jan. 24
84	Shohini Bhattacharya (BNL)	RBRC Seminar First global QCD analysis of the worm-gear TMD g1T (virtual)	Feb. 3
85	Giovanni Chirilli (Regensburg U.)	RBRC Seminar Pseudo- and quasi-PDFs in the BFKL approximation (virtual)	Feb. 4
86	Chandrodoy Chattopadhyay (North Carolina State U.)	RBRC Seminar Far-from-equilibrium attractors in boost-invariant plasmas (virtual)	Feb. 10

87	Simon Catterall (Syracuse U.)	RBRC Seminar Symmetric mass generation and anomalies in particle and condensed matter physics (virtual)	Feb. 11
88	João Barata (U. Lisbon)	RBRC Seminar Jet quenching in anisotropic media (virtual)	Feb. 17
89	Michael Wagman (Fermilab)	RBRC Seminar Few-nucleon systems in lattice QCD (virtual)	Feb. 18
90	Paul Caucal (BNL)	RBRC Seminar Anomalous diffusion in QCD matter (virtual)	Feb. 24
91	Takumi Doi (RIKEN)	RBRC Seminar Hadron interactions from lattice QCD (virtual)	Feb. 25
92	Yasutaka Taniguchi (Kagawa College)	SNP Seminar $^{12}C+^{12}C$ fusion astrophysical S-factor in a full-microscopic nuclear model (virtual)	Feb. 25
93	Mendel Nguyen (NC State U.)	RBRC Seminar Noninvertible symmetry and string tensions beyond N-ality (virtual)	Mar. 3
94	Farid Sazalar (UCLA)	RBRC Seminar Promoting gluon saturation to higher precision with dijets at the EIC (virtual)	Mar. 4
95	Bing-Nan Lu (China Academy of Engineering Physics)	SNP Seminar Ab initio nuclear physics on the lattice (virtual)	Mar. 4
96	Christian Schmidt (U. Bielefeld)	RBRC Seminar Lee-Yang edge singularities in lattice QCD (virtual)	Mar. 10
97	Andrei Alexandru (The George Washington U.)	RBRC Seminar Three hadron scattering from lattice QCD (virtual)	Mar. 11
98	Yuya Tanizaki (YITP)	RBRC Seminar Semiclassical description of confinement via center vortices and anomaly-preserving T^2 compactifications (virtual)	Mar. 17
99	Xabier Feal (BNL)	RBRC Seminar Infrared structure of QED as a many-body theory of worldlines (virtual)	Mar. 18
100	Alexander Rothkopf (U. Stavanger)	RBRC Seminar Static interquark potential from Euclidean and real-time lattices (virtual)	Mar. 24
101	Ihsse Friederike (BNL)	RBRC Seminar Towards resolving the QCD phase structure with discontinuous Galerkin methods (virtual)	Mar. 31

SNP Seminar → http://snp.riken.jp/seminar.html
RIKEN/BNL Lunch Time Talk → https://www.bnl.gov/riken/events/

Events (April 2021—March 2022)

RNC

Apr. 23	Wako Open Campus
May 26	The 28th RBRC Management Steering Committee (MSC)
Jul. 7	The 17th Industrial Program Advisory Committee (In-PAC)
Dec. 1–3	The 22nd Program Advisory Committee for Nuclear Physics Experiments at RI Beam Factory (NP-PAC)
Dec. 8–27	The 18th Industrial Program Advisory Committee (In-PAC)
Dec. 9–Jan. 4	The 21st Program Advisory Committee for Materials and Life Science Researches at RIKEN Nishina Center (ML-PAC)

CNS

Aug. 16–20	20th CNS International Summer School (CNSSS21) https://indico2.cns.s.u-tokyo.ac.jp/event/145/

Press Releases (April 2021—March 2022)

RNC

Apr. 16	New precise spectroscopy of the hyperfine structure in muonium with a high-intensity pulsed muon beam	K. Ishida, M. Iwasaki, Meson Science Laboratory
Apr. 26	Proton-^{3}He elastic scattering at intermediate energies	H. Sakai, RNC
May. 11	Measurement of neutron rich high dense matter pressure —Reproducing the inside of neutron star matter in a laboratory—	T. Isobe, M. Nishimura, H. Sakurai, H. Otsu, H. Baba, Radioactive Isotope Physics Laboratory, SAMURAI Team, Computing and Network Team
May. 19	Discovery of a charge symmetry breaking —Large difference in the shape between Kr-70 and Se-70—	P. Doornenbal, H. Sakurai, Radioactive Isotope Physics Laboratory
Aug. 30	Most charming dibaryon, "Charmed di-Omega" —Theoretical calculation using supercomputers predicts a new hexaquark state—	H. Tong, Y. Lyu, T. Doi, Quantum Hadron Physics Laboratory
Sep. 1	First high-precision direct determination of the atomic mass of a superheavy nuclide evinces a new means to unambiguously determine atomic numbers	K. Morimoto, Superheavy Element Device Development Team
Oct. 15	Measurement of gluon's motion inside the proton via "direct photon" —Data reveal that the dynamical motion of gluons is not very large—	Y. Akiba, Y. Goto, S. Ralf, I. Nakagawa, Experimental Group, RIKEN BNL Research Center
Nov. 29	難治性甲状腺がんに対する医師主導治験を開始 ーアスタチンを用いた新しい標的アルファ線治療ー	H. Haba, Nuclear Chemistry Research Team, RI Application Research Group
Dec. 8	Succeeded in creating a new breed of Satsuma mandarin orange	T. Abe, Ion Beam Breeding Team, Beam Mutagenesis Group
Feb. 28	Negative string tension of higher-charge Schwinger model via digital quantum simulation	E. Itou, Strangeness Nuclear Physics Laboratory
Mar. 28	Measurements of strong-interaction effects in kaonic-helium isotopes at sub-eV precision with X-ray microcalorimeters	F. Sakuma, Meson Science Laboratory

KEK

Aug. 31	超重元素の初めての精密質量測定に成功 ー新元素の新しい原子番号決定法の証明ー https://www.kek.jp/ja/press/202109010000/	P. Schury, M. Wada

List of Preprints (April 2021—March 2022)

RIKEN NC-NP

	Not Applicable	

RIKEN NC-AC

7	First Beam from SRILAC	O. Kamigaito *et al.*

RIKEN MP

	Not Applicable	

RIKEN QHP

494	Photonic quantum kinetic theory in curved spacetime and the spin Hall effect	K. Mameda *et al.*
495	Complex Langevin study for polarons in an attractively interacting one-dimensional two-component Fermi gas	T. M. Doi *et al.*
496	Emergence of the rho resonance from the HAL QCD potential in lattice QCD	Y. Akahoshi *et al.*
497	Quantum hydrodynamics from local thermal pure states	S. Tsutsui *et al.*
498	Unitary p-wave Fermi gas in one dimension	H. Tajima *et al.*
499	Effects of finite-light-speed correction for the Coulomb interaction on nuclear binding energies and radii in spherical nuclei	T. Naito
500	Three-body crossover from a Cooper triple to bound trimer state in three-component Fermi gases near a triatomic resonance	H. Tajima *et al.*
501	Construction of energy density functional for arbitrary spin polarization using functional renormalization group	T. Yokota and T. Naito
502	New constraints on the neutron-star mass and radius relation from the terrestrial nuclear experiments	H. Sotani *et al.*
503	Persistence of cluster structure in the ground state of ^{11}B	N. Itagaki *et al.*
504	Optical spin transport theory of spin-1/2 topological Fermi superfluids	H. Tajima *et al.*
505	Perturbative predictions for color superconductivity on the lattice	T. Yokota *et al.*
506	Color superconductivity in a small box: a complex	S. Tsutsui *et al.*
507	On the validity of the complex Langevin method near the deconfining phase transition in QCD at finite density	S. Tsutsui *et al.*
508	Isovector density and isospin impurity in ^{40}Ca	H. Sagawa *et al.*
509	Investigations of decuplet baryons from meson-baryon interactions in the HAL QCD method	K. Murakami *et al.*
510	Flavor number dependence of QCD at finite density by the complex Langevin method	Y. Namekawa *et al.*
511	Emergence of the rho resonance from the HAL QCD potential	Y. Akahoshi *et al.*
512	Most charming dibaryon near unitarity	Y. Lyu *et al.*
513	Finite volume analysis on systematics of the derivative expansion in HAL QCD method	T. Doi *et al.*
514	Optimized two-baryon operators in lattice QCD	Y. Lyu *et al.*

515 Isospin symmetry breaking in the charge radius difference of mirror nuclei T. Naito *et al*

CNS-REP

100	CNS Annual Report 2020	H. Nagahama

Nishina Center Preprint server (not including Partner Institution) can be found at
http://nishina-preprints.riken.jp/

理化学研究所
埼玉県　和光市　広沢
RIKEN 2022-039
ISSN 0289-842X